

IAVCEI 2017

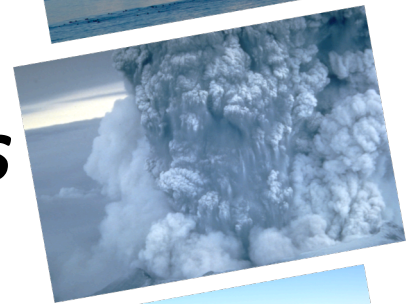
Scientific Assembly

August 14-18

Portland, Oregon, U.S.A

ABSTRACTS

***Fostering Integrative
Studies of Volcanoes***



Roberta Adamo, Milton Ivan Ordóñez, Cristian Mauricio Lopez, Maurizio Battaglia

Submission 71

2010 – 2016 geodetic monitoring of Nevado del Ruiz, Colombia

Nevado del Ruiz volcano is part of a 50 kilometer chain of volcanoes aligned N-S along the Colombian Central Cordillera. Due to its past eruptive history (i.e., the Armero tragedy in 1985), studying this volcanic complex using ground deformation data has considerable value for understanding the physical processes controlling its behavior. Furthermore, this information is essential for reducing the volcanic risk in the region. The deformation of Nevado del Ruiz has been monitored since 1985 and recently the geodetic network has been enhanced with electronic tiltmeters (since 2007) and permanent GNSS stations (since 2011). The monitoring record shows that Nevado del Ruiz has been continuously active since 2010, including an increase in seismicity, large gas and ash emissions, deformation, and moderate explosive eruptions (VEI = 2) such as those in May and June 2012. Analyzing and modeling the time-series from the GPS network allows us to trace the evolution of the deformation trend of Nevado del Ruiz. . Specifically, analysis of GPS and tilt recorded between 2007 and 2012 suggested the migration of magma from a deep reservoir to a shallower one, which is the source of the present unrest. In this work, we present the complete GPS time series from 2010 to the present. This longer data set enabled to study the evolution of the deformation infer the changes in the volume and depth of the magma reservoirs and instigating the unrest. Comparison with seismic and tilt data ensures a further check on the validity of the interpretation of the existing models of unrest, will help in forecasting eruptions and estimating the volcanic hazard in this area.

Brian James Aggangan, Teresito Bacolcol

Submission 983

Revisiting the Ground Deformation of Mayon Volcano during the 2004 and 2009 Eruptions using GPS

Mayon volcano, one of the most active in the Philippines, has erupted frequently in the past decades and poses risks to many residents at its vicinity. This study undertaken within the Philippine Institute of Volcanology and Seismology (PHIVOLCS), the national agency mandated in monitoring the country's most active volcanoes, revisits the ground deformation of Mayon volcano during the 2006 and 2009 magmatic eruptions. We start with the postprocessing of the Global Positioning Satellite (GPS) data from seven Mayon sites from 2004 to 2010 using GAMIT- GLOBK. After which we analyzed the interstation baseline lengths and east, north and up (ENU) displacements by realizing 3 local reference frames which aims to filter out the tectonic and active fault motion present in the local region. To further analyze the local deformation attributed to the volcano, we computed for GPS velocities at Mayon volcano by selecting time windows coinciding with identified trend changes in the baseline length and ENU displacement time series. Lastly, we identify and model the time windows that correspond to the ground deformation that preceded the 2006 and 2009 eruptions.

Using dModels, a MATLAB source code developed by the United States Geological Survey (USGS), we performed inverse modelling on both time windows that span the precursor ground deformation for both magmatic eruptions. Based on a reference frame constraining the position of one GPS site in the southwest of the vent, we observed the deformation during both precursor phases are characterized by deflation and interstation baseline lengthening. Seven months prior to the 2006 eruption, the ground deformation can be explained by a sill-like source centered 3.5 km southeast of the volcano vent with a volume change of -6.51×10^7 m³ and 283 m deep. Three months prior to 2009 eruption, the ground deformation can be explained by a sill-like source centered 3.5 km southwest of the volcano vent with a volume change of -3.42×10^5 m³ and 723 m deep.

For both eruptions, we were able to associate the closing of a shallow sill-like crack as the driving force for deflation. The results of this study, however limited GPS and the past two magmatic eruptions, are a useful reference in the understanding and predicting the behavior of Mayon volcano during unrest. Moreover, integrating other monitoring data from geophysics and remote sensing techniques may be key in enhancing our forewarning capabilities.

Gerardo J. Aguirre-Díaz, Aída López-Hernández, Eduardo González-Partida

Submission 933

The graben-type caldera of Tulancingo-Acocolco complex, central-eastern México: New caldera boundaries and their implications for geothermal exploration

The Tulancingo-Acocolco caldera complex (TACC) is a silicic center located at the eastern sector of the Mexican Volcanic Belt, in Puebla State. Previous studies indicate that Acocolco is an elliptical-shaped, classic caldera, with 18 by 15 km in diameter, nested within the 32 km in diameter Tulancingo caldera (López-Hernández et al., 2009, Geothermics). Tulancingo caldera was active at 3.0-2.7 Ma and Acocolco at 1.7-0.24 Ma, with the youngest rocks rather associated to mafic volcanism linked to regional faults in the area. Acocolco is a potential site for geothermal energy and has been studied since the 1980s by Comisión Federal de Electricidad Mexican agency, then, in 2015 by researchers from UNAM's Institute for Geophysics, and currently, by the group of GEMex project (European Union-Mexico consortium). The ignimbrites from Tulancingo and Acocolco calderas are mostly buried by younger volcanic rocks and thus these ignimbrites are little exposed. Two deep exploration wells (2000 m deep) carried out in Acocolco caldera shows the intracaldera sequence, but intense hydrothermal alteration has obscured the original textures in many units, although several of them are still recognizable, including a skarn at depth, densely-welded ignimbrites, and lava domes. A review of the geological and geophysical data of TACC resulted in a different interpretation involving the regional and local faults of this part of Mexico, such as NW- and NE- trending normal and strike-slip faults, respectively, which are both observed at surface and at depth by means of geophysics. Gravity studies indicate a rectangular caldera, much larger than previously thought for TACC, with 50 km by 37 km dimensions, elongated NW. The new caldera complex boundaries are represented by major faults that may have acted as the main vents during caldera collapse. This new interpretation for TACC, as a graben-type caldera (following Aguirre-Díaz, 2008, IOP), controlled by the trans-tensional tectonics of the region, has important consequences, in particular, by establishing new caldera boundaries, new caldera shape and size, new caldera type and origin, and a new paradigm to follow in the current studies of GEMex group involving geothermal exploration in this area, pointing towards the graben's boundary faults as well as the intra-caldera block faults as the main objectives for geothermics. Financed by GEMex grant for Working Group 4.

Thorbjorg Agustsdottir, Robert S. White, Tim Greenfield, Jennifer Woods, Tom Hudson, Bryndis Brandsdottir

Submission 1216

An overview of the 2014-2015 Bárðarbunga-Holuhraun volcano-rifting episode: Intrusive, co- and post-eruptive seismicity in Bárðarbunga caldera, central Iceland.

Bárðarbunga subglacial volcano, central Iceland, has remained seismically active since the first deployment of seismic instrumentation in Iceland in the 1920s. From 1974 seismicity rates were highly elevated, activity peaking in 1996 with the subglacial Gjálp eruption, SE of Bárðarbunga. Since 2004 seismicity rates have been increasing again, and on 16 August 2014 an intense swarm of seismicity marked the onset of a large dike intrusion. The dike exited the caldera at the SE corner, then taking a 90° turn and propagating laterally NE from the volcano at the brittle-ductile boundary ~6 km b.s.l., creating over 30,000 earthquakes along a 48 km path. Two weeks later a fissure eruption began at Holuhraun. The 6 months long eruption was the largest eruption in Iceland for over 200 years. During the eruptive period, Bárðarbunga experienced over 70 earthquakes greater than M5 that correlate with the gradual 66 m caldera subsidence.

During the dike intrusion seismicity progressively started in the caldera, confined to the northern rim and close to the dike exit. Throughout the eruption the caldera experienced high levels of seismicity, activating both the north and south side of the caldera rim. At the end of the eruption, caldera seismicity decreased drastically. We present accurate earthquake relocations, showing that during the study period the caldera seismicity was confined to shallower levels than ~7 km b.s.l. We investigate the different source failure mechanism between earthquakes occurring in the dike and those occurring in the caldera, using a Bayesian full moment tensor inversion, comparing the change throughout the intrusive, co- and post-eruptive periods.

Martin Airey, Giles Harrison, Keri Nicoll, Paul Williams, Graeme Marlton

Submission 1067

VolcLab: A balloon-borne instrument package to measure ash, gas, electrical, and turbulence properties of volcanic plumes

Release of volcanic ash into the atmosphere poses a significant hazard to air traffic. Exposure to appreciable concentrations (≥ 4 mg m⁻³) of ash can result in engine shutdown, air data system loss, and airframe damage, with sustained lower concentrations potentially causing other long-term detrimental effects (Safety and Airspace Regulation Group, 2014). Disruption to flights also has a societal impact. For example, the closure of European airspace following the 2010 eruption of Eyjafjallajökull resulted in global airline industry losses of order £100 million daily and disruption to 10 million passengers. Accurate and effective measurement of the mass of ash in a volcanic plume along with in situ characterisation of other plume properties such as charge, turbulence, and SO₂ concentration can be used in combination with plume dispersion modelling, remote sensing, and more sophisticated flight ban thresholds to mitigate the impact of future events.

We have developed and tested a new disposable instrument package that may be attached to a standard commercial radiosonde, for rapid emergency deployment on a weather balloon platform. The payload includes a newly developed oscillating microbalance to measure mass of ash directly without assumptions about particles' optical properties. The package also includes an SO₂ gas detector, an optical sensor to detect ash and cloud backscatter from an LED source (Harrison and Nicoll, 2014), a charge sensor to characterise electrical properties of the plume (Nicoll, 2013), and an accelerometer to measure in-plume turbulence (Marlton, et al., 2015). VolcLab uses the established PANDORA interface (Harrison, et al., 2012), to provide data exchange and power from the radiosonde.

There are several benefits of using this instrument suite in this design and of using this method of deployment. It is an all-in-one device requiring minimal expertise on the part of the end user. It is cheap and disposable, having been designed with software at the heart of device operation, which controls basic electronic components. The single package allows several plume properties to be measured and transmitted simultaneously. These systems can be deployed rapidly as part of a wider network of launches allowing spatially referenced datasets to be integrated with remotely sensed data. These measurements provide in situ plume characteristics for airspace risk management planning as well as providing valuable scientific information on plume dynamics.

Alessandro Aiuppa, Marcello Bitetto, Maarten Moretti, Gaetano Giudice, Marco Liuzzo, Giancarlo Tamburello, Gabriela Velasquez, Angelo Battaglia, Claudia Bucarey Parra, Vincenzo Francofonte, Andrea Mastrolia, Elvis Mendoza, Roberto Moretti, Armando Saballo

Submission 61

A volatile (CO₂) trigger for eruptions of mafic arc volcanoes: Insights from instrumental gas observations (2014-2017) at Villarrica and Masaya volcanoes

A major advance in volcanic gas studies has recently been achieved due to the advent of the Multi-component Gas Analyser System (Multi-GAS) technique. The improved temporal resolution of Multi-GAS-based volcanic gas observations has initially allowed capturing precursory leakage of CO₂-rich gas prior to eruption of Italian volcanoes. This success has motivated expanding the permanent Multi-GAS network to monitoring other volcanic regions, using funding from the DECADE program of the Deep Carbon Observatory (<https://deepcarboncycle.org/decade/>). Here, we present novel Multi-GAS results taken at two DECADE volcanoes, Villarrica in Chile and Masaya in Nicaragua, to show that pre-eruptive release of CO₂-rich gas is a recurrent precursor to volcanic eruption. At Villarrica, our results demonstrate a temporal evolution of volcanic plume composition in a 3-month period prior to the March 2015 paroxysm, the largest since 1985. In the period of escalating volcanic activity that culminated into the paroxysm, the gas evolved from low (CO₂/SO₂ ratios of 0.65-2.7) to rich (CO₂/SO₂ ratios up to \approx 9) in carbon. Similarly at Masaya, a pulse of unusually CO₂-rich gas (CO₂/SO₂ ratios > 20) was passively vented in the weeks prior to formation of the lava lake in December 2015. In contrast, the CO₂/SO₂ ratio was systematically 2-enriched gas was caused by a larger-than-normal supply of deeply sourced gas bubbles into the shallow conduit feeding system. Our results provide novel constraints on degassing mechanisms of carbon-poor (Villarrica) to intermediate carbon-rich (Masaya) arc magmas, and contribute to our understanding of lava-lake degassing dynamics. We conclude that the separate ascent of CO₂-rich gas, possibly sourced by intrusion of deep magma, may be a recurrent driver for the transition from quiescence to eruption.

Helena Albert, Fidel Costa, Jason Herrin, Andrea Di Muro, Nicole Metrich

Submission 620

Timescales of the 2007 caldera-forming eruption of Piton de la Fournaise (La Réunion Island) recorded in olivine crystals and their melt inclusions

Collapse of a small summit caldera is a rare event at Piton de la Fournaise (PdF). It occurred in 2007 during one of the largest eruptions (>200 Mm³ of magma). Effusion of aphyric basalts initiated at the summit area in mid-February, followed by the migration of active vents in March and early April to progressively lower elevations. Summit collapse occurred on April 5th while effusion of crystal rich lava continued until May 1st. Here we investigate the processes and timescales recorded in olivine crystals and their melt inclusions (MIs) based on their H₂O content.

Olivine cores from the early tephra emitted just before caldera collapse display compositional plateaus at Fo₈₄₋₈₆ [%Fo=100*Mg/(Mg+Fe)], but three different groups of olivine can be distinguished: (1) unzoned in Fo, Ca, Mn, or Ni, (2) Fo and Ni concentrations decreasing towards the rim (normal zoning), and (3) increasing Fo and Ni (reverse zoning), followed by normally zoned rims. Phosphorus concentrations and 2D X-Ray maps show complex patterns that can be interpreted as early skeletal growth that probably created the MIs. Olivine crystals from the post caldera collapse lava (April 25) are very similar to those of the tephra except that a few show lower Fo (82) at their rims, and next to MIs.

Diffusion modeling of the Fo, Ca, and Ni yield magma residence timescales for the olivine of the tephra that vary from a few days (normally zoned crystals), to up to a few months (reversely zoned crystals). Olivine crystals from the late-erupted lava yield timescales of only a few days.

The H₂O contents of the olivine-hosted MIs range from 0.67-1.16 wt% for the early tephra and from 0.35-0.87 wt% for the lava. This variation in the H₂O content has been previously ascribed to a multi-step ascent, degassing and crystallization. However, the selective loss of water in some MIs from the lava could suggest diffusive re-equilibration between MIs and their olivine hosts. We are applying an H₂O diffusive re-equilibration model to better understand the plumbing system processes that occurred before the eruption. The timescales obtained by using this method will be compared with the Fo, Ca and Ni timescales.

We infer that the early erupted crystals with the longest timescales could record a pre-existing intrusive body sitting below the volcano summit that was fluidized to lead to caldera collapse, while the normally zoned crystals grew more recently at shallow depth from the new mafic input that triggered the eruption.

Paul Albert, Victoria Smith, Emma Tomlinson, Takehiko Suzuki, Masataka Yamada, Takeshi Nakagawa, Suigetsu 2006 Project Members

Submission 870

Constraints on the tempo of volcanism at Daisen and Sambe volcanoes (SW Japan) from the Lake Suigetsu sedimentary archive

Pyroclastic deposits erupted from Daisen and Sambe stratovolcanoes located on south-west Honshu Island, Japan, are heavily weathered which makes reconstructing their volcanic histories using proximal terrestrial sequences challenging. Here we use volcanic ash (tephra) layers preserved in the down-wind, Lake Suigetsu (SG06 core) sedimentary archive, Honshu Island, to help elucidate both the chemical evolution and the tempo of volcanism at these two volcanic centres to better inform hazard assessments. The sequence from Lake Suigetsu spans approximately the last 150 ka and records tephra layers from volcanoes all over Japan. Volcanic glass shards from the visible tephra layers recorded in SG06 have been subject to detailed major and trace element geochemical characterisation. Glass geochemistry confirms nine tephra layers are from Daisen and four are from Sambe. The unrivalled temporal resolution of the SG06 record, owing to its integrated varve (annually layered) and ^{14}C chronology, provides high-resolution chronological constraints on the Daisen and Sambe explosive activities. The SG06 record reveals two main periods of unrest at Daisen volcano, characterised by multiple closely spaced eruptions. Differential dating in the varved portion of the SG06 record allows precise repose intervals to be calculated. Through integrating the proximal and distal records we now have a much more detailed understanding of the tempo and magnitude of volcanism from these volcanoes.

Fabien Albino, Falk Amelung

Submission 1058

Can rainfall trigger volcanic eruptions? The example of Cerro Azul volcano.

Many works have shown a correlation between rainfall and landslides or rainfall and earthquakes. This correlation can be explained by the increase of pore water pressure, which reduces the normal stress and trigger shear failure. However, the correlation between rainfall and eruptions is not widely studied. Mechanically, the formation of tensile failure around the magma reservoir is also pore pressure dependent and in theory an increase of pore pressure in the host rocks should favour the failure of the magma reservoir and the initiation of magma intrusion. Here, we will investigate this hypothesis at Cerro Azul volcano (Galapagos) where we observe that both last eruptions (1998 and 2008) occurred just after heavy rainfall events. In addition, based on Landsat dataset, the crater lake formed at Cerro Azul seems to be drained before eruptions. Using numerical models, we investigate how rainfall influences the stability of magma reservoir by combining (i) diffusion model to quantify how pore pressure changes from surface to depth after heavy rainfall events and (ii) poro-elastic numerical model to quantify the evolution of failure conditions of the magma reservoir as a consequence of these pore pressure changes. Sensitivity analysis is performed to characterize the influence on our results of the poro-elastic parameters (hydraulic diffusivity, permeability and porosity) and the geometry of the magma reservoir. In the event eruptions can be triggered by pore pressure changes, meteorological records and water table measurements would be an important information to improve eruption's forecast, especially in tropical regions where heavy rainfall events frequently occur, such as in Indonesia, Philippines or Central America.

John Albright, Patricia Gregg, Jeff Freymueller, Zhong Lu

Submission 347

Hindcasting the 2008 eruption of Okmok, AK using multi-data stream statistical data assimilation

Over the past few decades increasing effort has been spent monitoring active and potentially dangerous volcanoes, resulting in large, multi-instrument datasets including geophysics, remote sensing, geodesy, seismology, and geochemistry. In analyzing such datasets, statistical model-data fusion techniques such as the Ensemble Kalman Filter (EnKF) provide a robust and flexible framework that can match a variety of observations to increasingly sophisticated predictive models of magma chamber dynamics. In particular, the EnKF data assimilation framework can incorporate any observations that can be reasonably constrained by a chosen model while accounting for the uncertainties in both model and data. The EnKF has been used successfully in many fields, such as climate and hydrologic modeling, to provide model forecasts and hindcasts of dynamic systems. In this study, we use the EnKF to analyze geodetic data from Okmok Volcano, Alaska, in the years leading up to its July 2008 eruption, combining data from 4 continuous GPS stations, yearly GPS campaigns through 2005, and 46 Envisat InSAR interferograms. As new data become available for assimilation, the EnKF updates the parameters (e.g., chamber position and volume change) for an elastic model of a deforming magma reservoir. Using the misfit between the EnKF forecast and surface deformation observations, the model is nudged towards the more successful outcomes, eventually converging to a best-fit approximation. Furthermore, the elastic finite element model calculates stress evolution along the magma reservoir wall to determine whether or not tensile and/or Mohr-Coulomb failure has occurred. Finally, the results of the EnKF analysis are compared to previous deformation and finite element modeling investigations from Okmok, showing comparable results. Moving forward, increased computing power will allow the use of the EnKF technique with more advanced thermomechanical models capable of predicting and assimilating a wider variety of data types, with the ultimate goal of rapidly assimilating data in real time to provide forecasts of volcanic unrest.

Ellen Alexander, Johan Varekamp, Alejandro Rodriguez

Submission 1135

The chemical heartbeat of a volcanic hydrothermal system at Copahue volcano, Argentina

Copahue is an active arc volcano at 37.8° S in the Argentine Andes with an acid crater lake. Near-summit hot springs contaminate the Upper Río Agrio, glacial Lake Caviahue, and the Lower Río Agrio. The compositional time trends of the acid hot spring fluids reflect conditions within Copahue's shallow magmato-hydrothermal system. We used water flux measurements of the Upper Río Agrio and its river water chemistry to compute element flux variations between 1997 and 2013. Copahue had eruptions in 2000 and late 2012, and a failed eruption/intrusion in 2004. The flux data show a consistent pattern of pre-eruptive enrichment in volcanic volatiles (Cl, F, S) followed by enhanced fluxes of rock-forming elements and very rapid post-eruptive attenuation of all element fluxes. The Cl export rate from the system varied from 1700 Mg Cl/month prior to the 2012 eruption to 280 Mg Cl/month a few months after it. The Al fluxes varied from 650 Mg Al/month during the 2000 eruption to 70 Mg Al/month in early 2013. Similarly, the K flux varied from 100 Mg K/month prior to the 2012 eruption to 20 Mg K/month in early 2013. We hypothesize a "two valve" model for the hydrothermal system with a bottom valve that lets volcanic gas and heat enter from the underlying magma, conditioned by the permeability of the magma-fluid interface. A second 'valve' is represented by the overall permeability of the hydrothermal system that allows the export of fluids into the ambient world. Prior to eruption, the system acidifies and heats up, followed by magma intrusion and/or eruption, and reaction of the newly emplaced rock with the hot acid fluids. This leads to enhanced export rates of all elements, quickly followed by precipitation of secondary minerals such as alunite. This reduction in the system's permeability is reflected in highly reduced fluxes of all elements, but especially K and Al, as indicated in strong decreases in Al/Cl and K/Cl after the eruptions. In the longer aftermath of the eruption, the alunite starts to redissolve again. The annual flux measurements are tuned for annual variations with non-steady state dynamic calculations in Lake Caviahue. Saturation modeling of the hot spring fluid compositions allows the identification of the minerals that ultimately clog up the system. This alternation of enhanced acidification – rock dissolution – mineral precipitation – redissolution is the 'heartbeat' of the Copahue magmato-hydrothermal system.

Marco Antonio Aliotta, Mauro Amore, Stefano Messina, Flavio Cannavò, Carmelo Cassisi, Rosa Anna Corsaro, Marcello D'Agostino, Emanuela De Beni, Mario Dolce, Cinzia Federico, Andrea Mastrolia, Salvatore Mangiagli, Giuseppe Messina, Placido Montalto, Antoni

Submission 1010

Time Series Database Management System (TSDSystem) of Istituto Nazionale di Geofisica e Vulcanologia (INGV, Italy): a powerful tool for the management of volcano monitoring

One of the institutional duties of INGV is monitoring the active volcanoes of Italy. It consists in the systematic collection, analysis, and interpretation of visual observations and instrumental measurements before, during, and after eruptive activity. Monitoring is fundamental to forecast potential unrest scenarios in order to help the Italian Civil Protection Department (DPC) to evaluate volcanic risk and plan mitigation strategies.

Multiparametric monitoring is the winning strategy to investigate the complex dynamics of the volcanic systems. We developed a framework called TSDSystem (Time Series Database System), which allows to acquire data streams from several geophysical and geochemical permanent sensor networks (representing different data sources), located on the main volcanic areas of Southern Italy, and relate them within a relational database management system. Furthermore, spatial data related to different dataset are managed using a GIS module for sharing and visualization purposes. Starting from the GIS geodatabase used to create the geological map of Etna volcano (1:50.000), we have achieved a web-geodatabase. GIS modules can share data using common OGC web service such as WMF, WMTS and WFS.

Data standardization provides the ability to perform operations, such as query and visualization, of many measures synchronizing them using a common space and time scale. Finally, the structure of TSDSystem can manage several kinds of data such as chemical composition of volcanic rocks collected during an ongoing eruption and the chemical composition of volcanic fluids monitored during periodical surveys. The parameters and associated metadata are organized in a hierarchical standardized architecture.

In order to share data among INGV observatories, and also with DPC, we designed a "Master View" system that, starting from the implementation of a number of instances of TSDSystem (one for each observatory), makes possible the joint interrogation of data, both temporal and spatial, on instances located in different observatories, using web services technology. Similarly, it provides metadata for equipments using standard schemas (such as FDSN StationXML). The "Master View" manages the data policy through a "who owns what" system, which allows to associate viewing/download of spatial or time intervals to particular users/groups. TSDSystem is also able to provide data to different big projects such as EPOS (European Plate Observing System).

Patrick Allard

Submission 45

Terrestrial lava lakes: remarkable windows into inner magma dynamics and degassing at open-conduit volcanoes

Persistent lava lake activity is a quite rare phenomenon on Earth, during which molten magma continuously outcrops and degasses at the open air while losing little to no solid mass. Such an activity provides volcanologists with an exceptional opportunity to directly observe and investigate what is normally hidden within persistently active volcanoes: the innermost dynamics of an open magma reservoir/conduit system capable to sustain continuous gas and heat flow. Persistent lava lakes currently occur at only seven subaerial volcanoes worldwide: Nyiragongo and Erta'Ale (Eastern Africa), Kilauea (Hawaii), Erebus (Antarctica) and, in subduction zones, Masaya (Nicaragua), Villarica (Chile) and Ambrym (Vanuatu). These lava lakes display variable lifetime (from a few years to more than a century) and distinct dynamical patterns (from quiescent convective overturn, vigorous bubbling, cyclic upheaval and drain back due to gas-piston effects, to pulsated explosive disruption). Over the past decades lava lake behavior and source mechanisms have increasingly been investigated through field measurements at the above volcanoes – combining direct analysis of gas emissions and solid products with real-time recording with remote sensing tools – and analogue/numerical modelling. Comparison between measured parameters, models and volcanic activity reveal common features but also differences relying on the corresponding magma composition, volatile content and viscosity, the rates of magma supply, convection and degassing, as well as the system geometry. Here I'll present an overview of the main observations and results obtained in investigating/understanding terrestrial lava lake activity.

Patrick Allard, Alessandro AIUPPA, Philipson BANI, Nicole METRICH, Antonella Bertagnini, Michael Burton, Pierre-Jean GAUTHIER, Francesco PARELLO, Hiroshi SHINOHARA, Georgina SAWYER, Emanuela BAGNATO, Esline GARAEBITI

Submission 46

Volatile budget, magma dynamics and plumbing system of a top-ranking basaltic gas emitter: Ambrym volcano, Vanuatu Arc.

Ambrym basaltic volcano, in central Vanuatu arc, is one of the most active volcanic systems of the Southwest Pacific region. Lava lake activity and voluminous gas release occur from two main cones, Benbow and Marum, in its 12 km-wide summit caldera. We realized the first detailed investigations of gas emissions from this very active but remote and hardly accessible intra-oceanic arc volcano, combining both in situ and remote sensing tools during ground-based and airborne measurements. The degassing budget of major, minor, trace and radioactive volatile species reveals that Ambrym ranks amongst the three most powerful persistent emitters of magmatic volatiles at global scale [1]. Coupled with analysis of dissolved H₂O, CO₂, S and Cl in the feeding basalt (olivine-hosted melt inclusions), the gas emission rates imply a very high average magma supply/degassing rate of 25 m³/s – 6 times the rate at Mount Etna - from a reservoir emplaced at about 4 km depth beneath the caldera floor. The chemical composition of emitted volcanic gases is compatible with prevalent closed-system ascent and degassing of the basalt, followed by open degassing at shallow depth as water exsolution becomes extensive. Mass balance calculations imply that most of the degassed (denser) magma is convectively recycled downward in ca. 6 m wide conduits, in agreement with textural features of erupted tephra [2]. High resolution OP-FTIR remote sensing of hot volcanic gases from Benbow lava lake reveals different periodic oscillations in the degassing process associated with convective basalt overturn in the lake and the feeding conduits [3]. The ratios and fluxes of short-lived radioactive daughters of radon-222 (²¹⁰Po, ²¹⁰Bi, and ²¹⁰Pb) in the volcanic gases and ²¹⁰Pb activity in the basalt constrain that the 4 km-deep magma reservoir has a volume of 0.5 km³, is entirely renewed in about 240 days, and that gas bubbles raise up to the surface in less than 10 days.

[1] Allard et al., *JVGR* 322, 119–143, 2016; [2] Polacci et al., *JVGR* 233–234, 55–64, 2012;

[3] Allard et al., *EPSL* 448, 69-80, 2016.

Chelsea Allison, Kurt Roggensack, Amanda Clarke

Submission 1206

Thermodynamic modeling of H₂O-CO₂ solubility experiments in alkali-rich mafic magmas at mid-crustal pressures

Volatile solubility in magmas is dependent on both composition and pressure. In mafic magmas, high concentrations of alkali elements (Na and K) are known to increase H₂O-CO₂ solubility. These alkali-rich mafic magmas can consequently erupt explosively due to the exsolution of abundant gases. While existing volatile solubility models for alkali-rich mafic magmas are well calibrated below ~200 MPa, at greater pressures the experimental data becomes sparse. Melt inclusions (MIs) from some highly explosive mafic eruptions record CO₂ contents above this calibrated volatile solubility range for alkali-rich mafic magmas, which inhibits interpretation. Additionally, recent studies on volatiles, primarily CO₂, sequestered in MI bubbles have found as much as 90% of the total MI CO₂ content in the MI bubble, further demonstrating the need for higher pressure volatile solubility data. To allow for detailed interpretation of MI data at higher CO₂ contents and better understand magmatic plumbing systems, we conducted a set of mixed H₂O-CO₂ volatile solubility experiments at 1200°C in several mafic compositions with variable alkali contents. We targeted CO₂-rich fluid compositions at pressures between 400 and 600 MPa. The magma compositions cover a range of total alkali contents (~4 to 9 wt.%), but also varying ratios of Na vs. K to study the effects of different alkali components and produce a robust volatile solubility model. We analyzed the fluid composition of our experiments by vacuum manometry and the volatile content by Fourier transform infrared spectroscopy. Results from our experiments suggest that existing volatile solubility models for alkali-rich mafic magmas, if extrapolated beyond their calibrated range, over-predict CO₂ solubility at mid-crustal pressures. Physically, these results indicate that volatile exsolution can occur at deeper levels than what lower-pressure experiments would suggest. We have utilized an existing thermodynamic model and defined compositional relationships for the input parameters to accommodate our higher-pressure experimental data. Our revised model indicates deeper magma storage in this mid-crustal region than previously interpreted from MIs with high CO₂ contents.

Jorge Armando Alpala, Rosa Liliana Alpala, Maurizio Battaglia

Submission 68

Monitoring remote volcanoes: the 2010 - 2012 unrest at Sotar volcano (Colombia).

Sotar is a little known andesitic-dacitic stratovolcano in southern Colombia (Central Cordillera, Cauca Department). Its remote location and the lack of accessible roads make studying and monitoring Sotar volcano difficult. No historical eruptions are known, though there is current geothermal activity. Between the fall of 2010 and the fall of 2012 a small magma intrusion (inversion of tilt data indicate a depth ~ 1 km and $\Delta V \sim 106$ m³) triggered surface deformation and volcano-tectonic earthquakes but failed to reach the surface. This episode of unrest started with the volcano-tectonic earthquake of September 2010 (ML 4.4). Although one electronic tiltmeter recorded significant deformation between Jan 2011 and July 2012 (137 ± 7 μ rad), seismic activity remained at background levels until May 2012. Between June and September 2012, seismicity increased dramatically with an average of 120 volcano-tectonic events per day of magnitude up to 2.2. The epicenters of these events were initially located 6 km NE of the volcano but then migrated along a linear fracture towards the NW summit of the volcano. At the same time, the hypocenters moved closer to the surface as well: from a depth of 3 - 6 km for the initial events to a depth of 1 - 4 km for the events at the end of the summer. Although the dike intrusion did not culminate in an eruption, and seismicity and deformation returned close to background levels by January 2013, this episode of unrest is a reminder that Sotar is an active volcano and must be carefully monitored.

Salvatore Alparone, Alessandro Bonforte, Salvatore Gambino, Francesco Guglielmino, Francesco Obrizzo, Rosanna Velardita

Submission 799

Interaction between tectonic and volcanic dynamics at volcano island revealed by multiparametric monitoring data

Vulcano island is a composite volcanic edifice located in the south-central sector of the Aeolian Archipelago (Tyrrhenian Sea, Italy). Historic activity has been characterized by frequent transitions from phreatomagmatic to minor magmatic activity. The last eruption in 1888-90 was characterized by energetic explosive pulses and defines the “vulcanian” type of activity. After the 1880-90 eruption, La Fossa has been affected by two main episodes of increasing fumarolic activity; the first occurred in 1913–1923, when the maximum temperature of the crater fumaroles increased until to 615°C and the second episode began in the 80’s when fumarole temperature progressively increased to 690°C recorded in May 1993. The last unrest was marked by the two most energetic seismic episodes occurred at Aeolian Archipelago in the last century: the April 15, 1978 (M=5.5) and the May 28, 1980 (M=5.7); between late 70s and beginning of 90s, La Fossa was characterized by increasing temperature and output of crater fumaroles, chemical changes in fumaroles and waters, opening of new fractures on the cone and local seismicity.

We investigate Vulcano dynamics through ca. 40 years of ground deformation and seismicity data collected by the discrete and continuous INGV monitoring networks. We consider levelling, GPS, EDM, seismic and tilt data.

We distinguish three main superimposed dynamics, related to three main sources and acting at three different space and time scales: 1) A tectonic lithospheric fault system continuously, widely and slowly deforming the island that, sometimes, can be disturbed by local strong earthquakes temporarily changing the local stress field. These changes in the stress field can favor magma transfer from different storage levels and can disturb the magmatic fluid circulation at depth, triggering 2) a shallower pressure source beneath Vulcanello at 3-6 km depth, usually deflating in rest periods but that can release hot magmatic fluids coming up towards the surface. These fluids inevitably intercept the 3) shallowest hydrothermal system, interacting with the water table and increasing the temperature and pore pressure, defining the shallowest ground deformation source beneath La Fossa cone that inflates due to the increase in fluid circulation, causing very local seismicity, and deflates when all the excess of pressure has been released.

Falk Amelung, Alfredo Terrero, Bhuvan Varugu, Patricia Mothes, Yunjun Zhang, Dario Solano, Yosuke Aoki

Submission 1297

InSAR monitoring of volcanoes in Ecuador, Japan, Hawaii and Mexico

Several international space agencies are operating SAR satellites that provide data for volcanology, including the European Sentinel-1 sensors and Japan's ALOS-2. Some of the data sets are open access and directly available from the space agency, some are available from initiatives such as the Geohazard Supersites and Natural Laboratory initiative (GSNL) of the Group on Earth Observation, whereas others are available through research projects with space agencies. These data support routine data analysis approaches using automated workflows.

The Ecuadorian and Hawaiian volcanoes are among the selected volcano Supersites and therefore have excellent coverage by SAR satellites. Here we present the monitoring infrastructure put in place for the Supersites as well as results for recent crises and deformation periods. The SAR data are downloaded using Unavco's seamless SAR archive web services (SSARA). Networks of interferograms are processed into displacement time-series using the PySAR software (<https://github.com/yunjunz/PySAR>) and displayed using a time-series viewer at <http://insarmaps.miami.edu>, from which they are accessible to interested users via webservice. Case studies presented include the 2015 eruption of Cotopaxi volcano, the 2017 crises at Cerro Azul volcano in the Galapagos Islands, and the ongoing inflation periods at Mauna Loa and Kilauea volcanoes in Hawaii.

We also present results for volcanoes in Japan and Mexico. Japan's volcanoes are well covered by the L-band ALOS-2 mission of the Japanese Space Agency. The Mexican volcanoes are observed by the TerraSAR-X satellite of the German Space Agency (DLR).

Alvaro Amigo, Daniel Bertin

Submission 1190

Recent eruptions in the Andean Southern Volcanic Zone: surveillance, processes and impacts

In the last decade, several volcanic eruptions have occurred in the Andean Southern Volcanic Zone, which have affected regions in both Chile and Argentina. Some of them have been characterized by explosive behavior such as Calbuco (April, 2015) and Villarrica (March, 2015), while others are examples of explosive-effusive transitions and long-lasting bent-over plumes such as Chaiten (2008-2009) and Puyehue-Cordon Caulle (2011-2012). In addition, minor explosive activity have occurred in Planchon-Peteroa, Nevados de Chillan, Copahue, Llaima and Hudson volcanoes. Despite the fact that magnitudes of these eruptions are far below the largest historical eruptions documented for this segment of the Andes, for instance Quizapu in 1932 and Hudson in 1991, they are relevant due to the following features:

- They have generated notable tephra fall deposits in the proximal areas

- All have produced significant amount ash which have been dispersed thousands of km downwind

- Collection of distal fine ash allowed accurate volume estimations

- Near real-time assessment of ash clouds concentration and column heights

- Most of them were forecasted through the Chilean multiparametric network for volcanic surveillance

In this contribution, we describe the dynamics of the eruptions, characterize deposits in the field and their grain-size distributions, delineate atmospheric dispersals, update volume estimations and, finally, discuss about early warnings orientated to the mitigation of impacts related to tephra fallout. A discussion will be done on the size of expected eruptions in the near future and the comparison with the geological record, along with the compilation of a new dataset of volcanological parameters in order to better forecast ash dispersal and surface accumulation during future explosive activity in the Andes.

Nathan Andersen, Brian Jicha, Brad Singer, Wes Hildreth

Submission 1252

Recognizing signal through the noise: pre-eruptive incorporation of ^{40}Ar in Bishop Tuff sanidine revealed by single-crystal $^{40}\text{Ar}/^{39}\text{Ar}$ incremental heating

Accurate and precise eruption ages are critical to interrogating the timescales of magma emplacement and crystallization preceding caldera-forming eruption. Owing to the mobility of Ar in sanidine at magmatic temperatures, $^{40}\text{Ar}/^{39}\text{Ar}$ ages are typically interpreted to date the eruption without the ambiguity imparted by the protracted crystallization recorded by U-Pb dates of accessory minerals. Notwithstanding, dispersion of sanidine $^{40}\text{Ar}/^{39}\text{Ar}$ fusion dates—attributed to xenocrysts, excess Ar, or lost Ar—is common and thus data interpretation and eruption age assignment have become more problematic with the advent of multi-collector mass spectrometers. Whereas pooling many low precision dates frequently yields a statistically valid weighted mean age, the petrologic processes underlying dispersed sanidine datasets have not been explored.

Precise $^{40}\text{Ar}/^{39}\text{Ar}$ incremental heating of 49 individual sanidine crystals within five fall and flow units of the Bishop Tuff (BT) quantitatively recognizes and excludes intra-crystal domains compromised by Ar excess or loss that would bias ages calculated from single-crystal fusion data. The nominal range of plateau dates is 2.5 times less than that of recent fusion datasets. Yet dates up to 9.2 kyr older than the eruption, which are produced by crystals found throughout the BT deposits, imply that local thermal or chemical heterogeneity impacts the K-Ar clock in sanidine. Hypotheses to explain the older sanidine dates include: 1) Cooling of reservoir marginal domains below $\sim 550^\circ\text{C}$, accumulation of radiogenic Ar, and remobilization shortly prior to eruption, or 2) uniform incorporation of excess Ar during crystal growth or equilibration with melt enriched in Ar owing to its proximity to ancient reservoir wall rock.

The youngest sanidine dates are likely most representative of the BT eruption. Thus, common statistical filters that favor the mean or median of the aggregate population of single crystal dates are inappropriate. We propose a BT eruption age of $764.8 \pm 0.3/0.6$ ka (2σ analytical/full uncertainty; relative to 1.1864 Ma ACs) that is more precise and slightly younger than other recent estimates. Single-sanidine step heating provides new leverage with which to interpret U-Pb ID-TIMS zircon dates, indicates that pooling dispersed sets of dates from either technique can yield inaccurate eruption ages, and offers a new tool to probe the evolution of large silicic systems.

Kyle Anderson

Submission 780

Probabilistic short-term forecasting of eruption rate at Kīlauea Volcano using a physics-based model

Deterministic models of volcanic eruptions yield forecasts of future activity conditioned on uncertainty in the current state of the system. Physics-based eruption models are in principle well-suited for deterministic forecasting as they allow the current state of the system to be constrained using diverse observations, and future states of the system are derived naturally from the magma physics which underlie the model. However, physics-based eruption forecasting is strongly limited by our ability to model complex and often poorly-understood volcanic processes.

At Kīlauea Volcano, hours- to days-long cycles of magma system depressurization (termed deflation-inflation, or “DI” events) generate correlated, quasi-exponential variations in ground deformation and surface height of the active summit lava lake, as well as variations in eruption rate which partly control downslope lava inundation hazard. Because more than 600 of these events have been recorded to date, they offer an unusual opportunity to refine and test a physics-based eruption forecasting approach and apply it to lava effusion rates over short time periods.

A simple model of transient reductions in magma supply to Kīlauea’s shallow reservoir explains, to first order, DI event evolution. A Bayesian formulation together with a Markov chain Monte Carlo algorithm is used to simultaneously estimate uncertain model parameters, the time-evolving state of the system, and its state at future times. The evolution of an ongoing event is derived naturally from deterministic model physics and the current state of the system, but because the mechanism that triggers the onset or cessation of magma supply reductions is unknown, event durations are modeled stochastically from the statistics of previous events. Forecasts take the form of probability density functions which are thus conditioned on uncertainty in model parameters and stochastic event durations. Using past data, I perform hundreds of thousands of simulated forecasts and compare with observed outcomes. Forecast errors generally agree with estimated uncertainties, but uncertainties are relatively large – due chiefly to uncertainty in event duration. These results both validate the mixed probabilistic-deterministic eruption forecasting approach and also demonstrate some of the challenges inherent in using magma physics to forecast behavior at real systems.

Emily S. Anderson, Curtis M. Oldenburg, Michael H. Ort

Submission 914

An investigation of the role of thermal conditions, hydrologic processes, and country rock permeability in phreatomagmatic maar eruptions

Direct interaction of magma with external water often results in explosive eruptions due to molten fuel-coolant interaction. The explosivity of these eruptions is largely controlled by the extent to which water mixes with magma and the location in the conduit where this interaction occurs. Recently published experimental studies show that most phreatomagmatic tuff ring deposits are produced by explosions occurring above ~200 m depth, while those between ~200- 500 m are rarely energetic enough to displace material at the surface. It is thus uncertain how phreatomagmatic eruptions occur where depth to the water table is far below this critical depth as it is in some desert environments. While many studies have examined characteristics of magma in phreatomagmatic events, few have focused on questions regarding the details of thermohydrologic processes that control the eruption. To address this problem, we have investigated two maars in the San Francisco Volcanic Field of northern Arizona, Colton Crater and Rattlesnake Crater. Colton Crater appears to have formed by a prolonged cinder-cone-building eruption with only a brief late period of phreatomagmatic activity, while Rattlesnake Crater's deposits display characteristics of sustained magma-water interaction. Hydrologic, structural, and stratigraphic data of the subsurface beneath each volcano were used to construct conceptual models of groundwater flow and heat transfer within each eruptive system. The relevant thermophysical flow processes were then modeled using TOUGH2 simulation software. Preliminary results indicate that the continued phreatomagmatism of Rattlesnake Crater may have resulted from the formation of a "heat pipe" that carried water to the near-surface. Vertical heat pipes form when heat at depth vaporizes water, which rises until reaching cooler temperatures where it condenses, transfers latent heat to the surroundings, and falls back down due to gravity to repeat the cycle. This method may provide both a mechanism for moving liquid water through the overburden to a region shallow enough to produce efficient explosions, as well as for maintaining a wet eruption. By contrast, a heat pipe does not appear to have formed in the brief phreatomagmatic stage of Colton Crater's eruption. This suggests that the amount of time required to produce a large-scale heat pipe exceeds the duration of this eruptive phase, or that water supply was limited, though the short-lived explosions were very powerful.

Kyle Anderson, Takehiro Koyaguchi, Tomofumi Kozono

Submission 563

What can we learn by inverting monitoring data from explosive eruptions? Insights from a fast, physics-based eruption model

Our ability to monitor explosive volcanic eruptions has improved greatly in recent years. Time-dependent observations of ground deformation and eruption rate are now both increasingly available, and often show remarkable correlations, as recently observed at Grimsvötn and Shinmoedake volcanoes. Multiphysical (physics-based) eruption models link diverse observations such as these with magma physics, and may be used in a Bayesian inverse to estimate properties of volcanic systems. Yet, this approach has not yet been applied to explosive eruptions, in part due to the computational expense of explosive conduit flow models. Quantitatively interpreting and utilizing diverse observations from explosive eruptions remains a tremendous challenge.

In this work we couple a fast, 1D explosive/effusive conduit flow model [Koyaguchi, 2005; Kozono and Koyaguchi, 2009] with a simple elastic reservoir model and use it to predict time-dependent observations of ground deformation and mass eruption rate. In our eruption model, the interplay between magma ascent rate and the rate of gas loss from the conduit results in a non-monotonic relationship between reservoir pressure and mass eruption rate. This behavior can result in rapid changes in eruption rate, the cessation of eruptions, and in the presence of reservoir recharge, cycles of eruptive activity.

Analytical approximations to the flow equations yield a computationally-efficient model, and also insight into the parameters which control – and may therefore be constrained by – observations. Utilizing these relationships as well as a Markov chain Monte Carlo inverse technique, we explore how simulated observations may be used to constrain model parameters. As in the case of observations from effusive eruptions, erupted volume and ground deformation data from explosive eruptions yield constraints on magma system compressibility, but constraining conduit properties is more challenging. However, in certain flow regimes, observations from effusive eruptions and explosive eruptions may yield insight into different parameters. Therefore, eruptions which exhibit explosive-effusive transitions, as at Shinmoedake in 2011, should yield particularly rich information. Although it will remain a challenging problem for the foreseeable future, inverting monitoring data using increasingly sophisticated multiphysical explosive eruption models should yield important new insights into eruption physics and the properties of erupting volcanoes.

Jacob Anderson, Jeffrey Johnson

Submission 598

Nonlinear infrasound models and explosive gas flux

Gas flux during volcanic explosions is an important parameter with implications ranging from serving as a measure of eruption magnitude to predicting the size and fate of the plume. Infrasound waveforms relate directly to gas flux history and therefore--in theory--can be inverted to estimate the volume of gas erupted. However, many difficulties remain in estimating gas flux from infrasound. In particular, nonlinear propagation of high-amplitude waves near the vent is currently ignored in gas flux inversions and is a potential source of error, especially for large or intense eruptions.

We address this problem with numerical models of the Navier-Stokes system of equations, the governing equations of fluid dynamics to which the acoustic wave equation is a low-amplitude approximation. Numerical modeling allows us to simulate the conditions of a volcanic eruption, predict nonlinear propagation effects, and assess the accuracy of normal infrasound analysis. We investigate a range of eruptive conditions ranging from small bubble bursts to major vulcanian eruptions to determine conditions in which nonlinear effects are significant. We then discuss the implications of these models for infrasound analysis in recent eruptions, most notably the intense vulcanian eruption of Tungurahua (Ecuador) in July 2013. The results of this project will improve the accuracy of infrasound-based inferences of volcanic processes.

Póra Andrésardóttir, Armann Höskuldsson, Joan Marti Molist, Ingibjörg Jónsdóttir, Thor Thordarson

Submission 1312

Evaluating volcanic hazard at the Reykjanes Peninsula, Iceland. Use of Vetools software bundle for geological data analyses and hazard predictions

The project VETOOLS aims at improving and developing volcanic risk assessment and management capacities in active volcanic regions by using universal methodologies, scenario definitions, response strategies and alert protocols to cope with the full range of volcanic threats and improving quantitative methods and tools for vulnerability and risk assessment. The software bundle was used to approach hazard assessment for the Reykjanes peninsula. Reykjanes peninsula marks the merging step of the Mid Atlantic ridge to surface and the birth of Iceland. Along this peninsula there are up to 4 volcanic systems that all have been active during the past 1 ka. The area has been extensively mapped in the past due to geothermal exploration. This enhances the hazard analysis. Here we shall present results that identify high hazard regions and future scenarios for eruption in the area. Further we shall estimate the hazard in the area prior to last eruption period (1000-1240 AD) to see how well it would have predicted last events in the area. As an important factor of this analysis we shall discuss pros and cons in the universal methodology and reliability of assumptions drawn from existing data and how we could possibly strengthen our hazard analysis.

Benjamin Andrews, Edward Venzke

Submission 674

Incorporating stratigraphic, granulometric, and image data into Volcanoes of the World

Physical volcanology data include observations collected at the outcrop scale (e.g. stratigraphic sections, photographs) and at the sample scale (e.g. granulometric and/or componentry analysis of bulk samples, or textural and compositional analysis of individual pyroclasts). These data underlie much of our knowledge of explosive eruption processes and they provide important constraints and boundary conditions for hazard assessments and numerical models. Unfortunately, there is currently no central collection or compilation of these data. Instead, the data are generally maintained by individual investigators with varying degrees of discovery, accessibility, and dissemination; in most instances, only a small fraction of the data that inform any particular publication are available in that manuscript (for example, only “representative stratigraphic section(s)” are published). The Global Volcanism Program is currently developing the ability to incorporate physical volcanology data into the Volcanoes of the World (VOTW) database and make those data available for discovery and download. Data are associated with the relevant eruption as cataloged in VOTW. Each stratigraphic section includes its location (UTM or Lat. / Long.) and the original descriptions (thickness, unit type, notes, etc.) made by the investigator. Relevant images (which may include photographs, sketches, or schematic illustrations) are associated with the section, and samples are associated with the specific layer from which they were collected. Sample specific data can include grain size distribution, componentry, compositional analyses (e.g. glass composition), and textural descriptions such as vesicularity or crystallinity; the current locations of samples are also maintained. Images of samples, including field photos, photomicrographs, or XRCT scans are associated with the sample they describe. Individual sections can be displayed in a traditional schematic format with accompanying descriptions and links to samples and/or images, or all sections can be viewed at once in a map view. All of the new types of data incorporated into VOTW will be downloadable and publicly available.

Daniele Andronico, Gilda Currenti, Sergio Longo, Lorenzo Brusca, Sergio Calabrese, Tommaso Caltabiano, Antonino Cristaldi, Walter D'Alessandro, Cinzia Federico, Ferruccio Ferrari, Filippo Greco, Alessandro La Spina, Manfredi Longo, Lucia Messina, Rosalba

Submission 927

SEW – Save the Etna World

At more than 3,330 m high and ~40 km wide, Mount Etna in Sicily, Italy, is the highest volcano in Europe and one of the most active in the world. Etna stands majestic wherever you look at it, showing a distinctive skyline from each side. More than 200,000 people live around its mid-slopes, while another 300,000 are in the biggest city, Catania, located at its southern lower slope. The volcano is so imposing that there are many different landscapes and habitats, often highly dissimilar. Ente Parco dell'Etna (Etna Park) is the institution, started in 1987, covering the core of the volcano, protecting its biodiversity, ecosystems and landscapes, and lastly promoting the sustainable development of local populations. Within this framework, Etna has recently been added to the list of the World Heritage sites of UNESCO, which described it as "an iconic site encompassing 19,237 uninhabited hectares on the highest part".

Save the Etna World (SEW) is an Italian National project funded by "Fondazione CON IL SUD", which through a multidisciplinary approach aims at implementing a common strategy for monitoring and protecting unique habitats and biodiversity at Etna. Istituto Nazionale di Geofisica e Vulcanologia, Osservatorio Etneo (INGV-OE) is one of the partners of the project. Our main duties are monitoring and assessing the impact of the volcanic activity on the environmental elements. The territory surrounding Etna is frequently affected by tephra fallout and volcanic gas dispersion, which may alter the chemical-physical features of the ecosystem but also provides excellent nutrients for soils and vegetation. The data collected will advance our understanding of the relationships between the environment and volcanic activity and will help towards defining the best practices for a more efficient use of economic resources with implications for the socio-economic activities in the Etna area.

A broad-spectrum of outreach activities will promote the environmental, social, economic and cultural heritage of Etna and raise awareness towards the environment among the local population. INGV-OE will participate in the "information, education and governance" of SEW activities, providing modules dedicated to volcanology, organizing seminars and workshops, and developing teaching tools for schools. Furthermore, INGV-OE will play a scientific support role in the dissemination of the monitoring activity results and collection of best practices in the field of environmental risk.

Daniele Andronico, Boris Behncke, Antonella Bertagnini, Emanuela De Beni, Paola Del Carlo, Alessio Di Roberto, Massimo Pompilio

Submission 912

Pyroclastic density currents at Mt. Etna: the 11 February 2014 case study

Over the last decade, the deposits ascribable to pyroclastic density currents (PDCs) have been identified on the flank of an increasing number of volcanoes fed by basaltic magmas, which are commonly thought to be less prone to experience this type of volcanic events. At Mt. Etna (Italy), small-volume flows have been repeatedly observed since 1998, when frequent summit paroxysmal activity led to the rapid growth of the Southeast Crater (SEC) and, after 2011, of the New Southeast Crater (NSEC).

The largest PDC ever witnessed at Etna occurred on 11 February 2014, when a quite large volume of unstable and hot rock detached from the lower-eastern flank of the NSEC. The flow descended the eastern flank of Etna and the Valle del Bove for about 2.3 km at an average speed of >45 m/s. We investigated this event by merging data from visible and thermal camera provided by monitoring and surveillance activities at Istituto Nazionale di Geofisica e Vulcanologia, Osservatorio Etneo, with detailed stratigraphic, textural, and petrographic studies of the PDC deposits.

Thermal recordings showed that the 11 February 2014 flow had apparent temperatures >300 °C, while visible images pointed out the formation of a relatively hot elutriated cloud that dispersed over a wider area. Field observations on the main PDC deposits, carried out on 2016, showed that the deposit consists of 3 stratigraphic units. The base of the deposit consists of a ~5 cm-thick reddish ground layer of poorly sorted, massive ash and minor fine lapilli. It is overlaid by a 10-cm-thick, massive, poorly sorted brown-red coarse ash layer with dispersed small lapilli. The topmost unit is clast supported, massive to faintly inverse graded and poorly sorted, and consists of a polymictic breccia with clasts from different origin. In addition, we identified the deposit of the elutriated cloud made up of a few millimeters-thick layer of reddish fine ash. Deposits have been characterized for grain size, components, clast morphometric parameters and textures. This multidisciplinary approach allowed to investigate source and triggering mechanisms of the 11 February PDCs, and their flow dynamics. Our results contribute to improving the hazard assessment from this type of events at Etna, thus reducing the potential risks to volcanologists and tourists attending its summit area.

Mario Angarita, Jillian Pearse, Scott Henderson

Submission 913

Deformation processes in the region Galeras volcano using InSAR Images

A theoretical model of deformation was developed for Galeras Volcano, Colombia, applying the Finite Element Method (FEM) to Interferometric Synthetic Aperture Radar (InSAR) ALOS-1 images from June of 2007 to September of 2008. Using a time series inversion with 8 dates and 7 interferograms, we discover a 4 cm of maximum line-of-sight subsidence on the east flank of the Volcano covering an area of 8 km x 3 km. Parks et. al. (2011) found similar results in an independent analysis using the same ALOS-1 data. The deformation was presumably related to the eruption that took place January 2008, between the two acquisition dates, so we modelled the deformation as a depressurizing reservoir within the volcanic edifice. Two analytical models were tested: a spherical pressurized reservoir and a closing sill. The sill model better fits the observed data with a collapse of -2.6cm, width of 2.6km, length of 6.7km, a depth to 1.1km and the strike of -13 degrees. These findings give us a volume of $4.5 \times 10^5 \text{ m}^3$ that don't match the total volume of the products at 2008 eruption which was $1.1 \times 10^6 \text{ m}^3$. However the deformation pattern and magnitude change when topography is incorporated in a finite element model because the modelled reservoir is shallow relative to the free surface. These changes show a decrease between 20% and 30 % in the subsidence magnitude and a shift in the center of the deformation pattern. This study seeks to assess the importance of incorporating more realistic parameters in volcano deformation models, and in particular to improve our understanding of the magmatic sources at Galeras volcano, which has had minor eruptions every year after the eruption of 2008 until 2014.

Carlos A. Angeles De La Torre, Julie Roberge, Gilles Levresse, Celestine N. Mercer, Kevin G. Pedroza-Aldana

Submission 700

Comparing melt inclusions preparation methods in crystals from Popocatepetl Volcano

The most accurate and precise way to obtain estimates for magmatic pre-eruptive H₂O and CO₂ contents is through transmission-FTIR spectroscopic analysis of doubly intersected melt inclusions (MI). However, sample preparation is tedious, time consuming and sometimes impossible if the MIs are too small (H₂O and CO₂ contents of quartz-hosted MIs that have been intersected on both sides, on one side, and not intersected at all. But the comparison was not done on the same MI, leaving interpretation of the results somewhat ambiguous. Here, we present a comparison of 3 spectra obtained from the same MI for both quartz and olivine crystals. Each MI was prepared using the following procedure: 1) Prepare and analyze a doubly polished wafer containing a non-intersected MI; 2) Intersect the same MI on one side; 3) Analyze the singly-intersected MI; 4) Intersect the same MI on the second side; and 5) Analyze the doubly-intersected MI. For each MI, the concentration obtained with the final “traditional” doubly-intersected method is considered the “true” concentration for comparison with the singly and non-intersected methods.

For olivine, all 3 water peaks at 3550 cm⁻¹ are similar in shape and relative absorbance. As expected, the water peak measured on the non-intersected MI displays the highest absorbance due to the dispersion of the signal at the curved crystal-inclusion interface (28% more). In contrast, the water absorbance peaks from the singly- and doubly-intersected MIs give absolute H₂O concentrations that are within analytical error of each other (2 could only be successfully completed on the doubly-intersected MI because the olivine absorption peak at 1770 cm⁻¹ interferes with the CO₃ doublet at 1430-1515 cm⁻¹).

For quartz, water was measured as the sum of the 5230 cm⁻¹ and 4520 cm⁻¹ absorbance peaks and CO₂ was measured at 2350 cm⁻¹. All peaks have similar shape and relative absorbance for both water and CO₂. Again absolute concentrations for one and two side intersected MIs are within analytical error of each other (

Libby Anthony

Submission 1146

Fluorine behavior in trachyte-phonolite rocks, Suswa volcano, Central Kenya Peralkaline Province (CKPP), East African Rift

Mount Suswa is a Quaternary shield volcano with two nested summit calderas that erupted peralkaline trachyte and phonolite. The eruptive products are divided into two series: an early series (C1) built the shield volcano and erupted tuffs, pumices, and lavas associated with initial caldera collapse. The second series (C2), associated with the inner caldera, is dominated by ne-normative trachyte and phonolite. MELTS and trace-element modeling demonstrate that C1 is the result of protracted fractional crystallization of alkali basalt under relatively high pressure (400 MPa), low water content (less than 1 wt % H₂O), and low oxygen fugacity (FMQ to FWQ-1). Recharge, assimilation of C1 residual syenite (Ma/Mc=0.1), and renewed fractional crystallization produced nepheline trachyte of early C2. The final phonolitic, phase of magmatism is the result of additional recharge, as evidenced by resorption and reverse zoning of feldspar and linear compatible trace element patterns (White et al., 2012, *Lithos* 152, 84-104).

We have measured fluorine in fluorapatite (F = 4.5-6.5 wt.%), matrix, and melt inclusion glass. The initial stages of C1 have fluorine concentrations (0.08-0.78wt.%) for both melt inclusion and matrix glass. The tuffs associated with caldera eruption range to higher F concentrations (0.1 to 2.0 wt %) in the matrix glass, while the concentrations in melt inclusions remain less than 1 wt %. We interpret this behavior to indicate that the increased matrix concentrations are due to a phenomenon in addition to fractional crystallization. These syn-caldera tuffs also show carbonate-silicate liquid immiscibility (Macdonald et al., 1993, *CMP* 114, 276-287) and/or fluorite in the silicate matrix. Fluorine concentrations in C2 eruptions initially return to those observed in C1 units and then increase (to 0.2-1.3 wt.%) during the second caldera collapse.

Pórður Arason, Sara Barsotti, Mattia de' Michieli Vitturi, Sigurdur Jónsson, Hermann Arngrímsson, Baldur Bergsson, Melissa Pfeffer, Gudrun Nina Petersen

Submission 94

Real-Time Estimation of Mass Eruption Rate and Ash Dispersion During Explosive Volcanism

The Icelandic Meteorological Office (IMO) is responsible for monitoring over 30 active volcanic systems. For explosive volcanic eruptions, the principal scale parameters are plume height and mass eruption rate. IMO operates two fixed position C-band weather radars and two mobile X-band radars, which are crucial in monitoring plume height, due to their independence of daylight, weather and visibility. During initial phases of an explosive eruption, all available radars will be set to a more detailed scan, optimized to observe the volcanic eruption plume. Radar volume data above the active volcano are automatically analyzed at IMO-headquarters in Reykjavík. These data are available for the natural hazard specialists and meteorologists at IMO's 24/7 monitoring room in near real-time, and are communicated to London VAAC to support their ash transport simulations for aviation safety purposes. The newly-developed VESPA software uses the plume height estimates to calculate the eruptive source parameters through an inversion algorithm. This is done by using the coupled system DAKOTA-PlumeMoM which solves the 1D plume model equations iteratively by varying the input values of vent radius and vertical velocity. The model accounts for the effect of wind on the plume dynamics, using atmospheric vertical profiles extracted from the ECMWF numerical weather prediction model. Furthermore, the estimate of mass eruption rate provided by VESPA are used to initialize the VOL-CALPUFF dispersion model to assess the local-scale hazards due to tephra fallout.

Naoki Araya, Michihiko Nakamura, Satoshi Okumura, Atsushi Yasuda

Submission 368

Repeated Plinian eruptions from the shallow thick conduit in Sakurajima Volcano

At Sakurajima volcano, three historical eruptions starting from a VEI-4 Plinian eruption followed by more voluminous lava flows were repeated in similar sequence in AD 1471–1476, AD 1779–1782, and AD 1914–1915. We analyzed volatile contents and major element compositions of melt inclusions and their host phenocrysts from these historic Plinian eruptions. The chemical compositions of most of the melt inclusions were dacitic to rhyolitic. The H₂O contents of 85 melt inclusions encompassing all of the historic Plinian eruptions were determined by FT-IR reflectance spectroscopy to be 1.4–3.5 wt% irrespective of eruption age. The CO₂ contents of selected melt inclusions from the 1914–1915 eruption were below the detection limit of FT-IR transmission spectroscopy (i.e. less than a few tens of ppm). Volatile saturation pressures of >95% of the melt inclusions from the three historic Plinian eruptions were calculated to be 19–74 MPa, which corresponds to depths of 0.9–3.3 km assuming a density of the upper crust of 2300 kg/m³. Given the analytical accuracy of FT-IR reflectance spectroscopy (<0.3 wt%; Yasuda, 2014), the error in depth is estimated to be less than 0.6 km assuming a magma temperature of ~1000°C and a melt H₂O content of <3.5 wt%. Recent geophysical observations have revealed that the shallowest magma reservoir is located at a depth of 4 km beneath the Minamidake summit. Therefore, the magma storage depths estimated from the melt inclusions of the historic Plinian eruptions are shallower than the depths of magma reservoirs. Based on the hypocenter distribution of volcanic earthquakes in the 1970s–80s, at which violent Vulcanian explosions occurred repeatedly, the conduit was widened to a diameter of 300–500 m at a depth of 1–4 km beneath Minamidake crater. The apparent volumes of the historic Plinian tephra are estimated to be 0.3–0.8 km³ (Kobayashi et al., 2013), which can be converted into dense rock equivalent volumes of 0.1–0.3 km³; the volume of this shallow and thick conduit (0.2–0.6 km³) approximately corresponds to the tephra volumes. This indicates that magmas were pre-eruptively “loaded” in a region shallower than the present magma reservoirs prior to the Plinian eruptions of Sakurajima volcano.

Alejandra Arciniega-Ceballos, Francisco Sanchez-Sesma, Laura Spina, Ursula Iturraran-Viveros, Bettina Scheu, Donald Dingwell

Submission 988

Elasto-Acoustic Signatures within Viscous Flows

Viscous flow is frequently assumed as an underlying process in which several volcanic phenomena take place and it is the current explanation behind long-lasting oscillations like those producing tremors. Pressure changes that trigger long-period (LP) signals may be accounted for using viscous incompressible fluids and the Navier-Stokes equation provides a description of the non-linear behavior of these oscillations. Moreover, pressure variations produce elasto-acoustic signals that travel in the fluid much faster than the flux speed but the source and its associated frequencies are roughly the same. Because of the different time scales and the ensuing mechanics, it is assumed here that various phenomena co-exist independently. To examine the elasto-acoustic response in flow experimental settings we model the pressure within the fluid and the displacement field due to a monopole source within the fluid. The source is at the center of a circular infinite fluid cylinder and the discrete wavenumber (DWN) method is used to solve the integral representation of the source and the refracted, scattered potentials. This modeling exercise allows evaluating the relative importance of the acoustic phenomena in the intrinsic non-linear LP behavior.

Katie Ardill, Scott Paterson, Valbone Memeti, Jonathan Stanback, Sabrina Green, Evelyn Gutierrez

Submission 886

Hypabyssal porphyry intrusions across the central Sierra Nevada: characterizing vertical links between focusing plutonic and volcanic fields

The central Sierra Nevada (CSN) contains several 105-95 Ma hypabyssal intrusions, emplaced during the peak of the Cretaceous arc flare up and during a regional magma focusing event. Areal proportions of Cretaceous plutons, hypabyssal bodies and volcanic units exposed in the CSN are approximately 30:1:5, respectively. Most hypabyssal intrusions, between 10m² – 20 km² in areal extent, are much smaller than exposed Cretaceous CSN plutons and remnant volcanic packages. Hypabyssal bodies in the CSN are commonly porphyritic, one indication of their shallow emplacement, but are otherwise internally texturally variable, reflecting a transition between plutonic and volcanic domains. Hypabyssal stocks are often in intrusive contact with contemporaneous plutons and volcanic packages, providing a three-dimensional view of a focusing magma plumbing system.

Four field sites in the CSN are promising candidates to investigate the relationship between plutonic and volcanic rocks, where plutonic-hypabyssal and volcanic aliquots of the magma plumbing system are temporally and spatially associated: the Tioga Pass complex, the Iron Mountain pendant, the Minarets caldera and the Beartrap Lakes complex. These sites concentrically surround the voluminous 95-85 Ma Tuolumne Intrusive Complex (TIC), and map relationships and U-Pb zircon ages indicate each system is older than the TIC (between 100-98 Ma), consistent with regional spatio-temporal focusing patterns. We present new mapping and U-Pb zircon geochronology to establish the temporal connection, and bulk rock element geochemistry from plutonic, hypabyssal and volcanic samples to characterize the volcanic and subvolcanic plumbing system.

At each site, hypabyssal porphyry intrusions have sharp to gradational intrusive contacts with coeval volcanic and plutonic rocks. Compositions of hypabyssal intrusions at the field sites are dominantly intermediate-felsic andesites, dacites and granite porphyries ranging 62-76 wt.% in SiO₂, with few mafic bodies containing 2. Geochemical indices of differentiation, such as Rb/Sr, suggest volcanic samples may be fractionated from hypabyssal samples. Understanding the vertical relationship between plutonic, hypabyssal and volcanic components in arc systems is critical to better understand how magma focusing functions in the plutons of the CSN in comparison to well-established examples of magma focusing in volcanic systems.

David Arnold, Juliet Biggs, Silvia Vallejo Vargas, Kyle Anderson, Geoff Wadge, Susanna Ebmeier, Patricia Mothes

Submission 761

Lava extrusion rate and magma supply rate at El Reventador Volcano, Ecuador

Lava extrusion at erupting volcanoes can cause rapid changes in surface topography and morphology on the order of tens to hundreds of metres. Repeat-pass satellite radar provides a method for measuring topographic height change during a given time interval to an accuracy of metres, either by measuring the width of the radar shadow cast by steep sided features, or by taking the difference between radar phase recorded at two sensors separated in space. We measure surface elevation changes and hence estimate extruded lava volume flux at El Reventador, Ecuador between 2011 and 2016, using data from the Radarsat-2 and TanDEM-X satellite missions. We find 42 new lava flows were extruded between February 2012 and August 2016, with a cumulative volume of 44.8M m³ dense rock equivalent and a decreasing time-averaged extrusion rate. This diminishing extrusion rate can be well represented by exponential curves equivalent to the behaviour of a depressurising magma reservoir, either with no magma recharge or magma resupply at a constant rate. The average dense rock rate of lava extrusion during this time was 0.31 ± 0.02 m³s⁻¹, which is similar to the long-term average from 1972 to 2016 and also the inferred constant magma supply rate. Apart from a volumetrically small dyke-opening event between 9 March and 10 June 2010, lava extrusion at El Reventador is not accompanied by any significant ground deformation. We use the time evolution of eruption rate in conjunction with simple physics-based models to determine likely parameters of the magmatic system underneath El Reventador. We also discuss variations in the morphology of new lava flows through time that are observed with the high-resolution satellite data. Our results highlight the advantage of using satellite radar for tracking changes in eruption behaviour and characterising the magmatic system at long-lived volcanic eruptions.

Maria Carmencita Arpa, Bruce Christenson, Georg Zellmer, Ian Schipper, Jonathan Procter, Robert Stewart

Submission 722

Volatile Content of Tongariro Volcanic Complex Magmas

Composition of volatiles (H₂O, CO₂, S, Cl) in melt inclusions collected from several past eruptive deposits of Tongariro Volcanic Complex can provide insights into magmatic activity, eruption style and the ongoing degassing activity. The sample set for this study includes deposits from effusive (Te Maari 1500 A.D. lava flow) to explosive (Wharepu Tephra) eruptions of Tongariro from the past 10,000 years. Variations in volatile content from deposits of different eruption styles may indicate an influence of magmatic volatiles. The volatiles were measured from melt inclusions in pyroxene and olivine host minerals. The host minerals are in equilibrium with the magma or are considered xenocrysts. Melt inclusions from xenocrysts may provide the volatile content of a more primitive magma. Majority of melt inclusions are from the Upper Te Maari Crater 1500 A.D. lava flow. Because volcanic degassing data is available for the area of the Te Maari Craters as part of the volcano monitoring program of GNS Science, the melt inclusion volatiles data from the past deposit can be used as a set of parameters to interpret the depth and composition of the presently degassing magma. Initial data show that H₂O content is highest in the most explosive eruption deposit, but shows no clear trend among the other deposits in the data set. CO₂ is non-detected to low and may have already degassed before melt entrapment. S and Cl show slight differences between deposits, which may be explained by magmatic processes.

Fabio Arzilli, Margherita Polacci, Daniele Morgavi, Maurizio Petrelli, Mike Burton, Giuseppe La Spina, Margaret Hartley, Jorge Romero Moyano

Submission 755

Conduit dynamics and triggering mechanism of the April 2015 sub-Plinian eruption of Calbuco volcano, southern Chile

The April 2015 sub-Plinian eruption of Calbuco volcano, southern Chile, occurred after a quiescent period of 54 years since its last major eruption in 1961. The main explosive phase consisted of two pulses lasting ~1.5 h and 6 h on 22nd and 23rd April, producing stratospheric (>15 km height) eruption columns. Here we report textural and chemical features of tephra products. The bulk composition of erupted materials corresponds to basaltic andesite (~55 wt.% of SiO₂). Microprobe data show that melt inclusions in plagioclase phenocrysts are characterized by an andesitic composition (~5822plg = ~30%), orthopyroxene and clinopyroxene (∑px = ~12%) and titanomagnetite (∑mt = ~3%); olivine is present as an accessory phase. Microlites in the matrix consist of plagioclase (∑plg = ~20%) and orthopyroxene (∑px = ~5%). The rapid crystallization at shallow depths, due to the decompression during the ascent of magma in the conduit, produced a sudden exsolution of volatiles, generating an overpressure of the system which, in turn, triggered the sub-Plinian eruption.

María Asensio-Ramos, Cecilia Amonte, Marta García, Gladys Melián, Fátima Rodríguez, Mar Alonso, Rubén García-Hernández, Ernesto García, Verónica Vela, Pedro A. Hernández, Nemesio Pérez

Submission 846

Surface geochemical network to monitor diffuse degassing for the volcanic surveillance of the oceanic active volcano island of Tenerife, Canary Islands

Tenerife is the largest of the Canary Islands and has a geological history involving several constructive and destructive episodes. The emerged part of Tenerife was formed from subaerial deposits dated between 12 Ma and 100 years old. Three main volcanic rift-zones (NE, NW, and S) are identified, with five volcanic historical eruptions occurred along the NW, NE rifts and Teide-Pico Viejo (TPV) complex. The intersection of the three rifts occurs at the central part of the island, Las Cañadas Caldera, which host the TPV that has grown in the last 180 ka. At summit of Teide, low temperature fumaroles ($\sim 85^{\circ}\text{C}$) occur being the only surface geothermal manifestation at Tenerife. In order to strength the geochemical program for volcanic monitoring in Tenerife, in summer 2016 a network of 31 closed static accumulation chambers was installed along the three volcanic rifts as well as Cañadas. This method is based on the absorption of soil CO_2 through an alkaline solution placed in the closed chamber. The interest of measuring the diffuse CO_2 flux lies in that it is, after water vapor, the most abundant gas dissolved in magma and has a low solubility in silicate melts, which make CO_2 an ideal gas for volcano monitoring. To do so, 50cc of 0.1N KOH solution is placed inside the chamber to absorb the released soil CO_2 . The solution is replaced weekly and the trapped CO_2 is later analyzed at the laboratory by titration. Results are expressed as weekly integrated CO_2 efflux values, and ranged from 2.3 to 12.9 $\text{g m}^{-2} \text{d}^{-1}$, with average values of 6.8, 6.2 and 6.4 $\text{g m}^{-2} \text{d}^{-1}$ for the NE, NW and S rift-zone, respectively. The most significant CO_2 efflux values were observed at the NE rift-zone, with maximum of 12.9 $\text{g m}^{-2} \text{d}^{-1}$. To investigate the origin of the soil CO_2 , soil gas samples were weekly taken on the head space of the closed chambers to study the chemical and isotopic composition of the CO_2 . Collected gas samples can be considered as CO_2 -enriched air, showing concentrations of CO_2 in the range 355-22,448ppmV. The CO_2 isotopic composition, expressed as $\delta^{13}\text{C}-\text{CO}_2$, indicates that most of the sampling sites exhibited CO_2 composed by different mixing degrees between atmospheric and biogenic CO_2 with slight inputs of deep-seated CO_2 . Mean values are -16.4‰ -13.6‰ and -15.9‰ for the NE, NW and NS rift-zones, respectively. The methodology presented here represents an inexpensive method that might help to detect early warning signals of future unrest episodes in Tenerife.

James D. Ashworth, Jackie E. Kendrick, Anthony Lamur, Felix W. von Aulock, Paul A. Wallace, Rebecca Coats, Nick Varley, Yan Lavallée

Submission 1046

The effect of strain on the formation and connectivity of bubbly magmas

The exsolution of volatiles and the formation of porosity can radically modify a magma's rheological properties; whether that porosity is connected affects the degassing pathways available for fluids and the likelihood that pore pressure may build within the system. During ascent and eruption, magma is subjected to a variety of stress conditions and resulting strain. In this study, we investigate the effects of strain on the development of vesicles and associated evolution of a permeable network during vesiculation of a volatile-bearing obsidian.

Herein we study rhyolitic obsidian obtained from the Pochetero lava dome at Ceboruco volcano, Mexico. Simultaneous thermal analysis (STA) indicates that the obsidian has a glass transition temperature (T_g) of ~ 663 °C (at a heating/cooling rate of 10 °C/min).

To investigate the process of foaming during heating of volcanic glass, we produced several cylindrical cores (26 x 50 mm) and heated them to different dwelling temperatures with and without confinement. We then measured volume changes using image analysis and helium pycnometry. We found that when unconfined at 930 °C the material began to vesiculate within 1 hour, reaching a maximum total porosity of 70-73 vol.% after ~ 11 hours (the porous region is enclosed within a dense outer skin); beyond this, the foamed samples began to shrink slowly as gas was lost by diffusion. When we removed the skin, we found that only 2-3 vol.% of the pores were connected to the outside of the sample; the permeability was below the detection limit of our apparatus (i.e. $\lesssim 10^{-17}$ m²). We repeated the foaming process in a uniaxial press, on cores axially confined by two pistons prior to the onset of vesiculation. Foaming achieved similar total porosity values (ca. 70-73 vol.%); however, 13-16 vol.% of pores were connected, indicating that the porous network of a constricted magma body may be more permeable than those of free standing lava bodies. Permeability remained below the detection limit in the direction of confinement, but was on the order of 10-16 m² perpendicular to confinement. Further experiments with different geometries of confinement and applied stresses during vesiculation may allow us to better characterise the development of permeability anisotropy, with important implications for the evolution of gas pressure during eruptions of aphyric magmas.

Robert Askew, Thor Thordarson, Phil Gans

Submission 1097

Geological mapping of Breiðdalur volcano: Evolution and structure of a Neogene central volcano in Iceland

This study revisits the lithostratigraphy, petrology and age span of the c.a. 9.5 My old Neogene central volcano of Breiðdalur in East Iceland, which was first studied by George L.P. Walker in the 1960's. Breiðdalur is a well-exposed, 800 m-high, central volcano with well-defined mafic lava dominated flank sequences and a 10-12 km diameter caldera that is largely filled in with pumice breccia. The pumice breccia is in turn is intruded by mafic to dacitic dykes and sills and capped by a 100 m thick layered ignimbrite sequence. In the proximity of the summit, the mafic flank sequences are topped by silicic and composite lava flows, while further down slope the sequence was intruded by a series of silicic plugs; some resulting in formation of silicic lava domes on the outer flanks of the volcano. Mafic lavas erupted in the early stages of formation of Breiðdalur were dated to 10.1 My, the silicic sequences erupted in the last ~300 Ky the youngest being around 9.1 My. Olivine basalt lava flows, erupted from the Breiðdalur fissure swarm and which wrap around the youngest of the volcano's deposits, were dated to 9.1 My. The Breiðdalur dyke swarm, which spans the age range 9.8 to 8.1 My, cross cuts much of the volcano. Dyke density north and south of the caldera is around 15-20 % over 100 m intervals, a dyke shadow exists in the caldera sequence where density decreases to

Major and trace element composition of the Breiðdalur volcanic succession indicates an enriched tholeiitic magma suite, similar to that of the currently active Askja volcanic system (located in the axial rift of Iceland near the southern end of the North Volcanic Zone). The compositional and lithological resemblances of Askja and Breiðdalur suggest that the latter volcano was linked to magma sources, and situated in a volcano-tectonic setting, like that occupied by the Askja volcano. Furthermore, since dyke injections outlasted the activity at the central volcano, this implies that the mafic magma reservoir feeding the dyke swarm is separate and longer lived than the magma storage zone feeding the central volcano. Remapping of the entire volcanic succession has enabled an updated version of the 1:60.000 geological map of Breiðdalur.

Rebecca L. Astbury, Maurizio Petrelli, Daniele Morgavi, Chiara Maria Petrone, Diego Perugini

Submission 800

Using compositional zoning and chaotic mixing experiments to constrain timescales of plumbing system dynamics: Soufrière Hills Volcano, Montserrat

Compositional zoning within crystals is used to trace the history of a magmatic system, the dynamic processes that govern it, and the timescales over which these processes occur. In petrology, these compositional zones are often linked to the mixing of two or more geochemically distinct magmas within the volcanic system. Variation in these zoning patterns e.g. thickness or resorption, are indicators of the extent of mixing within the system prior to eruption. Understanding the formation of these textural variations is fundamental for reconstructing timescales of magma mixing.

In this study, we investigate natural samples of two events from the Soufrière Hills volcano (SHV), Montserrat; the 1997 final eruptive phase and the 2010 dome collapse. SHV samples contain multiple geochemically and texturally distinct plagioclase populations. From core to rim, in each plagioclase population, we analyse major and trace element concentrations e.g. Sr and Ba, and combine the data with diffusion modelling, to estimate the timescales of pre-eruptive magmatic processes.

SHV products also contain several, geochemically distinct enclaves. We use these enclaves (basalt, basaltic-andesite and andesite) as end-member compositions to perform a series of chaotic mixing experiments. By varying the ratio of end-members, mixing rate, and time, we attempt to reproduce the geochemical complexity found within natural SHV products. Textural variation, compositional zonation, and the subsequent timescale estimations from natural and experimentally produced crystals are then compared in order to gain a better understanding of the mixing processes within the SHV system.

Furthermore, the combination of studying natural samples alongside experimental techniques could be used to successfully develop a new geochronometric tool to interpret the evolution of volcanic plumbing systems.

Thomas Aubry, A. Mark Jellinek

Submission 120

Evaluation of entrainment and condensation parameterizations in integral models of volcanic plumes using a new database of eruptive parameters

Integral models of volcanic plumes are widely used due to their simplicity and computational efficiency. In these models, both turbulent entrainment of atmosphere into the plume and condensation of entrained water vapor contribute significantly to the strength of a plume (i.e., its buoyancy flux) and must be parameterized. Various models exist for both processes and uncertainties on the parameters on which they rely are large. Despite a recent “intercomparison” of model results for conditions representative of two eruptions, no extensive evaluation and comparison using a large database of eruptive parameters yet exists.

Here, we use a new database of 94 eruptive phases with independently constrained plume heights and source conditions to evaluate four integral models of volcanic plumes. Using a Monte Carlo approach to account for uncertainties in eruption parameters, we evaluate the best set of entrainment and condensation parameters for each model, and compare their performance. Our work provides guidance on the best integral plume model to use, and places constraints on each entrainment or condensation parameter, as well as the associated uncertainties. Critically, the hypothesis that a wetter atmosphere results in higher volcanic plume height is rigorously tested. We will expand our database with the total grain size distribution for each eruption, and test parameterization of particle sedimentation and re-entrainment, which are ignored in this study.

Muhammad Aufaristama, Armann Hoskuldsson, Ingibjorg Jonsdottir, Thorvaldur Thordarson

Submission 1035

A New Insight of Thermal Eruption Index (TEI) for Detecting and Deriving Thermal Properties of Active Lava Using Infrared Satellite during 2014-2015 Eruption at Holuhraun, Iceland

Holuhraun is a lava field in the Icelandic Highlands, north of Vatnajökull which is the largest effusive eruption in Iceland in the last 230 years, with an estimated lava volume of $\sim 1.2 \text{ km}^3$ covering an area of $\sim 84 \text{ km}^2$. Satellites based remote sensing commonly used as preliminary assessment of the large scale eruption since it is relatively efficient to collect and process the data. Landsat 8 infrared datasets (SWIR and TIR bands) were used in this study to determine thermal structure of the eruption within Holuhraun. We develop a new spectral index called Thermal Eruption Index (TEI) based on SWIR and TIR bands to differentiate thermal domains within lava flow field. TEI shows that active lava has value > 0.4 meanwhile warm-hot crusts have value range from 0.10 - 0.39. This threshold then applied in the dualband method to derive hot component temperature (T_h) from the lava. The preliminary result show hot crust has the T_h between $300^\circ\text{C} - 499^\circ\text{C}$ and $> 500^\circ\text{C}$ for active lava. Active lava such as breakout and closed lava pathway have higher T_h and occupied lower fraction coverage. We create assumption of flow interior from T_h to estimate radiative and convective flux densities (M_{rad} and M_{conv}), then we solve for crust thickness model of lava flow (Δh). This study has been successfully produced radiant flux (Φ_{rad}) and thickness model based on TEI and dual band method. Multiple infrared satellites data were being processed to get better temporal resolution of the development lava flow and the plan is to continue this research to derive thermal structure of multicomponent for better understanding lava flow emplacement mode.

Allison Austin, Robin Matoza, David Tessier, Art Jolly, Alex Iezzi, Richard Johnson, Geoff Kilgour, Bruce Christenson, Esline Garaebiti, Ben Kennedy, Rebecca Fitzgerald, Nick Key, Adrien Tessier

Submission 721

Flashing arcs at Yasur Volcano, Vanuatu and their relationship to strombolian eruption mechanics

Luminous, flashing arcs are quickly moving manifestations of pressure waves generated by explosive eruption processes. These visible phenomena are thought to result from density changes in the local atmosphere during rapid successions of pressure-wave compression (causing evaporation) and rarefaction (causing condensation), ephemeral effects that have eluded even modern-day photographic capture. However, flashing arcs can be recorded on video, which provides a unique opportunity to directly image and characterize near-source acoustic wavefield characteristics and directivity associated with volcano-acoustic source processes. Luminance differencing is a technique that enables the temporal and spatial extraction of flashing arcs from a static background video, from which acousto-luminance wavefield reconstruction and quantification are possible (Yokoo and Taniguchi, 2004; Genco et al., 2014). Here we apply this method to two digital-single-lens-reflex (DSLR) videos of flashing arcs recorded as part of a multi-parameter dataset generated during a field experiment at Yasur Volcano, Vanuatu from July 26th to August 4th, 2016. During this time, flashing arcs increased in intensity and frequency with heightened activity, and were observed both in connection with and separate from explosion events. The unique approachability and regularity of Yasur's strombolian eruptions (on the order of minutes), coupled with the presence of a constant plume, make this location an ideal place to see and record flashing arcs and evaluate the source processes that create them. Resultant acoustic-luminance waveforms from each type of flashing arc will be compared with seismic and acoustic data from the same time periods in order to analyze wavefield dynamics and directionality and gain insight about depths and mechanics of strombolian eruptions.

References

Genco, R., M. Ripepe, E. Marchetti, C. Bonadonna, and S. Biass (2014), Acoustic wavefield and Mach wave radiation of flashing arcs in strombolian explosion measured by image luminance, *Geophys. Res. Lett.*, 41, 7135–7142, doi:10.1002/2014GL061597.

Yokoo, A., and H. Taniguchi (2004), Application of video image processing to detect volcanic pressure waves: A case study on archived images of Aso Volcano, Japan, *Geophys. Res. Lett.*, 31, L23604, doi:10.1029/2004.

Geoffroy Avarad

Submission 359

Turrialba Volcano, Costa Rica: Transition to Magmatic Activity

Turrialba volcano, Costa Rica, presents an uncommon long reawakening period that started in 1996 and progressively turned into a more magmatic activity. In 2010 started phreatomagmatic eruptions that intensified in frequency and amplitude after 2014. At the same time the juvenile component passed from 1% to around 20% in the ash between 2010 and the end of 2016. That activity was alternating explosive events and periods of weak ash-venting to relative quiescence. The explosive events seemed to be escalating in frequency and amplitude until a climax on September 19, 2016, when ash reached 4 km above the crater (~7500m asl). These events deepened the crater to close to 200m as observed in January 2017. However, since October 2016 ash emissions decreased and juvenile strombolian material was observed for the first time on the rim of the crater on November 1, 2016. This tendency increased since then with more juvenile ballistics and less intense ash emissions. Moreover this increase of the magmatic component in the volcano activity is observable in the modal analysis of the rare ash emissions with an increase to >30% juvenile while the bombs are glassy and vesicular albeit with altered rinds. Hence the phreatomagmatic behavior of these last years may correspond to a gas-fed opening of the conduit as the magma was slowly moving toward the surface and since the end of 2016 beginning of 2017 the conduit should be considered almost totally opened. Ash emissions were not so much the result of a fragmentation of the magma induced by decompression than the pulverization of the edifice by the gas escape or interaction with hydrothermal fluids while opening the conduit under the slow motion upward of the magma in the column or dikes. Today the continued inflation of the edifice suggests the magmatic activity may slowly increase.

Denis Ramón Avellán López, José Luis Macías Vázquez, GIOVANNI SOSA CEBALLOS, PAUL LAYER, JOAN MARTI

Submission 1296

GEOLOGY OF THE ACOCULCO CALDERA COMPLEX AT THE EASTERN SECTOR OF THE TRANS-MEXICAN VOLCANIC BELT, MÉXICO

The Acoculco caldera complex is located in the northern part of the State of Puebla, México. The complex is located at the intersection of the NE Tenochtitlan-Apan, NW Taxco-San Miguel de Allende, and E-W Chapala-Tula fault systems that generate a regional extensional regimen. These fault systems controlled the caldera collapse and exerted the main control on the location of post-caldera vents. Acoculco was built upon a basement formed by a hornblende granite, Cretaceous limestones and marbles, the Zacatlan-Chignahuapan basaltic plateau of unknown, and Miocene Pre-Caldera hypabyssal domes and lavas (10-3 Ma). The caldera-forming eruption occurred 2.7 Ma ago with an explosive event that dispersed pyroclastic density currents that emplaced the Acoculco andesitic ignimbrite with a volume of $\sim 127 \text{ km}^3$. The activity was renewed dominantly inside the caldera complex producing several volcanic units that formed the Early post-caldera volcanism (2.6-2.1 Ma). This volcanism consist of lava and domes dominantly of basaltic trachyandesite to basaltic composition with an erupted volume of 32.8 km^3 . The activity migrated dominantly to the periphery provoking the emplacement of Late Post-caldera volcanism domes and lavas of rhyolitic composition with 70.6 km^3 in the period between 2.03 and 1 Ma. Finally, extra-caldera activity occurred between 0.9-0.06 Ma through venting of scoria cones and lava flows that erupted basaltic trachyandesites to basaltic andesites with a volume of 31 km^3 . The minimum total volume exposed of the ACC is circa 157 km^3 that was erupted at an average rate of $0.058 \text{ km}^3/\text{ka}$.

Effusive eruptions dominated the evolution of the complex (79 %) with the emission of basaltic to rhyolitic composition. All of these rocks are calc-alkaline, although some post-caldera rhyolitic lavas have peralkaline compositions. The calcic nature of the local basement enriched in ^{87}Sr dictate the final composition of the rocks of the ACC.

Dulcinea Avouris, Simon Carn, Gregory Waite

Submission 355

Triggering of volcanic degassing by large earthquakes

Statistical analysis of temporal relationships between large earthquakes ($M_w > 7$) and volcanic eruptions suggest that seismic waves may trigger eruptions over great (> 1000 km) distances from the epicenter, but a robust relationship between volcanic and teleseismic activity remains elusive. Here, we investigate the relationship between dynamic stresses propagated by surface waves and a non-eruptive volcanic response, manifested by changes in sulfur dioxide (SO_2) emissions measured by the Ozone Monitoring Instrument (OMI), onboard the NASA Aura satellite. Surface wave amplitudes for a catalog of 69 earthquakes in 2004-2010 are modeled at eleven persistently degassing volcanoes detected by OMI. The criteria for inclusion in the catalog was $M_w > 7$, depth $w > 8$, all depths. The volcanic response is assessed by examining daily OMI SO_2 measurements in 28-day windows centered on earthquakes meeting a variable Peak Dynamic Stress (PDS) threshold. The PDS value for each earthquake was calculated from the synthetic seismogram, which was modeled using the Computer Programs in Seismology software, and incorporates distance and azimuth in the computation. A positive volcanic response is identified if the average post-earthquake SO_2 mass was at least 20% larger than the pre-earthquake SO_2 mass, while a negative response is identified if the average post-earthquake SO_2 mass was at least 20% smaller than the pre-earthquake SO_2 mass. We find two distinct volcanic responses, correlating strongly with eruption style. Open-vent, basaltic volcanoes exhibit a positive response to earthquake-generated dynamic stress (i.e., the earthquake triggers increased SO_2 discharge), while andesitic volcanoes exhibit a negative response. We suggest that the former is consistent with partially solidified magma breaking as the yield strength is exceeded by dynamic stress, or a magma sloshing process acting on pre-existing gas bubbles in low-viscosity magmas, whereas the latter observation may reflect more dominant controls on degassing in viscous magmas or a post-earthquake reduction in permeability. Overall this analysis suggests that the potential effects of large earthquakes should be taken into account when interpreting trends in volcanic gas emissions.

Marek Awdankiewicz, Ryszard Kryza, Krzysztof Turniak, Maria Ovtcharova, Michael Wiedenbeck

Submission 738

CA-ID-TIMS ages and oxygen isotope signatures of zircons from the Sudetic Ophiolites – constraints on the origin of Palaeozoic oceanic domains in the Variscan Belt

The Sudetic Ophiolites, positioned on the NE margin of the Bohemian Massif in Central Europe, are relics of the Palaeozoic Rheic Ocean lithosphere emplaced into the Variscan Belt during Late Devonian – Carboniferous continental collision. The Sudetic Ophiolites range from dismembered slices, such as the serpentinite Szklary Massif, to nearly complete successions, from serpentinites to cherts, such as the Ślęza Ophiolite. Previous results summarized by Kryza and Pin (2010; *Gondwana Research*, 17, 292-305) confirm N-MORB like geochemical and isotopic affinities of mafic members of the ophiolites along with an Early Devonian age (c. 400 ± 10 Ma; U-Pb SIMS) for the magmatic crystallization of the Ślęza Ophiolite. The origin of the Sudetic Ophiolites has been linked to a mid-ocean ridge, although a subduction-related setting has also been considered a possibility. This study provides initial results of new precise CA-ID-TIMS U-Pb dating and oxygen isotope determination in three zircon separates (from a felsic segregation in the Ślęza metagabbro and two plagiogranites of the Nowa Ruda and Braszowice Massifs), which constrain in more detail the age and magmatic evolution of these ophiolites. Two populations of zircons from the Ślęza metagabbro were dated at 404.67 ± 0.35 Ma (including tracer calibration uncertainties) and 402.61 ± 0.24 Ma. An age of 402.69 ± 0.25 Ma, identical with the younger Ślęza population, was obtained from the Nowa Ruda plagiogranite, while the zircons from Braszowice plagiogranite yielded the youngest age of 401.28 ± 0.29 Ma. These results confirm the earlier SIMS data and provide further details, suggesting magmatic crystallization of the Ślęza gabbro at c. 404.7 Ma followed by infiltration by plagiogranite melts at c. 402.6 Ma, contemporaneous with plagiogranite magmatism in the Nowa Ruda Massif, and a younger plagiogranite emplacement at c. 401.3 Ma in the Braszowice Massif. The mean $\delta^{18}\text{O}_{\text{VSMOW}}$ determined by SIMS is 5.2 ± 0.14 ‰ (1sd, n=89) in zircons of the Ślęza gabbro, and 4.69 ± 0.21 ‰ (n=12) and 4.79 ± 0.26 ‰ (n=42) in the Nowa Ruda and Braszowice plagiogranites, respectively. The mantle-like values in zircons from gabbro are in line with the well-recognized N-MORB affinity of the mafic members of the Sudetic Ophiolites, whereas the lighter values in zircons from plagiogranites may reflect an involvement of sea water in the formation of the plagiogranite melts, or lower-temperature crystallization of zircon in the high-silica plagiogranite melts.

Mathilde Bablon, Xavier Quidelleur, Pablo Samaniego, Jean-Luc Le Pennec, Pierre Lahitte, Céline Liorzou, Jorge Eduardo Bustillos, Silvana Hidalgo

Submission 831

Eruptive chronology of Tungurahua volcano (Ecuador) revisited from new K-Ar ages and geomorphological reconstructions

Reconstruction of the past eruptive history of active volcanoes is essential to better understand the functioning of eruptions processes. The northern part of the Andean arc presents a very active volcanism since about 2 Ma. Seismic and volcanic hazards are high in Ecuador, where about 85 volcanic edifices were active during the Quaternary. Our study focuses on the Tungurahua volcano, one of the most active edifices from the northern Andean range. We have combined K-Ar ages and geomorphological reconstructions to refine the eruptive history of the volcano, to constrain through time its three construction stages, and to quantify their magmatic productivity and erosion rates. Moreover, geochemistry analyses allow us to scrutinize the long-term evolution of the lavas composition, as well as a possible influence on the magmatic signature of the two flank collapses experienced by the volcano.

The groundmass unspiked K-Ar dating method is particularly suitable for dating young subduction lavas, with low K and high Ca contents. Our new ages question the previously published K-Ar ages performed on whole-rock, and show that the volcano is much younger than expected. The first edifice was built from about 300 to 80 ka, with an eruptive rate of 0.6 ± 0.3 km³/kyr, and a volume of ~125 km³. After 50 kyr of quiescence, followed by a flank collapse ~33 ka, the second edifice filled the resulting amphitheater. Although its volume was significantly lower than the first edifice one, its eruptive rate was similar. The third and still active edifice was rapidly constructed during the last 3 kyr, after a new western collapse. It is characterized by the lowest volume of deposits, but displays a relatively high eruptive rate of 2.5 ± 1.0 km³/kyr, which may be explained by its recent construction and rather continuous activity, without periods of quiescence. In addition, deposits of the first edifice not affected by the collapses were eroded with a rate of 0.2 ± 0.1 km³/kyr. Major and trace elements contents of lavas from these three edifices are rather similar, and the magmatic signature do not seem to have been significantly affected either by the flank collapses experienced by the volcano, or by changes of the deep magmatic source through time.

Finally, our results show that the K-Ar dating method performed on groundmass can be successfully applied to volcanoes from the Ecuadorian arc, with many of them remaining without knowledge of the timing of their past activity.

Amelia Bain, Eliza Calder, Joaquín Cortés, Gloria Patricia Cortés, Diego Mauricio Gómez, Roberto Torres, Susan Loughlin

Submission 478

Repeated emplacement and destruction of stratified andesitic magma plugs in the shallow conduit of Galeras volcano between 2004-2012

The eruption of andesitic-dacitic magmas at arc volcanoes is often characterised by periods of cyclic vulcanian explosions thought to result from the repeated development of overpressure beneath degassed, highly-crystalline plugs in the shallow conduit. The timing, magnitude and nature (gas-rich to block-rich) of these explosions are highly variable and building understanding of the processes that control this spectrum of activity is necessary for hazard assessment during what are often prolonged volcanic crises.

We report results from a combined textural and volatiles study of time-constrained andesitic ballistic bombs from the 2004-2012 period of activity of Galeras volcano, Colombia. Our results show that degassed plugs of magma repeatedly developed in the shallow conduit prior to vulcanian explosions. These magma plugs were stratified with respect to volatile content, vesicularity and groundmass crystallinity. We show that vesiculation events occurred repeatedly at shallow levels, resulting in the development of permeable porous networks that facilitated efficient degassing of denser, more volatile-rich magma. The viscous collapse of these porous networks resulted in the formation of a densified cap. Block-rich explosions subsequently reamed out these volcanic plugs to a maximum depth of 500 m.

Our results show that explosions that varied with respect to magnitude ($8 \cdot 10^4 - 3.56 \cdot 10^6$ m³) and repose time (6–554 days) were sourced from magma plugs with similar structures and physical properties. Ongoing work aims to characterise the second-order textural and chemical differences between plugs that may explain the range of explosive activity observed at Galeras in 2004-2012, and to relate these differences to monitoring datasets.

Madison Ball, James Watkins, Leif Karlstrom

Submission 868

Vapor–melt equilibration rates in silicic magmas

The solubility of H₂O and CO₂ in silicate melts depends on temperature, pressure, melt composition and vapor-phase composition. Perturbations to any of these variables can result in bubble nucleation, growth, or resorption, which in turn affects rheological properties such as density and viscosity. Ultimately, these factors control whether magmas erupt effusively or explosively. Conduit models assuming vapor–melt equilibrium during magma ascent may be valid for slowly rising magmas in which H₂O and CO₂ have adequate time to diffuse into or out of bubbles and fractures. In rapidly ascending magmas, however, volatile transport can be limited by slow diffusion, and the assumption of vapor–melt equilibrium may be oversimplifying.

We are investigating the vapor–melt equilibration time using decompression experiments and numerical diffusion models. We define the time required for a bubble to diffusively equilibrate with its host melt (τ_{diff}) to be the e-folding time of the difference in CO₂ concentration between bubble–melt interface and the concentration in the melt halfway between hexagonally close-packed bubbles. This timescale depends primarily on temperature, ascent/depressurization rate, initial volatile-content, as well as bubble spacing and size. At fixed temperatures, the equilibration time increases exponentially with the distance between bubbles. For a 70 MPa pressure drop at 800°C with 2 wt.% initial H₂O, we find that τ_{diff} increases by two orders of magnitude from ~103 s for closely spaced bubbles (~50 μm) to ~105 s with a tenfold increase in spacing (~500 μm). Equilibration time has a lesser but still noticeable sensitivity to the bubble size, which affects diffusive transport across the bubble–melt interface due to vapor buffering. Larger bubbles on their own increase τ_{diff} but also deform the melt and shorten the distance between bubbles leading to faster overall equilibration. We anticipate that our parameterization of the vapor–melt equilibration time will be useful for assessing the assumption of maintained vapor–melt equilibrium during degassing/resorption in the interpretation of volatile concentration data and gas measurements. These results should also be useful as an input to conduit flow models that consider unsteady motions on timescales similar to bubble growth, such as those occurring during the propagation of acoustic waves generated by distant earthquakes, rock falls into the conduit, or impulsive (de)pressurization.

Jessica Ball, Margaret Mangan, Nathan Wood, Laura Dinitz

Submission 260

Crafting Effective Messaging for Volcanic Hazard Exposure and Vulnerability Studies in California

The California Volcano Observatory (CalVO) in Menlo Park, California is one of five United States Geological Survey (USGS) volcano observatories dedicated to enhancing public safety and minimizing societal disruption. Their work includes delivering long- and short-term hazard assessments and forecasts based on scientific research and monitoring of volcanic unrest. Volcanic eruptions occur in California about as frequently as the largest earthquakes along the state's infamous San Andreas Fault Zone, with 10 eruptions occurring in the past 1000 years. Even though the likelihood of renewed volcanism is high—chances are one in a few hundred to one in a few thousand, annually—volcanoes have been a “forgotten hazard” in the minds of government, industry, and public stakeholders.

In an effort to increase awareness and community resiliency to volcanic threats in California, the USGS established CalVO in February 2012. CalVO's mission is to build a targeted program of hazard research, volcano monitoring, community outreach, and inter-governmental coordination.

Current CalVO outreach and coordination efforts focus on a statewide assessment of California's exposure to hazards from future eruptions at eight volcanic centers ranked as Moderate, High, and Very High threat by the USGS (NVEWS, 2005). We will discuss our partnership with the California Office of Emergency Services, who commissioned the project, and our plans to incorporate social science, user-centered design, and modern communications theory in the development and rollout of the assessment.

Michael Barber, Nick Deardorff

Submission 1219

Characterization of volcanic terrains using lidar return amplitudes and other data: a statistical approach

In recent decades, lidar has revolutionized topographic mapping of the Earth and planets through the use of digital elevation models (DEMs). However, the return amplitudes of the reflected laser pulses, typically collected as part of a lidar dataset, have seldom been used as a means of identifying and characterizing volcanic surface features such as lava flows, rafted tephra and agglutinate, and pyroclastic deposits consisting of tephra and ashfall. Here, we find an effective process for remotely characterizing volcanic terrains using a simple but rigorous cluster analysis of lidar return amplitudes and DEM data to define the parameters for a self-organizing mapping routine. The data used for this study, collected from the Northwest Rift Zone on Newberry Volcano in central Oregon, has been accurately geo-referenced, providing 1 meter horizontal and 4.5 centimeter vertical resolution. In addition, the return amplitude values were recorded with a horizontal resolution of 50 centimeters. An appropriate number of terrain categories is found by applying an incremental within-cluster sum of squares algorithm to generate clusters from subsets of lidar DEM and reflectivity data, chosen in a completely randomized experimental design from the study area. From these results, a silhouette analysis determines the optimum number of clusters to be used as a necessary input parameter for the categorization of each data cell by means of a self-organizing mapping function. These results, confirmed by comparison with field work conducted at Mokst Butte and its associated lava flows, is then applied to other, less accessible volcanic terrains. The resulting false-color imagery allows precise identification of volcanic morphologies that are otherwise unrecognizable in remote sensing data such as lidar, InSAR, and orthorectified color photography, and in regions where traditional field work is difficult or unfeasible.

Nicholas Barber, Anne Jay, Loïc Vanderkluisen

Submission 183

Using Geographic Information Systems to Refine Estimates of Deccan Lava Flow Volumes (India)

The Deccan Traps is a continental flood basalt province that covers large areas of the Indian peninsula, extending from southern India to the border of Pakistan. The province is composed of hundreds of individual lava flows and flow fields, largely emplaced over the course of 3 for the whole of the Malwa Plateau. This estimate is but a small fraction of the entire Deccan volume (estimated at ~500,000 km³): the lava flow sequence of the Malwa sub-region is much less laterally extensive than the main province further south. To complement the work being done in these two subregions, we also used ArcGIS to trace digitally the boundaries of the 11 major chemostratigraphic formations in the main Deccan region, south of the Malwa. Initial results on the volume of individual lava flow packages indicate that Geographic Information Systems (GIS) can be a key tool for interpreting the architecture of large igneous provinces (LIPs) like the Deccan Traps. We plan to integrate rock core and stratigraphic data into updated volume estimates to determine long-term average eruption rates for individual Deccan flow formations. Consequently, the work presented here will help inform our understanding of the tempo of gas release to the atmosphere resulting from the Deccan volcanic eruptions, and the role they may have played in the end-Cretaceous extinction and post-extinction ecosystem recovery.

Jenni Barclay, Jonathan Stone, Maria Teresa Armijos, Anna Hicks

Submission 168

Citizen Science in Volcanology: analysing benefits for communities at risk

Citizen science involves volunteers, regardless of scientific background, in progressing scientific investigations. Their degree of involvement in the design, execution and analysis of these investigations varies. In volcanology the potential benefits for citizen science are not just restricted to the generation of new knowledge, projects can act as a vehicle to increase public awareness or confidence in scientific data, and to provide 'real-time' windows into the impacts of long-term change, rapidly evolving events or recovery from volcanic eruptions.

Citizen science projects around volcanoes thus have the potential to act as catalysts for the reduction of risk for communities around volcanoes, particularly in developing countries, where increasing the volume of scientific data and community empowerment are priorities. A global survey of volcano monitoring institutions and the ways in which they currently use the broad family of techniques that can be allied with 'citizen science' provides us with some insights into their current utility. Around two-thirds of respondents were involved in citizen science initiatives with > 85% of those involving some type of direct observation of eruptions or impacts, but less evidence for involvement in further data gathering or analysis. However our analysis suggests there are good reasons for stronger collaborations: all participants tend to benefit more when they adapt to and learn from one another, in response to ongoing activity. At best, citizen science projects can help both scientists and community members cope with the inherent uncertainties around volcanic phenomena by enabling them to devise strategies that minimise impacts on lives and livelihoods. However, sustaining interest can be hard out with periods of eruptive activity.

We also present a comparison of volcanological projects with similar initiatives (aimed at reducing risk from other natural hazards) and reflect on how evidence across these projects might be deployed to improve the utility of citizen science in reducing volcanic disaster risk in developing countries.

Jenni Barclay, Katie Preece, Katy Chamberlain, Richard Brown, Darren Mark, Charlotte Vye, Ben E. Cohen, Sue Loughlin

Submission 306

Integrating volcanology, geochemistry and petrology to understand magmatism on Ascension Island

Building on the geochemical work of Jon Davidson and his colleagues in the 1990s, the 'Ascension' project aimed to understand the control of magmatic processes on eruption duration, style and magnitude for a previously poorly constrained system. Our ambition was a holistic study of an ocean island volcanic system integrating Jon's existing knowledge, with physical volcanology, high-precision $^{40}\text{Ar}/^{39}\text{Ar}$ geochronology and geochemical and isotopic fingerprinting of magma supply through time.

The sub-aerial eruptive history of Ascension Island demonstrates an extraordinary cornucopia of volcanic activity. The last 1Ma has seen: > 80 explosive silicic eruptions and at least 40 mafic eruptions. We have shown that the most recent eruptions occurred at

The 'crystal cargo' of each deposit is as extraordinary for its uniformity as the eruptive activity is for its variety. There are strong petrological and geochemical signatures of closed-system behaviour; silicic eruptions are largely generated by fractional crystallization of mafic melt in the lower crust (> 6 km depth). Mafic eruptions also demonstrate little evidence for shallow or intermediate storage and rapidly ascend from depth scavenging crystals from plutonic bodies during ascent with insufficient time for the development of new compositional rims in response to their new host melt. We identified only two examples of significant interactions between differing magmas prior to or during eruption: a zoned pyroclastic deposit and a mixed magmatic eruption. Melt inclusions are volatile rich and eruptions are likely triggered externally or by volatile over pressurization, rather than interaction with further magmatic input.

Joseph Bard

Submission 365

What's the story with Mount Rainier? Taking a narrative approach to explaining Mount Rainier's volcanic hazards to general audiences using ESRI Story Maps.

Volcanic hazard information products developed by scientists, but intended for general audiences, are at risk for inheriting the characteristic inflection and default structure of expository scientific writing. By portraying volcanic hazard information in this fashion, volcano observatories, and analogous agencies, may be overlooking an opportunity to communicate more effectively with their intended audiences.

Taking a narrative approach when presenting scientific information to general audiences has a few critical advantages over employing a traditional scientific format. Narrative texts are often linked with shorter reading times, are more easily understood, and are associated with increased recall in comparison to information presented in an expository form. In addition, narratives may also allow people to mentally simulate critical scenarios and model possible outcomes without having to experience the scenario themselves.

ESRI's Story Maps are an emerging media platform uniquely suited for communicating inherently complex volcanic hazard information in a format that's relatable to general audiences. Using Story Maps, important volcanic hazard information can be explained through narratives and integrated with web maps, images, and videos within an intuitive web-based application. On the technical side, web map content can be served from observatory GIS databases and easily updated to keep pace with rapidly changing situations.

This talk will focus on the process of creating a Story Map to communicate hazard information about Mount Rainier, Washington for general audiences. This is a new product intended to complement existing products developed by the USGS Cascades Volcano Observatory (CVO) and its partners, such as prepared presentations for public outreach, interpretive signs and museum exhibits, videos, educational curricula, USGS Fact Sheets, and content on the CVO website. The discussion will include the use of narrative and cartographic techniques to describe the hazard context, increase awareness, and highlight actions the public can take to reduce their vulnerability to the hazards present at Mount Rainier.

Florian Barette, Caroline Michellier, Sophie Mossoux, Sam Poppe, Benoît Smets, Éléonore Wolff, François Kervyn, Matthieu Keryvn

Submission 413

Assessing lava flow risk at Nyiragongo volcano, DR Congo. Part 2: Lava flow hazard map

Nyiragongo volcano, located at the boundary between the Democratic Republic of Congo and Rwanda, is characterised by intra-crater lava lake activity interrupted by flank eruptions. Over the last 120 years, two disastrous flank eruptions occurred at Nyiragongo volcano, in 1977 and 2002. In 2002, two lava flows inundated the densely-populated city of Goma, destroying about 10% of the city, one third of the airport runway and most of the business centre. Between 300,000 and 400,000 people evacuated the city and the eruption caused several tens of fatalities.

Within the framework of the GeoRisCA project, we computed a new lava flow hazard map for Nyiragongo volcano. The vent opening susceptibility at Nyiragongo volcano was assessed with the QGIS for Volcanic Susceptibility (QVAST) plugin, using historical and non-historical eruptive fissures and vents as structural elements. Distinct probability density functions were calculated for these structural elements, and these were subsequently combined to derive the spatial probability of future vent opening along Nyiragongo flanks. The lava flow hazard was computed using the Quantum-Lava Hazard Assessment (Q-LavHA) model using a high accuracy and up-to-date TanDEM-X derived Digital Elevation Model (DEM) as topographic base. The model parameters were calibrated by simulating the 2002 lava flow of Nyiragongo volcano, using the 30 m SRTM DEM. The length of the historical lava flows was analysed to statistically constrain the terminal lava flow length of the simulations. A corrective factor based on the calibration of the model was used to account for the impact of the DEM resolution on the simulated lava flow length.

Our results indicate that the probability of vent opening is very high on the southern flank of Nyiragongo volcano, along the north - south oriented fissure system. The lava flow hazard is high on the southern flank of Nyiragongo volcano, and particularly in the western and eastern part of Goma. The latter was already destroyed during the 2002 eruption of Nyiragongo volcano. Our results, combined with the assessment of the exposure and vulnerability of the population and built elements (Part 1), shows that the lava flow risk is particularly high in the eastern part of Goma.

Simon Barker, Michael Rowe, Joel Baker, Colin Wilson, Shane Rooyakkers, Chris Conway

Submission 1000

MELT INCLUSIONS IN OLIVINE XENOCRYSTS PROVIDE A 'WINDOW' THROUGH LARGE SILICIC MAGMA SYSTEMS

The Taupo Volcanic Zone (TVZ) is globally unique amongst volcanic arcs in the intensity of its magmatic–volcanic–geothermal flux. However, the causes of this anomaly are not yet understood, as primary magmas (basalts) are extensively modified in the TVZ during their ascent to the surface, overprinting the geochemical features required to infer conditions under which they formed. Moreover, the small amounts of basalt that do erupt are likely buried or destroyed by explosive and voluminous rhyolitic (super)eruptions. Our novel study addresses this issue by applying forensic geochemical techniques to glassy melt inclusions trapped within olivine crystals, separated from volcanic rocks throughout the TVZ, ranging in age from 0 to 350 ka. Our approach is motivated by the recent identification of high-Mg olivine xenocrysts inherited from primitive basalts in large-volume TVZ rhyolites, which contain trapped basaltic melt inclusions with the most primitive magma compositions ever recorded in the TVZ. These data provide a novel and unique "window" into mantle processes driving voluminous rhyolitic volcanism. Here we present melt inclusion major and trace element data from olivine melt inclusions from across and along the arc and, for the first time, quantify the spatial and temporal compositional variability of magmas feeding TVZ volcanoes. Our data reveals the unique differences between mafic magmas feeding rhyolitic caldera volcanoes with those feeding discrete basaltic scoria cones or andesitic stratovolcanoes, suggesting there is a fundamental mantle control on the types of volcanoes and their spatial and geographic distribution. We consider the unique subduction and rifting processes behind the extreme, globally unique heat flow in the TVZ and how this is reflected in the composition of primary magmas in time and space.

Abigail Barker, Eric Andin, Valentin Troll, Börje Dahren, Steffi Burchardt, Michael Krumbholz, E Albers

Submission 644

Explaining Hekla's short eruption onset from the mineral record

Most volcanoes provide signals of unrest in the weeks to months leading up to an eruption. Hekla volcano on Iceland however, does not show perceivable warning signals in seismicity or deformation until typically a few hours or less before an eruption. In order to explain Hekla's unusual eruptive behaviour, we explore mineral chemistry in samples from the 1980/81 and 2000 eruptions to investigate cryptic signs of magmatic charging beneath the volcano.

The lavas are highly vesicular and contain sparse crystals of plagioclase, orthopyroxene, clinopyroxene and titanomagnetite, which often form clusters. The groundmass is very fine grained and composed of plagioclase, pyroxene and titanomagnetite. The samples from the 1980/81 eruption are andesitic in composition, whereas the samples from the 2000 eruption are basaltic andesites. Plagioclase from the 1980/81 eruption has An 20 to 96, whereas the 2000 eruption hosts plagioclase with An 53 to 75. Pyroxene compositions range from 52 to 99 Mg# and 90 to 98 Mg# for the 1980/81 and 2000 eruptions respectively.

Preliminary thermobarometry places plagioclase crystallisation between 1075 and 1095°C and 3 to 266±247 MPa. Clinopyroxene microphenocrysts in turn crystallise at temperatures of 1040 to 1095°C with corresponding pressures from near surface down to 387±160 MPa.

This wide range of mineral chemistry suggests complex differentiation and mixing processes occurred beneath Hekla preceding the eruptions. Estimates of crystallisation conditions imply depths of magma storage between 0 and 10 km below the volcano. The shallow level storage and cooling rates are likely key factors to explain Hekla's short warning times prior to impending eruptions.

Talfan Barnie, Ashley Gerard Davies, Gezahgen Yirgu, Chris Moore, Simon Carn, David Pieri, Clive Oppenheimer, Juliet Biggs, Tim Wright

Submission 452

The 2017 eruption of Erta 'Ale volcano, northern Afar, Ethiopia

The Erta 'Ale shield volcano lies in the eponymous rift segment in northern Afar, Ethiopia, and has hosted multiple lava lakes in its summit caldera over the past century. It has been proposed that a rise in the lava lake height since 2005 is linked to the increase in magmatic activity in the broader Red-Sea rift – Afar – Gulf of Aden region. Here we report on further remarkable eruptive activity involving both the lava lake and a larger caldera south-south east of the summit caldera (hereafter referred to as the “southern sink” after Barberi et al.), which we reconstruct using eyewitness accounts and satellite imagery. The eruption appears to have progressed in three phases: (i) an initial period of lava lake overflows in the summit caldera starting on the 19th January, (ii) a major fissure eruption in the southern sink starting on the 21st of January, and (iii) a sustained low level of effusion from the fissure from the 29th of January. Patterns of ground deformation revealed by radar interferometry using the Sentinel 1 satellite are consistent with a dike stretching from the southern sink to the summit caldera, intruded between the 11th and 28th of January. The early stages of the eruption were captured in high resolution ALI and Hyperion images from NASA's Earth Observing 1 satellite, automatically tasked by the NASA volcano sensor web, revealing 2.5 km of discontinuous eruptive fissures in the southern sink on the 23rd of January, approximately 95 m below the level of the overflowing lava lake. Subsequent images from these and other sensors have tracked the evolution of the flow field, which had reached a distance of 3.1 km from the fissure and an area of 3.3 km² by the 10th of March. High frequency SEVIRI images revealed a rapid waxing and exponential waning pattern in activity during the main phase of the fissure eruption, as well as the pre-eruptive lava lake overflows and co-eruptive pulsatory activity at the lake and/or fissure. Peak power output during this phase as recorded by EO-1 is approximately 5000 MW. Observations from OMPS and OMI during the fissure eruption suggest SO₂ emissions were modest, with a maximum plume load of approximately 1000 tonnes detected on January 22nd. This study highlights the importance of satellite remote sensing for eruption surveillance, and furnishes new insights into the behaviour of the axial volcanic ridges in Afar.

José Barrancos, Germán Padilla Hernández, Luca D'Auria, Rubén García Hernández, Nemesio M. Pérez Rodríguez, Fiona Anne Burns, Pedro A. Hernández Pérez, Aarón Pérez Martín

Submission 842

A new seismic monitoring system for Canary Islands

Canary Islands are an active volcanic archipelago located along the western coast of Africa in the Atlantic Ocean. The islands hosted various historical eruptions, the last one being the submarine 2011 El Hierro eruption. The increasing population density and the consistent number of tourists are constantly raising the volcanic risk. Along with seismo-volcanic activity, a significant seismicity occurs along a strike-slip fault located between Tenerife and Gran Canaria islands and along other minor regional tectonic structures. Therefore the islands are subject to a moderate seismic risk as well.

In June 2016 Instituto Volcanológico de Canarias (INVOLCAN) started the deployment of a seismological volcano monitoring network consisting of broadband seismic stations with real-time data transmission. The network began its full operativity in November 2016. Currently 13 stations are operating on the island of Tenerife and two in Gran Canaria. This seismic network complements a permanent GPS network of more than 30 stations, co-owned by INVOLCAN, GRAFCAN and Univ. of Nagoya and a network of 18 permanent continuous geochemical monitoring stations, managed by INVOLCAN. In the next years it is planned the deployment of more stations on other islands and a densification of the seismic network of Tenerife, the island with the highest volcanic risk among the Canaries.

The aim of the network are both volcano monitoring and scientific research. Its scientific objectives cover also the study of the potential geothermal resources of the islands, though the improvement of the knowledge about the spatial characteristics of the microseismicity and the definition of the structural models. Currently data are continuously recorded and processed in real-time. Seismograms, hypocentral parameters, statistical informations about the seismicity and other data are published on a web page also through weekly short reports and monthly detailed bulletins. We show details about the technical characteristics of the network, an estimate of its detection threshold and earthquake location performances. We present other near-real time procedures on the data: analysis of the ambient noise for determining the shallow velocity model and temporal velocity variations, detection of earthquake multiples through massive data mining of the seismograms and relocation of events through a double-difference technique. Furthermore we show some example of seismo-volcanic events recorded in the past months.

Julien Barrière, Adrien Oth, Nicolas d'Oreye, Nicolas Theys, Jeffrey Johnson, François Kervyn

Submission 501

Monitoring volcano seismicity, infrasound and SO₂ degassing patterns in the Virunga Volcanic Province, Democratic Republic of the Congo

The Virunga Volcanic Province (VVP) in the Democratic Republic of the Congo hosts two of the most active and hazardous volcanoes in Africa, Nyiragongo and Nyamulagira. Nyiragongo is a stratovolcano hosting the largest persistent lava lake on Earth. Only 13 km separate Nyiragongo from its neighbor Nyamulagira, which is a large shield volcano characterized by frequent eruptions. Following its 2011-2012 voluminous eruption, significant seismic and degassing activity persisted in the central crater leading to the intermittent resurgence of surface activity since mid 2014 (lava fountains and lake). The recent and progressive deployment of the broadband seismic network KivuSNet since 2014, currently composed of fourteen telemetered seismic stations and three infrasound arrays within the VVP and Lake Kivu area, opens new monitoring opportunities.

Automatic, picking-free location routines of seismic sources (continuous volcanic tremor, individual earthquakes) have been implemented, allowing a first overview of the seismicity patterns at Nyamulagira and Nyiragongo. Since magma movements at active volcanoes are commonly associated with changes in seismicity as well as modifications in SO₂ degassing levels, we combined the seismic dataset with space-based SO₂ emission estimates from the Ozone Monitoring Instrument (OMI) to set a continuous tracking methodology for magma migration over the last years. We find that such a multidisciplinary approach allows for a robust discrimination of magma migration in and out of the shallow plumbing system, improving our ability to interpret signs of volcanic unrest on a daily time scale. Moreover, infrasound signals should help to better understand the superficial magmatic processes. Preliminary analysis reveals significant explosion events at Nyiragongo recorded at tens of kilometres, making this acoustic component of the KivuSNet an important monitoring prospect.

Anna Barth, Megan Newcombe, Elizabeth Ferriss, Erik Hauri, Terry Plank

Submission 1027

Control of magma ascent rate on the explosivity of basaltic eruptions

Magma ascent rate plays a crucial role in modulating the dynamics of explosive basaltic eruptions. This control is imparted through the kinetics of crystallization and bubble nucleation, rheological changes, and dynamics of the multiphase flow. In particular, for basaltic systems the degree to which bubbles and melt remain coupled (a requirement for explosive eruptions) is largely controlled by ascent rate. Yet despite its clear physical significance, very few estimates of ascent rate exist. We explore here whether the transition from Strombolian to Sub-Plinian intensity could be the result of an increase in magma ascent rate. To constrain ascent rate, we exploit the incomplete diffusive re-equilibration of water through olivine. The novel aspect of this study is that we record water loss during ascent from both melt inclusions and the olivine crystals that host them. In order to isolate the effects of ascent rate from other controls on eruption style, we focus on two eruptions at the same volcano, Cerro Negro – the 1992 Sub-Plinian and the 1995 Strombolian eruptions.

Olivine-hosted melt inclusions (MIs) from the 1992 Sub-Plinian eruption show a negative correlation between MI size and diffusive water loss, as predicted for diffusive re-equilibration. Diffusion modelling of water through the host olivine coupled with a degassing model in the host magma yields ascent times on the order of several hours. MIs from the 1995 fire fountaining extend to comparable maximum H₂O and CO₂ contents (~4.5 wt.% H₂O, ~500 ppm CO₂), suggesting similar magma source conditions. However, for similar MI to olivine size ratios, the 1995 MIs are offset to lower water by 0.5-1 wt.%. Indeed, modelling results indicate that the 1995 olivines ascended four times more slowly on average than those from the 1992 eruption. We have also obtained among the first water profiles across olivine phenocrysts using SIMS and FTIR. Water concentrations decrease away from MIs and towards crystal edges. Preliminary 1D diffusion modelling gives diffusion timescales in agreement with the MIs. Diffusion anisotropy shows faster diffusion along the a direction than along c, consistent with the fast 'proton-polaron' diffusion mechanism. Using FTIR, we have been able to resolve which crystal defects are accommodating the diffusion. The olivine-melt inclusions system together presents a powerful tool for assessing magma ascent rate as a driver for explosivity.

Daniel Basualto, Pablo Gonzalez, Loreto Cordova, Jonathan Quijada, Gabriela Velásquez, Diego Lobos

Submission 1066

Megathrust and Volcanic Reactivations, Evidence, Correlations and Eruptions in the Chilean Volcanic Belt

The Chilean Volcanic Belt has shown evidence on the interaction between megathrust and volcanic eruption. One of the most described examples was Cordón-Caulle eruption in 1960, which occurred 42 hours after the Valdivia megathrust Mw9.5. There is some research that discusses this issue, however there still are questions about how the volcanic reactivation takes place after a megathrust. The continuous seismic monitoring network installed since 2010 by OVDAS, has allowed study those issues with the detail that is required. In all the extensive volcanic arc, Chillan (CHI), Copahue (COP) and Villarrica (VIL) recorded changes in volcanic activity levels after Illapel megathrust Mw8.4 09/16/15. These changes, can be summarize in an abrupt increase in the number of local volcano-tectonics events (650 COP and 85 VIL in 15 days), an increase in the values of RSAM (Realtime Seism Amp) and DR (Reduced Displacement) of the tremor (CHI, COP & VIL), increase of SO₂ (COP), variations in the GPS signal trend of deformation (COP), changes in the dominant frequencies of the seismicity and eruptions (CHI & COP). Chile has 45 volcanoes monitoring along its volcanic belt, which is the peculiarity of these volcanoes that reacted to the seismic waves of the earthquake? The analysis with different monitoring methodologies (seismology, geodesy, chemistry & webcams) for several years (2010-17), have allowed to define levels of background in volcanic activity and identify subtle changes, that generate instability in volcanic systems. Using this criterion, it was possible to establish that these three stratovolcanoes, whose geochemical in the magmatic chambers compositions are different from each other, share a common characteristic. All of them had recorded an increase in volcanic activity above the background level, few months before the megathrust. If we consider that the reactivated volcanoes are located 560, 670 & 850 km away from the epicenter, they are outside of the rupture zone, discarding static stress as a possible triggering. On the other hand, the dynamic stress (rectified diffusion, faults orientation) in an active volcanic system could be able to reactivate an unstable volcano outside of the rupture zone. Finally it should be mentioned that correlations do not generate causality by themselves, however, all these evidences suggest that the destabilization of volcanoes triggered by a megathrust occur in cases where the volcanic systems are in a previous unstable process.

Ahmad Basuki, Dannie Hidayat, Hendra Gunawan

Submission 949

Preliminary results 3D local earthquake tomography at Gede Volcano, West Java, Indonesia

Gede Volcano is a representative of plugged arc volcanoes. Gede exhibits seismic swarm every few years, but only minor visible degassing. The last eruption at Gede was 1957. Due to its proximity to the large population around the volcanoes, the Center for Volcanology and Geological Hazard Mitigation (CVGHM) closely monitored them since 1985. In collaboration between Earth Observatory of Singapore, and CVGHM, we are upgrading geophysical, geochemical and hydrological monitoring on Gede and Salak Volcano. Recent swarms occurred on this volcano and recorded by our network. A key question for Gede and Salak: are the seismic swarm suggest magma intrusion or tectonic? If it is magma intrusion, when will it lead to any eruption? Previous studies of swarms of earthquakes and tilt shed light into possible periods of magma intrusion that did not reach the surface with some control of the tectonic forces around Gede Volcano. Three-dimensional seismic P-wave travelttime tomography is used to image the magma source beneath Gede Volcano. We used travelttime arrivals from hundreds of VT earthquakes that occurred beneath the volcano over the period 2012-2016. Our aim is to further find the magmatic body under the volcano with some limitations to the available data and stations' configuration.

Angelo Battaglia, J. Maarten De Moor, Alessandro Aiuppa, Geffroy Avar, Marcello Bitetto, Gaetano Giudice, Hindeleh Henriette Bakkar, Hairo VILLALOBOS VILLALOBOS

Submission 848

First Multi-Gas time series of Rincon de la Vieja volcano, Costa Rica

Rincon de la Vieja (10.49 N, 85.19 W) is the furthestmost northern active volcano in Costa Rica about 25 km upwind from Liberia. It hosts a hot acidic lake and has produced large phreatic to phreatomagmatic eruption. It is poorly monitored due to remote location and field conditions. For the first time a Multi-GAS instrument does continuous measurements of gas concentrations at the edge of the degassing crater allowing to investigate its activity and the chemical composition of plume. The station performs four acquisitions per day, and the data are compared to the seismic monitoring results. The Multi-GAS station registered 5 phreatic eruptions between February 3 and March 16, 2017, which were also recorded seismically. The Multi-GAS data indicate that Rincon de la Vieja volcano base degassing level is characterized by a low level of magmatic gas concentrations with an arithmetic mean of $CO_2/SO_2 = 121$ and $SO_2/H_2S = 1.16$. The Phreatic eruptions are characterized by (1-2 minute) gas pulse with observed concentrations more than an order of magnitude higher than ground base (up to ~ 52 ppm SO_2 and > 3000 ppm CO_2). We note an increase in SO_2/H_2S from 0.85 to 1.5 prior to the largest eruption which occurred at 15:21 (UTM) on 20/02/2017. The SO_2/H_2S of the gas released during the phreatic eruptions is consistently > 5 , whereas CO_2/SO_2 ratio ranges from 50 to 232. These preliminary data suggest that injection of SO_2 -rich magmatic gas is the trigger for phreatic eruptions and that real time Multi-GAS monitoring could provide precursors to phreatic eruptions at Rincon de la Vieja.

Maurizio Battaglia, Mike Lisowski, Dan Dzurisin, Mike Poland, Steve Schilling, Angie Diefenbach, Jeff Wynn

Submission 66

Magma Intrusion at Mount St. Helens, Washington, from Temporal Gravity Variations

Mount St. Helens is a stratovolcano in the Pacific Northwest region of the United States, best known for its explosive eruption in May 1980 – the deadliest and most economically destructive volcanic event in US history. Volcanic activity renewed in September 2004 with a dome forming eruption that lasted until 2008. This eruption was surprising because the preceding four years had seen the few earthquakes and no significant deformation since the 1980-86 eruption ended. After the dome forming eruption ended in July 2008, the volcano seismic activity and deformation went back to background values.

A high-precision gravity monitoring network (referenced to a base station 36 km NW of the volcano) was set up at Mount St Helens in 2010 since time-dependent gravimetric measurements can detect changes in the subsurface mass flow long before this may cause earthquakes or deformation of the volcano's edifice.

Measurements were made at 12 sites on the volcano (at altitudes between 1200 and 2350 m a.s.l.) and 4 sites far afield during the summers of 2010, 2012, and 2014. The repeated gravity measurements revealed an increase in gravity between 2010 and 2014 at all the sites on the volcano. Positive residual gravity anomalies remained after accounting for changes in surface height, in the Crater Glacier, and in the shallow hydrothermal aquifer. The pattern of residual gravity changes, with a maximum of 57 ± 12 μGal from 2010 to 2014, is radially symmetric and centered on the 2004-08 lava dome. Inversion of the residual gravity signal points to a source 2.5-4 km beneath the crater floor (i.e., in the magma conduit that fed eruptions in 1980-86 and 2004-08). We attribute the gravity increase to re-inflation of the magma plumbing system following the 2004-8 eruption. Recent seismic activity (e.g., the seismic swarm of March 2016) has been interpreted as a response to the slow recharging of the volcano magma chamber.

Peter Baxter

Submission 233

Health effects of volcanic ash: still looking for answers

Preparedness for volcanic eruptions should include health sector planning for responding to concerns over potential acute and long term effects to human health from ashes, especially where dry and windy conditions can lead to regular, high exposures to ash in the air from the persistence of deposits in the environment. The evidence base for health effects from inhalation exposure to volcanic ashes is weak due to a shortage of reliable studies since the Mount St Helens eruption in 1980, with the exception of Montserrat, and it is necessary to extrapolate, with varying degrees of applicability, from occupational settings (silicosis risk from silica), and recent advances in urban and indoor air pollution epidemiology that focus on fine particulate matter, PM 10 and PM 2.5 (e.g., by raising mortality from respiratory and cardiovascular causes), which are also abundant in ashes from explosive eruptions. A review of the volcanic evidence base, its strengths and weaknesses, is undertaken to support preventive health interventions and health risk assessments, and to justify costly measures to reduce ash exposure on a population-wide basis.

Mark Bebbington, Mark Stirling, Shane Cronin, Ting Wang, Gill Jolly

Submission 173

National-level long-term eruption forecasts by expert elicitation

Estimation of volcanic hazard (medium-long term eruption forecasting) is becoming an increasingly quantitative science, potentially allowing the effect on land use decisions and facility design to be embodied in a similar manner to current seismic codes at a national level. The initial step is to characterize the possible hazard sources in a time-varying manner, quantifying the likely timing, size and, in some cases, location of the next eruption from each possible volcanic centre. Because of the long time-scales often involved, particularly for rhyolitic centres, it is desirable to take account of the elapsed time since the last eruption, a process that is only possible for certain data-rich faults in seismic hazard analysis. Incomplete and uneven records of past activity at various volcanoes motivate an approach based on expert elicitation. Here we report on an exercise conducted to quantify volcanic hazard in New Zealand, which has 10-12 'active' volcanoes.

A total of 28 experts (19 volcanologists and 9 non-volcanologist controls) provided estimates of the VEI of the next eruption and, conditional on the VEI, the repose to that eruption and its duration, and in some cases location. The expert opinions were combined using Cooke's classical method to arrive at a consensus hazard estimate. This required a set of 'seed' questions to calibrate and weight the various experts.

The resulting estimates of time to the next eruption were comparable with estimates from existing time-varying models. The elicited median dates for the next eruptions ranged from AD 2020 (White Island, which actually erupted a few months after the elicitation workshop) to AD 4000 (Mayor Island). In all cases bar one, the elicited eruption duration increased with VEI, and was correlated with expected repose. There was surprisingly little difference in elicited eruption duration between volcanoes. Excepting Taranaki, which is in an extended repose and expected to resume activity with a larger eruption, the andesitic volcanoes (Ruapehu, Ngauruhoe, Tongariro and White Island) had very similar elicited distributions for the VEI of a future eruption. Elicited future vent locations for Tongariro and Okataina reflect strongly the most recent eruptions. In the Bay of Islands volcanic field, the elicited spatial distribution is centred on the centroid of the vent locations, while in Auckland it has picked out two 'empty' regions within the field.

Mark Bebbington, Susanna Jenkins

Submission 172

So you have an eruption – how do you forecast what happens next?

Forecasting eruption onsets has received much attention, in both the short- and long-term. However, unlike an earthquake, an eruption is not easily reduced to an instant in time. Any usable definition of an eruption has to allow for activity over scales ranging from minutes to decades, and can do so only by allowing for multiple eruptive phases. These phases can be defined by having different styles (e.g., effusive and/or explosive) of activity and/or quiescent periods between them. A vital question then presents itself: given what we have seen so far of the eruption, what is likely to happen next? We have re-coded a GVP/USGS database of multiple-phase eruptions into 8 major styles, some of which have sub-styles (e.g., dome extrusion versus lava flows) and a further series of 'marks' such as presence of pyroclastic flows or new vents. The result contains c. 700 multi-phase eruptions, with eruptions having up to 33 non-quiescent phases.

The resulting record of transitions between states is relatively dense, and so a probability tree is infeasible to model the $O(8^{33})$ possible phase sequences. Instead we will turn to Markov chain models. Markov chains describe the state path under the assumption that only the present state determines the probability of the next state, but the definition of 'state' can be extended. The 'order' of a Markov chain is the number of consecutive phases that define the current state controlling the next transition, and thus higher order Markov chains can account for a greater degree of memory. We show how first- and second-order Markov chains can be used to calculate likelihoods for the next step of the eruption, conditional on the elapsed duration of the current phase, and the duration of the one preceding it. In a further elaboration, these can be used as building blocks to estimate the probability of the current eruption producing various hazardous phenomena.

Frances Beckett, Arve Kylling, Sibylle von Lowis, Claire Witham

Submission 196

Modelling and Observing Ash Plumes from Remobilisation Events

Ash plumes can be generated for years after an eruption as tephra deposits are resuspended into the atmosphere. The resulting ash clouds can pose a hazard to local populations, ground transportation and airports. The atmospheric dispersion model NAME includes a resuspension scheme and is used to provide daily forecasts to the Icelandic Met Office to warn of possible significant remobilisation events. NAME is also used by the London VAAC to forecast the transport and dispersion of volcanic ash clouds from explosive eruptions; ash clouds generated from resuspension events can provide a useful analogue for validating and developing VAAC modelling and observing capabilities. In this study we use satellite based measurements in combination with radiative transfer and dispersion modelling to quantify mass loadings of volcanic ash remobilised from tephra deposits in southern Iceland during September 2013. The resulting ash cloud was transported to the south-east over the North Atlantic Ocean and, due to clear skies at the time, was exceptionally well observed in satellite imagery. The timing and location of the ash cloud identified from measurements made by VIIRS on-board the SUOMI satellite agree well with model predictions using NAME. Total column mass loadings are determined from the VIIRS data using an optimal estimation technique which accounts for the low altitude of the resuspended ash cloud and are used to calibrate the emission rate of ash in the resuspension scheme in NAME. We estimate that ~ 0.2 Tg of ash was remobilised during this event. The newly calibrated scheme will be used to provide more accurate quantitative forecasts of future remobilisation events.

Kenneth Befus, Miguel Cisneros

Submission 253

Bringing Raman thermobarometry to the people

Raman spectroscopy of solid inclusions is becoming a reliable tool for constraining the pressure-temperature (PT) conditions of host mineral growth. The shape and position of Raman spectra are a consequence of the crystal lattice environment. Changes in temperature or pressure cause frequency shifts to the unique spectral fingerprint of any mineral. Crystal inclusions have special utility because host crystals act as containment vessels that preserve residual pressures in the inclusions. The residual pressure is directly related to entrapment PT conditions and is a function of the compressibility and expansivity of both phases, and the shear modulus of the host phase (Guiraud and Powell 2006; Kohn 2014). We developed a script that rapidly performs quantitative entrapment pressure calculations for any inclusion-host pair in the Holland and Powell (2011) thermodynamic database by implementing the Tait Equation of State, Guiraud and Powell (2006) elastic model, and linear mixing of molar volumes and shear moduli for solid-solution compositions. This script rapidly weaponizes unversed petrologists, and can be used to make predictions about inclusion-host pairs that will be sensitive to temperature and/or pressure. Most importantly, it expands the application of Raman thermobarometry to new magmatic, metamorphic, and mantle environments. Elastic modeling is only informative if the pressure-dependent Raman frequency shift for the inclusion phase is known a priori. To that end, we used a diamond anvil cell to incrementally measure Raman spectra for feldspars, pyroxene, and titanite at pressures up to 3.5 GPa. Our new data supplements past studies that have constrained pressure dependent Raman shifts of quartz, magnetite, forsterite, Al₂SiO₅ polymorphs, and diamond. Raman thermobarometry is now readily applicable to low- to high-grade metamorphic rocks, lithospheric and asthenospheric mantle environments, and mafic to felsic magmatic rocks. Future studies must analyze inclusions in crystal hosts from diverse environments, and compare Raman PT estimates with well-known entrapment conditions. Such comparisons will allow Raman thermobarometry to quantify PT conditions of the unconstrained geologic underworld.

Boris Behncke, Emanuela De Beni, Daniele Andronico, Antonella Bertagnini, Marina Bisson, Mattia De' Michieli Vitturi, Paola Del Carlo, Alessio Di Roberto, Tomaso Esposti Ongaro, Augusto Neri, Massimo Pompilio

Submission 1177

A geo-database of “pyroclastic avalanches” at Mount Etna, 1999-2017

Computer simulations of hazardous volcanic phenomena (e.g., lava flows, pyroclastic density currents) can significantly aid in Civil Defense action during eruptions in populated areas. Such simulations can benefit from input of data from existing databases of such phenomena. At Mount Etna (Italy), a broad variety of “pyroclastic avalanches” has been observed in recent years, representing a previously unknown hazard to areas close to its summit and on its upper flanks. We present a preliminary database of the best documented events recorded in 1999-2017, including the geometry (length, volume, direction, etc.) of the deposits and their physical and temporal features, by using thermal/visible imagery from the monitoring network, direct observation and photographic documentation, and when possible, analysis and field mapping of deposits.

Almost all “pyroclastic avalanches” included in the database occurred during the frequent paroxysmal eruptive episodes (more than 150 from 1998 to 2017) at Etna, which led to the rapid growth of the Southeast Crater (SEC) and, since 2011, of the New Southeast Crater (NSEC). The latter grew above the east flank of the SEC cone facing toward the Valle del Bove (VdB), a wide (5 x 6 km) valley on the eastern side of the volcano. Such paroxysmal episodes are characterized by strong Strombolian to lava fountaining activity accompanied by lava flow emission, constantly changing the morphology of the SEC-NSEC apparatus, today reaching a height of ~200 m with an elliptical-shaped base of ~1000x850 m.

Both craters have generated abrupt and rapid flowing of volcanoclastic material along the flanks of cones, mostly characterized by >30° slopes. These phenomena affected distances variable from a few to several hundreds of meters. The most hazardous event occurred on 11 February 2014, when a debris-avalanche traveled up to 2.3 km distance. Continuous overlapping of tephra and lava layers, together with the opening of ephemeral lateral vents on the SEC-NSEC cones, are causes of their potential high instability. The emplacement of the cones on the steep and unstable western VdB wall, where most of the lava flows descend, further enhance the weakness of their slopes.

Understanding the triggers of the events, the estimation of the main parameters of the deposits and the definition of their transport dynamic are crucial to correctly assess the hazard from volcanoclastic flows in the summit area of one of the most visited volcanoes of the world.

Sonja Behnke, Ronald Thomas, Harald Edens, Alexa Van Eaton, Stephen McNutt, Cassandra Smith, Corrado Cimarelli

Submission 880

Volcanic Lightning Observations and Applications: Recent Progress and Future Directions

The past decade has seen an increasing interest in the investigation of volcanic lightning. Recent studies include optical and radio frequency measurements of volcanic lightning, experimental studies of electrical charging of ash, and even experimental generation of volcanic lightning in the laboratory. The recent observational studies have revealed that volcanic lightning is a common phenomenon that occurs during explosive volcanic eruptions over a wide range of eruption size. Measurements of very high frequency (VHF) electromagnetic radiation from volcanic lightning have shown that volcanic plumes can be electrically active starting from the moment of injection and lasting beyond the transition to buoyant convection. Different types of volcanic lightning have been identified (e.g., near-vent lightning and plume lightning) and are categorized by their physical extent and when and where they occur within a plume. VHF measurements also show that the quantity of electrical activity occurring in a plume scales with plume height. As an integral part of an explosive eruption, volcanic lightning observations are both a metric that can help characterize eruptions and a tool for detection. We present a review of recent progress in volcanic lightning research and examine future research directions.

Caroline Bélanger, Pierre-Simon Ross

Submission 201

Origin of non-bedded pyroclastic rocks in the Cathedral Cliff diatreme, Navajo volcanic field, New Mexico

Most of the previous studies on maar-diatreme volcanoes describe the crater and the pyroclastic ring. However, these deposits provide only partial information about the processes that occur within the diatreme, since not all explosions eject material into the atmosphere. Studying well-exposed diatremes directly remains one of the best ways to better understand how they work. The Cathedral Cliff diatreme, in the Navajo volcanic field (Navajo Nation, New Mexico), provides an opportunity to examine the transition between the bedded and the non-bedded pyroclastic rocks in diatremes, as well as their relationships and emplacement processes. A detailed geologic map of Cathedral Cliff has been prepared with surveying tools. Each pyroclastic facies was described using field and microscopic observations combined with line counts and petrographic point counts, to quantify the proportion between the types of fragments, and the percentage of tuff matrix.

Pyroclastic rocks from Cathedral Cliff range from bedded to non-bedded (occupying 49% and 45% of the mapped area, respectively, with sedimentary megablocks occupying the balance) and from lithic-rich to juvenile-rich. Two types of bedded rocks are recognized. (1) Continuous beds comprise hundreds of layers ranging from a few millimeters to several decimeters in thickness and dipping 71° to 90° toward the diatreme centre. They locally display low-angle cross-bedding, dunes and bomb sags, suggesting deposition by surges and fall at the bottom of the crater, followed by subsidence. (2) In the disrupted beds, which occur in the SW portion of the diatreme, bedding is rarely continuous, and sometimes entirely destroyed.

Non-bedded pyroclastic rocks range from coarse tuff to tuff breccia (mostly lapilli tuff) and are mostly rich in juvenile fragments. They are poorly sorted and massive. The lapilli are mainly juvenile and their average size varies from 2 to 8 mm. Sub-vertical contacts within the non-bedded rocks and sub-vertical columns of non-bedded rocks cross-cutting the bedded rocks are interpreted as produced by the passage of debris jets through the diatreme. Isolated domains of bedded pyroclastic rocks found in non-bedded pyroclastic rocks, and the presence of partly to entirely destroyed bedding in the disrupted beds, suggest destruction, recycling, and mixing of the bedded pyroclastic rocks during phreatomagmatic eruptions, to produce some of the non-bedded pyroclastic rocks.

J. Belart, Gro Pedersen, F. Kizel, E. Magnusson, O. Vilmundardóttir, N. Falco, F. Sigurmundsson, G. Gísladóttir, S. Tarquini, M. Vitturi, J. Benediktsson

Submission 400

The evolution of Hekla volcano in the 20th century: Integrating remote sensing data from the past 70 years

Hekla volcano is one of the most active volcanic systems in Iceland and has erupted ~23 times since the settlement of Iceland in AD 874. The historical Hekla eruptions have been studied from written records and field data, especially tephra chronology. These eruption records show that the total erupted volume correlate with the length of the preceding repose period revealing a very constant magma production, which over the last millennium have produced a total of at least 7 km³ (DRE) of eruptive material.

In the 20th century Hekla mountain erupted five times (1947-1948; 1970, 1980-1981, 1991, 2000), the eruptions were well documented and it has been estimated that ~80% of the total erupted volume was lava. However, the lava flow thicknesses used in the volume calculations are uncertain due to coarse sampling at selected lava thickness profiles or at flow fronts. Accurate lava volume estimates are therefore crucial in order to assess the volume of eruptive material in the 20th century.

In the Hekla area, repeated aerial stereo-photography surveys have been conducted since 1945 allowing creation of Digital Elevation Models (DEMs) and ortho-photographs using digital photogrammetric techniques. We selected seven photogrammetric surveys (1945, 1946, 1960, 1979, 1984, 1987, 1992) to construct historical DEMs (5m/pixel) and ortho-photos (0.5-1m/pixel). Together with modern radar-based DEMs (1998 and 2012-2013) and a lidar-based DEM (2015) these data sets provide pre- and post-eruption topography of Hekla for each of the five eruptions in the 20th century. These DEMs allow creation of thickness maps and thereby unprecedented estimation of lava flow

The DEMs are also used for mapping of lava flow morphology by contextual spatial analysis providing an opportunity to link lava morphology with flow thickness, volume and eruptive history. Finally, the pre-emplacment topography together with lava volume provide a unique possibility to calibrate the lava flow models to the last five Hekla eruptions as well as correlate lava flow morphology with lava flow modelling.

Andrew Bell, Stephen Hernandez, H. Elizabeth Gaunt, Patricia Mothes, Mario Ruiz, Santiago Aguaiza, Daniel Sierra

Submission 417

Drumbeat earthquakes and related quasi-periodic low frequency seismicity at Tungurahua volcano, Ecuador

Highly periodic 'drumbeat' long period (LP) earthquakes have been described from several andesitic and dacitic volcanoes, commonly accompanying ascent and effusion of viscous magma. However, the processes controlling the occurrence and characteristics of drumbeats, and LP earthquakes more generally, remain contested. In recent years, the andesitic Tungurahua volcano, Ecuador, has displayed a wide and interesting range of variably periodic LP signals that broaden the phenomenology of this type of seismicity, and provide new insights to some of the physical processes that underlie it. Here we report on the results of analysis of seismic, geodetic, infrasound, and gas monitoring data recorded by the networks of the Instituto Geofísico of Ecuador during episodes of quasi-periodic LP seismicity. We describe new methods to model the temporal characteristics of quasi-periodic earthquakes that allow quantitative comparison between different episodes and systems. These analyses reveal a variety of progressive and stepwise changes in periodicity, magnitude, event rates, source locations, and waveform types during different episodes. Episodes which may or may not be associated with significant eruptive activity or notable changes in other monitoring signals can last from a few minutes to several days. Continuous tremor often evolves to or from quasi-periodic discrete LP earthquakes, through either changing event rate or modification (changing impulsiveness) of event waveforms. We argue that the observations are best explained by an LP source mechanism at Tungurahua involving partly-coupled gas and magma ascent, and with characteristics that are controlled by factors including the rheology of the magma column and its margins, gas permeability, and the gas and magma ascent rates.

Karen Bemis

Submission 340

Why craters exist: an exploration of scoria cone construction

Small explosive eruptions, from bubble bursts to ash plumes, deliver significant scoria proximally to the vent and build a scoria cone through the accumulation and subsequent grain flow of scoria. A crater remains prominent around the vent throughout such eruptions. However, crater size, relative to volcano size, varies widely. Cone profiles vary from pointy cones with no crater to flat cones with broad craters. Cone plan views vary from ideal circles to indented circles (horseshoes) to ellipses. Such morphometric characterizations of scoria cones treat craters as intrinsic features created as a volcano was constructed. This study explores constructional controls on crater size and cone shape.

Numerical simulations of cone construction (based on ballistics and grain flow) tend to make pointy cones with no significant crater when naively using realistic distributions of ejection angles based on quantitative observations of Strombolian-style eruptions. In these models, crater development stems from the specification of the ejection angles such that limited material falls back into the crater; that is, creating a crater with a 2D model requires the specification of a two peak distribution of scoria ejection angles centered over the crater. Visibly, this creates a gap in ejection in the vertical direction. In extending the modeling to 3D, models would need to specify an annulus of ejection.

In contrast, observations both qualitative and quantitative of Strombolian-style eruptions show fairly narrow ranges of ejection angles with no particular gaps in the vertical or elsewhere. The mean ejection angle varies significantly and is not necessarily vertical. Such narrow uniform ejection angle distributions should produce pointy cones. Instead, cones may represent the sum of many variably directed eruptions, consistent with the relative prevalence of non-ideal shaped cones over ideal (circular) shaped cones. On the other hand, the observations may represent the outer layer of a burst with an empty core. Recent studies of bubble bursts suggest they produce mainly outward rather than upward directed fragments. So, cones may represent the accumulation from an annular distribution. Finally, craters may form when the gas thrust regime blasts material that fell back into the crater out again. This study extends a 2D model to consider 3D effects such as 3D ejection distributions, wind, and gas thrusts in order to explore crater construction and cone shape.

Mary Benage, Benjamin Andrews

Submission 1068

Near-vent dynamics of volcanic jets: insights from analog experiments

Explosive volcanic eruptions eject turbulent jets of hot volcanic gas and particles into the atmosphere. The volcanic jet is initially negatively buoyant and decelerates with height above the vent. The jet can become buoyant through entrainment of ambient air, allowing it to rise tens of kilometers, or it may not entrain sufficient air before initial momentum is lost and the jet collapses, forming destructive pyroclastic density currents. Quantitative estimates of entrainment in volcanic jets and plumes are essential for understanding the dynamics of explosive eruptions. With this goal, we use scaled analog experiments to examine entrainment processes and dynamics of particle-laden jets with initial negative buoyancy. Through the experimental setup, we explore the transition from a momentum jet to a collapsing jet or a buoyant plume by varying initial gas velocity, particle flux, particle diameter, and gas temperature. The experiments are performed in a 1.22 x 1.22 x 2.44 m tank with a 4.76 cm diameter pipe that injects a multiphase current of air and alumina particles to form turbulent jets with Reynolds numbers exceeding 7×10^3 . The alumina particles are monodisperse distributions with peak sizes ranging from 10-60 μm diameter and vary from 1×10^{-5} to 1×10^{-3} particle volume fraction in the jet. A laser sheet illuminates the center of the jet and a high-speed camera records the experiments at 3000 frames/sec with pixel resolutions ranging from 0.33 to 1.2 mm/pixel. Using feature tracking velocity algorithms, we track the fluctuating turbulent velocity component, velocity field, and entrainment velocities illuminated within the 2D plane of the laser sheet. Preliminary results demonstrate that at similar gas and particle fluxes, only heated jets become buoyant. The jets that are within 1 °C of the ambient temperature collapse around 15 vent diameters (slightly above the end of the momentum driven jet height), whereas jets that are ~ 5 °C hotter than the ambient environment do not collapse or partially collapse. During partial collapse, falling particles are re-entrained into the jet as the jet rises above the momentum-driven jet height of ~ 10 -15 vent diameters. We continue to explore the entrainment coefficients through these varying conditions to examine how entrainment varies through space and time in the near-vent region of heated, particle-laden jets.

Sylvana Bendaña, Wendy Bohrson, Megan Graubard, Nicole Moore, Anita Grunder

Submission 350

Quantification of Mantle vs. Crustal Contributions to the Steens Flood Basalt Magmatic System

Flood basalts produce such large intrusive and extrusive volumes that crustal addition and modification must be significant. Changes in whole-rock major- and trace element and isotopic systematics provide clues to the relative contributions of crustal and mantle input, while mass and energy-constrained computational tools allow for quantitative examination of these contributions. The Steens Basalt is the oldest and most mafic member of the Columbia River Basalt, and records time-transgressive changes in composition of two geochemically distinct packages of flows. The lower Steens is MgO-rich (~4-12 wt.%) with low incompatible trace element concentrations (~7-21 ppm La) and isotope ratios ($^{87}\text{Sr}/^{86}\text{Sr}$ of 0.7033-0.7039). The upper Steens is MgO-poor (~3-7.5 wt.%) with high incompatible trace element concentrations (~12-35 ppm La) and isotope ratios ($^{87}\text{Sr}/^{86}\text{Sr}$ of 0.7035-0.7041). These changes suggest that recharge dominated during production of lower Steens lavas whereas upper Steens magmas experienced greater crustal interaction.

We explore the influence of recharge, assimilation, and fractional crystallization on the evolving major- and trace element and isotope geochemistry of stratigraphically constrained flows of Steens Basalt using the Energy-Constrained-Recharge, Assimilation, Fractional Crystallization (EC-RAFC) and Magma Chamber Simulator (MCS) models. Successful EC-RAFC models that recreate the [Sr] and Sr-isotope changes up section require (1) sub-equal masses for recharge and crustal assimilation in lower and upper Steens and (2) a critical role for crustal assimilation in lower Steens magmas. In contrast, successful MCS models that recreate select packages of major element changes up section suggest (1) recharge is dominant and slight crustal assimilation is required in the lower Steens, whereas assimilation dominates the chemical signature in upper Steens and (2) a significant decrease in recharge from lower to upper Steens. Both models predict large cumulate abundances, and thus significant additions to crust through cumulate formation. These quantitative results reflect model assumptions, illuminate how trace element/isotope vs. major element/phase equilibria models can yield different interpretations of RAFC, and emphasize the difficulty of assessing mantle and crustal contributions. Ongoing modeling informed by these results will better delimit crust vs. mantle mass contributions by integrating constraints from elemental and isotopic data.

Maria A. Benito-Saz, Michelle M. Parks, Freysteinn Sigmundsson, Andrew Hooper, Laura García-Cañada, María Charco, Carmen López

Submission 1026

El Hierro Island: an example of volcano island growth by deep magmatic intrusions

El Hierro Island is the smallest and youngest of the seven main volcanic intraplate islands that form the Canary archipelago. The island rises 1500 m above sea level, built up by repeated eruptions and intrusions, and shaped by at least three giant rockslides that have produced abrupt topography. Between July 2011 and March 2014 (after more than 200 years of quiescence) El Hierro experienced a period of volcanic unrest that lasted 3 months, a submarine eruption lasting >4 months, and six post-eruptive magmatic intrusions of between 3 and 20 days. Bathymetry surveys revealed that during the October 2011 submarine eruption, a total volume of erupted material of 0.33 km³ accumulated ~2 km off the southern coast.

We have observed, quantified, and modeled the ground surface deformation produced by the June 2012 – March 2014 post-eruptive volcanic activity. The island has grown vertically by up to 27 cm as revealed by observations from a network of ten continuous GPS stations and InSAR analysis of RADARSAT-2 and COSMO-SkyMed images. Geodetic modelling of the magmatic post-eruptive intrusive events suggest sill-like bodies trapped at a depth of ~14-16 km are responsible for the observed deformation and seismicity. The total intruded volume associated with these intrusions is 0.32-0.38 km³.

The ascent, emplacement, and movement of these magmatic intrusions has been affected by the internal structure of the island. Despite being more energetic and producing larger amounts of surface deformation than the pre-eruptive intrusion, these post-eruptive events did not culminate in an eruption. We propose that a discontinuous layer, probably the mantle-lower crust discontinuity, has been impeding the ascent of magma to the surface.

The recent activity at El Hierro provides important insight into the growth of a volcanic intraplate island through repeated magmatic intrusions installed at depth, where the subsurface structure of the island is influencing the volcanic activity. Continued integrated volcano monitoring and near-real time modeling of any changes in activity (such as renewed melt supply to these post-eruptive intrusions) is essential for forecasting the likelihood of a new eruption and to assess the growth of the island and the corresponding hazard of flank instability and collapse.

Ninfa Bennington, Paul Bedrosian, Matthew Haney, Kerry Key

Submission 1142

Magnetotelluric and Seismic Investigations of Magma Storage Beneath Okmok Volcano, Alaska

Alaska accounts for nearly 99% of the seismic moment release within the US. Much of this is associated with the Aleutian volcanic arc, the most tectonically active region in North America, and an ideal location for studying arc magmatism. Okmok volcano, characterized by a pair of overlapping 10 km diameter calderas, is one of the most active volcanoes in the Aleutian arc with the most recent major eruption occurring in 2008. Okmok is believed representative of volcanoes both within the Aleutian arc and worldwide, where extended periods of effusive eruptions are punctuated by much larger explosive caldera forming eruptions. The subdued topography of Okmok, relative to other Aleutian volcanoes, improves access and permits dense geophysical sampling of the volcanic edifice.

During the summer of 2015 we acquired an array of onshore and offshore magnetotelluric data and installed a temporary year-long seismic deployment. Analysis of these data include a suite of seismic and magnetotelluric modeling efforts (ambient noise and earthquake tomography, surface wave anisotropy, 3D onshore and 2D amphibious magnetotelluric inversions, joint ambient noise/body-wave and integrated seismic/magnetotelluric tomography). In this presentation, we present preliminary models of the 3D resistivity and seismic structure of the volcano from analysis of the onshore data. These data will be used to test hypotheses regarding the crustal magmatic plumbing and storage system beneath Okmok caldera.

Thomas Benson

Submission 509

Large lithium deposits hosted in intracontinental rhyolitic calderas

Global consumption of lithium (Li) is expected to meet or exceed current reserve levels by 2050 due to the increasing demand for Li-ion batteries used in mobile electronics and the growing fleet of hybrid and electric vehicles. Securing additional Li reserves is therefore essential for meeting future demand, especially for countries other than Australia and Chile, who together produce ~80% of current global Li. To elucidate the magmatic and volcanic processes involved in concentrating Li to economically extractable levels, we determined Li concentrations of rhyolitic magmas formed in a variety of tectonic settings by analyzing homogenized quartz-hosted melt inclusions in situ using secondary ionization mass spectrometry. Rhyolite magmas that contain a large proportion of felsic continental crustal material have high Li concentrations (>1,000 ppm) similar to rare-metal granites and an order of magnitude greater than magmas formed in thinned continental crust. Although the largest Li deposits worldwide occur in brines within basins adjacent to peraluminous rhyolites extremely enriched in Li (>2,000 ppm), our new data demonstrate that large Li deposits can form associated with calderas that collapse on eruption of relatively more common, voluminous, intracontinental rhyolites only moderately enriched in Li. Lithium leached from the eruptive products by meteoric and hydrothermal fluids becomes concentrated in clays (e.g., hectorite) within caldera lake sediments. The largest Li resource in the United States (~2 Mt Li) within the Mid-Miocene McDermitt Caldera, Nevada follows this model, with the resource being hosted in lacustrine sediments spatially coincident with caldera ring fractures. Cenozoic calderas with preserved lake sediments throughout western North America and ones newly identified ~15 km northwest of the McDermitt Caldera are therefore promising new exploration targets that can potentially help meet the rising demand for strategic Li resources.

Philip Benson, Marco Fazio

Submission 297

Generation mechanisms of fluid-driven seismic signals related to volcano-tectonics: a laboratory approach

A wide range of signals are generated from the volcano plumbing system, ranging from volcano-tectonic earthquakes driven by pure fracture, long period harmonic tremor at shallow and deeper levels driven by rock fluid interaction and resonance, longer lasting tremor activity, drumbeat activity in lava domes. Although there are a wide range of models that point to the resonance of the rock-fluid being the primary cause of the signals, the precise generation mechanics of volcano seismic signals, how they vary with subsurface conditions or fluid pressure (for instance), and their evolution with time, remains poorly understood.

In an attempt to image the source process, we have conducted a wide ranging laboratory study aiming to better constrain the time evolution of such signals across temperature conditions 25 to 175°C in order to simulate multiphase fluids. Simulations used pressures equivalent to volcanic edifices up to 1.6 km in depth using a triaxial deformation apparatus equipped with an array of acoustic emission sensors. We investigate the origin of fluid-driven seismic signals by rapidly venting the pore pressure through a characterized damage zone. During the release of water at 25°C broadband signals were generated, with frequencies ranging from 50 to 160 kHz. However, the decompression of a water/steam fluid at 175°C generated signals with a bimodal spectrum, in the range 100–160 kHz. This is consistent with natural signals from active volcanoes, such as Mount Etna, and highlight the role of fluid and gas phases (such as bubbly liquids) in generating different types of volcano-tectonic seismicity. Finally, when using dry gas (Nitrogen) we recover waveforms strikingly similar to the classic Tornillio signals.

By superimposing the known pore pressure evolution over the seismic signal envelope, we additionally find a strong correlation, providing further evidence that the fluid initiates the signal source. Finally, a simple application of the Kumagai & Chouet (2001) model suggests that a higher quality factor (Q) accompanies 'bubbly' liquid and gasses: this trend is seen across the frequency spectrum.

Olga Bergal-Kuvikas, Caroline Bouvet de la Maisonneuve

Submission 438

Geodynamic setting of volcanoes in Southeast Asia: Comparing slab and crust parameters with magmatic productivities

The location, size, and composition of volcanoes reflect inner processes of the Earth and can thus be used to explore the effect of large scale tectonics on eruptive dynamics. We have compiled an extensive database of Quaternary volcanoes (total of 159) and volcanic eruptions (total of ~1500) for Indonesia and the Philippines. Our database includes general information about each volcano, such as its geographical position (latitude, longitude), elevation, type (e.g. stratovolcano, caldera, cinder cone, intrusive dome), volume (assuming a cone shape) and a short geological summary. To identify the age of a volcanic edifice, we used geological maps and the geological summary of each volcano. The database also includes the geodynamic setting and parameters of the subduction zone: the depth of the mantle column for each volcano, the distance to the trench, the age of the incoming plate, locations of fracture zones and sea mounts on the slab, the thickness and age of the crust, and the stress regime (i.e. extensional, compressional or transform setting). For the eruptions, we report the age, magnitude (Volcanic Explosivity Index - VEI), volume and some meteorological observations of ash dispersion when available. Because Southeast Asia is a densely populated region, records of historical observations (2 ka BP to present) are available for almost all volcanoes. Meteorological observations of the strongest eruptions were used to describe the elevation of ash clouds, the ash transport directions, and the possible areas of ash fall. Preliminary analysis of our database reveals that across arc variations show a tendency toward a larger number of volcanoes in the frontal part of the arc but larger edifice volumes in the rear part of the arc. Along arc variations, on the other hand, show possible correlations between geodynamic setting and the source of voluminous (VEI > 6) eruptions. With the goal to understand interactions between geophysical parameters, magma generation, and the type (frequency and magnitude) of volcanic activity, we are adding all published geochemical and isotopic data for these Indonesian and Filipino volcanoes to the database. This should enable a greater understanding of volcanic hazards on the scale of an arc, and provide some constraints on the spatial distribution of geochemical fingerprints that can be useful for tephrostratigraphic reconstructions.

George Bergantz, Jillian Schleicher, Alain Burgisser

Submission 383

Unpacking the Crystal Cargo: Getting to the Bottom of Magma Dynamics

One significant legacy of Prof. Jon's Davidson's prolific career was the recognition that a tremendous amount can be learned from detailed studies of the crystal record. Whether sitting around a smoky campfire in Yosemite, in his office at UCLA or Durham, or in a pub, he was always encouraging about progress to unify chemical and physical descriptions of magmatic processes. This work is dedicated to that inspiration.

In partially molten rocks, often called a mush, the dynamics are controlled by both fluid and crystal-crystal interactions. An obstacle to progress in understanding high-temperature crystal-rich systems has been the lack of adequate levels of description of microphysical (crystal scale) processes. The problem is that most attempts to describe the physics of crystal-rich magmas rely on averaged volume fractions (or porosity) as the dominant state variable, sometimes the only state variable. This is inadequate, as it contains no information about the granular (crystal) modes of dissipation, and the character of the force chain fabric. To describe the microscale kinematics of a crystal-rich system we introduce the coordination number and the fabric tensors of particle contacts and forces. We will show how to quantify the changing contact and force fabric anisotropy, coaxiality, and the connectedness of the crystals within the mush, under dynamic conditions. To describe the dynamics, particle and fluid characteristic response times are derived. These are used to define local and bulk Stokes numbers, and viscous and inertia numbers which quantify the multiphase coupling under crystal-rich conditions. We employ the Sommerfeld number, which describes the importance of crystal-melt lubrication, with a viscous number to illustrate the dynamic regimes of crystal-rich magmas. Collectively, this framing unifies the dilute and crystal-rich description of magma dynamics into a common framework that can be extended to particle-rich explosive eruptions.

For example we show that the notion of mechanical "lock up" is not uniquely identified with a particular crystal volume fraction and that distinct mechanical behaviors can emerge simultaneously within a crystal-rich system. We also posit that this framework describes magmatic fabrics and processes which "unlock" a crystal mush prior to eruption or mixing.

Deborah Bergfeld, Kurt Spicer, William Evans

Submission 198

Evidence for intrusion of undegassed magma during the 2004-08 eruption of Mount St. Helens, USA; subtle signals from the hydrothermal system.

Low gas-emission rates during the 2004–08 dome-building eruption of Mount St. Helens imply a volatile-depleted magma, possibly remnant from the 1980s eruption. We performed annual geochemical monitoring between 2002 and 2015, including chemical analyses of gas and water from Loowit hot springs and discharge measurements on Loowit Creek downstream of the springs. The geochemical data indicate the presence of volatiles from 2 different batches of magma, the shallow degassed magma that erupted, and a deeper magma in its initial stages of degassing.

Changes in hot spring chemistry have been subtle and only became apparent toward the end of the eruption, in part due to groundwater residence times. Some of the changes, such as spikes in hot spring Cl and SO₄ concentrations were rapid and short-lived. Other changes evolved over many years, including a large spike in spring-water temperatures that remained elevated for 5 years before declining after August 2012, and isotopic shifts in hot spring δD and $\delta^{18}O$ that began in 2005 and ended after July 2010. All of these changes can be related to release of residual heat and volatiles associated with the 2004-08 eruption, and don't require injection of a new batch of magma.

Carbon isotope data, on the other hand, indicate that CO₂ from a deeper magma, unfractionated by previous degassing, began to enter the hydrothermal system by 2006. Dissolved inorganic carbon (DIC) in the hot springs and CO₂ gas both show a gradual increase of ~1.5‰ in $\delta^{13}C$ values between 2005 and 2009, with the maximum $\delta^{13}C$ - DIC values approaching the $\delta^{13}C$ -CO₂ values of 1980s dome gas. In addition, ³He/⁴He ratios of 10 hot spring gases and two fumaroles collected after the start of the 2004–08 eruption are as high as 6.5 RA compared to a range between 4.2 and 5.7 RA for five samples from 1986-2002. Nine of the recent samples (2005-2016) are greater than pre-eruptive ³He/⁴He ratios and support the undegassed magma hypothesis.

Kim Berlo, Vincent van Hinsberg, Pak Suparjan, Bambang Heri Purwanto, Hendra Gunawan, Sri Budhi Utami, Bassam Ghaleb

Submission 938

Gypsum at Kawah Ijen: a record of degassing in a crater lake

The crater lake of Kawah Ijen volcano rises 2100 m above the city of Banyuwangi and the agricultural heartland of the Asembagus plain in East-Java, Indonesia. It occupies the summit crater of Kawah Ijen and is the largest naturally-occurring hyperacid lake in the world. Lake waters are concentrated brines (6.5 wt% SO₄, 2.2 wt% Cl, 0.6 wt% Al, pH ~ 0) that obtain their composition from volcanic gases and water-rock interaction. During the most recent eruption in 1817, the lake was expelled, leading to devastating acidic lahars to both Banyuwangi and the Asembagus plain. Even in times of quiescence, the lake waters seep through the western flank of the volcano to form the hyperacid Banyu Pahit river, which is used for irrigation downstream. Where these waters emerge, gypsum precipitates as stalactites and plateaux.

The river water composition varies and can be used to monitor the magmatic activity, but the interpretation of these compositional variations requires knowledge of the background variability and inputs. Regular sampling of the river is now taking place. River water is being monitored for its SO₄/Cl ratio at the Ijen observatory using BaSO₄ turbidity and AgCl gravimetry to monitor the relative contribution of magmatic-hydrothermal waters to the river. A seasonal variation is observed in the signal with a volcanic control superimposed. Samples are subsequently sent to Canada for analysis of major and trace elements by ICP-MS.

The most recent eruption occurred 200 years ago and there are no water compositions from that time or other times of volcanic crisis with which to compare the current river water samples. Here we use the chemistry of gypsum deposits forming the plateaux as a proxy for the composition of the water from which these precipitated, and hence as a record of the magmatic degassing of the system. The gypsum is stratified and preserves a record dating back > 90 years. ²¹⁰Pb dating was used to determine the ages of individual growth zones, which were analysed for major and trace elements by LA-ICP-MS. Results indicate that there are significant variations in the metal ratios that can potentially be linked to periods of increased magmatic activity. The gypsum record can therefore provide both a measure of the background variability during quiescence and identify the compositional indicators of increased activity. This approach can potentially be extended to other volcanic crater lakes and acid rivers where gypsum precipitates.

Benjamin Bernard, Krupskaja Acuña, Diego F. Narvaez, Alicia Guevara, Marjorie Encalada, Santiago Santamaría, Jean Battaglia, Daniel Sierra, Stephen Hernandez

Submission 1038

Cracking the ash code at Tungurahua volcano

The compositional and textural diversity of volcanic ashes can be puzzling when trying to interpret old deposits in terms of eruptive dynamics. Contemporary eruptions help greatly to assess the origin of volcanic ash, particularly when geophysical data, direct observations and near real-time ash sampling are available. Three ash types are commonly reported at Tungurahua outside paroxysms: light toned, dark toned, and reddish. An important issue is that Tungurahua ash types have significantly contrasting impacts on farming and human health according to the local populations. Here, we investigate their characteristics through granulometry, mineralogy, chemistry, and componentry analysis. We selected the samples that best represent each endmember and compared them to the eruptive dynamics described using the monitoring network data. A first important observation is that there are no significant mineralogical or chemical differences between the three ash types, suggesting a common and homogeneous magmatic source. Nonetheless, the light toned ash presents the highest amount of amorphous phase, most probably volcanic glass, potentially associated to a higher magma ascent rate. Light toned ash is generally the finest-grained while reddish ash is typically the coarsest, being the dark toned ash an intermediate term. These grain size differences might arise from contrasting efficiency of the fragmentation processes and different discharge rates. The juvenile material, both dense and vesiculated, is dominated by honey-colored glassy particles in the light toned ash, while the others have principally black glassy particles. The accidental material is dominated by oxidized particles in the reddish ash while the other types have low amount of grey lithics and oxidized particles. When comparing these results with the monitoring data and direct observations, we found that light toned ash is generally associated to intense seismic tremor during long-lasting ash venting episodes, while dark toned ash is commonly observed during Vulcanian phases and reddish ash is typically associated to violent Strombolian activity. In conclusions, tracking the amount and nature of juvenile and accidental material as well as characterizing the grain-size distribution of ash fallouts at Tungurahua are useful tools to obtain insights on its eruptive dynamics.

Alain Bernard, Edgardo Villacorte, Katharine Maussen, Raymond Maximo, Corentin Caudron, Ma. Antonia Bornas

Submission 748

Carbon dioxide in Taal volcanic lake: a simple gasometer open to the atmosphere.

Taal Volcano island hosts an active crater which contains a lake (volume of 42 million m³) of warm (~32°C) and acidic waters (pH: 3.1). The crater lake (MCL) is fed by hydrothermal waters from a subsurface magma-hydrothermal system. It integrates most of the flux of heat and volatiles released by the volcano.

Since January 2013, a miniaturized NDIR CO₂ gas analyser is used for continuous monitoring of the pCO_{2aq} in the lake and show that the surface waters are highly supersaturated in CO₂ with respect to the atmosphere (with dissolved concentrations up to 430mg/l).

Large temporal variations observed in dissolved concentrations suggest that pCO_{2aq} is a very sensitive indicator of activity at Taal volcano compared to other lake's parameters that remained almost constant during the same period (i.e. temperature, pH, chemistry).

Contrary to sulfates, chlorides and other solutes which are largely conservative species in MCL waters; dissolved free CO_{2aq} has a more dynamic behaviour in the lake (much like temperature). Taal MCL lake acts as a simple gasometer where pCO_{2aq} reflects a steady-state equilibrium between CO₂ supplied to the lake by hot springs and by direct degassing and CO₂ lost by diffusion at the air-water interface.

Spot measurements carried over the entire lake surface show that pCO_{2aq} is very homogeneous, except for a positive anomaly in the northeast sector of the lake where upwelling of hydrothermal water occurs.

Taal volcano has experienced several episodes of increased seismic activity (swarms), notably in 1992-1994, 2000-2004 and 2010-2011. A minor swarm of Volcano Tectonic (VT) earthquakes occurred again in 2015 associated with ground deformation recorded by the GPS network (see M. Sayco et al. abstract). During this event, pCO_{2aq} rose above 0.25 atm, the highest recorded value since the start of continuous monitoring.

Since 2011, CO₂ flux measurements using a floating accumulation chamber were also carried out in order to study the diffusion of CO₂ at the air-water interface. The CO₂ fluxes obtained from 12 individual field campaigns ranged from 400 to 2,900 T.day⁻¹ and revealed that pCO_{2aq} and CO₂ flux are strongly positively correlated (R²: 0.94). This suggests that most of the CO₂ is transferred to the surface (lake) in a dissolved state to finally diffuse to the atmosphere and confirm the significant role of the hydrothermal system as an efficient trap for any volatile species.

Marc Bernstein, Eliza Calder

Submission 356

Empirical Method for Determining the Solar Heating Correction for Handheld Thermal Imagery: An Example from Soufrière Hills, Montserrat

Brightness temperatures of volcanic features and edifices obtained with handheld thermal imaging cameras are usually corrected for atmospheric transmissivity (distance between target and detector, mid-path air temperature and relative humidity), and thermal emissivity. These corrections yield the radiation and kinetic temperatures respectively. Corrections that are not typically done are for mixed pixels (pixel is small relative to the target), attenuation from ash and gases (imaging in clear air), viewing angle (normal to the surface of the target) and solar heating. Daytime solar heating is ideally dealt with by imaging at night, preferably before dawn, when it is not an issue. As this may not always be possible, it is helpful to have a method to obtain the temperature increment due to solar heating. This allows a comparison between thermal data obtained at different times of the day, and importantly, to evaluate the significance of temperature differences between thermal images, so as not to confuse solar heating for magmatic heating.

The empirical method described here, replicates the sun-volcanic edifice-camera location geometry on a smaller scale. At Soufrière Hills, an andesite boulder, of the same composition as the lava dome, was imaged at 10-minute intervals over several days (25 July to 1 August 2009) from a distance of 30 m in the same sun-camera-target orientation as existed between the sun-Montserrat Volcano Observatory-Soufrière Hills. The maximum temperature of the boulder was extracted from each image, and the results plotted for 24 hours. This allows the solar heating correction to be determined for any time of the day.

The average and maximum diurnal amplitudes were 22.6 °C and 26 °C respectively. The maximum diurnal amplitude is achieved on cloudless days. Minimum temperatures are between 04:00 and 06:00 local time, and the maximum temperatures are between 12:00 and 14:00 local time (sunrise and sunset were 5:48 and 18:42 respectively). This particular set of curves was derived for andesite at the latitude of Montserrat at a time of year when the sun is nearly directly overhead at local noon. The correction curve is broadly applicable to other volcanoes of similar composition, and with similar daily solar orientations and illuminations. For volcanoes of different compositions, at different latitudes, at different times of the year or with a different viewing direction, a new solar heating correction curve would need to be obtained.

Manuel Berrocoso Dominguez, Alberto Fernandez-Ros, Gonçalo Prates, Belen Rosado Moscoso, Amos De Gil Martinez, Luis Miguel Peci Sanchez, Raul Paez Jimenez

Submission 735

The 1990-2017 Deception volcano's geodynamic mechanism from GNSS data (Antarctic Peninsula)

The GNSS observations in Deception Island have started along the 1988 austral summer. The REGID network established in 1990 initially constituted by 4 geodetic benchmarks allow the determination of the first ground-deformation models of the geodynamic behavior both volcanic and tectonic of the Island. During the period 1990-2017 the network has experienced a large transformation considering the number of benchmarks, semi-permanent stations, data link by WIFI, and multi-constellation registry (GPS, GLONASS and GALILEO). Today the REGID network has 16 geodetic benchmarks around Port Foster and an additional semi-permanent reference station in Livingston Island. During the austral summer, 3 benchmarks in Deception are also semi-permanent stations.

Ground-displacement time series analysis depict the combined influence of the South Shetland Islands central block tectonic regime, thus from the extension present in the Bransfield basin rift and from the slow subduction of the former Phoenix micro-plate under the Antarctic plate. The 1998-1999 austral summer volcano reactivation was the most significant of this period. The ground-deformation and ground-displacement velocities are compatible with an accentuated process of extension and uplift. From 2001-2002 benchmarks are added to the REGID while 3 become semi-permanent stations that constitute the volcanic surveillance system based on ground-deformation with near real-time data link and data processing and analysis. In 2016-2017 this system was active. Several extension-uplift, compression-subsidence and transition periods have been observed. The extension-uplift periods correlation with higher seismicity and the higher volcanic activity precursory signal of ground-deformation have been applied to establish volcanic processes forecasts.

Therefore, the ground-displacement velocities and related ground-deformation models, and the location and evolution of point source models are presented. From them the geodynamic mechanism and evolution of Deception's volcanism is discussed.

Håvard Svanes Bertelsen, Frank Guldstrand, Olivier Galland, Luc Girod, Rikke F. Johannessen, Fanny Bjugger, Steffi Burchardt, Karen Mair

Submission 525

Application of open-source photogrammetric software MicMac for geodetic monitoring in laboratory models

Quantifying deformation has become essential in modern laboratory models of geological systems. Although a number of methods exist to quantitatively monitor deformation in geological laboratory models, none of them combines the following advantages: low cost, high resolution, high precision, both topography change and horizontal displacements and ease of set up in the laboratory. Moreover, with the exception of expensive XCT scanners, none of these techniques have successfully integrated (1) surface deformation with (2) the underlying structures after the end of the experiments. This contribution presents a new laboratory monitoring method through the implementation of the open-source software MicMac, which efficiently implements photogrammetry in Structure-from-Motion (SfM) algorithms. To describe the use and possibilities of MicMac, we apply this program to monitor surface deformation in two characteristic laboratory geodesy scenarios: magma emplacement and strike slip faulting. MicMac automatically processes images from four synchronized cameras (standard DSLR) to compute time series of digital elevation models (DEMs) and orthorectified images of model surfaces. MicMac also implements Digital Image Correlation (DIC) to produce high-resolution displacements maps. The resolution of DEMs and displacement maps corresponds to the pixel size of the processed images. Using 24 MP cameras, the precision of DEMs and displacements is ~ 0.05 mm on a 40×40 cm surface. Calculating divergence maps from the displacement maps with Matlab[®] scripts allows automatic fracture mapping on the monitored deforming surfaces. MicMac also offers the possibility to integrate 3D models of excavated structures with the corresponding surface deformation data. The high resolution and high precision of MicMac results coupled with the ability to generate virtual 3D models of complex structures make it a very promising tool for quantitative monitoring of laboratory models of geological systems.

Håvard Svanes Bertelsen, Frank Guldstrand, Olivier Galland

Submission 486

Dyke tip processes and large-scale deformation: implications for geodetic modelling

There are numerous examples of geodetic measurements associated with the emplacement of dykes in active volcanic areas. Systematically, geodetic models used to model these geodetic measurements assume that (1) dykes are tensile fractures and (2) the host is purely elastic. However, recent field observations and laboratory results suggest that dykes can also propagate as viscous indenters; the dyke tip propagates by pushing ahead its host rock, which fails by both shearing and tensile opening. In both the tensile fracture and viscous indenter models, dyke tip processes are restricted to a very small area compared to the size of the dykes. On this basis, dyke tip processes are usually neglected in dyke emplacement models, justifying the purely elastic assumption of geodetic models and dyke emplacement models. In this contribution, we show that dyke tip processes should not be neglected to interpret geodetic measurements. We performed two series of laboratory models of dyke emplacement, during which we monitored surface deformation using high-resolution and high-precision photogrammetry setup. In the first series, a fluid was injected in elastic gelatine and produced a dyke that propagated as tensile fracture; the resulting surface deformation was comparable with the predictions of the elastic Okada model, i.e. an elongated topographic trough above the dyke apex, surrounded by two uplifted zones. Conversely in the second series, a fluid was injected in cohesive silica flour and produced a dyke that propagated as viscous indenter; the resulting surface deformation was only uplift.

The first-order differences between the two series of models show that local tip processes do control large-scale deformation induced by propagating dykes, and so surface deformation patterns. Our results question the systematic use of tensile elastic fracture geodetic models to interpret geodetic measurements associated with dyke emplacement. Finally, our results show that relevant interpretation of geodetic measurements requires a proper physical understanding of dyke propagation mechanisms.

Elisabeth Bertolett, Darren Gravley, Rachel Beane, Guil Gualda, David Prior, Elizabeth Teeter, Chad Deering

Submission 1292

Compaction and fractionation revealed in a suite of plutonic lithics: a structural, textural and compositional study of the Akaroa Volcanic Complex, New Zealand

Plutonic lithics in volcanic rocks offer unique insight into the magma bodies that feed eruptions. Such lithics are found in lava flows and volcanic flank domes in the Akaroa Volcanic Complex (AVC), Banks Peninsula, NZ. Goat Rock, a basaltic, flank dome, has the largest diversity of plutonic chemistries and textures in one location. A geochemical and quantitative textural approach is used to explore the magmatic processes responsible for this diversity and provide insight into the AVC magmatic system.

Plagioclase in gabbroic samples from Goat Rock Dome were analysed with Electron Backscatter Diffraction (EBSD), Energy Dispersive Spectrometry (EDS), and colour-cathodoluminescence (CL) methods. EBSD was used to quantify the type and strength of plagioclase orientations. Lithic plagioclase Crystallographic Preferred Orientations (CPOs) are characterized by a girdle about {100} and clusters at {010}, indicative of uniaxial compaction, and range in strength (J index range from 5.77 to 45.38). With decreasing fabric strength, there is an accompanying whole rock compositional progression from 45.4 to 54.9 SiO₂ wt%: the most primitive sample shows strong compaction and the most evolved shows less compaction. Colour-CL images reveal an interstitial, fine-crystalline material, not observed optically, that is interpreted as late stage melt crystallisation between the larger plagioclase crystals. The area of interstitial material increases from 2.6% in the most compacted example to 7% in the least compacted, suggesting a correlation with melt extraction. Further, preliminary EDS scans reveal more evolved compositions for the interstitial material relative to the whole rock composition (i.e. 45.4% SiO₂ and 4.7% Na₂O for whole rock and 61.6% SiO₂ and 9.0% Na₂O for interstitial material in the most compacted sample). Combined textural and compositional data provide a compelling framework that links erupted plutonic lithic material to fractionation processes coincident with compaction. This adds significantly to our understanding of the magmatic processes, evolution, and structure of the AVC magmatic system(s). Continued research on AVC plutonic lithics will employ these combined SEM techniques along with MELTS modelling to advance our understanding of the conditions at which magma was stored and deformed in an, otherwise, 'invisible' AVC magmatic system.

Andrea Bevilacqua, Marcus Bursik, Abani Patra, E. Bruce Pitman

Submission 634

Multi-model probability assessments in the Long-Valley volcanic region (CA)

The Long Valley volcanic region is an active volcanic area situated at the east base of the Sierra Nevada escarpment, and dominated by a 32-km wide resurgent caldera of ~760 ka. Eruptions during the last 180 ka have been localized at Mammoth Mountain on the western rim of the caldera, and along the Mono-Inyo Craters volcanic chain stretching about 45 km northward. The past eruption record is characterized by significant acceleration during the last 6 ka. In 1325 - 1350 AD there was a ~1 km³ eruption along a 25 km section of the Mono-Inyo Craters chain. The most recent eruption in ~1700 AD created Paoha Island in Mono Lake. The last eruption in the southern part of the system was ~10 ka (Red Cones), but continuous CO₂ degassing, potential precursory signals and recent geophysical studies suggest that the Mammoth Mountain area could be active again.

Multiple spatial probability models were developed, based on past vents locations. One of the models couples this information with pre-existing faults, sampling a fault outcrop site as a parameter of proximity to the vent location forecast. Similarly, different Poisson-type models have been developed for modeling the temporal sequence of eruptions and making estimates for the current volcanic intensity of the system (i.e. the expected rate of eruptions per year). The models implement various self-excitement features, assuming that the expected volcanic intensity is increased by past events and is instead decreased by prolonged periods of quiescence.

All the available models can be considered as different “experts”, and this has significant analogies with “Structured Expert Judgment” problems. “Bayesian Model Averaging” is presented as a flexible technique for combining the results of multiple models, relying on their performance in hindcasting the past record. The analysis is set-up in a doubly stochastic framework, enabling us to incorporate some of the main sources of epistemic uncertainty - these include the effects of the unknown relevance of Mammoth Mountain area, the incompleteness of the past record and mapped faults, and the uncertain age (and location) of past events. Our findings provide a rational basis for hazard mapping of the next eruption in the Long Valley volcanic region, suggesting that the hazard associated with Mammoth Mountain volcanism should be carefully re-evaluated.

Joseph Biasi, Claire Bucholz, Paul Asimow

Submission 548

Death of a Subduction Zone: Alkaline Volcanism on the Antarctic Peninsula

This presentation will provide an overview of alkaline volcanism on the Antarctic Peninsula (AP), including eruptive styles/products, geochemistry, geochronology, and modeling of mantle sources.

From the Permian – 4Ma, a long-lived subduction zone existed to the West of the AP. Subduction ceased when the Phoenix-Antarctic ridge collided with this subduction zone. During active subduction, eruptive products on the AP had calc-alkaline geochemistries. After ridge-trench collision, calc-alkaline volcanism disappeared entirely and new alkaline shield volcanoes appeared. The origin of these alkaline volcanics is highly uncertain. Rifting, subduction, hotspots, slab windows, and even LIPs have been invoked to explain the presence of alkaline volcanics on the AP and elsewhere in Western Antarctica. Here, we combine fieldwork, geochemistry, modern geophysical data, and thermodynamic mantle modeling (with MELTS) to test the proposed origin of these volcanics. Our data suggests that low-degree melting of a heterogeneous mantle can produce the range of observed alkaline geochemistries. These results are most consistent with a slab window model for the origin of these alkaline lavas. During active subduction, dehydration of the lower plate produces a metasomatized mantle wedge. After ridge-trench collision, depleted MORB mantle comes in contact with metasomatized sub-arc mantle via the slab window. Partial melting of depleted MORB mantle and localized melting of metasomatic veins results from this interaction, producing alkaline magmas that later reach the surface of the AP. These results can be applied to other ridge-trench collision settings, where more complex tectonic histories make such relations difficult to determine.

Sébastien Biass, Andrea Todde, Raffaello Cioni, Marco Pistolesi, Nobuo Geshi, Costanza Bonadonna

Submission 275

Potential impacts of tephra fallout from a Plinian eruption at Sakurajima volcano, Japan

We present an exposure analysis to tephra fallout for a future Plinian eruption scenario at Sakurajima volcano developed based on a new field characterization of the last Plinian eruption and a review of reports of the eruptions that occurred in the past 6 centuries. A scenario-based probabilistic hazard assessment is performed using the Tephra2 model, considering various eruption durations to reflect complex eruptive sequences of all considered reference eruptions. A quantitative exposure analysis of infrastructures and lifelines is presented primarily using open-access data. Observations drawn from a detailed impact assessment after the 2011 VEI 2 eruption of Shinmoedake (Magill et al. 2013), providing a unique illustration of the impacts from tephra fall in a similar socio-economic context, are used in parallel of the hazard and exposure analyses to identify and discuss potential vulnerable and resilient infrastructures for a future eruption of Sakurajima.

Results indicate a main eastward dispersal, with higher eruption duration increasing the hazard in proximal and reducing it in distal areas. The exposure analysis reveals that 2300 km of road network, 18 km² urban areas and 306 km² of agricultural lands have a 50% probability to be affected by an accumulation of tephra of 1 kg/m² and identifies the municipalities of Kagoshima, Kanoya and Tarumizu as the most likely impacted. Finally, the 2011 eruption of Shinmoedake demonstrated that a range of mitigation measures are implemented, increasing the resilience and improving the recovery of the affected infrastructures. Nevertheless, the extent to which these mitigations actions will perform during the VEI 4 eruption presented here is unclear, and our hazard assessment indicates very high hazard levels on the Sakurajima peninsula and the neighboring municipality of Tarumizu.

Sébastien Biass, Don Swanson, Bruce Houghton

Submission 276

A new perspective on the 19th century golden pumice deposit of Kīlauea

The golden pumice represents one of the latest episodes of fountaining in the Keanakākoʻi Tephra and is the product of the first Hawaiian fountaining eruption at Kīlauea summit in ca. 300 years. The deposit has been observed by many authors but has never been studied in detail from a volcanological perspective, so little is known of its dispersal or eruptive sequence. We present a new physical characterization of the deposit based on the field study of over 200 sites detailing stratigraphic and structural relationships. Due to the absence of any overlying deposit of significant thickness, the field mapping is complicated by severe surface erosion, alteration and silicic encrusting of the deposit.

Our sections lie in an area of 20 km², extending 6 km N-S, and reaching 4.5 km W of Kīlauea caldera. Basic componentry analyses reveal a dominance of pumice lapilli and bombs associated with achneliths, Pele's hair and, in proximal areas, rare dense outgassed clasts. The isopach map for the entire deposit, elongate both in a dominant SW dispersal direction associated with trade winds and in an atypical NNW direction, is difficult to resolve with only one fountain. Proximal sections reveal at least two episodes of fountaining from sources in the present caldera and intense syn-eruptive erosion, suggesting major rainfall events during deposition. Fountains must have been sufficiently high to deposit outgassed bombs with diameters up to 30 cm on the caldera rim. This new characterization of the golden pumice increases the knowledge of the Keanakākoʻi stratigraphy and contributes to a better understanding of the explosive history of Kīlauea prior to the renewal of dominantly fountaining and effusive activity in the early 19th century.

Juliet Biggs, Yelebe Birhanu, Atalay Yirgu, Kathy Cashman, Marie Edmonds, Karen Fontijn, Joachim Gottsmann, Tim Greenfield, Juliane Huebert, William Hutchison, Fiona Iddon, Derek Keir, Michael Kendall, Elias Lewi, Ryan Lloyd, Tamsin Mather, Keri McNamara,

Submission 143

Rift Volcanism: Integrating Geological And Geophysical Constraints On Restless Volcanic Systems.

Our current understanding of volcanic systems is largely derived from our knowledge and experience of activity in arc and intra-plate oceanic settings, but continental rift settings, pose a different suite of challenges. The RiftVolc project aims to understand what controls volcanism in continental rifts by addressing the following questions 1) how does rifting influence magma generation, storage, migration and eruption? 2. What drives the unrest at rift calderas? 3. What are the potential volcanic threats? We carried out a range of geological and geophysical studies at Aluto, Corbetti, Tullu Moye and Bora-Berecha in the Main Ethiopian Rift. However, the question remains how to integrate these diverse observations into a physical model of a volcanic system, and whether the same model is appropriate to all rift calderas. In this talk, I will review observations from InSAR, seismology, magnetotellurics, dynamic gravity, geological mapping, petrology and tephrochronology and discuss what we have and haven't learned about the magmatic and hydrothermal systems under these volcanoes.

Juliet Biggs, Marie Edmonds, Brendan McCormick-Kilbride, Matthew Pritchard

Submission 144

Statistical and physical approaches to interpreting satellite observations of volcanic activity.

The growth of the satellite earth observation community means that we now have more observations of volcanoes than ever before. This provides a wealth of data, but provides new challenges to interpretation. In some cases, observations of different parameters appear to conflict, for example, the atmospheric sulfur yields of eruptions are variable and not well correlated with eruption magnitude and for many eruptions the volume of erupted material is much greater than the subsurface volume change inferred from ground displacements. This raises the question should we use the same framework everywhere, or is each volcano essentially unique? Here we apply both statistical and physical approaches to such datasets.

First, we show that the statistical link between deformation and eruption varies between types of volcanoes, and also between different characteristics of deformation. Although there is no clear threshold at which eruptions occur, a probabilistic approach shows that rapid deformation is more likely to result in an eruption and longer-lasting deformation is less likely to do so. Secondly, we present a model that allows the inferred volume change of the reservoir and the sulfur mass loading to be predicted as a function of reservoir depth and the magma's oxidation state and volatile content, which is consistent with the array of natural data.

Ilya Bindeman

Submission 430

Ice burial by caldera collapse: Thermal and isotopic effects on hydration of volcanic glass

Large-scale silicic volcanism has occurred frequently in regions mantled by thin to very thick glacial ice cover. Several notable examples took place during the Pleistocene (Yellowstone, Long Valley, Iceland), and high altitude calderas in Cascades and Kamchatka. Caldera-forming events must have occurred during long-lasting (ca 10-50Ma) episodes of snowball Earth glaciation in the Neo- and Paleo-Proterozoic; and on other ice-covered planets and moons. The process of caldera collapse typically lasts hours to weeks, during which the caldera floor with ice drops by 100-1000s of meters and is covered by hot tephra and ash layers of similar total thickness. Here we investigate tephra-ice interactions following the ice burial in calderas of various specified thicknesses, initial temperatures, and porosities. Energy is lost through the upper surface via conductive, radiative and convective transfers and by escaping vapor. Scaling arguments, augmented by a simplified 1D finite difference model, suggest that ice should often survive for decades to centuries while gradually melting beneath a thick layer of cooling intracaldera tuff. The liberated glacial water (both liquid and vapor) is expected to hydrate volcanic glasses as it ascends and cools prior to escape. Glass saturation occurs at a few wt% water in the middle of the tephra deposit. Using reasonable estimates for O and H isotope fractionation factors and water diffusion coefficients below the glass transition, we demonstrate that tephra layers should often become fully hydrated to water saturations of 2-5 wt% and infer that the escaping water will have exchanged δD and $\delta^{18}O$ in a retrogressive manner along predicted T-t-z paths. The tephra/ice contact representing the lower boundary of our model domain is expected to move downward at a typical rate of meters per year, possibly promoting slumping and lake formation above. Our theoretical treatment is motivated in part by our recent measurements of lower than modern δD values in products of several Pleistocene eruptions in the western U.S. occupying regions that were likely glaciated during eruption. We are developing $\delta^{18}O$ - δD criteria to recognize synglacially hydrated intracaldera tephra, potentially including samples that have buried, altered and subsequently exposed either by fault uplift or by drilling.

Ben Black, Michael Manga, Benjamin Andrews

Submission 267

Ash production and dispersal from sustained low-intensity eruptions: An example from Mono-Inyo craters

Recent rhyolitic volcanism has demonstrated that prolonged low-intensity ash venting may be a widespread process during predominantly effusive dome-forming eruptions. Such weak venting has received less attention than larger-scale explosive eruptions, despite the potential for relatively commonplace occurrence. As an example, we examine the possibility and some consequences of episodes of extended, weak ash venting at the rhyolitic Mono-Inyo chain in Eastern California. We describe ash-filled cracks within one of the youngest domes, Panum Crater, which provide a textural record of ash venting during dome effusion. We use synchrotron-based X-Ray Computed Tomography to characterize the particles in these tuffisites. Particle sizes in well-sorted tuffisite layers agree well with grain size distributions observed during weak ash venting at Soufrière Hills Volcano, Montserrat, and yield approximate upper and lower bounds on gas velocity (10^{-4} – 100 m/s) and mass flux (10^{-1} – 10^4 kg/s) during the venting episodes that formed the layers. We simulate ash dispersal with Ash3d to assess the consequences of long-lived Mono-Inyo ash venting for ash deposition and the accompanying volcanic hazards. Dispersal is especially sensitive to grain size and aggregation, exemplifying the influence of small-scale processes on the large-scale outcomes of volcanic eruptions.

Joshua Blackstock, Matthew Covington, Joseph Myre, Phillip Hays

Submission 1110

Direct dissolved CO₂ measurement in low-temperature waters using a low-cost measuring and data logging platform for a diverse range of hydrogeologic settings

A large portion of CO₂ degassing from volcanic-geothermal systems may occur as diffuse migration through shallow, relatively low-temperature groundwater. Identifying and quantifying these CO₂ emissions are paramount to developing accurate regional and global CO₂ inventories. High-resolution, long-term records are needed to define natural variability (e.g. seasonality) and to determine and understand high-variability events. To-date, the majority of globally cataloged emission inventories are derived from 'snapshots' of single monitoring events or short-term periodic monitoring; hence, tectonomagmatic, hydrogeologic, and geochemical factors that control CO₂ variability are often poorly understood. The high cost of gas analyzers and data loggers has limited the number and spatiotemporal scales in studies of such CO₂ emissions. This study conducts direct measurement and data logging of dissolved CO₂ in low-temperature waters using a non-dispersive infrared gas sensor interfaced with an Arduino-microcontroller for data logging and power cycling functionality at a cost of less than \$300 USD per unit. Hourly dissolved CO₂ measurements were carried out in a headwater stream (Elise Falls, Arkansas) and cave stream (Blowing Springs, Arkansas) from the southern Ozark Plateaus region. Dissolved CO₂ concentrations at the sites ranged from 13 to 56 and 18 to 36 mmol/L, respectively. Major ion chemistry (bicarbonate-type), pH (5 to 8), and dissolved CO₂ concentration ranges observed at the study sites are similar to low-temperature, high-CO₂ bicarbonate-type waters documented at numerous volcanic-geothermal environments, globally (e.g. Mammoth Mountain, California, USA; 20 to 50 mmol/L). The measuring platform presented demonstrates an accurate and low-cost methodology for assessing dissolved CO₂. Moreover, the platform could be implemented across an array of hydrogeologic environments, particularly, volcanic-geothermal environments where large short- and long-term variability may exist.

Madalena Blum-Oeste, Gerhard Wörner

Submission 463

Tracing magma components in mineral compositions from lavas of the Central Andes

In his “Crustal forensics in arc magmas”, Davidson et al. (2005, *JVGR* 140, 157-170) emphasized the need of careful evaluation of geochemical approaches in the context of petrographic observations. Indeed, as Jon’s work has shown, the nature and composition of magmatic components involved in arc magma genesis often cannot be extracted solely from analyses of powdered rock. Searching for magmatic end-member compositions of hybrid lavas of Taapaca volcano, in the Andean Central Volcanic Zone (CVZ, 18°S), polytopic vector analysis (Blum-Oeste & Wörner, 2016, *TN* 28, 434-440) has revealed two mafic and one silicic end-member magmas involved in the petrogenesis of Taapaca: a strongly LREE and HFSE enriched basalt (EB), a high-Al basaltic andesite (BA), and a HREE-depleted rhyodacite (RD). Here, we present supporting evidence based on petrography and mineral chemistry to validate the compositions extracted from the statistical approach.

Two distinct forsterite (Fo)-Ni trends and two initial olivine core compositions (Fo81, ≈1500-2500 ppm Ni; Fo74,

Jon Blundy, Duncan Muir, Luca Ziberna, Richard Brooker

Submission 339

Dacite Petrogenesis at Cerro Uturuncu Volcano, Bolivia

The Altiplano-Puna Magma Body (APMB) is the largest (~500,000 km³) known active magma reservoir in Earth's continental crust. It is presumed to be the source of the >12,000 km³ dacitic to rhyodacitic volcanic material erupted in the Altiplano Puna Volcanic Complex (APVC) over the past ~11 Ma, including the Pleistocene Cerro Uturuncu volcano in Southern Bolivia. Silicic magmas at Uturuncu, erupted 1.04 to 0.25 Ma, comprise chemically monotonous dacitic lava flows bearing abundant mafic enclaves of andesitic composition and rare xenoliths of crustal metamorphic rocks. Phase relationships of an Uturuncu andesite were determined between 890 and 980°C, 0.5 and 1.1 GPa and at $f_{O_2}=NNO$ under volatile-saturated and -undersaturated conditions in order to explore the conditions in the andesite source region. The natural andesite assemblage of plagioclase (An₈₀) + amphibole + cpx + opx + Fe-Ti oxides is reproduced only at 950-980 °C and 0.5-0.8 GPa with a dissolved H₂O content in the melt of 7.3 to 8.3 wt%. These conditions, melt composition and H₂O contents are consistent with electrical conductivity measurements of the APMB, suggesting that it comprises 10-20 vol% water-rich andesite melt in a solid matrix.

The experiments confirm that Uturuncu dacites cannot be generated from the andesite by simple fractional crystallization, in keeping with the differences in their Sr and Nd isotope ratios, that show a significant component of crustal melt is implicated in dacite petrogenesis. Isotope analyses of a crustal gneiss xenolith from Uturuncu provides an excellent match to the required crustal end-member. Using pseudosections for the bulk chemistry of the gneiss we show that its mineralogy of cordierite + sillimanite + biotite + Kspar + qtz + hercynite + biotite + ilmenite is consistent with the onset of dehydration crustal melting at pressures of 0.4 to 0.5 GPa and temperatures approaching 950 °C. We propose that Uturuncu dacites form at the upper surface of the APMB where hot wet andesites melt the Andean crust. Mixtures of ~50% crustal melt and 50% andesite reproduce the dacites in major, trace and isotope chemistry. The low H₂O content of dehydration crustal melts lead to dacite H₂O contents that are significantly less (≤4 wt%) that those in the andesite endmember. We suggest that water-poor dacites of the APVC may be characteristic products of silicic melt generation in the upper reaches of the APMB.

Jon Blundy, Oleg Melnik, Natasha Gorokhova, Ralf Dohmen

Submission 342

Rapid Destabilisation of the Magma System Beneath Mount St Helens prior to 1980-86 Eruption

Zoned plagioclase phenocrysts are ubiquitous in arc volcanic rocks. Their zoning patterns are hold clues to the magmatic processes that shaped their host rocks. An enduring question is whether this information pertains to kinetic processes, changes in intensive variables, open system behaviour, or combinations thereof. The challenge is to unpick the testimony of zoned plagioclase as an archive of pre-eruptive processes occurring in the sub-volcanic magma reservoir. For Mount St Helens (MSH) dacites from the 1980-86 eruption, we have approached the problem using a combination of ion microprobe (SIMS) analysis of zoned plagioclases, experimentally-derived models for plagioclase-melt equilibrium and element partitioning, and numerical models of intracrystalline diffusion.

Using phase equilibrium experiments on MSH dacites to parameterise plagioclase composition as a function of pressure (P), temperature (T) and melt fraction (F), we have developed a numerical method to invert zoned MSH plagioclase phenocrysts for their core-rim evolution in P-T space prior to eruption. We remove ambiguity in the family of plausible P-T paths by solving simultaneously for F using the Sr and Ba contents of the plagioclase as measured by SIMS. This approach is valid at MSH because of the relative monotony of magma composition and the absence of significant mafic magma inputs to perturb the bulk composition. Data from a representative set of crystals from the 1980-86 eruption record the same evolution – an abrupt change from plagioclase core crystallisation at ~12 km depth to rim growth at ~4 km.

Simultaneous with crystal growth, trace element diffusion occurs in an attempt to restore chemical potential equilibrium across the zoned plagioclase. Using correlations between anorthite and Sr we show that the cores are >10,000 yrs old, whereas the rims pre-date eruption by ≤ 3 yrs. The core-rim interface, that is related to the time of magma ascent from 12 to 4 km, can be precisely dated using high spatial resolution SIMS Sr profiles (2 μm spacing). A picture emerges of a long-lived, vertically extensive, mushy, magmatic system that became abruptly destabilised, probably gravitationally, in the months to years before eruption, a timescale commensurate with volcano monitoring. Mush destabilisation appears to be a key process in volcano rejuvenation and eruption triggering.

Wendy Bohrson, Frank Spera

Submission 353

Rejuvenation of Crustal Magma Mush: Constraints on Multiply Nested Processes and Timescales

Relatively crystal rich silicic volcanic deposits can preserve evidence of a past where a rheologically locked magma was rejuvenated through heat exchange with recharge magma. The erupted product reflects an array of processes that includes unlocking (i.e., melt formation) via heat transfer, crystal growth/resorption, ascent, and eruption. We assess conditions and timescales under which unlocking (the transition from near-solidus to ~50% melt of silicic mush), occurs and provide phase equilibria context for melt formation and crystal growth/resorption during unlocking. For a case of unlocking through heat transfer from recharge, MELTS computations provide the mass ratio of recharge magma to mush (MR/MM) when the two magmas achieve thermal equilibrium and the changes in melt and mineral masses and temperatures as unlocking progresses. For unlocking of 'dry' (0.5 wt.%) and 'wet' (3.9 wt.%) rhyolitic mush by basaltic recharge at upper crustal pressures, MR/MMR/MM than dry, and therefore wet rejuvenated magmas may be more abundant in the volcanic rock record. Temperature changes in dry mush as it defrosts are pronounced (>150°C) compared to those in wet (~15°C). As required, the net volume of crystals decreases during unlocking, but some phases (i.e., plagioclase) may increase in abundance. We estimate thermal unlocking timescales by 2 methods, one that calculates the time to reach thermal equilibrium for recharge magma dispersed in mush as 'clumps' of various sizes, and the second where the required volume of recharge magma is initially a single clump and evolves to smaller size through stretching and folding in host magma. For magma volumes from 0.1 to 5000 km³, unlocking times are 10-2 to 106 yrs. Shorter timescales require a large number of relatively small clumps (n>106); thus, large volumes of mush purported to unlock over short timescales should exhibit evidence of intimate magma mingling. Literature unlocking timescales are typically 2 to 105 yrs., and some estimated from diffusion are particularly short. But this diffusive timescale may not capture the entire unlocking process. To appreciate how these types of timescales inform unlocking timescales, these 'events' must be understood in context with the spectrum of unlocking processes. In the absence of this context, rejuvenation timescales may be incorrectly inferred, which may hinder effective eruption forecasting and hazard mitigation.

Xavier Bolós, Gerardo Cifuentes, José Luis Macías, Giovanni Sosa-Ceballos, Felipe García, Víctor Gámez, Mariela Albor, Mónica Juárez

Submission 1079

Hydrothermal system of Cerritos Colorados geothermal field (La Primavera caldera, Guadalajara, Mexico) inferred from an electrical resistivity tomography survey

Hydrothermal activity in volcanic calderas is a consequence of the energy transfer between the deep magmatic chambers and the subsurface layers saturated in water. This hydrothermal system is generated by convection of the groundwater supplied by meteoric water recharge and the ascent of hot volcanic gasses exsolved from deep magma reservoirs. Calderas are very heterogeneous geological structures due to its formation and evolution that produced a complex stratigraphy. The different stratigraphic units of the caldera promote the formation of more permeable levels. All of these heterogeneities can be affected by deformation and also by the presence of fractures and faults which constitute the main pathways whereby hydrothermal fluids can move easily through the surface as fumarolic activity and thermal springs.

Geoelectrical methods, and especially electrical resistivity tomography, have been used in the last decades to investigate the relationship between structural geology and hydrothermal systems in different volcanic areas around the world. In this work we have focused on the role of the subsurface structures to understand and localize the pathways of fluids in the hydrothermal system of the Cerritos Colorados geothermal field. We study the central area of the caldera (P12 well and Cerritos Colorados graben), where active hydrothermal activity is evidenced by fumaroles, thermal anomalies, CO₂ diffuse emission and sulfur precipitation. There are several geological studies of the volcanic evolution of La Primavera caldera, mainly about their general stratigraphy and eruption dynamics, however there are not studies focused on the structural geology and the hydrothermal system by applying geophysical surveys. In this sense, we have applied ERT in two selected places. The first profile (2.4 km in length) is located in the P12 well area. In the Cerritos Colorados graben area, we have carried out a 3D resistivity model using the equatorial method. Combining the results of the electrical resistivity tomography data with the detailed structural map of this area allowed us to identify the main degassing zones (i.e. fumaroles) correspond to the higher permeability zones located along normal faults. In conclusion, a strong structural control of the surface manifestation of these hydrothermal systems is deduced from our new data. Then, our results emphasize the importance of old structural boundaries mainly controlled by intra-caldera tectonic structures.

Xavier Bolós, Gerardo Cifuentes, José Luis Macías, Giovanni Sosa-Ceballos, Denis Avellán

Submission 1086

Eruption dynamics, internal structure and hydrothermal system of Parícutin volcano (Mexico). Insights from ERT 3D model combined with historical and geological evidences

Parícutin is one of the most famous monogenetic volcanoes around the world because is the youngest volcano of the Michoacán-Guanajuato Volcanic Field (MGVF). MGVF has an area of about $\sim 40,000$ km² that contains the largest concentration of monogenetic vents on Earth associated with a subduction-related continental arc, holding more than 1,100 edifices. The eruption of Parícutin volcano started on February 20, 1943 and ended on March 4, 1952. It produced a volume of ~ 2 km³. The volcano started with a fissural eruption emitting ash, sulfur-rich gases, and incandescent bombs. The main cone grew rapidly, reaching ~ 150 m in height at the end of the first month. Explosive activity was intense and often associated with lava effusion with different vents along an eruptive fissure. Its activity changed the style during the eruption producing effusive and Strombolian activity, as well as sub-plinian eruptions. probably related to phreatomagmatism.

A new methodology was developed to carry out electrical resistivity tomography (ERT) profiles with any geometry. We applied this method for the first time in volcanology in order to assess the Parícutin eruption dynamics and the role of the basement in the area attempting to understand the behavior of the feeder dyke and the plumbing system, which until now lacked any detailed geophysical data. We present this analysis in a 3D resistivity model to interpret the main structures observed. We detect high resistivity values corresponding to spatter facies and proximal well welded pyroclasts. We also found that the main intrusion might be aligned with the orientation of the eruptive fissure. Our data shows that the hydrothermal system is generated by convection of groundwater supplied by the recharge of meteoric water in specific areas of the cone. The main volcanic edifice of Parícutin presents normal faults produced by overburden of pyroclastic materials deposited during the eruption. The resistivity model suggests that these faults constitute the main pathways whereby hydrothermal fluids rise to the surface through the volcanic cone. The results obtained in this study will help to explain changes in the explosive behavior during monogenetic eruptions and can be extrapolated to other volcanoes of similar characteristics lacking of direct information of the eruption.

Costanza Bonadonna, Sebastien Biass, Jean Luc Falcone, Federico Di Traglia, Marco Pistolesi, Mauro Rosi, Pierino Lestuzzi, Sam Isgett, Bruce Houghton

Submission 264

Ballistic hazard assessment: so far, so good?

Developments in volcanic hazard assessments for ballistic projectiles suffer from several limitations across a range of key concepts in volcanology. Firstly, they are often associated with short, impulsive events within long-lasting eruptive sequences originating from complex conduit heterogeneities. Fragmentation in such a context typically results in unsteady, nonsustained plumes that are challenging to model. Secondly, our understanding of processes generating ballistic particles suffers from the lack of characterization of the total ballistic components of pyroclastic deposits. Most physical and hazard models are developed and calibrated using a small fraction of the total ballistic population inferred either directly from field measurements or indirectly (e.g. from the geometry of impact craters or remote sensing), which limits our empirical understanding of ejection conditions at the scale of a total deposit. Finally, although ballistic particles are unanimously recognized as a critical hazard in proximal areas, little debate has occurred regarding the purpose(s) of ballistic hazard assessment and few efforts have explored alternative approaches to delineating concentric hazard zones.

Here, we first present a new approach developed to probabilistically assess the hazard and physical impact of ballistics associated with Vulcanian explosions at La Fossa volcano (Vulcano, Italy). Limited field observations were inverted to define an eruption scenario, and various approaches to quantifying probabilities of impacts are explored and discussed. The vulnerability of the built environment to roof perforation is assessed based on field studies and the existing literature to allow the first quantitative pre-event impact assessment for ballistics. Second, we take advantage of the ballistic field formed in Episode IV of the 1912 eruption of Novarupta (Alaska, USA), which is constrained with an unprecedented degree of detail, to discuss the shortcomings of current approaches to probabilistic hazard assessments for ballistic impacts and to identify future research needs.

Christina Bonanati, Heidi Wehrmann, Kaj Hoernle, Steffen Kutterolf, Maxim Portnyagin, Maryam Mirzaloo, Dirk Nürnberg, Karen Strehlow

Submission 997

A 68,000 year tephra record in marine sediment cores offshore southeast Iceland

Large Icelandic explosive eruptions inject pyroclastic material and gases into the atmosphere, modifying its composition even on a global scale. Regionally, they affect infrastructure, air-traffic and human health. The 2010 Eyjafjallajökull eruption demonstrated that even medium-size eruptions can have a major societal impact beyond Iceland. Reconstructing the time-series of past eruptions is of key importance for understanding the temporal evolution and dimensions of Icelandic volcanic activity. Here we report detailed down-core investigations of tephra in four up to 10 m long marine sediment gravity cores obtained during RV Poseidon Cruise 457, at distances of 60 to 180 km southeast of Iceland. We analyzed major element compositions of volcanic glass shards and used geochemical fingerprinting to determine their provenance. We identified 52 primary basaltic ash layers, complemented by minor amounts of rhyolitic to basaltic-andesitic glass shards within these layers and in the background sediment. For the tephra identification, chronostratigraphy and inter-core correlation, we applied color-scans, AMS 14C dating and the tuning of proxy records to the $\delta^{18}\text{O}$ NGRIP reference climate record.

The succession of medium to large volcanic events as preserved in our cores reaches back to 68 ka BP. Therewith, we extend the Icelandic eruption record much further back in time than previously inferred from terrestrial Iceland and in more detail than determined from distal deposits. Grímsvötn-Lakagígar volcanic system was most active in the periods between 68 and 52 ka BP and between 40 and 35 ka BP. A phase of high activity at Kverkfjöll volcanic system since 30 ka BP culminated in the event producing the wide-spread Fugloyarbanki tephra at 27 ka BP, after which the explosive activity at Kverkfjöll almost ceased. Thereafter, we observe a shift towards higher activity at Bárðarbunga-Veiðivötn and Hekla volcanic systems. The investigated tephra record also points to a possible climate forcing component in Icelandic volcanism, with increasing activity during stadial-interstadial transitions and towards the end of Marine Isotope Stage 3.

Estelle Bonny, Þorvaldur Þórðarson, Robert Wright, Ármann Höskuldsson, Ingibjörg Jónsdóttir

Submission 661

What can the synergy of satellite- and ground-based measurements tell us about eruption processes: case study of the 2014-15 eruption at Holuhraun, Iceland

The August 31st 2014 to February 27th 2015 lava-producing eruption at Holuhraun (on Dyngjúsandur) produced an 84 km² and 1.2 km³ lava flow-field, the largest in Iceland since the one produced by 1783-4 Laki eruption. Emplacement of a basaltic flow-field of this size onto an effectively flat surface (3/s, ground-based) and include a secondary peak (150 m³/s, satellite-based) in mid-November. This is in disagreement with the asymmetric waxing/waning behavior from the Wadge (1981) theory, which tells us that this eruption is more complex. We found that the span of this secondary increase in TADR correlates with a large lava pool existing at the surface of the lava flow field. Interestingly, the ratio of saturated pixels at 11 μm over the total number of anomalous pixels also increases in correspondence with this bulge, which could be explained by the high radiant surface produced by this lava pool. The satellite-based technique yields a total erupted volume of about 1.27 km³ in good agreement with the above given estimate derived from field observations.

Frances Boreham, Katharine Cashman, Alison Rust

Submission 84

Linking Inflated Flow Margins, Lava-Water Interactions and Rootless Cone Formation

Littoral cones, scoriaceous rootless cones, spatter cones and hornitos all form by the explosive interaction of lava with environmental water, i.e. lakes, rivers, swamps or seas. They exhibit a range of morphologies and compositions; implied variations in the dynamics of the lava-water interaction may reflect differences in lava flux, lava rheology, available water and sediment properties. We link the different types of rootless features to the conditions in which they form to constrain both the dynamics of lava-water interactions and the hazards associated with lava flows in wet environments.

Using aerial photographs from Google Earth, and DEMs from ArcticDEM and drone surveys, we mapped 12 rootless cone sites in Iceland, categorised cones based on morphology and composition (scoria or spatter) and analysed their spatial distribution. We find that lava flows with a relatively high mass flux and access to lots of water build relatively larger and finer-grained cones. This relationship is clearest in transitional areas where the conditions of the lava-water interaction change due to changes in either the lava flow properties or the wider environment.

We present a case study in Aðaldalur, NE Iceland, where rootless features on the Younger Laxá lava flow change abruptly from large scoriaceous cones to small, closely-spaced hornitos made of spatter. This transition coincides with an inflation front in the parent lava flow, with the inflated flow margin hosting the rootless cones. The change in cone type from scoriaceous cones to hornitos suggests a reduction in explosive energy, likely related to an abrupt change in dynamics of the lava-water interaction. We hypothesise that the lava flow stalled and inflated as it entered part of the valley with a plentiful but dispersed water supply, e.g. a bog or floodplain. The constant supply of lava caused flow inflation, while the plentiful supply of water at the flow margin created the rootless cones. When the lava flow broke out and continued down the valley, dispersed water sources in the floodplain created large numbers of hornitos instead of rootless cones. Our analysis of other sites suggests that it is common for rootless cones to be concentrated at the margins of inflating flows or at a boundary where a lava flow meets water.

Ma. Antonia Bornas, Danikko John Rivera, Robjunelieaaa Lim, Renato Solidum, Alain Bernard

Submission 491

Reconstructing the 1754 eruption of Taal Volcano, Philippines: First results from deposit stratigraphy, particle analysis and geochemistry

The chronology and surface dynamics of the most violent historical eruption of the Decade Volcano Taal in south central Luzon, Philippines in 1754 are reconstructed using detailed stratigraphy, granulometry, SEM analysis and geochemistry. Documents from the Spanish colonial period describe a $VEI \geq 4$ explosion series spanning ~7 months that generated voluminous tephra fall and pyroclastic currents that obliterated coastal settlements around Taal Lake. The 1754 deposit consists of a distinct succession of thin wet surge ash, highly vesiculated vitric scoria lapilli fall interlayered with partially to highly indurated base surge units, lithic-bearing and lithic-rich scoria lapilli fall and indurated base surge tuff. Dispersal, stratigraphic and textural characteristics of tephra fall units are consistent with Plinian and sub-Plinian activity occurring across two monsoonal seasons. Base surge tuff consists mainly of vesiculated tachylite to sideromelane glass, broken crystals and sparse to rare hydrothermal and vent fragments. Emplacement and textural characteristics of base surge tuff indicate origin from phreatomagmatic processes in excess of peak magma-to-water ratios at breached vent conditions. Juvenile scoria and base surge glass are basaltic andesite in composition. Preliminary results demonstrate that the 1754 eruption commenced with a short-lived phreatomagmatic onset closely followed by Plinian and sub-Plinian activity that cycled with phreatomagmatic phases with changing eruption mass rates. The eruption progressed into paroxysmal Plinian activity that led to vent destruction and culminated in intense phreatomagmatic activity. These results are in general agreement with historical accounts and underscore significant challenges to current volcanic hazards assessment and eruption early-warning.

Joseph R. Boro, Owen K. Neill, John A. Wolff, Frank C. Ramos, Corey A. Dimond

Submission 572

Diffusion modeling of Ti-in-quartz from the Bandelier Tuff and Cerro Toledo Formation, Valles caldera, Jemez Mountains, New Mexico, USA

The 380 ± 170 km³ Otowi Member of the Bandelier Tuff erupted during formation of the Toledo caldera (the first phase of the Valles caldera), NM, at 1.60 ± 0.02 Ma. The Otowi Member consists of compositionally zoned high-silica rhyolitic pumice, exhibiting an approximately 4-fold increase in incompatible element concentrations from top to base. Phenocrysts are dominantly sanidine and quartz, with lesser amounts of Fe-rich clinopyroxene, magnetite, fayalite and accessory minerals. Quartz and feldspar crystals show increasingly prominent Ti zoning from first-erupted to last-erupted pumice, with cathodoluminescent-bright Ti-rich rims jacketing darker Ti-poor cores. The Ti-rich rims represent influx of new melt(s) with higher [Ti]. The very latest stage of the eruption is represented by a fallout unit, which overlies co-ignimbrite ash on top of the Otowi ignimbrite, and is mapped as the lowest unit of the Valle Toledo Member of the Cerro Toledo Formation.

We applied the method of Costa et al. (2008) and the Ti-in-quartz diffusion coefficient expression of Cherniak et al. (2007) to model times of diffusional relaxation of the boundary between Ti-rich and Ti-poor zones in quartz from the fallout and underlying ignimbrite. Zone boundaries were assumed to be initially sharp. Crystals were prepared for the electron microprobe as oriented grain mounts and sectioned through the center of the grain. Crystals were first selected by cathodoluminescence imaging and [Ti] were obtained along transects across diffusional boundaries using Kramers' Law and blank correction methods after Donovan et al. (2016). We find times on the order of 140-330 years between the onset of rim growth and quenching, with some indications of different magmatic residence times of individual quartz crystals. This may either represent the timescale between a triggering event and eruption, or alternatively the time between a prior recharge event and a more immediate eruption-triggering event.

References: Cherniak, D.J., Watson, E.B., Wark, D.A. (2006) *Chemical Geology* 236, 65-74; Costa, F., Dohmen, R., Chakraborty, S. (2008) *Reviews in Mineralogy and Geochemistry* 69, 545-594; Donovan, J.J., Singer, J.W., Armstrong, J.T. (2016) *American Mineralogist* 101, 1839-1853.

Claire Bouligand, Svetlana Byrdina, Marceau Gresse, André Revil, Jean Vandemeulebrouck, Shaul Hurwitz

Submission 154

Joint interpretation of magnetic and electric resistivity surveys in Yellowstone and Campi Flegrei vapor-dominated hydrothermal systems

We focus on two vapor dominated hydrothermal systems in silicic calderas: Solfatara di Pozzuoli, Campi Flegrei caldera (South Italy) and Solfatara Plateau thermal Area in the Yellowstone caldera (USA). Both of these areas have several fumaroles with native sulfur precipitation and a mud pool. We performed in both areas dense 2D magnetic surveys and high resolution 3D electric resistivity tomography (ERT). Magnetic surveys are effective in imaging horizontal contrasts of subsurface magnetization, but sensitivity decreases rapidly with depth and their interpretation is non-unique. ERT can provide a 3D image of the subsurface electric conductivity but the method is limited in resolution due to the relatively small number of profiles that can be acquired. Although magnetization and electric conductivity are two different quantities with no direct physical relationship, we investigate how the combination of such surveys can help better constrain the geometry of the hydrothermal plume and/or of geological features controlling hydrothermal flow. In particular, hydrothermal plumes are expected to have low electric resistivities due to a higher water and gas content and high degree of hydrothermal alteration that may also modify the subsurface magnetization.

Jade Bowers, Shanaka de Silva, Adonara Mucek, Indyo Pratamo, Armen Putra

Submission 686

Understanding resurgence and restlessness at calderas: insights from climatic vs post-climatic eruptive compositions with particular reference to Toba, Sumatra

Although calderas and the caldera cycle are well studied, the relationship between caldera-forming eruptions and post-caldera volcanism is poorly understood. The chemical characteristics of the erupted products suggest that two end-member compositions are involved during resurgence: (1) remnant magma of similar composition to the magma of the climactic eruption; and (2) a more mafic magma. Remnant magma may motivate uplift due to recovery of isostatic, lithostatic, and magmatic equilibrium after the climactic eruption, or be rejuvenated by recharge magma. Often a mixing trend suggests mixing between the end members. Resurgence at Toba Caldera, Indonesia, involves significant structural uplift with associated volcanism (in and around the caldera) since the caldera-forming eruption ~74 ka. The Samosir lava domes, on the eastern flank of the resurgent dome, compositionally overlap with the Youngest Toba Tuff (YTT; 70-75 wt. % SiO₂) suggesting remobilization and eruption of the remnant YTT magma. In the north, the Sipisupisu lava dome represents the most mafic post-collapse volcanism around the caldera (52-60 wt. % SiO₂) while the Pardepur lava domes in the south show compositions between Sipisupisu and the YTT (65-67 wt. % SiO₂), suggesting they might represent more hybrid compositions of remnant YTT and recharge magma. Age and spatial relations suggests in the Toba system, the signal of recharge is muted in the central part within the caldera where mainly remobilized remnant magma erupted. On the periphery, the signal of mafic recharge is much stronger possibly suggesting less remnant magma involvement. 35 km north of Toba is an actively erupting volcano, Sinabung, that has strong isotopic and age links to Toba Caldera. Sinabung lavas overlap with Toba's compositions, but are proportionally more towards the mafic end member (55-60 wt. % SiO₂). Sinabung may, therefore, be part of Toba's post-caldera history, but located outside the magmatic shadow zone and tapping the recharge magma in the resurgent Toba system. The silicic, remnant YTT magma is centered under the Samosir domes, while the mafic recharge signal gets stronger further away from the center of the caldera.

Esteban Bowles-Martinez, Paul Bedrosian, Adam Schultz, Jared Peacock, Graham Hill

Submission 1280

Magnetotelluric imaging reveals conductive connections within the southern Washington Cascade arc

A large-scale broadband magnetotelluric study was carried out as part of the iMUSH project, covering Mt. St. Helens (MSH), Mt. Adams, Mt. Rainier, and areas in between including the Holocene Indian Heaven Volcanic Field and the eroded Plio-Pleistocene Goat Rocks volcano. While the densest data collection is centered about Mt. St. Helens, the large array of over 300 stations constrains a detailed 3D model of the entire region. A primary goal of this study is to characterize the South Washington Cascades Conductor (SWCC), a highly conductive body that has been alternately interpreted in earlier studies as conductive accreted meta-sediments and as a zone of partial melt. We present preliminary 3D inversion results, showing that the SWCC is highly complex. Our model shows high conductivity associated with each volcano as well as conductive connections between them. West of Mt. Adams a prominent conductive zone begins around 8 km depth, with a less conductive connection extending to depths of at least 60 km. This is possibly a pathway for dehydration fluids released from the subducting Juan de Fuca slab. At shallower depths, this conductive zone appears to stretch outward toward the volcanic centers. The branch of this conductor going toward Indian Heaven as well as high conductivity near MSH both match zones of high V_p/V_s seen prominently in iMUSH seismic models, suggesting high fluid content. Our resistivity model shows how these anomalies connect to the greater Cascade arc. Other areas of high conductivity are attributed to the presence of altered volcanic rock, especially at Goat Rocks, as well as Eocene accreted metasediments, such as where the Morton anticline brings conductive sediment close to the surface. The elevated conductivity of the SWCC is thus attributed to a combination of sources of varying depth and spatial extent, including dehydration fluids, partial melt, alteration clays, and marine metasediments.

Luke Bowman, Camila Velastegui, Carlos Lara

Submission 1233

What do we say, when do we say it, and who do we tell it to? Volcanic hazard awareness and risk reduction at Cayambe Volcano, Ecuador

Cayambe Volcano is an ice-covered stratovolcano northeast of Quito, Ecuador. Its last known eruption occurred in 1786 with limited impacts on the town of Cayambe located ~15 km to the West. In the last ~230 years, the town of Cayambe's population has increased to over 45,000 individuals in the urban district—roughly half of whom could be impacted by lahar hazards. Since June 2016, Cayambe has demonstrated anomalous seismic activity suggesting volcanic unrest, and the possibility of a future eruption was made public by the Geophysical Institute of Ecuador and media.

We conducted semi-structured qualitative interviews with two groups in Cayambe: 1) individuals in two neighborhoods along the banks of Rio Blanco identified as “high risk” and 2) representatives from Cayambe's Risk Management Unit. Preliminary results suggest that hazard awareness among the residents is high—especially among homeowners that have lived in the area for many years—even though only small flooding events have occurred in the living memory of residents. Levels of disaster preparedness, however, are low for many reasons.

Authorities in Cayambe rely on approved contingency plans from eight technical groups that manage discreet components of disaster management. The current strategy is to postpone community-based disaster preparedness and risk management efforts until all eight contingency plans are in place. Results show that at-risk communities prefer immediate, small-scale interventions in order to begin preparing for future emergencies. Moreover, authorities wait to approach communities until an official alert is made in order to maintain calm and avoid panic among the population. This approach has an important unintended consequence. Interviewees describe the lack of information as unsettling and helps seed rumors that lack a scientific basis. Residents prefer to be continuously informed about the state of volcanic activity. Waiting to share information creates greater uncertainty in the population that is eager to better organize their communities and prepare themselves for a future hazard event. Results from this study are informing the design of new strategies to improve disaster risk reduction and communication efforts in Cayambe.

Brittany Brand, Michael Lindell, Alexa Dietrich

Submission 697

Promoting household preparedness to natural hazards using active-based learning

“What I hear, I forget. What I see, I remember. What I do, I understand.” Xunzi (340 – 245 BC).

Reducing the impact of disasters through the development of resilient communities is a top national priority. Resiliency refers to a community’s ability to proactively mitigate, prepare, respond, and recover from events such as natural (and man-made) hazards. Promoting the adoption of individual household preparedness represents a critical step toward building resilient communities. However, despite the efforts of federal, state and local agencies to provide hazard information and preparedness recommendations to the public, the level of disaster preparedness across the United States remains low.

We hypothesize that engaging individuals in active-based learning of natural hazards, developed for specific subpopulations, allows individuals to personalize risk and develop positive attitudes toward the efficacy of taking preparedness actions. This hypothesis is based in the Protective Action Decision Model (PADM), which integrates approaches in social influence, persuasion, behavioral decision making, and attitude-behavior relationships to demonstrate the phases through which an individual must typically pass before taking preparedness actions.

We will present tested and validated examples of natural hazard education strategies based in active learning and PADM, and provide recommendations for creating similar tools for volcanic hazard education programs. Our efforts will provide effective strategies to increase household preparedness, thus promoting community resilience to natural hazards.

Brittany Brand, Nicholas Pollock, Andrew Gase, Damiano Sarocchi, Olivier Roche

Submission 791

The erosive nature of pyroclastic density currents – A summary of findings from the 18 May 1980 Mt St Helens (USA) deposits

Our understanding of the mechanisms and conditions that promote substrate erosion by pyroclastic density currents (PDCs) is evolving through the combination of field data and analogue experiments. However, many questions remain as to how particle current concentration, topography, and the nature of the substrate influence erosive capacity. PDC deposits from the afternoon of the 18 May 1980 eruption of Mount St Helens provide insight into the role of these parameters on erosive capacity of the parent currents. We combine depositional characteristics from PDC deposits across slopes of 5-30° with componentry and granulometry studies to elucidate (1) how topography influences current dynamics, and (2) where and into what substrate the PDCs eroded. Blocks up to 0.29-m in size, eroded from the underlying substrate, are found within the cross-stratified deposits along the steep flanks of the volcano. We interpret that acceleration, partial confinement and high surface roughness increased basal shear stress, resulting in substrate erosion. In the shallow-dipping pumice plain, blocks of 0.64-1.2-m in size were eroded from upstream debris avalanche (DA) hummocks. Eroded blocks are most prevalent just above the base of unit contacts, consistent with experimental findings that erosion is favored by a pore pressure gradient at base of currents. Eroded blocks located meters above unit contacts indicate entrainment occurs within currents whose deposits aggrade upwards. Stratification and grain fabric at the PDC-DA contact also suggest basal shear stress due to irregular topography is important. Wave-like features, interpreted as the development of shear-induced waves within or near the flow boundary interface, are common across shallow slopes and within flow units. The wave-like features further suggest that shear is an important process, even in currents with pore gas pressure. Finally, an extensive ground penetrating radar study tracks a 200-m-wide scour-and-fill channel from an exposure in the distal region toward source, providing evidence of self-channelization and insight into the consequences of channelization on later PDCs. Our work demonstrates that topography and the nature of the substrate strongly influence PDC dynamics and erosive capacity, and motivates the need to further understand the consequences of substrate erosion on runout.

Carolyn Branecky, Tobias Keller, Peter Huybers, Wim Degruyter, Michael Manga

Submission 701

The relationship between deglaciation and volcanism in arc settings: the example of the Mount Mazama volcanic system, Crater Lake, Oregon

On a global scale, volcanic eruptions were more frequent during the last deglacial period than during the last glacial period (Huybers and Langmuir 2009). There are diverse hypotheses for what physically produces this correlation on the scale of an individual volcano. This study evaluates the hypothesis that crustal stress changes caused by ice mass changes make it more likely that eruptions will occur during periods of ice loss. Investigating ice-volcanism correlations can also reveal the sensitivities of the magma chamber and host rock to perturbations. We focus on a glaciated arc setting, Mount Mazama, Oregon, where pulses of volcanism have been suggested to follow major deglaciations (Bacon et al. 2006). The effect of ice mass changes on crustal stress conditions is tested by further developing an existing thermo-mechanical magma chamber model (Degruyter and Huber 2014). We developed a statistical approach to compare the degree of correlation between ice loss and eruption frequency between the modeled and observed eruption records. The correlation is quantified using a hypothesis-driven index representing the rate of change of ice unloading. This approach accounts for errors associated with the age of erupted deposits as well as the timing of ice load changes. By using a combination of magma chamber modeling and statistical methods, we evaluate the conditions under which crustal stress changes can explain the observed correlation between ice loss and volcanism.

Eric Breard, Gert Lube, Joe Dufek, Ermanno Brosch, Tomaso Esposti Ongaro, Jim Jones

Submission 867

Constructing a benchmark for pyroclastic density currents

Pyroclastic density currents (PDCs) are amongst the most dangerous natural phenomena known and volcanologists are faced with the challenge to forecast PDCs hazards in future eruption crises. In addition to traditional approaches of mapping PDC deposits and deriving event probabilities using eruption frequency/magnitude records, a range of computational PDC models were developed over the past decades to allow simulating PDC dynamics in various scenarios. To date, there is an urgent need to validate these computational PDC models to build sufficient confidence around them (or adapt them) so that they can be used reliably for hazard decision making.

This task is impeded by two major obstacles: PDCs are highly complex multiphase flows; and there are only fragmentary observations and measurements of their inner workings limiting our ability to constrain the underlying physics. To overcome similar challenges in other areas of science, experimental or numerical benchmark studies have been developed to guide model validation and advancement. Creating a benchmark for PDCs has not yet been attempted.

Here we present the first results from an international effort to create a benchmark for dilute PDCs via large-scale experiments and use this to validate existing multiphase codes for PDCs. During the last Australasian summer, we conducted a series of four large-scale experiments (35m long) at the eruption simulator PELE in New Zealand. The experiments created ground-hugging, hot and fully turbulent mixture flows of natural pyroclasts and air by column collapse onto an instrumented runout section. In the four scenarios we synthesized a range of PDC behaviours that scale dynamically and kinematically to natural dilute PDCs, but differ systematically in the following key parameters: temperature (from ambient to 120 degrees), substrate roughness (

Sarah Brehm, Rebecca Lange

Submission 1261

Temperature at the onset of phenocryst growth in basalts from the Big Pine Volcanic Field, CA: application of an olivine-melt thermometer based on DN_i

48109-The Big Pine volcanic field is located along the western margin of the Basin and Range province and is notable for containing basaltic lavas with mantle xenoliths. As a consequence, the phenocrysts in these basaltic liquids must have grown during magma ascent and not in a stalled magma chamber; otherwise they would have dropped their mantle xenoliths. This is consistent with diffusion-limited rapid-growth textures in many olivine phenocrysts in these flows. Additionally, these basalts contain up to 2.6 wt% H₂O, based on analyses of olivine-hosted melt inclusions (Gazel et al., 2012). This makes the Big Pine basalts excellent candidates for application of a new olivine-melt thermometer based on the partitioning of Ni (Pu et al., 2017), which has a weak dependence on melt water concentration, unlike that based on DM_gol/liq, which requires a correction for melt water content. In this study, analyses of the olivine population in eight different basalt flows were obtained, including their Ni contents. A histogram of all analyzed olivines in each sample allows the most Fo-rich composition to be identified. These were compared to the composition of liquidus olivine predicted by MELTS (Ghiorso & Sack, 1995; Asimow & Ghiorso, 1998), using the basalt whole-rock compositions as the starting liquid composition at $\Delta\text{NNO}=0$. The results show excellent agreement, consistent with the conclusion that the phenocrysts grew rapidly during magma ascent and the first olivine composition to crystallize at the liquidus is often preserved in the erupted sample. This allows the Ni content of the whole-rock to be used together with the Ni content in the most Fo-rich olivine to calculate temperature using DN_{iol}/liq (Pu et al., 2017). The results range from 1080-1247°C for basalts with 7-13 wt% MgO, whereas those calculated using DM_gol/liq give from 1177-1316 °C. The lower DN_{iol}/liq temperatures reflect the effect of water, which lowers the temperature of the olivine liquidus. In contrast, the DM_gol/liq thermometer gives temperatures that are too high (i.e., anhydrous conditions) because a correction for H₂O is needed. In this study, DN_{iol}/liq temperatures are combined with analyses of plagioclase in several basalts with ~7 wt% MgO, which enables the plagioclase-liquid hygrometer to be applied to the most calcic plagioclase in each sample. The results lead to melt water contents (≥ 2 wt%) that are consistent with those determined by direct analysis in Gazel et al. (2012).

Hans Brenna, Kirstin Krüger, Steffen Kutterolf

Submission 236

Halogen and sulfur rich explosive eruptions in the tropics: A potential threat to the future ozone layer? Halogen and sulfur rich explosive eruptions in the tropics

Large Plinian volcanic eruptions can inject large amounts of atmosphere-relevant gases (e.g. S, Cl, Br) and solid particles (e.g. ash) into the stratosphere. If those eruptions occur in the tropics, they can have a global impact due to the dispersal through the large scale meridional overturning circulation. Most modelling studies concentrate on the sulfate aerosol effects on climate and ozone. In contrast, the role of volcanic halogens from tropical eruptions is believed to play an insignificant role for the global atmosphere, based on observations from the recent El Chichon and Pinatubo eruptions. New results regarding the halogen release by paleo Plinian eruptions, as well as recent volcanic plume observations and model simulations facilitate our investigation into what effect the combined chlorine and bromine emissions from large tropical eruptions have on ozone and the atmosphere in general.

Here, we present the first modeling study of combined chlorine and bromine from tropical halogen and sulfur rich volcanic eruptions using a state-of-the-art coupled chemistry climate model. A complete halogen and sulfur data set for the last 200 ka, derived by the petrological method from paleo-eruptions of the Central American Volcanic Arc (CAVA), is used to force simulations with WACCM (Whole Atmosphere Community Climate Model). Based on the petrological data we simulated 3 forcing scenarios: Sulfur, halogen and combined injections. The goal is to quantify the impact of volcanic halogen and sulfur on the preindustrial atmosphere when the background chlorine level was low compared to the present day with the main focus on stratospheric ozone. We carried out 5 model simulations of each of the 3 forcing scenarios assuming that 10% of the Cl and Br emitted from an average CAVA eruption is injected into the tropical stratosphere during January. The model response reveals a global impact on the ozone layer affecting, through radiation, atmospheric circulation for more than 7 years. Total ozone drops below 220 DU, the present-day ozone hole threshold, in the tropics, Arctic and Antarctica. The increase in biologically active UV caused by the global ozone depletion is found to be more than 80% over much of the northern hemisphere during the first two years post eruption. Given the current decline in anthropogenic chlorine, halogen and sulfur rich explosive tropical eruptions may result in a major threat to the ozone layer in future.

Marco Brenna, Shane Cronin, Ian Smith, James Scott, Elaine Smid

Submission 591

Rapid magma ascent following complex storage in the monogenetic Auckland Volcanic Field

Eruptions in monogenetic volcanic fields are unpredictable both spatially and temporally. Nonetheless as magma makes its way to the surface to erupt seismic signals are produced, which can give some indication of unrest. The timescale between initiation of unrest and eruption onset is not clear, and depends on magma ascent rates. Understanding these relationships is paramount when eruptions may occur within densely populated areas such as the city of Auckland, New Zealand. Auckland is situated within the confines of the Auckland Volcanic Field consisting of 53 eruptive centres active over the last 250 kyrs.

Magma ascent rates can be estimated in monogenetic basaltic volcanoes by investigating their crystal cargo. Olivine xenocrysts from the mantle lithosphere that have been entrained by the ascending basaltic magma are not in equilibrium with the melt, and will therefore exchange chemical elements with the host through diffusion. The time necessary for this process to occur can be quantified through element diffusion modelling, and hence a residence time for the mantle xenoliths and xenocrysts can be estimated.

We sampled a suite of olivine xenocrysts from a strombolian fall deposits at Pupuke Maar, in the Auckland Volcanic Field to understand the magma ascent mechanisms and duration from mantle depths. Olivine xenocrysts have forsteritic cores (Fo#91-92) and chromian spinel inclusions indicative of their upper mantle origin, as opposed to ultramafic portions of the Dun Mountain belt present in the crust beneath Auckland. Diffusion profile lengths range from few tens of microns up to ~200 microns. Fe-Mg, Ca, Ni and Mn diffusion modelling of the observed profiles results in residence times for the mantle derived xenocrysts of mostly less than a week. A few crystals have more complex diffusion profiles that may indicate longer periods of storage up to two years and interaction with magmas with different compositions.

We propose a model for the plumbing system of Pupuke volcano, applicable to other monogenetic basaltic volcanoes which display similar chemical and petrologic variability, in which magmas ascend from their mantle source and interact with magmas with variable composition derived from different levels within the mantle. Trigger for ascent is given by the arrival of a final magma batch, generally more alkaline, which raises rapidly and promotes ascent of other ponded magmas.

Christopher Bronk Ramsey, Victoria Smith, Rebecca Kearney

Submission 511

The RESET tephra and INTIMATE chronological databases: Resources for tephrochronology and volcanology

The RESET and INTIMATE databases contain a lot of detailed geochemical and chronological information that could be exploited by volcanologists. The RESET database includes glass chemistry data from all the large eruptions in Europe in the Late Quaternary. The database of glass (melt) compositions developed for tephra correlation includes data generated for the RESET project and some previously published data. The dataset includes more than 22,000 major analyses and nearly 4000 trace element analyses of individual glass shards. These glass analyses are from proximal (sampled vertically through eruption sequences) and distal deposits of approximately 240 eruptions from volcanoes all over Europe, including the productive centers in Italy, Iceland, Greece, and Turkey. The database also includes secondary standard data from each analytical run providing information on accuracy. Tools for plotting and comparing the geochemical data are available in a web-based application associated with the database.

This RESET database is linked to the INTIMATE chronological database, which was initially developed to generate chronological sequences for environmental research. The INTIMATE database includes information of tephra occurrences in a range of sedimentary archives (paleoenvironmental sequences and archaeological sites) and ice cores. Tephra in these records can be used to constrain the age of the eruptions and provides insight into the dispersal of tephra.

Both of these databases are being developed further, including the addition of interfaces to extract data in JSON format, and tools for users to work with data in the database, stored in their own work area, or held on other data servers. These developments, along with the ability to transfer data through JSON files, should make sharing of the wider geochemical dataset for volcanology and tephrochronology much simpler for researchers.

References:

RESET database: <http://dx.doi.org/10.1016/j.quascirev.2014.11.008>

INTIMATE database: <http://dx.doi.org/10.1016/j.quascirev.2014.05.028>

Ermanno Brosch, Gert Lube, Eric Breard, Kevin Kreutz, Jim Jones, Tomaso Esposti Ongaro

Submission 954

Synthesizing hot pyroclastic surges to link flow dynamics and deposit characteristics

Dilute pyroclastic density currents (dPDCs) are fully turbulent fast-moving mixtures of particles and gas that travel great distances and surmount topography. Their high frequency of occurrence, high velocities, dynamic pressures and temperatures in combination with their ability to overcome large topographic obstacles generate high hazard potential globally.

Because pyroclastic surges are too dangerous to probe in real-life, there are no quantitative data to study their inner workings directly. On the other hand, current models of dPDCs, which are derived from first principles, are still difficult to validate, because of the incomplete knowledge of the small-scale, internal dynamics and of initial/boundary conditions. Comparison of model predictions with the sedimentary characteristics of dPDC deposits thus remains mostly qualitative, as the relationships between flow dynamics and deposit characteristics are largely unknown.

Here we present results of large-scale experimental simulations of pyroclastic surges at the eruption simulator PELE in New Zealand. We generated a range of dynamically-scaled dPDC flow conditions through systematic variation of the following parameters: temperature difference between flow and ambient air, substrate roughness, substrate erosivity and flow confinement. Other experimental parameters such as initial mass, mass flux, velocity and grain-size distribution are kept constant to allow comparison. More than 200 sensors capture the gas-particle transport and sedimentation characteristics over a surge runout length of up to 35 m. Aside from time-series data of the temperature, turbulence, velocity and concentration fields, we obtain high-speed video sequences of the deposition mechanisms and deposition rates as well as data of the flowing and depositing grain-size distribution.

In all experiments we observe alternation between erosion and deposition events, whose positive and negative deposition rates vary by more than four orders of magnitude. We visualize how these lead to the formation of a broad spectrum of natural deposit characteristics, including erosive unconformities, low-angle regressive and progressive dune bedforms, massive and graded beds, laminated beds and lapilli covers. We also identify a standard deposit unit for surges, which we link to the space- and time-variant flow structure, and which can be used to interpret natural deposits quantitatively.

Sarah Brown, Steve Sparks, Anna Stewart, Jenni Barclay, Carolyn Driedger, John Pallister, Elizabeth Westby, Gill Jolly, Julian Thomson, Katcho Karume, Mony Murongani, Jean-Christophe Komorowski, Iain Stewart, Patricia Mothes, Richie Robertson, Stacey Selm

Submission 57

VolFilm: educational films to increase resilience to risks from volcanic hazards

Many volcanoes erupt infrequently and many have had no eruptions in living memory. Communities near such volcanoes can have increased vulnerability due to their inexperience of volcanic hazards, lack of preparedness and knowledge of hazards and risk. The VolFilm project brings together volcanologists and film-makers to develop a series of short educational films on volcanic hazards, impacts and the experiences of communities in past eruptions or living with volcanic activity. Film is a very effective tool for communicating risk knowledge. The films are freely available to all, online and through project partners in a variety of languages. They are designed to be a useful educational tool for volcano observatories and those responding to developing volcanic emergencies, as a simple product that can be used to educate and distribute amongst local at-risk populations. The films are intended for a global audience, as about one tenth of the world's population are exposed to volcanic hazards, but are chiefly aimed at communities living or working near volcanoes with little or no experience of volcanic hazards. The aim is to inform and empower these communities to respond appropriately to volcanic activity and to reduce the impacts to their lives and livelihoods. Basic methods for self-protection and mitigation are included and further resources are made available through an accompanying website.

Phase 1 of the project saw the development of films on pyroclastic flows and lahars, as these are the volcanic hazards that historically have been responsible for the greatest loss of life. Phase 2 sees the creation lava flows, ash fall and gas hazards films. These historically have resulted in fewer casualties, but considerable disruption and economic losses. A simple questionnaire was used to evaluate the efficacy of the first films, in community groups and amongst partners in the UK, USA, Reunion, France, Vanuatu, St. Lucia, Ecuador and Turkey. The response was positive, with most agreeing that their knowledge had been improved by the films and that the films prompted consideration of their own evacuation plans.

We will discuss the films, dissemination plans, feedback received and lessons learned, and seek input from the volcanological community to ensure that the relevant information is effectively conveyed and the films efficiently disseminated, to both help save lives and improve the lives of those living alongside volcanoes.

Richard Brown, Brian Bell, David Reynolds, Sam Clark, Jonny Dietz, Clayton Grove, Richard Hobbs, Dougal Jerram, Niall Mark, Simon Passey, Bansri Raithatha, Heather Rawcliffe, Peter Reynolds, Oliver Sanford, Nick Schofield, Richard Walker, Sapphire Wanmer,

Submission 774

Unravelling the Impacts of Volcanic and Intrusive Igneous Rocks on Hydrocarbon Systems in Sedimentary Basins: examples from the North Atlantic

Hydrocarbon exploration in sedimentary basins containing volcanic and intrusive igneous rocks faces significant extra risk than non-volcanic basins. That risk derives from: (1) the effects of igneous rocks on the thermal history of basins and thus on the efficacy of initial hydrocarbon generation and maturation; (2) on complications arising from the poorly understood porosity and permeability values and diagenetic history of geochemically complex volcanic and intrusive igneous rocks (lava flows, intrusions and volcanoclastic sediments); (3) poor understanding and predictability of volcanic facies associations in mixed volcanic-sedimentary environments and of volcanic rock distribution; and (4) geophysical masking of target hydrocarbon traps by thick layers of volcanic sequences (e.g. lava flows, hyaloclastites). Subsurface exploration is costly and is largely achieved with remote datasets. Field-based studies of onshore volcanic rocks can provide critical insights into volcanic rock properties and facies distributions, and can significantly help improve, refine and de-risk exploration, and build more realistic 3D models. Here we present examples from the Faroe-Shetland Basin, North Atlantic: a hydrocarbon-bearing basin containing igneous intrusions and volcanoclastic and pyroclastic rocks, and which is locally covered by up to several kilometre thick basaltic lava flows. We demonstrate how analogue field studies have helped refine the geological understanding of the basin and improve the understanding of the roles that volcanic and intrusive igneous rocks play in hydrocarbon systems.

Karalee Brugman, Christy Till

Submission 1211

Investigation of the Applicability of Clinopyroxene Geothermometers to Silicic Igneous Systems

Clinopyroxene's widespread occurrence—it is found in both igneous and metamorphic rocks and in low- and high-silica systems, as well as in meteorites—means the mineral has the potential to be a powerful tool for petrologists seeking information about the P-T-X history of a system or sample. There is broad variability in clinopyroxene compositions in igneous systems, beyond what is represented in the traditional pyroxene quadrilateral, but a limited range of these compositions has been investigated experimentally. It is thus important to understand the validity of different petrologic tools to the range of clinopyroxene in natural igneous systems. We investigate the utility of different geothermometers for application to a range of clinopyroxene found in silicic igneous systems, and use Fe-rich clinopyroxene from the Scaup Lake flow from the high-silica Yellowstone Caldera as a case study. Scaup Lake clinopyroxene is distinctive in that it is moderately high in FeO_{tot} ($\text{Mg\#} = \sim 56$) but very low in Al_2O_3 (0.53–0.73 wt%), a composition not well represented in experimental data, and thus not calibrated for when developing geothermometers. Natural clinopyroxenes of a similar composition are found in the Rattlesnake Tuff (~ 0.35 wt% Al_2O_3), Bandelier Tuff (0.28–0.91 wt% Al_2O_3), Paektu Millennium eruption pumice (0.14–1.78 wt% Al_2O_3), and Pantelleria trachyte (0.25–0.72 wt% Al_2O_3). Of the existing geothermometers, PyMELTS (Sack and Ghiorso, 1994a, b, c) is calibrated on a range of similarly Fe-rich clinopyroxene to those in silicic igneous systems, however, these pyroxenes are significantly more enriched in Al_2O_3 (5.4–14.75 wt%) compared to those from Yellowstone. Furthermore, as the post-caldera magmatic system at Yellowstone has evolved, clinopyroxene compositions have diverged further from the bulk of experimental clinopyroxene data (e.g., become even higher in FeO_{tot} and lower in Al_2O_3), exemplifying the need to identify a fitting geothermometer to use to calculate temperature from Fe-rich clinopyroxene in silicic igneous systems.

Hannah Buckland, Julia Eychenne, Katharine Cashman, Alison Rust

Submission 292

Relating the physical properties of volcanic rocks to the characteristics of ash generated by experimental abrasion

Within the hot and turbulent flow of a pyroclastic density current (PDC), interactions between clasts generate volcanic ash. This co-PDC ash can be dispersed to the atmosphere presenting a risk to aviation. Moreover, due its small grainsize it is often the furthest travelled ash from an eruption.

We designed a series of experiments that imitate natural abrasion to determine the effects of pyroclast vesicularity and crystal content on the efficiency and type of ash generated by abrasion. Two different pyroclastic materials were used in the experiments: (1) basaltic-andesitic pyroclasts from Fuego volcano (Guatemala) with ~26-46% vesicularity, high phenocryst and microlite content and (2) tephri-phonolite Avellino pumice (Vesuvius, Italy) with ~55-75% vesicularity, intermediate-low phenocryst content and low groundmass crystallinity.

Bimodal grain size distributions were produced by the experimental abrasion with fine ash modes between 4 and 5 ϕ . The low density vesicular Avellino pumice typically generated more ash than the Fuego pyroclasts. However, we found that the ash generating potential of a single pyroclast can be independent of density, and is instead governed by differences in crystallinity and vesicularity. Heterogeneities in crystal content also increased the likelihood of Avellino clasts splitting which can enhance abrasion efficiency.

Pyroclast vesicularity and crystallinity influences the componentry and shape of ash generated by abrasion e.g. vesicular irregularly shaped Avellino ash versus groundmass-dominated blocky Fuego ash. Although abrasion can also alter ash shape by reducing grain roughness, we find that the Adherence Factor of attached matrix on phenocrysts best distinguishes between ash samples that have experienced different degrees of abrasion. Low Adherence Factor values for Avellino ash, in particular, demonstrate the efficient matrix stripping of the low crystallinity vesicular melt.

The results of the abrasion experiments highlight the need to evaluate the vesicularity and crystal content of pyroclasts to predict the potential for co-PDC ash formation in a PDC. We conclude that abrasion is an effective mechanism for generating fine ash as the experimental grain size data reproduces natural co-PDC fine ash modes that are ~5 ϕ (30 μ m).

David Buesch, Olivier Roche, Greg Valentine

Submission 439

Locally derived clasts, topography, and clasts high in stratigraphic sections of the ~18.8 Ma Peach Spring Tuff, southwestern USA

Lithic clasts in many ignimbrites vary in size, abundance, and composition within the deposits, and some clasts can be correlated to local sources whereas others cannot, so the question is “can locally derived clasts help with understanding flow processes in pyroclastic flows?” The ~18.8 Ma Peach Spring Tuff ignimbrite resulted from an eruption in the Silver Creek caldera, has a dense-rock equivalent volume of ~1300 km³, and the pyroclastic flow traveled more than 150 km west and east of the caldera. Roche et al. (2016) described field examples of locally derived clasts in the ignimbrite where the parent pyroclastic flow traversed alluvial deposits; that work focused on clasts in the lower few meters of the deposits. Analog laboratory experiments with fine (80 microns) and coarse (1600 microns) showed how clasts were captured, lofted into and transported by the flow, and then were deposited on an aggrading bed at the base of the flow. These processes occur in the lower and denser gas-particle parts of the flow, and result in a “zone of entrainment” with a critical flow velocity for different particle sizes. Once pyroclastic flow deposits cover the substrate, how do clasts continue to be incorporated into the flow and then get deposited high in the accumulated section? Topographic highlands (possibly with varied rock types) in a pre-eruptive landscape typically project well up into a flow, and can be the source area for local substrate-derived clasts. During the initial encounter of a density stratified flow, the part with the highest density and capability of forming a zone of entrainment for larger clasts is restricted to the valley bottom and lower elevations of the adjacent highlands, whereas the middle to upper parts of the flow could have zones of entrainment for smaller clasts. As aggradation of the deposits progresses, the highest density parts of the flow (as do all parts of the density stratified flow) migrate up the flanks of highlands thereby exposing higher elevations to the clast-size-specific zones of entrainment and greater carrying capacity. Once clasts from higher on the slopes are entrained, they are transported out across the aggraded valley-filling deposits. This process continues until the pyroclastic flow wanes and results in deposits that contain relatively large substrate-derived clasts distributed throughout, even at the highest stratigraphic levels and far from their outcrop sources.

Steffi Burchardt, Octavio Palma, Olivier Galland, Karen Mair, Dougal Jerram

Submission 622

Syn-emplacement ductile/brittle deformation within the Cerro Bayo laccolith, Chachahuén volcano, Argentina

When viscous magma intrudes at shallow depth in a volcanic edifice, it can form dome-shaped intrusions, called laccoliths or cryptodomes. Laccoliths form when sills inflate and lift the overlying rocks, which initially produces a mushroom-shaped intrusion. Successive inflation of the laccolith increases the stresses at the lateral ends of the intrusion, which may lead to faulting, producing a steep-sided or “punched” laccolith geometry. Generally, punching-related deformation, such as fracturing and faulting, has been assumed to occur in the host rock only. However, here we present field evidence indicating that host-rock deformation is not the only significant mechanism of strain accommodation during laccolith emplacement.

We studied four laccoliths composed of evolved andesite emplaced within lavas and pyroclastic flows of the Miocene Chachahuén Volcano, Argentina. Despite the size of the laccoliths (hundreds of m - 1 km across), their host-rocks show little evidence of deformation, such as upbending or faulting, whereas the laccoliths themselves contain considerable amounts of brecciated laccolith rock. Detailed mapping of the Cerro Bayo laccolith shows that the breccia forms a thick belt at the outer laccolith margin opposite of what we identified as the laccolith feeder. Magma inflow in Cerro Bayo can be traced by abundant flow indicators, such as flow banding. The relationship between the flow banding and the breccia suggests that brecciation occurred during laccolith inflation. A sharp boundary between the breccia and the essentially unfractured laccolith interior may indicate that brittle deformation during inflation was not simply due to cooling. A strain-related rheology change may offer a potential explanation for our observations.

The mechanics of laccolith emplacement should therefore be reevaluated taking into account strain in both the host-rock and the intrusion itself.

Yannick Buret, Joern-Frederik Wotzlaw, Stan Roozen, Marcel Guillong, Albrecht von Quadt, Christoph Heinrich

Submission 325

Volatiles at the plutonic - volcanic connection: An example of an explosive eruption terminating porphyry copper ore formation

Bridging the gap between the plutonic and volcanic realms is essential for understanding a variety of magmatic processes from caldera-forming eruptions to the formation of porphyry copper deposits. Porphyry copper deposits are commonly associated with large and long-lived volcanic centers, but the temporal and dynamic link between mineralized intrusions and volcanic eruptions has remained controversial. Based on the combination of high precision zircon U-Pb geochronology and trace element geochemistry with plagioclase textures we discovered an intimate connection between ignimbrite eruption and a nearby world-class porphyry deposit (Bajo de la Alumbrera in the Late Miocene Farallón Negro Volcanic Complex of Argentina). Our results indicate that the magmatic-hydrothermal deposit and explosive volcanism were derived from a common magma reservoir that evolved over a minimum duration of 200 k.y. before the final eruption. We show that the volcanic pile represents the inverted magma reservoir, recording systematic differences in plagioclase textures and juvenile clast content from bottom to top, suggesting that deposit formation and volcanic eruption were both triggered by the injection of a volatile-saturated primitive magma into the base of the magma chamber. A short, but significant time-gap of ~20 k.y. between porphyry mineralization and the onset of explosive volcanism indicates a minimum duration of magma rejuvenation that led to the explosive eruptive event. This previously undocumented genetic relationship between porphyry copper formation and explosive volcanism allows us to track the volatile evolution of the upper crustal magma reservoir prior to both events. Catastrophic loss of volatiles by explosive volcanism terminated the ore forming capacity of the upper crustal magma chamber, as evidenced by the intrusion of a syn-eruptive barren quartz-feldspar porphyry. Our results demonstrate that porphyry copper deposits provide critical information to understand how volatiles control the fate of hydrous magmas, between pluton formation and explosive volcanism.

Seth Burgess, Jonathan Hagstrum, Michael Sawlan, Jorge Vazquez, Matthew Coble, Terrence Blackburn

Submission 362

Constraining the rate and duration of Columbia River flood basalt magmatism using coupled SHRIMP-RG and CA-ID-TIMS U-Pb zircon geochronology

Accurate and precise radiogenic timing and tempo models for large igneous province (LIP) magmatism provide critical constraints on the location and processes of LIP melt generation, and on the efficacy of magmatism as a driver of environmental change. Although a powerful constraint, obtaining maximum achievable age accuracy and precision is difficult, and on Cretaceous and older LIPs where these models exist, maximum age precision ($\sim 0.02\%$) is insufficient to resolve dates on successive flows or flow groups, which limits interpretation. The Columbia River flood basalt province (CRB) is well preserved, exposed, and characterized with respect to geochemistry, petrology, and paleomagnetism and the maximum precision on radiometric dates potentially can reach the ~ 3 ky threshold due to its young age (~ 16 Ma). Temporal resolution at this threshold has yet to be realized for the CRB due to the absence of zircon in CRB lavas. Zircon-bearing silicic tephra/ash deposits are intercalated with CRB lavas, however, and provide an opportunity for application of high-precision U-Pb dating techniques. Development of an age model with maximal precision is predicated on (1) isolating and dating autocrystic zircon from silicic tephra/ash deposits via CA-ID-TIMS U-Pb geochronology, (2) dating tephra that bracket both narrow and extended stratigraphic intervals, and (3) integrating the new U-Pb dataset with existing $^{40}\text{Ar}/^{39}\text{Ar}$ datasets to build an accurate and comprehensive age model.

Toward this goal, we have isolated zircon from silicic ash beds intercalated with the upper half of the Grande Ronde Basalt (GRB) from well-characterized stratigraphic sections. To mitigate zircon contamination via pre-/syn-/post-eruptive admixing, we employ the Stanford-USGS SHRIMP-RG U-Pb technique, and follow this work with dating of identified zircon autocrysts via CA-ID-TIMS at the University of California at Santa Cruz. Coupled SHRIMP-RG and TIMS analysis on the same crystals provides (1) relatively rapid initial age determinations, (2) identification of a single age population representative of the time of eruption, (3) trace-element characterization of crystals, and (4) weighted mean dates precise to the

Alain Burgisser, Laure Chevalier, Marielle Collombet

Submission 407

Upgrading conduit flow models with coalescence, percolation, and permeability laws

During eruptions involving viscous magma, the changes that ascent imposes on the magma flowing up the conduit are dominated by retro-actions between ascent rate, bubble growth, coalescence, and gas escape. Numerical models, which are useful guides to explore such intricate retro-actions, are now bi- or multiphase, and they have not only been fed by experimental data but also inspired new research directions. It is now commonly accepted that separation from the connected network of growing bubble is a process that involves both horizontal and vertical directions. To date, three types of 2D conduit flow models have been proposed. The first type focuses on crystallization and does not include gas escape and the second type includes outgassing but not gas escape through conduit walls. The third type, which we treat herein, attempts to take into account both outgassing and gas escape through the walls.

We show how recently proposed laws of bubble coalescence, percolation and permeability have the potential to be integrated into the third type of conduit flow models. We describe coalescence thanks to a kinetic model that statistically describes the growth by decompression, exsolution and coalescence of a polydisperse population of gas bubbles in a silicate melt. The model tracks the time evolution of the distribution of bubble mass and volume. We formulate four coalescence mechanisms: thinning of the inter-bubble planar films, film deformation by differential bubble pressure, coalescence-induced, and buoyancy-driven collision. These four kernels yield distinct evolutions of the size distributions, and we show how they can be integrated into the conduit flow model.

We describe percolation thanks to analyses of 3D tomographic images of bubbles produced by decompression experiments. Our percolation threshold formulation recovers the behavior of a wide range of volcanic samples by separating permeable samples from impermeable ones with a success rate of 88%. We use this threshold to propose simplified permeability laws that can be integrated into the conduit flow model. These laws are valid within one order of magnitude for the viscous permeability coefficient and within two orders of magnitude for the inertial coefficient. They recover the ranges of values previously covered by isolated laws, reassembling disjointed sets of measurements within a single framework.

Dale Burns, Shanaka de Silva, Frank Tepley

Submission 1182

From the crystal to the arc: Using crustal forensics to understand the development and evolution of continental magmatic arcs

The pressure-temperature-time pathways associated with continental arc magmas can be very difficult to evaluate owing to complex interactions between ascending mantle-derived melts and the overriding continental lithosphere. In the past 25 years, pioneered by Jon Davidson, the advent and proliferation of techniques that utilize compositional and isotopic information from individual crystals has greatly enhanced our understanding of these systems. In this study, we build on Jon's early efforts at crustal forensics and utilize a combination of in situ intra-crystalline radiogenic isotope ratios and mineral thermobarometry to determine how P-T-t pathways changed over the lifetime of the Purico-Chascon Volcanic Complex (PCVC) in northern Chile. The PCVC is of particular interest as it records the transition from flare-up to steady-state arc magmatism over ~800 kyr. The transition recorded at the PCVC is characterized by a progression from erupting large volumes (~100 km³) of homogeneous crystal-rich dacite ignimbrite 1.0 Ma, to erupting small volume (3), basaltic-andesite to dacite lava domes by 0.2 Ma. Crystals within the ignimbrite have high, restricted radiogenic isotope ratios and major element compositions consistent with prolonged storage and considerable magmatic contributions from the upper continental crust (no mantle signatures were preserved). In contrast, crystals from the late-stage lava domes are isotopically and compositionally heterogeneous, with some crystals exhibiting clear upper mantle/lower crustal affinities. The crystal-scale variations observed in the PCVC record the thermal death (i.e., cooling) of a large upper crustal MASH zone that had been active in the region since ~10 Ma. Magmatism at the PCVC is microcosm for activity in the central Andes, where from 10-4 Ma magmatism was dominated by a large regional ignimbrite flare-up. Since 4 Ma, eruption rates and eruptive volumes have decreased and magmatic activity appears to have returned to a steady-state more typical of continental arcs globally. Interestingly, the entire transition from flare-up to steady-state is recorded in single crystals from the PCVC. Plagioclase crystals in the late-stage lava domes have interiors with isotopic and compositional signatures consistent with crystal growth in an upper crustal flare-up magma. These interiors are surrounded by growth rims with distinct upper mantle/lower crustal signatures characteristic of regional steady-state magmatism.

Mike Burton, Antonio Chiarugi, Francesco D'Amato, Silvia Viciani, Manuel Queisser, Gayatri Marliyani, Ferian Anggara, Agung Harijoko

Submission 773

New constraints on volcanic CO₂ emissions from Java, Indonesia

One of the main objectives of the ERC-funded CO₂Volc project was the airborne measurement of volcanic gas emissions from volcanoes in Java, Indonesia, for which limited flux information is available. This provides a snapshot of volcanic CO₂ emissions from a large proportion of the Banda-Sunda arc, and allows comparison with models of CO₂ subduction and recycling. This airborne campaign required the development of a new suite of volcanic gas instruments, capable of high frequency (2-5 Hz), high precision and high accuracy, whilst measuring multiple gases, including H₂O, CO₂, SO₂, HCl and HF. This development work has been completed successfully, with a suite of four instruments capable of measuring the target gases at the concentrations expected in dilute volcanic plumes. The airborne campaign was conducted in September 2016, following a complex permitting process, using a fixed wing aircraft. Gas measurements were conducted on 18 volcanoes and one mud volcano complex. Here we present the results of this survey, and use them to assess the CO₂ release from subduction processes along the Banda Sunda arc.

David Butterfield, Marvin Lilley, John Lupton, William Chadwick

Submission 1234

Estimates of magmatic CO₂ flux at Axial Seamount using magmatic and hydrothermal budgets

In the effort to monitor subaerial volcanoes for public safety and scientific understanding, techniques have been developed to monitor and quantify the flux of magmatic gases (SO₂ and CO₂) to the atmosphere. Changes in magmatic gas flux to the atmosphere can signal increased magmatic activity. The subaerial spectral techniques do not work under water and no practical methodology has been implemented to monitor chemical mass flux or heat flux from submarine volcanoes. Consequently, there is virtually no information on how and when magmatic gas is transported from magma chambers to the overlying ocean at mid-ocean ridge volcanoes. Until the large technical obstacle of monitoring heat and chemical mass flux in near real-time from a submarine volcano is overcome, alternative methods may help constrain the transfer of magmatic gases from magma chamber to ocean. Here we compare CO₂ mass flux estimates from independent geophysical/geochemical and hydrothermal approaches. The CO₂ mass flux calculated from magma delivery rates is similar to the estimated total hydrothermal CO₂ mass flux (~20 to 200 mol CO₂ per second), suggesting that a large fraction of the magmatic CO₂ is transported by the steady-state hydrothermal system. Furthermore, eruptions at Axial Seamount may not be associated with massive bursts of magmatic CO₂. Axial Seamount is arguably the only submarine volcano with enough data to take this approach, and because it is the site of a fiber-optic cabled observatory, it may become the first submarine volcano with near real-time heat and mass flux monitoring capable of directly observing the transient effects of a mid-ocean ridge eruption.

Paul Byrne

Submission 242

The volcanic histories of Mercury and the Moon are distinct from those of Earth, Mars, and Venus

Recent spacecraft observations of Mercury have shown that large-scale effusive volcanism—a major process by which the planet’s crust was built—came to an end within the first billion years after accretion. Further, most flood basalts emplaced toward the end of this phase were restricted to pre-existing impact structures. This record of volcanism is similar to that of the Moon, where the bulk of volcanic activity had concluded by about 3 Gyr ago and was constrained to antecedent impact craters and basins; indeed, the majority of the lunar surface is a flotation crust, rather than being volcanic in nature. Yet the volcanic histories of Earth, Mars, and Venus are markedly different. On Earth, effusive volcanism and the production of oceanic crust takes place today (albeit at substantially lower rates than in the Archaean). Mars also has a protracted history of effusive volcanism: the youngest flows on the planet are only a few million years old, but much of the mighty Olympus Mons volcano was emplaced by 2.4 Gyr ago, and some of the oldest portions of the planet’s crust are volcanic. And on Venus, a conspicuous dearth of impact craters suggests an average surface age of about 700 Myr, with vast, effusive volcanism the dominant resurfacing mechanism; moreover, the second planet may still be volcanically active. Importantly, both Mercury and the Moon have experienced long-lived global contraction arising from interior secular cooling, a process likely to have begun relatively early on. Superposition relations of tectonic and impact structures on Mercury indicate, for example, that the onset of global contraction was coincident with the end of widespread volcanism, which is consistent with decades-old models of that planet’s thermal evolution. The evidence for long-lived volcanism on Earth, Mars, and Venus suggests that global contraction, should it have operated at all, has not affected these worlds to the same extent as it did Mercury and the Moon, possibly because of these bodies’ larger masses and greater absolute amounts of heat-producing elements in their mantles. If so, then the threshold for a planet to experience a multi-billion year record of effusive volcanism from radiogenic heating may correspond to a mass somewhere between that of Mercury and Mars. Quantifying this threshold will improve our ability to predict the geological properties and processes of terrestrial-sized extrasolar planets.

Haley Cabaniss, Patricia Gregg, Eric Grosfils

Submission 348

Tectonic triggering of large caldera eruptions in the Taupo Volcanic Zone

Many have documented an apparent relationship between the abundance, volume, and chemistry of collapse-caldera eruptions and the localized tectonic regime in which they are found. The observed correlations suggest a link between tectonic setting and eruption triggering mechanisms, which may indicate the potential for far-field tectonic stress to either trigger eruption or promote stable storage conditions of large silicic magma reservoirs. To investigate the role of tectonic stress in the evolution and longevity of shallow magma bodies, we utilize 3D temperature-dependent viscoelastic finite element models (FEM) of an expanding magma reservoir undergoing regional extension or compression. The mechanical response of the host rock to tectonic stresses is calculated to predict the maximum eruption recurrence intervals and magma flux rates that large collapse caldera systems (>100 km³ reservoirs) may experience before system failure is attained as determined by through-going Mohr-Coulomb Failure, excessive overpressures (> 40 MPa), or tensile failure of the magma reservoir boundary. A series of numerical experiments are conducted to evaluate the impact of varying magma flux rates (0.0001 km³/yr – 0.15 km³/yr) and tectonic stresses (5-20 mm/yr of extension and 5-20 mm/yr of compression) for a variety of magma reservoir sizes (1 km³ – 105 km³). Numerical results indicate that regional extension decreases the stability of the roof-rock overlying a magma reservoir and may promote early-onset of caldera collapse. Alternatively, applying moderate amounts of compression (\leq 10 mm/year) on relatively short time scales (3/year, our models reproduce observed Taupo recurrence intervals of 24,700 yrs to within a few thousand years. These analyses provide further constraints on maximum recurrence intervals and magma generation rates, and offer insight into tectono-magmatic generation dynamics for a variety of reservoir sizes and stress regimes.

Ryan Cahalan, Josef Dufek

Submission 939

What controls pumice raft development? Numerical modeling of pumice transport during subaqueous eruptions

The relationship between heat transfer and pumice transport in the presence of water is an important topic to the volcanological community. Experiments show that cold pumice introduced to water can remain afloat for days to months, whereas heated pumice sink in seconds. However, in the case of the 2012 Havre Seamount eruption the majority of erupted pumice was transported through ~900 m water to form extensive pumice rafts at the surface (Jutzeler et al., 2014). Thus, a disparity exists between experiments and field observations that precludes proper evaluation and interpretation of deposits, and can lead to underestimation of erupted volumes and associated hazards from subaqueous eruptions.

We have developed a numerical model to independently assess the physical processes leading to this disparity. This calculation adapts an Eulerian-Eulerian-Lagrangian (EEL) approach for submarine environments and includes clast scale heat transfer, disequilibrium bubble growth, hydrous phase change, and advection through porous media (Syamlal, 1987; Dufek and Bergantz, 2007; Benage et al., 2014). The heat transfer model has been verified against an analytical model for spherical conduction and external convection, and compared to pumice-scale experiments. Modeled simulations cover a range of clast sizes, vesicularities, vesicle distributions, and eruption conditions to identify the dominant controls on pumice transport and to quantify mass partitioning in the water column.

The modeled results yield insight to subaqueous eruption transport dynamics and quantitative estimation of the amount of erupted material transported away from the near-source region. We can now begin to preemptively assess a subaqueous eruption's potential impact on maritime shipping and navigation, and local biota due to rafting pumice.

Emily Cahoon, Martin Streck

Submission 69

Reevaluating distribution area and composition of the Picture Gorge Basalt CRBG, eastern Oregon

Our focus is on un-studied, yet extensive, mid-Miocene basaltic lavas and dikes exposed between the southern extent of the known Picture Gorge Basalt (PGB) and the northern extent of Steens Basalt in a wide corridor of the Malheur National Forest, eastern Oregon. The age of sampled basaltic units is indicated by stratigraphic relationships to the 16 Ma Dinner Creek Tuff. These basaltic lavas provide an opportunity to revisit distribution area for either CRBG unit and explore the petrogenetic transition between them and the Miocene Strawberry Volcanics located immediately east of our study area. How PGB relates to other CRBG units has been debated over the years with one view that PGB is sourced from a discrete, back-arc like mantle distinct from other main phase units.

New compositional data from our study area indicate numerous basaltic lavas can be assigned as PGB, but also to a compositionally transitional group. This 'transitional' group has a large-ion lithophile and high-field strength element signature similar to the Strawberry Volcanics, and a heavy rare earth element signature similar to the Upper Steens Basalts. This transitional signature and the geochemical variability of individual lavas (as opposed to compositional averages of basalt members) suggest mantle sources of PGB and Steens Basalt are gradational rather than distinct. On a Ba/Th vs La/Ta plot, our samples fall within the Steens and PGB fields but also span the distance in between these fields. Geographically, samples with PGB composition extend lava flows and dikes of this CRBG unit much further south/southeast- and northeastward closing the exposure gap between PGB and Steens Basalt, and PGB and Imnaha Basalt, respectively. What has been viewed as Steens Basalt along the southern margin of our study area is in fact PGB and these exposures may have extended eastward into the Malheur Gorge where we find lavas with PGB compositions below local Grand Ronde equivalents (Birch Creek flows). We can also extend PGB distribution eastward from the John Day valley with identifying PGB compositions at the base of Dooley Mountain near Baker City.

The broader significance of this work will be to revise distribution area of PGB and to obtain a clearer picture of spatial relationships and character of mantle reservoirs for PGB, Steens Basalt, as well basaltic magmas of the Strawberry Volcanics in eastern Oregon where units come in contact.

Biao Cai, Rebecca Coats, Lavallée Yan, Jackie Kendrick, Felix Von-Aulock, Nolwenn Le gall, Paul Wallace, Robert Atwood

Submission 681

4D Synchrotron Imaging of Viscous Flow of Crystal-bearing Magma Melts

The style of volcanic eruptions reflects the rheology of magma during ascent in volcanic conduit. To model magma transport, our descriptions require an in-depth understanding of the flow properties of magma, including a quantitative description of its phases during shearing. Using a unique in situ thermo-mechanical cell (P2R rig), we performed 4D synchrotron imaging (high speed X-ray tomography plus time at Diamond Light Source, UK) on crystal-bearing melts subjected to shear. This procedure allows us to observe and quantify the crystal motion and crystal-crystal interaction during shear, which leads to strain localization, dilatancy and rupture. The work demonstrates that 4D X-ray imaging of magma shearing is a powerful tool to advance our rheological models of magmas relevant to lava flows and dome eruption, highlighting new phenomena which may have remained hidden from traditional analysis of eruptive products.

Antonina Calahorrano-Di Patre, Glyn Williams-Jones, Maurizio Battaglia, Patricia Mothes, Silvana Hidalgo, Santiago Aguaiza, Francisco Mejía, Helen Gaunt

Submission 664

Linking Gravity Change at Cotopaxi Volcano with the Volcanic Processes Responsible for the 2015-2016 Period of Unrest

We investigate the link between observed temporal gravity changes with the physical processes involved in Cotopaxi's episode of unrest of 2015-2016.

In April 2015, Cotopaxi, an active stratovolcano located 50 km south of Ecuador's capital city of Quito, began showing signs of unrest after 135 years of quiescence. The Instituto Geofísico of Ecuador reported an increase in the number of seismic events and daily SO₂ flux, as well as a change in the type of seismicity (an increase in the proportion of LP and VLP events). This increase in activity peaked on August 14, 2015, with the initiation of mild eruptive activity. The eruption was characterized by phreatomagmatic explosions with ash plumes that rose up to 8000 m above the summit: ash emissions affected the nearby communities until November 2015. The activity declined after December 2015, and seismicity and SO₂ emissions returned to background levels by April 2016.

Gravity monitoring at Cotopaxi began in June 2015, with campaign measurements taken approximately every two months across a network of eight stations around the volcano. Gravity data was corrected for tide and free-air effects as well as instrumental and daily drift. A maximum gravity increase of 30 μ Gal between stations was detected before the August 2015 explosions. Gravity decreases up to 52 μ Gal were observed at several stations around the volcano between October 2015 and March 2016, after which they stabilized towards background levels.

Preliminary calculations for a simple sphere-like source, using the largest observed gravity change, suggest the increase can be linked to mass variations up to $3.3 \pm 0.5 \times 10^{11}$ kg with an estimated depth of 2-3 km under the summit, and likely represent a magmatic intrusion preceding the initiation of eruptive activity.

Marta Lucía Calvache, Adriana Agudelo

Submission 840

From the tragedy of Nevado del Ruiz eruption to the Nevado del Huila disaster risk reduction

Building trust and credibility in the relationship between scientists, authorities and institutions is one of the bases needed for successful communication and social engagement, during volcanic crisis. The main challenge is to work together, in a coordinated and effective way, in a multi-disciplinary, multi-institutional approach, learning from past experiences. Colombia has had success with building powerful ties of confidence, especially in regions that have had problems by earthquakes, volcanic eruptions, landslides and very large mudflows. In Colombia the Nevado del Ruiz (5320 m) erupted in 1985 and mudflows completely destroyed the town of Armero and other towns around the volcano, with more than 25,000 people dead. In contrast, Nevado del Huila volcano (5360 m), in 2007, had a volcanic crisis, after more than 500 years of inactivity. On February that year, a small eruption produced a North-South direction fracture approximately two kilometers long at the top of the volcano. Small mudflows formed along the rivers that drain the volcano. A second eruption in April was accompanied by a second Northeast-Southwest directional fracture of equal length. This second fracture opened on top of the volcanic edifice, and a large mudflow originated from it. This mudflow was big enough to destroy most of the infrastructure along the rivers of the region. A total of 15 bridges were destroyed. No one was killed. In November 2008, a new eruption took place (VEI 3), this time forming a crater with the extrusion of a lava dome, and a very large volume mudflow. This new mudflow reached the first populated area, located 14 kilometers from the volcano in 8 minutes. The mudflow reached the town of Belalcazar located 35 kilometers within approximately 30 to 35 minutes. Some parts of Belalcazar town was destroyed by the mudflow, as well as all vehicular and pedestrian bridges. Twelve people were killed. This is a great improvement over an earlier tragedy. In 1994, river basins near the volcano, had been shaken by a M6.2 earthquake that triggered landslides and formed a debris flow that affected the same towns. However, more than 1600 people died or are missing. The more favorable outcome in 2007 occurred because of continuous volcano monitoring, work with authorities and other institutions and communities, early warnings, and the improved perception of risk by the community.

Marta Lucia Calvache V., Ivan Dario Nova V., Carlos Alonso Escobar P., Jorge Contreras, Gloria Patricia Cortes J.

Submission 1112

The Omaira Sanchez Park in Armero-Guayabal town, Colombia, an opportunity for reconciliation with the territory.

The town of Armero, in Colombia, is an emblematic place to learn about volcanic processes and our day-to-day life. More than 31 years ago, a relatively small eruption of Nevado del Ruiz volcano generated a mudflow or lahar, which traveled more than 80 kilometers down to the low planes of the Magdalena River, where the town of Armero was located. Its destruction in 1985 was the third time that the settlement was destroyed by volcanic eruptions. Prior to 1985, it had been destroyed in 1845 and in 1595. In 1985, when the volcano had the first signs of activity, most of the authorities and community did not perceive that their place was in danger from an eruption of Nevado del Ruiz because they did not have any experience with active volcanoes and every day necessities were more real than a possible eruption of the volcano. After the tragedy, the people from Armero-Guayabal, named Armeritas, wanted to reconstruct the social fabric and collective memory lost in the 1985 disaster, especially in the rescue of intangible culture and its reinsertion in the new populated centers. Now the authorities of Armero have a park named after the 13-year-old girl Omaira Sanchez, trapped in debris caused by the mudflow following the eruption of the volcano. This park is intended to be part of the meeting for the reconciliation of people with their territory, not only for the Armeritas, but for the Colombians who do not know their territory and therefore, cannot make decisions that are consistent with the place where they live. The communities do not have the opportunity to be exposed to volcanic processes, especially since these natural phenomena do not occur frequently. Armero and its surroundings are an excellent opportunity to see exposed evidence of geological processes that modify the territory and sometimes trigger great tragedies. One of the main objectives of the park is to become a center of learning about the territory and environment where we are living.

Andrew Calvert, Judy Fierstein, Wes Hildreth

Submission 1169

Middle and South Sister volcanoes—products of an unusual 35 kyr eruptive episode

Comprehensive studies of arc volcanoes show that volcanism is commonly episodic, and study of this behavior informs understanding of magmatic processes. The Three Sisters volcanic cluster in the Oregon Cascades includes three stratocones and numerous smaller vents that produced ~80 km³ over the past 200 ka. Much of this volume erupted from mafic centers North Sister and The Husband, ~28 km³ from the chemically-diverse South and Middle Sisters, and the rest from abundant distributed centers in the volcanic field. An episode of at least 57 eruptions at South and Middle Sisters between 50–15 ka is both relatively voluminous and silicic in composition. Prior to 50 ka, eruptive volumes for the whole field averaged 0.25 km³/1000 years and compositions were predominantly basaltic andesite. In contrast, during the 50–15 ka episode the eruptive volume increased nearly fourfold and compositions were mostly rhyolite, dacite and andesite. The episode is divided into periods A-D. (A) Early in the episode (50–37 ka) eruptions were primarily rhyolite and basaltic andesite localized north of Middle Sister, including a 38 ka high-silica rhyolite. Rhyolite windows beneath younger flows at South Sister suggest as much as 5 km³ of its unexposed core is rhyolite that erupted in this time range. (B) Eruptions from 37–27 ka are mostly andesite and dacite lava flows, restricted to the South Sister edifice. (C) Between 27–21 ka andesite and dacite erupted at the summit of South Sister and rhyolite, dacite and andesite domes and flows erupted from and adjacent to Middle Sister. (D) The youngest eruptions (21–15 ka) are mainly basaltic andesite with subordinate dacite, including the Middle Sister basaltic andesite eruption at 20 ka that forms the upper 2/3 of this edifice. Since 15 ka, eruptive volumes have returned to pre-50 ka rates and mafic compositions, with the exception of a pair of 2 ka rhyolite eruptions. The unusual volume and composition of Middle and South Sister eruptive products in the 50–15 ka range may represent an unusually large pulse of subduction-derived magmatism, or may represent arrival of the westward sweep of rhyolite across the Oregon High Lava Plains (Hill and Taylor, 1989, USGS Open-File). Rhyolite in the cluster has been tied to crustal melting rather than fractional crystallization (B.E. Hill, 1991, OSU dissertation) and its sudden appearance suggests that this unusual 50–15 ka episode is related to the High Lava Plains rhyolite trend.

David Calvo, Luca D'Auria, José Barrancos, Eleazar Padrón, Germán Padilla, Rubén García, Fiona Burns, Aarón Pérez, Pedro A. Hernández

Submission 1005

GUAYOTA: a weekly multi-language chart information on the seismo-volcanic activity at Tenerife, Canary Islands

Tenerife is one of the most prevalent touristic "hot spots" in Europe, and at the same time is crowned by the third largest volcano on earth, Teide, in a dormant state that makes it a huge attraction both for tourists and locals. This situation is a challenging task for volcanologists in order to raise resilience among the community living with the volcano. One of the actions that must be taken as stated by the UNESCO's work on risk reduction is to communicate and keep the people informed about the activity of the volcano. For that purpose a weekly, multi-language chart information on the seismic-volcanic activity at Tenerife has been released by the Instituto Volcanológico de Canarias (INVOLCAN). This chart is called Guayota, honoring the Guanche (aborigins from Tenerife living before the Castillian conquest) legend about the devil living inside the volcano, that was named that way.

This chart consists on a Tenerife map display where monitoring stations are pointed, and seismic epicenters are shown on a seven days interval, in addition to geochemical, geophysical and geodesy data provided by the instrumental permanent stations network of the INVOLCAN, and that are displayed on a background multiple scale. There's also a four position "volcanic semaphore", following the Special Plan of Civil Protection and Emergency Response for Volcanic Risk in the Canary Islands (PEVOLCA), as well as a small, depicting text about the chart, that also contains a QR Code that links to our website for free download.

Updated every friday, this chart is shared through our web, social networks, and released for free for local newspapers that are willing to publish this info. Being such a huge touristic destination, we actually provide the Guayota in multiple languages, ranging from english and german, that make the core of our tourists nationality, to other languages such as Portuguese, Italian, French and soon in Japanese, Polish and Russian. Our aim is to provide an understandable, reliable and friendly interaction between the people and the activity of the volcano, in order to ease and get better knowledge of how to live with an active volcano in the backyard.

Michal Camejo, Jon Blundy, Elena Melekhova, Richard Robertson, Thomas Christopher

Submission 274

Petrology of plutonic and volcanic rocks from Bequia, Lesser Antilles arc

Bequia is the northernmost island of the Grenadines archipelago, Lesser Antilles. Although Bequia has been volcanically inactive since the Pliocene, products of past eruptions record the conditions and processes operating within its magma reservoir. This archive is important for assessing along-arc variations in magmatism. We present the mineral textures and compositions of plutonic xenoliths and lavas from Bequia. The xenoliths represent the frozen by-products of magmatic differentiation whereas lavas are the complimentary melt-rich differentiated end product of pre and syn eruptive processes.

The xenoliths range from adcumulate to orthocumulate with inconsistent mineral crystallisation sequences. Bulk compositions of xenoliths deviate from the liquid line of descent of lavas suggesting a cumulate origin. Lavas are glomeroporphyritic, entraining an inferred cumulate and phenocryst component. Both suites contain assemblages of iddingsitized olivine, unaltered plagioclase, clinopyroxene and spinel with rare orthopyroxene and ilmenite. Iddingsite may result from percolating hydrothermal liquids through an olivine rich mush, with later fractional crystallization or new melt introduction producing unaltered, more evolved phases. Mineral zoning is widespread but more protracted in lavas than xenoliths. Plagioclase cores and olivine have high anorthite ($An \approx 90$) and low forsterite ($Fo \approx 63$) compositions respectively, implying crystallisation from a hydrous melt that was already fractionated. Amphibole, notably absent from lavas, is a common feature of xenoliths, together with minor biotite and apatite. Amphibole paucity in lavas may reflect instability at low pressures while its abundance in xenoliths hints towards its importance in mid-crustal differentiation. Amphibole textures were used to organize the xenoliths into 4 groups, corroborated by compositional similarities: interstitial, subhedral poikilitic, prismatic and amphibole-free. The wide range of amphibole compositions (Mg#79-56) implies infiltration of diverse melts through anhydrous crystal mushes.

Eruption temperatures of lavas were estimated to be ≤ 820 °C. Geothermobarometry calculations for xenoliths indicate mid-crustal crystallization (≤ 1046 °C, 260-830 MPa) under oxidizing conditions. A complex magmatic system was inferred beneath Bequia involving multiple melts percolating through accumulated crystal mushes. During eruption, the mush body became disrupted and incorporated into ascending magmas.

Cheryl Cameron, Katherine Mulliken, Scott Crass, Kristi Wallace, Janet Schaefer

Submission 132

Geologic Database of Information on Volcanoes in Alaska (GeoDIVA): integrating diverse datasets supports research and Observatory operations

GeoDIVA maintains complete, flexible, timely, and accurate information on Pleistocene and younger Alaska volcanoes, and supports the mission of the Alaska Volcano Observatory (AVO). This database is the backend of AVO's public (<https://www.avo.alaska.edu>) and internal websites, and assists AVO's scientific investigations, crisis response, and public information responsibilities. Since 2002, GeoDIVA has developed as a series of interlocking modules. Advanced modules with well-developed content include: bibliography (~5,000 references), basic volcano information (~150 volcanoes), historical and prehistoric eruption information and unrest events (~850 entries), images (25,000+), geologic sample metadata (17,000+ samples), tephra data (2,000+ EMPA analyses, named tephtras), whole-rock geochemistry (7,500+ analyses), internal remote sensing and seismic observations, citizen science ashfall observations ("Is Ash Falling?"), volcanic vent inventory (1,200 Quaternary vents), petrographic data, and physical sample storage metadata. Because each dataset contains key joins on items such as eruption, volcano, publication, image, geologist, and sample, we can write flexible queries to display AVO's geologic information for specific contexts (e.g., sample analyses tied to specific eruptions; images of stations; timelines of data observations).

This broad collection of diverse datasets is now used in support of many research goals, including a collaboration with the USGS VDAP Eruption Forecasting Information System. Our newly populated tephra data module provides integrated Alaska tephra data not just for AVO's volcano-hazard assessment work, but also for climate geologists, archaeologists, and other disciplines.

GeoDIVA provides critical and timely information to observatory staff, especially during eruption response. During the recent eruption of Bogoslof, we utilized the database to quickly access historical eruption accounts, photographs, existing rock samples, geochemical analyses, and the physical location of those samples and thin sections. Citizens used GeoDIVA to report ashfall to AVO, and AVO geoscientists use the database to store and distribute monitoring observations, images, and figures and accomplish numerous internal tasks necessary during eruption monitoring and response.

As GeoDIVA continues to mature, we want to increase our interoperability with other volcano datasets, and provide user-driven, complex queries of the database from our public website.

Cheryl Cameron, Kristi Wallace, Michelle Coombs, David Schneider, Hans Schwaiger, Donald Moore, Louise Fode, Christina Neal

Submission 1126

Interagency communication at the Alaska Volcano Observatory: A case study of the 2016-17 eruption of Bogoslof volcano

Drifting ash clouds and ashfall from North Pacific volcanoes can threaten aircraft operations over Alaska, its surrounding waters, and beyond. Volcanic ash also can significantly impact Alaskan communities, infrastructure, and human health. A well-coordinated response that includes consistent messaging is required to facilitate the flow of timely, useful information to those at risk. A formal Interagency Operating Plan provides guidance for an integrated, multi-agency response to the threat of volcanic ash in Alaska. It describes the roles and responsibilities of each agency during volcanic ash events, and is supported by more detailed, standard operating procedures maintained by each agency.

During the recent eruption of Bogoslof volcano in the Aleutian arc, the Alaska Volcano Observatory (AVO) and its interagency partners worked closely to issue timely warnings of volcanic activity and its impacts. AVO monitors volcanic activity at Bogoslof using scheduled checks of geophysical and remote sensing data. Automatic alarms on these data as well as reports of observations by pilots or mariners can alert AVO staff to volcanic activity. Upon the onset of explosive activity at Bogoslof (37 explosive events to date), AVO coordinates eruption source parameters such as timing and, cloud altitude and dispersal direction with the National Weather Service (NWS) Anchorage Volcanic Ash Advisory Center, who issue volcanic ash warnings and forecasts to the aviation industry within the Alaska Flight Information Region. For the purpose of warning people on the ground and at sea, AVO provides guidance about ashfall to the NWS Anchorage Forecast Office, who issue ashfall statements, advisories, and warnings for the public and marine communities. For events that may affect communities, the Alaska Department of Homeland Security & Emergency Management initiates multi-agency coordination calls with communities, focusing on impacts to health and infrastructure. In addition to the agencies where close coordination is required, AVO is in direct contact with numerous other aviation and non-aviation-sector agencies during events. Sharing of information is facilitated by AVO's web tools such as Volcview for visualizing satellite data, and volcano-specific web pages consolidating data streams, including ash fallout and cloud dispersion model results. The interagency effort is maintained by semi-annual updates to the Plan, training, after-action discussions and tabletop exercises.

Dante Canil

Submission 1090

Diffusivities of volatile trace metals (Au, As, Bi, Cd, Cu, Tl, Pb, Mo, Re, Sn, Sb) in melts over a range of oxygen fugacity with applications to their degassing behaviour

Many volatile trace metals can occur in considerable concentrations in gases and volcanic aerosols, and their behaviour could shed light on the re-filling of magma reservoirs, the chalcophile budget of volcanic eruptions, and the loading of the environment with trace metals. The concentration of trace metals in volcanic gases is dictated by fluid-melt partitioning, and by kinetics - the metals must diffuse to the melt-gas interface in order to partition. The diffusion rates (D , m^2/sec) of some of volatile trace metals vary substantially (5 orders of magnitude) inviting possible kinetic effects that can be exploited to inform the nature of bubble growth, degassing, mixing or precursory behavior of magmas. Previous diffusion coefficients were all measured in melts in equilibrium with air. To this end, the diffusion rates of several trace metals of varying volatility (Li, Au, As, Bi, Cd, Cu, Tl, Pb, Mo, Re, Sn and Sb) were measured at 0.1 MPa in basalt, dacite and rhyolite between 1200 – 1400 C over a range of $f\text{O}_2$ from air to 2 log units below the FMQ buffer. Evaporation of metals dissolved in the melts in open ended capsules create concentration gradients, allowing extraction of D values. The diffusion of Cu, Cd and Bi are incredibly rapid ($\log D > -10$). Order of magnitude variations are observed for $\log D$ of Au and Re, (-12 to -14) with $f\text{O}_2$, likely due to speciation changes in the melt or at the gas interface. The data are used to model observed changes in Pb/Tl of volcanic gases from Etna as either kinetic fractionation during bubble growth or by changing magma reservoir time. A number of trace metals (Li, As, Cd, Cu) are being measured with increasing frequency in lavas, fumaroles and in plumes from volcanic settings. The new D values for these elements can be applied to understand magma reservoir histories prior to eruption.

Flavio Cannavo, Andrea Cannata, Carmelo Cassisi, Placido Montalto, Danila Scandura

Submission 815

Towards an Automatic Volcano Instrumental Early Warning System (a-ViEWS) for Mt. Etna

The importance of monitoring active volcanoes, especially in case of energetic paroxysms that usually come with tephra emissions, is crucial not only for exposures to the local population but also for airline traffic. This is the reason why continuous evaluation of the status of potentially hazardous volcanos plays a key role for civil protection purposes. Presently, real-time surveillance of most volcanoes worldwide is essentially delegated to one or more human experts in volcanology, who interpret data coming from different kind of monitoring networks. Unluckily, the high nonlinearity of the complex and coupled volcanic dynamics leads to a large variety of different volcanic behaviors. Moreover, continuously measured parameters (e.g. seismic, deformation, infrasonic and geochemical signals) are often not able to fully explain distinctly the ongoing phenomenon, thus making the fast volcano state assessment a very puzzling task for the personnel on duty at the control rooms. With the aim of aiding the personnel on duty in volcano surveillance, here we present a system based on an ensemble of data-driven classifiers to infer automatically the ongoing volcano status from all the available different kind of measurements. The system consists of a heterogeneous set of independent classifiers, each one built with its own data and algorithm. Each classifier gives an output about the volcanic status. The ensemble technique allows weighting the single classifier output to combine all the classifications into a single status that maximizes the performance. We tested the model on the Mt. Etna (Italy) case study by considering a long record of multivariate data from 2011 to 2016 and crossvalidated it. Results indicate that the proposed model is effective and of great power for decision making purposes.

Elisa Carboni, Roy Grainger, Tamsin Mather, Anja Schmidt, Iolanda Ialongo

Submission 1022

Satellite-derived sulfur dioxide (SO₂) emissions from the 2014-2015 Holuhraun eruption (Iceland).

The 2014-2015 Holuhraun eruption was a major source of sulfur dioxide (SO₂) to the troposphere. Yet the number of ground-based SO₂ measurements was limited in particular during Icelandic winter. Here we present a time series of volcanic SO₂ atmospheric loading and vertical distribution from the Infrared Atmospheric Sounding Interferometer (IASI) over the entire eruption period from September 2014 to February 2015.

We simultaneously use all the IASI spectral range from 1000 to 1200 cm⁻¹ and from 1300 to 1410 cm⁻¹ (the 7.3 and 8.7 μm SO₂ absorption bands), to retrieve both the SO₂ amount and altitude of the plume. The SO₂ band around 8.7 μm (1000 to 1200 cm⁻¹) is within an atmospheric windows range, where radiation from the surface can reach the satellite measurements through all the atmospheric layers. This allow us to retrieve the SO₂ amount down to the surface and lower troposphere. A comprehensive error budget for every pixel is included in the retrieval.

To check the validity of our retrieval we compare the IASI dataset against Brewer ground measurements located at Sodankylä (Finland). This shows that all the SO₂ episodes, are consistent between satellite and ground measurements.

We present the evolution of the plume (maps of amount and altitude) for the 6-month period where volcanic SO₂ was transported in the lower troposphere all over the north hemisphere from 30 to 90 deg. North.

We developed a new optimal estimation scheme that uses the atmospheric loadings time series to retrieve emission fluxes together with the average lifetime of SO₂. We obtain emission fluxes reaching values up to 200 kt/d and a 'minimum' total mass emitted of SO₂ of 3.7±0.8 Tg with an average lifetime of 2.4 ±0.6 days.

Rebecca Carey, Adam Soule

Submission 1253

The role of the ocean in submarine silicic volcanism: morphologic and quantitative data from the Havre 2012 submarine eruption compared to subaerial analogues

The 2012 submarine eruption of Havre volcano in the Kermadec arc, New Zealand, is the largest and deepest in history. It was recognized from a gigantic 400km² pumice raft seen in satellite imagery, however the complexity of this event was concealed beneath the sea surface. Mapping, observations, and sampling by submersibles has provided the highest fidelity record to date of an eruption of this type, which included lava sourced from 14 vents at 900 – 1220m water depth, and fragmental deposits including giant pumice clasts up to 9m in diameter. All 2012 products analysed are rhyolitic (69-73 wt.% SiO₂).

The timing and development of the pumice raft is captured in a sequence of MODIS images, which constrains the timing to a period of 21.5 hours. The volume of the raft is also estimated via measurements of the area of the raft, and an estimation of its thickness, 1.2 km³. The time-averaged volumetric discharge rate is 1.5 x 10⁴ m³s⁻¹, or in terms of mass, 9 x 10⁶ kgs⁻¹ (using an averaged bulk density of 550 kgm⁻³). Given the erupted volume of 1.2 km³ is equivalent to subaerial VEI 5 eruptions, we suspect that the Havre instantaneous discharge rates were equivalent to moderate-sized VEI 4 – 5 Plinian eruptions in the subaerial setting, e.g., May 18 1980 Mount St Helens and Chaiten in 2008. Seafloor lavas at Havre show no morphological differences compared with subaerial silicic analogues. The volumetrically largest dome O-P (0.11 km³) has a time-averaged effusion rate of > 14 m³s⁻¹, or > 3.3x10⁴ kgs⁻¹.

By combining the Havre satellite eruption record with our seafloor stratigraphic and volumetric constraints, we calculated the first estimates of eruption mass and volumetric discharge rates at a silicic submarine volcano. The similarities of eruption rates and the morphology of the effusive products highlights a less than expected modulating role of the ocean and high hydrostatic pressures. However, voluminous deposits dominated by vesicular giant pumice clasts appear to be unique to submarine eruptions.

Rebecca Carey, Sharon Allen, Jocelyn McPhie

Submission 1236

Vesiculation in deep submarine silicic dome-forming magmas: Sumisu Dome Complex, Izu-Bonin Arc, Japan.

Hydrostatic pressure suppresses volatile exsolution and the vesiculation of magma on the seafloor. Silicic magmas erupted at high hydrostatic pressures are therefore expected to erupt effusively at low vesicularities with high residual volatiles in the melt. However, seafloor ROV investigations of deep submarine environments have revealed rhyolitic highly pumiceous dome and lava carapace at depths between 1300 - 800 mbsl at Sumisu (Izu-Bonin Arc, Japan) and Havre volcanoes (Kermadec Arc, NZ).

At Sumisu, two deep rhyolite domes at depths of 900 (Dome B) and 1300 mbsl (Dome C) were observed and sampled via ROV. At Dome B no dense dome rock was encountered, however intact highly pumiceous carapace (67 to 85 vol% vesicles) is preserved. At Dome C dense (5-16 vol.% vesicles) rhyolite is encased by a thin (~2 m-thick) partially intact highly pumiceous carapace (67 to 85 vol% vesicles). Initial volatile contents measured in melt inclusions hosted by Quartz are 5-5.8 wt% H₂O and

Pumiceous clasts from both domes are remarkably uniformly microvesicular with rare round coarse vesicles up to 5 mm in diameter. Quantitative vesicularities and permeability measurements from all clasts within and between domes carapace are also uniform: vesicle number densities (VND) range from 3 - 9 x10⁸ cm⁻³, with one exception where collapsed vesicles are clear (1.4 x 10⁹ cm⁻³). There is no obvious change in bulk vesicularity associated with the presence/absence of jointing and quenched margins. Furthermore, connected porosities, Darcian and Inertial permeabilities of pumiceous clasts broadly overlap regardless of eruption depth/hydrostatic pressure.

These data suggest similar histories of nucleation, growth and coalescence of bubbles throughout magma ascent and lava emplacement. The Sumisu VNDs are similar to explosive sub-plinian rhyolitic eruptions (e.g. Chaiten 2008; Unit 1, Taupo 181 AD eruption; Askja 1875 B). The decompression rates inferred from our VNDs are very high for an effusive silicic eruption. Measured glass volatile contents (FTIR) reveal up to 2 wt.% residual H₂O and 2. Viscosity calculations suggest that the melt viscosity at pressures of 9 - 13 MPa are ~10⁵ Pa s upon eruption and quenching, which together with lower specific volume of the vapour phase likely suppress explosive fragmentation.

Luca Caricchi, Tom Sheldrake, Jon Blundy

Submission 124

CO₂-triggered destabilisation of magmatic systems

Explosive volcanic eruptions and porphyry type ore deposits occur at convergent margins and are the result of the sudden and violent release of magma and magmatic fluids, respectively. The replenishment of magma reservoirs in the upper crust by mafic magma is generally considered as an essential element for triggering volcanic eruptions and the release of mineralising fluids. Here, we take a complementary approach and quantify the effect of the interaction between CO₂-rich gases and magma in upper crustal magma reservoirs (fluxing or flushing). We show that although magma input alone has the potential to destabilise volcanic systems, the input of magmatic CO₂ is a considerably more potent agent of destabilisation. Considering a mafic magma rising from depth with an initial CO₂ content of 1wt.%, its input in a magma reservoir generates overpressures that are up to one order of magnitude smaller than those generated by the input of CO₂ released during its ascent. Dissolution of just a few hundred parts per million of CO₂ in H₂O-rich magmas stored within the shallow crust drives exsolution of H₂O that is up to 100 times greater in mass, resulting in reservoir volume increase of up to 25% over timescale of tens to hundreds of years. Depending upon magma crystallinity, its physical properties and the duration of CO₂ input, flushing of CO₂-rich gases can trigger volcanic eruptions or the violent release of water and metal rich fluids, which is essential for the genesis of porphyry-type ore deposits.

Richard Carlson, Timothy Grove, Julie Donnelly-Nolan

Submission 429

The Origin of Calc-Alkaline and Tholeiitic Primary Magmas: The Example from Primitive Basalts of Newberry Volcano, Oregon

Newberry Volcano is a large (~600 km³) composite shield-shaped volcano located in central Oregon ~60 km east of the Cascades arc axis. Over the last 0.5 Ma, the volcano has erupted lavas ranging in composition from primitive basalt to rhyolite. The primitive basalts include end members with compositional characteristics typical of calc-alkaline, subduction-influenced basalts, but also others similar to the tholeiitic basalts erupted in the extensional High Lava Plains east of Newberry. The tholeiitic end members are high-alumina olivine basalts that are diktytaxitic and aphyric. These lavas are dry (20) with shallow-sloped primitive-mantle-normalized incompatible element abundance patterns. They are produced by anhydrous adiabatic decompression melting of convecting mantle asthenosphere at depths of 50 – 55 km and temperatures of 1350 oC based on the melting model of Till et al. (JGR, 2012). The calc-alkaline end members contain 2-4 vol. % olivine, calcic plagioclase, and high-Ca clinopyroxene as phenocrysts. These lavas contained 2 to 4 wt. % H₂O prior to eruption, based on plagioclase hygrometry. They show strong enrichment in the LREE, Ba, and Sr, and deficits in high-field strength elements such as Nb, Ta, Hf and Zr. Compared to the tholeiitic end member, the source of the calc-alkaline basalts is interpreted to include a component derived from the wet melting of eclogite, most likely the upper crust of the subducting Juan de Fuca oceanic plate. To simultaneously match the Sr, Nd, Hf and Pb concentration and isotopic differences between primitive tholeiitic and calc-alkaline basalts, the component added to the calc-alkaline source is calculated to have a Ba/Nb ratio near 530, a chondrite normalized La/Sm near 6, with $^{87}\text{Sr}/^{86}\text{Sr} = 0.70395$, $^{143}\text{Nd}/^{144}\text{Nd} = 0.51291$, $^{206}\text{Pb}/^{204}\text{Pb} = 18.99$. These isotopic compositions are only slightly different than those of the tholeiitic magmas. The calc-alkaline basalts have significantly more radiogenic Os than the tholeiites, implying that the slab component either had very high Os concentrations or was added not to mantle-wedge peridotite, but to a basaltic melt in the wedge. The similar, high, compatible element concentrations of both the calc-alkaline and tholeiitic primitive basalts are typical of melts in equilibrium with peridotite, indicating that the compositional difference between the two parental magma types was established in the mantle, not the crust.

Simon Carn, Vitali Fioletov, Chris McLinden, Can Li, Nickolay Krotkov

Submission 899

A decade of global volcanic SO₂ emissions measured from space

The global flux of sulfur dioxide (SO₂) emitted by passive volcanic degassing is a key parameter that constrains the fluxes of other volcanic gases (including carbon dioxide, CO₂) and toxic trace metals (e.g., mercury). It is also a required input for atmospheric chemistry and climate models, since it impacts the tropospheric burden of sulfate aerosol, a major climate-forcing species. Despite its significance, an accurate inventory that captures the spatial and temporal variability of passive volcanic degassing is very difficult to produce, due largely to the patchy coverage of ground-based SO₂ measurements. We report here the first volcanic SO₂ emissions inventory derived from global, coincident satellite measurements, made by the Ozone Monitoring Instrument (OMI) on NASA's Aura satellite in 2005-2015. The OMI measurements permit estimation of SO₂ emissions from over 90 volcanoes, including new constraints on fluxes from poorly monitored regions such as Indonesia, Papua New Guinea, the Aleutian Islands, the Kuril Islands and Kamchatka. On average over the past decade, the volcanic SO₂ sources consistently detected from space have discharged a total of ~63 kt/day SO₂ during passive degassing, or ~23±2 Tg/yr. We find that ~30% of the sources show significant decadal trends in SO₂ emissions, with positive trends observed at multiple volcanoes in some regions including Vanuatu, southern Japan, Peru and Chile. This new volcanic emissions inventory should improve constraints on volcanic CO₂ emissions discharged via passive degassing, and can also be used to prioritize targets for future ground-based CO₂ measurements. Furthermore, using older satellite measurements from the Total Ozone Mapping Spectrometer (TOMS) and other sensors, it may be possible to extend the emissions inventory back to 1978 for some of the strongest volcanic SO₂ sources and create unique multi-decadal records.

Brett Carr, Amanda Clarke, Mattia de' Michieli Vitturi

Submission 457

Earthquake induced variations in extrusion rate: a numerical modeling approach to the 2006 eruption of Merapi Volcano (Indonesia)

Extrusion rates during lava dome-building eruptions are variable and eruption sequences at these volcanoes generally have multiple phases. Merapi Volcano, Java, Indonesia, exemplifies this common style of activity. Merapi is one of Indonesia's most active volcanoes and during the 20th and early 21st centuries effusive activity has been characterized by long periods of very slow (3 s^{-1}) extrusion rate interrupted every few years by short episodes of elevated extrusion rates ($1 - 4 \text{ m}^3 \text{ s}^{-1}$) lasting weeks to months. One such event occurred May – July 2006, and previous research has identified multiple phases with different extrusion rates and styles of activity during the eruption. Using input values established in the literature, we apply a 1D, isothermal, steady-state numerical model of magma ascent in a volcanic conduit to explain the variations and gain insight into corresponding conduit processes. The peak phase of the 2006 eruption occurred in the two weeks following the May 27 Mw 6.4 earthquake 50 km to the south. Previous work has suggested that the peak extrusion rates observed in early June were triggered by the earthquake through either dynamic stress-induced overpressure or the addition of CO_2 due to decarbonation and gas escape from new fractures in the bedrock. We show that, in order to explain the observed change in extrusion rate, the chamber overpressure increase must have been approximately 5-7 MPa. We find that the addition of ~ 1000 ppm CO_2 following the earthquake is sufficient to reduce the solubility of water in the magma such that sufficient water would exsolve to generate an overpressure on the order of 7 MPa. Thus, it is feasible and reasonable to state that the peak phase of the Merapi 2006 eruption was caused by the May 27 earthquake in that the resulting CO_2 release facilitated the generation of the overpressure necessary to increase the extrusion rate to the levels observed. A time-series of extrusion rate shows that the rate increased suddenly three days following the earthquake. We explain this three-day delay by the combined time required for the effects of the earthquake to develop in the deep system (1-2 days), and the time we calculate here for the affected magma to ascend from storage zone to surface (40 hours). The increased extrusion rate was sustained for 2-7 days before dissipating and returning to pre-earthquake levels.

Alexandre Carrara, Alain Burgisser

Submission 177

Numerical simulations of silicic magmatic chamber reawakening and mixing

The reawakening of volcanoes being asleep for several hundred years is generally marked by Plinian eruptions (e.g. Komagatake 1640, Pinatubo 1991...). Petrological analysis of juvenile deposit associated with such events often shows evidences of mixing between a resident, highly crystalline mush and a newly injected, less crystalline magma. The process of mixing that leads to the formation of an eruptible, mobile magma is not yet well understood. Recent studies (Bergantz et al., 2015; Schleicher et al., 2016) developed a Computational Fluid Dynamic – Discrete Element Method (CFD-DEM) model for basaltic magma chambers with low (0.2 Pa.s) interstitial liquid viscosity. The aim of this study is to adapt this CFD-DEM model to higher melt viscosities in order to simulate the remobilization of silicic magmatic chambers.

When viscosity increases, the relative importance of the forces acting on crystals change (Trulsson et al., 2012). Drag and gravitational forces dominate over collisional forces. Lubrication forces, which act like a buffer between particles to reduce the collisional energy, become also more important and can affect the dynamics. That is why we need to validate the CFD-DEM approach of our model by reproducing rotating tumbler experiments in fluids from Pignatel et al. (2012). We implemented into our model the normal and tangential lubrication forces and found that they only play a minor role in such experiments. This may be explained by the fact that the cascading of particles in the tumbler flow is in the frictional regime. In parallel with such validation runs, we simulated pure liquid injections in particle-rich suspensions with liquid viscosities of ~10-100 Pa.s. We use these preliminary results to explore the relationship between injection rate and the incorporation of particles from the resident suspension into the injected liquid and to discuss how this relates to observations of crystals content in the petrological records.

Gerardo Carrasco

Submission 592

U/Th and $^{40}\text{Ar}/^{39}\text{Ar}$ dating revealing a new evolutionary model of Los Humeros caldera formation: Implications for its geothermal potential

A former evolutionary scheme for the Los Humeros caldera, Mexico, based on K/Ar dating (Ferriz and Mahood, 1984) indicated that the initial caldera-forming eruption occurred at 460 ka, followed by the emplacement of peripheral rhyolitic domes at 360-220 ka, and an intense period of activity with alternating stages of explosive and effusive eruptions. New U/Th and Ar/Ar dates reported here for pre-, syn- and post-caldera volcanics allow a reappraisal of the volcanic evolution of the active, Los Humeros geothermal field. The age of the voluminous (115 km³ DRE) Xaltipan ignimbrite (160-180 ka) associated with the formation of Los Humeros caldera, obtained by two geochronometers (U/Th and Ar/Ar dating), is much younger than previously reported and post-dates an intense eruptive episode of pre-caldera volcanism. The other main explosive events are also much younger than previously reported. The remarkable Plinian activity that produced the Faby Formation is now dated at ~60 ka, which is followed by the second caldera-forming eruption, which is associated with the eruption of the 15 km³ Zaragoza ignimbrite. Resurgent activity occurred at the center of the caldera at different times (45-74 ka) producing isolated rhyolitic domes. Late Pleistocene-to-Holocene activity has been documented in different sectors of the caldera, including a remarkable episode of contemporaneous bimodal eruptions of trachydacite and basaltic andesite magmas (Cuicuiltic Member,

Eduardo Cartaya, Lee Florea, Andreas Pflitsch

Submission 574

Systematic Investigations of the Summit Fumarole Caves of Mount Rainier, Washington State, U.S.A.

The glaciers in the twin summit craters of Mount Rainier (one of the 16 Decade Volcanos identified by the IAVCEI) in the Cascade Volcanic Arc of the Pacific Northwest, U.S.A., contain the largest and most extensive example of a glacier fumarole cave system in the world—glacier caves that have persisted in comparable equilibrium since their discovery in 1870. Expeditions mounted in August 2015 and 2016 mapped more than 3 km of cave passages developed primarily along the contact between the ice and the crater floor that span more than 100 m of vertical relief. Complementing this multi-national mapping effort were data collections to offer preliminary insight into the geochemistry, microbiology, climatology, and thermodynamic relationships of these unique caves.

Future changes in volcanic thermal activity will influence the dimensions, ablation features, and ablation rates of the caves. Survey data for this research include inter-annual measurements of the volume of key cave passages as one measure of the ablation of glacial ice. Interior and deeper cave passages are in near equilibrium with heat flux from fumaroles, potentially making the cave ice dimensions a sensitive indicator for thermal changes not otherwise detectable from surface observation. Higher level passages near the crater rim change annually in response to yearly snow accumulation. Vertical movement of reference stations in the cave wall provides an estimate of downward ice motion with preliminary values of almost 8 meters. Detailed thermal images of fumaroles combined with data from an array of temperature-humidity data loggers will ultimately contribute to a detailed model of convective heat flux and advection of moisture. In-cave wind flow study, combined with data logger measurements of water level, temperature, fumarole output, and specific conductivity of water from in-cave meltwater pools, provide a spectrum of information that can help scientists better understand the dynamics of the glacial plugs in the summit craters, and the interaction of this glacial melt with the magmatic source. Information collected during this project may subsequently establish a relationship between the cave volume / lake levels / rate of ice cap downward movement, and the heat flux from the fumaroles, thus potentially establishing a unique subglacial monitoring system of the volcano's thermal and chemical activity which could be integrated into hazard monitoring and rescue pre-planning.

Raymond Cas

Submission 78

Why deep water volcanic eruptions are so different from subaerial eruptions

Deep water (>500m depth) eruptions experience very different physical constraints than subaerial eruptions. Exsolved volatile content will be lower because magmas decompress to pressures orders of magnitude higher than atmospheric pressure. Higher retained volatile content and higher eruption pressure makes subaqueously erupted magmas less viscous, making them more prone to erupt by fountaining, and lavas to be more fluidal. The high heat capacity and thermal conductivity of water will lead to rapid cooling, and in many cases, quench fragmentation of lavas and lofted pyroclasts. Hyaloclastite breccia will be common, especially in shallow to intermediate water depths. Increasing hydrostatic pressures with water depth will increasingly suppress volatile exsolution, growth rate of exsolved volatile bubbles, and so explosive fragmentation. However, slow steady vesiculation of magma, under lower volatile overpressure can produce highly vesiculated, coherent pumice lava carapaces. Quench fragmentation can then produce pumice hyaloclastite breccia, clasts of which can be buoyant. Under increasing hydrostatic pressure, implosions of under-pressured, condensing volatile bubbles in magma, the water column, or in cavities in lavas increase. At water depths/pressures greater than the critical pressure for H₂O (22MPa, ~ 2.2 km) and CO₂ (7.4 MPa, ~ 0.7 km), exsolved volatiles are supercritical fluids, with limited ability to expand explosively, or only weakly so. The intensity of subaqueous explosive eruptions will also be low because of the much higher bulk modulus of water than air. Subaqueous eruption columns driven by supercritical fluids or gas are initially buoyant, are subject to condensation erosion, slowing to rise as plumes of hot water. They are unlikely to have the dynamics, height and dispersal capacity of subaerial eruption columns. In air, no pyroclast is buoyant, whereas in water clasts -1, are buoyant, can float, be rafted away, and may never settle to the seafloor. Dispersal and sedimentation of buoyant pyroclasts in water are affected by the rate at which they become water-logged, oceanic current patterns, wind push and wave directions, which can be very circuitous. Large volumes of pumice can float for months or years and can abrade in floating rafts, generating in transit ash fallout unrelated to explosive intensity. New concepts and terminology are required for all phenomena; comparison with subaerial eruption styles is misleading.

Ana Casas, Fabian Wadsworth, Jeremie Vasseur, Paul Ayriss, Corrado Cimarelli, Donald B. Dingwell

Submission 793

In-plume gas scavenging: An insight into gas adsorption, ash-surface chemistry and the role of water

Although many studies have investigated the occurrence of gas scavenging (by ash particles) during large volcanic eruptions, the mechanisms involved in these processes are not completely understood. Our work seeks to constrain the particle properties that lead to gas adsorption onto ash surfaces, through a combined experimental and modelling approach. We carry out sets of experiments, using three different grain size distributions (>90, 90-63 and 2, HCl, in anhydrous and hydrous conditions), at high temperatures (200-800°C), for different amounts of time (1-60 min). These experiments were performed with the AGAR (ash-gas advanced reactor), a unique apparatus that allows simulation of in-plume conditions. Post-experimental leaching of our samples showed that, for the SO₂ experiments, up to 80% of the calcium in the particles diffused towards the surface to form soluble salts (mainly CaSO₄). We use a 1D diffusion equation for polydisperse spheres with a concentration-dependent diffusivity to model our leachate time-series. We find that the model gives consistent diffusivities when each grain size distribution is taken into account, and provides a rigorous expression for the diffusivity as a function of the total local calcium concentration and temperature. By addition of H₂O (to the SO₂ experiments), we noticed a negligible impact on calcium diffusion, whereas sodium diffusion was measurably greater than that in anhydrous conditions. We attribute this difference in the effect of water between the calcium and sodium mobility to the role of H⁺ in sodium mass transfer, which is not relevant to calcium mass transfer. Furthermore, we find that at high temperatures above which iron oxidizes, sodium mobility is further reduced. This is attributable to the charge balancing effect of sodium on Fe³⁺ cations. These results could be used in conjunction with large-scale plume simulations to estimate the total mass of gases removable (due to high temperature adsorption) from the hot-plume, during the largest volcanic eruptions.

Montserrat Cascante, Maarten DeMoor, Cyril Muller, Geoffroy Avard, Maria Martinez, Javier Paheco, Jorge Brenes

Submission 24

Development of a volcanic crisis protocol for the Observatorio Vulcanologico y Sismologico de Costa Rica, OVSICORI

During the 2016 volcanic crisis at Turrialba volcano, the Observatorio Vulcanologico y Sismologico de Costa Rica (OVSICORI-UNA) saw the need for the development of a volcanic crisis protocol for a successful coordination and a better approach to problem-solving during a crisis. Thanks to the USAID-VDAP program, we used event trees for probabilistic short-term scenarios to compare different volcanic crises around the world and establish a baseline for the state of the volcano. During the crisis we tried different ways to maintain 24/7 monitoring, also the fastest way to response and the people that we need to inform changes as soon as something happened. We perceived the need to internally improve the organization of our observatory in order to more efficiently communicate with the government, press, and communities. First we create internal alert levels, just for the use of the observatory, to define the schedule and the assignments that the observatory must do during these levels. After that, small groups were assigned with group leaders, and every leader had to assign a job to every person which they must complete during 24 hours of monitoring. In this type of crisis, the internal structure was key to maintaining consensus with the updated information within the volcano monitoring group. Different steps were taken to inform changes; for example, we created a protocol to talk to the press and a list of key individuals that we should contact as soon as a change is perceived. We achieved a direct line of communication between the central and local government, the airport, and the national parks in case of an eventual change. We generated automatic reports when changes were detected. All of this was achieved through a collaborative effort between the staff of the observatory and VDAP. We managed to establish the guidelines so that during future volcanic events we are prepared and alert to be able to activate the protocols efficiently.

Katharine Cashman, Stephen Sparks, Jon Blundy, Jenny Riker, Guido Giordano

Submission 488

What's the mush? Physical insights into mush structure provided by crystal cargo

Jon Davidson demonstrated that the chemical evolution of magmatic systems is preserved in the variable cognate crystal cargo – cumulate nodules, glomerocrysts, and antecrysts – transported within many melts. Subsequent detailed studies of these crystals and crystal assemblages have created a paradigm shift in our views of magmatic systems. Key to the new view is the notion that magmatic systems are dominated by crystal mush that is not eruptible but retains some percentage of melt. Important questions arising from this view relate to the dominant state of the mush: Under what conditions is the mush held at near-solidus conditions (consistent with zircon evidence for cold storage), and when is the mush held at relatively high melt fractions (and thus easily mobilized by new inputs of melt and/or volatiles)? What is the spatial distribution of melt and crystals throughout the mush? Answering these questions has important hazard implications, particularly for large super-solidus bodies detected by tomography, which can provide estimates of average melt content only.

Here we explore ways in which the crystal cargo provides insight into the physical structure of the mush zone. Cumulate nodules come from near-solidus parts of the magmatic system, and typically contain small amounts of melt distributed along crystal margins. These low melt fractions are consistent with experimental evidence from granites showing a rapid drop in strength at melt fractions greater than approximately 7%, the point at which the melt phase becomes fully connected. Antecrysts are ubiquitous, and can be entrained from either hotter (and more primitive) or cooler (and more evolved) parts of the magmatic system. Limited data suggest that the former are common in mafic open systems, while the latter are more common in evolved magmas. Glomerocrysts have received the least systematic attention, but may shed the most light on mush structure. Monomineralic glomerocrysts are commonly interpreted to form by synneusis, and thus may not bear directly on mush structure. Poly-mineralic glomerocrysts, in contrast, may reflect original crystal growth as poly-mineralic aggregates rather than as isolated crystals, and may thus derive from disruption of melt-rich (5-50%) mush. If true, this suggests that the interstitial melt phase is likely back-mixed into the transporting melt and may form an important part of the mixing signature common to many magmatic suites.

Mike Cassidy, Jonathan Castro, Christoph Helo, Susanna Ebmeier, Sebastian Watt

Submission 777

Combining experimental petrology with InSAR deformation constraints on the magmatic system prior to eruptions at Kelud volcano, Indonesia

The parameters that govern the eruptive style at volcanoes are critical to understand, since the volcanic threat posed to the nearby populations are directly related to whether an eruption is explosive or effusive. Eruptions from Kelud volcano, located in East Java, Indonesia are difficult to forecast in that sense, because the eruptive style varies considerably, from effusive eruptions e.g. 1920 & 2007 to explosive eruptions in 1990 and 2014, despite near identical bulk rock compositions. Experiments were undertaken to constrain the magma storage conditions such as pressure, temperature and volatile contents prior to both explosive and effusive eruptions at Kelud. A gas-pressurized TZM cold-seal pressure vessel was used, whereby the sample (coarsely-crushed aliquots of the 2014 Kelud pumice contained in a AgPd capsule) were held at upper crustal P-T conditions for several days to equilibrate, and then rapidly quenched using a water-cooled coupling system to prevent further crystallisation. The experiments were held near the NNO oxygen buffer using a double-capsule method. A range of pressures (25-200 MPa), temperatures (950-1100 °C), H₂O-saturated and mixed H₂O-CO₂ conditions were explored in this study. Experimental matrix glass and mineral rim compositions, as well as crystal contents were measured and compared to the natural mineral and groundmass characteristics in explosive (1990, 2014 & undated pumice fall) and effusive (2007) eruption products. Both the experimental constraints and deformation assessed from a set of CosmoSkymed SAR interferograms suggest the pre-eruptive 2014 magma was stored at low pressure (20, where $X_{H_2O} = H_2O / (H_2O + CO_2)$ in moles) between 0.55 and 1. Experiments showed that the magma stored before effusive eruptions had lower initial fluid X_{H_2O} than magmas that generated the explosive eruptions, which were near water saturation. These data suggest that eruptive style at Kelud may be controlled by temperature and the degree of water saturation before eruptions. This coupling between pre-eruptive deformation monitoring data and experimental petrology may help to constrain the magmatic conditions that precede explosive eruptions at Kelud.

Jonathan Castro, Yves Feisel, Hugh Tuffen, C. Ian Schipper

Submission 1101

Dynamics of obsidian flows inferred from surface folds on Cordón Caulle (Chile) rhyolites

Lava flow emplacement modifies the Earth's surface and can damage infrastructure and upset ecological balance. Unstable silicic lava domes and flows are also hazardous, as they often collapse and may generate explosions related to structural deformation and degassing. In order to better understand how silicic lavas are emplaced—specifically rhyolites—we use a combination of high-resolution imagery, geometric analysis of macroscopic structures, and lava sample analyses to constrain the rheology and the dynamical regime under which the 2011 and 1960 rhyolitic lava flows of Cordón Caulle (Chile) were erupted. These two lava flows have virtually identical compositions and petrologically inferred eruption temperatures, yet are morphologically distinct in that the 2011 flow is two to three times thicker than the 1960 lavas, is flat-topped, and exhibits a peripheral facies of darker lava that forms “breakouts” [1]. Surface folding—common on both lava flows—comprises distinctive meters-tall ridges that are laterally extensive over hundreds of metres. Similar features on Holocene obsidian flows in the Pacific Northwest (USA) were interpreted to arise from buckling of a stiff flow surface in response to cooling and advance [2]. The arc wavelengths of such ridges are primarily controlled by the surface-to-interior viscosity gradient in the flow and its deformation rate. Thus, we used the geometry of surface folds, as constrained by a 1-m resolution DEM of the Cordón Caulle flows and observations of emplacement velocities, to predict viscosity contrasts during emplacement. Using a newly developed Matlab code that applies buckling theory, we find that on average the 2011 flow had higher interior viscosities ($\log \mu \approx 9.5$ Pa s) than the 1960 flow ($\log \mu \approx 8.1$ Pa s), although both appear to have developed a similarly viscous surface ($\log \mu \approx 11.5$ Pa s). As the extrusion rates for both flow systems were similar (tens of cubic meters per second), the important difference in folding characteristics, namely an average 10 m longer arc wavelength in the 2011 flow, likely arose from the different slopes on which the flows were emplaced. Viscosity assessments are currently being reconciled with independent estimates that account for groundmass microlite textures of representative interior (breakout) and surface lava, in addition to thermal models that track these flows' respective cooling histories.

[1] Tuffen et al 2013 Nature Communications 4, 2709.

[2] Fink 1980 Geology 8, 250-254.

Angelo Castruccio, Mikel Diez

Submission 871

The influence of magmatic system properties on volcano morphology and evolution: A comparison between the Central and Southern Volcanic Zones of Chile

Volcano edifices have generally been studied from a geomorphological descriptive point of view. In this work we pursue a different approach, where we view volcano edifices as indicators of magmatic system properties. We present a model that allows us to estimate the maximum height, volume, topographic profile and time of construction that a volcano edifice can attain for a given set of conditions of the magma system such as depth and size of the magma chamber.

We applied the model to study volcanic edifices from the Central (28 volcanoes) and Southern (36 volcanoes) Volcanic Zone of Chile (CVZ and SVZ respectively) to explore the differences between the dimensions, morphologies and longevity of volcanoes from both zones. The two zones possess contrasting characteristics regarding crustal thickness, average chemical compositions and morphologies of volcanoes. Composite volcanoes from the CVZ usually have volumes 3×10^3 km³, heights $>2,500$ m and basal radii of > 15 km. Compositions range from andesites to basalts.

We propose that these differences are due to a different nature of the architecture of magmatic systems characterizing both zones. In the CVZ, the large crustal thickness (~ 70 km) and tectonic regime promote a slow crustal ascent of magma. The small size of volcanoes of this zone is a combination of the higher viscosity of magmas, which favor low effusion rates and shorter lava flows, and because eruptions are triggered from shallow (20 km depth) with low viscosity magmas. Henceforth, these characteristics promote edifices that are built with longer lava flows and reach higher altitudes from its base.

Our work suggests that the longevity of volcanic centers can be controlled not only by the magma output rate from source, but also by the location of reservoirs, rheology of magma and dimensions of the volcanic edifice. Supported by FONDECYT 11121298 and FONDAP 15090013 projects.

Corentin Caudron, Tártilo Girona

Submission 625

Towards forecasting phreatic eruptions using volcano-seismic tremor

Gas-driven eruptions (including phreatic and hydrothermal eruptions in this study) are small-scale volcanic events that have the potential of causing substantial casualties. For example, the 2014 phreatic eruption at Mt Ontake, Japan, killed several dozens of hikers. The destructive potential of phreatic eruptions lies in the difficulty of identifying clear warning signals. Only some phreatic eruptions were preceded by physico-chemical changes, but these were extremely short-term (a few hours), and no long-term trends were clearly evidenced so far. In this work, we identify distinct features in the spectrum and the amplitude of seismic tremor emerging months to years prior to phreatic eruptions at Kawah Ijen (Indonesia), Ruapehu and Tongariro (New Zealand) volcanoes. We show through a mechanistic model of shallow volcano seismicity that this precursory activity reflects significant modifications of the shallow subsurface due to the overpressurization of the shallow crust by volcanic or hydrothermal gases, which eventually leads to phreatic eruptions. Our results highlight the feasibility to assess the onset and the end of an unrest episode, which is of paramount importance for the agencies in charge of volcano monitoring.

Jaime Cavazos, Gerardo Carrasco

Submission 844

Vertical and lateral lithofacies variations of a caldera-related ignimbrite and their implications in an active geothermal system: The case of Los Humeros geothermal field, Mexico.

Los Humeros Volcanic Field (LHVF) is a silicic volcanic complex that records a period of intense magmatic activity since the Pleistocene. It is located in the eastern portion of the Trans-Mexican Volcanic Belt, and actually is one of the main and most studied active geothermal fields in Mexico. The eruptive history of LHVF is marked by a succession of several large explosive events, which include multiple plinian eruptions and the formation of two nested calderas. The larger caldera is Los Humeros, whose structure encloses the geothermal system. This was followed by the nested and smaller caldera: Los Potreros. The voluminous eruption associated with Los Humeros caldera collapse (160-180 ka), generated the Xáltipan ignimbrite. This is a potent sequence of PDC deposits with an estimated volume in order of 115 km³ (DRE), composed mainly of rhyolitic ignimbrites. The deposits of this unit are widely exposed in the outer caldera areas, but mostly buried by younger pyroclastic fill-deposits inside the caldera. The conventional geothermic model refers to Xáltipan ignimbrite as a homogeneous and impermeable unit, which acts as a seal cap. Nevertheless, recent subsurface data obtained from drilling wells in the caldera, shows important vertical and lateral welding heterogeneities. These variations affect directly the permeability conditions and therefore the geothermic efficiency. This work shows the preliminary map of lithofacies of the Xáltipan ignimbrite on the outflow caldera deposits. This new data is based in a reviewed stratigraphic reconstruction and in the application of new generation X-Ray microtomography techniques. These results explain the relation between the facies variations (particularly welding and permeability conditions) with the different emplacement conditions of the PDC currents. This new approach has the potential to be applied to the intracaldera fill deposits and provides a more efficient control of the permeability conditions of the seal unit, which is key in modern geothermic exploitation.

Valerie Cayol, Aurelien Augier, Sébastien Court, Jean-Luc Froger, Sarah Menassian

Submission 1197

Improved Cluster of Volume Strain Method Applied to Volcano Deformation

Interpretation of surface displacement induced by reservoirs, whether magmatic, hydrothermal or gaseous, can be done at reduced numerical cost and with little a priori knowledge using cluster of volume strain methods, where reservoirs are represented by a population of volume strain sources embedded in an elastic half-space. Most of the time, the solution representing the best trade-off between the data fit and the model smoothness (L-curve criterion) is chosen. Our study relies on synthetic tests to improve cluster methods in several ways. Firstly, to solve problems involving steep topographies and medium heterogeneities, we construct unit sources numerically. Secondly, we show that the L-curve criterion leads to several plausible solutions where the most realistic are not necessarily the best fitting. We determine that the cross-validation method, with data geographically grouped, is a more reliable way to determine the solution. Thirdly, we propose a new method, based on source ranking according to their contribution and minimization of the Akaike information criteria, to retrieve reservoirs geometry more accurately and to better reflect information contained in the data. We show that the solution is robust in the presence of correlated noise and that the reservoir complexity that can be retrieved decreases with increasing noise. We also show that it is inappropriate to use cluster methods for pressurized fractures. Finally, the method is applied to the summit deflation recorded by InSAR after the caldera collapse which occurred at Piton de la Fournaise in April 2007. The deformation source is found to be very shallow. Comparison with other data and models indicates that the deflation source is probably related to ongoing fracturing and poro-elastic compaction subsequent to the crater collapse.

Valerie Cayol, Marine Tridon, Jean-Luc Froger, Aurelien Augier

Submission 1209

Inversion of Coeval Shear and Normal Stress of Piton de la Fournaise Flank Displacement

The April 2007 eruption of Piton de la Fournaise was the biggest volcano eruptive crisis of the 20th and 21st centuries. InSAR captured a large (1.4 m) co-eruptive seaward slip of the volcano's eastern flank, which continued for more than a year at a decreasing rate after the end of the eruption. Co-eruptive uplift and post-eruptive subsidence were also observed. While it is generally agreed that volcano flank displacement might be induced by fault slip, we investigate whether this flank displacement might have been induced by a sheared sill, as suggested by observations of sheared sills at Piton des Neiges. To test this hypothesis, we develop a new method to invert a quadrangular curved source submitted to coeval pressure and shear stress changes. This method, based on boundary elements, is applied to co-eruptive and post-eruptive InSAR data. Post-eruptive displacement is well explained by slip and closure of a large fracture sub parallel to the topography (5 km by 8 km), and probably coincident with a lithological discontinuity. The amount of closure is too large and the closure time too short to be explained by a thermally compacting sill, allowing to rule out the sill hypothesis. Co-eruptive displacement can be explained by a smaller (2 km by 2 km) fracture at the same location, submitted to a zero overpressure and a 3 MPa shear stress drop, which confirms that the determined structure is not a sill. We conclude that the fracture is a detachment fold, shallow enough to induce the observed coeval uplift. This finding confirms a previous determination obtained using a decision tree based on ratios of maximum displacements. The determined shear stress change of 3 MPa is consistent with the eastern flank loaded by previously intruded rift dikes.

Matteo Cerminara

Submission 1102

Comparing and understanding volcanic plume models: can integral approaches reproduce 3D simulations?

A recent inter-comparison between integral (1D) and three-dimensional (3D) volcanic plume models has been carried out in the framework of a study promoted by the IAVCEI Commission on Tephra Hazard Modeling. The study highlighted important differences amongst models in estimating both local and global properties of the plume: maximum plume height, neutral buoyancy level and local quantities along the plume axis. This raises questions about the hypothesis behind 1D models and whether it is possible to reduce their discrepancies with respect to averaged properties of 3D simulations. A deeper understanding of this theoretical problem would have an immediate impact on mass flow rate estimates and, consequently, hazard assessment.

To address these questions, a 3D compressible multiphase-multicomponent computational fluid dynamic model for the Large Eddy Simulation (LES) of plumes at geophysical scale is used (ASHEE, ASH Equilibrium-Eulerian model). Results are firstly averaged in time, using all the time steps in a temporal window wide enough to smooth out turbulent fluctuations. Then, they are spatially averaged using a method defined coherently with the hypothesis behind the ASH1D integral model. In this way, it is possible to arise and understand the critical points affecting the accuracy of both 3D and 1D approaches. Indeed, even if 3D models with dynamical LES do not need empirical parameters, they are affected by numerical sub-grid scale error. On the other hand, 1D models enable deeper understanding of the physical phenomenon through a simple theory, but they are strongly dependent on the entrainment parametrization. Theoretically justified modifications to the averaging procedure and to the integral equations significantly improves the agreement between models.

The comparison has been carried out using a wide set of initial conditions, from the experimental scale up to the scale of Plinian eruptions.

Matteo Cerminara, Stella V. Paronuzzi Ticco, Tomaso Esposti Ongaro

Submission 1188

Reconstructing sub-Plinian eruption dynamics by combining field observations, remote sensing data and three-dimensional numerical simulations: the case of April 2015 Calbuco (Chile) eruption.

The three-dimensional ASHEE (ASH Equilibrium Eulerian) model simulates compressible multiphase-multicomponent volcanic plumes. The volcanic mixture, including gas and ash particles finer than about 1 mm is described with a Eulerian quasi-equilibrium approach, able to resolve particle clustering and gravitational settling. In the new version of the model, particles coarser than a few mm can be treated with a Lagrangian approach and one-way/two-way coupling. More realistic atmospheric conditions can also be used, allowing to accurately simulate turbulent plume dynamics and lateral transport of tephra by wind. As a result of gravitational settling and wind advection, particles lost from the plume eventually form a deposit. In the model, deposit mass and thickness are evaluated by removing tephra that reach the bottom boundary. This assumption holds if ash resuspension due to strain and deposit mobilization due to the topography can be disregarded.

The new code has been used to perform Large Eddy Simulations to reconstruct the eruptive conditions of the 25 April 2015 Calbuco sub-Plinian eruption. Detailed field measurements, laboratory analyses and remote sensing data (plume height, umbrella cloud thickness and height, proximal deposit thickness and grain size distribution) have allowed to estimate erupting source parameters and, in particular, to put constraints on the mass eruption rate. Preliminary results show that numerical plume model provide a very effective tool for interpreting observational data. However, to complete the analysis, long range transport under variable atmospheric conditions should be described, e.g. by coupling 3D plume models with atmospheric advection-diffusion model such as the Lagrangian HYSPLIT or the Eulerian FALL-3D models.

Amy Chadderton, Hugh Tuffen, Peter Sammonds, Philip Meredith, Rosanna Smith

Submission 513

The influence of temperature on permeability evolution in Volcán Chaitén rhyolite: An experimental approach

Rhyolitic volcanic eruptions are amongst the largest and most explosive eruptions worldwide, yet due to their rarity have not been directly observed or monitored to the same extent as more common types of volcanism. Two recent rhyolitic eruptions in Chile, Volcán Chaitén in 2008-09 and Cordón Caulle in 2011-12, allowed the first direct observation and monitoring of rhyolitic activity with modern techniques and provided insights into the evolution of highly silicic eruptions, particularly the explosive-effusive transition. Both eruptions exhibited at one stage simultaneous explosive and effusive behaviour with both lava and ash columns being emitted from the same vents. The ability of gas to efficiently decouple from magma in the shallow conduit is believed to control such behaviour, and evolving modes of conduit outgassing and their respective efficiencies hold the key to understanding such hybrid activity.

This study reports the results of a systematic experimental investigation into the permeability of dome material from Volcán Chaitén at magmatic temperatures and shallow conduit pressures, with various pore fluids, using the Rocchi Cell (a high temperature triaxial deformation rig at UCL). Tests were conducted at temperatures up to 600°C with an effective pressure of 5MPa using the steady-state flow permeability technique. The influence of cyclicity and temporal variation on the development of permeable networks was also explored through the experimental program. The results show a complex permeability evolution that includes a reduction in permeability by approximately 3 orders of magnitude up to 600°C with further decreases over periods of several hours at high temperature. Together with porosity data, P and S wave velocities, acoustic emissions and SEM analysis these experimental permeability results are applied to not only draw general conclusions regarding the permeability of volcanic material at high temperature, but also to enhance our understanding of the specific setting of Volcán Chaitén and the observed evolution of eruptive behaviour.

Axial Seamount: Recent results from the most active volcano in the US Pacific Northwest

William W. Chadwick, Jr.

Plenary Talk

Axial Seamount, located 470 km offshore Oregon and Washington and 1400 m below sea level, is one of the most active and is now the best-monitored submarine volcano in the world, via a new cabled observatory. It is a basaltic hot spot volcano superimposed on the Juan de Fuca spreading ridge, giving it a robust magma supply that is continuous but variable with time. Since systematic observations and monitoring began in the 1980s, Axial Seamount has had three effusive eruptions in 1998, 2011, and 2015. Magma is stored in a shallow reservoir beneath the summit caldera. Eruptions are fed by dikes that intrude laterally from the summit 10s of km down either the north or south rift zones. High-resolution mapping of the seafloor with autonomous underwater vehicles (AUVs) have been used to determine the thickness, morphology, and volume of new lava flows from before-and-after surveys, and to document the last 1000 years of summit eruptions in combination with dating and petrologic sampling. Seismicity at Axial Seamount has been monitored both remotely and in-situ by hydrophones and seismometers. Seismic monitoring before and during the 2015 eruption showed that most earthquakes are located along outward dipping caldera faults which apparently also channel magma to the surface. The rate of seismicity builds sharply before eruptions and drops abruptly afterward. Deformation measurements have been conducted at Axial Seamount since the late 1980's with precise pressure sensors that can detect vertical movements of the seafloor. This monitoring has produced a time-series of inflation and deflation that can be used to model deformation sources and constrain the magma supply rate over time. The 2015 eruption was successfully forecast based on this deformation pattern and, in combination with tiltmeter data, revealed the timing, location, and volume of eruption-related magma movements. The vertical deformation cycle at Axial Seamount is large enough (2-3 m) that it can also be measured by repeated AUV bathymetric surveys, opening up new ways to monitor the volcano's behavior. Recent results from the combination of geologic mapping and sampling from ships and submersibles, multi-channel seismic surveys, real-time seismic monitoring, and the long-term deformation time-series have provided new insights into the internal magmatic plumbing system at this excellent natural laboratory for the study of active basaltic volcanism.

William Chadwick, Susan Merle, Carl Kaiser, Edward Baker, Sharon Walker, Joseph Resing, David Butterfield, Tamara Baumberger, Melissa Anderson, Patrick Shore, Doug Wiens, Kenneth Rubin

Submission 1141

A recent volcanic eruption discovered on the central Mariana back-arc spreading center

The first known historical eruption on the Mariana back-arc spreading center was discovered during exploration of the back-arc axis for new hydrothermal vent sites during expedition FK151121 on R/V Falkor in December 2015. A CTD tow-yo along the back-arc axis showed hydrothermal plumes over the site characterized by low-particle concentrations but relatively high reduced-chemical anomalies from an oxidation-reduction potential (ORP) sensor. A dive with the autonomous underwater vehicle (AUV) Sentry (dive 367) collected high-resolution (1-m) multibeam sonar bathymetry over the site, followed by a near-bottom photographic survey over a smaller area. The photo survey revealed the presence of a pristine, dark, glassy lava flow on the seafloor with no sediment cover. Venting of milky hydrothermal fluid was photographed, indicating the lava flow was still warm and therefore very young. The hydrothermal plume sensors on AUV Sentry also measured anomalies over the lava flow. A comparison of multibeam sonar bathymetry collected by R/V Falkor on December 1, 2015, to the most recent previous survey of the area by R/V Melville on February 14, 2013 (expedition MV1302a), revealed large depth changes in the same area, effectively bracketing the timing of the eruption within a window of less than 3 years. The multibeam comparison shows the eruption produced a string of lava flows with thicknesses from 38 up to 127 m along a distance of 7.3 km (from latitude 15° 22.3' to 15° 26.3'N) along the back-arc axis at a depth of 4050 to 4450 m. The cross-axis width of the lava flows is 300-600 m. The AUV Sentry bathymetry shows that the new lava flows are constructed of steep-sided hummocky pillow mounds and are surrounded by older flows with the same morphology. In April and December 2016 two remotely operated vehicle dives were made on the new lava flows by ROV Deep Discoverer (on Okeanos Explorer EX1605L1) and ROV SuBastian (on R/V Falkor FK161129), respectively. The pillow lavas display an extraordinary number of delicate fingers and buds on their surfaces and small cones of radiating pillows were found at the tops of the mounds. Remarkably, the pillows also cascaded down vertical cliffs in some areas without disruption. Only minimal hydrothermal venting was observed during the 2016 ROV dives, suggesting that the eruption had occurred only months before its discovery in December 2015. Samples of the lava flows were collected for geochemical analysis.

Isabelle Chambefort, Colin J.N. Wilson, Julie V. Rowland

Submission 955

New (Zealand) perspectives on continental arc geothermal systems

An enduring question is: what controls the longevity and position of geothermal systems in areas of active volcanism and rifting? Can deep-seated crustal discontinuities focus the upwards transport of subduction volatiles and influence the compositional variability in magmatic and geothermal fluids? Rifting arc models of the Taupō Volcanic Zone (TVZ, New Zealand) are still challenged to link disparate observations, including deep seismic anisotropy and tomography, 3D magnetotelluric inversions, the location and evolution of geothermal systems, magmatic and aqueous fluid compositions, locations of caldera formation and the North Island tectonic environment. By combining recent geophysical, geological, geochemical and structural studies we here consider an integrated model to suggest future research avenues. We present a new hypothesis that the deep feed zones for geothermal systems are located at the crest of ridges on top of the ductile crust.

The TVZ is an extensional arc, representing the on-land continuation of the Tonga-Kermadec arc/back-arc system, marked in its central part by intense magmatism associated with 23 geothermal systems. To accommodate the slightly oblique extension, the brittle crust is segmented, controlled by accommodation zones orientated perpendicular to the arc. These accommodation zones may be the expression of cross-arc magmatic migration as seen just north of the TVZ in the Havre Trough, and commonly elsewhere in arc/back-arc settings, e.g. Japan.

Published 3D inversion magnetotelluric (MT) models of several TVZ geothermal fields show deep feeder zones with a NW-SE orientation (perpendicular to the overall arc alignment) below 5 km depth. These MT anomalies have been interpreted as resulting from fluids (magma or aqueous) in the crust. We hypothesise that deep, long-lasting, crustal cross-arc discontinuities (occurring to accommodate the oblique extension), favour permeability in the ductile crust. These permeable zones are oriented NW-SE; perpendicular to the NE-SW rift elongation. These discontinuities enable vertical mass transport from the mantle wedge, enhancing crustal melting and creating a ridge on the surface representing the brittle–ductile transition. This ridge creates a locus for groundwater convective cells, and explains the persistence of many of the geothermal systems, despite interruption in some cases by caldera collapse, and the variability of geothermal fluid chemistry and magma compositions.

Duane Champion, Drew Downs, Patrick Muffler, Michael Clynne, Andrew Calvert

Submission 1149

Geologic Mapping of the Burney - Pit River Area, California, Using a Multidisciplinary Approach

We use a multidisciplinary approach to elucidate the eruptive history of a gap between Quaternary calc-alkaline volcanoes in the Cascades Volcanic Arc where the Pit River crosses the arc north of the Lassen Volcanic Center and south of Mt. Shasta and Medicine Lake Volcano. This gap leaves intermittent low-potassium olivine tholeiite (LKOT) lava fields as the dominant volcanic expression. These voluminous eruptions fill and level the topography and where faulted, record tectonic strain. LKOTs range from 24 ka to >1 Ma in age; older lava flows are deeply weathered and show few outcrops. Locally, rounded boulders protruding through soils are all that are available. We begin with a thorough search for outcrops and with collection of samples for thin-section petrography and chemical analysis. Discrimination of LKOT units by examination of hand specimens or by thin-section petrography is very difficult owing to intra-flow textural variation being similar to inter-flow variation. Chemical data plotted on Pearce elemental and trace-element variation diagrams reveal affinities and differences among outcrops that help to define eruptive units. Paleomagnetic sampling is done at any outcrop that appears in-situ since it was erupted. Distinctive mean magnetic directions constrain unit correlation. Comparison of chemical and paleomagnetic data generally affirms unit correlations despite minor deflections of the mean remanent magnetic direction owing to deformation of some sites along or near fault scarps. Robust correlation occurs when data from independent and intrinsic chemical and paleomagnetic analyses of samples concur. Samples for $^{40}\text{Ar}/^{39}\text{Ar}$ dating are selected from fresh, dense flows with crystalline groundmass. Argon age experiments on LKOT samples are difficult, due to low K_2O content, common diktytaxitic textures, and low ^{40}Ar rad percentage. Nevertheless, we have experienced success with these experiments, producing ages in conformity with interpreted stratigraphic order. We shall present examples showing how data from these different field approaches support and affirm each other. Over the last 1 Myr, 11–12 areally extensive LKOT lava flows have dominated the eruptive history of this arc gap. They vented from both the north and south sides of the gap, and flowed downhill toward the long-lived topographic low of the Pit River valley.

Sylvain Charbonnier, Charles Connor, Laura Connor, Jacob Richardson, Elodie Macorps

Submission 1065

Assessing the performance of volcanic mass flow models using well-constrained geological data, validation metrics and Bayesian statistics

We propose a methodology for evaluating key flow metrics for a variety of volcanic mass flows. Numerical simulations of volcanic mass flows such as pyroclastic density currents (PDCs), lahars and lava flows have become useful tools for modeling future scenarios of volcanic eruptions (forward modeling) and to constrain eruption parameters using data gathered from deposits (inverse modeling). However, current mass flow hazard assessment at active volcanoes is still often limited to field observations of deposits from past events. Statistical and numerical mass flow models now exist, capable of approximating the motion of a given flow volume from its source to the deposition area. Because of the high impact that modeling and simulations can have, their credibility needs to be assessed. To assess the adequacy of numerical models for volcanic mass flows, a consensual validation procedure should be established. Here, a suite of test cases with validation metrics and Bayesian posterior functions are used to account for and quantify uncertainties related to the numerical simulations of: (1) well-constrained concentrated PDC-forming eruptions from the 2006 and 2010 Merapi volcano eruptions (Indonesia) and July 2015 events at Volcán de Colima (Mexico), (2) lahars from the 2005 Panabaj event (Guatemala), and (3) lava flows from the 2012-13 Tolbachik eruption (Russia). Each of these test cases uses a combination of various geological data (through both field-derived and remote sensing mapping) to define a particular solution to which numerical results from various statistical and numerical models are compared. Results obtained highlights inherent sources of model uncertainties related to (1) initial and boundary conditions including digital topography accuracy, (2) estimation of other input parameters that cannot be directly constrained from geological data (i.e., flow rheology) and (3) complex rheological behavior of these flows over natural terrain. Moreover, the most important source of uncertainty relates to how flow rheology is encapsulated and parameterized in the models, and how associated input or tuning parameters are constrained. Through a series of such similar comparisons, it is hoped that a general validation methodology emerges that can be used in the future to maintain a measure of models' accuracy regarding the simulation of various mass flow events and prediction of their related impacts.

Sylvain Charbonnier, Elodie Macorps, Fenghui Deng, Jean-Claude Thouret, Eliza Calder

Submission 1057

Integrating high-resolution digital mapping and field-derived data to investigate the dynamics and hazards of volcanic mass flows

Volcanic mass flows such as pyroclastic density currents (PDCs), lahars and debris avalanches are responsible for most fatalities during or between volcanic eruptions. Currently, mass-flow hazard assessment at active volcanoes is often limited to field observations of deposits from past events. The topography at these volcanoes largely controls the dynamics of volcanic mass flows, and rugged terrains can greatly affect the flow mobility metrics (volume, inundation areas, run-out distances) and final impacts of these events. Compilation of pre-, syn- and post-eruptive data obtained from four selected, well-constrained, major PDC and lahar events at active volcanoes from Indonesia and Latin America allows us to better understand the influence of varying topographic parameters on the internal flow dynamics. Results include (1) careful mapping of the stratigraphy, distribution, thicknesses and surface morphologies of the different deposit units, (2) identification of longitudinal and lateral lithofacies variations based on changes in grain-size distribution, coarse-tail grading and matrix componentry inside each stratigraphic unit, and (3) a geomorphic characterization of the variations of local topography (i.e. slope, curvature, surface roughness) and channel geometries (sinuosity, width and cross-sectional areas) along the flow paths. Combining the data sets from the four targeted eruptions led to the identification of quantifiable relationships between deposit footprint and surficial/sedimentological features, retaining capacity of the receiving landscape and scale-dependent tendencies for flows to overspill confined channels. It can also be shown that the use of high-resolution satellite datasets and digital elevation models, produced through various remote sensing techniques (using both optical and radar satellite data), is vital for an accurate characterization of areas prone to such currents and their associated hazard and impact capacity, thereby reducing their potential risk. These findings aim to: (1) define new semi-empirical relationships between the processes that control the emplacement and deposition of volcanic mass flows and their potential for overspill/avulsion related to channel geomorphic parameters; (2) invert some key flow parameters at critical locations that will constitute part of the source database needed for enhancing and calibrating standard mass-flow hazard models.

Lauriane Chardot, Benoit Taisne

Submission 984

Testing an alternative model to explain results from the Material Failure Forecast Method

Common signs of volcano unrest include changes in monitoring data including geodetic data, geochemistry data and/or seismicity data. For the latter, increasing seismicity is often observed prior to volcanic eruptions, but not all seismicity increases are followed by an eruption. Assessing the effect of increasing seismicity on the likelihood of an eruption is therefore challenging. Several options can be explored to tackle this challenge including optimizing monitoring networks to get more useful data, developing robust methods to analyze these data and proposing new models to explain the data.

The Material Failure Forecast Method (FFM) can allow us to get the potential timing of an eruption from the evolution of an observed seismic increase. This method relies on a model involving failure of an edifice (e.g., volcanic conduit) due to loading (e.g., magma pressurisation), similar to slope failure following rainfall events. It doesn't account for the seismicity location for eruption forecasting, only the rate of the seismicity increase. What insights can the FFM give in the case of migrating seismicity, e.g., due to upward magma migration?

As seismicity gets shallower, the distance between the seismic source and the monitoring site decreases, as does the attenuation. This leads to an increasing seismic intensity recorded at the site. Would this apparent increase be captured and well explained by the FFM? This alternative interpretation of increasing seismicity preceding eruption, might provide a robust explanation to the success/failure of the FFM to predict the onset time of an eruption.

We will present applications of the FFM on synthetic seismicity increases due to upward seismicity migration. The aim is to offer a potential alternative and robust model to explain the results of the FFM. Ultimately, our results will help understand precursory activity to eruptions.

Danielle Charlton, Christopher Kilburn, Stephen Edwards

Submission 95

Communicating hazard information to varying audiences

Hazard maps are among the most commonly-used communication tools, yet they are often distributed without regard for the preferences and needs of different audiences. Incorporating audience preferences in map design is a simple, but underused, method that allows users to feel included in the process of hazard mapping. Few studies have investigated the preferences of those using volcanic hazard maps and so few maps have been constructed with any appreciation for user preference.

Here we present the results of a global online survey of 217 individuals, from 27 countries. The survey was used to understand map user preferences in a volcanic hazards mapping context. Participants were categorised by audience group, age, location and mapping experience. The two biggest audience groups were the general population (53%) and scientists (33%). Emergency responders, government officials, and the media also responded. We compared participant's preference for five types of hazard map and the option to see them all. The maps were geological, integrated, administrative, probabilistic and those that included timings. Overall, respondents clearly preferred geology-based maps, where the hazard is clearly labeled. However, when divided by the user there were differences in preference. 21% of the scientists chose the administrative map as their top choice compared to only 8% of the general population surveyed. 24% preferred the option to be able to see all the hazard information available to them, which was the top choice for respondents from New Zealand. Evacuation information clearly stood out as being important to 44% of respondents and was second in terms of importance after hazard type. In terms of design and formatting, we found that 73% of respondents preferred to see a hazard map online over a paper map.

Many of our findings, coupled with the increasing volume of information delivered online both suggest an inevitable progression to online hazard mapping. Results demonstrated preferences in how users would like to see hazard information. However, clearly one map will not suit the needs of all map users. To address this challenge, the development of interactive online hazard maps with which users can integrate the information of specific interest should be investigated further. These maps can provide different users with quick access to mapping information and accommodate both different preferences and levels of user involvement.

LiLu Cheng, Fidel Costa

Submission 607

Quantification of multiple plagioclase crystal populations using fractal analysis of mineral and glass inclusions

Many plagioclase phenocrysts from volcanic and plutonic rocks display quite complex chemical and textural zoning patterns. Understanding the zoning patterns and variety of crystal populations holds clues to the processes and time scales that lead to the formation of the igneous rocks. Here we provide a new technique using the fractal spectra analysis of mineral and glass inclusion textures to quantitatively characterize the crystal populations. We first analyze the random sections of single crystals, and then calculate the fractal spectra of 2D plagioclase sections produced by the same 3D model. Base on these results, we use the cluster dendrogram to group them to discuss the effect of random cuts. We contrasted our models to 3 dimensional images of Fe-Ti oxide inclusions obtained by X-ray computer tomographic scans. Using the fractal spectra and cluster dendrogram to samples from 1947 eruption of Mayon volcano indicate there are two main plagioclase populations, despite the large variety of plagioclase crystals seen in two dimensional electron backscattered (BSE) images. These results are compatible with our statistical analysis of plagioclase populations based on anorthite distributions (Cheng et al., 2017). Application of statistical petrological analysis of volcanic rocks can provide unique insights into decoding the crystal record thus unraveling magmatic processes.

Cheng, L., Costa, F., Carniel, R. (2017) Unraveling the presence of multiple plagioclase populations and identification of representative two dimensional sections using a statistical and numerical approach. *American Mineralogist*, doi: 10.2138/am-2017-5929CCBYNCND

Oryaëlle Chevrel, Jérémie Labriquère, Andrew Harris, Scott Rowland

Submission 505

PyFLOWGO: an open-source platform for simulation of channelized lava thermo-rheological properties

Lava flow advance (velocity, morphology) may be modeled through tracking the evolution of the lava's thermo-rheological properties, which are defined by viscosity and yield strength which in turn evolve with cooling and crystallization. Harris and Rowland (2001) conceived a 1-D model (FLOWGO) in which flow velocity is computed via the Jeffreys equation as modified for a Bingham fluid by Moore (1987). Solution depends on rheological properties computed following the lava cooling and crystallization path estimated via a heat balance. Originally FLOWGO was written in the programming language IDL (Interactive Display Language) and the script was owned by Harris and Rowland (2001) who would share it if requested. Due to license price and other issues this code was set aside and an Excel version was written (Harris et al. 2015). This was freely shared with other scientists. Although Excel is a convenient tool, easily and widely used by geologists, it has limited applications, poor flexibility for model evolution, cannot be easily incorporated into other software and, when many equations and input parameters are stacked in sequence, it becomes too easy to key in a hidden (or very-hard to find) error.

We thus provide FLOWGO in a modern and flexible language, while providing input cards that reduce the likelihood of erroneous parameter or relation entry. Python was chosen because it is open-source, it provides useful libraries, and its object-oriented approach allows for great flexibility. Furthermore, Python is available on any operating system which removes the problem of portability, so that it has been widely adopted in scientific computing during recent years. We describe here the code (PyFLOWGO) and the various models that can be chosen to run a lava flow simulation (heat flux, rheology, crystallization rate, crust temperature, crust-cover fraction). As validation, several cases are tested (Mauna loa 1984, Mauna Ulu 1974, and Piton de la Fournaise 2010) and results are discussed in terms of model convergence, errors and limitations. We finally provide a detailed user-guide for the software that is open-source and can be download via GitHub, making all aspects of PyFLOWGO freely available to the community.

Oryaëlle Chevrel, Nanci Reyes Guzman, Claus Siebe, Marie-Noëlle Guilbaud

Submission 1153

Emplacement characteristics of thick andesitic lava flows: Case of the western part of the Zacapu basin in the Michoacán-Guanajuato Volcanic Field, Mexico

Thick andesitic flows are common within the 40,000 km² Michoacán-Guanajuato Volcanic Field (MGVF) yet their emplacement characteristics are poorly known. The youngest of these are sparsely vegetated and locally called “malpaíses” (badlands in Spanish). They reach up to 100 m in thickness and up to 3 km³ in volume, and have a rough blocky surface almost devoid of soil cover.

The western part of the Zacapu lacustrine basin in the central part of the MGVF contains over 36 thick andesitic lava flows within an area of 400 km². The youngest of them, Malpaís Prieto, is dated at AD900 and is in average 3. El Infiernillo (the oldest) is 3). Malpaís Las Víboras is 80 m thick and 3. El Capaxtiro covers >21 km² and consists of 10 flows which are 150 m thick in average. This later represents the largest eruption in that area during the Holocene with a volume of ~3.2 km³. All these lava flows share a similar texture and petrography: they are dense (

Curiously the western-Zacapu lavas are very similar in petrography and bulk composition to late lavas from AD1250 El Metate shield volcano, although El Metate lavas are larger in size, the longest of these being 15 km long and 2.5 km wide, 77 m thick in average, and 3.4 km³ in volume. At El Metate lava viscosity was estimated at 109 to 1011 Pa.s and emplacement duration at 2 to 7 years, which likely correspond to a higher bound for western-Zacapu lavas. We aim to discuss here how the explosive behavior was avoided during the eruption of such evolved, crystalline magmas, suggesting an efficient open system degassing (outgassing) of the magma as it was stored temporally at shallow depth within the thick upper crust underlying the central part of the MGVF.

Massimo Chiaradia, Luca Caricchi

Submission 126

Crustal magmatic processes controlling the formation of porphyry copper deposits

Porphyry deposits, our main source of copper and of significant amounts of Mo, Re and Au, form at convergent margins in association with intermediate-felsic magmas. Although it is accepted that copper is transported and precipitated by fluids released by these magmas, the magmatic processes leading to the formation of economic deposits remain elusive. Here we perform Monte Carlo petrological and geochemical modelling to quantitatively link crustal magmatic processes and the geochemical signatures of magmas (e.g., Sr/Y) to the formation of porphyry Cu deposits of different sizes. Our analysis shows that economic deposits (particularly the largest ones) may only form in association with magma accumulated in the lower-middle crust ($P > \sim 0.5$ GPa) during $\geq 2-3$ Ma, and subsequently transferred to and degassed in the upper crust over periods of up to ~ 2.0 Ma. Magma accumulation and evolution at shallower depths (

Brandon Chiasera

Submission 311

Magmatically assisted off-rift extension – a study of the Galema range

Within continental rift settings, extensional strain is initially accommodated along the nascent rift margins, subsequently localizing to zones of focused magmatic intrusion. The migration of strain from rift border faults to diking, places an emphasis on constraining the magmatic plumbing system of focused intrusion zones to resolve how extension is accommodated in the rift lithosphere. Existing rifting models concentrate on the relationship between extension and focused magmatism within the rift, but there are interesting cases of contemporaneous magmatic focusing immediately outside the rift margins. We examine the Galema Range, an area of focused magmatic intrusion along the eastern margin of the Ethiopian Rift, which is morphologically similar to areas of focused magmatism within the rift. We find that whole rock thermodynamic modeling and thermobarometric calculations suggest that fractionation (and hence magma stalling depths) within the magmatic plumbing system of the Galema Range is polybaric (~25 and ~11 kbar). These results, when compared with zones of focused intrusion within the rift, are strikingly similar. Lithospheric extension acting along the Galema Range, and possibly taking advantage of a basement suture, provided precursor to focused magmatism within the rift zone.

Giovanni Chiodini

Submission 470

Modelling the effects on the hydrothermal system of Campi Flegrei of magma degassing approaching the critical pressure

An ascending magma batch, upon decompression, selectively releases dissolved volatiles depending on their solubilities so that, while barely soluble CO₂ dominates “deep” degassing, more soluble H₂O prevails at shallow depths. This selective release of volatiles from magma implies that heat transfer to overlying hydrothermal systems exhibit a non-linear pressure dependence. By applying a gas-melt degassing model, we find that there is a narrow pressure interval (CDP, critical degassing pressure) over which the total amount of separated fluid and of the associate thermal energy steeply increases by more than one order of magnitude. Evidence of critical degassing, and consequent heating of the hydrothermal system, are clear at Campi Flegrei caldera. Large variations in the N₂-He-CO₂-Ar fumarole compositions, indicative of degassing in open-system conditions at increasingly lower pressures, are in fact accompanied by a 15 years long exponential increase of the fumaroles’ CO indicating a generalized heating up of the hydrothermal system. Based on these observations Campi Flegrei magmatic system may be approaching the CDP, i.e. a depressurising magma batch is releasing fluids of progressively more H₂O-rich (and CO₂-poor) compositions, perturbing the thermal structure of the hydrothermal system. This hypothesis was tested by comparing the observed geochemical and geophysical signals with the results of TOUGH2 models of a hydrothermal system affected by the input of magmatic fluids, which increase their H₂O/CO₂ ratio during time. Ground deformation, background seismicity and gas geo-indicators proceed following surprisingly well the simulated time pattern of temperature increase of the hydrothermal system. We conclude that magma degassing approaching CDP and heating of the system are controlling the ongoing volcanic unrest of Campi Flegrei caldera.

Bruce Christenson, Agnes Reyes, Ben Kennedy, Richard Henley, Aaron Farquhar

Submission 619

Processes leading to hydrothermal seal formation and failure in “wet” volcanic vents: Insights from some recent NZ phreatic eruption events.

Phreatic eruptions are amongst the most poorly understood and least predictable hazards from active volcanic systems. Three such eruptions from NZ volcanoes over the last 11 years resulted in either loss of life, serious injury, and/or infrastructural damage, and all occurred with little or no warning (Raoul, 17-3-2006; Ruapehu, 25-9-2007 and White Island, 27-4-2016). Evidence suggests that these were gas-driven events, the principal cause for which was permeability reduction through progressive hydrothermal mineralization in the vent conduits. Fluid inclusion data from ejecta from each of these events define temporal patterns of temperature and pressure cycling of fluids in the respective vent environments, with rapid transitions from low temperature liquid, through two-phase (vapor + liquid) conditions, to higher temperature gas-dominant (CO₂-rich) gas mixtures. These observations are consistent with periodic development of high pressure, non-condensable gas columns beneath sealed or partially-sealed vents prior to eruptive release.

Where degassing magma lies close to the surface, as at White Island and Ruapehu, dissolution of evolving magmatic acidic volatiles (SO₂, H₂S, HCl) into the enclosing hydrothermal fluids leads to the formation of hyper-acidic fluid regimes, and aggressive fluid-rock interaction. Mineral phases involved in seal formation in this aqueous environment include elemental S, sulfate minerals (anhydrite, gypsum, alunite, natroalunite) and Fe(Cu) sulfide phases. Fast high temperature reactions may also occur directly between magmatic SO₂ and Ca-bearing mineral phases, also leading to the formation of anhydrite. At Raoul, deeper level water-rock interaction scrubs out SO₂ and HCl, leaving the less reactive and less soluble CO₂ to condense into shallow aquifers leading to the formation of carbonate-dominant (i.e., aragonite and calcite) seals with minor anhydrite.

We propose that explosive decompression (and eruption) occurs when gas pressures exceed the critical tensile strength (t) of the seals. Pressures within such gas columns are stepped between hydrostatic (liquid water density $\sim 1000 \text{ kg/m}^3$) and vapor-static (vapor density 3) such that column development transmits increasing pressure to higher level sealed fractures until the condition, $P_{\text{gas}} > P_{\text{lithostatic}} + t$. Pressure-temperature conditions at a seal, as modelled with TOUGH2, are defined by heat and mass flux through the evolving column.

Annemarie Christophersen, Lauriane Chardot, Nico Fournier

Submission 443

Bayesian Networks as potential decision support tools in monitoring volcanoes and forecasting eruptions

For many years, Bayesian Networks (BNs) have been advocated as decision support tools in volcanic crises. However, so far BNs have not been implemented as operational eruption forecasting tools. We explore the potential use of BNs for volcano monitoring to forecast eruptions by adapting a previously published model for a volcano in New Zealand and by involving the volcano monitoring team to modify the model and elicit the necessary probabilities in a workshop setting.

BNs are probabilistic graphical models that represent a set of random variables and their conditional dependencies. The random variables are represented by nodes and can be described by discrete states or by continuous probability density functions. The dependencies between nodes are illustrated by arrows and quantified by conditional probabilities for discrete variables and correlations for continuous variables. BNs provide a framework to model complex systems and are used as powerful tools in hazard and risk assessment in many different domains.

A small team with expertise covering volcanology, social science, earthquake forecasting, neural networks and BN modelling modified the published BN structure from the La Soufrière volcano (Guadeloupe) to White Island volcano (New Zealand). The team also developed a questionnaire to elicit the conditional probabilities for the BN. Other members of the volcano monitoring team then reviewed and modified the structure to present the current conceptual model of White Island, including the monitoring data that are regularly collected.

A workshop was held in December 2015 and included nine experts from within the volcano monitoring team, one from the University of Auckland and one from Massey University. The workshop was interactive with discussions on structured expert elicitation and BN modelling. The experts estimated 120 conditional probabilities and their uncertainties and answered questions on thresholds for monitoring data as well as general comments on the BN and the process.

For many conditional probabilities there is a wide spread of answers indicating large uncertainties about the variable in question. Overall, the probabilities for monthly eruption are higher than observed. This might be a consequence of the challenge to estimate small probabilities. Estimating the probabilities within a model context allows for testing the forecasts and calibrating with observations.

Jong-Hwa Chun, Yuri Kim

Submission 465

Tephra layers in deep-sea UBGH cores derived from submarine explosive volcanic eruptions at the South Korea Plateau, East Sea

Geophysical studies established the existence of submarine volcanoes on the South Korea Plateau (SKP) in the East Sea based on magnetic anomalies and Chirp sub-bottom profile data. The SKP tephra layers derived from submarine volcanoes (at a water depth of about 1,000 m) at the South Korea Plateau have been identified in deep-sea UBGH cores from the Ulleung back-arc basin since the early Pleistocene. The SKP tephras composition indicates an origin from phonolitic or trachytic alkali magam with high alkali and low silica contents. Fine-grained scoria and pumice lapilli exhibit a distinctly bimodal grain size distribution. The vesicular microstructure of SKP tephras includes bridge forms, coalesced bubbles, distorted circular forms, and highly fractured circular form, which are quite different from the elongated circular forms of Ulleung tephra from subaerial volcano. Scoria vesicles have distinctive isolated circular forms with thick walls. The vesicle characteristics of SKP tephras indicate that the SKP tephras formed under high hydrostatic pressure during explosive volcanic eruptions. The SKP tephra layers are thicker in cores from the South Korea Plateau than in cores from the deep Ulleung basinplain, and accumulated from both fallout and gravity currents. The eruption column from a submarine volcanic eruption is similar to those of subaerial eruptions, except for the development of a buoyancy-driven convection column caused by the density contrast between the eruption column and cold seawater. Floating volcanic particles are commonly transported at the sea surface. Such particles are most abundant near vents, but also form high concentrations in density flows on the sea bottom of the South Korea Plateau. The remaining floating particles were transported to the deep Ulleung Basin predominantly by surface currents. The spatial distribution of the SKP tephras in the East Sea would be influenced by explosiveness and prevailing wind or currents directions.

Valeria Cigala, Ulrich Küppers, Juan Jose Pena Fernandez, Jacopo Taddeucci, Joern Sesterhenn, Donald B Dingwell

Submission 326

What is controlling pyroclast ejection dynamics? Analyzing the boundary conditions affecting velocity and trajectory via shock-tube experiments.

The variability of pyroclast ejection dynamics observed during explosive volcanic eruptions is due to complex interactions among different parameters defining the boundary conditions. Scaled and repeatable laboratory experiments come in hand to characterize the effect of such parameters on eruption features.

Here, we focus on the dynamics of pyroclast ejection of impulsively released gas-pyroclast mixtures (i.e., mimicking processes in the gas-thrust region during unsteady eruptions). Gas-particle mixtures were released in a series of shock-tube experiments with varying 1) tube length, 2) vent geometry, 3) gas-particle ratio, 4) initial temperature and 5) particle size distribution. The tube length was varied by changing the starting sample load, allowing for variable time for particle acceleration. Additionally, four vent geometries were employed, a nozzle with converging walls (5°), a cylinder and two funnels with walls diverging at 15° and 30°, respectively. The experiments were performed at 25 and 500°C using particles from 2 to 0.125 mm in diameter. The initial pressure was always 15 MPa.

The temporal evolution of particle velocity as well as the spreading angle of the exit trajectory and their dependence on boundary conditions was analyzed from high-speed videos of the ejections. Max velocity of 300 m/s was observed together with a non-linear decay of exit velocity over time. The exit trajectories were found to deviate from the vertical by 5° to 45° and display a non-linear evolution with time. Moreover, the velocity decay was used to investigate the accuracy of the empirical fragmentation depth model from Alatorre-Ibargüengoitia et al. (2011) when different gas-particle ratios are employed.

We observed a) positive correlation of particle velocity with diverging vent walls and temperature and b) negative correlation with starting tube length and particle size. On the other hand, the spreading angle showed negative correlation with 1) diverging walls, 2) starting tube length, 3) temperature and 4) particle size. Moreover, gas-particle ratio strongly affects the temporal evolution of both ejection velocity and trajectory. These results highlight the importance of scaled and repeatable laboratory experiments for an enhanced understanding of volcanic phenomena that bear direct observability. Establishing a close link between governing parameters and observed behavior will enhance volcanic hazard assessment.

Corrado Cimarelli, Damien Gaudin, Joshua Méndez-Harper

Submission 821

From ashes to flashes: experimentally mapping the conditions for electrification and lightning in volcanic plumes.

Volcanic explosive eruptions can produce intense electrical activity and volcanic lightning. As in thunderclouds, lightning in volcanic plumes generates electro-magnetic pulses that allow their location from safe distance and in all weather conditions. Volcanic lightning mapping is thus emerging as a powerful volcano monitoring tool. A thorough understanding of plume electrification is yet hampered by the lack of i) systematic instrumental observations and ii) constrained laboratory experiments.

We have first achieved electrical discharges in particle-laden jets simulating volcanic explosions by rapid decompression experiments (Cimarelli et al., 2014 *Geology*). Our effort is now in mapping the conditions at which electrical discharges happen. We have so far explored the influence of grain size distribution, the chemistry of the material, the mass eruption rate, the overpressure conditions at the vent and the influence of shock waves generated by the explosions. In addition, the basic microphysics processes underlying particle electrification have been investigated by contrasting the effect of triboelectrification versus fractoelectrification in constrained experiments. The experimental results show a good correspondence with field observations (Cimarelli et al., 2016 *GRL*) and point at the dynamic of the volcanic explosion as the main responsible for the electric structure of volcanic plumes, where “internal” parameters of the volcanic jets prevail on ambient atmosphere “external” parameters. Our experiments thus further highlight the importance of volcanic lightning monitoring not only as a tool for locating and tracking volcanic plumes but also, and more importantly, for deriving fundamental intrinsic plume source parameters otherwise difficult to retrieve at erupting volcanoes.

Benjamin Clarke, Eliza Calder, Joaquin Cortes, Mark Naylor, Firawalin Dessalegn, Ian Butler, Karen Fontijn, William Hutchison

Submission 330

Achneliths with Evidence of Post-Emplacement Vesiculation at Aluto Volcano, Main Ethiopian Rift: New constraints on Fragmentation and Eruptive Styles at Peralkaline Rhyolite Volcanoes

The fragmentation of peralkaline rhyolites is considered somewhat enigmatic. Peralkaline rhyolitic melts, due to their high Na⁺, K⁺ and halogen contents, have low melt viscosities relative to metaluminous melts of equivalent silica content. While typical rhyolite viscosities are around 108 Pa S, the viscosity of H₂O free peralkaline rhyolites at eruptive temperatures are around 105.5 Pa S, and with 1 wt % H₂O this value drops to 103 Pa S. Such viscosities necessitate unrealistically high strain rates to undergo brittle fragmentation, despite showing significant evidence of doing so.

Our discovery of some unusual, globule-shaped pyroclasts in a peralkaline rhyolite pyroclastic deposit sheds light on these poorly understood processes. These pyroclasts occur within an unconsolidated pyroclastic succession associated with a pumice cone at Aluto volcano in the Main Ethiopian Rift. The clasts are lapilli to ash sized, often have a droplet-like morphology and are characterised by a distinctive obsidian skin indicative of having been shaped by surface tension. We adopt Walker's term 'achneliths' for these clasts. These achneliths however, unlike their mafic counterparts, are highly vesicular (up to 92 vol % vesicle), and the glassy skin often shows a thinly bread-crust texture. Importantly, there is strong evidence for post-depositional, in-situ, inflation, including expanding against other clasts and in some cases fusing together. Similar clasts, referred to as 'globules', have been found in welded pyroclastic deposits at other peralkaline volcanoes, however, the unconsolidated nature of the Aluto deposits means that these clasts are easily separated providing an opportunity to study their features in 3D using μ CT, SEM and EPMA.

Textural observations, in addition to numerical cooling models for these pyroclasts, provide constraints on the eruptive styles and fragmentation processes associated with different clast types found at Aluto. These models could be applicable to peralkaline rhyolite eruptive products elsewhere. We also suggest that the post-deposition inflation of pyroclasts is a principal contributory factor in the welding of peralkaline pyroclastic deposits.

Laura Clor, Peter Kelly, Steven Ingebritsen, William Evans, Deborah Bergfeld, Christoph Kern, Michael Doukas, Aaron Rinehart

Submission 331

Gas emissions monitoring at Mount Hood volcano, Oregon, USA

We present chemical and isotopic gas monitoring data and emission rates from Mount Hood, Oregon. Mount Hood (3,426 m) is an iconic, glacier-clad Cascade Range volcano located approximately 70 km east of Portland, Oregon (pop. ~600,000). It is designated a “high threat” volcano by the US Geological Survey’s National Volcano Early Warning System (NVEWS) assessment due to its eruptive history and close proximity to regionally-significant population centers and infrastructure. Mount Hood’s last confirmed eruption was in 1865 but it sustains an active hydrothermal system, as evidenced by numerous fumaroles and elevated ground temperatures in the summit crater, and also by the discharge of thermal waters (T up to ~25°C) from springs on the south flank up to ~10 km from the summit.

The direct gas sampling record from Mount Hood spans over 80 years (1935–present) and includes 33 samples for bulk chemistry, 7 samples for ^{13}C -CO₂ collected between 1997–present, and 11 samples for $^3\text{He}/^4\text{He}$ collected between 1978–present. Most of the samples were collected irregularly, but annual samples have been systematically collected from 2009–present. The measured gas compositions and fumarole outlet temperatures (~89°C; boiling point for 3200 m) have remained generally stable over the period of record. Undiluted, dry fumarole gases are predominantly CO₂, up to 96.7% by volume. Sulfur is present as H₂S, consistent with a developed hydrothermal system, with a maximum of 7.4% in our samples. CO₂/H₂S ratios range from 12–35 and recent samples (2009–present) average ~17, which is also typical of hydrothermal emissions (CO₂/Stotal > 10; Stotal = SO₂ + H₂S). As an indicator of source components for these gases, N₂/He ratios are intermediate between “mantle-derived” and typical “arc-type” gases, suggesting a strong mantle component in the source of the gases from this arc volcano. Helium isotopic ratios (R_c/R_a) at both Crater Rock near the summit and at Swim Warm Springs on the volcano’s lower flank have remained very stable over time at 7.18 ± 0.42 , also consistent with a mantle source for the He. Calculated reservoir temperatures range from 300–380°C, derived from the D’Amore and Panichi (1980) gas-geothermometer. Airborne measurements performed in 2014 reveal a CO₂ emission rate of ~120 tonnes/day, and an H₂S emission rate of ~1 tonne/day for gases emitted from the summit area. These emission rates are similar to those for other quiescent Cascade Range volcanoes.

Michael Clynné, Duane Champion, Maren Wanke

Submission 506

Stratigraphy and Age of the Castle Creek Eruptive Period, Mount St. Helens, Washington

The Castle Creek Eruptive Period (CCP) at Mount St. Helens (MSH) was one of the most active and complex periods in the volcano's history and was the only one that produced basalt. Based on new stratigraphy, ¹⁴C ages and paleomagnetic data, we redefine the previous CCP definition of Crandell (1987) and Mullineaux (1996). We also report new lithologic and compositional data. Based on composition and age, we divide the CCP into: 1) Early CCP, 2) Middle CCP, and 3) Late CCP. Early CCP comprises a group of lithologically similar pyroxene andesite/dacite domes (e.g., Northwest Dome), lava flows, tephra Bi, and associated lahars that are found on all but the southeast flank of MSH; all were emplaced around 2,000 B.P. Middle CCP comprises 3 groups of lithologically distinct olivine basalt lava flows (e.g., Cave Basalt), and tephra Bu1 found on the south flank of MSH that were emplaced ~1895 B.P. Late CCP comprises 9 units of lithologically diverse olivine basalt (e.g., Castle Creek basalt) basaltic andesite and pyroxene andesite lava flows and tephras Bu2 and Bu3, that are mostly found on the north flank of MSH. Late CCP units were emplaced between ~1800 and 1700 B.P. Paleomagnetic secular variation data for CCP units are distinct from the preceding Pine Creek and the subsequent Sugarbowl Periods and are consistent with the path of the virtual geomagnetic pole for western North America. These secular variation-data aid in the placement of several units that lack definitive stratigraphic relationships, especially for the Late CCP lava flows.

Middle and Late CCP units include three compositionally distinct mafic end-members: 1) high-K basalts that are enriched in K, Ti, P and incompatible elements (resembling Cascades OIB-like basalts), 2) low-K basalts with comparatively low incompatible-element compositions akin to Cascades low-K tholeiites, and 3) arc-type basaltic andesites, similar to typical calc-alkaline Cascades basalts but more evolved. Early CCP andesite/dacites may be related to a single or closely related magma batches. Middle CCP units can be related by mixing between two distinct batches of basalt. The array of Late CCP units cannot be simply related but require multiple batches of compositionally distinct basalt, mixing with more felsic magmas, and fractionation to explain their compositions. The close temporal and spatial eruption of diverse CCP lavas has important implications for understanding the origin, evolution and ascent paths of MSH magmas.

Rebecca Coats, Biao Cai, Jackie E Kendrick, Paul A Wallace, Taka Miwa, Adrian J Hornby, James D Ashworth, Felix W von Aulock, Peter D Lee, Jose Godinho, Yan Lavallée, Robert C Atwood

Submission 1008

An experimental investigation into magma rheology using natural and analogue materials

Laboratory experiments on natural and synthetic magmas allow us to systematically vary parameters to investigate the way they may flow or fail. Such understanding of the rheology of magma is vital to gain an insight into the controlling factors on eruption style.

Concerned with the effect crystals and bubbles have on the non-Newtonian rheology of magmas, we carried out uniaxial compressive experiments on a suite of both natural and synthetic samples.

Experiments, carried out on variably porous (9-32 vol.%) and highly crystalline (> 50 vol.%) dacites from Mt. Unzen, Japan, demonstrated that uniaxial compressive strength systematically decreases with porosity, a finding which is widely accepted in the scientific community. In addition to this result, tests have also revealed strength to be strain rate dependent, and, more critically, to increase at higher temperatures (900°C), an outcome not previously observed in glass-bearing volcanic rocks. By applying Gent's (1960) parallel plate theory, viscosities were calculated for experiments that resulted in a viscous response. Apparent viscosity decreased with increasing strain rate, known as a shear-thinning response. However, we also found that for the materials investigated, viscosity showed no dependence on porosity (within the ranges of porosity, temperature stress and strain tested).

As the nature of three-phase volcanic materials is complex we recently sintered glass materials, analogical to natural magma, with atmospheric air filled pores (2 particles (0-50 vol.%)). We performed a series of high-temperature compression experiments on those 'simpler' synthetic magmas. These were conducted in the laboratory and key experiments were repeated whilst performing in-situ x-ray tomographic imaging at the Diamond Light Source, UK. We Preliminary results have shown that at room temperature strength is independent of crystal content, but at higher temperatures, strength decreases with increasing crystal volume. A possible explanation of this strength reduction is that the surrounding glass becomes increasingly brittle with the addition of particles. Work on synthetic samples is on-going and results are expected to shed light on the way in which crystal-bearing magma may flow and fracture.

Gent, A. N. (1960). Theory of the parallel plate viscometer. *British Journal of Applied Physics*, 11(February), 85–87. <http://doi.org/10.1088/0508-3443/11/2/310>

Matthew Coble, Seth Burgess

Submission 893

New zircon U/Pb and (U-Th)/He eruption age for the Rockland tephra from Lassen Volcanic Center in the southern Cascade arc

Eruption ages for a number of widely distributed Quaternary volcanic deposits remain inaccurately and/or imprecisely constrained, despite their importance as regional stratigraphic markers in paleo-environmental reconstructions and as evidence of climate-altering eruptions. Accurately dating volcanic deposits presents challenging analytical considerations, including poor radiogenic yield, scarcity of datable minerals, and contamination of crystal populations by magma, eruption, and transport processes. One prominent example is the Rockland tephra, which erupted in the Quaternary from the Lassen Volcanic Center in the southern Cascade arc. Despite a range in published eruption ages from 0.40 to 0.63 Ma, the Rockland tephra is extensively used as a marker bed across the western United States. To improve accuracy and precision of the age of the Rockland tephra-producing eruption, we present new U/Pb zircon crystallization dates from the outermost $\sim 2 \mu\text{m}$ of crystal faces (surfaces) using secondary ion mass spectrometry (SIMS). As an independent test of the accuracy of this age, we determined new (U-Th)/He dates from individual zircon grains. Our data yield good agreement between our new U/Pb and (U-Th)/He zircon ages, which reinforces accuracy of these methods and confirms that zircon surface U/Pb dates sample zircon growth up to the time of eruption. We compare these results to previously published $^{40}\text{Ar}/^{39}\text{Ar}$ ages and U/Pb zircon measurements performed on polished grain interiors, as well as discuss the broad applicability of coupled U/Pb zircon-surface and single-grain zircon (U-Th)/He geochronology to accurate dating of Quaternary tephra.

Simone Cogliati, Sarah Sherlock, Alison Halton, Kerry Reid, Tiffany Barry, Mike Branney, Simon Kelley

Submission 401

Noble gases: a tool to track the degassing of active volcanic systems

He, Ne and Ar are widely used to characterize magmatic reservoirs and to study volcanic processes. Their isotopic signature and fractionation (e.g. $4\text{He}/40\text{Ar}$ ratio) provide information on magma source, differentiation, contamination and degassing. Several studies have investigated sources, reservoirs and chemical controls of noble gases, but few efforts have been made to study which factors control noble gas incorporation, partition and release during degassing episodes.

The aim of this research is to identify these factors and to test how they influence noble gas behaviour in volcanic rocks with different degassing histories. This will help improve our understanding of how noble gases are recycled into the atmosphere during volcanism. Particular attention will be given to the behaviour of Ar because of its use in $40\text{Ar}/39\text{Ar}$ dating. A better knowledge of how Ar is trapped and released from volcanic rocks will help find a solution to the 'excess argon problem': the presence of an excess portion of 40Ar inside rocks that is not related to atmospheric Ar nor to the radiogenic decay of 40K , which complicates $40\text{Ar}/39\text{Ar}$ age dating. Younger volcanic rocks are more affected by this problem due to their lower concentrations of radiogenic 40Ar with respect to non-radiogenic Ar.

Samples from 0 to 1 Ma are used to study rocks with different proportion of radiogenic and excess 40Ar . A variety of materials (pumice, ash, non-vesicular glass, crystals) and deposit types (pyroclastic fall, ignimbrites, lavas, and Pele's hairs) from Tenerife (Spain), Etna (Italy) and Masaya (Nicaragua), will be used to test how noble gases vary in response of cooling rate (Pele's hairs vs. lavas vs. mode of pyroclastic emplacement) and physical characteristics of the deposit (crystals vs. bubbles, rock porosity).

Noble gas mass spectrometry results from Pele's hairs/tears collected in 2015-2016 at Masaya Volcano, a persistent degassing system, show an inverse degassing trend with 2016 samples less degassed (low $4\text{He}/40\text{Ar}$ ratio) than 2015 samples (high $4\text{He}/40\text{Ar}$ ratio).

Causes and factors controlling this trend have been investigated. Mineral assemblages and sample textures have been characterised by petrographic and SEM analysis; samples chemistry have been determined by electron-probe and NANO-SIMS analysis; further studies on the internal structure of the considered material will help to understand the role of bubbles in noble gas distribution and release during degassing episodes.

Rosemary Cole, James White, Graham Leonard, Dougal Townsend

Submission 252

A physical volcanology study to determine the glaciovolcanic evolution of an andesitic edifice, Tongariro Volcano, New Zealand

Summit or flank glaciers on ice-clad volcanoes can play an active role in the emplacement of erupted products by physically confining lava flows and by directing pyroclastic material along meltwater channels, or in lakes. However, glaciovolcanic interactions at andesitic centres are poorly understood, reflecting the hazardous nature of contemporaneous field study and because few products of such interactions have been studied at source.

Recent mapping and dating of ice-contact lavas and pyroclastic flows on Ruapehu volcano, and moraine ridges on Ruapehu and Tongariro, demonstrate growth of these edifices during the last and penultimate glacial periods. With glaciers now melted away, Tongariro volcano's South Crater provides an ideal site for the study of past subglacial volcanic processes, of both explosive and effusive behaviour, on an andesitic cone. Although previously given the name 'crater', this amphitheatre-shaped structure is a glacial feature and the inferred accumulation centre for the former Mangatepopo Glacier that we now term South Cirque.

Detailed mapping, stratigraphic logging and lithofacies analysis of deposits exposed in this cirque were undertaken in order to understand the physical eruption and emplacement processes of individual erupted units, and the potential glaciovolcanic evolution of this edifice. These deposits were previously either undescribed, or interpreted as subaerial pyroclastic flows, surges and lava flows. By reinterpreting these units, we present a chapter of Tongariro's history that has formerly gone unrecognised. Hyaloclastite breccias indicate eruption into ponded water, that at ~1700-1900 m above sea level, on steep topography, plausibly reflects an eruption-formed lake which was partially dammed by an ice cap or summit glacier. Coarse lapilli tuffs bearing quenched, fluidal blocks exhibit numerous sedimentary structures that suggest water-lain deposition and wet sediment deformation. Deposition from dilute PDCs is unlikely since they lack ash-draped dunes and accretionary lapilli. Rather, they are interpreted as syn-eruptive, water-lain sediments deposited along meltwater channels carved through an ice cap. The morphologies of intercalated and cross-cutting coherent lava bodies also indicate confinement and deflection of this lava by a summit glacier.

Results presented here form part of a wider project into the physical mechanisms and thermodynamics associated with andesitic eruptions beneath or against a glacier.

Meredith Cole, Emily Johnson, Frank Ramos, Andrew Calvert

Submission 1134

Evaluating Subduction Component Contributions in the Cascades: Melt Inclusion Volatile Contents and Compositions, and Whole-rock Isotopic Compositions of Cinder Cones in California and Southern Oregon

Contributions from a subduction component (fluids and/or melts) play an important role in magma generation beneath the southernmost Cascades as indicated by basaltic magmas with elevated H₂O contents associated with Mt. Shasta and Mt. Lassen (1-8 wt.% H₂O, Grove et al., 2002; 2.6-3.4 wt.% H₂O, Walowski et al., 2015). However, within the southern Cascades north of Mt. Shasta, subduction component contributions have not been well constrained. Lower H₂O contents of basaltic magmas in central Oregon (1.8-2.7 wt.% H₂O, Ruscitto et al., 2010) may indicate that subduction components decrease to the north of Mt. Shasta. This project evaluates volatile, major, and trace element compositions of olivine-hosted melt inclusions and assesses whole-rock Sr, Pb, and Nd isotopic compositions of associated lavas to evaluate subduction inputs to three cinder cones in the southern Cascades between Mt. Shasta and Mt. Bachelor. ⁴⁰Ar/³⁹Ar ages of basalts from this area additionally constrain temporal variations in subduction contributions. Primary melt compositions derived from melt inclusion geochemistry are used to investigate mantle compositions along the arc. Volatile, trace element, and isotopic data are used to estimate the magnitude and compositions of subduction component contributions. Melt inclusions (Fo₈₆₋₇₉) show variable maximum H₂O (0.7-2.6 wt.% H₂O) and CO₂ contents (120-800 ppm CO₂); however, there is evidence for significant H₂O and CO₂ degassing prior to melt inclusion entrapment. Melt inclusion Cl and SO₂ concentrations are highest to the south (≤ 600 ppm Cl, ≤ 4500 ppm SO₂) and lowest to the north (≤ 400 ppm Cl, ≤ 2400 ppm SO₂). Similarly, melt inclusion Ba, Sr, and Pb are more enriched (relative to NMORB) in the southernmost cinder cone when compared to the northernmost and Cl/Nb and Sr/Nd are highest to the south. Basalt ⁴⁰Ar/³⁹Ar ages (29.0 \pm 6.4 to 1249.8 \pm 27.1 ka) do not show a correlation with Sr/Nd, suggesting no temporal variations in subduction inputs in the past \sim 1.2 Ma. ⁸⁷Sr/⁸⁶Sr of basalts (0.70336 \pm 2, 0.70384 \pm 2, and 0.70362 \pm 2 from south to north) overlap published ⁸⁷Sr/⁸⁶Sr ranges for the southern Cascades and may indicate influence of subducted sediments with cratonic ⁸⁷Sr/⁸⁶Sr signatures, especially in southern Oregon. Together, these trends are consistent with a northward decrease in the subduction contributions in the southern Cascades north of Mt. Shasta, though the ⁸⁷Sr/⁸⁶Sr trend may indicate a complicated influence of subducted sediments.

Joseph Colgan, David John, Christopher Henry, Kathryn Watts

Submission 425

Implications of field relationships, geochronology, and zircon geochemistry for the emplacement of upper crustal plutons and their relationship to large silicic calderas, western Nevada, USA

Geologic mapping, U-Pb zircon ages and trace elements, and $^{40}\text{Ar}/^{39}\text{Ar}$ sanidine ages document at least six nested silicic calderas in the southern Stillwater Range, Clan Alpine, and Desatoya Mountains of western Nevada. Locally extreme Miocene extension has exposed crustal depths locally ≥ 9 km and revealed granitic plutons that underlie four calderas. Oligocene igneous rocks were emplaced in two episodes about 4 m.y. apart. Caldera-forming ash-flow eruptions of the older episode include the 30.4 Ma, >120 km³ tuff of Deep Canyon, the 28.9 Ma, ≥ 1200 km³ tuff of Campbell Creek, and the 29.2 Ma, >110 km³ tuff of Job Canyon. Caldera-forming eruptions of the younger episode include the small-volume 25.2 Ma tuff of Louderback Mountain (previously mapped as outflow tuff of Job Canyon), the 25.2 Ma, ≥ 360 km³ tuff of Poco Canyon, and the giant (2500-5000 km³) 25.1 Ma tuff of Elevenmile Canyon. The Elevenmile Canyon caldera is exposed across the Stillwater, Clan Alpine, and Desatoya Mountains and includes at least five tuffs mapped as different units by previous workers. Voluminous plutons beneath the calderas are the 28.2 Ma IXL pluton (Job Canyon caldera), Chalk Mountain granodiorite and rhyolite (both 25.0 Ma; Louderback and Elevenmile Canyon calderas), Freeman Creek granodiorite (25.2 Ma) and granite (24.8 Ma) (Poco and Elevenmile Canyon calderas). Plutons intruded in part along the same structures that accommodated caldera collapse, but field relationships and zircon trace element geochemistry indicate that only the Freeman Creek granodiorite underlying the Elevenmile Canyon caldera may represent residual magma. The other plutons were derived from different magmas than overlying tuffs and have no known ignimbrite equivalents, suggesting that large resurgent magma bodies beneath calderas do not necessarily presage additional catastrophic eruptions. Caldera collapse and emplacement of underlying plutons were accommodated by floor subsidence of largely intact country rock blocks, resulting in almost complete replacement to Mesozoic upper crust to depths ≥ 9 km by Oligocene intrusive and extrusive rocks over an estimated total area of ~ 1500 km² (pre-extension) during Oligocene magmatism. If other Great Basin calderas are similar, the dense concentration of shallowly exposed calderas in central Nevada is underlain by a complexly zoned mid-Tertiary batholith assembled in discrete pulses that coincided with formation of large silicic calderas.

Mathieu Colombier, Fabian Wadsworth, Katherine Dobson, Jeremie Vasseur, Francisco Cáceres, Bettina Scheu, Manuela Tost, Shane Cronin, Tim I. Yilmaz, Kai-Uwe Hess, Bernhard Ruthensteiner, Donald Bruce Dingwell

Submission 747

The percolation threshold in magma: Insights from laboratory measurements, in situ synchrotron experiments and numerical simulations

The percolation threshold in magma is the critical porosity above which system-spanning pore connectivity and fluid permeability occurs. It therefore dictates the onset of outgassing potential in magma, and potentially influences the shift between explosive and effusive activity. During magma ascent, the percolation threshold can be reached by vesiculation or fracturing or a combination of both. Magma crystallinity, pore geometry, pore size distribution, shear strain, and surface tension are among the parameters that dominantly control the porosity at which percolation is onset. We performed in-situ high temperature synchrotron-source X-ray tomography vesiculation experiments to track an evolving pore network. We additionally perform stochastic numerical simulations in which we populate 3D volumes with spherical “pores” that are allowed to freely overlap. This method is analogous to heterogeneous random nuclei and excludes bubble-bubble interaction dynamics. We compare our experimental and numerical results with pore structures and connectivities measured for a vast suite of volcanic rocks, covering those formed in a range of eruption styles from mild to vigorous explosivity.

We find that the percolation threshold determined for structurally isotropic volcanic rocks covers a wide range from a lower limit of ~30 vol.% porosity for the stochastic simulations, to an upper limit of ~75 vol.% for isotropic pumices from explosive eruptions. We attribute this range primarily to crystallinity and polydispersivity in pore size. Samples from our vesiculation experiments exhibit a similar range depending on crystallinity. Contrastingly, for samples with elongate, structurally anisotropic pore networks, we constrain a percolation threshold as low as 20 vol.% porosity, illustrating the influence of shear deformation on the percolation threshold. Our vesiculation experiments demonstrate that the presence of crystals results in a lower percolation threshold compared with crystal-free melts. In the case of high surface tension, such as for vesiculating low-water content rhyolite, foam formation and the resultant bubble-bubble flattening can yield very high percolation thresholds up to ~82 vol.% porosity. Further experimental work, in concert with numerical models of two-phase conduit flow, will allow a systematic assessment of the percolation threshold and its controlling parameters providing a powerful tool to assess volcanic activity and shifts therein.

Dylan Colon, Ilya Bindeman, Taras Gerya

Submission 1295

Crustal rheological controls on melt distribution in continental hotspot volcanoes: modeling Yellowstone magma chambers

We introduce a new high-resolution model of magma movement through the crust in the Yellowstone hotspot system in western North America by adding a crustal rheology-based melt extraction protocol to the I2VIS thermomechanical modeling program. This model causes rising melts to stop and accumulate at rheological barriers where local maxima in the ratio of melt overpressure to local rock viscosity are overlain by colder and more rigid material. In a situation where a mantle plume underlies continental crust, as at Yellowstone today, the model naturally produces two melt bodies at depths of 5-15 km and 30-45 km, matching recent tomographic studies of the system under Yellowstone. The lower melt body is comprised of basaltic melts rising from the mantle being stopped at the major rheological barrier at the Moho, and then gradually percolate up through thermally weakened and partially molten crust. The shallow magma body is produced by melts accumulating beneath the rigid top 5 km of the crust, which resists thermal weakening due to its ability to be rapidly cooled by the surface. Between these melt bodies, a 10-15 km thick gabbroic sill complex forms, which remains mostly solid because of the high solidus temperature of the intruding basalts, meaning that melts both in the upper and lower crust are overwhelmingly rhyolitic. This structure arises almost purely from rheological constraints, and the depth of the upper magma bodies are much less sensitive to density contrasts in the upper crust. In thinner and more mafic crust, the high melting point of the crust suppresses the formation of these tiered magma chambers, leading to most basalt being erupted at the surface, suggesting that a change in crustal composition may have been the primary driver of the transition from primarily basaltic to primarily rhyolitic volcanism as the Columbia River Flood Basalt group gave way to volcanism in the Snake River Plain. Finally, we note that erupted melts at each volcanic center become more isotopically mantle-like with time as new intrusions overwhelm country rocks in terms of crust available to be melted to create new rhyolites, a trend which has been observed on the Yellowstone hotspot track as well as in our models.

Pier Paolo Comida, Pierre-Simon Ross, Bernd Zimanowski, Ralf Büttner

Submission 80

Artificial juvenile pyroclasts from wet and dry “eruptions”: impact of magma composition on grain sizes and particle shapes

Maar-diatremes are the second most common volcanic landform on continents and a direct expression of phreatomagmatic explosions, characterized by high explosivity and commonly associated with potentially devastating pyroclastic density currents. Beyond the hazard implications, some diatremes are associated with major ore deposits. Yet eruptive processes especially for the diatreme portion are still poorly understood as they occur largely underground.

Juvenile pyroclasts in maar-diatreme volcanoes come in a range of sizes, shapes, surface features and internal textures (e.g., for basalt, sideromelane versus tachylite). These parameters are influenced by how magma deforms, fragments and cools, which is controlled by factors such as magma viscosity, surface tension, crystallinity, volatile content, and interaction with external water, including Molten Fuel Coolant Interactions (MFCI) and less explosive interactions.

To understand how both silica content and interaction with external water impact on magma fragmentation and the resulting juvenile pyroclasts, a series of laboratory scale experiments were performed at the Physikalisch Vulkanologisches Labor in Würzburg (Germany). In each run, 200-250 g of volcanic rock was re-melted to 1200°C within 1-2 hours using an induction furnace. The melt was fragmented and expelled from the steel crucible through the use of compressed argon ($\approx 500 \text{ cm}^3$, 10 MPa driving pressure) injected from the base; this is known informally as a “dry blowout”. In wet blowouts, a layer of liquid water ($\approx 100\text{-}250 \text{ ml}$) was added on top of the magma about 2 s before the start of deformation. Dry and wet blowouts were performed on four melt compositions ranging from olivine-melilitite to rhyolite and the artificial pyroclasts collected. The next steps are to analyze the size, texture and shape of particles. These results will be compared to data on artificial pyroclasts from classic “water entrapment” MFCI experiments on the same and similar melts, as well as with data from natural juvenile pyroclasts from selected diatremes and maars. This will hopefully allow us to better link processes and products in maar-diatreme volcanoes.

Richard Conrey, David Sherrod, William Leeman

Submission 1227

Relation between extension, volcanic production rates, and arc rock geochemistry, Cascades volcanic arc, USA

The post-8 Ma Cascades volcanic arc, which extends from N. California to S. British Columbia, hosts a variety of eruptive styles and compositions. From Mount Rainier north the arc comprises isolated intermediate composition stratovolcanoes with minor flanking mafic lavas of calc-alkaline arc (CAB) and intraplate-like (IPB) basalt. In S. Washington and N. Oregon the arc broadens and comprises intermediate-composition volcanoes Mounts St. Helens, Adams, and Hood, plus widespread and more abundant mafic lavas of low-K, mid ocean ridge (MORB)-like, tholeiitic basalt (LKT) as well as CAB and IPB. South of Mount Hood intermediate composition stratovolcanic centers are surrounded by thick fault-bounded piles of mafic lava erupted from monogenetic vents and shield volcanoes. These rocks include the aforementioned compositions, but proportions change in response to inferred extension and volcanic production rate.

Extension rates along different arc segments are estimated from balanced cross sections with sparse drill hole control and age determinations. Rates are highest in Oregon for approximately 2 m.y. before and during initiation of graben-bounding normal faulting. They decline as faulting diminishes. The estimated post-0.8 Ma extension rate in north-central Oregon (1 mm/a) agrees with heat flow estimates.

High extension rates favor overall volcanic production rate and the abundance of LKT relative to CAB and IPB. The higher rates also influence the geochemistry of stratovolcanoes; intermediate and silicic magmas are more potassic and incompatible trace element-enriched, and there is a broader compositional range of erupted lava. In contrast, surrounding mafic lavas include more incompatible trace element-poor LKT. At low production and extension rates amphibole is common in silicic rocks; it is rare to absent at high rates.

LKT composition is sensitive to extension rate, with the highest Ca/Al ratios and lowest Na concentrations at high rates and vice versa. The correlation of these parameters appears to mimic relations in MORB to extension rates of 1 mm/a, suggesting that a minimum rate is required for entrapping LKT magma in the middle to shallow crust. Fractionated Fe-rich intermediate lava is also restricted to rates >1 mm/a, as is the eruption of large-volume ash-flow tuffs.

Claudio Contreras, Alison Rust, Katharine Cashman

Submission 599

Quantification of bubble heterogeneities in pumice: Application to Los Espejos Pumice Fall, Laguna del Maule Volcanic Complex

The kinetics of vesiculation and the mechanics of bubble deformation are strongly linked to magma ascent conditions and eruptive explosiveness. Many studies have analyzed pyroclast textures to assess bubble nucleation, growth and coalescence. However, despite the common occurrence of textural heterogeneities within pumice, they are rarely considered, although they also provide clues to dynamic conduit processes. As a case study, we characterize the textures of crystal-poor rhyolitic fallout pumice from Los Espejos (Laguna del Maule, Chile) with a range of densities (0.67–1.57 g cm⁻³) and textures. The bubble number density (BND) does not correlate with pumice density. X-ray tomography reveals that BND varies spatially within pumice clasts, with domains of higher BND occurring around quartz phenocrysts, around the largest bubbles, or as clots of small bubbles not associated with large bubbles or crystals. The distribution of the largest bubbles is also heterogeneous; some large-bubble domains surround quartz (but not biotite, amphibole or plagioclase) phenocrysts, suggesting that quartz acts as a site for heterogeneous bubble nucleation. Most bubbles are spherical or ellipsoidal but there are some with lobate forms. The distribution of ellipsoidal bubbles indicates that strain localization occurs heterogeneously on a small scale. There can be multiple domains of parallel, elongate bubbles within a single lapilli-sized clast, with contrasting domain orientations. This texture indicates complex strain localization, only some of which is associated with shearing around phenocrysts. To quantify the geometry and properties of domains with distinct textures we characterize bubble heterogeneities in 2D from SEM images. We present Gaussian distribution contour maps of: 1) BND; 2) bubble area; 3) bubble convexity = convex hull perimeter/bubble perimeter; and 4) bubble aspect ratio and bubble orientation. These are considered proxies for nucleation, size, coalescence and strain localization, respectively. The 2D bubble property contour maps of Los Espejos pumices reveal that: 1) Bubble coalescence mainly occurs in domains of high BND around relatively large round bubbles, but not around phenocrysts; and 2) Strain is mainly localized at boundaries between large-bubble domains and small-bubble domains. This 2D analysis is a step towards our ultimate goal of quantifying the geometry and textures of domains with distinct textures in 3D from X-ray tomography data.

Chris Conway, Graham Leonard, Dougal Townsend, Colin Wilson, Andrew Calvert, John Gamble, Shaun Eaves

Submission 945

Lava-ice interaction at Mount Ruapehu, New Zealand: implications for reconstructing glacier extents, edifice growth histories and magma flux rates at stratovolcanoes

The presence of ice exerts a primary control over the emplacement, distribution and preservation of volcanic products that form glaciated stratovolcanoes through both constructive (ice-marginal lava emplacement) and destructive (glacial erosion) processes. This interplay produces complex stratigraphic relationships and edifice morphologies, especially as glacier extents have varied in response to global climate fluctuations (glacial and interglacial periods) during the growth histories of long-lived volcanoes over hundreds of thousands of years. We have combined detailed field and geochronological studies in order to unravel this complexity at Ruapehu, a glacially eroded andesite-dacite stratovolcano at the southern end of the Taupo Volcanic Zone, New Zealand. Mount Ruapehu has a total history for the exposed edifice of >190 kyr. In particular, though, contemporaneous effusive volcanism and glaciation from 50–15 ka resulted in the impoundment of lava flows that were chilled against valley-filling glaciers. $^{40}\text{Ar}/^{39}\text{Ar}$ ages for these lavas coupled with field observations of evidence for lava-ice interaction provide novel constraints of former glacier extents that complement paleoclimate reconstructions from moraine ^3He chronology. Conversely, ages of lava flows emplaced on the floors of glacial valleys indicate wholesale deglaciation of Ruapehu occurred from 15–10 ka. Revised magma flux rates constrained by new mapping and geochronological data reveal that glacial unloading of the edifice did not result in any increase in eruption rates. However, the post-glacial destabilisation of the upper edifice, due to retreat of glaciers that were formerly buttressing summit cones, was a major factor in generating a large sector collapse at ~10 ka. This new account of the glaciovolcanic evolution of Ruapehu serves as a case study for comparison to other large glaciated cones located along the circum-Pacific arcs.

Michelle Coombs, Alaska Volcano Observatory Staff

Submission 533

Forecasting and detection during the 2016-2017 eruption of Alaska's Bogoslof volcano

We describe a multidisciplinary approach developed to rapidly detect, characterize, and sometimes forecast explosive events during the ongoing eruption of Bogoslof volcano, a back-arc submarine volcano with an emergent summit in Alaska's Aleutian arc. The eruptive sequence began in December 2016 and has to date featured 37 discrete explosive eruptions. Because the volcano has no local monitoring stations, we use stations on the nearest volcanoes, Okmok (50 km) and Makushin (72 km), combined with regional infrasound sensors and lightning detection from the Worldwide Lightning Location Network (WWLLN). Monitoring has been accomplished using a combination of scheduled checks and automated alarms, instead of 24/7 staffing. Automated alarms include Realtime Seismic Amplitude Measurement (RSAM); infrasound detections from several arrays, the closest being on Okmok (2 min travel time); and lightning strokes detected within a 20-km radius of the volcano. During any increased signs of unrest, a multidisciplinary team of four scientists responds by fulfilling specific roles pertaining to monitoring of geophysical and remote-sensing data, event-specific ash-cloud dispersion modeling, interagency coordination, and development and distribution of formalized warning products.

Since the start of the eruption, patterns in seismicity have allowed AVO to provide short-term (hours or less) forecasts prior to 10 of the 37 explosive events. For events with no detectable precursors, RSAM +/- lightning alarms have issued alerts within minutes of the start of an explosion, allowing AVO to provide timely notification at all hours of the day. Lightning has been a reliable indicator of explosive activity, occurring prior to 21 explosions with no false positives. After an explosion event begins, we use near-real-time satellite data for event confirmation, to estimate volcanic cloud height, and to track the dispersion of the resulting volcanic cloud. AVO uses ash-dispersion model Ash3D to predict ashfall and ash-cloud movement based on either hypothetical or actual eruption information.

Non-real-time data inform our longer-term forecasts. Such data include: high-resolution satellite imagery for tracking changes at the island and the nature of the shallow submarine or subaerial vent; satellite retrievals of SO₂ emissions during specific events; and morphology and composition of ash samples. These longer-term forecasts also include information about proximal hazards at the volcano.

Claire Cooper, Graeme Swindles, Ivan Savov, Anja Schmidt

Submission 125

Volcano-Climate Interactions in the Holocene: The Effect of Deglaciation on Volcanic Eruption Frequency

A link between large volcanic eruptions and variations in regional and global climate variability has been surmised to exist for at least several centuries. Changes to global climate and weather patterns following several historic eruptions, such as Mount Tambora (Indonesia, 1815), El Chichón (Mexico, 1982) and Mount Pinatubo (Philippines, 1991) have proved that explosive volcanic eruptions may cause annual or interannual surface cooling on regional and global scales through stratospheric injection of aerosols and fine ash particles. However, in recent years many studies have suggested that, on a centennial scale, an increase in global temperature may affect the frequency of large-magnitude eruptions through deglaciation. Many models use the example of Iceland to suggest that post-glacial isostatic rebound will significantly increase decompression melting, and may already be increasing the amount of melt beneath Vatnajökull and several other Icelandic glaciers. Evidence for such a relationship existing in the past may be found in cryptotephra records from peat and lake sediments across northern Europe. At present, such records are incomplete, containing spatial gaps. Nonetheless, the current trend of rising global temperatures and contemporary projections of future climate change make understanding the long-term interactions between the atmosphere and the geosphere a highly pertinent issue. A significant increase in volcanic activity in Iceland would result in more frequent ash clouds over Europe, disrupting aviation and transport. Given the current extents of ice sheet and glaciers and the spatial distribution of active volcanic centres, the unloading effect may also be felt in parts of western North America, South America and coastal Antarctica. Further research into this field will allow the development of an understanding of the relationship between the global climate and volcanism, greatly improving our ability to forecast and prepare for future ash- and aerosol-cloud events.

Kari Cooper, Adam Kent, Christian Huber, Kevin Schrecengost, Allison Rubin, Wim Degruyter, Richard Bradshaw

Submission 823

Reconciling “cold storage” and “warm storage” in crustal magma reservoirs

Magma temperature is one of the main variables controlling crystallinity, which in turn exerts a major influence on bulk viscosity and therefore mobility. A long-standing debate centers on the thermal conditions of magma storage in the crust. For example, some data suggest storage over tens to hundreds of kyr at temperatures where the magma is melt-dominated (“warm storage”), whereas other data suggest that magmas are stored largely in a crystal-dominated (or even sub-solidus) state and remobilized in the decades to centuries prior to eruption (“cold storage”). We propose that these apparently contradictory results can be reconciled, at least for the silicic systems on which most of these interpretations are based, by considering the following:

Crystallization temperatures do not necessarily reflect storage temperatures. For example, we present zircon data from the Taupo Volcanic Zone, New Zealand, that shows Ti-in-zircon crystallization temperatures that are inconsistent with preservation of Li concentration gradients across the same crystals over the duration of crystal storage.

The presence of melt sufficient to grow zircon does not require that a large body of magma be held at high temperatures for long durations. In fact, many of the Ti-in-zircon data sets interpreted to reflect warm storage show >100 °C variations in crystallization temperatures at a given time. This is consistent with previous observations showing that zircon crystals in a single eruption sample many compositionally (and likely thermally) diverse regions of the reservoir.

Numerical models which suggest high-T storage over long durations either assume that the magma reservoir is homogeneous, or effectively average gradients in thermal conditions over larger spatial scales than that captured by individual crystals. Therefore the crystal-scale data need not be inconsistent with the numerical results.

The fundamental observations interpreted to reflect long durations of warm storage do not necessarily contradict those interpreted to reflect long durations of cold storage. In fact, by combining all of the available data, a more complete picture of the compositional and thermal variations of magma reservoirs in both time and space can emerge. These data coupled with numerical modeling at multiple spatial scales could provide fundamental insights into the physical processes of heat and mass transport in magma storage systems.

Alisha Coote, Phil Shane, Claudine Stirling, Malcolm Reid, Michael Palin

Submission 118

Origin of plagioclase phenocrysts and crystal cargos in small volume intraplate basalt magmas: Kaikohe-Bay of Islands Volcanic Field, New Zealand

Intraplate, monogenetic, basalt volcanoes are characterized by small scale eruptions, where magma is thought to ascend rapidly from the mantle. Commonly there is little storage in the crust and the magma undergoes minimal crustal assimilation. Presumably, some eruptions would provide little warning in such rapid ascent conditions. However, basalts from some centres such as the Kaikohe-Bay of Islands (KBI) Volcanic Field, New Zealand, contain large phenocrysts, requiring growth during ascent. This provides a unique opportunity to investigate the dynamics of basaltic ascent in such settings.

KBI basalts are porphyritic (10-22% crystals) with crystals up to 10 mm in size. Plagioclase represents 40-70% of the phenocrysts, and display a wide diversity of textural features. Some crystals record three stages of growth comprising: (1) a high-Anorthite (An), disequilibrium, resorbed core (An75-80), from a high pressure and temperature mafic magma in a lower crustal/upper mantle region; (2) a disequilibrium, resorbed, low-An (An40-60) mantle growth from a more evolved source, presumably in the upper crust; and (3) a high-An (An65) rim with oscillatory zoning. MgO and FeO zonation is consistent with late-stage mafic magma recharge. Thus, crystallization occurred in multiple stages involving magma mixing and recycling, and stalling within a multi-level magmatic system. Other crystal textural groups include low-An (An35-45) resorbed relic cores that grew in a more fractionated melt or are foreign to the basaltic system, and display high-An (An60) rims. MgO and FeO zonation indicates late-stage entrainment into ascending basalt melts. Strontium isotope ratios determined using an excimer laser ablation system coupled to a multiple-collector ICP-MS (MC-ICPMS) instrument reveal wide diversity among the crystals, giving $^{87}\text{Sr}/^{86}\text{Sr}$ values ranging from ca. 0.70261 to 0.70556 and thus indicate variable crustal contributions. Individual crystals are also zoned at the 0.1 to 0.2%-level. Low-An resorbed cores have the most radiogenic $^{87}\text{Sr}/^{86}\text{Sr}$ ratios, and display the most isotopic heterogeneity, implying these cores are xenocrysts, originating from a more evolved and crustal-like source. The plagioclase-rich basalts carry a crystal cargo of various origins. The multi-stage storage and recycling during ascent means that magmas in future eruptions may be able to be detected by geophysical phenomena.

stefano corradini, luca merucci, dario stelitano, matthieu poret, antonio costa, mario montopoli, simona scollo

Submission 1028

Improvement of volcanic cloud detection, retrievals and source characterization by means of remote sensing data integration

Volcanic eruptions are one the most important sources of natural pollution due to their large emission of particles and gases into the atmosphere. Such phenomena affects the environment, climate, public health but represents also a threat for aviation.

The volcanic activity is monitored worldwide using both satellite and ground-based systems having different spatial resolutions, sensitivities and working at different spectral ranges. The high phenomenon complexity implies that it doesn't exist a single remote sensing system able to give a complete description of a particular geophysical parameter, then an integrated approach is needed.

In this work, the complementarity between geostationary, polar satellites and ground based measurements is exploited in order to improve the eruption source characterization as well as the volcanic cloud detection and retrievals.

The integration is accomplished at the space-time scale of typical geostationary observations through polar satellite and in-situ measurements. The typical ash retrievals realized in the thermal infrared are integrated by using a wider spectral range from visible to microwave and the ash detection is extended also in case of cloudy atmosphere or steam plumes.

As test cases, the 23 November 2013 Etna (Italy) and the 24 April 2015 Calbuco (Chile) eruptions have been considered. Finally the 23 November 2013 Etna integrated eruption source parameters have been used as input for the FALL3D dispersion model to improve the volcanic cloud forecast through an inverse problem methodology. Indeed, while the model is controlled by the inputs, the results validated against the field deposits and the satellite observations are of help to assess the satellite detection limits by comparing the computed and observed volcanic clouds.

Joaquin Cortes, Stephen Blake

Submission 502

Forecasting in real-time Volcanic Eruptions Based on Ground Deformation Data

We present a new real-time forecasting methodology for volcanic eruptions, using Krafla volcano, Iceland, as a case study. Krafla's last volcanic eruptive cycle occurred between 1975 and 1984 and can be divided into 18 periods of ground inflation, each concluded by deflation accompanied by either an eruption event or a shallow dyke intrusion (Buck et al., 2006). Our methodology uses pre-eruptive inflation data to calculate the probability of an eruption or a dyke intrusion occurring during a time window of length Δt , given that a time t_i has passed from the beginning of an inflation period.

As at Kilauea and Mauna Loa (Dvorak and Okamura (1987), Lengliné et al. (2008)), inflation events at Krafla are measured as changes in elevation and/or radial tilt and follow a decaying exponential relationship with time with a characteristic timescale τ and scale factor α . Pooling all available data, we have found that the duration of an inflation event before an eruption or dyke intrusion (t^*) is comparable to the timescale parameter (0.99 i within an on-going inflation period it is possible to estimate, within a given confidence, t^* based on the value of $\tau(t_i)$ (i.e. the timescale parameter calculated at time t_i) and the cumulative distribution function (cdf) for t^*/τ . Our methodology applied to the 1975-84 Krafla activity uses the inflation data of Björnsson and Eysteinnsson (1998) and the cdf for t^*/τ is modelled as a log-logistic distribution. The procedure is as follows: Given an ongoing inflation period, We calculate $\tau(t_i)$ at the time t_i by fitting a exponential decay model on the inflation data, using the Levenberg-Marquardt non-linear fitting approach. Conditional probability identities are then used to estimate the probability that t^* will occur during Δt , given that a time t_i has passed. Our method of calculating probabilities of eruption within given time windows during ongoing pre-eruptive unrest is equally applicable to any precursor phenomena with a known cdf.

Guillermo Cortés, Philippe Lesage, Roberto Carniel, Carmen Benítez, Javier Almendros, Raúl Arámbula-Mendoza

Submission 928

Unsupervised volcano-seismic event recognition as a tool for real-time monitoring and eruption forecasting: the VULCAN.ears project

The most promising approaches for Eruption Forecasting are based on the precursory increase of the seismicity. In order to analyze this seismic activity, it is necessary to classify the volcano-seismic signals, i.e. to label each event with its corresponding class according to its physical origin. The manual classification carried out by experts is a time-consuming and not always reliable task, being impossible to carry out during seismic crises.

The aim of the European Union funded VULCAN.ears project (Volcano-seismic Unsupervised Labelling and CIAssificatiON Embedded in A Real-time Scenario) is to build an automatic Volcano Seismic Recognition (VSR) system designed to detect and classify signals in unsupervised scenarios (without having any prior knowledge of the signals to recognize), and portable enough to be integrated into various monitoring equipments. The system is based on state-of-the-art VSR technologies, using statistical structured models as Hidden Markov Models (HMMs) and a parallel approach (Parallel System Architecture, PSA-VSR) composed of specialized recognition channels to detect and classify the most significant types of events for eruption forecasting.

Promising results have been obtained in different areas:

Efficient description of events via robust feature designing and selection in PSA-VSR systems, increasing the recognition class accuracy (cAcc) in more than 40% compared to usual serial VSR (SSA-VSR) solutions.

Joint databases, built from several volcanoes, allow the building of robust models able to perform unsupervised VSR (U.VSR) scoring 65%cAcc in continuous blind recognition.

Unsupervised classification of already isolated events, via PSA-VSR, reaches 80%cAcc (vs. 60% with SSA-VSR) at Deception volcano. Joint detection and unsupervised recognition of events in continuous data streams overpasses the 60%cAcc in PSA-VSR (35% in SSA-VSR).

Integration of VSR into Bayesian approach of the material Failure Forecast Method allows processing of large databases and improves success rate of forecasts.

Antonio Costa, Matthieu Poret, Daniele Andronico, Simona Scollo, Mathieu Gouhier, Antonio Cristaldi

Submission 795

Integrating tephra dispersal models with field, airspace, and airborne observations: the case of 23th February 2013 Etna paroxysm

Eruptive plumes generated from Mt. Etna, in Italy, are affected by prevailing winds typically blowing eastwards, driving volcanic ash over the Ionian Sea. As a consequence, tephra is commonly sampled within ~15-20 km from the vent, making the assessment of total grain-size distribution (TGSD) and fine ash fraction highly uncertain. On 23 February 2013, an intense lava fountain episode produced a buoyant plume that reached ~9 km a.s.l. according to the visible and thermal camera images. During this event, the wind dispersed the volcanic cloud towards North-East, causing tephra fallout over a large area extended from the vent to the Puglia region (South Italy). This allowed us to collect tephra samples and evaluate their load on the ground from proximal to very distal locations, i.e. up to the city of Brindisi located more than 400 km far from Etna.

In this study, firstly the TGSD is estimated using only the analysis of the field deposit. Second, the TGSD is extended empirically adding mass into the PM10 classes to account for the fine ash content observed from satellite multispectral imager SEVIRI using the thermal infrared range (MSG-SEVIRI). The tephra dispersal and fallout are reconstructed integrating modelling and observations using the FALL3D tephra dispersal model. All the available information, concerning tephra deposits, airborne loadings, and plume heights estimated by satellite, were used to evaluate the Eruption Source Parameters (e.g. total erupted mass, mass eruption rate, TGSD) through a best fitting procedure. Best guess estimations give a column height of ~8.7 km a.s.l., a mass eruption rate of ~ 1.2×10^6 kg/s, a Total Erupted Mass (TEM) of ~ 4.7×10^9 kg, and a PM10 content of ~1.8% with respect to the TEM. Fall3D results also indicate an aggregate fraction of ~1.7% of the TEM. The results were also compared with the AERONET aerosol network. The integration of numerical models with field, airborne, and airspace observations has allowed a robust estimation of the fine ash fraction of the eruptive plume at Etna, crucial for aviation hazard assessment.

Antonio Costa, Giovanni Macedonio

Submission 783

Modelling particle charge and electrostatic field effects on volcanic ash aggregation

During explosive eruptions ash particles are mainly charged by fractoemission and triboelectric processes. Triboelectric charging occurs when two initially neutral surfaces come into contact, transfer charges, and remain charged with opposite polarity when they separated. The amount of charge that can be transferred through tribologic processes is relatively large. Triboelectric charging also occurs in granular insulating systems even when all particles are composed of identical material. Charging in insulator systems composed of particles of identical material can be attributed to particle size distribution: smaller particles tend to charge negatively and larger particles tend to charge positively. Theoretical and experimental results show that humidity decreases electrostatic charging. Indeed water vapour affects surface properties increasing the surface conductivity and lowering the electrical breakdown strength of air. Observations show significant electrostatic fields in volcanic plumes and indicate three regions: an upper part with positively charged aerosol, a middle part with negatively charged fine ash particles, and a lower part with positively charged coarse ash particles (PNP model).

In order to model the effects of electrostatic fields on charged ash clusters (e.g. due to Coulomb fields, van der Waals, etc.) during aggregation processes, the Smoluchowski equation, describing the rate of change of number density of particles, has to be generalized in order to conserve both total mass and total charge before and after the collisions. To determine the aggregation kernel, it is necessary to derive the merger cross-section and introduce a correction factor, which depends on the effective potential energy of the particle interaction and on the relative collision energy.

Here, first we shortly review the basic theory behind the model then we show some examples of the effect of the corrections on the coagulation kernel due to electrostatic forces for typical volcanic plume conditions.

Fidel Costa, Lili Cheng

Submission 605

A statistical approach to identify plagioclase crystal populations and applications to subduction zone magmas

To anticipate whether the next eruption at an already active volcano will be similar to the previous one, and the extent to which magma is completely new or recycled from the existing plumbing system is among the most difficult problems in volcanology. For example, how much of the 2004 Mt St Helens erupted rocks were simply left over from the previous events? Another point in case was the 2010 Merapi eruption, which was much more explosive and larger than that of 2006, suggesting new arrival of a different magma type. However, the juvenile blocks of both eruptions show a very large variety and complexity of mineral paragenesis and textures. This makes it very difficult to establish the extent to which the 2010 erupted magma was leftover and “gas-remobilized” from 2006 sitting shallow levels, versus new magma from depth. To address this question we have developed a new statistical approach based on the anorthite area of a large number of 2D sections of plagioclase crystals to quantitatively determine the similarity between plagioclase populations (Cheng et al., 2017). We will provide various examples to illustrate our approach to identify the crystal populations and quantify the similarity between them among different eruptions and volcanoes.

Cheng, L., Costa, F., Carniel, R. (2017) Unraveling the presence of multiple plagioclase populations and identification of representative two dimensional sections using a statistical and numerical approach. *American Mineralogist*, 10.2138/am-2017-5929CCBYNCND

Jason. P. Coumans, Edward. W. Llewellyn, Madeleine. C. S. Humphreys, Marcus Nowak, Richard. A. Brooker, Simon. A. Matthias, Iona. M. McIntosh

Submission 991

A new robust numerical water diffusion model with applications to rhyolitic volcanism

Volcanic eruption behaviour is strongly influenced by mechanisms of volatile exsolution and escape from magma. Of particular importance are the rates and timing of bubble growth and the development of gas escape pathways which, in turn, control eruption dynamics. Bubble growth in magma is controlled by diffusive transport of dissolved volatiles (predominantly water) and viscous deformation of the melt, whilst both the melt viscosity and the water diffusivity are themselves strongly dependent on the melt water content. Consequently, an accurate, quantitative description of the behaviour of water in silicate melt is an essential pre-requisite for modelling of many eruptive processes, and for interpretation of the spatial distribution of water in quenched glass to infer syn-eruptive pressure–temperature pathways.

Water is present in silicate melts as both molecular (H_2O_m) and hydroxyl (OH) species. Diffusion of molecular water is much faster than hydroxyl water because H_2O_m is a small molecule that moves relatively easily while OH is bonded to the silicate network. Diffusion of ‘total water’ ($H_2O_t = H_2O_m + OH$) can be described by a process where H_2O_m diffuses and the two species re-equilibrate as defined by the equilibrium constant (K_{eq}). The equilibrium constant and the kinetics of the speciation reaction are both strongly temperature dependent; consequently, the quench rate of a melt strongly influences the final species abundances. This significantly complicates analysis since, even at high quench rates, final species concentrations may not represent equilibrium conditions. Furthermore, previous determinations of K_{eq} have depended on separate determinations of H_2O_m diffusivity, and vice versa, compounding uncertainties.

To address these problems, we have developed new numerical models that determine both H_2O_m diffusivity and K_{eq} simultaneously from the same experimental dataset. Using species data from diffusion-couple experiments on rhyolites, we have determined both quantities as functions of pressure and temperature, while eliminating uncertainties associated with disequilibrium speciation arising from quench. We also present a rigorous bootstrapping approach to quantifying errors in diffusivity and K_{eq} . Our approach, which can be applied to diffusion-couple experiments for other compositions, therefore yields high-quality parameter values for modelling and analysis of diffusion in silicate melts with applications to eruptive processes.

Fiona Couperthwaite, Daniel Morgan, Thor Thordarson, Jason Harvey

Submission 813

Diffusion chronometry: potential and problems as a volcano eruption monitoring tool

Diffusion chronometry applied to elemental exchange across minerals is a successful method used to interpret and quantify the timescales of magmatic processes pre-, syn- and post eruption. Typical methodologies make diffusion challenging as an eruption monitoring tool due to the time it takes to complete the processing workflow for a single set of timescales (1 week+). However, by unpicking the different geometric and crystal-chemical corrections, we have created a user-friendly, easy-to-deploy methodology operating on populations of crystals providing monitoring-relevant interpretations within a matter of hours (25 hours). This provides a new magmatic perspective to better inform hazard mitigation that has not been routinely possible previously on an eruption timescale.

For diffusion chronometry to be successfully implemented, especially as a monitoring tool, it is paramount that the user understands what to expect from the eruption products collected and the extracted data with which they will be working. The required number of timescales needed to reliably interpret a magmatic process is important to know in a time-pressured scenario such as an ongoing eruption, together with many other considerations. Using both synthetic datasets and natural datasets from Piton de la Fournaise, Hawaii and Iceland, diffusion of olivine crystals has been considered to explore;

- a) the variability of timescales extracted from various eruption products – preparation time and viability of crystals/crystal faces vary markedly by material type
- b) the type of information that can be retrieved from various erupted materials e.g. tephra compared to lava flows
- c) the variations within the same material type i.e. pahoehoe lava flows vs. a’ā lava flows and,
- d) ultimately the counting statistics required. Our study suggests >30 crystal faces are required, to produce a meaningful dataset when under time pressure to be incorporated with other monitoring datasets. This compares well with other methods (Costa et al, 2008, Shea et al, 2015).

Armed with these constraints and the new methodology, diffusion chronometry can truly be utilized as an efficient and effective eruption monitoring tool.

Leah Courtland, Carlos Laverde

Submission 1184

Quantifying Differences in Methodologies for Forecasting Tephra Fallout

Tephra is the most far-reaching of volcanic hazards and therefore poses a significant threat to human populations even at distances on the order of 100 km. Tephra fallout models are commonly used to determine the accumulation of ejected volcanic material across a region given an eruptive scenario, enabling scientists to make the type of reliable forecasts crucial to hazards assessment. A subset of these fallout models, advection-diffusion models, describe the solution to the transport, diffusion, and sedimentation equations to calculate the mass loading of tephra on the ground relative to a particle release source. Advection-diffusion models are well-suited for civil protection purposes, such as planning mitigation measures. For this reason, they are most often employed in long-term forecasting of volcanic hazards. This work examines in detail three methodologies commonly utilized in long-term tephra forecasting: (1) Worst Case Scenario: this methodology envisions the worst possible eruption parameters and wind field and executes the model for this single case; (2) Minimally Probabilistic: either the most likely or worst case scenario is utilized and the wind field is varied such that the full range of possible wind fields is sampled from local atmospheric data; (3) Fully Probabilistic: eruption parameters vary based on a set of probability density functions while the wind field is also varied such that the full range of possible wind fields is sampled. While each of these methodologies has merit, each also has drawbacks. The Tephra2 numerical models is here employed to quantify the differences in the resulting hazard maps given each of these techniques. By determining the degree to which the choice of methodology impacts the actual hazard map, this work provides valuable information regarding the applicability of each methodology to tephra forecasting generally.

James Cowlyn, Josef Dufek, Julian McAdams, Ben Kennedy

Submission 526

What happens when pyroclastic density currents travel over ice? Insights into transport processes and hazards at glaciated volcanoes

Sudden melting, scouring and mass failure of summit ice due to volcanic activity can pose severe hazards to populations near glaciated volcanoes. Pyroclastic density currents are a particular concern as both a primary hazard and also because they can rapidly entrain and melt glacial ice and generate hazardous debris flows. Here, we present experimental determinations of rates of water and steam production when hot pyroclasts contact ice, and use these results to inform a series of high-resolution multiphase numerical simulations to assess the effects of over-ice pyroclast transport. Using the example of a well-preserved PDC deposit at Ruapehu volcano (NZ), we show that complex thermal interactions, meltwater and steam generation, and changes in the PDC mass and energy balances significantly change the flow structures, velocities and runout distances that define the primary hazard. Furthermore, we show that near-instantaneous meltwater generation can produce debris flows equivalent in volume to that of the source PDC. Therefore even relatively small eruptions at ice-covered volcanoes can represent a significant hazard to distal communities if they generate PDCs. These results are important for volcanic hazard assessments at high-risk glaciated volcanoes in the US Cascades and worldwide.

Shane Cronin, Magret Damaschke, Rafael Torres-Orozco, Michael Turner, Thomas Platz, Anke Zernack, Jonathan Procter, Geoff Lerner, Mark Bebbington, Ian Smith, Richard Price

Submission 691

Stratovolcano “pulse” observed through a decadal multicomponent, high-resolution volcanic study at Mt. Taranaki, New Zealand.

Over the last decade a coordinated suite of PhD studies have targeted various aspects of the eruption history of Mt Taranaki (Egmont), a >170 ka andesitic stratovolcano that last erupted between AD1800-1820. The 2518 m-high cone is mainly 7 km³. Chemical compositions of rock suites from the well-exposed ringplain record show that each major sector collapse engendered a re-invigorated pulse of magmatism. There is a general trend toward erupting higher-silica andesites over time, with a distinctive steady increase in whole-rock K₂O contents (from ~2 to ~5 wt%). The petrographic and geochemical properties of these hornblende-andesites and pyroxene-andesites (rare opx and ol) indicate a complex magmatic system with amphibole fractionation inferred in the upper-mantle or base of the ~35 km-thick crust. Each ~10-14 ka magmatic cone-growth cycle has included a wide range of explosive and effusive volcanism, with the last 30 ka investigated in greatest detail through a combination of proximal to distal studies into volcanoclastic deposits along with swamp- and lake-deposits containing tephra. In this period >235 eruptions are documented, with >56 in the last 5 ka alone. Roughly one sub-plinian >0.5 km³ event occurs every 300 years, with the remainder 3 explosive or dome-forming eruptions. There is a five-fold variation in eruption intensity (events/yr), on a cycle with a period between 1000-1500 yrs. This cyclicity coincides broadly with pulses of magma feeding the basal part of the magmatic system. Distinctive chemical “batches” are seen in tephra mineral and glass chemistry, often with overlaps between successive batches. The last 5 ka of activity has also seen eruptions from two vent areas, each with distinctive chemical and physical signatures. Using the combined sedimentary and volcanic record time-varying forecasts of volcanic events were constructed, including annual eruption probability as well as that for sector collapse. Through this broad team study, the big picture is beginning to emerge of the factors influencing the growth, development and predictable aspects of volcanic activity at one of the most hazardous types of volcano known.

Kayla Crosbie, Geoffrey Abers, Kenneth Creager, Helen Janiszewski, Eric Kiser, Carl Ulberg, Roger Denlinger, Seth Moran

Submission 1230

Velocity structure of Mount St. Helens, WA region from the joint inversion of ambient noise and earthquake surface waves

Mount St. Helens (MSH) lies trenchward of the main arc front in Cascadia, on the edge of the cold forearc. The imaging the Magma Under St. Helens (iMUSH) experiment is probing the deeper magmatic plumbing system of MSH, in part to understand how magmas could be generated in this setting. A 70-element broadband array was deployed for 2 years with a dense 10 km station spacing and 100 km grid aperture. Ambient noise tomography and earthquake surface wave tomography provide fundamental-mode Rayleigh wave phase velocity maps of the region from 0.01 to 0.18 Hz. From these, shear velocity (V_s) structure is estimated down to 80 km depth. Initial attempts at integrating ambient-noise and earthquake datasets have been complicated by the lower resolution of earthquake-derived phase velocities compared to ambient noise, resulting in ambiguous mantle velocities; care is being taken to minimize this incompatibility. Crustal structure, mostly determined by ambient noise, is better constrained than mantle structure. For depths of 0-5 km, fast V_s zones (3.3 km/s) are imaged that correspond well with Spud Mountain and Spirit Lake plutons. Crust at 10-30 km depth has higher V_s (4.2 km/s) west of MSH than east and north of it. Crustal temperature variations from a cold forearc to a hot volcanic crust could partly explain the crustal velocity pattern. For example, V_s east of MSH is typical of hot continental crust. However, the exceedingly high V_s west of MSH requires a strong change in crustal composition, most likely revealing the mafic Siletzia terrane, which has a predicted V_s similar to that observed. Just below the Moho the pattern reverses, and V_s is low west of MSH and high east of MSH. The V_s contrast across the Moho is weak to absent in the forearc Moho and strong farther east. Previously, a P-wave reflection study interpreted this pattern as a serpentinized cold nose (Hansen et al., 2016). However, the anomalously high crustal velocities we observe west of MSH contribute more to this forearc Moho absence more than these mantle velocity variations. These results confirm not only that MSH lies on a notably cold forearc, but also that crustal composition varies markedly. Speculatively, the sharp crustal terrane boundary may help localize volcanism here.

David Crown, Daniel Berman, Thomas Platz, Stephen Scheidt

Submission 554

Lava Flow Fields on the Western Flanks of Alba Mons, Mars

This investigation utilizes high-resolution imaging and topographic datasets to provide new constraints on the distribution, styles, and timing of volcanism in the northern Tharsis region of Mars. The volcanic geology of the vast flow fields that comprise the western flanks of Alba Mons is being documented through generation of a 1:1M-scale geologic map (230-245°E, 37.5-47.5°N). Mapping and analyses using GIS software allow for synthesis of morphologic, morphometric, and spatial characteristics as well as interactions and age relationships between the different types of lava flows, graben, and erosional valleys. Current research focuses on identification and characterization of individual lava flows and lava tube systems.

Using THEMIS IR (~100 m/pixel) and CTX (~6 m/pixel) images, 154 lava flows, many with lengths of 100 km or more, have been identified across the western flanks. Discrete flows are indicated by observed flow fronts or the distal extents of parallel lateral margins. Preliminary analyses of flow morphology indicate a diversity in flow types consistent with that described in past Viking Orbiter studies. High-resolution images show adjacent flank surfaces that exhibit morphologic characteristics suggesting the presence of additional smaller lava flows with poorly defined margins.

Lava tube systems are discontinuous and characterized by sinuous chains of elongate depressions. Mapping of more than 200 segments of lava tube systems shows that they occur throughout the western flanks, are concentrated in some locations, and can extend for 100s of km. Lava tube systems include both topographically prominent ridges with central distributary features and lateral flow textures and more subtle features denoted by a central distributary feature within the flat-lying flow field surface.

Relative and absolute model age constraints for individual lava flows and flow sequences are being derived from detailed examination of cross-cutting relationships combined with compilation and assessment of crater size-frequency distributions for populations of superposed impact craters. Preliminary results using craters ~300 m and larger identified on CTX images demonstrate that distinct ages can be derived for different parts of flow field surfaces.

Matthew Cruz, Martin Streck

Submission 1098

The elusive eruptive sources of the mid-Miocene Dinner Creek Tuff, eastern Oregon.

Silicic volcanism associated with the Columbia River Basalt Group (CRBG) started synchronous with mafic volcanism and lasted to ~15 Ma. The Dinner Creek Tuff (DIT), one of the main silicic units, is a widespread tuff originally covering more than 30,000 km², and consists of a minimum of four cooling units (DIT 1–4) erupting between 16.1 – 15 Ma. Cooling units 1 to 3 are rhyolite distinguished by age, mineral data, and bulk tuff compositions. Bulk tuff of the youngest unit 4 is dacitic consisting of co-mingled rhyolitic, dacitic, and andesitic glass.

Since the 1960's, a possible eruptive source was postulated based on thick tuff at Castle Rock near the town of Juntura, Malheur county for a single cooling unit restricted to ~2000 km². Our data on all outflow units led us to define a broad eruptive source area, the Dinner Creek Tuff Eruptive Center (DITEC), from which all cooling units were sourced. This project is aimed at pinpointing field evidence for source areas of specific units of the Dinner Creek Tuff within the DITEC.

DIT1 erupted from a caldera with its western margin at Castle Rock. Field evidence for a caldera includes over 300 meters of intra-caldera tuff, overlain by pumice lapilli tuffs that show evidence of re-working by water, and palagonitic basalt. Vertically foliated, breccia filled tuff dikes were mapped along the northwest margin of the caldera. Younger andesite and rhyolite vents occur along the dikes. The northern margin of the caldera is rimmed by mega-breccia composed of pre-caldera fragments over 2 meters in length. The western and northern margins of the caldera have been uplifted, possibly due to resurgence and regional tectonic uplift, but the southern boundary appears to be buried underneath the existing Beulah Reservoir basin. We call this newly identified eruptive center the Castle Rock Caldera.

DIT2 and DIT3 appear to have been erupted from a caldera centered at Ironside Mountain, named here the Ironside Mountain Caldera, which consists of over 1000 meters of DIT2 & 3 that have been uplifted and tilted towards the southwest, along a normal fault on the northern margin. Tuff dikes are exposed along the south and east flanks, intruding into granodiorite and shale country rock. Icelandite and andesite sills and dikes intrude into the tuff, and along the ring faults.

No field evidence has been found for a source for DIT4 that overlies aphyric basaltic andesites within the Castle Rock Caldera.

Adam Curry, Luca Caricchi, Peter Lipman

Submission 584

Determining the physical and chemical processes behind four caldera-forming eruptions in rapid succession in the San Juan caldera cluster, Colorado, USA

A primary goal of volcanology is to understand the frequency and magnitude of large, explosive volcanic eruptions to mitigate their impact on our society. Recent studies show that the average flux of magma (Q_{av}) and the time period between magma injection into a given magmatic-volcanic system fundamentally control the frequency and magnitude of volcanic eruptions, yet these parameters are unknown for many volcanic regions on Earth. We focus on the petrography, geochemistry, and geochronology of four caldera-forming ignimbrites from the San Juan caldera cluster in the Southern Rocky Mountain volcanic field, Colorado, to determine the physical and chemical processes leading to large eruptions. We collected outflow samples along stratigraphy of the three caldera-forming ignimbrites of the San Luis caldera complex: the Rat Creek Tuff (~150 km³), Cebolla Creek Tuff (~250 km³), and Nelson Mountain Tuff (>500 km³); and we collected samples of both outflow and intracaldera facies of the Snowshoe Mountain Tuff (>500 km³), which formed the Creede caldera. Single-crystal sanidine ⁴⁰Ar/³⁹Ar ages show that these large eruptions occurred in rapid succession between 26.91 ± 0.02 Ma (Rat Creek Tuff) and 26.87 ± 0.02 Ma (Snowshoe Mountain Tuff), providing an opportunity to investigate the temporal evolution of magmatic systems feeding large, explosive volcanic eruptions. Major and trace element analyses show that the first and last eruption of the San Luis caldera complex (Rat Creek Tuff and Nelson Mountain Tuff) are rhyolitic to dacitic ignimbrites, whereas the Cebolla Creek Tuff and Snowshoe Mountain Tuff are crystal-rich, dacitic ignimbrites. Trace elements show enrichment in LREE over HREE, and while the trace element patterns are similar for each caldera cycle, individual trace element values show variability (HREE concentrations) within a single ignimbrite. This may indicate that these large eruptions sampled a magmatic system with some degree of internal heterogeneity. This whole-rock and pumice geochemistry will be combined with detailed petrography, microprobe analyses of multiple phases, zircon ID-TIMS analyses, and cross-correlation of mineral chemistry for each ignimbrite. The quantitative Q_{av} and magma injection periodicity results obtained from this study will be used in conjunction with similar studies of other, smaller volcanic systems to better understand the role of these parameters in modulating the frequency and magnitude of volcanic eruptions.

Aaron Curtis, Philip Kyle

Submission 1281

Satellite and LiDAR monitoring of ice-covered volcanoes to detect volcanic unrest

One fifth of volcanic centers active in the Holocene host perennial ice masses (Curtis and Kyle, 2017). Initiation of unrest at these volcanoes can disturb the overlying ice in styles ranging from subtle to catastrophic. Jokulhlaups and phreatomagmatic explosions are easily observed, but here we focus on subtle and often overlooked interactions: ice mass loss, formation of subsidence cauldrons, and fumarolic ice caves. These processes, often occurring beneath only tens of meters of ice, can represent early indicators of unrest which may be of use for volcano monitoring.

We present MODIS snow cover data in which a change in snow-covered area is apparent during periods of activity at several volcanoes. We discuss the extent to which the unrest signal in snow area can be separated from seasonal patterns and noise. Ice area is a difficult signal to use as an unrest indicator, but it may provide an unrest detector if coupled with observations of topography.

For a case study in how volcanic degassing leads to basal melting and results in an ice subsidence cauldron, we present three-dimensional models of a fumarolic ice cave on Erebus volcano, Antarctica. Annually between 2009 and 2014 we recorded the geometry of Warren Cave. In 2011, 2012 and 2013, we also scanned the ground surface (snow) above the cave. In one chamber, an energy balance change led to an observed increase in the ceiling height on the order of 0.5 to 1m annually during the period of investigation, with resulting subsidence occurring directly above the chamber of about 5 cm per year. These observations show that sub-surface melting does give a subtle surface signal that could possibly be detected by satellite observations or other remote sensing. We discuss the extent to which existing remote sensing and geodetic techniques can be applied to detection of subtle unrest signals expressed in ice.

Curtis, A., Kyle, P., 2017. Methods for mapping and monitoring global glaciovolcanism. *J. Volc. Geoth. Res.* 333-334, 134-144. <http://dx.doi.org/10.1016/j.jvolgeores.2017.01.017>

David Damby, Claire Horwell, Claire Natrass

Submission 1119

Origin of a public health concern: Cristobalite in ash from the 18 May 1980 eruption of Mount St Helens

Abundant cristobalite, a toxic crystalline silica polymorph, in respirable volcanic ash was an unforeseen hazard prior to the 18 May 1980 eruption of Mt. St. Helens. Its presence prompted repeated toxicological testing of ash to establish the consequence of exposure for human health. Despite these efforts, the toxicity of volcanic cristobalite remained enigmatic, adhering to a well-established paradigm of crystalline silica being variably reactive, governed by its origin and history. Cristobalite in the ash derived from fragmentation of the cryptodome, where structural substitutions of aluminum facilitated metastable crystallization, and incorporation of the pre-existing, altered edifice. Cristobalite abundance in cryptodome samples is bimodal, with visually-distinguishable 'black' dacites containing considerably more than 'gray' dacites (11-13 wt.% vs. 3-6 wt.%). As cristobalite in these samples predominantly formed through devitrification, this bimodality aligns with assertions that the gray dacite was sufficiently ductile to undergo a secondary vesiculation event upon depressurization, thereby also limiting sub-solidus cristobalite crystallization. Well-constrained samples from the series of external domes from the 1980-1986 and 2004-2008 eruptions reveal that cristobalite crystallization can commence immediately upon dome formation, and abundance is associated with dome residence time. Accordingly, the resultant cristobalite content in ash derived from discrete eruptive events can vary. Substantial effort led to a consensus of ~7 wt.% cristobalite in ash from the 18 May eruption, but ash from later dome collapses and vent explosions contained up to 20 wt.%. Medical studies, at the time and since, show that cristobalite-bearing ash is less reactive than anticipated for a mixed-mineral dust containing crystalline silica but can initiate a sample-dependent pro-inflammatory response, with cristobalite being a reactive component. This diminished reactivity has been tied, in part, to Al impurities, which are known to dampen crystalline silica reactivity. Therefore, lattice substitutions of Al appear to mediate both the existence and suppression of the volcanic cristobalite hazard, but are insufficient to abrogate reactivity completely. These constraints on the origin and reactivity of cristobalite in volcanic ash, garnered in the wake of the 18 May 1980 eruption, strengthen our capacity for health risk assessments during volcanic crises worldwide.

Martin Danišik, Shan de Silva, Adonara Mucek, Axel Schmitt, Indyo Pratomo

Submission 366

Eruptive history of the Toba Volcanic Complex (Indonesia) revisited: new constraints from (U-Th)/He ages and comparison to Ar/Ar and fission track dating results

Accurate and precise dating of Quaternary volcanic rocks is often difficult because, due to a lack of datable material or sufficient resolution, the application of traditional dating tools (e.g., radiocarbon, Ar-Ar, K-Ar, fission track, cosmogenic nuclides or luminescence) may not be always feasible. Hence, there is a critical need for new dating methods appropriate to Quaternary volcanic rocks and (U-Th)/He dating offers a viable alternative for rocks that contain zircon or apatite. This method has been successfully used for dating volcanic eruptions as young as a few thousands years. Perhaps the major advantage of (U-Th)/He dating is that it allows dating of silicic rocks that typically contain zircon but are often not datable by Ar-Ar methods due to a lack of K-rich minerals. (U-Th)/He methods are based on the accumulation of radiogenic Helium produced by decay of Uranium and Thorium, and may involve a correction for disequilibrium in samples younger than 1 Ma. This is facilitated through the determination of crystallization ages for (U-Th)/He dated single crystals by using secondary ion mass spectrometry (SIMS).

Despite being successfully used in Quaternary volcanic geochronology for ~15 years, there is still some hesitation within the vulcanological community in using (U-Th)/He dating as the tool of choice for zircon or apatite-bearing Quaternary volcanic rocks. This may be due to the relatively small number of studies demonstrating the reliability of (U-Th)/He data. In order to further test the efficacy of (U-Th)/He dating, in this presentation we will report on a cross-validation experiment in which we applied (U-Th)/He method to strategically selected rocks from the Toba volcanic complex (Indonesia) that have been dated by other means and can be used here as a natural calibration sites. We will report a new set of (U-Th)/He ages generated for the Old Toba Tuff, the Middle Toba Tuff and the Harrangoal Dacitic Tuff and compare these to the available eruption ages obtained by high-precision Ar-Ar and fission track dating methods. The overarching goal of this presentation is to promote the (U-Th)/He method to the vulcanological community and demonstrate its usefulness for dating of many previously undatable Quaternary volcanic rocks.

Fiona D'Arcy, Étienne Boucher, Maarten De Moor, Jean-Francois Helie, John Stix

Submission 970

Isotopes in tree rings as a proxy of volcanic degassing: A geochemical study of the gas plume at Turrialba volcano, Costa Rica

Trees are useful archives of past atmospheric conditions. They have most commonly been used to infer large-scale changes in climate, industrial pollution, and in the magnitude and frequency of geological hazards. Though geochemical changes in tree rings have been linked to localized smelter pollution, never has their potential to track geochemical changes in volcanic plumes been realized on a local scale. In recent years, technology has allowed real-time monitoring of volcanic gases to aid in eruption prediction, which, if coupled with dendrogeochemical studies, would allow the development of a new proxy.

Turrialba volcano is an ideal location where this new method can be developed. Turrialba is an historically explosive stratovolcano located at the southern end of Costa Rica's central volcanic range, and is currently in a phase of re-awakened activity which has developed into a degassing crisis over the past two decades. Since 2010, Turrialba has emitted a near constant plume of gas and there have been increasingly frequent explosions and ash emissions as activity continues to accelerate.

In this study, fluctuations of gas output in the volcanic plume are being examined using dendrogeochemical analysis of a robust montane species, *Alnus acuminata*, which is found in abundance around the volcano. This is the first study of this species in a tropical montane setting, and after a successful campaign of non-destructive sampling we have found that they possess traits suitable for dendrochronological studies. Given their exposure to the volcanic gas plume, these trees should contain a geochemical fingerprint of local atmosphere as recorded in seasonal tree rings. Pollution studies have shown that exposure to high levels of SO₂ can affect the stable carbon and stable sulphur isotopes, $\delta^{34}\text{S}$ and $\delta^{13}\text{C}$, in trees. Preliminary analysis of $\delta^{13}\text{C}$ has revealed a shift of about -0.5‰ in volcanic trees after onset of degassing, whereas background trees show a shift of +0.5‰ in the same time frame. With further analysis at biannual resolution, we will be able to measure $\delta^{34}\text{S}$ and $\delta^{13}\text{C}$ both before and throughout the degassing episode and compare these results with the corresponding fluctuations of CO₂ and SO₂ from the plume during this time. After this standardization, the new proxy can then be applied to other volcanoes as a novel method of obtaining a temporal record of degassing, a crucial tool for volcano monitoring.

Amberlee Darold, Benjamin Pauk, Weston Thelen, Rebecca Kramer

Submission 545

Geophysical Monitoring of Oregon and Washington Cascade Volcanoes

Despite the present quiescence of the Cascade Range, eight volcanoes in Oregon and Washington have been classified as very high-threat by the 2005 National Volcano Early Warning System (NVEWS) threat assessment. The NVEWS recommended monitoring level for very-high threat volcanoes includes utilizing seismic, GPS, gas, hydrologic and remote sensing data. Seismicity, deformation and gas emissions are principal signs of volcanic unrest and integrating the monitoring of each of these signals gives us a more comprehensive understanding to characterize unrest. Over the last 10 years CVO has upgraded and expanded its monitoring capabilities by adding 50+ seismic and GPS stations throughout the Cascade Range. Through these upgrades and expansions, CVO has moved from the stand-alone monitoring site model of seismic or GPS to a co-located integrated monitoring approach combining GPS and seismic monitoring tools. Thus the new integrated approach to station installations allows for tilt, infrasound, and volcanic gas monitoring instruments to be easily incorporated into stations with specific monitoring requirements. Despite the improved approach to monitoring, only Mount St. Helens and Newberry Volcano meet the NVEWS standard. CVO plans include major network upgrades to Glacier Peak and Mt. Baker and enhancement of existing networks at Mt. Rainier, Mt. Hood, and the Three Sisters volcanic complex. Utilization of multiple geophysical parameters in times of quiescence provides verification of background behavior and provides an opportunity to build conceptual models of these volcanoes to help recognize and better interpret periods of unrest. CVO continues to develop more reliable and robust monitoring stations, expand existing networks, and establish new networks at under-monitored very high-threat volcanoes. CVO's monitoring networks provide both a foundation and an infrastructure for more detailed temporary research projects and experiments that can further our understanding of Cascade volcano structures and processes.

Luca D'Auria, Susi Pepe, José Barrancos Martínez, Raffaele Castaldo, Claudio De Luca, Pedro A. Hernández Pérez, Gladys Melián Rodríguez, Germán Padilla Hernández, Eleazar Padrón González, Nemesio M. Pérez Rodríguez, Pietro Tizzani

Submission 839

Novel insight into the 2004 seismo-volcanic unrest at Tenerife through finite-element modelling of ground deformation

The active volcanic island of Tenerife has the highest volcanic risk among the Canaries. Currently it hosts a population of about 900,000 with a significant population density (442/km²). Furthermore the island is a major touristic destination, with more than 5 million visitors every year. Tenerife hosts three major active volcanic systems: the Teide-Pico Viejo complex, the NW and NE dorsals. At least four eruptions have been observed on the island in historical times. They showed a moderate explosivity and some of them were preceded by a significant, destructive, seismicity. The last one occurred in 1909 along the NW dorsal: the Chinyero eruption. During the Holocene, however, the island experienced also explosive eruptions.

In 2004 Tenerife suffered a seismo-volcanic crisis with earthquakes, geochemical anomalies and ground deformation, mostly along the NW dorsal volcanic system. Earthquakes started increasing since mid-2001. In April 2004, IGN observed a significant increase in the seismicity NW of Teide-Pico Viejo volcanic complex, with about 372 located events. Some of these earthquakes ($M > 2.5$) were strong enough to be felt by the inhabitants of villages located close to the epicenters. This seismic crisis started to decline toward the end of 2004. The crisis was preceded since 2001 by various geochemical anomalies: increase of the CO₂ fluxes and changes in the composition of the fumaroles on the Teide crater and increase in the radon emission at a monitoring station. Between 2004 and 2005 it was observed also an increase in the diffuse CO₂ emission along the NW dorsal. Geochemical data hints toward a magmatic origin of the unrest.

The analysis of radar images acquired by the ERS sensors from 1992-2005 and processed through DInSAR-SBAS technique, revealed a ground uplift episode in 2004. The episode was hidden within the long term subsidence trend of the whole island. Hence we first processed the data to remove the nearly-linear subsidence component and then studied the source of the ground uplift. We performed a non-linear inversion, allowing different source geometries and a model selection through robust statistical model selection tools. The forward modeling kernel has been implemented using a Python finite-element code, which allows to perform FE analysis on 3D models with topography, variable mechanical properties and a wide range of possible source geometries (ellipsoids, crack, pipes).

Ashley Davies, Sarath Gunapala, David Ting, Sir Rafol, Alexander Soibel, Paul Hayne, Megan Blackwell, Michael Kelly

Submission 517

Measuring Lava Eruption Temperatures Remotely with a Novel Infrared Detector and Digital Readout Circuit: Implications for Observing Planetary Volcanism

Determining lava eruption temperature by remote sensing is problematic. Unexpected, intense thermal emission can saturate detectors. This has implications for observing ongoing volcanic activity on Io, Earth and Venus[1]. One method of determining lava eruption temperature of Io's dominant silicate lavas is by measuring radiant flux at two or more wavelengths and fitting a black-body thermal emission function. Only certain styles of volcanic activity are suitable, those where thermal emission is from a restricted range of surface temperatures close to eruption temperature[2]. Problems that must be overcome are (1) the cooling of the lava between data acquisitions at different wavelengths; (2) the unknown magnitude of thermal emission, which often led to detector saturation; and (3) thermal emission changing on a shorter timescale than the observation integration time. We can overcome these problems by using the HOT-BIRD detector[3] and an advanced digital readout circuit (D-ROIC)[4]. We have created an instrument model that allows different instrument parameters (including mirror diameter, number of signal splits, exposure duration, filter band pass, and optics transmissivity) to be tested to determine eruption detectability. Focusing on Io's extreme volcanism as an example, we find that a short-wavelength infrared instrument on an Io flyby mission can achieve simultaneity of observations by splitting the incoming signal for all relevant eruption processes and obtain data fast enough to remove uncertainties in accurate determination of the highest lava surface temperatures exposed. Observations at 1 and 1.5 μm are sufficient to do this. Lava temperature determinations are also possible with a visible wavelength detector[2] so long as data at different wavelengths are obtained simultaneously and integration time is very short. This is especially important for examining the thermal emission from lava tube skylights[2] due to rapidly changing viewing geometry during close flybys.

References: [1] Davies et al., 2017, LPSC48 abstract 1263. [2] Davies et al., 2016, Icarus, 278, 266-278. [3] Ting et al., 2012, Barrier infrared detector, U.S. Pat. No. 8217480. [4] Schultz et al., 2014, LL Journal, 20, 2, 36-51. Acknowledgements: This work was performed at the Jet Propulsion Laboratory-California Institute of Technology, under contract to NASA. This material is also based upon work supported at MIT-LL under Air Force Contract FA8721-05-C-0002.

Pablo Davila-Harris, Graham D.M. Andrews, Sarah R. Brown, Nick Moreno, Linda Anderson, Brenda Pack

Submission 1246

Stratigraphic architecture of a voluminous succession of rhyolitic ignimbrites from the central Sierra Madre Occidental (SMO) Silicic Large Igneous Province, Mexico

We present new advances from an ongoing project on the central part of the Sierra Madre Occidental (SMO), silicic large igneous province. Two main transects have been developed; a southern one, between Parral and Guadalupe y Calvo and a northern transect between Balleza and Guachochi towns, Chihuahua. Both transects comprise ca. 250 km long of superb exposures of silicic ignimbrites, through the extended and non-extended core of the SMO. The suite comprises a set of 41 silicic ignimbrites, acidic and mafic lavas. The southern transect comprises at least 20 ignimbrites, from intensely welded to non-welded tuffs and fall deposits, as well as continental sediments. It also includes, at least three volcanoclastic units, five acidic and six basaltic-andesite lavas. From this transect we present 30 detailed logged sections, recording vertical and lateral variations, grouped into a final set of 13 stratigraphic columns that define the general vertical stratigraphy. Ignimbrite lithologies comprise variably thick (5 to 60 m thick), cream-brown, welded and non-welded tuffs. They are separated intermittently by paleosols, erosion surfaces or just as stacked successions overstepping unconformably, at places slightly tilted and locally normal-faulted. Very few units contain fall deposits at the base. Lateral and vertical variations are not ubiquitous, thus they comprise mainly massive, fines-rich lapilli tuff. Ignimbrite compositions include crystal-rich rhyolites, rhyodacites and dacites, with mineral assemblages of plag., quartz, K-feldspar and biotite, amphibole and pyroxene, with 3% to 50% phenocryst proportion. Sedimentary packages occur intercalated, mostly stratified fluvio-lacustrine sandstone and conglomerate. The succession is locally disrupted by silicic domes and locally capped by basaltic andesite lavas forming shield-like plateaus. At the deepest barrancas, the ignimbrite succession can reach up to 1,500 m thick, uninterrupted sequence of ignimbrites. Preliminary data suggests a migration of the volcanism towards the southwest, in good agreement with previous works elsewhere in the SMO. The age range of the rhyolites from the northeast starts from Eocene, then Eocene-Oligocene at the centre, and in the southwest mainly Oligocene rhyolites. Huge unconformities were recognized as well as resumption of younger volcanism (24-22 Ma). For the northern transect, several U/Pb and Ar/Ar ages have been acquired recently, recognizing ages not older than Oligocene.

Vesta Davydova, Vasily Shcherbakov, Pavel Plechov

Submission 419

Magma storage and mingling conditions for the 2006–2010 eruptions of Bezymianny Volcano (Kamchatka): insights from mafic enclaves

The 2006-2012 eruption products of the Bezymianny volcano (Kamchatka) are represented by two-pyroxene andesites with 56.5 to 57.5 wt. % SiO₂. Andesites contain evidence for magma mingling, caused to the intrusion of different magma in andesitic magma chamber. Such petrological evidence are plagioclases and pyroxenes with complex reverse zoning and dissolution surfaces; non-equilibrium xenocrysts (relicts of Hbl and Ol); different enclaves, which show signs of molten state at time of interaction with andesite. This study devoted to mafic enclaves (50 to 57.5 wt. % SiO₂). We subdivide their into four distinct types (A-D) with different morphological, textural, chemical and petrological features.

Type A-C interpreted as products of predominant crystallization parental magma during ascent and after injection to the shallow andesitic magma chamber. Differences between them correspond to different crystallization rate and different andesitic contamination degree. Type D interpreted as products of early crystallization at depth.

All enclaves have non-equilibrium phenocryst assemblages, which correspond to crystallization at different levels of magma plumbing system. We subdivide three major mineral paragenesis:

“shallow chamber paragenesis” – Pl-Opx-Cpx-Ti-Mt (T: 940-980oC, P ~ 1 kbar)

“deep paragenesis” – Hbl-Pl±Px (T: 960-1040oC, P: 5-9 kbar)

“mantle paragenesis” – xenocrysts of Ol with Cr-Spl or detritus of spinel

harzburgites

This paragenesis meet two-chamber magma plumbing system, which was proposed by result of geophysical and geochemical studies, and allow to specify the P-T conditions of magma interaction.

Shallow magma chamber (andesitic, T ~ 940-980°C и P ~ 1 kbar) periodically provide by more water and mafic magma, which comes from deem magma chamber (andesibasaltic, T: 960-1040oC, P: 5-9 kbar). In deep magma chamber forming Hbl-Pl cumulates (type D enclaves). Injection of mantle-derived magma into deep chamber leads to heat up 1050-1090°C and partial melting of cumulates. Injection of mantle-derived magma and partial melting of cumulates resulted in the displacement of andesibasaltic magma into shallow chamber. In turn, this injection resulted to heat andesitic magma up 1000-1020°C and initialization of eruption.

Mattia de' Michieli Vitturi, Tomaso Esposti Ongaro, Kae Tsunematsu

Submission 778

Phreatic explosions and ballistic ejecta: a new numerical model and its application to the 2014 Mt. Ontake eruption

The recent eruptions at Upper Te Maari Crater, Tongariro volcano (2012) and Mt. Ontake volcano (2014) have shown that volcanic ballistic produced during hydrothermal and phreatic explosions pose a significant hazard in areas proximal to the eruption vent. In order to assess those hazards to people and infrastructures, it is important to adequately model the processes determining ballistic trajectories, as their initial acceleration phase and the interaction of particles with the carrier multiphase flow. In addition, a detailed knowledge of such coupling allows to better constrain the pre-eruptive conditions of the eruptive gas-particle mixture.

For this reason, we have developed a new three-dimensional numerical model based on OpenFOAM, a C++ toolbox for the development of customized numerical solvers. The model describes the gas and finest particles mixture with a two-phase non-equilibrium Eulerian-Eulerian formulation, and the ballistic particles, coupled one-way with the mixture, with a Lagrangian approach. At the initial simulation time, a pressurized, high-temperature mixture (initially confined within the shallow vent) is allowed to decompress and expand in the atmosphere forming an eruptive cloud, while ballistic particles are rapidly accelerated by the coupling effect of drag and pressure forces.

The application of the model to the phreatic eruption of Mt. Ontake volcano in 2014 is discussed and model results are compared with the distribution of ballistics derived from geological observations. Furthermore, to better quantify the hazard posed by such explosions, a study of the effect of the initial overpressure, temperature and crater/fissure geometry on the distance and landing energy of the ballistics is presented.

J. Maarten de Moor, Cyril Muller, Javier Marso, Mauricio Mora, Geoffroy Avard, Alessandro Aiuppa, Guillermo Alvarado, Christoph Kern, Peter Kelly, Jeremy Pesicek, Heather Wright, John Pallister, Jeff Marso

Submission 540

The slow awakening of Turrialba Volcano: An increasing challenge for eruption forecasts

Turrialba volcano is located directly upwind of San José, the capital of Costa Rica. First signs of unrest occurred in 1996 and since Turrialba has become progressively more active with increasing societal impact. The slow awakening behavior at Turrialba challenges monitoring and crisis management strategies as well as conventional models of volcano reactivation, however it also allows detailed documentation of the transition to magmatic activity. Gas monitoring has shown strong changes in both composition and flux, from hydrothermal-dominated emissions to voluminous magmatic degassing. Pulses of CO₂-rich gas have been observed prior to eruptive periods by high-frequency MultiGAS monitoring. Seismicity at Turrialba has shown an array of low to medium frequency signals whose origin and relation to the evolution of eruption dynamics are not well understood. Eruption precursors have been difficult to identify within this diversity, though LP, VLP, and VT earthquakes precede some of the more explosive events, consistent with formation of a blocked conduit that can precede Vulcanian eruptions. Relatively low SO₂ fluxes prior to some events also suggest pre-eruptive pressurization due to conduit blocking. Despite years of vent-opening eruptions, the majority of ash particles (>60%) is still non-juvenile. However, low viscosity and highly vesicular spatter bombs were observed near the vent in early 2017, consistent with development of a more open-system Strombolian eruptive style. Gas, seismic, deformation, and eruption frequency data have all shown sudden increases, but precursors have become increasingly difficult to distinguish with more open-system behavior. A continuation of this trend implies the likelihood of a future abrupt transition to further escalated activity. Sequential semi-quantitative probabilistic scenario assessments (event tree analyses) suggest slowly increasing probability of a VEI \geq 3 eruption with time, primarily driven by the hypothesis that continuing degassing and inflation suggest accumulation of more magma with time. However, the SO₂ flux record suggests that \sim 0.3 km³ of magma has degassed since 2008 whereas deformation modeling suggests that only \sim 0.05 km³ of magma has been emplaced. These disparate results highlight the large uncertainties in constraining the volume of eruptible magma and therefore a broad range of scenarios must be considered for the future eruptive evolution of Turrialba.

Raphael De Plaen, Corentin Caudron, Thomas Lecocq, Andrea Cannata, Valérie Ferazzini, Flavio Cannavo

Submission 186

Single-station monitoring of volcanoes using seismic ambient noise: Application to different types of volcanoes

Volcanic eruptions can be predicted by monitoring deep changes and early aseismic processes associated with magma pressurization and/or migration. Seismic noise correlation is now largely used as a non-destructive way to map heterogeneities and to continuously measure the temporal variation of seismic velocity associated with stress field variation and fluid movement. Seismic noise is correlated to retrieve an estimate of the Green's functions between pairs of stations. Subtle structural changes associated with volcanic activity would cause variations of seismic velocity ($\sim 0.1\%$) which can then typically be measured from the cross-correlation functions.

Although it is increasingly used, this classical technique is usually limited to volcanoes equipped with large and dense networks of broadband stations. We, therefore, use a single-station approach as an alternative to measure variations of seismic velocity on volcanoes and detect pre-eruptive signals. This approach takes advantage of the three components of the sensor with two types of processing: Single-station cross component (SC) and each component with itself or autocorrelation (AC). Furthermore, using Phase Cross-Correlation in place of the Classical cross-Correlation allows to dispose of any kind normalization in the processing workflow. Ultimately, the single station approach was successfully implemented on volcanoes that differ in types and dynamics.

Elske de Zeeuw-van Dalftsen, Reinoud Sleeman, Láslo Evers

Submission 296

Combining monitoring techniques at the volcanoes of Saba and St. Eustatius, the Caribbean Netherlands.

The tiny islands of Saba (13 km²) and St. Eustatius (21 km²) are located at the northernmost end of the active arc of the Lesser Antilles. A large part of each island consists of a volcano: Mt. Scenery (887 m elevation) at Saba and the Quill (600 m elevation) at St. Eustatius. The last eruptive activity at the Quill occurred 1600-1800 years ago but Mt. Scenery erupted as recent as in 1640. Deposits indicate that the eruption style has been mostly Pelean, but Plinian style eruptions also occurred. Furthermore, the existence of heated groundwater at St. Eustatius and hot springs at Saba indicate that both the Quill and Mt. Scenery are active, but quiet, rather than extinct. To ensure the safety of the local populations (~5500 people), an expansion of the monitoring network is crucial.

Currently four broadband seismometers are already deployed on each island. To define background levels of a range of geophysical parameters, it is important to combine several monitoring techniques. We thus aim to expand the monitoring effort with continuous and campaign style GNSS measurements, the analyses of InSAR data, the study of a TanDEM-X DEM and temperature measurements of the hot springs/wells.

We will install the first two permanent GNSS stations in 2017 and plan to integrate those with the existing Continuously Operating Caribbean GPS Observational Network (COCONet). The local geological features of Saba and St. Eustatius islands can be identified and described in detail through thorough analysis of the TanDEM-X DEM.

We aim to create a 'baseline' for future monitoring at the islands of Saba and St. Eustatius in the Lesser Antilles. This 'baseline' is needed to be able to detect unrest in the future, but also to continue to assess the potential hazard at the islands.

Nick Deardorff, Cyrielle Humbert, Daniel Golus, Alexander Patch

Submission 889

Determining the effect of composition on timescales and extent of crystallization in recycled tephra through heating experiments

Microcrystalline inclusions within microlite-poor matrix are surprisingly common in low intensity eruptions around the world, yet their origin is poorly understood. Inclusions are commonly interpreted as evidence of crystallization along conduit margins. Alternatively, these clasts may be recycled from low level eruptions where they recrystallize by heating within the vent. We conducted a series of heating experiments using untreated basaltic andesite and basaltic lapilli, as well as basaltic lapilli encrusted with NaCl. All samples were heated from temperatures below the glass transition ($\sim 690^{\circ}\text{C}$) to $\geq 1100^{\circ}\text{C}$ for 2 to >60 minutes. In basaltic andesite samples at 690°C 800°C , crystallization occurs in

Timescales of crystallization are similar for untreated and NaCl-encrusted basaltic samples. However, the extent of crystallization appears greater in samples with NaCl, including localized areas of extensive crystallization; a texture not observed in untreated samples. These localized crystalline areas strongly resemble microcrystalline inclusions observed in lapilli from the submarine volcano NW Rota-1, Mariana arc, both of which have increased Cl concentrations within the matrix of the crystalline areas (determined through EDS element maps), which suggests Cl diffusion during heating and a potential signature of submarine recycling. Local extensive crystallization may be due to interaction with NaCl through encrusted salt or seawater, creating an increased availability of Na which allows more rapid plagioclase crystallization, leaving residual Cl within the matrix.

From our experiments, more evolved compositions begin to crystallize at shorter timescales and lower temperatures than basalt, while all samples crystallized extensively at $T \geq 1000^{\circ}\text{C}$. The compositional dependence of heating-induced crystallization may be due to small quantities of preserved H_2O , which can suppress crystallization (particularly of plagioclase). Once heated any residual volatiles will be further degassed which may induce additional crystallization.

Wim Degruyter, Christian Huber, Olivier Bachmann, Kari Cooper, Adam Kent, Francesca Forni, Andrea Parmigiani

Submission 246

Insights into the eruptive history of volcanoes from a lumped-parameter magma reservoir model

Volcanoes often show complex variations in eruption frequency, magnitude and style making eruptions difficult to predict. This complexity stems from the interplay between various processes occurring in the volcanic plumbing system before and during an eruption. We attempt to disentangle these processes with a thermo-mechanical reservoir model that includes (i) transient recharge of new magma from below, (ii) crystallization, (iii) volatile exsolution, (iv) heat loss to the crust, (v) visco-elastic response of the crust, (vi) gas loss from the chamber, and (vii) mass withdrawal due to eruptions. The model highlights the importance of (1) reservoir size, and (2) the presence of exsolved volatiles in controlling the pressurization of the reservoir following recharge. The ability of large and bubble-laden reservoirs to better accommodate stresses associated with recharge events provides an explanation for (1) the evolution from small-frequent strato-volcano to larger caldera-type eruptions in long-lived systems (e.g., Santorini, Kos-Nisyros, Campi Flegrei) and (2) a shift in eruptive style between successive eruptions observed at Volcàn Quizapu (1846-47 lava flow and 1932 Plinian eruption, both dacitic in composition with an andesitic recharge, similar storage depth: 130-180 MPa, and water content: 4-6 wt.%). In the latter example, we find that the presence of exsolved volatiles not only allows for larger recharge events prior to reaching the critical overpressure, but it also affects the partitioning of thermal energy (sensible to latent heat), leading to significantly different thermal signals recorded in response to magma recharges.

Elisabetta Del Bello, Jacopo Taddeucci, Jonathan Merrison, Stefano Alois, Jens Jacob Iversen

Submission 861

Modelling volcanic ash resuspension by environmental wind tunnel experiments: the effect of grain size and humidity.

Resuspension of volcanic ash from ground and infrastructures constitutes a source of environmental hazard both during and after the course of an explosive volcanic eruption. An exhaustive description of the factors that influence and promote the resuspension of particles over large distances is crucial for an adequate management of the risks connected to this problem.

Existing resuspension models of ash-sized particles rely on empirical relationships that are derived from geo-materials (e.g. desert or marine sands and dusts) that may have a different behaviour from that of volcanic ash. Also, most of the observations are made at the visible scale and may fail to capture important processes occurring at the single grain scale. Here we explored these observables by conducting wind-tunnel erosion experiments aimed at parameterizing the first-order processes controlling the removal of a homogenous layer of volcanic ash particles from a plate placed downwind a boundary layer setup. Our experimental approach includes the use of high-speed imaging equipment to capture the removal dynamics at 2000 fps and down to 25-micron pixel resolution, and the weighting of the plate pre and post-experiment. Explored variables include: 1) wind speed and boundary layer structure; 2) particle grain size distribution and sorting; 3) sample chemistry; and 4) sample relative humidity. We found that in addition to grain size distribution, the humidity exerts the strongest control on the threshold friction velocity, i.e. the local wind speed required to remobilise a mass of ash from the plate surface. Samples with particles > 90 micron have a lower remobilization threshold and a detachment dynamics characterized by particles entering the airflow individually. Conversely, removal of <90 micron particles occurs at much higher friction velocities, occurring in clumps of aggregates that are either disaggregated and dispersed or redeposited. For a given size distribution, the remobilization threshold and boundary between the two dynamics may shift greatly as a function of ambient humidity, this effect being an order of magnitude greater for smaller particles than for larger ones.

Brent Delbridge, Tushar Mittal

Submission 1304

Dispersion relations for multi-physics wave propagation

The geophysical response of volcanic-hydrothermal systems to forcing is complicated by the variety of processes operating. Specifically, the coupling of magmatic and hydrothermal systems lead to responses on a variety of length and timescales which may be difficult to disentangle observationally. We address this complexity by using a multi-physics framework that incorporates the coupling of a visco-poro-elastic solid with its corresponding temperature field.

We first present a self-consistent set of governing equations which account for the coupling of a non-isothermal visco-elastic skeleton to an interstitial fluid. We non-dimensionalize these equations and scale them to obtain non-dimensional groupings, each of which is associated with a specific physical process. Our framework allows us to test which processes would dominate at the spatial and temporal scales observed in the field. This allows us to simplify the equations in a self-consistent manner and estimate the magnitude of error associated with common assumptions.

Secondly, we present semi-analytic results for the dispersion relation for the normal modes with the effect of thermo, poro, and visco-elastic couplings explicitly included. These relations allows us to go from the physical properties of the magmatic system such as temperature and pore-pressure directly to wave speed. While traditional elastic waves are not dispersive, in the case of poro-elastic and thermo-elastic waves the traditional P- and S- waves are dispersive, and we distinguish between these different effects. Further, in addition to the traditional elastic waves, we derive and identify a variety of additional waves, including slow diffusive waves which may be relevant to understanding ultra-long period seismicity, tilt and other deformation signals in volcanic settings. We analyze the mode coupling and non-normality of the system. We examine the transient growth processes and explore the amplitude and type of waves that a given source will optimally excite. Finally, we present preliminary results for the inclusion of a free surface in a half-space and the resulting dispersion relation for Rayleigh waves in realistic media.

Audray Delcamp, Hannes Mattsson, Lucia Gurioli, Christian Bircher, Engelbert Sakoma, Lore Steyaert, Houria Belkus, Matthieu Kervyn

Submission 328

Towards an understanding of the North Tanzanian maar crater formation from a cross-disciplinary perspective.

About 350 maar craters and tuff cones are spread along the Manyara rift escarpment, and clustered around the Hanang and Kwahara volcanoes in North Tanzania. They lie in an active tectonic setting, the East African Rift, where the magma composition are moderately to highly alkaline, carbonate-rich, and are extracted from a metasomatised mantle.

By using a multi-disciplinary approach, we investigate how such settings influence the formation of the North Tanzanian maars and if it controls the volcano spatial distribution and the resulting deposit morphology. The preliminary outcomes of this long-term project are presented below.

Our preliminary results suggest that the maar distribution is partially controlled by faults parallel to the rift orientation, but strike-slip faults that accommodates rift opening influence the most maar distribution.

Evidence for phreatomagmatic fragmentation and deposition in a wet environment, such as accretionary lapilli and impact sags, are scarce. Juvenile particle shapes vary from one maar to another but are mostly rounded, with few to no vesicles. Juvenile lava balls are common throughout the deposits and some of the maar deposits are mostly made of those melt blobs. The juvenile pyroclasts range in chemistry from melilitites to basanites, and they are often coated with clay minerals. No direct correlation between the textures of the juvenile pyroclasts and magma composition has been noticed.

Most of the maar deposits are made of mm to few cm thick not continuous layers and lenses which implies that the deposits have been mostly emplaced through small scale pyroclastic density currents, suggesting numerous and not-sustained eruptions formed the maar craters.

Because the deposits lack evidence for phreatomagmatic fragmentation, we suggest that water might not have been the primary trigger for a large portion of the maars in northern Tanzania. Instead, we interpret rapid decompression (ascent) of gas-rich magmas to be responsible for maar formation in the area. Further investigations, specifically melt inclusion analyses in olivines, are envisaged to determine the original volatile content of these mantle-derived magmas.

Francisco Delgado, Matthew Pritchard

Submission 266

Renewed post-eruptive uplift following the 2011-2012 rhyodacitic eruption of Cordón Caulle (Southern Andes, Chile): evidence for transient episodes of magma reservoir recharge

The 9-month 2011-2012 eruption of Cordón Caulle (CC) volcano in the Southern Andes of Chile is the best scientifically observed rhyodacitic eruption to date and is thus a key place to understand the dynamics of these rare but powerful explosive eruptions. The eruption was immediately followed by ~ 0.77 m of InSAR-detected exponentially decaying post-eruptive uplift between March 2012 and May 2015, that we interpret as being produced by magma recharge due to an increase in the pressure gradient between a shallow chamber and a deeper reservoir. However, exponential decay in ground deformation can also be produced by viscoelastic relaxation, as the material surrounding a magma chamber behaves viscously rather than brittlely, producing a delayed response due to transient pressure changes in the reservoir. In order to test the idea that post-eruptive uplift is related to other mechanisms than magma recharge, we have developed a set of numerical simulations that include viscoelastic relaxation and volatile exsolution.

Finite element models of a pressurized magma chamber surrounded by a viscoelastic shell embedded in a layered linear elastic medium were calculated with exponential pressure evolution as predicted by magma recharge models. We varied the shell viscosity and find that the best-fit figure ($\sim 10^{17}$ Pa s) does not provide a better fit to the InSAR time series than an exponential function. Further, a numerical model of the reservoir pressure coupled with time and pressure dependent gas exsolution predicts a signal different than the observed time series. Hence we consider these effects as less likely mechanisms than magma recharge to explain the post-eruptive uplift. Indeed, the exponential fit predicts higher rates in the final months than the InSAR data, suggesting that the end of the uplift period could be caused by clogging of the conduit by solidifying magma intruded from a deeper source towards the shallow reservoir.

After a little more than one year with no deformation, several InSAR satellites detected renewed uplift at CC since July 2016. The preliminary maximum rate is ~ 24 cm/yr, intermediate between the ~ 45 cm/yr during 2012-2013 and the ~ 16 -17 cm/yr during 2013-2015. The spatial pattern of deformation is similar to the 2012-2015 inflation, but the cause of uplift is under study. The inflation has not been related to abnormal seismicity and we speculate the Kaiser effect might explain the mostly aseismic ~ 0.9 m of total post-eruptive uplift.

Natalia Deligne, Gill Jolly, Tony Taig, Nico Fournier

Submission 207

Quantifying life-safety risk at active volcanoes: a decision support tool for volcano observatories

When is it safe, or at least, not unreasonably risky, to undertake fieldwork on active volcanoes? Fieldwork anywhere, and especially in mountainous areas - which many volcanic environments are - contains an element of risk. However, a volcanic eruption, and in some cases, heightened unrest, produces hazards with a high fatality rate among exposed people. During a large eruption, an obvious measure to prevent fatalities is to evacuate people from areas from probable hazard zones. However, what can be done to minimize fatalities during periods of unrest, when a volcano may, but probably won't, erupt in the immediate future? This is a question faced by volcano observatories, as despite the increasing coverage and scope of remote monitoring methods, in-person field data collection is still required for comprehensive volcano monitoring. As an employer, a volcano observatory is morally and sometimes legally obligated to take reasonable measures to ensure staff safety and to minimise occupational risk. We will present how GNS Science manages life-safety risk for staff engaged in fieldwork on New Zealand volcanoes in unrest. The primary concerns are ballistics, pyroclastic surges, and/or near-vent processes from eruptions with no useful precursory activity. Our method includes several key elements: (1) an expert elicitation for how likely an eruption is within a specified time frame, (2) quantification, based on historical data, of the likelihood of exposure to volcanic hazards various distances from the vent for small, moderate, or large eruptions, and (3) estimate of fatality rate given exposure to these volcanic hazards. The final product quantifies the hourly risk of a fatality for an individual at various distances from the volcanic vent. Various thresholds of risk (for example, zones with more than 10⁻⁵ hourly risk of fatality) trigger different levels of required managerial approval to undertake work. Although an element of risk will always be present when conducting fieldwork on potentially active volcanoes, this is a first step towards providing objective guidance for go/no go decisions for volcanic monitoring.

Fanghui Deng, Charles Connor, Rocco Malservisi, Laura Connor, Jeremy White, Aurélie Germa

Submission 83

A numerical model for the origin of vent clusters in a Colorado Plateau volcanic field

Volcanoes within distributed volcanic fields are often thought to be monogenetic, with each volcano, or alignment of nearby volcanoes, representing a single, relatively short-lived magmatic event. Volcano vent clusters have been identified in numerous distributed volcanic fields globally, but the origin of these vent clusters remains uncertain. We show with new gravity data and numerical modeling that vent clusters in the Quaternary Springerville volcanic field (SVF), Arizona, correlate with gradients in the gravity field. Inverse modeling of gravity anomaly data in and around the SVF using parameter estimation software PEST indicates that gravity anomalies are explained by density discontinuities transecting nearly the entire crust. These discontinuities are interpreted to be caused by boundaries in the North American crust accreted during the Proterozoic. Spatial density of volcanic vents is low in regions of high density Proterozoic crust, and high in areas of relatively low density Proterozoic crust. 2D and 3D numerical models of magma ascent are developed to simulate long-term average magma migration leading to the development of vent clusters in the SVF. We assume that viscous flow of a fluid in a porous media (Darcy's Law) is statistically equivalent to full field scale magma migration averaged over geological time through the lithosphere. Changes in the model conductivity, associated with changes in the bulk properties of the lithosphere, can simulate preferential magma migration paths and alter the estimated magma flux at the surface. Using this model, we find variation in vent density, and occurrence of vent clusters, are explained by changes in conductivity associated with the Proterozoic crust. The implication is that in some distributed volcanic fields large-scale crustal structures, such as inherited tectonic block boundaries, influence magma ascent and the clustering of volcanic vents. Like SVF, volcanic vents in another two volcanic fields in Colorado Plateau, San Francisco volcanic field and Zuni-Bandera volcanic field, are distributed at areas with low gravity and /or large gravity gradient. Probabilistic models of volcanic hazard for distributed volcanic fields can be improved by identifying crustal structures and assessing their impact on volcano distribution with the use of numerical models.

Roger Denlinger, Alexa van Eaton, Þórður Arason

Submission 581

The significance of segregation and clustering of ash particles for ash aggregation in volcanic plumes and clouds

Volcanic plumes and clouds transport volcanic ash in a turbulent suspension, and the spatial distribution of ash in these suspensions on scales from microns to kilometers is structured. Both clustering of particles and segregation of clusters are produced by coupling of the particles with the turbulent structure of the flow. Several decades of research in gas-particle suspensions shows that coupling depends primarily on particle size and concentration, with shape and density playing secondary roles. Our study examines two aspects of this coupling: (1) how solid particles change the energy scaling and structure in turbulent suspensions, and (2) how the turbulent structure affects the formation of ash aggregates. For particle-laden atmospheric clouds, dissipation of turbulent kinetic energy typically defines Kolmogorov scales between 0.1 mm and 1.0 mm. As fine micron-size ash is added to a volcanic plume, energy dissipation increases at scales less than a few hundred microns, causing clusters of particles tens of microns in diameter to form and be trapped within and between small eddies. Much larger (mm-size) particles, if present, are transported by much larger eddy structures and take separate paths. This segregation of different aggregate sizes and paths, a consequence of the turbulent structure of the suspension, produces collisions between different size clusters on different paths, and can quickly build aggregates hundreds of microns or more in diameter. These interactions within the turbulent structure of a plume explain the observed differences between core and rim structures in well-preserved ash aggregates from Redoubt volcano in 2009. Here cores rich in clusters of large particles have multiple rims of much finer particles. Additional evidence for segregated clusters comes from the 2011 eruption of Grimsvotn, in which clear hailstones several mm in diameter that fell from the volcanic plume were photographed. These photos show randomly distributed, irregular clusters of fine ash up to 200 microns in size trapped in each hailstone. The irregular distribution of clusters of different sizes within the hailstones demonstrates that the distribution of ash in the plume was neither random, nor homogeneous, but rather was segregated into clusters by the turbulent structure of the plume.

Benjamin Devenish

Submission 187

A co-flowing two-plume model of a volcanic eruption column

The co-flowing two-plume model of Bloomfield and Kerr (JFM 2000), which was originally developed for turbulent fountains in a stratified environment and consists of coherent upward and downward interacting plumes, is extended to volcanic plumes. Equations for the variation with height of the mass flux, vertical momentum flux, enthalpy flux and moisture flux are presented for both the upward and downward plumes which are then solved numerically following an iterative approach. The interaction between the upward and downward plumes is modelled by entrainment and detrainment from one to the other. This necessitates the introduction of two extra entrainment coefficients representing detrainment from the upward to the downward plume and entrainment from the downward to the upward plume. The model may produce a more accurate estimate of the mass flux at the lateral outflow of the volcanic plume which could be important for initialising simple models of intrusions (gravity currents).

The model is applied to two realistic cases: the weak and strong cases considered in the volcanic plume model intercomparison exercise by Costa et al. (JVGR 2016). They are respectively the 26 January 2011 Shinmoe-dake eruption in Japan, that produced a plume that reached about 8 km above sea level, and the climactic phase of the Pinatubo eruption, Philippines, on 15 June 1991, during which the eruption column reached about 39 km above sea level.

Two sets of entrainment coefficients are used in the model: the first set are the original values of Bloomfield and Kerr (which were determined from experiments) and the second set are revised values which were determined by Devenish et al. (JFM 2010) from comparisons of the original Boussinesq model with large-eddy simulations (LES). Results from the new model are compared with equivalent results from a recent LES of the same two realistic cases described above (Esposti Ongaro and Cerminara, JVGR 2016). In particular, vertical profiles of the mass and momentum fluxes will be presented. While significant differences exist, the model captures some aspects of both the weak and strong eruptions such as the order of magnitude of the fluxes and, to a lesser extent, the relative magnitudes of the upward and downward fluxes, with the revised entrainment coefficients slightly better at capturing the shape of the profiles.

Rossella Di Napoli, Alessandro Aiuppa, Stefano Valenza, Giovanni Chiodini, Attilio Sulli, Valerio Acocella, Giuseppe Ciralo, Mauro Antonio Di Vito, Francesco Interbartolo, Marco Milazzo, Carmelo Nasello, Gabriele Turco, Mariano Valenza

Submission 117

A NOVEL METHOD FOR QUANTIFYING THE CO₂ OUTPUT FROM SUBMARINE VOLCANO-HYDROTHERMAL SYSTEMS

Characterizing the degassing behaviour of volcano-hosted hydrothermal systems in coastal areas requires investigation of their offshore sectors. Unfortunately, information on hydrothermal setting of submarine volcano sectors still lags behind studies onshore. In particular, the CO₂ output is yet to be quantified for most of the several known submarine hydrothermal gas vents worldwide. Here, we show the ability of a novel CO₂ sensor (HydroC) to mapping the CO₂ anomaly in seawater generated by submarine hydrothermal vents. The HydroC sensor was initially validated against results from conventional direct sampling in a campaign at Baia di Levante (Vulcano Island). The CO₂ distribution in the seawater column was also reconstructed. A more systematic seawater CO₂ profiling study was then carried out in the Pozzuoli bay (offshore of Campi Flegrei), where 47 geochemical vertical profiles were acquired along a quasi-regular measurement grid around the Secca delle Fumose (SdF), the largest submarine thermal manifestation in the area. In each vertical profile, measurements were taken every 5cm depth, allowing us to obtain a high-resolution 3D spatial distribution of pCO₂ in seawater. The acquired data identified a sizeable CO₂ anomaly in the seawater column, due to hydrothermal venting on the seafloor. The CO₂ distribution map was finally processed to derive the total C mass in the seawater volume (in excess to normal ambient seawater), finally converted into a CO₂ output of 52±10 tons/day. This CO₂ output, although corresponding to circa 3% of the present-day Campi Flegrei gas budget, remains substantial (e.g., within the range of the CO₂ output from recently active volcanic systems). We conclude that further investigation of the Campi Flegrei offshore is critical to evaluating its hydrothermal setting and volcanic hazard(s).

Sara Di Salvo, Riccardo Avanzinelli, Roberto Isaia, Lorella Francalanci

Submission 241

Unravelling plumbing system dynamics generating explosive eruptions through in situ isotopic micro-analyses: insights into the Campanian Ignimbrite activity (Campi Flegrei, Italy)

Compositional variations in ignimbrites record significant zoning in shallow magma reservoirs and represent an excellent source of information on magma storage conditions and volcanic evolutionary processes. Configuration of these magma chambers is still not clear, so its knowledge represents an important task to better understand how emptying dynamics work during large explosive eruptions.

The Campanian Ignimbrite (CI) eruption, from Campi Flegrei volcanic field, Italy, represents a typical example of such events, producing a voluminous pyroclastic sequence of trachytic to phonolitic magma around 39 ka ago. Whole-rock geochemical variations are reported in literature, both horizontally and vertically along the sequence of CI. A considerable isotopic dataset exists for products from medial CI outcrops, suggesting Sr-isotope disequilibria. Nevertheless, less is known about the isotopic variations in stratigraphic sections of CI from proximal outcrops, despite its more detailed sequences in the field and the more remarkable heterogeneity of its components.

To provide a complete picture of the compositional variability within the proximal CI sequences, we have performed geochemical and isotopic micro-analyses on matrix glasses and minerals of all juvenile components of the proximal CI. Samples were collected along six different proximal CI outcrops and are representative of all the six stratigraphic units (PPF, USAF, Piperno, LPFU, BU/SU, UPFU) recognised for the proximal CI sequence.

Our major and trace element data on matrix glasses and crystals, and Sr-Nd isotopes on matrix glasses point out a much larger geochemical heterogeneity than that already displayed by whole-rock data. Moreover, our detailed micro-analytical data show a compositional complexity even at the micro-scale ($K_2O\%$: 2.71-11.09; $Na_2O\%$: 3.43-8.24; $^{87}Sr/^{86}Sr$: 0.707316-0.707487; $^{143}Nd/^{144}Nd$: 0.512461-0.512521), possibly revealing the presence of multiple magma components in the CI system interacting in a complex magmatic network.

Recent hypotheses have suggested that the CI magma reservoir evolved by incremental addition of deeper recharge into a high-crystallinity region (i.e. crystal mush), from which crystal-poor melts were extracted. In this light, the present work also contributes to better understand crystal mush systems linked to highly explosive eruptions, through a detailed in situ isotopic micro-analytical study.

Rosa Didonna, Fidel Costa, Heather Katherine Handley, Simon Turner, Jenni Barclay

Submission 918

A new view of mafic-silicic magma interactions at Soufrière Hills Volcano, Montserrat

Mafic magma intrusion into silica-rich crystal mushes is commonly proposed to drive the eruption of andesitic magma at arc volcanoes. Geological and petrological evidence for such processes include quenched mafic inclusions, and at microscopic level, bimodal crystal populations and chemical zoning. However, given the contrasts in physical and chemical properties between the resident and intruding magmas, it is still unclear what are the dynamics and time scales of such interactions and how they may relate to eruption. Here, we present a geochemical and petrological study of samples from the last eruption (February 2010) of Soufrière Hills Volcano to elucidate the dynamics of magmatic recharge. We find that the eruption itself can facilitate magma mingling and mixing and produce andesitic compositions, rather than the other way around as commonly proposed. Large area backscattered electron images reveal five textural types of plagioclase phenocrysts, all of which are present in both the enclaves and the host, attesting to a high degree of interaction. Detailed electron microprobe traverses of plagioclase crystals reveal two main compositional groups: (1) An₅₀₋₈₀ and low MgO (60-90 and high MgO (> 0.1 wt%). The low MgO phenocrysts are in equilibrium with melts of around 1 wt% MgO, similar to that of the evolved glass and host rocks. In contrast, high MgO phenocrysts preserve record of melts with up to 5-6 wt% MgO, higher than the bulk-rocks but likely to record the mafic melt composition. The low MgO plagioclases are well re-equilibrated with an evolved melt in a crystal mush over years to decades, in accord with previous studies. The abrupt compositional transitions between low and high MgO concentrations towards plagioclase rims indicate timescales of a few days. In our current model, mafic magma intrudes a crystal-rich evolved reservoir, which has been equilibrating for at least years or decades. Such intrusions drive overpressure of the system. Thus, the eruption may have been the driving force that allowed extensive silicic magma interactions by mechanically pooling and exchange crystals and melts from the various end-members. Although andesitic eruptions may be triggered by intrusion of mafic magma, the andesite bulk-rock compositions are only made during the eruption and final magma transport towards the surface.

Angela Diefenbach, Steve Schilling

Submission 1202

Thirty six years of topographic change at Mount St. Helens viewed through consistent high-resolution terrain modeling

Mount St. Helens (MSH) has undergone remarkable topographic change over the past 36 years. The cataclysmic eruption on May 18, 1980 produced one of the most dramatic and swift landscape changes in US history as the north sector of the volcano collapsed to produce a massive landslide. The sector collapse triggered a lateral blast that devastated the heavily forested landscape over hundreds of square kilometers and left a 2 km wide horseshoe-shaped crater. Episodic lava dome growth ensued within the crater until 1986 after which the volcano entered an 18 year period of quiescence. During this time, a new glacier developed within the crater, growing quickly over time to surround the 1980-1986 lava dome. In 2004, MSH erupted again with continuous lava dome extrusion that ended in 2008. Lava dome growth during 2004-2008 split the crater glacier in two, pushing it against the surrounding crater walls, eventually forcing the two arms of the glacier to flow northward. By the end of the 2004-2008 eruption, the arms of the glacier had reconnected on the north side of the 1980-1986 lava dome. Since 2008, the glacier has continued to advance northward at a declining rate.

Vertical and oblique aerial photography have been employed to visually monitor landscape changes at MSH since the 1970s. During the 1980-1986 and 2004-2008 eruptions, aerial photography was captured at various time intervals and processed using a variety of photogrammetric techniques to monitor lava dome growth. Since the end of the 2008 eruption, annual aerial photogrammetry surveys have been conducted to monitor ongoing topographic change at MSH, most notably the continued advancement of the glacier. Images from these annual surveys are processed using structure from motion photogrammetric algorithms and software to create high-resolution (1 m) digital elevation models (DEMs) of the crater of MSH. Modern photogrammetry workflow has been applied to images of MSH going back to 1980 to create a consistent, high-resolution time-series of DEMs that spans 36 years. The time-series allows quantitative measurements of topographic change within the crater of MSH, including improved estimates of lava dome growth, geomorphic evolution, and glacier dynamics, at unprecedented temporal and spatial resolutions. These data help to provide a better understanding of dome growth mechanics at MSH as well as to provide baseline information for assessing future changes within the crater.

Hannah Dietterich, Drew Downs, Mark Stelten

Submission 358

Reconstructing lava flow emplacement histories with implications for hazard assessment within the Harrat Rahat volcanic field, Saudi Arabia

The Harrat Rahat volcanic field in western Saudi Arabia covers an area of $\sim 20,000$ km², has a volume of $\sim 2,000$ km³, and is historically active (last eruption in 1256 CE). Mafic lava flows make up the bulk (>95%) of the volcanic deposits and represent a future risk to property and infrastructure in the region, particularly along its northern limit near the city of Al-Madinah. To assess expected future lava flow behavior, we have carried out mapping, geochronology, geochemistry, petrologic analysis, and morphologic analysis of past lava flows to reconstruct eruptive histories and lava flow emplacement conditions. Lava flow behavior is fundamentally controlled by rheology, effusion rate, and underlying topography, and combining petrologic and morphologic analyses has allowed us to estimate these parameters for past flows. Quenched lava samples from a suite of flows have provided phase equilibria relationships between crystals and melt to estimate eruptive temperatures and water contents. Combining these with crystallinity and vesicularity, calculated from image analysis, yields estimates of bulk rheology, with viscosities increasing from 10² to 10⁷ Pa s along flow. Morphologic analysis of flow thickness, channels, and levees allows calculation of eruptive volumes, as well as independent estimates of rheology and indicators of effusion rates. Airborne lidar, satellite photogrammetry, and TanDEM-X satellite interferometry across the volcanic field provide high-resolution (0.5 to 12 m) digital elevation models from which we have extracted morphology and interpolated pre-eruptive surfaces. Analytical and numerical models relating flow morphology to flow properties have been applied in order to infer effusion rates and rheology. Within the suite of studied flows, preliminary volume estimates range from 0.07–0.5 km³, with fluxes on the order of 10s to 100s of m³ s⁻¹. These combined analyses offer insights into past lava flow emplacement conditions and dynamics, which we use as inputs for numerical lava flow simulations for hazard assessment.

Antoine Dille, Sam Poppe, Sophie Mossoux, Hamidi Soulé, Matthieu Kervyn

Submission 798

Small scale lahars at Karthala volcano: comparing probabilistic Q-LavHA and LAHARZ simulations

Karthala, on Grande Comore Island, is a basaltic shield volcano characterised by sporadic ash-forming phreatic eruptions. In 2005, two of such mildly explosive episodes emplaced large quantities of tephra on the summit area, initiating the repetitive occurrence of small-scale secondary lahars up to 2012. In this study, we aim to characterise and model these rain-triggered flows which heavily impacted the settlements situated at the foot of Karthala, damaging infrastructures and affecting thousands of inhabitants.

We mapped the lahar deposits and surveyed the morphology of eight flow-guiding ravines in the field during the summer of 2015. We compared for the first time numerical lahar simulations from the widely used LAHARZ with results from Q-LavHA, a recently developed probabilistic model initially designed for lava flow emplacement modelling. The depositional extent mapped in the field served as input for a fitness index which assessed the accuracy of the resulting simulations. Additionally, we updated the virtual topography (Digital Elevation Model) that is used as model input, by considering the measurements of the ravine geometry acquired in the field and assessed its impact on the accuracy of the simulated lahars.

Our study allows to define the flows as small-scale, rain triggered and low sediment concentration lahars, i.e. with a total volume of 2-5.10⁵ m³ and a peak discharge of ca. 10 m³/s. The comparison of the simulation outputs shows that Q-LavHA is a suitable model for such small-scale lahar simulations, with accuracy values similar or higher to the ones obtained by LAHARZ. Its strengths lie principally in its accurate simulation of the lateral spread of the flow downslope from concave break-in-slopes and its ability to model flow bifurcation. Our results also indicate an accuracy increase, with more accurate flow trajectories, of the modelled outputs of LAHARZ and Q-LavHA when detailed channel topography is used to update the virtual topography on a small spatial scale. The numerical simulation results highlight their added value as part of an integrated volcanic hazard assessment. Based on this case study, we recommend the use of Q-LavHA and updated virtual topography as the base for the production of lahar inundation hazard maps for highly populated volcanic islands such as Grande Comore.

John Dilles, Nansen Olson, Michelle Campbell

Submission 258

Zircon geochemistry as a recorder of arc magmatic processes related to porphyry copper formation: Evidence from SHRIMP-RG and LA-ICP-MS data

Zircon geochemical compositions from a variety of plutons in the Americas include both pre-ore and post-ore granitoids and mineralizing Cu±Au±Mo porphyries in a single district. Zircons from non-mineralized intrusions, similar to other arc magmatic rocks, have a wide range of Ti-in-zircon temperatures, and evolve from high to low temperature with increased Hf content, decreased REE and Y contents, decreased Th/U ratio, and increased negative europium anomaly (EuN/EuN*). Ore-related porphyries differ by having low Ti-in-zircon temperature estimates (750 to 650°C) and EuN/EuN* >0.4. As Ti-in-zircon temperature decreases, EuN/EuN* is constant or increases, REE and Y contents decrease by a factor of ca. 10, and the middle REE/heavy REE ratio decreases.

Zircon compositional diversity in arc granitoids largely reflects initial melt composition and evolution via crystallization, but U- and Th-rich growth zones document contamination by crustal melts. At temperatures of ≤1,000° to 760°C, melt cooling accompanied by crystallization of either hornblende or apatite causes a decrease in the Gd/Yb ratio of zircon, and can be distinguished on Ce/Sm vs Gd/Yb plots via small versus large increases of Ce/Sm, respectively (Lee et al., 2017). Evolution to low temperature produces a large negative europium anomaly (EuN/EuN* 2+-rich plagioclase from relatively water-poor melts, which commonly do not produce ores.

Mineralizing granitoid melts likely separated from lower- to middle-crustal source regions at low crystal content, high water content, and low temperature (850-800°C), and lack high temperature zircon (Lu et al., 2015). The small negative EuN/EuN* anomaly attests to high water content and suppression of plagioclase crystallization (e.g., high Sr/Y of whole rock). At temperatures REE XI/m = 200-1000; Colombini et al., 2011), and decreases the REE content of melt and zircon. Consequently, zircon crystallizes with low Gd/Yb (N/EuN* in mineralized porphyries during crystallization at near solidus temperatures of 750-650°C is a complex process; oxidation of melt (Eu) via degassing of SO₂-rich ore fluids (Dilles et al., 2015) and titanite crystallization both cause an increase in EuN/EuN*, and crystallization of observed Na-plagioclase causes a decrease.

Fabio Dioguardi, Pierfrancesco Dellino, Daniela Mele

Submission 1100

A new model for quantifying the flow and depositional characteristics of dilute pyroclastic density currents based on deposit data

Dilute pyroclastic density currents (DPDCs) are ground-hugging turbulent gas-particle flows that move down volcano slopes under the combined action of density contrast and gravity. DPDCs are dangerous for human lives and infrastructures both because they exert a dynamic pressure in their direction of motion and transport volcanic ash particles, which remain in the atmosphere during the passage of a DPDC and its waning stage. DPDCs' deposits show peculiar characteristics that can be linked to flow field variables by means of sedimentological models.

Here we present a new model for the quantification of the flow and depositional properties of DPDCs based on field data. The model is implemented in PYFLOW_2.0, a significantly improved version of the code of Dioguardi and Dellino (2014) that was already extensively used for the hazard assessment of DPDCs at Campi Flegrei and Vesuvius (Italy). In the latest version the code structure, the computation times and the data input method have been updated and improved. A set of shape-dependent drag laws has been implemented as to better estimate the aerodynamic drag of particles transported and deposited by the flow. A depositional model for calculating the deposition rate and time of the ash and lapilli layer formed by the pyroclastic flow has also been included. The model links deposit (e.g. componentry, grainsize, thickness) to flow characteristics (e.g. flow average density and shear velocity). The deposition rate is calculated by summing the contributions of each grainsize class of all the components constituting the deposit (e.g. juvenile particles, crystals, etc.), which are in turn computed as a function of particle density, terminal velocity, and volumetric concentration. In this way, realistic estimates of the deposition rate can be obtained.

Results from the validation of the models against large scale experiments and its application to field data of past DPDCs at Campi Flegrei and Vesuvius will be presented. Dioguardi, F. and P. Dellino (2014), PYFLOW: A computer code for the calculation of the impact parameters of Dilute Pyroclastic Density Currents (DPDC) based on field data, *Comput. Geosci.*, 66, 200-210, doi:10.1016/j.cageo.2014.01.013

Thy P. Do, Maurizio Battaglia

Submission 72

dMODELS: A software package for modeling volcanic deformation

dMODELS is a software package that includes the most common source models used to interpret deformation measurements near active volcanic centers. The emphasis is on estimating the parameters of analytical models of deformation by inverting data from the Global Positioning System (GPS), Interferometric Synthetic Aperture Radar (InSAR), tiltmeters and strainmeters. Source models include: (a) pressurized spherical, ellipsoidal and sill-like magma chambers in an elastic, homogeneous, flat half-space; (b) pressurized spherical magma chambers with topography corrections; and (c) the solutions for a dislocation (fracture) in an elastic, homogeneous, flat half-space. All of the equations have been extended to include deformation and strain within the Earth's crust (as opposed to only at the Earth's surface) and verified against finite element models. Although actual volcanic sources are not embedded cavities of simple shape, we assume that these models may reproduce the stress field created by the actual magma intrusion or hydrothermal fluid injection. The dMODELS software employs a nonlinear inversion algorithm to determine the best-fit parameters for the deformation source by searching for the minimum of the cost function (chi square per degrees of freedom). The non-linear inversion algorithm is a combination of local optimization (interior-point method) and random search. This approach is more efficient for hyper-parameter optimization than trials on a grid. The software has been developed using MATLAB, but compiled versions that can be run using the free MATLAB Compiler Runtime (MCR) module are available for Windows 64-bit operating systems. The MATLAB scripts and compiled files are open source and intended for teaching and research. The software package includes both functions for forward modeling and scripts for data inversion. A software demonstration will be available during IAVCEI. You are welcome to contact the author at mbattaglia@usgs.gov for additional information, and the software can be downloaded from the USGS website at pubs.usgs.gov/tm/13/b1/.

Flavio Dobran

Submission 892

VESUVIUS PENTALOGUE: Five key objectives for developing resilience and sustainability of populations surrounding Vesuvius

The plan for dealing with an impending eruption of Vesuvius is to resettle all over Italy one million people surrounding the volcano and for the past 20 years the Italian and European governments failed to support more reliable and culturally acceptable strategies. The Vesuvius evacuation plan was politicized by Italian geologists to marginalize the interdisciplinary volcanic risk reduction initiative VESUVIUS 2000 whose central objective is to produce resilient and sustainable areas around the volcano.

VESUVIUS PENTALOGUE requires the development of five key objectives of VESUVIUS 2000: (1) Produce “temporary settlements” for the inhabitants within the areas close to their native homeland until the volcanic crisis subsides and minimize the effects of the eruptions on the built environment; (2) Divide the danger zone into an exclusion nucleus that prohibits all future human settlements and discourages the existing ones, a resilience belt that houses most of the current populations, and a sustainable area beyond the resilience belt that allows for both sustainable practices and temporary resettlements of the “resilience belt” citizens following the volcanic crises; (3) Develop the built environment construction codes for the population of the danger zone by utilizing plinian eruption scenarios, scenario-based seismic hazard assessment and zonation, global volcanic simulator, and dynamic structural analysis; (4) Implement volcanic risk information and education campaigns for different risk areas surrounding the volcano; and (5) Produce a memorandum of understanding between the authorities and scientific communities, and produce periodic progress reports for keeping the populations informed on the developments leading to the realization of the above objectives.

The VESUVIUS 2000 risk mitigation initiative is resisted by the cultural barriers between different professional disciplines, complacent population, and many special interests that fear losing their privileges. In spite of these difficulties we have, during the past 20 years, achieved notable successes through volcanic risk information and education campaigns directed at both the general public and at the schools of the Vesuvius area, and developed multi-dimensional global volcanic simulation capabilities for designing the resilience and sustainability areas surrounding the volcano. This development work is being periodically updated on our website www.gvess.org

Katherine J. Dobson

Submission 898

Taking the strain: Quantifying 3-phase microstructural evolution during flow using ultra fast X-ray tomography

The microstructural evolution of bubble and crystal rich magmas during magmatic flow is the critical control on both local and bulk behaviours. Rheological experiments typically define a range of non-Newtonian strain dependent behaviours but do not allow observation of the movement and interactions between the bubble and crystal phases in the suspensions. The physics of the interactions, and their dynamic reordering to accommodate strain localisation are unknown. Important processes that include the coalescence and the creation and collapse of permeable networks, and the formation and breakage of load transmitting crystal networks remain poorly understood; as are the mechanisms and processes that enable, or prevent the mobilisation of highly viscous crystal rich magmas in response to internal and external forcing. Here we present state of the art 4D imaging that enables the observation of these processes. We use ultra high speed X-ray tomography – with 3D image acquisition rates of 2.00 – 0.07 sec (performed at the TOMCAT (Swiss Light Source) and JEEP (Diamond Light Source) synchrotron beamlines) with in situ rheological testing (XRheo) to observe and quantify the movement of all crystals and bubbles. We present a set of data of variable crystal and bubble content during variable strain under both isothermal and dynamic heating conditions (at constant pressure). Using this unique 4D (3D + time) data we present 3D and 4D maps of local microstructure, and discuss how the mechanisms, magnitude and frequency of the interactions and localisation controls the macroscopic properties of the system. This information must be integrated into numerical and conceptual models of magmatic flow if we are to better understand the conditions that permit eruption, the movement of magmas in the crust and the conduit processes that control eruption behaviour.

Chad Dodge, Rachel Teasdale, Jennifer Wenner

Submission 146

Groundmass Crystallinities of Proximal and Distal Lavas of the Poison Lake Chain in the Lassen Region of the Southern Cascades

The Poison Lake Chain (PLC) is a group of 39 calc-alkaline basaltic volcanoes located east of the crest of the Cascades arc in the Lassen Volcanic Center, approximately 30 km east of Lassen Peak. Previous work describes PLC cones to be monogenetic and representative of primitive magmas (Muffler et al., 2011). The goal of this work is to characterize PLC lava flow emplacement. Approximate effusion rates for 28 PLC flows range from 0.6-40 m³/s, and eruption durations from 20-205 hours. Rates and durations were determined from flow lengths and cone heights respectively, using methods of Walker et al. (1973). These results suggest eruptions of PLC lavas were relatively fast, with effusion rates comparable to the early and late stages of the 1999 eruption of the summit crater Bocca Nuova on Mt. Etna (Harris, et al., 2007). Relatively high eruption rates are likely influenced by the location of the PLC on the western edge of the Basin and Range extensional region. We can also constrain the emplacement of PLC lavas through investigation of cooling rates, which can be approximated from groundmass crystallinities. SEM backscatter- electron (BSE) images of crystallinities from vent and flow samples were analyzed to obtain 2D measurements of groundmass plagioclase using ImageJ software. Measurements were converted to 3D Crystal Size Distributions (CSD, Higgins, 2000). Vent samples exhibit smaller crystal sizes and widths for groundmass plagioclase (e.g., flow unit br2 has an average groundmass crystal area of 381µm² and average width of 10µm) and distal samples show larger crystal sizes and widths for groundmass plagioclase (e.g., flow unit br2 has an average groundmass crystal area of 1100µm² and average width of 18µm). Crystal sizes and population densities indicate that crystallization of groundmass plagioclase in vent samples are nucleation-dominated while crystallization of groundmass plagioclase in distal samples are growth-dominated. With these measured crystallinity patterns of natural samples, 1- atmosphere cooling experiments will help constrain cooling rates for PLC flows during emplacement.

Jacqueline Dohaney, Ben Kennedy, Thomas M. Wilson, Erik Brogt, Darren Gravley

Submission 454

Simulating a volcanic crisis to teach students emergency management, volcanic forecasting concepts, and communication skills

Traditional teaching of volcanic science tends to omit the key roles, responsibilities, protocols, and communication needs that accompany volcanic crises. The Volcanic Hazards Simulation¹ is a complex volcanic crisis role-play that is used to enhance upper-year undergraduate students' volcanic forecasting, communication and teamwork skills. The scenarios are based in New Zealand with one built for regional impacts from an explosive Mt Tongariro eruption and the other from the Auckland Volcanic Field to explore urban/local impacts from volcanoes.

During the role-play, students assume authentic roles and responsibilities of professionals. One team monitors the volcano and is focused on recording, processing, and interpreting real volcano monitoring data (e.g., seismic activity, gas output, etc.), while the other team forecasts and manages likely impacts. A primary goal of the simulation is to improve students' communication skills in a pressured and evolving scenario, through interdisciplinary team discussions, media releases, and press conferences.

Results from observations and interview data indicate that the role-play is a highly challenging and engaging learning experience for students. Students struggled to initiate and maintain effective communication pathways, especially during times of stress, and reported difficulties with communicating uncertainty, use of jargon, and the amount of and appropriateness of information content to differing stakeholders. However, overall, students self-reported an improvement of their teamwork and communication skills through experience with the crisis scenarios.

Additionally, we measured the students' (n=37) confidence (self-reported) and perceptions of volcanic crisis communication (i.e., awareness of crisis communication best practice) using a mixed methods research design. Results showed a statistically significant improvement in both communication confidence and perceptions of crisis communication. Additionally, students reported a comprehensive and diverse set of best practices but focussed primarily on the mechanics of science communication delivery.

This curriculum is a successful example of how to improve students' communication confidence and perceptions. We invite more volcanic teaching groups to use the scenarios in their classrooms. Please see the link below for more information.

1 <http://serc.carleton.edu/introgeo/roleplaying/examples/125523.html>

Clare Donaldson, Corentin Caudron, Robert Green, Bryndís Brandsdóttir, Þorbjörg Ágústsdóttir, Jenny Woods, Robert White

Submission 1108

Volcano monitoring with seismic noise-based methods: insights from the Northern Volcanic Zone, Iceland and Kīlauea, Hawai'i

Cross-correlation of a pair of seismic traces is the first step for a variety of novel monitoring techniques in volcanic regions. Here we present results from the Northern Volcanic Zone, Iceland and Kīlauea, Hawai'i, which show some of the potential of such noise-based methods.

In both studies, we analyze volcanic tremor using cross-correlation functions from local seismic networks. During the 2014 Bárðarbunga-Holuhraun dyke intrusion and sustained eruption (2014-2015) we locate long-period (0.5-2.0 Hz) volcanic tremor at the central volcano itself, the main eruption site and at sub-glacial eruption sites. We have also detected and located shallow long-period earthquakes in these areas. This long-period activity reveals insights into eruption dynamics which are missed by location methods solely using the higher-frequency (2.0-16.0 Hz), brittle-failure earthquakes. In particular, sub-glacial eruptions can be difficult to detect, often only manifested by surface ice cauldrons possibly days later. Tremor location from cross-correlation has the potential to be run automatically in real-time, providing useful assessment of ongoing eruptions.

At Kīlauea, we locate a very active tremor source at or below the eruptive vent during the period of study (2011-2015). This tremor source is stable enough to be used for noise interferometry. Our resulting time series of relative seismic velocity in the shallow crust shows a remarkable correlation with the tilt record measured at Kīlauea summit, consistently correlating on a timescale of days to weeks for almost the entire time-period of study. As the summit continually deforms in deflation-inflation events the velocity decreases and increases respectively. Modeling of strain suggests that during inflation of the shallow magma reservoir (1-2 km below surface), most of the edifice is dominated by compression – hence closing cracks and producing faster velocities – and vice versa.

The concept of velocity being controlled by strain is being tested further in the Northern Volcanic Zone of Iceland by measuring velocity changes associated with the 2014 Bárðarbunga dyke intrusion and seasonal load variations. Comparing seismic velocity variations associated with different causes of deformation provides an opportunity to understand better the mechanisms causing seismic velocity changes in volcanic areas, which currently limits the scope of passive interferometry as a monitoring tool.

Franck Donnadieu, Valentin Freret-Lorgeril, Julien Delanoë, Jean-Paul Vinson, Thierry Iatchimy, Frédéric Peyrin, Claude Hervier, Christophe Caudoux

Submission 243

The mass load of Strombolian ash plumes: first retrievals from a mm-wave radar

A set of cutting edge instruments were deployed at Stromboli volcano in 2015 to retrieve various physical properties of the ash plumes, especially the ash mass load. We mainly focus on measurements of over 200 ash plumes from three radars and a laser disdrometer. A 1.2 GHz volcano Doppler radar (VOLDORAD 2) was set up at about 2.2 km in slant distance NNE of the eruptive craters recording at 0.15 s in 60 m-deep volumes the signature of ballistics and small lapilli in the upper part of their trajectory. Typical maximum radial velocities were 25 m/s. The mini-BASTA Doppler radar at 95 GHz (3.2 mm wavelength), originally designed for atmospheric studies of clouds and fog, was configured to have its fixed beam observing from the same location successive volumes above the SW crater with an unprecedented spatio-temporal resolution of down to 12.5 m and 1 s. Ash emissions typically last a few tens of seconds to over a minute and along-beam plume widths range from a few tens of meters to over one hundred meters. Internal reflectivity gradients are clearly imaged and appear uncorrelated to internal velocities. Plume reflectivities are in good agreement with those recorded by a 24 GHz micro rain Doppler radar (MRR Metek) from a point 400 to 650 m NE of the active craters (10 s sampling rate, 25 m radial resolution). Reflectivity factors measured inside the ash plumes above the source vent by the mm-wave radar range from -9 to +21 dBZ. Comparing these measurements with reflectivity factors calculated from disdrometer proximal records of particle sizes and settling velocities reveal ash concentrations unsurprisingly exceeding by several orders of magnitude the aviation safety thresholds, up to several hundred meters from the vent. Fallout could sometimes be tracked during several minutes within the beam, providing stringent constraints on particle sizes and sedimentation processes from ash clouds, revealing sedimentation waves (see IAVCEI 2017 communication by V. Freret-Lorgeril). Proximal ash samples constantly show a unimodal distribution ranging from 44 microns to 1 mm (more rarely 2 mm), with a mode around 0.3 mm. This is expected to be representative of the coarse content of the ash plumes generated by Strombolian explosions at Stromboli, i.e. mainly coarse ash. Particle size and morphometry statistics will be further used to refine radar mass loading retrievals using inversions of the backscattered power.

Franck Donnadieu, Valentin Freret-Lorgeril, Mauro Coltelli, Simona Scollo, Mathieu Gouhier, Patrick Freville, Claude Hervier, Michele Prestifilippo

Submission 289

Lava fountaining paroxysms generating tephra plumes at Mt. Etna: Remote sensing retrievals

Between January 2011 and December 2015, Etna volcano has produced 50 eruptive episodes characterized by lava fountains which generated tephra plumes rising up to 15 km (a.s.l). Those paroxysms were recorded by a 23 cm-wavelength Doppler radar (VOLDORAD 2B), located at the Montagnola station, about 3 km south from the New SE Crater and integrated into the INGV-OE instrumental network. It has been continuously monitoring the explosive activity of Etna's summit craters since 2009. We analyzed several lava fountain paroxysms using the radar signals from 13 successive 150 m-deep probed volumes, in combination with ground- and satellite-based thermal and visible imagery.

The range gating allows us to discriminate the active summit craters and to roughly estimate the lava fountain widths reaching up to 450 m. The radar echoes, related to the tephra mass load, and Doppler velocities help to mark the transition from Strombolian activity to lava fountain, providing duration of the paroxysms. Importantly, the combination of the radar parameters measured at high rate (0.2 s) provides a proxy for the mass eruption rate, which is found to follow the time variations of tephra plume height given by visible imagery, and which can be used in real-time for monitoring purposes. Oscillations of the echo power are found at several time scales, reflecting pulsations in the emission of the lava fountains likely originating in the conduit or shallow reservoir. Ejection velocities retrieved from positive along-beam velocities measured near the emission source, are found to range from 140 to almost 350 m.s⁻¹ during the climax. Maximum Doppler velocity components from fallouts allow us to infer maximum proximal particle sizes (pluri-decimetric), while the modal value of the power spectral distribution corresponds to lapilli-sized particles. Ejecta from lava fountains are found to follow fan-shaped trajectories with fast-speed blocks ejected up to over 1.5 km from the vent. A reliable absolute quantification of the source mass loading parameters requires more stringent constraints on the complete ash size distribution erupted during the paroxysms. Comparison with independently validated measurements from other sensors such as radar and satellite, whose data provide spatio-temporal information on distal plume dispersion in terms of content (ash and SO₂), relative cloud thickness and height, are also necessary.

Julie Donnelly-Nolan, Robert Jensen, Duane Champion, Mark Stelten

Submission 528

Impact of lidar on geologic mapping of Newberry Volcano, Oregon, USA

In 2010, after >10 yrs of effort, a new geologic map of Newberry Volcano was presented at AGU. Mapping of the >3,000-sq-km volcano utilized a topographic base with 20- to 40-ft contours. Air photos were nearly useless on this volcano, where trees grow thickly in a mantle of Mazama tephra from the ~7,700-yr eruption of Mt. Mazama that created the Crater Lake caldera ~100 km to the SW. In 2011, the USGS purchased lidar coverage over the central part of the volcano, soon followed by additional purchases by the Forest Service and the USGS. Quite suddenly, 1-m topography illuminated previously hidden cinder cones, small canyons, buried flow margins, and individual outcrops otherwise lost in large areas of deadfall and thick forest. Faced with new high-resolution data including enhanced detail in hard-to-reach upper parts of the volcano, revision of the 2010 map was required. Use of georeferenced lidar pdfs that enable location tracking in real time on iPads has facilitated the second generation of mapping. The same iPads are loaded with scanned field notes and pdfs of chemical analyses, etc., and act as notebooks and cameras. The enhanced topography has also helped with the search for localities where sufficient exposure permits sampling for paleomagnetism and argon chronology. This largest Cascades Arc volcano has erupted lavas ranging in composition from basalt (tholeiitic and calcalkaline) to rhyolite over ~500 ka and suffered multiple caldera collapses, most recently at ~75 ka. Situated in a strongly E-W extensional environment east of the arc axis, most mapped eruptive units (>250) reflect tectonic control and have NE- to NW-trending vent alignments. The ~7-ka post-Mazama mafic lavas of the NW rift zone erupted over ~35 km, but in a short time interval as indicated by paleomagnetism. This compositionally zoned Holocene event is one of many episodes documented by a combination of paleomagnetism and mapping. Argon dating has also defined eruptive episodes including a time of numerous rhyolites at ~140 ka in the center of the volcano. Newberry erupted most recently ~1300 yrs ago in the central caldera with the Big Obsidian Flow and tephra. Potential hazards include explosive interaction of magma with lake water in the heavily used caldera, and lava flows that could extend 10s of km beyond the main edifice, block highways, railroads, and the nearby Deschutes River, and overrun property in the city of Bend, where over half of the city sits on Newberry lavas.

Nicolas d'Oreye, Dominique Derauw, Halldor Geirsson, Benoît Smets, Sergey Samsonov, Julien Barrière, Adrien Oth, Nicolas Theys, Celestin Kassereka, Ludibvine Libert, Adriano Nobile, François Kervyn

Submission 312

Recent activity in Nyiragongo active crater, Democratic Republic of Congo – remote sensing and in-situ measurements.

Nyiragongo volcano in the Virunga Volcanic Province is one of the rare volcanoes that host a semi-permanent lava lake. Being ~220 m wide, the lava lake nested in 1.2 km wide crater is the largest on Earth. Recurrent lava overflows inundate the crater floor, which after solidification make the floor to rise up to several dozens of meters per year. After its drainage during the last eruption in 2002, the crater filled up on ~400 m thickness until 2008. Since then, the activity reduced and was mostly characterized by lava level fluctuations of various amplitude and time scales within the pit hosting the lake (Smets et al., this meeting).

Incidentally, at the time of a large volume eruption in 2011-2012 at neighboring Nyamulagira volcano located 13 km away, the level of the lava lake progressively lowered, reaching ~70 m below the crater floor. It remained at that low level until the end of 2015. Early in 2016 a new vent opened within the crater, at the contact point between the crater floor and the sub vertical rim. Such an activity, still visible at the time of writing, has never been observed since the discovery of the volcano in the late 19th Century. The intermittent activity at the vent emits an important volume of degassed lava that now blankets the crater and flows back into the lava lake.

Here we analyze the rise of the crater floor and the lava lake level fluctuations measured from the module of hundreds of SAR images (ENVISAT, RADARSAT, TERRASAR, COSMOSKYMED, SENTIEL 1) and digital elevation models obtained from SplitBand Radar Interferometry. We compare these measurements with other parameters: seismicity (Oth et al., this meeting), gas emission (Barrière et al., this meeting), ground deformation (Geirsson et al., this meeting) and visual observations. We will discuss possible interactions between that crater activity and tectonic and volcanic activity at neighboring Nyamulagira volcano.

Advanced InSAR time series method as well as photogrammetry-derived DEM models (see Smets et al, this meeting) also show a near-field, meter-scale deformation signal affecting the crater floor and bordered by ring-fractures. We will compare and contrast plausible models of processes contributing to this near-field deformation, including thermal contraction, elastic response, block rotation, structural weaknesses, and subsurface shape of the lava lake.

Domenico Doronzo, Joan Marti, Silvina Guzman

Submission 138

A thermo-mechanical model of high-grade ignimbrites at the Coranzuli volcanic complex, Argentina

High-grade ignimbrites are pyroclastic flow deposits that generally show a lava-like lithofacies, with the presence of welding and rheomorphic features, columnar joints, vitrophyres, and fiamme in agglutinated massive tuffs. The parental density currents are thermally-conservative, dense multiphase flows of hot pyroclasts and gas generated in large-volume explosive eruptions (e.g. 100-1000 km³), and they can cover distances of tens of km from the source. An example of high-grade ignimbrites are the Late Miocene dacitic deposits of the Coranzuli volcanic complex in Argentina. Here we present a field-based theoretical model of high-grade ignimbrites, linking for the first time sedimentation and thermal aspects in pyroclastic flows. Then, we make a parametric study for our case-study, the 7 Ma ignimbrites of Coranzuli. Considering mass eruption rates (MERs) between 10⁹ and 10¹¹ kg/s in a large-volume, explosive super-eruption of a thousand km³ of silicic magma, the eruption will result a few hours to a few days long (terupt), which is well longer than typical small-to-intermediate volume eruptions at tuff cones (3) and stratovolcanoes (3). Inside this timeframe there must be the timescale of the emplacement of the ignimbrites (t), so that $t \ll t_{\text{erupt}}$. On the other hand, we find an upper threshold for the sedimentation rate to enter the ductile deformation in the shear zone during the deposit formation, which is characterized by $t > 10^4$ s. This implies that ductile deformation and rheomorphism are thermo-mechanically possible only in large-volume and long-lived, caldera-forming eruptions. Also, the sedimentation rates vary from site to site, although we can consider an upper magnitude of a few tens of kg/m² s as representative of the emplacement of the ignimbrites at Coranzuli, using the thermal constraints on ductile deformation and rheomorphism. Therefore, pyroclastic flows in large-volume explosive eruptions would move as a caterpillar sustained by high and long-lived MERs, while emplacing thick massive ignimbrites at sedimentation rates not exaggeratedly high. In this way, both high transport and deposition can simultaneously occur at the same site.

Guilhem Douillet, Mélanie Bouyssou, Lukas Gegg

Submission 1228

Overtured strata in deposits of dilute pyroclastic density currents, field and analogue data.

The sedimentary print of a dilute pyroclastic density current, and in particular the variety of stratification patterns it contains, is a huge source of information about the parental flow's dynamics. Here, we present and analyze overturned strata, a type of structures that has, to date, only been sporadically recognized, but may be widespread in the sedimentary record.

Overtured strata are defined as "laminations or layers that show a coherent recumbent overturning, generally aligned with the parent flow direction". They can be divided in two types: 1. overturned whirls, and 2. overturning truncations, where several laminae or bedsets cut by an erosion are overturned at the preserved limit of the truncation. Both can only be explained as soft sediment deformation structures. Here we describe and report on various outcrops and present a set of experiments that reproduce the patterns and give preliminary constrains on their formation.

Analogue experiments producing overturned whirls are present in the literature from granular flows and they are linked to shear instabilities. New analogue experiments were performed and permitted to reproduce overturning truncations. A short lived, transient burst was generated by "shooting" an air jet with a compressor-gun into stratified beds of loose particles. The resulting truncation planes contain all characteristics of natural overturning truncations. Experiments were filmed with a high speed camera, and the experimental deposits were sectioned for cross-sections. By varying the inlet pressure of the incoming jet (1 to 5 bar), and the grain size of the erodible bed (3 distributions), conclusions can be drawn on the formation of overturned truncations:

- Fine-grained beds (
- Using successive laminae of varying grain size, overturning was blocked.
- A lower pressure threshold exists but no upper limit was found.
- Coarse-grained beds (0,3-1 mm) produced "shallower" overturning, i.e. confined to the vicinity of the erosion plane.

Overtured truncations demonstrate that the fluid's velocity profile penetrates into the deposit. These features indicate rapidly evolving velocities, undeveloped boundary layers (or a squeezed velocity profile), and a diffuse flow-bed interface. The quantification of these processes would permit to infer energy transfers between flow and ground, and scale to the intensity of turbulence.

Drew Downs, L.J. Patrick Muffler, Michael Clynne, Duane Champion, Andrew Calvert, Ingvar Fridleifsson

Submission 210

Emplacement of the largest Quaternary monogenetic silicic dome complex in the Cascades Arc: the Burney Mountain dacite in northern California

At ~ 9 km³, the Burney Mountain dacite comprises the largest monogenetic silicic dome complex emplaced within the Cascades Arc during the late Quaternary. Reconnaissance mapping in the 1980s defined 6 dacite domes, which erupted from a single vent or multiple closely spaced vent locations. Dome exposures consist of angular clasts ranging from several meters to half a meter in size with rare bulbous lobes of in-situ lava. There is no evidence of an explosive phase (e.g., lapilli or ash), except for a single small-volume pyroclastic deposit with moderately inflated juvenile clasts. This pyroclastic deposit is inferred to be related to the youngest dome based on its location near the summit and diagnostic juvenile clasts. While a dome emplacement sequence was proposed based on field mapping and geomorphology (db1 oldest to db6 youngest), the lack of radiometric and paleomagnetic constraints precluded determining whether the Burney Mountain dacite domes erupted as a single pulse or as a protracted episode of magmatic activity. New ⁴⁰Ar/³⁹Ar analysis on groundmass from 3 of the 6 domes span an age range of ~ 20 kyr, which overlap with a previous age of 280 ± 6 ka from dome db1 (by M.A. Lanphere in Muffler and Clynne, 2015). In addition, our ages contradict the geomorphically inferred stratigraphic order. Dome emplacement occurring in less than ~ 20 kyr is supported by paleomagnetic, petrographic, and geochemical data. In particular, paleomagnetic secular variation measured via drilling of in-situ lavas strongly indicates eruption of all 6 domes as a single eruptive event. Additionally, these domes contain similar major-oxide and trace-element geochemical compositions, and mineral assemblages of euhedral, unzoned orthopyroxene in greater abundance than clinopyroxene, and abundant mm- to sub-mm, normally zoned, euhedral to corroded plagioclase (micro-)phenocrysts, as well as comparable mineral chemistries for orthopyroxene (averages of En72, 74, 70, 71, 68, 67), clinopyroxene (averages of En45, 47, 46, 42, 44, 42), and plagioclase compositions (averages of An59, 63, 66, 62, 59, 63) for db1 to db6, respectively. Integrating paleomagnetic, petrographic, and geochemical datasets provide evidence that all 6 dacite domes of Burney Mountain erupted as a nearly simultaneous episode, and we use ~ 280 ka for the age of emplacement of the Cascades' largest monogenetic silicic dome complex.

Carolyn Driedger, Peggy LovellFord, Jay Wilson, Maximilian Dixon

Submission 673

Preparing with Partners and Populations for Communications during Volcanic Crisis in Washington and Oregon, USA

Pre-crisis planning is an essential component of effective communication and coordination during a volcanic crisis. Authorities can create crisis-communication strategies and anticipate expectations of the public when they become knowledgeable about hazards and risks, and when they develop trusted relationships among themselves, with scientists, and the public. In the USA, delivering information to the public about volcano emergencies and pertinent response measures is the responsibility of multiple agencies representing science, land and emergency management, and emergency response. All groups benefit from a pre-crisis 360-degree knowledge of the others' roles, expectations, and information needs.

Internally, each agency develops mechanisms for rapid updating and dispersal of information. The USGS disperses volcano information on its websites, and near real-time volcano status through its Volcano Notification Service (VNS). Land and emergency management groups prepare to deliver information about closure zones and recommended responses by a variety of local broadcast and notification mechanisms. Agency personnel participate in training about volcano hazards, multi-agency incident command protocols, and effective news-media interactions.

Externally, scientists, and land and emergency managers prepare coordinated protocols for presentation of complementary science and response information. During a crisis, agency representatives might present information side-by-side, but each presents facts within its own 'information lane'. This synchronized information dispersal requires long-term inter-agency coordination and almost constant dialogue, but it is necessary to maintain the public's trust.

In Washington and Oregon, public officials, emergency and land managers, first responders, educators, and scientists maintain ongoing conversations through participation in long-standing regional volcano-hazard work groups. These groups develop, exercise, and maintain volcano emergency coordination plans, and they agree upon specific protocols for crisis communication internally and with the public. In the perception of the public, various government agencies and information sources are often indistinguishable. The success of an eruption response by governmental authorities is judged in part by the seamlessness of inter-agency response, which depends on the effectiveness of communication strategies conceived during pre-crisis planning.

Vincent Drouin, Freysteinn Sigmundsson, Sigrun Hreinsdottir

Submission 319

Inflation events and quiescent periods since 1993 at Theistareykir central volcano, Iceland: role of magma intrusions for geothermal utilization

The Theistareykir volcanic system is the northernmost of the five main volcanic systems in the Northern Volcanic Zone of Iceland (NVZ). It is located near the junction between the divergent plate boundary in the NVZ and the Husavík-Flatey Fault. Eruptive activity of the central volcano is low, the last eruption taking place about 2500 years ago. Other lava flows are older than 10,000 years. Rifting events without eruptions may have occurred in the area in 1618 and 1885 but it is uncertain if these originated from the Theistareykir central volcano or from a nearby off-shore volcano.

We investigate ground deformation in the area since 1993, using campaign GPS surveys, continuous GPS monitoring, and several InSAR time-series from different satellites. It appears that the central volcano is located at the western boundary of the present extension zone across the NVZ. Observations show two possible inflation periods in the central volcano, the first one during 1995-1996 and the second one during 2006-2009. No clear increase in seismicity is observed during the inflation episodes. However seismicity has been low in the area since it is in the earthquake shadow zone of the 1975-1984 Krafla rifting episode. ERS InSAR time-series indicate an uplift of up to 20 mm between 1995 and 1996. For the second inflation period, an uplift of over 50 mm is inferred from both InSAR and GPS observations, and the inflation pattern appears to be more complex than during 1995-1996. However, an uplift of over 20 mm comparable to the 1995-1996 one is observed between 2007-2008 using Envisat data. Using a single Mogi source model, the first inflation relates to a 8.0-13.6 km deep source with a volume change of $5.7-14.2 \times 10^6$ m³, and the 2007-2008 interval of the second inflation period relates to a 7.6-12.8 km deep source with a volume change of $5.0-15.3 \times 10^6$ m³. The horizontal distance between the inferred center of the two sources is about 2.5 km, both are less than 4 km away from the main geothermal area. Since 2008, subsidence of a few mm/yr is observed in the Theistareykir area.

The area is of critical interest as a new geothermal power plant will start production there at the end of 2017. We interpret the two inflation events to relate to magma injection near the brittle-ductile boundary in the crust, fuelling energy into the geothermal system lying above in the long-term.

Timothy Druitt, Maxime Mercier, Taya Flaherty, Etienne Deloule, Juan Andujar, Anita Cadoux, Fidel Costa, Bruno Scaillet

Submission 1009

Plumbing system architecture and magma ascent timescales at Santorini caldera

Santorini is one of the most explosive arc calderas in the world. This paper reviews what we have learned about the plumbing system through a combination of phase equilibria experimentation, melt inclusion (MI) volatile barometry, and multi-mineral diffusion chronometry. Phase equilibria show that basalt fractionates to basaltic andesite at about 400 MPa (lower-upper crustal transition), andesite fractionates to silicic compositions at 400-250 MPa, and silicic melts are stored prior to plinian eruptions in magma reservoirs at about 200 MPa. H₂O+CO₂ contents of phenocryst-hosted inclusions of volatile-saturated melt refine and extend these pressures. MIs from plinian eruptions record entrapment over a wide range of pressures, from 100 to 320 MPa, whereas those in eruptions from interplinian periods record pressures of 4 km depth by a pluton that extends into the lower crust and which is overlain at

The timescales of silicic melt ascent and ponding in shallow magma reservoirs prior to plinian eruptions has been investigated for the 3.6 ka Minoan eruption. MIs in plagioclase cores were entrapped at pressures of up to 320 MPa, while those in rims record 110-170 MPa. The antecrystic cores were transported from the middle to upper crust, then overgrown by the rims. Diffusion modelling using Mg in plagioclase and Mg-Fe in orthopyroxene and clinopyroxene shows that rim growth on all three phenocryst phases began 3 DRE eruption underwent rapid polybaric ascent into the upper crust, where it accumulated in a single sill-shaped reservoir of well mixed melt. The existence of this reservoir is shown by the compositional uniformity of the erupted magma: pumice and glass compositions, phenocryst rim compositions and residence timescales, plagioclase CSDs, and Fe-Ti oxide temperatures. The final magma inputs took place within a few years of the eruption. Following prolonged generation and storage of silicic melts in the middle crust, destabilization of mush layers in the sub-caldera pluton caused interconnectivity of melt pockets. Successive batches of melt then ascended rapidly to the top of the pluton where they injected to form the transient magma reservoir that was erupted a few decades to years later.

Kyriaki Drymoni, Alison Rust, Katharine Cashman, John Browning, Agust Gudmundsson

Submission 637

Dyke propagation through heterogeneous successions

In subduction zone volcanism, magma travels through a considerable thickness of continental crust providing opportunities for a range of physical and chemical interactions with surrounding rocks. As volcanic successions (e.g. stratovolcanoes) often consist of sequences of intercalated effusive and pyroclastic deposits, sometimes with variations in primary chemistry or alteration (e.g. by hydrothermal fluids), a propagating dike may encounter rocks of a wide variety of chemical, physical and mechanical (e.g. Young's modulus) properties along its path.

To study how such heterogeneous successions affect dikes, we have mapped sections of the northern caldera wall at Santorini volcano, Greece, which includes a dike swarm through a complex stratigraphy of lava flows, welded pyroclastics, nonwelded scoria deposits, and sedimentary units. The dikes vary in thickness, orientation and colour, and there is clear evidence of incorporation and assimilation of pyroclasts into dikes.

By coupling the field and geochemical data with numerical and analytical models we aim to 1) understand stress distributions within the edifices 2) to define and address variables that contribute to dike propagation 3) group the different dike populations according to their age, time of propagation and geochemical evolution, and 4) assess the degree of mechanical entrainment and chemical assimilation of wall rock materials.

Eliecer Duarte

Submission 35

Summit Geomorphological Changes Due to Ash and Pyroclasts Emplacement, Near the Active Crater of Turrialba Volcano: Costa Rica.

Turrialba's sustained activity, over 20 years, have produced dramatic changes near the active crater. Recently, emplacement of mainly ash and larger pyroclasts has been documented 360° around the west crater showing: edges, inner structures, nearby hills and other features. Special emphasis was given to the east and west; where most of the deposition occurred. To the east because of the infilling of central crater and potential implications for the future activity of this feature. To the west due to the potential of the area to accumulate voluminous materials becoming ready to conform lahars down the northern distant plains.

Spatially, changes documented, will not exceed 500 horizontal meters from the active crater, in all directions. Ash and pre-existent sediments range from few micras to 2mm. Ballistics, scoria and blocks range from several cms. to several meters.

Sequential photos from several key points will depict surface changes from the very beginning (vegetated surroundings) to actuality (total devastation). Despite rapid erosion (due to heavy rain) and gravity; thickness in most locations, remain above several meters. Still images will show rapid topographical changes that in some cases occurred within weeks or even days.

Photographic material collected over 20 years has been gathered from similar viewpoints at the same angle. Reoccupation of key points has been difficult due to the very same topographical changes, enhanced activity and mainly due to obvious risks.

Josef Dufek, Nathan Andersen

Submission 943

The Growth, Dynamics and Longevity of Silicic Magma Bodies: Crustal Forensics in Two Restless Andean Magmatic Systems

The compositional diversity observed in igneous rocks and the growth of continental crust is ultimately driven by physical process including multiphase convection in magmatic systems, melt-crystal separation, and concurrent phase change in magmas and the surrounding crust. As described by Davidson et al. (2005), crustal forensics that account for the relative importance and timescales of each process have a bearing on the eruptability of magmas and the evolution of the crust. Here, we use multiscale numerical models in conjunction with recent information from the on-going geophysical and geochemical investigation of a large silicic magmatic system, Laguna del Maule (Chile) and bimodal (andesitic-rhyolitic) volcanism of the Cotopaxi-Chalupas system (Ecuador).

To evaluate the timescales of silicic magma production, a 3D multiphase dynamics model was implemented that includes heat transfer, phase change and magma dynamics. To compare simulations to a range of data, major element chemistry, phase assemblage, and tracking of representative crystals are made through time. A particular focus of this presentation is a comparison of dynamic processes to proxies used as chronometers in the spirit of Jon Davidson's work. This includes recording the timescale of appearance of different phases that can be compared to timescales inferred from diffusion profiles and monitoring zircon saturation and dispersal. Both the differentiation timescale and timescales of the major growth of zircons are a relatively small fraction of the melt-present lifetime of magma reservoirs, and in particular, typically represent relatively smaller fractions for larger magmatic systems. These reservoirs can be assembled incrementally with magma fluxes in the ranges estimated for arcs. A mid-upper crust location is important to have phase assemblages with sufficient leverage to produce the most silicic magmas. We compare predicted seismic, gravity, and other geophysical signals from these simulations with a particular emphasis on the Laguna del Maule system. We also compare volume, composition and timescales inferred from both the LDM and Cotopaxi systems (Garrison et al., 2011; Andersen et al., 2017). A generalized view from these simulations is one in which magmas reside for long periods at low melt fraction, but where many chronometers and dynamics operate on much shorter timescales, reconciling some apparently inconsistent observations on the duration of magmatism.

Stéphanie Dumont, Freysteinn Sigmundsson, Andy Heimisson, Kristín S. Vogfjörd, Sigrún Hreinsdóttir, Benedikt G. Ófeigsson, Melissa A. Pfeffer, Diego Coppola, Sara Barsotti, Maurizio Ripepe, Eva P.S. Eibl, Chris J. Bean, Elías R. Heimisson, Michelle M. Par

Submission 639

Spatial and temporal evolution of the plumbing system feeding the 2014-2015 fissure eruption at Holuhraun (Iceland) inferred from a multi-disciplinary approach

Over 14 days propagating seismicity and deformation revealed the onset of a rifting event with the formation of a 47 km-long segmented dyke extending from subglacial Bárðarbunga caldera to the flood plain located ~10 km north of the Vatnajökull ice cap in Iceland. A major effusive eruption started on August 31, 2014 and lasted 6 months, producing an extensive lava field of ~1.4 km³ which is the largest in Iceland since the 1783-84 Laki eruption. Continuous draining of magma from a reservoir located below the Bárðarbunga caldera caused a gradual caldera collapse forming a subsidence bowl up to 65 m deep covering an area of 110 km², by the end of the eruption (February 27, 2015).

To better understand the spatial and temporal evolution of the volcanic plumbing system feeding the eruption at Holuhraun, we carried out a study integrating geodetic, seismics, remote sensing and gas observations for the entire eruption. This allows us to investigate the link between ground deformation, magma transfer at depth and the eruptive activity. A large data set of synthetic aperture radar (SAR) images, acquired by the TerraSAR-X, CosmoSky-Med and RADARSAT-2 satellites, has been used for interferometric analysis (InSAR). This data is complemented with three-dimensional displacements observed by continuous GPS in the area. Using the series of interferograms, we perform a joint inversion of InSAR derived line-of-sight changes and GPS using a Bayesian approach to characterize the temporal evolution of the dyke opening at depth and the slip along the fractures bordering the dyke.

From late August to early September 2014, dyke emplacement induced widening of 1.3 m and 4-5 m subsidence dominated the surface deformation in the flood plain. From early to mid-September 2014, a transition period occurred characterized by a significant decrease for numerous observables including seismic activity, tremor character, deformation rates and gas release. This period ends with a peak in the radiated power, reflecting a maximum heat radiated by the lava field newly created. The following months show small scale variations with a general decreasing trend for all the observables that seem to be correlated with the eruptive activity. We investigate the role of magma transfer as direct source of these variations for the different observables.

Melanie Duncan, Katy Mee, Samantha Engwell, Anna Hicks, Sue Loughlin, Richard Robertson, Michelle Forbes, Idelia Ferdinand

Submission 1093

Increasing resilience to multiple natural hazards through citizen science: piloting the myVolcano app in St Vincent and the Grenadines

The British Geological Survey (BGS) has been working with Caribbean partners on the role of citizen science in increasing resilience to natural hazards. The work has largely built upon the example of the myVolcano app, which was designed by BGS after the 2010 Eyafjallajökull and 2011 Grímsvötn eruptions. During these eruptions BGS asked the UK public to collect dust samples, subsequently analysing these for ash presence to map the distribution of ash fallout across the UK and Europe. The app was designed to be able to capture transboundary observations of volcanic ash and emissions and to assist collection of future observations, which are made visible to other users via an interactive map built into the app. The map interface has global coverage and the data collection methods (free-text descriptions and photographs) are such that information about any natural hazard anywhere in the world could be captured. A case study of St Vincent was subsequently undertaken with the UWI Seismic Research Centre on using the app in proximal environments and capturing a wider variety of observations for use by the public, operational scientists and civil protection. The study of St Vincent emphasised the potential and challenges of such an app.

In March 2017, a workshop and school activities were held in St Vincent to collect feedback from potential users of myVolcano. Workshop attendees were from across government and monitoring agencies (including civil protection and the leading mobile phone network operator). As part of the workshop, a multi-hazard scenario was 'played out' to stimulate discussions on usability of the app, data gathering and processing, and existing applications of citizen science. Discussions developed around data validation and quality assurance, data sharing and presentation, local data management by nominated scientists (real-time applications) and the associated need for a locally appropriate app (i.e. no one size fits all). This last point is particularly significant when considering the utility of an app in several countries – the front end, at least, requires specific tailoring to the country needs. Using this feedback, we are currently modifying the app to meet the local requirements, widening the multi-hazard application and enhancing two-way information sharing, including how best to share critical information with those making observations and how to make observations available to decision-makers and monitoring scientists in real-time.

Michael Dungan, Stephen Turner, Charles Langmuir, Leif Karlstrom

Submission 921

Mantle sources of lithospheric components in Quaternary magmas of the northern, thick-crust portion of the Andean Southern Volcanic Zone (33-36°S), Chile

An ultimately asthenospheric mantle origin for the vast majority of arc magmas is established, but in certain situations, such as the northernmost Chilean SVZ, mantle geochemical signatures may be masked by lithospheric contributions. Subcrustal subduction-erosion and incorporation of crustal material during magma evolution both have been advocated in this case, wherein the arc has migrated eastward onto crust that is undergoing thickening and shortening in conjunction with decreasing slab-dip northward due to subduction of the oceanic Juan Fernandez Ridge (Quaternary volcanism disappears north of 33°S). Crustal contributions are important here, but we offer an alternative scenario to continental margin retreat, arc migration, and mantle wedge 'pollution' due to large-scale subduction-erosion of the continental margin, a hypothesis about which we have independent concerns. We ascribe the late Cenozoic eastward migration of the active arc (36-33°S) onto the continental divide as the inevitable consequence of changes in the mantle wedge as the upper-plate lithosphere thickened due to increased coupling with an increasingly shallow slab and the addition of mantle-derived melts. Thus, the arc has been 'chasing' a migrating mantle-melting region eastward as the asthenospheric wedge has been impinged upon from above and below. Our recent assessment of mantle contributions to SVZ magmas (34.5-41°S) reveals a northward increase, from 38°S, in the contributing fraction of OIB-like mantle (EM1) that reaches an estimated maximum of 90% in reliably mafic compositions, relative to ambient subduction-modified asthenospheric mantle. We infer that the EM1 component originates as enriched material added over time to the base of the mantle lithosphere beneath southern South America, which was then advected westward by virtue of asthenospheric corner-flow. Decompression melting of the EM1 component is inferred to become increasingly important as the wedge thins and slab-dip decreases. This scenario explains northward decreases in $^{143}\text{Nd}/^{144}\text{Nd}$ of least-contaminated magmas. Overprinting of mantle-derived signals by assimilated crust makes this arc segment difficult to interpret on the basis of any petrologic model, but geochemical data must be assessed in the correct geodynamic framework.

Susanna Ebmeier

Submission 1020

Testing the independence of volcanic signals: application of Independent Component Analysis to volcanic deformation

The geophysical signals caused by magmatic, hydrothermal and tectonic activity at active volcanoes are complex, and originate in multiple related and independent processes. Separating out signals of different origin, as well as linking them to the underlying volcanic process, is a priority for volcanologists.

Interferometric Synthetic Aperture Radar (InSAR) allows measurement of the displacement of the Earth's surface on a sub-centimetre scale over weeks to months. It is a powerful research tool for volcanologists investigating magmatic plumbing systems, and is increasingly widely used for monitoring deformation at active volcanoes. A challenge in the analysis of InSAR data is distinguishing and separating magmatic, hydrothermal, tectonic and anthropogenic displacements from each other and from atmospheric noise. I demonstrate an approach for addressing this using Independent Component Analysis (ICA) to investigate the spatial and temporal properties of apparent volcanic deformation.

ICA is a computational signal processing method that describes random variables as a linear combination of statistically independent components. It has previously been applied to remote sensing applications including cloud identification and the detection of thermal hotspots. I present results from a recently published validation of the applicability of this approach to InSAR datasets. A particularly useful property of ICA is that it provides a robust test of signal independence in space or time. Deformation sources caused by different processes result in independent displacement patterns, and are decomposed into distinct independent components. I demonstrate the use of ICA to assess the relationship between different parts of deformation signals, and assess statistical significance using cluster analysis of spatial patterns identified as independent components. This approach is particularly useful for interrogating the large volumes of satellite radar imagery, such as the European Space Agency's Sentinel-1 rapidly expanding archive.

I present analysis of volcano deformation using ICA and cluster analysis, including tests of end-member examples of rapid co-eruptive subsidence during the April 2015 eruption of Calbuco (Chile) and the long-term compaction of lava flows at Parícutin (Mexico). This approach is likely to be most useful at volcanoes experiencing a sustained period of unrest, where multiple magmatic and hydrothermal processes contribute to a complex deformation field.

Marie Edmonds, Tamsin Mather, Emma Liu

Submission 304

Tracking metal pathways in magmas using volcanic gases

As well as gases that have regulated climate over geological time such as carbon and sulfur dioxides, volcanoes also outgas prodigious quantities of metals into the atmosphere and oceans. Here these metals play important roles as catalysts, bioessential nutrients and oxygenation markers in the geological record. Some of these metal species present significant hazards to human health when present in air and groundwater. Volcanic plume metal fluxes are similar to those into hydrothermal ore deposits, making them a significant, yet poorly understood, part of the metal cycle. We show, using a global dataset, that arc basaltic volcanoes outgas high fluxes of metals with plumes rich in copper, lead, zinc and tin; ocean island volcanoes, in contrast, outgas lower metal fluxes but with plumes comparatively enriched in strongly chalcophile metals. The metal compositions of volcanic gases in different tectonic settings are remarkably consistent. We propose that volcanic plume metal outputs are controlled by vapor and sulfide saturation systematics: in arc settings, deep vapor saturation and no (or limited late) sulfide saturation promotes the formation of metal-rich magmatic vapor (and later, volcanic gases). In ocean island volcanoes, reworking and resorption of sulfides formed prior or synchronous to vapor saturation feeds the metal component of volcanic plumes. It follows that submarine arc volcanoes would have been important sources of bioessential metals in the oxygen-limited oceans of Earth's past. There are important implications of these observations for understanding how copper porphyries form. Mafic underplating of arc magma reservoirs may supply sulfur and metals to reservoir roof zones over long timescales via a magmatic vapor phase, with no requirement for sulfide reworking and resorption.

Marie Edmonds, Emily Mason, Alexandra Turchyn

Submission 286

Earth's exhaust pipe: understanding carbon budgets at arc volcanoes

Of the total amount of carbon contained in Earth, the mantle is the largest reservoir. Cycling of carbon between the surface environment and the mantle takes place via carbonate subduction and volcanic outgassing. Imbalance in this cycle has huge significance for atmospheric CO₂ concentration and consequently for atmosphere-ocean temperature over geological timescales. Carbon isotopes, combined with other geochemical tracers, may provide a means to isolate sources and mechanisms of carbon cycling. Carbon in subducting slabs takes the form of organic sediments (with a $\delta^{13}\text{C}$ of -40 to -20‰) and carbonate fixed in the oceanic crust during hydrothermal circulation (with $\delta^{13}\text{C}$ of ~0‰). The $\delta^{13}\text{C}$ composition of the depleted upper mantle has been proposed to be -4±2.5‰. Volcanic gases might be expected to be influenced by these sources, as well as by crustal contamination and interaction with hydrothermal systems. We have created an updated compilation of $\delta^{13}\text{C}$ values of emissions from arc volcanoes, in tandem with He and N isotopic data to provide additional constraint on subduction inputs and crustal contamination. While a small number of arc volcanoes emit gases that fall within typical mantle values, there is a dominance of heavier-than-mantle values in much of the compiled arc volcanic data, particularly when weighted by CO₂ flux. Heavy carbon volcanic outputs, with low $^3\text{He}/^4\text{He}$, are particularly common in continental settings. We propose that whilst the heavy carbon signature of arcs may be influenced by a contribution from subducted inorganic carbon, there is also a strong signature of contamination by carbonate contained within the overriding crust (accreted as carbonate platforms during ocean closure), particularly among volcanic arcs of the Tethyan margin. Observations of modern day volcanic carbon isotope systematics may be used to infer how the volcanic signal might have changed accompanying Wilson cycle supercontinent formation and rifting through the Phanerozoic.

Ben Edwards, Meagen Pollock, William Kochtitzky, Ellen Was

Submission 1267

Constraints on the evolution of glaciovolcanic pillow-dominated tindars from Iceland and British Columbia

Recent field observations at several pillow-dominated tindars in Iceland and British Columbia are revealing the complexities of structures and stratigraphy at volcanoes that were once considered to be simple, monogenetic edifices. Detailed fieldwork at Pillow and Tsekone ridges in British Columbia and along Undirhlíðar ridge in Iceland show that these ridges dominantly comprise multiple eruption units of pillow lava, with intercalated lapilli tuff and tuff-breccia, although locally vitric tuff breccia is volumetrically dominant. Periods of pillow effusion are locally preceded by vitric deposits dominated by fluidal clasts interpreted to form from subaqueous fire fountaining, as opposed to tuff-breccia made by collapse of over-steepened pillow lavas, which is also present at most ridges. Dikes are common at all observed ridges, and are seen to feed overlying pillow lava flows. At several locations dikes are exposed close to present day ridge axes, indicating that many ridges have had material removed from their upper surfaces. Within quarries in Iceland exposed lava tubes and 'master' pillow lavas likely formed along-axis feeder systems. Construction of 3-dimensional surfaces from field images using Photoscan software show that some parts of the feeder system maintain laterally consistent relative elevations along the axis of the ridge. The presence of shelving structures and collapsed shelving structures record smaller-scale changes in lava supply during evolution of individual pillow tubes. Detailed mapping of individual pillow lava morphologies along quarry walls and naturally exposed cross-sections suggest that individual pillow lava units show variation in average pillow dimensions related to lateral positions: closer to flow centers large pillows (>2 m in diameter) are present, whereas towards flow edges pillow diameters are smaller (

Gabriel Eggers, James Wray, Josef Dufek

Submission 537

Feldspathic Rock on Mars: Compositional Mapping of Nili Patera, Syrtis Major

Decades of studies via remote sensing and landed observation of the igneous Martian crust concluded that it is predominantly basaltic. However, new meteorite analyses and mission data indicate this is an incomplete understanding. Nili Patera caldera at Syrtis Major volcano provides one of the best examples of a wider Martian compositional range, exhibiting feldspathic rock as interpreted from data from the Compact Reconnaissance Imaging Spectrometer for Mars (CRISM) instrument. These feldspathic outcrops are subject to many interpretations, including silicic rock formed from multiple cycles of magma evolution, spectrally similar anorthosite, or porphyritic basalts with large feldspar phenocrysts. These feldspathic rocks are distinct from Martian basalts and indicate unique magmatic processes.

To complement existing geomorphologic mapping, we present a thorough compositional mapping of the Nili summit caldera, using all extant CRISM images to investigate the mineralogical diversity of this site. CRISM summary parameters were used to identify major mineralogic constituents, which are then confirmed via direct spectral sampling. Attention is given to tracking the extent of the feldspathic unit using a broad absorption centered at $\sim 1.25\text{-}1.3\ \mu\text{m}$, a unique feature of feldspars only present in the relative absence of mafic minerals. Relations between compositional units were explored further by correlating CRISM data with images from the High Resolution Imaging Science Experiment (HiRISE) instrument.

We find that the Nili Patera feldspathic unit is much larger than first reported: 75 km² of clear contiguous exposure with an additional 75+ km² of obscured exposure beneath the southwestern dune fields. The surrounding terrains are mafic with sundry proportions of high-calcium pyroxene, Mg-olivine, and Fe-olivine in crater ejecta at one locale. The contacts between the feldspathic unit and mafic terrain are varied: some are sharp and look like flow fronts while others are diffuse with a gradational change, and elsewhere the two surfaces are interlaced. Still, all contacts indicate that the feldspathic unit lies beneath and appears to predate the mafic terrain.

Knowing the size and compositional context of the Nili Patera feldspathic unit will inform future modeling of its formation. This unit is potentially the most highly evolved composition on Mars, and further study could revolutionize our understanding of Martian magmatic history and magma evolutionary processes.

Eva P. S. Eibl, Christopher J. Bean, Ingibjörg Jónsdóttir, Ármann Höskuldsson, Thorvaldur Thórdarson, Diego Coppola, Tanja Witt, Thomas R. Walter

Submission 515

Multiple Eruptive Seismic Tremor Sources During an Effusive Eruption: Implications for Monitoring of Lava Flows

We studied the seismic signals that accompanied the 6 month-long, effusive eruption at Holuhraun in 2014/15 in Iceland. The eruption started along a nearly 2 km long fissure, soon focused on fewer vents and had after 20 days focused on one single vent that fed a lava flow field growing to a final size of 85 km².

We analysed the accompanying, long-lasting, seismic signal called tremor using a seismic array at 15 km distance from the vents. Our results surprisingly indicate that there are three tremor sources moving at different speeds and generated by three different processes at different locations. We interpret them after comparison with mappings of the growing lava flow field, effusion rates deduced from MODerate resolution Imaging Spectroradiometer (MODIS) and ground video monitoring data.

We observed a tremor source stable in back azimuth and link it to a process below open vents. We observed a tremor source moving by a few degrees per month and correlate it with the growing margins of the lava flow field. And finally we observe a tremor source moving by more than 10 km in 4 days and interpret it as lateral intrusions at depth as no correlating superficial observations were made.

Our results indicate that care must be taken when using the tremor amplitude in order to derive for example effusion rates, but they also suggest that seismic arrays can be used to monitor the growth of a lava flow field in near real-time.

John Eichelberger, Paolo Papale, Yan Lavallee

Submission 1306

KMT – Krafla Magma Testbed, an international infrastructure for game-change research

The serendipitous encounters with magma in 2009 during drilling at the Krafla caldera, Iceland, is opening the door to a game-change enterprise gathering tens of academies, institutes and industries and represented by KMT, a permanent international infrastructure for engineering, sampling, observing, and manipulating magma and its surrounding system. This unprecedented science project will provide unparalleled information on the geothermal potential of magma-coupled “supercritical” systems; on the behaviour of coupled magma-rock systems during natural or induced, controlled volcanic unrest; on crystallization and heat loss, and the possibility of direct intervention during volcanic crises; at the same time triggering technological developments and feedback between geoscience and industry. The potential benefits to fundamental understanding of the Earth system, to volcano monitoring and hazard evaluations, and to geothermal energy production, are enormous. Examples of revolutions provided by ground-truth evidence through KMT include overcoming tens of years of speculation on the physical state of magmas at depth, on the magma-rock transition, on the mechanisms of fluid loss from magma and magma-geothermal system coupling, etc.; truly testing geophysical and geochemical inverse models to image and characterize deep magmatic bodies; accessing a next level in understanding volcanic unrest dynamics; exploring energy generation directly from magma, the ultimate source of geothermal energy, or from its immediate surroundings, with efficiency gains of order(s) of magnitude; and many others, individually and together qualifying KMT as a potentially gigantic game change in volcano-related science.

Catherine Elder, Paul Hayne, Timothy Glotch

Submission 361

Low Thermal Inertia Volcanic Deposits on the Moon

The Moon has a long and complicated volcanic history ranging from ancient silicic eruptions to mare flood basalts (>1 Gya) and possibly extending to recent (2500 km²) pyroclastic deposits have a low thermal inertia, which is consistent with the hypothesis that they are composed of small glass beads. The thermal inertia of localized (2) pyroclastic deposits generally does not differ from their surrounding terrains. This could be due to the incorporation of a large fraction of country rock during eruption or due to post eruption modification by impacts. Silicic domes on the Moon have a thermal inertia lower than their surrounding terrain which is the opposite of what would be expected for coherent rock, suggesting that they may be highly vesicular. Of the four IMPs large enough to be covered by multiple Diviner pixels, three do not have thermal inertias significantly different from their surrounding terrains, but Ina has a thermal inertia significantly lower than its surrounding terrain. The area with the lowest thermal inertia is located on the largest smooth mound within Ina. This may imply that pyroclastic eruptions or highly vesicular material were a component in the formation of Ina. For each of these volcanic features on the Moon, their thermal inertia tells us about their material properties and provides an important constraint in understanding their formation.

Tamar Elias, Elizabeth Tam, Claire J. Horwell, A. Jeff Sutton

Submission 1181

Volcanic air pollution in Hawai'i: a closer look at air quality, self-reported respiratory symptoms, and measured health outcomes

Kīlauea Volcano on the Island of Hawai'i, has been erupting nearly continuously since 1983, emitting 500-15,000 tonnes of SO₂ per day during periods of sustained activity. The copious gas emissions affect Hawai'i Island air quality, and impact human health, agriculture, and infrastructure. An acidic volcanic haze, known locally as 'vog', is comprised mainly of SO₂ gas and acid and neutral sulfate aerosols, arising from the gas to particle conversion of SO₂ in the atmosphere. In 2008, an additional vent opened at the summit of Kīlauea. This resulted in a several-fold increase in SO₂, as well as an increase in the scope of air quality impacts on the island. Gas and particle monitoring on the island of Hawai'i records SO₂ concentrations in excess of US EPA health standards on a regular basis at proximal, downwind communities. Particulate concentrations (PM_{2.5}) are rarely above federal health standards, but measurements indicate that distal PM composition is very acidic. Health symptoms among Island residents and visitors are formally and informally documented in studies, surveys, and media reports. These symptoms frequently involve the upper respiratory tract, a known target for SO₂ and sulfate irritation. A cross-sectional health study looking at respiratory symptoms and lung function in children prior to 2008, showed a trend toward FEV₁/FVC 1/FVC

While vog contains high concentrations of SO₂ and acidic PM_{2.5}, Hawai'i Island's remote location and light urban development yields volcanic air pollution that lacks the additional contaminants contained in traffic-related and industrial pollution. Vog's limited chemical composition provides an opportunity to compare lung health associated with exposure to anthropogenic pollution as compared to SO₂ and acid aerosol pollution. Further study of Hawaiian and other persistently degassing volcanoes is needed to better understand how volcanic air pollution interacts with environmental factors such as mold, pollen, and environmental tobacco smoke, and to determine acute effects of episodes of increased emissions.

Ben Ellis, Dawid Szymanowski, Tomas Magna, Julia Neukampf, Olivier Bachmann, Peter Ulmer, Marcel Guillong

Submission 753

Post-eruptive behaviour of Li in volcanic rocks: implications for element cycling

Lithium remains a key element in terms of quantifying the cycling of various components through subduction zones. Despite this, much remains unknown about the behaviour of Li in shallow magmatic and volcanic systems.

Here, we use a suite of eight welded ignimbrites from the Yellowstone-Snake River Plain (YSRP) volcanic province to illustrate how post-eruptive effects control the lithium inventory of a deposit. YSRP ignimbrites have a common lithological stratigraphy with rapidly quenched glassy vitrophyres found at the top and base of individual units separated by a more slowly cooled microcrystalline lithology. In all cases, plagioclase and sanidine phenocrysts from the slowly cooled ignimbrite interior contain more Li than the same crystals from the quenched part. The increase in Li between crystals from the two lithologies may be greater than an order of magnitude. This variability is restricted to Li with all other elements unaffected by differences in post-eruptive cooling rate. Such a relationship suggests that the ranges in Li abundance do not reflect a pre-eruptive process. Rather, we interpret the higher Li contents in slowly cooled lithologies to reflect increased partition coefficients due to the lower temperatures and water contents prevailing in the post-eruptive realm.

We further investigated these processes using Li isotopes from glassy and microcrystalline portions of the Tuff of Knob. Bulk and groundmass samples from the microcrystalline lithology had lower Li contents and higher $\delta^{7}\text{Li}$ values than their glassy counterparts. These data are consistent with degassing during slow post-eruptive cooling. In addition, the $\delta^{7}\text{Li}$ in the high-Li feldspar crystals from the microcrystalline lithology was several per mil lighter than that of the low-Li feldspar crystals from the glassy lithology. This indicates that the ingress of Li into the feldspars primarily involves the movement of ^6Li .

These results indicate that the post-eruptive cooling history of a deposit may have a profound effect on both where Li resides in the deposit and the isotopic character of bulk samples. Given this post-eruptive over-printing, studies using Li isotopes to address deeper, magmatic processes should be attempted with caution.

Samantha Engwell, Melanie Duncan, Susan Loughlin, Andrew Tupper

Submission 980

Informing eruption source parameters from volcanic ash advisories

Notifications describing an ongoing eruptive episode and its characteristics are crucial for communicating potential hazard to at risk communities. Reports are designed to provide tailored information according to different stakeholder needs. An example of one such report is volcanic ash advisories (VAAs). VAAs are provided every 6 hours in the event of an eruption, and are provided by the Volcanic Ash Advisory Centre (VAAC) responsible for the affected airspace. These reports are designed to communicate height and distribution of ash in the atmosphere, and forecasts for dispersion for the following 18 hours, predominantly to the aviation industry. In addition to this information, remarks regarding the style of eruption and observations (e.g. from the volcano observatory, pilots and satellite imagery) are also included. Given the frequency of distribution of these reports, and the contained information, analysis of the contained information can provide information not only on reporting, but also on eruptive activity. Here, we show how analysis of available reports can provide information on the information sources, but also on eruption source parameters crucial for application of ash dispersion models.

Application of numerical models for hazard analysis is dependent on accurate assessment of a number of key input parameters. For ash dispersal modelling, such parameters include plume height, erupted grainsize distribution, mass and duration. These parameters are typically estimated from analysis of past eruptive behaviour; from direct observation of eruptive activity or from interpretation of resultant deposits. During an eruption, emphasis is placed upon volcano observatories to provide input parameters to operational forecasters in VAACs. While databases exist that contain such parameters (e.g. the Eruption Source Parameter database, Mastin et al. 2009), operational modelling is increasing calling for a range or distribution of input parameters. Using information within past VAAs, we assess the utility of information contained within volcanic ash advisories (VAA's) to inform distributions of key input parameters, in particular plume height and duration, and investigate how these parameters change both during an eruption, but also over a number of different eruptive events. Our research demonstrates the value of analysing previous advisories for the purpose of understanding eruptive behaviour, but also allows some insight into reporting practises.

Tomaso Esposti Ongaro, Mattia de' Michieli Vitturi, Marco Pistolesi, Federico Di Traglia, Costanza Bonadonna, Mauro Rosi

Submission 995

Physical modelling and numerical simulation of a shallow hydrothermal explosion: PDC generation and ballistic ejection during the 13th century “Breccia di Commenda” eruption (Vulcano island, Italy).

We investigate, by numerical simulation, the initial stages and eruptive mechanism of the 13th century “Breccia di Commenda” eruption at the Vulcano island (Italy). Complementary to this study, recent field work analysis and literature review (Pistolesi et al., session 3.10) allowed to accurately characterize the eruptive sequence and products and to put quantitative constraints to the physical model.

To simulate the eruption, we adopt a new three-dimensional numerical model describing the eruptive mixture as a Eulerian-Eulerian two-phase non-equilibrium gas-particle fluid plus a one-way coupled Lagrangian ballistic particle phase. At the initial simulation time, a pressurized, high-temperature mixture (initially confined within the shallow vent) is allowed to decompress and expand in the atmosphere forming an eruptive cloud, while ballistic particles are rapidly accelerated by the coupling effect of drag and pressure forces. After an initial expansion stage (lasting only 2-3 seconds), the eruptive cloud collapses (while ballistic particles tend to keep their trajectories) forming lateral pyroclastic density currents (PDCs). We show that PDC features and ballistic ranges (up to 2.2 km) are consistent with an exploding body having a mass of about 109 kg, an initial overpressure above 10 MPa, a maximum temperature of about 250°C and a maximum depth less than 200m. We also show that the observed deposits are consistent with explosion from an elongated fissure oriented North20°East, with preferential ballistic ejection and pyroclastic density current generation occurring in the directions orthogonal to the fissure orientation.

We finally discuss present findings in the framework of volcanic hazards posed by phreatic explosions like those occurred at Ontake (Japan) in 2014 and Tongariro (NZ) in 2012.

Tomaso Esposti Ongaro, Mattia de' Michieli Vitturi, Giacomo Lari, Alvaro Aravena Ponce, Augusto Neri

Submission 996

A new depth-averaged flow model for pyroclastic avalanches dynamics and hazard.

Pyroclastic avalanches (PA) are gravity-driven flows of pyroclastic material, typically confined within steep volcanic slopes, whose dynamics are controlled by the balance between the longitudinal component of gravity and friction, and by their interaction with the topography. Physical and numerical modelling is a key tool for studying their behaviour and for evaluating their hazards, but it is particularly challenging because of the complex (and relatively poorly understood) rheology of the basal, concentrated flow and its interplay with the substrate and the overriding, more dilute, turbulent ash cloud.

We present here a new depth-averaged two-dimensional flow model and a numerical solver designed for simulation of shallow PA on rough and steep topographies. In the present implementation, the model solves the mass and momentum equations for a granular fluid having constant density and specific rheological laws (Voellmy-Salm or constant stress). Model equations are written in conservative form in a geographic Cartesian coordinate system, thus avoiding the need of metric corrections (e.g. curvature) on complex topographies. On steep slopes, non-hydrostatic formulation of the vertical momentum equation can also be implemented to provide accurate modelling of avalanches with non-negligible vertical acceleration.

The numerical code is designed to facilitate the implementation and testing of a variety of rheological laws and transport equations, including two-layers or multi-fluid formulations and transport of scalars (e.g., temperature or turbulent energy). In particular, the implicit treatment of the (non-hyperbolic) friction terms is shown to be essential to avoid the problems typically associated to operator-splitting or predictor-corrector algorithms in the regime of flow stoppage.

We present here a preliminary application of the new model to the simulation of PA generated by the partial collapse of scoria cones at Mt. Etna volcano (Italy) and discuss the potential application of the model in hazard assessment studies.

Ben Esse, Mike Burton, Simona Scollo, Giuseppe Salerno

Submission 811

Mitigating volcanic ash risks through ground based ultraviolet spectroscopy

Volcanic ash can pose a serious hazard to health and infrastructure; if inhaled, ash can cause short term breathing difficulty or aggravate pre-existing conditions, while heavy ash fall can damage transportation and electricity networks, or cause buildings to collapse. Aircraft are particularly at risk from ash; exposed components can be damaged through abrasion while ash ingested into jet engines can cause them to fail. The 2010 eruption of Eyjafjallajökull in Iceland is a good example of the widespread disruption large ash clouds can cause to air travel, costing the air industry over US\$1.7 billion and stranding approximately 10 million passengers.

By detecting and characterising ash remotely these risks can potentially be reduced. Here we examine the possible application of ultraviolet absorption spectroscopy to the detection and quantification of airborne ash loading. Existing detection methods can be bulky or expensive (such as LIDAR) or require prior knowledge of the plume characteristics (such as infrared). Ultraviolet spectrometers are relatively cheap and extremely portable, making them easy to deploy to on-going eruptions, as well as potentially to airborne applications. The retrieval method utilises scattered solar light backlighting the plume, so the radiative processes are relatively simple. Furthermore, utilisation of the polarized nature of scattered solar light may also allow for discrimination ash, which is highly non-spherical, from other volcanic aerosols in the plume, as these are predominantly spherical.

Compact ultraviolet spectrometers are already used in the monitoring of volcanic gasses, such as in the FLAME network for monitoring SO₂ fluxes at Mt Etna in Italy. The gas retrieval processes often remove the broadband effects of volcanic aerosols; however incorporation of these effects into the model could provide information about the ash loading of the plume. At present there is no quantification of ash emission using these data, so the development of ultraviolet ash retrieval potentially offers a large source of untapped information on volcanic processes and risk mitigation.

We will present an overview of the state of the art methods in volcanic ash detection using UV absorption spectroscopy, as well as preliminary results from ground based field experiments.

Russell Evarts, Richard Conrey, William Leeman, Martin Streck

Submission 1232

Insights Into Magmatic Diversity in the Columbia Cascades Transect (CCT)

The CCT straddles the Columbia River and includes major stratovolcanoes (Hood, Adams, St. Helens) and many dispersed monogenetic vents and lava fields. These include prominent back-arc (Simcoe, Tygh Valley VFs), intra-arc (Indian Heaven VF), and forearc (Portland Basin) activity spanning late Pliocene to recent times. It is unique in its diversity of magmatic compositions, that range from mainly andesite to dacite in the stratovolcanoes to mainly basalt and basaltic andesite from lesser vents. The latter are the focus of this study. They comprise two broadly distinct chemical groups: [1] intraplate-like basaltic lavas distinguished by low Ba/Nb (~ 20) and variable enrichments of LILE and depletions of HFSEs. Group 1 can be further divided into an almost MORB-like low-K (and other LILE) subset (LKTs) and a higher-K, OIB-like subset. These chemical variants of mafic magmas are widely distributed across the CCT and overlap extensively in age. Because MgO in many of these lavas exceeds 8% MgO, we infer that they came from the underlying mantle wedge in a quasi-continuous manner and are widely available. An exception is near the stratovolcanoes where eruption of mafic magmas is impeded by shallow accumulations of evolved felsic magmas. Occurrences there of mixed or hybrid magmas attest to interactions between these magmatic end members. Frontal arc activity in the CCT sector may reflect tectonic controls in the fore-arc.

How did the diverse mafic magmas form? How did they retain their distinctive compositions? And what do these imply about the nature of the mantle wedge? Flux-melting processes have been invoked to account for some of the diversity, but cannot readily explain the strong contrasts in trace-element compositions within Group 1, and it appears to conflict with evidence for limited inputs of slab-derived fluids to the mantle wedge. Mantle heterogeneity could play a significant role but is difficult to reconcile with the nearness in time and space of distinct primitive magmas. The Cascadia subduction zone is extremely warm, and the slab strongly dehydrated. Thus, we consider decompression melting of upwelling mantle domains to be a dominant factor in CCT magmatism.

John Ewert

Submission 657

A history of volcano hazard maps

The Volcanological Survey of Indonesia produced the first volcano hazard maps following the 1919 eruption of Kelud. These maps were prepared for some of the most frequently active and deadly volcanoes in Indonesia. The nature, scale, and areas affected by well-observed historical eruptions defined the hazard zones. These direct observation-derived hazard maps were standard practice for decades in Indonesia and at the few other volcanoes where hazard maps were prepared.

Volcano hazard assessments were rare and not primary subjects of scientific inquiry until the 1960s. On the basis of careful field geology and laboratory work, USGS volcanologists Rocky Crandell and Don Mullineaux developed the first modern volcano hazard maps for Cascade Range volcanoes in the mid-1960s. Their volcano hazard mapping arose organically from their geological studies of surficial geology and eruption history of dormant Cascade volcanoes. They extended the observational basis of hazard area definition by developing a more comprehensive history of eruptive frequency, style, and magnitude. The primary purpose of their studies was to provide a basis for long-range land-use planning in areas near volcanoes. Degree of hazard was indicated with a simple low-moderate-high schema. These early USGS hazard maps included a companion geologic map from which the hazard map was derived. Such volcano hazard maps encompass the entire range of past eruptive behavior and show all areas exposed to some degree of hazard from future eruptions. They were essentially unconditional hazard maps. In addition to land use planning, these hazard maps were intended to provide context for monitoring data and associated forecasts, on the basis of which conditional or scenario-based hazard assessments and maps could be developed.

The hazard assessment and mapping approach pioneered by Crandell and Mullineaux was validated during the response to the 1980 eruption of Mount St. Helens, USA. Subsequently, volcano hazard mapping and hazard assessment were broadly adopted by the volcanological community and grew rapidly to become a significant part of modern volcanological practice, incorporating sophisticated process models and increasingly quantitative statistical analysis, particularly for times of unrest. Given the uncertainties in outcomes that accompany the reactivation of long-dormant volcanoes, unconditional, geology-based hazard maps remain as fundamental elements of hazard assessments and communication.

Julia Eychenne, Alison Rust, Katharine Cashman, Wolfram Wobrock

Submission 288

Distal enhanced sedimentation from volcanic plumes: insights from the secondary mass maxima in the 1992 Mount Spurr fallout deposits

Some tephra fallout deposits show an increase of mass and thickness at distances from the source > 100 km, hereafter referred to as Areas of Secondary Mass Maximum (ASMM), which demonstrate distal enhanced sedimentation from volcanic plumes. To assess the volcanic ash transport and sedimentation processes that cause such depositional variations, we focus on the 1992 August and September Mount Spurr eruptions, Alaska, which produced fallout deposits with conspicuous ASMMs beyond 150 km from vent. We compare the crosswind and downwind variations of mass and grainsize within the two fallout deposits, and show that the increase of sedimentation at the ASMM does not result from preferential settling of fine (<100 μm) ash relative to coarser grain sizes, as has been suggested elsewhere. Simulations of individual particle settling through a homogeneous and horizontally stratified atmosphere indicates that fine ash reached the ground much closer to the vent than the theory predicts, as observed in many other fallout deposits. However, these simulations show that the mechanism leading to enhanced settling at ASMMs affected the sedimentation of both fine ash and coarser particles. Moreover, measurement of the particle fall velocities in a sample from the August deposit shows that the texture and morphology of the particles has only a minor effect on settling within the ASMM. But we find a clear link between the ASMM and the topography: in both deposits, the mass local minimum occurs on the windward flank of a 2 km-high mountain range, while the local maximum (i.e. the ASMM) appears on the leeward flank. Mesoscale models of the three-dimensional wind field that include the effect of the underlying topography highlight stagnant zones of the atmosphere above the leeward flank of the topography highs, where the horizontal wind field is quasi null. We suggest that the lack of horizontal ash transport results in a local increase of the sedimentation rate and causes ASMMs to form on the leeward flank of the mountains. More generally, we conclude that questions of ASMM formation must be decoupled from questions about controls on sedimentation of fine ash, and that topography may play an important role in controlling depositional patterns of tephra.

Gareth Fabbro, Chris O. McKee, Mikhail Sindang, Caroline Bouvet de Maisonneuve

Submission 611

Variation in the magmatic plumbing system of Rabaul (Papua New Guinea) across space and time

Caldera volcanoes commonly show cycles, in which repeated ignimbrites are interspersed with long periods of minor activity when the caldera-forming magma bodies must develop. Also, calderas can have multiple vents, which may tap different melt bodies. To understand the behaviour of silicic calderas, we must ensure our sampling is representative both in time and in space. Rabaul is an ideal location to study these variations, as it has had at least five caldera-forming eruptions in the last 20 ky and has multiple vent locations. Several overlapping calderas make up the Rabaul Caldera Complex (RCC), while to the north and east lies a zone of five dominantly mafic stratocones (the Watom-Turagunan Zone, WTZ). Historical activity has taken place at several locations within the most recent caldera. We have focused on activity during the Late Pleistocene–Holocene, a period that includes the most recent complete caldera cycle, from the ~10.5-ka Vunabugbug Ignimbrite until the ~1.4-ka Rabaul Pyroclastics. Between these two caldera collapses lie the Talwat and Talili subgroups, a sequence of at least 11 explosive eruptions. These include both basaltic scoria fall deposits and dacitic fall, flow and surge deposits. The deposits are well constrained by ¹⁴C, allowing us to trace temporal variations in the plumbing system. In addition, the eruptions occurred from multiple vents, permitting us to explore the spatial variations in the plumbing system.

During the post-Rabaul Pyroclastics era, basalt has been free to enter the shallow silicic magma reservoir. Basaltic enclaves and mafic mineral assemblages are found in dacitic magmas, and low-Ti hybrid andesites have also been erupted. However, prior to the Rabaul Pyroclastics, during the period of emplacement of the Talili Pyroclastics (4.2–1.8 ka), basalt was prevented from entering the silicic reservoir. Although basalt continued to reach the surface (until at least 3.4–2.5 ka), it did not interact with any dacite, and most likely erupted from the WTZ. In the RCC, the only evidence for mixing is aphyric andesitic inclusions in dacitic tephra of an early-erupted phase of the Talili sequence, and at the end of the dacitic Rabaul Pyroclastics eruption. The high Ti content of these andesites implies that they were formed by fractional crystallisation. Rheology contrasts between a large dacitic melt body and basaltic recharge could have prevented mingling and mixing, allowing a caldera-forming silicic melt body to form.

Erickson Fajiculay, Nang Thin Zar Win, Christina Widiwijayanti, Fidel Costa, Christopher Newhall, Antonius Ratdomopurbo

Submission 974

Improving WOVOdat Online Tools For Eruption Forecasts

During periods of volcanic unrest, volcanologists need to interpret monitoring data to be able to forecast whether an eruption is likely to occur, to anticipate to the evolution of the unrest, and to implement timely mitigation actions. Some volcanoes are regularly active and closely monitored, while other aren't. Often, the record of precursors to historical eruptions of a volcano isn't enough to allow a forecast of its future activity. Therefore, volcanologists must refer to monitoring data of unrest and eruptions at similar volcanoes. WOVOdat is the World Organization of Volcano Observatories' (WOVO) Database of worldwide volcanic unrest. Through WOVOdat, users will be able to search analogous historical unrest that can be compared to ongoing unrest, to find the range and rough probabilities of possible outcomes. WOVOdat is intended to provide reference data useful during volcanic crises, for comparative studies, and basic research on pre-eruption processes. We have now incorporated data from 317 volcanoes, 75 of which covered by more than 650 episodes of unrest since 1950.

To improve and promote the use of WOVOdat, we are creating a robust online-interface allowing users to explore and use the database. Main tools in WOVOdat (www.wovodat.org), currently include: (1) Spatio-temporal interactive visualization tools including 2D and 3D hypocenter distribution and a plot of multi-parameter time-series data. (2) Data search and data download tools, by applying variety of filter criteria and threshold value into selected unrest datasets. (3) Application tools for advanced analyses of WOVOdat.

WOVOdat application tools are a web service application that employs various statistical and machine learning algorithms. The tools allow users to perform statistical analysis of various types of temporal monitoring data i.e. RSAM, seismic counts, gas emission rate, tiltmeter, GPS, etc. The development aims to identify signals of unrest indicators from the baseline with supervised and unsupervised learning. Data processing and trend analysis procedures includes filling up data gaps, time series prediction, inverse and logarithmic function, 1st or 2nd derivatives, time averaged, cumulative value over time, and user inputted custom function. Integration of the web service to other URLs and to desktop application will be develop to support users who wish to process data on their personal computer.

Jamie Farrell, Robert Smith

Submission 1174

The Yellowstone crustal magmatic system: Our current understanding and what's next

The Yellowstone magmatic system has been imaged from the mantle through the crust to the surface hydrothermal systems using seismic tomographic methods of local and teleseismic data. Results show that the Yellowstone crustal magmatic system consists of a lower crustal basaltic reservoir at depths of 20-40 km and an upper crustal rhyolitic reservoir at depths of 5-15 km. Based on the magnitude of the reduced P-wave velocity (VP) from ray paths through the partial melt, the lower crustal magma reservoir, about 4.5 times larger than the upper crustal reservoir, has a melt fraction of about 2% while the upper crustal reservoir has a melt fraction of about 5-15%. The upper-most crustal reservoir in turn provides magma for the youthful rhyolitic-basaltic Yellowstone volcanic system and the extraordinarily high heat flux, up to 30 times the continental average, that drives Yellowstone's extensive hydrothermal system. The presence and volume estimate of the lower crustal basaltic reservoir is supported by the amount of CO₂ that is released at the surface, which requires a deeper crustal basaltic magma reservoir in addition to the upper crustal rhyolitic reservoir to produce the observed quantity of CO₂ at the surface. Unlike the P-wave velocity structure, the S-wave velocity (VS) structure for the crustal magmatic system is less well constrained because there are less S-wave arrival times identified in the Yellowstone earthquake data. However, having a better VS model would better constrain the amount of melt in the Yellowstone magma reservoirs and allow for a VP/VS model. We show preliminary VS results for Yellowstone data for body waves and compare that to a VS model from surface wave ambient noise tomography.

Kristen Fauria, Michael Manga, Michael Chamberlain

Submission 121

Effect of particle entrainment on the runout of pyroclastic density currents

Pyroclastic density currents (PDCs) can erode soil and bedrock, yet we currently lack a mechanistic understanding of particle entrainment that can be incorporated into models and used to understand how PDC bulking affects runout. Here we quantify how particle splash, the ejection of particles due to impact by a projectile, entrains particles into dilute PDCs. We use scaled laboratory experiments to measure the mass of sand ejected by impacts of pumice, wood, and nylon spheres. We then derive an expression for particle splash that we validate with our experimental results as well as results from seven other studies. We find that the number of ejected particles scales with the kinetic energy of the impactor and the depth of the crater generated by the impactor. Last, we use a one-dimensional model of a dilute, compressible density current—where runout distance is controlled by air entrainment and particle exchange with the substrate—to examine how particle entrainment by splash affects PDC density and runout. Splash-driven particle entrainment can increase the runout distance of dilute PDCs by an order of magnitude. Furthermore, the temperature of entrained particles greatly affects runout and PDCs that entrain ambient temperature particles runout farther than those that entrain hot particles. Particle entrainment by splash therefore not only increases the runout of dilute PDCs but demonstrates that the temperature and composition of the lower boundary have consequences for PDC density, temperature, runout, hazards and depositional record.

David Fee, Keehoon Kim, Arthur Key, Robin Matoza, Alexandra Iezzi, Allison Austin, Richard Johnson, Geoff Kilgour, Bruce Christenson, Esline Garaebiti, Ben Kennedy, Rebecca Fitzgerald, Nick Key

Submission 1082

High-resolution explosion localization and characterization at Yasur Volcano, Vanuatu using the Time Reversal Mirror algorithm

Localization of volcano seismic and acoustic sources remains a topic of great interest. However, dynamic sources and complex wave propagation often makes accurate and precise localization difficult. Advances in numerical waveform modeling and data quality have permitted the location of volcano acoustic sources within tens of meters using a network distributed within ~5 km of the source (Kim and Lees, 2015). Resolution on this scale provides detailed information on not only the timing and location of activity, but also valuable information on the eruption dynamics. Here we apply the Time Reversal Mirror (TRM) algorithm to infrasound data collected at Yasur Volcano, Vanuatu. TRM has been applied broadly in medical imaging and underwater acoustic communications, and more recently seismology and airborne acoustics. The algorithm relies on the relation between the observed waveforms and the time-reversed wavefield computed through numerical modeling, as well as reciprocity in the Green's functions between the source and receiver. TRM therefore accounts for complex topography and crater morphology often present at volcanoes that other algorithms (e.g. semblance) do not. Here we compute the numerical Green's functions using a 3-D Finite Difference Time Domain (FDTD) algorithm and a high-resolution Digital Elevation Model (DEM) constructed from structure from motion.

At Yasur we deployed six single infrasound sensors around the active vents within 750 m and two 3-element infrasound arrays along a line extending out to 1 km, as well as multiple acoustic sensors on tethered balloons above the vents. We anticipate source resolution on the scale of meters for the thousands of diverse explosions we recorded during our 8-day deployment. This will permit not only discrimination between the multiple active vents but inferences on source processes in the shallow conduit and surface. The different vents at Yasur have different eruption characteristics (e.g. gas-rich vs. ash-rich), but often erupt in succession and appear to be connected at shallow depth. Comparison of the TRM results with seismic, video (including UAV), infrared, and geochemical observations will also permit characterization of the eruptive processes, including eruption style and emissions information.

References

Kim, K., Lees, J.M., 2015. Imaging volcanic infrasound sources using time reversal mirror algorithm. *Geophysical Journal International* 202, 1663-1676.

Rui M.S. Fernandes, Stéphanie Dumont, José Madeira, João Mata, Machiel Bos, Fernando Carrilho, Graça Silveira, Ricardo S. Ramalho, Carla Candeias

Submission 647

A Multidisciplinary approach for studying an active volcano: the example of Fogo volcano (Cape Verde)

Fogo volcano is one of the most active volcanoes in the Atlantic with 27 eruptions since settlement, in the early 15th century, and a return period of ~20 years. It is a stratovolcano with a summit depression (Chã das Caldeiras) 9 km in diameter open to the east, where a secondary cone rises 1 km above the depression. The almost vertical wall surrounding the depression is interpreted as resulting from two caldera collapses followed by an eastward flank collapse to the east or as the headwall of the giant lateral collapse at ~65 to 84 ka. The dimension of such event (estimated as involving 90 to 150 km³) may have changed the internal stresses within the volcanic edifice impacting its plumbing system. To better decipher its impact on the eruptive activity, it is necessary to understand the plumbing system of Fogo. This is even more critical since the last three eruptions (1951, 1995, 2014-15) have produced extensive lava flows that threatened the local populations resulting in the total destruction of two villages in 2014-15.

Following the latest eruption, the project "FIRE - Fogo Island volcano: multi-disciplinary Research on 2014/15 Eruption" was conceived to understand the structural evolution of the volcano, its eruptive dynamics, and to contribute to the hazard assessment and risk mitigation in collaboration with local institutions. The structural characterization of Fogo is targeted through geophysical and geological studies including gravimetry, seismology, geodesy, paleomagnetism, geochemistry, and morpho-structural analysis. It will allow understanding the evolution of the plumbing system (pre- and post-collapse) over the last hundreds of kyr. A wide range of eruptive behaviours was recognized at Fogo volcano, namely during the last eruption that shown a variety of eruptive styles with a dominant effusive component, accompanied by hawaiian, strombolian and vulcanian manifestations. Multi-disciplinary observations collected during this eruption are of prime importance to decipher the eruptive dynamics and the conditions of magma storage. Petro-geochemical analysis of the eruptive products will address these points and will be complemented by geological mapping to reconstruct Fogo's eruptive history. FIRE project includes also societal aspects using environmental analyses that will allow evaluating the impact of volcanic activity on the ecosystems and in human health.

This is a contribution to Project FIRE (PTDC/GEOGEO/1123/2014) funded by FCT.

Judy Fierstein

Submission 447

Multi-faceted tephra studies and mapping as complementary tools in establishing eruptive histories of explosive volcanic centers

Combining the study of pyroclastic deposits with geologic mapping of edifices provides more complete eruptive histories than either approach can separately. While tephrostratigraphy that focuses on sourcing and dating distal ash-fall layers can establish useful time markers and can inform hazards considerations to a degree, much more can be learned from a “whole-volcano, vent-to-distal-extremes” approach that includes detailed stratigraphy, chemistry, mineralogy, deposit characteristics and physical volcanology. Such studies can establish chronologies, scales, and styles of eruptive sequences and emplacement processes. When including whole-edifice field mapping, the complementary studies can develop an integrated view of magmatic and eruptive processes, decipher the eruptive history of each center, and place eruptive histories into time-volume-composition stratigraphic contexts. Synthesis of such data provides a better understanding of how volcanoes work, as well as helps to develop more advanced evaluations of eruption potential and hazards assessments. Examples to be discussed include: (1) Study of the 1912 plinian deposits of Novarupta (Alaska), for which compositional changes in fall layers deposited during the 3-day event were correlated with packages of pyroclastic-flow deposits emplaced during the same time interval. This evidence unequivocally documented for the first time the eruptive synchronicity of plinian falls and pyroclastic flows; that the pyroclastic flows were density stratified; and that phreatic mud layers intercalated in the Novarupta plinian deposits were derived from collapsing Mt. Katmai, thus establishing the timing of fitful subsidence at Katmai caldera. (2) Detailed stratigraphy and deposit characteristics at Ubehebe Crater cluster in Death Valley, California show that eruptions from all 14 phreatomagmatic vents lasted a total of days to months, not millennia as has been previously suggested. (3) A combination of mapping the Laguna del Maule volcanic field in Chile and tephra studies on both sides of the Chile/Argentina border establish that >50 postglacial silicic events (several of which are plinian) erupted from multi-vent complexes that were each recurrently active for decades to millennia. Integration of the effusive and explosive records for numerous silicic vents in both space and time highlights the potential hazard from this volcanic field on the Andean crest.

Judy Fierstein

Submission 1113

Postglacial eruptive history from tephra-lava correlations provide window into magmatic system beneath Laguna del Maule, Chile

Laguna del Maule (LdM) volcanic field on the Chile-Argentina border (36° S) is a unique focus of postglacial rhyolitic eruptions. Study of tephra and related lavas has established its postglacial eruptive history. Spatial and temporal distribution of the eruptive vents can be used as a window into the magmatic system that supports the volcanic field. Stratigraphy, chemistry, and grain-size distributions yield tephra-to-vent correlations for most of the >60 postglacial silicic LdM eruptive events. These correlations, combined with radiocarbon dating, show that each of the 24 postglacial silicic vents identified by Hildreth et al. (2010, SNGM Boletín 63) were built intermittently over decades to millennia by multi-stage eruptive sequences between ~15 ka and 2 ka. The most voluminous eruption that began ~15 ka is newly named the “rhyolite of Laguna del Maule” (rdm) and is inferred to have erupted at the site of the subsequent lake. The aphyric, high-silica rhyolite produced as much as 20 km³ of pyroclastic flows and fallout impacting both sides of the border at least as far as 80 km downwind (~E). Rhyolite and rhyodacite eruptions that followed issued from vents that surround the lake, nearly all within 5–11 km of the rdm vent site. The exception is also the largest and most long-lived—the multi-vent Barrancas complex—with 2 edifices and as many as 17 vents that erupted episodically between ~14.5 and ~3.5 ka, ~16 km SE of rdm. All of the rhyolites are crystal-poor and some are truly aphyric, but most of the rhyodacites include 5-25% phenocrysts (pl, hb, bt). In the LdM basin, an additional 13 mafic vents (53-61% SiO₂) and one dacite (66% SiO₂) erupted during the same time interval, most in a sector west to southwest, 6–11 km from the lake center. Notably, one scoria ring along the SE lakeshore, and a cluster of 3 scoria rings on the NW shore are only 4 and 5.5 km, respectively, from the rdm vent site. Mafic components are clearly present in each of the rhyodacite eruptions as enclaves and mixed pumices, but are not typically seen in the rhyolites. One exception is rdm itself, which has mafic enclaves in the rhyolite pumice and cognate cauliflower-shaped mafic clasts (53-61% SiO₂) in the deposits that were comagmatic liquids. The established sequence of events shows rhyolite, rhyodacite, and mafic magma erupted throughout the entire postglacial interval, sometimes concurrently, with no systematic trends in either vent location or composition through time.

Jonathan Fink, Steven Anderson

Submission 1284

Unanswered questions about silicic lava flows fed from dikes

Silicic lava flows receive considerable attention because many preserve evidence about explosive eruptions that precede or follow their emplacement, and some may generate their own pyroclastic activity through flow front collapse or explosive release of concentrated volatiles. Additional interest has recently come from observations of rhyolite and rhyodacite eruptions at Chaitén and Cordón Caulle, in Chile; a submarine rhyolitic eruption at Havre Seamount north of New Zealand; recognition of the increasing potential for a major explosive eruption from the silicic dome-covered Laguna del Maule volcanic field in Chile; and plans for a program to drill into an active rhyolitic system at Krafla Volcano in Iceland.

Despite this new scrutiny, scientists have still not observed active dike-fed eruptions of glassy rhyolite lava flows and domes like those exquisitely exposed in the Cascades of central Oregon and northern California and in the Mono-Inyo chain of eastern California. In this presentation, we discuss evidence bearing on the following unanswered questions about these eruptions:

What causes dike-fed explosive eruptions to localize to individual point-source dome extrusions?

What controls the spacing and volumes of different domes fed by a single dike?

What influences if domes can generate pyroclastic flows by flow front collapse?

How can the morphology and structure of domes be related to extrusion rate and rheology, and how do these relationships vary for magmas with differing silica contents or in submarine or extra-terrestrial environments?

Do glassy and pumiceous textures preserved in rhyolite domes form by the collapse of an originally extruded foam or by inflation of an original dense glass, and does this mechanism affect how much explosive activity can occur during dome emplacement?

How and where does magma mixing occur for large dike-fed domes that show compositional transitions during a single eruption?

How is endogenous and exogenous growth partitioned in the evolution of individual silicic domes?

How do brecciation and other fracture processes relate to dome emplacement rates?

Given the renewed interest in silicic eruptions, our goal is to use these questions and an assessment of earlier work to map out a new agenda for future research on silicic lava flows and domes.

Emily First, Julia Hammer, Philipp Ruprecht

Submission 917

Experimental constraints on dacite magma storage beneath Volcán Quizapu, Chile

Volcán Quizapu, in the Andean Southern Volcanic Zone, has erupted twice in historic times. Lava flows in 1846-7 and a Plinian eruption in 1932 each discharged 4-5 km³ of dominantly dacite (67 wt% SiO₂) magma. The drastic difference in eruptive styles motivates our study, which includes first evaluating the pre-eruption magma storage conditions. A suite of water-saturated phase equilibrium experiments ranging from 800-900 °C and 35-200 MPa were performed using isochemical 1932 pumice and 1846-7 lava samples. Experimental products contain all phases present in the starting materials, including plagioclase, amphibole, pyroxene, titanomagnetite, ilmenite, apatite, and glass. Amphibole is stable above 125 MPa, at temperatures ≤ 875 °C. Fe-Ti oxides, though frequently cited as fast-equilibrating phases that record short-term thermal excursions, display disequilibrium textures in all experiments. Thus, in Quizapu dacite at temperatures and pressures typical of arc volcano reservoirs, coexisting Fe-Ti oxides in the 10-100 mm size range require > 14 days to equilibrate. Experimental glass compositions match natural dacite glass compositions within a narrow, negatively-sloping band of pressure-temperature space, centered near 160 MPa and 835 °C. At 835 °C, the water-saturated stability curve for the dominant natural plagioclase (An₃₅) falls at the outer edge of the band, ~ 135 MPa. However, application of the plagioclase-liquid hygrometer (Waters and Lange, 2015) indicates that water undersaturation by ~ 0.5 wt% (melt H₂O content of 4.75 wt%) shifts the An₃₅ isopleth to lie centrally within the band. Additional evidence for water undersaturation in the magma storage environment comes from experimental glasses, which contain less chlorine (0.09 wt% Cl) than pumice glass (0.17 wt% Cl). This discrepancy suggests that chlorine in the water-saturated experiments was partitioned into a hydrous magmatic volatile phase that was not present in the natural storage region. Thus, the total pressure at which Quizapu dacite magmas were stored is higher than the P_{H₂O} indicated by the An₃₅ water-saturated stability curve, by ~ 25 MPa. Our study suggests that both batches of Quizapu dacite magma were undersaturated with respect to an H₂O-rich vapor phase while stored at ~ 835 °C and ~ 160 MPa (total pressure), slightly colder than the ~ 860 °C that has been estimated from geothermometers applied to natural Quizapu samples.

Tobias Fischer, Patrick Allard, Alessandro Taran, Bo Galle, J. Maarten de Moor, Taryn Lopez, Giovanni Chiodini, Brendan McCormick, Hiroshi Shinohara, Nicole Bobrowski, Erik Hauri, Marie Edmonds, Yuri Taran, Elizabeth Cottrell, Kerstin Lehnert

Submission 536

Deep Earth CARbon DEgassing: Results from the Deep Carbon Observatory DECADE initiative

Since 2012 the DECADE initiative has brought together gas geochemists and volcanologists to significantly advance our understanding of volcanic fluxes of deep carbon. This is being achieved through building of a permanent volcanic gas monitoring network, conducting targeted campaigns to remote volcanoes, developing linked databases and constraining diffuse volcanic degassing. Current DECADE monitored volcanoes include: Turrialba and Poas, Costa Rica; Masaya, Nicaragua; Galeras and Nevado del Ruiz, Colombia; Popocatepetl, Mexico; Villarrica, Chile; Merapi, Indonesia; and White Island, New Zealand. The success of the DECADE initiative hinges on the commitment of local scientific staff that enables sharing of data and instrument maintenance. Most monitoring stations include a MultiGAS instrument for plume CO₂ and SO₂ measurements and multiple NOVAC scanning DOAS stations for quantifying SO₂ flux.

In addition to better constraining global volcanic CO₂ fluxes, observed changes in CO₂/SO₂ ratios and SO₂ fluxes by DECADE networks have provided key precursors to eruptions. Such changes preceded explosive eruptions at Turrialba and phreatic eruptions at Poas. In both instances the compositional changes provided new insights on the dynamics of the volcanic-hydrothermal system in response to magma degassing at depth. CO₂/SO₂ changes weeks prior to the explosive eruption of Villarrica in March 2015 and prior to increased lava lake activity at Masaya in 2016 are consistent with injection and degassing of new magma.

Campaign-style measurements include determination of volatile fluxes at Ambrym (Vanuatu), Bromo and Krakatau (Indonesia), Piton de la Fournaise (Reunion), Tavurvur, Bagana, Ulawun

(Papua New Guinea). An expedition to the Western Aleutians was enabled through collaboration with NSF GeoPRISMS and the USGS and resulted in gas measurements at previously unmeasured volcanoes. The 2016 expedition to the Kuriles set the stage for the planned 2017 expedition. Campaigns also deployed pioneering instrumentation (drones, isotope spectroscopy). Data obtained by DECADE initiatives are accessible through IEDA and Smithsonian GVP databases. Linkages between these and other databases are being developed. As more volcanoes are measured and monitored for gas emissions we expect that integration of continuous high-frequency gas monitoring with geophysical time series data will greatly improve dynamic volcano models and yield fundamental new insights on magmatic-tectonic processes.

Richard S. Fiske, Benjamin J. Andrews, Alex Nichols

Exceptionally energetic pyroclastic-fall eruptions at Kīlauea Volcano, Hawai'i, ca 900 CE. Evidence for jet-driven events

Kīlauea is typically the site of gentle effusive activity punctuated by moderately explosive phreatic and phreatomagmatic eruptions, but we show the volcano can erupt far more energetically. The Kulanaokuaiki-3 (K-3) eruption consisted of two ~VEI-3 events that dispersed lithic clasts and scoria southeastward from the volcano's summit, a direction at a high angle to prevailing northeast trade winds. A 110-site sampling grid extending over ~65 km² southeast of the summit shows that dense, 12-cm blocks fell 8-10 km from the interpreted summit vent area, and 2-4 cm lithic lapilli reached the south coast of the island, 17 km distant. These long-distance dispersals, far beyond ballistic range, are evidence for the energy of the K-3 eruptions.

Southeastern tephra dispersal implies involvement of jet-stream winds, currently between 4 and 17 km altitude and generally traveling at 20-50 m/s toward the east and southeast; we assume the jet stream had a similar velocity profile and orientation during K-3 time. Both K-3 events were sufficiently energetic to carry the wide variety of K-3 clasts to (or near) the top of the jet stream, where their rise and fall were deflected toward the southeast. The energy of the K-3 eruptions and their modest ~VEI-3 volumes suggest that jets of CO₂ and/or steam, the two most abundant gases currently released from the volcano's summit, were the eruption drivers.

Lithic clasts from conduit-wall reaming and rock-fall talus sheets were erupted during both eruptions. FTIR spectroscopy shows K-3 scorias were derived from a magma body within a kilometer of the surface; we suggest this body was accidentally intersected by the K-3 conduit and supplied scorias to both eruptions. Quench-rind remnants on many scorias are evidence that fragmentation was followed by vesiculation. We interpret K-3 scorias were eruption "passengers" and were entrained passively in the erupting jets. A notable finding is that the second of the two K-3 scoria deposits contains inverted, cm-scale compositional zoning over an area of ~60 km², implying gradual top-down tapping of a crystallizing magma body and orderly tephra dispersal.

Erin Fitch, Sarah Fagents

Submission 990

Ash Formation Mechanisms Associated with Lava–Water Explosions: Implications for Estimating Explosion Energy

During phreatomagmatic eruptions, the energetics of explosive magma–water interactions is difficult to constrain due to the competing effects of juvenile degassing-induced fragmentation. However, during explosive melt–water experiments and natural lava–water explosions only external water drives explosive activity. Experiments indicate that the high surface-area-to-volume ratio of ash-sized grains enables heat transfer rates rapid enough to cause explosive detonation. Based these experiments, workers have derived a quantitative empirical relationship between the mass of ash-sized ejecta and explosion energy, and have applied this relationship to phreatomagmatic eruptions in order to estimate magma–water explosion energy. However, we have found that larger lava–water explosion ejecta derived from molten spatter display fragmented surfaces generated during transport, including fine-scale abrasion, which may result in the production of ash-sized grains. Therefore, secondary fragmentation may result in over-estimations of the mass of ash-sized grains, and therefore explosion energy, in natural systems. Previous work on lava–water explosions has found that ash-sized grains with a glassy groundmass can form at the interaction interface between lava and water, and these grains may efficiently contribute heat at a fine scale to drive lava–water explosions. Therefore, we investigated the crystal textures of ash-sized grains and found that roughly 50–90% have glassy textures, and must have quenched rapidly or fragmented from a source that quenched rapidly. Additionally, we performed laboratory experiments to simulate abrasion of medium lapilli-sized grains and investigated the crystal textures of the grains produced. We found that abrasion produces an amount of glassy ash-sized grains similar to that present in the original sample. Although these results help us constrain the mass of ash that may have been energetically significant, abrasion of the glassy rind of larger grains may also contribute to the mass of ash-sized grains deposited. This work highlights potential issues that limit the scaling of empirical relationships from laboratory experiments to natural systems, due to uncertainties of ash-sized grain origin. However, additional analysis will allow us to further constrain parameters as inputs for energy modelling and to apply these results to the study of explosive magma–water interactions.

Rebecca Fitzgerald, Ben Kennedy, Thomas Wilson, Graham Leonard, Amy Jeffrey, Ame McSporran

Submission 739

Ballistic hazard and vulnerability quantification using a pneumatic cannon

With many people living close to or on volcanoes and a growing volcano tourism industry, better understanding and quantification of ballistic hazard and risk is needed. Mapping the ballistic particles ejected from explosive eruptions is a key method in defining ballistic hazard zones. Yet this is often problematic as they do not always remain where they originally landed, bouncing or rolling downhill, burying themselves or shattering on impact. This makes it difficult to assess the true distribution (travel distance and density of impacts) and size of particles ejected. However, they usually leave behind an impact crater, allowing impact location to be recorded. Craters vary in morphology with the size, shape and energy of the ballistic and the characteristics of the substrate they impact. Craters can therefore reveal information about the ballistic and its subsequent impact (e.g. impact angle, ballistic shape, velocity, substrate, ballistic lithology/density and surface slope). To understand the factors that control crater morphology and what relevant hazard information can be observed from craters, we performed empirical experimental testing using a pneumatic cannon. Volcanic blocks of varying size and elongation were fired toward varying substrate types and hardness at varying impact angle and velocity. Each test was recorded by multiple cameras. These same experiments also provided data on the hazard footprint produced, specifically by shrapnel from shattering blocks or mobilised substrate debris. This information is important when assessing risk to people, although has rarely been recorded or accounted for in risk assessments. These experiments will improve understanding of ballistic hazard and risk and subsequently improve hazard and risk assessments.

Taya Flaherty, Tim Druitt, Gareth Fabbro, Fidel Costa, Katie Preece, Chad Deering

Submission 766

Timescales of final magma chamber assembly prior to the Minoan eruption of Santorini from Fe-Mg diffusion chronometry in pyroxenes

Understanding the timescales on which large volumes of eruptible magma mobilize below caldera volcanoes prior to eruption is critical to understanding their future behavior. We have used Fe-Mg diffusion chronometry in orthopyroxene (opx) and clinopyroxene (cpx) phenocrysts from the Minoan eruption of Santorini to find timescales of pre-eruptive magma storage and ascent prior to the caldera-forming event. The Minoan eruption occurred in the late 17th century BCE and ejected 30-80 km³ DRE of rhyodacitic magma containing up to 20 wt% of plagioclase, opx (Wo₂-3En₅₂-70Fs₂₈-45), cpx (Wo₄₄En₃₆-41Fs₁₅-24), apatite and Fe-Ti oxides. Fe-Mg diffusion profiles were extracted from zoned pyroxenes by two methods: (1) high-resolution backscattered electron images calibrated for Mg# or (2) electron microprobe. The 1D diffusional gradients were modelled assuming a step-like starting condition, with published diffusion coefficients for each pyroxene and a magmatic temperature ($855 \pm 25^\circ\text{C}$) and $f\text{O}_2$ determined from touching Fe-Ti oxide pairs. We quantitatively explored potential sources of uncertainty in the diffusion chronometry technique such as cut effects and growth zoning.

Observed in both pyroxenes are common occurrences of distinct magnesian cores mantled by less-magnesian, often oscillatory or multiply zoned rims. Our final dataset (quality-controlled via least squares profile fitting) includes a total of 32 opx models and 26 cpx models across core-rim boundaries and within zoned rims. Some profiles, including core-rim and $R_{22} > 0.98$) are found to be

Ashton Flinders

Submission 668

Seismic evidence for a possible deep crustal hot zone beneath Southwest Washington

Crustal pathways connecting deep sources of melt and the active volcanoes they supply are poorly understood. Beneath Mounts St. Helens, Adams, and Rainier these pathways connect subduction-induced ascending melts to shallow magma reservoirs. Modeling predicts that these melts may first be emplaced as a succession of sills into the lower crust, generating deep crustal hot zones. While these zones are increasingly recognized as a primary site for silicic differentiation at a range of volcanic settings globally, imaging them remains challenging. Near Mount Rainier, ascending melt has previously been imaged ~28 km northwest of the volcano, while to the south, the volcano lies on the margin of a broad conductive region in the deep crust. Using 3D full waveform tomography, we reveal an expansive low-velocity zone, which we interpret as a possible hot zone, linking ascending melts and shallow reservoirs. This hot zone may supply evolved magmas to Mounts St. Helens and Adams, and possibly Rainier, and could contain approximately twice the melt volume as the total eruptive products of all three volcanoes combined. Hot zones like this may be the primary reservoirs for arc volcanism, exerting partial control on compositional variations and spatial-segmentation along the entire 1100 km-long Cascades Arc.

Ashton Flinders, David Shelly, David Hill, Phillip Dawson, Yang Shen

Submission 666

Full-Wave Ambient Noise Tomography of the Long Valley Volcanic Region (California)

In the late 1970s, and throughout the 1990s, Long Valley Caldera (California) experienced intense periods of unrest characterized by uplift of the resurgent dome, earthquake swarms, and CO₂ emissions around Mammoth Mountain. While modeling of the uplift and gravity changes support the possibility of new magmatic intrusions beneath the caldera, geologic interpretations conclude that the magmatic system underlying the caldera is moribund. Geophysical studies yield diverse versions of a sizable but poorly resolved low-velocity zone at depth (> 6 km), yet whether this zone is indicative of a significant volume of crystal mush, smaller isolated pockets of partial melt, or magmatic fluids, is inconclusive. The nature of this low-velocity zone, and the state of volcano's magmatic system, carry important implications for the significance of resurgent-dome inflation and the nature of associated hazards. To better characterize this low-velocity zone we present preliminary results from a 3D full-waveform ambient-noise seismic tomography model derived from the past 25 years of vertical component broadband and short-period seismic data. This new study uses fully numerical solutions of the wave equation to account for the complex wave propagation in a heterogeneous, 3D earth model, including wave interaction with topography. The method ensures that wave propagation is modeled accurately in 3D, enabling the full use of seismic records. By using empirical Green's functions, derived from ambient noise and modeled as Rayleigh surface waves, we are able to extend model resolution to depths beyond the limits of previous local earthquake studies. The model encompasses not only the Long Valley Caldera, but the entire Long Valley Volcanic Region, including Mammoth Mountain and the Mono Crater/Inyo Domes volcanic chain.

María Fernanda Flores, Julie Roberge, Arturo Ortiz-Ubilla, Dougal A. Jerram, Roberto Hernández-Zúñiga, Carlos A. Angeles-De la Torre

Submission 692

Understanding Popocatepetl's last plinian eruption: A Volcanological and petrological study of the Pink Pumice

Popocatepetl volcano is located 46 km East of Mexico City in the central part of the Trans-Mexican Volcanic Belt. Since it reawakened in 1994, it has been one of the most monitored volcano in the world. In the past 23,000 yrs, Popocatepetl has had 7 plinian eruptions, the last one producing the Pink Pumice fall deposit, ~1100 years ago. To date, little detailed work on this deposit has been reported and so far no pyroclastic flow deposits have been linked to this eruption. Previous works has provided a general description dividing the eruption into 4 fall events (Pink 0 to 3) separated by surges and characterized by various amount of pumice, dark lithics, and crystals (Pl, Px, Ol and Ox). This work presents a detailed volcanological and petrological study of the Pink Pumice based on 5 outcrops at different distance from the vent. Within this outcrop dataset only two included Pink 1 to 3 events, with no outcrops found to have all 4 events present at the same location. Granulometry data revealed a bimodal distribution of Pink 1 and 2 and a unimodal distribution of Pink 3. It is shown that the pumice and crystal sizes diminish and the amount of lithics decreases as the sections move away from the crater. Pink 1 is recognized by the presence of elongated black volcanic fragments that appeared to have been shaped while still ductile. This indicate that these black fragments are in fact part of the Pink 1 event (instead of coming from old material e.g. conduit wall) and their random orientation in the deposit can be attribute to deformation at the time of magma fragmentation. Such fragments are very rare or absent in Pink 2 and 3. Pink 2 is characterized by crystal-rich pumice (~15%) with the majority of crystals being plagioclase whereas Pink 1 and 3 both have less than 5% crystals which are mainly pyroxene. In all 3 deposits, individual pumices show a two-colored texture (light and dark beige), which is partially distributed but in Pink 3 the colors are mixed in mosaic-like pattern. Further image analysis and compositional data should define whether these colors are due to composition or texture of the glass. Popocatepetl's recent activity has been of relatively low explosivity, making the surrounding population believe that it is harmless and fairly predictable. The truth is that the volcano has had periods of more explosive eruptions, and charactering Popocatepetl's plinian deposits will highlight the explosive potential of this volcano.

Verity Flower, Ralph Kahn

Submission 406

Volcanic plume characterization using space-borne multi-angle imagery.

Volcanic eruptions represent a significant source of atmospheric aerosols and can display local, regional and global effects, impacting earth systems and human populations. The regional-to-global nature of volcanic hazards make satellite observations a valuable resource for observing eruptions. In this work, we exploit the NASA Earth Observing System's Multi-angle Imaging SpectroRadiometer (MISR) to investigate and compare volcanic plumes generated by seven volcanoes in Kamchatka, Russia. MISR multi-angle imaging facilitates the calculation of plume height and dispersion characteristics, in addition to providing some details of microphysical properties of observed plumes. The over 17-year record of MISR, deployed on NASA's Terra satellite, captured over 110 volcanic plumes from these volcanoes. Plumes were observed in visible imagery dispersing up to 400 km in length at a spatial resolution of 1.1 km, facilitating the characterization of injection heights and the downwind development of plume particle microphysical properties. The capabilities of MISR were tested on the Kamchatka region due to multiple active volcanoes (Shiveluch, Kliuchevskoi, Bezymianny, Tolbachik, Kizimen, Karymsky and Zhupanovsky) during the analysis period (2000-2017), displaying both ongoing and intermittent eruptive activity. The retrieval of features generated from multiple volcanoes, facilitated the comparison of multiple plumes with the same source, of plumes emanating from different sources, and plumes produced by varying eruptive characteristics.

Arnau Folch, Alejandro Martí

Submission 332

Solutions on real time for air traffic management (SORT-ATM)

Atmospheric dispersion of hazardous substances is a sporadic (e.g. volcanic eruptions, sandstorms) but important risk influencing many economic markets, as well as society in general. The impact associated to these extremes has been demonstrated worldwide by eruptive events such as those in Europe (2010 Eyjafjallajökull and 2011 Grímsvötn eruptions) and the southern hemisphere (2011 Cordón Caulle and 2015 Calbuco eruptions); all of which attracted global attention and concern. For example, due to the extent of the ash clouds generated by the 2010 Eyjafjallajökull eruption, more than 100,000 flights were cancelled, causing a loss exceeding US\$1.7 billion airline revenues, and more than 10 million stranded passengers. Past events have shed light on two issues related to the provision and use of the atmospheric hazard dispersal information in Air Traffic Management (ATM): information overload of aviation stakeholders during the event and accessibility of the provided information. In addition to disruptions to the ATM and losses from aviation stakeholders, these events can also severely disrupt transportation systems over extremely large areas for hours to days (e.g. ground and marine transportation); cause damage to buildings and their support systems; lead to a widespread loss of power supply, communication equipment and water and wastewater systems. These catastrophic impacts pose a variety of problems for the insurance companies. Losses from insured property and infrastructure first affect primary insurers, who in turn rely on reinsurers to absorb peak risks – low-probability, high-impact events. Despite of the high demand on risk management solutions for the atmospheric dispersion of hazardous substances such as volcanic ash and mineral dust, to date, there are no commercial tools capable to integrate and analyze all the necessary information to provide short-term emergency management for ATM, or long-term planning solutions for the reinsurance (RE) industry. Solutions On Real-Time for Air Traffic Management (SORT-ATM) and REinsurance industry (SORT-RE) is a software product capable to assess the impact of these natural hazards, offering real-time and long-term tailored solutions at the individual end-user level. This new product is expected to lead to: i) a more efficient ATM management and individual airlines' operations management (SORT-ATM) and; ii) a pioneering risk assessment tool to secure resilient and efficient insurance markets (SORT-RE).

Karen Fontijn, Keri McNamara, Amdimichael Zafu, David Pyle, William Hutchison, Gezahegn Yirgu, Tamsin Mather

Submission 514

Contrasting styles of volcanic activity along the Main Ethiopian Rift: Implications for contemporary volcanic hazards

The Main Ethiopian Rift (MER) is the type example of a magma-assisted continental rift. We focus on the central MER (~7-9 °N), which includes regularly spaced silicic caldera complexes and central stratovolcanoes on the rift axis, as well as large fields of small eruptive centres, predominantly scoria cones of basaltic composition. The recent history of volcanism in the central MER is poorly known, and no eruptions have occurred in the living memory of the local population. The only way to assess contemporary volcanic hazards and associated risk is therefore in the first instance based on the volcanic geology. We present a compilation of new field observations and geochemical data on tephra deposits from the main centres of Late Quaternary volcanic activity in the central MER, as well as existing literature data, and discuss the most recent styles of activity at each, with implications for contemporary volcanic hazards.

Most central MER volcanoes host large calderas with associated widespread ignimbrite flow sheets of trachyte and peralkaline rhyolite composition. Several of these caldera-forming events are mid-Pleistocene in age. Our observations show that these systems have displayed highly contrasting eruptive behaviour in their most recent post-caldera stages of activity, despite similar magma compositions and tectonic controls. Post-caldera activity is dominated at most centres by eruptions of peralkaline rhyolitic magmas, which have generated obsidian flows and domes, and pumice cones. The frequency and magnitude of explosive events however varies up to an order of magnitude between individual volcanoes. Some systems suggest a strong dominance of basaltic volcanism in their post-caldera stage, which may be controlled by the tectonic development of different rift segments.

This work indicates that (1) relatively low-cost reconnaissance of the volcanic geology of poorly known volcanoes can yield a wealth of crucial information about potential hazards; (2) seemingly similar volcanoes in a given tectonic context display highly contrasting behaviour, which raises concerns about the use of analogues to inform hazard and risk mitigation policies.

*Daniel Fornari, Patricia Gregg, Michael Perfit, Emma McCully, Megan Lubetkin,
OASIS Science Team*

Submission 694

High resolution mapping using the submersible Alvin and Sentry AUV at the 8° 20'N Seamounts: Morphostructural analysis and volcanic history

High-resolution Sentry AUV-based mapping and in situ sampling using Alvin was recently carried out along the ~160 km-long seamount chain near 8°20'N, west of the East Pacific Rise (EPR) axis and parallel to the northern margin of the Western Siqueiros Fracture Zone. At 8° 20'N, seamount volcanism appears to initiate ~11 km from the EPR axis, on the west flank of the first major abyssal hill. The eastern 60 km of the seamount chain has prominent volcanoes each with southern rift zones impacted by the curvilinear structures associated with the RTI at the western Siqueiros - EPR intersection. The northern rifts are nearly parallel to abyssal hill / EPR axis fabric (~350°). The central section of the chain extends ~40 km – to 105° 27'W, and does not exhibit sweeping rift zone ridges, instead fields of small satellite cones are either aligned along the EPR-parallel 350° strike or randomly distributed north and south of the main edifices. The western portion of the chain consists of a group of ~4 relatively isolated seamounts (i.e., few satellite cones), extending ~40 km along a strike of ~240°, ending in Ivy Seamount at 105° 44'W. The westernmost seamount in the chain, Liona Smt., occurs ~50 km NW (300°) of Ivy and sits ~22 km north of the trend of the main - 8 20'N seamount chain.

Morphological and slope analysis of EM122 multibeam data over the entire span of the 8° 20'N seamount chain includes calculation of seamount basal diameters, height, morphology, presence of craters/calderas (and sizes), plan-view edifice shape characterization, and aspect ratio; all as a functions of distance from the EPR as well as distance from each major edifice center and distance from adjacent abyssal hill faults. Ongoing analysis includes georeferencing and cataloging ~90,000 hi-res. digital images acquired during 15 Alvin dives and conducting quantitative analysis to generate volcanic facies and geological maps of each seamount. Slope analysis and textural analysis of Sentry near-bottom multibeam and sidescan sonar data will be correlated to volcanic morphology and sediment distribution derived from digital still imagery analysis. These data will allow us to assign relative age estimates to features throughout the 8° 20'N seamounts, based on contact relationships with adjacent cones/edifices and faults, at both regional and local scales, and deduce the history of volcanism over the past ~3 MY on the flank of this fast-spreading MOR.

Francesca Forni, Wim Degruyter, Olivier Bachmann, Gianfilippo De Astis, Silvio Mollo

Submission 750

Long-term magmatic evolution at the Campi Flegrei caldera (Southern Italy)

Understanding the mechanisms that lead to the accumulation of large silicic upper-crustal magma bodies, potentially resulting in high volume caldera-forming eruptions, is pivotal for assessing the eruptive potential at active volcanic centers. Campi Flegrei is an excellent example of active and restless volcano, located in one of the most densely populated area on Earth. Over the last 60 ka, Campi Flegrei has gone through two cycles of activity, each of which produced numerous small eruptions and culminated in a cataclysmic caldera-forming eruption. Here we combine the results of a detailed petrological survey conducted on a number of eruptions representative of the geological record of Campi Flegrei with a magma reservoir thermo-mechanical model to understand the past, present and future evolution of the magmatic system. Our data reveal that during the two major eruptions most of the eruptible crystal-poor magma and part of the cumulate crystal-mush were efficiently evacuated from the upper crustal reservoir, leading to a caldera collapse. Subsequently, the magmatic reservoir was replenished by mafic magmas of deeper origin, which evolved through time towards more evolved, colder and volatile-rich compositions and produced relatively frequent, small-volume eruptions. The most recent eruption at Monte Nuovo (1538 AD), characterized by highly differentiated, low temperature and wet magmas akin to those that fed the pre-caldera activity and the initial phases of the caldera-forming eruptions, suggests that a potentially explosive magma reservoir might be currently accumulating underneath Campi Flegrei.

Pablo Forte, Jonathan M. Castro

Submission 300

H₂O evolution in rhyolitic systems: the case of the 2008 Chaitén eruption, Chile

H₂O is one of the key parameters controlling explosivity of volcanic eruptions. Studies performed on several Holocene rhyolite eruptions throughout the Pacific Northwest have elucidated degassing systematics of silicic systems, and generally show that H₂O content of the magma evolves with eruption progress. The 2008 eruption at volcán Chaitén was the first opportunity to scientifically observe a complete rhyolitic eruption cycle and therefore relate volcanic activity to H₂O contents preserved in deposits. The eruption started on 1 May 2008 and lasted for almost 3 years. The first ten days were characterized by explosive eruptions that were followed by lava effusion over a period of several months. Interestingly, a protracted transitional phase between the purely explosive and effusive stages was identified, with the simultaneous emission of tephra and the emplacement of a degassed obsidian lava body.

We sampled deposits formed during each of the three eruptive phases in several field campaigns spanning 2010 to 2016. Our samples comprise: distal Plinian tephra fallout, PDC deposits, an obsidian bomb field, a tephra cone developed around the vent during the hybrid activity and the lava dome. We characterized how H₂O concentrations varied during the eruption by applying Fourier transform infrared spectroscopy (FTIR). We analyzed more than 500 pyroclastic obsidians from time-constrained stratigraphic sections and mapped the H₂O content of the obsidian bomb field. We also evaluated cooling rates using hydrous speciation and textural variations (crystalinity and vesicularity). Preliminary results show a well-defined trend of H₂O depletion from the explosive to the effusive deposits. Bulk H₂O contents range from 2.5 to 0.5 wt.% across the pyroclastic sequence, while values of the lava dome are consistently 20 content values. These water content windows shift with stratigraphic position and demarcate clear H₂O gaps with respect to effusive obsidians. We are currently investigating the meaning of such chemical patterns in a broader set of Chaitén pyroclastic samples.

Marine Foucher, Eric Engel, Katie Bristol, Aleksey Smirnov

Submission 1161

Evolution of large lava flows in rift setting: Paleomagnetic and rock magnetic insights into the Greenstone flow.

One of the world's largest lava flows, the Greenstone flow (GSF), was emplaced at ~1094 Ma as a part of a series of basaltic lava flows (the Portage Lake Volcanics) erupted during the extension phase of the North-American Mid-Continent Rift (Cannon and Nicholson, 2001). The GFS outcrops on the Keweenaw Peninsula and Isle Royale Island in Michigan. Although the extent of GFS on the surface (~5000 km²) is limited in comparison to other large flows (e.g. Columbia River basalt), its aggregated volume has been estimated at ~1650 km³ (Longo, 1984). As a result, lava accumulated in a thick, up to ~500 m layer, taking centuries to millennia to solidify. During this long solidification period, the GSF differentiated into three main units: the upper ophite, pegmatitic center, and ophitic basal zones (Cornwall, 1951).

The GSF represents a rare opportunity to investigate eruption and emplacement mechanism of flood basalts. We have conducted a number of rock-magnetic and paleomagnetic analyses of 114 oriented core samples from 17 sites across the GSF, representing the main lithological units. The angular variation of paleomagnetic directions between different stratigraphic layers within the GSF may provide an insight into the timing of solidification sequence. The magnetic fabric and rock magnetic properties provide information about the crystallization patterns and may facilitate development of a precise model for the GSF formation. Overall, the combination of paleomagnetic and rock magnetic method may prove a useful tool for improving our understanding of crystallization and emplacement of ancient large lava flows.

Nicolas Fournier, Bradley J Scott

Submission 759

Volcanic Alert Bulletins 2.0: integrated volcano communication in New Zealand

For a volcano observatory, effective communication can save lives. Preserving the accuracy of any messaging is therefore absolutely essential. Yet, the explosion of the number and variety of information sources available to all presents significant challenges to observatories and to the wider scientific community. Issues such as fact distortion or perception bias are commonly encountered and can be substantial barriers to the observatories' main mission - providing timely and accurate information about volcanic activity.

Here we present how we overcame such challenges by rethinking the way official information on volcanic activity is provided via Volcanic Alert Bulletins in New Zealand. We also show how creating a range of communication products not only allows effective communication across ever-changing levels of "seriousness" of volcanic activity, but also substantially speed-up communication channels. Finally, we discuss how social media can effectively complement official bulletins and be used to feed specific societal needs and target groups, ultimately leading to a modern, integrated, and comprehensive communication strategy around active volcanoes.

Jodi M. Fox, Jocelyn McPhie, Rebecca J. Carey

Submission 710

Basaltic cryptodomes and daily records of phreatomagmatic eruption – Miocene submarine volcanism at Cape Grim, Tasmania, Australia

Cape Grim in far north western Tasmania, Australia, was a site of submarine intraplate basaltic volcanism during the Cenozoic. The succession extends 10 km along the coast and is exceptionally well preserved and exposed in rock platforms and steep coastal cliffs. The succession is 30-110 m thick and dominated by pillow lava, massive lava and pillow fragment breccia. Field relationships are consistent with effusive submarine volcanism from multiple vents on the seafloor in

The succession includes two facies that are particularly striking and rare worldwide. The first facies is part of the oldest unit in the Cape Grim succession, the Woolnorth Tuff (WT). It is composed almost entirely of devitrified basaltic glass shards and olivine crystal fragments. The facies is at least 25 m thick and consists of multiple (>100), 5-20 cm thick beds. Each bed consists of climbing-ripple cross laminated tan tuff overlain by 1-2 cm of grey tuff. We interpret this facies as a tidally influenced basaltic ash deposit fed by phreatomagmatic explosions at a shallowly submerged or emergent vent. Assuming semi-diurnal tide, each set of 4 beds could represent a single day of accumulation and deposition of the entire facies may have occurred over ~35 days.

The second facies comprises basaltic sills within the WT. The sills are oval in plan view with complexly jointed cores. The outermost margins consist of two layers of columnar joints, the axes of which are sub-horizontal on the sides and progressively fan upwards to a vertical orientation at the top of the sills. The column orientations are consistent with the sills having domed upper surfaces.

Apophyses of basalt extend up into the overlying WT. The apophyses have quenched, glassy margins and are 5-80 cm in diameter. At the contacts between the sills and the WT, beds in the tuff are absent or disrupted and there are abundant faults and clastic dykes. We interpret the basaltic sills to be basaltic cryptodomes that intruded and updomed the WT when the tuff was wet and not fully lithified.

Jodi M. Fox, Rebecca J. Carey, Millard F. Coffin, Sally J. Watson, Paul Olin, Richard Arculus, Erica Spain

Submission 714

McDonald Islands – An example of submarine and subaerial phonolitic volcanism on the Kerguelen Plateau, the southern Indian Ocean.

McDonald Islands, located in the southern Indian Ocean atop the submarine Kerguelen Plateau, were discovered in 1854 ~43 km west of Heard Island. They originally comprised three islands: McDonald Island, Meyer Rock, and Flat Island (Stephenson et al 2005). In 1980, the sole geological expedition to McDonald Islands collected phonolitic rocks (Clarke et al 1983). All previous and subsequent observations have been from passing ships or satellites.

Unwitnessed explosive and effusive eruptions in 1992 and 1997 doubled the area of McDonald Island to 2 km long x 2 km wide, and created an isthmus between Flat Rock and McDonald Island (Stephenson et al 2005). Fumaroles are active on the flanks of McDonald Islands, and ongoing submarine hydrothermal activity is suspected in the surrounding area. In 2016, scientists aboard the RV Investigator conducted the Heard Earth-Ocean-Biosphere Interactions expedition that aimed to identify submarine hydrothermal activity in the Heard and McDonald islands region. We acquired detailed multibeam bathymetry/backscatter and water column acoustic data, together with high-resolution still and video photography, dredged rock dredges, and grab sediment samples, around McDonald Islands.

Mapping revealed that McDonald Islands are central to a field of >70 submarine sea knolls interpreted as submarine volcanoes. Rocks dredged from the sea knolls included vesicular phonolite lavas, phonolite obsidian, and phonolite pillow lava fragments. The sea knolls are circular to ovoid in plan view, ≤ 3 km in diameter and ≤ 120 m high, and rise to 20 to 150 m below the sea surface.

Post-voyage analytical work has included petrography, geochemistry, and $^{40}\text{Ar}/^{39}\text{Ar}$ geochronology. These data, combined with shipboard observations, reveal a complex history for the McDonald Island volcanic field involving submarine and subaerial explosive and effusive eruption of predominantly phonolite in an environment characterised by glaciation, strong ocean currents, and high winds.

Richard Freeman, Chris Gregg, Matt Patrick, Tim Orr

Submission 1196

Continuous Tracking of Lava Effusion Rates with Single Receiver Differential Very Low Frequency (VLF) Monitoring

Determination of real time volcanic eruption rates is one of the great challenges in volcanology, because it would help constrain geophysical models for magma dynamics, conduit geometry and both deep and shallow volcano processes. It would also be of infinite help in assessment of eruption hazards and risk management. A variety of methods are currently used to estimate average effusion rates and while results are in basic agreement, significant discrepancies are common and do not allow measurements at time scales below tens of minutes to hours. Furthermore, measurements are generally made during daylight hours and can only be made intermittently, not continuously. Measurement of effusion rates is facilitated at Kīlauea Volcano, Hawai'i because a significant percentage of basaltic lava frequently travels through a single, master lava tube. We developed a Differential VLF (DVLF; Freeman et al, in review) instrument to continuously monitor the cross-sectional area of lava in a lava tube and estimate the instantaneous effusion rate (IER). The design utilizes two stationary very low frequency (VLF) radio receivers and is designated the Freeman DVLF. One of the VLF receivers, referred to as the on-tube receiver, is located above the lava tube and measures the sum of the primary VLF signal and the secondary VLF signal that is radiated from the molten lava in response to the primary signal. The other receiver (i.e., off-tube), is positioned a short distance from the lava tube and measures the primary signal from the remote transmitter and a relatively small secondary VLF signal emitted from the lava. In normal operation, data from the off-tube receiver is used to remove the primary signal from the signals recorded by the on-tube receiver at the lava tube and isolate the secondary signal. This secondary signal represents and tracks the cross-sectional area of molten lava in the lava tube and, when combined with a velocity measurement or calculation, is a proxy for effusion rate. We describe data from a 14-day test of the Freeman DVLF instrument during which the on-tube receiver became inoperable. However, the off-tube receiver continued to collect data. We use these data to demonstrate that by mathematically filtering the data, variations in the secondary VLF signal are detectable with a single stationary off-tube VLF receiver. We conclude that those variations track volcanic tilt and likely are tracking changes in lava effusion rate.

Peter Frenzen

Submission 212

Land Use and Response Coordination: Lessons from the 2004 Eruption of Mount St. Helens

The onset of renewed volcanic activity in October 2004 ended an 18-year period of quiescence and provided the first real test of emergency response plans that were established following the May 18, 1980 eruption. Close collaboration between US Forest Service land managers, USGS scientists and local sheriff's and response officials was a key ingredient to the success of the emergency response effort. Uncertainty regarding the likelihood of explosive activity, together with logistical challenges associated with 24/7 live media coverage and the thousands of people who gathered at viewpoints and visitor facilities, posed significant challenges to federal, state, and local officials.

The 2004 eruption response was successful, in part, because of forward-looking planning during establishment of the Mount St. Helens National Volcanic Monument. This included post-1980 federal acquisition of private and leased lands and use of hazard maps to locate roads and facilities on ridges above valleys draining the volcano. In 2004, these factors contributed to the timely evacuation of 2,500 visitors and implementation of 5, 8 and 11 km radius volcanic closure zones around the volcano. While not required during the 2004 eruption, monument facilities were also constructed with roofs designed to support the combined weight of projected ash fall and precipitation.

Forward looking land use and facility planning greatly reduced potential hazards and simplified the situation faced by emergency responders during rapidly evolving volcanic events and public responses to the 2004 eruption. Mount St. Helens provides a compelling example of the successful application of multi-agency planning, application of hazard mapping and appropriate placement of tourism development and public infrastructure near a volcano.

Interfacing with the Public: Lessons Learned from 30 Years of Science Messaging at Mount St. Helens

Peter Frenzen

Plenary talk

Interfacing with the public is an important activity that can be accomplished in many ways. Effective communication involves understanding and adapting to the way people relate and respond to technical information. In this presentation I offer a few simple techniques and lessons learned over three decades working with reporters, filmmakers, exhibit designers and park ranger interpreters at Mount St. Helens.

Probably the hardest concept for a scientist to grasp is that shorter is better and less is more. In a world of online video and rapid-click-browsing people have developed incredibly short attention spans, so developing an effective way to capture and hold their attention is critical. Studies show that most exhibit viewers decide if they're interested or walk away after only 12 words. Experience also suggests that science communication is most effective if it's presented in a meaningful context and relatively brief, bite-sized junks. A favorite saying in the development of effective messaging is 'You can include all the detailed graphics and text you want in an exhibit or PowerPoint presentation as long as you don't care if anyone reads it or pays attention.'

Successful science communication is about transforming technical information into meaningful stories that relate to people's personal experience and spark their interest. The choice is ours, we can take the time to develop programs that inspire people and draw them into the exciting world of science discovery and wonders of our dynamic planet . . . or . . .

Valentin Freret-Lorgeril, Franck Donnadieu, Julien Delanoë, Thierry Latchimy, Jean-Paul Vinson, Christophe Caudoux, Frédéric Peyrin, Claude Hervier, Sébastien Valade

Submission 178

Sedimentation waves from weak ash plumes recorded by optical disdrometer and millimeter-wave radar at Stromboli, Italy

Several studies have shown that ash sedimentation rate from ash plumes can be non-homogeneous spatially, including along the plume dispersion axis. For instance, instability features such as ash curtains and ash fingers have been described under sustained volcanic plumes, that may lead to ash deposition rate fluctuations and fine ash sedimentation close to the eruption source. Novel combined observations of ash fallout at Stromboli volcano in 2015 with a new millimeter-wave (95 GHz) Doppler radar and an optical disdrometer highlight that sedimentation rate variations from short-lived weak ash plumes are common during normal Strombolian activity. 96 % of the disdrometer proximal fallout records show ample phases of increased sedimentation rate 20-60 s apart characterized by a higher contribution of coarse ash with bulk concentrations up to 0.12 g.m⁻³. Particle size distributions are in the range 0.20 to 0.80 mm with a modal value at 0.35 ± 0.05 mm consistent with measured settling velocities of 2.4 m.s⁻¹. The high spatio-temporal resolution (12.5 m, 2 s) radar also reveals multiple trends inside the ash fallout interspersed by 30 to 60 s. These sedimentation waves are about 80 m thick, last up to 5 min, and have inferred ash concentrations up to three times higher. Being pulsed or not, volcanic eruptions seem to produce ash plumes whose sedimentation originate from early thermodynamicself-structuration or from atmospheric interactions or both. Sedimentation waves seem to be a feature common to other sustained tephra plumes like fountain-fed plumes of Etna. This finding may challenge interpretations of changes in volcanic deposits in terms of eruptive conditions and evaluation of source term parameters such as the mass eruption rate, and thus significantly impact hazard assessment of large tephra plumes.

Valentin Freret-Lorgeril, Franck Donnadieu, Julia Eychenne, Thierry Latchimy

Submission 247

Physical characterization of ash at Stromboli volcano: Implications on terminal settling velocity

Ash particle terminal settling velocity is an important parameter to measure in order to constrain the internal dynamics and dispersion of volcanic ash plumes and clouds and their relationships with fallout deposits from which eruption conditions are often inferred. Spatio-temporal variations of the settling velocity have implications as regards the mass eruption rate and the particle size distribution during ash plume dispersion. Many studies have empirically highlighted the need to consider form factors such as the sphericity to better constrain ash fall velocity as a function of size. During radar remote sensing measurements of weak volcanic plumes of Stromboli volcano in 2015, an optical disdrometer was used to measure falling ash particle sizes and their settling velocities, and several fallout ash samples were also collected 400 m from the vents and another one 2 km away. Ash particles sizes and shapes were characterized using an optical, automatic morpho-grainsizer MORPHOLOGI G3 and density was determined by water pycnometry. We focus here on the physical characterization of ash and on implications for settling velocities.

Manually sieved samples from the summit show sorted and coarse particle size distributions (PSD) ranging between less than 63 μm to at least 2000 μm with modal values between 250-355 μm . All PSD are offset compared to the indicated sieve limits, 26.2 % up to 96.2 % of the distributions being higher than the sieve limits. So we use the diagonal of the upper mesh sizes as the upper sieve limit for particle higher than 63 μm . Morphologically, particles show decreasing average convexity from 0.96 to 0.85 with increasing circle-equivalent diameter, the latter being equal to 0.8 times the particle longest axis in average. Measured particle densities increase from 2645 kg.m^{-3} to 2811 kg.m^{-3} with decreasing particle size. Ash terminal settling velocities were determined using tests in laboratory conditions and using the best empirical model (Ganser, 1993). Our results on ash characterization validate field disdrometer measurements above the instrument detection threshold and the capability for such an instrument to monitor volcanic ash sizes and falling velocities. Finally, complete ash characterization can be used to constrain radar data inversions to estimate the mass loading parameters of the ash plumes.

Holli Frey, Matthew Manon, Katherine Swager

Submission 1074

Accessory minerals and magma chamber storage conditions: constraints from zircon chronology and apatite chemistry in tephra deposits from Dominica, Lesser Antilles

U-Th zircon geochronology, coupled with apatite and matrix glass chemistry, and oxide temperature data suggests numerous distinct magmas erupted that shared a common magmatic plumbing system beneath central Dominica. Thick sequences (up to 200 m) of ignimbrite deposits fill the Roseau Valley and were estimated to have a cumulative volume of 58 km³ (Carey and Sigurdsson, 1980). Based on stratigraphy within the units (Sigurdsson, 1972), ¹⁴C dates, and (U-Th)/He ages of zircons (Howe et al., 2014), it was suggested that the Roseau Ignimbrite was comprised of at least six smaller homogeneous eruptions (24 to 61 ka). Based on similar whole-rock geochemistry (andesite-dacite) and major mineral compositions, it was proposed that the Roseau eruptions shared a common source (Smith et al., 2013; Howe et al., 2014). We extracted zircon, apatite, and oxides from pumice clasts in five distinct pyroclastic flow units within the Roseau Valley. U-Th dating of 67 unpolished zircon rims yielded complex, polymodal distributions from three of the units (~25 to 200 ka), with rare zircons matching (U-Th)/He eruption ages. The other deposits have a unimodal population (35 +/- 6 ka) and a bi-modal distribution (6 +/- 6 ka and ~100-200 ka). Matrix glasses from the pumice clasts showed distinctive chemistry (i.e. FeO, CaO). One of these units yielded a Fe-Ti oxide temperature >125°C lower than a comparable age deposit and had much more abundant and larger zircons, likely due to being well below the zircon saturation temperature of 750°C. Textural evaluation of >200 apatites using CL and subsequent analysis by LA ICP-MS further supports the hypothesis that each eruption is a chemically distinct magma batch. All of the apatites feature fine-scale oscillatory zoning and several have detrital cores with variable luminescence. In one of the older deposits, ~30% of the apatites have dark cores, which is correlated to elevated Ce/Lu and Sr/Y values compared to other units. The deposit with the youngest zircons has distinctive apatites with bright rims (~25%), unseen in the older units, and contains the most compositionally homogeneous apatites. Collectively, this study demonstrates that tephra deposits in very close spatial and temporal association must have evolved in isolation prior to eruption. Similar distributions of zircon antecrysts suggest the magmas have a shared deeper history, but the unique apatite and glass compositions reflect more recent magmatic conditions.

Michael Fromm

Submission 1159

On Being Prepared for the Next Big Volcanic Eruption via Syngistic Satellite Remote Sensing

Volcanic eruptions can have a global impact on weather and climate in addition to local effects/hazards. The young volcanic plume is, by its nature, extreme in abundance, concentration, and complexity of composition. The state-of-the-science regarding volcanic-plume remote sensing is critically flawed; measurement systems are generally not geared for the extremes. Each legacy satellite-based measurement technique has a significant weakness in the face of extreme plumes or clouds—and each has been misinterpreted in past volcanic cases. Even at present there are systemic misunderstandings of eruption parameters such as injection height, plume composition, and mass. The future is uncertain from a satellite deployment standpoint and eruption-event timing, prompting certain science questions. What are the unique advantages of past, current, and planned satellite-based volcanic-aerosol remote sensing strategies? What are the critical weaknesses of past, current, and planned satellite-based volcanic-aerosol remote sensing strategies? How have past eruption scenarios been mischaracterized? How has that impacted the science status-quo? How can the shortcomings in past measurements/interpretations be mitigated in the future? What are the recommendations for future remote-sensing strategies that will be relied on for rapid, accurate volcanic plume monitoring? This paper will critically address these questions and survey historical, current, and future remote sensing methods applicable to volcanic aerosol plumes. In addition we will identify potential “Achilles heel(s)” of certain aerosol measurement strategies and show how these weaknesses may be transformed into unrealized advantages in the future through a synergistic approach to satellite data analysis.

Maria Furtney, Matt Pritchard, Simon Carn, Susi Ebmeier, Jennifer Jay Hsu, Brendan McCormick

Submission 589

Assessing volcanic unrest from space: a global integration of multi-sensor satellite data

Owing to economic and practical limitations, roughly half of Earth's 1400 sub-aerial volcanoes have no ground monitoring, and few are monitored consistently and extensively. Earth-observing satellite missions provide global, frequent, and unprecedented measurements of volcanic activity which are closing these gaps in coverage. We have created databases of global, satellite-detected unrest for ground deformation (1992-2016), SO₂ emissions (1978-2016), and thermal anomalies (2000-2016) in order to better characterize measurements of volcanic unrest worldwide. Each database has limitations in terms of spatial and temporal resolution, and we are working to improve them. We compare the timing between the onset of unrest for deformation (N=116 episodes), thermal anomalies (N=19286 episodes), and SO₂ emissions (N=74 episodes) to eruption start dates. We analyze these data in two ways: first, without any a posteriori knowledge regarding whether the unrest was eruptive or benign in order to contextualize volcanic unrest within the eruptive process, and second, by considering only pre-eruptive unrest to elucidate the amount of warning time a precursory unrest episode provides. In the first scenario, we find that deformation is more often observed in the pre-eruptive period whereas available databases of thermal anomalies and SO₂ emissions are predominantly observed in the co-eruptive period. In the second scenario, we find that deformation, thermal anomalies, and SO₂ emissions each occur over one year prior to an eruption. We additionally compare our database to the past few decades of eruptions and note that satellites measure unrest at erupting volcanoes at a higher rate than eruptions naturally occur (54% versus 17%). We find that most erupting volcanoes without satellite-detected unrest are associated with low VEI eruptions, and any unrest could be below the detection threshold of the satellites.

Andrea Gabrieli, John N Porter, Robert Wright, Paul G. Lucey

Submission 648

Validation Studies of the Accuracy of Various SO₂ Gas Retrievals in the Thermal InfraRed (8-14 μm)

Detecting and quantifying hazardous sulfur dioxide (SO₂) in volcanic plumes and in the atmosphere is important for predicting volcanic eruptions and public health. Thermal Infrared (8-14 μm) remote sensing measurements of spectral radiance of plumes contain information on the path abundance of SO₂. Reliable inversion algorithms are needed in order to convert plume radiance measurements into SO₂ path-concentrations. Various techniques have been used for this purpose. Gabrieli et al., 2016 and Prata and Bernardo, 2014 employ dual view techniques where radiances or calculated temperature brightness inside the plume are compared with those just outside of the plume. These dual view approaches suffer from several issues. They assume the plume background (adjacent sky) is homogeneous. Furthermore, clouds are often present in the background and these techniques assume clear sky background conditions. This paper introduces a new method to derive SO₂ path-concentrations, which allows for single point SO₂ path-concentration retrievals, suitable for hyperspectral imaging with clear or cloudy background conditions. The SO₂ Amenable Lookup Table Algorithm (SO₂ –ALTA) is based on a lookup table of MODTRAN5 spectral radiance calculations for a variety of plume and atmospheric conditions. Rather than searching an extensive lookup table for each retrieval, the lookup table was used to train a Partial Least Square Regression (PLSR) model. The use of PLSR models provides a fast and efficient way to implement an otherwise time consuming inversion. In this paper, we compare the two dual view techniques and the new single point approach by studying their accuracy for different environmental conditions. In order to validate the algorithms, thermal infrared hyperspectral measurements (8-14 μm) were carried out by measuring sky radiance when looking through gas cells filled with known amounts of SO₂. For cloud free conditions, all three techniques worked well. In cases where background clouds were present, then only SO₂ –ALTA was found to provide good results, but only under certain conditions.

Catherine Gallagher, Thorvaldur Thordarson, Bruce Houghton, Maria Janebo, Zoë Decker, Kevin Burton

Submission 1050

Shallow conduit processes during the 2014–15 Holuhraun and 1783–84 AD Laki flood basalt eruptions, Iceland.

Large Flood Basalt (FB) events induce significant atmospheric perturbations, through the volatiles they release, but are infrequent and thus poorly constrained events. Smaller modern flood lavas are valuable analogues to constrain shallow conduit processes, including degassing, within these larger scale eruptions. This study compares and contrasts eruption dynamics, and the modulating role of shallow conduit processes, in the two most recent flood lava eruptions in Iceland.

The 6 month-long 2014–15 event at Holuhraun was Iceland's largest effusive eruption in the last 231 years, and created a lava flow field of 1.45 ± 0.04 km³. It has yielded, through near continuous on-site monitoring, an un-paralleled dataset for a flood lava eruption and the tephra fall samples collected are linked to direct observation of styles of vent activity.

The 1783–84 AD Laki flood lava eruption produced a 14.7 km³ of lava and 0.4 km³ of tephra, with a significant atmospheric impact. Unlike Holuhraun, activity at Laki propagated along a 27 km-long fissure in 10 eruptive episodes: seven are magmatic and episodes 4 and 6 are phreatomagmatic. Previously unidentified phreatomagmatic activity in episode 10 gives way to magmatic activity in the waning phases of the eruption. Each episode featured a short-lived explosive initial phase followed by longer-lasting lava effusion.

Bulk density/vesicularity analysis and vesicle size distributions of juvenile lapilli constrain the influences of vesiculation on the explosive activity starting each episode and allow comparisons between explosive phases.

Vesicularities at Holuhraun are high, 85% in September, increasing to 90–95% in October. Laki lapilli exhibit somewhat more variable vesicularity, with skewed unimodal and bimodal distributions. Despite calculated rise velocities in the Laki eruption (75–100 cm/s) being an order of magnitude greater than in Holuhraun (5 cm/s), the modal vesicularities are similar, ranging up to 90% irrespective of the nature of eruptive style. Laki vesicle number densities for both phreatomagmatic and magmatic phases are consistent with subplinian to Plinian intensities, and suggest that phreatomagmatic ash was generated by late stage water interaction with a mature and fragmenting magmatic foam at near to atmospheric pressures. This implies that water-magma interactions did not contribute significantly to the mass eruption rates.

Elisabeth Gallant, Charles Connor, Laura Connor, Jacob Richardson, Paul Wetmore

Submission 890

Probabilistic lava flow hazard assessment for the Idaho National Laboratory

We present a probabilistic lava flow hazard assessment for the Idaho National Laboratory (INL) and adjacent municipalities. This is the first study to use computational modelling to quantitatively assess lava flow hazards on the eastern Snake River Plain (ESRP), one of the largest North American volcanic provinces active during the Holocene. A new method for clustering single vents into eruptive events based on spatial and temporal relationships was developed for this study to examine the potential biasing of spatial density maps towards eruptions with multiple points of effusion. Conditional probabilities of new vents and events occurring on the ESRP were modelled using the the Sum of Asymptotic Mean Squared Error (SAMSE) optimal pilot bandwidth estimator with a bivariate Gaussian kernel function. Monte Carlo analyses of potential eruption scenarios for both the vent and event datasets were performed using MOLASSES, a cellular automata fluid flow simulator. Annual probabilities of the inundation of INL by a lava flow and the initiation of an eruption within the property boundaries range from 1.1×10^{-4} to 7.6×10^{-5} . These values are greater than those of previous studies and exceed the screening threshold established by the International Atomic Energy Agency by several orders of magnitude.

Gabriel Garcia, Brittany Brand, Joshua Bandfield

Submission 672

Identifying explosive volcanism on Mars through geomorphologic and thermophysical observations

Accurately identifying the products of explosive volcanism on Mars is critical for unraveling the evolution of the martian crust and interior. Recent work using high-resolution datasets suggest explosive processes may have dominated over effusive activity in early martian history. However, distinguishing the products of explosive volcanism from non-volcanic sediments remains challenging since both are similar in thermophysical and geomorphologic datasets.

Apollinaris Mons (APM) is one of the best-known candidates for an explosive volcano on Mars. This study seeks to identify geomorphologic and thermophysical characteristics of possible explosive volcanic deposits on APM using visible and thermal infrared imaging datasets. These geomorphic and thermophysical characteristics are compared to terrestrial analogs within volcanic settings to more accurately identify evidence for explosive volcanism on Mars.

Thermal inertia values throughout the region are low ($\sim 90 \text{ J}\cdot\text{m}^{-2}\cdot\text{K}^{-1}\cdot\text{s}^{-1/2}$) consistent with fine particulate and weakly indurated material at the surface. The most important findings thus far include planar bedding, cross-bedding, and breccia deposits within exposed crater walls along the debris fan, and within the caldera. Breccia deposits are also present along a valley wall on the southwestern flank, where boulders grade from coarser to finer with distance from source.

Planar bedding could be consistent with fall deposits, or discrete lateral flow events. Cross-bedding is consistent with traction transport in dilute mass flows, such as dilute pyroclastic density currents. However, such cross-bedding could also be formed due to truncation of earlier deposits by later erosive flows. Breccias also form during mass flows, such as concentrated pyroclastic currents, debris avalanches or debris flows. Gradation of blocks down slope is further evidence for lateral transport since heavier blocks are dropped out of the flow at more proximal regions due to decreasing carrying capacity with distance from source.

Our evidence for extensive friable deposits, combined with consistently low thermal inertia, further supports an explosive volcanic history for APM. We see no evidence for effusive activity, although we recognize that we cannot access the entire volcanic history. Therefore, we suggest that features such as bedded deposits, cross-bedding and breccias may be used to help identify the deposits of explosive volcanism elsewhere on Mars.

Michael Garcia, Kendra Lynn, Aaron Pietruszka, Jared Marske, J. M. Rhodes

Submission 450

Using the Jon Davidson Approach for Deciphering Magmatic Processes during the Ongoing Eruption of Kilauea Volcano, Hawaii

Kilauea's 34 year old, voluminous (4+ km³) Puu Oo eruption has been investigated using the Jon Davidson approach: careful field work followed by comprehensive petrologic analysis of rocks. Its lava shows a wide variation in major and trace element concentrations, and Pb, Sr, O and U-series isotope ratios providing unique insights into the dynamic processes during a single magmatic event that result from the interplay between crustal and mantle processes. Compositional zoning generated by the diffusive re-equilibration within olivine phenocrysts provides insights into magma mixing, storage and transport within the crust. Timescales modeling of Fe-Mg and Ni indicates that Puu Oo olivine crystals can be stored at magmatic temperatures for a few months to years before eruption (e.g., Shea et al. 2015). Whole-rock compositional variation through 2004 involved mixing of two, rift-zone-stored magmas and a new, continually changing mantle-derived magma. The resulting hybrid magma has shown a temporal evolution with progressively lower MgO-normalized CaO, K₂O, Ni concentrations, and Nb/Y and ²⁰⁶Pb/²⁰⁴Pb ratios that were accompanied by an increase in SiO₂ and ⁸⁷Sr/⁸⁶Sr (Marske et al. 2008). These systematic compositional and isotopic variations document rapid changes in the parental magma composition which are unrelated to crustal processes. At least three source components are involved in producing Puu Oo magmas. Three short (20, CaO and Nb/Y) indicating the incorporation of a new source component (or mixture of sources). These changes are superimposed on a long-term decrease in MgO (10-6.5 wt%) despite a factor of two or more variation in eruption rate (e.g., Poland et al. 2012). The ongoing Puu Oo eruption provides a superb natural laboratory for evaluating models for the generation and evolution of basaltic magmas.

Marske et al., 2008, *J. Petrology*, 49, 1297-1318; Poland et al., 2012, *Nat. Geosci.* 5, 295-300; Shea et al. 2015, *Geology*, 43, 935-938.

Thomas Garden, Darren Gravley, Isabelle Chambefort, Chad Deering, Ben Kennedy

Submission 690

Calderas and their volcano-tectonic controls on hydrothermal fluid flow: A case study from Lake City caldera, Colorado, U.S.A.

Silicic caldera volcanoes are often associated with hydrothermal systems economically important for electricity generation and localization of ore deposits. However, the underlying influence that caldera structures have on permeability is not fully understood. In this study, we use field mapping, scanline transects, vein textures, alteration mineralogy, fluid inclusion microthermometry and reflectance spectroscopy to better understand and reconstruct the shallow fossil hydrothermal system associated with the 22.9 Ma Lake City caldera, Colorado, U.S.A. Field mapping reveals previously undocumented complexities along the caldera margin, which is a wider and more polygonal zone than previously thought. The geothermal system in the western half of the caldera was dominantly high-temperature (up to $\sim 300^{\circ}\text{C}$), low salinity (

James Gardner, Fabian Wadsworth, Edward Llewellyn, James Watkins, Jason Coumans

Submission 141

Sintering of Ash Under Conduit Conditions: Experiments and Implications for the Longevity of Tuffisite Fractures

Volcanic eruptions often fluctuate between highly explosive events and less explosive lava effusions. The transition to effusive behavior is thought to result when magmatic gases escape before they can cause the magma to fragment into pumice and ash. One mechanism by which gases can escape is through fracturing of the magma; tuffisite veins – ash-filled fractures – are interpreted to be relict gas-escape pathways. The efficiency of degassing along fractures depends in part on the timescale over which the fractures remain open. Sintering of ash that fills the fracture greatly reduces its permeability. Sintering occurs when viscous droplets that share contacts coalesce, driven by the interfacial tension between the droplets and the ambient fluid in the interstitial pore space. How quickly molten ash particles sinter depends on their viscosity and sizes. Because tuffisites have been shown to seal at vapor pressures >8 MPa, we carried out experiments in which ash-sized particles of natural obsidian were sintered in H₂O fluid at 20–40 MPa. Obsidian particles of known size were inserted into H₂O fluid at temperatures up to 800°C, held for variable time, and then quenched rapidly. The extent of sintering, as measured by porosity reduction, was found to vary with time, temperature, and initial grain size. At 40 MPa, the time taken for porosity to decrease to 3 vol.% is less than 10 minutes at 800°C, but almost one hour at 700°C. Coarser samples take longer to sinter, all else being equal. The viscosity of the droplets depends on temperature and dissolved water content; the ash is initially undersaturated, hence its water content increases during the experiment. We quantify the evolution of the dissolved water content in the ash via a diffusion model, and verify results against measured H₂O in the quenched products. We compare the measured time evolution of porosity during sintering against an existing sintering model, and find excellent agreement when the viscosity of the ash is computed from the spatial integral of the water distribution within them, calculated using the diffusion model. We use the validated sintering model to infer the potential longevity of tuffisite veins and open-system degassing of ascending magma. In addition, the experiments show that trapped vesicles become completely isolated from the outside of the system only after the sintering ash pack reaches low total porosity.

James Gardner, Caroline Nazworth, Mark Helper, Benjamin Andrews

Submission 148

Standing Trees in the Midst of Destruction: Insights into the 18 May 1980 Pyroclastic Density Current

On the morning of 18 May 1980, a laterally directed pyroclastic density current (PDC) was generated when a cryptodome inside Mount St. Helens exploded while the north flank of the volcano avalanched. The dilute, turbulent PDC rapidly expanded outwards, devastating about 600 km² of thick conifer forest. Most witnesses agree that the PDC was 150–300 m thick, hugged the ground, and followed topography. Over much of the area, most large trees were uprooted or broken off near the base (referred to here as the blowdown zone), but at its distal margins trees were scorched but left standing (the scorched zone). Throughout the blowdown zone, there are more than 40 patches, between 0.01 to ~1.4 square kilometers, where groups of trees were left standing. We have analyzed post-eruption digital topography and patch distribution, and constrained flow directions near the patches from toppled trees. More than half of the patches occur within 1020 meters of the closest scorched zone, and most occur where the PDC had reached 94±5% of its runout, regardless of how far it had travelled. Patches as close as 4 to 7 km to the volcano occur at 90–93% of the runout. Despite the strong coincidence of where they occur, there is no correlation of the size of a patch with its position relative to runout. There is also no relationship of patch area with the relative velocity of the PDC, based on satellite measurements of the flowfront movement. The ground on which the patches stand slopes away from the direction that the PDC was locally traveling, with the most common occurring slope in each patch being 25 degrees. The trees are thus standing on topographic leesides, where they were likely protected from the brunt of the flow. In some cases, trees are blown down in same direction both upstream and farther downstream of the leeside, but are chaotically directed just beyond the leeside. Despite being protected, the standing trees were scorched and killed by the PDC, and some accounts suggest that the tops of the standing trees were sheared off by the flow. We envision that the patches occur where the ground-hugging PDC detached from the ground upon reaching an abrupt steepening of the slope downstream. The prevalence of patches near the end of the PDC runout suggests that detachment became easier as the PDC started to become buoyant.

Steph Gates, Ben Kennedy

Submission 717

Modelling ballistic hazard based on partial ballistic deposit fields : exploring limitations and possibilities.

Volcanic ballistics are a major hazard in areas proximal to volcanic eruptions. Assessing the ballistic hazard of active vents with incomplete ballistic deposit field preservation is a challenge faced by volcanologists wishing to provide vent specific hazard assessments. Mt Tongariro, New Zealand is an active composite cone which receives over 100,000 visitors per year on the Tongariro Alpine Crossing hiking trail. This trail passes close to multiple vents which have been active in the last 150 years, many of which have a history of small phreatic eruptions which occur with little, if any, warning. For example in 2012 a phreatic eruption at Upper Te Maari Crater, ~1.5km's distance from the Tongariro Alpine Crossing trail, ejected blocks over 2.3km from the vent with ballistics impacting along ~2.6km of the trail.

Red Crater is an active vent of Tongariro Volcano which has erupted at least 16 times within the last 300 years in Strombolian and phreatic styles. It lies directly adjacent to the Tongariro Alpine Crossing, with the path traversing the crater rim. To date, no vent specific ballistic hazard assessment has been undertaken beyond a generalised summit hazard zone, which was based on literature and other vent studies. Recent 3D modelling of Upper Te Maari Crater's ballistic field, informed by detailed field mapping of deposits and eruption dynamics has a) demonstrated the suitability of 3D modelling to successfully inform vent specific ballistic hazard assessment, and b) emphasised the importance of using previous deposits to inform vent specific eruption parameters within such models. We present detailed field mapping and desktop image analysis following UAV image collection of Red Crater's remnant ballistic field. Using this data we assess the ability of 3D modelling to recreate past ballistic distributions, within the constraints of the ballistic field and with reasonable eruption conditions. The applicability of remote image collection for ballistic hazard mapping is also assessed through comparing ballistic size distribution and spatial density as measured directly versus using UAV image collection and image analysis through ImageJ. This technique has potential to reduce the time requirements of ballistic hazards assessments. This study addresses some of the issues faced by hazard scientists trying to produce meaningful, vent specific ballistic hazard assessments, based on past eruptions with incompletely preserved ballistic fields.

Damien Gaudin, Corrado Cimarelli, Sonja A. Behnke, Valeria Cigala, Harald Edens, Stephen R. McNutt, Cassandra M. Smith, Ronald Thomas

Submission 487

Volcanic lightning vs. plume dynamics: Integration of multi-parametric observations from the explosive activity of Sakurajima Volcano (Japan)

Recent eruptions –and in particular that of Bogoslof Volcano (2016-2017)– have demonstrated the great potential of volcanic lightning for detection and monitoring of ash plumes at remote volcanoes. Variations in lightning characteristics during an eruption imply a relationship between the dynamics of the plume and its electrical structure. However, any such correlation remains poorly constrained to date, preventing the detection of lightning as a quantitative monitoring tool of explosive eruptions.

In order to bridge this gap, during summer 2015, we deployed a multi-parametric set-up at Sakurajima volcano (Japan) to monitor explosive and associated electrical activity. The instrumental set-up included: i) a lightning mapping array (LMA) composed of ten very high frequency (VHF) antennas recording the electromagnetic waves produced by lightning (sample rate of 25 Msps); ii) a visible light high-speed (VL-HS) camera (5000 frames per second, 0.5 m pixel size, 300 m field of view) recording lightning discharges at different stages of the plume evolution; and iii) a thermal infrared (TIR) camera (25 fps, 1.5 m pixel size, 800 m field of view) continuously recording the plume and allowing the estimation of its main source parameters (volume, rise velocity, mass eruption rate, etc.).

The TIR and VL-HS cameras are used jointly to estimate the ash concentration, temperature, velocity and turbulence characteristics of the plume. A statistical analysis of the data shows how the structure of the plume influences the locations of the flashes and their lengths.

LMA and VL-HS data are compared to locate and characterize volcanic lightning discharges in the plume. In particular, the correlation between VL-HS camera and LMA data suggests a direct relationship between flash length and intensity of the electromagnetic signal. At the inception of the explosion, the high-speed camera records discrete small discharges that appear in the LMA data as peaks superimposed on a continuous radio frequency (CRF) signal. At later stages, flashes happen less frequently and increase in length with the growing dimensions of the plume.

This study demonstrates how evolution of the electromagnetic signals –from CRF to small, frequent peaks, to large discharges– could be used to monitor the plume location, as well as to distinguish various phases of plume development (gas-thrust vs buoyant) and its main characteristics.

Maxim Gavrilenko, Michael Krawczynski, Philipp Ruprecht, Wenlu Li

Submission 829

Are melt inclusions a robust tool for understanding H₂O content of deep hydrous arc magmas?

Dissolved in magma, H₂O plays a significant role in generation, evolution, and eruption of arc magmas. Estimating pre-eruptive H₂O content is challenged by near-surface H₂O degassing during ascent and eruption. Currently, the 'gold-standard' for determining pre-eruptive volatile contents in magmas is the study of mineral-hosted glassy melt inclusions (MIs). They act as tiny pressure capsules potentially preserving maximum dissolved water contents, while the matrix melt degasses on ascent and gets modified by mixing and differentiation processes. Despite the widespread use of glassy MIs, it has yet to be tested whether they underlie a systematic maximum limit resulting in potentially biasing the inferred magmatic H₂O budget in subduction zones. Natural glassy MIs have been found to contain no more than ~8-9 wt.% of dissolved H₂O, and the question remains, is this limit representing a natural limit or a preservation limit? Here we explore the limits of mineral hosted glassy MIs as hydrous magma recorders based on an experimental study of quenching water-bearing silicate melts and show that 9 wt.% of dissolved H₂O is a physical limit that quenched melt inclusions cannot exceed, while still quenching to a single-phase glass. Our results demonstrate that the maxima of 8-9 wt.% H₂O from glassy MIs studies is linked to the ability of quenched glass to incorporate H₂O/OH⁻ in its structure, while excess water exsolves as bubbles and/or promotes devitrification through crystallization of quench crystals or hydrous alteration of the glass. Hydrous melts with H₂O >9% will not form glassy MIs. As a result glassy MIs are only faithfully recording magmatic pre-eruptive H₂O contents in the upper-most part of the Earth's crust where H₂O-solubility is below 9 wt.%. They have no sensitivity to estimate volatile budgets neither in deep/primitive arc magmas nor in mid-crustal evolved magmas. Such magmas may contain much larger amounts of water than currently recognized imparting also additional buoyancy on ascent. For dense primitive magmas this may solve a conundrum often found in convergent margins; the fact that such magmas can reach the surface despite a low-density filter in the form of evolved magmas and crust in their path. These results show that we might be drastically underestimating the volatile budgets in subduction zones and they highlight the necessity of using and developing alternative methods for estimating pre-eruptive H₂O contents.

Halldor Geirsson, Nicolas d'Oreye, Adriano Nobile, Benoît Smets, François Kervyn

Submission 1061

Volcano-tectonic deformation in the Kivu Region, Central Africa, observed by continuous GNSS observations of the Kivu Geodetic Network (KivuGNet) and InSAR time series analysis

The Kivu Region in Central Africa is in the western branch of the East African Rift, where the Nubia plate and the Victoria micro-plate are diverging by approximately 2-3 mm/yr. Two closely spaced and frequently active volcanoes, Nyiragongo and Nyamulagira, are located at the plate boundary. Nyamulagira is a volcanic shield volcano in formation, while Nyiragongo is more known for its persistent large lava lake. Since 2009 the KivuGNet (Kivu Geodetic Network), comprised of now 15 continuously operating GNSS stations, has been tasked with monitoring deformation in the area. The subtle gradual plate motion is superimposed by co-eruptive deformation from the 2010 and 2011-2012 eruptions of Nyamulagira, and deformation from the Mw5.8 August 7, 2015 Katana earthquake at the western border of Lake Kivu. Importantly, the GPS data also show an ongoing deformation signal, which is most readily explained by long-term magma accumulation under the volcanic region. We use the GNSS and InSAR time series analysis (MSBAS) of the deformation signals to constrain and compare source parameters of simplistic elastic models for the different time periods. Although not well constrained, most of the time periods indicate the presence of a deep (deeper than approximately 10 km) magmatic source centered approximately under Nyamulagira or to the southeast of Nyamulagira, that inflates between eruptions and deflates during eruptions. Both the 2011-12 co-eruptive and inter-eruptive deformation fields show a horizontal asymmetry which may be modelled as an ellipsoidal-shaped source striking roughly along the Nyamulagira-Nyiragongo "transform" zone. The total volume changes of these deeper parts of the magmatic system are uncertain and highly dependent on the depth of the source, however, given that the inflation and deflation sources are the same, the source has (in 2017) recaptured less than half of the deflation that occurred during the 2011-2012 eruption.

Kimberly Genareau, William Back, Carol Stewart, Shane Cronin

Submission 262

Chemical Impacts of Remobilized Volcanic Deposits on Water Quality: The Role of Mineralogy

Disaggregation of existing volcanic material can occur from days to centuries after an eruption due to landslides, mudflows, avalanches, and entrainment in fluvial systems, but little research has been done on the impacts of mechanically milled volcanic deposits, both explosively and effusively produced, on water quality. Forty samples from seven different volcanoes with variable bulk compositions (ultramafic, 42 wt % SiO₂; mafic, 49 wt% SiO₂; intermediate, 56 wt% SiO₂; and felsic, 73 wt% SiO₂) were collected, milled to produce grain sizes <32 micrometers, and a standard ash leachate protocol was performed. The bulk compositions of the milled samples were determined using a Phillips PW 2400 X-ray fluorescence (XRF) spectrometer and the cation concentrations of water leachates were determined using a Perkin Elmer Optima 3000 DV inductively coupled plasma-optical emission spectrometer (ICP-OES). The leachate solutions were also analyzed by ion chromatography (IC) to obtain anion concentrations. Na shows the highest concentrations in all leachates (200-400 mg/kg), except those derived from ultramafic samples (<25 mg/kg). Ca (30-150 mg/kg) and Mg (13-58 mg/kg) concentrations are highest in leachates derived from mafic and intermediate samples. Si concentrations (30-250 mg/kg) overlap for all leachates, regardless of bulk magma composition. Mafic samples produce the highest concentrations of leachate anions (chloride, sulfate, and nitrate 95-120 mg/kg). These analyses indicate that mineral phases and glass present in different types of volcanic samples are both contributing factors to leachate chemistry, after the loss of the initial adsorbed salts on tephra surfaces. Results of this work pose important implications for hazard assessment following remobilization of deposits in volcanically active regions, as sudden influx of certain elements may be either beneficial or deleterious to the local flora and fauna and may directly impact water supplies for regional populations, agriculture, and livestock.

Aurelie Germa, Christopher Perry, Xavier Quidelleur, Andrew Calvert, Michael A. Clynne, Charles Connor, Laura Connor, Rocco Malservisi

Submission 493

New geochronological constraints of the Lassen segment's regional volcanism

A new set of 18 unspiked K-Ar and $^{40}\text{Ar}/^{39}\text{Ar}$ ages, obtained on groundmass separates, demonstrates that regional mafic eruptions within the Lassen segment are more recent than anticipated, and suggests a potential for future mafic eruptions. Since ~ 3.5 Ma mafic to intermediate calc-alkaline magmas have erupted from hundreds of cinder cones, building lava flows and small shield volcanoes, all spatially scattered, whose locations are consistent with magnetotelluric and gravity data showing mid-crustal anomalies in the back-arc. Most shields were dated at about 2.5 Ma (Clynne and Muffler, 2010) and are commonly dissected by erosion. We obtained younger K-Ar ages of 395 ± 27 and 280 ± 12 ka for lava flows at the summit and base of Crater Mountain shield, respectively, indicating that its eruptive activity overlapped that of the Lassen Volcanic Center (LVC), which has been active from 825 – 0 ka. Volcanic activity within the Caribou Volcanic field (CVF) at the eastern boundary of the Lassen segment was contemporaneous with activity at the LVC (Clynne and Muffler, 2010). We obtained Lower Pleistocene K-Ar ages (1.34 ± 0.02 Ma) on the basaltic andesites of Hay Meadow and Indian Meadow, preceding the activity of the rest of the Caribou sequence, restricted to 425 ka and younger. The Beauty Lake sequence, whose timing was not constrained until this study, erupted between 595 and 245 ka. A new K-Ar age on Red Cinder chain indicates activity in the Middle Pleistocene, an age consistent with the heavily glaciated surface of the chain. Our K-Ar and $^{40}\text{Ar}/^{39}\text{Ar}$ ages indicate that the Bidwell Spring Chain was active between 70 and 50 ka. We dated the basaltic andesite tuya of Turnaround Lake at 13 ± 11 ka, consistent with the timing of the Tuya chain (15 - 18 ka). Additionally, four regional basaltic flows west of LVC, including Inskip Hill, also yielded Upper Pleistocene ages. Finally, the tholeiitic basaltic flow of Highway 44, reversely polarized, yields $^{40}\text{Ar}/^{39}\text{Ar}$ and K-Ar ages consistent with the Pringle Falls magnetic excursion. These results warrant a regional volcanic hazard assessment, not just one focused on the LVC, and additional geochemical studies are required to better constrain petrogenetic processes of the regional volcanism within the Lassen segment.

Adelina Geyer, Alex Marti, Arnau Folch, Santiago Giralt

Submission 428

Antarctic volcanoes: A remote but significant hazard

Ash from Antarctic volcanoes may pose a bigger threat than previously believed. Amongst all volcanoes located in Antarctica, at least nine are known to be active and five of them have reported previous volcanic activity. However, to date, no attention has been paid to the potential consequences of an ash-forming eruption occurring at high southern latitudes. This paper evaluates the significance and impacts from an eventual 1970-like scenario at Deception Island, one of the most active volcanoes in Antarctica. Simulations using the on-line NMMB/BSC-ASH meteorological and atmospheric dispersion model demonstrate that volcanic ash resulting from Antarctic volcanoes and, in particular, those located at lower-latitudes, could potentially encircle the globe even for moderate size eruptions, resulting in significant consequences in the context of global aviation safety. These results recall the need for further research to quantify the possible hazards associated to Antarctic volcanoes.

This research was partially funded by the MINECO grants VOLCLIMA (CGL2015-72629-EXP) and POSVOLDEC(CTM2016-79617-P)(AEI/FEDER).

Emanuele Giacalone, James D.L. White, J. Michael Palin, Marco Brenna

Submission 553

An unusually coarse basaltic lava with extremely coarse segregation structures, Swinburn, Waipiata Volcanic Field, Otago, New Zealand.

The Miocene Waipiata Volcanic Field, South Island, New Zealand, is an eroded Miocene volcanic field (c. 25 – 9 Ma), belonging to the broader Dunedin Volcanic Group. The largest Waipiata volcano is represented by the little-known Swinburn Volcanic Complex, in Central Otago. Here we present new petrographic and geochemical results of an unusually coarse type of lava common at Swinburn and its extremely coarsely crystalline segregation structures. Lava flows at Swinburn are underlain by bedded, bomb-bearing scoriaceous pyroclastic rocks. Highly vesicular basalt at the basal contact and equivalent-aged sediment depositionally overlying it, confirm an effusive origin. Swinburn lava has crystals of augite and olivine that enclose random plagioclase laths. Crystal sizes average 0.5 – 1 mm, with some bigger crystals reaching 2 mm. Centimetric domains crystallised from residual liquid and metre-scale pegmatitic segregation veins have been found at the bottom and at different heights inside the lava flow, respectively. They show the same mineralogy and ophitic texture of their host basalt but are much more coarsely crystalline (crystals 0.5 – 2 cm long). Inside the segregations, plagioclase compositions are more sodic, also olivine and augite crystals have enriched FeO and depleted MgO and CaO compared to host basalt crystals. There is also an enrichment in incompatible elements such as Ba, REE, Zr, Nb, Th and a depletion in compatible ones (e.g. Cr, Co, Sc, Ni). Field and textural observations along with geochemical features of the Swinburn lavas suggest that they had an effusive emplacement. During cooling, within the partially solidified lava, a slighter more evolved and less dense residual liquid moves from the bottom to upward, through the flow. Segregation domains formed by accumulation of the residual melt at different levels inside the flow. A higher water content inside the residual melt and destruction of the majority of crystal nuclei during the ascent, could explain the extremely coarse crystals forming the segregation structures.

Thomas Giachetti, James Gardner, Helge Gonnermann, Sahand Hajimirza

Submission 585

Coalescence of gas bubbles and percolation threshold in rhyolitic melt: insights from decompression experiments

Experiments of homogeneous nucleation, growth, and coalescence of bubbles in rhyolitic melt during decompression provide new constraints on time scales for bubble coalescence and acquisition of a permeability, two processes controlling open-system degassing of magma. Rhyolitic melts were hydrated at 190-250 MPa and 850 °C to water contents of 5.3-6.0 wt% before decompression at rates of 45-150 MPa.s⁻¹. Samples were held at the final pressure for 6-90 s, allowing for different amount of bubble growth and coalescence.

Scanning Electron Microscopic (SEM) images of the twenty-four decompressed glasses were analyzed for bubble size distributions, with isolated bubbles being discriminated from those quenched while coalescing. Samples total porosity varies from 11 to 2.7x10¹⁶ m⁻³. Coalescing porosity is positively correlated with total porosity once the latter reaches approximately 30%, independently of bubble number density. A “burst” in coalescence occurs below an average bubble wall thickness of approximately 2 μm. Time scales show that bubble coalescence in these samples is driven by bubble growth rather than due to gravitational or capillary forces, while Ostwald ripening does not affect sample texture. The rather short length of the experiments does not allow for complete coalescence (i.e., complete bubble relaxation and full retraction of the thin film of glass initially separating the two coalescing bubbles).

A percolation model was used to overcome the fact that two bubbles may appear isolated from one another on the SEM images while actually coalescing in the third dimension. The percolation model allows to retrieve the actual coalescing porosity in 3D and to predict the percolation threshold, which is the porosity at which a sample becomes permeable. Percolation threshold of the decompressed rhyolitic melt is predicted to be about 0.9, slightly higher than what is predicted for natural pyroclasts with similar chemistry (~0.7). This illustrates the importance of bubble deformation in enhancing bubble coalescence and reducing the percolation threshold, a process that is not accounted for in our experiments but that largely occurs while magma ascents during a volcanic eruption.

Salvatore Giammanco, Pietro Bonfanti, Alessandro Bonforte, Francesco Guglielmino

Submission 322

The “Salinelle” mud volcanoes at Mt. Etna (Sicily, Italy) periphery: possible correlation between local ground deformation and gas flux

Some well-known and monitored mud volcanoes fields are located on the south-west foot of Mt. Etna volcano. These mud-volcanoes are locally known as “Salinelle” because of the salty hot water emitted by the vents.

Together with the hot water, many different gases are also emitted in large amounts; they are mostly composed of CO₂ (reaching up to 90 % of total gas) and CH₄ (10-50 % of total, depending on the site).

The source of CO₂ is deep magma (depth > 10 km), whereas methane is from shallow hydrocarbon reservoirs. Geochemical studies have clearly assessed the relationship between the activity of the Salinelle and the dynamics of the deep magmatic system of Mt. Etna.

The activity of the Salinelle volcanoes is continuous, although with highly variable intensity. The morphology of these volcanoes is also highly variable, due to the frequent opening of new vents replacing older ones and the consequent formation of new cones and mud deposits. Depending on the variable gas flux, mud eruptions can become more intense, with sporadic paroxysmal episodes that emit fluids with temperature up to about 50 °C.

The most recent paroxysmal episode occurred between early January and June 2016 at the mud-volcanic field closer to the village of Paternò, with a violent mud eruption from new vents that opened beneath a private house.

Between June 2016 and March 2017, for the first time since routine satellite InSAR monitoring is performed over Mt. Etna, a clear ground deformation has been detected on the whole southern periphery of the volcano. The observed deformation includes the area where the mud volcanoes fields develop and peaked in September 2016.

A new, though less intense, eruption at the Salinelle was then observed since late January 2017 until present. We report on the InSAR data and imagery and on its time series, showing this particular ground deformation, together with the geochemical and geological information about the “Salinelle” mud volcanoes.

The aim is to try to interpret the ongoing dynamics in terms of interplay between local tectonics and over-pressure of magmatic gas, looking for its potential indication on new magma accumulation beneath Mt Etna.

Johanand Gilchrist, Johanand T. Gilchrist and A. Mark Jellinek

Submission 854

Sediment Waves in Analog Experiments Simulating Explosive Eruption Columns

Explosive volcanic eruptions are multiphase jets that inject mixtures of gas, ash and entrained air high into the atmosphere. Analog experiments (Veitch and Woods, 2000; Carazzo and Jellinek, 2012) indicate that these multiphase jets occur in the "Buoyant Plume" (BP), "Total Collapse" (TC) and "Partial Collapse" (PC) regimes depending on source and environmental conditions. Natural eruption columns may transition among these regimes in one episode. The 1912 Novarupta, 1980 Mt. St. Helens and 2015 Calbuco plinian eruptions produced partially collapsing eruption columns during phases with quasi-steady source conditions, emplacing alternating tephra fall and pyroclastic flow deposits near their vents (Hildreth and Fierstein, 2012; Carey and Sigurdsson, 1985; Castruccio et. al, 2015). The deposit architecture suggests a mechanism by which a sustained multiphase jet will collapse while simultaneously feeding an umbrella cloud.

To understand this behavior, we conduct analog laboratory experiments on turbulent sediment laden jets of water injected into stratified saltwater layers. We vary the jet velocity, buoyancy flux and particle concentration at the nozzle and identify a continuous transition between the BP and TC end member regimes marked by an increasing extent of PC. Periodic "Sediment Waves" (SWs), which drag buoyant interstitial fluid to the tank floor, are a key feature of all TC and PC regimes. On deposition of the sediment, entrained fluid is released and rises as a phoenix cloud. PC jets consequently produce multiply layered clouds composed of an umbrella cloud underlain by spreading phoenix clouds due to the action of SWs. The size, velocity and wavelength of SWs increase monotonically as jet source conditions are varied from the BP to the TC regime. The large SWs distinguishing the TC regime produce axisymmetric terraced deposits proximal to the vent. These results suggest an alternative explanation for deposits previously characterized as pyroclastic surge-type. Conversely, BP jets near the PC regime produce small SWs that disperse prior to reaching the tank floor and release entrained buoyant fluid to the umbrella cloud base. These jets produce a deposit with a thickness that decreases monotonically away from the nozzle, consistent with continuous sedimentation.

James Gill, Everton Bongiorno, Takashi Miyazaki, Martin Jutzeler, Cedric Hamelin, Ann-Sophie Jonas, Susan DeBari, Megan Yakavonis

Submission 31

Tuffaceous mud is a volumetrically important volcanoclastic facies of submarine arc volcanism

Unexpectedly, about 2/3 of the 1806 m of rock drilled during IODP Exp 350 on the flank of an Upper Miocene andesitic seamount in the Izu reararc was “tuffaceous mud or mudstone” (versus ash or tuff) that accumulated at carbonate-free sedimentation rates of 6-12 cm/ky for the last 9 m.y. This rate is high even for submarine arcs. Except during Pleistocene glacial periods, tuffaceous muds consist mostly of 10-40 μm dense glass shard elongate bubble walls \pm plag,cpx,hb crystals and bioclasts. Most are dacitic in bulk composition on an anhydrous, carbonate-free basis. They are intercalated with thin discrete ash or tuff beds. The trace element and Sr-Nd-Hf-Pb isotope geochemistry of carbonate-free tuffaceous mud and mudstone indicates that they consist >70% and sometimes >90% of local volcanic materials that range from basalt to rhyolite. Consequently, submarine arc volcanism can produce large quantities of very small, mostly silicic glass shards. The resulting thick tuffaceous mud is an important but infrequently recognized submarine volcanoclastic facies destined to become shale or slate in the geological record while retaining geochemical information about its provenance. Even though the drill site was

Amy Gilmer, R. Stephen J. Sparks, Jon D. Blundy, Alison Rust

Submission 490

A hypabyssal perspective: magmatic processes in the Don Manuel igneous complex and porphyry copper system, central Chile

The Don Manuel igneous complex (DMIC) in the Andean Cordillera of central Chile provides a window into a trans-crustal magmatic system and the igneous processes involved in magmagenesis associated with porphyry copper-style mineralization. The DMIC was emplaced episodically between ca. 4 and 3.6 Ma with intrusions progressing from quartz monzonite through rhyolite and biotite tonalite to intermediate porphyritic and basaltic andesite dikes. The time scale for intrusion of DMIC units is similar to observed episodicity of eruption and degassing events in active arc volcanoes. Mineral chemistry, coupled with thermobarometry, constrains the petrogenesis of the DMIC. Amphibole compositions indicate polybaric differentiation of the magmas, and geochemical signatures are consistent with cryptic amphibole fractionation. The DMIC magmas were wet ($H_2O >> 4\%$), but the parental magmas for these units likely had variable initial water contents. Plagioclase Sr concentrations define two main trends, interpreted to result from variation in the point at which plagioclase saturates during magma differentiation. One trend represents wetter magma in which initial plagioclase crystallization is suppressed, and the other represents less wet magma in which plagioclase crystallizes early. Intermediate porphyry dikes associated with copper mineralization contain diverse crystal cargoes indicating significant mixing of crystals from different parts of the magmatic system. These crystal cargoes represent samples of crystal mush entrained at different depths, as well as crystals originating in different magmas and crystals grown in-situ from hybridized magmas. Mafic enclaves within the biotite tonalite indicate magma mingling and have plagioclase and amphibole compositions similar to that of the basaltic andesite in the Don Manuel system. Sulfur and chlorine contents of apatite in the intrusive units suggest variable degassing and decoupling of volatile components. This decoupling is consistent with mafic magma as the source of sulfur for DMIC copper mineralization. The DMIC provides insight into the processes that influence porphyry-type ore formation, as well as into what is sampled from the trans-crustal mush and subsequently emplaced into the sub-volcanic system, but ultimately not erupted.

Guido Giordano

Submission 520

Volcano Geology and mapping

The complex internal architecture of volcanic successions, both at individual volcano scale and at volcanic province scale, is controlled by the interplay between the evolution over time of the volcanic activity, essentially related to the evolution and structure of the magmatic plumbing system, and both climatic and tectonic factors. Volcanic edifices may be simple (monogenetic or associated with fixed and short-lived point sources) or very complex (e.g. stratovolcanoes or caldera complexes), where polygenetic activity spans over long time periods and feeding systems are both time- and space-variable. Volcano-tectonic and gravitational collapses may not only substantially and instantaneously change the topography of volcanoes but also affect the feeding system by changing the lithostatic load. Erosion and remobilization of volcanic material during inter-eruptive periods and longer quiescent periods build large volcanoclastic aprons that grade into other continental and marine sedimentary environments. In order to represent such complexity, the common lithostratigraphic approach to mapping of volcanic areas may be sided by other stratigraphic tools able to organize the stratigraphic successions based on the hierarchy of unconformities and on the morphology of the volcanic structures. Formal units that can be used to this purpose are the Unconformity Bounded Stratigraphic Units (UBSU) and Lithosomes. UBSU are able to represent objectively the extent and physical expression of unconformities, implicitly related to the extent and duration of the associated geological processes, e.g. an unconformity related to the change of global climate affecting the sea level versus a regional tectonic uplift versus a local caldera collapse. Lithosomes may represent individual edifices at various scales allowing to associate parts of the volcanic successions to specific sources and eruption styles. The experience of the last twenty years of mapping in volcanic areas of the Italian volcanological community has established a sound approach for the representation of volcanic successions, which greatly enhances the role of geological maps as ground reference work for civil protection purposes in active areas and resource assessment in recent or extinct areas.

Guillaume Girard

Submission 424

Complex crystal populations in lava flows erupted in the early stages after caldera collapse at Yellowstone: implications for magma chamber composition and dynamics.

Most rhyolite lava flows in Yellowstone have mineralogy dominated by sanidine-quartz-clinopyroxene±plagioclase with uniform major and trace element crystal compositions that closely follow temporal magma compositional changes, with constant mineral-melt partition coefficients that suggest equilibrium crystallization in the melt. These data argue for crystal formation in isolated magma batches, previously extracted from a larger differentiating reservoir. By contrast, lava flows erupted shortly after two caldera collapse events, the Mesa Falls and Lava Creek eruptions at ~1.3 Ma and 0.64 Ma, deviate from this pattern and exhibit more complex, multimodal crystal morphologies and compositions. In two of such units, the 1.28 Ma Osborne Butte lava, and the ~0.6 Ma East Biscuit Basin lava, euhedral, isolated clinopyroxene and plagioclase with sieve textures coexist with plagioclase-clinopyroxene-oxides glomerocrysts with crystal size 23 to An₄₆ vs An₂₀₋₂₅ in isolated plagioclase. Clinopyroxene in glomerocrysts is En₂₅₋₃₁Fs₃₁₋₄₃Wo₃₄₋₃₈ vs. En₂₁₋₂₃Fs₄₀₋₄₁Wo₃₇₋₃₈ in isolated crystals. Rare earth elements also are more enriched in the isolated clinopyroxene, while a distinct behavior of Eu suggests different crystallization sequences. Clinopyroxene-melt partition coefficient of Eu in glomerocrysts is similar to other MREE while in individually occurring clinopyroxene, Eu has lower concentration and partition coefficient which may indicate a later stage crystallization in presence of feldspar. In the Osborne Butte lava, a third population of >cm-sized, euhedral plagioclase with patchy textures similar to plagioclase in the Mesa Falls tuff has a heterogeneous trace element composition that suggests disequilibrium with melt, and antecrystic origin from the Mesa Falls eruption. These unusual lavas were erupted shortly following caldera formation, thus it is plausible that collapse disturbs the magma reservoir system, enhancing its capability to erupt. While during much of the magma system history, extracted melt is the only material to reach the surface, during these disturbed episodes, some crystallized material (the glomerocrysts) may be carried to the surface, possibly also with crystal-rich remnants of the magma chamber(s) that fed the earlier caldera-forming eruption.

Társilo Girona, Corentin Caudron, Christian Huber

Submission 217

Source of volcanic tremor at openly-degassing volcanoes

Connecting volcano-seismic signals, magma degassing, and subsurface processes is crucial to properly interpret volcanic activity. One of the most enigmatic signals is shallow volcanic tremor, a long-lasting (minutes-to-years) ground vibration that frequently appears during periods of volcanic unrest. In this work, we show that shallow tremor can arise from spontaneous pressure oscillations occurring in gas pockets embedded in the upper part of volcanic conduits; these pressure oscillations result ultimately from the transient porous flow of gases through permeable caps or lava domes. Our model is consistent with geophysical data showing that the seismic source is localized at a fixed region and can explain the characteristics of shallow volcanic tremor, including the typical range of dominant frequencies (~ 0.1 -15 Hz); the distinct amplitude spectra observed (i.e., monochromatic, harmonic, and broadband); the gliding of the spectral peaks when volcanic activity increases; and the variations of seismic amplitude as a system approaches an eruption. The dynamics of subsurface gas pockets provides a consistent explanation for the genetic correlation observed between volcanic degassing and shallow seismicity, as well as a link between tremor and the processes leading to volcanic eruptions. In particular, we find that different eruption mechanisms (e.g., magma ascent vs cap sealing) have distinct footprints in terms of tremor properties, thus opening new perspectives to forecast the type, style, and potential danger of forthcoming eruptions.

Margaret Glasgow

Submission 1289

Upper crustal long period microseismicity at Mount St. Helens during volcanically inactive period

A dense array of 904 continuously recording, short-period geophones deployed in the summer of 2014 within ~15 km of Mount St. Helens is used to investigate seismicity. An initial catalog of 212 shallow earthquake detections and locations was obtained from a continuous reverse-time imaging (RTI) method. From those detections, two distinct types of signals are identified, volcanic-tectonic (VT) and long period (LP) through visual and automated classification methods. Prior to this study, upper crustal LP earthquakes have only been detected at Mount St. Helens during volcanically active periods. Surprisingly, we find an average LP occurrence of 2–3 daily during this experiment. A concern in robust identification of subsurface LP earthquakes is the ability to distinguish them from surface generated signals (e.g., rockfalls). To investigate absolute locations, manual phase picks and a grid search with travel time grids from a 3-D velocity model are used. Most LP earthquakes lack clear S arrivals, which increases location uncertainty relative to VT events. A minority of LP earthquakes have clear enough S arrivals to improve hypocenter estimates. RTI locations for LP events are within error of absolute locations from manual phase picks. Thirteen of the LP signals are used as waveform templates to detect 28 additional LP events. Double-difference relative relocation results in the location of VT and LP earthquakes predominately distributed beneath the eastern edge of the summit crater from 0–4 km below sea level. Their source volumes overlap, suggesting multiple source mechanisms at an interesting depth, just above a tomographically imaged high V_p/V_s body (~5–15 km below sea level) consistent with where most melts from the 1980 eruption last equilibrated. Ongoing and future studies will seek to estimate source mechanisms for the newly identified upper crustal LP earthquakes.

Jonathan Glen, Calvin Chopra, Pattawong Pansodtee, Mircea Teodorescu, Christoph Kern, Peter Kelly, Laura Clor, Brent Ritzinger

Submission 1258

High-precision spatial positioning of rotary wing UAS for volcanic gas measurements

Gas emissions monitoring is a fundamental technique for tracking activity and detecting unrest at volcanoes. In particular, routine characterization of gas emission rates (CO₂, SO₂, H₂S) has proven to be an extremely useful approach for monitoring magmatic and hydrothermal systems. Existing methods allow for accurate emission rates to be determined for volcanoes with relatively large gas plumes, and ground-based approaches (e.g. CO₂ soil efflux surveys, Eddy Covariance) allow for measurements of diffuse hydrothermal (CO₂, H₂S) gas emission rates from soils. However, these existing techniques do not allow for measurements of gas emission rates from smaller vents, such as fumaroles, geysers, and mudpots. This is because manned aircraft typically fly too high and too fast to sample these relatively subtle emissions and because equipment to measure diffuse soil degassing cannot be applied to vents with focused gas emissions. As a result, this class of gas emissions has generally been omitted from gas emission surveys despite the possibility that they may constitute a significant and overlooked component of many systems' degassing budgets.

Small rotary wing UAS present a new opportunity to measure gas emissions from small gas vents using smaller non-commercial aircraft. Although recent efforts have been successful in detecting volcanic gases using small UAS systems, these state-of-the-art systems are unable to accurately measure fumarolic gas emission rates due to the inherent inaccuracy in their GPS guidance systems. We are developing a rotary wing UAS with a gas sensor payload to fly a pre-programmed flight track with a spatial precision of better than 1 meter, that could perform plume contouring flights at small volcanic vents. The improved spatial positioning is achieved with a network of nodes that utilizes ultra-wide band RF localization to map node locations. This system has advantages over other wireless localization systems because of its wide bandwidth (500MHz) and range (100's m) that is suitable for the scale of this application and is not prone to signal interference from other WiFi devices. Such measurements would broadly improve our ability to monitor gas emissions and also help improve our estimates of total gas flux from large hydrothermal systems where current estimates include diffuse degassing from soils, but neglect degassing from active vents. We will present our latest efforts in developing, testing, and deploying this system.

Robert Goldman, Darren Gravley, Eric Grosfils, Patricia Gregg

Submission 345

Reconstructing the paleo-stress field of New Zealand's Akaroa Volcano: Insights from field, petrographic, seismic and numerical methods

A fundamental question in volcanology is predicting the location of the next eruption. On conical edifices, eruptions are commonly depicted as originating from a central vent. However, the summit is often one of many eruptive regions, most of which occur along the volcano's flanks. These peripheral eruptions are fed by magmatic sheet intrusions that may propagate several kilometers from the central vent before breaching the surface. Therefore, flank eruptions increase the area of an active volcano that volcanologists must monitor for signs of unrest. However, we can significantly reduce the spatial uncertainty of eruption forecasts with a firm understanding of the factors governing intrusion formation and propagation. The magnitude and orientation of stresses acting within a volcano control where active intrusions will propagate. Thus, we can learn how the stress state of a growing volcano evolves with time if we analyze the paths of solidified intrusions exposed within an ancient eroded edifice. The present study applies field, petrographic and seismic data of New Zealand's Akaroa volcano to elastic finite element models, built in COMSOL Multiphysics 5.2a, that map the system's paleo-stress field. Dikes exposed along Akaroa's erosional crater rim have predominantly radial orientations, suggesting the existence of a stress barrier along which ascending, radially aligned dikes deflected before emplacement. Simulations of the Akaroa system imply that this barrier sloped downward away from the edifice center; however, thin sections of two dikes reveal plagioclase crystals aligned diagonally upward away from the center, suggesting the dikes were emplaced well below the stress barrier. Models incorporating a downward sloping boundary along the base of the volcano, consistent with seismic data of the underlying Tokama siltstone strata, address this discrepancy by placing the stress barrier roughly 100 m above the elevation of the sampled dikes. This result indicates the importance of accurately defining the shape of the boundary between the base of the volcano and underlying units that predate its construction. Temperature-dependent viscoelastic models of Akaroa, in which mechanically distinct layers of the edifice and underlying substrate are deposited at discrete time steps and subsequently allowed to deform, are expected to further constrain the geometry of its magma plumbing system and provide a foundation for simulating flank eruptions on active volcanoes.

Alejandra Gomez-Ulla, Marie Edmonds, Olgeir Sigmarsson, Maria Jose Huertas, Eumenio Ancochea

Submission 803

Volatile elements in Lanzarote melt inclusions and their mantle source heterogeneity caused by recycling of mafic lithologies

Volatile abundances of oceanic basalts can provide insight into the volatile composition of their mantle source. Olivine-hosted melt inclusions (MI) may constrain degassing and magma differentiation during ascent from the magma source and through the lithosphere before eruption at the surface. Here, we report volatile concentrations (H₂O, CO₂, S, Cl and F) coupled with those of trace elements from olivine-hosted MI from two historical eruptions on Lanzarote, Canary Islands. These MI range in composition from basanites to tholeiites. Both Cl and F concentrations correlate with those of K ($R^2 = 0.9$ and 0.8 , respectively) and other incompatible trace elements, demonstrating the non-volatile and incompatible behavior of Cl and F. Therefore, ratios of Cl and F against other incompatible elements can be used to trace the magma source assuming dominantly pyroxenitic-source melting (Gomez-Ulla et al., 2017). The Cl/K ratio in Lanzarote MI ranges from 0.06 to 0.18, which exceeds the uncontaminated OIB and MORB literature values (between 0.05 and 0.12; e.g. Philippot et al., 1998). The F/Nd of the inclusions varies between 15 and 37 in marked contrast with the canonical mantle value of 21. Highest CO₂ and S concentrations (~4800 and ~4170 ppm respectively) are observed in MI having the highest Cl/K and, surprisingly, the lowest F/Nd. Assuming a fluid-saturated melt, an estimated minimal entrapment pressure for those MI is ~550 MPa. This pressure corresponds to the crust-mantle boundary beneath Lanzarote, strongly suggesting that the compositional variability is indeed a deep signature. These results, therefore, reveal that the variable Cl/K and F/Nd are most likely linked to the magma source composition rather than to incorporation of superficial brine or a potential assimilation product of an altered oceanic crust. Consequently, the mantle beneath the Lanzarote is remarkably heterogeneous in volatile composition, perhaps due to diverse recycled material. We highlight that ratios such Cl/K or F/Nd, as well as the halogen concentrations in the mantle beneath Lanzarote display significant variability, extending to higher values than the 157-322 ppm of Cl proposed by Philippot. This variability may reflect a heterogeneous mantle source influenced by recycling of halogens.

Martha Gabriela Gómez-Vasconcelos, Pilar Villamor, Shane Cronin, Alan Palmer, Jon Procter, Bob Stewart

Submission 1106

Spatio-temporal associations between dike intrusions and fault ruptures in the Tongariro Volcanic Centre, New Zealand: insights from the geological record and static stress analysis.

In the southern Taupo Rift, in the Central North Island of New Zealand, crustal extension is mostly accommodated by normal faulting and occasionally by dike intrusions. Here the Tongariro Volcanic Centre coexists with faults from the Ruapehu and Tongariro grabens. This close coexistence and volcanic vent alignment parallel to the regional faults has always raised the question of their possible interaction. In this study we have explored temporal associations between volcanic eruptions and fault activity in the geological record for different time frames. Many periods of high fault slip-rate seem to coincide with explosive volcanic eruptions. For some periods these coincidences are shown to be unrelated; however, it remains important to evaluate the potential link between them. In order to gain a better understanding if these interactions are causative or coincidental, Coulomb stress transfer models are examined. Eight faults and four dikes were modelled as the main sources of regional stress changes in the Tongariro Volcanic Centre for the last 100 ka. Models integrating geological and modelling results are used to explain time associations and short-term variations in fault slip-rates and volcanic activity. These short-term rifting variations could be influenced by static stress transfer between adjacent faults (within

Angel Gomez-Vazquez, Servando De la Cruz-Reyna, Ana Teresa Mendoza-Rosas

Submission 145

The ongoing process of consecutive lava dome emplacements and destructions at Popocatepetl volcano, Central Mexico

The activity of Popocatepetl over the past 22 years has been characterized by a sequence of dome emplacement and destruction episodes within the crater. A previous lava dome eruption in 1919-1927 had similar features that were amply reported at the time. The current sequence of lava dome emplacements began in March 1996 and continues to the present. With information extracted from different types of aerial photographs and from seismic and other data from the monitoring system operated by CENAPRED, we have estimated the volumes, thicknesses and growth rates of 38 domes emplaced from the onset of the activity in 1996 to February 2015. The total volume issued in that time is $\sim 40.5 \times 10^6$ m³. The loss of material within the crater fragments by explosions is $\sim 27 \times 10^6$ m³. The resulting mass balance of material deposited within the crater is $\sim 13.5 \times 10^6$ m³. The average volume of the 38 domes is $\sim 1 \times 10^6$ m³ with a wide range of variability. The volumes and thicknesses of the domes show a clear exponential distribution. Lava effusion rates during emplacement of the domes (short-term rates) were estimated from the measured volumes and the duration of related seismic signals (tremors, LP's) yielding a mean value ~ 8.3 m³ / sec. The average emission rate (long-term rate) for the total duration of the lava dome eruption process is ~ 0.07 m³ / sec. Analysis of the data indicates that the cyclic lava dome eruption develops as a succession of alternate regimes of high and low rates of dome emplacement, fluctuating around a mean value. This led to a condition of some balance between the rates of accumulation and loss of material within the crater that has kept its volumetric capacity almost constant since 2003. The Popocatepetl magma production rates, even in the "high" regimes are lower than in other volcanoes such as St. Helens or Redoubt. Since 2015, two new growth episodes have been observed in January and December of 2016.

Helge Gonnermann, Céline Fliedner, Thomas Giachetti

Submission 1288

The effect of hysteretic permeability during open-system degassing of erupting magma

When bubbles within ascending magma coalesce and form a permeable network, exsolved magmatic volatiles can flow through the magma, which is no longer a closed system. If such permeable flow allows for the escape of magmatic volatiles from the erupting magma, a process called outgassing, the volume fraction of bubbles and their pressure may be reduced, which may be a necessary requirement for the effusive eruption of silicic magmas. We measured the porosity and permeability of rhyolitic pumices from the Plinian phase of the 1060 CE eruption of Medicine Lake Volcano, CA. We then deformed the samples under combined shear and normal stress at temperatures above the glass transition, and the pumices compacted to a lower porosity. The resultant porosity-permeability relationship is hysteretic. In other words, upon outgassing the magnitude of the change in permeability, with respect to porosity, is substantially smaller than the trend in permeability vs. porosity of the un-deformed samples. This implies that magma can retain a relatively high permeability during outgassing, enabling higher gas loss than would be inferred otherwise. We also measured shear stress and strain rate during sample deformation, in order to estimate the relative viscosity, which is the measured viscosity of the bubbly magma, normalized by the melt viscosity. The functional relation of relative viscosity with respect to Capillary number is non-Newtonian and similar to highly concentrated bubble suspensions in other Newtonian liquids, regardless of sample porosity. Together with suspension viscosity, the hysteretic porosity-permeability relationship was incorporated into a numerical model of eruptive magma ascent, which allows for open-system permeable gas flow, both vertically and radially into conduit walls. We present model results that assess this effect on eruptive dynamics, in particular the potential buildup of gas overpressure, which is thought to result in magma fragmentation.

Robert Gooday, Andrew Kerr, David Brown, Kathryn Goodenough

Submission 485

The Central Arran Igneous Complex: structure and evolution of a Scottish Palaeogene caldera system

The Isle of Arran in the Firth of Clyde, western Scotland, contains one of the onshore 'central complexes' of the British Palaeogene Igneous Province. The Central Arran Igneous Complex (CAIC) is exposed in the middle of the island, and comprises several suites of coarse-grained intrusions and a well-preserved volcanoclastic sequence interpreted as a caldera fill. The intermediate-silicic hybrid intrusions around the north and east of the caldera, as well as the granite preserved in the centre, pre-date the caldera and a basaltic dyking event. A series of geochemically homogeneous granites around the margins of the caldera were intruded into the caldera-fill succession and are not cut by any dykes. U-Pb dating of zircons from the silicic intrusions within the CAIC, as well as some ignimbrites from the volcanoclastic succession, indicate that the whole complex was formed very rapidly between 58.9 – 58.7 Ma.

The volcanoclastic and sedimentary rocks of the caldera-fill (the Arran Volcanic Formation) record a complex history of eruption and caldera subsidence. The lowest preserved unit comprises an extensive blanket of massive lapilli tuffs, which is thought to record a significant highly-explosive caldera-collapse event. This is overlain by a series of conglomerates which we interpret as evidence for collapsing caldera walls. The overlying units are a complex series of lapilli tuffs and crystal-rich lava-like ignimbrites of varying composition, extent, and thickness. The presence of fluvial systems during periods of volcanic quiescence is shown by erosional unconformities, coarse fluvial conglomerates, and localised phreatomagmatic tuffs.

The intrusions of the CAIC are geochemically and isotopically distinct from the North Arran Granite (NAG), a large laccolithic intrusion of a similar age exposed around 3 km to the north. All intrusions within the CAIC (apart from a syn-volcanic dolerite sill) have Pb-Sr-Nd- Hf isotopic signatures consistent with contamination by the crustal units into which they were intruded. The NAG was intruded into a different terrane, across a large regional-scale fault (the Highland Boundary Fault) from the CAIC, and has isotopic values suggesting a different ascent history through the crust. The dolerite sill which intrudes the caldera-fill succession has an isotopic signature resembling a small terrane fragment exposed 75 km to the north west.

Natalia Gorbach, Maxim Portnyagin, Tatiana Filosofova

Submission 448

Amphibole record of the ongoing dome-forming eruption of Young Shiveluch volcano (Kamchatka)

Young Shiveluch is the most productive, highly explosive and hazardous andesitic volcano on the Kamchatka peninsula. The present phase of Shiveluch volcanic activity started in 1964 with an edifice collapse and subsequent strong Plinian eruption. Lava dome have been growing in the 1964 crater since 1980 and producing block-and-ash and more rare pumice flows, lahar and ash falls. Since 2001 five strong explosive eruptions (May 2001 and May 2004, February and September 2005 and in October 2010) accompanied the lava dome growth and produced large 20-25 km long pyroclastic flows. In 2007, 2008, 2009, 2013 and 2016, moderate explosions also occurred and formed small-volume 6 to 12 km long pyroclastic flows.

The most recent erupted products of Young Shiveluch are amphibole-bearing andesites of narrow compositional range of whole rocks ($\text{SiO}_2=60-64$ wt. %) and matrix glasses ($\text{SiO}_2=74-80$ wt. %). The rocks exhibit, however, a large textural heterogeneity and multiple crystal populations. Here we present the results of study focused on the composition of amphibole from andesites of the 1964 Plinian eruption, dome-building eruption with slow (in 1980-81 and 1993-95) and high discharge rates (2001-current time). The goal of the study was to decode a complex zoning of amphibole crystals to reconstruct the most recent evolution of the volcano plumbing system.

The dataset comprises ~1000 amphibole analyzes of high-resolution core-to-rim profiles across crystals with point spacings ranging between 10–15 μm . The amphiboles have variable compositions, ranging from low-Al Mg-hornblende to high-Al pargasitic and magnesiohastingsitic amphiboles on the scale of the entire dataset as well as within single rock samples or even within single crystal. The data were interpreted using petrographic information and geo- and thermobarometric models. The P-T estimates from three different models (Holland, Blundy, 1994; Ridolfi et al., 2010; Putirka, 2016) provide mostly comparable results but show some discrepancies in the case of hybrid rocks. Our data reflect P-T-fO₂ variability in the Young Shiveluch plumbing system and provide insight into mixing and convective processes in shallow magma chamber. This work was supported by the Russian Foundation for Basic Research (grant # 15-05-06640)

References:

- Holland, Blundy, 1994. *Contrib Mineral Petrol*, 116: 433-447;
Ridolfi et al., 2010. *Contrib Mineral Petrol*, 160. P: 45-66.;
Putirka, 2016. *American Mineralogist*, 101 (4):841-858.

Yoshihiko Goto, Jocelyn McPhie

Submission 26

Tectonics, structure and resurgence of the largest Quaternary caldera in Japan: Kutcharo, Hokkaido

Kutcharo is the largest Quaternary caldera in Japan. It is subcircular with a diameter of 20–26 km and formed by repeated violent rhyolitic explosive eruptions since 340 to 35 ka. We have revealed that Kutcharo has a resurgent dome (10–12 km across, 360 m high) that was produced by re-inflation of the underlying magma chamber. The resurgent dome comprises lacustrine deposits and overlying dacite lavas, and is transected by an L-shaped graben 3 km wide. A rhyolite lava flow and eleven rhyolite lava domes occur around the resurgent dome and within the graben. The architecture of Kutcharo caldera closely resembles that of Valles caldera. Geological and geochronological data suggest that the resurgent dome formed by the uplifting of caldera floor between 28 and 23 ka, and subsequent extrusions of rhyolite lava flow/domes. Kutcharo is one of the youngest resurgent calderas in the world. Kutcharo has shown signs of unrest (earthquakes and ground deformation) since AD 1938. Seismic, geodetic, geothermal, and resistivity data all indicate that large-volume molten magma occurs beneath the resurgent dome. Kutcharo is located at the intersection of two regional faults that accommodate the ongoing movement of the Kurile forearc sliver, caused by oblique subduction of the Pacific plate. The structure and activity of the resurgent dome are linked to this tectonic setting. Kutcharo remains a potential for future volcanic eruptions. Our new view of the architecture of the Kutcharo caldera may provide invaluable information for hazard assessment of caldera volcanoes.

Alison Graettinger, Dave McGarvie, Ian Skilling, Armann Hoskuldsson

Submission 195

Growth of a long-lived multi-vent ice-confined basaltic volcano: Austurfjöll, Askja, Iceland

Austurfjöll is the largest basaltic glaciovolcanic massif of Askja volcano and provides excellent exposures of the overlapping deposits of multiple spatially disperse subaqueous fissure eruptions as part of a prolonged ice-confined eruption history. This massif was constructed through a Weichselian (Pleistocene) ice sheet over two major phases and seven eruptive episodes. This history was reconstructed through a detailed study of the stratigraphy, geomorphology, and geochemical characteristics of the massif. Austurfjöll is composed of large pillow lava sheets, numerous (>50) overlapping tindars and only localized emergent deposits, forming a broad stepped construct covering 48 km² that was cut by Holocene calderas. This history of multiple dispersed fissure eruptions of modest volume has strong parallels with Holocene volcanism at Askja, where modest fissure eruptions have occurred in and around the Askja caldera to present. The disperse geometry of the glaciovolcanic construct contrasts with previous descriptions of tuyas and tindars. The earliest eruptive episode involved poorly-exposed subaerial lavas succeeded by six glaciovolcanic episodes involving pillow lava sheets and numerous overlapping tindars produced by fissure eruptions. Evidence of localized subaerial lithofacies associated with subaqueous deposits indicates the growth of some eruptive centers above local water levels, followed by flooding and a return to subaqueous activity. Localized ice-contact facies, paleowater levels, and glacial diamictite indicate the position and thickness of the ice varied during the construction of Austurfjöll massif. The distribution of emergent, ice-contact, and subaqueous facies indicates that eruptive activity occurred in multiple and variable-extent melt-water lakes confined by ice. Lithofacies evidence, including gradational transitions from effusive to explosive deposits, superposition of fragmental facies above coherent facies, and drainage channels suggest that changes in eruptive style were driven largely by external factors such as ice cover, drainage, and the increasing elevation of the massif. This new glaciovolcanic geometry should be considered in the future identification of glaciovolcanic massifs on Earth and on Mars. This uncommon structure raises important questions about the tectonic setting of central Iceland or perhaps the role of other eruptions on the structure of the glaciovolcanic massif.

Alison Graettinger, Greg Valentine

Submission 188

A new approach to phreatomagmatic explosion depth estimation from tephra rings

Phreatomagmatic tephra rings are composed of pyroclastic deposits displaying variations in bed thickness, structure, grain size characteristics and sorting. Recent experiments suggest that these variations can be produced by a single explosion mechanism through changes in the depth and energy release of an explosion and the presence or absence of a crater above the explosion. Fieldwork on two tephra rings in the Hopi Buttes Volcanic Field focusing on these deposit variations evaluated eruption reconstructions from tephra ring deposits in light of evolving conceptual models of phreatomagmatic-dominated eruptions. Facies interpreted to be the product of discrete phreatomagmatic explosions, closely timed phreatomagmatic explosions, and magmatic activity were observed in these two tephra rings and previously published stratigraphic columns from tephra rings in 14 volcanic fields. Massive tuff breccias with jigsaw clasts and basal loading structures overlain by cross-bedded tuffs form distinctive couplets and are commonly preserved in tephra rings. Bed sets composed of repeating layers of massive tuff breccia or cross-bedded tuff were also observed above and below couplets. The massive tuff breccias are interpreted to be the result of the ballistic transport of poorly sorted debris from discrete explosions, called ballistic curtains. The cross-bedded tuffs show evidence of lateral transport in a dilute current and could be formed through the collapse of a dilute eruption column, the expulsion of fines from a collapsing poorly sorted eruption column, and from the segregation of fines from ballistic curtains. The relationships between these facies were used to interpret the relative depth of discrete explosions that formed bed sets within the tephra sequence. These deposits contrast with matrix supported coarse-tail graded tuff breccias with erosive basal contacts and gas escape structures that are interpreted to be the result of more sustained activity, likely multiple closely timed phreatomagmatic explosions. The variable order of deposits reflecting discrete explosions, more sustained activity, and magmatic volatile driven processes in the 18 stratigraphic sections highlights that grain size variations in tephra rings are not strictly related to a systematic evolution of the hydrological conditions in the vent.

Jacques Grangeon, Philippe Lesage

Submission 192

A new, robust, low-cost and well-calibrated infrasound sensor for volcano monitoring

Volcano acoustic signals contain valuable information on shallow magmatic and hydrothermal processes. In some cases, the detection of acoustic waves is the only clear evidence of the occurrence of volcanic explosions. Their study is thus complementary to that of seismic signals. For this reason, acoustic sensors are more and more frequently integrated in volcano monitoring systems as well as in temporary instrumental deployments.

We have developed a low-cost infrasound sensor designed for the detection and analysis of acoustic waves on volcanoes. It is based on a small temperature-compensated micromachined differential pressure transducer. The reference pressure is balanced through a pneumatic high-pass filter the corner frequency of which can be set down to 5 mHz or lower. Its amplitude range is ± 400 Pa and its sensitivity is 10 mV Pa⁻¹, with a noise level of ~ 0.05 Pa RMS. The power consumption is 28 mW (2.3 mA with 12V voltage). Two outputs are available: a low-pass filtered one with corner frequency of 40 Hz and another one with the complete frequency range of the transducer of up to 500 Hz.

The instrumental response of each infrasound sensor is carefully measured using an especially designed calibration system which delivers sinusoidal pressure variations in the frequency range from 1 mHz to more than 100 Hz. The mechanical elements of the sensor are produced by 3D printer and filled by epoxy resin which guarantees high robustness in the aggressive environment of most volcanoes. The sensor dimensions (26x45x80 mm) and weight (130 g) makes it very easy to handle and install.

Darren Gravley, Guilherme Gualda, Chad Deering

Submission 1269

High-resolution mantle-crust feedback demonstrated in a 'quick' ignimbrite flare-up, Taupo Volcanic Zone, New Zealand

Tempos in arc magmatism ('flare-ups' and 'lulls') are thought to occur at such large timescales (>10 Myrs) that it is difficult to find direct geologic evidence for how the mantle and crust are communicating. Magmatic 'flare-up' timescales are much shorter than 'lulls' and represent a disproportionate production of magma (90% of the arc). These flare-ups are related to large-scale changes in the geometry of the converging plates, dramatically increasing mantle melt production. However, constraining how the vertical extent of the crust modulates an increase in mantle production, and whether it translates to a 'volcanic' flare-up can be elusive.

The Taupo Volcanic Zone (TVZ) of New Zealand is the modern manifestation of one of the fastest trench-ward migrating arcs in the world. An increase in spreading at the Pacific-Antarctic ridge at ~8 Ma was matched by a step change in arc migration in the North Island of New Zealand from 4 to 18 mm/yr. In total, the arc has shifted ~150 km to the southeast over this timeframe as the Pacific Plate has been rolling back and steepening. The upper plate response has been an increase in mantle flux and crustal thinning that has culminated in the rifted TVZ arc and its unparalleled rate of silicic volcanism. Notably, >3000 km³ of high silica rhyolite erupted from 7 different calderas (at a rate of 43 km³/kyr) during a 'quick' ignimbrite flare-up from 350 to 280 ka. Magma extraction and crystallisation pressures were calculated using rhyolite-MELTS and depict a vertical mush column from the lower to upper crust. Trace element geochemistry depicts a marked change in magma compositions partway through the flare-up suggesting part of the mush system may have been built over a similar and remarkably short 10 to 100 kyr timescale. The depth of eruptible rhyolite became progressively shallower (>200 MPa to

Patricia Gregg, Daniel Fornari, Michael Trim, Dorsey Wanless, Valentina Romano, Dennis Geist, Steven Shirey, William Ridley, Matthew Smith, Craig Lundstrom, Yan Zhan, Emma McCully, Charelle Trim, Haley Cabaniss, John Albright, Bridgit Boulahanis, Yen Joe

Submission 414

Emplacement of the 8° 20'N Seamount Chain: Preliminary results from the 2016 OASIS Expedition

Understanding how melts are generated and focused hundreds of kilometers through the upper mantle to erupt at the narrow mid-ocean ridge axis is fundamental to determining the processes that form the Earth's crust. Using near-axis seamount as mantle probes provides critical information to constrain the three-dimensional mantle melt region feeding crustal accretion at an adjacent ridge segment. The OASIS (Off-Axis Seamount Investigations at Siqueiros) Expedition is a multidisciplinary investigation to survey and sample the 160 km-long, 8° 20'N Seamount Chain situated ~15 km north of the Western Siqueiros Fracture Zone. The goal of this study is to provide constraints for melt generation and migration in the mantle adjacent to the well-studied 9°N segment of the East Pacific Rise (EPR). In November 2016, the OASIS expedition mapped over 7000 km² of seafloor, collecting 50-m resolution EM122 Multibeam data, SeaSPY marine magnetics data, and a BGM-3 gravimeter data. Multibeam data were used to guide sampling and near-bottom data collection for 15 HOV Alvin dives, 19 dredges, and 12 AUV Sentry dives. The 367 cataloged rock samples (145 from dredges and 222 from Alvin) are primarily basaltic lavas ranging from aphyric to plag- and olivine-phyric, with ample glass. Initial microprobe glass analyses indicate significant geochemical variation along the seamount chain from N-MORB to E-MORB (see Perfit et al., this conference, for more details). Preliminary analysis of the EM122 and AUV Sentry multibeam data indicate that preexisting seafloor fabric heavily influences seamount morphology and structural evolution (see Fornari et al., this conference, for more details). Constraining the timing of seamount formation is critical for linking compositional and structural observations with geodynamic models. As such, gravity-derived elastic plate thicknesses are used to determine approximate age ranges for seamount emplacement. Preliminary results indicate that some seamounts, such as Coral Seamount (105°W, ~ 90 km from the RTI), may have formed near their current location. However, others, such as Ivy Seamount (the most distal seamount located ~175 km from the RTI at 105° 45'W), appear to have had a much thinner elastic plate thickness at the time of formation. Future efforts will systematically compare the timing of loading along the chain and inform geodynamic models of melt migration for this fast-spreading mid-ocean ridge.

Chris Gregg, Ashleigh Reeves, Michael Lindell, Frank Trusdell, Bruce Houghton, Andrew Joyner

Submission 1224

Resident stakeholder perceptions of lava flow hazard diversion strategies and protective measures for infrastructure and commercial and private property on Kīlauea and Mauna Loa volcanoes, Hawai'i

Decisions to interfere with the natural path of lava are constrained by geological, engineering and logistical factors; and legal, environmental and socio-cultural considerations. Lava flows erupted from several volcanoes around the world have threatened people and their property, motivating them to take actions to prevent or slow its advance by diverting the flow direction using channels, berms and explosives or obstructing the lava by quenching with water or armoring. Property to be protected has included government, public, commercial and private property ranging from cities and harbors to personal property.

The earliest known attempt to influence the path of lava occurred in 1669 on Mount Etna, Italy, but more recent diversion experience there occurred in the 1980s-90s. Several eruptions of Kīlauea and Mauna Loa volcanoes, Hawai'i provided abundant experience in 1881, 1935, 1942, 1955, 1960 and repeatedly during the on-going 1983-present eruption of Kīlauea. Additional experience relates to experimental tests and an untested berm on Mauna Loa. In 2014-2015 local residents on Kīlauea constructed berms to protect their property and the local utility authority constructed novel protective structures around electric utility poles.

Decisions to use mitigation strategies may be based on expert scientific opinion, but public opposition has been reported to alone be able to prevent lava diversion. In 2014, public opinions about the use of traditional mitigation strategies (diversion by berms or bombing) to protect commercial and residential areas of Puna were mixed among residents, but there appeared to be no opposition to the new mitigation strategy that protected key areas of the electrical infrastructure and supply of electricity. To help understand prevailing public opinions about this and their acceptance of additional risk to personal property necessary to protect important elements of their community, we are conducting questionnaire surveys among resident householders on Kīlauea and Mauna Loa as part of a multi-university NSF Hazards SEES project. We evaluate crisis experience, hazard zonation, and community bonding, in addition to socio-demographic and cultural factors, with beliefs concerning mitigation, including effectiveness of mitigation strategies for lava flows and other hazards; financial and legal considerations; and requirements for specialized knowledge, skills and cooperation.

Stephanie B. Grocke, Thorvaldur Thordarson, Anja Schmidt, Elisa Carboni, Estelle Bonny, Rob Wright, Ármann Höskuldsson, Ingibjörg Jónsdóttir, Tamsin A. Mather

Submission 579

Integrating the empirical petrologic method, satellite retrievals, and model simulations to evaluate sulfur degassing processes at the 2014-2015 basaltic flood lava eruption at Holuhraun (N-Iceland)

The 2014-2015 basaltic flood lava eruption at Holuhraun, North Iceland was an archetypical Icelandic eruption and the largest by volume in the country for more than 200 years. With a high-resolution, ground-based time-series of magma discharge now in place, the eruption is an ideal event at which to compare petrology-based estimates of volcanic SO₂ with those derived via satellite remote sensing and model simulations. We use the empirical relationship between TiO₂/FeO and initial and residual sulfur (S) contents, established for basaltic melts in the range of 4-8 wt% MgO, to establish pre- and post-eruptive S contents and reconstruct the SO₂ emissions of the 2014-2015 Holuhraun eruption. The average TiO₂/FeO value in melt inclusions (0.156) yields initial and residual S concentrations in the melt of 1422 and 436 ppm, respectively. This is in excellent agreement with published S concentrations measured directly in melt inclusions and matrix glasses (1400 and 425 ppm, respectively). The difference between the initial and the degassed values implies ~70% S degassing upon venting. This value, when applied to the total volume of lava produced (1.2 km³, dense rock equivalent), gives a total mass of SO₂ emitted of 7.6 ± 1.1 Mt (6.4 Mt at the vents, 1.2 Mt by the lava). Integrating petrology-based estimates of SO₂ fluxes (2 for September 2014, we calculate an average daily SO₂ mass burden of 53 ± 8 kt, assuming a SO₂ lifetime of 0.4 days. This value is in good agreement with the published average daily SO₂ mass burdens of 99 ± 49 and 61 ± 18 kt calculated for September 2014 using the Ozone Monitoring Instrument (OMI) and the Infrared Atmospheric Sounding Interferometer (IASI), respectively. Observations show that vigorous lava fountaining, while prevalent during September and into October, diminished steadily during the course of the eruption, and by mid-October activity was best characterized as variably intense bubbling. Hence, it is possible that the efficiency of vent degassing decreased in par with diminishing eruption vigor. For this reason we consider our estimates to be maximum values. Extending the comparison between satellite retrievals, model simulations, and petrologic estimates of volcanic SO₂, for the entire 6-month Holuhraun eruption, will elucidate the processes controlling S degassing behavior during an archetypical basaltic fissure eruption in Iceland.

Carter Grondahl, Zoltan Zajacz

Submission 1278

Magmatic controls on the genesis of the giant Bingham Canyon porphyry Cu-Mo-Au deposit

Bingham Canyon, Utah, is one of the world's largest porphyry Cu-Mo-Au deposits. Previous studies proposed that magma mixing and sulphide saturation were key steps to enhance the fertility of ore-related latitic magmas. We analyzed bulk rocks, minerals, and silicate melt inclusions (SMI) from a co-genetic, ore-contemporaneous volcanic package (~38 Ma). Whole rock trace element signatures (e.g. Be/B, Ba/Th, Th/Nb) preclude shoshonite-latite genesis via mixing of melanephelinite and trachyte or rhyolite. In addition, core to rim compositional profiles of clinopyroxene phenocrysts from latite lavas identified Mg, Cr and Ni-rich cores with trace element signatures near identical to clinopyroxene from shoshonite but dissimilar to those from the melanephelinites. Major and trace element and Sr-Nd isotopic signatures indicate that the ore-related shoshonite-latite series magmas were generated by partial melting of an ancient metasomatized mantle source. The latite and SMI compositions can be reproduced by MELTS modeling assuming 2-step lower and upper crustal fractionation of a primary shoshonite magma with minimal country rock assimilation. In concert with the enrichment in fluid mobile trace elements, high oxygen fugacities (fO_2) on the order of 1-2 log units above the Ni-NiO buffer are prevalent in the magmatic system as evidenced by olivine-spinel oxybarometry, high SO_3 in apatite, and anhydrite saturation. With respect to ore metals and volatiles, the SMI data show that the latites were Cu-rich, with Cu concentrations as high as 300-400 ppm in the silicate melt at about 60 wt. % SiO_2 , which then sharply dropped with further differentiation. The Au and Ag concentrations are also high (1.5-4 ppb and 50-200 ppb, respectively), but show less variation with SiO_2 . The concentration of S closely follows the values predicted for anhydrite saturation, whereas most Cl concentrations fall between 1200 and 3000 ppm. The high Au, Ag, and Cu concentrations at ~60-65 wt. % SiO_2 preclude significant sulphide saturation, consistent with the high fO_2 in the system. The sudden drop in Cu and S in the presence of high Cl, Mo, Ag, and Au in the silicate melt at around 65 wt. % SiO_2 must have been induced by degassing at depth and likely represents the main stage of ore fluid release from the magma. Thus our data show that fluid exsolution during relatively simple magmatic differentiation of oxidized alkaline magmas is capable of producing giant porphyry Cu-Mo-Au deposits.

Gianluca Groppelli, Gerardo Carrasco, Pablo Davila-Harris, Roberto de Franco, Gianluca Norini, Claudia Pellicioli, Claudia Principe, Roberto Sulpizio

Submission 1213

New geological, structural and volcanological data of the Los Humeros Volcanic Complex: implications for reconstruction of the 3D model volcanic structure and geothermal exploration

The Los Humeros Volcanic Complex (LHVC) is an important geothermal target in the Trans-Mexican Volcanic Belt. Understanding the recent geological evolution of the LHVC and its associated volcano-tectonic structures and its influence on the hydrothermal fluids are important goals to get insights into the characteristics of the geothermal resources in the area and to improve the recent structural model proposed by Norini et al. (2015). In the framework of the EU GEMex project we are carrying on a detailed geological survey of some key areas inside the caldera depression to obtain an in-depth knowledge of the recent activity, constrained by archaeomagnetic data. In the same areas we will perform also structural studies to obtain a well stratigraphic constrained volcano-tectonic model for the recent feeding system and caldera resurgence. The LHVC is characterized by a nested caldera, with at least two main collapses: Los Humeros Caldera (460 ka) and Los Potreros Caldera (100 ka). In between there are some important plinian eruptions characterized by thick fallout deposits and lava dome emplacements. Also later on Potreros Caldera, the volcanic activity is characterized by explosive and effusive activity, with a final activity made of widespread basaltic flow fields covering the western floor of the caldera depression. Both caldera collapses appear to be controlled by an active fault system of volcano-tectonic origin NW-SE striking, one of the main geothermal targets, recently controlled by active resurgence of the caldera floor. The resurgence of the caldera floor could be induced by a magmatic intrusion, representing the heat source of the geothermal system and feeding the simultaneous monogenetic basaltic flow fields around the deforming area.

Eric Grosfils, Patrick McGovern, Nicolas Le Corvec, Gerald Galgana, Debra Hurwitz, Shelley Chestler

Submission 39

Revisiting the Mechanics of Radial Dike Swarm Formation: Some Limitations of Past Approaches and an Overview of New Insights Derived from Recent Numerical Models

Complementing extensive documentation of edifice- and regional-scale examples on Earth, numerous radial dike systems have been identified on Mars, Venus and possibly Mercury. Since such systems are typically linked to magma reservoirs and/or larger-scale plume activity—and because dike geometry tends to reflect stress conditions at the time of intrusion—understanding how radial dike systems form provides direct insight into fundamental volcanotectonic processes operating at multiple scales within the solar system. Most quantitative attempts to investigate radial dike system formation have relied upon either analytical equations or 2D plan view numerical models. Recently, however, some key findings upon which our understanding of radial dike emplacement has long rested have been called into question by results obtained using both axisymmetric and fully 3D numerical simulations. For example, rather than analytically determining rupture location as an ellipsoidal magma reservoir inflates and then presuming, if the failure location is near the reservoir midsection, that a radial dike will result, analysis of the full stress field using a numerical model leads one to conclude that laterally propagating sills, not radial dikes, are the intrusion type produced during such an inflation-driven reservoir rupture event. In short it is not easy, mechanically, to produce a radial dike system; this finding is contrary to what is reported in much of the published literature. After extensive numerical examination of reservoir inflation, however, under conditions ranging from a simple halfspace to complex flexural loading, we have identified four scenarios that produce radial dike systems. Two of these scenarios yield dike systems akin to those often associated with shield and stratocone volcanoes on Earth, while the other two are more consistent with the giant radial dike system geometries catalogued on Earth, Venus and Mars. It is encouraging that the insights we have gained thus far are broadly consistent with key observations, but it is important to recognize that the simplicity of the models used to date suggests there is far more to be learned. In this presentation we will (a) illustrate why it is not easy to produce a radial dike system, (b) summarize the four volcanological circumstances we have identified that do allow a radial dike system to form, and (c) discuss current model limitations and potentially fruitful directions for future mechanical analyses.

Legacy of Cenozoic Volcanism in the Pacific Northwest: One of myriad versions.

Anita Grunder

Plenary Talk

The Pacific Northwest boasts an active volcanic arc above a young slab, a nearby ocean ridge, the youngest flood basalt province and extension-related volcanism. The western margin of North America was sculpted through translation and accretion of mainly proximal island-arc terranes stitched to the margin by Mesozoic arc batholiths. Magmatism ceased with shallowing of the slab and the crust thickened eastward. North to south slab foundering created an E-W belt of Eocene, arc-like magmatism including the ~ 50 Ma Clarno Formation and the Challis and Absaroka Volcanics to the east. Delamination, volcanism and orogen collapse moved south as the ~57-49-Ma oceanic Siletzia terrane docked. Subduction moved west of Siletzia at ~40 Ma establishing the Cascades arc. From ~35-17.5 Ma, abundant ignimbrites and mafic to intermediate lavas erupted from broadly distributed vents. Thick volcanoclastic sections formed the John Day Formation with a famous mammalian fossil record.

At 17 Ma the Columbia River Basalt (CRB) began to erupt from northward-younging vents near the edge of the craton. The CRB culminated at 16-15 Ma. Inflated flows travelled > 600 km to the Pacific coast. A halo of silicic calderas increases the thermal footprint of the CRB province. The CRB event may be the initial expression of the track of ENE-younging rhyolite calderas of the Yellowstone hotspot track, or the re-expression of the hotspot (possibly Siletzia) obscured by Cascadia subduction as North America migrated across the plume. Also at ~17 Ma, modern Basin and Range-style extension (B&R) began. The arc shortened through northward propagation of the Mendocino triple junction on the right-lateral San Andreas fault system. Around 8 Ma, slower, increasingly oblique subduction and clockwise rotation of the south Cascades forearc coincided with impingement of B&R on the arc and more abundant basaltic activity between composite volcanoes. More orthogonal subduction and compression in the north Cascades focused volcanism at major centers. Coupled with slab rollback and steepening, the differing tectonic regimes results in geomorphologic, seismic and petrologic segmentation of the arc. Temporal Ba/Nb in the arc indicates persistent mantle fluxing by subduction. Slab-rollback, -steepening, and -edge flow have led to a domain of strong E-W mantle anisotropy associated with westward-younging of rhyolites in the bimodal High Lava Plains east of the arc, at the northern margin of the B&R.

Guilherme Gualda, Darren Gravley, Chad Deering, Mark Ghiorso

Submission 1290

Magma extraction and storage pressures over time in the Taupo Volcanic Zone flare-up: The changing architecture of magmatic systems retrieved using rhyolite-MELTS geobarometry

Silicic magmatic systems are crustal-scale features. We use rhyolite-MELTS geobarometry to rebuild the crustal architecture of magmatic systems by calculating extraction and storage pressures for pumiceous volcanic rocks. We retrieve glimpses of the regions in the crust at which rhyolitic magmas are extracted from crystal-rich residues, and of the locales in which storage and pre-eruptive crystallization take place. We apply our method to decipher the evolving structure of the crust during the 350-280 ka Taupo Volcanic Zone (TVZ) flare-up in New Zealand. We focus on 4 caldera-forming eruptions, totaling ~400 km³ of magma.

We derive pre-eruptive magma storage pressures by applying the rhyolite-MELTS geobarometer to matrix glass compositions determined with a Tescan VEGA3 SEM at Vanderbilt University. Analyzed glass serves as a proxy for melt that equilibrated with quartz and plagioclase. We find that storage pressures decrease over the course of the flare-up, from ~250 MPa for the oldest system (Chimpanzee) to ~75 MPa for the youngest (Ohakuri).

To derive source extraction pressures, we apply the rhyolite-MELTS geobarometer to whole-pumice compositions compiled from the literature. We assume: (1) that extraction from the crystal-rich source is perfect (no crystals present in the extracted magma), and (2) closed-system behavior since extraction (no new crystals lost since extraction). Both assumptions are reasonable for the crystal-poor deposits of the TVZ flare-up. The assemblage in equilibrium with the extracted melt has to be independently constrained. We consider quartz-plagioclase and plagioclase-orthopyroxene sources, consistent with the amphibole-poor nature of the TVZ crust. We find that extraction pressures are deep and span a relatively small range early in the flare-up (~300-350 MPa for Chimpanzee), and they become more widespread with time (150-350 MPa for Ohakuri).

We demonstrate that extraction and storage pressures do not always coincide. While the "Mush Model" is broadly applicable to the TVZ flare-up systems, eruptible magma can be mobilized and completely segregated from the crystal-rich source, being stored at shallower levels in the crust prior to eruption. Repeated input of material and heat gradually conditions the crust and allows segregation over a growing range of pressures with time. Rapid segregation, storage, and eruption of magmas during the flare-up provide a view into the growth and architecture of magmatic systems with time.

Roberto Guardo, Luca De Siena

Submission 1155

Integrating passive seismicity with GIS for a new perspective on volcano imaging and monitoring: the case study of Mt. Etna

The timely estimation of short- and long-term volcanic hazard relies on the existence of detailed 3D geophysical images of volcanic structures. High-resolution seismic models of the absorbing uppermost conduit systems and highly-heterogeneous shallowest volcanic layers, while particularly challenging to obtain, provide important data to locate feasible eruptive centers and forecast flank collapses and lava ascending paths. Here, we model the volcanic structures of Mt. Etna (Sicily, Italy) and its outskirts using the Horizontal to Vertical Spectral Ratio method, generally applied to industrial and engineering settings. The integration of this technique with Web-based Geographic Information System improves precision during the acquisition phase. It also integrates geological and geophysical visualization of 3D surface and subsurface structures in a queryable environment representing their exact three-dimensional geographic position, enhancing interpretation. The results show high-resolution 3D images of the shallowest volcanic and feeding systems, which complement (1) deeper seismic tomography imaging and (2) the results of recent remote sensing imaging. The study recovers a vertical structure that divides the pre-existing volcanic complexes of Ellittico and Cuvigghiuni. This could be interpreted as a transitional phase between the two systems. A comparison with recent remote sensing and geological results, however, shows that the anomaly is related to volcano-tectonic structures active during the last 15 years. We infer that seismic noise measurements from miniaturized instruments, when combined with remote sensing techniques, represent an important resource to monitor volcanoes in unrest, reducing the risk of loss of human lives and instrumentation.

Roberto Guardo, Ariel Uzal, Andres Colubri, Carola Dreidemie

Submission 1152

Integrating spatial earthquake distribution and 3D modelling analysis in a customizable GIS for a new perspective in volcano preliminary imaging: the case study of Mt. Etna

Modeling and visual imaging of the interior of a volcano is a crucial step to the comprehension of its dynamics and to the development of an efficient eruption forecasting system; among these models, high-resolution seismic image modelling yields important data to locate possible lava ascending paths, eruptive centers and forecast flank collapses.

Here, we modelled the lava ascending path and feeding system of Mt. Etna (Sicily, Italy) using the Marching Cubes algorithm (MC) method, usually applied to medical visualization and 3D modelling, combining 30-years spatial earthquakes distribution data within a new customizable Geographic Information System (GIS).

The development of this new volcano oriented-GIS, offers the possibility to analyze, model and visualize geological and geophysical data in an interactive 3D and 4D environment, representing their exact spatial position, and incrementing considerably the possibilities of multiple new interpretations.

The results show 3D high-resolution structures that describe the shape and location of the feeding system. Those results (1) increase the detail of the previous deeper seismic tomography imaging in a span between sea level and 8 km beneath it and (2) confirm the results of recent remote sensing imaging.

This multidisciplinary approach combining geophysical and geological data with 3D graphics analysis integrated with a geographic information system and remote sensing techniques, represents an important new resource to preliminary imaging of volcanoes analysis. It also reduces costs and the risk of loss of equipment and human lives during field trips. We believe that this tool can show new outcomes related to the study of the volcanoes and, due to its clear visual representation, could strongly increase the ability to communicate and understand volcanological phenomena.

Esther Ruth Gudmundsdóttir, Gudrun Larsen, Jón Eiríksson, Ólafur Ingólfsson

Submission 1210

Periodicity in Icelandic volcanism – What do tephra layers tell us?

Volcanism is a major force in shaping the Earth Environment. Understanding volcanic processes is therefore an important goal, which can benefit significantly from a thorough knowledge of past behaviour of volcanoes and the course of volcanic events.

Eruption frequency is high in Iceland and has been estimated to exceed 20 eruptions per century on average during the Holocene. The majority of the eruptions are mafic (~90%) and predominantly explosive (~70%). The dominating explosive volcanism in Iceland allows for the history and behaviour of volcanic provinces to be studied in detail through tephra stratigraphy.

To extend and fill in gaps in the eruption history and investigate behaviour of Icelandic volcanoes, the project presented here aims to unravel the activity of volcanic systems in Iceland as far back as 50.000 years, as expressed by tephra layers from soil, lacustrine and marine archives.

There are strong indications that volcanism in Iceland during the Holocene has been periodic at several timescales with apparent periods of 140, 500, and 4-5000 years. Preliminary results from a high-resolution lake record from east Iceland, soil sections from north and northeast Iceland and marine records from the north Iceland shelf, reveal volcanic periodicity even further back in time. Basaltic tephra layers dominate the records investigated and the vast majority originate from the volcanic systems most active in the Holocene, Grímsvötn, Bárðarbunga and to a lesser extent Katla, Kverkfjöll and Hekla. The 4-5000 year period is prominent in the tephra records, where eruption frequency peaks are observed between 1-2000, 5-7000, 9-10.000 and 12-14.000 years ago. The early Holocene and Late-glacial peaks have not been observed before and suggest that volcanism has been periodic as far back as 15.000 years. The eruption frequency peak between 9-10.000 years ago occurred at the time of a major environmental change associated with deglaciation and rapid isostatic rebound, but the two younger peaks cannot be related to such changes. A more plausible explanation is periodicity in magma supply from the mantle, given the location of the two systems above the centre of the Iceland mantle plume.

Marie-Noelle Guilbaud

Submission 500

Magmatic controls on monogenetic activity in a continental arc: Insights from a geochemical study at the trenchward margin of the Michoacán-Guanajuato Volcanic Field (México)

The Michoacán-Guanajuato Volcanic Field (MGVF) is an atypical vast region of monogenetic activity located in the western-central part of the subduction-related Trans-Mexican Volcanic Belt (TMVB). New petrographic, geochemical, and isotopic (Sr-Nd-Pb-Os) data on recent volcanics and the outcropping Eocene basement at the southern trenchward edge of the MGVF (Jorullo and Tacámbaro areas) are used to constrain the origin and en-route evolution of magmas in this region. Plio-Quaternary rocks (205 (0.4-1.2 wt.%). Mineral textures, compositions, and assemblages when compared with phase equilibria data indicate that, with few exceptions, magmas were initially hot (>1000°C) and hydrous (>2.5 wt.% H₂O) and crystallized at shallow levels. Both medium- and high-alkali rock types have trace element patterns typical of subduction zones, but high-alkali ones show extreme enrichments in incompatible elements that vary linearly with P₂O₅. Sr, Nd, and Pb isotopic ratios correlate with SiO₂ for medium-alkali rocks whereas they vary linearly with La/Sm for high-alkali rocks. Primitive (MgO>8 wt.%) medium- and high-alkali rocks plot on opposite ends of a trend in a Sr vs Nd isotopic plot. Diverse degrees of melting of a heterogeneous veined mantle and cryptic assimilation and fractional crystallization at upper crustal levels can account for the differences between the two rock types. The long duration of the TMVB-related activity in this area (5 Ma) argues against the previous hypothesis that postulates a southward migration of the volcanic front across the MGVF during the last 3 Ma.

Frank Guldstrand, Steffi Burchardt, Erwan Hallot, Olivier Galland

Submission 771

Dynamics of Surface Deformation Induced by Dike and Cone Sheet Emplacement in a Cohesive Coulomb Brittle Crust

The analysis of surface deformation associated with intruding magma has become an established method to study subsurface processes and intrusion architecture. The monitored deformation is commonly modeled using static elastic models. However, the upper crust also deforms as a brittle Coulomb material. To what extent Coulomb failure of the brittle crust affects intrusion-induced surface deformation remains largely unexplored. In this contribution, we present quantitative laboratory modeling results of surface deformation induced by the emplacement of shallow magma intrusions in a cohesive Coulomb material, here dikes and cone sheets. We show that the surface deformation exhibits complex dynamics that reflect the evolution of the magma path and emplacement at depth.

Our laboratory setup uses compacted fine-grained silica flour and a vegetable oil to simulate host rock and magma, respectively. The oil is injected at constant flow rate by a volumetric pump. Each experiment lasts for ~1 min or less ending with oil erupting at the surface. The model topography is monitored through a moiré projection method, projecting a set of moving fringes recorded by a camera, enabling monitoring ever 1.5 s. After eruption, the model intrusion cools down and solidifies for ~45 min, after which it is excavated to verify intrusion geometry. This setup allows us to simulate the emplacement of various intrusion geometries, in this case, either sub-vertical planar dikes or inverted cone sheets in a controlled systematic manner (Galland et al., 2014).

We produced 35 monitored experiments, among which 18 produced cone sheets and 17 produced dikes. We performed a quantitative analysis of the associated surface deformation data set, and reveal the dynamic evolution of surface uplift associated with dikes and cone sheets. The analysis incorporates the dynamics of the maximum uplift, the uplifted area, and uplifted volume, and quantified the asymmetry of the uplifted pattern, and shows that the surface deformation exhibits clearly distinctive, systematic signatures for the two intrusion types: dikes exhibit a two-phase behavior while cone sheets develop gradually. The results are highly relevant in the context of volcano geodesy for comparison, evaluation and development of current geodetic models.

Hendra Gunawan

Submission 604

Volcano Monitoring System, Data Management, and Data Processing Automation for Crisis Response at Sinabung Volcano, Indonesia

A small explosion on 28 August 2011 marked the start of Sinabung Volcano's ongoing, now 7-years-long eruption. This first eruptive phase ended by mid September 2010. After the 2010 eruption, persistent fumarolic emissions continued for almost 3 years. On 15 September 2013, a new eruptive phase began and continues to the present. In second phase Sinabung has exhibited various styles of activity ranging from phreatomagmatic, pyroclastic density current deposits, lava extrusion, and ash explosion. The long duration of eruption posed a constant hazard and also impacted the social and economic conditions of people around the volcano. Responding to this, Center for Volcanology and Geologic Hazard Mitigation (CVGHM) provides volcano alerts, generates hazard maps, and recommends exclusion zones. Throughout the eruption, the activity has been continuously evaluated based on monitoring data, which includes instrumental and visual information. Started with four seismic stations in the early stage of eruption, then with partnership of CVGHM-USGS-USAID Volcano Disaster Assistance Program and the Disaster Prevention Research Institute of Kyoto University, the monitoring system in Sinabung has been expanded to 11 seismographs, 5 cGPS, 2 tiltmeters, 3 EDM lines, SO₂ flux measurements with DOAS, and 2 webcams. Such large numbers instruments have generated an increasing volume of data to archive and process, an efficient and robust method of managing and processing, and that poses significant challenges. Therefore, an efficient and robust method of managing and processing large volume of data is crucial to achieve good quality surveillance and provide accurate and timely mitigation action. For multi parameter data repository, CVGHM monitoring division adapts database archiving system on the basis of WOVodat schema for data archiving. To increase efficiency in deformation and seismic data processing, CVGHM developed INVDEF2WOV (a deformation data processing automation utility in collaboration with ITB) and adopted SEI2WOV (a seismic data processing automation utility developed by PHIVOLCS). The seismic utility has also been implemented in other volcano observatories e.g. Ijen, Guntur etc. Multiparameter monitoring datasets are currently processed, archived, and analysed in a near-realtime. The customized web tools adapted from WOVodat also allow users to interactively visualize earthquake hypocenters in 2D and 3D plot, display various time series monitoring datasets in a synchronized graph plots that also include observed events e.g. ash explosion, pyroclastic flow, and rock falls. The SEI2WOV automation and WOVodat database system served to process and display, in near real time, the recent seismic swarm around Sinabung area followed the Mb5.7 Deli Serdang tectonic earthquake ~20km NE of Sinabung on 16 January 2017. This kind of facility allows CVGHM scientists to evaluate, assess, and disseminate information on the progress of unrest activities around Sinabung.

Jóhann Gunnarsson-Robin, Andri Stefánsson, Shuhei Ono, Sæmundur Ari Halldórsson, Martin Whitehouse

Submission 314

Sulfur chemistry and isotopes in geothermal fluids and crustal minerals in Iceland

The sulfur isotope ratios were measured in geothermal fluids and sulfide minerals within Icelandic geothermal systems to assess the source(s) and reactions of sulfur. The geothermal systems studied had reservoir temperatures of 56-296°C and Cl concentrations of 18-21000 ppm. Dissolved sulfide ($\Sigma\text{S-II}$) and SO_4 concentrations in liquid water were 2S(g) concentrations in the vapor 4.9-2000 ppm. The $\delta^{34}\text{S}$ and $\Delta^{33}\text{S}$ values for different geothermal fluids were highly variable: $\delta^{34}\text{S}_{\Sigma\text{S-II}} = -11.6$ to 10.5‰ ($n=99$), $\Delta^{33}\text{S}_{\Sigma\text{S-II}} = -0.12$ to 0.00‰ ($n=45$), $\delta^{34}\text{S}_{\text{SO}_4} = -1.0$ to 24.9‰ ($n=125$), $\Delta^{33}\text{S}_{\text{SO}_4} = -0.04$ to 0.02‰ ($n=50$), $\delta^{34}\text{S}_{\text{H}_2\text{S(g)}} = -2.6$ to 5.9‰ ($n=112$) and $\Delta^{33}\text{S}_{\text{H}_2\text{S(g)}} = -0.03$ to 0.00‰ ($n=56$). The $\delta^{34}\text{S}$ values for sulfide minerals ranged from -1.93 to 1.68‰ ($n=18$) in the Krafla geothermal system (dilute), and from 3.35 to 19.65‰ ($n=25$) in the Reykjanes geothermal system (saline). The multiple sulfur isotope values of the thermal fluids are interpreted to reflect various sources of sulfur, as well as isotope fractionation occurring within the geothermal systems associated with fluid-rock interaction, boiling, and redox reduction reactions. In low-temperature fluids, the $\delta^{34}\text{S}$ and $\Delta^{33}\text{S}$ values reflect the various sources of sulfur such as leaching from rock sulfur and seawater sulfate. High-temperature fluids are, however, taken to be the result of fluid-rock interaction, $\Sigma\text{S-II}$ oxidation and SO_4 reduction and sulfide and sulfate mineral formation, resulting in a large range of $\delta^{34}\text{S}$ and $\Delta^{33}\text{S}$ values for $\Sigma\text{S-II}$ and SO_4 in the fluids and minerals. This highlights the importance and effects of chemical reactions on the isotope systematics of reactive elements like sulfur, and how these effects need to be quantified to discover the various sources of an element.

Sarah H. De Angelis, Paul A. Wallace, Jackie E. Kendrick, Adrian J. Hornby, Felix W. Von Aulock, Stephen Clesham, Takehiro Hirose, Donald B. Dingwell

Submission 1034

Impact of mineralogy on frictional melting in the conduit: An experimental study of Soufrière Hills Volcano and Volcán de Colima

The eruption of highly viscous magma provides the ideal opportunity for strain localisation and frictional heating as a consequence of slip along shallow conduit margins. Heating during deformation can lead to chemical changes occurring out of thermodynamic equilibrium. Diffusion is central to the understanding of such highly dynamic processes and may exert important rheological controls on slip dynamics. In order to understand melt homogenisation during friction, high-velocity rotary shear experiments were performed under controlled conditions. Three sample sets were used to investigate the mineralogical effects on melting dynamics during slip: amphibole-bearing andesites (Soufrière Hills) and pyroxene-bearing andesites (Volcán de Colima and Santiaguito). For each sample, five experiments were performed, stopping (1) at the onset of melting; (2) after a full melt layer had formed; (3) after 5 m of slip; (4) after 10 m of slip; and (5) after 15 m of slip. Proto-melts were analysed using synchrotron based micro X-ray spectroscopy focusing on concentrations of REE. EPMA was performed on bulk glass, bulk crystals, proto-melt and remnant proto-melt crystals to quantify the degree and timescales of chemical homogenisation. Melt onset shows the greatest degree of heterogeneity, representing non-mixed patches of melt. However, with increasing slip distance the melt begins to homogenise towards the bulk composition. Element standard deviations decrease with slip distance owing to increased mixing efficiency with time, although different major elements homogenise at different rates (Na fastest, Si slowest). The preferential melting of mineral phases contributing to melt chemistry is seen dominantly in the amphibole-bearing andesites, with adjacent melt becoming enriched in amphibole-bearing elements (e.g., Ca). Owing to amphibole-melt interaction, we find pyroxene-bearing andesites show less melt heterogeneity from the onset. Preferential mineral melting plays a clear role in frictional melt composition via decomposing during flash heating. Although initial slip promotes disequilibrium melting and mixing in the melt zone, the time-dependence of melt homogenization means slip behaviour can be related to chemical diffusion once steady state conditions are achieved via double-diffusion convection. These changes have important rheological implications, with melt chemistry and mineral comminution having fundamental controls on the mechanical forces associated with slip.

Baptiste Haddadi, Olgeir Sigmarsson, Marion Carpentier, Gudrun Larsen

Submission 1150

The magma system of Grímsvötn volcano and eruption magnitudes

Eruption sizes vary by an order of magnitude at the subglacial Grímsvötn volcano, Iceland. Large and small eruptions occur after repose periods of similar length, their duration is also similar and the emitted magma is of tholeiite composition. These factors are thus unrelated to the eruption sizes, which in turn might be due to magma system configuration controlling crystallization depth and/or magma recharge from depth. Here, we present compositional time-series on historical tephra from Vatnajökull ice-cap and detailed geothermobarometry on two large and two small Grímsvötn eruption products. In-situ analyzes of matrix glass from the last large eruption (2011) reveal bimodal distribution of MgO (at 4.8 and 5.6 %), whereas those of clinopyroxene (cpx) melt inclusions (MI) show a considerable range (3.2-6.7 %). This variability is caused by magma mingling of deep-derived basalt recharge into residing basaltic magma higher up in the magma system. Most cpx crystallization pressure, as calculated from pairs of matrix glass and cpx rims as well as MI and host cpx, from two small (CE 1823 and 2004) and two large eruptions (CE 1873 and 2011) indicate pre-dominant mid-crustal depth regardless of eruption size. Precise trace element concentration measurements of tephra from CE1200 to 2011, with uniform Sr-, Nd, and Pb-isotope ratios, reveal a general increase of incompatible element concentrations with time, whereas compatible elements show less regular decrease. Fine-scale irregularities are observed on a plot of Th vs time that correspond to spikes in Cr and Ni concentrations. These irregularities suggest magma recharges of deeper-derived and more primitive tholeiite and correlate in time with large seismic events on a transform fault in S-Iceland. Cyclic increase in eruption frequency observed by Larsen et al. (1998) has a period of approximately 150 years. This periodicity may correspond to readjustment of the stress regime in the deep crust beneath Grímsvötn volcano causing increased magma flux from depth and larger eruptions than usual.

Gregor Hahn, Mike Branney, Philip Leat

Submission 99

Geochemical fingerprinting and the correlation of welded ignimbrites: A case study from the nested calderas of the Borrowdale Volcanic Group, U.K.

The >4 km thick Ordovician Borrowdale Volcanic Group in the Lake District, north-western England, is a remnant of a Palaeozoic subaerial volcanic arc. Central to this volcanic group is a caldera complex dominated by the well-documented >140 km² Scafell caldera, exceptionally exposed by glacial erosion at the volcanic/subvolcanic level. A large number of welded calc-alkaline-high-K silicic ignimbrites and andesite units are associated with this caldera and other more poorly documented calderas within this nested complex, e.g. Langdale caldera. Correlation of the ignimbrites from calderas to the outflow, distal facies is poorly known for most of the units and many of the outflow ignimbrites have yet to be correlated with their potential source areas. Correlation of units has been hampered by the large number of units, prehnite-pumpellyite regional metamorphism, local cleavage and thrust fault development during the Acadian orogeny.

In order to correlate outflow facies to units within and proximal to the Scafell and Langdale calderas trace-element geochemical fingerprinting is utilised. This is supported by detailed stratigraphic mapping and textural interpretation of the andesite to rhyolite caldera-forming succession. A similar methodology has resulted in correlations of ignimbrites over long distances being achieved in more recent systems (e.g. Snake River Plain, USA). This study is a test in using such geochemical correlations using elements that were immobile during the low-grade regional metamorphism in a Palaeozoic succession.

Improved correlation of the outflow sheets is enhancing understanding of ignimbrite volumes and eruption parameters, relative age relationships of ignimbrite eruptions, caldera collapse events and intracaldera lacustrine sedimentation in the nested caldera complex. Because caldera fills, faults and eruption conduits are outstandingly exhumed at Scafell caldera, the aim is to correlate outflow sheets to caldera fills and ultimately to individual vents. Initial results show that some outflow sheets can be traced to their sources, whereas others are 'exotic' and derived from as yet unidentified sources. The study illustrates that understanding the stratigraphic succession is of fundamental significance for our understanding of ancient volcanic complexes, but can be resolved even where there has been locally intense tectonic deformation and alteration.

Sahand Hajimirza, Helge Gonnermann, James Gardner, Thomas Giachetti

Submission 1240

Predicting homogeneous bubble nucleation rate

Classical nucleation theory has been used to infer magma decompression rates during volcanic eruptions from bubble number density in pyroclasts. We have tested the accuracy of such predictions against a suite of homogeneous bubble nucleation experiments in rhyolitic melt and find discrepancies between observed and predicted bubble number densities of up to four orders of magnitude. We hypothesize that this is due to the known curvature dependence of surface tension for the nucleating bubble. To test this hypothesis, we first performed a suite of decompression-nucleation experiments in rhyolitic melt and subsequently numerical modeling of bubble nucleation during the experiments.

For the experiments we first hydrated rhyolitic melt at pressures between 141 and 250 MPa, corresponding to water concentrations of 4.8-6.1 wt.%. Following equilibration, samples were decompressed to pressures ranging between 8 and 122 MPa over time intervals of 1 to 35 seconds. In the quenched samples there was no evidence for heterogeneous nucleation. Measured bubble number densities ranged from approximately 10^8 to 10^{16} m^{-3} , correlating positively with the difference between initial and final pressures, decompression rate as well as initial pressure.

We then modeled the experiments by integrating the coupled system of equations for the rates of bubble nucleation and growth. Model predictions are bubble number density, average dissolved water concentration and mean bubble radius as functions of time. By minimizing the discrepancy between observed and predicted bubble number densities for all experiments we obtain a supersaturation-dependent correction to the macroscopically measured surface tension. This correction provides a significant improvement in the predictability of homogeneous bubble nucleation in rhyolitic melts and, hence, our ability to constrain magma decompression rates from pyroclast bubble number densities. In addition to presenting aforementioned experimental and modeling results, we will discuss implications for bubble nucleation during silicic eruptions.

Morgan Haldeman, Thorvaldur Thordarson, Enikő Bali, Steven Carey

Submission 1033

Degassing-induced crystallization as a proxy for pressure in subaerial and submarine basaltic glassy selvages

The physical characteristics of subaerial versus subaqueous lavas are well-known and perhaps best exemplified by the difference between pahoehoe and pillow lava. Pahoehoe is typically fairly vesicular (30-60 vol%) and features glassy selvages with significant amounts of microlites up to 20-35 vol%. Deep-sea pillow lava lobes are effectively vesicle-free (i.e. undegassed due to the relatively high external pressures) and their glassy selvages are essentially free of microlites. In general, the most abundant volatile phase to dissolve in basaltic magmas is water (H₂O), which while dissolved in the magma lowers its liquidus temperature. Upon venting in vigorously fountaining subaerial eruptions, the bulk of the H₂O (≥70% in primitive MORBs) is exsolved from the magma and released into the atmosphere. This degassing-induced drop of dissolved water raises the liquidus temperature of the magma and promotes crystal nucleation and formation of microlites. These observations are suggestive of a relationship between amount of microlite crystallization and degree of magma degassing upon venting. Magma degassing is a function of the pressures exhibited by the external environment (i.e. water and air) on the eruption site, which in our case ranges from 0.1-15.1 MPa. In this study we aim to examine whether the degree of microlite crystallization in glassy selvages from pahoehoe and pillow lavas correlate with the water contents in the groundmass glass, or, in other words, test whether crystallinity can be used as a proxy for degree of magma degassing in subaerial and subaqueous basaltic eruptions. For the purpose of this study we have collected glassy selvages from pahoehoe and pillow lavas in the Western and Reykjanes volcanic zones in Iceland. The pahoehoe are representative of atmospheric conditions, while the pillow lavas were formed beneath ice up to 500m in thickness. We have also acquired glassy selvages from deep sea pillows collected from water depths > 1500m. The crystallinity of the lava selvages will be determined by analysis of SEM images using IMAGEJ, while the H₂O ± CO₂ concentrations of the groundmass glass will be determined by FTIR. We also plan to measure the sulphur content and S₆₊/totalS ratios in the groundmass glass to examine the relationship between S and H₂O concentrations and test whether sulphur or its speciation can be used as a proxy for the water contents.

Minard Lane Hall, Patricia A. Mothes, Alexandra P. Alvarado

Submission 593

HAZARDS OF REMOBILIZED TEPHRA SEQUENCES DOWNWIND OF ACTIVE VOLCANOES

Areas downwind from active volcanoes can accumulate significant quantities of airfall tephra that can be remobilized as dangerous slides. Immediately west of Cotopaxi volcano, Ecuador, thick deposits of rhyolitic tephra were formed during the Holocene. This tephra accumulated upon the pre-existing hilly topography of Yacupungo mountain, characterised by 200-500 m-high hills with slopes of 10-30°. The total tephra accumulation, 10-20 m thick, consists of many pumice clast-rich layers, each 10 to 200 cm thick, interbedded with finer-grained ash beds and soils. Sometime between 1000 and 800 yBP this tephra accumulation (~1 km³) became destabilized and slid downslope and across the adjacent flat areas for several kilometers, affecting an area of ~12 km².

The triggering event was probably seismic in origin, as a major SW-NE regional fault traverses this area which also suffered a 5.7 M (Richter) earthquake in October 1976. More than 5000 houses were destroyed. A factor in the slide's mobility may have been due to the interbedded layers of coarse pumice clasts that may have acted initially like ball-bearings and aided differential movement. Once started, the slide depended upon gravity and the steep slopes for its runout. The presence of folded tephra beds suggests that some tephra sequences slid coherently downhill like a blanket but became folded as they slowed and stopped. Little evidence of water participation in the slide's initiation and movement was observed. The danger continues while the vulnerability increases as now hundreds of people live in the disturbed area where they mine the pumice as a light-weight aggregate for brick making.

Downwind ash distributions and maps are an invaluable guide for evaluating hazardous ash accumulations.

Christopher W. Hamilton, Stephen P. Scheidt, Andrew P. Keske, Alexandra E. Huff, William H. Speiser, Debra H. Needham, Ethan I. Schaefer, Sarah S. Sutton, Jeffrey E. Moersch, Corbin L. Kling, Erika Rader, Andrew J. Ryan, Amber L. Keske, Danielle K. Moyer

Submission 432

Sinuuous Channel Formation within the Laki Lava Flow: A Consequence of “Fill and Spill” Emplacement

In aerial and satellite imagery, sinuous lava channels can resemble fluvial channels incised into bedrock. These two channel types can be distinguished using field observations, but their similarities complicate remote sensing interpretations of channel systems on Mars. This study characterizes a sinuous channel in the Laki lava flow in Iceland as a baseline for planetary remote sensing studies. Our results show that the channel resulted from a “fill and spill” mechanism whereby the temporary storage of lava formed a perched-lava pond, which drained in response to a dam failure event. This breach caused a surge in the local lava discharge rate, relative to the effusion rate at the vent, and has implications for assessing volcanic hazards.

The Laki eruption began on 8 June 1783 and lasted for 8 months, erupting 14.7 ± 1.0 km³ Dense Rock Equivalent (DRE) of lava and covering 600 km². Approximately 25% (3.7 km³ DRE) of the total lava volume was extruded during the first eight days from Fissures 1–3. Much of this lava flowed through the Varmádalur valley before entering the Skaftá river gorge, forming a 30-km-long channel. This study focuses on a 5.2-km-long segment of this channel near Fissure 3, which active was between 14–18 June.

Using ground-based observations, Differential GPS, and unmanned aerial vehicles, we identified 17 facies in a 5 km² region near Fissure 3. These facies are primarily associated with the lava channel and adjacent cone row, and were mapped at a scale of 1:400. We also measured lava high-stand marks in the channel (to infer the depth and volume of the lava pond) and the thickness of 2258 crustal slabs (to estimate the duration of the pond’s stability based on its cooling history).

We infer that mass wasting of the scoria cones near the vent introduced tephra blocks into the channel system. This material rafted down-flow until it stranded to form a temporary barrier that confined a lava pond. Based on the 0.18 m mean thickness of its crust, the pond was stable for at least 5.3 hours. Then, during a drainage event, the lava level within the channel dropped by an average of 3.6 m and the local discharge rate suddenly increased, leading to the development of rubbly and slabby lava down-flow. The resulting sinuous channel appears to have incised into the surrounding volcanic plain, but is the product of a “fill and spill” process involving an initial stage of construction, followed by partial drainage in response to a dam-breaching event.

John Hamilton, Kayla Iacovino, Tobias Fischer, Armando Saballos

Submission 167

Application of a Thermodynamic Model Resolving Volatile Concentration Differences Between Melt Inclusions and Surface Degassing

Given direct subsurface measurements of volatiles in magmas are not possible, analysis of melt inclusions provide constraints for the inner working of volcanic systems. Melt inclusions record dissolved volatile concentrations at various depths in the volcanic plumbing system, which can be used to model the pressures and temperatures of magma storage regions. Connecting the chemistries of surface gases with their source regions is crucial for interpreting active gas monitoring data but is challenging since melt inclusions only record dissolved volatiles, but not changes to the gas composition between depth and surface. Observations show that CO₂/H₂O ratios are higher in surface degassing compared to melt inclusions raising questions about whether volatile loss occurs during gas ascent. We use fumarole and melt inclusion compositions from Cerro Negro and El Hoyo volcanoes (Venugopal et al. 2016) to examine magma degassing and volatile mixing processes to explain differences in surface and subsurface volatile chemistries. Measurements show CO₂/H₂O ratios are up to an order of magnitude greater in fumaroles compared to melt inclusions here, suggesting alteration of gas chemistry between melt inclusion entrapment and surface degassing.

We use a thermodynamic model of Iacovino, 2015 to compare surface and subsurface volatile compositions at these two volcanoes. This model calculates all possible subsurface C-O-H-S fluid combinations from volatile differences in melt inclusions at discrete depths to match surface degassing measurements within ± 2.0 mol%. At Cerro Negro and El Hoyo, magma reservoirs at 2 and 8 km (Venugopal et al., 2016) may show contribution of CO₂ from co-existing fluid based on surface gas measurements. Model results help to determine actual CO₂ concentrations prior to volatile loss in melt inclusions and investigate the connection between these two volcanic systems in terms of their volatile sources and initial concentrations. Successful application of the model to a wider range of magma compositions and open-system degassing scenarios could be the first step in reconciling the missing CO₂ at active volcanic systems.

References:

Iacovino, K., 2015, *Earth and Planetary Science Letters*, v.431, p.59-74.

Venugopal et al., 2016, *Journal of Volcanology and Geothermal Research*, v.325, p.211-224.

Christopher W. Hamilton

Submission 412

Explosive Lava–Water Interactions: Tephrostratigraphy and Eruption Processes

Volcanic rootless cones (VRCs) are the products of explosive interactions between lava (fuel) and external sources of water (coolant). The thermodynamics of rootless eruptions are generally attributed to molten fuel–coolant interactions (MFCIs), but the relationships between MFCI efficiency, processes of fragmentation, and tephra dispersal are poorly constrained.

This study examines a 13.55-m-thick vertical section through an archetypical rootless tephra sequence in the Rauðhólar VRC group in Iceland. The deposit includes a rhythmic succession of twenty-eight bed-pair deposits. Each bed-pair consists of a fine-grained basal component and a coarse-grained upper component. This succession is interpreted to be the result of discrete explosion cycles, with material emplaced through a combination of tephra fall (during an energetic opening phase), and ballistic ejecta (during a weaker coda phase). Nine additional layers are interleaved throughout the stratigraphy and include abundant lacustrine sediment with cross-stratified internal laminations. These layers are interpreted to result from episodically erupted dilute pyroclastic density currents (i.e., surges).

Overall, the stratigraphy divides into four units with a depositional pattern that is consistent with a decrease in MFCI efficiency as locally available groundwater was gradually depleted. However, the rhythmic nature of the bed-pairs also suggests that water-to-lava mass ratios periodically increased during cycles of groundwater recharge. The depositional sequence also provides insight into other aspects of VRC formation. For instance, the abundance of coarse-grained clasts, which lack evidence of lava–sediment intermingling, suggests that only a small fraction of the overall volume of erupted lava directly participated in the MFCI process. Additionally, mud-rich surge beds, in some cases including less than 5% juvenile (i.e., lava-derived) material, implies that VRCs include the products of both phreatomagmatic and phreatic explosions.

These observations are placed into the context of understanding the triggering of rootless explosions, eruption mechanisms, and deposit characteristics for rootless tephra sequences within Rauðhólar and other VRC deposits observed in the Laki lava flow. Together these examples also provide insight into rootless eruption processes and establish a framework for interpreting the geological and paleo-environmental significance of similar tephra deposits identified on Mars.

Rachel Hampton

Submission 166

The Middlesex Fells Volcanic Complex: A Revised Tectonic Model based on Geochronology, Geochemistry, and Field Data

The Boston Bay area of Eastern Massachusetts is composed of several terranes originating on the paleocontinent of Avalonia, which accreted as an arc onto the continent of Laurentia during the Devonian. Included in these terranes is the Middlesex Fells Volcanic Complex, a bimodal complex composed of both intrusives and extrusives. When originally studied this volcanic complex was believed to have been erupted during a rift event as the Avalonian continent separated from its parent continent between 700-900 Ma. However, this study collected geochemical and geochronological data and combined it with field relationships to create a new tectonic model for this Volcanic Complex. U-Pb laser ablation zircon (LA-ICPMS) data on four samples from different units within the complex revealed that the complex erupted around ~ 600 Ma. ICP-MS geochemical analysis of the metabasalt member of the complex carried a strong N-MORB back arc basin signature, while the felsic units had an arc related signature when plotted on tectonic discrimination diagrams. Combined with the field relationships, this data suggests that the Middlesex Fells Volcanic Complex was erupted as part of the arc-sequence of volcanism on Avalonia and as part of the formation of a back-arc basin well after Avalonia separated from its parent continent. Further work is needed to determine the exact chronology of events within the complex, but this model gives a much younger eruption scenario for the Middlesex Fells Volcanics and may be used to study and compare to other volcanics from Avalon Terranes in localities such as New Foundland and the greater Boston area. When combined with other areas, this study will provide more rigorous constraints on the tectonic history of the Avalonian continent.

Heather K. Handley, Jon P. Davidson, Colin G. Macpherson

Submission 575

Separating crustal and mantle signatures in Sunda arc subduction zone volcanic rocks

Understanding magma genesis and evolution in subduction zone environments is crucial for understanding the formation of the continents and crustal recycling in the mantle. However, determining the original source compositions of volcanic arc rocks can be challenging, as lavas rarely reach the Earth's surface without experiencing some processes that modify their composition, for example, fractional crystallization, magma mixing and crustal assimilation. Despite the apparently simple tectonic setting of the northward subduction of the Indo-Australian Plate beneath the Eurasian Plate, understanding magma genesis and evolution at the Sunda arc is complicated by along-arc changes in the composition and thickness of the overriding Eurasian plate, the changing age of the subducting oceanic crust and variation in the type and amount of sediment entering the trench. This contribution highlights work on Sunda arc volcanic petrogenesis to show that through detailed geochemical and isotopic studies of individual volcanoes it is possible to resolve 'shallow' versus 'deep' crustal inputs. Differentiation processes play a major role in modifying the geochemical composition of Sunda arc magmas. The distinct intra-volcanic complex differentiation trends observed at several volcanoes are spatially controlled and explained by independent conduits and multiple magma reservoirs at different depths in the crust. Deep fractionation of a phase in which HFSE and HREE are compatible (e.g. amphibole) is inferred in the evolution of most Javanese magmas. Two crustal assimilants are identified in West and Central Java: a low $\delta^{18}\text{O}$ and relatively low Pb and Sr isotopic composition assimilant in West Java, likely representing more primitive arc rocks or mafic-ultramafic ophiolitic rocks, known to outcrop in West (and Central) Java and, a higher $\delta^{18}\text{O}$, higher Sr isotope composition assimilant in Central Java, which is consistent with the proposed assimilation of crustal carbonate material for Merapi in Central Java. Once the effects of crustal-level processes are accounted for, strong East to West Java regional variations in Ba concentration, Ba/Hf ratio and Pb isotopic composition are evident. These differences are attributed to heterogeneity in the subducted source input component along the island. The subduction of the Roo Rise, an area of oceanic basement relief, is thought to contribute significantly to the spatial geochemical source input variations exhibited by Javanese volcanoes.

Heather Handley, Lucy McGee, Rosa Didonna, Karoly Németh, Rebecca Griffis, Michael Turner

Submission 627

Multiple vent eruptions at monogenetic volcanoes: Waitomokia volcano, Auckland Volcanic Field, New Zealand

Waitomokia volcano (also named Mt Gabriel, Gabriels Hill, and Moerangi), is a basaltic tuff ring and scoria cone complex located in the southern lowlands of the Auckland Volcanic Field (AVF). Extensive quarrying and urban developments have resulted in the near-complete removal of three intra-tuff ring scoria cones, incision of the original tuff ring rim and some degree of infilling of the original crater floor, hindering a full understanding of the formation of the volcano. In this work, historical records are combined with detailed field studies of the remaining pyroclastic deposits to reconstruct the formation and evolution of Waitomokia, with special reference to the nature of explosive magma and groundwater interactions. The proximal sequence of the tuff ring consists of a coarse massive-to-weakly bedded pyroclastic breccia and lapilli tuff that alternates with a well-bedded, cross- and/or dune-bedded tuff. The clast-supported nature of juvenile lapilli layers and the presence of scoriaceous bombs within the tuff ring deposits suggest repeated magma discharge through an open but slurry-laden vent. The irregular and flame-like boundaries of lithic clasts within magmatic bombs indicate that coarse mixing occurred between intruding magma and water-saturated sediments (e.g., peperitic domain). Juvenile scoria fall and spatter deposits within the tuff ring crater provide evidence for a more sustained magmatic phase towards the end of Waitomokia's eruption leading to a scoria cone building phase. Several lines of evidence such as 1) the overall wide, oval-shaped, shallow nature of the tuff-ring crater, 2) presence of individual explosion craters preserved in the tuff ring rim on the north-east side, 3) significant scoria fall deposits, peppered with mm-scale rounded lithic clasts, 4) the presence of rounded (milled) large accidental lithic clasts, and 5) an unconformity in the tuff ring proximal succession suggest that the tuff ring was formed by volcanic activity at multiple, closely-spaced vents with some aspect of vent migration through time. This eruption model is in good concert with inferred eruptive histories of other large tuff ring complexes from the AVF, especially those formed in the low-lying coastal areas of the field, suggesting the influence of the external environment on volcano growth and the potential volcanic hazards involved in such type of evolution can be associated with vent migration and unstable vent/crater and conduit conditions.

Matthew Haney, David Fee, Robin Matoza, Alexa Van Eaton, Peter Cervelli, David Schneider, Alexandra Iezzi

Submission 878

Plume-tremor hysteresis: Analogies between fluvial seismology and co-eruptive volcano seismo-acoustics

Scientists at volcano observatories have long sought to estimate plume height and mass eruption rate from commonly available real-time observations such as seismic data. The standard view is that stronger eruption tremor corresponds to higher volcanic plumes since both are assumed to scale with mass eruption rate. However, in practice such a straightforward relationship is often not observed. Many factors can lead to a lack of scaling between tremor strength and plume height such as a weak plume, deeply-sourced co-eruptive seismicity, and atmospheric effects.

Here we report on a newly observed phenomenon in which the amplitude of volcanic tremor and the height of a volcanic plume do not scale in a simple way during an eruption and instead depend on the stage of the eruption (Fee et al., 2017). We describe variations between plume height and amplitude of co-eruptive seismo-acoustic recordings observed during the 2016 eruption of Pavlof Volcano in Alaska. Connections exist with the emerging field of fluvial seismology, which has established a characteristic hysteresis pattern between the strength of seismic shaking radiated by a river and its discharge. We find a similar hysteresis pattern between co-eruptive seismo-acoustic tremor amplitude and plume height at Pavlof Volcano. The source of the tremor is closely linked with erosion of the volcanic vent and upper conduit. The hysteresis effect means that at late stages of an eruption, volcanic tremor may decline even while the height of the plume remains at high altitude. This conceptual model informs forecasting of ash cloud height when only seismo-acoustic data are available. Building on the results at Pavlof Volcano, we discuss the possibility of plume-tremor hysteresis during recent eruptions at other volcanoes. Future progress in this field will depend on the availability of high-quality plume height data and mass eruption rate estimates with high temporal resolution.

Fee, D., M. M. Haney, R. S. Matoza, A. Van Eaton, P. F. Cervelli, D. J. Schneider, and A. M. Iezzi (2017), Volcanic tremor and plume height hysteresis from Pavlof Volcano, Alaska, *Science*, 355(6320), 45-48, doi: 10.1126/science.aah6108.

Szabolcs Harangi, Réka Lukács, Balázs Kiss, Axel K. Schmitt, Olivier Bachmann, Kata Mészáros, Ioan Seghedi, Christoph Hauzenberger, Paul R.D. Mason

Submission 992

Petrologic constraints for a warm magma storage prior to the latest eruption of the Ciomadul volcano, eastern-central Europe

Determination of the conditions, processes and timescales of magma storage prior to volcanic eruptions contributes to our understanding on the state of a volcano and to the evaluation the style and magnitude of possible further eruptions. Ciomadul (Carpathian Mountains, Romania) is classified as a volcano with a potentially active magma storage (PAMS volcano). Although the last eruption occurred at 32 ka, geophysical studies indicate the presence of a melt-bearing magma body in the crust. Volcanism at Ciomadul is divided into a lava dome extrusion phase from 150 to 100 ka, followed by a dominantly explosive eruption phase from 57 to 32 ka. Petrologic studies imply that presumably fast remobilization of a long-lasting cold felsic crystal mush body by hot basaltic magma led to effusive eruptions, whereas we propose here that the most recent explosive volcanic activity was preceded by a protracted period of heating.

Pumiceous blocks of the youngest pyroclastic flow deposit have a crystal content of ca. 30 vol. % and comprise phenocrysts of plagioclase, amphibole and biotite in addition to accessory FeTi oxides, apatite, titanite and zircon. Two generations of compositionally homogeneous plagioclase are present with An = 40-50 mol% and FeO contents of 0.2-0.3 wt%. Amphibole phenocrysts show various zoning patterns and cover a wide compositional range. Three groups can be distinguished: low Al-Mg hornblendes, high Al-Mg pargasites and an intermediate group. Remarkably, the latter type characterizes always the outer rim of the usually euhedral amphibole phenocrysts. Trace element composition of amphiboles indicates that at least three distinct magmas interacted in the volcanic plumbing system. Amphibole-plagioclase and FeTi oxide thermometry yields 800-830 oC equilibration temperatures prior to eruption, whereas zircon and titanite have crystallization temperatures of 650-730 oC. Spot analyses of zircon interiors give a wide range of crystallization ages between 360 ka and 100 ka. Depth profiling of the outermost rims of the zircons indicates crystallization ages >65 ka, significantly predating the eruption age of 32 ka. Thus, we propose a magma storage at temperatures >800 oC over several 10's kyr prior to the last explosive eruption. This condition could have produced greater melt fractions in the magma reservoir what is an important constraint for geophysical modelling of the present magma body.

This research belongs to the NKFIH K116528 and PD121048 projects.

Lydia Harmon, Guilherme Gualda, Darren Gravley, Chad Deering

Submission 1178

Deciphering Whakamaru group storage conditions and magma mingling/co-eruptive magma bodies via glass geochemistry and rhyolite-MELTS geothermobarometry

The Whakamaru group magmas erupted as a series of large events over ~10 ky at 350 ka, with the total ignimbrite and associated fall deposit volume exceeding 2000 km³. The objective of this study is to better understand the magmatic storage conditions of the system that fed the Whakamaru group eruptions. We combine detailed sampling of the volcanic stratigraphy with geochemical data and geothermobarometric calculations to characterize the evolution of this large magmatic system.

These relatively crystal-rich magmas (up to 35 wt.% crystals) erupted during several large events and were emplaced as six distinct ignimbrite units. The sectorial distribution of the ignimbrite units makes correlation difficult, so we focus on co-erupted fall deposits to determine the time-progression of eruptions. These fall deposits are key to understanding the timing and differences in magma types and storage conditions tapped during the entire eruptive sequence.

Small, lapilli-sized juvenile clasts (~2-4 mm), collected in a sequence of fall deposits, were used to derive magma storage conditions. Major-element geochemistry of minerals and glass were obtained by energy-dispersive X-ray spectroscopy (EDS) via SEM. Several samples have two distinct glass populations, indicating magma mingling prior to eruption or co-eruption of two distinct magma types from different vents. Glass compositions within the pumice clasts were averaged (after separating distinct glass populations), and geothermobarometric estimates were calculated from samples with SiO₂ values between 77.2 and 77.8 wt.% SiO₂.

We utilize rhyolite-MELTS geothermobarometry using major-element glass compositions to obtain crystallization pressures, under the assumption that melt equilibrated with quartz and two feldspars (q2f) or quartz and plagioclase (qp). Of the 43 compositions, 5 yielded q2f pressure calculations, and an additional 25 compositions yielded qp pressure calculations. There does not appear to be a systematic difference between pressures calculated for q2f and qp assemblages.

For the entire fall deposit sequence, pressure estimates range from 50 MPa to 200 MPa, with the majority of pressures distributed between 75 MPa and 150 MPa. The pressures range from 50 MPa to 150 MPa in a single fall unit, indicating a complex storage history for the Whakamaru group. There does not appear to be a systematic relationship between depth through the eruption sequence, but instead there is a range of pressures within most units.

Claire Harnett, Mark Thomas, Matthew Purvance, William Murphy, Jurgen Neuberg

Submission 113

Why do lava domes fall down? New insights from numerical modelling

Structural instabilities of lava domes generate pyroclastic flows and debris avalanches that can be devastating to areas surrounding the edifice. Numerous mechanisms have been reported to trigger collapse, with several of the most common being: increased magma flux; resulting in gravitational instabilities caused by additional loading or over steepening; mechanical erosion of the dome slopes again leading to over steepening; significant internal gas overpressure, and interaction of the dome with rainfall. Given the numerous potential causes of collapse, the complex interactions between the underlying failure mechanics and the volcanic processes occurring means our understanding of dome collapse is still limited.

Following an investigation into the global and historical causes of dome collapse using the Global Archive of Dome Instabilities (GLADIS) database, developed by the author, we combine these results with mechanical testing of dome rock to inform a suite of new numerical models that represent the most commonly cited collapse triggers. We use ITASCA's Particle Flow Code (PFC) to create a model with material properties that are fully calibrated to dome rock samples collected in the field. This allows a more accurate estimation of dome strength than used in previous dome stability modelling, and ultimately the ability to evaluate the importance of the different trigger mechanisms identified by the GLADIS database on the relative stability of lava domes.

Andrew Harp, Greg Valentine

Submission 129

Emplacement controls for the basalt-andesite radial dikes of Summer Coon Volcano, CO, USA

Dike fed flank eruptions pose a significant hazard to life and property due to the uncertainty linked with new vent locations and their potentially close proximity to inhabited areas. Beneath and within a volcano, lateral variations in host rock stress combined with the driving pressure of ascending dikes may play a significant role in controlling dikes' along-strike propagation direction. However, this process is difficult to investigate in active systems.

Erosion at the Oligocene age Summer Coon volcano, CO has exposed a radial dike sequence of over 700 basalt-andesite dikes. The density of dike outcrops is highest within a ~2 km-wide-zone centered ~3 km from the volcano's center. Oriented samples were collected from the outermost chilled margins of 82 dikes located throughout the sequence. Samples were thin sectioned and analyzed to determine the inclination of along-strike plagioclase fabrics and infer the dike's emplacement angle. A total of 71 samples survived analysis and 41 possessed statistically significant fabrics. Mean flow fabric angles, which are lines with no implied flow direction, are separated into three groups based on their plunge direction. In group 1 (37 percent of dikes) the mean fabric angles plunge away from the volcano's center 10-60 degrees from horizontal. Group 2 (12 percent) has sub-vertical fabric angles from 60-90 degrees from horizontal. Finally, in group 3 (51 percent) the mean fabric angles plunge in toward the volcano's center 09-60 degrees. There is no clear correlation between a dike's measured fabric angle and its petrography, geometry, or distance from the volcano's center.

Dikes of group 1 likely originated from the conduit and upon nucleation propagated in a down-sloping angle toward the flanks. The sub-vertical flow fabrics of group 2 indicate primarily vertical propagation of each dike, presumably in the upward direction. The inclination of dikes in group 3 indicates oblique upward propagation toward the volcano's flanks and may represent the dominate process for ascending basalt-andesite dikes at Summer Coon. The lack of correlation between fabric angles and other dike attributes of group 3, such as petrography, combined with the zone of higher dike density indicates a relatively stable balance existed between dike overpressure and edifice induced stresses. This is possibly a result of consistent reservoir rupture pressure and edifice geometry during a majority of dike emplacement events.

Christopher Harpel, Kus hendratno, James Stimac, Sofyan Primulyana

Submission 708

The Orange Tuff: a late Pleistocene tephra-fall deposit emplaced by a silicic VEI5 eruption in West Java, Indonesia and its hazard implications

The Orange Tuff crops out over at least 2,000km² of West Java, Indonesia. The unit is usually orange with a white base, but is locally cream colored. Black Fe/Mg concretions with white halos are often present in the lower part of the unit. The unit is moderately sorted and mantles the paleotopography suggesting a fall origin. No pyroclastic-flow deposits appear associated with the Orange Tuff. Lithic isopleths suggest that Salak is the unit's likely source, but the Perbakti-Gagak system is also a possibility. From isopachs and lithic distribution, we infer a 2km³ minimum bulk volume, 28–37km column height, 2–6x10⁸kg/s mass eruption rate, and 1–3hrs minimum eruption duration. Such data imply a VEI5 Plinian eruption. The unit's glass, including in relict pumices, is altered to clay and only sparse lithics are present. Andesine, enstatite, Fe-Ti oxides, and rare augite, apatite, and zircon are present, giving the unit a gritty texture. Coexisting Fe-Ti oxides' compositions suggest a magmatic temperature of about 800°C. The phenocryst assemblage, high immobile element concentrations, and temperature suggest a dacite magma. The lack of amphibole and conditions needed to maintain an eruption column without producing pyroclastic flows suggest H₂O contents between 1.5–3.5%. Calibrated ¹⁴C ages on overlying and underlying units constrain the Orange Tuff's age between 34ka and 17.5ka. The Orange Tuff crops out near the modern surface, but several paleosols and an erosional unconformity separate it from the underlying dated unit, suggesting that it is closer in age to its younger limit. No pervasive tephra-fall deposits overlie the Orange Tuff, suggesting that it represents Salak's or Perbakti-Gagak's most recent VEI5 eruption. Tens of millions of people, including those in the city of Bogor, live within 30km of either vent, and critical infrastructure is within close proximity. More than 100 million live within 100km of both vents, and the unit's volume and column height suggest that ash fall likely occurred to such distances. Both Salak and Perbakti-Gagak are fumarolic and produced small-volume pre-historical and historical phreatic/phreatomagmatic eruptions. The lack of subsequent VEI5 eruptions and Orange Tuff's age temper its hazards significance, so Salak's and Perbakti-Gagak's hazards assessments should be primarily based on recent activity. Nonetheless, the severe consequences of an Orange Tuff-scale eruption suggest that such an event should be considered.

Karen Harpp, Darin Schwartz, Emily Wilson, Maggie McGuire, Zachary Cleary, Jake Mahr, Regina Pimentel, Rita Van Kirk, Hannah Bercovici, Eric Mittelstaedt, Mark Kurz, Dennis Geist

Submission 155

The Evolution of Galapagos Volcanoes

The Galapagos Islands exhibit remarkable diversity in morphology, eruptive behavior, and magmatic composition. Among the most striking variations is the dichotomy between the young western shields, characterized by large calderas with diameters up to several kilometers and depths of several hundred meters, and the older eastern volcanoes, which lack calderas. Instead, the eastern volcanoes have aligned vents that are parallel to fault networks, suggestive of dikes with strong tectonic control. Our recent gravity studies of Santa Cruz and San Cristobal confirm that neither volcano has any evidence of a refilled caldera or a dense subcaldera intrusion. Most Galapagos eruptions are Hawaiian or Strombolian-style, although in at least two cases, Alcedo volcano and Rabida Island, pumice-rich, rhyolitic fall and PDC deposits indicate Plinian explosive activity. San Cristobal and Santiago have anomalously young volcanism, which occurred after hiatuses of 1-2 My and migration of >150 km from the hotspot center. On San Cristobal, ~200 km downstream of the hotspot, the young phase dates from 5 to 175 ka. In a different style of late-stage volcanism, Floreana volcano is covered by xenolith-laden scoria deposits of alkaline basalts, attributed to contributions to the plume source from ancient, recycled ocean crust. The compositional homogeneity of lavas from many of the western volcanoes suggests that their magmatic reservoirs are long-lived and in a steady thermal state. With distance from the plume, compositions become increasingly variable, consistent with a shift to a network of small, ephemeral magma reservoirs. The extent of shallow fractionation and depth of melt generation also become more variable as the volcanoes age. Much of the morphological, eruptive, and compositional diversity in the Galapagos can be attributed to a progressively waning magma supply, as the volcanoes are carried away from the plume center. Other observations, such as the lack of evidence for calderas on the eastern islands and the variability in rejuvenescent volcanism styles, cannot be explained by a simple evolutionary model. Instead, the style of volcanism may be governed by changing tectonic environments owing to the near-ridge environment. The evolution of ocean islands is complex, influenced by numerous factors, including distance from the plume, magma supply rate, spatial and temporal variations in the mantle source, and tectonic configurations, especially plume-ridge distance.

Andrew Harris, Stefano Mannini, Simon Thivet, Lucia Gurioli, Nicolas Villeneuve

Submission 308

Unexpected rheological regime measured down an active lava channel

We here present results from simultaneous sampling and thermal imaging down the near-vent reach (the first 500 m) of an active lava channel at Piton de la Fournaise during July-August 2015. Between 10:00 and 15:00 on 1 August 2015, four channel stations were set up down the distal section of the flow system. From each station, thermal imagery of the channel could be collected over a line of site distance of 2-6 m; and water quenched samples were obtained from the first (at-vent) and second (70 m down-channel) stations. While thermal video was used to extract flow velocity profiles and cooling rates, sample analysis yielded flow chemistry, vesicularity and crystallinity. We found that, between, a distance of 25 and 70 m from the vent, flow increased in velocity (from 0.05 to 0.1 m/s) and increased in width (from 2 to 4 m), in spite of there being no change in slope (it being steady at 5°). To conserve volume the flow depth would thus, also, have had to decrease from 1.75 to 0.63 m between the two stations. This implies a down flow decrease in viscosity from 3500 to 1400 Pa s, in spite of cooling rates of 190-290 °C/km. In addition, the velocity profile switched from parabolic to one with a broad central plug with narrow marginal shear zones. The only way we can account for the trend in the viscosity is if we treat the vesicles as a population of rigid spheres, and interpolate between an at-vent vesicularity of 53 % and the lowest value measured (23 %) at 100 m. We thus argue that we have a situation whereby vesicles are steadily removed from the mixture over the first 100 m of flow, with the effect on mixture viscosity offsetting that of cooling, so that viscosity actually decreases over the proximal reach of the channel. Thereafter, vesicularity is stable so that the effect of cooling takes over to push the mixture viscosity upwards and through 104 Pa s by 500 m. Sample analysis suggests that this effect is aided by the formation of the plug (which is vesicle-rich) and shear-zones (which are vesicle-poor). We thus suggest that, with progressive flow, vesicles are increasingly partitioned between a vesicle-rich plug and low-vesicularity marginal shear zones. These vesicle-poor, low viscosity shear zones then carry the vesicle-rich, high viscosity plug between them. This effectively causes the flow to accelerate over the proximal reach of the channel, and then begin to de-accelerating once partitioning has been completed.

Margaret Hartley, Emma Liu, Marie Edmonds, Fabio Arzilli, Margherita Polacci, Samantha Bell, Nolwenn Le Gall, Evgenia Ilyinskaya, Mike Burton, Michael Drakopoulos, Nghia Vo

Submission 184

The role of sulfides in controlling volcanic SO₂ emissions from Icelandic eruptions: a textural approach

The 2014-2015 Holuhraun eruption, Iceland, emitted on average ~100 kt/day of SO₂ [1]; more than any other recent Icelandic eruption. Petrologic models assume that crystal-hosted silicate melt inclusions preserve a record of the undegassed S content of the pre-eruptive melt; for Holuhraun, this has been quantified at ~1500 ppm S. However, the Holuhraun tephra contains abundant sulfide globules, ranging in size from 2 emissions from Icelandic eruptions.

We have used synchrotron X-ray computed microtomography (μ CT) at Diamond Light Source to image the 3-dimensional (3D) structure of a series of scoria lapilli in the size range 3-10 mm, collected over the course of the Holuhraun eruption. The voxel size of 1.3 μ m means that we can reliably resolve sulfides >10 μ m in diameter. Initial 3D spatial distribution analysis reveals that the majority of sulfides are found close to plagioclase macrocrysts or clinopyroxene-plagioclase glomerocrysts, but they do not directly wet the crystal surfaces. Sulfides are also found as inclusions in olivine, plagioclase and clinopyroxene macrocrysts, and within melt inclusions. By quantifying the volumetric proportions of sulfides, crystals and glass in scoria samples, we aim to constrain the minimum pre-eruptive S content of the Holuhraun magma. We will also quantify the spatial and textural relationships between sulfides, crystals and bubbles, and explore temporal changes in sulfide abundance or texture that might be indicative of changes in the magmatic transport pathway or ascent rate during the eruption. Finally, by comparing the pre-eruptive magmatic sulfur and sulfide contents with in situ field FTIR measurements of SO₂ in the eruption plume, we aim to assess the contribution of sulfide breakdown to the outgassed SO₂ budget of the Holuhraun eruption.

[1] Schmidt et al. (2015) JGR Atmospheres 119:14180-14196.

Eva Hartung, Luca Caricchi, David Floess, Davide Roggero, Simon Wallis, Satoru Harayama

Submission 510

Linking plutonic and volcanic realms using plagioclase chemistry: Insights from the Takidani Pluton and the Nyukawa-Chayano-Ebisutoge volcanics (Central Japan)

The Takidani pluton in Central Japan (~1.5 Ma) is potential source of volcanic deposits of the Nyukawa and Chayano-Ebisutoge eruptions (1.76-1.75 Ma) whose total estimated eruptive volume exceeds 300 km³. In this study we investigate major and trace element variations in core to rim profiles in plagioclase crystals from both the Takidani pluton and the volcanic products to (1) investigate whether a genetic relationship exists between the Takidani pluton and eruptive products and (2) to understand the magmatic processes that preceded the caldera-forming eruptions.

Europium variations in plagioclase are used to distinguish two main crystal groups: low-Eu (3.5 ppm) plagioclase typical of the rhyolitic Chayano-Ebisutoge pyroclastic deposits (PD). Plagioclase grains in the Takidani pluton are typically oscillatory zoned (An₄₀₋₅₀) and show a normal zoned sodic overgrowth rim (An_{>20}) with high La and low Mg, Sr, Ba and Eu concentrations. Plagioclase grains from the andesitic and crystal-rich Nyukawa PFD are oscillatory zoned (An₄₀₋₆₀) with a rimward increase of An content and Fe and Mg concentrations. Plagioclase grains from the overlying rhyolitic and crystal-poor Chayano Tuff contain resorbed low-An cores (An₃₀) and a normal zoned overgrowth rim (An₂₅₋₃₅). Plagioclase grains from the youngest Ebisutoge PD are typically normal zoned (An₃₀₋₄₀) and contain two types of resorbed cores, low-An (An₃₀, Eu >3.5 ppm) and high-An cores (An₄₀₋₆₀, Eu

Overall, plagioclase chemistry indicates a petrogenetic relationship between the Takidani pluton and the Nyukawa-Ebisutoge-Chayano deposits. Trace element variations and the low-Eu signature suggest that the Nyukawa eruption was sourced from the Takidani magmatic reservoir. Moreover, low-Eu plagioclase with high-Eu overgrowths present in the Chayano-Ebisutoge PD suggest that remelting of remnants of the crystal-rich Takidani-Nyukawa magma body occurred before the eruption of the crystal-poor Chayano-Ebisutoge rhyolite. The Takidani pluton and its associated volcanic products present an extremely rare and exciting location to investigate upper crustal silicic magmatism and the generation of large caldera-forming eruptions.

Takeshi Hasegawa, Hiroki Hasegawa, Tetsuo Kobayashi, Darren Gravley

Submission 1192

Emplacement of highly mobile and 'cool' block-rich PDCs from the Mashu caldera-forming eruption, eastern Hokkaido, Japan

The Mashu volcano, eastern Hokkaido, has a Holocene caldera (7.5 x 5.5 km) formed on the edifice of a pre-caldera stratovolcano, within the larger Kutcharo caldera. The caldera-forming eruption of Mashu occurred 7.6 ka and the eruption deposits (18.6 km³) consist of a plinian fall sequence overlain by pyroclastic density current (PDC) deposits (Ma-f). Ma-f can be divided into 6 units (Ma-f1 to Ma-f6, top to bottom) with no interbedded soil layers. Here, we focus on the transport and emplacement of an unusual deposit (Ma-f3) in the middle of the PDC sequence.

Ma-f3 has a limited distribution from the west to the southeast of Mashu volcano. Proximally, Ma-f3 is up to 100 cm thick, and it can be recognized as a ~5 cm layer in distal areas 30 km from source and atop the 500 meter-high wall of the older Kutcharo caldera. It consists of a moderately sorted and fines-depleted lower part with a high concentration of dacitic lava blocks, and a pumice-rich upper part. Impact sag structures from large (> 50 cm) dacitic bombs can be recognized at the base of Ma-f3 10 km from source. In addition, Ma-f3 incorporates large rip-up clasts from the underlying substrate. Ma-f3 is compositionally homogenous with its lava blocks exhibiting the same range in whole rock chemistries as the overlying pumice (SiO₂=68~72%, K₂O=0.6~0.75%). Progressive thermal demagnetization was performed on the lava blocks, and their remanence directions exhibit random orientations in an equal area plot that suggests the blocks had cooled down below blocking temperature (500~600°C) prior to emplacement in Ma-f3.

Our results suggest that despite no interbedded soil layers within the PDC sequence, there was sufficient time (following eruption of Ma-f4 through Ma-f6) for a dacitic lava edifice to build and sufficiently cool prior to a violent blast that sent ballistics 10 km from source. The sectorial distribution of the overlying PDC deposits suggests it was a directed blast. In addition, despite the relatively cool nature of the lava blocks in the lower part of Ma-f3, a directed blast is a reasonable explanation for highly mobile and fast PDCs that were able to overcome high obstacles. The eruption episode culminated with the emplacement of the compositionally similar pumice-rich PDC deposit on top, suggesting the initial blast opened the conduit for fresh magma to explosively fragment and erupt.

Toshiaki Hasenaka, Kosuke Shiihara, Yasushi Mori, Natsumi Hokanishi, Atsushi Yasuda

Submission 1283

Petrological constraints on the precursory event of Aso-4 caldera-forming eruption

We examined petrological characteristics of a precursory volcanic products of Aso-4 caldera-forming eruption in Kyushu Island, Japan. Compositions of phenocrysts, glass and melt inclusions in minerals suggest that the precursory event formed a separate, slightly SiO₂-poor, and volatile-poor magma reservoir outside the caldera.

Aso-4, dated as 8.9 ka, was the last of four large pyroclastic eruptions, and produced >600 km³ pyroclastic flows and co-ignimbrite ash. Omine scoria cone and associated Takayubaru lava flow, dated as 9.0 ka, produced >2 km³ lava and pyroclastic materials. Soil did not develop between two volcanic products, however, reconnaissance paleomagnetic measurement of the two suggested a slight secular variation time gap. Omine scoria cone is located on the active Futagawa fault zone which extend NE toward the western end of the caldera. Caldera rim there was probably destroyed open by the old repeated fault movements. The 2016 Kumamoto Earthquake produced max 2 m right-lateral displacement on and around Omine cone. Futagawa fault passes across Takayubaru lava flow, where 100 m north-dipping vertical displacement is observed. Akai scoria cone, a precursory volcanic event for Aso-2 eruption is also located on the Futagawa fault. Thus, active fault system probably plays an important role for caldera-forming eruptions.

Aso-4 pumice and Omine-Takayubaru volcanic products are both hornblende two pyroxene dacite. However, they show different trends, thus indicating fractionation process at different reservoirs. In addition, compositions of plagioclase and pyroxenes show different peak patterns. Melt inclusions hosted in these minerals are also slightly different between Aso-4 and precursory products. All these suggest that the magma probably did not branched out from the main Aso-4 magma reservoir to form Omine volcano. Isotopic study shows Aso-4 and Omine have nearly the same Sr isotopic ratios. Both magmas possibly originated from the common deep reservoir, and separated near the surface. Whether the eruption from this separate Omine magma reservoir activated the main Aso-4 reservoir is difficult to prove. Active fault system definitely is an important factor for triggering of caldera-forming eruption at Aso caldera.

Takeshi Hashimoto, Masami Matsumoto, Risa Okamoto, Hiroshi Koyama, Atsushi Morii, Wataru Mishima, Tagiru Ogino, Ryo Takahashi

Submission 372

Long-term Correlation between Geomagnetic Field Changes, Ground Deformation and Gas Composition at Mt. Tarumae Volcano, Northern Japan

Mt. Tarumae is an active volcano in Hokkaido, northern Japan, that started erupting about 9 ka. Although magmatic eruption sequence is recognized from historical records and geological studies, it has only exhibited small phreatic explosions since the 1909 eruption that extruded the summit lava dome. Here we discuss the volcanic activity of recent two decades by means of multi-parameter monitoring such as magnetic field, ground deformation, volcanic gas composition, and so on.

The lava dome is located at the center of the 1km-across summit atrio. In the atrio, repeated measurements of geomagnetic total field and GNSS have been conducted since the late 1990's, and some other monitoring such as volcanic gas composition, fumarolic height and temperature have also been performed. Geomagnetic total field and ground deformation are highly correlated to each other. In the years around 2000, baseline extension was observed with clear demagnetization. From 2001 to 2006, both of them were almost stagnant, but after 2010 the tendency has been reversed, showing the contraction that accompanied remagnetization. The high correlation between the two recalls the possibility of a stress-induced magnetic effect, but it is more natural to interpret it as a thermomagnetic effect in view of the polarity of changes. Both geomagnetic field and ground deformation imply their sources are shallow, estimated to be about 300-500 m deep relative to the dome top.

Meanwhile, there is a focal region of micro earthquakes at a depth of around 0.5 km below the dome. The micro-seismicity has been activated since 1996, keeping a moderate level with fluctuation since then. Considering that the fumarolic temperature beside the dome sharply elevated since 1997, we infer that hot gas started to rise from a depth in the mid 1990's and reached the ground surface in some years. Since the fumarolic temperature was kept high thereafter, it seems that gas supply continued. We suspect that the gas flux began to wane from 2010, considering that recent tendencies of remagnetization and contraction are due to cooling and deflation. Elevated C/S ratio and depleted total sulfur concentration in the gas since 2010 onward seems consistent with the interpretation. In other words, waning of the gas supply may have allowed meteoric water intrude around the vents in the shallow subsurface. We believe that we have observed an activity cycle in a non-eruptive period through long-term multi-parameter monitoring.

Kana Hashimoto, Ikuro Sumita

Submission 42

Model experiments of degassing process in a crystal-bearing magma

As the magma cools and its crystal content increases, the rheology becomes non-Newtonian which affects the degassing style. This problem has been investigated using a gel (Divoux et al., 2011). However the effect of the particle volumetric fraction ϕ on the degassing process is still unknown. Here we use a transparent mixture of liquid and particles, which models a crystal-bearing magma, and inject air from the bottom orifice. We conduct experiments using fluids with different ϕ in the range of 0 to 0.5 to study how the degassing styles transition as ϕ increases. First, we inject a single bubble to study the dependence of the bubble ascent velocity U on its volume V . We fit the measurements to a power-law relation ($U \propto V^n$) and obtain the power-law exponents n , for each fluids with different ϕ (0-0.4). From the Stokes' law, n in a Newtonian fluid is $n = 2/3 \sim 0.67$. At $\phi = 0, 0.1$, we find that n and U is smaller than the Stokes' velocity U_s . These results can be interpreted as a consequence of turbulent drag becoming important at large V . On the other hand for $\phi = 0.3, 0.4$, n is $n > 0.67$ and the measured U is $U \sim U_s$ calculated using the shear-thinning viscosity alone, since the turbulence drag is negligibly small. Here we note that n increasing with ϕ implies that the coalescence of bubbles with different sizes are enhanced in fluids with large ϕ , which we also confirmed in our experiments. When the particle content in the fluid becomes large as $\phi = 0.5$, the bubble ascent is strongly inhibited because the fluid yield stress becomes comparable to the bubble buoyancy. Second, we studied the pattern of the bubbly flow and the fluctuations of air pressure at several flow rates. In a fluid with $\phi = 0.4$, bubbles form and coalesce periodically. In a fluid with $\phi = 0.5$, slugs form followed by a narrow crack which originate at the orifice. The pressure measurements show a coexistence of long and short period pressure fluctuations which arise from the air flowing into a slug and a crack. Our experiments suggest that when the bubble size exceeds a critical value such that they can ascend in a fluid with large ϕ , coalescence of bubbles with different sizes are enhanced which promotes degassing. Furthermore whenever a bubbly flow occurs, an increase in ϕ results in pressure fluctuations having two time scales.

Reza Firmansyah Hasibuan, Tsukasa Ohba, Mirzam Abdurrachman, Takashi Hoshide

Submission 762

MAGMAS CHARACTERISTICS OF RAJABASA VOLCANIC COMPLEX INFERRED BY PETROLOGICAL APPROACH

Rajabasa is a stratovolcano located in the southern tip of Sumatra Island, Lampung Province, and uniquely situated in the same lineament with Krakatau volcanic complex and Sukadana basalt plateau. This volcano yet still yields some magmatic activities, such as solfatara and hot springs. These facts lead to that the understanding of magma characteristics becomes significant either for across arc variation of magmas or geothermal development. Methodologies done are microscopic study, X-ray fluorescence, K-Ar isotope dating, and EPMA analysis. Plagioclase is a dominant constituent in the samples, followed by pyroxene, opaque, and some hornblende. Groundmass is occupied dominantly by lath plagioclase, clinopyroxene, and glass. Plutonic rock xenolith is also encountered as the evidence of assimilation process. Whereas, the rock chemistry or TAS plot shows a heterogeneity of magmas, ranging from basaltic (51 wt.%) to rhyolitic (75 wt.%). When SiO₂ contents are correlated with the relative ages, we found a broad tendency that SiO₂ contents progressively decrease with age. Rajabasa volcano lifespan is known formed at 0.31 Ma while one of the youngest lava is identified erupted at 0.12 Ma. However, it's found that the older product was developed at 4.33 Ma, from Gunung Tangkil. Some plagioclase crystals exhibit disequilibrium textures, such as highly sieved core and clear rim regions, also overgrowth of the calcic plagioclase and Mg-rich pyroxene rims on the sodic plagioclase and Fe-rich pyroxene cores, indicating magmatic recharge events. Reverse zoning and resorption textures associated with compositional step zoning in addition to progressive zoning are quite common as well in clinopyroxene and plagioclase crystals. Considering these evidences, injection of a hotter basaltic magma into colder and more felsic magma is estimated to occur beneath the volcano. Temperatures and depths have been measured using pyroxene pairs geothermobarometer. For mafic end-member in Gunung Tangkil, it's found that the Pliocene's magma has temperature of 1046.3°C. Meanwhile, the temperature of magmas beneath Rajabasa volcano is averagely 894.6°C. From calculation, pressures of magma chambers range from 4.1 kbar to 5.5 kbar.

Maki HATA, Nobuo MATSUSHIMA, Shinichi TAKAKURA, Mitsuru UTSUGI, Takeshi HASHIMOTO

Submission 388

3-D electrical resistivity model beneath Aso caldera in the Southwest Japan Arc for clarifying magmatism in the crust

Aso caldera, with dimensions of 18×25 km, lies on the island of Kyushu in the Southwest Japan Arc. The caldera was formed during 270–90 ka by four huge eruptions that produced hundreds of cubic kilometers of pyroclastic deposits. Thereafter, a number of post-caldera cones/volcanoes were formed at the central part of the caldera by smaller eruptions. Naka-dake, which is the active cone with emitting several hundred tons of SO₂ per day, has cyclically erupted since the sixth century. The latest magmatic eruption, which is an explosive eruption with spewing volcanic ash 11,000 m into the air, occurred in October 2016. The crustal structure beneath Aso caldera has been studied by electromagnetic and seismic surveys. Seismic tomography of the crust has identified low-velocity anomalies beneath the caldera that may correspond to magma chambers [e.g., Sudo and Kong, 2001; Abe et al., 2010, 2017]. Sudo and Kong [2001] reported a spherical low-velocity anomaly centered at 6 km depth that flattens at 10 km depth to the west of Naka-dake. Abe et al. [2010, 2017] reported a large low-velocity layer at a depth of around 20 km in and around Aso caldera.

We had carried out a magnetotelluric (MT) survey of 55 sites mainly at the inner part of the caldera from Nov. to Dec. 2015. By applying three-dimensional inversion analyses to the MT data of a period range between 0.005 and 2,380 s, we revealed a possible magma pathway in the form of a significant series of electrical conductive anomalies, extending north from Naka-dake at depths of >15 km, in the obtained electrical resistivity structure/model [Hata et al., 2016]. A sill-like deformation source inferred from GPS data [Geographical Survey Institute, 2004] has been detected at a depth of 15.5 km beneath the conductive anomalies. However, the space resolution of the MT survey was insufficient to examine the lower crustal structure for a deep-seated magma reservoir associated with the post-caldera magmatism beneath Aso caldera. Thus, we carried out an MT survey of 45 sites mainly at the outer part of the caldera from Nov. to Dec. 2016 in addition to the previously obtained 55 sites. An initial result based on the phase tensor analysis [Caldwell et al. 2004], in which we use its coordinate invariants to visualize phase information on the MT data for 100 sites, show that the conductivity beneath the northwestern part in and around Aso caldera increases significantly with depth corresponding to periods of >100 s.

Øystein Thordén Haug, Olivier Galland, Alban Souche, Pauline Souloumiac

Submission 638

Shear failure versus tensile opening at sill tips: insights from limit analysis modeling

Sills are common features in many sedimentary basins worldwide, and described as flat-lying intrusions that may differ in shape from flat to saucer-shaped. Intrusions make room for themselves by bending, breaking and fracturing their host rocks, and the resulting structures can have important implications for fluid (e.g. hydrocarbons) transport and storage in sedimentary basins. Commonly, models of sill emplacement account only for the elastic deformation of their overburden, and to a large degree neglect any plastic deformation or damage related to the emplacement. However, field observations show that significant damage, such as shear fractures, accommodate sill emplacement. The aim of this study is to explore how damage in sill overburdens affects the emplacement of sill intrusions.

We study the condition for shear failure and the distribution of damage in the overburden of sills using the limit analysis software Optum G2. The numerical setup consists of an elongated pressurized cavity within a Mohr-Coulomb material. Through a parameter study, we investigate the effect of the length-to-depth ratio L/D of the sill and the cohesion of the host rock on the over-pressure within the sill at failure.

The damage related to the sill is generally localized in an inclined band from the sill tip towards the free surface. However, significant differences are observed in the damage distribution for varying sill lengths (at the same depth). Short sills display linear bands of damage from the sill tips toward the surface, creating V-shaped patterns. For long sills, the damage is oriented orthogonally to the sill tip and curve towards shallower angle closer to the surface, leading to a characteristic saucer shape. The over-pressure required for shear failure scales linearly with the host cohesion and as a power-law of L/D with an exponent of $3/2$. From these observations, we propose a scaling law for a new shear failure criterion in the overburden of a sill.

Our simulations suggest that shear failure of the overburden can play a dominant part in the creation of V-shaped and saucer-shaped intrusions. Further, our results can be used to infer whether shear failure is favorable compared to other failure mechanisms. Specifically, we will discuss the conditions required to shear failure in sill overburden and those for commonly assumed tensile opening of sill tips.

Brian P. Hausback, Drew T. Downs, Andrew T. Calvert

Submission 1162

Improved $^{40}\text{Ar}/^{39}\text{Ar}$ Dating Analyses of Intermediate Intrusions and Domes from the Sutter Buttes Volcano, California

The Sutter Buttes comprise a Pleistocene dome field in the Sacramento Valley ~80 km north of Sacramento, California. The field is circular, ~15 km in diameter, and composed of a central core of volcanic domes surrounded by a large fragmental apron. Most of the dome complex is andesite/dacite, with rhyolite domes forming a discontinuous peripheral ring around the central andesite/dacite domes.

Field mapping of the domes, and stratigraphic study of the fragmental apron, indicate that the rhyolites were extruded prior to the andesite/dacite domes. The relative timing is illustrated at individual contacts between rhyolite and andesite/dacite; where rhyolite is hydrothermally altered and unaltered andesite/dacite is sheared. In addition, andesite/dacite fragmental rocks overlie rhyolitic fragmental rocks in the peripheral apron. Single-crystal, total-fusion $^{40}\text{Ar}/^{39}\text{Ar}$ dating of sanidine from rhyolite domes have yielded ages of 1.55 to 1.58 Ma (Hausback et al., 1993). Dating of the andesite/dacite domes by $^{40}\text{Ar}/^{39}\text{Ar}$ analyses of hornblende yielded aberrantly old ages (all >1.7 Ma) compared to U/Pb zircon dates of 1.7 to 1.4 Ma from the same domes. Excess argon compromises hornblende and biotite dating from this magmatic system (Swisher et al., 2000).

Fifteen new high-precision $^{40}\text{Ar}/^{39}\text{Ar}$ analyses from the USGS Argon Lab in Menlo Park, California on both plagioclase and groundmass separates from andesite/dacite domes yield ages ranging from 1.67 to 1.41 Ma. The new dates overlap in uncertainty with the previous zircon dates from the andesite/dacite domes. Due to the fine-grained groundmass of these andesite/dacite domes, all groundmass $^{40}\text{Ar}/^{39}\text{Ar}$ experiments are strongly affected by ^{39}Ar recoil and yield complicated results. Plagioclase separates generally yield acceptable plateau ages despite having low K_2O concentrations. Although groundmass recoil-model ages and plagioclase plateau ages overlap at the 95% confidence level, the plagioclase results are generally younger and interpreted as more reliable. Plagioclase results are slightly older than U/Pb zircon ages, but are indistinguishable within 95% confidence. These analyses indicate that andesite/dacite domes erupted within 150 ky of cessation of rhyolite eruptions and help determine the detailed eruptive sequence of the assemblage of andesite/dacite domes at the Sutter Buttes volcano.

Catherine Hayer, Lucy Ventress, Elisa Carboni, Roy Grainger, Simon Carn

Submission 825

Satellite observations of atmospheric emissions from the April 2015 eruption of Calbuco volcano, Chile

Calbuco volcano (41.3°S, 72.6°W) is an andesitic volcano, located within the Chilean Andes and is one of the most active volcanoes in Chile.

The most recent large eruption of the volcano occurred in three distinct phases between 22nd and 30th April, 2015. The first two phases, on 22nd and 23rd April, produced large ash and gas eruption columns, reaching approximately 12 and 15 km respectively. The third phase of the eruption, on 30th April, produced a weak ash column not exceeding 4.5 km. The plume was observed by numerous satellite instruments, including IASI, OMI, OMPS, MLS and CALIOP. Data from all of these instruments are analysed and compared allowing for a detailed description of the evolution of the plume over time.

The IASI-retrieved altitude data are compared to those from the CALIOP lidar overpasses as well as limb-view measurements from the MLS and OMPS instruments. SO₂ atmospheric loading measurements from IASI, OMI and OMPS are compared.

The maximum ash loading measured by IASI was 2.0 Tg in the evening overpass on 23rd April 2015. This measurement included contributions from both the Phase 1 & 2 plumes. The ash plume was visible for 8 days prior to dropping below the detection limit of the IASI instrument. A secondary peak of 1.8 Tg was observed following the eruption in Phase 3.

The SO₂ plume was visible for a lot longer than the ash plume – it was observed by the IASI instrument for 36 days, during which time it had circled the globe. The maximum IASI-derived SO₂ atmospheric loading of the plume was 0.3-0.4 Tg over the first two days, following the initial two phases of the eruption. The third phase does not appear to have produced any detectable injection of SO₂.

When the plume reached the west coast of S. Africa, it was caught in a cyclonic system for several days. This system kept the plume in a constrained area and significantly reduced the effects of dispersal due to wind, allowing the study of the chemical conversion of SO₂ into H₂SO₄. A conversion rate for SO₂ to H₂SO₄ is calculated from this data. The volcanic aerosols produced in the plume are believed to have contributed significantly to the record size of the Antarctic ozone hole in 2015. Satellite observations of the ozone hole over the past 15 years show that the impact of the Calbuco plume was unprecedented (Ivy et al., 2016, doi:10.1002/2016GL071925).

Josh Hayes, Thomas Wilson, Natalia Deligne, Graham Leonard

Submission 973

Embracing deep uncertainties to transparently develop plausible scenarios for volcanic impact and risk assessment

Volcanic eruptions are multi-hazard events that cause a variety of impacts to exposed societies. One challenge scientists face is communicating intricate interactions between various eruption hazards and societal elements. Complex eruption scenarios that include multiple likely eruption hazards have been found to be an effective tool for communicating this information. These eruption scenarios are of relevance to end-users because they provide a more in-depth picture of a potential future eruption than those analyses that focus on a single eruption hazard. However, deep uncertainties within the analysis must be addressed to unravel the multifaceted interactions between an eruption and societal elements for the development of scenarios. Deep uncertainty manifests when probabilities of an event are poorly constrained, unknown, or unknowable. How can volcanic risk analysts provide appropriate decision support when fundamental probabilistic relationships are unknown or at best poorly understood? What if you must rely on limited information or case studies to develop scenarios? What are the implications if fundamental assumptions or scientific data the analysis heavily relies on turn out to be incorrect? These are some of the challenges volcanic hazard / impact / risk analysts must overcome to develop multi-hazard volcanic eruption scenarios and impact assessments. Here, we propose a transparent and structured framework for scenario development that provides guidance for analysts to not only develop robust hazard, impact and risk scenarios in the face of deep uncertainty, but to also ensure that they accurately report and communicate findings to end-users and the research community. Our approach borrows concepts from traditional gap-analysis methodologies where we identify and rank the degree of scientific knowledge the scenarios are based on. We demonstrate how this process has been used to develop seven new eruption scenarios in the Auckland Volcanic Field.

Patrick Hayman, Ray Cas, Rick Squire, David Douch, Ian Campbell, Mimi Chen

Submission 54

Archean 'Dolerites': stratigraphic architecture, emplacement origins and association with orogenic gold

'Dolerites' make up a significant proportion (~30-50%) of Archean greenstone belts and are hosts to major orogenic gold deposits, yet their emplacement origins, internal architecture, and relationship to mineralization remain contentious and poorly documented. We present results of field mapping (drill core), whole rock geochemistry and magnetic susceptibility of several mineralized and barren 2.7 Ga 'dolerites', including the world class Golden Mile Dolerite (54 Moz), from the Eastern Goldfields Superterrane (Yilgarn Craton, Western Australia). 'Dolerite' (cf diabase) is a colloquial term used to describe any medium to coarse-grained mafic rock and includes other products of differentiation that formed together as one cooling unit. The examined 'dolerites' range from 30 to 450 m thick (~200 m average), are primarily hosted in mudstones or basalt, are concordant, and most extend for 10's of km's. There is a general stratigraphy, from base to top, starting with a lower chilled margin that grades from basalt into peridotite +/- pyroxenite, a middle gabbro/dolerite, and an upper quartz gabbro/dolerite, which grades into an upper chilled basalt margin. Granophyric veins and pods are common in the upper third of 'dolerites'. Within this framework there is variability in the relative thickness and the number of lithofacies (eg, several examples also include basalt in the middle), and all 'dolerites' exhibit numerous groundmass grain size fluctuations. Comparison with young ponded lavas demonstrates the ambiguity of many features for distinguishing intrusions from extrusions. The top contact can provide the key evidence for an intrusive origin (apophyses and peperitic margins), but for many Archean examples the evidence is unclear and/or has low preservation potential (e.g., ropy surfaces). Most internal characteristics of 'dolerites' are not unique to intrusions, however, the maximum groundmass grain size (excluding granophyres) of the Archean 'dolerites' (>2 mm) is significantly coarse than that for young ponded lavas (40 Ma younger than the host, is spatially associated with quartz dolerite/gabbro and granophyric veins and pods, all of which are exceptionally voluminous in the mineralized examples. We speculate on how these 'dolerites' developed such thick quartz-rich intervals. The outcomes of this research have implications for gold exploration as well as understanding the volcanic evolution of greenstone belts.

Elisabet Head, Antonio Lanzirotti, Matthew Newville, Steve Sutton

Submission 606

Vanadium, Sulfur, and Iron Valences in Melt Inclusions as a Window into Magmatic Processes at Nyamuragira Volcano, Africa

Micro X-ray absorption near edge structure (μ -XANES) spectroscopy measurements of sulfur (S), vanadium (V), and iron (Fe) in olivine-hosted melt inclusions (MI) preserved in tephra (1986 and 2006) and lava (1938 and 1948) from Nyamuragira volcano (D.R. Congo, Africa) are used to constrain the evolution of oxygen fugacity (fO_2) and sulfur speciation for the entrapped melts. Average calculated melt fO_2 s based on S, V, and Fe valence state oxybarometry for the 1938, 1948, and 2006 MI are all \sim FMQ-1. XANES data show that the sulfur in MI from these three eruptions is also sulfide-dominated (fO_2 and S μ -XANES data indicate more variable sulfate content. In addition, S and V μ -XANES spectra suggest they record the effects of post-entrapment crystallization within the MI. The 1986 data are best explained by water loss driven by diffusive loss of H from the entrapped melt, which results in the crystallization of sub-micron magnetite and sulfide crystallites within the MI prior to eruption. This may signify a different magma storage history compared to the other eruptions. Results demonstrate that coupled S, V, and Fe μ -XANES analysis of alkalic MI can provide accurate measures of the fO_2 of entrapped melts, and that V and S μ -XANES spectroscopy are potentially highly sensitive tools for identifying diffusive water loss in olivine-hosted MIs.

Ben Heath, Emilie Hooft, Doug Toomey, Joanna Morgan, Costas Papazachos, Paraskevi Nomikou, Michael Warner

Submission 1158

Upper crustal structure of Santorini Volcano and the surrounding region from dense, active-source seismic data

Magma body depth and geometry as well as regional tectonic setting control magma evolution and eruptive behavior. To image the entire crustal magmatic system of a continental arc volcano, we collected a dense active-source, marine-land seismic dataset at Santorini Volcano, Greece, using 155 seismic stations (90 ocean bottom seismometers and 65 land seismometers) and over 14,000 marine sound sources. We present a P-wave travel time tomography model of the upper crustal structure beneath both Santorini and the surrounding, tectonically extended region. The preliminary upper crustal velocity model includes over 100,000 Pg travel time picks. Regionally, we find the shallow (<2 km) velocity structure is dominated by sediment filled grabens (low-velocity anomalies) bounded by horsts of metamorphosed basement (high-velocity anomalies). Below southeastern Santorini, we recover high-velocity seismic anomalies, which correspond to a metamorphic block. Within the northern caldera basin of Santorini, we find a low-velocity anomaly that directly overlies the area of 2011-2012 inflation; this anomaly is shallower (~1-2 km depth) than the inferred inflation source (4-4.5 km depth). At 4-5 km depth beneath the northern caldera basin strongly attenuated arrivals and associated low velocity anomalies provide preliminary evidence for magma associated with the deformation source. These tomography results are compared with geodetic and petrologic models of the upper crustal magmatic system.

Elias Heimisson, Paul Segall

Submission 151

Imaging a propagating dike through joint inversion of seismic and geodetic data: Application to the 2014 Bardarbunga dike, Iceland.

Seismicity and deformation have been successfully used to study volcanic processes, for many years. Yet, most studies do not jointly interpret the two types of data in a quantitative manner, although they are signatures of the same underlying mechanism. Those that do consider deformation and seismicity usually only do so in a qualitative sense. In this study, we develop a method to jointly invert the seismicity and deformation data in a quantitative manner, and apply the method to image the 2014 Bardarbunga dike in Iceland using a physics based dike model.

In order to predict both deformation and seismic data the model must both accurately capture the far field deformation and near field stresses, the latter requirement negates the use of the conventional kinematic dislocation models with ad hoc regularization. We formulate a physics based boundary element crack model with only two time dependent free parameters, magma pressure and dike length, which, nevertheless, fit the GPS time-series well. A novel aspect of the model is the introduction of an under pressured crack tip cavity, the length of the cavity is solved for such that the stress singularity is cancelled everywhere around the periphery of the dike. We related the stress changes as the dike propagates to cumulative number of earthquakes by implementing the seismicity rate theory of Dieterich (1994), which we compare to the observed time series of cumulative number of events within discrete volume elements. We find GPS and seismic data to be complimentary, were GPS is sensitive to dike overpressure and rough dimensions, but seismic data is more sensitive to the location of the dike tip. The model allows us to simulate seismicity and investigate how governing parameters, such as magma density, crack tip cavity pressure, in situ stresses and frictional constitutive parameters, alter the space-time evolution of the seismicity. We thus show that by quantitatively combining geodetic and seismic data to image a physics based dike model we not only attain additional constrains on dike geometry, but also gain insight into a wide range of processes from earthquake triggering to tectonic loading of the crust.

Jussi S. Heinonen, Tobias Fusswinkel

Submission 444

High Ni and low Mn/Fe in olivine phenocrysts from peridotite-derived magmas from the Karoo LIP

Nickel contents and Mn/Fe in olivine phenocrysts have been suggested to reflect the mineral composition of the mantle source of the host magma. Specifically, absence of olivine in the source (i.e. pyroxenitic source) lowers KD for Ni and increases KD for Mn relative to Fe thus resulting in elevated Ni and low Mn/Fe in the partial melt, which is then recorded by olivine phenocrysts. Initially these “pyroxenite source tracers” were suggested to be inert to variations in mantle melting conditions, but recent studies have highlighted the effects of temperature, pressure, and wetness of the source. Here we present high-precision LA-ICP-MS olivine trace element data for a well-characterized suite of meimechitic (or Ti-rich komatiitic) dikes from the Jurassic ~180 Ma Karoo large igneous province. The studied Fo_{82–92} olivines show relatively high Ni (2430–3570 ppm) and low 100*Mn/Fe (1.32–1.5; Mn = 890–1570 ppm) that are compatible with pyroxenite-rich (37–75%) sources. In contrast, many other source indicators such as parental melt MgO and whole-rock Zn/Fe, MgO/CaO, FC3MS, Zr/Y vs. Nb/Y, and radiogenic isotope (Sr, Nd, Pb, Os) compositions strongly favor a depleted peridotite source similar to those of MORBs. Instead, the high Ni and low Mn/Fe in the olivines are likely to reflect anomalously high temperatures and pressures of mantle melting and high water contents (evidenced by kaersutite-bearing inclusions in olivine) in the peridotite source of the studied rocks. Our findings suggest that olivine Ni and Mn/Fe are rather poor pyroxenite source indicators on their own and they should only be used for qualitative comparison of primitive volcanic rocks that originated under fairly similar mantle conditions.

Jussi S. Heinonen, Arto V. Luttinen, Teal R. Riley, Sanni Turunen

Submission 446

Sublithospheric mantle sources of the Karoo LIP

Two decades of research in the Antarctic portion of the Karoo large igneous province (LIP) has revealed at least four Mg-rich magma types that represent near-primary melts derived from the deep mantle beneath the Gondwanan lithosphere. Two of the magma types record evidence of recycled pyroxene-rich source lithologies, but they seem to have sampled anomalous mantle heterogeneities rather than essential source components for the Karoo LIP as a whole. Two other magma types represent relatively high- and low-pressure partial melts from long-term depleted mantle sources resembling those of some modern mid-ocean ridge basalts (MORBs) from the Southwest Indian Ridge. This MORB-source affinity is contrasted by the high crystallization temperatures calculated on the basis of Al-in-olivine thermometry (~1500 °C), which may have been caused by a mantle plume or internal mantle heating. Energy-constrained assimilation-fractional crystallization modeling suggests that magmas from such depleted sources could have been parental to many Antarctic flood basalts that show geochemical indications of interaction with continental lithospheric materials. The majority of the Karoo flood basalts, especially from Africa, show even stronger affinity to continental lithosphere and their possible relationships to sublithospheric sources may have been overprinted beyond recognition. Recent findings of picrites with chondritic isotope characteristics from Mozambique, Africa, may shed light on this issue. They may turn out to be the first example of Karoo magmas that can be associated with primordial sources similar to those recognized for some (plume-related) LIPs and oceanic islands.

Scott Henderson, Matthew Pritchard, Francisco Zoffoli, Michael Poland, Juliet Biggs, David Arnold, Susanna Ebmeier, Christelle Wauthier, Kirsten Stephens, Kendall Wnuk, Falk Amelung, Eugenio Sansosti, Simona Zoffoli, Patricia Mothes, Orlando Macedo, Luis

Submission 962

Lessons learned from coordinated regional multi-satellite volcano observations 2013-2017: The CEOS Latin America pilot project

Within Latin American, about 315 volcanoes have been active in the Holocene, but 202 (>60%) of these volcanoes have no seismic, deformation or gas monitoring. Following the 2012 Santorini Report on satellite Earth Observation and Geohazards, the Committee on Earth Observation Satellites (CEOS) developed a 3-year pilot project to demonstrate how satellite observations can be used to monitor large numbers of volcanoes cost-effectively, particularly in areas with scarce instrumentation or difficult access. The pilot aims to improve disaster risk management by applying a full spectrum of remote sensing data and techniques to track volcanic unrest and eruption, working directly with both the volcano observatories that are governmentally responsible for volcano monitoring as well as with international space agencies that collect and distribute data (ESA, CSA, ASI, DLR, JAXA, NASA, CNES).

Here we highlight several case studies where CEOS data have successfully been used by volcano observatories to monitor volcanoes and respond to crises: For example, Chiles / Cerro Negro, Ecuador and Colombia; Nevado de Ruiz, Colombia; Sabancaya, Peru; and Calbuco, Chile. InSAR and other remote sensing data have served as an independent check on ground sensors, guided the deployment of new instruments, and ultimately provided input to help local authorities determine appropriate alert levels. We describe several lessons learned about the type of data products and information that are most needed by the volcano observatories in different countries. We propose a strategy for regional satellite volcano monitoring for use by volcano observatories in Latin America and elsewhere.

Christopher D. Henry, Stephen B. Castor, William A. Starkel, Ben S. Ellis, John A. Wolff, Joseph A. Laravie, William C. McIntosh, Matthew T. Heizler

Submission 596

The McDermitt caldera, northern Nevada and southeastern Oregon, USA: Diverse 16 Ma, silicic magmatism during initiation of the Yellowstone Hotspot

Based on detailed and reconnaissance geologic mapping, extensive petrographic and chemical analysis, and high-precision $^{40}\text{Ar}/^{39}\text{Ar}$ dating, a single McDermitt caldera formed from eruption of the 16.39 ± 0.02 Ma (FC-2 sanidine at 28.201 Ma, $\lambda_{\text{total}} = 5.463 \times 10^{-10} \text{ yr}^{-1}$) McDermitt Tuff, during a voluminous, ~ 16.7 - 16.1 Ma pulse of silicic magmatism focused around the caldera. Rhyolite lavas erupted as early as 16.69 Ma, interbedded with late Steens Basalt, and the proportion of rhyolite increased steadily up to eruption of the McDermitt Tuff. Precaldera silicic activity was almost entirely effusive and consisted of metaluminous to mildly peralkaline, sparsely anorthoclase-phyric rhyolite to peralkaline, aphyric rhyolite to peralkaline, quartz-sanidine-sodic amphibole-phyric rhyolite at 16.41 Ma. Metaluminous to peraluminous, quartz-sanidine-plagioclase-biotite rhyolite lavas and domes were emplaced around what is now the caldera wall in four areas at 16.62, 16.49, and 16.38 Ma. The McDermitt Tuff is strongly zoned from peralkaline, aphyric, high-Si rhyolite (comendite) to metaluminous, abundantly anorthoclase-phyric, trachydacite or icelandite. The diversity of silicic rocks emplaced over a few 100 ka implies multiple independent magma chambers.

The McDermitt caldera is irregularly keyhole-shaped, 40 x 30 to 22 km. Collapse occurred mostly along a narrow zone of discrete ring faults with variable downwarp into the caldera between faults. Minor, parallel faults locally widen the zone to as much as 6 km. We find no evidence that the McDermitt caldera consists of multiple, nested calderas, as previously postulated. Total collapse was no more than about 1 km, and total erupted volume was $\sim 1000 \text{ km}^3$ (DRE), of which 50 to 85% is intracaldera tuff. Mega- and mesobreccia are common in intracaldera tuff. Intracaldera tuff is strongly rheomorphic as is outflow tuff where it was deposited over steep topography. Post-collapse resurgence was driven by intrusion of icelandite magma that produced widespread lavas from two major vents until ~ 16.1 Ma.

Our data and published work show that silicic volcanism around the McDermitt caldera is amongst the oldest of the Yellowstone hotspot. Silicic activity ≥ 16 Ma is widespread across $\sim 40,000 \text{ km}^2$ of northern and northwestern Nevada and southeastern Oregon to southwestern Idaho attesting to a wide footprint for the hotspot.

Richard Herd, Marie Edmonds, Julia Woitischek, Bruce Houghton, Andrew Woods

Submission 354

Understanding the geochemical evolution of gas bubbles and slugs in outgassing basaltic conduits

Of the top volcanic outgassers on Earth, a large fraction are basaltic, open vent volcanoes, persistently delivering volatiles to the atmosphere through magma-filled conduits. Our ability to obtain high resolution observations of the composition of gas emitted during such activity has undergone rapid improvement in recent years, allowing time series of ratios between different gas species to be generated, e.g. the ratio of carbon to sulfur. It has been observed empirically that the bursting of large gas slugs and bubbles is associated with CO₂-rich gases and that lower energy outgassing, involving smaller bubbles, are more H₂O- and sulfur-rich. The dependence of the gas composition on bubble size and rate of ascent has not however, been modelled quantitatively. Here we present a model to illustrate the evolution of the gas composition of bubbles during rise through melt in a conduit, using a range of initial bubble populations and sizes. We allow the bubbles to undergo coalescence, expansion and growth through mass diffusion, limited by the rate of ascent. We vary the initial bubble size distribution to account for new results from analogue experiments showing that larger gas bubbles may be generated under crystal-rich conditions. We generate synthetic volcanic gas time series that may be compared with data from a range of natural outgassing volcanoes such as Kilauea and Stromboli, to understand their variability in style and intensity and their dependence on bubble dynamics in the conduit.

Stephen Hernandez

Submission 1173

Material changes at Guagua Pichincha, Ecuador gleaned from coda wave interferometry

Volcán Guagua Pichincha is an active stratovolcano of dacitic composition located 12 km west of nearly 2 million urban inhabitants. Seismic activity at Pichincha is characterized by regularly reoccurring, short duration (8000 individual events over a span of 24 months. Via a hierarchical clustering analysis, multiple groups are discovered with differences in waveforms manifesting primarily in the coda, indicating possible material changes over time. One abrupt change in particular occurs soon after the occurrence of the 16 April Mw7.8 Pedernales earthquake off the coast of Ecuador. We investigate the origins of this change as they relate to dynamical stresses imparted by the large coastal mainshock and/or its numerous aftershocks.

Pedro A. Hernández, Gladys Melián, Nemesio García, Luca D'Auria, María Asensio-Ramos, Eleazar Padrón, Mar Alonso, Fátima Rodríguez, Marta García-Merino, Germán Padilla, Cecilia Amonte, Aarón Pérez, Rubén García, David Calvo

Submission 836

Observed anomalous changes of diffuse CO₂ emission at the summit crater of Teide volcano (Tenerife, Canary Islands): evidence of volcanic unrest or increase gas release from a stationary magma body?

The summit crater of Teide volcano is characterized by the presence of a weak fumarolic system and high rates of diffuse volcano-hydrothermal CO₂. Diffuse CO₂ emission surveys have been performed since 1999 at the same 38 observation sites homogeneously distributed within an area of about 6,972 m², to determine CO₂ emission rate and to evaluate the relation between its temporal variations and seismic-volcanic activity. Measurements were carried out following the accumulation chamber method with a non-dispersive infrared (NDIR) CO₂ analyzer LICOR LI-820. Sequential Gaussian simulations (sGs) were used for mapping and estimate the volcanic diffuse CO₂ emission rate at each survey. From the beginning of this study in 1999 to March 2017, estimated diffuse CO₂ emission rates from summit crater of Teide have ranged between 2.0 and 176.1 t d⁻¹, with an average value of 27 t d⁻¹. Until November 2016, diffuse CO₂ emission rates ranged between 2.0 and 42.2 t d⁻¹, but from that month a sharp increase is observed reaching the maximum of the time series in February 2, 2017. Historical seismic activity in Tenerife has been characterized by low- to moderate-magnitude events (M 2 emission was registered, from 21.3 to 101.7 td⁻¹. This signal preceded the occurrence of a ML=2.5 seismic event in January 6, 2017, the strongest earthquake located inside Cañadas caldera since 2004. No significant horizontal and vertical displacements were registered by the Canary GPS network belonged to INVOLCAN. This increase in the emission rate was followed by a decrease to 70.4 td⁻¹ and a new continuous increase to the maximum recorded value of 176.1 t d⁻¹ on February 2, 2017. After this date, the time evolution shows a continuous decrease in the emission rate. The January 6 seismic event was probably due to the increase of fluid pressure in the hydrothermal-magmatic system of Tenerife. The anomalous increase observed on the diffuse CO₂ emission rate from summit crater of Teide suggests the occurrence of a volcanic unrest episode or an increase of gas release from a stationary magma body and could be a precursory geochemical signal of future increase in the seismic-volcanic activity of the island.

Julie Herrick, Sarah Henton De Angelis, Marguerite Toscano

Submission 843

Provenance of Floating Pumice in the Caribbean: Big Data and Hierarchical Clustering

Pumice rafts have not been observed in the Caribbean Sea since the delta-forming stages of the Soufrière Hills eruption of Montserrat (1995–2005). Pyroclastic flows reached the sea in 1996, allowing strands of pumice to drift from shore. The rare occurrence of pumice rafts cannot account for the high frequency of pumice findings along the Caribbean shore, particularly those of Colombia, Panama, Belize, Mexico, and Florida where rhyolitic pumice (floating and stranded) has been observed as early as 1947. Our collection of these samples represents a correlation challenge and we have developed a method to statistically determine the provenance based on geochemical “fingerprinting.” Possible pumice contributors to the Caribbean Sea include numerous geographically dispersed volcanic centers. The very large number of possible source volcanoes/eruptions discourages simple techniques for identifying matching samples (e.g., TAS and Harker diagrams); these methods were found to be time consuming, inefficient, and inaccurate. To better identify the provenance of the floating pumice, we compiled a database of glass and whole rock major and trace element geochemical data from volcanoes throughout Central America, northern South America, the Atlantic Ocean, and the Mediterranean. Data were sourced from the GEOROC database (maintained by the Max Planck Institute for Chemistry), the RU_CAGeochem database (compiled by Rutgers University), and selected published studies identified through our own literature review. In total, our database includes 435 lines of volcanic glass data and 2,949 lines of whole rock geochemical data. These data represent 290 discrete volcanoes, volcanic groups, and/or eruptions. Caribbean pumice compositions were added to the database, which was then analyzed using simple cluster analysis and hierarchical cluster analysis techniques using the MATLAB software package. The results produced a short-list of possible source volcanoes/eruptions. From this short-list, we were able to use simple criteria (e.g., possible transportation paths, eruption size, eruption age) to identify Atitlan Volcano, Guatemala, as the most likely source for the floating pumice.

Richard Hey, Ármann Höskuldsson, Fernando Martinez

Submission 1309

Shallow and deep submarine volcanoes at the Vestmannaeyjar archipelago and southern end of the Reykjanes Ridge

We shall present bathymetric data from the Vestmannaeyjar Archipelago, off shore south Iceland and from the southernmost tip of the Reykjanes ridge across the Bight transform fault. In Vestmannaeyjar water depth is between 0 and 200 m and the area is characterized by fluctuation in sea level during the past 11 ka. Most of the volcanic formations are thus representing shallow water submerging explosive volcanic eruptions. At Reykjanes ridge water depth is considerably higher, or between 1500 and 3000 m. At high water depths, magmatic volatiles at MORB compositions are kept in magma solution, thus preventing explosive activity and favoring effusive eruptions. Therefore pillow ridges and sheet lavas are commonly observed with occasional caldera or pit crater formation along the ridge axis. Further volcanic ridges and tectonics within the axial rift valley are perpendicular to the rift directions. Tectonic faults bounding the rift valley and away from it are however, highly oblique to the rift. Off rift volcanic formations are commonly observed in the area, they are less faulted and overprint the oblique striking boundary faults. These volcanic formations show well developed pyroclastic crater formations with or without associated lava flow. This suggests higher volatile content of the erupted magma.

James Hickey, Ryan Lloyd, Juliet Biggs, David Arnold, Patricia Mothes, Cyril Muler

Submission 399

What's causing asymmetric flank deformation at Tungurahua volcano, Ecuador?

Tungurahua volcano, a steep stratovolcano in the Eastern Cordillera of the Ecuadorian Andes, has been persistently active since 1999. The current volcanic edifice (5023 m) is built upon the remnants of two former edifices that were partially destroyed by large-scale flank collapse. The most recent collapse occurred approximately 3000 years ago and resulted in loss of the western flank. This flank has again been built up to its current extent and has steep slopes of 30 – 35°. During the ongoing post-1999 eruptive activity, this western flank has undergone significant surface deformation, with the highest rates contained within the modern amphitheatre-shaped scar from the 3000-year-old failure. The surrounding flanks are relatively undisturbed. Previous studies have investigated the cause of this asymmetric deformation using analytical models but have not considered topographical or heterogeneous mechanical effects. A dipping magmatic source has been inferred as the likely cause. Here we present a range of models using the Finite Element Method to examine this and other possible causes of the uneven deformation, including asymmetric subsurface material properties, surface topography effects, and shear stress along a fracture. Our models are informed by InSAR measurements of the deformation episode in October/November 2015, using the Sentinel-1, Cosmo-SkyMed and ALOS-2 sensors with a combination of descending and ascending line-of-sight scenes. These data show a maximum displacement of around 3.5 cm over a period of roughly 4 weeks. Analysis of the models and the physical mechanisms that can cause the asymmetric deformation will have different implications for future potential flank collapse hazard and magma ascent mechanics. Data was sourced from the CEOS Volcano Pilot and GEO Supersites projects.

Anna Hicks, Teresa Armijos, Jenni Barclay, Jonathan Stone, Richard Robertson, Gloria Patricia Cortes

Submission 1088

Risk Communication Films: Process, product and potential for improving preparedness & adaptation

Film is a well-established medium for education and communication about hazardous phenomena; providing engaging ways to directly view hazards and their impacts. Empirical analysis can help to understand films' effectiveness in informing populations at risk and catalysing actions to reduce risk.

We present an evidence-based methodology to create, use, and track the outcomes of digital film tools designed to raise hazard and risk awareness and develop preparedness efforts. Experiences from two contrasting eruptions were documented (Nevado del Ruiz, 1985 and Soufriere St Vincent, 1979), with a secondary purpose of fostering social and cultural memories of eruptions, developed in response to demand from at-risk communities during field-based research. The films were created as a partnership with at-risk populations and local volcano monitoring scientists (Servicio Geológico Colombiano and the Seismic Research Centre), who consequently became the leading focus of the films, thus providing a contrast with other types of hazard communication.

We shared the final productions with communities at several local film screenings in both St Vincent and Colombia. Over 700 people attended local film screenings in at-risk areas around Nevado del Ruiz and seven screenings were held in communities located in the high hazard zones in St Vincent.

These screenings were also designed to be fora for discussion about the films, so we surveyed the audience to evaluate immediate influence of the films on learning and affect. Results indicate that the use of local content and actors to share experiences and teach valuable lessons were impactful. Recognizable faces and spaces helped to convey the disaster risk reduction messages. They also motivated audiences to consider their ownership of risk and potential actions to reduce risk and strengthen resilience.

We present evidence of the effectiveness of co-production in the design and execution of these volcanic risk reduction intervention strategies. Co-production of films with local agencies resulted in products that are contextually appropriate, meaningful for audiences, and useful risk communication tools. For example, in St Vincent, they were used to support the roll out of 'household emergency plans' and have formed part of the communication strategy for the national emergency management organisation.

This research is part of the Strengthening Resilience in Volcanic Areas (STREVA) project.

Silvana Hidalgo, Jean Battaglia, Santiago Arellano, Daniel Sierra, René Parra, Pablo Samaniego, Peter Kelly, Benjamin Bernard

Submission 1256

The Cotopaxi 2015 eruptive phase: insights from gas and glass

Cotopaxi volcano (5,897 m) is located 50 km south of Quito, the capital of Ecuador. In April 2015, a progressive increase in the amplitude of transient seismic events initiated volcanic unrest. Starting on May 20, an increase in SO₂ emissions from ~500 t/d to ~3000 t/day followed the increased seismic activity. Both SO₂ emissions of up to 5000 t/day and seismic tremor were observed until August 14 when a swarm of volcano-tectonic earthquakes preceded the first hydromagmatic explosions.

Unrest continued after August 14, with three episodes of ash emission. However, the intensity of ash fallout, average seismic amplitude, and SO₂ emissions during each successive episode progressively decreased. Both, BrO and HCl were detected in the plume by ground-based DOAS and FTIR remote sensing, and airborne direct measurements with a Multi-GAS indicated a CO₂/SO₂ (molar ratio) of ~1 - 2. These measurements showed that sulfur was speciated almost completely as SO₂. The gas composition of the plume clearly indicates a shallow magmatic source driving the activity of this period. Since late November 2015, surface manifestations and all monitored parameters have shown marked decreases.

We analyzed juvenile glass and plagioclase microlites rim compositions from the emitted ash using an electron microprobe and calculated the last equilibrium pressures and temperatures of the magma using an empirical plagioclase-liquid thermometer and barometer (Putirka, 2008). Our results record three different equilibrium pressures around 5, 3, and 2 kbar, indicating a slow or “stepwise” ascent from a deeper reservoir. Calculated equilibrium temperatures are around 1050 °C, in agreement with the andesitic composition of the juvenile magma. Chlorine is still present in the glass (up to 1115 ppm) but sulfur and fluorine were below detection limits, which suggest that they had nearly completely degassed from the ascending magma. From May-November 2015 about 470 kt of SO₂ degassed from Cotopaxi. Based on S balance between inclusions (1800 ppm) and S-free glass, we estimate that 65 million m³ of magma were intruded assuming that all of the emitted SO₂ was of a magmatic origin. Compared to eruptive volumes of 4.8×10^5 m³ (Bernard et al., 2016) this equates to eruption of less than 1% of the intruded magma.

Dannie Hidayat, Cahya Patria, I Gede Suantika, Warseno Warseno, Hendra Gunawan, Benoit Taisne, Dini Nurfiani, Chiou Ting Tan

Submission 736

Precursory long-period events and tilt signals to the explosion events at Marapi Volcano, West Sumatra, Indonesia

Marapi Volcano's activity is characterized by Strombolian to small Vulcanian explosions with occasional VEI 2 events producing tephra and pyroclastic flows. Currently in collaboration between Earth Observatory of Singapore (EOS) and Centre for Volcanology and Geological Hazard Mitigation (CVGHM), the volcano is seismically monitored with 7 broadband stations, and 2 short-period stations. In addition, we deployed 2 tiltmeters and an experimental soil CO₂ sensor. These stations are telemetered by 5.8GHz radio to Marapi Observatory Post where data are archived and displayed for Marapi observers for their daily volcano activity monitoring work. We also archive the data in the EOS and CVGHM main offices. Data are being utilized by volcano scientists of CVGHM and researchers in both institutes as well as university students in and around them. We present correlation between tornillo events, a kind of long-period earthquakes that are often recorded at Marapi, and tilt signals prior to explosion events at this volcano. Tilt changes mostly occurred before tornillo events. Of the two tilt stations, the flank station recorded changes earlier than that the summit station suggesting a shallowing pressure source. These changes followed by increased numbers of tornillo and tremor events a few days later. In the more ideal case, swarms of shallow VT events occurred prior to the explosion. Possible mechanisms will be discussed to explain the observations. Our study attempts to understand the state of the volcano based on monitoring data, which will enable us to better estimate the hazards associated with future small explosions or eruptions.

Kaylon Higgenbotham, Ben Kennedy, Thomas Walter

Submission 740

Shake and wake: investigating how earthquakes trigger volcanic activity by shaking bubbles in shear thinning fluids as an analogue for magma chambers during earthquakes.

Shaking bubbles in a shear-thinning magma analogue provides insight into how seismic shaking affects magma bodies. Volcanic eruptions connected to earthquakes have been recorded since the 19th Century. Anecdotal evidence, statistical studies, and numerical modelling indicate that both near- and far-field earthquakes can trigger volcanic activity. However, little experimental work has been done to constrain the dynamic interaction between the seismic trigger and the bubbly magma. Bubbles were injected into homogenous, silicon oil with a shear thinning rheology in a sealed tank and then subjected to shaking. The viscosities of the fluids tested were 2,000 Pa s, 10,000 Pa s, and 30,000 Pa s, simulating different magmas. Duration (s), displacement (mm), and frequency (Hz) of shaking were varied and the rate of bubble rise measured and bubble deformation recorded. Results indicate that bubble rise rate is affected by shaking exceeding accelerations over 0.5 g during which bubble rise rate increased by 1.91 % to 13.33 %. A positive correlation exists between increasing rise rate and higher acceleration of shaking. However, viscosity, bubble size, and displacement of shaking do not appear to directly affect bubble rise rate. Duration indirectly affects bubble rise as the rise rate increase occurs only during shaking. Measured increase in rise of bubbles has implications for advective pressure increases and outgassing of magma following earthquakes. Rheology data for the fluid indicates that at the strain rates of the experiments some shear thinning behaviour could be expected to lower the measured viscosity, which may be reflected in the increased rise rates of bubbles. During shaking bubble shear was measured as bubbles became slightly deformed by dominantly simple shear and contraction. Higher accelerations in our fluids result in a greater range and maximum value of shear strain. This gives rise to a capillary number allowing bubbles to deform. Fluid dynamics offer additional explanations for an increase in bubble rise rate associated with asymmetric bubbles such as a net lift that develops associated with lateral fluid flow around asymmetric bubbles, similar to aircraft wings, which promotes upward movement of bubbles. Therefore, bubble shear, combined with lowered viscosity due to the shear strain rate viscosity dependence of the fluids, may be mechanisms driving increased bubble migration during shaking.

Anthony Hildenbrand, Fernando Ornelas Marques, Aurore Sibrant, Ana Costa, Christian Hübscher, Benedikt Weiß

Submission 421

Tectonic control on volcano growth and large landslides near the Azores Triple Junction

The Azores volcanic archipelago in the Atlantic has developed near the Azores Triple Junction (ATJ), where North America (NA), Eurasia (Eu) and Nubia (Nu) plates meet. It constitutes a natural laboratory of major interest to constrain the relationships between magmatism and tectonics, and to relate magmato-tectonic processes and volcano flank instability. Most of the recent volcanism (<1.5 Ma) is constrained along the present eastern branch of the ATJ (Eu-Nu boundary), which comprises a hyper-slow active oceanic rift in the east (Terceira Rift, TR) and a series of horst and graben structures closer to the ATJ, where deformation is diffuse. From geomorphological, structural, geochronological, geochemical, geophysical and geodetic data, we show that (1) volcano growth has been influenced by regional tectonics through the gradual development of narrow volcanic ridges and elongated islands, with dominant orientation in the range N110-N150, i.e., consistent with the main directions of the regional tectonic structures and the distribution of earthquakes; (2) no significant age progression is evident over a distance of ca. 300 km; (3) instead, all the islands have grown through successive, partly coeval brief episodes (<50 kyr) of intense volcanism, which supports distinct major episodes of deformation at the regional scale; (4) most islands are cut by normal faults and dyke swarms striking N110 to N150, plus an additional N050-N070 trend interpreted as the transform direction accommodating the present differential movement between Eu and Nu in the Azores; (5) central volcanoes are generally located at the intersection between the various trends, whereas individual trends are highlighted by linear chains of strombolian cones, which often deviate from the main pattern, likely due to local perturbation of the stress-field by adjacent volcano load; (6) at least ten major flank collapses and one active slump during the last 1 Myr have been recently recognized, often repeatedly cutting a given island; (7) flank collapses have affected edifices of small/moderate size (<5 km tall from seafloor), and occurred along major structural directions, suggesting that flank destabilization not solely results from gravitational instability, but was controlled by volcano-tectonic processes. Similar link between tectonics, volcanism and landslides is observed for Santa Maria extinct island (>2.8 Ma), which can be used to track the earlier position of the Eu-Nu plate boundary.

Wes Hildreth, Judy Fierstein

Submission 441

Constructing an Eruptive History Demands Detailed Mapping

Our mapping of volcanic areas produces eruptive histories that characterize magnitudes, styles, and episodicity of all past activity. We ultimately construct time-volume-composition records that distinguish great eruptions from small and document variation of inter-eruptive intervals, thereby avoiding simplistic or misleading averages. Recognizing the full range of past behavior of an edifice or volcanic field provides an essential complement to real-time instrumental monitoring. Meaningful definition of eruptive units and temporally clustered eruptive groups requires ample compositional data, radioisotopic dating, and paleomagnetic determinations. Lab work is synchronous with field mapping and iterative over several seasons, not deferred until mapping approaches completion. We plan at the outset to map the whole volcanic system, including peripheral vents. Grouping of eruptive units is by temporal and sectorial packages from each vent site, whether point source or fissural. Robust definition of packages relies on recognizing chemical, mineralogic, and lithologic affinities and on establishing timelines by precise dating, tephra deposits, weathering surfaces, or special contact relations. Because nearly every contact in a volcanic terrain is rough and irregular, contacts are walked and scrutinized for the influence of preeruptive topography, syneruptive scour, and constructional morphology, not merely for long-term weathering, erosion, and deformation. Sectorially distinct depositional sequences need to be correlated and dated in order to reconstruct adequately the eruptive history of the whole system.

Methods emphasized in each volcano-mapping project evolve empirically as needed. Eruptive units are subdivided into complex proximal facies, pyroclastic flows and lava flows, and distal fragmental flows, fall units, and sediments. We favor splitting, because lumping can obscure details or lead us to overlook or neglect features that may later be realized important. We avoid defining "formations," as this can inhibit new perspectives and invites bureaucratic impediments to revision. Volcanoes come in many forms, sizes, proportions of lithologically varied products, degrees of exposure, eruptive episodicity, and magnitudes and styles of eruption. We reject the straightjacket of formalizing field-mapping procedures.

Wes Hildreth, Judy Fierstein

Submission 442

Simcoe Mountains Intraplate Volcanic Field East of the Cascades

The Simcoe Mountains volcanic field of south-central Washington drapes ~1,660 km² of the Yakima Foldbelt. Its eruptive products are mostly mildly alkalic intraplate basalts, along with a continuum of intermediate alkalic fractionates, subordinate subalkalic basalts, and sparse rhyolites and low-K tholeiites. They erupted at ~205 exposed vents, mostly scoria cones and small shields that range from ~4 Ma to 0.6 Ma. Only a modest fraction of the field is Pliocene; most of it is early Pleistocene. A common error lumps the Simcoe volcanic field with the Cascade arc, which lies adjacent to its west. It is, instead, a distributed field dominated by intraplate basalts that have OIB-like chemical signatures and fractionate to alkalic intermediates, not to arc andesites. Some carry mantle xenoliths and xenocrysts. The volcanic field is divisible geographically into three parts by a parallel pair of east–west trending basement anticlines—elements of the Yakima Foldbelt—which consist of Miocene flood lavas of the Columbia River Basalt Group and form the basement through which Simcoe volcanoes erupted. The southern part is a 460-km² area that extends from the southerly anticline nearly to the Columbia River and is largely on private lands. It has ~50 vents and two main components—a 35-km³ Pliocene tholeiitic shield and a 5-km³ scattering of Pleistocene alkalic scoria cones. The 950-km² central part, now mapped in detail, extends 60 km east–west, drapes both anticlines, and has ~110 vents, mostly alkalic, including several multivent shields. The 250-km² northern part extends 25 km northwest from the northern anticline to the rugged headwaters of the Klickitat River, where it adjoins the Goat Rocks arc-volcanic cluster. It has ~25 vents, including several small shields, is largely mafic subalkaline, is older than 3 Ma, and is deeply incised by canyons. The northern and central parts are within the Yakama Indian Nation and open only to enrolled members and permittees. Most products, whether alkalic or tholeiitic, are high-Fe, high-K, and enriched in Nb, Zr, and Ti relative to Cascade arc suites. About 25% of 1300 samples are mafic subalkaline. Only a few units are rhyolites, low-K basalts, and trachytes. Activity was concentrated 4.1–3.2 Ma, 2.2–1.2 Ma, and 1.0–0.6 Ma. No units are known to have erupted 3.1–2.3 Ma. No systematic space-time distribution is recognized in the central and southern parts, where the oldest and youngest vents are clustered and overlapping.

Nicholas Hinz, Mark Coolbaugh, Pete Stelling, Lisa Shevenell

Submission 1303

Structural–Tectonic Characteristics as indicators of geothermal potential on active subduction zone volcanoes

There are currently 74 productive geothermal systems associated with volcanic centers (VCs) in arcs globally, including actively producing systems, past producing systems, and systems with successful flow tests. These 74 productive VCs constitute 10% of 732 VCs distributed across more than a dozen major arcs around the world. The total installed or tested capacity of these 74 geothermal systems is 7,605 MWe, ranging from 0.7 to 795 MWe per system, and averaging 90.5 MWe per system. The intra-arc tectonic setting is highly variable globally, ranging from extension to compression, with varying strain rates, and structural styles of accommodating strain. This study looked to see if there is a correlation between structural and tectonic characteristics of individual volcanic centers and geothermal potential. Five summary parameters were characterized; tectonic setting (e.g., extensional or compressional), angle of plate convergence relative to the arc axis, distribution of Quaternary fault activity, fault slip rates, and local structural setting. Results demonstrate that each of these parameters have associations with the electrical productivity of volcanic centers (MWe/VC). The regional tectonic setting of the 74 VCs include 11 (15%) extensional, 43 (59%) transtensional, 4 (5%) transpressional, 7 (9%) compressional, and 9 (12%) unknown environments. Importantly, 73% of the VCs are in extensional or transtensional environments and these are responsible for 88% of the total known MWe capability in global arc settings. At a local scale the VCs are associated with a number of structural settings, including 10 (14%) in pull-aparts along strike-slip fault zones, 15 (20%) in association with displacement transfer zones where strike-slip faults merge with normal faults, 4 (5%) in normal fault accommodation zones, 7 (9%) in normal-fault step-overs, 22 (30%) associated with major fault intersections, 4 (5%) in other settings, and 12 (16%) in unknown settings. Of these structural settings, the pull-aparts, displacement transfer zones, step-overs, and accommodation zones accounted for 49% of the productive VCs and 76% of the total MWe. In contrast, the fault intersections included 30% of the VCs but only 16% of the total MWe. One primary conclusion is that productive geothermal systems associated with arc VCs are mining convective heat flow co-located with areas of active, extensional, intra-arc strain, and local structural complexity.

Kirsten F. Hodge, A. Mark Jellinek

Submission 534

Mixing magmas: A mechanical recipe for Earth's continental crust

The extensive mechanical mixing of injections of hot, low viscosity basaltic magma into relatively cool, highly viscous silicic magmas is apparently required in the production of andesite, the predominant rock type of Earth's continental crust. Furthermore, varied observations show that mixing of basaltic and silicic magmas also plays a key role in triggering explosive volcanic eruptions from andesitic stratovolcanoes. However, the stirring together of magmas with widely different viscosities is virtually impossible on fluid mechanical grounds. Thus the petrologic, geochemical, and volcanological requirement of extensive magma mixing is an enduring enigma, making the origin of andesitic magmas one of the grand challenges in Earth science. Our work shows that although large viscosity variations inhibit mixing by the steady accumulation of pure and simple shear strains, the process is enhanced if crystallization of the injected basalt causes it to acquire a yield strength and a relatively high effective viscosity. Indeed, for very large viscosity variations we show that a yielding rheology favors the breakup of mafic dikes entering a convecting silicic chamber into blobs (enclaves), which are at or comparable to the crystal scale immediately after injection, consistent with observations. Such small initial scale lengths obviate the restrictive requirement of extensive stirring and stretching to cause mixing and intensify a rapid exchange of heat and volatiles, which can drive eruptions. We argue that arc andesites are an inevitable consequence of the mechanical behavior of mafic dikes as they enter silicic crustal magma chambers. Our results explain the heterogeneous character of erupted andesitic magmas at all scales and predict well-known features including compositional gaps, textural variability and irregular populations of crystal phases strongly out of chemical equilibrium. Our work also predicts the compositionally homogeneous character of more evolved (dacitic) magmas and suggests links to their tendency to erupt effusively rather than explosively.

Jenni L Hopkins, Graham Leonard, Colin J N Wilson, Marc-Alban Millet, Christian Timm, Lucy E McGee

Submission 382

Reconstructing the evolution of the monogenetic Auckland Volcanic Field, New Zealand, using a multi-criteria approach to correlate tephra deposits to their source centres

Linking tephtras back to their source centre(s) in monogenetic volcanic fields is crucial not only to reconstruct the eruptive history and evolution of the field but also to understand tephra dispersal patterns and thus the potential hazards posed by a future eruption scenario. Here we present a multi-disciplinary approach to correlate distal basaltic tephra deposits to their source centres in the Auckland Volcanic Field (AVF), New Zealand. In order to achieve these correlations, major and trace element compositions from distal tephra-derived glass are compared with published and newly obtained proximal whole rock geochemical data for the entire field. The results show that incompatible trace element ratios (e.g. (Gd/Yb)_N, (La/Yb)_N, (Zr/Yb)_N) vary widely across the AVF but show a more restricted range within samples from a single volcanic centre. These ratios are also the least affected by fractional crystallisation and are therefore the most appropriate geochemical tools for correlation between tephra and whole rock samples. However, findings for the AVF suggest that each volcanic centre does not have a unique overall geochemical signature, thus preventing unambiguous correlation of tephtras to source centre using geochemistry alone. A number of additional criteria are therefore combined to further constrain the source centres of the distal tephtras including age, eruption scale, and location (of centres, and sites where tephra were sampled). The combination of tephrostratigraphy, ⁴⁰Ar/³⁹Ar dating and morphostratigraphic constraints allow, for the first time, the relative and absolute age ordering of 48 of 53 volcanic centres of the Auckland Volcanic Field to be resolved. Eruption frequencies are shown to vary between 0.13-1.5 eruptions/kyr and repose periods between individual eruptions vary from

John Hora, Gerhard Wörner, Andreas Kronz, Axel Schmitt

Submission 1036

Progress toward Crystal Thermal Stratigraphies: relative and quantitative constraints on T-t evolution of long-lived magmatic systems

Zoned minerals record information about changing environments encountered during their growth. Changes in chemical and isotopic compositions e.g. at resorption horizons are powerful indicators of open system processes. Thermobarometers that only require analysis of one phase (while making assumptions about the melt), have been shown to provide a record of thermal inputs into a magmatic system that are comparable in resolution to records of mass inputs provided by chemical and isotopic tracers.

Near-equiline bulk U-Th suggest that rhyodacite domes comprising an early stage in the evolution of Paríacota Volcano in the Central Andes come from magmas that stagnated in the upper crust for an extended period of time. Near-eutectic bulk composition means a relatively narrow crystallization T interval for minerals from these magmas. Whereas this provides some thermal buffering at temperatures approaching the eutectic, the system's long-term persistence and eventual eruption requires that final solidification would have been counteracted by repeated heat input.

Paired U-Th disequilibrium and Ti measurements by SIMS in zircon yield snapshots of (T, t) of the magmatic system. Taken in aggregate, these frame a protracted crystallization history spanning >300ka prior to eruption, including several excursions to near-liquidus temperatures.

Titanite and amphibole provide a complementary and potentially higher-resolution record of T (albeit with only relative t): these minerals are relatively large, and like zircon, slow diffusion preserves zoning through thermal excursions. Intergrowths of small zircon and large titanite crystals provide tie-points between absolute ages provided by zircon and the high-resolution thermal record from Zr zoning in titanite. Repeated oscillations in temperature recorded by core-to-rim profiles in both titanite and amphibole indicate that these phases, like zircon, can survive recharge and pass through the same crystallization T interval several times. Intergrowths/inclusions of titanite with/in amphibole allow comparison of T recorded in each, a potentially useful cross-check of the thermometry calibrations used.

These results support (1) extended cold storage of minerals near the solidus, (2) persistence of crystals in magma chambers, encountering several different transiting melts, and (3) modulating the balance of crystallization vs. recharge is a primary control on whether a magma system changes from a storage- to eruption-dominated regime.

Adrian Hornby, Yan Lavallée, Stephen Clesham, Gavyn Rollinson, Ulrich Kueppers, Jackie Kendrick, Alan Butcher, Corrado Cimarelli

Submission 696

Advanced Characterization of Volcanic Ash using QEMSCAN® particle mineralogical analysis (PMA)

The physical and chemical properties of volcanic ash are a fingerprint for pre-, syn- and post-fragmentation processes in volcanic eruptions. However, detailed ash particle analyses are typically labor-intensive and limited by particle number and particle size range. Here, we show that QEMSCAN® PMA (an SEM-based automated mineralogy technique that maps the distribution of minerals and glass in each particle at a micron scale) can rapidly discriminate thousands of ash particles and dramatically improve the efficiency and sample size of ash analyses. We use data from two ash samples collected 500 m from the vent at Santiaguito, Guatemala to compare ash deposited following 1) a Vulcanian explosion and 2) a dome collapse with associated pyroclastic density currents. We use image analysis to measure size-dependent variation in ash particle properties. Particle size distribution is unimodal for the dome collapse ash deposit, while the ash derived from a Vulcanian explosion has a more complex size distribution and more complex particle shapes. We present novel analysis showing that the ash produced by Vulcanian activity contains a higher total fraction of glass, but particles are preferentially bordered by plagioclase, while ash deposited after the dome collapse contains less glass, but a preferential distribution of glass at particle boundaries. These observations may represent fracturing focused in differing phases under varying fragmentation regimes (e.g. abrasion, overpressure, faulting). However, trends in the properties described above cannot be directly linked to fragmentation mechanisms due to a lack of empirical data. Therefore, the same properties will be measured for ash produced experimentally under controlled conditions using shock tube, abrasion and friction apparatuses. These analyses will be compared to natural samples from Volcán de Colima (Mexico) and Mt. Etna (Italy). Diagnostic properties can then be used to predict the characteristics of ash produced in well-monitored eruptions in order to contribute to timely risk assessments to aviation. This novel characterization protocol can define links between particle properties and fragmentation triggers and processes, furthering our understanding of eruptions and associated hazards. We discuss potential applications of QEMSCAN® using the PMA mode and encourage further development of the technique within volcanology.

Claire Horwell, Andrew Apsley, Stephanie McPherson, Karen Galea, Will Muller, Susanne Steinle, Anne Sleuwenhoek, Martie Van Tongeren

Submission 1019

Testing the effectiveness of respiratory protection used to prevent inhalation of volcanic ash: filtration efficiency experiments

At the onset of a volcanic eruption, there is often great concern from the public as to whether inhalation of ash is harmful. Given that it is not usually possible to provide specific information on the pathogenicity of ash in a useful timeframe, the World Health Organization, and other agencies, take a precautionary approach and recommend that people stay indoors or, if they must go outdoors, that they wear a light-weight, disposable mask. However, there is currently a lack of evidence on the types of masks which might be effective at blocking fine particles in non-occupational settings.

The Health Interventions in Volcanic Eruptions project (<http://community.dur.ac.uk/hive.consortium/>) is building the first evidence base on the effectiveness of the range of forms of respiratory protection worn by communities exposed to ash. These range from T-shirts and bandanas, through surgical masks, to high-efficiency N95-style masks, although their use is rare. For the most part, agencies distribute surgical masks, or more basic, single-layer, non-woven masks.

At the Institute of Occupational Medicine, Edinburgh, we have characterised the material (thickness, composition and thread count of each layer) of 18 forms of respiratory protection and then subjected each mask to filtration efficiency tests. These tests were performed (3 repeats) with three dusts (volcanic ash from Sakurajima and Soufrière Hills volcanoes and aluminium oxide, chosen as a low-toxicity surrogate dust of similar particle size distribution for the following human volunteer studies) at two concentrations (1 mg.m⁻³ and 2.5 mg.m⁻³) and 2 flow rates (equivalent to 40 and 80 l.min⁻¹). Each material was held in a sample holder, within a chamber, and dust concentrations measured by TSI Sidepak, outside the mask material (challenge conc., mg.m⁻³) and also inside the sample holder (penetration conc., mg.m⁻³), to determine percentage penetration. We also tested the effect of wetting a bandana.

Overall, 4 masks performed very well with mean penetration of 2.5 mask, Indonesian basic mask provided by the Red Cross). Surgical masks had ~12% penetration and all other materials had 25-83% penetration, including wetted bandanas. The FFP2, Japanese PM2.5, Indonesian basic and a surgical mask from Mexico will now be tested for effectiveness on human volunteers with the surgical mask also being tested for improved effectiveness through adaptation with an elasticated outer layer.

Armann Höskuldsson, Thor Thordarson

Submission 1310

Debris avalanche and fluctuation in geothermal output a sign for unrest at Askja volcano Iceland

During winter 2012 ice on lake occupying Askja caldera melted at end of February. The lake normally freezes over late December and does not thaw until in June/July. Multibeam observations carried out in September 2012 reveal several large solfatara fields at the bottom of the lake, three of the solfatara fields were unknown up to fall 2012. During winter 2013 and 2014 the lake froze over as usually. In July 2014, a 20 million m³ debris avalanche occurred in the SE corner of the caldera and ran into the lake. Tsunami generated by the avalanche ran up 60-80 m in places along the coast of the lake. The avalanche is originating in an area of an old lava dome that is half buried in the SE rim and associated solfatara fields. Multibeam observations carried out in August that year reveal that about 10 million m³ of avalanche deposits are at the bottom of the lake. Further it revealed that the three of the larger solfatara field observed in 2012 on the bottom of the lake had no more activity. In both events, seismic activity was not above normal. We argue that these are signs for future eruptions at Askja.

Alicia Hotovec-Ellis, David Shelly, David Hill, Andrew Pitt, Phillip Dawson, Bernard Chouet

Submission 524

Investigating the relationship between deep long-period and deep high frequency seismicity at Mammoth Mountain, California, 2012 – 2014

Deep long-period (DLP) earthquakes are a relatively common type of seismicity observed at volcanoes worldwide, yet remain poorly understood. These events are thought to be related to the movement of magma and exsolved gases as they work their way to the surface from the mantle, and may be among the first indicators of volcanic unrest and potential eruption. Mammoth Mountain, situated on the southwestern boundary of Long Valley Caldera, California, produces prolific DLP seismicity, with long-lived clusters of activity at cataloged depths of 8 – 20 km in 1989, 1997 – 1998, and 2012 – 2014. We focus on the most recent DLP activity, the onset of which was coincident with several brief high-frequency swarms a few kilometers deeper than the DLPs. The deep seismicity occurred during a temporary deployment of 11 broadband seismometers at Mammoth Mountain, which provided improved sensitivity and location accuracy. The potential relationship between these swarms, based on their spatiotemporal coincidence, provides an opportunity to investigate the underlying physical mechanism(s). Because these DLP earthquakes occur close to each other, source—rather than path effects—control the frequency content. We use waveform cross-correlation techniques to improve the catalog’s completeness and better isolate individual clusters of repeating sources. We then use these additional observations to clarify each swarm’s structure in space and time with precise relative relocations. Initial relocations of the high-frequency seismicity since 2000 form a nearly vertical, inverted wishbone-shaped pattern in a plane striking WSW away from the summit of Mammoth Mountain. The best-relocated DLPs then form a more shallowly dipping plane spanning the two tips of the wishbone at 10 – 15 km depth.

Bruce Houghton, Tim Orr, Bianca Mintz, Jacopo Taddeucci, Elisabetta Del Bello, Damien Gaudin, Ullrich Kueppers, Rebecca Carey, Marie Edmonds

Submission 278

Transitions in style and intensity during Strombolian and Hawaiian eruptions: examples from Kīlauea in 2011-2017

Most eruption styles are distinguished by constraining mass eruption rate (or intensity). However a second rigorous criterion for defining style, especially for basaltic explosive volcanism, is the contrast between impulsive short-lived explosions and emergent prolonged episodes of fountaining. On this basis, many weak basaltic eruptions have been cataloged as either Strombolian or Hawaiian. A small number of events worldwide do not fit this two-fold classification comfortably and either have intermediate characteristics or show temporal shifts between transient and sustained behavior. These events are disproportionately significant in terms of constraining shifts in shallow conduit behavior that drive rapid transitions in activity.

Many eruptions at Kīlauea include intervals of eruption informally termed ‘spattering’ which consist of rapid bubble bursting, often through magma stagnated over the vent. This activity can precede high fountaining eruptions and/or be interspersed in time or space with fountaining. Spattering bubble-bursting occurs at frequencies 1-2 orders of magnitude higher than normal Strombolian explosions but is not sustained or steady like Hawaiian fountaining.

Activity at Halemaūmaū lava lake in 2013-2017 has permitted us to quantify patterns of extended spattering eruption. Spattering bubble-bursts occur either as isolated events, lasting typically for seconds or less, as short-lived clusters of events from point sources, or as prolonged episodes of closely spaced events that can last for tens of minutes or hours. We present here grain size, duration, MER, and velocimetry data for examples of all 3 patterns of spattering activity.

The 4-day-long 2011 Kamoamoā eruption at Kīlauea shows a temporal and spatial evolution from such closely spaced spattering to sustained low-fountaining as the discharge of melt and gas became focused in only two of the 11 segments along the 2.4 km-long fissure system. The transition was driven by an increase in the frequency and intensity of bubble bursts until sustained behavior ensued.

These two eruptions demonstrate that differences in style and intensity are driven by the degree of mechanical coupling of the largest of the bubble population to the melt, in turn mostly modulated by changes in the size and frequency of arrival of the largest bubbles in the shallowest conduit.

Keith Howard, Tom Simkin, John R. Filson

Submission 1091

Hydromagmatic Eruption Related to the 1968 Collapse of Fernandina Caldera, Galápagos

The VEI-4 hydromagmatic eruption that heralded the June, 1968 caldera collapse of basaltic Volcán Fernandina offers a case study of the power of hydromagmatic eruptions when basaltic magma interacts with caldera water. Ground water flowing toward a lowering magma column likely triggered the eruption.

Fernandina's violent eruptive sequence originated from a previously fuming alcove in the caldera wall that likely overlay shallow magma. Explosive venting began on June 7 and climaxed in the VEI 4 event on June 11.

The eruption records an early stage of the 1.5 km³ magmatic withdrawal that led the caldera floor to lower 350 m over the next two weeks. The vent surface area had been a few tens of meters above and away from a shallow lake in the caldera floor. Ground water was readily available below the floor, as shown when 0.1 km³ of stored ground water discharged into the lake as it and its floor lowered post-eruption, increasing the lake's volume 12 fold. The ground-water storage area was confined within dikes that encircle the caldera.

Tephra from the hydromagmatic eruptions accumulated to a thickness of 17 m on the caldera floor, 5 m on the high western caldera rim, 15 cm on the coast 11 km to the west, and a light dusting on a ship >300 km to the west. The lithic-rich tephra contained a small proportion of Pele's tears and other juvenile basaltic glass. Lava and gabbro blocks were ejected. Blocks as large as 2 m thrown out of the 700-m deep caldera formed impact craters into the finer ash on the volcano's flank 1 km away. Assuming air drag, trajectories suggest initial ballistic velocities >225 m sec⁻¹. Surge formed dune bedding in rubbly ash on the caldera floor, plastered ash on trees on the caldera rim, and blew small trees over radially outward on the rim.

Venting and collapse increased the alcove volume by 0.3 km³, crudely comparable to the mass ejected. Subsidence of an adjacent small block (~0.06 km³) after the venting may represent space evacuated by vented magma. Small rimmed craters reflect late eruptions in the sequence.

Lake and ground water also undoubtedly triggered earlier hydromagmatic eruptions that had built pre-1946 tuff cones on the caldera floors of Fernandina and neighboring Cerro Azul volcanos and deposited tephra on the caldera rims, including a pre-1968 accretionary lapilli-bearing tuff bed up to 2 m thick on Fernandina's caldera rim.

Erin Hoxsie, Thomas Giachetti, James Watkins, James Gardner

Submission 104

Evidence for CO₂ fluxing from CO₂-H₂O anticorrelations in obsidian pyroclasts

Measurements of volatile species (e.g., H₂O, CO₂, S, F, Cl) in melt inclusions and pyroclast matrix glass are widely used to investigate how magma loses volatiles on its way to the surface. During magma ascent, pressure generally decreases and volatile species partition into the vapor phase. Therefore, parcels of melt that are more degassed have lower dissolved volatile concentrations. Regardless of whether the magma undergoes open-system degassing (gas is continuously extracted from the melt and new bubbles form) or closed-system degassing (gas is not extracted from the melt and bubbles continuously evolve in composition), in equilibrium or non-equilibrium, a positive correlation between dissolved CO₂ and H₂O among variably degassed samples is expected. Contrary to the expectation from simplified degassing models, recent measurements from the 1340 AD eruption of the Mono Craters chain in California show that individual obsidian pyroclasts often exhibit a negative correlation on a CO₂-H₂O diagram. We attempt to explain this observation by presenting a detailed chemical and textural analysis of a composite pyroclast from that eruption. This clast exhibits several distinct textural domains that link the negative slopes on the CO₂-H₂O diagram to regions of melt where CO₂ and H₂O have counter-diffused. Two-dimensional diffusion modeling of both H₂O and CO₂ reproduces the CO₂-H₂O anticorrelation and yields a diffusion timescale of approximately one hour, assuming a magmatic temperature of 800°C. We conclude that the conduit process most likely to generate parcels of melt with distinctly different dissolved volatile concentrations is fluxing of a CO₂-rich vapor into a relatively H₂O-rich melt/gas/ash column.

Christian Huber, Andrea Parmigiani, Olivier Bachmann, Wim Degruyter

Submission 597

Outgassing in shallow arc magma reservoirs

Volatile exsolution and migration play a significant role in their thermo-mechanical evolution of shallow magma reservoirs and impact the dynamics and magnitude of forthcoming eruptions. We focus here on two sets of questions related to outgassing (1) how does vapor migration influence the evolution of the reservoir? And (2), what are the physical processes and optimal conditions that allow efficient outgassing out of crystal-rich magma as they solidify to form plutons? We approach these questions by investigating the pore-scale fluid dynamics that controls the transport of the vapor in crystal-rich and crystal-poor magmas. We show that the vapor tends to migrate efficiently in crystal-rich parts of a magma reservoir and accumulate in crystal-poor regions in a heterogeneous magma body. Moreover, under in-situ degassing conditions (crystallization-driven exsolution), we find that outgassing by permeable buoyant migration is most efficient between 50 and 70 vol. % of crystals for typical arc (wet) conditions, but that a large fraction of volatiles remains trapped before being finally expelled by capillary fracturing at very high crystal content (significantly >75 vol. %). We parameterize our pore-scale results in a thermo-mechanical magma reservoir model and show that the pore-scale results provide a good estimate of outgassing efficiency when considering large reservoirs and/or a hot compliant crust. Contrarily, in small reservoirs and/or considering a stiff crust, the mechanics of outgassing is shown to be largely controlled by mechanical feedbacks between the crust and the reservoir. In the latter case, we find that estimates of outgassing based on pore-scale flow models significantly underestimate the amount of volatiles that remain trapped in the reservoir up to very high crystallinity.

Michael Hudak, Ilya Bindeman

Submission 1180

Extreme δD and $\delta^{18}O$ depletion of glass in Mt. Mazama pinnacles: Developing a snapshot paleoclimate tool using H and O isotopes in hot and cooling glass

Silicic volcanic rocks and glasses are degassed during eruption and subsequent cooling to ~ 0.1 wt% H₂O with δD range of -80 to -115‰. Higher concentration of water in glass is due to secondary hydration below the glass transition. As the meteoric water interacts with and hydrates volcanic glass, it imparts its isotopic composition to the glass. Because δD and $\delta^{18}O$ in meteoric water are strongly temperature-, altitude-, and latitude-dependent, δD in hydrated volcanic glass may be a robust proxy for paleoclimate. Hydration rates at ambient T are very slow (0.1-1 $\mu m/1000$ years) and are not fully understood theoretically. They cannot provide a true “snapshot” of the climate at the time of the eruption. Here, we investigate glasses hydrated in fumaroles in the transient hydrothermal systems hosted in ignimbrite outflow sheets, which should provide a more instantaneous climate record because glasses are hydrated in days to months at high temperatures.

We report bulk δD and $\delta^{18}O$ in pumices from fumarolic pinnacles in Mt. Mazama tuffs as well as the $\delta^{18}O$ of water-in-glass ($\delta^{18}O_{\text{water}}$) extracted by rapid thermal decomposition. Pumices have δD values as low as -152.9‰ and rarely lighter than -140‰. Bulk $\delta^{18}O$ is considerably more variable (0.95 to 5.55‰), with an even greater range of $\delta^{18}O_{\text{water}}$ (-13.7 to +3.5‰). Water contents cluster around ~ 1.8 wt%. The narrow range of δD is consistent with the assumption that effectively all the water in these glasses is meteoric and not magmatic and that the meteoric water had a relatively consistent, stable δD composition. The comparative range in $\delta^{18}O$ and $\delta^{18}O_{\text{water}}$ of these samples suggest variable water-rock interaction and isotopic exchange. The two $\delta^{18}O$ measurements have a positive linear relationship, suggesting rapid equilibration of $\delta^{18}O$ between the secondary water and the glass with lighter $\delta^{18}O$ and $\delta^{18}O_{\text{water}}$ recording a higher degree of isotopic exchange. This is also demonstrated by δD vs $\delta^{18}O$, which extends to progressively lighter δD at near constant $\delta^{18}O$ before dropping to lower $\delta^{18}O$ at a lower threshold for δD .

These data demonstrate that δD in hydrated silicic glasses record meteoric water H isotopes at the time of the eruption. For 7.6 ka Mt. Mazama ignimbrites, the low δD signature of glass suggest that pre-climactic edifice could have been higher than 5 km based on δD change with altitude. Since many silicic eruptions are also easy targets for geochronological analyses, this technique may prove to be a useful paleoclimate tool.

Eric Hughes, Nickolay Krotkov, Arlindo da Silva, Robert Hoffman, Tim Myers

Submission 1242

Real-Time Modeling of Volcanic Clouds and their Application to Air Traffic Flow Algorithms

Correctly forecasting the dispersion of volcanic clouds is essential for predicting potential aviation hazards. However, constructing accurate forecasts of volcanic SO₂ and ash clouds is difficult as many parameters necessary to initialize model simulations are not well understood at the time of a volcanic eruption. Analyses that combine observations and model simulations provide useful constraints on volcanic emission source terms and can progressively improve the modeled dispersion. Recent developments in the NASA GOES-5 model allow for the dual simulation of volcanic ash and SO₂ clouds. In what follows, we demonstrate that column SO₂ and aerosol profile observations from the Ozone Monitoring and Profiler Suite (OMPS) Nadir Mapper and limb profiler instruments on board NOAA-NASA Suomi NPP satellite provide early estimates of the total SO₂ mass and aerosol cloud altitude, and with backward transport analysis, we estimate initial volcanic emission height to initialize the volcanic SO₂ cloud into the GEOS-5 model. We assimilate successive column SO₂ observations into the GEOS-5 model to minimize differences between the model simulations and observations. We use the April 2015 eruption of Chilean volcano Calbuco to demonstrate how our method improves forecast accuracy.

Producing real-time volcanic cloud forecasts requires rapid inclusion of volcanic eruption events into the GEOS-5 Aerosol and SO₂ Forecasting System. Air traffic flow algorithms can use real time quantitative forecasts of volcanic SO₂ and ash clouds to manage navigation around hazardous regions. We propose implementing a parallel “dormant” model to simulate the initial eruption off-line and update the operational model’s state to report more up-to-date information about volcanic emissions locations. Metron Aviation has developed tools that use GEOS-5 volcanic simulations to estimate the impact to aviation of volcanic ash and/or SO₂ avoidance. The details of the proposed system to process real time volcanic cloud forecasts is presented, and the application of GEOS-5 volcanic emissions forecasts within the Metron Aviation air traffic flow algorithms is demonstrated.

Ery Hughes, John Blundy, Roman Botcharnikov, Richard Brooker, Pierre Cartigny, EIMF -, Geoff Kilgour, Heidy Mader

Submission 822

Quantifying the initial volatile contents of basaltic magmas using stable isotope fractionation

As magmas ascend to the surface, volatiles exsolve into a vapour phase, expanding and driving volcanic eruptions. By the time the magma reaches the surface, it is possible that some portion of the volatile content has decoupled from the magma and escaped to the atmosphere. To trace the degassing history of the magma, most studies rely on phenocryst-hosted melt inclusions (tiny pockets of melt trapped inside crystals as they grow in the magma) assuming these approximate a close representation of the initial volatile content in the magma at depth. However, magma crystallisation may occur after the initiation of degassing and therefore the volatile concentration measured in melt inclusions is a minimum estimate for the initial volatile content, especially for CO₂, which is significantly less soluble than H₂O.

As fluid is released from the magma, CO₂ isotopically fractionates between vapour and melt phases providing a record of the magma degassing history. Thus, the carbon isotope signature can be used as a tool for volatile budget determination. The melt becomes enriched in the lighter isotope (¹²C), with the amount of enrichment being controlled by the melt-vapour isotopic fractionation factor ($\Delta_{\text{vap-melt}}[\text{CO}_2] = R_{\text{vap}}/R_{\text{melt}}$ where $R = ^{13}\text{C}/^{12}\text{C}$). By measuring the CO₂ and $\delta^{13}\text{C}$ of a suite of melt inclusions, the initial CO₂ content and $\delta^{13}\text{C}$ value of the magma and the degassing pathway can be estimated. To date, the only measurements of $\Delta_{\text{vap-melt}}[\text{CO}_2]$ have been carried out using anhydrous melts.

To investigate the influence of H₂O, pressure and initial CO₂ content on $\Delta_{\text{vap-melt}}[\text{CO}_2]$, we performed IHPV experiments on a basaltic starting composition with initial CO₂ and H₂O ranges of 2000 – 5000 ppm and 0 – 5 wt.% respectively. Experiments were run at 100, 300, 500 and 700 MPa and 1250 °C. The $\delta^{13}\text{C}$ of the carbonate in the starting material ranged from -5.43 – +1.99 ‰. The resultant glass chips have been analysed for their CO₂ and H₂O using SIMS and demonstrate that the experiments follow a closed-system degassing path. These experiments also provided a series of $\delta^{13}\text{C}$ SIMS standards as their bulk $\delta^{13}\text{C}$ values have been measured using stepped-heating C extraction. The range of CO₂ and H₂O will be used to assess whether H₂O effects ionisation yield. Finally, we analyse phenocryst-hosted melt inclusions with high CO₂ contents (e.g., from arc settings) for $\delta^{13}\text{C}$, CO₂, δD and H₂O to show the applicability of this method for estimating the initial volatile content of magmas.

Amy Hughes, Jackie Kendrick, Yan Lavallee, Adrian Hornby, Giulio Di Toro

Submission 1023

The role of porosity and glass content on the frictional properties of volcanic rocks

Volcanic materials are often heterogeneous, with widely varying porosities, interstitial glass contents and crystallinity amongst other factors. This results in edifice building materials with very different mechanical properties, which is a key factor in understanding the process of volcanic flank collapses, both their initiation and runout. Experimental data suggests that at speeds associated with volcanic flank and sector collapses are capable of producing frictional melt (Lavallée et al. 2012), which is supported by rare field evidence of pseudotachylytes found at the base of volcanic slide deposits (Legros et al. 2000).

In volcanic materials, interstitial glass remobilises at temperatures above the glass transition temperature (e.g. Lavallée et al. 2012) and the development of frictional heat during slip has been commonly observed to exceed this temperature. Interestingly, rotary shear experiments examining frictional heating in glass show that samples with high glass content tend to fail at relatively low frictional stresses, the mechanism for which is currently not well constrained. In addition, the high porosities encountered in volcanic materials act to reduce the effective contact area at the slip surface, promoting both comminution of a material and flash heating at contacts. By combining porosity calculations with 3D tomography, a relationship between the porosity, effective contact area and frictional behaviour may be found. Further, by systematically varying both porosity and glass content, we can test their influence on the mechanical properties of fault slip and on the physical evolution of the slip surface, thickness of shear zone and magnitude of temperature change. The tests are performed using synthetic samples of solid glass and variably sintered glass beads (which exclude the effects of crystallinity, mineralogy and chemistry), compared to a wealth of data from frictional experiments on natural samples with a wide range of porosities. The data will feed discussion on the development of faults, cataclasis, granular flow and frictional melting in volcanic systems.

Lavallée, Y., et al. (2012). "Experimental generation of volcanic pseudotachylytes: Constraining rheology." *Journal of Structural Geology* 38(0): 222-233.

Legros, F., et al. (2000). "Pseudotachylyte (Frictionite) at the Base of the Arequipa Volcanic Landslide Deposit (Peru): Implications for Emplacement Mechanisms." *The Journal of Geology* 108(5): 601-611.

Eugene Humphreys, Jonathan Perry-Houts, Matthew Morriss, Nicholas Wogan

Submission 864

The Columbia River flood basalts: Initiated from below, driven from above

The Yellowstone-Columbia River flood basalt system has many classic attributes of the plume-head-plume-tail hypothesis. It also has some outstanding anomalies: prominent pre-eruptive uplift is not evident; eruptions propagated rapidly off track (northward); and volcanism was dominated by eruptions ~350 km off track. By putting Yellowstone in a regional tectonic context, we argue it is a plume, and the rapid off-track magmatic propagation and large eruptive volumes are consequences of melt-enabled lithospheric foundering.

More specifically, Columbia River group flood basalts eruptions initiated ~16.8 Ma with arrival to SE Oregon of a small plume head (generated by an already-active Yellowstone plume). The associated mantle melt enabled foundering of two relatively dense bodies. First was a fragment of Farallon slab left beneath NE Oregon following the ~53 Ma accretion of Farallon lithosphere to the Pacific Northwest. Yellowstone asthenosphere was drawn north by the S-to-N delamination of this lithosphere, and we image this lithosphere as a prominent high-velocity slab hanging vertically to ~300 km beneath NE Oregon.

The second foundering was a foundering of the Wallowa batholith restite root. Root loss is evidenced by Wallowa batholith uplift, which (eventually) elevated the overlying Imnaha basalts 2 km relative to the same flows nearby. We infer an initial partial foundering caused Yellowstone asthenosphere upwelling into the middle and upper crust, creating the 16.5-16.0 Ma Grande Ronde magmatic flareup. This event occurred prior to Wallowa Mt faulting and it appears to have created an upper-crustal sill and domal uplift. We think the sill extended ~80 km from the Wallowa Mts to the margins of the circular topographic uplift that surrounds the Wallowa Mts.

The volume of Imnaha and Grande Ronde basaltic dikes, and their generally northerly trend, requires significant west-directed tectonic extension during the course of their emplacement; the pole of rotation appears to have been in the vicinity of the Washington-Oregon border. Wallowa Mt faulting occurred later, at ~10 Ma, under SW-oriented tension. The result was Wallowa Mt uplift (to ~2 km) and coincident downdropping of the surrounding moat-like depression.

Madeleine Humphreys, Richard Brooker, Jenny Riker, Victoria Smith, Cees-Jan de Hoog, Michael Stock

Submission 398

Apatite as a tool to investigate the changing pre-eruptive volatile compositions of magmas

Minerals such as apatite can generate new insights into the volatile compositions of the systems from which they crystallise. Apatite has a very flexible mineral structure and igneous apatites can accommodate all the major volatile species of magmatic importance, i.e. H, C, F, Cl and S. Apatite may therefore be helpful in evaluating the variability of volatile compositions in hydrous magmas and any coexisting volatile phase. Because apatite crystallises relatively early in many magmas, it is commonly trapped as inclusions within phenocrysts, and can therefore preserve a temporal record of changing magmatic volatile contents prior to eruptions.

New high-P-T experiments and direct analysis of the major volatile components (including C and OH) show that apatite can accommodate high CO₂ concentrations. In halogen-free experiments carbonate is accommodated primarily in the channel site (Type A substitution) but in halogen-bearing experiments it is incorporated onto the phosphate site (Type B substitution). Experimental apatite-melt KDs for H₂O-CO₂ exchange are 0.381 ± 0.054 for haplobasaltic andesite and 0.246 ± 0.057 for trachyte. Equivalent apatite-melt KDs for OH-Cl and OH-F exchange are in the range 0.08-0.11 and 0.02-0.09 respectively. Our new data, combined with data from the literature, show a clear log-linear dependence of K_{DOH-Cl} and K_{DOH-F} on temperature, with increased preference for the OH component at higher temperatures.

Modelling suggests that apatite volatile compositions may be sensitive to the composition of a coexisting magmatic volatile phase and to the onset of volatile saturation in magmas. This is a significant advantage over melt inclusion studies and provides additional constraints on the role of volatile exsolution in pre-eruptive processes. We illustrate this using the volatile compositions of apatites from eruptions of Laacher See, Germany and Campi Flegrei, Italy, as well as data from the literature. Apatite chemistry therefore has great potential for investigating temporal variations in magmatic volatiles prior to eruption, and for understanding the nature of exsolved volatile phases.

Tony Hurst, Cory Davis, Natalia Deligne

Submission 268

Handling uncertainties in volcanic ash forecasts from HYSPLIT atmospheric modelling

A product of GeoNet, New Zealand's geological hazard monitoring system run by GNS Science, is forecasting where volcanic ash would be likely to travel and be deposited in the case of a volcanic eruption. If any volcano is erupting, ashfall forecasts for that volcano are distributed to relevant organisations and the public; at times these forecasts are also distributed for volcanoes in heightened unrest.

A major source of error in volcanic ash forecasting is the wind pattern above and around the volcano. Our current forecasts are produced by the program ASHFALL, originally described in Hurst (1994), which uses 1-Dimensional wind models, i.e. it cannot allow for horizontal variations in the wind pattern. Given New Zealand's dynamic meteorology, this is a major limitation. GNS Science, in conjunction with New Zealand's MetService, is working to move its routine ash forecasts to HYSPLIT, which uses a full 4-D atmospheric model. We are now routinely producing forecasts with HYSPLIT of where ash would be deposited if particular volcanoes erupted.

Because of the simple wind model, and the way ash diffusion is allowed for, ash contours produced by ASHFALL are ellipses which usually cover a much wider area than more sophisticated models forecast. Conversely, HYSPLIT often forecasts narrower deposited ash distributions with smaller spatial features, so minor errors in input wind conditions can result in ash falling where it was not forecast. This higher level of detail can give a false impression of accuracy. This problem is apparent in hindcasting ash deposition from the 6 August 2012 Te Maari eruption from Tongariro volcano (Hurst & Davis, 2017).

Prior to making these new forecasts public, we will explore ways of displaying the uncertainty in the atmospheric modelling to avoid inappropriate reliance on deposit forecast details. We are investigating using multiple atmospheric models to make our ash forecasts take better account of the uncertainties in the atmospheric modelling.

Shaul Hurwitz, Steven E. Ingebritsen, Mark E. Reid, Jessica L. Ball, Joshua M. Taron, Carol A. Finn, Paul A. Bedrosian

Submission 199

Groundwater in stratovolcanoes of the Cascade Range, USA – what we do and do not know

Water saturation increases the potential for explosive phreatic and phreatomagmatic eruptions. If volcanic edifices are partially altered to clay, they also become mechanically weak and may be prone to catastrophic flank collapse and destructive lahars. The steep stratovolcanoes in the Cascade Range potentially pose a significant threat to large populations and infrastructure, and most are classified by the USGS-National Volcano Early Warning System (NVEWS) as “very high threat”. Their summits host extensive glaciers that have been shrinking considerably in recent decades, but none currently hosts a summit crater lake. Holocene phreatic eruptions at Mts. Adams, Baker and Rainier suggest that these volcanoes contained near-surface groundwater. Results from electromagnetic and magnetic surveys and alteration mapping at Mts. Adams, Baker, Rainier and St. Helens, combined with measurements of rock physical properties, suggest that many edifices are extensively altered and/or contain large amounts of water. However, hydrothermal alteration is minimal at Mt. St. Helens, and the failure surfaces of the 1980 collapse were not localized in weak, hydrothermally altered rocks. Seasonal modulation of seismicity rates and seismic velocity at Mt. St. Helens may reflect pressure changes deep in the underlying groundwater system. Drillhole information is available only for the Mt. Hood edifice, owing to geothermal reconnaissance in the 1970s and early 1980s. There, the 1130-m deep Pucci hole had a static water level 573 m below land surface after drilling. This deep static water level is subject to alternative explanations; either the water table is relatively deep (unless there is dike-impounded water beneath the summit region) or the water table is shallow, with a large potential gradient for downward flow. These dichotomous interpretations highlight the fact that, despite a handful of observations and inferences, a large knowledge gap remains. Limited qualitative inferences from numerical simulations provide only partial guidance for hazard assessments. The existing knowledge gap could usefully be addressed by a program of deep drilling combined with continuous measurements of seismic velocity and electric resistivity at high spatial and temporal resolution.

Shaul Hurwitz, Jacob B. Lowenstern, James J. Thordsen, Jeffrey T. Cullen, Jaime D. Barnes, Emma G. McConville, Mark E. Szymanski

Submission 197

The source and fate of the halogens fluorine, chlorine, and bromine in the Yellowstone Plateau Volcanic Field hydrothermal system

In the Yellowstone Plateau Volcanic Field (YPVF) the Cl/F ratio observed in both glass inclusions in quartz crystals and in rhyolitic matrix glass (~0.5 by mass) is significantly lower than the ratio in the rivers draining the YPVF (~8) or in the thermal springs (up to 140). Within the YPVF, Cl/F in neutral-alkaline-chloride waters (pH>6) in Norris Geysir Basin (NGB) north of the Yellowstone Caldera is substantially higher (80-140) than the ratios in thermal waters within the Yellowstone Caldera and along the caldera's southern boundary (<15). Potential explanations include: 1) preferential degassing of chlorine (as HCl) compared to fluorine (as HF) from the underlying silicic magmas into the overlying thermal waters, 2) a crustal source of chlorine that contributes to the thermal waters, and/or 3) a mineralogical sink for fluorine between magma and the ground surface. To test the three possible explanations, we carried out laboratory experiments where powdered Yellowstone obsidian was reacted with water at temperatures of 150°C to 350 °C for ~90 days. Experimental results suggest that at temperatures of 150-250 °C, the Cl/F in reacted waters is <1, but at temperatures of 300 °C and 350 °C, Cl and Br are more readily leached from the rock. At 350 °C, Cl/F (~11) and Cl/Br (~400) are similar to the ratios in many thermal springs of the Yellowstone caldera. The slow decrease of F concentration in the reacted waters during the experiments suggests incorporation into secondary phases. Pyrohydrolysis of altered rocks from drillcores in NGB (<331 m) and in the caldera (<74 m) suggests that Cl is significantly more depleted in comparison to F, and both are depleted compared to Yellowstone obsidian. We used a scanning electron microscope (SEM) to identify secondary minerals containing fluorine in core samples obtained during research drilling by the USGS in the 1960s. Fluorine-bearing minerals were found in all drillcores. Fluorite was identified in Y-2, Y-7 (in the caldera) and in Y-12 (in NGB) and fluoroapatite was found in Y-7 and Y-8 (in the caldera). The REE fluorocarbonate minerals bastnaesite and parisite are predominantly found in Y-12 at depths >276 m where temperatures are >170 °C. Initial results from the experiments, pyrohydrolysis, and SEM imply that Cl/F is mainly modified in the shallow crust at T>250 °C by leaching chlorine from rhyolite and by incorporating fluorine into secondary minerals.

David Hyman, Marcus Bursik

Submission 779

Transient Lava Dome Pressurization and Degassing at Volcán Popocatépetl, Mexico: Numerical Analysis and Degassing Flux Calculations from Thermal Infrared Images

The collapse or explosive breakup of growing and degassing lava domes may result in the formation of dense, mobile pyroclastic flows and thus presents a significant hazard. Because of the reduction in effective stress due to pore-pressurization, the transient distribution of elevated gas pressure is critically important to understanding dome break up. The nearly continuous cycles of lava dome growth, pressurization, and failure that have characterized the last two decades of eruptive history at Volcán Popocatépetl, Mexico provide an excellent case study of these processes with the use of modern tools and integration of measurements into new models of transient dome pressurization.

We combine mathematical and numerical analysis with infrared observations and measurements to gain a better understanding of the temporal variation in gas flow through the dome system. In doing so, we develop and analyze new governing equations describing transient pressurization of a deforming dome with an evolving porosity field. To test this model, we compare the models with degassing mass flux data derived from ground-based infrared imagery of the volatile plume at Popocatépetl. Mass flux calculations are obtained by a simple thermal energy flux conservation method using thermal data from FLIR image sequences and show significant oscillations in degassing rate or ash-free puffing activity. Time series analysis of the degassing flux estimates reveal two dominant short-term oscillation modes of ~2 and 10 min cycles. These measurements were made during a period of non-explosive degassing from the dome and do not reflect development of new gas flow paths, nor plume eddy processes within the crater and thus can be compared directly with our model of permeable gas flow.

Numerical analysis suggests that such short-term oscillations cannot arise within the dome and must be the result of an oscillating source of gas flux below the dome. The oscillating source of gas may be the result of alternating gas-rich and gas-poor regions of rising magma, so-called "porosity waves" within the conduit. Additionally, these internal pressure fluctuations must lead to periodic reductions in the stress required to fracture the dome and induce explosion, and may play a role in the cyclic growth and destruction behavior at Popocatépetl.

Fiona Iddon, Marie Edmonds, Karen Fontijn, Juliane Hübert Hübert, William Hutchinson, Charlotte Jackson, Tamsin Mather, David Pyle

Submission 483

Mush architecture beneath peralkaline volcanoes in the Main Ethiopian Rift

Our understanding of magma reservoirs has improved dramatically over the past decade through advances in analytical techniques and by combining petrology with geophysics. Geochemical studies have shown that crystal mushes are often disaggregated and magmas mingled, leading to heterogeneous crystal cargoes not in equilibrium with their carrier liquids. Seismic tomographic and magnetotelluric surveys of the crust beneath volcanic centres have in some cases highlighted large bodies of interconnected melt; in other cases, enigmatically, an absence of melt, despite the presence of active volcanoes at the surface.

The Main Ethiopian Rift features peralkaline calderas that have erupted frequently during the Pleistocene and Holocene. Caldera forming phases produce feldspar rich ignimbrites, whilst post caldera eruptions give rise to crystal poor lavas and pumice cones. Despite seemingly simple geochemical relationships dominated by fractional crystallisation, there is evidence for more complex processing prior to eruption and geophysical surveys have struggled to locate appropriate bodies required for fractionation of large quantities of melt. Similar centres along the East African Rift system have revealed evidence for phenocryst zoning and resorption and heterogeneous glass compositions. Eruption of xenoliths and xenocrysts has been cited as evidence for remobilisation of solidified material in the system.

Here we conduct a systematic comparison between whole rock, glass and feldspar compositions for a suite products from Aluto and Kone volcanoes. It is hypothesised that the nature of peralkaline melts allows for the efficient segregation of small residual melt lenses from crystalline mush areas, causing the net downward transport of compatible elements. These lenses may be small enough to avoid detection, but significant enough to feed the crystal poor eruptions. The crystalline material is only significantly tapped during highly explosive eruptions, often associated with caldera formation. We will evaluate the relationship of crystal cargoes to their carrier liquids and use this to determine the relative importance of entrainment of crystals from a disaggregating mush system and elucidate to the processes that drive this.

Alexandra Iezzi, David Fee, Robin Key, Arthur Jolly, Keehoon Kim, Bruce Christenson, Richard Johnson, Geoff Kilgour, Allison Austin, Esline Garaebiti, Ben Kennedy, Rebecca Fitzgerald, Nicholas Key

Submission 550

3-D acoustic waveform simulation and inversion at Yasur Volcano, Vanuatu

Acoustic waveform inversion shows promise for improved eruption characterization that may inform volcano monitoring. Well-constrained acoustic source inversions can provide robust estimates of volume and mass flux, increasing our ability to monitor eruptions and characterize volcanic emissions (potentially in real-time). Previous studies have assumed variations of the multipole source mechanism, which can be thought of as the combination of pressure fluctuations resulting from either a point mass-outflow source (isotropic monopole) or combination of monopoles (dipoles and quadrupoles). However, to date, infrasound source mechanisms have not been well constrained in three dimensions due to infrasound sensors only being deployed on Earth's surface, and the assumption of no vertical dipole component has been made. In this study, we deployed a high-density seismo-acoustic network around Yasur Volcano, Vanuatu, including multiple acoustic sensors along a tethered balloon above the volcano. Yasur has frequent strombolian eruptions from any one of its three active vents within a 400 m diameter crater. The third dimension (vertical) of infrasound sensor coverage allows us to begin to constrain the vertical acoustic source components in a profound way, primarily the horizontal and vertical components and their previously uncharted contributions to volcano infrasound. The deployment also had a geochemical and visual component, including FLIR, FTIR, two scanning FLYSPECS, and a variety of visual imagery. Our analysis employs Finite-Difference Time-Domain (FDTD) modeling to obtain the full 3D Green's functions for each propagation path. This method, following Kim et al. (2015), takes into account realistic topographic scattering based on a high-resolution digital elevation model created using structure-from-motion techniques. We then invert for the source location and source-time function for numerous explosions from multiple vents, constraining the contribution of the vertical sound radiation to the source by incorporating the infrasound data collected from the balloon. The final outcome of this inversion is an infrasound-derived volume flux as a function of time, which we then compare to those derived independently from geochemical techniques as well as the inversion of seismic data.

Kim, K., Fee, D., Yokoo, A., & Lees, J. M. (2015). Acoustic source inversion to estimate volume flux from volcanic explosions. *Geophysical Research Letters*, 42(13), 5243-5249.

Masato Iguchi

Submission 375

Probabilistic forecasting of amounts of volcanic ash ejected by vulcanian eruptions at the Sakurajima volcano, Japan

Vulcanian eruptions frequently occurred at the Showa crater, east of the summit of Sakurajima volcano during the period from 2008 to 2016. Total number of the eruptions reached 5811. Strainmeters are installed in the underground tunnel 2.1 km apart from the crater. Inflations prior to 89% of the vulcanian eruptions were detected by the instruments and co-eruptive deflation are detected, too. Here, durations and amounts of inflation and deflation strains are statistically analyzed. Duration of the precursory inflation shows lognormal distribution. This indicates occurrence time of the eruptions can be forecasted by probability density function of lapse time from the start of inflation. Logarithm of amount ratio of deflation to inflation shows normal distribution with the peak of amount ratio of 1 and more than 2 of the log value share only 1% of the total number. Coeruptive deflation is examined in relation with weight of volcanic ash ejected by the eruptions. Total amounts of volcanic ash is estimated from spatial distribution of volcanic ash density at 63 monitoring sites, which provide data monthly. It is estimated that weight of volcanic ash ejected from the crater amounted 43 million ton in 2008-2016. We examined ground deformation and seismic amplitude as they relate to monthly sums of volcanic ash weight ejected from craters. We found that in monthly sums, both deflation ground deformation and the amplitude of volcanic tremors correlate positively with the weight of ejected volcanic ash. A linear combination of terms for ground deformation, seismic amplitude and a correction factor correlates better than single parameter of deflation or seismic amplitude with volcanic ash weight. For individual vulcanian eruption, it is found that the amounts of deflation correlate volcanic ash weight by removing ash weight emitted by post-vulcanian continuous eruption accompanied by only volcanic tremor. Log of amount ratio of deflation to inflation shows normal distribution. Therefore, it is possible to probabilistically forecast volcanic ash weight of vulcanian eruption from precursory inflation.

Fumihiko Ikegami, Rebecca Carey, Jocelyn McPhie

Submission 32

Topographical and structural controls on the Havre 2012 submarine rhyolitic lavas

The Havre 2012 eruption in the Kermadec arc produced 14 submarine rhyolitic lavas (70~73% SiO₂) at depths between 650~1550 meters. It was the largest deep submarine effusive eruption ever documented on the modern Earth. The eruption took place along the southern margin of a 5-km wide caldera and the lavas (Lava-A~D, F~I, K~P from west to east) have a total volume of >0.24 km³. We described and characterized the diverse morphology and facies architecture of the lavas utilizing high-resolution bathymetry and extensive visual observations and sampling at the seafloor during the MESH cruise in 2015.

The lavas at the southwestern margin of the caldera (Lava-A~G) are all “lobate” shaped low-aspect ratio (

The lavas at the southern (Lava-H~N) and southeastern margin of the caldera (Lava-O/P) are “dome” shaped and have higher aspect ratios (>0.3) than the lobate lavas. Lava-H~N are small lava domes on the crest of an elongate mound along the caldera rim, suggesting their partly intrusive nature. Lava-O/P on the other hand is a large dome complex which has half of the total volume of the entire Havre 2012 lavas (~0.12 km³). All lava domes have spiny structures (~40 m height) at the top, steep margins and aprons of talus. At least two of the 8 lava domes that were sampled have pumiceous carapaces, represented by either pumiceous breccia covering the surfaces (Lava-G) or pumiceous coherent facies exposed in a vertical section (Lava-L).

The rhyolitic lavas of the Havre 2012 eruption have morphologies which are both structurally and topographically controlled by the caldera rim. The alignment of the vents suggests magma ascent along dykes which could be occupying caldera-related ring faults. Lavas that flowed down the steep caldera-wall formed a distinctive narrow ridge morphology whereas on horizontal surfaces, the lava formed domes and lobate morphologies.

Tehnuka Ilanko, Tobias Fischer, Laura Crossey, Aaron Curtis, Philip Kyle, Hyunwoo Lee, Yuji Sano

Submission 34

Subnivean degassing in the summit area of Erebus volcano, Antarctica

Erebus is one of only a few volcanoes where subnivean degassing through perennial snow and ice is known, though such systems may be far more widespread than the documented examples (Curtis & Kyle 2017). The degassing forms unique environments where magmatic gas and heat interact with permanent snow or ice and surface air. At Erebus, this manifests as ice caves and warm ground, typically due to vent and diffuse degassing respectively. Their locations may be associated with shallow magma intrusions or permeable rock around the Erebus summit caldera, as indicated by seismic tomography (Zandomenghi et al. 2013).

Based on gas sampling around the summit plateau of Erebus, we suggest that hydrothermal modification is a significant influence on the flank degassing. Two gas compositions are identified: the first has N₂/O₂ ratios of 3.0 – 4.4, resembling air or air-saturated water; the second is oxygen depleted but nitrogen-rich, with N₂/O₂ up to 1000. Both contain up to 2% CO₂. We report the first nitrogen isotope ratios from Erebus, which show that N₂ in both gas types is predominantly air-derived ($\delta^{15}\text{N} = -0.1 - 0.8\text{‰}$), consistent with helium isotope ratios (1.0 – 1.2 Ratm).

Carbon isotope ratios indicate mixing of air with two CO₂ endmembers distinguished by $\delta^{13}\text{C}$ of -5‰ and -1‰. The CO₂ fluxes, measured on warm ground and cave floors, consist of a higher flux population of 100 – 930 g.m⁻².d⁻¹ (mean of 260 g.m⁻².d⁻¹), and backgrounds (.m⁻².d⁻¹). The distinct isotopic compositions likely reflect CO₂-rich magmatic gas from shallow intrusions, modified by interaction with air and meltwater. We consider the lightest ratios (-5‰) to reflect magmatic degassing, ultimately from the upper mantle, while fractionation to heavier values results from CO₂ dissolution in water, and subsequent degassing associated with precipitation of minerals such as calcite.

Although meteoric recharge is limited by the dry Antarctic environment, melting, steam emission, and re-freezing occur in the warmth of ice caves and at the base of the snowpack. Gas measurements are one way to investigate and monitor hydrothermal systems resulting from volcano-ice interactions such as at Erebus. As warming and deglaciation raise the potential for volcanism in areas presently beneath the Antarctic ice cap, flank degassing through ice or snow may be a valuable early indicator of reactivation; and it also becomes more important to characterise the magmatic-hydrothermal plumbing of glaciated volcanoes.

Takumi Imura, Tsukasa Ohba, Mitsuhiro Nakagawa

Submission 900

Volcanic fluids-rock interaction inferred from characteristics of altered minerals in volcanic products at Tokachidake volcano, central Hokkaido, Japan.

Altered volcanic products from Tokachidake were mineralogically observed to interpret interaction between volcanic fluids and rock, by using XRD, Raman spectroscopy, and SEM-EDS. We collected samples from the 4.7 ka pyroclastic flow deposit (Gfl-0), lower and upper units of the 3.3 ka pyroclastic flow deposit (Gfl-1 and Gfl-2), and the 1926AD eruption deposits consisting of the lower debris avalanche deposit (Unit A), the middle hydrothermal surge deposit (Unit B), and the upper debris avalanche deposit (Unit C). Each product contains unaltered ash grains consisting of primary igneous minerals and volcanic glass, weakly-altered ash grains in which unaltered part coexists with altered minerals, and intensely-altered ash grains consisting only of altered minerals. Individual ash grains have one of three types of altered mineral assemblages: silica mineral (silica type), silica mineral-alunite±kaolin (alunite type), and silica mineral-kaolin (kaolin mineral type). Most ash grains in Gfl-0 have undergone alteration that produces the alunite type. The samples from Gfl-1 contain abundant kaolin mineral type ash, subordinate alunite type ash, and minor unaltered ash grains. Alteration types in the Gfl-2 deposit are similar to those of Gfl-1, but unaltered ash grains are more abundant in Gfl-1. Most of the ash grains in the 1926AD products underwent alteration which produced mainly silica and alunite types. These mineral assemblages in every product indicate only acidic alteration. The presence of unaltered parts in the most abundant weakly-altered ash indicates rock alteration by a brief, incomplete chemical reaction. For such brief and incomplete reaction, the followed two fluid-rock interactions can be available. One is water-rock interaction which acid hydrothermal water reacts with rocks. Another is vapor-rock interaction which volcanic vapor separated from magma reacts with rocks. Thus, the presence of weakly-altered ash suggests that rock alteration occurred by the brief, incomplete fluid-rock interactions was undergoing an acid-hydrothermal system and/or a volcanic vapor-dominated system developed under the crater when a magma intrudes and degasses. This concluded that the conditions of rock alteration at Tokachidake volcano can be controlled by a magma intrusion.

Rodrigo Iriarte, Shanaka de Silva, Néstor Jiménez, Axel Schmitt

Submission 405

The Cerro Guacha Caldera Complex: A long-lived, multicyclic resurgent caldera complex in the Altiplano-Puna Volcanic Complex of the Central Andes

Four multicyclic calderas and smaller ignimbrite shields located within the Altiplano Puna Volcanic Complex of the Central Andes (APVC) erupted >15000 km³ of magma within the last 11 Ma. One of the largest and most complex of these is the 60x30 km Cerro Guacha Caldera Complex (CGCC). ⁴⁰Ar-³⁹Ar and ²³⁸U/²⁰⁶Pb in zircon age determinations reveal the history of the CGCC is recorded in two climactic eruptions with caldera collapse, resurgence cycles and several smaller eruptions. Characteristic remanent magnetization data for the ignimbrites show that the Guacha has reverse polarity, while the Tara is normally polarized and the magnetic fingerprints have allowed their current full extents to be identified. The two climactic ignimbrites are: 1) the 5.65 ± 0.01Ma, 1300 km³ (magma volume) Guacha ignimbrite and 2) the 3.49 ± 0.01Ma, 800 km³ Tara ignimbrite. The last major eruption from the CGCC occurred on the western flank producing the 1.72 ± 0.02 Ma Puripica Chico Ignimbrite and dome with a volume of 10 km³. The most recent eruption is the 1.52 ± 0.07 Ma ⁴⁰Ar/³⁹Ar age Negreal andesite lava dome. A conspicuous lineament of volcanic structures in the eastern part of the caldera, bordering the caldera moat, filled with welded ignimbrites and sedimentary lacustrine sequences marks part of the first 60x40 km caldera collapse associated with the Guacha ignimbrite. A central graben formed by the Guacha welded ignimbrite is related to a first episode of resurgence. Evidence of a second 30x15 km inner collapse includes offset welded Guacha ignimbrites and alignment of lava domes associated with the Tara ignimbrite. A second resurgence episode is suggested by the presence of an uplifted central block consisting primarily of welded Tara ignimbrite. Juvenile clasts from all three ignimbrites share the same petrological/geochemical characteristics: high-K series, compositional ranges from dacite to rhyolite, indicating a remarkably homogeneous magma chemistry through time. U/Pb in zircon ages are combined with Ar/Ar ages and allowed us to estimate residence times of 256, 115 and 379 kyrs respectively for the Guacha, Tara, and Puripicar Chico magmatic systems. The dacite reservoirs were characterized by fO₂ -13.06 to -13.38 and Fe-Ti oxide equilibration temperatures of 714° to 801°C. Storage depths based on amphibole geobarometry yielded pressures of 133 to 242 MPa equivalent to 5.3 and 9.2 km consistent with the uppermost zones of the regional Altiplano Puna Magma Body.

Roberto Isaia, Daniela Mele, Roberto Sulpizio, Giovanni Macedonio, Antonio Costa, Fabio Dioguardi

Submission 1132

Tephra fallout hazard scenarios at Campi Flegrei caldera (Italy) as deduced from combined use of geological data, laboratory analysis and physical modeling

Tephra fallout represents the most recurrent phenomena in the recent eruptions of the Campi Flegrei (Southern Italy). Previous studies reconstructed probability maps of fall deposits of three different eruption scenarios, representative of past activity: a high-magnitude event similar to the ~4.5 ka Agnano-Monte Spina eruption, a medium-magnitude event, similar to the ~4.1 ka Astroni 6 eruption, and a low-magnitude event similar to the ~4.2 ka Averno2 eruption. A semi-analytical model (HAZMAP) was used to estimate the Eruption Source Parameters (ESP), such as total erupted mass, eruption column height, and Total Grain-Size Distributions (TGSD) associated to these eruptions. ESP were obtained by best-fitting field data of proximal and medial outcrops. However, sensitivity studies of the dispersion of fall deposit showed that TGSD, fine-ash mass and particle aggregation processes are the main cause of the uncertainty.

Here we integrate the previous works using new field data including samples of medial-distal outcrops to better reconstruct the TGSD of the reference eruptions. Moreover 3D particle shape parameters obtained by microtomographic technics is used to better characterize drag law and hence particle settling velocity. The new data set is used to feed tephra dispersal models in order to produce a series of maps of tephra loading on the ground for the most representative eruptive scenarios accounting for different meteorological data and the eruptive parameters.

Samantha Isgett, Bruce Houhgtton, Alain Burgisser, Laurent Arbaret, Thomas Shea

Submission 679

Extreme complexity of a shallow conduit: the case study of the 1912 Vulcanian block apron at Novarupta, Alaska

The uniquely well-preserved block apron from the 1912 eruption of Novarupta provides a snapshot of degassing and outgassing processes occurring prior to and after Vulcanian fragmentation. Extreme conduit heterogeneity is expressed in a diverse textural range of pumiceous, dense, brecciated, and mingled dacitic blocks. Variable proportions of each category exhibit breadcrusting in the form of a cracked, dense rind. Non-breadcrusted blocks and breadcrust rinds preserve syn-fragmentation vesicularities and volatile contents, whereas interiors of breadcrusted clasts have undergone a second, renewed vesiculation after outgassing and fragmentation. Residual H₂O contents for all block types measured by Raman spectroscopy and gas chromatography range from

Vesiculation of portions of the melt has up to three distinct phases: early primary degassing, outgassing to variable extent (and at variable but always shallow depth), and renewed degassing. The non-breadcrusted pumices have vesicle number densities and size distributions comparable to the three preceding Plinian phases indicating their rapid ascent to shallow levels and fragmentation without the opportunity to outgas. We suggest the vesiculation of this portion of the melt largely powered the explosions. The breadcrust rinds and the dense dacite blocks show extensive coalescence and collapse of bubble populations implying their magma reached advanced states of outgassing. The variability amongst these pyroclasts suggests contrasting degrees and depths of stagnation within the shallowest conduit. Depth of stagnation controlled the residual volatile content of the melt and hence the extent of the first degassing. Duration of stagnation controlled the extent of outgassing of this primary bubble population. A strong proviso is that the existence of mingled blocks (with cm- to mm-scale banding between domains of dense and pumiceous dacite) suggest that not all melt had time to equilibrate at the depth of fragmentation.

We propose a very complex qualitative model of a dynamic conduit at Novarupta in which domains of chemically uniform magma with widely contrasting degrees of degassing, outgassing, and melt equilibration co-existed on short length and time scales at the shallowest levels immediately before and during eruption.

Kensuke Ishii, Toshiki Shimbori, Yuta Hayashi, Eiichi Sato, Tesuo Tokumoto, Akihiro Hashimoto

Submission 271

A volcanic ash data assimilation system based on the three dimensional variational method

Volcanic ash forecasts are important for world aviation safety and also for populations living around volcanoes. The Japan Meteorological Agency (JMA) has two major operations for volcanic ash forecasting. The Volcanic Ash Fall Forecast (VAFF) provides information for local communities and populations who may be affected by ash fall from volcanoes (Hasegawa et al., 2015), and the Volcanic Ash Advisory (VAA) issues information to the airline industry and aviation authorities to ensure safe aviation.

The JMA uses atmospheric transport models to calculate forecasts. Within forecasting, the initial condition of volcanic ash is one of most important and uncertain factors and it has been based on the empirical model of Suzuki (1983). Unfortunately, such empirical models often fail to reproduce the actual plumes of volcanic eruptions which indicates an empirically derived assumption is too simple to be applied to actual variety of volcanic eruptions. For example, actual large eruptions often create umbrella clouds. However, in the operational model, umbrella clouds are not created, and the initial condition is almost a vertical line source compared to actual ash distribution.

We have begun using the three-dimensional variational data assimilation method (3D-Var) so that we may obtain a more accurate initial condition. 3D-Var has low computational cost and can provide initial conditions immediately after an eruption. Weather radar and Himawari-8 (geostationary meteorological satellite) observation data are used as input for analysis. The mutually independent analysis variables of concentration of ash and size distribution parameters are used (Ishii et al., 2016).

We expect that we can obtain three-dimensional ash concentration and parameters of ash particle size distribution from the radar observation. From satellite observation, retrieval of ash clouds provide two-dimensional parameters such as mass loading, top height and effective radius of ash particles (Hayashi et al, 2016). Because accurate forecasts need an initial condition having an accurate vertical profile, estimation of the thickness of ash clouds is required. We estimated the thickness of ash clouds using vertical wind shear, and derived the observation operators for the Himawari-8 satellite retrieval data in the 3D-Var.

Acknowledgement

This work is supported by Integrated Program for Next Generation Volcano Research and Human Resource Development.

Shelby Isom, Erik Shafer, Martin Streck, Ilya Bindeman

Submission 614

The voluminous, low $\delta^{18}\text{O}$, and strongly trace element zoned high-silica rhyolite reservoir of the Devine Canyon Tuff, eastern Oregon: Reality check for the mush model.

The Devine Canyon Tuff represents a large-volume ($>300 \text{ km}^3$), high-silica rhyolite magma body that erupted $\sim 9.7 \text{ Ma}$, from the Harney Basin of southeastern Oregon, forming a simple cooling unit after an initial plinian phase. Bulk rock and pumice analyses indicate nearly all of the tuff ($>99\%$) is strongly trace-element zoned high-silica rhyolite, except sparse dacite and dacite/rhyolite banded pumices. Data ranges of bulk tuff is slightly less than compositional range defined by rhyolite pumices, which are [ppm]: e.g. Zr 611-1600, Nb 46-112, Rb 52-180, Y 75-204. Pumices lie in compositional clusters with or without gaps. $\delta^{18}\text{O}$ values of quartz and feldspar vary among phenocrysts of single pumices of all rhyolite compositions, from most to least evolved, as well as for dacite pumice. Converted $\delta^{18}\text{O}$ melt values indicate a max. range of 1.5‰ from 4.28‰ to 5.76‰. Quantitative mineral data on pumices, including fallout, indicate rhyolite magmas vary in crystallinity from 3 to 19% and dacite is at 22%. However, size distribution of phenocrysts among rhyolites changes progressively with each rhyolite, with narrow and overlapping compositions across rhyolites (sanidine with Ab: 54-59, Or: 46-41; cpx with En: 57-58 Wo: 41-41.5) and slightly wider range of minerals from dacite.

Tight mineral compositions, banded pumices composed of different rhyolites, and low $\delta^{18}\text{O}$ strongly suggest different rhyolites erupted from a contiguous and shallow reservoir rather than separated reservoirs. The low $\delta^{18}\text{O}$ values point to hydrothermally altered material and we hypothesize that addition of this material occurred prior to the development of trace element zonation of highly fractionated rhyolites ($\text{Eu}/\text{Eu}^* 0.08\text{-}0.16$). Intermediate rhyolites cannot be solely generated through the mixing of the end-member rhyolite melts but require, as minimum, some subsequent modification. Similar but distinct minerals of dacites argue against a direct cumulate-extracted melt relationship with any observed rhyolite and low $\delta^{18}\text{O}$ of rhyolites precludes a dominant origin through melt extraction from an intermediate magma body. Dacitic magma appears to have resulted from mixing with more mafic magmas rather than from remobilized crystal mush. All this suggests magmatic evolution occurring within melt rich rhyolite magma(s) and nearby evolution of intermediate magmas rather than punctuated extraction of melt from intermediate crystal mush.

Ima Itikarai

Submission 1044

Application of high frequency volcano-tectonic earthquakes for forecasting volcanic eruptions.

Volcanic eruptions occur as a result of pressure build-up inside a shallow magma reservoir beneath a volcanic edifice. Pressure build-up in the shallow magma reservoir is normally caused by intrusion of new magma and the occurrence of certain volcanic processes that occur inside the magma body. The pressure build-up generates detectable eruption precursor phenomena such as various types of volcano seismicity, surface deformation, volcanic gases, and others. This work focuses on high frequency volcano-tectonic earthquakes and its application in forecasting volcanic eruption. A number of observations have been made at a number of volcanoes in Papua New Guinea, including Rabaul, Manam and Ulawun between the two between 1995 and 2014 and they seem to have a strong correlation. The lead-time between the occurrence of high frequency volcano-tectonic earthquakes and an eruptions ranges between weeks to months. Furthermore, the observations suggest the lead-time is shorter for open and partially open volcanic systems and longer for partially closed and completely closed systems. The outcomes of this work suggest it is possible that the lead-time to an eruption is not restricted to weeks to months only, but can extend into years. In this case the volcano would have been quiet for an extended period of time.

Ima Itikarai

Submission 1054

Challenges of routing monitored volcano parameters to a central facility for effective volcano monitoring.

In many under-developed and developing volcano-prone countries monitoring volcanoes in an effective and efficient manner is very challenging. There are multiple reasons for this including, lack of financial resources, lack of appropriate volcano monitoring equipment, lack of relevant national infrastructure and others. Rabaul Volcanological Observatory (RVO) in Papua New Guinea that has a mandate to monitor 15 active volcanoes in the country has had many of these challenges. But since 1995 assistance provided by the Governments of USA and Australia through the Volcano Disaster Assistance Program under the auspices of USGS and the PNG-Australia Volcano Support Project undertaken by Geoscience Australia has addressed some of these issues progressively in a cost efficient way to a state where RVO is now routing real-time seismic waves from two of its remote volcanoes to its central facility at RVO. It has plans to install similar facilities at three volcanoes in the next 1-2 years.

Hisatoshi Ito

Submission 371

Entire magmatic history of the Kikai Caldera as revealed by zircon U–Pb method

The Kikai Caldera, a mostly submerged caldera ~50 km off Kyushu Island, Japan, is well-known as a caldera whose eruptive products devastated prehistoric human activities in southern Kyushu at ~7.3 ka. It is of prime importance to reveal magmatic history of this caldera to assess the next gigantic eruption. Zircon U–Pb dating using LA-ICP-MS should be a viable tool for this purpose because it can date both old (xenocrystic) and young (autocrystic) ages with high throughput from a single tephra layer. Recently, we investigated three tephra layers in the nearby Yakushima Island and assumed that the Kikai Caldera initiated its gigantic magmatic activity at ~0.7 Ma, followed by ~0.6 Ma, ~0.1 Ma and the latest 7.3 ka gigantic eruptions (Ito et al., 2017). This conclusion was obtained mainly because the ~0.1 Ma tephra (K-Tz from the Kikai Caldera) contained zircons of ~0.7 Ma and ~0.6 Ma (Ito et al., 2017). In order to further establish magmatic history of the Kikai Caldera, we collected tephtras from another nearby island, Tanegashima Island and the Satsuma Iwo-jima Island, a small island that constitutes parts of the caldera rim. To date, zircon U–Pb data from the Tanegashima Island were obtained: the data confirmed that two (~0.6 Ma and ~0.1 Ma) magmatic activities occurred presumably in the Kikai Caldera. Adding zircon U–Pb data from the Satsuma Iwo-jima, the source area of the Kikai Caldera, we expect that the entire magmatic history of the Kikai Caldera will be further established.

Reference: Ito, H., Uesawa, S., Nanayama, F., and Nakagawa, S., 2017, Zircon U–Pb dating using LA-ICP-MS: Quaternary tephtras in Yakushima Island, Japan: *Journal of Volcanology and Geothermal Research* (in press).

Hideyuki Itoh, Hidekazu Kakuno, Morio Tsuji, Seima Ichikawa, Shinya Narita, Fumihiko Takasaki

Submission 277

Radiographic measurements of the internal structure of the Iwate Volcano using cosmic – ray muons and groundwater chemical composition .

Muon radiography is a recently developed technique with several successful applications being reported, such as Satsuma-Ioujima, volcano and Asama volcano (Tanaka, et.al, 2009a, 2009b).

The Iwate volcano is located in north - east Japan. Following 1998 - 2003 eruption crises of volcano, earthquake swarm and inflation were observed due to magma intrusion into a shallow zone.

The authors built a muon detector, which has been operational since October 14, 2016 in the east foot of the Iwate volcano, approximately 6 km from the Yakushi-dake crater. On the other side, we analyzed the chemical composition of spring water recharged from the Iwate volcano, to clarified deep underwater flow systems in the interior of the volcano. In addition, we investigated the relationship between chemical composition of spring water and the image of the internal structure of the Iwate volcano obtained from muography.

From the observations, two-dimensional images were obtained. However, the measured value of the density length of the volcano deviated considerably from the actual thickness of the volcano, which was apparently owing to the influence of the electromagnetic shower. We explored the redact technics that influence the electromagnetic shower.

From the chemical composition of the spring water can be divided into two groups $\text{Ca}(\text{HCO}_3)_2$ and SO_4^{2-} in addition to $\text{Ca}(\text{HCO}_3)_2$. Tritium dating gives values of 13.9-23.5 years. In particular, for the Oide and Kanazawa springs, the values were 19.4 years and 23.5 years, respectively. This indicates the possibility of the groundwater being recharged during the 1998-2003 eruption crises to flow out from now onwards.

Richard Iverson, David George

Submission 87

Modeling the massive 2010 debris avalanche/lahar at Mount Meager, Canada: seamless simulation from initiation to deposition

On 6 August, 2010, about 50 million cubic meters of wet, hydrothermally altered rock slid off the south face of Mount Meager volcano in southwestern British Columbia, Canada, and transformed into a lahar that traveled about 13 km along a tortuous path before it temporarily dammed the Lillooet River. Extensive geological documentation of the event (Guthrie et al., *Natural Haz. Earth Sys. Sci.*, 2012, doi:10.5194/nhess-12-1-2012) and its seismic signature (Allstadt, *J. Geophys. Res. Earth Surf.*, 2013, doi:10.1002/jgrf.20110) makes the Mount Meager debris avalanche/lahar well-suited for assessing numerical simulations. We have simulated the event using D-Claw, a depth-integrated two-phase flow model we previously developed and tested against data from large-scale debris-flow flume experiments (Iverson & George, *Proc. Royal Soc. London A*, 2014, doi: 10.1098/rspa.2013.0819, and doi: 10.1098/rspa.2013.0820). A key feature of D-Claw, crucial for modeling lahar mobilization from landslides, is the model's ability to seamlessly simulate transitions from statically balanced states to rapidly flowing, liquefied states without employing unrealistic dam-break initial conditions or adjusting parameter values along flow paths. This ability results from the model's computation of evolving granular dilatancy and pore-fluid pressure, which in turn influence evolution of basal friction. As a consequence of the close coupling of these variables, D-Claw predictions of flow dynamics depend largely on the values of two dimensionless parameters: the difference between the initial solid volume fraction and static critical-state volume fraction, $m\text{-}m_{\text{crit}}$, and the ratio of timescales for downslope debris motion and slope-normal pore-pressure diffusion, Trat . Neither parameter was independently measured for the Mount Meager event. Therefore, we chose values of $m\text{-}m_{\text{crit}}$ and Trat that were consistent with the debris avalanche's composition and also with the requirement that forces must have been statically balanced in debris that was initially poised in the steeply sloping source area. When constrained in this way, D-Claw yields predictions that successfully mimic the major features of slope failure and lahar dynamics at Mount Meager. In particular, model simulations are broadly consistent with flow speeds inferred from seismological interpretations, runup and superelevation heights observed along the runout path, and the final distribution of lahar deposits.

Nels Iverson, Nelia Dunbar, Andrei Kurbatov, William McIntosh

Submission 1282

Antarctica's englacial tephra record: linking source volcanoes, ice cores and blue ice areas

Developing an integrated tephrochronology framework for Antarctica has been an ongoing project over the past several decades. This framework integrates limited exposures on volcanoes with proximal blue ice areas and more distal ice core tephra records. The tephra fallout from explosive volcanic eruptions in Antarctica provide isochronous time markers called "pinning points" that can be correlated between different ice records. These pinning points allow for time to be translated from one location to another on a time scale more precise (

Local volcanic sources dominate the englacial tephra record; mainly large stratovolcanoes in Marie Byrd Land (Mt. Berlin and Mt. Takahe) and Northern Victoria Land (Mt. Melbourne). Although, these volcanoes have produced numerous eruptions, very few are widely distributed enough to provide robust regional markers. Precise and accurate geochemistry is required to distinguish between the many trachytic tephra layers sourced from local volcanoes and even more difficult to distinguish are different eruptions from the same volcano. Often, only one geochemical component is different (i.e. MgO at Mt. Berlin (~0.05 wt. %) and Mt. Takahe (> 0.20 wt. %)) and allows for volcanic source to be determined. Mt. Berlin, which has produced 35 distinct tephra layers in the past 100 ka, shows an increase in Fe over time, which can help distinguish between different layers. Tephra from local volcanoes are difficult to correlate across Antarctica and we look to more unique tephra compositions for robust correlations, many of which are cryptotephra from non-Antarctic volcanoes. One such tephra is the ~25 ka Oruanui tephra from New Zealand, which is the first direct link between Antarctica and New Zealand climate records.

There are very few tephra layers that can be found in both East and West Antarctic ice cores and recent advancements in analytical techniques have proven valuable in obtaining meaningful geochemistry of fine grained cryptotephra. Identifying and analyzing cryptotephra, particularly from the centrally located South Pole ice core, will allow for more correlations to be made across the continent and provide better understand of paleoclimate.

Katrina Jacobs, Nico Fournier, Charles Williams, Martha Savage, Colin Wilson

Submission 473

Signatures of Regional Tectonics in Local Volcano Responses in the Taupo Volcanic Zone, New Zealand

An increasing number of studies globally are recognising that regional tectonic processes can have a major influence on volcano behaviour. How can broad scale tectonic processes be incorporated into volcanic monitoring and hazard assessment? A first step towards an answer is a better analysis of volcano-tectonic interactions. Here we consider the far-field processes that may affect volcanic activity by examining the impact of regional, large-scale tectonic events on volcano behavior in the Taupo Volcanic Zone (TVZ). Our main study area is Taupo caldera volcano and the southern TVZ. We focus on the response to slow slip events (SSEs) located on the subduction interface and two recent $M > 7$ earthquakes (East Cape 9/2016 and Kaikoura 11/2016). We use data from continuous GPS instruments to determine strain induced by the SSEs. The loci of these SSEs are mostly relatively far away (~ 100 km) from Taupo caldera, but the resulting surface deformation is clearly seen on local GPS sites around the volcano. We have applied existing SSE slip distributions to a finite element model for two small SSEs within 100 km of Taupo caldera, as well as for several large SSEs farther away from the TVZ. The finite element models allow us to get a continuous picture of predicted strain through the region. The strain changes are also compared to seismicity rates in the TVZ to determine their influence, if any, on the timing of volcanic unrest. The area around the Taupo caldera is seismically active and includes several geothermal fields. However, the timing of seismicity inside and outside the caldera appears distinct and independent. To help determine what physical processes occur around the volcano we also examine several individual earthquake sequences for fluid diffusion and spatial expansion patterns. We also look for evidence of temporal changes in ambient noise to quantify the background fluctuation of velocity changes and the sensitivity of Taupo to strain induced by SSEs and large earthquakes. Volcanic responses are not observed for all SSEs. The strain results indicate that dilatational strain may increase the likelihood of observing a local volcanic response. Strain is relatively easy to measure, and increasing dilation could trigger additional monitoring protocols in the future. The difference in volcanic responses to the large earthquakes and SSEs will be used to estimate thresholds for observed responses, and the importance of strain-rate over absolute strain.

Mike James, Stuart Robson, Mark Smith

Submission 741

How precise are your SfM topographic surveys? 3-D uncertainty-based surface change detection with structure-from-motion photogrammetry and precision maps

The increasing availability of aerial imagery collected from drones offers substantial opportunities for detecting and measuring surface change in volcanic environments. However, such data are usually processed into 3-D products or DEMs using structure-from-motion (SfM) software which doesn't provide the detailed error metrics characteristic of rigorous photogrammetry, and thus can limit the interpretation of detected change.

Here, we present a novel approach to generate maps of 3-D precision for SfM-based surveys that have been georeferenced either directly using camera positions or by ground control (James et al. 2017). The maps illustrate the spatial variability in precision that is associated with the relative influences of photogrammetric (e.g. image network geometry, tie point quality) and georeferencing considerations (e.g. number and distribution of control points, quality of their ground survey measurements). They then enable confidence-bounded quantification of 3-D topographic change that, for the first time, specifically accounts for the precision characteristics of repeated photo-based surveys through an adapted state-of-the-art point-cloud comparison (M3C2; Lague, et al., 2013). The utility of the approach has been demonstrated in a geomorphology context (eroding badlands).

Our method not only enables confidence-bounded 3-D change detection and uncertainty-based DEM processing, but also provides covariance information for all parameters. Thus, we now open the door for SfM practitioners to use the comprehensive analyses that have underpinned rigorous photogrammetric approaches over the last half-century.

James et al. (2017) 3-D uncertainty-based topographic change detection with structure-from-motion: precision maps for ground control and directly georeferenced surveys, <http://dx.doi.org/10.1002/esp.4125>

Lague et al. (2013) Accurate 3D comparison of complex topography with terrestrial laser scanner: application to the Rangitikei canyon (N-Z), <http://dx.doi.org/10.1016/j.isprsjprs.2013.04.009>

Maria Janebo, Thorvaldur Thordarson, Sébastien Biass, Costanza Bonadonna, Bruce Houghton

Submission 626

Estimating eruption source parameters for explosive eruptions in Iceland

Eruption source parameters (ESPs)—such as magma volume/mass, discharge, and plume height—are critical information for the physical characterization of eruptions and as input parameters for numerical simulations of tephra dispersal used for real-time forecasting and long-term hazard assessments. Most ESPs are traditionally derived from field measurements via a range of empirical methods. A common feature of these approaches is that they require detailed mapping of the tephra deposits, which is time consuming and expensive in terms of man hours. The problem is particularly acute in Iceland, which is one of the volcanically most active regions in the world, with over 20 events per century of which a majority (>70%) feature significant explosive activity. Even moderate explosive eruptions from Icelandic volcanoes (e.g., the 0.17 km Eyjafjallajökull summit eruption in 2010) can have significant impact on international air traffic.

About 700 tephra-producing events are preserved in the post-glacial soil and lake sediments in Iceland and the last 3 ka contains about 200–250 events. ESPs, however, have yet to be determined for most of these eruptions. Dispersal maps have only been published for <45 of these tephra layers, and there is good control on the ESPs for <20. Establishing a statistically robust data set of ESPs for explosive eruptions in Iceland is a critical task for both fundamental understanding of eruptive processes and for ash forecasting. An alternative approach of determining ESPs is provided by inversion modeling. We will present results for selected test-case eruptions from Hekla volcano, which is one of the historically most active volcanoes in Iceland. The selected events span the explosive spectrum of hybrid eruptions at Hekla, covering a range of magma compositions and eruption magnitude. The eruptive volume was estimated using the TEPHRA2 model in inversion mode. The number of data points used for the inversion was systematically reduced to determine the minimum number/spacing of data points required to produce first order estimates of eruptive volume. Applying the approach in the future to a much larger set of eruptions for which ESPs have not yet been determined will enable the construction of a more robust data series on explosive eruptions in Iceland, allowing for assessment of spatial and temporal distribution of eruption magnitude and intensities, and systematic hazard assessments of events.

Maria Eva Jankovics, Szabolcs Harangi, Balazs Kiss, Karoly Nemeth, Theodoros Ntaflos

Submission 1124

High-resolution mineral-scale analysis to unravel the complexity of the subvolcanic magmatic systems beneath monogenetic basaltic volcanoes

Investigation of the textures, zoning and chemistry of rock-forming minerals is an essential tool in discovering the evolution of subvolcanic magmatic systems. Since minerals respond both texturally and compositionally to changing magmatic environments, in their crystal growth stratigraphy they preserve a wealth of information concerning their history of magmatic processes and compositions. Detailed mineral-scale analyses allow us to detect distinct crystal populations and the origins of single crystals and portions of crystals. Despite this, the detailed studies focusing on single monogenetic basaltic centres generally only rest on whole-rock geochemistry. These revealed significant compositional variations through the successions that were interpreted as the result of complex melting and mixing processes within the mantle sources, variations in melting conditions or mixing of different magma batches during ascent.

We present the results of an approach that provides a unique, more direct and detailed insight into the evolution of these “simple” magmatic systems. This includes the integrated analysis of olivine crystals and their spinel inclusions as well as of clinopyroxenes. Through this high-resolution mineral-scale investigation applied for monogenetic volcanic centres in the western Pannonian Basin we demonstrate the remarkably complex evolution of these subvolcanic magmatic systems enabled by the fact that crystal growth stratigraphy and compositions yield direct evidence for various petrogenetic processes which are usually obscured in the whole-rock geochemistry.

With the stratigraphically ordered sampling and the detailed petrogenetic analysis of the individual eruptive units of volcanic centres we revealed the features and evolution of the successively erupted magma batches as well as the processes operated in the magmatic system. The intra-crystal compositional variations of olivine crystals characterised by various textural and zoning patterns and the diverse chemistry and position of their spinel inclusions indicate several distinct magmatic environments and bear evidence of magma accumulation, storage, fractionation, replenishments and mixing. Our results imply that the petrogenesis of a single magma batch – usually defined as representing a given eruptive unit – can be as complex as involving multiple magma packets and various, closed- and open-system magmatic processes which finally result in the whole-rock (erupted magma) composition.

Anne Jay, Matthew Balme

Submission 635

A new 3D map of the Main Deccan Province constraining the current and original volumes of the geochemically defined formations.

The Deccan large igneous province (LIP) is one of the best preserved and most studied LIPs on Earth. It was emplaced before, during and after the end-Cretaceous mass extinction event (KPB), so constraining the volumes of lava erupted is vital for understanding the role the Deccan played in end-Cretaceous climate change and the mass extinction event itself. The Deccan LIP has been well-studied and a geological map produced (e.g., Beane et al. 1986, Devey and Lightfoot, 1988 and Khadri et al. 1999) using a chemostratigraphy which has 3 sub-groups and 12 formations. However, useful formats of this map have limited availability, and, as many of the formations are exposed in steep cliffs, these are difficult to display on a paper map.

To improve our understanding of the role the Deccan played in the KPB it is essential that the spatial distributions of variations in the lavas (e.g. physical volcanology, mineralogy, and geochemistry) are studied in higher detail than the formation-level. Significant detailed work has been done, and incorporating this into the stratigraphy is important, but it is challenging to display these data in conjunction with the current geological maps.

This study uses GIS (Geographic Information System) and new Digital Elevation Models (DEM) to display the current Deccan geological map in a more useful form. This allows a better understanding of the gross structure of the province and can provide a higher resolution, more useful geological map for future workers. The DEM used for the GIS is the newly released, 12 m per pixel TanDEM-X data. This work is some of the first to use these high resolution DEMs.

This project concentrates on the Main Decan Province (MDP), as this contains the KPB lavas. Chemostratigraphic data have been compiled from multiple published sources, including various Ph.D. theses, that provide the elevations and positions of the boundaries of the 12 formations across the MDP. These “XYZ” co-ordinates are imported into the software ArcGIS and projected onto the DEM. In addition to providing a new 3D map, these data allow the formation boundaries to be used to estimate the current volume of the formations. Furthermore, the formation boundaries can also be projected beyond the outcrop, to predict the original volumes of lava in each formation.

Beane, et al. (1986). DOI 10.1007/BF01073513

Devey, & Lightfoot, (1986). DOI 10.1007/BF01087674

Khadri, et al. (1999).MEM. GEOL. SOC. INDIA, (2), 179-202.

Mark Jellinek, Thomas Aubry, Wim Degruyter, Costanza Bonadonna

Submission 329

Evaluation of future volcanic SO₂ emissions into the stratosphere and consequences for future volcanic forcing experiments in Global Climate Models

Stratospheric volcanic sulfate aerosols modify Earth's radiative balance and are a key climate forcing. Our understanding of volcanic sulfate aerosol forcing and the ability of climate models to simulate their impacts has continuously improved in the past decades. However, due to the absence of reliable forecasting of future eruptions at timescales relevant for climate projections, incorporation of volcanic forcing in global climate model (GCM) projections remains rudimentary.

Here, we explore a method to estimate future volcanic SO₂ emissions into the stratosphere using a statistical model of eruption source conditions, a volcanic plume model, and atmospheric conditions retrieved from CMIP5 climate models for various greenhouse gas emission scenarios. Our statistical model for source conditions is based on a 2500-year ice core record of "large eruptions" and a 37-year satellite record of "small eruptions", and assumes that the probability distribution of eruption source parameters will not change at timescales relevant for climate projections.

First, we show that as a consequence of changes in the tropospheric lapse rate and the tropopause height driven by anthropogenic greenhouse gas emissions, fewer volcanic plumes are expected to reach the stratosphere in the coming centuries due to a decrease in the tropospheric lapse rate and the tropopause height driven by anthropogenic greenhouse gas emissions. This effect reduces the flux of volcanic SO₂ into the stratosphere, particularly in the tropics. For the scenario with the largest greenhouse gas emission (RCP8.5), such changes may be significant despite large uncertainties in projected SO₂ flux at centennial timescales.

Secondly, the uncertainties themselves pose challenges for climate model projections. Indeed, our results suggest that the flux of volcanic SO₂ into the stratosphere at centennial timescales could vary by up to a factor 4, mostly due to variability in the distribution of frequency and magnitude of explosive eruption suggested by our statistical model of eruption source condition.

We discuss the consequences of our results for designing volcanic forcing scenarios for GCM projections and test whether the changes in average flux and uncertainties projected would significantly affect future climate projections.

Susanna Jenkins, Harvey Goldstein, Steve Sparks, Takehiro Koyaguchi

Submission 285

Forecasting explosion repose intervals with a Bayesian survival model: Application to Sakura-jima volcano, Japan

With increasing population densities and expanding urban boundaries, the potential for explosive volcanic eruptions to adversely impact upon urban areas is increasing. This is particularly true for volcanoes along subduction zones as they are almost exclusively explosive and often coincident with large populations and population densities. Explosive eruption hazards such as tephra fall have the potential to impact very large areas and potentially very large numbers of people. The tephra fall hazard at any one site may be the sum of potential hazards from more than one volcano. For example, Tokyo in Japan has at least 40 Holocene active volcanoes within 500 km. In addition to considering the cumulated hazard at any one site, there is an emerging need from international agencies, industries and governments for hazard and risk information to be available at regional or global scales, allowing at-risk areas to be compared on a like-for-like basis. In this study, we have carried out site-specific probabilistic tephra fall hazard assessments for 16 major cities in the Asia-Pacific region, one of the world's most densely populated and volcanically active regions. Tephra fall footprints from large numbers of plausible explosive eruptions were simulated for 141 volcanoes within 500 km of the cities, and the results aggregated for each city. There is a clear distinction in hazard levels between cities near subduction zones and those farther away resulting from the higher number and density of volcanoes and the increased probability of more explosive eruptions in subduction zone settings. By combining the resulting site-specific hazard with a number of different indicators describing the exposure and vulnerability of people and infrastructure, we have calculated tephra fall 'risk scores' for each city. These relative scores, or rankings, provide overview information on cities in the Asia-Pacific region most at risk from tephra falls. The highest hazard and risk scores are in Manila, Surabaya, Tokyo and Jakarta. While this study provides a transparent and consistent method for assessing regional volcanic hazard and risk, there are challenges associated with the data-poor setting and we conclude the paper by discussing what is required in order to improve regional volcanic hazard and risk assessments.

Max Jensen, Luca Caricchi, Jon Blundy, George Cooper, Othmar Müntener

Submission 1118

The temporal evolution of an arc volcano through zircon petro-chronology of intrusive and volcanic products

Eruptible magma (magmas with

The volcanic islands of St Kitts and Nevis, situated in the northern part of the Lesser Antilles Volcanic Arc in the Caribbean Sea, offers a rare opportunity to study coeval plutonic and volcanic rocks from the same magmatic system. Erosion of the islands eastern portion has exposed the intrusive part of the volcanic systems. Additionally, cumulates, which indirectly sample the intrusive rocks, are also abundant in the volcanic products.

The statistical analysis of populations of zircon ages provides insights on the thermal evolution of magmatic systems. However, while this analysis has been proven useful for intrusive rocks, its applicability on volcanic rocks has yet to be thoroughly tested. Preliminary investigation of the samples from St Kitts and Nevis revealed that zircons are present in volcanic products but also in mafic cumulates, making zircons suitable tracers for chemical fluctuations throughout the systems' magmatic history.

We focus on a combined geochronology and geochemical study of zircons separated from the volcanic and intrusive (plutonic + cumulates) products to trace the temporal evolution of the magma chemistry. Analysis of U/Pb, U/Th and trace elements composition of zircons will be determined using LA-ICP-MS. The results will be used to compare the geochemistry of coeval zircons from volcanic and intrusive products to determine if the zircons, when integrated, provide a complementary picture of the temporal evolution of magmatic systems.

Keywords: Zircon petro-chronology; zircon age populations; LA-ICP-MS; temporal evolution; magma reservoirs

David Jessop, Josef Dufek, Mark Jellinek, Olivier Roche, Johan Gilchrist

Submission 994

Particle-plume coupling and vent-shape effects on volcanic plume stability

Explosive volcanic eruptions produce turbulent, particle-laden jets that can loft material several tens of kilometres or undergo gravitational collapse to produce ground-hugging pyroclastic density currents. The key to determining which of these two phenomena will occur is the turbulent entrainment of atmospheric air, which adds buoyancy to the jet. We demonstrate how two important factors, vent shape and particles critically coupled to the flow, affect turbulent entrainment, and hence jet stability.

Natural volcanic vents can have a variety of shapes including circular, flared (craters), elongated (fissures) and annular (calderas). Recent work using scaled analogue experiments, has tested the effect of these different vent geometries on the entrainment rates into jets laden with inertial particles [Jessop and Jellinek, 2014; Jessop et al., 2016]. This work shows that the smallest gap size sets the initial eddy size, which governs the entrainment rate and that the aspect ratio (e.g. gap size/diameter for annular vents) of these more complex vent shapes has a strong influence on the stability of the jet, with more extreme aspect ratios causing the jets to collapse more readily. These findings make explicit predictions for deposit architectures which can be tested using field data.

The coupling of particles to a turbulent flow is determined by how rapidly it responds to fluid accelerations. This coupling depends on the particles' size, density, the fluid's viscosity, and the speed and size of turbulent eddies. Critically-coupled particles have a response time approximately equal to the time scale for fluid accelerations. We use scaled analogue models and numerical simulations to show that the presence of critically-coupled particles, even in low concentrations, can dramatically alter the dynamics of turbulent entrainment by changing the size and intensity of the eddies that are responsible for entraining ambient fluid into the flow.

Ingrid Johanson, Asta Miklius, Michael Poland

Submission 1165

Unraveling the contributions of multiple sources during a 2015 intrusive sequence at Kīlauea Volcano

A sequence of magmatic events in April-May 2015 at Kīlauea Volcano produced a complex deformation pattern captured by Hawaiian Volcano Observatory monitoring networks, which include continuous GPS stations and tiltmeters. The sequence began with inflation in the volcano's summit caldera near Halema`uma`u (HMM) Crater, which continued over a few weeks, followed by rapid deflation of the HMM source and inflation of a source in the south caldera region during the next few days. Separating the magnitude and time history of each source's contribution to the overall deformation pattern is an important step towards describing the underlying volcanic processes.

We used principle component analysis of daily GPS time series from the 2015 intrusion sequence to determine three basis vectors. These vectors are combined with InSAR data from the COSMO-SkyMed and Sentinel-1A satellites. The InSAR data provide additional constraints on the geometry of the sources, while the GPS data inform how much each of the three sources contributes to the interferograms given their individual timespans. The three basis vectors correspond with three sources: 1) a shallow source near Halema`uma`u Crater that is consistent with a known zone of magma storage, 2) a body in the south caldera region that has long been recognized as a location for long-term magma storage, and 3) a deformation source near Keanakāko`i Crater, which has been previously noted as an intermittent source of magma accumulation. Unraveling when and to what extent each of these sources was active during the 2015 intrusive event provides insight into the structure and connectivity of Kīlauea's shallow magmatic system.

Jessica Johnson

Submission 1087

Changes in scattered seismic energy associated with eruptions at Mt Ruapehu detected using repeating earthquakes

For two earthquakes to have seismograms that are indistinguishable to within uncertainties, they require near-identical source parameters (hypocentre and moment tensor) and invariant seismic properties along the propagation path. We have identified 29 sets of similar earthquakes from the Waiouru swarm to the south-east of Mount Ruapehu Volcano in New Zealand. These multiplets are identified using the permanent geonet network of seismometers and span 15 years from 1995 to 2010. The multiplets have P-wave code with cross correlation coefficient of 0.99. However, most multiplets display a discrete change in S wave coda (from 0.95 to less than 0.5) at times around the last two eruptions of Mount Ruapehu in 2006 and 2007. The changes in S coda correlation are due to a single pulse of energy, signifying a change in scattered energy. We have located the source of the scattered energy by simply subtracting the seismograms and locating the residual.

Preliminary results suggest that the source of the changing scatterer locates near another cluster of earthquakes to the North West of Mount Ruapehu, named the Erua cluster. The Erua cluster is associated with the delamination of the lithosphere as the Pacific plate is subducted beneath the Australian plate. This cluster of earthquakes has also shown to have changing properties (seismic anisotropy and b-value) at times of volcanic unrest at Mount Ruapehu. We suggest that small changes in the character of the lithosphere at this location as the lithosphere delaminates create inhomogeneities that scatter seismic energy. These small changes in scattered energy can be detected using extremely similar earthquakes from the Waiouru swarm.

Jeffrey Bruce Johnson, Leighton Miles Watson, Eric Dunham, Jose Luis Palma, Luis Franco Marin, Carlos Cardona, Alexander Miller

Submission 976

Forecasting Paroxysmal Eruptions at Volcán Villarrica (Chile) Using Infrasond

On the morning of March 3rd, 2015 Volcán Villarrica (Chile) erupted suddenly and with a powerful 30-minute-long lava fountain reaching more than 1.5 km above the summit crater. It was the first explosive eruption from the volcano in about thirty years and a dramatic departure from its steady state, which is characterized by an open-vent configuration and roiling lava lake situated ~102 m below the crater rim. The eruption was presaged by anomalous seismicity and acoustic radiation beginning in January 2015 and exhibiting an uptick in early February. Though this was recognized as a sign of increasing volcanic unrest the precise timing and suddenness of the March 3rd paroxysm was unanticipated.

In hindsight we have carefully examined the seismo-acoustic records and found that the infrasond character - in particular - showed dramatic changes during the 52-hour interval preceding the paroxysm. The low frequency sounds from regular Strombolian-type explosions exhibited both changing frequency content (0.75 to 1.3 Hz) and resonance 'quality' (4 to 1) over the course of several days. Through corroboration from aerial structure-from-motion (SFM) analysis and numerical modeling we are able to relate these variations to changing crater morphology associated with a lava lake rising in the crater. This presentation focuses on how infrasond can be used to quantitatively detect changes in the morphology of a volcano's crater and permit remote tracking of a lava lake stage. Such monitoring has important implications for other potentially hazardous open-vent volcanoes. Although Villarrica's changing infrasond character was not recognized prior to the March 3rd eruption we propose that the infrasond network operated there by the University of Concepcion may be helpful to forecast that volcano's future eruptions.

Jeffrey Johnson, Jose Luis Palma, Nick Varley

Submission 977

Monitoring Lahars with Infrasond

Volcanic mudflows are well suited to infrasound-band and low-frequency audio band monitoring and can be detected using arrays of microphones deployed many kilometers away from a flow path. As an example, the paroxysmal 2015 eruption of Volcán Villarrica (Chile) produced a lahar, which descended more than 20 km within the Rio Correntoso/Turbio drainage and destroyed two small bridges. A single three-element infrasound array located 10 km from the summit, and 4 km from the lahar's closest approach, was used to detect and map the passage of the initial flow front, which moved from 2 km to 12 km downslope at an average speed of 38 m/s. After its initial advance the lahar infrasound remained detectable for more than two hours and was manifested as broadband tremor with exponentially decreasing amplitude. Additional arrays located near other Villarrica drainages recorded contemporaneous and smaller, more local lahars, including a sequence of more than six distinct pulses that were mapped in one drainage. Infrasond surveillance of lahar channels is a promising new technology and should provide an important complement to seismic monitoring because of its capability to track sources of sound with a high degree of precision and from significant distances. Outstanding challenges remain for developing processing techniques and sensor topologies that will optimize detection of lahars. Ongoing work includes modeling the flow mechanisms, which are able to ensonify the atmosphere. Additional field experiments are also needed to match acoustic recordings with multiparametric observations of flow parameters. Toward this objective, work is planned at Volcán de Colima (Mexico) to detect secondary lahar events common during the rainy season.

James Jolles, Rebecca Lange

Submission 1139

A re-examination of temperature and mineral-melt equilibrium across Early to Late Bishop Tuff: Insights from all possible pairs of Fe-Ti oxides per pumice clast

The Bishop Tuff, >600 km³ of high-SiO₂ rhyolite that erupted ~0.77 Ma in eastern California, is one of the most intensively studied volcanic deposits in the world. Among its defining features are marked changes in composition and mineralogy between earliest and latest erupted material (Early and Late Bishop Tuff). There is on-going debate, however, whether there was a corresponding thermal gradient (~700-800°C), inferred on the basis of Fe-Ti oxide thermometry. Typically, only one Fe-Ti oxide pair per pumice clast has been used to calculate temperature. In this study, Fe-Ti oxide separates from 24 single pumice clasts sampled from across units of the Bishop Tuff (Early to Late) have been analyzed. On the basis of all possible pairs that pass the Mg/Mn equilibrium test, the results confirm average Fe-Ti oxide temperatures per pumice clast of ~700-735°C for the Early BT, ~735-755°C for the Middle BT, and ~775-800°C for the Late BT. However, three surprising results include: (1) temperatures in each pumice clast, whether from Early, Middle, or Late Bishop Tuff, span a continuous range of ~50 degrees, on average; thus nearly half the thermal gradient documented for the entire Bishop Tuff is present in each pumice clast; (2) the temperature range is independent of number of Fe-Ti oxide pairs used (35 to 5188), % crystals, or evidence of magma mixing; (3) there is no difference in the average temperature and ΔNNO values calculated from Fe-Ti oxide pairs that pass vs. fail the Mg/Mn test (in 23 of 24 cases). Plagioclase was also analyzed in each clast, and there is an abrupt (not continuous) change in its average composition between Early/Middle (~An₁₆) and Late (~An₂₃) Bishop Tuff. Application of the plagioclase-liquid hygrometer, when combined with the average Fe-Ti oxide temperature calculated for each clast, leads to water contents that match those analyzed in quartz-hosted melt inclusions. This supports the Fe-Ti oxide thermometry results, which also allow melt ferric-ferrous ratios to be calculated. Compositions of orthopyroxene in clasts from Middle/Late Bishop Tuff result in Fe²⁺-Mg KD values that match those from phase-equilibrium experiments from the literature. The combined evidence supports Fe-Ti oxide equilibrium between ilmenite and titanomagnetite across all units of the Bishop Tuff, although individual pumice clasts consistently sampled melts that spanned a pre-eruptive temperature interval.

Joshua Jones, Wendy McCausland, Javier Pacheco, Randall White

Submission 979

Identifying coupled explosion events with a hybrid matched-polarization filter

Coupled explosion events, comprising a signal in the subsurface conduit followed by a near-surface event seconds to minutes later, are seen at a handful of persistently active volcanoes. The second signal of each pair often corresponds to observed surface activity and has a high signal-to-noise ratio (SNR); the first is typically emergent and low-SNR, making reliable identification of the signal onset a challenge. Solving this problem could serve as a proxy for tracking changes in the shallow magma system because the differences in onset times might act as a proxy for changes in magma column height or conduit permeability; however, richer data sets are needed to explore these possibilities. Matched filtering detects signals at SNR < 0 dB in a variety of environments, from volcanic regions to microseismic monitoring; in addition, we recently introduced a quantitative measure of polarization similarity that appears comparably robust with respect to SNR. In this work we develop a detector that uses polarization similarity to augment matched filter detection of coupled explosion events. We investigate detector robustness using synthetic data, then apply our technique to real data from Turrialba, Costa Rica. Using the high-level, high-performance Julia language, with a novel data architecture developed for rapid data analysis, we demonstrate real-time detection and tracking using the SeedLink data protocol.

Thomas Jones, Edward Llewellyn, Laura Höltgen

Submission 420

In-conduit magma convection during basaltic fissure eruptions

Basaltic eruptions often initiate as a fissure – the surface expression of the feeder dyke – then localize to a small number of vents on timescales varying from hours to days. This study addresses the subsurface processes that operate during localization. Measurements of SO₂ released during basaltic eruptions indicate that the volume of magma that is degassed in the subsurface is typically much greater than the volume of magma that is erupted. Furthermore, plagioclase crystals may show zonation that indicates repeated cycles of ascent and descent of the magma. These observations suggest that there is a convection system within the dyke that constitutes an exchange flow between upwelling, gas-rich magma, and downwelling, gas-poor magma. Under these conditions, the upwelling magma has low viscosity and density, whilst the descending magma has high viscosity and density.

We investigate in-conduit convection through scaled analogue experiments. Previous work has focused on exchange flow of two Newtonian fluids in a pipe, replicating the simplified geometry of a cylindrical conduit. Here, we investigate exchange flow in a slot (a rectangular duct of high aspect ratio) which replicates a more realistic dyke-like geometry. We stratify two Newtonian fluids – e.g. air, vegetable oil, glycerol, golden syrup and dilutions thereof – such that initially the lower density, lower viscosity fluid lies on top, then invert the apparatus to initiate overturn. The resulting exchange flow is documented videographically. The convective system is characterized via the dimensionless Grashof number (Gr) which is a ratio of viscous to buoyancy forces (at $Gr > 1$ buoyancy dominates). Our experiments span the range (10-32) covering most of the range expected in the natural system (10⁻³ to 10⁴). At low Gr we observe laminar flow with narrow, well-defined fingers of upwelling low density, low viscosity fluid separated by broad regions of downwelling dense, viscous fluid. As Gr increases, the flow becomes increasingly turbulent and chaotic, and no stable fingers or regions of coherent flow are established. We find that exchange is much more efficient at low Gr than at high Gr , and that upwelling regions of buoyant material – of the sort that might underlie regions of localization along a fissure – form only in low Gr systems. The convective regime therefore has implications for melt and crystal recycling, fissure localization and eruption longevity.

Meghan Jones, Samuel Soule, Mark Kurz, Dorsey Wanless, Harry Brodsky, Darin Schwartz, Veronique Le Roux, Frieder Klein, Eric Mittelstaedt, Joshua Curtice, Dan Fornari

Submission 1235

Formation and distribution of popping rocks from the Mid-Atlantic Ridge near 14N

Popping rocks are unusually vesicular mid-ocean ridge (MOR) basalts that explode upon recovery from the seafloor due to the release of trapped volatiles. The best-studied popping rock was recovered from the Mid-Atlantic Ridge (MAR) near 14°N during a 1985 Russian dredging cruise. This popping rock has been inferred to be representative of undegassed magmas from the upper mantle due to its high volatile concentrations. The 1985 sample has been used to constrain CO₂ flux from the MOR system, upper mantle volatile concentrations, and magma degassing dynamics. Here, we offer new insight into the geologic context and origins of popping rocks based on a 2016 R/V Atlantis cruise to the Mid-Atlantic Ridge near 14°N, which was the first to recover popping rocks in situ. The popping rocks were recovered by the submersible Alvin from lightly sediment-covered pillows near east side of the rift valley, proximal to an oceanic core complex. The newly recovered popping rocks display unique volatile concentrations, vesicularities, and noble gas contents relative to non-popping samples. The popping samples contain low dissolved CO₂ concentrations (161-178 ppm), moderate dissolved H₂O concentrations (.44-.50 wt%), and are at equilibrium with their eruption depth based on solubility calculations. Non-popping samples collected by Alvin from lava flows in the rift valley near 14°N display a broader range in dissolved CO₂ concentrations (154-265 ppm) and H₂O concentrations (0.21-0.76 wt %), and are commonly CO₂ supersaturated. X-ray microtomography reveals that popping rocks have vesicularities ranging from 6-21% and vesicle size distributions that reflect complexities in degassing dynamics. The popping rocks exhibit extremely high, variable total CO₂ concentrations (3000-12000 ppm) and helium concentrations (18-76 micro-cc/gram). In contrast, non-popping rocks exhibit low vesicularities (2 concentrations (

Joshua Jones, D. Sarah Stamps, Christelle Wauthier, Elifuraha Saria, Kang Hyeun Ji

Submission 1137

Investigating volcano-tectonic stress interactions in a youthful continental rift.

Volcano-tectonic processes are prominent in multiple stages of rift evolution, however their interaction is little known, especially in rift initiation settings. Previous work supports that magma-tectonic interactions can affect the regional stress state and that stress perturbations on the order of ~ 0.1 MPa may trigger the occurrence of active volcanism. These subsequent volcanic events may cause fault slip and destabilization of surface structures including volcano's flanks. This work investigates the 2007 Tanzanian rifting episode in the Natron Rift and quantifies the associated Coulomb stress change along a major border fault. We hypothesize that the 2007 rifting event caused a positive stress change that induced slip on the border Natron fault causing possible destabilization. This project uses Coulomb 3.4 to model the 2007 Tanzania rifting events and takes advantage of the Coulomb failure hypothesis to calculate the stress accumulated or released on the Natron Fault. The resulting static stress change modeling shows that there is a Coulomb stress change of ~ 0.2 MPa induced by the 2007 Tanzanian rifting episode, with the positive stress change primarily associated with volcanic activity from the Ol Doinyo Lengai volcano. We also present newly processed InSAR and GNSS/GPS data from February - September 2008, of slip coinciding with an eruption that is in agreement with our created model. This work suggests that small stress perturbations caused by volcanic activity can drive fault slip in rift initiation.

Erouscilla Joseph, Denise Beckles, Viveka Jackson, Leonette Cox, Stacey Edwards

Submission 149

Community-Based Volcano Monitoring Approach at Sulphur Springs, Saint Lucia: A Lesson in Good Stakeholder Engagement.

Many volcano-monitoring institutions face the financial and human resource challenges of providing ongoing services to economically burdened small island states. The Lesser Antilles arc includes 21 potentially active volcanoes, spread across 11 volcanically active islands. In many of these islands, large subsistence-based communities often live for generations directly adjacent to volcanoes with active hydrothermal systems. Hydrothermal activity has an influence on their water supplies, crops, air and livestock. Sulphur Springs Park (SSP), in Saint Lucia, is an active hydrothermal system that caters to a large number of recreational visitors (>200,000 annually), and has a full-time complement of staff as well as vendors, who are exposed to a continuous source of volcanic emissions. In response to concerns about the volcanic emissions and its possible health effect the UWI-Seismic Research Centre (SRC) established a monitoring network for quantifying the ambient sulphur dioxide (SO₂) concentrations at Sulphur Springs in order to assess the potential risk of unsafe exposure. The operation of this network required collaboration with local stakeholders, including the staff and management of the Soufrière Regional Development Foundation (SRDF), management of the SSP. Local staff measured the levels of ambient concentrations of SO₂ at Sulphur Springs, using both commercially available passive diffusion tubes, as well as regionally available low-cost SO₂ samplers. The main objective was to quantify the concentrations of ambient SO₂ present in the Park, to assess the potential associated health risks. Investigations of the reliability and accuracy of the low cost sampler as a possible economic alternative to the commercial samplers was also undertaken. This type of approach was thought to be an effective option for scientists to engage communities as partners in disaster risk reduction. Lessons learnt from this experience are presented for the benefit of other citizen science monitoring projects, including its use as a tool for promoting volcanic hazard education, and enhancing communication and understanding between geoscientists and the community they serve.

Martin Jutzeler, Michael Manga, James White, Peter Talling

Submission 48

Pyroclastic flows traveling over the sea and their seafloor deposits, IODP 340

Expedition 340 of the Integrated Ocean Drilling Program (IODP 340) cored a ca. 4 Ma, very thick pumice lapilli-ash unit on a bathymetric high 35 km offshore Montserrat. By its thickness, complex stratifications, poor sorting, components, and coarseness, this unit stands out from all other volcanoclastic units of the core. The pumice lapilli-ash is interpreted to be the first recognized record of submarine deposition from hot, pumice-rich pyroclastic density currents that traveled above the water surface. The pumice lapilli-ash comprises three main depositional units, with a framework-supported base overlain by matrix-supported middle and top sections; lithic clasts are present everywhere, and pumice clasts are sub-rounded. Detailed sedimentological analysis and experimental data from floatation and settling experiments show evidence for multiple episodes of settling in the water column in

Maren Kahl, Þorvaldur Þórðarson, Enikő Bali, Guðmundur Heiðar Guðfinnsson

Submission 1076

Constraining P-T-X-t paths for magma and volatile evolution within distinct volcano-tectonic environments in Iceland

Tracking the storage and transfer of magmas and volatiles through volcanic plumbing systems prior to eruption is an important goal in volcanology. Most information about magma migration within sub-volcanic plumbing systems is obtained with geophysical methods such as geodetic and seismic monitoring. However, as magma ascends towards the surface, its physico-chemical properties change, affecting the style, extent and intensity of future eruptions. Tracking how, where and over what timescales gas and magma chemistry change as the magma moves underground is essential for the long-term goal of better anticipating future volcanic hazards and risks. To this end, we apply an integrated method, linking Systems Analysis, a time-integrated study of zoned olivine populations, and a micro analytical study of melt inclusion geochemistry. This enables us to constrain the pressure-temperature-composition-time (P-T-X-t) paths for magma and volatile evolution within distinct volcano-tectonic environments across Iceland. For this purpose, a representative suite of basaltic samples (alkaline to tholeiitic) from different volcano-tectonic settings in Iceland is being studied. Here, we present first preliminary results of samples from the North Volcanic Zone (NVZ) and from the Snæfellsnes peninsula in W-Iceland, a typical intra-plate system (IPS). The record preserved in 61 olivine macrocrysts from Búðahraun, Berserkjahraun (IPS) and Bóndhólshraun (NVZ), spans a wide compositional range, from Fo68 up to Fo91. Bóndhólshraun olivines are normally zoned with extended core plateaus between Fo86 and Fo90, and rims of uniform composition at Fo80-81. Berserkjahraun and Búðahraun olivines display mainly two types of zoning with variable core (Fo75-91) and rim (Fo68-80) compositions: (i) Normal zoning with high forsteritic core plateaus compositions at Fo88-91 (Berserkjahraun), Fo85-89 and Fo76-81 (Búðahraun). The rim compositions are at Fo68-75 (Berserkjahraun) and Fo72-76 (Búðahraun). (ii) Complex zoning, with reversely zoned cores (Fo80, Berserkjahraun; Fo76-80 Búðahraun), followed by high forsteritic 'shoulder' parts (Fo84, Berserkjahraun; Fo79-84 Búðahraun), and normally zoned rims (Fo70, Berserkjahraun; Fo74-76 Búðahraun). The observed compositional and zoning record of olivines from Snæfellsnes suggests sub-surface magma transport and olivine evolution within different magmatic environments (characterized by a different set of intensive thermodynamic variables) prior eruption.

Wataru Kanda, Yasuo Matsunaga, Takao Koyama

Submission 299

Geomagnetic evidence for the episodic fluid intrusion associated with the 2014 unrest of Kusatsu-Shirane volcano, Japan

In Kusatsu-Shirane volcano, the elevated seismic activity, which accompanied a remarkable deformation and a change in the chemical compositions of volcanic gas, was observed from March 2014. In May 2014, a rapid change in the total geomagnetic intensity was observed. The amount of change was about 1 nT at the maximum, but the rate of change was rapid: the total intensity decreased only for about three weeks and did not show a significant change in the following two years. In this study, we attempted to infer temperature change accounting for this rapid geomagnetic variation within the volcanic edifice by a numerical simulation of hydrothermal fluid. We used HYDROTHERM ver.3.1.1 developed by the USGS for the simulation. The calculation was made within a cylindrical domain of 5km in height and 5km in radius. A high-temperature fluid was emplaced along the center axis as a source of temperature and flow fluctuations. A uniform permeability structure was assumed except for the low-permeable clay layer proposed by resistivity structure at the depth of 100 to 400m. Parameters such as permeability were adjusted so as to explain the average heat discharge at the surface, and the magnitude and time-scale of geomagnetic variation. We assumed that the hydrothermal fluid and the surrounding rocks were in an equilibrium state. The temperature dependence curve of the magnetization of rocks, which was used to transform temperature distribution into the magnetization distribution, was made from the experimental data for the volcanic rocks sampled in the summit area (Yamazaki et al., 1992). Changes in the geomagnetic total intensity were calculated by the input of the high-temperature fluids at the depths. The geomagnetic variation occurred from the onset of fluid input and terminated when the fluid input was interrupted. Then, little change was calculated also after 100 days. The temperature distribution showed almost no change after 100 days, and the high temperature state was maintained beneath the clay layer. After numerous simulations were performed with changing several parameters, we found that the geomagnetic variation observed in May 2014 and the subsequent stagnant state of the total intensity could be explained by the temporary input of high-temperature fluid of higher than 400 degrees with a flux of 20 ton/sec for about three weeks. This possibly detected the discharge process of magmatic fluids caused by a breach of the sealing zone (Ohba et al., 2008).

Yo Kanno, Mie Ichihara

Submission 136

Chamber-pipe flow experiment as a mathematical analogue for flow-induced volcanic oscillation systems

Geodetic signals resembling sawtooth waveforms have been observed in data from many active volcanoes, including tilt and displacement records (e.g. Ohminato et al., 1998; Voight et al., 1998; Genco and Ripepe, 2010; Anderson et al., 2010). We found similar sawtooth wave-like pressure change in slug flow experiments with a chamber-pipe system and have studied the system as an analogue for flow-induced volcanic oscillation system. However, our experiment cannot be directly compared with the actual volcanic systems contrasting with scaled experiments such as slug flow experiments for basaltic eruptions (e.g. James et al., 2004, 2006). Here we clarify mathematical similarities between our system and existing models for volcanic oscillation.

The following non-dimensional equations represent our experimental system: $dP/dt = Q_{in} - \alpha Q$, $P = (L + \Gamma L) Q + \rho g L$, where t is time, P and Q are the chamber pressure and the mass flux, respectively, Q_{in} is the given flux into the chamber, α is the void fraction at the gas slug, L is the length of liquid slugs, ΓL is a function of L representing the surface tension effect, and ρg is the hydrostatic pressure gradient in the liquid. All quantities are in non-dimensional forms. The first equation represents the pressure capacitance of the chamber while the second represents pressure loss in the pipe.

Our system has the same mathematical structures as the existing models for lava dome eruptions in non-dimensional forms: $dP'/dt' = Q'_{in} - Q'$, $P' = \mu' Q' + Gr$, where μ' and Gr are the effective viscosity and the magma-static pressure term, respectively. Both or either of μ' and Gr are functions of state variables such as bubble and crystal fractions and depend on Q' and P' . Their functional forms determine the oscillatory (or non-oscillatory) behaviors of the system. The individual models consider different physical processes that control μ' and Gr . The controlling state variable is L in our system. Time evolution of L is determined by interaction between upward and downward flow.

We experimentally reveal importance of downward-flow effects in generating both periodic and non-periodic behaviors. Existence of “downward flow” has been proposed in actual volcanoes. The examples are magma convection in a conduit (Kazahaya et al., 1994), lava drain back, and recycled ejecta that fall back and cover the vent (Capponi et al., 2016). We infer that downward-flow effects could be relevant to periodic and non-periodic oscillations of volcanoes.

Kazuhiko Kano

Submission 577

Internal structures and growth of an early Miocene deep submarine tephra cone at Morokui, Shimane Peninsula, SW Japan

An early Miocene submarine tephra cone is exposed for a distance over 1 km along the Morokui coast of the Shimane Peninsula, providing a good opportunity to examine the internal structures and growth of submarine tephra cones. Rising more than 600 m above a deep marine mudstone this cone consists mainly of fallout deposits characterized by poorly vesicular, water-chilled bombs and lapilli of andesite composition and is accompanied by water-chilled, brecciated lava flows and intrusions of andesite to dacite compositions. Water-chilled bombs are less than 1 m in length with a thickness less than 10–30 cm and are shaped like a ribbon, spindle, tadpole, or hollow pillow. They are accumulated together with a minor amount of lapilli and ash without any specific orientation and form 2-to-30-m-thick beds poorly defined by different grain-size populations. Composed mainly of blocky, polyhedral lapilli and ash with variably disintegrated water-chilled bombs and/or blocks including pseudo-pillows, density current deposits are successively accumulated to a thickness of 1 to 10 m in-between the fallout successions and thicken toward the downslope side. They are individually massive or inversely-to-normally-graded and stratified, presumably representing gravitational or explosive slope collapse of the cone. Graded and stratified centimeters-thick layers of lapilli tuff to tuff are repeatedly accumulated for a thickness of 5 or 6 m in association with these deposits, even though they can be observed only at one location. They predominantly contain blocky, polyhedral grains and are interpreted as the dilute density current deposits derived from local phreatomagmatic explosions. Andesitic to dacitic intrusions occupy the root zone of the tephra cone, feeding the water-chilled and brecciated lava flows emplaced on the eastern slope of the cone. Lava fragments brecciated in situ and associated pseudo-pillows are relatively many in the density current deposits proximal to these lava flows and intrusions, presumably reflecting gravitational collapse of the lava effused or protruded near the surface. A low vesicularity of 15–19 % for the water-chilled bombs is too low to disrupt the melt explosively, but coalescence of earlier-formed gas bubbles could have enabled large gas slugs to grow, ascend, burst, and break the surrounding melt into bombs and fine fragments. The Morokui tephra cone thus grew with these explosive activities and syn-eruptive mass-wasting processes.

Ozge Karakas, Jörn-Frederik Wotzlaw, Zack McIntire, Olivier Bachmann, George Bergantz, Julian-Christopher Storck, Peter Ulmer, Josef Dufek

Submission 857

Constraining the heat budget and lifetime of crustal-scale magmatic systems: Insights from the Ivrea-Verbano Zone and Serie dei Laghi, Italy

Crustal-scale magmatic systems feed hazardous volcanic eruptions while generating and recycling continental crust. The Ivrea-Verbano Zone and Serie dei Laghi volcanic system of the Southern Alps, collectively referred to as the Sesia Magmatic System (SMS), provides a complete record of a magmatic plumbing system where upper and lower magmatic units as well as the erupted material are exposed on the Earth's surface. In this system, partial melting in the mantle during lithospheric extension generated hot mafic magmas that intruded and differentiated at various crustal levels, ultimately leading to at least one large-scale rhyolitic eruption fed from a shallow-crustal magma reservoir. Although recent studies have revealed clear spatial and temporal kinship of all these magmatic units, the total duration of magmatism, and the main processes controlling chemical differentiation, are still debated. In particular, the relationship between lower and upper crustal magmatism still needs to be better determined. Here we integrate high-precision ID-TIMS U-Pb zircon geochronology and thermal modeling to quantify the heat and mass budget of magmatism in the SMS. The ages gathered from high-precision ID-TIMS U/Pb zircon geochronology provide more precise estimates on the duration of magmatism for the different magmatic units. The thermal model involves emplacement of magmas by dykes and sills in an extensional environment at both lower and upper crustal levels, using fluxes constrained by field relations and geochronology. We are testing the possibility of constructing a crustal-scale magmatic system, largely by AFC processes, as melting of pre-existing wall rocks appears thermally limited to ~15-30 % of injected mantle-derived magma volume.

Leif Karlstrom, Scott Paterson, Mark Jellinek

Submission 689

A reverse energy cascade for crustal magma transport

Direct constraints on magma ascent through Earth's crust come primarily from exhumed intrusions. Connecting these structures to transport processes that ultimately control the occurrence, longevity, and style of volcanism remains a seminal problem. In long-lived provinces such as arcs, it is particularly unclear why so much mantle-derived melt is ultimately stored and not erupted at the surface. We combine an exhaustive field data analysis with new theory to show that this tendency for magma storage is a crustal property which evolves in response to magma transport. Intrusions preserved as plutonic complexes in the North American Cordillera exhibit two dominant classes of structures that are consistent with a transition in the rheological response of crustal rocks to intrusion. We propose that, in a long-lived crustal magma transport network, energy delivered from the mantle to open small dikes and sills will be transferred to intrusions of increasing size through a "reverse energy cascade" via mechanical merging, assimilation and mixing of small intrusive bodies into larger ones, as well as by cooling and solidification. Although the size distribution of intrusions less than ~100 m in minimum dimension is complex, larger intrusion sizes follow a power law scaling consistent with model predictions. Continuous, distributed mantle magma supply over 10s to 100s of kyr should trigger the reverse energy cascade. Magmatic systems evolving within this regime preserve mantle input fluctuations that occur more slowly than the crust can mechanically mix, or that are large enough to activate transport pathways throughout the crust. The reverse magmatic energy cascade provides both a framework for interpreting surface patterns of volcanism in terms of deep magma transport and for interpreting the plutonic record. A young arc, erupting near the rate at which magma is supplied, should exhibit intrusions dominated by elastic deformation and no energy exchange between scales. Surface eruptions should mimic the spatial distribution of mantle input. For the same mantle supply, a longer-lived transport network will evolve to a rheological regime favoring storage, and a power law intrusion size distribution with maximum intrusion scales approaching crustal thickness. This is consistent with evidence for interactions among intrusions in the central Sierra Nevada batholith (Paterson et al., this meeting) as well as the spatio-temporal clustering of eruptions in the Cascades.

Kyoko Kataoka, Yoshitaka Nagahashi

Submission 965

Frequent lahars and hidden eruptions at Adatara and Bandai volcanoes unraveled by volcanic sediment density flow deposits in Lake Inawashiro-ko, Fukushima, Japan

Records of volcanic eruptions are often incomplete due to preservation potential of eruption deposits. The deposits can easily be reworked and/or eroded by the influence of vegetation, pluvial, and glacial activities. The present study shows the reconstruction of eruption records of two important volcanoes in the northeast Japan (Adatara and Bandai), approaching from analysis of subaqueous volcanic density current deposits in a lacustrine sequence. Bandai volcano is well known for a large-scale debris avalanche event following the phreatic eruption in AD1888 that took > 400 fatalities, and the AD1900 eruption at Adatara volcano caused > 80 casualties. Appropriate evaluation for recurrent intervals of high frequency eruptions is essential for populated areas surrounding the volcanoes. The studied sedimentary core (INW2012) was drilled out from off Lake Inawashiro-ko (~90 m deep), the largest volcanic dam lake in Japan, which was formed by the 50 ka Okinajima debris avalanche at Bandai volcano. In the 29 m long core, 19 tephra-fall layers and 71 event deposits, in contrast to background offshore sediments, are recognized. The event deposits, of a subaqueous density flow origin, such as gray muddy/sandy (Gm/Gs) units and brown muddy/sandy (Bm/Bs) units show that Gm is usually mms to cms thick, blue-gray color, homogenized, and finer than background sediments. Especially, Gm/Gs units contain pyrite, sulfate minerals and smectite, and are characterized by high sulfur contents, and can be correlated with muddy lahars in the Sukawa River catchment of Adatara volcano. High-sulfur contents indicate syn- or post-eruptive lahars in relation with phreatic eruptions sourced from hydrothermally altered rocks. Bm/Bs, thicker than those of gray units (1 to 6 cm), suggests more proximal origin. It contains fresh glass shards and is normally graded with a sharp erosive base. Chemical composition of fresh glass shards indicates that brown units originated from Bandai volcano rather than reworking of pre-existing old tephra. With muddy nature and glass shards, the brown units are attributed to phreato-magmatic eruptions at Bandai volcano. Since depositional rates of background lake sediments are stable, the ages and frequency of eruption-related events both from Adatara and Bandai volcanoes can be well constrained. Such event deposits reveal the unknown eruptive history of Adatara and Bandai, as they were more active during the last 50,000 years than previously known.

Kyoko Kataoka, Yoshitaka Nagahashi, Atsushi Urabe

Submission 1279

Traceable cohesive lahar deposits in volcanic fan, delta, and lake floor environments, Adatara volcano, northeast Japan

Adatara volcano in northeast Japan erupted in AD1900 that caused > 80 fatalities. The known eruptive history of Adatara comprises at least 6 Vulcanian and 5 phreatic eruptions during the last 10,000 years (Yamamoto and Sakaguchi, 2000). In the Sukawa River system, western slope of Adatara volcano, there are 17 muddy lahar units that were formed during the last 14,000 years (Kataoka et al., 2015). The lahar units are characterized by muddy matrix-rich facies and are very poorly sorted with pebble to cobble sized andesite clasts and hydrothermally altered clasts. The high clay content (8-14%) in clay + silt + sand fraction of the deposits suggests cohesiveness of the lahar flows.

The Sukawa River joins Nagasegawa River debouching into Lake Inawashiro-ko. Sedimentary cores drilled on the deltaic area (KBR2015) and lake floor (INW2012, 2013) revealed a number of intercalations of muddy units which are correlatives of cohesive lahar deposits in the Sukawa River. In the KBR2015 core, one of the units is 45 cm thick, massive, moderately sorted, and blue-gray muddy matrix-rich facies with very coarse sand to granule grains partly composed of hydrothermally altered lithic fragments. Muddy units in the INW2012 and 2013 cores were deposited in offshore environments. The units are usually mms to cms thick, blue-gray color, and homogenized, and partly consist of several subunits. Some of these units contain very small amount of glass shards with high SiO₂ content in chemical composition.

XRF and XRD analyses of these muddy units in proximal (Sukawa River), medial (delta) to distal (lake floor) areas indicate similar characteristics in chemical composition and mineral assemblages. High sulfur contents of the sediments are partly derived from pyrites in the matrix. Presence of clay minerals such as smectite and kaolin minerals in muddy deposits contributed to cohesiveness of lahar flows.

By the lithology, sedimentary facies, and chemical composition, we consider that these muddy units found in proximal to distal areas are derived from a lahar origin from Adatara volcano that travelled a long distance (~30 km) without major flow transformation probably due to cohesiveness of the flow. High-sulfur contents and presence of altered rock fragments and silicified glass shards indicate that cohesive lahars were related with phreatic eruptions sourced from Numanotaira crater where hydrothermally altered rocks are recognized.

Koji Kato, Jun'ichi Miyamura, Yoshiro Masuda, Yoshihiro Ueda, Takahiro Yanada

Submission 964

Volcano monitoring and evaluating system in Japan Meteorological Agency (JMA)

There are 110 active volcanoes in Japan and JMA monitors them. Among 110 active volcanoes, 50 volcanoes in need of more intensive observation are monitored with seismometers, GNSS, tiltmeters, infrasonic microphones and cameras by telemetry. Based on these observed data, if an unusual event is detected and deemed to be the precursor of an eruption that may affect residential areas or areas around the crater, JMA issues Volcanic Warnings or various information to mitigate the damage of volcanic disaster. The data are processed in the Volcanic Observation and Information System (VOIS) and warning/information messages are created and disseminated from VOIS. This year, VOIS will be updated and the new system, called VOIS3, will start operation in August. In this poster, We introduce JMA's volcano monitoring and evaluating method using VOIS3.

Precursors of an eruption and the process of volcanic activity are rich in variety. To evaluate volcanic activity appropriately it is important to understand the condition inside a volcano by making the most use of experiences of past eruptions and outcomes of volcanic research. In previous system, observed data such as volcanic earthquakes and crustal deformation was displayed individually and the alarm sounded automatically. Volcanic activity evaluation was conducted by gathering analyzed results of each data that was inefficient and took time. In order to respond against anomaly events more quickly and accurately, analysis capability of the system was expected to be improved.

In the new system, observed data such as hypocenters of earthquakes, sources of crustal deformation, thermal information obtained from geomagnetic or fumarole data are superimposed on the known model of velocity structure, resistivity structure. The structure inside a volcano such as magma chamber or geothermal water chamber and the condition inside a volcano related to the magma plumbing/hydrothermal system are visualized with simple models. These models support quick and appropriate volcanic activity evaluation by illustrating the activity transition with clear images inside a volcano.

VOIS3 has a database in which precursor observed at past eruptions, volcanic activity transition as well as observed data or research results on the urgency of eruption in the mid to long term are archived. If an event occurs, similar cases are searched and picked in the database and those data are used as a reference for evaluation of volcanic activity.

Janine Kavanagh, Simon Martin, Suraya Hilmi Hazim, Elliot Wood, David Dennis, Alec Burns, Andrew Biggin, Megan Phillips

Submission 763

Interpreting magma flow and host-rock deformation during magma ascent: A multidisciplinary study

The study of magma ascent dynamics in the crust is challenging as syn-emplacement and post-emplacement measurements often capture only a partial record of conduit and volcanic plumbing system processes. Indirect measurements of magma flow can be garnered using geophysical techniques that track the deformation of the host-rock as magma is intruded, and ancient volcanic plumbing systems can be studied post-emplacement by analysing the host-rock structures and crystallised magma within intrusions. However, deciphering how sub-surface and surface rock deformation and crystallised magma bodies record dynamic processes of magma ascent towards eruption is not straightforward.

We present results from a multidisciplinary study that uses analogue experiments and field studies to explore the interaction between magma and host-rock during the development of volcanic conduits and plumbing systems. Using case studies from the Isle of Skye (Scotland), Utah (USA) and Patagonia (Chile) we explore how magnetic and petrographic fabrics within solidified dykes and sills relate to the macro- and micro-structural deformation of their host rock. Scaled analogue experiments then provide a tool to interpret and explore the physical processes that control magma ascent in nature. The experiments consider magma intrusion within a mechanically-layered host material, where the Young's modulus and fracture toughness of the layers and their bonded interfaces are controlled. Digital image correlation and the use of polarised light enables the internal deformation of the gelatine host-material to be mapped as the magma analogue is intruded, and the evolving surface deformation is quantified using an overhead laser scanner. Fluid flow within the evolving model volcanic conduit and plumbing system is analysed using particle image velocimetry. Our results reinforce the necessity of multidisciplinary studies and increased interaction between analogue modelling, numerical modelling, geophysical and petrologic research communities to study conduit processes and volcanic plumbing systems.

Ryohei Kawaguchi, Tetsuya Yamamoto, Shin'ya Onizawa

Submission 728

Modeling of gas bubbles rise in a magma chamber and its application to periodic ground deformation at Izu-Oshima volcano

Recently, geodetic observation succeeded in detecting ground deformations associated with volcanic activity with high time-resolution. These observation data are useful to understand the dynamics of volcanic activities. In this study, we present the model of magma chamber inflation due to gas bubbles rising in the magma and apply this model to explain the periodic ground deformation observed at Izu-Oshima volcano.

Izu-Oshima is a volcanic island located in the Izu-Bonin arc, Japan and its repeatedly erupt basaltic magma with a time interval about few decades. Geodetic observation network installed around Izu-Oshima Island detected the long-term ground inflation of the island and periodic inflation and deflation cycle with period of 1 to 1.5 years. The location of pressure source of periodic deformation was estimated at about 4-5 km depth beneath the Izu-Oshima Island and the amount of its volume changes in one cycle was also estimated to be order of 10^6 m^3 .

This periodic deformation cycle is modeled as follow. First, the volatiles accumulating the upper part of the magma chamber are suddenly degassed and the pressure of magma chamber decreases. As the pressure decrease, the volatiles exsolve and form small gas bubbles in magma. Then, small gas bubbles rise in magma due to their buoyance force and expand their volume as decreasing the pressure of surrounding magma. The volume of magma chamber increase due to expansion of gas bubbles in the magma. According to the Stokes law, the gas bubbles rise in viscous melt with a velocity proportional to the square of their radius and the radius of gas bubbles is depended on the static pressure of surrounding magma. The amount of volume increase of magma chamber due to gas bubbles rising is determined by the height of gas bubbles rising and the ratio of bulk modulus of melt and the rigidity of surrounding elastic medium. Assuming the initial radius of gas bubbles, the temporal changes of the volume increase of magma chamber is calculated by finite difference method. We compare the observed data and calculated result on the amount and time scale of magma chamber expansion. As a result, the volume increase of 106 m^3 and the duration of a hundred days are expressed by the initial gas bubble radius of $2 \times 10^{-4} \text{ m}$ and distance of gas bubbles rising of 1 km.

Masataka Kawaguchi, Toshiaki Hasenaka, Atsushi Yasuda, Natsumi Hokanishi, Yasushi Mori

Submission 1111

High-sulfur basalt hosted in olivine as an indicator of magma supply beneath Aso, central Kyushu, Japan

We analyzed the bulk rock, melt inclusion (MI) of minerals and host minerals, and determined the volatile concentrations (H₂O, Cl, S) and major elements of MI of Holocene volcanic products from Aso central cones (Ojodake and Kamikomezuka) to obtain the information of magma supply system. Holocene activity of Aso is mainly basalt-basaltic andesite. Our data suggest that existence of a shallow reservoir and volatile-rich mafic melt injection.

MIs of the phenocrysts were divided into two compositionally different groups. One is mafic (SiO₂ 46.7-57.5 wt. %) and high-S (2 52.3-59.8 wt. %) and low-S (2O ratios indicate that MIs hosted in Ol has high volatile contents initially. The S contents of Ol hosted MI tend to decrease with decreasing hosted-Ol Mg#. Measured H₂O contents in felsic MIs from Ojodake are the highest (2O values (2, high-Mg# and volatiles in the mafic MIs indicate that the mafic group derived from a deep-reservoir.

These observations suggest the injection of high-S basaltic magma into a shallower reservoir. High-S mafic magma was found by melt inclusion studies beneath the frontal volcanoes in central and northeastern Japan (Yamaguchi et al., 2003; Yamaguchi, 2010). It has become clear that primary melts of arc island are enriched in volatiles by subduction (Wallace, 2005; Zellmer et al., 2015). In general, the high S contents of basaltic melt require oxygen fugacity (fO₂) greater than FMQ+1 (Wallace, 2005; Jugo et al., 2005; Jugo, 2010). The concentration of S in basaltic magmas is strongly depends on temperature, fO₂, fS₂, and Fe content in melt (Wallace & Carmichael, 1992). The compositional gap of S contents between mafic and felsic group probably reflects the different degree of degassing.

Tatsuhiko Kawamoto, Jun-Ichi Kimura, Qing Chang, Masako Yoshikawa, Mitsuru Okuno, Tetsuo Kobayashi

Submission 55

An oxidizing agent of the mantle wedge: sulfate in saline fluid inclusions in harzburgite xenoliths from Pinatubo

Sulfate ion and minerals were found in the H₂O–CO₂–(Na_{0.75}K_{0.25})Cl fluid inclusions in the harzburgite xenoliths from Pinatubo, a frontal volcano located at the Luzon arc, the Philippines (Kawamoto et al. PNAS 2013). The Na/K ratio was determined in the fluid inclusions (>0.02 mm) in olivine using a quadrupole inductively coupled plasma-mass spectrometry equipped with a 266 nm femtosecond laser ablation system. Thanks to a newly installed Raman mapping system, SO₄²⁻ ion, gypsum (CaSO₄ · 2H₂O) and/or anhydrite (CaSO₄) or hexahydrate (MgSO₄ · 6H₂O) were found (Frezzotti et al. JGE 2012) in one fourth of the fluid inclusions. Kumagai et al. (2014 CMP) reported a presence of Mg-sulfate hydrate in CO₂–H₂O–Cl fluid inclusions in the Ichinomegata lherzolite xenoliths from northeastern Japan; however, we had found no sulfur in the Pinatubo in our previous work (Kawamoto et al. PNAS 2013).

Sulfur contents in the Pinatubo fluid inclusions can be 20 wt based on the method of Binder and Keppler (2011 EPSL). This is consistent with those in serpentinites (Alt et al. 2012 EPSL). Origin of the fluids in the Pinatubo harzburgite is supposed to be from serpentinites whose water was originally brought via sedimentary pore fluids on the basis of halogen systematics (Kobayashi et al., 2017 EPSL). High Pb contents in the amphiboles from the Pinatubo harzburgite (Yoshikawa et al. 2016 Lithos) can be explained by such sulfate bearing saline fluids.

Olivine-hosted melt inclusions show a positive correlation between water contents and Fe³⁺/Fe²⁺ ratios (Kelley and Cottrell 2009 Science). Presence of sulfate ions in the slab-derived fluids further supports their observation. This also provides insights into the genesis of calc-alkaline rock series characterized by a high oxygen fugacity (Miyashiro 1974 Am J Sci). Our observation solves the missing link between high-S in arc magmas (Le Voyer 2010 J Petrol) and presence of sulfate in the slab serpentinites (Alt et al. 2012) and high-pressure metamorphic rocks (Frezzotti and Ferrando 2007 Per Mineral). Current estimate of S content in the aqueous fluids in forearc (20) is more than an order of magnitude lower than that in melt inclusions in arc basalts (0.06-0.6 S/H₂O; Le Voyer 2010). Sulfur can be enriched during partial melting of the mantle with larger S/H₂O than that of slab-derived fluids. Alternatively fluids released beneath sub-arc contain larger amount of S by supercritical fluids (Kawamoto et al. PNAS 2012).

Ryunosuke Kazahaya, Hiroshi Shinohara, Toshiya MORI, Masato IGUCHI, Akihiko YOKOO

Submission 110

Pre-eruptive inflation caused by gas accumulation: Insight from detailed gas flux variation at Sakurajima volcano, Japan

Volcanic gas measurements provide crucial insights for the condition of conduit system at a volcano. Sulfur dioxide (SO₂) emission rate observations were made at Sakurajima volcano, Japan, to quantify the relationship between the SO₂ emission rate and inflation prior to Vulcanian explosions. The explosions associated with precursory inflation events were preceded by decreases in SO₂ emission rates by 10–60 min. The amounts of accumulated gas were calculated using time series of SO₂ emission rate. The amounts of accumulated SO₂ and increases in strain records before the explosions showed a positive relationship. The volume increase of a deformation source calculated using the strain records was of the comparable order of magnitude as the volume of the accumulated volcanic gas. The results suggest that the inflations before the explosions were caused by the gas accumulation.

Karim Kelfoun, Valentin Gueugneau

Submission 25

A two-fluid depth-averaged model for block-and-ash flows and ash-cloud surges.

Pyroclastic currents are very destructive and their complex behaviour makes the related hazards difficult to predict. A new numerical model has been developed to simulate the emplacement of both the dense and the dilute parts of pyroclastic currents using two coupled depth-averaged approaches. Interaction laws allow the dense current (pyroclastic flow) to generate a dilute current (pyroclastic surge) and, inversely, the dilute current to form a dense current or a deposit.

The model is first explored theoretically using simplified topographies. It reproduces the relationships observed in the field between the surge genesis and the topography: the increase in surge production in constricted valleys, the decoupling between the dense and the dilute currents and the formation of surge-derived dense flows. The strong non-linear link between the surge genesis and the velocity of the overlaid dense flow could explain the sudden occurrence of powerful and destructive surges.

The model is then tested with two real events: the 5 November 2010 eruption of Merapi volcano (Indonesia) and the 25 June 1997 eruption of Soufriere Hills (Montserrat). The model is able to reproduce the dynamics of the currents and the characteristics of the deposits: thickness, extent, volume, and trajectories.

Franziska Keller, Sebastian Mueller, Christoph Helo, Jonathan Castro

Submission 809

Experimental evidence for geochemical and morphological alteration of ash particles by volcanic lightning

Lightning discharge in ash plumes is a common but to-date still poorly studied phenomenon related to explosive volcanic eruptions. Genareau et al. (2015) found glass spherules and glass aggregates in ash deposits of two explosive eruptions where volcanic lightning was highly observed (Eyjafjallajökull, 2010 & Mt. Redoubt, 2009). They hypothesized that the extreme heat released during the lightning discharge (potentially > 30,000 K) leads to the transformation of volcanic ash particles into glass spherules and linked them to short-time melting processes similar to fulgurite formation.

Using a specifically designed volcanic lightning simulator, we performed laboratory experiments in order to investigate the behaviour of air-suspended ash struck by lightning. In a first set of experiments natural ash from Sakurajima volcano (Japan) in distinct size fractions between 36 and 300 μm was used to examine morphological changes of the particles caused by lightning-induced melting. The resulting morphologies range from spherical shapes, to incompletely melted particles, as well as particle aggregates. The individual morphologies were linked to different peak temperatures and melting histories caused by varying impact of the electric arc on particles.

In a second set of experiments, ash-sized fragments of homogenised Laacher See phonolite (Eifel, Germany) were subjected to the electric arc. Careful electron microprobe analyses of the lightning-melted particles display vaporisation and loss of distinct elements (e.g. Cl, S, Na) in the glass. Analyses of the resulting diffusion/depletion profiles within fragments affected by the electric arc allow constraints on peak temperatures experienced by the glass during flash-melting.

Genareau K, Wardman JB, Wilson TM, McNutt SR, Izbekov P (2015): Lightning-induced volcanic spherules. *Geology*, doi:10.1130/G36255.1.

Cyndi Kelly

Submission 1214

Back-Projection Imaging of extended diffuse pre-, co-, and post-eruptive seismic sources at El Jefe Geyser, El Tatio Geyser Field, Chile

El Tatio Geyser Field in the Antofagasta region of northern Chile is the third largest geyser field in the world. It is comprised of 3 basins that span ~ 10 km x 10 km at an average elevation of ~ 4250 m. The field contains at least 80 active geysers and several hot springs, perpetual spouters and fumaroles. Its relatively non-pristine condition from geothermal exploration and heavy tourist traffic makes it an ideal place to perform minimally invasive geophysical experiments. We deployed a dense array of 51 L-28 3-component geophones (1-10 m spacing, corner frequency 4.5 Hz, 1000 Hz sampling rate), and 6 Trillium 120 broadband seismometers (2-20 m spacing, long period corner 120 s, 500 Hz sampling rate) in a ~ 50 m x 50 m grid in the central Upper Geyser Basin (the largest basin in area at ~ 5 km x 5 km) during October 2012 as part of a collaborative effort to study hydrothermal system dynamics between Stanford University; U.C. Berkeley; the University of Chile, Santiago; the University of Tokyo; and the USGS. The seismic array was designed to target El Jefe Geyser (EJG), an easily accessible columnar geyser (eruption height ~ 1 -1.5 m) with a consistent periodic eruption cycle of $\sim 132 \pm 3$ s. Seismicity at EJG was continuously recorded for 9 days during which ~ 6000 total eruptions occurred. Excluding eruptions during periods of high anthropogenic noise (i.e. tourist visits, active field work), the array recorded ~ 2000 eruptions that we use to study the evolution of seismic source locations before, during and after EJG eruptions. We use a new back-projection processing technique to locate geyser signals, which tend to be harmonic and diffuse in nature, during 5 key phases of the EJG eruption cycle. We obtain V_p and V_s from ambient-field tomography and use these velocities to back-project and correlate seismic signals from all available receiver-pairs to potential subsurface source locations assuming straight-line raypaths. We then create 4D time-lapse images of individual and concurrent geyser sources throughout an entire EJG eruption cycle and over multiple eruption cycles. We use spectral analysis to target specific seismic observations (i.e., high or low frequency bands) and use our results to evaluate changes in source distributions before, during and after eruptions and compare them to complementary, and synchronous, surface (downhole temperature/pressure, discharge rate, thermal video) observations.

Peter Kelly, Ugan Saing, Sofyan Primulyana, Suparjan, Bambang Heri Purwanto, Sulus Setiono, Hendra Gunawan, Aaron Rinehart, Allan Lerner, Christoph Kern, John Paskievitch

Submission 433

Continuous Multi-GAS monitoring yields new insights into gas emissions from Kawah Ijen volcano, Indonesia

Kawah Ijen is a basaltic to dacitic stratovolcano located in East Java, Indonesia, that possesses a host of notable features, including the largest natural acid crater lake in the world (28 x 106 m³, T > 30°C, pH 2, SO₂, H₂S) of the fumarolic gas plume. After one year we exchanged the temporary unit for a permanent station capable of measuring H₂O, CO₂, SO₂, and H₂S, and added a second permanent Multi-GAS at another location to better monitor emissions from the acidic crater lake.

The >1.5 years of continuous Multi-GAS data include a number of novel observations that provide new insights into geochemical processes occurring at Kawah Ijen during normal background levels of activity. Over the measurement period, the CO₂/STotal ratio (STotal = SO₂ + H₂S) of the fumarole plume remained steady at 2-3, and was relatively oxidized with an average H₂S/SO₂ = 0.4. However, the data include remarkable short-term (hours to days) variations to much more reduced values (H₂S/SO₂ = 1.8) that correspond to periods of wet and rainy weather. Constant CO₂/STotal ratios during rainy periods argue against preferential scrubbing of SO₂ as a mechanism for explaining the observed H₂S/SO₂ variations. These observations lead us to suggest that heavy rain can temporarily extinguish the fumaroles' flames and thereby alter the H₂S/SO₂ ratio in the plume.

Gas emissions from the lake are compositionally distinct from the fumarole gases and are primarily composed of H₂O, CO₂, and SO₂; lake-derived H₂S has not been detected. Lake gas compositions show broad seasonal variations with CO₂/SO₂ ranging from 30-90. The data also show that lake gas emissions are strongly modulated by precipitation and suggest that prolonged periods of rain can "cap" the lake, eventually leading to discrete CO₂-rich limnic gas expulsion events. At least three such limnic expulsions have occurred in Jan-Feb 2017. In our presentation we will explore these data and their implications for monitoring and understanding processes and hazards at Kawah Ijen and other "wet" volcanoes.

Melanie Kelman

Submission 1198

Modeling potential lahar inundation zones at Mount Garibaldi and Mount Cayley in southwest British Columbia's Garibaldi Volcanic Belt

Mount Garibaldi, Mount Cayley, and Mount Meager, three large stratovolcanoes in the Garibaldi Volcanic Belt of southwest British Columbia, Canada have steep unstable slopes, glaciers, and significant hydrothermal alteration. All have evidence for prehistoric and historic mass flows of a range of sizes, although the prehistoric records, especially for Garibaldi and Cayley, have not been well studied with respect to age, volume, and spatial extent of deposits, nor is it clear how many events were synvolcanic. Thus, the lahar hazard to nearby populated areas (15-40 km downstream from potential sources) and transportation infrastructure (7-13 km downstream) is not well quantified. Only for Mount Meager have lahar inundation zones been estimated, using the semi-empirical ArcGIS tool, LAHARZ.

I used LAHARZ to model potential lahar inundation zones for Garibaldi and Cayley, choosing lahar volumes in consideration of Mount Meager's largest known historic (49 million m³) and prehistoric (likely much larger than 100 million m³) debris flows, since there is significant information about both (including drill cores). One challenge was the choice of lahar starting points at Cayley, since the asymmetry of the volcano made choosing them using the intersection of a height/length cone impossible. I instead used sharp decreases in slope on stream topography profiles to choose starting points, since these may represent where net erosion changes to net deposition.

For all volumes, the differences between maximum and minimum inundation zones at the 95% confidence level are significant. Thus, this modeling provides only a crude first estimate of possible lahar inundation zones for Cayley and Garibaldi. It does, however, show that relatively small lahars (3), especially from Garibaldi, may affect the Sea to Sky Highway, while larger lahars (≥ 100 million m³) from either volcano may impact the town of Squamish. This work highlights the need for more studies of lahar and debris flow deposits at Cayley and Garibaldi. I plan to expand this work by remodeling lahar inundation zones from Mount Meager using LAHARZ and a higher resolution DEM. I also hope to eventually redo modeling for Cayley and Garibaldi either with LAHARZ and a higher resolution DEM, or by using newer lahar flow models. The ultimate goal is to produce comprehensive hazard maps for all three volcanoes.

Stuart Kenderes

Submission 1092

Exploring the thermal effects of country rock type on the mobility of magma through conduits

Whether a magma is mobile or not largely depends on the time spent as a liquid, when the magma flows under any stress. Therefore, understanding the thermal history of sheet intrusions can provide insight into the mobility of magma in sub-volcanic plumbing systems. Recent studies (Whittington et al., 2009; Nabelek et al., 2012) have demonstrated that temperature-dependent thermal properties can significantly affect the heating and cooling rates of igneous and metamorphic systems in the Earth's crust. Numerical models of these systems, however, often over simplify the nature of the "country rock", and therefore the thermal history of sheet intrusions.

We measured the thermal diffusivity (D) and isobaric heat capacity (CP) of shales from 20°C to 300°C. Preliminary data show that shales have considerably lower D and greater CP values than other sedimentary rocks. The D of sandstone (Branlund and Hofmeister, 2008), limestone (Merriman et al, in review), and shale (this study) at 20°C are 3.1, 1.5, and 0.8 mm²·s⁻¹ respectively, and decrease to 1.1, 0.5, and 0.4 mm²·s⁻¹ at 300°C. The changes in D and CP also result in a decrease in thermal conductivity (k) with increasing temperature, where $k = D \cdot CP \cdot \rho$, and where ρ is density. The decrease in D and k with increasing temperature creates a thermal feedback loop causing the country rock to become more insulating as its temperature increases. The more insulating the country rock, the slower an intrusion will cool, allowing magmas to remain mobile for longer periods of time. Finite difference thermal models of a basalt sill intruding granite, sandstone, limestone, and shale using the newly acquired data, suggest sills that intrude shales cool to their solidus the slowest. This suggests that models need to use thermal properties for the appropriate country rock types in order to correctly model thermal histories of sheet intrusions.

Jackie Kendrick, Yan Lavallée, Paul Wallace, Rebecca Coats, James Ashworth, Adrian Hornby, Amy Hughes, Oliver Lamb, Felix von Aulock, Sarah Henton De Angelis, Silvio De Angelis

Submission 1047

Shear zone development during the ascent of highly viscous magma

The ascent of highly viscous magma often leads to the growth of lava domes. Such eruptions are prone to rapid shifts from effusive to explosive behaviour, yet the factors responsible for this potentially predictable behaviour remain poorly understood. Magma rheology is governed by composition, porosity and crystal content, which during ascent evolves continuously via the exsolution of volatiles and nucleation of crystals, to yield a rock-like, viscous suspension in the upper conduit. Here, we review how geophysical monitoring, laboratory experiments and detailed field studies offer the opportunity for unravelling the complexities associated with the ascent and eruption of such magmas.

Studies using analogues and natural magmas indicate that crystal interaction during flow results in strain-partitioning and shear-thinning behaviour of the suspension. In a conduit, such characteristics favour the formation of localised shear zones as strain is concentrated along conduit margins. These areas of strain localisation can be preserved in deposits, including the margins of erupted magma spines, which may variably display evidence of complex fracture-healing cycles in the form of: grain size reduction; anisotropic permeable fluid pathways; mineral reactions; injection features; recrystallisation; magnetic anomalies etc. Evidence suggests that such fracture-healing mechanisms in ascending magma are responsible for the release of repetitive earthquakes often observed during lava dome eruptions, which can be mimicked by damage accumulation that releases acoustic signals on the laboratory scale. The repetitive fracture of magma at (~fixed) depth in the conduit and the fault-like products exhumed at spine surfaces indicate that the last hundreds of meters of ascent may be controlled by frictional slip. Experiments on a low-to-high velocity rotary shear apparatus indicate that shear stress on a slip plane is highly velocity dependent, and that mechanical work which induces comminution of asperities and heating can lead to melting in just a few cm of slip. In a volcanic conduit, as slip-rate along the margin (ascent rate) fluctuates, the magma rests at a pivotal position with regard to the glass transition, allowing it to either flow or fracture. Velocity-dependence then acts as an important feedback mechanism, accentuating pulsatory (stick-slip) cycles that bring the magma to the surface accompanied by characteristic repetitive seismic events.

Adam Kent, Kari Cooper

Submission 565

Can zircon crystallization really record the thermal history of magmas?

Magmatic zircons can record both the time and temperature of their formation. Thus a relatively common approach is to interpret the crystallization temperatures of zircons formed at different times in an individual magmatic system in terms of the thermal history and evolution of stored magma. However it is also important to consider how adequately this approach records the thermal history of the magma in which they occur. While zircon thermometry records the temperature at which they crystallized - it provides no explicit information about the temperatures experienced since crystallization occurred.

There are a number of factors to be considered. Firstly the growth of magmatic zircon is non-random, and strongly focused in periods where compositional and temperature conditions promote zircon saturation. As a result zircons are highly unlikely to provide a representative sampling of the thermal state of a magma body throughout its residence. In many magmas, zircon saturation occurs near the solidus and thus the higher temperature portions of thermal evolution are less likely to be recorded. Secondly, uncertainties in measured zircon U-Th or U-Pb ages are large relative to the time that it takes for the analyzed volume of zircon to grow (a few hundred to thousand years at typical growth rates for the volume sampled by ion probe analyses). Thus a limited number of short-lived zircon growth events can produce a broad apparent range of ages, and can appear to define a trend. Finally, where temperature and/or compositional variations occur within a magma reservoir, zircon crystallization may occur only in restricted locations. Later mixing of zircons derived from different portions of the magma reservoir during eruption may produce zircons with an apparent range of temperatures and ages that are not representative of the overall conditions within the reservoir.

Investigation of these issues using probabilistic models of zircon crystallization over a range of thermal histories suggests that zircons are unlikely to comprehensively record thermal evolution. For example several zircon data sets currently interpreted in terms of progressive thermal evolution can be readily explained by a restricted number of episodes of zircon growth interspersed with long periods of no growth. In these cases the total duration of zircon growth is less than a few percent of the total magma residence, and thus much of the thermal history goes unrecorded.

Gabor Kereszturi, Jonathan Procter, Lauren N. Schaefer, Reddy Pullanagari, Stuart Mead, Ben Kennedy, Ian Yule

Submission 106

Airborne hyperspectral imaging for monitoring active volcanic system – Lithological and hydrothermal alteration mapping of the Upper Te Maari craters, Tongariro Volcanic Complex, New Zealand

Hyperspectral imaging acquires light intensity readings in hundreds of contiguous spectral bands at Visible to short-wave infrared wavelengths (370 nm to 2500 nm). This region of the electromagnetic spectrum can be used to identify surface minerals, such as sulphates, carbonates, micas, and clay minerals. Hyperspectral sensors can be mounted on an airborne platform that allows us to map a region of interest quickly and in a cost-effective way. Airborne and ground-based hyperspectral imaging can offer a new approach to map volcanic terrains, and to monitor active volcanic systems such as hydrothermally altered areas, prone to flank instabilities (e.g. generating debris flows and landslides) that can pose hazards to the communities living around volcanoes.

This study develops a methodology of fusing hyperspectral and Light Detection and Ranging (LiDAR) data together to provide detailed insight into the shallow-surface architecture and topography of Tongariro Volcanic Complex in New Zealand. The Upper Te Maari crater and its surroundings were used as a case study to assess the capability of this new methodology to be used in volcanic hazard assessment. Specifically, we focus our efforts on a violent hydrothermal eruption in 2012 that was preceded minutes before by a ~700,000 m³ landslide and debris avalanche on the western flank. The airborne hyperspectral imaging was carried out using a push-broom AisaFENIX hyperspectral sensor (Specim Ltd, Finland) in autumn 2016. The imagery has a 2 m spatial resolution and a spectral sampling interval of 3.3–5.7 nm, covering the full spectrum (370–2500 nm). Ground truthing of the imagery was carried out by sampling and mapping of the hydrothermal alteration zones. The altered samples were analysed using lab-based spectroscopy and X-ray diffraction (XRD) to identify the dominant type of clay minerals. A detailed lithology/geological map based on hyperspectral imagery was produced using machine learning algorithms. The hyperspectral imagery was complemented with topographic data from a LiDAR survey in 2012. The geological map was then analysed in conjunction with the topographic data from LiDAR to highlight areas that are susceptible to flank instabilities in the future. The developed methodology is found to be suitable for volcano monitoring purposes (e.g. changes in the hydrothermal alteration zones), geological mapping and for volcanic surveillance using airborne remote sensing.

Christoph Kern, Pablo Masias, Fredy Apaza, Kevin Reath, Ulrich Platt

Submission 103

High water vapor emissions detected at Sabancaya Volcano prior to its 2016 eruption by differential optical absorption spectroscopy

Water is by far the most abundant volcanic volatile species and plays a predominant role in driving volcanic eruptions. However, various difficulties associated with making accurate measurements of water vapor in volcanic plumes have limited their use as a diagnostic tool. Instruments measuring water vapor in-situ are susceptible to condensation in the sampling line, thus skewing the results. Remote measurements have been restricted to active-source experiments which require a thermal source (e.g. lava lake) or access to both sides of the volcanic plume and are therefore limited in their applicability.

Here we present the first detection of water vapor in a volcanic plume using passive visible-light differential optical absorption spectroscopy (DOAS). The measurements were conducted at Sabancaya Volcano, Peru. With a summit elevation of 6,000 m, this study site allowed us to locate DOAS instruments at 5,000 m, thereby reducing the overhead water vapor column by almost two orders of magnitude below the average column at sea level. After carefully correcting for the remaining atmospheric water vapor background, we were able to detect the absorption of water vapor in the Sabancaya plume. We find that the plume contained an exceptionally high water vapor abundance six months prior to its November 2016 eruption. Using both ultraviolet and visible-light spectrometers, we obtained emission rates of 900 t(SO₂)/d and 250,000 t(H₂O)/d averaged over the two-hour measurement window. Our plume measurements yielded an H₂O/SO₂ molecular ratio of 1,000 which is about an order of magnitude larger than the ratio typically found in high-temperature volcanic gases.

We attribute the large water vapor emission rate and high H₂O/SO₂ ratio to a boiling-off of Sabancaya's hydrothermal system caused by an intrusion of magma to shallow depths. This hypothesis is supported by a significant increase in the thermal output of the volcanic edifice detected in infrared satellite imagery leading up to and after our measurements. Though the measurement conditions encountered at Sabancaya were exceptionally favorable for our experiment, we show that visible-light DOAS systems could be used to measure water vapor emissions at numerous other high-elevation volcanoes. Such measurements would provide observatories with an additional, independent parameter particularly useful for forecasting eruptions at "wet" volcanoes harboring significant hydrothermal systems.

Laszlo Kestay, Colin Dundas

Submission 1041

Recent Quantitative Insights from Field Investigations of Lava-Water Interactions

It is very challenging to obtain any direct observations of lava-water interactions because the key processes take place underneath an active lava flow. Quantitative measurements are even more difficult to obtain. We have had the good fortune to be involved in two recent studies with various colleagues that have provided new quantitative insights into lava-water interactions. The first, reported on by Baker et al (2015) JVGR 302: 81-86, involves a 1-m thick shallow sill of the Columbia River Basalt Group intruded into wet lake sediments. By measuring the discoloration of pollen, profiles of maximum heating above and below the sill were obtained. The profiles are identical above and below the sill, showing a disregard for gravity/buoyancy forces. This rules out convective processes. The heating profiles are also very uniform with distance from the sill, ruling out thermal conduction as the dominant heat transfer process. In an opaque medium, thermal radiation is also unimportant. The only process that can fit the observations is the "heat pipe" process where liquid water is moved by capillary forces. The second field site is the lava flow from the 2014-2015 eruption at Holuhraun, Iceland. This large (>1 km³) basaltic lava flow entered the channel of the Jokulsá á Fjöllum river. Multiple glacial meltwater streams and groundwater springs feed cold water into the base of the lava flow. This water emerges as hot springs at the terminus of the flow. We initiated a campaign to monitor the heat and water fluxes in the summer of 2016, installing a few permanent sensors in the around the flow. We plan to expand this monitoring network in the summer of 2017. We hope to present preliminary results at this meeting. These field constraints have demonstrated that the numerical models we have used to date, relying heavily on thermal conduction, are wrong to the point of not being useful. Armed with the insights from these sites we are beginning to create a new generation of numerical models for lava-water interaction on Earth and Mars.

Myriam Khodri, Takeshi Izumo, Jérôme Vialard, Serge Janicot, Christophe Cassou, Matthieu Lengaigne, Juliette Mignot, Guillaume Gastineau, Eric Guilyardi, Alan Robock, Michael J. Mcphaden

Submission 837

El Niño–Southern Oscillation Response to tropical stratospheric volcanism

Over the past few years, efforts have focused on resolving the relationship between natural radiative forcing and tropical Pacific climate variability, to determine El Niño–Southern Oscillation sensitivity to tropical volcanism. This is a critical question that also bears on the future response of ENSO to future climate change, including both anthropogenic and natural radiative forcings. The effect of such eruptions on the El Niño Southern Oscillation (ENSO) is however still debated. Observations and proxies suggest that tropical volcanic eruptions favour an El Niño within two years following the eruption. Modelling studies have, however, so far reached no consensus on either the sign or physical mechanism of ENSO response to volcanism.

This contribution further investigates the possible mechanisms of ENSO response to tropical explosive volcanism through a hierarchy of atmosphere and ocean models numerical experiments. We evaluated in particular the sensitivity of tropical Pacific internal dynamics to the applied same volcanic forcing and by doing so, evaluate the robustness and limits of the simulated results across different models physics.

Christopher Kilburn, Richard Wall, Robert Robertson

Submission 343

Forecasting eruptions after long repose intervals

Short-term forecasts of eruptions at long-quiescent volcanoes currently depend on qualitative and empirical evaluations of precursory sequences. Here we show how the uncertainty in such forecasts can be reduced using a new and quantitative, physical model of crustal deformation and faulting before eruptions.

Precursory signals show a range of variation with time. They are not all independent and the mutual variation among related signals significantly constrains evaluations of eruptive potential. Thus, the behaviour of an elastic-brittle crust being deformed by magmatic pressure evolves from quasi-elastic (deformation with minor faulting) to inelastic (deformation dominated by faulting) before bulk failure. Using volcano-tectonic (VT) events to measure fault movement, the quasi-elastic and inelastic regimes are distinguished by exponential and linear increases in VT event number with deformation. They reflect faulting under an increasing and constant maintained stress, and can be quantified with field proxies for the ratio of applied stress to the crust's tensile strength. The associated changes of VT event rate and deformation rate with time are determined by the rate of pressurization in the deforming source.

The regimes have been identified at long-quiescent volcanoes at timescales from ~0.1-1 years at stratovolcanoes to ~10-100 years at large calderas, and over ~0.1 years before flank eruptions at frequently-erupting volcanoes. The longer timescales reflect slower mean rates of stress increase, including intervals of stasis between episodes of rapid unrest. All the studied eruptions have occurred in the inelastic regime. The transition to inelastic behaviour begins when the ratio of applied stress to tensile strength (obtained from the characteristics of the exponential VT-deformation trend for quasi-elastic behaviour) reaches values of 3-4, consistent with limiting deformation in tension.

The results show that rates of crustal fracturing with deformation are essential, quantitative measures of the approach to bulk crustal failure, and that the probability of an eruption increases significantly with the start of inelastic behaviour. However, bulk crustal failure alone does not guarantee that magma will be fed to the surface. An outstanding goal therefore remains to establish whether pre-eruptive bulk failure can be distinguished from non-eruptive conditions.

Geoff Kilgour, Ian Hamling, Ben Kennedy, Gert Lube, Stephanie Gates, Jonathan Proctor

Submission 1225

Understanding small, phreatic eruptions: Ballistic ejecta, dilute pyroclastic currents and delineating ejecta from space after the 27th April, 2016 eruption of White Island

White Island erupted on the 27th April, 2016 during a period of heightened volcanic tremor and moderately elevated gas flux. Furthermore, the level of Crater Lake had dropped significantly over the two weeks prior to the eruption. The eruption itself took place at around 9:30 pm (NZT) without any visual observations possible. Subsequent analysis of the acoustic and seismic signals indicates that there were at least 5 pulses of ejections over the ~ 1.5 hr period of the eruption.

The volcanic gas flux was similar before and after the eruption, which implies that the trigger of the event was most likely related to hydrothermal rather than magmatic processes - consistent with the analysis of the eruption deposit. The eruption deposit contains variably altered rock fragments, sulphur-infused breccia and minor lake sediments with no juvenile material.

Ground visits to the island were made within days of the eruption to assess the resulting deposit. Thickness measurements, grain size analysis and image analysis have been used to determine the volume of ejecta, the relative timing of phases and the components present. Based on these data, the eruption generated a dilute pyroclastic density current (DPDC) that reached ~ 800 m from the vent. Soon after the current was initiated, a jet of ballistics was ejected onto the tail of the DPDC. These ballistics landed up to 450 m from the vent.

We then assessed the correlation between ground-based dispersal measurements against satellite radar data to investigate the sensitivity of the technique for mapping recent eruption deposits. We found that the satellite data matched the deposits with promising results despite the eruption generating a very small volume of ejecta (3). Radar incoherence data matched the lateral extent of the deposit in most places where the thickness did not exceed 5 mm, showing its utility as a potential monitoring tool at remote volcanoes.

Balazs Kiss, Szabolcs Harangi, Christoph Hauzenberger, Theodoros Ntaflos, Paul R. D. Mason

Submission 1051

Petrological mapping of Volcanic Plumbing Systems using amphiboles in mixed intermediate magmas: a case study from the Ciomadul Volcano (E-Carpathians)

The pathways and storage zones in the crust beneath volcanoes are called as a Volcanic Plumbing System (VPS) can be mapped by volcano geophysics and petrology. The petrological mapping of the VPS is essential to determine the feeding magmas and their storage conditions. Amphibole is a powerful tool to map the VPS of dacitic volcanoes because their major and trace element composition is influenced by the p , T , fO_2 , fH_2O , X_{melt} .

Ciomadul volcano is the youngest volcano in the Carpathian-Pannonian region and it were active in the late Pleistocene and the last eruption occurred only ~30 kyrs ago. The eruptions were fed by monotonous dacitic magma with small compositional variation ($SiO_2 \sim 63-69wt\%$) but there is no systematic change through time. The dacites are crystal-rich (25-30% phenocryst content) and show several textural evidence (e.g. coexisting quartz and olivine, resorption textures, multiple phenocryst populations) for open system evolution.

The erupted dacites contain abundant amphibole phenocrysts coexist with all of the rock forming minerals (e.g. with quartz or with olivine) additionally amphiboles show large compositional variation (e.g. Al_2O_3 : 6-15 wt%, Cr: 10-3000 ppm, Sr: 55-855 ppm, Eu/Eu^* : 0.62-1.19) suggesting that they were crystallized at different conditions from different melts. The large variation of the major elements can be covered by amphiboles were produced experimentally from dacitic magmas were found in the literature. The published partition coefficients of amphiboles were used to reveal the observed trace element variation. The model calculations indicate that amphiboles were crystallized from similar melts to the host dacite regardless to the large observed variation. Based on the amphibole only thermobarometers, the amphiboles were crystallized at ~750-1000°C and ~100-400 MPa.

Our results indicate that amphibole phenocrysts were crystallized from dacitic melts in an upper-mid crustal magma mush column 4-16 km below the volcano. This magma capture zone experienced incremental growth during continuous intrusion of dacitic melts more probably originate from a lower crustal hot zone. Zoned amphiboles indicate that repeated intrusions of fresh hot melts initiated the eruptions.

Koji Kiyosugi

Submission 1285

Frequency of volcanic eruptions and long-term magma discharge rate in sub-regions in Japan

Frequency of volcanic eruptions is a fundamental parameter to evaluate volcanic activity. Together with mass of ejecta, it gives long-term magma discharge rate, providing an insight into material circulation through volcanoes. Calculating frequency of eruptions is, however, a challenging problem due to difficulty of estimating the amount of under-recording of volcanic eruptions. The main mechanisms of under-recording are absence of historical records, erosion and alteration of tephra deposits, burial of tephra deposits by younger deposits, disappearance of the source volcano itself due to burial or erosion, deposition of majority of tephra on the sea surface, and occurrence of submarine eruption. The relative importance of these mechanisms may vary in different regions. In this study, therefore, I calculated frequency of volcanic eruptions and estimated long-term magma discharge rate in sub-regions (subduction zones) in Japan. The investigated datasets consist of age and magnitude, M , of volcanic eruptions ($M \geq 2$), which occurred in the Hokkaido, Tohoku, Izu, Central, and Kyushu regions in Japan in recent about 2 million years. For the estimation of the frequency of eruptions, under-recording of events was taken into account by modeling a decreasing trend of recording rate of analyzed volcanic eruptions with time.

The results of the analysis show that the frequency of eruptions ($M \geq 2$) in those regions varies more than one order of magnitude. For larger eruptions ($4 \leq M \leq 6$), frequency of eruptions decays by a factor of about 10 for each successive eruption magnitude category. On the other hand, frequency of smaller eruptions ($2 \leq M \leq 4$) decays by a factor of about 1.5 - 2.6, showing that the smaller eruptions are less frequent than the frequency expected from the magnitude-frequency relationship of the larger eruptions. The long-term magma discharge rate, normalized by the length of those subduction zones, show similar value (2×10^{10} kg/ka/km) in the Kyusyu, Central, and Tohoku regions. On the other hand, the long-term magma discharge rate in the Hokkaido and Izu regions is about one third of that of the other regions.

These results show the influence of magma ascending process and tectonics on the magnitude-frequency relationships and long-term magma discharge rates, as well as the relative importance of the different under-recording mechanisms in various regions.

Johannes Klein, Sebastian Mueller, Jonathan Castro

Submission 82

The influence of crystal size distributions (CSD) on the rheology of magma: new insights from analogue and petrological experiments

Knowing the flow properties, or rheology, of magma is of great importance for volcanological research. It is vital for understanding eruptive and depositional features, modelling magma flow rates and distances, interpreting pre-eruptive volcanic unrest and earthquakes, and ultimately predicting volcanic hazards related to magma motion. Despite its key role in governing volcanic processes, magma rheology is extremely difficult to constrain in time and space within a natural volcanic system, because it is dependent upon so many variables. Therefore, both analogue and experimental studies of permissible yet simplified scenarios are needed to isolate different rheological influences.

Despite significant progress in understanding the rheological properties of silicate melts and two-phase mixtures (e.g., melt+crystals), as well as the impact of the volume fraction (e.g. Pinkerton & Stevenson, 1992; Caricchi et al., 2007; Mueller et al., 2010) and shape (Mueller et al., 2011) of crystals on magma rheology, the effect of the crystal size distribution (CSD) is still poorly constrained. A highly disperse CSD (i.e., a great variety of different crystal sizes) leads to a much more efficient packing of crystals in a flowing magma which predominantly controls the rheological behavior of magma in a sheared particle Accounting for, or neglecting, the size distribution of crystals can therefore make a considerable difference in magma flow models.

We present the results of systematic rheometric experiments using multimodal analogue particle suspensions of well-defined size fractions of micrometer-sized glass beads in silicone oil as magma-analogue material, as well as HP/HT experiments producing artificial CSD's. The dataset of analogue experiments also contains the analysis of multimodal Gaussian distributions with varying variance ('broadness') as well as with varying skewness ('tailed distributions'). These results were applied to natural as well as experimentally produced CSD's by decompression experiments to 'map' the evolution of the rheological properties in a magmatic feeding system. Finally, those CSD's were simulated and reproduced in analogue experiments to combine the idea of CSD's directly with the rheological changes occurring during the rise and crystallization of hydrous magma in order to link that with an observed eruption behaviour and to confirm the previously developed (semi-)empirical model.

Barbara I. Kleine, Andri Stefánsson, Saemundur A. Halldórsson, Martin J. Whitehouse, Kristján Jónasson

Submission 820

Origin of quartz in the Icelandic crust evident from $\delta^{30}\text{Si}$ and $\delta^{18}\text{O}$ isotope

Here, we report an investigation of quartz formation processes within the Icelandic crust. The studied sample set contains (1) igneous quartz from crustal xenoliths and micro-granites ($>550^\circ\text{C}$), (2) high-temperature hydrothermal quartz ($\sim 200\text{--}400^\circ\text{C}$) and (3) low-temperature hydrothermal quartz and amorphous silica (in-situ using SIMS and trace elements of the same grains using EMPA).

Trace elements in quartz are in agreement with existing data from similar crustal settings and do not provide any distinct trends to further distinguish different formation conditions for quartz. However, the measured $\delta^{30}\text{Si}_{\text{NBS28}}$ values are strongly correlated with quartz formation conditions and the source of Si to the system and range from (1) -0.2‰ to -0.7‰ when formed under magmatic conditions, (2) -0.9‰ to $+0.7\text{‰}$ when formed under high-temperature hydrothermal (HTH) conditions and (3) -4.6‰ to $+0.5\text{‰}$ when formed under low-temperature hydrothermal (LTH) conditions. Corresponding $\delta^{18}\text{O}$ values were: (1) -5.6‰ to $+6.6\text{‰}$ for magmatic quartz (2) -9.3‰ to -12.1‰ for HTH quartz and (3) -0.9‰ to $+30.1\text{‰}$ for LTH quartz and amorphous silica.

Results of quantitative isotope modelling demonstrate that the range of $\delta^{30}\text{Si}$ values observed are caused by isotope fractionation between fluids and quartz upon various processes occurring in hydrothermal systems with progressive fluid-rock interaction. Boiling for HTH and boiling followed by cooling for LTH systems of a geothermal fluid have been shown being a significant process that can explain extremely low $\delta^{30}\text{Si}$ values in quartz and amorphous silica. Furthermore, kinetic isotope fractionation may also be important at low temperature. The $\delta^{18}\text{O}$ values of the same mineral grains were found to be dependent on the source of the water, either meteoric or seawater, and fractionation between liquid, vapour and secondary minerals. The results of this study demonstrate $\delta^{30}\text{Si}$ and $\delta^{18}\text{O}$ values of quartz can be utilized to constrain and quantify various hydrothermal processes occurring in the Earth's crust.

Erik Klemetti, Michael Clynne, Adam Kent, Frank Tepley

Submission 114

Magmatic storage conditions over the past 825,000 years at the Lassen Volcanic Center revealed in zircon model ages, compositions and melt inclusions

Zircon are ideal vessels for capturing T-t-x conditions across the history of a magmatic system as they are easily dated using U-Th and U-Pb techniques and their trace element compositions provide indirect evidence of T-t-x change in magmatic systems. Melt inclusions in zircon can be used to give us direct compositional evidence of melts that can be linked to the zircon chronology to map the changing magmatic conditions. The Lassen Volcanic Center (LVC) in the Cascades of California records ~825 k.y. of basaltic andesite-to-rhyolite volcanism: the silicic Rockland Sequence (RS; ~825-610 ka), andesitic Brokeoff Volcano (BV; ~550-350 ka) and 3 groups of silicic and mixed rocks of the Lassen Domefield (LD; ~315-0.1 ka). We sampled erupted products from the LVC and extracted zircon from all samples. U-Th and U-Pb ages, along with trace element compositions, were collected on zircon (n=301) via SHRIMP-RG. These data show two main populations of zircon crystallization ages: RS and BV, from ~820 to 350 ka, with small peaks at ~675 and ~570 ka and the LD, with most zircon crystallizing between ~250 and 50 ka and the youngest being 14 ka. Ti-in-zircon temperatures calculated from zircon peak during the transition from the BV to LD periods. Since ~350 ka, the highest zircon temperatures have dropped from >800°C to

Melt inclusions (MI) from selected zircon, along with adhering glass, were analyzed via electron microprobe for a suite of elements. MI in LVC zircon are relatively homogenous: ~74-76 wt% SiO₂, ~11.5-12.5 wt% Al₂O₃, 2 (76-79 wt%) and lower Cl (0.01-0.08 wt%). MI and adhered glass from the RS plot as overlapping fields with 0.10-0.15 wt% Cl while almost all adhered glass has slightly lower SiO₂ compared to MI. These data from RS-age zircon suggests that the RS magma body did not change significantly between zircon crystallization conditions and entrainment of zircon prior to eruption. The increased Cl content of the RS-age zircon glass might indicate little degassing prior to eruption compared to eruptions during the LD, thus producing a more explosive eruption.

Andreas Kluegel, Markus Schmid, Simon Day, Bruno Faria

Submission 749

Magma plumbing during the 2014-2015 eruption of Fogo (Cape Verde Islands)

The latest eruption of Fogo (Cape Verde Islands), one of the world's most active oceanic island volcanoes, occurred from 23 November 2014 to 7 February 2015. It produced lava flows and tephra of basanitic composition, as well as minor phonotephrite at the early and late phases of the eruption. Zoned phenocrysts and mingled lavas in some samples indicate a magma mixing event that may have initiated the eruption. We have carried out thermobarometric investigations of a suite of samples to place constraints on the depths of pre-eruptive and syn-eruptive magma storage and transport. The samples cover all main stages of the eruption; their dates of emplacement have been determined from the date of incandescence of each sample site in high-resolution thermal infrared emissivity maps collected by satellite instruments (Landsat-8 OLI and EO-1 ALI) during the eruption. Phenocryst and groundmass compositions of basanites indicate equilibrium pressures of 540-740 MPa (average 640 MPa), equivalent to ca. 19-25 km depth, within the uppermost mantle. Phonotephrites yield slightly shallower depths. The data do not indicate systematic changes in equilibrium pressures during the course of the eruption. We suggest that this depth range reflects a magma reservoir system from which the eruption was fed. Fluid inclusions in clinopyroxene phenocrysts indicate a well-defined shallower depth range of 250-340 MPa (average 300 MPa), equivalent to ca. 9-13 km depth. This data is interpreted to reflect a section of lateral magma flow within the lower oceanic crust, plausibly in a short-lived storage subsystem that became filled prior to eruption. Remarkably, pre- and syn-eruptive seismic data do not reflect these depth ranges, as almost all events were at less than 5 km below sea level, mostly within the volcanic edifice rising above the ocean floor that is some 4 km below sea level. The bimodal depth distribution of our barometric data shows complete overlap with data from the preceding 1995 and 1951 eruptions, which suggests that similar magma storage systems and pathways in the uppermost mantle and lower crust are repeatedly used. The lack of pre-eruptive seismicity within the oceanic crust and uppermost mantle may reflect re-use of an existing magma conduit, with new dike propagation only taking place in the edifice itself.

Tetsuo Kobayashi

Submission 734

Precursory sequence to the caldera-forming eruption deduced from the outcrops of two caldera volcanoes in Kyushu, Japan

There are active caldera volcanoes in Kyushu, from north to south; Aso, Kakuto, Aira, Ata, and Kikai calderas. These calderas are now partly occupied by active volcanoes. Large volumes of felsic magma erupted from these calderas which formed vast pyroclastic plateaus around the area. I present two examples of precursory eruptions at Kikai and Aso calderas which are characterised by the effusion of lava with small amount of tephra, probably erupted within several hundred years before the caldera-forming eruptions.

Kikai caldera, which is now submerged, is located about 40 km south of the Kyushu mainland. The latest caldera-forming eruption (Akahoya) occurred ca. 7.3 ka, which produced the rhyolitic Koya pumice fall deposit, intra-plinian flow and the Koya ignimbrite (Naruo and Kobayashi, 2002). The Nagahama lava on the north-western caldera rim is overlain by the Akahoya tephra without any intervening soil, suggesting they were erupted successively (Kobayashi et al., 2010). However, a thin vulcanian ash, which is correlated to the Nagahama lava, is overlain by a thin soil layer underneath the Koya pumice. This indicates that the interval between the effusion of Nagahama lava and the start of Akahoya eruption is stratigraphically estimated to be longer than 100 years, and the eruption of Nagahama lava was mainly effusive. The chemical composition of the Nagahama lava is similar to the ejecta from the Koya eruption. This field evidence suggests that the precursory eruption of the same magma occurred more than 100 years before the climactic Akahoya eruption (Kobayashi, 2008).

Aso caldera is located in northern Kyushu, and the latest caldera-forming eruption (Aso-4 eruption) occurred ca. 90 ka. Precursory eruption occurred outside of the Aso caldera rim. The vent is located along the active fault, which traverses the northern caldera from SW to NE. The eruption started with a strombolian eruption then changed to effusive, generating the voluminous Takayubarua lava flow. The blocky surface of the lava is overlain by the Aso-4 ignimbrite with intercalating soil, suggesting that there was a time interval between their depositions, probably several hundred years. Takayubarua lava is dacitic which is similar to the ejecta from the Aso-4 eruption deposits.

These field evidence will contribute to the modelling of large-volume magma reservoir prior to caldera-forming eruptions.

Danielle Koebli, Aurelie Germa, Zachary Atlas, Paul Wetmore, Austin Arias, Charles Connor

Submission 410

A Geochemical and Petrological Investigation of dikes and sills from the San Rafael Volcanic Field, Utah.

The Pliocene San Rafael Volcanic Field (SRVF), Utah, is an exposed dike swarm with comagmatic sills and conduits. Silicate liquid immiscibility promoted extraction of the felsic phase from the mafic melt (Williams, 1983), resulting in syenite (~50.84 wt% SiO₂) being enclosed in shonkinite (~45.8 wt% SiO₂) within the sills. To determine magma petrogenesis, storage, evolution, crystallization parameters and causation for liquid immiscibility within the sills, we compared mineral major element composition to corresponding whole rock major and trace element data. Results support the hypothesis of a hydrated magma with hornblende (4% vol. in shonkinite, and 23% in syenite, 2mm-1.5 cm), biotite (10% vol. in shonkinite and 21% in syenite, 0.5mm – 4 mm), altered olivine (20% vol. in shonkinite with 10% serpentine, and 5% vol. in syenite with 2% serpentine, 1-3 mm), pyroxene (30% vol. in shonkinite and 17% in syenite, 1-4mm), and plagioclase (17% vol. in shonkinite – mostly matrix – and 30% in syenite, 80-90) and calcic-plagioclase (An₉₅₋₃₅) indicate a relatively hot magma (~1300°C), confirmed by thermodynamic calculations and Rhyolite-MELTS modeling (Ghiorso et al, 2012, and Ghiorso et al, 2015). Thermodynamic modeling also supports liquid immiscibility occurring within the sills due to mineral phases (olivine>magnetite>pyroxene) repeatedly forming at different depths and temperatures (example: olivine at 700 bar and 100 bar). Our results indicate a single lithospheric magma source that later differentiated in-situ within the sills as a result of liquid immiscibility at a shallow depth (~50-27bar), resulting in two melts: a mafic, volatile-poor melt (shonkinite), and a felsic, viscous, volatile-rich melt (syenite) visible as veins, ocelli and lenses.

Gualda G.A.R., Ghiorso M.S., Lemons R.V., Carley T.L. (2012) Rhyolite-MELTS: A modified calibration of MELTS optimized for silica-rich, fluid-bearing magmatic systems. *Journal of Petrology*, 53, 875-890.

Ghiorso M.S., Gualda, G.A.R., (2015) An H₂O-CO₂ mixed fluid saturation model compatible with rhyolite-MELTS. *Contributions to Mineralogy and Petrology* 2015
Williams, J. D. (1983). *The Petrography and Differentiation of a Composite Sill from the San Rafael Swell Region, Utah*. Arizona State University.

Jean-Christophe Komorowski, Marc Peruzzetto, Marina Rosas-Carbajal, Anne Le Friant, Anne Mangeney, Yoann Legendre

Submission 427

New insights on flank-collapse and directed explosions hazards from hydrothermal eruptions at La Soufrière de Guadeloupe (Lesser Antilles)

Detecting unrest that could herald the onset of non-magmatic collapse of a hydrothermally-altered and pressurized volcano constitutes a significant challenge. Recent eruptions of Ontake (2014) and Tongariro (2012) underscore the hazards and risks associated with sudden, often unpredictable non-magmatic hydrothermal eruptions at volcanoes characterized by long-lasting non-magmatic unrest. At La Soufrière de Guadeloupe, exegesis and re-analysis of historical chronicles has shown that 3 of 6 historical non-magmatic hydrothermal eruptions (1797-1798, 1836-1837, 1976-1977) have produced: 1) small-volume laterally-directed explosions; 2) small-volume highly mobile high-energy dilute turbulent pyroclastic density currents (PDCs) with runouts ≤ 1.5 -2 km; 3) small-volume collapses of parts of the dome that formed rockslides and/or debris avalanches; and 4) the exurgence of pressurized warm to hot acid hydrothermal fluid from eruptive fractures. We reinterpret the available data on historical eruptions at La Soufrière de Guadeloupe in light of new field data and the recently published electrical conductivity 3D tomography of the hydrothermal system (Rosas-Carbajal et al., 2016) to determine the parameters for likely scenarios (geometry, volume, friction angle) of partial edifice collapse for La Soufrière. We model, using the SHALTOP code, the emplacement of associated debris avalanches as granular flows for different collapse scenarios. Intensifying since 1998, persistent evolving hydrothermal unrest at La Soufrière involves degassing and circulation of very acid pressurized hydrothermal and magmatic fluids that favor pervasive alteration and mechanical weakening of the core of the dome within structurally controlled low-strength regions. Results show that debris avalanches and associated dilute turbulent non-magmatic pyroclastic density currents could reach several kilometers from the dome into populated areas of the southern flanks of the volcano. Given that flank instability of hydrothermally altered and pressurized regions of a volcano can be triggered by seismic, hydrothermal, magmatic, and meteorologic forcings, our results have implications for hazard and risk assessment as well as for continuing multi-parameter monitoring strategies on La Soufrière of Guadeloupe volcano

Szabolcs Kósik, Karoly Nemeth, Jonathan Procter, Mark Bebbington

Submission 89

Hazard implications of silicic small-volume volcanism within the Taupo Volcanic Zone, New Zealand: spatial, temporal, volumetric and eruptive style distribution of the eruptive vents

Silicic small-volume volcanoes emerging from the extensive ignimbrite sheets of the Taupo Volcanic Zone (TVZ) have produced at least 220 km³ DRE volume of volcanic material within the last 500 ky. However, drill cores obtained from the geothermal field as well as pyroclastic successions relating to deep-seated phreatomagmatic eruptions have uncovered many edifices adding up to significant volume that are totally buried within the area of the ancient Lake Huka and the Whakamaru caldera. The estimated number of total vents suggests that small-volume eruptions occur 100-200 times more frequently than climactic eruptions that caused caldera collapses. In the past 250 ky the average frequency was one small-volume eruption in every thousand years, characterized by decreasing total volumes from 30 to 13 km³ for sequential 50 ky periods. In the first half of the past 50 ky the erupted volume continued to decrease, but the eruption rate of the past 25 ky saw a significant increase with the eruption of 55 km³ of lava and a related additional 35-40 km³ pyroclastic deposits. The spatial distribution of the activity was highly uneven as 90-95 % of the total erupted volume was sourced from the Okataina Volcanic Centre. This corresponds to the typical volume of ignimbrites of the TVZ relating to caldera formations. The low contemporaneous total erupted volume from the remaining parts of the TVZ is noticeable and may imply the accumulation and merging of melt lenses that are necessary for large climactic eruptions. The magma source of small-volume eruptions is identical to the source of caldera volcanism, thus the product of such volcanism provides snapshots, which may reflect the changing conditions preceding the formation of calderas. Besides being possible precursors of large eruptions, small-volume volume eruptions pose a significant threat to their neighbourhood or broader areas, especially in eruptions of gas-rich magmas or strong magma/water interaction as documented at the 16 ka Puketerata and 0.7 ka Kaharoa eruptions. In other cases such eruptions produce lava domes as demonstrated by the TVZ having about 300 lava domes. The morphometric features of lava domes imply a wide range of lava emplacement styles which are often associated with explosive activity. The spatial distribution of the eruptive vents and the elongation of volcanic structures display the influence of fissural activity indicating a strong linkage to the fault system of the Taupo Volcanic Zone.

Marinel Kovacs, Alexandrina Fulop, Ioan Seghedi, Zoltan Pecskay, Masatsugu Yamamoto, Maria Jurje

Submission 170

P-T evolution of the Miocene magmatic system from Gutai Volcanic Zone (Eastern Carpathians, Romania)

Gutâi Volcanic Zone (GVZ) belongs to the Neogene-Quaternary volcanic chain of the Carpathians which stretches over the north-western part of the Romanian territory (Eastern Europe). A complex, predominantly andesitic volcanism with a four stage evolution developed in GVZ between 13.4-7 Ma. The volcanism reached its climax in the second stage (11.6-9 Ma) when subalkaline, predominantly medium-K basaltic andesites, andesites and dacites are emplaced. A small composite dome comprised of high-silica andesites and dacites (8.5-8 Ma, stage III) and small-sized intrusive bodies of olivine-bearing basalts (8.1-7 Ma, stage IV) ceased the volcanism. GVZ is the surface expression of magmatic processes dominated by assimilation-fractional crystallization (AFC) and magma-mixing processes, controlled by the evolution of the lithospheric mantle-source magmas in an intra-crustal magmatic system. This study is a first time attempt to model the magma plumbing system. Amphiboles and clinopyroxenes, selected from different rock-types (basalts, basaltic andesites, andesites, dacites and MME/mafic microgranular enclaves hosted by dacites) formed during stages II, III and IV, were used to calculate P and T parameters based on the new geothermobarometers for amphibole and clinopyroxene. The calculated P and T are characteristic for different types of amphiboles and clinopyroxenes: magnesiohastingsite (Mg# 70-79): P=6-8.5 kb, T=965-10150C; thschemakite (Mg# 65-71): P=3.2-3.7 kb, T=895-9200C; magnesiohornblende (Mg# 54- 65): P=1.6-2.0 kb, T=850-8950C; Ti, Cr diopside (Mg# 83-92): P=7.0-8.2 kb, T=1120- 11450C; Ti augite (Mg# 74-77): P=6.5-6.7 kb, T=1100-11250C. A remarkable P-T correlation is noticed for the coexisting amphiboles and clinopyroxenes (at equilibrium). Based on the obtained P-T data, three level magmatic reservoirs, deep (20-27 km depth), intermediate (10-13 km) and shallow (5-7 km), were constrained as part of a complex plumbing system comprised of multi-level interconnected magmatic reservoirs. P-T data correlated with geochronological data indicate the long-live activity of the deep reservoirs (11.6-7 Ma). Basaltic magmas (Mg hastingsite+Cr diopside/Ti augite) from these reservoirs repeatedly ascended into the intermediate and shallow-level reservoirs, mixed and mingled with the more evolved magmas hosted at shallower levels, and subsequently triggered volcanic eruptions.

Takehiro Koyaguchi, Kyle Anderson, Tomofumi Kozono

Submission 175

Determination of conduit-flow model parameters based on inverse analysis of ground deformation and mass eruption rate data: the effects of mathematical structure of the conduit flow model

Recent development of conduit-flow models has revealed that the eruption style (e.g., evolution of magma discharge rate etc.) is sensitively dependent on model parameters related to geological and petrological conditions such as volume and depth of magma chamber and magma properties. In order to validate these conduit-flow models, the model parameters need to be estimated from inverse analysis of time-varying observations. Generally, because a sophisticated conduit-flow model includes many model parameters, it is mathematically and computationally difficult to investigate the influence of each observation on the parameter estimation. Here, we have developed an approximate time-dependent eruption model utilizing a steady analytical conduit-flow model (e.g., Koyaguchi, 2005; Kozono and Koyaguchi, 2009), and have systematically investigated how the mathematical structure of the conduit-flow models affects the estimates of the model parameters.

We carried out a series of resolution tests as follows. First, we simulate the evolution of eruptions using a model of a magma plumbing system composed of a conduit and a magma chamber, where pressure of a magma chamber in elastic rocks is determined by the balance between magma influx and outflux. The conduit-flow model is based on analytical solutions so that it describes complex features of an eruption sequence by a minimum number of parameters. Secondly, we generate a set of pseudo-data of ground deformation and magma extrusion, and add artificial noise to these results. Finally, posterior probability density functions of the model parameters for given pseudo-data are obtained using a Markov chain Monte Carlo (MCMC) algorithm (Anderson and Segall, 2013).

Through the above resolution tests, we identified the key parameters that affect the time evolution of magma discharge rate and magma chamber pressure for explosive and effusive eruptions. Some key parameters are fundamentally different between explosive and effusive eruptions, because the characteristic mass flow rate is strongly controlled by sound velocity of gas-pyroclast mixture for explosive eruptions whereas it is basically governed by viscous resistance for effusive eruptions. Because of this difference, model parameters constrained from the observations also depend on whether the eruption is effusive or explosive.

Tomofumi Kozono, Hideki Ueda, Taku Ozawa, Toshiki Shimbori, Keiichi Fukui, Takehiro Koyaguchi, Eisuke Fujita, Akihiko Tomiya

Submission 561

The dynamics of the 2011 Kirishima-Shinmoe-dake eruptions, Japan, revealed by tiltmeter, satellite, and weather radar observations

Multiple observations during volcanic eruptions provide important information about eruption styles, magma plumbing systems, and eruption column dynamics. During the 2011 eruptions of Kirishima-Shinmoe-dake volcano in Japan, the type and intensity of eruption drastically changed within a week, with three major sub-Plinian eruptions on January 26 and 27, a continuous lava effusion from January 29 to 31, and intermittent Vulcanian explosions. Some of these events were well captured by borehole-type tiltmeter, a synthetic aperture radar (SAR) satellite imaging, and weather radar observations. We investigated the dynamics of the Shinmoe-dake eruptions by combining these observations.

In the Shinmoe-dake eruptions, combining the tiltmeter and the satellite imaging data enabled us to precisely estimate a magma discharge rate which is a key parameter controlling eruption styles. The tiltmeters detected a deflation of a spherical magma chamber caused by magma movement to the surface during the three sub-Plinian and lava effusion events, leading to estimate a geodetic volume change within the magma chamber caused by each eruptive event. The erupted volume and discharge rate during lava effusion were constrained using SAR satellite imaging of lava accumulation inside the summit crater. By combining the geodetic volume change and the volume of lava effusion, we successfully determined the erupted volume and discharge rate during each sub-Plinian event. The above precise estimates revealed that the Shinmoe-dake eruptions occurred in a critical state between explosive and effusive eruption.

A combination of the tiltmeter with the weather radar data in the Shinmoe-dake eruptions, which enables us to obtain the correlation between the magma chamber deflation and the height of the eruption cloud echo, also provided strong constraints on the eruption dynamics: we detected whether a column-forming eruption is accompanied by magma migration from the magma chamber (e.g., sub-Plinian eruption), or not (e.g., Vulcanian explosion). By using well-correlated chamber deflation and echo height data, we found a one-quarter power scaling relationship between cloud height and magma discharge rate even with a low discharge rate and strong wind during the Shinmoe-dake eruptions, and revealed that a stable magma plumbing system connecting the magma chamber and the surface did not change substantially during the eruptions.

Rebecca Kramer, Andrew Lockhart, Aaron Rinehart, Christopher Lockett, Amberlee Darold

Submission 1163

Keep the data flowing: an improved, integrated station design and implementation for Mount Rainier lahar detection and warning

The U.S. Geological Survey Cascades Volcano Observatory and Pierce County, Washington are upgrading the existing lahar detection and warning network installed in the 1990s along the Puyallup and Carbon River Valleys on the west flank of Mount Rainier. More than 100,000 people live in Mount Rainier lahar hazard zones. Included in the upgrades are four new broadband seismic stations. For the new stations we improved on existing infrastructure designs in ways that reflect years of refinement through installations on volcanoes in the United States and abroad. The modified design is intended to support long-term, solar-powered, telemetered, multi-sensor volcano monitoring with infrastructure that can be installed rapidly and relatively inexpensively. The basis of the station design is a single, large (1.2m x 0.65m x 0.6m) aluminum enclosure framed by 2" pipe driven to refusal and cemented into the ground. The frame supports six 55 Watt solar panels and can be instrumented with a radio antenna, dual frequency GPS antenna, camera, weather station, or other equipment without increasing the station footprint. The enclosure houses the data acquisition, power, and telemetry equipment and provides protection against water, rodents, and nominally against vandalism. Our power system comprises dual power supplies using Maximum Power Point Tracking solar charge controllers to provide redundancy and maximize battery life. The compact and rigid structure reduces vibratory wind noise contamination of seismic data compared to previous design iterations, provides single-point grounding, and acts as a faraday cage for protection against lightning or electrostatic discharge. The relatively small footprint is ideal for confined locations or sensitive natural areas with strict guidelines for ground disturbance. Principles of the design can be easily reproduced for permanent or temporary deployments requiring substantial solar capacity with the ability to optimize solar panel angle and expand the power system. The flexibility of the design allows for easy instrument additions or upgrades. For example, plans for the four recently installed seismic stations include the addition of cameras and tripwires. The new stations will improve lahar detection on Mount Rainier and the implementation of our design will safeguard integrated monitoring stations in the harsh environments commonly found on volcanoes.

Stepan Krasheninnikov, Lilya Bazanova, Maxim Portnyagin, Maarten Blaauw

Submission 770

Record of the Holocene magmatism of Avachinsky and Koryaksky volcanoes: geochemical and tephrochronological approach

Avachinsky (AV) and Koryaksky (KOR) volcanoes are the largest in the Avachinsky volcanic group situated 30 km to the north from Petropavlovsk-Kamchatsky city. Proximal composite tephra sequences for these volcanoes comprise 156 units (eruptions) of AV and 54 units for KOR. In order to date the eruptions, more than 189 radiocarbon dates as well as 53 dates for marker tephra layers [Braitseva et al., 1993, 1995; Bazanova and Pevzner 2001] from 50 localities from the studied sections and across all Kamchatka were compiled and run through the OxCal calibration procedure [Bronk Ramsey, 2009], using the terrestrial northern hemisphere IntCal13 model [Reimer et al., 2013]. The erupted tephra volumes were estimated for 40 Holocene eruptions.

Pyroclastic rocks from AV and KOR volcanoes were studied geochemically to reconstruct their temporal compositional variations. The dataset comprises the major and trace element composition of bulk tephra samples and matrix glasses for 63 samples representing 38 eruptions of AV volcano and 12 eruptions of KOR volcano. AV compositions have low- to medium-K₂O compositions while KOR tephra are medium- to high- K₂O, correlating with increasing distance to the trench and the depth to the Benioff zone from AV to KOR volcano [Kuno 1966]. Chemically contrasting glass shards were found in the samples of different ages and often in single lapilli samples. The data testify an important role of magma mixing in the origin of AV rocks that occurred along with fractional crystallization. Compositions of bulk tephra span a much narrower range compared to matrix glasses and represent magmas formed by effective mixing of compositionally contrasting melts, crystallization and accumulation of phenocrysts. Tephra samples from KOR eruptions have more homogeneous compositions.

Whereas magmatic system of KOR appears to have been in quasi-steady state during the Holocene, AV is characterized by a change in tephra compositions from low-K andesites to medium-K basaltic andesites started more than 5000 cal BP. The processes of fractional crystallization associated with periodic injections of mafic middle-K magmas into the shallow low-K silicic magma chamber formed in the early Holocene are thought to control the compositional variability of the Holocene tephra compositions.

Research supported by RSF grant 16-17-10035.

Mike Krawczynski, Maxim Gavrilenko, Philipp Ruprecht

Submission 1272

Possible existence of deep super-hydrous arc magmas: implications from high-Mg amphibole

The importance of quantifying the amount of H₂O dissolved in magmas is obvious. However, pre-eruptive dissolved H₂O in magmas is difficult to estimate due to nearly complete degassing of magmas during ascent, eruption, and cooling. Currently, magmatic H₂O content estimations are based mostly on two methods: 1) measurements of water dissolved in melt inclusions; 2) plagioclase chemistry 'hygrometers' that are thermodynamically derived models which use composition and/or phase stability as a function of dissolved water content. There is compelling evidence that these methods are only applicable to magmas in the upper-most part of the Earth's crust. Thus, the tools, which are commonly used for magmatic pre-eruptive H₂O estimations are not able to provide information about deep/primitive arc magmas, which may contain much larger amounts of water than normally recognized.

In many ways amphibole may be complementary to plagioclase in its potential use as a hygrometer-type phase. In water-bearing magmas plagioclase crystallization gets suppressed, but amphibole crystallization does not. This leads to amphibole being an early crystallizing phase in deep-crustal hydrous systems, and in particular it crystallizes before plagioclase, and under certain circumstances, coeval with olivine. Primitive amphiboles crystallizing with or possibly even before olivine is a rare but globally ubiquitous assemblage, and has a lot to reveal about just how hydrous are subduction zone magmas when they leave the mantle. The primitive setting for amphibole discussed here is very different from the more typical use of amphibole as a barometer in evolved acidic rocks. Here we present a survey of published data from plutonic and volcanic rocks that shows magma processing in the lower to middle crust often involves dissolved H₂O contents >12 wt%. We also outline how petrologic investigations of primitive igneous amphibole could be carried out to highlight the importance and ubiquity of amphibole as an early crystallizing phase. Amphibole's lack of a stability field at low pressure and the positive correlation between pressure and H₂O solubility are likely major contributing factors to the underestimation of the global significance of H₂O-rich primitive melts that are processed through volcanic arc systems. Ongoing and future experiments will help to better interpret the global array of primitive amphibole samples.

Janine Krippner, Alexander Belousov, Marina Belousova, Michael Ramsey

Submission 307

Correlating dome collapse events with block and ash flow deposits at Shiveluch volcano, Kamchatka

Shiveluch volcano in Kamchatka, Russia, is one of the world's most active dome-building volcanoes and has produced some of the largest historical block and ash flows, globally. The current eruption phase of Shiveluch volcano has been ongoing since 2001 in a cycle of dome growth and collapse. Understanding these prolonged dome growth episodes and describing the largest of these deposits to understand the extreme end of the deposit size and runout range is important for determining the maximum hazard extent of other dome collapse events. The spatial and temporal trends of eight dome eruptions and the resulting block and ash flow deposits were investigated using ASTER thermal infrared (TIR), shortwave infrared (SWIR), visible-near infrared (VNIR), and digital elevation model (DEM) data. The block and ash flows are a result of partial collapse events and their flow direction is controlled by the location of collapse on the 1,350 m-wide dome and the topography at the base of the dome. Runout distances of the largest flows extend to 18 km from the dome summit and deposited boulders with a maximum diameter of 11 m to over 11 km away. Planimetric areas of the dome collapse scars range from 0.24 to 1.71 km². There is no correlation between scar area and deposit size, indicating that the deposit size is largely dependent on the depth of the collapse area. Maximum pixel-integrated brightness temperatures within the collapse area are recorded up to 465°C (where SWIR data is available) with the temperature decreasing rapidly towards the outer dome surface. When pre-event data are available, an increase in thermal output occurs within the area of collapse, although the areal extent of the thermal anomaly does not correlate with the size of the collapse area. Not every thermal anomaly is followed by a partial collapse. Field and satellite data show evidence of retrogressive, pulsatory collapses, in which the dome collapsed in multiple phases over the hours of the eruptions to produce one large deposit. Over the 16 years of this ongoing eruption phase of Shiveluch volcano there has been no apparent trend in aerial extent or runout distances of the flows through time, although the largest events occur when the dome is at a maximum size. Linking the block and ash flow deposit distribution and runout distance to the size, location, and temperatures of the dome collapse area provides a basis for determining the distribution and extent of future hazards at similar volcanoes.

Nickolay Krotkov, Simon Carn, Bradford Fisher, Steven Taylor, Can Li, Pawan Bhartia, Fred Prata, Eric Hughes

Submission 1017

First observations of volcanic eruption clouds from L1 orbit by DSCOVR/EPIC

Volcanic emissions of sulfur dioxide (SO₂) and ash have been measured by ultraviolet (UV) sensors on US and European polar-orbiting satellites since the late 1970s. Although successful, the main limitation of these UV observations from low Earth orbit is once a day temporal resolution. Timeliness can be crucial when detecting hazardous volcanic eruption clouds that threaten aviation, and most currently operational geostationary satellites cannot detect SO₂, a key tracer of volcanic plumes. In 2015, the launch of the Earth Polychromatic Imaging Camera (EPIC) aboard the Deep Space Climate Observatory (DSCOVR) provided the first opportunity to observe volcanic clouds from the L1 Lagrange point. EPIC is a 10-band spectroradiometer spanning UV to near-IR wavelengths with two UV channels sensitive to SO₂, and a ground resolution of ~25 km. The unique L1 vantage point provides continuous observations of the sunlit Earth disk, from sun rise to sunset, potentially offering multiple daily observations of volcanic SO₂ and ash clouds in the EPIC field of view. When coupled with complementary retrievals from polar-orbiting UV and infrared (IR) sensors such as the Ozone Monitoring Instrument (OMI), the Ozone Mapping and Profiler Suite (OMPS), and the Atmospheric Infrared Sounder (AIRS), the increased observation frequency afforded by DSCOVR/EPIC will permit more timely volcanic eruption detection, improved trajectory modeling, and novel analyses of the temporal evolution of volcanic clouds. No large tropical eruption has occurred to date during the DSCOVR/EPIC mission. Hence, we demonstrate the sensitivity of EPIC UV radiances to volcanic clouds using examples from several recent mid- to high-latitude eruptions including Etna (Italy), Aso (Japan) and Bogoslof (Alaska, USA). Detection of these relatively small events proves EPIC's ability to provide timely detection of volcanic clouds in the upper troposphere and lower stratosphere.

Pooja Kshirsagar, Karoly Nemeth, Raúl Miranda-Avilés

Submission 908

Structural control of an eroded mafic alkali monogenetic volcanic field associated with flood basalt volcanism: Central Kachchh (NW Deccan Traps of India)

The late Cretaceous Deccan volcanics in Kachchh are represented not only by typical tholeiitic flows and dikes, but also eroded plug-like bodies of alkali basalt, basanite, melanephelinite and nephelinite commonly containing mantle xenoliths, intruding the Mesozoic sandstones. These rocks form the base of the local Deccan stratigraphy and the ^{40}Ar - ^{39}Ar ages of 65-66 Ma make them contemporaneous with the bulk of the Deccan Traps to the south. The ensemble has been studied extensively for their geochemical and petrogenetic history however their volcanological context is poorly understood. The eruptive centers are heavily modified and eroded to the level of exposures of shallow subsurface architecture of small volcanoes with limited preservation of anything associated with the former volcanic edifices. The identified vents form clusters and alignments in Central Kachchh typical for a dispersed, monogenetic volcanic field. The exposed crater-filling to conduit filling successions are inferred to be necks, sills, dikes, crater-filling lava sheets, shallow laccoliths, associated lava flow, peperites and proximal mafic alkali lapilli tuff deposits. Central Kachchh in this respect shows analogy with other younger, but still eroded monogenetic volcanic fields such as those in Central Europe, posing a question about the link between large igneous province formation and normal monogenetic volcanic field evolution. The km-scale volcanic edifices in Central Kachchh show correlation with the location of major lithospheric structural elements of the region suggesting that the vent opening was influenced by the position of pre-existing local faults within the peri-cratonic rift basin that is bounded by the Nagar Parker fault in the north and the Kathiawar fault in the south. The rifting is inferred to have started along major Precambrian trends in the Early Jurassic. In Late Cretaceous–Early Paleocene time, the Kachchh rift was again subjected to deformation prior at ~66 Ma the Deccan volcanism took place. Preliminary observation indicates at least two generations/cycles for the formation of the vents in Central Kachchh, which is also witnessed in the geometry, morphology and geochemistry of the mafic alkali plugs. It seems there is clear relationship between the pre-existing structural elements of the region and the spatial distribution and the variation in the chemistry of the volcanics of the vents in Central Kachchh.

Stephen Kuehn, Eric Arrington, Jared Rose, James Frye, Savannah Ballengee, Addison Hostetler, Cameron McNeely

Submission 1255

Pyroclastic eruptive history of the Three Sisters volcanic cluster, Cascade arc, Oregon, USA

The Three-Sisters–Tumalo volcanic region, located in central Oregon, USA, is associated with one of the most active segments of the Cascade volcanic arc. This region's potential for future eruptions was thrust into public consciousness by a period of ground deformation and earthquakes during the late 1990s to early 2000s. The region is also a known locus of rhyolitic volcanism. Although several late Holocene (e.g. ~2.2 ka Rock Mesa tephra) to late Pleistocene (e.g. ~300 ka Bend Pumice/Tumalo tuff, and ~600ka Desert Springs tuff) pyroclastic deposits are well known, the overall pyroclastic eruptive history of the area has remained poorly understood. New field studies and analyses of tephra glasses by EPMA are currently underway. Because of extensive erosion, the most proximal samples available are preserved primarily on unglaciated high ridges. Other samples come from a limited number of exposures at lower elevations to the east. EPMA data reveals more than a dozen distinct geochemical populations, and each of these likely represents a separate eruptive event. Geochemical similarities suggest that at least two of these eruptions deposited ash at Carp Lake, Washington, about 200 km to the north-northeast. At least five tephra beds (II1, JJ, JJ0.2, G, and E1) at Summer Lake, Oregon, located 170 km to the southeast, also match the chemistry of Three Sisters area tephra deposits. Although an exact geochemical match has not yet been located, close geochemical affinity and known tephra distributions suggests strongly that the Three Sisters volcanic cluster is also the source region for the widespread, ~30-35 ka Wono tephra, a key regional time marker in Oregon, California, and Nevada, which forms a visible tephra layer more than 500 km from the inferred source.

Ulrich Kueppers, Valeria Cigala, Julia Holzmueller, Juan Jose Pena Fernandez

Submission 757

Size matters, shape too: The significance of pyroclast characteristics

Explosive volcanic eruptions eject variable amounts of gas, pyroclasts and lithics into the atmosphere. The dynamics can surely be changed by extrinsic factors (e.g. external water) but are ab initio controlled by magma properties (temperature, crystallinity, porosity, gas overpressure etc.) and the geometry of the plumbing system. Late-stage magma deformation and eventually fragmentation frequently lead to brittle fractures as manifested by angular clast shape in primary fall deposits.

Here we investigated the transport and abrasion properties of porous volcanic clasts: 1) The mechanical strength has been investigated by tumbling and fall experiments. Results show that porous clasts lose weight and achieve significant rounding easily without the need for energetic events. Break-up upon impact occurred rarely and was found to occur more frequently for scoriaceous than pumiceous clasts. In general, weight loss and shape changes are both negatively correlated with sample weight and surface roughness. 2) The ejection dynamics of gas-particle mixtures from laboratory experiments following rapid decompression have been analysed from high-speed videos. Although most particles are not coupled to the gas phase, we observe that clasts from 1-15 mm leave the setup at comparable velocities and only start following different trajectories when affected by the Kelvin-Helmholtz vortices in the gas-entrainment mixing layer.

During explosive volcanic eruptions, the gas-particle mixtures are ejected in a quasi-unidirectional way. Accordingly, particle-particle collisions are more likely oblique than head-on, leading to abrasive processes overruling comminution. As angular clasts are by far the most dominant shape fraction in fall deposits, we conclude that size reduction and shape changes play a minor role during conduit and gas-thrust region transport. Accordingly, grain size characteristics found in primary fall deposits are controlled by energy conversion during magma fragmentation and can be used as a proxy for eruption characterisation.

Hiroyuki Kumagai, Yuta Maeda, John Londoño, Cristian López, Lina Castaño, Beatriz Galvis, Lina García

Submission 902

Magma conduit system beneath Nevado del Ruiz volcano, Colombia, inferred from seismic waveform analyses

Nevado del Ruiz volcano located in the Colombian Andes continues its eruptive activity. To enhance monitoring capabilities at this volcano, broadband seismometers and other equipment have been deployed. Using waveform data from the seismic network, source locations of volcano-tectonic (VT) earthquakes, very-long-period (VLP) events, and tremor were systematically determined by the amplitude source location (ASL) system since March 2016. We conducted waveform inversion of VLP events to estimate their source mechanisms. In this paper, we discuss the magma conduit system beneath Nevado del Ruiz volcano based on results of these seismic waveform analyses.

At Nevado del Ruiz volcano, 13 broadband and 3 short-period seismic stations have been maintained. We have operated an automated event trigger system using seismic amplitudes in a low-frequency band of 0.3-1 Hz. Source locations of triggered events and tremor have been automatically determined by the ASL system using high-frequency (5-10 Hz) seismic amplitudes. The quality (Q) factor of the volcano and site amplification factors at the individual stations used in the ASL determinations were estimated by minimizing the hypocenters and ASLs of VT earthquakes that occurred at the volcano.

Our ASL results indicated that VT earthquakes occurred in localized regions surrounding the volcano and the sources of tremor and VLP events were distributed from the summit crater (5311 m) to a depth of about sea level in the NW direction. We found that some tremor episodes showed moving sources along the tremor and VLP source region. The waveform inversion of VLP signals points to tensile cracks dipping toward the NW direction. Tomographic images of the volcano estimated by Londoño and Kumagai (this meeting) display that the tremor and VLP source region corresponds to the region with high V_p/V_s ratios, implying the existence of fluids in this region. These results suggest that this source region represents an active crack-like conduit inclined toward NW, in which tremor and VLP events were triggered by magma fragmentation processes. The inclined conduit may correspond to the Palestina fault intersecting Nevado del Ruiz volcano, along which magma ascends from a deep magma chamber.

Syegi Kunrat, Martin Streck, Heather Wright

Submission 719

Soputan volcano, Indonesia: petrological systematics of volatiles and magmas and their bearing on explosive eruptions of a basalt volcano

Soputan volcano is one of the few basaltic volcanoes among the 127 active volcanoes in Indonesia. It is part of the Sempu-Soputan volcanic complex located south of Tondano Caldera, North Sulawesi and commonly produces both explosive eruptions with VEI 2-3 and effusive lava dome and flow eruptions. Over the last two decades, Soputan had thirteen eruptions, the most recent in 2016. Most eruptions started explosively, followed by dome growth and in some cases pyroclastic flows. Our study focuses on understanding the magmatic system of Soputan and what processes are responsible for its highly explosive eruptions given the basaltic magma composition. Our study includes tephra samples predating the 1911 eruptions, lava flow from the 2015 eruption, and ash from a 2015 fallout deposit.

Our whole rock major and trace element data are virtually identical to lava flows and select pyroclastic deposit compositions of Kushendratno et al. (2012) for the 1911–1912 and 1991–2007 eruptions. Bulk rocks contain 49 to 51 wt.% SiO₂, whereas 2015 ash samples are slightly more silicic with 53 wt.% SiO₂, consistent with segregation of groundmass from phenocrysts in the eruption cloud. Mantle normalized incompatible trace elements indicate strongly depleted HFSE and REE signatures but with spikes at Pb and Sr and mild enrichment of Rb and Ba.

Fo68-79 olivine-hosted melt inclusions range from basaltic (48–52 wt.% SiO₂) to basaltic andesite (54-55 wt.%) as compared to 54 - 65 wt.% SiO₂ glass in Fo68-74 olivines reported by Kushendratno et al. The compositional range of melt inclusions is consistent with 30-40% fractionation of multiple minerals rather than a single phase (e.g. olivine), which is in line with observed phenocrysts of olivine, plagioclase, pyroxene and oxides of phenocryst-rich magmas and excluding compositional effects of post-entrapment crystallization. New volatile concentration data from melt inclusions are higher than previously reported from younger samples (S max. ~0.07 wt.%, Cl max. 0.2%, H₂O max. ~1 wt.%) with S max. 0.21 wt.%, Cl max. 0.17%, H₂O max. 4.1 wt.% (FTIR data). H₂O is relatively constant (~3-4 wt.%) for individual tephra samples (data by FTIR and difference method). Our inclusion data suggest that more volatile-rich magmas exist at depth and this is consistent with a model whereby recharge of deep, volatile-rich magmas into a more degassed and crystal-rich magma initiates a new, highly explosive eruption.

Kushendratno, et al (2012): BV 74:1581-1609

Andrei Kurbatov, Nelia Dunbar, Nels Iverson, Mark Royer, Martin Martin

Submission 1273

Antarctic tephra database AntT, lessons learned

Paleoclimate research relies on establishing accurate timing, notably timing related to rapid shifts in Earth's climate system, with the aim of correlating these events at local to global scales to assess phasing. Many key questions in climate research (e.g. relative timing of climate events in different geographic areas, climate-forcing mechanisms, natural threshold levels in the climate system) are dependent on accurate reconstructions of the temporal and spatial distribution of past rapid climate change events in continental, atmospheric, marine and polar realms. Tephra-producing volcanic eruptions are geologically instantaneous events that are largely independent of climate, and unresolved potential for tephrochronology still exists within the framework of paleoclimate research in the Antarctic.

We report results of a collaborative effort between groups at the University of Maine (UM) and New Mexico Tech (NMT) to build the Antarctic tephrochronological database (AntT).

The database was designed to integrate all publicly available tephrochronological data sets from Antarctica, and has a search and geochemistry-based tephra correlation tools. It provides a robust, easy-to-use, and publicly available platform assisting in characterization and correlation of regional and global tephra layers known to be present in Antarctica.

We will report system design and philosophy, discuss available data sets, and outline future research plans.

Support through NSF awards 1142007, 1142069 is acknowledged.

Steffen Kutterolf, Julie Christin Schindlbeck, Marion Jegen, Armin Freundt, Susanne Straub

Submission 629

Milankovitch frequencies in tephra records at volcanic arcs: Does climate control volcanism?

Systematic changes in eruption frequencies since the last glacial maximum in Iceland and elsewhere suggest that deglaciation may have an effect on volcanism. Tephra records form continuous time series that are particularly useful to investigate relationships between frequency of volcanic events and glaciation/deglaciation cycles. However, most studies of regional volcanic time series cover just one glacial cycle not sufficient enough to detect reliable statistically relationships between volcanism and global climate throughout the Quaternary. As a first attempt to that effect, we had collected and combined the Pleistocene through Holocene tephra records from along the Pacific Ring of Fire, encompassing widespread ash deposits of sub-Plinian to Plinian eruptions and occasionally co-ignimbrite origin recorded in marine sediments. This combined volcanic data set was necessary in order to 1) increase the overall data density for significant statistical analyses and 2) to facilitate the detection of globally occurring variations opposed to regional ones. Spectral analysis yielded a statistically significant spectral density peak at the obliquity (41 kyr) period and but only a weak spectral density increase at the ~ 100 kyr eccentricity period.

In a second approach, we analyze the 1.1 Myr long tephra time series of IODP Hole U1437B drilled near the Izu-Bonin Arc in the northwestern Pacific that combines a high background sedimentation rate (>11 m/Ma) with the frequent emplacement of tephra fallout from the nearby Izu-Bonin and Japan Arcs. Interestingly, this record, which covers 13 glacial periods, yields a statistically significant, prominent spectral density peak at the eccentricity period (~ 100 kyr, the prominent periodicity of glacial cycles) whereas the 41 kyrs periodicity is not clearly recognized in these data and may be obscured by the control of regional geological conditions on the volcanism.

Statistical analyses of the tephra and global $\delta^{18}O$ records suggest increased volcanism during the periods of fastest sea level rise and deglaciation rate. This suggests that changes in the lithospheric stress distribution may play a crucial role assisted by a comparison of the most complete Late Pleistocene-Holocene Central American tephra time series with the regional stress changes obtained from a global stress model for the last glacial period which shows a significant increase in eruption frequency where the rate of change in lithospheric stress is highest.

Giuseppe La Spina, Amanda Clarke, Mattia de' Michieli Vitturi, Chelsea M. Allison, Kurt Roggensack, Fabrizio Alfano, Mike Burton

Submission 751

1085 AD sub-Plinian eruptions at Sunset Crater: a numerical study through a 1D transient conduit model of magma ascent

Volcanoes exhibit a wide range of eruption styles, from relatively slow effusion to intense explosions, in which very large volumes of volcanic gas and particles are ejected into the atmosphere. As magma rises through the conduit towards the surface, the confining pressure decreases, causing dissolved volatile species, such as water and carbon dioxide, to exsolve from the melt forming gas bubbles. Gas bubbles in the melt expand as the pressure decreases and the magma will fragment to generate explosive eruptions if and when a threshold gas volume fraction, bubble overpressure, or strain rate is exceeded. Ascent and fragmentation are influenced not only by the nucleation and growth of gas bubbles, but also by magma rheology and its behaviour under a wide range of strain rates. Here we employ a multiphase multicomponent 1D transient numerical model to better understand subsurface processes that controlled and characterized the 1085 AD sub-Plinian eruptions at Sunset Crater, Flagstaff, AZ. Specifically, we investigate the impacts of several model assumptions, such as isothermal conditions, instantaneous vs. finite-rate gas exsolution, and gas and melt coupling vs. decoupling, on numerical results. We focus our simulations on the dynamics associated with the sudden depressurization of an overpressured conduit sealed by a viscous, crystal-rich plug. Our numerical results show that, assuming perfect gas-melt coupling, the solution converges rapidly towards a steady-state explosive eruption, independently of whether the isothermal or instantaneous exsolution assumptions are made. As such, the isothermal and exsolution assumptions have little impact on fragmentation depth and mass eruption rate, and therefore appear to have limited bearing on simulated eruption style. However, when decoupling, due to permeable gas escape, is allowed between melt and gas, the solution does not reach steady-state. Our results, therefore, highlight the point that gas-melt decoupling is an important process that may control the eruption style and duration at explosive basaltic volcanoes.

Stefan M. Lachowycz, Diana C. Roman, Ioana A. Cosma, Mel Rodgers, David M. Pyle, Tamsin A. Mather, Nick Varley

Submission 37

Investigating temporal variations in volcanic activity by statistical analysis of observation time-series

Despite recent advances in collection and analysis of monitoring data from active volcanoes, and the resulting insights into volcanic processes, challenges remain in interpreting and forecasting volcanic activity from near-real-time analysis of observation time-series. Statistical methods have the potential to characterise the underlying structure and facilitate intercomparison of these time-series, and so inform interpretation of changes in volcanic activity. We explore the utility of multiple statistical techniques that could be widely applicable to observation time-series, including Shannon entropy and detrended fluctuation analysis, which quantify uncertainty and long-range correlations in data, respectively. We apply these techniques to various time-series from monitoring during periods of temporally variable activity at diverse volcanoes, including Soufrière Hills (Montserrat), Telica (Nicaragua), and Volcán de Colima (Mexico). Each analysis method reveals changes through time in the structure of some of the datasets that were not apparent from conventional analysis. For example, the Shannon entropy of real-time seismic measurements and some volcano-seismic event counts at Soufrière Hills and Volcán de Colima is found to be temporally variable. Generally, these data are found to have higher entropy during periods of lava effusion and/or large Vulcanian eruptions, with the entropy sometimes shifting prior to or coincident with changes in seismic or eruptive activity. Comparison with other statistics demonstrates the sensitivity of the entropy to the data distribution, but that it is distinct from conventional statistical measures such as coefficient of variation. Similarly, detrended fluctuation analysis of volcano-seismic event counts at Telica, a persistently restless volcano with highly variable seismicity rates, reveals temporal variation in the correlation extent of these data; some shifts in correlation extent precede or coincide with changes in eruptive activity. We conclude that each statistical analysis technique applied could provide valuable insights for interpretation of changes in volcanic activity inferred from diverse observation time-series.

Kathrin Laeger, Daniele Andronico, Maurizio Petrelli, Jacopo Taddeucci, Valeria Misiti, Piergiorgio Scarlato, Corrado Cimarelli, Elisabetta Del Bello

Submission 1085

Constraining the magma dynamics during the Eyjafjallajökull 2010 eruption by high-resolution geochemical mapping

The Eyjafjallajökull (Iceland) eruption in 2010 is marked by changes in eruptive style from effusive to explosive activity and therefore, was presumably triggered by replenishment of new basaltic magma migrating into the plumbing system. Eruptive products provide a great variability in compositions from basalt to rhyolite. Here, we present new EMPA and LA-ICP-MS data on groundmass glasses of ash particles and minerals erupted between 15 April and 22 May 2010. Major and trace element data of glasses imply magma mixing between compositionally different magma batches over the whole eruptive period. Resorbed inverse zoned crystals are in agreement with open system processes. In particular, the injection of fresh basaltic magma into the magmatic system of the volcano has led to remobilization of magma batches of trachyandesite and rhyolite composition. According to geophysical data, these batches might have been formed by intrusions over the past twenty years before eruption. We envisage two mixing processes that are responsible for the compositional variability of the ash samples. The first occurred between basalts and trachyandesites and the second between trachyandesitic and rhyolitic end-members. This hypothesis is supported by least squares modeling of major elements. Moreover, the analysis of compositional histograms of trace elements helps us to assess the initial proportions of the interacting melts that generated the compositional variability ranging from trachyandesites to rhyolites.

Kathrin Laeger, Armin Freundt

Submission 1094

Post-glacial magma storage conditions at Laguna del Maule, Chile

Laguna del Maule (LdM) volcanic field is of special interest due to its vigorous postglacial (<25 ka) activity, even though no historical eruptions have been identified. LdM is located in the Transitional South Volcanic Zone (34°30'-37° S) of South America, where generally andesite compositions further north gradually change to basalt compositions towards south but still comprise high amounts of rhyolites of postglacial age. This study deals with three separate explosively erupted units which consist of andesite to rhyolite compositions, contain zoned plagioclase (An₁₉₋₈₇), mixed phenocryst populations of amphibole of dominantly magnesio-hastingsite and tschermakite composition, clinopyroxene (Mg#=0.73-0.82), olivine (Fo₇₄₋₈₀) and orthopyroxene (Mg#=0.71-0.80). Amphibole gives crystallization conditions of 939-987 °C and 288-391 MPa, corresponding to a depth of 11-15 km. The water contents in the melts, based on amphibole chemistry calculations, is 5.2-6.0 wt. %. The occurrence of rhyolitic melt inclusions in dacites, several dissolved and reversely zoned phenocrysts including reverse FeO and anorthite-zoning in plagioclase, and additionally olivines and orthopyroxene yielding disequilibria conditions, suggest interaction of at least two different evolved magmas. Further, late-stage magma mingling is evident from banded pumice-clasts and inhomogeneous matrix glasses. Based on melt inclusions, the felsic resident melt had rhyolitic composition, whereas the hybrid magma is andesitic to dacitic. Olivine phenocrysts are stable in melt of Mg#=0.50-0.55 that might represent the less evolved component. We investigated three systems showing variable magma storage conditions, including replenishments of less evolved magma batches that are not in agreement with the hypothesis of a great homogenous silicic magma chamber underneath LdM volcanic field.

Joao Lages, Alessandro Aiuppa, Andrea Luca Bernard, Tobias Fischer, Diego Narváez, Philipson Bani, Yves Moussallam, C. Ian Schipper, Viviana Burbano, Silvana Hidalgo, Pablo Samaniego, Jean-Luc Le Pennec, Benjamin Bernard, Gustavo Garzón

Submission 617

Subduction dynamics, mantle and crustal processes at arc volcanoes, investigated by relative CO₂/ST abundances and ³He/⁴He isotope signatures.

The investigation of the relative abundance of volatiles allows for a better constrain of the origin and recycling efficiency of these elements via subduction. Here, we attempt to correlate along-arc and inter-arc variations of CO₂/ST gas ratios with noble gases and CO₂ compositional trends (in particular ³He/⁴He and d¹³C) with the aim to shine a light on the complex transfer of fluids through the mantle wedge to the partial melting zone, while tracking fluid's modification during magma ascent towards the surface. Our first approach reviews the available CO₂/ST gas data, along with their respective R/Ra and d¹³C from gas discharges and magmatic crystals, on a data set comprising 35 arc volcanoes. Then, we specifically focus on the Northern Andean Volcanic Zone, where we attempted compositional analysis of high T gases, sampled gas discharges from active vents and peripheral areas, as well as hydrothermal springs. We also collected rock samples from lava flows and pyroclastic deposits for analysis of elemental and isotope composition of Helium (and CO₂ when possible) in fluid inclusions hosted in olivine crystals. Our global review highlights lack of correlation between CO₂/ST gas ratios and noble gases compositional trends. This discrepancy may partly reflect the different sampling techniques and conditions (e.g., very low to high T gas emissions). We argue that the high variability in R/Ra (Min=3.60; Max=9.77) that follows may affect our ability to better estimate the extent of such relation, thus making the role/effect of crustal contamination and/or interaction of magmatic fluids with shallow hydrothermal systems a key assessment of this investigation. For instance in Ecuador, a mean R/Ra of 3.3 is estimated, far from the homogeneous MORB signature of 8 ± 1 Ra, highlighting the importance of newly collected data. With the research being carried out, we believe we can investigate: (i) at a local scale, temporal variations in noble gas composition throughout the course of an eruption, for a particular volcano (analysis of El Reventador products, from 2002 to present); (ii) subduction zone signature of the Ecuadorian-Colombian arc by looking at different subduction parameters possibly governing ratio's variability (e.g. different subduction angle and thermal regime within the NVZ); and (iii) improving our ability to use volatile and noble gas trends as geochemical and isotopic precursors of volcanic eruptions.

Oliver Lamb, Paul Wallace, Silvio De Angelis, Yan Lavallée, Anthony Lamur, Adrian Hornby, Felix von Aulock, Jackie Kendrick, Gustavo Chigna, Armando Pineda, Alejandro Diaz Moreno, Andreas Rietbrock

Submission 794

Geophysical and geochemical observations of explosion dynamics at Santiaguito, Guatemala

Santiaguito lava dome complex in Guatemala, presents an ideal location for the study of eruption dynamics at long-lived silicic eruptions. Here we present the first long-term seismic, infrasound and geochemical dataset over a period of significant activity at Santiaguito that can shed light on the deep and shallow volcanic processes that affect surficial activity. The geophysical instrument network, deployed in November 2014, comprises of seismometers and acoustic sensors located between 0.5 and 7 km away from the active vent. Ash and bomb samples collected during field campaigns over the subsequent two years were used to track changes in geochemistry during eruptive activity.

Since at least the early 1970s, activity at Santiaguito was characterised by regular, small gas-and-ash explosions from the summit crater, sometimes simultaneously with the extrusion of blocky lava flows. In mid-2015, a major shift in activity took place at Santiaguito where the regular gas-and-ash explosions were replaced by irregular, occasionally highly energetic, Vulcanian explosions sometimes accompanied by pyroclastic density currents. Furthermore, this sequence caused the lava-filled summit crater of El Caliente dome, the current eruptive centre at Santiaguito, to be excavated into a crater of ~150m depth. Differences in arrival times of seismic and acoustic waveforms suggest a deepening of the explosion initiation point during the sequence which may be linked to a change in bulk magma composition of eruptive products. The long-term trend in bulk chemical composition has seen a decrease from 66 wt% in 1922 to 61 wt% in recent years. Activity from early 2016 shows a rapid increase in SiO₂ of ~1.5 wt% over a 6-month period. Our dataset illustrates how deep magmatic processes can directly affect surficial activity during an ongoing silicic eruption. The results of the multi-parametric monitoring experiment have specific implications for hazard assessment at Santiaguito, and contribute to our understanding of the processes that control gas-and-ash explosive sequences at lava dome volcanoes.

Ellen Lamont, Andrew Meigs, Philip Wannamaker

Submission 850

Stress-state, slip-tendency, and magmatism along faults within the Cascadian arc-backarc region of central Oregon

The Cascade arc-backarc region in Oregon has unique potential for development of geothermal energy. North American plate deformation including Basin and Range extension and subduction-related magmatism are reflected by a complex system of heterogeneously oriented faults intermingled with Quaternary volcanic centers. Dense faulting contributes to regional permeability while hot springs along the length of the arc suggest an existing heat source at depth, two variables controlling geothermal systems. The goal of this study is to assess the propensity for fault slip and dilation, which dictate fluid transmissivity in extended terranes. Slip and dilation tendency models the likelihood of fault motion and tension given normal and shear stresses acting on individual fault surfaces. Faults displaying high slip and/or dilation tendency have greater failure potential and tend to be more fluid transmissive. We test conduit-like fault behavior by comparing fault models against the occurrence of observed fault-controlled magmatism such as aligned cinder cones, vents, and fissure flows.

One-meter resolution LiDAR imagery was used to map fault traces and volcanic edifices for the region from 42°N - 45.5°N. Three prominent fault strikes were observed: northwest, north, and northeast. Regional stress state compiled from borehole breakouts, earthquake focal mechanisms, vent/dike alignments, and the World Stress Map yields a range of minimum compressive stress trends (060° to 120°), with the majority of sources fitting a tighter range (085° to 095°). Due to the variations in stress orientations and fault trends, tendency analyses were conducted in 5° stress intervals to evaluate sensitivity. Slip and dilation tendency are maximized for the case of normal faulting with a least principal stress orientation of 080°. However, lack of observed fault-controlled magmatic activity on orientations of highest tendency suggests this maximized case might overestimate slip and dilation tendency. Conversely, a least compressive stress orientation of 100° under a strike-slip regime yields numerous high tendency fault traces that better relate to faults containing magmatic deposits. This suggests a transtensional model for stress orientations, related to Walker Lane shear zone and Basin and Range extension, that facilitate magmatism and potential fluid flow on a variety of fault orientations, which is supported by regional tectonic models and geodetic data.

Anthony Lamur, Jackie Kendrick, Gudjon Eggertsson, Fabian Wadsworth, James Ashworth, Richard Wall, Felix Von Aulock, Yan Lavallée

Submission 1071

Fracture, heal, repeat: timescales and implications for silicic systems eruptive behavior

Volcanic systems are often anisotropic environments. The development of anisotropic permeable pathways occurs through numerous processes (e.g. bubble growth, coalescence, shearing, fracturing and cooling/ contraction). Understanding the evolution of such features is of prime importance in building a quantitative picture of fluid migration and stress build-up in shallow volcanic systems, potentially describing eruptive cyclicity.

Here, we show the results of new experimental protocols that aim to understand the development of permeability through fracturing as well as the timescales required for magmatic strength recovery through fracture healing.

To assess the impact of macro-fractures on fluid flow in volcanic rocks, we measure the permeability of 77 samples (with initial porosities of 1-41 vol.%), intact as well as following tensile fracturing. We demonstrate that a macro-fracture has the ability to enhance fluid flow efficiency by increasing the permeability. In rocks with a low initial porosity (

In the second set of experiments, we monitor the stress recovery at the contact interface between two glass (synthetic or obsidian) rods at high temperature, as a function of time of contact. We demonstrate that fracture healing happens in short timescales (minutes to hours) and that (and therefore temperature) is the dominant limiting property in healing kinetics. We conclude that the relaxation of magmas allows for fast strength recovery of fracture planes, leading to the closure of permeable pathways which is more efficient than mechanical sealing.

In the light of these results, we surmise that rapid and dynamic permeability changes due to repeating fracture (permeability increase) and healing (permeability decrease) events can contribute to the cyclic eruptive behavior of silicic volcanic systems.

Rebecca Lange, Jameson Jolles

Submission 1276

The origin of two distinct geochemical gradients with temperature in the Bishop Tuff: resolution of unanswered questions

High-silica rhyolites are the most evolved magmas on Earth and constitute some of the largest eruptions. An example is the Bishop Tuff (BT), for which unanswered questions include what is the cause for: (1) the geochemical gradient in the earliest erupted (Early) BT, which is unrelated to magma mixing, (2) the systematic increase in ΔNNO ($\text{Fe}^{3+}/\text{Fe}^{\text{T}}$) with temperature across the BT, and (3) the greater crystal abundance in Late vs. Early BT and why qtz+sanidine is always dominant over plagioclase. In this study, 24 single pumice clasts were analyzed from Early to Late BT and average temperature obtained from Fe-Ti oxides. Correlations of element concentrations with temperature in Early BT are strong ($R^2 \leq 0.9$) and used to determine the relative compatibility and incompatibility of elements, by taking the slope of their gradient with temperature and dividing by their average concentration. Because Early BT contains nine minerals, segregation from a crystal-rich mush with these phases was modeled and their relative abundances were constrained by matching bulk partition coefficients to the relative compatibility and incompatibility of the various elements obtained from the pumice clasts. The data show that the geochemical gradient with temperature in Early BT can form by extraction of interstitial melt at various melt fractions/source depletion from a leucogranite that also contained ~3% biotite, ~0.9% tmte, ~0.4% ilm, ~0.08% allanite, ~0.04% apatite and ~0.015% zircon. This assemblage also explains the systematic increase in ΔNNO (i.e., $\text{Fe}^{3+}/\text{Fe}^{\text{T}}$) with temperature, because Fe^{3+} is more compatible than Fe^{2+} in this crystalline assemblage. For the Late BT, a low- SiO_2 rhyolite (extracted from a mush that included plagioclase, two pyroxenes, biotite, tmte and ilm) may have mixed with a high- SiO_2 rhyolite extracted from a leucogranite crystal-rich mush; both appear to have been at similar high temperatures and low water activities (relative to Early BT) when they formed and segregated. The location of the eutectic in a leucogranite at low water activity shifts toward K-spar, which is why qtz-hosted melt inclusions in Late BT have high $\text{K}_2\text{O}/\text{Na}_2\text{O}$ ratios. After segregation and ascent, the water activity in the melt progressively increases, causing the eutectic to shift back, thus initial crystallization is along the qtz-sanidine cotectic before reaching saturation with plagioclase. This explains the dominance of qtz and sanidine in all BT samples and their abundance in Late BT.

Federica Lanza, Clifford H. Thurber, Ellen M. Syracuse, Abhijit Ghosh, John Power

Submission 415

High-resolution seismic velocity structure of Makushin Volcano, Alaska

Located in the eastern portion of the Alaska-Aleutian subduction zone, Makushin Volcano is among the most active volcanoes in the United States and has been classified as high threat based on eruptive history and proximity to the City of Unalaska and international air routes. Seismic imaging of its complex plumbing system has been previously attempted, but the unfavorable network geometry presented a great challenge. Here we expand on previous work in order to improve the resolution of the seismic structure beneath the volcano. We supplemented the one-sided station coverage provided by the Alaska Volcano Observatory (AVO) permanent seismic network with a set of five individual stations and three mini seismic arrays of 15 stations each. It provides us better azimuthal coverage with higher signal-to-noise ratio. Data collected during the 2015-2016 deployment show an improved event detection capability, providing us with a larger earthquake dataset. Preliminary P-wave images confirm the presence of high Vp features in the upper 5 km beneath the caldera, possibly delineating a remnant magma pathway or conduit. Low-Vp regions are found at approximately 7.5 km depth, which have been identified as a possible long-term source of magma based on geodetic models using InSAR data.

Using this new dataset and performing both body wave and ambient noise tomography, separately and jointly, we provide a high-resolution tomographic image of Makushin volcano as well as better-constrained earthquake locations, thus enhancing AVO's monitoring and forecasting efforts.

Luis E. Lara, Lucy M. McGee

Submission 968

Small eruptive centres are decoupled from arc volcanoes in the Southern Andes

Holocene monogenetic volcanoes or small eruptive centres (SECs) are ubiquitous in the Southern Andes and are spatially related to the main branch of the Liquiñe-Ofqui Fault System (LOFS), a 1200 km long intra-arc fault, and/or the neighbours of major stratovolcanoes. Early hypotheses about the origin of SECs connected their genesis with the role of postglacial rebound, which should be higher at the LOFS, but systematic ¹⁴C dating shows a wider time span from early Holocene to almost historical. Instead, our results suggest that the generation of SECs could be a recurrent, perhaps time-predictable (and hence tectonically-controlled) process. On the other hand, petrological and compositional data show an unexpected variety, which suggests local-scale source heterogeneity and a range in the dominance of certain magmatic processes, such as deep crustal contamination, which occurs to different extents. There is no correlation between composition and distance to the arc front and SECs along the LOFS do not present fluid influenced isotopic signatures as do basalts from the stratovolcanoes or SECs around them. To integrate these findings we present a general model where tectonically-triggered decompression melting of a heterogeneous mantle source would be the key process over which local scale factors play a role.

Fondecyt projects No. 1110966, 1141303 and 11130296 are acknowledged.

Adam Large, Martin Streck, William McIntosh

Submission 1171

Rhyolite volcanism at the northern and western periphery of the Columbia River province rhyolite flare-up: The Buchanan and Dooley Mountain volcanic complex, eastern Oregon

Mid-Miocene (>16.5-15 Ma) rhyolite volcanism associated with the eruption of lavas of the Columbia River Basalt Group (CRBG) stretches from NE Nevada to SW Idaho to NE Oregon over an area with ~400 km diameter. Dooley Mountain and Buchanan rhyolite complexes are located along the northern termination near Baker City and along the western periphery near Burns of this rhyolite flare-up, respectively.

The focus of this study is to characterize eruptive units through field and laboratory analysis, to determine their extent, to establish an eruptive stratigraphy, and to constrain rhyolite activity by modern $^{40}\text{Ar}/^{39}\text{Ar}$ age dates. Our work builds on USGS mapping done in the 90's and earlier PSU thesis research at Dooley Mountain, and only on limited mapping done in a regional context at the Buchanan complex.

Both rhyolite complexes were prolific centers. At Buchanan, at least eight distinct eruptive units erupted over period of 600 kyr from 16.1 to 15.5 Ma producing a minimum of ~16 km³ of rhyolite lava flows with a subordinate amount of tuffs. Lava flows have relatively low aspect ratios and are low to high-silica rhyolites ranging from aphyric to containing ~10% phenocrysts. At Dooley Mountain, individual units are difficult to trace laterally due to disassembly, coverage, and erosion. Four eruptive packages based on rhyolite composition and petrography can be established and consist dominantly of lava flows and breccias with only limited ash-flow tuffs. Character of rhyolites became slightly more A-like with time. All rhyolites amount to ~35 km³ and our new radiometric ages indicate a minimum activity span from 15.6 to 15.4 Ma but regional tuffs reaching into the area allow for a longer activity period bracketing it to 16.1 to 15 Ma. However, rhyolites from the greater Dooley Mountain area have yielded ages greater than 16.5 Ma and thus indicate initiation of rhyolite volcanism along the northern periphery as early as in the southern part of the rhyolite flare-up.

Basalt lava flows are part of the stratigraphy of both complexes and we have correlated those with regional CRBG units. At Dooley Mountain, it was unexpected to identify most basalt lava flows, apparently under- and overlying rhyolites, as Picture Gorge Basalt based on incompatible trace element signatures and not Imnaha Basalt as previously thought. At Buchanan, we correlated an underlying basaltic andesite flow with upper Steens Basalt.

Patricia Larrea, HELENA ALBERT, FIDEL COSTA, ELISABETH WIDOM, CLAUS SIEBE

Submission 295

Magmatic processes of Paricutin volcano: rapid fractionation with no crustal assimilation?

Paricutin volcano is famous for its birth in a corn field and its historical eruption that lasted for nine years (February 1943 - February 1952). It is considered a classical example of magma differentiation by progressive crustal assimilation and fractional crystallization. However, recent multi-isotopic studies of its volcanic products point to mantle source heterogeneity together with fractional crystallization. We have started a detailed petrological study of the deposits to clarify the magma residence times and processes that lead to the chemically zoned eruption. The whole-rock composition progressively evolves from basaltic andesite to andesite. Major element variation diagrams show kinks that are indicative of crystal fractionation being a key process during the differentiation of the magmas. All the eruptive products have low phenocryst contents (typically 81-76). We do not find petrological evidence for crustal assimilation (no xenocrysts were found). Detailed core to rim olivine EPMA analysis of early, middle, and late erupted deposits shows that there is mainly one compositional population of crystals. Rather homogeneous cores (Fo81-79) have normally zoned rims (Fo71-52). Such simple zoning patterns (e.g. no reverse zoning has been observed) suggest that magma evolution did not include major open system events or magma replenishment, in contrast with other mafic monogenetic eruptions. Diffusion modeling of the Fe-Mg in olivine shows that the zoning could be created by high-temperature residence of 2 months prior to eruption. However, there is no increase of the residence time with eruption time, which suggests that magma differentiation may have occurred in 'real time' on similar time scales as the eruption itself. Together, the lack of xenocrystic components and the Sr-Nd-Pb-Os isotope data suggest limited to no crustal assimilation involved in the differentiation despite the presence of crustal xenoliths in some lavas.

Peter Larson, Jerry Fairley, Nick McMillan, Cary Lindsey, Brady Lubenow

Submission 832

A Comparison of Heat Transfer Modes from a Thermal Discharge Area in the Yellowstone Caldera

Volcanism is a manifestation of heat transport through the crust, yet evaluating the amount of heat discharged to the surface in a volcanic environment is difficult. Some heat can be transported to the surface through hydrothermal processes. A common, but untested, assumption is that heat transport at the land surface boundary of hydrothermal discharge areas is dominated by advection. To evaluate this assumption, we analyzed the partitioning of heat flow in the vicinity of LCBNN159, a small circumneutral hydrothermal spring in the Morning Mist Springs area of Lower Geyser Basin, in the Yellowstone caldera. We quantified the advective heat transport using time-series records of spring temperature and a novel deuterium-doping method to determine volumetric discharge. For comparison, we estimated conductive heat losses from the near-field surroundings of the spring using >600 shallow (20 cm depth) temperature measurements, made on a grid at a spacing of 3 x 3 m. We used a simple geostatistical analysis to obtain a best estimate of the distribution of shallow temperatures, and a similar analysis to estimate the distribution of thermal conductivity of the near-surface materials. We employed a 1D model of heat transfer between a flux boundary and a convection-conduction boundary, combined with a time-series record of air temperatures, to estimate conductive heat flux near the spring. A comparison of the two quantities shows that conduction may account for as much as 50% of the total heat transfer to the atmosphere across the land surface boundary, at least in the vicinity of spring LCBNN159. In acid-sulfate areas, this fraction may be much higher because of steam-heating of the land surface in areas adjacent to fumaroles and frying-pans.

Benjamin Latutrie, Pierre-Simon Ross, James DL White

Submission 128

Bedded to non-bedded transition at Round Butte diatreme, Hopi Buttes volcanic field, Arizona

The Hopi Buttes volcanic field (HBVF) in the Navajo Nation (Arizona, USA) provides excellent exposures of maar-diatreme volcanoes at different erosion depths, from the maar ejecta ring and crater infill (White, 1991, *Bull Volc* 53:239-258) to the deep diatreme (Lefebvre et al., 2013, *Bull Volc* 75:1-17). This makes it an ideal locality to better understand eruptive processes for this type of volcano. We are currently investigating the Round Butte diatreme in the eastern portion of the HBVF. This study provides the first insight of the composition of the deposits and the structure relationships and geometries. The current exposure lies at the top of the Owl Rock member of the Chinle formation (Upper Triassic) near the contact with the bottom of the Moenave formation (Lower Jurassic), at ~190 m below the eruptive paleosurface. At this depth, Round Butte is 130 m in diameter and the exposure is 30 m high cliffs and displays the contact between the lower (non-bedded) and the upper (bedded) portions of the diatreme. The contact is irregular, varying in apparent angle from sub-horizontal to vertical. Deformed mudstone blocks that underwent shearing are found in the non-bedded pyroclastic rocks, near the vertical contact with the bedded ones. A vertical contact suggests that the non-bedded pyroclastic deposits were emplaced after the bedded ones, whereas the sub-horizontal contact suggests the opposite. The upper part is composed of diffuse bedding with sometimes accumulation levels of juvenile and lithic blocks, while the lower part is massive and exposes blocks and pockets randomly scattered from Moenave formation and Bidahochi formation (Miocene). In the whole outcrop no evidences of blocks from Owl Rock member were found, that suggest the filling was possibly conducted by fallbacks and avalanches of upper materials from Moenave and Bidahochi formations and volcanoclastic products from the tuff ejecta ring. A huge avalanche in the southwest of the outcrop shows a succession of Moenave and Bidahochi blocks intercalated by pyroclastic tuffs from the ejecta ring. At Round Butte all the processes that lead to the formation of the current outcrop seem to work simultaneously.

Yan Lavallee, Jose Godinho, Jackie Kendrick, Biao Cai, Katherine Dobson, Felix von Aulock, Robert Atwood, Marian Holness

Submission 1105

Flow, fracture and vesiculation in shearing basaltic magmas revealed by synchrotron imaging

Our understanding of physical, chemical and rheological processes during magma shearing remains obscured due to a lack of syn-deformation visualization of physico-chemical interactions. Synchrotron-based x-ray tomography now allows us to image the inside of materials during testing under controlled conditions, revealing an unprecedented level of details on the state and configuration of materials as they evolve.

Here, we experimentally investigate the rheological behavior of basaltic magmas from Pacaya volcano (Guatemala) using shearing experiments at variable temperatures (940-1100 °C), during in situ x-ray tomographic imaging. In particular, we explore the physico-chemical development of multiphase magmas during shearing. These informative 4D reconstructions offer new insights, which combined with geochemical and physical characterizations, permit the description of crystals interact, fracture propagation and vesiculation during shearing. We will conclude with a discussion and reinterpretation of our models of magma shearing during transport and eruption.

Nicolas Le Corvec, Thierry Menand, Jean-Luc Froger, Valérie Cayol

Submission 294

Incremental growth of magma reservoirs: Insights on the room problem through the use of finite element models

Magma accumulation in the lithosphere leads to the formation of either plutonic rocks or magmatic reservoirs, which give birth to large volume of silicic volcanic rocks. The accumulation and sustainability of such reservoirs through time is believed to be controlled by the magma emplacement rate. The accumulation of large quantities of magmas in the crust is however not a trivial mechanism since it involves large deformation of the country rock. Such deformation is believed to occur currently in the Andes where InSAR data are showing large and persistent uplifts at seemingly constant rates of several centimetres per year over nearly two decades. The observed deformation can however reflect different rheological processes happening within the crust: either 1- an elastic response of an ongoing deformation, or 2- an ongoing viscoelastic response of a now ceased deformation. In this work, we aim to address this issue by studying the mechanical response of the country rock to the incremental growth of a magma reservoir using finite element models and seek to better constrain the interpretation made from remote sensing data.

Using the modeling capabilities of COMSOL Multiphysics®, we have developed a methodology allowing for incremental growth of a magma reservoir by successive sill intrusions. The methodology was developed using the module LiveLink™ for Matlab® to automatize the process which consider several stages of five successive steps: 1- building the geometry, 2- imposing the physics, 3- meshing the domains, 4- computing the model, and 5- exporting the state of stress and the deformed geometry. At the end of each stage, the exported data are used as initial conditions in the subsequent stage, for which the 5 steps are repeated. The methodology has been developed using axisymmetric elastic models with each intrusion having a radius of 500 m long.

We will present the methodology itself and the initial results obtained in the initial and simple case of an elastic domain.

Nolwenn Le Gall, Fabio Arzilli, Biao Cai, Robert C. Atwood, Peter Rockett, Sara Nonni, Richard Brooker, Margherita Polacci, Mike Burton

Submission 494

Time-resolved synchrotron tomography of basaltic magmas: successes and challenges

Synchrotron X-ray computed microtomography (sCT) allows 3D images of materials to be captured in a few seconds. Combining this technology with an environmental cell that replicates the temperatures and pressures experienced during magmatic processes offers to provide a tool to directly capture the kinetics of both crystal and gas phase formation in magma, termed 4D imaging (3D plus time). However, performing in situ sCT experiments on magma is challenging due to their high chemical reactivity, the range of temperature and pressure variations, and oxygen fugacities (fO_2) required to replicate natural conditions.

Currently, most experiments are conducted in air at 1 atm, and on silicic melts due to the lower range of temperatures and volatile diffusivity. However, working under controlled pressure and redox conditions, as well as with mafic magmas is essential when investigating volatiles that affect the rate and extent of degassing and crystallisation. We are currently working on this complex issue.

By using a high-temperature resistance furnace ('Alice'), able to achieve a maximum temperature of 1460 °C (at a max rate of 0.5 °C/s), we were able to quantify in 4D the nucleation and growth of crystals (clinopyroxene, plagioclase, oxide) in basaltic melts. Previous works in silicate melts, mainly focusing on degassing kinetics, were generally performed using a laser-based heating system that, although allows a rapid heating, induces thermal fluctuations and gradients.

As a first step, our cooling-type experiments were conducted in air, at 1 atm and between 1250 and 1100 °C, using high-speed sCT (I12 beamline, Diamond Light Source). As a second step, we are adapting a thermo-mechanical rig ('P2R') to create intermediate pressure (fO_2 at NNO). Combined with the Alice furnace and I12's high-speed microtomography, we hope to replicate, in situ, the ascent of basalt in the shallow volcanic conduit (

Hélène Le Mével, Patricia Gregg, Kurt Feigl

Submission 859

Characterizing magma pulses feeding Long Valley caldera using thermo-poroelastic models of magma injection into a magmatic mush

Long Valley caldera (California) has been experiencing unrest episodes characterized by intervals of increased ground deformation and swarms of seismicity. Since 1990, four main episodes of uplift were identified and recorded by geodetic techniques including Electronic Distance Measurement (EDM), GPS and InSAR. Geodetic studies using kinematic source models of a pressurized void in an elastic or viscoelastic domain have revealed that a vertically elongated source located at depths of 6 to 7 km explains most of the ground deformation signal. We hypothesize that this persistent source intermittently inflates as new magma arrives in the magmatic system that underlies the resurgent dome of the Long Valley caldera.

To test this hypothesis, we have developed and validated a dynamic poroelastic model that simulates the injection of magma into a mush zone, possibly topped with a long-lived magma reservoir. The porous rock matrix is characterized by its permeability and porosity, while the single-phase magma characterized by its viscosity and density flows through the crust following the application of a mass flux at the base of a conduit. The thermal effect of the magma injection on the resulting surface displacement is also investigated by solving the heat transfer equation through the crust following the application of a heat and mass flux. The models are used to match the spatial and temporal pattern of uplift for the episodes of 1990-1995, 1997-1998, 2002-2003, and 2011 to present. This new model allows us to quantify the volumes of magma feeding the magmatic system of Long Valley for each of the 4 historical uplift episodes. These magma flux estimates are then compared to those at other volcanic systems, giving us insight on the processes responsible for non-eruptive unrest episodes at other calderas worldwide.

Yannick Le Moigne, Glyn Williams-Jones, Karim Kelfoun, Philippe Labazuy, Kelly Russell, Nathalie Vigouroux-Caillibot

Submission 860

Investigating and modeling Canada's deadliest volcanic eruption

Tseax volcano (Wil Ksi Baxhl M'ihl) is a polygenetic cinder cone with associated basanite lava flow situated in Northwest British Columbia, Canada. It marks the southern extent of the Northern Cordillera Volcanic Province. Located in the Anhluut'ukwsim Laxmihl Angwinga'asanskwhl Nisga'a (Nisga'a Memorial Lava Bed Provincial Park), Tseax is the site of one of the youngest and deadliest volcanic eruptions in Canada; an eruption in the mid-1700s killed an estimated 2000 people of the Nisga'a Nation living in two villages near the volcano. A rich oral history has preserved detailed observational accounts of the eruption, however, the exact cause of the fatalities remains unclear. Moreover, there has been limited scientific investigation of Tseax volcano and its erupted products and thus, many questions still need to be addressed.

Detailed field mapping and sampling in 2016 and 2017 in conjunction with an aerial photogrammetry survey has enabled the development of a high-resolution 3D model (using Agisoft PhotoScan) of the volcano and lava flow. The Tseax lava flow is 32 km long with a volume of ~ 0.5 km³, and can be divided into several units based on surface textures such as blocky, slabby, rubbly, wavy or flat pahoehoe. There are notable features characteristic of a very low viscosity fluid and which suggest a rapid expansion of the flow. Indeed, numerous lava tubes up to 3 m in diameter are found along the entire flow and several mega-pillows (up to 4 m in diameter) are exposed along the Nass River. Furthermore, at least 150 accretionary lava balls (formed by rolling of viscous lava on the surface of an open channel) ranging from 1 m to > 5 m in diameter are found along the first 6 km of the flow. These field observations, along with petrophysical data, are combined with the high-resolution 3D photogrammetry model in order to numerically model (e.g., with VolcFlow, Q-LavHA) the emplacement of the lava flow.

As such we aim to establish the sequence and duration of the volcanic events responsible for one of Canada's worst natural disasters. Our models show that a large volume of low viscosity lava emitted over a short period of time (i.e., high flux) could effectively reach the location of the two ancient Nisga'a villages and thus be responsible for the large number of fatalities.

Elodie Lebas, Steffen Kutterolf, Anne Le Friant, Kai Fockenberg, Georges Boudon, Benoît Caron, Stephan Jorry, Patrick Bachèlery

Submission 1037

Extending the eruptive history of La Réunion Island to the Mid Pleistocene: Constraints from deep-sea sediments

La Réunion Island is an intraplate volcanic system located in the western part of the Indian Ocean. It is composed of two shield volcanoes: the older and extinct Piton des Neiges, and the younger and still-active Piton de la Fournaise. In 2011, sediment cores have been retrieved around La Réunion Island during the ERODER 4 cruise in order to investigate how large volcanoclastic turbidite systems are working. As a site project a 16.74 m long sediment core (MD11-3347) was recovered, ~42 km from the coast on the northern flank of Piton des Neiges on a submarine plateau at a water depth of 2890 m, to reconstruct a detailed eruptive history of La Réunion. Oxygen isotope measurements of planktonic foraminifera (*Globigerinoides Ruber*) allows us to assign an age of 433,000 years at the bottom of the core, representing the oldest sedimentary archive available offshore La Réunion. A detailed sedimentological and volcanological study has been done and identified with magnetic susceptibility at least 39 horizons potentially derived from explosive eruptions. This first investigation is complemented by compositional characterization of the volcanic products and correlation to known eruptions using extensive major and trace element measurements. For example, correlations of major element glass compositions from a pumice-rich marine tephra to on-land data facilitate the revision of the eruption age of the St Pierre ignimbrite to 213 ± 4 ka, which is significantly older and more precise than previously known. Using the combined data sets then the goals of our study are to (1) identify distal deposits from large previously known and unknown volcanic events (paleo-eruptions); (2) assign these deposits to on-land volcanic centers by chemical fingerprinting; (3) quantitatively and qualitatively investigate temporal changes in the geochemistry of the volcanic events; and (4) finally establish a compositional and temporal tephrostratigraphic framework for the region around La Réunion. Here, we report on the first results of this tephrochronostratigraphic study that are mainly based on major element chemistry and comprise >20 volcanic events of mugearitic to trachytic composition in the oldest part of core MD11-3347.

Hans Lechner, Mark Rouleau, Greg Waite

Submission 1170

To flee or not to flee? Lessons learned from the 2010 eruption at Pacaya volcano and factors affecting evacuation decisions

In 2010, Pacaya volcano in Guatemala experienced its largest eruption in over a decade and prompted the evacuation of roughly 2000 people from several communities. The eruption damaged hundreds of homes, injured dozens, and killed one person. During this volcanic crisis, individuals within the hazard zone faced the choice to evacuate or remain in a high-risk area. Many people chose not to evacuate. This study investigates evacuation decisions through the causal relationships between hazard warnings, risk perception, and evacuation behavior using a structured questionnaire survey. In October 2016, we conducted a door-to-door survey administered to households in eight communities surrounding Pacaya and asked participants to rank the factors that influence their decision to evacuate or not. Initial results suggest that while most participants trust information from emergency management agencies, official warning messages were distributed differentially to at-risk communities, which may have inhibited the evacuation decisions by households in some of the communities most affected by the eruption. The data also suggests that while official warning messages are important, the perceived risk to one's home and property may play a more important role in the decision not to evacuate. We will discuss these results as well as the need for improved communication strategies between scientists, emergency management agencies, and local communities to be prepared to cope with future eruption crises and facilitate more effective and successful evacuations.

Thomas Lecocq, Valérie Ferrazzini, Patrice Boissier

Submission 1305

Short term real time relative velocity variations prior to the Piton de la Fournaise eruptions since June 2014

The Piton de la Fournaise is one of the most active volcano worldwide. June 2014 "1 day" eruption was the first of a series of new eruptions that were different than those observed before, with much shorter (if any) precursory signals of unrest and rapid migration and eruptions.

In this communication, we propose to have a systematic look at the relative velocity variations observed in real time during the period January 2014 - March 2017. To be "fair" with true real time, we will first show an interpretation of the time series as they were recorded and presented on the OVPF intranet every morning (replay of real time), then we apply new filtering and predictive statistics (autoregression, anova, kalman filtering, granger causality, etc) to see if we could obtain a better precursory signal to the eruptions.

JooYong Lee, HyunA Son, SungSu Lee

Submission 390

Complementation of Lagrangian particle diffusion model for analysis of volcanic ash dispersion

This study presents numerical procedure to estimate volcanic ash concentration based on Lagrangian particle dispersion model. In order to compute the dispersion of ash particle, PUFF-UAF, a Lagrangian particle tracking model is employed, which simulate the turbulent diffusion by using random-walk model. In addition, gravitational effects on the individual particles are governed by Stoke's law. If a particle contacts with the ground surface during the unsteady computation, then it is regarded as fallout and requires a removal from the tracking. The particle tracking model presents the ash concentration by averaging the total mass loading in the grid system as a post processing. The Lagrangian-based PUFF-UAF model described above is useful because it is computationally fast, but it faces several problems. Lagrangian model suffers from the incomplete information on the spatial distribution of ash concentration because the model in nature assumes puffs or parcels of particles representing pre-assigned amount of ash with given distribution of particle sizes. This results in spatial discontinuity in the ash concentration with unrealistic distribution in some cases. In order to overcome this shortcoming, the ash concentration is calculated by using the method of Gaussian puff model in this study. It assumes that the diffusion takes place from the location of ash particles computed from Lagrangian model and the time scale for diffusion is considered as the elapsed time after the discharge. The calculated concentration results were compared with the method using the particle number. From those comparisons, we can observe the advantages and disadvantages of the methods for the calculation of ash concentration which lead to the efficiency of computation method.

This research was supported by a grant [MPSS-NH-2015-81] through the Disaster and Safety Management Institute funded by Ministry of Public Safety and Security of Korean government.

Rachel Lee, James Thompson, Michael Ramsey, Penelope King

Submission 781

Does the Emissivity of Basaltic Lava Surfaces Change with Temperature and Why Do We Care?

Infrared emissivity is an important physical property of a molten material because it directly affects the cooling efficiency, the determination of the bulk composition with cooling, and can therefore be significant in thermo-rheological models designed to study cooling and emplacement. Emitted energy from basaltic surfaces cooling from a molten to a solid state has been investigated in the past by several authors, yet remains enigmatic. Determining emissivity of active basalt surfaces in situ is a complex undertaking. As the lava cools, changes in surface glass content and vesicularity will occur, as does the simple mixing of temperatures within the field of view of the instrument, all of which introduce potential errors into the measurement. A series of high-resolution laboratory melting experiments on basalts has been conducted using a micro-furnace and thermal infrared (TIR) spectrometer, resulting in emissivity spectra of basalts at known temperatures both above and below the liquidus. Changes in spectral morphology can be seen with this transition, and have helped confirm that the emissivity of basalt does indeed change with cooling. In more recent work, the emissivity of the Kilauea lava lake surface was measured using a new ground-based miniature multispectral TIR camera system. This instrument collects multispectral data, which can be directly compared with the laboratory spectra, as well as with data acquired from TIR orbital sensors. The ground-based data of the lava lake surface show similar changes in emissivity with physical state. In an effort to test and calibrate this camera system under more controlled conditions, data will also be collected at the Syracuse University Lava Project facility, which conducts large-scale pours of degassed Palisades Sill basalt. These results, together with data from the laboratory and lava lake, should allow us to confirm the magnitude of emissivity change with the change of state for basaltic lava surfaces and also calibrate and test the efficacy of the camera system. These findings will ultimately provide a means to improve the accuracy of thermo-rheological models dependent on accurate cooling rates as well the ability of orbital TIR sensors to characterize future basaltic eruptions.

Hyunwoo Lee, Tobias Fischer, Maarten de Moor, Zachary Sharp, Naoto Takahata, Yuji Sano

Submission 1183

Geochemistry of volatiles in springs at the Costa Rican subduction zone

Subduction-zone fluids play a pivotal role in triggering earthquakes and generating arc magmas. Geochemical investigations on volatiles in the fluids offer information about contributing sources and various subduction processes. We report gas chemistry and isotope compositions (argon, helium, and nitrogen) of dissolved gases in forearc (FA) and arc front (AF) fluids in the Costa Rican subduction zone (CRS). Ten FA (Nicoya, Santa Elena, Osa, and Burica) springs ($T = 26.0 - 31.6^{\circ}\text{C}$) and nine AF springs ($T = 26.1 - 72.6^{\circ}\text{C}$) were sampled in 2012 and 2014. Based on gas chemistry, FA springs are subdivided into N₂-rich (62.4 – 98.3 vol. %) and CH₄-rich (36.1 – 96.8 vol. %) types, and AF springs have N₂-rich (88.0 – 98.5 vol. %) and CO₂-rich (47.2 – 98.4 vol. %) types. The N₂-Ar-He abundances indicate that volatiles in the FA and AF springs are mostly atmospheric, except for two AF springs (Cayuco and Rincon de la Vieja) showing more mantle-derived components. $^{40}\text{Ar}/^{36}\text{Ar}$ ratios (296.7 ± 7.5) which are close to air ($^{40}\text{Ar}/^{36}\text{Ar} = 295.5$) imply that argon is predominantly atmospheric. $^3\text{He}/^4\text{He}$ ratios of the Nicoya and Santa Elena FA springs range from 0.61 to 1.09 Ra, lower than the Rincon de la Vieja AF spring (7.88 Ra). This indicates that the major source of the FA fluids is predominantly crustal with atmospheric contribution. Nitrogen isotope compositions ($\delta^{15}\text{N}$ vs air) of the CRS springs (9-11N°) range from -4.4 to 1.6‰, except for Osa (4.7‰) and Burica (4.0‰) FA springs in the southernmost part of the CRS (8.4-8.6N°). Both the FA and AF springs at 9-11N° have a lower apparent sediment component ($\delta^{15}\text{N} = 7\text{‰}$) than the other Central American subduction zone samples at > 11N° (e.g., Nicaragua and Guatemala). In order to resolve the signals depleted in pelagic sediments-derived nitrogen in the CRS (9-11N°), several models (e.g., off-scraping, shallower subduction angle, and Cocos-ridge subduction) have been suggested. However, the ODP legs 170 and 205 of off-shore Costa Rica show pelagic sediments subducting beyond the trench. Moreover, subduction angles are shallower southward from Nicaragua to southern Costa Rica, and the center of the Cocos ridge subducts beneath the Osa and Burica areas rather than the CRS at 9-11N°. Instead, it is likely that subduction erosion occurs due to the Cocos slab off-shore at 9-11N° with abundant seamounts on the incoming plate. This results in contribution of the ophiolitic FA component (e.g., low-grade serpentinite) to the CRS fluids.

William Leeman, Rick Conrey

Submission 896

Along-strike Variations in Compositions of Cascades Primitive Mafic Magmas: Implications for Compositional and Thermal Structure of the Mantle Wedge

The Cascades Volcanic Arc (CVA) spans ~1000 km with complex along-strike variations in tectonic setting and basement geology. The subducting plate is young and warm, and the downgoing slab strongly volatile-depleted. Also, the extensional Basin & Range province has propagated into the S. end of the arc and rifting appears to have propagated at least to S. WA. Data for primitive basaltic magmas (>7% MgO) from along the arc constrain major, trace, and isotopic compositions of inferred mantle sources beneath the arc. Distinctive low Ba/Nb intraplate-like (IPB) and high Ba/Nb calcalkalic (CAB) basalts are common along the arc; and MORB-like low Nb/Zr and low-K tholeiites (LKT) are common from S. WA to N. CA sectors of the arc. All basalt variants have high eruptive T_s (most $\geq 1200^\circ\text{C}$). In a given sector, CAB variants appear to have slightly more refractory sources, and estimated depths of segregation from the mantle increase in the order CAB>IPB>LKT.

LKT eruptive T_s and equilibrium olivine Fo contents are highest in N. CA and decrease northward. Conversely, estimated T and P of melt segregation are lowest in N. CA and increase northward. These trends are consistent with shallower, more refractory mantle sources toward the south, as is also evident from southward decreasing Fe/Mg in calculated parental liquids. LKTs are plausibly derived from a 'DM' type mantle source in some cases ranging toward 'EM-1' enrichment, with negligible to small subduction component (e.g., available H₂O and B contents are low). LKTs may represent melting of upwelling little-modified asthenospheric mantle in response to extensional deformation in the arc. Their rarity in northern reaches of the arc may be tectonically controlled.

IPB lavas are distinguished by usually high Nb, Nb/Zr, and similar ratios, and absent to weak subduction signature. These lavas are most prominent in northern reaches of the arc. Their source domains are inferred to resemble asthenospheric mantle similar to sources for many OIBs. Melting of upwelling mantle wedge or sub-slab mantle (i.e., proximal to tears in the slab) are plausible scenarios to involve such sources.

CAB lavas are characteristic of most arcs, but segregation of such melts from the shallowest mantle domains is problematic for direct derivation of their 'subduction signature' from the modern subducting slab. Some may represent partial melts of previously melt-metasomatized domains in the shallow mantle wedge or lower crust.

Jonathan Lees, Daniel Bowman

Submission 1129

Volcano Infrasond From the Stratosphere

We have recently developed a new volcano observatory system by launching acoustic sensors into the stratosphere on free floating balloons. The value of balloon work is the development of a Lagrangian system for monitoring signals free of the disturbing effects of wind. For acoustic pressure, this can be a significant improvement over traditional land based observatories. The difficulty is, of course, the loss of control over the location of the system and retrieval of the data once data collection is over. Some of the technical difficulties can be overcome, and we are still in the initial stages of research and development. As a proof of concept, several experiments were conducted in the summer of 2016 to show that signals sourcing from the ground are recorded with high fidelity at between 30-40 km altitude hundreds of km from the source. This suggests that balloon platforms may be excellent sources of data collection for three-dimensional studies of volcanic explosions. An experiment in the Southern Ocean included a 10 hour flight over southern Chile, just north of Villarrica Volcano. Comparison of stratospheric floating balloon platforms with ground based (IMS) infrasond stations shows considerable improvement in the noise floor, suggesting that balloon borne signals offer a high-fidelity alternative to traditional acoustic installations. Numerous signals were detected throughout the flight, including high frequency arrivals during the Chile-Argentina cross flight. While the source of the high frequency signals is yet unknown we provide a statistical analysis of the content during the flight.

Nathalie Lefebvre, Juanita Rausch, David Jaramillo, Michael Ort, Hannes Mattsson

Submission 583

Textural and morphological studies of juvenile pyroclasts from the Ukinrek maars, Alaska: Insights into variation in eruption style of mafic monogenetic volcanoes

Mafic monogenetic volcanoes exhibit variation in eruption style at all scales and volcano structural levels. It is generally accepted that external water plays an important role in the explosive formation of maar-diatreme volcanoes. However, variation in eruption intensity observed at historical maar eruptions and recorded within the tephra rings down to the diatreme structures highlight that the combination of extrinsic and intrinsic factors that govern these eruptions are still poorly constrained. We characterize juvenile pyroclast textures and shapes of the most recent and best-observed maar-eruption, the Ukinrek 1977 eruption in Alaska. This eruption demonstrated fluctuating, discrete strombolian and phreatomagmatic activity of varying intensity at both maars formed and simultaneously from two proximal vents within the same maar. In addition, the magma composition remained nearly constant over the course of the eruption, making it an ideal locality to better understand variations in explosivity of a small-volume mafic system. This study examines juvenile ash and lapilli from 13 samples of phreatomagmatic and strombolian deposits spanning the entire eruption using classic petrographic techniques combined with 3D image analysis acquired by nano-CT and fractal analysis, in order to investigate the fragmentation conditions, and vesiculation and crystallization history.

Fluctuations in textural and morphological features are observed throughout the Ukinrek eruption, especially in the ash-size fraction and are distinct between strombolian and phreatomagmatic deposits. However, fine ash grains in all units show rare surface features indicative of interaction with external water. Phreatomagmatic pyroclasts are typically microlite-rich, vesicle-poor and blocky and ovoid in shape. Vesicles are irregular and show heterogeneous nucleation and size, high vesicle number density (VND) and lower interconnectivity. In contrast, strombolian lapilli have generally higher vesicularity, spinose and ragged shapes, and ash particles are dominantly microlite-poor, variably vesicular and blocky, ovoid and fluidal in shape. Vesicles in strombolian grains are coarser, have spherical to complex coalesced shapes, and show lower VND and higher interconnectivity. These observations suggest that small-scale horizontal and temporal variations in the physical properties of the magma along the shallow feeder system could be a factor in how efficiently magma and water can interact.

Graham Leonard, Andrew Calvert, Colin Charlier, Bruce Houghton, Dougal Townsend, Marvin Lanphere, John Begg, Darren Gravley, Drew Downs, Pilar Villamor, Julie Rowland, Michael Rosenberg, Bruce Charlier

Submission 999

The life and times of central Taupo Volcanic Zone: 15 years of mapping and geochronology illuminate the episodic evolution of Earth's most productive silicic volcanic system

The central Taupo Volcanic Zone can be considered in terms of its overall evolution as a single rhyolitic caldera complex of comparable longevity and scale to Yellowstone. It also has the largest time-averaged eruption rate on the planet over the last ~25 ka. We present an overview of results and discoveries obtained from 120 new $^{40}\text{Ar}/^{39}\text{Ar}$ ages combined with a decade of mapping for the QMAP regional mapping programme. These data shed new light on the tempo, style and hazards of the four largest supereruptions (Ongatiti, Kidnappers, Whakamaru, Oruanui) down to the frequent smaller magmatic (millennial) and hydrothermal (decadal) eruptions.

We have identified and interpreted periods of caldera-forming flare-ups, most recently from ~350 ka for at least 70 kyrs. In addition, previously unrecognised eruptive units have been identified in geothermal drill cores, dated, and fitted into the stratigraphic system. There appears to be not only spatial but also temporal clustering of smaller explosive and effusive eruptions, both following and apparently unrelated to caldera events.

There is a link of some Holocene vents with current shallow (~5km depth) areas of possible magma accumulation (e.g. Rotokawa), whereas other areas of low resistivity and high heat flow (e.g. Kapenga) appear un-associated with young eruptions. We can see a complex relationship of eruptive vents and rift faults to hydrothermal systems. There is clear temporal variability in rift faulting, including episodic narrowing, and sudden step-overs linked to caldera-related flare-ups in caldera volcanism. The rates of post-caldera volcanic and sedimentary infilling are remarkably rapid (kilometres of thickness in tens of thousands of years) and the distal landscape response to sedimentation has been equally dramatic.

Substantial multi-agency planning of responses and communication during future eruptive activity is underway. Preparing for future unrest and eruptions is challenging because of the extremely diverse behaviour (eruptive and unrest) shown within this unique area. Future hazard is not limited to past caldera locations, but their outlines dominate questions from both public and emergency managers. Unrest in our lifetimes is anticipated, but the challenge is in explaining that this translates to only a small probability of magmatic eruption.

Tanis Leonhardi, Kenneth Befus, Michael Manga, Nobumichi Tamura

Submission 663

Residual Stresses in Zircon from Bishop Tuff Record Volcanic Stresses

Quantifying subsurface magmatic processes is important for understanding the interplay between magma system architecture and volcanic eruptions. Forces from these processes stress magmatic crystals. Under certain pressure, temperature, and stress conditions, the mineral develops lattice strains that lock into the crystal's structure upon cooling. We use X-ray Laue microdiffraction (μ XRD) to quantify residual strains preserved in zircon grains in the 767 ka Bishop Tuff, California. Strain and composition were mapped across zircon grains with μ XRD and X-ray fluorescence respectively. We then used Hooke's Law to calculate the stress needed to produce the observed strain. Our measurements reveal a mean residual stress of 301 +/- 6 MPa. Zircon strain microstructures coupled with a lack of correlation between mapped trace elements and residual stress suggest that two main processes contribute to strain: (1) anisotropic distribution of the isotropic 'lithostatic' pressure in a crystal mush and (2) rapid decompression. Higher stresses recorded by subhedral cores (485 +/- 14 MPa) likely reflect formation at a greater depth and/or more damage from radioactive decay. These results show that zircon residual stresses may provide quantitative insights into magmatic processes.

Allan Lerner, Paul Wallace, Carl Thornber, Peter Kelly, Michelle Coombs, Charles Mandeville

Submission 982

Investigating the connection between sulfur degassing and the oxidation state of melt at Mount St. Helens, Washington, and Augustine Volcano, Alaska

Sulfur is a highly redox-sensitive element, and occurs as S(II-) in reduced melts ($\Delta\text{NNO} < 0$) in oxidized melts ($\Delta\text{NNO} > 0$), but exsolves as $\text{H}_2\text{S}(\text{II-})$ or $\text{S}(\text{IV+})\text{O}_2$ gases. Depending on the relative speciation of magmatic S and exsolving S gases, redox changes associated with S degassing can potentially affect magma $f\text{O}_2$ (Burgisser and Scaillet, 2007; Moussallam et al., 2016), which in turn can affect phase stability, S-solubility, and further degassing. We test whether S-degassing and $f\text{O}_2$ are linked in relatively oxidized systems (ΔNNO : ~ 0 to $+2$) by undertaking the first combined EMPA and μXANES melt inclusion study of recent eruptions from Mount St. Helens, Washington, and Augustine Volcano, Alaska.

We analyzed matrix glass and plagioclase-, amphibole-, and orthopyroxene-hosted melt inclusions from the 1980 dacitic plinian eruption, and the 2004–2008 dacitic dome forming eruption of Mount St. Helens. In accord with previous studies, we find relatively low S contents in matrix glasses and melt inclusions from both eruptions. For the 1980 and 2004–8 eruptions, plagioclase-hosted melt inclusions range from 40–120 ppm S, whereas amphibole- and orthopyroxene-hosted inclusions have 40–180 ppm S. A single analyzed clinopyroxene-hosted inclusion from the 1980 eruption has 340 ppm S. The collective melt inclusion suite shows that S concentration generally decreases with increasing melt SiO_2 (from 60–72 wt%), indicating that S-loss accompanies crystallization during decompression and H_2O -degassing (Blundy and Cashman, 2005).

Augustine is a more compositionally diverse system, with recent eruptions triggered by a basaltic intrusion into a shallow dacitic magma (Larsen et al., 2010). In melt inclusions from low-silica andesite samples of the 2006 eruption, S concentrations range widely, with 80–430 ppm S in plagioclase, 150–720 ppm S in orthopyroxene, and 150 to 2500 ppm S in clinopyroxene-hosted inclusions. Sulfur decreases appreciably with decreasing FeO (4–1 wt%), but is largely invariant across the analyzed SiO_2 range (55–64 wt%).

The ranges of S concentrations in Mount St. Helens and Augustine melt inclusions likely reflect entrapment during progressive stages of S-degassing. S-XANES and Fe-XANES analyses are being made in melt inclusions across these S ranges to directly determine whether S-loss, S-speciation, and $f\text{O}_2$ variations are coupled in these systems. These will be the first direct measurements of pre-degassed $f\text{O}_2$ at these well-studied volcanoes.

Philippe Lesage, Anaïs Boué, Guillermo Cortés Moreno, Bernard Valette, Raul Arámbula-Mendoza, Agus Budi-Santoso

Submission 190

Massive data processing and evaluation of the success rate of deterministic eruption forecasting

The material Failure Forecast Method (FFM, Voight, 1988) is the most frequently used approach for deterministic eruption forecasting. It is based on the use of accelerated increase of an observable, such as the rate of seismic event or ground deformation. An empirical power law is fitted to the observations and the predicted time of eruption is given by the location of the vertical asymptote of the function. Although the principle of FFM is relatively simple, the methodology for its implementation has still to be improved. For example, the choice of the observable, of the power law exponent, and of the fitting window, as well as the estimation of the uncertainties and confidence level of the time of eruption, are complex issues that must be carefully addressed. However, despite some encouraging results, the number of study cases published in international journals is still limited (~30 papers concerning 14 volcanoes). These papers generally describe forecasts in hindsight, i.e. using the whole sequence of observations until the eruption, and there are very few attempts in real-time. Furthermore, while the literature mainly presents successful cases, systematic studies including many eruptions with both successful and unsuccessful forecasts are still rare.

Statistically significant and unbiased evaluation of the success rate and reliability of FFM is thus needed. This task requires the processing of years of seismic records from a wide variety of volcanoes, which would imply international and cooperative efforts and access to large databases. As an example, we propose a rigorous Bayesian approach of FFM designed for real-time applications, coupled with an automatic recognition system of seismic events. 23 years of continuous recordings from 3 volcanoes, including 64 eruptions, have been analyzed. 36 % of the eruptions could have been forecast in real-time. However, when the reliability criteria are fulfilled, the success rate of forecast increases to 83 %.

Einat Lev, Camera Ford, Matt Patrick, Katharina Unglert

Submission 872

Cooling and degassing of lava lakes -- global and local perspectives

Active lava lakes, where cooling and outgassing at the surface are balanced by input of hot and gas-rich magma from below, are a rare occurrence. Yet, multiple lava lakes exist at present. Due to their longevity and visibility, lava lakes provide a natural laboratory for studying fundamental volcanic processes. We focus our work on two solidification and outgassing by investigating the cooling of a vesicular magma, and the penetration of gas bubbles through a solidified crust.

Using high temporal resolution (9Hz) thermal video captured at the Halema'uma'u lava lake at Kīlauea (Hawai'i, USA) we extract multiple time series of cooling at the lake's surface. We examine two geometries and data types: point-wise cooling following the bursting of large gas bubbles through the lake's solidified skin, and line-wise cooling as surface plates move away from spreading cracks (akin to mid-ocean ridges). We then compare the observed thermal histories with models of lava cooling, and invert for the effective thermal properties of the shallowest portions of the lake. Combining these observations with the thermal properties of the liquid melt, we infer the vesicularity of the shallow lake. Our results indicate very high vesicularity (over 80 vol.% gas), in agreement with values derived from measurements of the gravity and density of the lake when it was empty versus filled.

We also compare the behavior of the Halema'uma'u lava lake with five other lakes: Erebus (Antarctica), Nyiragongo (Dem. Rep. of Congo), Erta A'le (Ethiopia), Marum (Ambrym, Vanuatu), and Masaya (Nicaragua). We use both visible-light and thermal imagery collected by various groups to analyze activity at each of these lakes over time. Where possible, we go beyond lake-wide average values for temperatures and surface velocities by characterizing lake behavior using the machine-learning tool of Self-organizing Maps. We collate the data from the six lakes to compile a scale of circulation vigor, and find that the correlation between circulation vigor and total gas emission improves significantly when lake size is considered. We interpret this improvement to reflect the role of a surface crust (or the lack of) in modulating outgassing from lava lakes.

In summary, our work demonstrates that lava lakes are useful laboratories for studying lava properties and fundamental volcanic processes such as degassing, outgassing, and solidification.

Chelsea Leven, Lindsay Ellingson, Benjamin van Wyk de Vries, William Rose

Submission 1260

Supporting global geoheritage through international collaboration for a potential Ometepe Geopark in Nicaragua

Geoheritage is global, and although UNESCO Global Geoparks grow from local energy and commitment, international partners are important. We aim to combine international resources and experience to advance the idea of an Ometepe Global Geopark in Nicaragua. There are now 119 Global Geoparks in 33 countries. Many are in Europe and Asia, but there are only three in all of North and South America (Canada, 2; Brazil, 1). With its strong geoheritage and opportunities for related socioeconomic development, we are convinced that Ometepe Island could be a valuable addition to the Global Geoparks Network.

Ometepe has two imposing volcanoes that are obviously very different to any visitor. Strongly active Concepción illustrates a rapidly growing volcano, while Maderas tells the tale of a sleeping giant. Both are cut by very visible faulting, and the hills of Moyogapla are a classic example of uplift pushed up by Concepción's weight. Archaeological remains are preserved in the stratigraphic record of Concepción and built onto the rocks of Maderas.

Ometepe already is a UNESCO Biosphere Reserve, but has always drawn tourism with the volcanoes. However, public understanding of the geology and hazards is insubstantial. This is a global problem, where the very basis for biosphere existence is ignored, incapacitating a real preservation of the resource. Local conditions compound this, as educational resources are more difficult for locals than in neighboring areas with more developed tourism, e.g. Costa Rica. International and multicultural input for science communication, education, and geo-conservation and development could help foster the Geoparks plan, adding resilience to the reserve.

Some of us know Ometepe well and work for our own geoheritage sites. The first author has no direct experience of Ometepe yet, but was approached by a local NGO to assist, due to her experience in tourism and education. Thus, she has broad back up to develop this as part of an M.S. project.

International researchers have done much of basic geology and hazard analysis. Ways in which international partners might contribute include (1) making accessible geological results for a broad public, (2) helping engage local stakeholders, (3) obtaining resources to support the geoheritage infrastructure, (4) demonstrating effective strategies from other Geoparks, and (5) using their knowledge of Ometepe to describe and inventory geosites.

David Leverington

Submission 40

Constraints on the nature of the effusive volcanic eruptions that incised Kasei Valles, Mars

With a length of more than 2000 kilometers and widths as great as several hundred kilometers, Kasei Valles is the largest outflow channel on Mars. The scabland-like morphology of Kasei Valles is superficially evocative of terrestrial systems that were carved by aqueous floods, and has led to the widespread interpretation of this system as a product of catastrophic outbursts from aquifers. However, as at other outflow channels on Mars, clear examples of fluvial sedimentary deposits have proven difficult to identify here, and spatial correlations with hydrated minerals are not known to exist. Though Kasei Valles lacks numerous properties expected of aqueous systems, its basic morphological and contextual properties are closely aligned with those of ancient volcanic channels on Venus, Mercury, the Moon, and Earth. As with many of these channels, Kasei Valles heads at a topographic depression that marks sites of voluminous effusion of low-viscosity basalts or komatiitic basalts, shows evidence for having acted as a conduit for these magmas, and terminates at extensive mare-style ridged plains. Combined mechanical and thermal incision rates of at least several meters per day are estimated to have been readily achieved at Kasei Valles by 20-m-deep magmas flowing with viscosities of 1 Pa s across low topographic slopes underlain by bedrock. Incision rates in excess of 10 meters per day are predicted under these conditions for flow depths of 50 m. Effusion rates as great as tens of millions of cubic meters per second are expected to have been involved in channel incision here. The total volume of magma erupted at Kasei Valles is estimated to have been as great as five million cubic kilometers, a volume comparable in magnitude to those that characterize individual Large Igneous Provinces on Earth. Development of other large outflow systems on Mars is expected to have similarly involved eruption of up to millions of cubic kilometers of magma. Effusions of such magnitudes are likely to have involved deep and voluminous partial melting of mantle materials within long-lived plume-like environments, resulting in development of magmas with especially low viscosities and high potential temperatures. Accumulation of these magmas in large subcrustal reservoirs would have favored the existence of conditions capable of driving magmas to the surface at high rates of flow.

Steven Levesque, Frank Ramos

Submission 409

Geochemical Constraints on the Magmatic Evolution of the McCartys Flow, West-Central New Mexico

Geochemical signatures of intraplate tholeiites can be used to constrain the mineralogy of mantle underlying continents and identify potential open-system effects imposed during magma residence at crustal depths. Tholeiitic magmas are products of high degrees of partial melting, generally characterized by lower incompatible element abundances. Therefore, tholeiitic magmas may be highly impacted by open-system effects after mantle melt generation. Basaltic melts erupted along the Jemez lineament, a chain of northeast trending Late Cenozoic volcanic centers in southwestern U.S., have been attributed to mantle melting directly. The Zuni-Bandera volcanic field (ZBVF), located within the transition zone between the Colorado plateau and Rio Grande rift, contains both alkalic and tholeiitic basalts. The McCartys flow is the youngest tholeiitic basalt (3.9 ± 1.2 ka) within the ZBVF and consists of three petrologically distinct basalt types classified as olivine-phyric, plagioclase-phyric, and transitional. Whole-rock and olivine-hosted melt inclusion major elements, trace elements, and isotopes are evaluated to determine if McCartys basalts were generated from the mixing of magmas derived from multiple, distinct mantle sources. Alternatively, McCartys basalts could be derived from melt generated by a single mantle source that has undergone open-system assimilation of crustal material. Whole-rock major element variations of the McCartys basalt can be explained by $\sim 13\%$ crystal fractionation. However, incompatible trace element variations require $\geq 25\%$ crystal fractionation. Olivine-hosted melt inclusion compositions are generally more evolved than whole rocks and require $\sim 13\%$ crystal fractionation to account for major element variations. While melt inclusion incompatible trace element variations require $\geq 25\%$ crystal fractionation. McCartys whole-rock and olivine-hosted melt inclusion rare earth element variations also reflect the buffering effects of residual garnet during partial melting. Sr, Nd, and Pb isotope variations of McCartys basalts are consistent with crustal contamination involving mafic material. Results suggest McCartys magmas are derived from partial melting of garnet-facies mantle in which resulting magma was subsequently contaminated by mafic material at crustal depths. These conclusions are inconsistent with previous suggestions that McCartys basalt compositions result from spinel-facies mantle melts without accompanying contamination.

Jennifer Lewicki, Peter Kelly, Deborah Bergfeld, Jacob Lowenstern

Submission 130

Gas and heat emissions at Norris Geyser Basin, Yellowstone National Park, USA based on a combined eddy covariance and Multi-GAS approach

While basaltic magma intrusion and resulting gas-rich conditions in the subsurface likely drive cycles of uplift and deflation in Yellowstone Caldera, the specific mechanisms proposed by which this occurs have varied. Quantification of temporal variations in gas and heat emissions and their relationships to deformation and seismicity are required to improve understanding of caldera unrest. Norris Geyser Basin, located just north of Yellowstone Caldera and near an area of anomalous uplift, has displayed large variations in hydrothermal activity. We deployed an eddy covariance (EC) system that measured half-hourly CO₂, H₂O and sensible (H) and latent (LE) heat fluxes and a Multi-GAS station that measured H₂O, CO₂ and H₂S mixing ratios in Norris Geyser Basin from 14 May to 3 October 2016. We also measured soil CO₂ fluxes using the accumulation chamber method and temperature profiles on a grid and collected fumarole gas samples for geochemical analysis. EC CO₂ fluxes ranged from -68 to 758 g m⁻² d⁻¹. Using wavelet analysis, average daily CO₂ fluxes were locally correlated with average daily environmental parameters on several-day to monthly time scales. Multiplying the mean nighttime (to avoid daytime photosynthetic uptake) CO₂ flux (201 g m⁻² d⁻¹) by the ground-based measurement grid area (0.04-km²) roughly yielded a CO₂ emission rate estimate of 8.0 t d⁻¹, within 18% of that estimated based on accumulation chamber measurements (9.8 t d⁻¹). Nighttime H and LE were considered representative of hydrothermal heat fluxes and ranged from 3.3 to 176.9 and 38.2 to 465.5 W m⁻², respectively. Multiplying mean nighttime H and LE by the measurement grid area roughly yielded H and LE outputs of 2.4 and 7.7 MW, respectively, whereas the conductive heat output estimated based on soil temperature profile measurements was 3.2 MW. The Multi-GAS station measured low H₂O/CO₂ ratios (~20) and high ambient CO₂ values (> 800 ppmv) during nighttime periods with low wind speeds. During the daytime, southwesterly winds prevailed and gases with H₂S up to ~5 ppmv and strong mutual correlations of H₂O, CO₂, and H₂S were detected. The measured gas compositions define binary mixing trends between invariant end member compositions likely representing fumarole and soil gas sources. The average end member fumarolic gas ratios were H₂O/CO₂ = 101.7 and CO₂/H₂S = 27.1, which were within the range of values measured for in-situ gas samples.

Madeline Lewis, Paul Asimow, David Lund

Submission 507

Petrology of Explosive Eruptions from the Pacific-Antarctic Ridge and Ties to Sea Level Variation

Basaltic glass shards from sediment core OC170-26-159, retrieved 14km west of the Pacific-Antarctic Ridge (PAR) at 39°S, represent the products of large explosive submarine eruptions capable of ejecting material 7km from their axial source. Intervals in the core containing abundant glass shards indicate that volcanic activity peaked at 200 and 130ka, the latter of which is concurrent with glacial termination T-II and enhanced hydrothermal activity on the East Pacific Rise (Lund et. al., 2016). Based on our analyses of the glass and thermodynamic modeling, we propose that sea level changes alter the magmatic flux and consequently modulate the eruption style at mid-ocean ridges.

To evaluate whether sea level drives changes in magmatic flux and may be related to the frequency of large explosive submarine eruptions, we have collected major element, trace element, and volatile content data. Though more evolved (MgO 5.8-6.5wt%) and slightly enriched in H₂O and incompatible trace elements relative to effusively erupted basalts on the PAR axis (PetDB), the glasses are consistent with the axial liquid line of descent. Volatile saturation pressures range from approximately 2km crustal depth to the axial water depth of 2.26km, confirming that the shards erupted from the ridge axis. Using our maximum measured saturation pressure and fO_2 values consistent with MORB upper mantle conditions, we implemented the MELTS thermodynamic model (Ghiorso and Sack 1995, Asimow and Ghiorso 1998) to successfully predict the composition and volatile content of the glass shards through fractional crystallization of an axial magma and confirm the relation of the shards to the axial magmatic system. Fractionation from the most primitive axial composition results in over an order of magnitude increase in magma viscosity, suggesting that the explosivity was caused by higher viscosity in the fractionated melt and variations in magmatic flux over time. The period of energetic eruption near 130ka follows rapid sea level decrease and requires high magmatic flux to the ridge axis, while a period of fractionation between the explosive intervals, coincident with steady sea level, indicates low magmatic flux. Our fractionation model and the timing of explosive activity support modulation of mantle melting beneath mid-ocean ridges by sea level variation.

Weiran Li, Fidel Costa, Jason S Herrin, Kazuhide Nagashima

Submission 615

Contrasting eruption styles of Merapi volcano but similar magma pre-eruptive volatile compositions (CO₂, H₂O, S, Cl, F) and contents

Eruption styles of subduction-zone volcanoes may abruptly change. For example, Merapi Volcano (Indonesia) erupted effusively (VEI 2) in 2006, but explosively (VEI 4) in the following event in 2010. What caused this change in eruption style within such short period is still unclear, especially when considering that bulk rock compositions and major mineral assemblages of the 2006 and 2010 deposits are virtually indistinguishable. Here we address this question, by investigating the pre-eruptive volatile compositions and contents using apatite crystals located in various textural positions and hosted by different crystals.

All the major magmatic volatile species including CO₂, OH, S, Cl and F were measured in apatite using Cameca ims-1280 ion microprobe at the University of Hawai'i at Mānoa. We used apatite standards with known concentrations of volatile species. We find that volatile abundances in apatite fall into two groups: clinopyroxene-hosted crystals and microphenocrysts in the groundmass are depleted in CO₂ (~50-800 ppm) and H₂O (~0.5-0.6 wt. %), whereas crystals included in amphibole show distinctly higher CO₂ (>2400 ppm) and H₂O contents (~1 wt. %). Such differences in volatile concentrations indicate at least two magma reservoirs at different depths beneath Merapi, consistent with previous studies. Similar bimodality of apatite volatile content was observed in both the 2006 and 2010 deposits. We used thermodynamic models and exchange coefficients ($Kd_{Cl-OH}^{Ap-melt}$) from the literature to estimate melt volatile contents. We find that both 2006 and 2010 magmas had ~4-6 wt. % water and ~1000-2000 ppm Cl in the deep reservoir, and ~1-2 wt. % water and ~1500-5000 ppm Cl in the shallower one. These results overlap with the range of volatile contents in melt inclusions and measured gases found in previous studies. Moreover, we find that CO₂ concentrations are at least 3 times higher in the deep reservoir(s) than in the shallower ones. These results show that the main magma plumbing architecture (e.g. two main reservoirs) and the initial volatile abundances in the magmas of 2006 and 2010 were very similar. Thus, magma ascent rates, pre-eruptive accumulation and transfer of volatiles from depth, and/or rapid decompression after dome explosion are likely to be responsible for the contrasting eruption styles of the two events.

Long Li, Longqian Chen, Carmen Solana, Frank Canters, Matthieu Kervyn

Submission 280

Automated discrimination and mapping of lava flows through random forest classification of satellite imagery

Lava flow mapping is a key component of hazard assessment for volcanic regions and has benefited considerably from remote sensing. In recent years, satellite data from optical to thermal infrared and radar imagery, and techniques from manual mapping to elevation differencing and (un)supervised classification, have become increasingly available for discriminating and mapping lava flows at active volcanoes. Previous spectrum-based mapping studies often made use of traditional pixel-based classifiers, without much investigation into the added value of object-based approaches and into advantages of using machine learning algorithms.

In this study, Nyamuragira, characterized by a series of more than 20 overlapping lava flows erupted over the last century, was used as a case study. The random forest classifier was tested to map lava flows based on pixel and object scales. Image classification was conducted for the 20 individual flows using 30-m-resolution Landsat 8 imagery and ancillary data of the volcano.

Results show that object-based classification produces maps with continuous and homogeneous lava surfaces, in agreement with the physical characteristics of lava flows, while lava flows mapped through the pixel-based classification are heterogeneous and fragmented including much “salt and pepper noise”. In terms of accuracy, both pixel- and object-based classification performs well. It is concluded that despite spectral similarity, lava flows of contrasted age can be well discriminated and mapped through image classification. The classification approach demonstrated in this study only requires easily accessible image data and can be applied to other volcanoes as well if there is sufficient information to calibrate the mapping.

Keywords: Lava flows; Nyamuragira; Classification; Random forest

Long Li, Longqian Chen, Lien Bakelants, Carmen Solana, Frank Canters, Matthieu Kervyn

Submission 282

Using vegetation recovery as a lava flow age indicator

Vegetation as well as soil is destroyed during new lava flow emplacement. Vegetation starts regrowing on new lava surfaces after some time, suggesting that the stage of vegetation recovery can be linked to lava flow age, which is an important piece of information for assessing lava flow hazards from active volcanoes.

In this study, a statistical dating approach based on remote sensing characterization of vegetation on lava flows is constrained for three different volcanoes, i.e. Nyamuragira (the Democratic Republic of the Congo), Mt Cameroon (Cameroon) and Karthala (the Comoros). Using the normalized difference vegetation index (NDVI) to represent vegetation recovery on lava flows, factors controlling the NDVI spatial variation on lava flows are first analyzed for contrasted volcanic contexts. These topographic factors, i.e. elevation, slope gradient and orientation, together with NDVI are then used to constrain pixel-based regression models of lava flow age for the three volcanoes, using dated lava flows for calibration.

The models are shown to be volcano-specific as climatic and topographic conditions vary between volcanoes. Validation suggests that the obtained statistical models are reliable and can thus be applied for estimating the age of undated lava flow surfaces for these volcanoes, except for where vegetation is impacted by human activity. However, the results should be interpreted with caution when the models are applied to old lava flows because NDVI saturates for fully recovered vegetation and stop increasing with aging of lava flows.

Keywords: Lava flow age; NDVI; Nyamuragira; Mt Cameroon; Karthala

Chao Liang, Eric Dunham, Leif Karlstrom

Submission 467

Resonant waves in a coupled conduit-crack system: Application to very long period (VLP) seismicity at Kilauea volcano

Oscillation of magma in volcanic conduits connected to cracks (dikes and sills) has been suggested as an explanation for very long period (VLP) seismic signals recorded at active basaltic volcanoes such as Kilauea, Hawaii. Chouet and Dawson (2013) proposed a lumped parameter model, which captures several relevant processes and provides a reasonable match to the data. However, more sophisticated modeling that accounts for magma column stratification and dynamics in the crack is necessary to validate the many assumptions of the lumped parameter model and to gain deeper insights into the geometry, magma properties, and energy balance of the coupled system. The lumped parameter model is also specific to a single eigenmode, whereas a more general model predicts many modes (as required by the data). In this work, we investigate the VLP seismicity using a linearized model for waves in and associated eigenmodes of a conduit-crack system filled with multiphase magma. We extend the Karlstrom and Dunham (2016) quasi-one-dimensional conduit model with inviscid magma to a more general axisymmetric conduit model that accounts for viscous boundary layers near the conduit walls (Prochnow et al., 2017). At the bottom, the conduit is hydraulically connected to a magma-filled crack. The crack model accounts for inertia and viscosity of magma and elastic deformation of the crack walls. We have implemented a 2D plane strain crack model and are extending it to 3D. Acoustic-gravity waves in the magma column interact with crack waves, resulting in various resonant modes of a coupled system. An examination of the energetics of these modes reveals the complex interplay of different restoring forces (magma compressibility in the conduit, gravity, and elasticity of the crack) driving the VLP oscillations. Both viscosity and nonequilibrium bubble growth and resorption contribute to the damping of VLP signals. Displacements of the conduit and crack walls are convolved with elastic Green's functions to generate synthetic seismograms. Our model predicts different seismic signatures for excitation of the coupled system from the top (e.g., rock fall into the lava lake) and at depth (e.g., abrupt crack opening/extension, small earthquakes in the wall rock), which might be used to discriminate different source mechanisms for VLP events. Inversions based on this model will provide a means to infer physical properties of open-vent basaltic volcanoes from seismic observations of VLP events.

Yang Liao, David Bercovici, Mark Jellinek

Submission 894

Magma wagging & whirling in volcanic conduits, and their seismic signatures

Seismic tremor characterized by 0.5-7 Hz ground oscillations commonly occur before and during eruptions at silicic volcanoes with widely ranging vent geometries and edifice structures. The ubiquitous characteristics of this tremor imply that its causes are potentially common to silicic volcanoes. Here we revisit and extend to three dimensions the magma-wagging model for tremor [Jellinek and Bercovici, 2011, Bercovici et al., 2013], wherein a stiff magma column rising in a vertical conduit oscillates against a surrounding foamy annulus of bubbly magma, giving rise to tremor. While prior studies were restricted to two-dimensional lateral oscillations, here we explore three-dimensional motion and additional modes of oscillations. In the absence of viscous damping, the magma column undergoes 'whirling' motion: the center of each horizontal section of the column traces an elliptical trajectory. In the presence of viscous effect we identify new 'coiling' and 'uncoiling' column bending shapes with relatively higher and comparable rates of dissipation to the original two-dimensional magma wagging model. We also calculate the seismic P-wave response of the crustal material around the volcanic conduit to the new whirling motions and propose seismic diagnostics for different wagging patterns using the time-lag between seismic stations. We test our model by analyzing pre-eruptive seismic data

from the 2009 eruption of Redoubt Volcano. In addition to suggesting that the occurrence of elliptical whirling motion more than one week before the eruption, our analysis of seismic time-lags also implies that the 2009 eruption was accompanied by qualitative changes in the magma wagging behavior including fluctuations in eccentricity and a reversal in the direction of elliptical whirling motion when the eruption was immediately impending.

Chungwan Lim, Insung Lee

Submission 33

Eruption histories and genesis of Baekdusan volcanoes

The intraplate Baegdusan (Changbai) volcanoes located on the border of China and North Korea have been explained by either hotspots by mantle plumes or asthenospheric mantle upwelling (wet plume) caused by stagnation slab of the subducted Pacific plate. To understand the origin of the Baegdusan volcanism, we performed geochemical analyses on the volcanic rocks and tephra deposits erupted from the Baegdusan volcanoes. We propose that the intraplate alkaline volcanism associated with Baekdusan volcanic region is fed by a mantle upwelling originating below the discontinuity subducting slab. The upwelling is a result of a slab neck into the subducting slabs. The Baekdusan volcano relies on a slab neck within subducting slab at depth to allow for a focused upwelling. Therefore, the magmatic progression of back-arc magmatism in Baekdusan volcanoes can be explained by the interaction of this Philippine Sea Plate Slab and upwelling mantle.

Jan Lindsay, Eliza Calder, Mary Anne Thompson, John Ewert, Graham Leonard

Submission 135

State of the Volcanic Hazard Map: Development and preliminary results of a world-wide survey of official volcanic hazard maps. A presentation on behalf of the IAVCEI Hazard Mapping Working Group.

Volcanic hazard maps are visual, spatial depictions of the areas that could be potentially impacted by volcanic phenomena, and include information about expected magnitudes and/or likelihoods of events occurring. Developed, communicated and used appropriately for a given volcanic setting and cultural and political context, hazard maps can represent a common reference point that can play a major role in mitigating risk to vulnerable communities and thus disaster risk reduction by putting all parties quite literally “on the same page” of hazard information.

Although most volcanic hazard maps show similar types of content, such as hazard footprints or zones, they vary greatly in input data, communication style, appearance, and visual design. The diversity of hazard maps around the world stems from a whole range of factors, including differences in map purpose, the specific methodology used, the level of understanding of past eruptive history of the volcano, the prevailing scientific and cartographic practice at the time, the status of volcanic activity, and any local agency standards or policy requirements in place.

The Hazard Mapping Working Group of the IAVCEI Commission of Volcanic Hazard and Risk is facilitating a number of activities to enable sharing of volcanic hazard map experiences, including experiences of how volcanic hazard maps are developed and used around the world. The overall aim of the working group is to develop open-access source book: *Considerations for the Development of Volcanic Hazard Maps* that summarises these various approaches, methods and lessons learned for use throughout the map creation process.

One key activity is a currently active survey that aims to collect data about official, published volcanic hazard maps and how they were developed, to capture a snapshot of existing maps. The web and paper-based survey, available in English and Spanish, asks questions about map content, design and input data, as well as about the map development process. The responses will be used to quantitatively describe and summarise current practices in volcanic hazard map development. Here, we present the philosophy behind the survey, preliminary results, and explain how the knowledge gained from this global map review will provide valuable input into the *Considerations for the Development of Volcanic Hazard Maps*.

Peter Lipman, Matthew Zimmerer

Submission 76

Magmato-Tectonic Links: Ignimbrite Calderas, Regional Dike Swarms, and the Transition from Arc to Rift in the Southern Rocky Mountains

Compositionally diverse dikes and other intrusions, radiating westward from the polycyclic Platoro caldera (source of five large ignimbrites: 30.0-28.6 Ma) in the Southern Rocky Mountain volcanic field, merge in structural trend, composition, and age with the spectacular but little-studied Dulce swarm of trachybasalt dikes that trend SW and S for ~125 km along the east margin of the Colorado Plateau (San Juan Basin) from southern CO into northern NM. More than 100 dikes of the Platoro-Dulce swarm are depicted on regional maps. Some dikes, though only 1-2 m thick, are continuously exposed for 20 km or more; numerous smaller dikes are unmapped. Subhorizontal grooves on walls of some Dulce dikes suggest rapid lateral injection for distances of >10 km, perhaps farther, possibly originating from the Platoro locus. Five new $^{40}\text{Ar}/^{39}\text{Ar}$ mica and groundmass ages for Dulce dikes cluster tightly (25.34-25.97 Ma), are more precise than published K-Ar dates (23-27 Ma), and within the range of sanidine $^{40}\text{Ar}/^{39}\text{Ar}$ ages from radial dacite dikes (20.31-26.52 Ma) more proximal to Platoro. Bulk compositions of Dulce dikes become progressively more mafic and alkalic with increasing distance from Platoro.

We suggest the radial Platoro intrusions and Dulce dikes record interrelated effects of uplift associated with prolonged assembly and solidification of an arc-related granitoid batholith beneath Platoro caldera concurrently with the transition to weak extension along the east margin of the Colorado Plateau, satellitic to initiation of the Rio Grande rift and associated basaltic volcanism farther east. The potential genetic link between the Dulce swarm and Platoro radial dikes provides opportunities to examine the role of transitional tectonics (convergent arc to continental rift) on mechanisms of magma emplacement and strain partitioning during waning of a large caldera complex. The implied link between tectonic and magmatic regimes, and associated impacts of abrupt shifts in either over geologically short times, has implications for continental structural evolution and geologic hazards. Rapid emplacement of such an enormous dike swarm, in conjunction with late evolution of a caldera-related batholith, could have generated extension-related earthquakes and triggered dispersed volcanism. Documentation of such events would define a previously unrecognized magmato-tectonic hazard that could occur near active calderas in the western USA such as Valles, Long Valley, or Yellowstone.

Michael Lisowski, Rob McCaffrey

Submission 542

Time-dependent modeling of contemporary tectonic and volcanic deformation in the Cascade volcanic arc, USA

Ongoing ground deformation has been detected at 5 of 10 monitored volcanoes in the Cascade arc. The volcanic deformation is overprinted by regional tectonic block rotation, strain accumulation from the Cascadia subduction zone, and strain release from earthquakes and slow-slip events. We use the TDEFNODE software (McCaffrey, GRL, 2009) to distinguish tectonic and volcanic deformation. Cascadia margin-wide survey-mode GPS (sGPS) and continuous GPS (cGPS) time series are inverted to derive steady background tectonic deformation and transient deformation sources for ~100 tectonic and volcanic events. At Mount Baker in northwestern Washington, slow inward and downward station velocities (few mm/yr) are best fit with a shallow (3 km deep) slowly deflating (-0.1×10^6 m³/yr) Mogi source. At Mount St. Helens in southwestern Washington, slowing inward and downward station movements (a few cm) that accompanied the 2004–08 dome-building eruption reversed after the eruption ended. This cyclic deformation is fit with a deflating, ~8-km-deep prolate spheroidal magma reservoir that fed the eruption and has since partially recharged. At Three Sisters volcanic center in central Oregon, we invert 47 interferograms, leveling surveys, line length changes, and cGPS and sGPS time series. Outward and upward bulging of the ground centered ~5 km west of South Sister is fit by decaying inflation of ~6-km-deep spherical or slightly prolate spheroidal reservoir that was activated sometime in 1998. At Medicine Lake Volcano in northern California, inward and downward station movements (~1 cm/yr) are best fit by an ~8-km-deep deflating (-1.4×10^6 m³/yr) Mogi source or slightly deeper sill source. At Lassen volcanic center in northern California, inward and downward station movements (~1 cm/yr) are best fit by a ~10-km-deep deflating (-2.5×10^6 m³/yr) sill source. Our TDEFNODE analysis provides background rates of tectonic deformation and inverted source parameters for transient volcanic and tectonic deformation events throughout the U.S. Pacific Northwest.

Catherine Lit, Lucia Gurioli, Benjamin van Wyk de Vries, Pierre Boivin, Didier Miallier

Submission 327

How the Chopine eruption developed- a monogenetic trachytic eruption

The Puy Chopine volcano erupted about 8,000 years ago in the Chaîne des Puys, Auvergne, France. Trachyte was intruded into a pre-existing Scoria cone (Puy de Gouttes), which deformed and then collapsed. A dome might have already been at the surface before collapse. The collapse was followed by a directed blast and then vertical eruption, which formed a crater and breccia cone, still visible over 120 degrees. This crater contains the Chopine spine that is the final extrusion of the eruption. Extensive dense pyroclastic flows and surges formed the lobes and dunes of which can still be seen in the landscape. We have analysed the textural and lithological characteristics of the eruption deposits. There are six main layers, a basal coarse breccia, corresponding to the first collapse-related explosive fragmentation of the dome/cryptodome, then a less dense set of eruption, corresponding to the decompression on the magmatic column, and finally increased lithic layers relating to conduit erosion and collapse. The massive spine formed the last part of the eruption and uplifted large blocks of granite, schist and basalt from the country rock. The Chopine eruption occurred after 20,000 years of repose in this part for the Chaîne des Puys, and forms one possible scenario for a resumption of activity in the field.

Emma Liu, Thomas Richardson, Kieran Wood, Colin Greatwood, Ben Schellenberg, Helen Thomas, Matthew Watson, Alessandro Aiuppa, Gaetano Giudice, Marie Edmonds, Gustavo Chigna

Submission 302

In-plume measurements of volcanic emissions from Volcán de Fuego, Guatemala, using Unmanned Aerial Systems

Volcanoes are prodigious sources of volatiles and trace metals to the atmosphere, and therefore have an important role in the geochemical cycling of these elements through the Earth system. Measurements of gas flux and composition are also critical to volcano monitoring. However, CO₂ and volcanic gas metal fluxes, both of which require proximal sampling of a concentrated plume, are lacking for many volcanoes, particularly those where the near-vent region is hazardous or inaccessible. Unmanned Aerial Systems (UAS) offer a valuable solution to the challenges of in-situ sampling and routine monitoring of volcanic emissions.

We have developed an instrumented UAS based on customisation of a Thermik XXXL motor glider to enable simultaneous sampling of ash, gas and aerosol directly from the near-vent region of volcanic plumes. The instrument payload comprises a multiGAS (CO₂, SO₂, H₂S), four-stage filter pack (metal aerosol and acid gases), carbon stubs for ash sampling, thermal and visual cameras, and atmospheric sensors (temperature and humidity). Data is telemetered to a ground-station in real-time.

During initial field testing of the UAS and additional smaller vehicles in Guatemala (February 2017), we carried out beyond-visual-line-of-sight (BVLOS) flights to the summit of Volcán de Fuego, demonstrating the capability to fly at altitudes of 10,000 ft above ground level, and a range of 8 km from the ground-station. Full permissions for aerial work were given by the civil aviation authority of Guatemala (DGAC) for this and future field campaigns, with a request to communicate any data relevant to commercial flight operations. Clear visual and thermal images of the summit were acquired, and used to generate digital elevation models (DEMs) of the crater topography. These data confirm the existence of two active summit vents, from which explosive activity occurs simultaneously. Successive imaging surveys on 19 and 23 February captured a period of rapid cone growth in the week prior to the eruption paroxysm commencing 24 February, and calculated extrusion rates will be compared with near-continuous ground-based thermal imaging data collected over the same time period. Initial data from atmospheric sensors show a distinct change in temperature and humidity within the plume, such that we should be able to automate a system for in-flight plume detection. A future field campaign to measure erupted gas and metal emissions from Volcán de Fuego is planned for November 2017.

Ed Llewelin, Jen Truby, Tim Orr, Hugh Tuffen, Bruce Houghton

Submission 632

Does bubble suspension rheology control runout-length of lava flows?

The speed, run-out length, and morphology of a lava flow is primarily controlled by its viscosity. Lava viscosity is, in turn, a function of the composition of the melt, dissolved volatile content, temperature, volume fraction of suspended crystals, bubble volume fraction, and strain rate. Changes in these factors are known to occur as lava flows away from a vent, although there is no general model for determining their relative importance. We present a framework for calculating the viscosity of a lava, accounting for variations in vesicularity, crystallinity, composition, temperature, and strain rate. The approach is based on constitutive models, taken from the literature, for the impact of the component parameters on viscosity.

We apply our approach to the 27th June 2014 lava flow from Kīlauea, Hawai`i. The flow repeatedly threatened the town of Pahoa – approximately 20 kilometres from the eruptive vent – from late 2014 to early 2015. On several occasions, the flow appeared poised to reach the town or its infrastructure, but stopped short, begging the question: what were the physical controls on its run-out length? To address this question, we sampled active parts of the flow at three locations down the flow field, from breakouts that were very close to the lava tube that fed the flow. For each set of samples, we measured crystallinity, vesicularity, and dissolved water content, and used the results to quantify the viscosity of the melt and the rheological impact of the suspended phases for each site. We find that loss of bubbles (outgassing) has a much greater influence on viscosity than degassing of the melt or changes in crystallinity. This contrasts with previous studies, which typically assume that crystallinity is the more important factor.

Our calculations show that the down-flow decrease in bubble content (from ~70% to ~20%) leads to a marked reduction in its shear thinning behaviour. At the most proximal site, around 1km from the vent, the viscosity of the lava varies by a factor of ~30 depending on strain rate; by contrast, at the most distal site, around 20km from the vent, the variation is only a factor of 2. We propose that the strongly shear-thinning behaviour in the proximal lava favoured flow localization, and the formation of a robust lava tube. In the distal flow field, localization was less favoured, and we propose that this led to the formation of a less robust lava tube that was more prone to breakdown, limiting the run out length.

Ryan Lloyd, Juliet Biggs, Yelebe Birhanu

Submission 496

Sustained Uplift at a Continental Rift Caldera

In continental rifts, the accumulation of magma in the shallow crust is important in accommodating extension. The transport of basalt via dyking will have a distinctively different influence on the rifting process than storage of silicic magma at calderas.

The Corbetti caldera, in the Main Ethiopian Rift, is a large (~11 by 13 km) axial silicic center. Since Mid-2009 Corbetti has been uplifting rapidly. We use data from GPS and the ALOS-1, ENVISAT, Cosmo-SkyMed and Sentinel-1 satellites, to produce a time-series of deformation; totalling >40 cm of uplift. The duration and rate of this deformation has not been observed before at a continental rift caldera.

This prolonged deformation provides a unique opportunity to model the evolution of a continental rift magma reservoir over decadal timescales. We model the deformation using a Bayesian inverse modeling approach, incorporating a Markov Chain Monte Carlo algorithm, to estimate posterior probability distribution functions for the best fitting parameters of analytical source solutions.

We test inflating point (Mogi) and opening sill (Okada rectangular dislocation) sources for the deformation during its onset, after 5 years, and the present deformation. Specifically, we investigate the temporal evolution of both location and rate, and what factors may have influenced the formation and development of the source (e.g. stresses and pre-existing structures).

Interpreting the cause of this deformation is integral to understanding the dynamics of this magmatic system, and the implications of the observed deformation for potential post-caldera volcanism.

Andrew Lockhart, Tom Sharp, Chris Lockett, Rebecca Kramer, Ben Pauk, Kate Allstadt, Seth Moran, Amberlee Darold

Submission 529

The automated Puyallup and Carbon River (Mount Rainier) lahar detection system: current upgrades and possible future directions of an 18 year-old system.

An automated lahar detection and alerting system for the Puyallup and Carbon Rivers on the west flank of Mount Rainier USA was developed by the USGS and installed in a joint Pierce County (Washington) – USGS effort in 1998-99. The system is designed to provide advance warning of a dangerous lahar to Pierce County residents of the Puyallup River valley. After installation, the system was turned over to Pierce County Department of Emergency Management, which operates it in cooperation with the Washington State Department of Emergency Management.

The design goal is to detect a lahar larger than 40 million cubic meters ~ 40-45 minutes before it arrives in Orting (pop ~7,000) 50km from the west flank of Rainier. Although volcanic unrest should lead to an evacuation of Orting well before a large lahar, the system was designed to detect lahars absent recognized volcanic unrest such as the 250 million cubic meter Electron mudflow some 500 years ago.

The 1998-vintage system uses the USGS Acoustic Flow Monitor (AFM) for lahar detection and tripwires for lahar volume estimation. Data are telemetered to base station computers located at 24/7 Washington State and Pierce County facilities which would initiate a call-down and public warnings when a large lahar is detected.

The current system is now obsolete.

The USGS is upgrading the system in collaboration with Pierce County, in phases to avoid disruptions in detection capability:

1. Repace existing detection software
 2. Replace existing AFM stations with broadband seismometers and tripwires, replicating the functionality of the existing system
 3. Explore new algorithms and methods for lahar detection and volume estimation that would leverage new station locations including:
 - a. investigate and test new instrumentation ideas; cameras, etc
 - b. Develop and test new algorithms and techniques for seismic detection and characterization of moving sources, including modeling, small scale controlled experiments, and analysis of seismic data from natural events from other locations.
- The existing, still-functioning system will be left in place until such time as the new system can reliably replace it.

The upgrades may offer additional warning time for an unheralded lahar to the downstream population at Orting. Phase 2 may offer 4 minutes of additional warning time due to the much higher sample rate of broadband seismometers compared to AFMs. Phase 3 developments as yet unrealized may result in additional warning time.

John M. Londono, Hiroyuki Kumagai

Submission 182

4D seismic tomography for Nevado del Ruiz Volcano, Colombia. 2000-2016

A 4D seismic tomography for P, S waves, and Vp/Vs ratio was performed for Nevado del Ruiz Volcano (NRV), Colombia, for the period 2000 to 2016.

P and S arrival times data were divided into five data set: 2000-2006, 2007-2009, 2010-2012, 2013-2014, and 2015-2016. Similar number of earthquakes as well as similar spatial distribution for each period were selected in order to avoid misinterpretation due to data inhomogeneity.

Results showed that there is a temporal change in the magmatic system of NRV. The most clear changes were found for the periods 2013-2014 and 2015-2016, in agreement with the increasing of volcanic activity, after the unrest in 2010. Low Vp, low Vs, and high Vp/Vs (>1.9) regions were found beneath the active crater and to the NW of this crater, at 5-6 km depth, which were smaller in size for the other periods, suggesting a new input of magma to the volcanic system. Calculation of the ratio of fractional change (Rsp) of Vp and Vs caused by the liquid phase (Takei 2002, JGR, VOL. 107, NO. B2, 2043, 10.1029/2001JB000522) for the zones with high resolution of Vp and Vs anomalies suggested that partial melting zones are located beneath the active crater (5 km depth) and at 5 km away to the W (5-7 km depth). This zone has increased in size with time. Low Vp/Vs zones (1.3-1.6) were found to the upper part of the volcano (1-2 km), probably associated accumulation of vapor within the hydrothermal system and highly fractured zones. Low Vp/Vs zones were found surrounding the High Vp/Vs zone beneath the active crater, suggesting an old degassing and cooling magma body.

These results show that NRV have experienced important changes in the magmatic system in the last 16 years, associated with new input of magma, which still has not erupted, but it seems is moving up and interacting with the previous emplaced magma bodies. The current emplacement of a small dome at the bottom of the active crater seems to be related with a shallow old and small magma patch that has been moved up by the new magma.

The presence of new magma at similar depths and larger amount of those of the 1985 eruption implies that NRV could produce eruptions in the near future of larger, or at least, the same size of those of the November 1985 and September 1989 eruptions. Based on this, careful monitoring of the current activity of this volcano is critically important.

Marc-Antoine Longpre, Kelly Yong

Submission 881

Zoning patterns in olivine macrocrysts from Lanzarote, Canary Islands: Insights into magma ascent rate from the mantle during large basaltic fissure eruptions?

The nature and spatio-temporal evolution of magma plumbing systems feeding large basaltic fissure eruptions are poorly constrained. Here we present a detailed study of olivine macrocrysts from the 1730–1736 Timanfaya eruption (Lanzarote, Canary Islands) that aims to reconstruct the magmatic system of this eruption in space and time. The Timanfaya eruption involved 5 main eruptive phases and produced 3–6 km³ of unusually mafic (up to 14 wt% MgO) lavas and tephra that commonly host abundant peridotite xenoliths [1]. Backscattered electron images and high-precision EPMA data on >90 olivine crystals from basaltic lapilli from the earliest, main, and latest eruptive episodes reveal the occurrence of 3 macrocryst types in all samples. Type 1 macrocrysts typically show polyhedral morphologies — but sometimes also skeletal to dendritic shapes — and show gradual to steep normal zonation profiles (Fo_{86–81}). Type 2 macrocrysts are characterized by high-Fo anhedral cores and dendritic overgrowth rims and display pronounced gradual to steep normal zoning (Fo_{91–81}). Both Types 1 and 2 commonly feature a short plateau or reversal in Fo content within their rims. Rare reversely zoned macrocrysts (Fo_{77–84}) fall into a third category. In core–rim transects, Ni concentration generally co-varies with Fo content, whereas Ca and, particularly, P contents are moderately to strongly decoupled from Fe–Mg zoning. While we interpret Type 1 macrocrysts to have grown from the carrier melt and its parental liquids, Type 2 macrocrysts appear to represent grains of mantle origin that have acted as nuclei for rapid olivine growth from the carrier liquid, in agreement with [2]. This is strongly supported by the high Fo, low Ca, and high Ni contents of Type 2 cores matching that of olivine grains (Fo₉₁, 540 ppm Ca, 2980 ppm Ni) extracted from peridotite xenoliths within Timanfaya lavas. Type 2 macrocrysts thus provide the opportunity to derive timescales of xenolith transport from about 20–26 km depth [3] in the mantle — and therefore magma ascent rate estimates — via kinetic modeling of elemental diffusion within the core–rim compositional gradients. Our results have important implications for understanding the crystal cargo of mantle xenolith-bearing lavas and outline a novel approach to interrogate magma transport rates at basaltic volcanoes.

[1] Carracedo et al. (1990), *Est. Geol.*

[2] Gómez-Ulla et al. (2016), *Chem. Geol.*

[3] Neumann et al. (1995), *Lithos*

Rosaly Lopes, Jani Radebaugh, Robert Howell, Elizabeth Turtle, Ralph Lorenz, Julie Rathbun, Tracy Gregg

Submission 91

Extraterrestrial Lava Lakes

Lava lakes are rare on Earth but common on Jupiter's moon Io and likely occurred on other bodies such as Venus and Mars. Data from the Galileo spacecraft revealed that many Ionian paterae (calderas) are active, and several showed greater thermal emission around their edges (Lopes et al., 2004), which can be explained by the crust of a lava lake breaking up against the patera walls. Observations from both Galileo and ground-based telescopes reveal that several paterae, including Pele and Janus, have persistently high thermal output with regions of exposed, high-temperature lavas, indicative of large, vigorously active lava lakes similar to the Marum/Mbwelesu lava lake on Ambrym, Vanuatu. The volcano on Io that is the largest and has the greatest thermal output, Loki, has semi-periodic cycles of intense activity, interpreted as the foundering crust of a lava lake (Rathbun et al., *Geophys. Res. Lett.* 29; de Kleer et al., *DPS*, 2016), similar to the crusted, active lava lakes in Erta Ale, Ethiopia and Halemaumau, Hawaii. Alternatively, Loki Patera could be underlain by a thin, persistent magma "lens" that feeds thin, temporary lava lakes within the patera (Gregg and Lopes, 2008, *Icarus* 194). One significant and yet unexplained difference between Ionian and terrestrial paterae is the existence of cold "islands" in Ionian paterae that persist for decades (e.g., observed by both Voyager and Galileo) despite intense and likely continuous activity.

Field studies on Earth can help investigations into the nature and dynamics of Io's lava lakes. Remote, handheld observations of the Marum/Mbwelesu lava lake in May 2012 (Radebaugh et al., 2016) and Erta Ale in 2011 (Carling et al., 2015, *GeoResJ* 5) revealed exposed, high-temperature lavas at cracks and fountains. These observations help us identify similarities (or differences) between the morphology, temperatures, and eruptive behavior of lava lakes on Earth and those on Io.

Taryn Lopez, Lleven Clarisse, Simon Wallace, Fred Prata, David Fee, Hans Schwaiger, Alexa Van Eaton, Peter Cervelli, Cheryl Searcy, Matthew Haney, John Lyons, Aaron Wech, Kristi Wallace, Christopher Waythomas

Submission 1115

Insight into eruption processes at Bogoslof volcano, Alaska through evaluation of SO₂ masses and comparison with complementary datasets

Bogoslof volcano, Alaska, is a remote back-arc volcano that had 37 discrete eruptions between 12 December 2016 and 13 March 2017. Although no ground-based monitoring instruments are present on Bogoslof, these eruptions have been monitored through a combination of remote sensing and remote geophysical observations. SO₂ emissions from Bogoslof have been detected for about half of these eruptions by the infrared satellite sensors IASI and AIRS. Calculated SO₂ masses for individual events range from 0.23 to 16 kt, with no clear correlation in presumed eruption size/explosivity and SO₂ mass. While some variation in satellite detected SO₂ may be attributed to measurement conditions, we expect these differences to be minor compared to variations in eruption source processes. High-resolution satellite imagery acquired at different stages of the eruption indicate that Bogoslof's vents have been located predominantly just below sea level; however, changes in both seismic and infrasound energy suggest that the amount of water involved has varied among and within individual eruptions. Considering these complementary observations, we speculate that the diversity in eruptive SO₂ masses from Bogoslof events may be largely due to: (1) different degrees of seawater scrubbing of water-soluble SO₂ gas released during the eruption as a function of vent water content, and/or (2) variations in magma flux, as SO₂ flux is often used as a proxy for magma flux. Here we evaluate SO₂ emissions from Bogoslof throughout the eruption and consider atmospheric conditions and satellite overpass times to constrain uncertainties due to measurement conditions. We then compare eruptive SO₂ masses to complementary observations including: infrasound, seismicity, lightning, and tide water depths to help distinguish between the two proposed mechanisms contributing to the diversity in SO₂ emissions. We expect that correlations between SO₂ mass and time-integrated geophysical parameters may support magma flux as the controlling factor in SO₂ emissions; while geophysical indications of changing proportions of external water involved in individual eruptions may help fine-tune our understanding of SO₂ scrubbing by seawater. Additionally, we explore the use of IR satellite data to help constrain plume water content for high altitude eruption clouds. Through integration of these complementary datasets we aim to provide new insight into eruption processes at Bogoslof volcano and related systems.

Cristian Mauricio López Vélez, Lina Marcela Castaño, Lina Constanza Garcia Cano, Beatriz Elena Galvis Arenas, Oscar Sanabria, Alvaro Pablo Acevedo, Milton Ivan Ordoñez Villota, Carlos Andres Laverde, Zoraida Chacon, Claudia Patricia Durán, Gloria Patricia

Submission 727

SEISMIC ACTIVITY OF THE NEVADO DEL RUIZ VOLCANO DURING THE DOME EXTRUSION PROCESS (2015 - 2017)

During 2010, the Nevado del Ruiz Volcano (NRV) presented a significant change in its activity, in which there was an increase in seismicity rates of mainly low frequency (LF) and hybrid type seismicity (HB). It also had changes in the rates of SO₂ degassing and some changes in volcanic deformation. Pre-eruptive activity was recorded during the first months of 2012, with new swarms of higher energy (LF, VT, and HB), accompanied by higher rates of deformation and degassing with values up to 33,000 tons/day. Subsequently, two minor eruptions (VEI 1-2) were recorded, accompanied by constant volcanic tremor and gas and ash discharge.

After this activity, which was dominated by fluid-driven seismicity, new processes began. In late 2012 to the present, March 2017, significant fracture seismicity (VTs) began occurring mainly in distal areas of the volcano with rates up to 4900 earthquakes per day and magnitudes up to 4.6 ML.

The volcanic activity continues to evolve. In the period 2015-2017 in the NRV the ascent, placement and growth of two small lava domes occurred. This was accompanied by episodes of "drumbeat" type seismicity of low energy and short duration. The first episode occurred on August 20, 2015 and since then this type of seismicity has been present in different periods of time until now (March 2017). This seismic activity has been located in the Arenas crater, at depths less than 1 km. The process of dome extrusion identified from drumbeat seismicity has been confirmed through information from catalogs of publicly available satellite images and data shared by research groups worldwide. The satellite images show the growth of two domes in the Arenas crater, extruded between September 2015 and March 2016 and from September 2016 to the present day. The first dome has an approximate volume of $\sim 1.8 \times 10^5$ m³ and the second dome located on the south side of the first has reached a volume of $\sim 1.0 \times 10^6$ m³.

Finally, the morphological changes observed in the bottom of the crater, as well as the variations in deformation and the degassing rates of the NRV, show the complexity and instability presented by the system and corroborate that it continues to evolve.

Ainhoa Lorenzo, Marie-Noëlle Guilbaud, Julie Roberge

Submission 436

Violent-Strombolian eruptions at monogenetic volcanoes and their hazards: The case of the 10 ka Pelado shield, Sierra Chichinautzin, Central México.

Pelado volcano is a type example of an andesitic Mexican shield capped by (a) scoria cone(s) such as the hundreds that occur along the Trans-Mexican Volcanic Belt. It formed ca. 10 ka ago in the central part of an elevated plateau, in what is today the southern part of Mexico City. It is roughly circular, and consists of a 10 km-wide lava field crowned by two scoria cones and surrounded by thick fallout deposits that had not been studied previously. New cartographic, stratigraphic, granulometric, and textural data indicate that Pelado volcano was the product of a single, continuous eruption marked by three stages: an early explosive stage with multiple vents along an E-W fissure, an intermediate stage with simultaneous effusive and explosive activity, and a late stage, which began with concurrent effusive and explosive activity and ended with purely effusive activity from two vents opened at the base of the main cone. Tephra changed from relatively coarse, highly vesicular and glassy in the early stage, to poorly vesicular and crystalline in subsequent stages, whereas lava changed from olivine-bearing, highly-vesicular and massive to orthopyroxene-bearing, moderately to poorly vesicular and internally foliated with a discontinuous blocky carapace. The volcano emitted >0.9 km³ Dense-Rock Equivalent (DRE) of tephra and up to 5.3 km³ DRE of lavas. Pelado shares various diagnostic features with documented “violent Strombolian” style eruptions, specifically that of Parícutin (1943-1952). The total volume of magma erupted (~ 6 km³ DRE) is 6 times higher than Parícutin and if we consider similar average eruption rates, Pelado activity lasted three times longer (3 decades). Based on these results, we define the hazards caused by this kind of event, likely corresponding to a worst-case scenario for future monogenetic activity in México.

Charline Lormand, Georg Zellmer, Naoya Sakamoto, Karoly Németh, Alan Palmer, Hisayoshi Yurimoto

Submission 612

Pre- and syn-eruptive processes visualized through semi-automatic Crystal Size Distribution analysis of microlites from Tongariro Volcanic Centre tephras, New Zealand

Microlite Crystal Size Distributions (CSDs) in volcanic rocks have become a useful tool to assess pre- and syn-eruptive processes such as nucleation and growth at the onset of explosive eruptions. CSDs may provide information about rates of magmatic processes such as magma mixing and ascent. The Tongariro Volcanic Centre (TgVC), which includes Ruapehu, Ngauruhoe and Tongariro volcanoes, has produced historical explosive eruptions of different styles. A semi-automatic method for selecting microlites based on back-scattered-electron (BSE) images using Weka Segmentation, a machine learning tool available in ImageJ software, was employed on four tephra formations of the TgVC: Tufa Trig and Papakai (source: Ruapehu); Mangatawai (source: Ngauruhoe); and Pahoka-Mangamate (source: Tongariro). Tufa Trig and Mangatawai tephras are composed of glassy shards with well-defined microlites, whereas Papakai and Mangamate contain more complex grains of diverse petrographies and of potentially different origins. CSDs of plagioclase and pyroxene from individual glass shards of the same tephra are computed, compared, and combined to obtain total tephra CSDs. The same procedure is repeated with the four studied tephra sequences so as to assess the effect of eruptive style and the associated conditions (magma chemistry, water content, explosivity, etc.) on microlite CSDs. Manual selection of crystals is time consuming, but provides more accurate CSDs compared to the semi-automatic selection, which does not separate crystals that are part of clusters (e.g. tabular plagioclases). Also, pyroxenes typically display the same BSE greyscales as the groundmass, which may lead to inaccuracies in the computed CSDs. However, due to the reasonably low difference in CSDs and the significantly faster computing aspect of this method, the semi-automatic selection used for this study is preferable. Then, CSDs can provide a powerful tool to establish mixing histories of various magmas involved in the eruptions of the studied tephras, recognition of entrained antecrysts, as well as the timescale of these pre-eruptive processes. These microchemical processes will be presented from the perspective of contrasting volcano evolution within the TgVC.

Susan Loughlin, Anna Hicks, Jenni Barclay, Roger Few, Emily Wilkinson, Richard Robertson, Patricia Mothes, Gloria Patricia Cortes

Submission 1095

Integrating diverse datasets and applying new knowledge: the use of scenario exercises in the STREVA project

Preparing populations for eruptions at volcanoes without recent activity requires methods to enhance hazard and impact awareness, counter possible erosion of longer-term social memory and increase engagement in preparedness and planning efforts. If properly executed, scenario exercises offer the opportunity to explore a range of eruption scenarios and their evolution over time, discuss possible impacts, recognise the knowledge of different participants and how knowledge is applied, identify critical knowledge gaps (both social and scientific), and use these to guide further analysis and data gathering as well as to improve preparedness of all those involved. Developing and 'playing out' scenarios also presents an opportunity to integrate diverse datasets across the physical and social sciences. For those living around frequently active centres where familiarity may develop, preparedness efforts should acknowledge the possibility of eruptive and impact scenarios that have not been experienced in the recent past.

The Strengthening Resilience in Volcanic Areas (STREVA) project team have conducted scenario exercises in three case study settings: St Vincent, Ecuador and Colombia. The scenarios were designed by scientists and civil protection, and the scientists responsible for official advice led the exercises. We demonstrate how scenario exercises can raise awareness, acknowledge uncertainty, identify thresholds for action, engender collective responsibility, and strengthen the resilience of populations to future eruptions. Our scenarios were explicitly designed to explore the spatial and temporal dynamism of eruptions and their impacts, and to consider facets of preparation and response that were important to emergency response and medium and long-term recovery. In all instances, the scenarios not only uncovered areas to improve institutional, community, household and individual preparedness but also highlighted possible constraints to the application of scientific knowledge. In many cases, participants of the scenario exercises adjusted their 'mental models' of the likely evolution and impacts of eruptions and thus felt better able to make risk mitigation decisions.

We argue that our iterative approach to building dynamic scenarios and investigating them during exercises has provided a conduit not only for improved preparedness of communities and institutions but for the technical and scientific innovation necessary to enhance resilience to eruptions.

Mikkel Louis, Conner Toth, Wendy Bohrsen, Nicole Moore, Sylvana Bendaña, Megan Graubard, Anita Grunder

Submission 556

Phase Equilibria Constraints on the Magma Storage System with the Steens Basalt

The Steens Basalt (SE Oregon, USA), is the oldest, most mafic part of the Columbia River Basalt Group. Tholeiitic to mildly alkaline Steens Basalts range from ~3.5-12 wt.% MgO and are characterized by a mineral assemblage of olivine (ol), clinopyroxene (cpx), plagioclase (pl), and Fe-Ti oxides. Some flows contain up to 40 modal % giant pl (>2 cm). Phase equilibria modeling of whole-rock (WR) and pl compositional data constrain key intensive parameters of this flood basalt, including pressure, initial H₂O, and oxygen fugacity (fO₂) of the magma body, and contribute to understanding the origin of large, abundant pl. Over 60 MELTS (Gualda et al. 2012) models were run using fractional crystallization with temperature decrements of 5°C. Two high MgO parents (10.9 & 12 wt.%) were run isobarically from 0.8-0.1 GPa, with fO₂ of QFM and QFM±1 and initial H₂O of 0.5-1.0 wt.%. Numerous polybaric models were also completed. Best-fit simulations were identified by comparing observed and modeled WR mineralogy and major element data. High pressure (0.8, 0.6 GPa) runs produced abundant orthopyroxene, which is not consistent with observed mineralogy. Lower pressure (0.4, 0.2 GPa) runs produced mineralogies consistent with the rock samples. Most major element trends are reproduced by shallow simulations using initial H₂O of 0.5-1.0 wt.%; this range is necessary to describe the variable WR Al₂O₃. Polybaric models (e.g., 0.1-0.4 GPa, QFM, initial H₂O 0.5-1.0 wt.%) reproduced mineral assemblages and are generally consistent with WR data. The main exception is K₂O; model results are lower than observed values mainly at lower MgO. MELTS results yield pl with anorthite (An) content from ~66-76%, broadly consistent with the range observed in the samples (60-70, Toth et al., this meeting), though modal abundances in the MELTS models are lower than observed. Many samples with >7 wt.% MgO contain abundant pl, but in MELTS, pl begins to crystallize at ~7 wt.% MgO. Collectively, these models provide evidence for a relatively shallow (0.1-0.4 GPa), dry (0.5-1.0 wt.% initial H₂O) magma system that dominantly crystallizes ol, pl, and cpx. Best-fit models do not reproduce K₂O well, suggesting influence of crustal assimilation. In addition, models do not predict pl in magmas with >~7 wt.% MgO and modeled abundances are too low. To address these deviations, we will model isentropic ascent and assimilation of plagioclase-rich mush.

Jacob Lowenstern, Vincent Van Hinsberg, Kim Berlo, Heather Wright, Kayla Iacovino, Moritz Liesegang, Ilya Bindeman

Submission 208

Opal in pumice from the 1817 phreatomagmatic event at Kawah Ijen, Java (Indonesia): its origins and implications

At Kawah Ijen, vigorous SO₂ degassing sustains a hyperacid lake (pH ~0) and intensely acid-alters the subsurface, producing widespread residual silica and advanced argillic alteration products (Van Hinsberg et al., 2010). In 1817, a VEI 2 phreatomagmatic eruption evacuated the lake, depositing a widespread layer of muddy ash fall, and sending lahars down river drainages. We discovered at least three types of opaline silica in juvenile low-silica dacite pumice and laharic sediments. 1) Sedimentary aggregates are dominated by opal and are found as clasts within pumice, and also as a component of the laharic sediments. 2) Laminated, colloidal silica also forms rare clasts included within fresh pumice clasts. 3) Opal-replaced phenocrysts (ORP: pseudomorphs of plagioclase and pyroxene) are common in juvenile pumice. Matrix glass and melt inclusions remain pristine. Opal-bearing pumice has been found at numerous sites, including where post-eruption infiltration of acid water is unlikely.

Based on the types 1 and 2 opal in the pumice and laharic sediments, we conclude that ascending magma incorporated acid-altered opaline materials in the subsurface. Some of the glassy laharic sediments are more andesitic than the main pumice type and may represent older volcanic materials present at the lake bottom that were forcefully ejected by the 1817 eruption. Type 3 opal (the ORPs) have uncertain and possibly multiple origins. Fresh pyroxene and feldspar phenocrysts are adjacent to ORPs, implying syn-eruptive mixing of altered crystals into ascending dacite magma. Experiments at 750 to 850°C demonstrate that the opal begins to break down in tens of minutes, inconsistent with most observed ORP textures. Therefore, any incorporation of opal must have been followed rapidly by eruptive quenching. Some ORPs have delicate textures difficult to reconcile with forceful incorporation in ascending melt. And post-eruption replacement is possible: experiments at 25° and 100°C reveal that when pumice is bathed in strong acid for six weeks, similar ORPs are formed without altering either matrix glass or melt inclusions. We suggest that some opal was incorporated by ascending magma, and may have induced eruption by rapid dehydration of hydrous opal and generation of additional steam/volatiles. Some opal-altered volcanic materials were blasted out of the lake. And some opal formed post-eruption by infiltration of acid into the pumiceous deposits.

Jordan Lubbers, Chad Deering, Olivier Bachmann, Marcel Guillong

Submission 370

Rhyolite and Trachyte Formation at Lake City Caldera: Evidence from Quantitative Textural and Geochemical Analyses

Lake City Caldera (22.93 ± 0.02 Ma) is the youngest of 15 Tertiary calderas found within the Southern Rocky Mountain Volcanic Field (SRMVF). Extreme topographical relief of the area reveals the three-dimensional exposure of a complex, high-k calc-alkaline, magmatic system, which provides us with the opportunity to study, in detail, how large silicic magmas evolve in the subsurface. The Lake City igneous system is comprised of two major units: a resurgent syenite intrusion and the Sunshine Peak Tuff (Lower, Middle, and Upper). Bulk-rock analyses indicate that the Lower and Middle Sunshine Peak tuff (LSPT and MSPT) are crystal poor and rhyolitic in composition, while the Upper Sunshine Peak Tuff (USPT) is crystal rich and trachytic in composition. Rhyolite-MELTS modeling and geochemical analyses show that Lake City rhyolites were formed by fractional crystallization of the syenite magma reservoir once it reached ~40% crystallinity. Zoning of these ignimbrites LSPT (76 wt % SiO₂) to MSPT (74 wt% SiO₂) shows that further crystal fractionation occurred following melt extraction from the syenite magma. This is interpreted as occurring within a melt-rich rhyolite cap within the syenite magma reservoir. Geochemical and textural analysis suggests that the USPT was formed by later re-melting of a portion of the syenite cumulate. Crystal Size Distributions (CSDs) generated for both the syenite and trachyte suggest signs of textural coarsening, although trachytes exhibit these signatures to a more advanced degree. Syenite CSDs show characteristics of crystal accumulation, and both units are comprised mainly of glomerocryst networks. Titanium in quartz geothermometry gives temperature estimates for quartz formation across all units and shows that the majority of grains were formed between 735°C and 785°C, further providing evidence for a petrogenic relationship for all the rocks comprising Lake City Caldera. The presence of mafic enclaves within both the syenite and USPT trachyte coupled with reverse zoning noted in trachyte potassium feldspar grains alludes to mafic injection into the magma reservoir being responsible for both the re-melting of the syenite cumulate and the eruption mechanism for all three units of the Sunshine Peak Tuff. These models, for both rhyolite and trachyte production, are consistent with other models put forth for rhyolite production in the shallow crust and the origin of zoned ignimbrites.

Gert Lube, Eric Breard, Luke Fullard, Jim Jones, Shane Cronin, Ermanno Brosch

Submission 1011

A recipe for unleashing the infernal forces of pyroclastic flows

Pyroclastic flows exhibit astonishing fluidity, which allows them to transport large volumes of volcanic material across the Earth's surface bypassing tortuous flow paths, rough substrates, flat and up-sloping terrain. The high mobility is reflected in ultra-low coefficients of apparent friction. This mobility contrasts with the much higher internal friction of the pyroclastic material transported and has provoked a range of 'friction-cheating' theories to explain observed behaviour. A test of these theories remains outstanding because direct observations and measurements of the processes operating inside real-world flows cannot be realized yet.

Here we report on large-scale pyroclastic flow experiments run at the eruption simulator PELE in New Zealand. Flows of 1.5 tonnes of variably hot ignimbrite material and air are initiated by column collapse onto an instrumented runout section. The section comprises an upper 12 m-long, 6 degrees inclined, rough channel followed by a 23 m-long, flat, unconfined and rough plane. We view inside the flows and measure vertical profiles of velocity, particle concentration, pore-pressure, temperature and friction coefficients. The resulting multiphase flows develop a non-turbulent dense underflow below a fully turbulent dilute ash-cloud surge.

Through systematic variation of the initial mass flux (Q), temperature (T) and fine-ash content (F), we reveal transient behaviour of the underflow between two end-member flow regimes. At high Q , low T and F , flows de-fluidize over low fractions of their duration. They have short runout lengths and obey high friction coefficients typical for dry granular flows. Deposits comprise a single flow unit with thicknesses strongly decreasing with distance. With decreasing Q , increasing T and F the behaviour changes fundamentally. The underflow attains fluid-like behaviour, incl. surface waves, multiple flow units, frontal lobes, levee-and-channel structures and degassing pipes. Deposition rates are astoundingly low and at times negative emplacing deposits with markedly constant thickness over runout lengths of >28 m. We show that fluid-like behaviour is self-generated via downward advection of excessive pore-pressure into the lower underflow. This leads to full bed support, and ultra-low local friction coefficients (0.01-0.09) and mixture viscosities (0.04-2 Pa*s). We propose and test a new mixture rheology that replicates depth-variant friction coefficients from flow initiation to deposition.

Federico Lucchi, Lorella Francalanci, Gianfilippo De Astis, Claudio Antonio Tranne, Eleonora Braschi, Martijn Klaver

Submission 745

Recurrent collapse-driven blast eruptions during the mafic Holocene activity of Stromboli volcano, Italy

Stromboli is a 924 m-high active stratovolcano in Southern Italy, which has erupted mafic shoshonitic and more potassic magmas during the last 13 ky. In the latter 1300 years it has been characterized by basaltic, intermittent and moderately explosive, strombolian activity with sporadic higher-energy paroxysms and lava flows flowing down the Sciara del Fuoco collapsed flank. The latter is a multi-stage NW-dipping collapse structure resulting from recurrent flank instability events during the Holocene, at times associated with the development of landslides and/or tsunamis events. Here we present the geological evidence for three different collapse-driven blast eruptions that produced coherent to unconsolidated, ash-supported, accretionary lapilli-rich lapilli-tuff deposits from pyroclastic density currents (PDCs) and minor fallout. It is suggested that collapses have unloaded the magmatic system causing explosive decompression driven by rapid volatile exsolution and enabled external water to have access to the main conduit system and explosively interact with the magma, typically producing laterally-directed blast hydromagmatic eruptions and PDCs. The three successions have distinctive componentry, volcanologic and stratigraphic characteristics, and display an asymmetric areal distribution in distinct sectors of the volcano. Moreover, the juveniles of the three successions have slightly different trace element, isotopic and mineralogical characteristics, although they are all high-K shoshonites. The three hydromagmatic eruptions are thus associated with successive major collapses of Stromboli occurred in different time-stratigraphic windows during the Holocene (at about 13, 6 and 4 ka ago). Intriguingly, the three eruptions are fed by magmas with compositions that are among the most evolved (MgO: 2.4-4.0 wt%) in the prevalent mafic magmas of the same eruptive period (MgO: 4.2-6.6 wt%), and are generally associated with eccentric activity. A model linking the concomitant occurrence of several factors (evolved mafic magma composition, lateral activity, sector collapse, hydromagmatic explosive eruption) is proposed as an interpretation of the collapse-blast eruption link.

Réka Lukács, Szabolcs Harangi, Marcel Guillong, Olivier Bachmann, László Fodor, Yannick Buret, István Dunkl, Jakub Sliwinski

Submission 989

Early to Mid-Miocene syn-extensional massive silicic volcanism in the Pannonian basin (East-Central Europe): Zircon perspective age and isotopic constrains

The convergence between the Eurasian and African plates formed a compressional regime in the Alpine-Mediterranean region during the Late Cretaceous to Cenozoic and resulted in the formation of several extensional basins in association with retreating subduction. The Pannonian basin belongs to this system and has been characterized by major lithospheric thinning, basin subsidence, elevated heat flow and magmatism since the Early Miocene. The continental rifting was associated with massive silicic volcanism occurring mostly at the inner part of the Pannonian Basin. During the Early to Mid-Miocene this could have been one of the most significant volcanic activities affecting the European continent. Here, we present the results of a zircon perspective study to constrain the eruption ages, the compositional fingerprints of the eruptive products and the origin of the magmas.

The majority of the pyroclastic products of this volcanism (mostly ignimbrites) are covered by younger sediments in the Pannonian Basin, due to subsidence. However, they are exposed in several localities, including the Bükkalja Volcanic Field (BVF, North Hungary). Drilling cores of many boreholes revealed that their cumulative thickness could exceed 1000 m in many parts of the Pannonian Basin. The dacitic to rhyolitic volcanic products contain quartz, plagioclase and biotite with sporadic occurrence of amphibole, pyroxenes and sanidine. Zircon U-Pb ages indicate that the volcanism took place from 18.3 Ma to 14.4 Ma and at least 8 eruptive units can be distinguished. Within this, 4 eruptions could result in large volume (>10 km³) volcanic deposits. Miocene bentonites and volcanoclastic sediments around and within the Carpathian-Pannonian Region are potential distal deposits of this volcanism. Each of the eruption products has a specific zircon trace element compositional fingerprint, which helps the regional correlation, involving the Mid-Miocene sedimentary sequences at the northern part of the Mediterranean. Ash beds in the Paratethys subbasins appear to correlate well in age with the main identified volcanic events in the BVF that supports the large-volume plinian eruption events. The Hf isotope content of zircons and the bulk pumice Sr-Nd isotope ratios show a sharp change after 16.6 Ma, suggesting an increase of mantle influence in the genesis of the magmas and that a thinned crust already existed by this time.

This work was supported by NKFIH projects PD112584 and PD121048.

Paul Lundgren, Sergey Samsonov, Pietro Milillo, Jacqueline Salzer, Julia Kubanek, Cristian Lopez, Milton Ordoñez

Submission 530

Deep source model and dome growth analysis for Nevado del Ruiz Volcano, Colombia

Nevado del Ruiz (NRV) is part of a large volcano complex in the northern Andes of Colombia with a large glacier that erupted in 1985, generating a lahar killing over 23,000 people in the city of Armero and 2,000 people in the town of Chinchina. NRV is the most active volcano in Colombia and since 2012 has generated small eruptions, with no casualties, and constant gas and ash emissions. Interferometric synthetic aperture radar (InSAR) observations from ascending and descending track RADARSAT-2 data show a large (>20 km) wide inflation pattern apparently starting in late 2011 to early 2012 and continuing through at least 2015 at a LOS rate of over 3-4 cm/yr. Volcano pressure volume models for both a point source (Mogi) and a spheroidal (Yang) source find solutions over 14 km beneath the surface, or 10 km below sea level, and centered 10 km to the SW of Nevado del Ruiz volcano. The spheroidal source has a roughly horizontal long axis oriented parallel to the Santa Isabel – Nevado del Ruiz volcanic line and perpendicular to the ambient compressive stress direction. Its solution provides a statistically significant improvement in fit compared to the point source, though consideration of spatially correlated noise sources may diminish this significance. Stress change computations do not favor one model over the other but show that propagating dikes would become trapped in sills, leading to a more complex pathway to the surface and possibly explaining the significant lateral distance between the modeled sources and Nevado del Ruiz volcano. Since September 2015 COSMO-SkyMed (CSK) and TerraSAR-X (TSX) data track the dome growth in the summit crater, which appears to have occurred in at least two episodes, the first one ended in early 2016 and the second one is ongoing since August 2016, though slowing down somewhat by March 2017. InSAR time series may indicate deflation coincident with dome extrusion episodes, though deflation deformation amplitudes are low. We compare the InSAR (including Sentinel-1A/B) time series and dome growth analysis (CSK, TSX, and possibly TDX) with contemporaneous in-situ volcanic activity observations to guide future volcano system analysis of Nevado del Ruiz.

Craig Lundstrom

Submission 254

A new view of magmatic water in silicic plutonic-volcanic systems

Lundstrom (2016) reported experiments demonstrating that a very hydrous peralkaline melt coexists with quartz and two feldspars at 330-400°C and 0.5-1 kbar, consistent with previous literature (Tuttle and Bowen, 1958, Friedman, 1951). The melt contains >40 wt% H₂O, with its anhydrous composition being ~35wt% total alkalis, 2 wt% Al₂O₃ and 63 wt% SiO₂. If such melt exists in upper crustal silicic magma bodies (both plutons and magma chambers), it would have profound impact on magmatic processes, including water storage and eruption triggers of mushes. Observations of low temperatures indicated by 2 feldspar equilibria (in granitoids) and Ti in quartz (in both granitoids and ignimbrites) may evidence low temperature melt. Thermochronology shows that plutons cool rapidly below 500°C but then take >5 Myrs to cool below Ar-Ar biotite closure (Davis et al., 2012) providing time for low temperature melt to impact geochemistry and texture.

The presence of this melt could strongly increase the rate of heat loss from magma bodies by its buoyancy driven advection upward through granitic mush. Several studies have found that granitoid plutons are built top down, such that arriving magmas underplate previously emplaced sills; this provides a thermal gradient which leads to production of low temperature melt. One such pluton, the Torres del Paine intrusive complex, contains a dramatic lithologic boundary between contemporaneous granite and underlying mafic complex. The perfectly horizontal contact crosses the Valles Frances and produces two nearly perfect 135° bends on opposite sides of the valley, where granite forms the boundary layer with surrounding sedimentary country rock. This contact is logically interpreted as an isotherm (not an intrusive contact). Thermal modeling shows that in order to make a horizontal isotherm of several km length, heat conductivity must be >5x greater in the vertical direction than the horizontal direction. A possible explanation is that buoyantly rising low temperature melt carries heat toward the surface, providing a more effective cooling process than conduction alone. The presence of ubiquitous low temperature melt in upper crustal magma bodies may also explain the dramatic differences in melt inferred from seismic and magnetotelluric images of magma bodies.

Davis J et al., *CMP*. 163:449, 2012; Friedman I, *J. Geol.* 59:19, 1951; Lundstrom CC, *IGR* 58:371, 2016; Tuttle O & Bowen N, *GSA Mem* 74:1, 1958.

Rebecca Lynch, Dante Canil

Submission 336

Condensation behaviour of volatile trace metals in laboratory benchtop fumarole experiments

Volcanoes are natural polluters of trace metals. Volatile trace metals from natural systems are often collected on silica tubes in active fumaroles or on filters in a plume, accumulating precipitates that condense from the gas phase. We design a laboratory 'benchtop' fumarole to experimentally measure volatilization and condensation behaviours of volatile trace metals to emulate similar conditions to natural volcanic systems. A synthetic silicate melt composition with dissolved trace metals (V, Cu, Zn, As, Y, Mo, Cd, Sn, Tb, Pb and Bi) is degassed in air in a box furnace at 900oC over a period of days to weeks. The precipitates from the gas phase are collected on a silica tube along a thermal gradient from 725 to 125oC. The precipitates are analysed by SEM and ICP-MS. We observe variable crystallinity of condensates with elevated amounts of Li, V, Cu, As, Rb, Mo, Ag, Cd, Cs, W, Pt, Tl, Pb and Bi with peak concentrations at temperatures between 250 to 450oC. Mo is present in the largest quantity of up to 322 ppb at 410oC in a one week experiment with a Na-Al-silicate melt composition. We compare our experimental condensates to natural condensates and see good correlation with the behaviour of V, Cu, As, Ag and Pb. Future work is exploring the control of other ligands, atmospheres or melt compositions in the experiment on transport mechanisms for metals into the volatile phase.

Kendra J. Lynn, Thomas Shea, Michael O. Garcia, Fidel Costa

Submission 675

A new application of lithium diffusion in olivine to investigate late-stage mixing events at Kilauea Volcano (Hawaii)

The processes that lead to magma eruption and ascent involve a large range of timescales, from hundreds of years to only a few seconds. The timescales relevant to late-stage magmatic processes involving magma ascent, degassing, and magma mixing in basaltic systems are particularly challenging to quantify. Lithium, a monovalent cation that diffuses about an order of magnitude faster than Fe-Mg in olivine (Dohmen et al. 2010), provides a promising new means to recognize mixing events that occurred a few hours to weeks before an eruption. Here we present timescales derived from Fe-Mg and high-precision laser ablation ICPMS measurements of Li zoning in precisely oriented and sectioned euhedral olivine crystals from Kilauea's explosive Keanakakoi Tephra period (1500-1823 C.E., Swanson et al. 2012). Our previous work has revealed that Fe-Mg zoning styles (normal, reverse, hook, shoulder) generally record crustal mixing and storage durations of a few weeks to months. A number of profiles show 5-20 μm wide rims with Fe-Mg compositional reversals that are difficult to fit with diffusion models due to their limited spatial resolution. These compositional reversals suggest that an additional mixing event occurred shortly before eruption. Lithium profiles (10-300 μm long) are normally or reversely zoned and are inversely correlated with Fe-Mg, suggesting that Li zoning formed from mixing of primitive recharge magmas and older evolved magmas stored in shallower reservoirs. Modeling of Li diffusion profiles yields storage timescales that are generally a few hours to days. These short durations are interpreted to reflect the remobilization of stored reservoir magma as a result of a late-stage intrusion of mantle-derived recharge magma. Thus, Li zoning and Fe-Mg compositional reversals in olivine probably record the last mixing event occurring in the magmatic plumbing system prior to eruption.

Dohmen et al. (2010); *Geochimica et Cosmochimica Acta*, 74, 274-292.

Swanson et al. (2012); *Journal of Volcanology and Geothermal Research*, 215-216, 8-25.

John Lyons, Matthew Haney, David Fee, Alex Iezzi, Hans Schwaiger

Submission 936

Infrasound from the shallow submarine eruption of Bogoslof volcano, Alaska

After 25 years of quiescence, Bogoslof volcano began a new phase of eruptive activity in December 2016. Bogoslof is a back-arc submarine stratovolcano in the Aleutian Arc with a summit platform shallowly (37 significant explosive events (as of 21 March) were sufficiently energetic to be observed on one or more of the Alaska Volcano Observatory's infrasound arrays that range from 60 to 800 km from Bogoslof. Explosions have varied between discrete and sustained, sometimes within the same eruptive event, and have produced eruption clouds that reached a few to 11 km above sea level. The events have been dominated by low frequency energy (0.067-1 Hz), with notable exceptions that shed light on how seawater interaction affects infrasound production in shallow submarine eruptions. An event on 31 January that lasted more than 5 hours began with discrete, low frequency infrasound that after two hours transitioned into continuous, higher-amplitude, broadband infrasound. A satellite image captured shortly after the end of the event showed that a tephra ring was formed during the eruption that temporarily isolated the below sea level vent from the ocean, and resulted in the change in observed signal character. This event, and a similar event on 8 March, produced the most significant ash clouds of the eruption to date, highlighting the utility of regional infrasound for detection and rapid characterization of hazardous eruptions.

Luisa Macedo Franco, Marco Rivera Porras, Jersey Mariño Salazar

Submission 1194

Reducing Volcanic Risk in Arequipa City

El Misti is one of the seven active volcanoes in southern Peru, located 17 km from the main square of Arequipa city, which has ~1 million inhabitants. This volcano has presented diverse types of activity: explosive eruptions (VEI 1-7), effusive eruptions, and growing and collapsing lava domes. There have been episodes of flank collapse that generated at least two debris avalanche deposits (Thouret et al., 2001), and which illustrate the continued threat of flank instability. 2000 years ago, Misti volcano produced a VEI 5-plinian eruption emplacing pumice-lapilli fall deposit, PDCs, and debris flow (lahar) deposits (Harpel et al., 2011), which can be viewed in outcrops within the urban area. Ash deposits were also emplaced as a consequence of vulcanian eruptions (VEI 1-2) during 1440-1470 A.P. (Macedo, 1994). At present, El Misti shows sporadic fumarole emissions, and it is monitored by the Volcano Observatory of INGEMMET (OVI). The vulnerability of the city is increasing daily due to the expansion of the urban area toward the volcano. People are building their houses in hazardous zones such as Alto Selva Alegre, Miraflores, Mariano Melgar and Paucarpata districts. In these suburbs, houses are built on steep lands and close to streams. In 2007, INGEMMET developed the Misti volcano hazard map which shows three hazard zones related to volcanic activity described as high (red), moderate (orange) and low (yellow). Then, in 2016 the hazard map was printed in a simple and comprehensible A-3 version that now is widely distributed among the population. The OVI continues to provide presentations and hold conversations with people living in risk, scholars, and university students. These activities are intended to teach about volcanic hazards and how to act in case of eruptions. A part of this work includes communication and preparedness of authorities. This encourages development of municipal ordinances that regulate urban expansion in risk zones. Part of this effort is focused on working with the news media and journalists so that they can improve the communication of information responsibly. Finally, technical inspections have been carried out with the Crime Prevention Office in areas of volcanic risk, to urge the population not to invade these areas, and to maintain their personal integrity and that of their property. This work has been carried out for several years and shows good results.

Elodie Macorps, Sylvain J. Charbonnier

Submission 287

Using field investigations as proxies for interpreting the dynamics of concentrated Pyroclastic Density Currents

Pyroclastic density currents (PDCs) are highly hazardous mixtures of gas and particles, for which direct observations are nearly impossible. Deposits left after the emplacement of concentrated PDCs are generally composed of stacked units of poorly-sorted mixtures with centimeter- to meter-size volcanic fragments set in lapilli and ash matrix. Field investigations of these deposits can provide insights into the physical parameters that control their depositional regimes. We compile field-based studies of small-volume (3) concentrated PDC deposits generated from (1) sustained dome-collapses at Volcán de Colima in Mexico (July 2015) and at Merapi Volcano in Indonesia (June 2006), (2) recurrent vertical/lateral dome explosions at Merapi Volcano (November 2010) and (3) short-lived column collapses at Calbuco Volcano in Chile (April 2015). The diversity of source material spanned by these four major PDC-forming eruptions allow us to use deposit characteristics as proxies to infer deposition models of concentrated PDCs. Results show that the receiving landscape is the primary factor controlling the unsteadiness of these concentrated PDCs. Lobate morphology, decreased clast-size organization, and increased median particle size of the deposits with distance is observed in conjunction with a sudden decrease in channel confinement, consistent with a deposition model dominated by frictional freezing of the basal flow region during stepwise aggradation of different flow units. We identify the key deposit proxies for interpretation of concentrated PDC dynamics to be (i) distribution of deposit facies (i.e. valley-confined, unconfined overbank and associated surge deposits), thicknesses and surface morphologies over complex topographies; (ii) total grain size distribution and volumes of individual flow units; and (iii) longitudinal and lateral lithofacies variation in terms of local grain size distribution and componentry characteristics of the different units. The overarching goal of this study is to identify quantifiable relationships between deposit characteristics and geomorphic parameters (i.e. slope, width, cross-sectional area and sinuosity) that affect the resulting flow mobility metrics (i.e. runout and inundated areas). Coupling of these parameters will help developing new topography-dependent rheological models to enhance the performance of numerical models of concentrated PDCs and better predict the behavior and risk posed by such hazardous flows.

Fukashi Maeno, Shun Nakano, Mitsuhiro Yoshimoto, Takao Ohminato, Atsushi Watanabe, Atsushi Yasuda, Takayuki Kaneko, Setsuya Nakada

Submission 92

Emplacement of lava flows in the sea and creation of a new volcanic island at Nishinoshima, Ogasawara, Japan, revealed from first landing and survey

The island-forming eruption at Nishinoshima volcano, Ogasawara, Japan, began its activity in November 2013 and ended in late 2015. We investigated the emplacement of lava flows in the sea and creation of a volcanic island by analyzing aerial and satellite images during the eruption and surveying geological features of the new island after the eruption. In October 2016, we landed on the new Nishinoshima for the first time since the beginning of the eruption. Along the gravelly coast, we observed many lava lobes that were emplaced during the eruption. The front of lava lobe (a few to >10 m thick) is generally eroded by wave action and exposed its interior. The lava lobes consist of a black or dark gray, glassy clinker part and a massive inner part, some of which are highly fractured, vesiculated, and/or oxidized. Rubbly lava surface was commonly observed. The top of the pre-existed island is covered by ash and scoria fallout deposits with thickness of ~10 cm or more that were caused by Strombolian activities in early periods and ballistic ejecta from the latest Vulcanian activity in November 2015. One of lava lobes in the northern area has a chilled margin that is characterized by a few-cm-thick glassy rim with many fine cracks developed perpendicular to the lava surface. We also observed clefts along the axial crest of lobes, exposing the interior of massive part of lava flows. They are thought to be products from lava inflation driven by an increase of internal pressure by successive injection of new lava into the lobes during lava emplacement. The petrological features of the 2013–2015 lava flows (andesite with 2) are clearly distinguished from the 1973–1974 products and the pre-1702 products. Moreover, it seems that the SiO₂ (MgO) contents slightly decreased (increased) with time, indicating more differentiated magma was erupted in early stage. Although more geological and petrological analyses are needed to explain the origin of chemical variations in products, our findings from the first landing and survey at new Nishinoshima and aerial and satellite observations during the eruption offer important insights into understanding the eruption process of this volcano as well as other eruptions in marine and lacustrine settings.

Christina Magill, Russell Blong

Submission 966

Determining the magnitude of the 17th century Long Island eruption, Papua New Guinea

Tibito Tephra was first identified in the Western Highlands of Papua New Guinea in the 1970s. In 1982, Russell Blong published "Time of Darkness" (University of Washington Press), detailing the physical and geochemical characteristics of the deposit and linking the tephra fall with local oral histories. Blong concluded that the tephra originated from Long Island in the Bismarck Sea, and estimated a compacted volume for the deposit of $> 11 \text{ km}^3$. Assuming an average deposit density of $1,500 \text{ kg}\cdot\text{m}^{-3}$, gives a mass of $> 1.6 \times 10^{13} \text{ kg}$.

However, estimates of volume and mass are difficult given a lack of proximal data. Blong's inner isopach was derived from a single measurement on Crown Island, 25 km northwest of Long Island. All other measurements were taken on mainland New Guinea, $> 70 \text{ km}$ from source, and some from elevations exceeding 3,000 m. An updated isopach map and geometric approach gave a new mass of $3.2 \times 10^{13} \text{ kg}$; varying deposit density and extent of the inner isopach produces mass estimates between 2.0 and $3.6 \times 10^{13} \text{ kg}$. Inversion modelling of tephra dispersal has provided consistent estimates between 2.5 and $3.4 \times 10^{13} \text{ kg}$. We discuss uncertainties in our modelling and use results to refine eruption duration, environmental conditions and season.

Nathan Magnall, Mike R James, Hugh Tuffen, Charlotte Vye-Brown

Submission 754

The formation and classification of breakouts in the 2011-2012 rhyolitic lava flow at Cordón Caulle, Chile

The eruption and emplacement mechanisms of rhyolite lava flows remain enigmatic due to the infrequency with which these eruptions occur. The 2011-2012 eruption of Cordón Caulle in Chile provided the first opportunity to make detailed scientific observations of the active emplacement of an extensive rhyolite lava flow and thus offers an unparalleled opportunity to advance our knowledge of emplacement processes.

The lava flow initially advanced as a blocky flow before stalling, shortly followed by the formation of breakouts at the lava flow front and margins. This change to a cooling limited regime, with a transition from viscosity to crustal control, is common in more mafic lava flows but is rarely considered for high silica flows. As breakout formation can extend the footprint of a lava flow, and change its advance direction, full understanding of breakout processes is key to adequate hazard mitigation.

Here we present a multiscale study that combines satellite imagery, field observations, and microtextural characterisation to constrain the evolution of the Cordón Caulle lava flow and the processes controlling breakout formation. We show that breakout initiation was associated with a combination of 1) fracturing of the surface crust, due to spreading of the flow front and 2) internal pressurisation, due to material supply and vesiculation. The observed microtextures indicate significant in-situ crystallisation occurs within the lava flow core and breakout interiors, suggesting that vesiculation is driven by second boiling. Breakout development reflects the action of inflationary processes and we propose four morphological classifications (domed, petaloid, rubbly, and cleft-split) to describe their evolution. These stages are defined by the degree to which surface slabs are inflated and then fractured. Our insights into breakout morphology will assist interpretations of the emplacement mechanisms of other high silica lava flows.

Sue Mahony, Steve Sparks, Laura Wallace, Samantha Engwell, Ellie Scourse, Nick Barnard, Jessica Kandlbauer, Sarah Brown

Submission 303

Increased rates of large-magnitude explosive eruptions through the late Neogene and Quaternary in Japan, shown from ocean drilling core records.

Visible tephra layers in marine sediment cores from scientific ocean drilling, record high magnitude silicic explosive eruptions in the Japan arc for up to the last 20 million years. 180 tephra layers in a global data set were analysed for the presence of tephra, and layer thickness variation with distance from source volcano. This gives an understanding of the characteristic distances from source that various magnitude eruptions may reach, and still be recorded in ocean drilling records. Here, it suggests that the majority of the visible tephra layers used in this study are the products of caldera-forming eruptions with magnitude (M) >6 , considering their distances at the respective drilling sites (>100 km) to their likely volcanic sources.

The frequency of nearly 5000 visible tephra layers identified in IODP programs cores from around Japan, indicates a marked increase in rates of large magnitude explosive eruptions at around 8 Ma, 6–4 Ma, and further increase after 2 Ma. Comparison of the ocean core records with land-based tephra records from the last 4 Ma shows a similar pattern of changing rates of volcanism. The ocean record displays characteristics of being a more complete record than the land record, as we move back in time.

These changes in abundance of tephra layers with time are attributed to major changes in tectonic plate interactions. Lower rates of large magnitude explosive volcanism in the Miocene are related to a strike-slip-dominated boundary (and temporary cessation or deceleration of subduction) between the Philippine Sea Plate and southwest Japan, combined with the possibility that much of the arc in northern Japan was submerged beneath sea level partly due to previous tectonic extension of northern Honshu related to formation of the Sea of Japan. Changes in plate motions and subduction dynamics during the 8 Ma to present period led to (1) increased arc-normal subduction in southwest Japan (and resumption of arc volcanism) and (2) shift from extension to compression of the upper plate in northeast Japan, leading to uplift, crustal thickening and favourable conditions for accumulation of the large volumes of silicic magma needed for explosive caldera-forming eruptions.

Jon J. Major, Gordon E. Grant, Sarah L. Lewis

Submission 74

A volcano, a lake, and a recurring headache—the Spirit Lake conundrum

The 1980 eruption of Mount St. Helens spawned a massive landslide and subsequent pyroclastic currents, deposits of which blocked the outlet of Spirit Lake at the foot of the volcano. Consequently, lake level rose, threatening to breach the blockage, release a massive volume (to 0.5 km³) of water, and generate a lahar. Geological evidence shows exactly this mechanism—breaching of an ancestral Spirit Lake—generated the largest lahars in the Toutle River valley. Lahars of that magnitude, to about 1 km³ in volume and having flow depths to many tens of meters, would have catastrophic downstream consequences (possible life loss and \$billions in economic damages) should they occur again. To reduce the chance of this happening, the US Army Corps of Engineers in 1985 bored a 2.6-km-long tunnel through a bedrock ridge on the western edge of the lake. Locally, the tunnel crosses weak rock in broad shear zones. Slow, ongoing squeezing and heave along some shear zones have reduced tunnel conveyance capacity and necessitated periodic major repairs. Such repairs require extended closures of the tunnel, allowing Spirit Lake to rise and reducing the margin of safety against blockage failure. Extended closures that allow substantial lake rise and increase system vulnerability highlight the need for a reliable outlet that does not require repeated, prolonged, and expensive interventions. A Congressional request urged the US Forest Service, US Army Corps of Engineers, and US Geological Survey to analyze options for a long-term solution that maintains a safe lake level and minimizes the threat of catastrophic failure of the blockage. Amid institutional cultures and agendas, an interagency, interdisciplinary team evaluated the potential for complete failure of the current infrastructure and consequent breaching of the blockage, and potential risks associated with four alternative lake outlets. Under all options, the annual chance of lake release is mostly low to remote (10^{-5} to 10^{-6}) except after an extended outlet closure when the lake is artificially elevated and the chance of lake release increases to about 10^{-4} . Each outlet option has clear hazard exposure, known data and knowledge gaps, and nuanced risks. Known hazard exposures, nuanced risks, and potentially unknown risks must be weighed against the benefits each outlet option offers.

Rocco Malservisi, Fanghui Deng, Elisabeth A. Gallant, Nicholas Voss, Surui Xie, Mel Rodgers, Timothy H. Dixon, Sylvain J Charbonnier, Cristian M López

Submission 947

High-resolution DEM generation from multiple remote sensing data sources - a case study from Nevado del Ruiz, Colombia

High resolution DEMs are a critical parameter for hazard estimation in volcanic areas. For example, analysis of the expected pathways of lava flows, pyroclastic flows, lahars, and landslides strongly relies on the knowledge of accurate regional topography. While satellite coverage has greatly improved the quality of DEMs around the world, volcanoes remain a challenging target because of extremely rugged terrain with steep slopes and deeply cut valleys. In this study, we combine multiple types of remote sensing data sources with different spatial scales to generate a high resolution DEM (10 m) of Nevado del Ruiz.

Colombia's deadliest volcanic event in recorded history was caused by Nevado del Ruiz Volcano. On November 13, 1985, a VEI 3 eruption triggered large volume lahars (9 107 m³), killing over 23,000 people in the city of Armero and 2,000 people in the town of Chinchina. Meltwater from a glacier capping the volcano was one of the main contributors to the lahars. From 2010 to present, increased seismicity, surface deformation, ash plumes and gas emissions have been observed at Nevado del Ruiz. Since 2014 two small domes have been recorded in the Arenas crater. Analysis of data from remote sensing techniques including Synthetic Aperture Radar (SAR), terrestrial radar interferometry (TRI), and structure from motion (SfM)) were combined to generate a single high resolution DEM. Synthetic aperture radar images acquired by TSX/TDX satellites were applied to generate a DEM covering most of the study area. To reduce the effect of geometric distortion inherited from SAR images, TSX/TDX DEMs from ascending and descending orbits were merged to generate a 10×10 m DEM. Terrestrial Radar Interferometry is a technique that uses a scanning radar to measure the amplitude and phase of a backscattered microwave signal. It provides a more flexible and reliable way to generate DEMs in steep-slope terrain compared with TSX/TDX satellites. The TRI was mounted at four different locations to image the upper slopes of the volcano. A DEM with 5×5 m resolution was generated by TRI. SfM provides an alternative to reduce the effects of shadow zones in both TSX/TDX and TRI images. It is a low-cost and effective method to generate high-quality DEMs in relatively small spatial scales. More than 2000 photos were combined to create a DEM of the deep valley in the shadow zones. DEMs from the above three remote sensing data sources were merged into a final DEM with 10×10 m resolution.

Michael Manga, Chloe Michaut

Submission 90

Formation of lenticulae on Europa by saucer-shaped sills

Europa's surface contains numerous quasi-elliptical features called pits, domes, spots and small chaos. We propose that these features, collectively referred to as lenticulae, are the surface expression of saucer-shaped sills of liquid water in Europa's ice shell. In particular, the inclined sheets of water that surround a horizontal inner sill limit the lateral extent of intrusion, setting the lateral dimension of lenticulae. Furthermore, the inclined sheets disrupt the ice above the intrusion allowing the inner sill to thicken to produce the observed relief of lenticulae and to fracture the crust to form small chaos. Scaling relationships between sill depth and lateral extent imply that the hypothesized intrusions are, or were, 1-5 km below the surface. Liquid water is predicted to exist presently under pits and for a finite time under chaos and domes.

Margaret Mangan, Jessica Ball, Michael Clynne, David Damby, Hannah Dietterich, Larry Mastin, Manuel Nathenson, Joel Robinson

Submission 261

If Lassen Erupted Today: Using “what if” scenarios to focus volcanic risk management, societal resilience, and long-term mitigation of eruption impacts.

Motivating stakeholders to address risk mitigation in volcanic regions where eruptions are infrequent is a challenging, but important, end product of volcanologic research. The challenge is especially evident in California (USA), where mitigation of the more frequently occurring hazards from earthquakes, landslides, wild fires, and floods takes precedence. To increase awareness of volcanic hazards in the state, the USGS California Volcano Observatory is developing methodology to integrate Holocene eruptive histories, computational hazard modeling, volcanic impact research, and exposure analysis to engage stakeholders in ways that “make real” the serious ramifications of failing to plan for low probability - high impact events. The end product of this endeavor is the development of realistic “what if” scenarios examining the hypothetical consequences of well documented past eruptive events occurring today.

By way of illustration, we present a scenario from the Lassen Volcanic Center in northern California, asking stakeholders to consider: what if the 1100 BP Chaos Crags or the 1914-1917 C.E. Lassen Peak eruption were to occur today? We incorporate published data on the dynamics, properties, and deposits of these eruptions combined with numerical modeling of hazards under present-day conditions to constrain the footprint, intensity, and duration of hazards. Using simplified intensity descriptors (destruction; disruption; nuisance) we assess the impact on populations, lifeline utilities, infrastructure, human activities, agriculture, and natural resources and present a series of vignettes that provide stakeholders with a concrete jumping off point for risk mitigation and community resilience planning.

Michael Mann, Geoffrey Abers, Kayla Crosbie, Kenneth Creager, Carl Ulberg

Submission 1203

Geometry of the crust and subducting Juan de Fuca plate beneath the Mount St. Helens region using array-based receiver functions

A goal for the imaging Magma Under mount St. Helens (iMUSH) experiment is to resolve the deep controls on volcanism in the Cascade arc. Mount St. Helens (MSH) is unusual as a prolific arc volcano located 50 km towards the forearc of the main Cascade magmatic arc. The iMUSH broadband deployment featured 70 seismometers at 10 km spacing in a 50-km radius around MSH, spanning an along-strike width that is wide enough to test for along-strike variation in subsurface geometry as well as cross-strike structure. Using these data and seismic velocities from surface wave analyses, we generate P-to-S receiver functions to constrain the relative locations of the primary interfaces: the Moho of the Cascade arc and the dip and depth to the subducting slab as it descends beneath North America. Previous analyses of slab geometry beneath MSH are extrapolated from several hundred km to the north and south. We analyze both back-projected receiver functions from single earthquakes to provide high resolution and two-dimensional Born migrations of the full data set. The strongest coherent phase off the subducting slab is the primary reverberation (Ppxs; topside P-to-S conversion off of a slab interface), seen at nearly all stations across the array. Its polarity and similarity to interfaces seen elsewhere indicate that the Ppxs phase images the Moho of the subducting oceanic plate. A comparison with dipping-layer theoretical receiver functions that properly account for ray bending shows that the Juan de Fuca plate Moho dips at about 26 degrees, at a depth of approximately 85 km +/- 5 km beneath the volcano; presumably the plate interface is 6-8 km shallower. North and east of MSH we observe a clear upper-plate Moho conversion beneath the Cascades range at 40 km depth. That Moho signal is absent west and south of MSH, consistent with variations observed in high-frequency PmP data and other Cascades transects. The resulting interface geometry indicates a mantle wedge that is roughly 35 km thick directly beneath this volcano. Basaltic volcanic centers are found on all sides of MSH, presumably mantle-derived melts. Such magmas either form in this limited region of the mantle, despite low heat flow immediately west of MSH, or migrate from farther in the backarc. Overall, these data confirm the unusually shallow depth of the slab beneath this arc volcano and suggest a narrow vertical extent of the mantle melting region directly beneath MSH.

Kazutaka Mannen

Submission 213

Development of vt; a new simulation code to describe pyroclastic fall deposit from bending eruption column under windy condition

Most tephra fall simulation codes assume eruption columns that rise vertically from a source vent. This assumption is, in many cases, inappropriate since most eruptions occur under more or less windy condition. In windy condition, eruption columns, especially weak ones bend downwind and particle source locates downwind of the eruption centre. Recently, several models that formulate bending column under windy condition have been proposed. Here I include bending of eruption column modeled by Woodhouse et al (2013) in Tephra2. The modified code is named wt (=windy Tephra2).

Woodhouse (2014) calculate coordinate of column center, column radius, upward velocity of the column, column temperature and etc. as a function of height. Tephra2 calculate coordinate of distribution center as a function of released height and particle diameter. wt calculate coordinate of distribution center based on column bending (Woodhouse, 2014) and atmospheric advection (Tephra2). Also, distribution width in Tephra2 is a sum of column radius and atmospheric diffusion. In wt, column radius is based on Woodhouse et al. (2014).

In the presentation, difference of deposit distributions calculated by Tephra2 and wt will be discussed. Also application of wt to the 2011 Shinmoedake eruption and the comparison of calculation results and observation will be discussed.

Fabio Manta, Benoit Taisne

Submission 940

Open window into an Open system: a Bayesian approach for model validation

Real time data interpretation is key in crisis management. How to increase our level of confidence in data interpretation? How to design optimum monitoring network in order to get most of the data at a minimum cost? We aim to address those questions by mean of analog modelling.

Inverse procedures are commonly used to interpret observation data by estimating key parameters controlling volcanoes behaviour. The application of this technique requires a theoretical model that links observations (e.g. deformation, degassing, seismicity) with processes happening within the volcanic system. However, existing models are often imprecise and suffer of uncertainties related to approximations of the system. For this reason, conducting analogue experiment can contribute to bridge the gap between theoretical formulation and the complexity of natural systems, allowing us to quantify the uncertainties in the estimation of the key parameters.

Based on this principle, we have performed analogue experiments that simulate surface deformation related to conduit processes, and we have used the results to test the uncertainties of the theoretical model recently developed. The theoretical model, relates short time tilt signals recorded at the surface with strombolian activity. In particular, the surface deformation is linked to geometrical properties of the volcanic system (i.e. conduit diameter and dimension of the gas slug) as well as its physical properties (i.e. mass of the gas slug, viscosity and density of the magma). Nonetheless, due to the lack of direct observations related to system properties, the uncertainties of the proposed model are still unknown.

To this end, we applied the Bayesian inversion on data recorded during analogue experiments performed in a controlled environment with known parameters. The experiments simulated a typical open system that consist in a degassing volcanic conduit. The interaction between bubble rinsing the conduit with the stress and strain field in the surrounding medium generate deformation of the surface. Due to the quasi-controlled environment, the result of the inversion on the measured deformation can be directly compared with parameters of the experiment, allowing us to quantify the uncertainties of the model.

Alvaro Marquez, Raquel Herrera, Jose Luis Granja Bruña, Benjamin van Wyk de Vries, Pilar Llanes, Marta Rincón

Submission 802

Recent volcano-structural evolution of Teide volcano (Tenerife, Canary Islands): constraints from geological mapping and geochronological data of the summit zone.

Teide is the only active stratovolcano in the Canarian archipelago. Last summit eruption occurred at 1302-1414 AD forming the large phonolitic lava flow field known as "Lavas Negras". Current models for Teide evolution propose that Lavas Negras eruption is the only summit eruption occurred in the last 30 ky, the age proposed for the youngest so-called "Old Teide" lava flows which form the main edifice. From that age onwards the eruptive activity allegedly migrated from summit, first to construct Pico Viejo volcano (30-17 ky), and later to peripheral phonolitic lava domes (

Our results show that the youngest "Old Teide" lava flows affected by the tectonic scarps of the summit zone are around 40 ky old, and the youngest lava flow occurring at the eastern flank is 28 ky. However, at the volcano south flank we have obtained an age of 15 ky for one the youngest lava flows coming from the volcano summit. In addition, some short phonolitic lava flows showing surface breadcrust textures cropping out in the summit zone have produced radiometric ages of 14 ky. These results suggest, on one hand, that at least part of the Pico Viejo construction has been coeval to Teide summit eruptive activity. On the other hand, and since the published radiometric ages of Teide peripheral lava domes are younger than 6 ky, our results can not discard a possible shift of eruptive activity between summit and base volcano zones around 14-10 ky. Otherwise, our field data indicate that there was no eruptive activity from Teide summit between those breadcrust-texture flows and the Lavas Negras eruption. Since breadcrust lava flows are apparently affected by the bulging process attributed to the effect of a shallow intrusion, then the deformation of the volcano summit zone must be recent. That deformation should be produced by an undetected cryptodome emplaced between 14 and 0.6 ky ago or during the first stages of Lavas Negras eruption.

Lauren Marshall, Anja Schmidt, Matthew Tsigaridis, Ken Carslaw, Graham Mann, Michael Mills, Jean-Francois Lamarque, Fiona Tummon, Simone Tilmes, Sandip Dhomse, Davide Zanchettin, Myriam Khodri, Claudia Timmreck, Michael Sigl, William Ball, Slimane Bekki,

Submission 62

Multi-model comparison of the volcanic sulfate deposition from the 1815 Mt. Tambora eruption

The eruption of Mt. Tambora in 1815 was the largest eruption of the past 500 years. The eruption had significant climatic impacts, leading to the 1816 'year without a summer' and remains a valuable event from which to understand the climatic importance of large stratospheric volcanic SO₂ injections. It is also one of the strongest, and most easily identifiable volcanic signals in polar ice cores, which are widely used to reconstruct the timing and magnitude of past eruptions. As part of the Model Intercomparison Project on the climatic response to Volcanic forcing (VolMIP), 5 state-of-the-art aerosol climate models have simulated this eruption. We analyse both simulated background (no Tambora) and volcanic (with Tambora) sulfate deposition to polar regions and compare to ice core records. Background sulfate deposition is similar across all models and compares well to observations, with models capturing the east-west gradient in sulfate deposition in Antarctica and the north-south gradient in Greenland. Volcanic sulfate deposition, however, varies in timing, spatial pattern and magnitude between the models. Mean sulfate deposition to Antarctica in the Tambora simulations ranges from 19 kg km⁻² to 264 kg km⁻², and in Greenland from 31 kg km⁻² to 195 kg km⁻². Scaling factors between the average ice-sheet deposition and the corresponding hemispheric sulfate burdens vary between models. Sources of the inter-model variability include the formation and transport of sulfate aerosol, and differences in the treatment of wet and dry deposition in each model. These results highlight the uncertainties and difficulties in deriving historic volcanic forcing, estimated from the scaling of volcanic sulfate at the poles to atmospheric burdens.

Aaron Marshall, Brittany Brand

Submission 1117

When good volcanoes go bad - The causes and consequences of mafic explosive volcanism, Llaima volcano, Chile

Llaima volcano, in the south-central volcanic zone of Chile, is an active stratovolcano with a history of mafic explosive volcanism. At least two of these eruptions (~16 ka and ~15 ka) were catastrophic in explosivity and eruptive volume, and likely resulted in the formation of calderas. The products of these eruptions created the extensive Curacautín ignimbrite sequence deposited radially around Llaima volcano. While common in highly silicic systems, large-volume explosive eruptions are uncommon in mafic systems due to the lower melt viscosity of their magmas.

The objective of this study is to constrain the pre-eruptive conditions responsible for triggering the Curacautín eruptions. Twenty-seven samples were collected from ten locations on the east and west sides of the present-day Llaima edifice. Samples were selected from varying heights within each stratigraphic section to constrain differences in deposit features, granulometry, geochemistry, and pyroclast textures.

All outcrops are matrix supported and range from massive to diffusely stratified. However, we find that the eastern outcrops have 5-15% dispersed lithic blocks; whereas, the western outcrops have up to 35% accidental blocks in lenses and horizons. The juvenile pyroclasts in the eastern outcrops are finely vesicular, and contain ~1–2% euhedral crystal cumulates of olivine and plagioclase, and up to 3% accidental lithics (coarse ash in size). Juvenile pyroclasts in the western outcrops are dense, glassy, and many contain radial jointing. These juveniles contain 5–7% accidental lithics (coarse ash to fine lapilli in size) and ≤1% crystal cumulates. Future work includes combining depositional characteristics and geochemical analyses to determine the timing and nature of eruption. Textural analysis of the pyroclasts will include bubble and microlite number densities (2D and 3D), and measurements of bubble connectivity, throat diameters, and the tortuosity of pore pathways (3D). We hypothesize that the combination of geochemistry and textural analysis will allow us to constrain the pre- and syn-eruptive conditions that resulted in the explosive, mafic, caldera-forming eruptions.

Jacques Marteau, Marina Rosas-Carbajal, Kevin Jourde, Jean de Bremond d'Ars, Bruno Carlus, Dominique Gibert, Yves Le Gonidec, Jean-Christophe Ianigro

Submission 562

Monitoring the La Soufrière de Guadeloupe hydrothermal system with a regularly-spaced muon telescope network

Long-term muon tomography allows to track density changes in a volcano by continuously measuring the flux of cosmic muons traversing the geological body. In the context of volcanic hydrothermal systems, this approach can help to determine zones of preferred steam formation, condensation, water infiltration and storage. A single muon telescope provides an integrated 2-D average-density section of a volcanic system, leading to an intrinsically ambiguous inverse problem. To overcome this limitation, we present the first results of imaging the La Soufrière de Guadeloupe dome and shallow hydrothermal system with several simultaneous muon telescopes viewing the dome from different positions around its base. Our strategy provides better constraints on the spatial location of the density changes and an improved estimate of the amount of mass involved in these changes. Therefore, we can better characterize water phase changes and estimate pore pressures. We compare the temporal density variations extracted from different muon telescopes to time-series of rainfall on the summit recharge area and temperature profiles in the vicinity of ground thermal anomalies and summit fumaroles.

Alejandro Marti, Arnau Folch

Submission 416

Meteorological coupling on volcanic ash modeling: a first order source of error for operational volcanic forecast?

In the event of an eruption, ash modeling systems are used to simulate the atmospheric dispersion of volcanic ash and to generate operational short-term forecasts to support civil aviation and emergency management. At present, operational modelling systems are built on off-line approaches, where the meteorological model runs a priori and independently from the dispersal model to produce the required meteorological fields at regular time intervals. There is a concern that inconsistencies and shortcomings associated with this coupling strategy might lead to errors in the ash cloud forecast. These inconsistencies are anticipated to be more relevant in scenarios where the meteorological conditions change rapidly in time or distal ash cloud dispersal simulations are required. In the aftermath of the 2010 Eyjafjallajökull eruption in Iceland, substantial effort and progress has been done to quantify and reduce several ash cloud modeling and forecasting errors associated with a number of critical aspects including, among others, characterization of the source term and related uncertainties in model inputs, model parameterization of relevant physical phenomena, or satellite detection and retrieval algorithms. However and surprisingly, the quantification of modeling errors and shortcomings associated to the off-line coupling strategy has received no attention despite the fact that lessons from other communities (e.g. air quality) show that these can be substantial. In contrast, in an on-line modeling system, the meteorological model and the VATDM run concurrently and consistently, allowing the particle transport to be automatically tied to the model resolution time and space scales, and resulting in a more realistic representation. This work aims to identify model shortcomings and systematic errors associated to traditional off-line forecast and, to provide a quantitative assessment over time of these forecasting systems and their predictability limits. In that context, we compare the results from employing the off-line and on-line coupling strategies available in the NMMB-MONARCH-ASH model to: i) quantify the predictability limits of different off-line coupling intervals (e.g. 1h, 3h, 6h, 12h); and ii) assess how the magnitude of the model forecast errors implicit in the offline approach compares with other better-constrained sources of forecast error, e.g., uncertainties in eruption source parameters.

Joan Marti, Ármann Höskuldsson

Submission 1315

Why should Vatnajökull National Park, Iceland, become a UNESCO natural heritage site?

Vatnajökull National Park represents a geological system build up due to interaction between geosphere, hydrosphere/cryosphere and atmosphere. Internal geological forces originate deep within earth's mantle, the Icelandic hot spot. For the past 25 Ma the hotspot has coexisted with the Atlantic divergent plate boundary. Presumed focus of this activity is within the National park. Results are main rise of Iceland and variety of large active central volcanoes, faults and fissures. For the past 2.5 Ma the area has been periodically covered with ice sheet, namely Vatnajökull, currently the largest ice sheet on the Eurasian plate. The National park covers about 14000 km² within which subaerial and subglacial volcanic formations can be readily explored. Further tectonic and erosional processes linked to the divergent plate boundary, crustal formation, glacial erosion and water runoff are exposed. The national park is thus expressing a comprehensive evolution of a geological system involving volcanic crustal and plate formation to destruction and deposition by water/ice. This interplay of geological forces is not readily observed elsewhere in the world. Places within the National park are easily accessed, southern coastal areas all year and highlands during summer, making its educational and conservational value of extreme importance for future generations.

Bart Martin

Submission 1133

Small Volume Wanapum Basalt (Columbia River Basalt Group) Flows in SE Washington and NE Oregon: Integrating Fieldwork with Geochemistry to Constrain Flow Emplacement and Petrogenesis

The Shumaker Creek Member and the Basalt of Powatka are small volume (≈ 25 to 30 km^3) largely aphyric basaltic andesite flows overlying the Frenchman Springs Member (Wanapum Basalt) in SE Washington and NE Oregon. Both are notable for their high P₂O₅ and Ba (P₂O₅: ~ 1.00 and $\sim 1.23 \text{ wt}\%$; Ba: ~ 1200 and $\sim 1085 \text{ ppm}$, respectively) and lower TiO₂ (TiO₂: ~ 2.45 and $\sim 2.60 \text{ wt}\%$, respectively) abundances relative to the more voluminous Wanapum Basalt units (Frenchman Springs, Roza, and Priest Rapids Members). Recent fieldwork in NE Oregon, integrated with geochemistry, established that the Powatka is younger than the Shumaker Creek.

Wright et al. (1979, USGS OFR 79-711) identified a 23-meter wide Shumaker Creek dike in Joseph Creek Canyon, $\sim 25 \text{ km}$ SSE of the flow's southernmost outcrops. Topographic relief along the margin of the Sentinel Gap (Frenchman Springs Member) basalt probably limited the westward movement of Shumaker Creek lava in the Troy Basin (NE Oregon). North of the Blue Mountains in SE Washington, Shumaker Creek lavas form two large lobes that appear to have flowed around a topographic high associated with older N₂ Grande Ronde Basalt vents. The eastern flow lobe may have also followed the drainage of the ancestral Grande Ronde River into the Lewiston Basin.

Ross (1978, Ph.D. thesis, Idaho) and Swanson et al. (1981, USGS OFR 81-797) mapped the Powatka basalt throughout most of the Troy Basin, southward towards Elgin OR and westward to the Blue Mountains summit plateau near Tollgate OR. An eruptive source for the Powatka has not been recognized. Field relationships suggest that the older Shumaker Creek lavas probably formed a topographic barrier limiting the eastward advance of the younger Powatka flows in the eastern Troy Basin.

While abundances of most incompatible elements (e.g., K, P, Nb, Zr, Y, Ba) in the Shumaker Creek and Powatka lavas are greater than those observed in the voluminous Wanapum units, incompatible element ratios (i.e., Zr/Nb, Zr/Y) and normalized trace element patterns for all of these Wanapum flows are similar. This suggests that all of the flows were derived from similar sources and include contributions from both assimilated continental lithosphere and subducted material; however, higher Ba concentrations at similar incompatible element ratio values suggest that the Shumaker Creek and Powatka lavas represent melts formed by lower degrees of partial melting compared to the more voluminous Wanapum units.

Simon Martin, Janine Kavanagh, Andy Biggin

Submission 298

How are variations in magma flow recorded across the breadth of intrusions? Insights from magnetic anisotropy and petrological studies

Understanding the factors that influence magma transport and emplacement within the crust is vital for understanding the behaviour of volcanic systems. Studying extinct volcanoes where erosion has exposed their plumbing systems provides insights into a range of stages of magma movement, however unravelling which parts of the transport history are preserved is challenging. This study aims to understand how magma flow can be preserved over small distances by using magnetic anisotropy and petrographic analysis with high density sampling across the breadth of solidified intrusions. Fieldwork was conducted on well exposed sills near Inver Tote, Isle of Skye, Scotland, where 6 to >15 m thick olivine dolerite sills from the Little Minch Sill Complex (c.60 Ma) have intruded Jurassic sediments. Two basaltic dykes cross-cut the site in a NNW-SSE orientation. Closely-spaced sampling was undertaken across a 6 m thick sill for anisotropy of magnetic susceptibility (AMS) and anisotropy of anhysteretic remanent magnetisation (AARM) studies at 50 cm intervals, and at 1 m intervals for petrological analyses.

Results from the AMS tensors indicate a K1 axis (longest axis) parallel to the sill plane, originating from ferromagnetic crystals with hysteresis properties suggestive of multi- to pseudo-single domain titanomagnetite. With increased distance from the sill margins, >0.5 m, the orientation of the K1 axis rotates around the K3 axis (shortest axis) from a N-S orientation to NE-SW orientation, but remaining parallel to the sill plane. At the lower contact AARM K1 axes are parallel to AMS K1, suggesting a normal fabric and magma flow in a N-S orientation. However, the AMS and AARM tensors become progressively more oblique to each other towards the centre of the intrusion, suggesting an anomalous fabric and possible reorientation of magma flow direction. The results suggest the magma is related to the Cuillin Hills complex in southern Skye, and we propose that changes in magmatic flow recorded in magnetic fabrics occurred due to progressive channelization within the intrusion. Our results suggest magma flow may be highly variable within intrusions, and that interpretations of magma flow dynamics based on field evidence may require reconsideration.

Ma. Mylene Martinez-Villegas, Renato Solidum, Jean Saludadez, Ruben Lamela

Submission 290

Moving for Safety: A Qualitative Analysis of the Communication among the Scientists, Local Officials and the Affected Communities in the 2014 Mayon Volcano Eruption Evacuation

This study used qualitative analysis to examine interviews of people who experienced the August-December 2014 Mayon unrest and be able to understand the nature of communication that occurred and people's response during the period. There is direct communication among agency and office heads and various channels were utilized to disseminate information during the height of Mayon 2014 unrest –advisories were sent via official channels (fax, email). In addition, as part of redundancy, SMS were sent directly from the provincial office to barangay officials, unlike in the past that information had to go through the municipal offices. Another channel heavily used is the online posts from the provincial government office's website. In the communities, passing on of information facilitated by the barangay officials still remained the means of disseminating information to the populace.

Thematic analysis shows that people reacted to the information given to them in several ways-they evacuated, chose not to evacuate for various reasons (e.g. they did not believe they are in danger citing past experience, inconvenience in evacuation sites, etc), and evacuated even when not asked to. Officials were asked for possible reasons or motivations as to why people evacuated and common themes that emerged were fear emanating from experience of past eruptions, obeying order to evacuate because it is the law, and the potential to receive relief goods for those who are economically in need.

Key words: Communication, evacuation, affected communities, response

Silvia Massaro

Submission 582

Time evolution of magma feeding system during a Plinian eruption

The geometric feeding system evolution of large eruptions remains a big question mark in present day volcanological research. Here, for the first time, a dynamic picture of the evolution of the conduit system is provided for the Pomici di Avellino (PdA) Plinian eruption (Somma-Vesuvius, Italy). Such a picture was obtained coupling field data and numerical simulations. The physical data of the Avellino eruption, such as Magma Discharge Rate (MDR) and volume of lithic components in fall deposits, were used to constrain numerical simulations. The PdA eruption represents an ideal case study, having a continuous magma discharge feeding a sustained column. The fall deposits show a sharp change in colour (white to grey, phonolites to tephri-phonolites) reflecting magma withdrawal from a zoned magma chamber at 7 km depth. The CPIUD code was used to simulate three eruptive phases of the Plinian eruption, using as constraints the amount and lithology of the eroded lithics, together with the independently inferred MDRs. Three stable geometry configurations of the feeding system were assessed for the Eruptive Units 2 and 3 (EU2, EU3). They capture the EU2 base, EU2 top, and EU3 peak. A 7 km long dyke, connecting the magma chamber to the surface, characterises the feeding system at the onset of the Plinian phase (EU2 base). The feeding system rapidly evolved into hybrid geometry, with a deeper dyke and a shallower cylindrical conduit, during the eruption of the EU2 top. Both dyke and cylindrical conduit evolved during the progression of the Plinian phase, with the cross sectional area of the dyke that increased from $3.8 \times 10^3 \text{ m}^2$ at the onset of EU2 to $1.9 \times 10^5 \text{ m}^2$ during EU3. At the same time the cylinder radius passed from 0 m to 60 m, while its length from 0 m to 3000 m. The changes in feeding system geometry testify for partitioning of driving pressure of the eruption, which was used for both moving magma to the surface and for dyke growth. Descends that the lower dyke acted as a sort of magma capacitor in which the liquid was stored for a while before accelerating to the cylindrical conduit and erupted. The capacitor effect of the lower dyke guaranteed the magma feeding into the upper cylindrical conduit when the base of the dyke was closed for the drop in driving pressure due to progressive magma chamber emptying. These outcomes represent a new baseline for further geophysical studies devoted to the comprehension of processes driving volcanic eruptions.

Larry Mastin, Alexa R. Van Eaton

Submission 263

When do umbrella clouds matter? The effect of radial expansion on the distribution of ash clouds and tephra deposits

Powerful eruptions create their own radial wind field, driving an umbrella cloud outward in all directions. Most operational models do not consider these effects; they emit ash from a line source extending vertically from the vent, and allow it to advect passively with the ambient wind field. It is presently not well known how big an eruption needs to be for the umbrella cloud to significantly alter ash transport. To address this question we used the Ash3d model to examine umbrella-cloud spreading during eruptions of different size. The model considers an umbrella whose radius r grows with time t at $r=At^2/3$, where the constant A is mass eruption rate. Within the cloud radius, we also add a radial wind field to the ambient wind field. We simulated 5 hypothetical mid-latitude eruptions with volumes (V) of 0.1, 1, 5, 50, and 500 km³ dense-rock equivalent (DRE), respectively. For each case we ran two simulations; one with an umbrella cloud and the other without. Durations for these eruptions were 24, 24, 24, 24, and 72 hours, plume heights were 13, 20, 27, 27, and 27 km, and eruption rates (MER) were 0.01, 0.06, 0.14, 1.4, and 4.8×10^9 kg/s, respectively. Umbrella clouds were assumed to be located vertically at between 56% and 75% of the total plume height. In each case, we tracked the cloud for 72 hours and calculated the deposit distribution.

Results show that even the smallest (0.1 km³) eruption produced a cloud with twice the area of the no-umbrella simulation. The discrepancy of 2x (50k km²), was greatest in the first 2 hours and diminished through time. For larger eruptions, the maximum discrepancy was 6-10 hours after the eruption start, and produced clouds 2, 3, 7, and 20 times larger in area than their no-umbrella counterparts. Absolute area differences were 250k, 300k, 2.3M, and 7.7M km². Thus neglecting the umbrella in a 1-km³ eruption could underestimate the cloud area by an amount the size of the United Kingdom. There are similar impacts on the resulting deposit. Deposit areas (within the 1mm isopach) are 1.0, 1.5, 1.5, 2.5, and 7x greater than calculated without the umbrella, respectively. We conclude that, for $V > \sim 10^{-1}$ km³ DRE, involving sustained $MER > \sim 10^8$ kg/s, models that neglect umbrella-cloud growth may significantly underestimate the area of both the airborne clouds and deposits.

Tamsin Mather, Lawrence Percival, Micha Ruhl, Stephen Hesselbo, Hugh Jenkyns, Jessica Whiteside

Submission 882

Pulsed volcanism during the end-Triassic mass extinction: new evidence from mercury archives

Recent studies have demonstrated that mercury spikes in sedimentary sequences show promise as a proxy for large igneous province (LIP) volcanism. The end-Triassic extinction event (~201.5 Ma) is one of the five largest environmental perturbations of the Phanerozoic Eon. This event has long been proposed to be causally linked with the Central Atlantic Magmatic Province (CAMP), thought to revolve around a substantial increase in atmospheric pCO₂. In eastern North America and northern Africa, CAMP is preserved as multiple basaltic units interbedded with uppermost Triassic to lowermost Jurassic sediments. However, it remains unclear whether this apparent pulsing was a local feature, or if pulses in the intensity of CAMP volcanism characterized the emplacement of the Province as a whole. Here, six geographically widespread Triassic–Jurassic records, representing varied paleoenvironments, are analyzed for mercury concentrations and mercury/total organic carbon (Hg/TOC) ratios. Volcanism is a major source of mercury to the modern environment. Clear increases in Hg and Hg/TOC are observed at the end-Triassic extinction horizon, confirming that a volcanically induced global mercury-cycle perturbation occurred at that time. The established correlation between the extinction horizon and lowest CAMP basalts allows this sedimentary excursion in mercury to be stratigraphically tied to a specific flood basalt unit for the first time, significantly strengthening the case for volcanic mercury as the driver of sedimentary Hg/TOC spikes. Additional Hg/TOC peaks are also documented between the extinction horizon and the Triassic–Jurassic boundary (a time interval of ~100–200 kyrs), confirming that the intensity of CAMP volcanism was pulsatory across the entire Province, and providing direct evidence for episodic volatile release during the initial stages of CAMP emplacement. Pulsatory volcanism, and associated perturbations in the ocean–atmosphere system, may have had profound implications for the rate and magnitude of the end-Triassic mass extinction and the subsequent biospheric recovery.

Robin Matoza, Arthur Jolly, David Fitzgerald, Richard Johnson, Bernard Chouet, Phillip Dawson, Geoff Kilgour, Bruce Christenson, Eslie Garaebiti, Alex Iezzi, Allison Austin, Ben Kennedy, Rebecca Fitzgerald, Nick Key

Submission 344

Seismo-acoustic wavefield of strombolian explosions at Yasur volcano, Vanuatu using a broadband seismo-acoustic network, infrasound arrays, and infrasonic sensors on tethered balloons

Seismo-acoustic wavefields at volcanoes contain rich information on shallow magma transport and subaerial eruption processes and inform our understanding of how volcanoes work. Acoustic wavefields from eruptions are predicted to be directional, but sampling this wavefield directivity is challenging because infrasound sensors are usually deployed on the ground surface. We attempt to overcome this observational limitation using a novel deployment of infrasound sensors on tethered balloons in tandem with a suite of dense ground-based seismo-acoustic, geochemical, and eruption imaging instrumentation. We conducted a collaborative multiparametric field experiment at the active Yasur volcano, Tanna Island, Vanuatu from 26 July to 2 August 2016. Our observations include data from a temporary network of 11 broadband seismometers, 6 single infrasonic microphones, 7 small-aperture 3-element infrasound arrays, 2 infrasound sensor packages on tethered balloons, an FTIR, a FLIR, 2 scanning Flyspecks, and various visual imaging data; scoria and ash samples were collected for petrological analyses. The infrasonic signatures of Yasur's strombolian explosions consist of short-duration explosion waveforms with non-linear characteristics. The seismic signals are numerous repetitive long-period (LP) seismic events underlain by very-long-period (VLP) signals with periods of ~ 10 s. In addition to these dominant signal types, we also record a near-continuous broadband (~ 0.1 –20 Hz) infrasonic tremor associated with the vigorous degassing activity. This unprecedented dataset should provide a unique window into processes operating in the shallow magma plumbing system and their relation to subaerial eruption dynamics.

Akiko Matsumoto, Mitsuhiro Nakagawa, Masato Iguchi

Submission 557

Petrological monitoring of eruptive activity since AD 2006 at Sakurajima volcano, Southern Kyushu, Japan: Implication of the activation in AD 2015

Sakurajima volcano, located in southern Kyushu, Japan, has resumed its eruptive activity at Showa crater since June 2006. After that, the volcanic explosions has been continued until 2013. Although the number of explosions declined in 2014, the volcano had become higher level of eruptive activity accompanied with clear inflation since January 2015. In addition, the dyke intrusion event had occurred in August 2015. In order to reveal the magma plumbing system since 2006 as well as the reason for the activation in 2015, we have carried out the petrological monitoring of the dated juvenile lapilli and ash for 6 years since 2009. The juvenile lapilli (lithic, scoria, and pumice) have plagioclase, orthopyroxene, clinopyroxene, and Fe-Ti oxides, and a small amount of olivine as phenocrysts. The core compositions of olivine phenocrysts are Fo₈₀₋₈₁, compositionally disequilibrium with the co-existed pyroxenes. On whole-rock chemistry, all the juvenile lapilli are the most mafic since 20th century, and are plotted on the one linear trends on Harker diagrams, which agree with the compositional trends of the 20th juveniles. The SiO₂ content of juvenile lapilli slightly increases from 2009 (58.5 wt.%) to 2013 (59.6 wt.%), and clearly decreases in 2015 (58.3-59.0 wt.%). On matrix glass chemistry of juveniles from lapilli and ash samples, there exists the similar temporal variation to whole-rock chemistry. The silica content decreases from 2009 to 2010, and increase gradually until 2013, and again decrease clearly in 2015.

The existence of high-Fo olivine and the linear trends of whole-rock chemistry suggest that the magma mixing between basaltic and andesitic ones has been occurred since 2006. Therefore, it is considered that the silica contents of whole-rock and matrix glass chemistries reflect the ratio of basaltic magma in erupted magma. Comparing to the geophysical monitoring data, as the ratio of basaltic magma in erupted magma increased, the volcanic edifice inflated and the number of explosions became larger. Especially, the effect of basaltic magma is much large in 2015. On the basis of the zoning profiles of high-Fo olivine phenocrysts in the 2015 juveniles, the timing of the latest magma mixing is estimated at the period during late of 2014 to May 2015, agreeing with the beginning of the inflation of volcanic edifice. It is probable that the activation of the 2015 eruptive activity had been induced by newly input of basaltic magma since the late of 2014.

Tobias Mattsson, Steffi Burchardt, Bjarne Almqvist

Submission 746

Insights into cryptodome emplacement from the Sandfell laccolith, eastern Iceland – implications for seismic and geodetic monitoring

Cryptodome emplacement poses a considerable volcanic risk because it may lead to explosive eruptions and/or edifice collapse. Cryptodome emplacement is associated with surface deformation and, notably, characteristic seismicity consisting of thousands of small similar waveform-events [1]. Although the cause of the cryptodome seismicity is still debated, it is used to monitor and to estimate the size and volume of active cryptodomes [2]. Improved understanding of cryptodome emplacement and associated volcano deformation and seismicity therefore has the potential to significantly advance volcanic hazard assessment. Here we present new observations from the Neogene Sandfell laccolith in eastern Iceland, an exposed cryptodome that can be considered an analogue to active cryptodomes in volcanoes, such as Katla. Detailed mapping and 3D structural modelling of the Sandfell laccolith show very local uplift and deformation in the surrounding host-rock. Moreover, microstructural analysis and anisotropy of magnetic susceptibility (AMS) of the Sandfell rocks reveal that localized syn-emplacement shear fabrics developed in the magma, which are related to extensive planar fracture-rich layers observed within approximately half of the volume of the Sandfell laccolith. This indicates that cryptodome seismicity could be caused by widespread sub-solidus fracturing in large volumes of the magma body, and implies that size approximations of active cryptodomes based on seismicity may underestimate the actual dimensions of the intrusion. A detailed understanding of the syn-emplacement fracturing in cryptodomes and the associated seismicity are key to better assess volcanic risks in the future.

[1] White RA, Miller AD, Lynch L, Power J (1998) Observations of hybrid seismic events at Soufriere Hills Volcano, Montserrat: July 1995 to September 1996. *Geophys Res Lett* 25:3657–3660. doi: 10.1029/98GL02427

[2] Soosalu H, Jónsdóttir K, Einarsson P (2006) Seismicity crisis at the Katla volcano, Iceland—signs of a cryptodome? *J Volcanol Geotherm Res* 153:177–186. doi: 10.1016/j.jvolgeores.2005.10.013

Kate Mauriohooho, Shaun L. L. Barker

Submission 1045

Mapping lithology and hydrothermal alteration in geothermal systems: traditional versus portable techniques

Characterising the geology of geothermal fields involves visual description of cuttings, core, petrography and x-ray diffraction. New technologies like short wave infrared (SWIR) and portable x-ray fluorescence (pXRF) have emerged driven by demand from the mineral exploration industry. These technologies obtain mineralogical and geochemical information rapidly and inexpensively. Our aim was to evaluate their application to characterising geothermal drill cuttings. 304 samples from three drillholes in the Tauhara geothermal were analyzed. pXRF results from untreated drill cuttings were compared with laboratory XRF results from pressed pellet and lithium borate fused beads prepared from crushed powders. SWIR results were compared to x-ray diffraction results to evaluate hydrothermal alteration mineral identification.

Three main zones of alteration were recognised: a shallow argillic to intermediate argillic alteration zone, a transition zone as propylitic alteration begins to dominate with increasing depth and an intense propylitic alteration zone at the deepest levels. Mineral inferred temperatures are cooler than measured well temperatures in all wells except TH10. Here mineral inferred temperatures agree with hotter measured well temperatures (> 280 °C). Strong potassic alteration suggests TH10 is closest to the major upflow zone making south Tauhara a prospective area for geothermal production.

pXRF data downhole shows that immobile elements (Zr, Y, Nb) can be used to define lithological boundaries which are difficult to identify from visual logging alone. Downhole immobile element trends can separate lithology packets and distinguish subunits or internal stratigraphic variations. Conversely variations in mobile element concentrations (Ba, K, Ca, As, Rb and Pb) indicated feed zones or permeable zones of fluid movement by depletions or elevations in element concentrations.

Whole rock geochemistry is not carried out during geothermal well logging due to cost and time constraints. We suggest pXRF in particular should become a routine part of the characterization of drill cuttings during geothermal exploration and well drilling. The results can be used to correlate between drill holes therefore improving geologic, stratigraphic and hydrothermal alteration models of the geothermal field.

Katharine Maussen, Edgardo U. Villacorte, Raymond Patrick R. Maximo, Ma. Antonia V. Bornas, Alain Bernard

Submission 305

Geochemical evidence for magmatic intrusions at Taal Volcano, Philippines

Taal volcano (Luzon island, Philippines) has erupted 33 times since 1572, the last time in 1977. Out of these 33 eruptions, 31 have occurred after a rest period of less than forty years, making Taal volcano likely to erupt in the near future. Despite the lack of recent eruptions, Taal volcano has shown some remarkable activity with several seismic crises accompanied by rapid ground deformation (up to 20cm/day in 1994), temperature rise of the Main Crater Lake (MCL) by up to 9°C in 1994, the opening of fissures in 1991-1994 and a tenfold increase in carbon dioxide emission in 2010. We studied major, trace element and isotopic compositions of the MCL over a period of 25 years to investigate the nature of these seismic crises and to study the potential of geochemical monitoring for eruption prediction of Taal volcano.

Long-term evolution of MCL composition shows a slow but consistent decrease of acidity, SO₄, Mg, Fe and Al concentrations and a trend from light to heavy sulphate, consistent with a general decrease of volcanic gases dissolving in the hydrothermal system. Na, K and Cl concentrations remain constant indicating a different origin for these elements. A significant deviation from this baseline can be seen in two samples from 1995. pH dropped from 2.6 to 2.2, F, SiO₂ and Fe concentrations increased and Na, K and Cl concentrations decreased. Sulphate was depleted in 34S and temperature was 4°C above baseline level at the time of sampling. We attribute these changes to the injection of hot acidic fluids into the MCL caused by the intrusion of a shallow degassing magma body during the unrest in 1994.

More recent unrest periods, including 2004-2005 and 2010-2011, have not caused significant changes in the geochemistry of MCL waters. It seems unlikely that these seismic crises were caused by intrusion of degassing magma to shallow levels. New magmatic intrusions that might lead to the next eruption of Taal volcano are expected to change the geochemistry of MCL in the same way as in 1994, with the most notable effects being changes in temperature, pH, F and SiO₂ concentrations.

Raymond Patrick Maximo, Alain Bernard, Katharine Maussen, Ryan Rebadulla, Ericson Bariso, Deborah Fernandez

Submission 333

Insights into the magmatic-hydrothermal activity using major and trace elements and isotopic values of thermal spring waters from active volcanoes in the Philippines.

Geochemical surveys on thermal waters discharging from three geochemically distinct active volcanoes in the Philippines were carried out between 2014 and 2016. Thermal spring waters were collected from Kanlaon, Bulusan and Biliran volcanoes for chemical and isotopic analysis. Geochemical monitoring of these thermal springs can be used in short- and medium-term eruption forecasting.

Kanlaon volcano is linked to the coexistence of two hydrothermal systems evolving independently from each other, one being mature and the other being immature. The mature hydrothermal system known as Pataan is characterized by neutral Na-K chloride fluids whereas the immature system represented by Hagdan hot springs indicates the presence of acid sulfate waters. The heavy sulfur isotopic value of Hagdan hot spring ($\delta^{34}\text{S} = +8.2\text{‰}$) could reflect some magmatic contribution for the second hydrothermal system.

On the other hand, Bulusan hydrothermal system is characterized by neutral-pH thermal spring discharges (temperatures 42-) and chloride (Cl^-) compositions, thermal springs in Bulusan volcano can be classified into two categories: Group I, which are springs that show positive correlation with a possible hydrothermal end member, and Group II, which are springs that may have formed by simple dilution or mixing of two end-members, meteoric water and sea water.

Finally, Biliran volcano presents a significantly large magmatic-hydrothermal system, which is characterized by the presence of three categories of fluids: acid-sulfate-chloride, acid-sulfate (steam heated) and mixed fluids. Acid-sulfate-chloride fluids which are found near the summit of Biliran volcano, has an important influence in the magmatic degassing history resulting in strongly acidic pH values (pH 34S values (+16.5 to +26.6‰)). Acid-sulfate (steam heated) fluid is characterized by lighter isotopic composition ($\delta^{34}\text{S} = -5.2$ to -3.0‰), which excludes a magmatic origin for the sulfate ions. Lastly, the mixed fluids that are formed by the dilution of meteoric water and neutralization of acid-sulfate-chloride fluids with the surrounding rocks during lateral flow. They are characterized by near-neutral pH (pH ≈ 6.3), high concentrations of bicarbonate ions and similar isotopic values as the acid-sulfate-chloride fluids.

Gari Mayberry, David Ramsey, John Pallister

Submission 522

The Volcano Disaster Assistance Program's Performance Monitoring and Evaluation System: Coordinating, Capturing, and Communicating Progress in Building the Capacity to Respond to Volcanic Crises

August 2016 marked the 30th anniversary of the Volcano Disaster Assistance Program (VDAP), which is a joint project between USGS and the US Agency for International Development (USAID) with the goal of reducing loss of life and property from volcanic eruptions by responding to requests for emergency and non-emergency technical assistance and helping counterparts build capacity and awareness. One challenge of successfully administering a long-term interagency scientific program like VDAP is in quantitatively measuring progress towards achieving capacity building and crisis response goals and in effectively coordinating and communicating results to the respective scientific and humanitarian/civil protection funding agencies. VDAP began with about 5 team members in 1986 and has grown to more than 20 staff. Over time, changes in staffing and program direction, as well as the growth and maturation of partners' volcano hazard institutions, have made program management more complex than when VDAP began. Starting in 2014, VDAP began systematically capturing performance-monitoring information about VDAP activities. Performance monitoring is the ongoing systematic tracking of information relevant to strategies, projects, and activities. Monitoring data are used for learning, adaptive management, and accountability, all of which are important to achieving the goal of reduced loss of life and property. VDAP's Monitoring and Evaluation (M&E) team has been collecting monitoring data using 21 output and outcome indicators that VDAP staff have been reporting on for over a year. The monitoring data includes indicators that were designed to capture information about the quality of VDAP's crisis responses and capacity-building activities in order to communicate program progress with USAID, improve VDAP's performance by applying lessons learned from past responses, and share best practices with counterparts in volcano hazard institutions to improve crisis responses. Monitoring and evaluation activities add a significant amount of additional work for a program of VDAP's size, but M&E is recognized by the team as worthwhile for evaluating and improving performance internally, and demonstrating VDAP's effectiveness to the funding agencies that have different cultures and missions.

Klaus Mayer, Cristian Montanaro, Roberto Isaia, Marceau Gresse, Bettina Scheu, Tim Yilmaz, Jean Vandemeulebrouck, Tullio Ricci

Submission 730

On the role of the subsoil on surficial degassing processes at Solfatara crater, Campi Flegrei caldera

The Solfatara area and its fumaroles are the main surface phenomena of the vigorous hydrothermal activity within the active Campi Flegrei caldera system. A range of volcanic and structural processes dictate the actual state of the hydrothermal system below the crater. The presence of a large variety of volcanic products at shallow depth (including pyroclastic fallout ash beds, pyroclastic density current deposits, breccias and lavas), and the existence of a maar-related fault system appears to have a major control on the degassing and alteration behavior. In this already very complex environment the subsoil and its variation in permeability and porosity may additionally control the fluid flow toward the surface due to soil lithology and alteration effects.

Here, we report results from a field campaign conducted in July 2015, which aimed to characterize the in-situ physical (temperature, humidity) and mechanical (permeability, strength, stiffness) properties. The survey also included a mapping of the surficial hydrothermal features. Laboratory measurements (porosity, granulometry) of selected samples were also performed.

Results show that the crater floor area comprises very different kinds of soils, from fine grained, thin laminated deposits around the two bubbling Fangaia mud pools, to crusted hummock formations along the eastern border of the crater. A silica flat area is present in the western and southern part. Furthermore, we observed indication of an early-stage crust formation within the central part of the crater. Generally, the subsoils show alternation of levels with very high to very low permeability which seems to affect both the temperature distribution and the surficial degassing. A large range of surface temperatures, from boiling point to ambient temperature, were measured throughout the studied area. In the subsoil the distribution of temperature is more complex and is controlled by the presence of coarser, and more permeable sandy/pebbly levels. These act as preferred pathways for the circulation of hot hydrothermal fluids. On the contrary low permeability, fine-grained levels act as thermal insulators that remain relatively colder, and hinder the fluid escape to the surface. Hot gases mostly reach the surface along (vertical) fractures; when this happens, mound-like structures can be formed by a cracking and healing process, allowing significant degassing.

Jerome Mayeux, Barbara Tripoli, Michael Manga

Submission 588

Effect of deformation on the crystallization kinetics of magmas

Crystals and bubbles nucleate and grow in a magma that experiences a range of temperatures, pressures and strain-rates. We have a good conceptual and sometimes quantitative understanding of how crystallization and bubble nucleation are controlled by decompression and cooling. However, the effect of strain rate on the crystallization kinetics of magmas is at present poorly constrained.

In order to understand the interaction between deformation and crystallization, samples of basalt were deformed during their crystallization. We made measurements at subliquidus conditions (1080 - 1175°C) and deformed samples in compression at strain rates varying from 0 to $2 \cdot 10^{-4} \text{ s}^{-1}$ for a total strain of 0.31. We simultaneously imaged the samples using X-Ray micro-tomography at the Advanced Light Source, Lawrence Berkeley National Lab.

Under static conditions, there was no crystallization during the 260 minutes experiment. By increasing the strain rate to $1.0 \cdot 10^{-4} \text{ s}^{-1}$, crystallization occurs. However, the crystallization kinetics in our experiment does not depend on the strain rate. We hypothesize that deformation decreases the induction time for crystallization by affecting the diffusion coefficient, the activation energy and/or the activation volume for kinetics.

Agnes Mazot, Bruce Christenson, Tony Hurst

Submission 1179

Using a Tunable Diode Laser method for a better understanding of CO₂ degassing from New Zealand volcanic lakes

The Tunable Diode Laser (TDL) spectroscopy method has been used for monitoring CO₂ degassing in volcanic areas in New Zealand. The purpose is to have a better knowledge of the spatial and temporal dynamics of CO₂ degassing from volcanic lakes into the atmosphere, which can be used to monitor the underlying volcano-hydrothermal system. Examples from the crater lakes of Mt Ruapehu and White Island are presented.

Frequent mild-to-moderate explosive eruptions have occurred in historical time from the crater lake of Ruapehu with the last hydrothermal eruption occurring in September 2007. The pH of the lake is around 0.9 with lake temperatures ranging from 10 to 60 °C. The results from the TDL measurement campaign conducted on the 23 May, 2012 over Ruapehu's crater lake (630 m line distance) showed that the CO₂ concentration there was higher (420-470 ppm) than the CO₂ background (~400 ppm) measured well outside the volcanic lake. The method showed that CO₂ degassing was present over the lake and confirmed by CO₂ emission measurements (48 ± 2.6 t/day) made on 5 May, 2012 from an airborne platform at a constant distance from the summit.

The most recent eruption at White Island in April 2016, was a phreatic explosion through the shallow acidic (pH 2 concentration measurements were made above the active crater in April 2014 over a length of 729 m, when the crater lake was still present. The results showed CO₂ concentration up to 490 ppm above the crater. Airborne CO₂ emission measurements made in November 2013 and July 2014 showed an average value of 1400 t/day. The TDL method showed that even at a long distance measurement the mean CO₂ concentration was still higher than the mean CO₂ (~400 ppm) measured outside the volcano.

Rapid CO₂ concentration changes recorded above these lakes during surveys are caused mainly due to pulses of gases into the volcanic lakes, which are frequently observed as upwelling. Measuring CO₂ concentration using TDL technique and applying 2D and 3D tomography could help understand CO₂ degassing behaviour associated with the pulses at the surface of the lakes. A 2D tomographic reconstruction using CO₂ concentration data from forty-four paths performed at a small area of Wairakei geothermal field, highlighted different steaming areas. As a monitoring technique, TDL surveys could help discriminate between normal temperature and degassing cycles versus unusual gas discharges that could lead to phreatic eruption.

Agnes Mazot, Bruce Christenson, Brad Scott

Submission 1172

Mini-DOAS data processing for SO₂ emission measurements and monitoring volcanic degassing on White Island (Whakaari), New Zealand

Gas monitoring of New Zealand's active volcanoes has relied heavily on measuring volcanic gas emission by campaign and semi-continuous methods, with our most successful campaign method based on SO₂ emission rates using COSPEC. In June 2006, GeoNet installed two scanning mini-DOAS at White Island offering semi-continuous SO₂ emission data.

In 2010, we developed a new processing system for the mini-DOAS data using the DOASIS software package customised with Javascript code. The application allows processing to be almost fully automated, and calculates SO₂ emission rates for a wider range of wind directions by using plume modelling.

SO₂ emission data from the above analysis method is examined from 2006 to 2017. Volcanic unrest started at White Island in May 2012, 3 months before eruptions started in August 2012 with lake level decreasing and volcanic tremor increasing. From November 2006 to October 2011, the average SO₂ emission was about 100 t/day with a maximum of 300 t/day. From October 2011 to 4th August 2012 the average SO₂ emission increased to a mean of 430 t/day, with a maximum flux of 1500 t/day (19th June 2012). A small eruption with ash emission occurred on the 5th August 2012. Following the eruption, SO₂ emission ranged from less than 200 t/day to more than 400 t/day. In November 2012 a small lava extrusion appeared, followed by phreatic, steam driven activity in December which continued through January and February 2013. SO₂ emission in 2013 was lower than 2012 but higher than the emissions in pre elevated unrest and eruptions, going from 150 to 607 t/day only a few days before the 20th August 2013 eruption. Volcanic tremor remained at an elevated level until a moderate eruption occurred on 11th October 2013. Two days before the eruption, SO₂ emission increased up to 1000 t/day and was following the same trend as the increase in volcanic tremor. Tremor started to increase again in October 2015 and the lake level decreased at the beginning of April 2016. An eruption occurred on the 27th April 2016 with surge and ballistic phases. Before the eruption SO₂ emission ranged from 150 to 500 t/day. Currently, SO₂ emission has been fluctuating between less than 100 t/day to more than 700 t/day, due in part to the changes the April 2016 induced (removal of shallow crater lake) and also changes in the volcanic-hydrothermal system.

Julian McAdams, Josef Dufek, Joshua Mendez

Submission 649

Understanding the Dynamics of Bomb Sags: A High Velocity Impact Experimental Approach

Understanding the processes that occur during phreatic volcanic eruptions is key to decreasing risk of physical and cultural impact in areas of high human population density. Phreatic eruptions occur when magma interacts with ground or surface water and creates a rapid expansion of steam. These eruptions have the potential of being the most disastrous natural events due to their unpredictability and the large amounts of mass ejecta released in short timescales.

Impact craters originating from ballistically ejected lithics during phreatic eruptions regularly create sag-like features, known as “bomb sags”, in the underlying strata. Previous studies have related size, depth, composition, and grain size of these bomb sags to atmospheric density during eruption, assuming the ballistic impacts occur at terminal velocity. Furthermore, cohesion of the underlying strata is also key to understanding the observed bomb sag morphology, hence deciphering their impact dynamics.

To assess the effects of bed cohesion, we performed a series of experiments using a custom made air cannon and an impact bed comprised of spherical glass beads. Experiments are performed for both a dry and fully saturated bed using three varying grain size ranges and four impactors that vary in size and density. Impact velocity is observed by use of a high speed camera. Depth of impact measurements are made post impact as well as photo measurements of crater diameter.

Initial results show a significant diminution in the mass of ejecta when impacts occur in saturated media versus dry media. Cohesion of the impact bed alters the morphology of the impact crater and in some cases, depending upon level of saturation, increases the slope of the sag layer to create steep crater walls. Here we establish, a key relationship between velocity and depth of impact across each impact regime.

Results from experiments will be compared to an Eulerian-Eulerian-Lagrangian discrete element model utilizing similar parameters to that of the experiments. Ultimately, this model combined with experimental results will allow for the derivation of an ideal relationship of all parameters associated with impacts in dry and saturated media. This relationship will allow velocity and impact force of volcanic bombs during phreatic eruption to be back-calculated from observed deposits. This information is key to risk assessment and may help improve resilience to future phreatic events.

Wendy McCausland, Randall White

Submission 845

A Process-based Model of Pre-eruption Seismicity Patterns and its use for eruption forecasting at dormant stratovolcanoes

Forecasting the size, timing and style of volcanic eruptions is of primary interest to volcano observatories and civil authorities worldwide, yet long-term monitoring data and detailed eruptive histories are not available for most volcanoes. In such cases, many volcano observatories and the USAID-USGS Volcano Disaster Assistance Program (VDAP) have utilized extensive collective experience with geologic, geochemical, geodetic and seismic data over multiple eruption cycles and across volcano types to successfully forecast eruption size, style and onsets, as well changes in eruptive style and vigor within ongoing eruptions. We will show that seismic data, usually the longest term real-time monitoring data available at the majority of volcanoes worldwide, is a proxy for rate-dependent changes in the magmatic system from deep magmatic input to shallow eruptive processes. From observations of seismic signals prior to and during more than 60 eruptions at more than 45 volcanoes worldwide, we have developed a 4-stage process-based conceptual model based on Fournier's (2007) geologic model and Hill's (1977) fault-fracture mesh model that, when applied to the seismic data both prior to, and during volcanic eruptions, enables volcano seismologists to forecast eruptive style, size, and timing, especially for stratovolcanoes that have been dormant more than 20 years. We will describe each of these four stages of seismicity (deep, distal, vent-clearing, and repetitive) using examples from 25 eruptions at 21 well-monitored volcanoes.

Interfacing Science with Government: You Don't Always Get What You Want

Vicki S. McConnell

Plenary Talk

Science, government, and policy have long been strange and tumultuous bedfellows. Frequently neither sees the need for the other. Scientists think that all you need are the facts and the data and a clear decision can be made and implemented. Policy/government includes complex issues, multiple stakeholders, and a need to solve vexing problems in a limited timeline. You may or may not consider facts useful.

Policy making means bringing stakeholders together to solve problems or enact actions through developing guiding principles. Policy issues can be emotional and very personal to stakeholders and facts may appear to be antithetical to their ideas of what would be sound policy.

In the framework of government, science is generally considered a tool to making decisions and setting strategies, not the center point. Scientific advice is important but it isn't the only advice or advisor that will come into play. Economics and law will direct decision-making as well.

Timelines are usually drastically different with the policy-maker wanting relatively rapid information and actions and scientists seeing the long views and the need for "more data". These timeline discrepancies can spoil a fruitful collaboration if neither side is willing to hedge. In particular a scientist participating in policy decision making must be able to work with the data available or be able to explain why actions cannot be made now that might save lives or money.

A scientist will express uncertainty when explaining data and information as a primary part of ethical scientific behavior but this can be unduly confounding to decision makers. It is not that a government/policy-maker doesn't understand uncertainty, the scientific uncertainty should be clear.

Societal problem solving that includes science in the policy discussion and solutions that make sense in the natural world require both sides clearly articulate their needs and expectations. It is most helpful when the scientist and the policy-maker can view the problem through the other's lenses and communicate that way.

There are myriads of examples of successful and unsuccessful science and government interface in the natural hazards realm. My experiences have been that you have to keep the communications clear and open, be respectful at all times, provide relevant information, and accept that you can't always get what you want; but you might get what you need.

Lucy McGee, Heather Handley, Mark Reagan, Simon Turner, Kim Berlo, Michael Turner, Jenni Barclay, Steve Sparks

Submission 613

Testing the mafic trigger hypothesis at Soufriere Hills Volcano, Montserrat, using short-lived U-series isotopes

A prominent hypothesis for triggering large explosive eruptions is mafic recharge. The input of new mafic magma contributes heat and volatiles, which can lead to destabilization and overpressure. Evidence for this process includes the occurrence of mafic enclaves in silicic volcanic rocks. Ratios between short-lived isotopes in the uranium series decay chain (^{226}Ra - ^{210}Pb) can be used to investigate the relative timing of mafic recharge versus eruption and the timescale over which volatile transfer occurs prior to eruptions.

^{210}Pb - ^{226}Ra disequilibria can be used to trace gas movement within recently erupted (^{222}Rn) partitions into the gas phase of magmas. Consequently, excesses of ^{210}Pb (which has a half-life of 22 years) relative to ^{226}Ra in recently erupted rocks constrain the longevity and extent of gas transfer prior to an eruption. Deficits indicate persistent open system degassing of the magma, and equilibrium values suggest any significant gas transfer occurred more than several decades before eruption.

Soufriere Hills Volcano (SHV) on the island of Montserrat is the ideal place to test the theory that gas transfer from mafic material at depth triggers explosive eruption of silicic lavas, as it has been in a state of eruption since 1995 and is monitored by the Montserrat Volcano Observatory. Basaltic enclaves are a notable feature within andesitic dome material and have been well-characterised by recent studies. Nearly all measured ($^{210}\text{Pb}/^{226}\text{Ra}$) for enclaves from all five recent eruption phases were recently enriched in gasses, displaying elevated ($^{210}\text{Pb}/^{226}\text{Ra}$) ratios up to 2.2. In contrast, andesites have both excesses and small deficits with respect to ^{226}Ra . We observe a possible shift to lower ^{210}Pb -excesses from phase III onwards which coincides with changes in eruption characteristics, modal mineralogy and lava composition.

Our current work involves the analysis of cm-scale blocks through a sample of a phase V andesite and enclave in contact in order to assess (1) whether the enclave has ^{210}Pb excess indicating recent gas fluxing, (2) if a gradient of ^{210}Pb excess exists from enclave to host and (3) if so, the timescale over which gas is transferred from one to the other. This study has the power to show whether the incorporation of recently gas-charged mafic material is the effective trigger of explosive eruptions at SHV and potentially elsewhere.

Patrick McGovern

Submission 1200

Intra- and Trans-(Impact)-Basin Igneous Provinces on the Terrestrial Planets.

Impacts and volcanism are two fundamental processes that shape planets. Both provide inputs of material and heat to planetary crusts (although post-accretion impacts mostly remove or redistribute the former), and both are fundamental mechanisms of resurfacing well represented in the broad spans of history preserved on “one-plate” planets (those lacking plate tectonics). Recently, several prominent volcanic provinces associated with the margins of large impact basins have been identified and characterized. Further, new insights into impact and volcanic systems gained through analysis of high resolution datasets and advanced physical modeling of processes allow a thorough rethinking of the relationships between impact basins and volcanic systems that cover and flank them. Moon: The dark basaltic mare units are the most obvious expression of volcanism on the Moon. A large volume of mare material fills the large impact basins of the lunar nearside (Nectaris, Crisium, Serenitatis, and Imbrium), thus they constitute Intra-basin Igneous Provinces (I-BIPs). However, the vast Procellarum region is also covered by mare, and views of that region as a relict giant impact have been challenged by an alternative primordial thin-crust, magmatic rift-bounded zone. Stress modeling indicates that the lithosphere’s flexural and membrane responses to basin-filling loads enhances subsequent magma ascent in annular regions around the basins. While strictly annular zones of volcanism are not seen surrounding lunar basins, local mare regions such as Mare Tranquillitatis occur between basins, and thus we dub them Trans-basin Igneous Provinces, or T-BIPs. Mars: Most of the largest impact basins on Mars have large volcanic constructs and provinces associated with their margins in T-BIP style. Such pairings include [Hellas:Circum-Hellas Volcanic Province], [Isidis:Syrtis Major], [Utopia:Elysium Rise]. The locations of martian T-BIPs, which are not annular but occur at discrete locations on basin rims, may be structurally controlled by a combination of regional-scale tectonic and local-scale loading stress states. Only the Utopia and Isidis basins have infill large enough to be considered I-BIPs, although non-volcanic material (e.g., sediments) may contribute a substantial amount at the former. Mercury: the relatively young plains surrounding the Caloris basin may constitute a loading-stress-facilitated T-BIP, with a much more annular nature than the localized T-BIPs on the Moon and Mars.

Iona McIntosh, Alexander Nichols, Kenichiro Tani, Ed Llewellyn

Submission 560

Accurately measuring H₂O in volcanic glasses: application of a new FTIR spectroscopy method

Volcanic eruptions are driven by the exsolution and bubble growth of magmatic volatiles, of which water is particularly important due to its abundance and strong control on parameters such as melt viscosity. Dissolved magmatic water content changes throughout magma ascent, eruption and emplacement, and snapshots of this evolution are preserved in the dissolved water contents of volcanic glasses, which include both melt inclusions in crystals and matrix glasses in pyroclasts, dome rocks and lavas. These glasses record not only the total dissolved water content (H₂O_t), but also the water speciation, i.e. the amount of water dissolved as molecular water (H₂O_m) versus hydroxyl groups (OH). These H₂O speciation data are widely used to investigate the pressure-temperature-time histories of volcanic products, and are obtained using Fourier transform infrared spectroscopy (FTIR). We present here a new FTIR method that improves the accuracy, hence interpretation, of these data, and highlight its potential for reconstructing the original H₂O_t contents of hydrated glasses.

Due to the weak intensities of the near-IR water absorption peaks, many FTIR analyses of volcanic glasses must use the mid-IR 3500 cm⁻¹ H₂O_t and 1630 cm⁻¹ H₂O_m peaks, with OH concentration found indirectly as $OH = H_2O_t - H_2O_m$. However, large errors in H₂O_t and OH concentrations can occur due to the use of a fixed 3500 cm⁻¹ H₂O_t molar absorptivity coefficient (ϵ_{3500}), when ϵ_{3500} in fact varies with H₂O speciation. Our new method is a modified version of the Beer-Lambert law (which converts absorbance into concentration) that accounts for the species-dependence of ϵ_{3500} , without the need to know H₂O speciation a priori. This method requires no special equipment or procedure, and can also be used to reprocess existing FTIR data.

We demonstrate the improved accuracy of H₂O_t and OH concentrations obtained using this method, and present applications including H₂O diffusion profiles, melt inclusions, and hydrated glasses. FTIR (unlike other techniques that measure only H₂O_t) can identify hydrated glasses by their elevated H₂O_m contents, since low temperature hydration adds the diffusive species H₂O_m without altering OH. This 'disequilibrium' speciation makes the species-dependent ϵ_{3500} method critical for hydrated glasses. Moreover, by combining accurate OH contents of such glasses with existing models of H₂O speciation, we show that it is possible to reconstruct their original, pre-hydration H₂O_t contents.

Kathleen McKee, David Fee, Matthew Haney, John Lyons, Robin Matoza

Submission 551

Infrasound signal detection and characterization using ground-coupled airwaves on a single seismo-acoustic sensor pair

Here we aim to develop a minimalist infrasound signal detection and characterization technique requiring just one microphone and one three-component seismometer. Ground-coupled airwaves (GCA) are commonly sourced from volcanic eruptions, bolides, meteors and explosions and detected 100s of kilometers away across seismic networks and infrasound arrays. GCAs occur when an incident atmospheric pressure wave encounters the Earth's surface and part of the energy of the wave is transferred to the ground (i.e. coupled to the ground) as a seismic wave. This seismic wave typically propagates as a Rayleigh wave evidenced by the retrograde particle motion detected on a three-component seismometer. When these acoustic waves propagate along the surface exciting the assumed dominant Rayleigh waves in the subsurface and are recorded on a collocated microphone and seismometer, they can be coherent and have a 90° phase. If the sensors are separated, usually 10s to 100s of meters, then recorded wind noise becomes incoherent relative to wind speed and frequency and an additional phase shift is present due to the separation distance.

Determining a source azimuth should be possible using a single seismo-acoustic sensor pair by utilizing the phase difference, coherence, and exploiting the characteristic particle motion. The phase difference from 90° depends on the direction the pressure wave arrives from, as each back-azimuth will have a different apparent distance between the sensors. However, the apparent sensor separation determined from the additional phase alone does not provide a unique source azimuth. In turn, we incorporate the arrival times and particle motion to determine a unique solution. Here we use synthetic seismo-acoustic data generated by a coupled Earth-atmosphere 3D finite difference code to test and tune the detection and characterization method. These simulations have the expected high coherence, 90° phase and elliptical retrograde particle motion. The method is then further tested using various well-constrained sources (e.g. Antares Rocket, Chelyabinsk meteor, Pagan and Cleveland Volcanoes) and existing high signal-noise data (e.g. EarthScope Transportable Array, IMS infrasound network, USGS volcano monitoring networks). Our proposed technique would provide a new method to detect infrasound signals and determining the back-azimuth, and would be particularly useful in situations where resources are limited and large sensor networks or arrays are not feasible.

Danielle McLean, Paul Albert, Victoria Smith, Takeshi Nakagawa, Takehiko Suzuki, Keitaro Yamada, Ikuko Kitaba, SG14 Project Members

Submission 1025

Resolving the tempo of Holocene volcanism in East Asia using the Lake Suigetsu record (central Japan)

Proximal pyroclastic successions are typically used to establish the magnitude, tempo and recurrence intervals of past volcanic events. The stratigraphy and detailed mapping of these deposits, including ash fall, directly feeds into hazard and risk assessments for heavily populated regions. Unfortunately, proximal records can often be incomplete due to erosion or burial by more recent activity. Furthermore, proximal outcrops can lack the appropriate material for radiometric dating, necessary to reliably constrain the tempo of activity. Lacustrine cores from low energy environments are often underexploited archives of past explosive events, allowing smaller eruptions that are closely spaced in time to be distinguished, and thus used to better constrain the chronology and magnitude of activity.

The Lake Suigetsu core, obtained from a small tectonic lake in central Honshu, is the most precisely dated sediment record for Japan. Its high-resolution ^{14}C chronology allows us to precisely date the ash layers preserved within the sequence. Four visible layers are identified in the Holocene sediments, and we have used cryptotephra extraction methods to identify a further sixteen non-visible layers from smaller or more distal eruptions. Major element glass geochemistry obtained from these layers is compared to new and published proximal datasets to correlate them to their volcanic sources. These ash layers originate from numerous explosive eruptions from northern (Hokkaido) and southern (Kyushu) Japan, and notably other volcanoes to the west, such as Ulleungdo Island (South Korea) and Changbaishan (North Korea/China). The Lake Suigetsu chronology provides improved relative and absolute chronological constraints for the majority of the ash layers identified, which can be exported into proximal records to better constrain the tempo of activity, including repose intervals. This record indicates the region was covered by ash fall every 500 years. The presence of many of these tephra layers in the core considerably extends the known ash dispersal of the eruptions, for example, the archive provides the most southerly occurrence of ash fall from the highly-explosive Changbaishan 'Millennium' eruption. This new integrated tephrostratigraphy establishes the Lake Suigetsu archive as a comprehensive Holocene record of volcanism for East Asia, and highlights that distal tephrochronology can provide detailed information to refine hazard assessments in this heavily populated region.

Claire McLeod, Jon Davidson, Shanaka de Silva

Submission 518

Probing the Depths of Continental Arc Magmatism: Insights from the Minor Volcanic Centers of the Bolivian Andes

Keri McNamara, Karen Fontijn, Katharine Cashman, Alison Rust, Amde Micheal Zafu, Gezahegn Yirgu, Françoise Chalie

Submission 47

Constraining the Holocene eruptive history of Aluto volcano in Ethiopia

Ethiopia is home to around 60 volcanoes, many of which are fed from the Main Ethiopian Rift (MER), a northern section of the East African Rift System (EARS). A recent report on volcanic hazard for the World Bank has classified many of these volcanoes at the highest level of uncertainty due to the deficit of data in the region. Many of the volcanoes are populated and therefore understanding their eruptive history is important for hazard mitigation.

One such populated MER volcano that has been actively deforming is Aluto. We are examining the Holocene tephra record of this volcano that is preserved in lake beds (both in cores and now on land). The record displays at least 23 distinct eruptions in this period, highlighting the need to determine a robust eruption history.

We are addressing this by using tephtras to reconstruct the size and frequency of such Holocene eruptions by correlating deposits and analysing lake settling processes. The thickness and structures of deposits has been considered in the context of the lacustrine depositional environment in order to understand the secondary processes affecting the tephtras.

In addition, traditional methods of tephra correlations using glass major element geochemistry have proved somewhat ineffective for this volcano as the environment of preservation is shown to have an effect on major element concentrations. Alternative approaches were therefore adopted using textural morphology and componentry in combination with trace element geochemistry. This was applied within a ^{14}C dated sequence and combined with grain size data to inform the timing and size of previously unstudied eruptions. Our reconstruction of the frequency of these eruptions defines two main periods of activity in the mid and late Holocene- an observation that has important implications for hazard forecasting and management.

James McNeal, Graham Freedland, Larry Mastin, Raul Cal, Stephen Solovitz

Submission 423

Experimental insights into the role of turbulence in the entrainment and height of weak volcanic plumes

Volcanic eruptions can release significant amounts of ash into the atmosphere, impacting regions hundreds to thousands of kilometers away. Ash dispersal models are used to predict the location of ash clouds, but their accuracy depends strongly on estimates of the mass eruption rate (MER). The MER can be estimated using simplified one-dimensional models, which rapidly determine the exit parameters based on observed plume height H , known atmospheric conditions, and assumed vent and magma properties. However, these models require empirical entrainment coefficients for the vertical plume and the cross flow, α and β , whose accuracy and overall basis need refinement. We use wind tunnel measurements of jets in a cross flow, considering Reynolds numbers on the order of 10^3 to 10^5 and bulk jet-to-ambient velocity ratios from 5 to 40. In addition, we examine ambient flows with significant freestream turbulence. We conduct particle image velocimetry (PIV) measurements to determine the full-field, two-dimensional, instantaneous velocity fields in the symmetry plane to high accuracy. We calculate plume trajectories, flow profiles, and turbulence statistics from these flow fields, and we compare their behavior with the open-source plume model Plumeria. Our estimates of the entrainment coefficients, with $\alpha \sim 0.09$ and $\beta \sim 0.6$, agree reasonably with legacy data. However, the modeled trajectory has a significant offset in the near-exit region, likely due to the initial jet development. In addition, the cross flow coefficient shows some dependence on ambient turbulence, increasing the entrainment and lowering final plume trajectory.

Stephen McNutt, Glenn Thompson, Jochen Braunmiller, Stephen Holtkamp

Submission 1021

Peak Rates and Largest Magnitude Events in Volcanic Earthquake Swarms and Mid-Ocean Ridge Swarms

We present results of recent studies of volcanic earthquake swarms, with the focus on identifying diagnostics. One clear pattern is that peak rates often occur early in swarms, whereas the largest M event occurs late. Using a dataset of 20 swarms from the literature, swarm durations ranged from 12 h to 6 mos, measured from swarm onset to eruption onset. Data were normalized to percent duration. Peak rates occurred from 1-42 percent of the way through swarms (with 2 outliers), whereas the largest M event occurred from 32-99 percent of the way through. Additional evidence from 4 cases suggests that the seismic source size grows systematically, especially for events with similar waveforms (families). This is revealed in plots of M or amplitude versus time for event families. For comparison, 19 cases of mid-ocean ridge swarms were analyzed. These show durations of 1-42 days, with peak rates occurring 1-24 percent of the way through and largest M occurring 1-87 percent of the way through. In 6 cases largest M occurs before or at the same time as peak rate. Thus the pattern for MOR swarms differs significantly from that for volcanic swarms. Further work on volcanic swarms shows that the distribution of seismicity before the peak rate differs from after, suggesting two dominant processes. The durations of post-peak portions are roughly proportional to the peak rates. This is similar to the behavior of aftershock sequences and suggests that diffusion is a controlling process. The portions of the swarms prior to the peaks behave differently, however. These may represent the invasion of hot fluids and the opening or reopening of cracks prior to magma intrusion. We infer that the growth in event size reflects activation of a preferred magma pathway. Recognition of such patterns, linked to processes, may help to improve monitoring and reduce risks from eruptions.

Stuart Mead, Jonathan Procter

Submission 897

Comparing predictions of run-up and superelevation of the 2012 Upper Te Maari debris flow with analytical and numerical models

The accurate estimation of run-up and superelevation by numerical and analytical models is crucial for understanding the likelihood of debris flows overtopping topographic barriers, breaching protective structures or breaking the confines of channel banks. Run-up occurs when a debris flow encounters a roughly perpendicular topographic obstacle (e.g. ridges, channel side walls, dam) in its path. Superelevation occurs when the debris flow free surface is elevated on the outer bank of channel bends due to inertia of the debris flow. Run-up and superelevation heights have frequently been used to estimate flow velocities and infer the behaviour of debris flows (e.g. Pierson 1985; Sheridan et al. 2005; Procter et al. 2014) through the use of simple using analytical models. These post-event estimates of velocity, if accurate, can be used as validation points for numerical debris flow models. However, the validity of analytical models are limited by broad assumptions of flow criticality, frictionless energy transfer, uniform densities and one-dimensional flow (Pierson 1985; Iverson et al. 2016) and the estimates typically represent minimum emplacement velocities of mudlines (Pierson 1985; Procter et al. 2014).

This study focuses on the 2012 debris flow from the Upper Te Maari crater, Tongariro Volcano to investigate analytical run-up and superelevation models, compare velocity estimates to several debris flow numerical models and assess the utility of run-up predictions for the validation of numerical models. The Te Maari debris flow provides a well constrained and documented test bed to assess the utility of run-up height estimates from analytical models, compare and validate numerical models against the complexities of a real-world unsteady, inhomogeneous and three-dimensional debris flow. Analytical estimates of debris flow velocity, in addition to other metrics such as deposit depth, are used to compare several debris flow numerical models in order to highlight the strengths and weaknesses of each model when applied to debris flows.

Ezequiel Medici, Gregory Waite

Submission 1248

Scaling analog shock tube experimental observations to model explosive volcanic eruptions

Analog shock tube experiments can provide fundamental insight into the complex fluid dynamics and thermodynamics of explosive volcanic eruptions. A unique feature of shock tubes is their ability to suddenly accelerate a volume of fluid (liquid, gas, solid particles or a mixture of them), as observed in explosive volcanic eruptions, under controlled laboratory conditions. These experiments allow for a broad range of instrumentation and measurements such as pressure, velocity, acceleration, and temperature among others. Shock tube experiments can also provide proximal visual access to the accelerated fluid volume. These experimental observations are essential to determine the dominant physical processes of each stage of explosive eruption. The challenge is to extrapolate those experimental observations to actual explosive volcanic eruptions. The proper procedure to link analog shock tube experimental observations with actual explosive volcanic eruptions is through a scaling analysis of the most relevant physical parameters such as densities, viscosities, diffusivities, heat capacity ratios, velocities, sizes, temperatures, and pressures among others. Classical fluid dynamics and thermodynamics provide the theoretical scaling analysis that takes those physical parameters and combines them into dimensionless numbers. In this work, the dimensionless numbers needed to compare analog shock tube experimental observations and explosive volcanic eruptions are discussed and used to scale our experimental results.

Elena Melekhova, David Schlaphorst, Jon Blundy, Michael Kendall

Submission 404

Geophysical and petrological constraints on crustal structure variation along the Lesser Antilles arc.

The Lesser Antilles volcanic arc is distinguished by a wide range of magma types generated contemporaneously along strike and unusually abundant plutonic xenoliths, many with cumulate textures. Some volcanic centres (e.g. St. Vincent, Grenada) have erupted high-MgO basalts, which approximate primary magmas from the mantle wedge. Experimental petrology of such magmas provides insights into differentiation processes that gave rise to more evolved magma types. Experiments on a primitive St. Vincent basalt show clear relationships between the proportion and composition of the extracted melt, the cumulate mineral assemblage and the dissolved H₂O content of the parental basalt. For each experimental run product we calculated the seismic velocities of the solid residue (lower crustal layer) and of the solidified extracted melt (upper crustal layer) to explore variations in the depth and magnitude of seismic discontinuities within the crust and at the crust-mantle boundary (Moho). For parental H₂O contents ≥ 2.5 wt% the mid-crustal velocity contrast (between upper and lower crustal layers) is greater in magnitude than that at the Moho because the ultramafic cumulates of the lower layer are seismically indistinguishable from mantle peridotite. For H₂O contents ≤ 2.0 wt% give rise to along arc variations in the depth and magnitude of seismic discontinuities.

To test the inference from experimental petrology we used receiver functions, H-k stacking and modelling to investigate variations in crustal thickness and structure along the arc, using the existing network of seismic stations. The conventional H-k stacking approach did not allow us to resolve easily the two crustal layers. To tackle this problem we developed an inversion modelling approach that combines seismological and petrological results. We find that the Moho is the dominant seismic discontinuity from Martinique to the north end of the arc, whereas the mid-crustal discontinuity is stronger from St. Lucia to the south of the arc. The depths to the mid-crustal and Moho discontinuities lie at 10-25 km and 25-35 km respectively, with slightly deeper values for the mid-crustal discontinuity in the north and for the Moho in the south. These variations correlate well with magma and xenolith geochemistry and are ascribed to differences in magmatic H₂O content along the arc.

Gladys V. Melián, María Asensio-Ramos, Cecilia Amonte, Mar Alonso, Marta García-Merino, Fátima Rodríguez, Eleazar Padrón, José Barrancos, Pedro A. Hernández

Submission 1002

Diffuse H₂ degassing emission to monitor changes of volcanic activity

Hydrogen is one of the most abundant trace species in volcano-hydrothermal systems and is a key participant in many redox reactions occurring in the hydrothermal reservoir gas (Giggenbach 1987; Chiodini and Marini 1998). Because of its chemical and physical characteristics such as low weight and low solubility in groundwater and hydrothermal fluids, H₂ moves rapidly within the crust and escapes easily to the atmosphere. These characteristics make H₂ a potentially excellent tracer of processes operating deep in magmatic systems. Most of the diffuse degassing studies on active volcano-hydrothermal systems is mainly focused on CO₂. Unfortunately however, few studies of surface H₂ efflux measurements at active volcanoes have been performed to evaluate diffuse H₂ emission rates from active volcanic systems. Here, we report a time series on diffuse H₂ emission rates from surveys carried out in yearly basis at the summit cone of Teide volcano, where most obvious geothermal features at Tenerife occurs, during the 2006-2016 period. Thousands of samples of volcanic gases from the surface environment, at 40 cm depth, have been collected during this 2006-2016 period to estimate surface H₂ efflux values from 150 observation sites selected to cover the 0.5 Km² area of the summit cone Teide volcano. Most of the surveys showed diffuse H₂ emission rate values lower than 40 kg·d⁻¹ from the summit cone of Teide volcano. On the contrary, an increasing trend of diffuse H₂ emission rate from 35 ± 7 to 122 ± 36 kg·d⁻¹ was observed during the 2006 to 2009 period. This increase trend of diffuse H₂ emission rate was detected before a raise of seismic activity in and around Tenerife from November 2009 to June 2011, with about 1176 seismic events recorded by Spanish-IGN in 2010 (Pérez and Schmincke, 2016). The observed increased trend of diffuse H₂ emission occurs simultaneously with an increase trend of diffuse CO₂ emission at the summit cone of Teide volcano during the 2005-2009 period (Pérez et al., 2013) suggesting the ascent of deep-reservoir (CO₂-H₂-rich) gas bubbles. These geochemical observations seems to be clear evidences of changes of processes operating deep in the magmatic system of Tenerife.

Chiodini and Marini 1998, *Geochim. Cosmochim. Acta*,

Giggenbach 1987. *App. Geochem.*, DOI: 10.1016/0883-2927(87)90030-8

Pérez et al. 2013. *J. Geol. Soc.*, DOI: 10.1144/jgs2012-125

Pérez and Schmincke 2016, *Geophysical Research Abstracts Vol. 18, EGU2016-10379*

Oleg Melnik, Andrey Afanasyev, Ivan Utkin, Yulia Tsvetkova

Submission 228

Brine lens formation above degassing magma chamber

Formation of porphyry-type ore deposits is associated with degassing of crystal magma chambers. Saline rich-in-metals magmatic fluid penetrates into a shallow region saturated with cold meteoric water where the metals concentrate in brine lenses.

In order to investigate lenses formation, we developed an extension of our multiphase simulator MUFITS (www.mufits.imec.msu.ru) for NaCl–H₂O binary mixture flows in a wide range of pressures, temperatures and salinities. A fast method for calculation of the properties of the mixture under sub- and supercritical thermodynamic conditions including three-phase gas-liquid-solid states is developed. We consider a degassing of magma chamber into axisymmetric host rock with a high permeable vein zone in the central part of the domain surrounded by low permeability material. The degassing is simulated as a point source of hot supercritical fluid that ascends rapidly along the vein undergoing the phase transitions. At relatively low pressures the evaporation of H₂O results in enrichment of residual fluid in halite and metals. At a depth of 1–2 km halite precipitation as solid phase blocks the pore space and facilitates formation of concentrated brine lenses.

Results of parametric studies indicate that the size of a brine lens increases with increase in injection temperature of magmatic fluid. At temperatures below ~ 650 oC evaporation of the brine does not lead to precipitation of salt and blockage of the pore space, thus, formation of the concentrated brine lens is suppressed. Low permeability of the host rocks decreases the intensity of meteoric water convection resulting in smaller dilution of magmatic fluid. It favors formation of a larger brine lens.

This work was supported by the Russian Science Foundation under grant RSF-16-17-10199.

Valbone Memeti, Cal Barnes, Kevin Werts, Dustin Williams, Louis Oppenheim, Melanie Barnes, Scott Paterson

Submission 1207

Using mineral geochemistry to unravel waxing and waning magmatism in the Tuolumne Intrusive Complex plumbing system, central Sierra Nevada, California

Long-lived, composite intrusions represent horizontal sections of vertically extensive magma plumbing that preserves the record of compositionally varying and waxing and waning magmatism over millions of years. Quantifying the volumes and sizes of magma batches and potential existence of coalesced, melt-interconnected magma reservoirs from field evidence and whole rock studies becomes increasingly challenging due to overprinting, erosion, and mixing of early magmas by/with later ones. However, mineral compositions and zoning patterns have the ability to record geochemical changes associated with these processes and with fractional crystallization, thereby providing information on the scales of these processes at different stages of magma chamber construction and evolution.

The Tuolumne Intrusive complex (TIC) represents a long lived magmatic system in the upper middle crust. It is composed of three nested major units spanning a 10 myr long crystallization history. The margins of the TIC were constructed by intermediate to mafic, cm- to 10s of meter-scale sheeted intrusive bodies, whereas the younger, interior, homogeneous-looking granodiorite–granite units formed magma bodies at km-scales. Trace elements in calcic amphiboles from the TIC margins (Kuna Crest) and each major interior unit show distinct compositions and zoning patterns that suggest the increasingly larger magma bodies didn't necessarily mix across unit boundaries, but underwent broad intra-unit fractionation. Some mixed hornblende populations occur in transition zones, for example in the boundary between the Kuna lobe and the main TIC. In addition, trace element and Sr- and Pb-isotope data from growth zones of K-feldspar phenocrysts from the interior units indicate complex mineral zoning with overlapping element and isotope values, which suggest both intra- and inter-unit mixing and fractionation and thus extended melt interconnectivity. This is also supported by hybrid transition zones between adjacent units, evidence for mineral recycling by U-Pb zircon geochronology and the presence of local leucogranites.

These preliminary results indicate that for the first 1-2 myr, the TIC grew through the emplacement of small, heterogeneous magma batches resulting in smaller, discrete and none exchanging magma bodies. Subsequent (higher flux?) magmatism resulted in km-scale, more homogeneous-looking bodies with heterogeneous mineral histories, indicating complex and broad interacting magma mushes.

Joshua Méndez Harper, Josef Dufek, Corrado Cimorelli

Submission 1263

What volcanic lightning tells us about the near-vent dynamics

Volcanic plumes are often highly electrified and produce spectacular displays of lightning [Pliny (translation), 2003; Mather and Harrison, 2006; Thomas et al., 2007; McNutt and Williams, 2010; Arason et al., 2011; Nicora et al., 2013; Aizawa et al., 2016]. Observations of eruptions at Augustine, Redoubt, and Sakurajima reveal that volcanic lightning can be classified broadly into three modalities: vent, near-vent, and plume lightning [Thomas et al., 2007; Behnke et al., 2012, 2013; Cimorelli et al., 2016]. Because these electrification mechanisms are thought to be related to the dynamics of the eruption itself, remotely captured lightning signals may serve to extract information about the interior structure of plumes that would otherwise be opaque to observation [James et al., 2000]. While vent and near-vent lightning has been linked to overpressure conditions at the vent, no mechanism has been proposed to quantitatively explain such observations.

To explore near-vent electrical panorama, we employ experimental setups at LMU and Georgia Tech. These state-of-the-art setups are used to generate sonic, energetic flows of ash particles similar to those found in the conduit and gas-thrust region. We demonstrate that 1) the rate and location of vent discharges are closely related to the dynamics of the gas-thrust region upstream of the first normal shock; 2) that normal shocks in jets represent electrostatic barriers that decouple electrostatics process in the conduit from those in the plume; 3) that fracturing of material produces LF radio-frequency emissions that explain the signals detected during explosive phases of the Augustine (2006) and Redoubt (2009) eruptions; and 4) that triboelectric and fractoelectric processes generate vastly different electrostatic responses in terms of discharges.

Ana Teresa Mendoza-Rosas, Ángel Gómez-Vázquez, Servando De la Cruz-Reyna

Submission 1080

Statistical analysis of the lava dome emplacement sequences and dome dimensions at Popocatepetl volcano, central México.

Popocatépetl volcano reawakened in 1994 initiating a magmatic effusive phase that has emplaced a succession of at least 38 lava domes within the summit crater of this volcano rising 5454 m a.s.l. between 1996 and 2015. The domes have been irregularly emplaced and destroyed, with each dome reaching particular volumes and thickness at specific emplacement rates, and remaining for variable times before destruction. This sustained, irregular and non-stationary process is analyzed using statistical methods in an attempt to gain insight into the physics and dynamics of the still ongoing lava dome emplacement and destruction process, and to objectively assess the hazards related to that volcano. The time series of emplacements, dome residences, lava effusion lulls and emplaced dome volumes and thicknesses are modeled using the simple exponential and Weibull distributions, the non-homogeneous generalized Pareto-Poisson process (NHPPP) and the mixture of exponentials distribution (MOED). The statistical analysis of the ongoing episode has allowed to calculate the probability of emplacement of domes exceeding a specified volume in a given time interval, and also to establish objective criteria for recognizing an alteration or a different trend in the non-stationary sequence of emplaced domes that could be indicative of a change in the nature of the process.

Gary Michelfelder, Alicia Wilder, Emily Salings

Submission 1215

Geochemical and Isotopic Data from Micron to Across-Arc Scale in the Andean Central Volcanic Zone: Resolving Crustal Magmatic Differentiation and Modification Processes

Plagioclase phenocrysts from silicic (andesitic to dacitic) lavas and domes at Volcán Uturuncu, a potentially active volcano in the back-arc of the Andean CVZ (22.3°S, 67.2°W), exhibit large variations in An contents, textures, and core to rim $^{87}\text{Sr}/^{86}\text{Sr}$ ratios. Sr isotopic ratios in plagioclase cores record the hybridization and the homogenization of a mid-crustal reservoir. Uturuncu plagioclase cores record initial assimilation of crustal rocks with high $^{87}\text{Sr}/^{86}\text{Sr}$ ratios. These magmas subsequently modified the crust by frequent recharge of a magma with lower $^{87}\text{Sr}/^{86}\text{Sr}$ ratios. Typical Uturuncu silicic magma plagioclase populations are therefore a hybrid of xenocrystic plagioclase and inherited cores from the recharging magma. During the evolution of the system end-member plagioclase core compositions become more similar to the intermediate hybrid.

In the Lazufre region of active surface uplift (~25°14'S; Volcán Lastarria and Cordon del Azufre) closed system differentiation processes are not the only factors influencing silicic magma compositions. $^{87}\text{Sr}/^{86}\text{Sr}$ (0.70651-0.70715) and $^{206}\text{Pb}/^{204}\text{Pb}$ ratios (18.83-18.88) are highly elevated and $^{143}\text{Nd}/^{144}\text{Nd}$ ratios (0.512364 –0.512493) are low relative to similar composition rocks from the "southern Cordillera domain." Mineral chemistry supports a source location at mid crustal levels. These data, along with major and trace element trends, reflect a multitude of differentiation processes and magma sources including crystallization-differentiation of more mafic magmas, melting and assimilation of older crustal rocks, and magma mixing and mingling.

On an arc-wide scale silicic lavas erupted from six well-characterized composite volcanoes between 21oS and 23oS (Lastarria, Lascar, San Pedro-San Pablo, Aucanquilcha, Ollagüe, and Uturuncu) display systematically higher K₂O, LILE, REE and HFSE contents and $^{87}\text{Sr}/^{86}\text{Sr}$ ratios with increasing distance from the arc-front. In contrast, the lavas have systematically lower Na₂O, Sr, and Ba contents; LILE/HFSE ratios; $^{143}\text{Nd}/^{144}\text{Nd}$ ratios; and more negative Eu anomalies. Silicic magmas along the arc-front apparently reflect melting of relatively young, mafic composition amphibolitic source rocks with the continental crust becoming increasingly older with a more felsic bulk composition toward the east. We suggest this results from progressively smaller degrees of mantle partial melting, primary melt generation, and crustal hybridization with distance from the arc-front.

Caroline Michellier, Florian Barette, Sylvain Kulimushi Matabaro, Innocent Kadekere, Marcellin Bahati Bifuko, Delphin Ciza Assani, Fanny Hage, Eléonore Wolff, Matthieu Kervyn

Submission 460

Assessing lava flow risk at Nyiragongo volcano, DR Congo. Part 1: Vulnerability of population and assets in Goma

Goma is a ~ 800,000 inhabitants city, located 15 km south of the Nyiragongo volcano. This volcano last erupted in 1977 and in 2002, each time seriously affecting the surrounding villages and Goma. In 2002, lava flows devastated 10% of the city, not only triggering direct impacts – such as the evacuation of 300,000 to 400,000 people, several tens of fatalities, and the destruction of buildings and roads–, but also inducing long-term economic consequences, such as the International Goma Airport runway reduced by a third of its length for more than 10 years, commercial trading affected, and administrative buildings and archives destroyed.

The GeoRisCA project (Belspo, 2012-2016) has focused on mapping the volcanic risk for the population and assets of Goma by answering the following questions: How exposed are population, lifelines and buildings? How to assess their vulnerability? How people considered volcanic risk in their daily life? How to assess the risk associated to lava flows?

On the one hand, a baseline demographic database was developed in collaboration with the local scientists, based on an easy-to-reproduce methodology relying on remote sensing, quantitative household survey, in-depth interviews, and detailed knowledge of the studied area. The surveyed population samples were used to derive detailed population density for the whole urban area; and a social vulnerability index reflecting the local context was defined by combining, in a Principal Component Analysis (PCA), a wide range of socio-economic data collected. On the other hand, through intensive fieldwork, lifelines were mapped, and their vulnerability was assessed. Built elements were also digitalized thanks to remote sensing techniques; and, using spatial models and local experts' knowledge, their economic values were evaluated to constrain their exposure.

Our results show that if the population density and the related infrastructures are important in the eastern part of Goma, people living in marginal neighborhoods in the west and north of the city appear to be particularly vulnerable. Combined with the lava flow hazard assessment (Part 2) in a Geographic Information System (GIS), the results highlight that the highest lava flow risk area lies in the eastern part of Goma, which was already destroyed during the 2002 eruption. GeoRisCA risk map is provided to local authorities as a decision supporting tool, strengthening risk management of existing preparedness and mitigation institutions.

Sabina Michnowicz, Christopher Kilburn

Submission 623

Developing trust in hazard warnings and responses at long-quiescent volcanoes

Intervals of several generations between eruptions are a key obstacle to improving resilience against volcanic activity, because they are long enough for the collective memory of previous events to have faded. Exposed communities lose knowledge of the threats they may face and scientific advisors lose experience in responding to an emergency. The loss of knowledge and experience promotes misunderstandings when communicating advice - misunderstandings that can transform a crisis into a disaster.

We have investigated changing knowledge and experience of volcanic unrest at the Campi Flegrei caldera outside Naples in southern Italy. After four centuries of repose, the volcano has been through two major, non-eruptive emergencies in 1969-72 and 1982-94 and is continuing a pattern of unrest consistent with a progressive approach to eruption. Each of the emergencies triggered evacuations of some 40,000 people. The first was prompted by uncertainty in the possibility of eruption and the second by the perceived threat from persistent volcano-tectonic seismicity to the stability of buildings. They occurred within the professional lifetimes of the same monitoring scientists and emergency authorities and, whereas the first evacuation provoked scientific disagreements in the public arena, the second was co-ordinated through more unified channels of communication.

Our interviews in 2016-17 show that, three decades after the last emergency, public expectations of a future response to unrest remain coloured by memories and stories of previous emergencies. Recurring themes include: orders to evacuate will be conditioned by political considerations; the principal threat to communities will be the danger of building collapse caused by local seismicity; the State will pay the cost of recovery; and the threat from volcanic activity is remote and, in any case, cannot be prevented. Apparently, therefore, memories of the first emergency dominate views of how evacuations are decided, regardless of the second having been better organized. In addition, the threat from volcanic activity is considered secondary to that from local seismicity, in spite of public campaigns to raise awareness of volcanic activity. Encouraging trust in the scientific basis for evacuation and hazard assessment is thus a core goal in preparing for the next emergency at Campi Flegrei.

Richard Middlemiss

Submission 1043

Miniaturised Gravity Sensors for Remote Gravity Surveys

The ability to measure tiny variations in gravitational acceleration (g), allows one to see not just the Earth's gravitational pull, but the influence of smaller objects. The more accurate the gravimeter, the smaller the objects one can see. Gravimetry has applications in many different fields: from tracking magma moving under volcanoes before eruptions; to locating hidden tunnels. The top commercial gravimeters weigh tens of kg and cost at least \$100,000, limiting the situations in which they can be used. By contrast, smart phones use a MEMS (microelectromechanical system) accelerometers that can measure the orientation of the device. These are not nearly sensitive or stable enough to be used for gravimetry but they are cheap, light-weight and mass-producible.

At Glasgow University we have developed a MEMS device with both the stability and sensitivity for useful gravimetric measurements (maintaining a sensitivity of 40 micro-Gal/rt(Hz) over week time-scales). This was demonstrated by a measurement of the Earth tides – the first time this has been achieved with a MEMS sensor. A gravimeter of this size opens up the possibility for new gravity imaging modalities. Arrays of gravimeters could be networked over a survey site, storing data on an SD card or communicating wirelessly to a remote location. These devices could also be small enough to be carried by UAVs: airborne gravity surveys could be carried out at low altitude by multiple UAVs, or UAVs could be used to deliver ground based gravimeters to remote or inaccessible locations. Low-cost, miniature gravimeters could fundamentally change the way in which volcano gravity surveys are carried out - reducing the risk to personnel, whilst increasing the temporal and spatial coverage of the acquired data.

These devices are currently being packaged in a commercial process, with a total size comparable to a smart-phone. Field testing is expected to begin in the summer of 2017, with preliminary results to be presented at the IAVCEI.

Daniel Miggins, Anthony Koppers

Submission 1217

Look out ^{14}C ! Here comes high precision $^{40}\text{Ar}/^{39}\text{Ar}$ geochronology into the Holocene

Since the advent of multi-collector mass spectrometers, the ability to date very young volcanic events using $^{40}\text{Ar}/^{39}\text{Ar}$ geochronology has increased. $^{40}\text{Ar}/^{39}\text{Ar}$ geochronology is on the threshold of dating various rock types with low and high K_2O contents for historic eruptions and broadening the method from previous researchers. Additionally, being able to precisely date such recent events has major implications for recurrence intervals of tectonomagmatic processes and associated seismic hazards. This has major significance for the geochronology community as we now have the ability to compare and contrast different dating techniques using young chronometers such as ^{14}C , thermoluminescence, obsidian hydration, uranium-series, cosmogenic surface exposure dating (^3He and ^{21}Ne) and dendrochronology for samples ranging in age from 50 ka to as young as a few hundred years. We will present some recent dating results from 20 to 3 ka basaltic lava flows and rhyolites, as well as ^{14}C ages for the same flows dated by the $^{40}\text{Ar}/^{39}\text{Ar}$ method and discuss the pros and cons of dating young rocks such as excess argon, initial $^{40}\text{Ar}/^{36}\text{Ar}$ ratio, groundmass versus single crystal analysis, and the effect of melt inclusions on the resulting ages. A key to unraveling ages for young igneous systems, especially those younger than 20 ka, is the trapped initial $^{40}\text{Ar}/^{36}\text{Ar}$ composition and the effects of excess argon in melt inclusions and within crystalline lattices of minerals and groundmass concentrates. Understanding the significance of the sub-atmospheric $^{40}\text{Ar}/^{36}\text{Ar}$ ratios exhibited by some samples has ramifications on the interpretation of eruption ages.

T. Dylan Mikesell, Jordan Bishop, Luis Franco Marin, Jonathan Lees, Berk Biryol, Rebecca Rodd

Submission 1201

A seismic look at the internal structure of Llaima Volcano, Chile

Llaima Volcano in Chile is one of the largest and most active volcanoes in the South Volcanic Zone (ZVS) of the Andes (38.7° S and 71.7° W, Chile), with over 50 eruptions since the 1600s. Llaima is a stratovolcano of basaltic-andesitic composition, and after years of persistent degassing, Llaima recently erupted in a series of violent Strombolian eruptions in 2008-2009. This period had few precursory signals, which highlights the need to obtain accurate magma storage information. From January 2015 to March 2015, 24 broadband seismic stations operated continuously in an approximately 30km by 20km area surrounding Llaima. In this study we provide an overview of recent results from 2-D travel times, ambient seismic noise tomography, and receiver function studies to present a seismically-derived geophysical model of Llaima's internal structure. Ambient noise tomography (ANT) has become an important tool to image crustal structures and magmatic bodies at volcanoes, and in addition to traditional travel-time tomography and receiver functions, ANT provides complimentary data and improved resolution of volcanic structures. Arrival time perturbations from regional and teleseismic events are used to identify a low velocity anomaly at least 10km in diameter beneath the volcano edifice. Ambient noise tomography is used to estimate group velocity dispersion between receiver pairs in the array. Initial results reveal two low velocity zones beneath the volcano: one below the summit and a second eastward of the summit. Receiver function H-k stacking and common conversion point (CCP) stacking are conducted to obtain a crustal thickness estimate of 43km and to examine mid-crustal discontinuities. A seismic anomaly is imaged at approximately 8-13km depth to the south-east of Llaima, which we interpret to be the top of a body of partial melt. By combining these complementary results, we present a new geophysical model of Llaima's subsurface structure that is consistent with available petrologic data.

Calvin Miller, Michelle Foley, Lily Claiborne, Guilherme Gualda, Ayla Pamukcu

Submission 1151

PRE-ERUPTION MELT COMPOSITIONS REVEALED BY TEMPERATURE-SENSITIVE ZIRCON-MELT KDS: DIVERSITY IN THE PEACH SPRING TUFF MAGMA CHAMBER, SW USA

Characterizing diversity of melt compositions within silicic systems in space and time provides critical insights into physical and chemical processes in evolving and erupting magmas, but reconstructing this record is challenging. Model Ti-correlated Kds based on zircon rims and host glasses from Iceland, Mount St. Helens, and volcanic rocks from the Colorado River region of NV-AZ provide a promising approach for assessing this diversity (Claiborne et al 2016, 2017).

The 18.8 Ma Peach Spring Tuff (PST) is a zoned, supereruption-scale deposit in AZ-CA-NV (Ferguson et al 2013). Dominant outflow is phenocryst-poor high-silica rhyolite (HSR); exposed caldera fill and the youngest portion of the outflow is phenocryst-rich trachyte (TR). All PST contains a rich accessory mineral assemblage. We use the new zircon Kds to estimate melt compositions from which 164 SHRIMP-analyzed zircon zones grew; zircons were separated from six samples of pumice and fiamme (2 TR, 2 HSR, 2 low-silica rhyolite).

Estimated trace element concentrations in zircon-equilibrated melts are highly diverse. Some of the variability is undoubtedly a reflection of uncertainties in modeling of Kds, but we regard much, and probably most, of it as real. The model melts demonstrate compositional patterns consistent with those of analyzed PST glasses and whole-pumices, which have been interpreted to indicate crystal accumulation and cumulate remobilization (TR) and melt fractionation (HSR) from rhyolite magma (Pamukcu et al 2013; Foley et al 2014, 2016). They are, however, more diverse and display compositional patterns that suggest variability in crystal accumulation and subsequent partial dissolution during reactivation. Many model melts have superchondritic Zr/Hf (40-50, well above mean PST of ~37; analyzed TR glasses 40-45, HSR glasses 15-25); this documents dissolution of zircon from zircon-enriched cumulates during remobilization. Accompanying the high Zr/Hf in model melts is highly variable enrichment of Gd/Lu (~15-40; mean PST ~15; glasses: TR 22-25, HSR 5-8). The Gd/Lu indicates highly variable accumulation and dissolution of cumulate sphene (titanite). Zircon-modeled melts tend to reflect their host samples ("cumulate melt" compositions dominate in TR, "fractionated melts" in HSR), but in all 6 samples they spread from the fractionated melt field to that of reactivated cumulate melt, indicating mechanical interaction between cumulate and crystal-poor rhyolite.

Craig Miller, Glyn Williams-Jones, Dominique Fournier, Jeff Witter

Submission 85

3D gravity inversion and thermodynamic modelling reveal properties of shallow silicic magma reservoir beneath Laguna del Maule, Chile

Active, large volume, silicic magma systems are potentially the most hazardous form of volcanism on Earth. Knowledge of the location, size, and physical properties of silicic magma reservoirs, is therefore important for providing context in which to accurately interpret monitoring data and make informed hazard assessments. Accordingly, we present the first geophysical image of the Laguna del Maule volcanic field magmatic system, using a novel 3D inversion of gravity data constrained by thermodynamic modelling. We image a 30 km³, low density, volatile rich magma reservoir, at around 2 km depth, containing at least 85 % melt, hosted within a broader 115 km³ body interpreted as wholly or partially crystallised cumulate mush. Our model suggests a magmatic system with shallow, crystal poor magma, overlying deeper, crystal rich magma. Even though a large density contrast (-600 kg/m³) with the surrounding crust exists, the lithostatic load is 50 % greater than the magma buoyancy force, suggesting buoyancy alone is insufficient to trigger an eruption. The reservoir is adjacent to the inferred extension of the Troncoso fault and overlies the location of an intruding sill, driving present day deformation. The reservoir is in close proximity to the 2.0 km³ rln eruption at 2-3 ka, which we calculate tapped approximately 6 % of the magma reservoir. However, we suggest that the present day magma system is not large enough to have fed all post-glacial eruptions, and that the location, or size of the system may have migrated or varied over time, with each eruption tapping only a small aliquot of the available magma. The presence of a shallow reservoir of volatile rich, near liquidus magma, in close proximity to regional scale faulting, has important implications for volcano monitoring and hazard mitigation.

Victoria Miller, Matthew Garthwaite, Rikki Weber, Jonathan Griffin, Grant Cox

Submission 107

Volcanic-tsunami hazard assessment – A case study from Heard Island and McDonald Islands, Australia

Volcanic-tsunami can occur with little warning, travel quickly (up to 1000km/hr) and cover great distances causing devastating impacts. There are several mechanisms for volcanic-tsunami events, including underwater explosion, blasts, pyroclastic flows, caldera collapse, subaerial failure and submarine failure. For the latter two, volcanic activity is not a pre-requisite, which presents additional challenges when raising awareness and undertaking planning activities.

Volcanic-tsunami are often not considered in hazard and risk assessments, particularly as a far-field source. This can leave communities vulnerable to their impacts. It is estimated that 20-25% of fatalities directly attributable to volcanoes in the last 200-250 years have resulted from volcanic-tsunami (Latter, 1981; Auker et al., 2013) (e.g. ~36,000 deaths were a direct result of the tsunami generated from the 1883 Krakatau eruption). Moreover, volcanic-tsunami account for ~6% of tsunami events globally and can generate tsunami with a similar intensity to those from earthquake sources. In volcanically active regions the possibility of experiencing impacts from volcanic-tsunami is likely to be greater, highlighting a need for inclusion in hazard assessments.

A volcanic hazard assessment that includes volcanic-tsunami can be as fundamental as an identification and characterisation of potential source volcanoes. More in-depth hazard assessments can then be produced through numerical modelling of propagation and inundation from tsunami generated in volcanic regions. In combination, this can provide an evidence base for undertaking more extensive analysis, or to provide guidance to planners who wish to consider potential impacts from lower frequency/higher consequence events.

Here we present a method for classifying volcanoes for their potential to generate a tsunami and demonstrate the application of this method to the Heard Island and McDonald Islands (HIMI). HIMI are Australian Antarctic Territories located ~4000 km south west of Perth, Australia. Both of these eruptive centres have experienced violent, ongoing eruptive events; Heard Island as recently as 2016. Our analysis indicates that there is the potential for submarine mass failure at HIMI which could feasibly generate a tsunami detectable along the south-west Australian coast and in Antarctica. This poses a potential tsunami hazard to Australia, but more work needs to be undertaken to understand the mechanism and likelihood of such events.

Alex J.C. Miller, Jeffrey Bruce Johnson, Jacob Anderson, Matthew R. Von Lintig

Submission 640

Constraining plume velocity and pulsed emissions from two months of continuous video data at Volcán Villarrica, Chile.

Determining periods of active venting and quantifying the injection rate of material into the atmosphere are essential in scientific study and hazard mitigation. Though webcam and video datasets are often used qualitatively in volcano monitoring, simple image analysis techniques can yield substantial information about eruptive behavior including style, emission velocities, and timing. Eruption quantification is particularly important for long chronologies such as the months following the paroxysmal March 3rd, 2015 eruption of Volcán Villarrica, Chile.

Starting March 3rd and continuing throughout April, a visible and near-infrared surveillance camera was focused on the summit of Villarrica. The camera recorded continuous activity at 30 fps corresponding to a zoomed-in area (100 s of m field-of-view) above the crater rim 17 km away. The camera was installed just after Villarrica erupted with a 1.5 km tall lava fountaining event lasting 30 minutes. Video records from the weeks following the eruption show the evolution from a post-eruption sealed state to a more typical mode with open-vent and degassing lava lake. In order to analyze the large volume of data, video was decimated to 1 Hz still frames and cropped to highlight the summit region. By using a row and column projection image-analysis method, we identify eruptive periods lasting minutes to hours, which are punctuated by pulsed emissions and strombolian activity. Vertical and horizontal plume velocity components are calculated by examining the row and column projections during pulsed emissions. These components can then be used to calculate plume velocity and direction. We find that during periods of active degassing, emissions are preferentially ejected at about 20-s intervals and at velocities of 101 m/s. We correlate video results to infrasound time series data for a range of different eruptive styles. Video imagery is a powerful monitoring tool that provides important constraints on source parameters and multiparameteric observations. Processed data from long acquisition camera records can help to comprehensively quantify eruptive chronologies.

Samuel Mitchell, Bruce Houghton, Rebecca Carey

Submission 256

Giant Pumice: A window into the physical and geochemical heterogeneity of a deep submarine silicic volcanic conduit

Giant pumiceous blocks are commonly associated with the submarine volcanic environment. With limited field exposure and, until recently, no historical in situ record of formation, the process that yields these meter-scale clasts remains somewhat of a mystery. The current mechanism of giant pumice formation is the spalling of a vesicular, lava-dome carapace at the seafloor with a high flux of volcanic outgassing. In 2012, a deep submarine silicic eruption at Havre volcano on the Kermadec rear-arc produced 0.1 km³ of giant pumiceous blocks over >35 km² of seafloor. Detailed ROV sampling and in situ observation provides significant insight into how these clasts reflect shallow conduit conditions and pre-eruptive processes at Havre. Through a multi-analytical approach, we endeavor to constrain the shallow conduit conditions that would favor the spalling of a lava dome at hydrostatic pressure, or another explosive mechanism. We sampled exteriors of 10 giant pumice clasts to compare the macrotextural, microtextural and geochemical evolution between and within individual pumices. Major element geochemistry was obtained by XRF (bulk rock compositions) and electron microprobe (phenocryst, microlite and matrix glass compositions). Binary 2D-image nesting was used to compare the vesicle and microlite number densities and size distributions between the exteriors.

Consistency of phenocryst assemblages and bulk XRF implies a relatively homogeneous primary magma source during the 2012 eruption, whereas wide variation in densities, vesicular textures and types of banding suggest that textural heterogeneity developed in the shallow conduit or upon effusion on the seafloor. The close proximity of both spherical and highly-elongate tubular vesicles further imply localized viscous shearing and subsequent formation of permeable degassing pathways. Variations in microlite phase and number density also reflect heterogeneous cooling and crystallization histories between clasts attributed to variable thermal coupling with the submarine volcanic plume. Our study further reveals the complexity of submarine giant pumice, and highlights that every pumice clast in a single deposit preserves its own degassing, cooling and crystallization history; these observations are not readily compatible with classical explosive fragmentation mechanisms.

Tushar Mittal, Mark Richards

Submission 895

Volatile degassing from magma chambers as a control on the size and frequency of volcanic eruptions

The loss of volatiles from a magma reservoir affects the overpressure leading to and driving eruptions. Although the high-temperature metamorphic aureole around a magma chamber is typically considered to have low permeability due to ductile creep, recent theoretical, experimental, and field work (e.g. Weis 2015, Noriaki et al. 2017, Achtziger-Zupančič et al. 2017) have highlighted the role of dynamic permeability and ductile failure in magmatic systems. Consequently, the effective permeability of the crust when magma is present in the system can be many orders of magnitude larger than that of exhumed rock samples. In addition, new observations suggest that passive degassing is a significant component of total volatile loss in both basaltic and silicic volcanoes (Stefansson et al. 2016). We therefore infer that the loss of volatiles from a chamber can be more important than previously recognized. Short time-period dynamic permeability changes can be modeled as a competition between hydro-fracturing (increased porosity) and fracture closure by ductile creep and hydrothermal mineral precipitation (reduced porosity), leading to a porosity wave solution.

We use a fully coupled poro-thermo-visco-elastic framework to account for both the flow of volatiles as well as associated effects on the stress state of the visco-elastic crust in a high time-averaged permeability setting. We combine a magma chamber box model (modified from Degruyter & Huber 2014) with semi-analytical poro-thermo-visco-elastic solutions for the surrounding for flow of volatiles in the crust surrounding a magma chamber to analyze system-scale dynamics for both basaltic and silicic magmatic systems. We find that in addition to viscous relaxation, injection, and cooling time scales, there is a pore-pressure diffusion timescale that exerts a first-order control on the magnitude and frequency of volcanic eruptions. We describe a parameter space to identify which components dominate in different regimes for volcanic eruptions. Passive degassing affects the spatial distribution of effective pressure around the magma reservoir and thus influences the location and orientation of dikes transporting melt to the surface. Our models can help relate some surface observations of hydrothermal systems, e.g. episodic variations in the Campi Flegrei system, to deeper processes in magmatic systems.

Daisuke Miura, Mizuho Amma-Miyasaka, Shimpei Uesawa, Shingo Takeuchi

Submission 109

Kuttara caldera complex and its ignimbrites.

The Kuttara caldera complex (KCC), a silicic volcanic field in southwest Hokkaido, Japan, consists of multiple ignimbrite units, and a nested caldera complex with 3 and 8 km in diameters. The 3 km caldera is recognized as a topographically circular lake named the lake Kuttara. The larger and older 8 km caldera is obscured due to the lack of clear topographic margins. Twelve major eruptions have been recognized, separated by long dormant periods. Each dormant period has been inferred from the presence of volcanoclastic soil layers on the surfaces of the older deposits. Explosive eruption ejecta (tephra) episodes constitute 9 of the 12 episodes. The 9 tephra episodes, called as Kt-series tephras, are: Kt-1 (44.1 ka), Kt-2, Kt-Tk, Kt-3 (54.6 ka), Kt-Hy, Kt-4 (74 ka), Kt-6 (84 ka), Kt-7 (ca. 90 ka) and Kt-8 (90–110 ka).

Geochemical studies on the Kt-series tephras have been undertaken to examine the process of magma genesis in the KCC. The SiO₂ versus TiO₂ diagram shows that the KCC ejecta have a wide range of SiO₂ contents: 50 to 74 wt% or higher. For pyroclastic units, each episode has a relatively wide range of SiO₂ content; e.g., 64–74 wt% SiO₂ for Kt-1. Our glass component analysis for the tephras reveals a marked characteristic of the KCC ejecta, which is a relatively high K₂O content in the Kt-1 and the Kt-7 episodes. The TiO₂ versus K₂O diagram shows that the glass components for the Kt-2, -3, -4 and -6 fall into the almost same variation with low K₂O content. The Kt-1 and a piece of Kt-7 thus differ from the low K₂O content in the other Kt-series.

The caldera-forming eruption at the 3 km Kuttara caldera could have occurred in the Kt-3 episode, because typical sequence of caldera-forming eruption has been observed in the Kt-3 units. In contrast, the larger caldera margins have been inferred by the pieces of evidences indicating the caldera moat. Those evidences are the followings: (a) a line of topographic changes from the steep host-rock mountains to the flat-even volcanoclastic terrains, (b) the arrangement of a parasite crater, hot-springs, and lag-fall breccias (Kt-7), (c) downsag structure of the Kt-7 ignimbrite, filled up with the later deposit sequence. A depression shape of gravimetric data is coincident with the inferred large caldera moat. Therefore, the presences of the downsag structure and lag-fall breccias in the Kt-7 ignimbrite suggest that the large 8 km caldera was collapsed at least once at the Kt-7, and might be a couple of times.

Pranabendu Moitra, Ingo Sonder, Greg Valentine

Submission 272

Magma-to-water heat flux estimate: Insight from pool-boiling experiments

The heat transfer rates from magma to water are important to quantify in order to understand better the dynamics of explosive phreatomagmatic and effusive to explosive submarine eruptions. In this study, we performed pool-boiling experiments using natural magma submerged in a water bath, in order to constrain the heat transfer rates for a range of magma (upto 1120 0C) and water temperatures (0-100 0C). Spherical samples of about 3 cm diameter were produced from basaltic rock. These spherical samples were heated to 1120 0C inside a furnace purged with argon gas, and were submerged in distilled water. The water bath was maintained at a fixed temperature during each experiment. A thermocouple was inserted in the sample to record the sample temperature during the experiments. The boiling experiments were recorded using high-speed cameras (upto 1000 frames per second), where the temperature data and the video snapshots were synchronized for analysis. We find that a stable vapor film exists at large sample temperatures during our experiments. This stability decreases with decreasing water temperature with no vapor film observed at colder water temperatures (0C). With decreasing sample temperature, the pool-boiling regime shifts from stable vapor film- to transition- to nucleate-boiling to free convection, respectively. The transition and nucleate boiling regimes are defined by the formation of vapor bubbles surrounding the sample, where the onset of free convection regime is marked by the absence of vapor bubbles. In order to quantify the heat flux, we solve the heat equation in spherical coordinate with temperature-dependent thermal diffusivity and heat capacity of the sample material. The temperature data at the thermocouple position inside the sample was fitted with the model to obtain the sample surface temperature, as well as the heat flux. The minimum heat flux, required to maintain a stable vapor film, is determined and correlated for different water temperatures. Using our heat flux estimate, the cooling time scale of magma in the presence of external water and its implication for thermo-brittle fracturing of magma are discussed.

Jonathan Moles, Dave McGarvie, Sarah Sherlock, John Stevenson, Peter Abbott

Submission 630

Long-range tephra dispersal and ignimbrite emplacement from a large rhyolitic glaciovolcanic eruption

A rhyolitic eruption in Iceland dispersed tephra across much of the North Atlantic region in the middle of the last glacial period ($55,380 \pm 2368$ a b2k). In the Greenland ice sheet and in North Atlantic marine sediments, this tephra horizon is the dominant component of a complex ash zone known as North Atlantic Ash Zone (NAAZ) II. The tephra is a valuable chronostratigraphic marker that has been used to integrate palaeoclimatic and palaeoenvironmental information from sediment cores and ice cores. In the terrestrial realm, the tephra has been shown to correlate with the Thórsmörk Ignimbrite in southern Iceland. We aim to identify the source of this significant explosive eruption and to assess interactions between the eruption and ice.

Tindfjallajökull volcano, southern Iceland, has been accepted as the source of the Thórsmörk Ignimbrite for over 35 years. However, the major element geochemistry of the ignimbrite and NAAZ II suggests that they are instead derived from Torfajökull volcano, the outer margin of which is 25 km NE of the area of ignimbrite outcrop. In particular, we have identified a major element correlation between the Thórsmörk Ignimbrite/NAAZ II and the Torfajökull Ring Fracture Rhyolites, a set of rhyolitic tuyas believed to have been emplaced in one large-volume glaciovolcanic eruption (~ 18 km³ DRE) during the last glacial period. This potential correlation is being more fully assessed using geochronology ($^{40}\text{Ar}/^{39}\text{Ar}$) and trace element geochemistry (LA-ICP-MS).

If this correlation proves to be robust, it will lead to an improved understanding of the processes that can take place during large rhyolitic glaciovolcanic eruptions. For instance, it will confirm that these eruptions can produce widespread tephra layers following breaching of the ice. Where tephra from an eruption is found in an ice or sediment core, it allows a precise comparison between core-derived palaeoclimatic data and lithofacies-derived information on the eruptive environment. This correlation would also demonstrate the existence of a previously unstudied aspect of glaciovolcanism: the long-range propagation of pyroclastic density currents across (and beyond) a low-profile ice sheet.

Danielle Molisee, Sylvain Charbonnier, Aurelie Germa, John Bell

Submission 309

Cinder Cone Age Estimation Based on Cone Morphology Using Two-Dimensional Nonlinear Diffusive Numerical Modeling, Buffalo Valley Volcanic Field, Nevada, USA

Buffalo Valley Volcanic Field (BVVF; North-Central Nevada, USA) is composed of basaltic to trachybasaltic cinder cones and flows of Pliocene to Quaternary age. Perceived discrepancies between crisp cinder cone morphology and chronology inferred from $^{40}\text{Ar}/^{39}\text{Ar}$ ages (1.15 - 1.99 Ma) has prompted the development of a computational method for cinder cone age estimation based solely on morphometry and independent of radiometric dates.

Cinder cones typically form with exterior slope angles at or near the angle of repose (30°-33°) that subsequently erode, resulting in reduced slope angles with time. Based on this assumption, we use 2D nonlinear diffusive numerical modeling in Matlab and finite difference diffusive modeling (1D and 2D) in Python to estimate the age of four Quaternary BVVF cinder cones. We generate multiple topographic profiles for each cone and calculate their maximum external slope angle (MESA). Using a MATLAB cinder cone erosion simulation code (Vitturi and Arrowsmith, 2014) and our own finite difference Python script, for which input parameters (both methods) are the estimated diffusion constant ($k=3.9$ m/kyr; Lathrop Wells), cone base and/or height dimensions, simulation end time and adaptive time step interval, we estimate age ranges for each cone.

Matlab modeling results show that the age range based on MESA, is 0.7 –2.8 Ma which generally agrees with the radiometric dates. However, the two methods differ in regards to relative cone ages. The cone of youngest radiometric age (1.15 Ma) is modeled as oldest (2.5-2.8 Ma) which is consistent with morphological observations. Modeled age ranges for two other BVVF cones are 1.5-1.7 Ma and 1.2-1.5 Ma which support their radiometric ages of 1.76 Ma and 1.31 Ma, respectively. The age range of the fourth cone used in this study is modeled as 0.7-0.85 Ma which is ~1 Ma younger than the radiometric age (1.7 Ma). The base of this fourth cone has been altered by fluvial processes which may affect our modeling. Our set of modeled ages suggests that eruption of the Quaternary BVVF cinder cones began in the north and progressed southward with time. This trend is also supported by the chemical evolution of the erupted lavas from basalt to trachybasalt. These results show the importance of using various geochronological techniques and integrating age data with both geomorphological features and geochemical data to decipher the complex temporal and spatial histories of monogenetic fields.

Kata Molnar, Szabolcs Harangi, Reka Lukacs, Istvan Dunkl, Axel K. Scmitt, Mihaly Molnar, Agnes Novothny, Balazs Kiss

Submission 1031

A detailed eruption chronology of the Ciomadul lava dome field (Eastern Carpathians, Romania) based on (U-Th)/He zircon dating.

During the last decade, combined U-Th and (U-Th)/He zircon geochronology has become a promising method for dating young volcanic eruptions. It is proved to be particularly applicable when other dating methods encounter analytical or interpretational difficulties often caused by a lack of appropriate materials. The ~200 °C closure temperature for He diffusion in zircon enables determination of eruption ages based on (U-Th)/He systematics. However, for

We applied this method to obtain a detailed eruption chronology of the Ciomadul lava dome volcanic field composed of a central lava dome edifice with two explosion craters and a number of satellite domes surrounding it, situated in the Eastern Carpathians. We sampled all known eruption centers and eruption products. In a few cases, radiocarbon and thermoluminescence ages at the same locality were used and yielded concordant results with the zircon (U-Th)/He ages. The high spatial resolution zircon crystallization ages show a wide temporal range even for analyses that targeted only the outermost ~4 µm crystal rims. Therefore we determined first the (U-Th)/He ages and then we used the weighted-mean averages of U-Th and U-Pb spot analyses which targeted the mantles of zircon crystals for disequilibrium correction because these best represent the age of the bulk volume of the crystals. This correction is significant for eruption ages of up to 1.5 Ma.

Our new (U-Th)/He zircon ages refined considerably our knowledge on the eruption chronology of Ciomadul and showed that the active phases were often separated by long (>100 kyr) quiescence periods. The first lava dome extrusions occurred at ca. 1 Ma followed by four further lava dome building events until ca. 300 ka. Subsequently, the renewed volcanic activity became more productive. Numerous lava domes were developed between ca. 200 and 100 ka forming the 10-12 km³ central lava dome edifice of Ciomadul volcano. It was followed by a more explosive phase with minor dome building activity which occurred at ca. 80 and between 56 to 32 ka forming two explosive craters. Since then, the volcano is again in a dormant phase, however, the length of this quiescence is well within the usual repose times of this volcanic complex.

This research is supported by the NKFIH K116528 and PD121048 projects.

Cristian Montanaro, Shane Cronin, Bettina Scheu, Ben Kennedy, Bradley Scott, Donald B. Dingwell

Submission 726

Host rock influence on the energy partitioning and crater morphology of steam-driven eruptions

Blasts triggered by explosive vaporization of water in volcanic and hydrothermal settings are common on our wet planet and are termed steam-driven eruptions (SDEs). They occur mainly within geothermal areas or volcanic terrains with high heat-flow, and comprise subsurface explosions that produce differently shaped and sized craters. Craters commonly preserve evidence of multiple explosions with complex explosion clustering or migration patterns of explosion locus, or even coalesced craters with complex forms. SDEs are known from a wide range of host rock lithologies, alteration states, strength and permeability, etc. The impact of these substrates on eruption energetics, dynamic properties, and the final crater morphology has yet to be quantified.

Here the Lake Okaro (Taupo Volcanic Zone) explosion crater was examined. Reconstructions of its formation include a main phreatic eruption phase, along with successive secondary hydrothermal explosive events. The climactic event was hosted within the ~70m-deep Rangitaiki ignimbrite, whereas shallower welded tuff and unconsolidated sediments (including initial explosion breccias) hosted the shallow focused hydrothermal explosions.

Field characterization of breccia deposits on the crater rim, together with the shape analysis of craters from new bathymetrical data, point to multiple explosion sites. Additionally, drill core samples of Rangitaiki Ignimbrite and of breccia deposit material, were petrophysically characterized and experimentally exploded in rapid decompression experiments mimicking SDEs. The latter yield quantitative information on fragmentation and ejection behaviors, as well as estimates of the explosive energy for steam-driven explosive events. Through the combination of field observations, lithology studies, crater morphology analysis and experimental studies, we show a relationship between explosion energy and explosion dynamics, including crater-form, with the host rock properties.

Emily Montgomery-Brown, Mario Mattia, Valentina Bruno, Danila Scandura

Submission 49

A comparison of slow slip events at Kīlauea and Mt. Etna

Unstable flanks are common at volcanoes that have experienced large catastrophic sector collapses. Instability has also been identified on smaller arc volcanoes due to structural and magmatic sources. Increasingly, observations of slow, episodic flank slip events have been observed by geodetic instruments, suggesting that flank collapse can occur incrementally. Mt. Etna and Kīlauea are both large basaltic volcanoes with unstable flanks on which episodic slow slip events have been observed repeatedly by continuous GPS networks. The observed slow slip events (SSEs) at both volcanoes lasted about two days and released energy equivalent to a M5.5-M6 earthquake, but there are differences in the depths and recurrence intervals. At Kīlauea, SSEs have become more regular since 2005 with an inter-event time of about 2.4 years, although earlier events had more irregular intervals. At Mt. Etna, SSEs are more frequent (inter-event time of about 0.5 years). Ground deformation data suggest different mechanisms of slip at Mt. Etna and Kīlauea. Slip at Kīlauea occurs on a discrete decollement at about 8 km deep, coincident with a narrow band of seismicity. At Mt. Etna, a variety of data suggest that the sliding could be much shallower, more diffuse and often related to the main recharge phases of the volcano. In this work, we show new preliminary results of a kinematic block model of Mt. Etna's slow slip events. This block-model identifies the source of the flank displacements on the Giarre Wedge, a triangular section of Sicily's east coast slowly subsiding into the Ionian Sea. The documentation and comparison of flank slip events at Kīlauea and Mt. Etna can further the understanding of the possible range of flank instability at large basaltic volcanoes, including structural mechanics, gravitational stresses, and interactions with fluids or magma.

Sarah Moore, Christelle Wauthier, Yo Fukushima, Michael Poland

Submission 1243

Deformation sources in Kilauea's East Rift Zone During 1993-1997 revealed through InSAR modeling

The February 1993 dike intrusion in the East Rift Zone (ERZ) of Kīlauea Volcano, Hawaiʻi, was recognized from tilt and seismic data, but ground-based geodetic data were too sparse to constrain the characteristics of the intrusion. Analysis of Interferometric Synthetic Aperture Radar (InSAR) from the Japan Aerospace Exploration Agency (JAXA) JERS-1 satellite reveals ~30 cm of Line-of-Sight (LOS) displacements occurring near Makaopuhi Crater in the middle ERZ of Kīlauea. We model this deformation signal as a subvertical dike using a 3D-Mixed Boundary Element Method (3D-MBEM) paired with a nonlinear inversion algorithm to find the best-fit model. The best-fit dike is located just to the west of Makaopuhi Crater and within 100 m of the surface. The dike strikes N50°W, is ~1.3 km long, along-strike by ~2.7 km wide, down-dip, and has a total volume increase of $\sim 7.4 \times 10^6$ m³. Because it lacked precursory inflation of Kilauea's shallow magma system, we classify the 1993 dike intrusion as a passive intrusion, similar to those that occurred in 1997 and 1999. We also analyzed a post-intrusion interferogram from 1993-1997 in order to characterize the deep rift zones and decollement. Preliminary results suggest opening of the deep rift zones beneath the Southwest and East Rift Zones. The dike-like opening extends from 3 km depth to at least to the decollement. The décollement is modeled as a sub-horizontal detachment fault seaward of the rift zone with a calculated average slip of 0.4 m between 1993-1997.

Nicole E. Moore, Anita L. Grunder, Wendy A. Bohrson, Richard W. Carlson

Submission 1239

Source and Magma Processes During the Onset of Columbia River Basalt Volcanism, the Steens Basalt, SE Oregon

The Steens Basalts are exposed in spectacular relief at Steens Mountain and allow a flow-by-flow temporal reconstruction of volcanism during the early, and most mafic, phase of the Columbia River Flood Basalt event. Geochemical signatures can be explained by melting of a minimally enriched mantle source and differentiation by various combinations of recharge, assimilation and fractional crystallization processes. Samples from the most primitive flows have low $^{187}\text{Os}/^{188}\text{Os}$ (0.127-0.129) and high Os concentrations (>0.2 ppb), implying that the mantle source contains little to no pyroxenite, and the magmas suffered minimal contamination by modestly radiogenic crustal material in the region. The more radiogenic Os isotopic compositions (0.282) indicate that crustal assimilation took place in the more evolved upper Steens section. The high Os concentrations in the most primitive flows require melting conditions that consumed most Os-bearing phases in an ultramafic source, a contribution by some other Os rich component, or lack of fractionation of Os rich phases (e.g. sulfide, chromite) from a picritic parental magma. Os behaves compatibly, tracking Ni and Cr in the lower Steens suite.

The earliest Steens Basalt flows, stratigraphically below the lower Steens section, are as old as 16.9 Ma and fill paleotopography. Incompatible trace element and Sr-isotope enrichments (Rb 10-50 ppm; $^{87}\text{Sr}/^{86}\text{Sr}$ 0.7035-0.7037) with decreasing MgO from ~ 8 to 3.5 wt.% are consistent with modest contamination by crust of accreted mafic terranes accompanied by mid to upper crustal crystal fractionation. In the lower Steens, flow-to-flow compositions oscillate by ~ 4 -5 wt.% MgO, creating a zig zag stratigraphic pattern, in which the mafic flows increase from ~ 8 to 12 wt.% MgO and then decline, signaling an early mafic recharge dominated history followed by predominant fractionation. Assimilation of a plagioclase rich component is required to explain a linear mixing trend towards high Al_2O_3 , CaO, and NaO but lower Rb and constant Sr with decreasing MgO. We propose it is a cognate plagioclase cumulate with a few percent interstitial liquid. In the latter stages of Steens magmatism, magma chambers shoal, as indicated by assimilation becoming more pronounced following thermal priming of the crust, and assimilation plus fractional crystallization processes become dominant, as evidenced by lower MgO, higher K_2O and incompatible elements, and higher $^{87}\text{Sr}/^{86}\text{Sr}$ and $^{187}\text{Os}/^{188}\text{Os}$.

Chris Moore, Tim Wright, Andy Hooper, Juliet Biggs, Talfan Barnie

Submission 830

The 2017 eruption of Erta Ale, Afar, Ethiopia: Insights from Satellite Geodesy

Late-stage continental rifting in Afar, Ethiopia, provides the opportunity to observe magmatic spreading centres analogous to that of mid-ocean ridge systems. Erta Ale volcano, in northern Afar, has been the site of a sustained lava lake for over 90 years. Since 2005, a rise in lava lake height has been proposed to be attributed to wider scale magmatic activity throughout Afar and the Red Sea Rift. Previous studies have also shown the presence of a shallow magma system further north in the Erta Ale segment, which was the source for magma erupted in November 2008. In January 2017, Erta Ale erupted with lava lake overflows from the 19th, a vigorous fissure eruption on the south flank, c. 7 km SE and 95 m below the summit caldera, from the 21st, and sustained low-level effusion from the fissure from the 29th. Lava flows from the fissure eruption reached 3.1 km in length, and 3.3 km² in area by the 10th of March. We use Sentinel-1 and COSMO-SkyMed interferometric synthetic aperture radar (InSAR) observations of ground deformation during the 2017 Erta Ale eruption, and elastic models, to assess the magnitude and geometry of the sources of deformation occurring during, before and following the eruption. Initial results are consistent with a dyke intrusion between the 11th and 28th of January aligned with the ridge axis, extending from the summit caldera to the south flank eruption site, producing ridge-perpendicular extension of up to 30 cm. The timing of this intrusion is consistent with activity during the eruption, but due to temporal resolution, we cannot resolve at which point deformation occurred. Deformation patterns also indicate a component of ridge-perpendicular compression about the summit caldera of up to 10 cm, consistent with deflation of a shallow magma source. There is no clear sign of precursory deformation or any significant post-eruptive deformation. The deformation of Erta Ale during this eruption is significantly different to the behaviour during any previous overflow of the lava lake that has been observed with InSAR. We discuss the implications of the event for the plumbing system of Erta Ale, and for the behaviour of spreading centres in general.

Lyndsay Moore, Réal Daigneault, Dominique Genna, Claude Pilote, Claude Bernier, John Stix

Submission 174

Facies architecture, hydrothermal alteration and precious metal mineralization at submarine felsic volcanic complexes: insights from the felsic centres of the Abitibi greenstone belt, Quebec, Canada

Archean-aged sub-vertically- to vertically-dipping strata allow for the opportunity to study internal synvolcanic structures and architecture of ancient submarine felsic volcanic complexes. The 2704 – 2696 Ma Blake River Group in the Abitibi greenstone belt hosts numerous submarine felsic centres associated with economic, sub economic and barren volcanogenic massive sulfide deposits. Four volcanic centres clustered within the city limits of Rouyn-Noranda, Quebec - the Horne, Quemont, Glenwood and Delbridge complexes – all exhibit varying degrees of precious and base metal mineralization.

A multifaceted approach incorporating detailed facies mapping, core logging, petrography and geochemical analysis is employed to understand the similarities and differences at these centres. The Quemont, Delbridge and Glenwood complexes have facies consistent with effusive and autoclastic processes: massive to in situ brecciated flows intercalated with flow breccia facies and minor re-sedimented volcanoclastic units. Facies of the Horne (sampled from the Horne 5 zone) are distinctly different. Minor massive felsic flow facies are present but the centre is dominated by facies produced by combined pyroclastic and autoclastic processes. All felsic facies range in composition from dacitic to rhyolitic and all centres are affected by some degree of chloritic, sericitic, carbonate and silicic alteration. Hematization and albitization are variably present at some centres.

The Quemont, Horne and Delbridge centres all host Cu, Zn, Au and Ag mineralization, whereas the Glenwood has minor base metal mineralization and known Au mineralization. Pyrite is the dominant sulfide phase at all centres with lesser chalcopyrite, sphalerite and rare occurrences of pyrrhotite. The 54 million tonne Au-rich Cu deposit situated within the Horne complex is substantially larger in volume than those of the other neighbouring complexes. Its considerably larger size is likely directly related to the style and type of volcanism and host felsic volcanic facies. Gold mineralization within the deposit is found predominantly within the crystal structure of pyrite and is therefore largely invisible. A similar style of Au mineralization is present within stringer pyrite zones of the Quemont deposit and within pyrite phases of the Glenwood complex. This relationship will be further investigated in facies of the Delbridge complex.

Cindy Mora-Stock, Luca De Siena, Roberto Guardo, Gonzalo Carreño

Submission 1015

3D Attenuation Tomography at Villarrica volcano (Chile): Preliminary Results

Villarrica volcano, located in the southern Chilean Andes, is one of the most active volcanoes in the region. It is at the top of the list for most hazardous volcanoes in Chile, with its last recent eruption pulse occurring in March 2015. Villarrica volcano is strongly monitored for its activity, and highly studied to improve the knowledge of its processes.

Body-Wave Tomography provides information about the heterogeneous complexity of the region beneath the volcano edifice. In this occasion, we use the attenuation of body-wave amplitudes of volcano-tectonic events located inside the volcanic edifice recorded in March 2012. These events were obtained with a temporary network of 50 Short-Period stations, located at and around the volcano edifice. The events are in a N-S strike arrangement at about 4km to the east of the crater, between 3 and 5 km depth. This location and structure falls at the intersection of the two main crustal structures related to Villarrica volcano: Liquiñe-Ofqui fault (NS striking) and Villarrica-Lanin-Quetrupillan alignment (NW-SE striking).

The MuRAT (Multi-scale reasonable attenuation tomography analysis from De Siena, et al., 2014) code has been applied to other volcanic areas, such as Mt. Vesuvius, Mount St. Helens, Tenerife at Canary Islands, and Deception Island in Antarctica presenting valuable results complementing other tomography and velocity structure models. This method provides information from the full-waveform, adding information outside the direct path of the P-wave, as it is commonly used. We applied the MuRAT code at the selected dataset previously checked at local P-wave inversion tomography (Mora-Stock, et al. In Prep.), and we expect to complement the previous results found at Villarrica volcano.

Stanley Mordensky, Marlene Villeneuve, Ben Kennedy, Darren Gravley, Michael Heap, Graham Leonard, Jamie Farquharson, Thierry Reuschle

Submission 134

Shallow Intrusions and Their Effects on Permeability, Strength, and Jointing in Volcanic Strata

Magmatic intrusions alter host-rock strength and permeability by inducing fracturing in and alteration of the host rock. At Mt. Ruapehu, New Zealand, we mapped fractures and mineral alteration with respect to proximity of intrusions. Our aim is to compare these field analyses with laboratory strength and permeability measurements.

Mt. Ruapehu is an active andesitic stratovolcano with rockfall, landslide, and eruptive hazards. Our study focuses on the fossil hydrothermal system of Pinnacle Ridge in the Te Herenga formation (~170 ka). The Te Herenga is exposed in a nearly vertical sequence by glaciation (~10 ka). Pinnacle Ridge is composed of three distinct facies: variably altered coherent andesite lavas, variably altered andesite breccias, and several generations of dyke and stock intrusions.

We used several methods to observe a wide array of physical properties. These methods include UAV photogrammetry, ground-based scanline fracture mapping, field permeability (TinyPerm II), Schmidt Hammer analyses, and in-field rock mass classification. Data on samples prepared for the laboratory included porosity, permeability, elastic wave velocities, uniaxial compression strength, and triaxial compression strength. We completed a mineralogical assessment through the use of optical thin-section and TerraSpec analysis.

Together, these data show that primary lithology controls the fracture density, extent of smectitic alteration, and hence, the physical rock properties, to a greater extent than proximity to the intrusion. Alteration increases porosity and therefore reduces rock strength. Further, a change in the failure mode—from brittle to ductile—is observed in triaxial experiments due to alteration alone. The contrasting rock properties have implications for controlling fluid flow, and thus heat flow, in volcanic and geothermal systems. We suggest this type of detailed field study can provide important context to laboratory-based mechanical studies and hazard models.

William M. Moreland, Thorvaldur Thordarson, Bruce F. Houghton, Gudrun Larsen

Submission 1059

The nature of explosive activity during the 10th century Eldgjá fissure eruption, southern Iceland.

The 10th century Eldgjá flood lava event is the largest eruption in Iceland in historical time (i.e. the last 1140 years) and erupted 21 km³ of magma, 19.7 km³ as lava and about 1.3 km³ as tephra (all volumes are given as dense rock equivalent). Activity began in the southwest beneath the Mýrdalsjökull glacier and progressed to the northeast with time to form a 70 km long vent system. The tephra was formed in at least 13 separate explosive episodes originating initially from subglacial and later subaerial fissure segments along the vent system, producing a sequence of phreatomagmatic and magmatic tephra deposits more than 2.5 m thick at distance of 10 km from the vents. Unit 7 (magmatic) and unit 8 (phreatomagmatic) were studied in detail. Both units were dispersed to the east-southeast from 13 to 17 km high eruption columns. Unit 7 deposit has a volume of 0.02 km³ and has a positively-skewed unimodal total deposit grain-size distribution with a mode at -2.5 Φ and a median grain-size of -2.2 Φ . Unit 8 has a volume of 0.03 km³ and a bimodal total deposit grain-size distribution with broad peaks at 0.0 Φ and 5.0 Φ . The total deposit grain size distribution for the magmatic versus the phreatomagmatic units are distinct and record different fragmentation histories. However, the high clast vesicularity (61-80%) along with identical vesicle-size distributions for both units show that the magma erupted in the phreatomagmatic phase featured identical vesiculation (i.e. nucleation and growth of bubbles) as the magma erupted in the magmatic phase. Hence, in the case of the phreatomagmatic phase the external water encountered the magma after it was fully vesiculated or in other words at the time of venting. We take this to indicate that the contribution of the external water to magma interaction was confined to enhancing fragmentation an already formed lapilli-size foam of the magma upon venting via quenched granulation and its contribution to enhancing the intensity of the explosive phases was minimal.

Daniele Morgavi, Donald Swanson, Lucia Mancini, Marco Voltolini, Fabio Arzilli, Diego Perugini

Submission 742

3D Microtomography on accretionary lapilli from the 1790 CE Kīlauea volcano eruption

Kīlauea Volcano, mainly known for its effusive behaviour with the production of lava flows and fountains, produced an explosive eruption in November 1790 CE that killed a large number of people (Swanson et al., 2014). This eruption was probably the largest in a series of explosive events that formed the Keanakākoʻi tephra over a 300-year period starting in about 1500 CE. In previous studies, the upper part of the Keanakākoʻi section was divided into 14 stratigraphic units, I-XIV, from youngest to oldest (Swanson et al., 2014). The 1790 deposits, comprising at least units XI-VIII and possibly including XII-XIV, consist mainly of phreatic, lithic lapilli and ash falls and cross-bedded and laterally discontinuous lithic deposits of pyroclastic density currents. In this work we focus on the fall deposit X, containing many accretionary lapilli and informally named the “footprints ash” because of thousands of human footprints imbedded on its surface.

Accretionary lapilli were characterized by BSE images, and electron microprobe analyses of major elements were performed on glasses and minerals. Although BSE images provide accurate morphological information, they do not allow understanding the 3D microstructure of such a complex volcanic feature. Therefore, a non-invasive 3D characterization of the lapilli was performed by using X-ray microtomography (X-mCT). The novel results of the X-mCT measurements provide reconstructed volumes of the accretionary lapilli with an isotropic voxel size varying between 6.2 and 15.0 mm, depending on the sample size. This technique helped us for the first time to better constrain the volume and the spatial distribution of vesicles, cracks (between accretionary layers) and crystals inside the accretionary lapilli otherwise obscured in conventional 2D observation and analysis. Morphometric analysis clearly identifies a class of thin cracks connected to the outside, in the outermost region of the lapilli, and another class with wider (i.e. smaller aspect-ratio) cracks closer to the centre, and unconnected to the outside. Vesicles are typically much smaller in size, but are volumetrically as important as the cracks. X-mCT proved to be the ideal method to study the 3D microstructural characteristics of the lapilli in a non-destructive fashion, providing new insights about their growth history.

Azusa Mori, Hiroyuki Kumagai

Submission 43

High-frequency seismic source amplitude of eruption tremor and its use for estimating eruption plume height

We studied the relationship between eruption plume heights and high-frequency seismic amplitudes of eruption tremors and explosion events to understand eruption phenomena and to estimate eruption size. We estimated source amplitudes (A_s) of eruption tremors and explosion events using high-frequency seismic amplitudes based on the assumption of isotropic S-wave radiation. Using the envelope waveform corrected for geometrical spreading and medium attenuation in a frequency band of 5-10 Hz, A_s is estimated as the envelope amplitude averaged in a 10-s window including the maximum amplitude. We analyzed eruption tremors and explosion events at Sakurajima, Kuchinoerabu, Ontakesan, and Kirishima volcanoes in Japan and Tungurahua volcano in Ecuador. We found that the maximum eruption plume heights (H_{Max}) during eruption tremors are proportional to 0.21 power of A_s . We also compared time-series data of plume heights (H) for the sub-plinian eruptions at Kirishima volcano in January 2011 with individual A_s values in corresponding time windows. The estimated relation between H and A_s is not represented by a power law relation when H is less than 6 km, and H becomes zero when A_s is less than a certain value. Based on the physical process of buoyant plume rise for plinian eruptions, H is proportional to 0.25 power of the volumetric flow rate in the upper troposphere and the stratosphere, in which plume rise is controlled by buoyancy given by air entrainment. If we assume a seismic source with volume changes and far-field S-wave, A_s is proportional to the source volume rate. Moreover, if we assume that the volumetric flow rate is equal to the source volume rate, H is proportional to 0.25 power of A_s . This indicates that the power law relation between H and A_s is established in the upper troposphere and the stratosphere. When the speed of plume rise is slow, air entrainment in plume is not sufficient. In this case, plume rise is controlled by momentum and stops in the lower troposphere due to the lack of buoyancy. Therefore, the power law relation between H and A_s may not be established in the lower troposphere. This is consistent with our result that the relation between H and A_s is not expressed by a power law relation when H is less than 6 km. These results indicate that the scaling between H and A_s is universally established in the upper troposphere and the stratosphere, which may be used to estimate eruption plume height.

Yuichi Morita

Submission 293

Detection of rising volatile from multi-parameters of seismicity based on stress response of volcanic earthquakes

By extrusion of volatile components from magma reservoir, high temperature volcanic gases often rise up to the ground prior to eruptions and they heat aquifer and ground surfaces. It shows that increases in fumarolic activities, appearance of volcanic tremor and anomaly of magnetic field around a crater when the volatile reaches near the ground surface. But the volatile at the depth has not been sensed well by any method. To detect rising volatile at deeper zone, the concept of stress response of volcanic earthquakes is introduced here. Parameters of earthquake generation rate: seismicity, GR b-value and tidal response are used to monitor volcanic activities independently and have not been discussed fully on the mutual relations. Using the concept, I focus on the change in effective normal stress, that composed of tectonic normal stress and pore pressure.

I analyzed volcanic earthquakes occurring at the depth of 2-3km beneath the caldera and just above the magma reservoir of Izu-Oshima volcano, central Japan, where the ground inflation began several years after the latest eruption in 1986-87. From simultaneous analysis of seismic and geodetic data from 2003 till the present, it is confirmed that the seismicity correlates well with the ground deformation and is roughly predicted using rate and state friction law (RSF) for the all over period. This shows that the seismicity in the region is very sensitive to stress rate caused by inflation of magma reservoir and ambient stress. In addition, the temporal change in multi-parameters of seismicity: rate, b-value, and the tidal response appeared systematically. Before 2011, the seismicity well obeys the RSF and has no correlation with the tidal stress. After 2011, seismicity becomes greater than the value expected by the RSF, and tidal response appears after 2013. The b-value decreases slightly after the same time. One of the plausible models that can explain all above phenomena is an increase of pore-pressure at the hypocenter zone. Considering that the average interval of eruptions is 30-40 years at this volcano, the next eruption is expected in several years, even fumarolic activity and anomaly of magnetic field are not observed now. Increasing pore-pressure may be caused by the volatile components rising up from magma reservoir. In conclusion, the monitoring multi-parameters in seismicity may be able to detect the uprising volatile at the depth with the help of the concept of stress response of seismicity.

Kaori Morita, Takeshi Matsushima, Kazunari YOKOO, Rintaro MIYAMACHI, Yoshiko TEGURI, Shiori FUJITA, Manami NAKAMOTO, Hiroshi SHIMIZU, Hitoshi MORI, Masayuki MURASE, Takahiro OHKURA, Hiroyuki INOUE, Akihiko YOKOO

Submission 324

Vertical ground deformation of Ioyama, Kirishima volcanoes measured by precise leveling survey (during June. 2015 - Feb. 2017)

Ioyama of Kirishima Volcanoes is located in Ebino kogen volcanic area, southern Kyushu. This volcano has activated since December 2015. We conducted the precise leveling survey in the Ebino kogen volcanic area for 7 times from June 2015 to February 2017. The purpose of the survey is to reveal the vertical deformation and pressure source. Inflation of the Ioyama was detected since we initiated this observation to March 2016. Subsequently, the ground subsided from around June 2016. However, uplift is detected around the Ioyama again in November 2016.

From the surveyed leveling data in February 2017, the vertical displacements indicate the ground uplift at all bench marks. In this study, the reference bench mark is BM1120 at the western flank of Ioyama. The amount of maximum uplift is about 17.3 mm near the summit referred to BM1120 in February 2017. We estimated pressure source models based on the vertical deformation. We supposed the presence of an inflation spherical source as Mogi's model. As a result, the depth has been inferred about 700 m and the increase of pressure source volume since June 2015 is detected 4.5×10^4 m³ in February 2017. The lower limit of low resistivity layer assumed to be the clay layer is estimated in this depth (Aizawa et al., 2013). Accordingly, the inflation source by using precise leveling survey is located under the impermeable clay layer.

Aaron Morrison, Michael Zanetti, Christopher Hamilton, Catherine Neish, Einat Lev, Alan Whittington

Submission 873

Rheology of lunar highland and mare impact melt simulants: JSC-1a, Stillwater anorthosite, and Stillwater norite

Energy released during impact cratering events can rapidly heat silicate materials to superliquidus temperatures and generate gravity-driven melt flows that behave, ostensibly, like lava flows. However, the rheology of impact melt flows on the Moon and other planetary bodies is poorly constrained. To address this, we characterized three lunar simulant materials (JSC-1a representing mare basalt, Stillwater anorthosite and Stillwater norite representing lunar highlands) using differential scanning calorimetry (DSC) and viscometry. Liquidus and glass transition temperatures (T_{liq} and T_g) determined by DSC were 1325°C and 665°C for JSC-1a; ~1550°C and 840°C for the anorthosite; and 1452°C and 780°C for the norite. Superliquidus viscosity measurements were made for each by concentric cylinder viscometry and supercooled glass measurements by parallel plate viscometry just above T_g . These span viscosity (η , Pa s) ranges of -0.2–1.0 log units and 9.0–12.3 log units, respectively. The data were fit by Vogel-Fulcher-Tammann equations, allowing viscosity to be extrapolated to higher temperatures. At 2000°C the liquid viscosity of JSC-1a is 0.08 Pa s, anorthosite is 0.1 Pa s, and norite is 0.1 Pa s, suggesting most impact melts will have similar, extremely low viscosities if initially emplaced at these very high temperatures.

Subliquidus experiments were conducted for each composition to quantify how viscosity changes with crystal fraction. JSC-1a behaved like terrestrial basalts, remaining Newtonian until pseudo-plastic behavior began near 1250°C. Attempts at measuring the norite and anorthosite at subliquidus conditions proved difficult due to rapid crystallization. The MELTS model of Gualda et al. (2012) predicts rapid crystallization for both samples over a narrow subliquidus temperature range. This implies that thick flows of norite- or anorthosite-like materials on the Moon would become too viscous to flow after only a few degrees of undercooling. This rheological change is expected to occur quickly, in space and time, in impact melt sheets. However, anorthosite-like material is observed on the Moon flowing far from crater rims (e.g. Giordano Bruno) suggesting extreme superliquidus initial temperatures, slower than expected cooling rates, or a combination thereof. JSC-1a crystallized at a slower rate allowing measurement over a wider temperature range. Further data will be collected for chemical analyses, evolved compositions, crystal fraction and aspect ratio analyses.

Matthew Morriss, Leif Karlstrom, Morgan Nasholds, Kendra Murray

Submission 975

Constraints on the structural and thermal conditions of Columbia River Basalt feeder dikes from a comprehensive regional dataset

The Chief Joseph dike swarm (CJDS) fed the Imnaha and Grande Ronde flows of the Miocene Columbia River Basalt Group (CRBG) in SE Washington, NE Oregon, and W Idaho. The CRBG is the best-studied large igneous province (LIP) on Earth; however, the processes at work within the conduits that fed this LIP have not been fully characterized. We use digitized, unpublished maps by William H. Taubeneck (Oregon State U.) to interrogate the dynamics of the CRBG magmatic plumbing system. This dataset contains ~4400 dike segments in an area of ~15,000 km² and 40 years of field notes corresponding to most mapped dikes. We combine structural analysis with low-temperature thermochronometry to better characterize the magmatic flux through the CJDS.

Initial analysis of Taubeneck's maps indicates greater complexity within the CJDS than previously recognized. There is a well-recognized NW trend in the CJDS, sub-parallel to the cratonic boundary. Additional trends orthogonal or sub-parallel to the main trend also exist. Dike orientation shows no direct correlation with bedrock joints or regional faults; this does not preclude some involvement. The mean thickness of all segments is 9.2 ± 7.6 m; the mean length is 463 ± 423 m, with a maximum length of 3.8 km. Dike segmentation is an artifact of intermittent exposure and likely mixed-mode fracturing that resulted in en echelon segments. If the CJDS is dominated by Grande Ronde dikes, the variability in dike orientation implies abrupt transitions in the regional stress field and/or major reorganization of the magmatic plumbing system over several 100 kyr. We plan to investigate relative timing through cross-cutting relationships.

Only ~3% of Taubeneck's mapped CJDS dikes have evidence of prolonged conduit activity, which reflects how magma flux was partitioned through the swarm. Previous work on host-rock melt zones along the Maxwell Lake dike margins (Wallowa Mtns.) suggest several years of activity. Fluid flux estimates suggest that all CJDS segments could not have been active nearly as long. The extent of country-rock heating by individual dikes, documented by the pattern of low-temperature thermochronometer resetting, can constrain the timescale of magma flux through CJDS conduits. We explore this using apatite and zircon (U-Th)/He dating of country rocks in a transect perpendicular to the Maxwell Lake dike, which should determine the extent to which this method can constrain the overall emplacement rate pattern of the CRBG.

Adam Mosbrucker, Jon Major, Kurt Spicer

Submission 116

As decades roll by, Mount St. Helens' sediment keeps on truckin'

Explosive eruptions deposit sediment in topographically diverse environments—both on hillsides and in river valleys. Thus, sediment-response trajectories after eruptions commonly exhibit a two-stage evolution. Initial erosion of sediment from hillsides and channels, when systems are far from equilibrium, is typically very rapid and dramatic, thus rates of sediment delivery can be orders of magnitude above typical pre-eruption levels. If new sediment is not deposited by frequent eruptions, this initial phase of system response usually lasts only a few years before erosion and sediment delivery decline markedly. Subsequently, some catchments, especially those having severely disturbed channels, enter a secondary phase of sediment delivery greatly diminished from peak levels but persistently higher than pre-eruption levels. This secondary phase of diminished, but elevated, sediment delivery can persist for decades, perhaps centuries, depending on the magnitude of disturbance and local physiography. The Toutle River basin at Mount St. Helens exemplifies this two-stage conceptual response. In that watershed, a massive debris avalanche, extensive pyroclastic surge, and lahars during the volcano's 1980 eruption delivered abundant sediment that eroded rapidly. Initial suspended-sediment yield (SSY) from the Toutle River basin (>104 t/km²) was several hundred times greater than probable pre-eruption yields (~ 102 t/km²), owing mainly to channel incision across the debris-avalanche deposit. This extraordinary SSY decayed swiftly within a few years as rates and magnitudes of hillside and channel erosion declined sharply. After nearly 40 years, SSY remains elevated at ~ 103 t/km², yet the longitudinal profile of the upper North Fork Toutle River across the avalanche roughly stabilized about 10 years after eruption. Thus, channel incision is not the primary process driving this persistently abnormal yield. Repeat topographic surveys show persistent lateral channel processes owing to bed reworking, bank erosion, and mass wasting along the main fluvial corridor are principally responsible for maintaining abnormally elevated SSY. Persistently elevated sediment delivery from the upper North Fork Toutle River continues to beget significant monetary expenditures on hazard mitigation for downstream communities.

Sophie Mossoux, Mathijs Saey, Sam Poppe, Stefania Bartolini, Frank Canters, Matthieu Kervyn

Submission 498

Q-LavHA, a plugin to simulate lava flows: functioning and applications

Accurate simulation of lava flow extent is essential information in locations confronted with imminent or long-term lava flow hazard from basaltic volcanoes. As the world population grows and the exposed infrastructures increase, knowing what is the probability of an area to be inundated by lava flow becomes increasingly important. Models for estimating lava flow emplacement exist. Each of them has its strengths and restrictions but most of them are not easily available.

Q-LavHA is a new open access plugin which simulates channelized lava flow propagation on a Digital Elevation Model. The opportunity to choose between different options to model the eruptive vent(s), the lateral extension and the lava flow length enable its use in different environments where knowledge on lava flow properties varies.

The simulations are produced from one or multiple regularly distributed eruptive vents. This option enables lava flow simulations from a well-defined vent, an eruptive fissure or clusters of closely spaced vents. The spatial lateral extension is constrained by the steepest slope following the probabilistic approach of Felpeto et al. (2001). The corrective height factors which are included allow the lava flow simulation to overcome small topographical obstacles. The terminal length of the lava flow can be determined based on a fixed length value, a Gaussian probability density function, or based on the thermo-rheological properties of a cooling open-channel lava flow following the approach of the FLOWGO model (Harris and Rowland, 2001). Using susceptibility maps giving the probability of occurrence of different vent locations, lava flow hazard maps can be generated.

In this contribution, we demonstrate the functionalities of Q-LavHA. We confront the simulations produced by Q-LavHA with recent lava flow emplacements to discuss the implications of the main parameters of the plugin as well as the influence of the background slope and the DEM resolution. Contrasted level of input data are used to demonstrate the flexibility of the plugin. Additionally, we present lava flow hazard maps produced by Q-LavHA and investigate their reliability.

REFERENCES:

- Felpeto et al. (2001), Assessment and modelling of lava flow hazard on Lanzarote (Canary Islands), *Nat. Hazards*, 23, 247-257.
- Harris and Rowland (2001), FLOWGO: a kinematic thermo-rheological model for lava flowing in a channel, *Bull. Volcanol.*, 63, 20-44.

Patricia A Mothes, Elizabeth H. Gaunt, Mario C. Ruiz, Minard L. Hall, Silvana Hidalgo

Submission 957

Step by Step Awakening at Cotopaxi Volcano: A new look at the geophysical beginnings of recent and past eruptions and conduit processes

Cotopaxi's 2015 unrest culminated in low-level eruptions from August to November, producing ~0.8M m³ of ashfall before return to calm. This uptick was preceded in 1976 and 2001/02 by non-eruptive unrest. The dense monitoring network operating in 2015 recorded LPs, VTs, hydrothermal tremor, then followed by deep and energetic VLP's, and synchronous positive tilt and outward GPS displacements, signals thought to represent magma movement. Strong SO₂ degassing ensued post August 14th eruption. Petrologic study of erupted ashes showed that glassy ash expelled in mid August had low micro-crystallinities which suggests rapid ascent of juvenile magma. The abundance of hydrothermally altered ash also suggests that the juvenile magma interacted with a hydrothermal system, possibly triggering the first explosions. As the eruption progressed more microlite-rich material was erupted; microlites may indicate higher magma viscosity and lower magma ascent rates. Simultaneously the seismic energy levels and deformation rates decreased. Thus three parameters; ash petrology, reduced seismicity, and weaker flank deformation, jointly indicated the eruption's waning.

In retrospect, the initiations of Cotopaxi's 4 historical (1532-1877) eruptions of paroxysmal intensity began with ejection of ballistic blocks (~0.5m diam.) out to 4-6 km from the vent. These conduit plug rocks are dense highly-crystalline, vesicle-poor, with minor porosity and low permeability that led to the Vulcanian-style eruptions. This conduit and vent clearing left conspicuous layers of ballistic fragments, then followed by emplacement of juvenile products in the stratigraphy of these historical-age VEI 4 eruptions. Since the 2015 VEI 1 eruption products are now mostly eroded, it was thought that similar small, 2015-like eruptions might have occurred prior to the historical paroxysmal events; these were not recognized.

Using the near-field ballistic-juvenile sequences as a guide to inform on the possible timing and characteristics of future Cotopaxi eruptions, we postulate that significant "ratcheting up" of seismic energy levels, magma input and pressure release are necessary to blow out the dense, low porosity conduit plug rock that may have formed over the past ~75 years. We anticipate that synchronous strong seismicity and ground deformation, followed by increased degassing, and high infrasound values will be the fundamental precursors to announce proximity of future Cotopaxi eruptions.

Severine Moune, Olgeir Sigmarsson, Pierre-Jean Gauthier, Evgenia Ilyinskaya

Submission 792

Fractional magma degassing at Holuhraun, Bárðarbunga volcanic system, Iceland

The 2014-2015 Bárðarbunga rifting event in Iceland resulted in a 6-month long eruption at Holuhraun. This eruption was characterized by high lava discharge rate and significant gas emission. Indeed, the SO₂ flux, estimated at approximately 10Tg, is the largest yet measured for basaltic fissure eruptions (Gislason et al., 2015 ; Gauthier et al., 2016). The extended duration of this basaltic fissure eruption (6 months from 29 August 2014 to 27 February 2015) led to considerable major volatile (elevated S/Cl) and trace metal fluxes to the atmosphere (Gauthier et al., 2016).

After the eruption came to an end, the lava field continued to degas and the residual gas phase could be sampled from the principal crater. Gas and aerosol samples were collected early March 2015 and were subsequently analyzed for major gas species and trace element concentrations. Compared to the primary gas phase collected early October 2014, the residual gas has low S/Cl mass ratios (0.9-1.6 versus 40-52 in the primary gas) and elevated F/Cl, with 50 times more F released during the secondary degassing. All analyzed trace elements appear to be present in the gas plume with enrichment factors relative to Mg up to 105 (Se). Most of the trace element concentrations are depleted by 1 to 3 orders of magnitude compared to primary degassing, except for Sb, As, Re and Se, which have chalcophile behavior. However, REE patterns normalised to Holuhraun lava composition show an enrichment of LREE over HREE suggesting degassing as chlorides during both degassing phases.

The available results strongly support the earlier volatilization of sulfur compared to halogens at Holuhraun, as well as chlorine versus fluorine. They suggest also a pure fractional degassing process, or a Rayleigh distillation. The residual degassing is thus responsible for elevated F in precipitations (Stefánsson et al., 2017) collected during the eruption.

Yves Moussallam, Nial Peters, Philipson Oppenheimer, C. Ian Schipper, Talfan Barnie, Aaron Curtis, Alessansro Aiuppa, Giancarlo Tamburello, Joao Lages, Pablo Masias, Fredy Apaza, Silvana Hidalgo, FReddy Vasconez, Marco Almeida, Diego Narvaez, Alvaro Amigo

Submission 234

A snapshot of volatile degassing at the scale of an entire subduction zone; the “Trail by Fire” expedition.

Quantifying the total flux of volatiles emitted by active volcanoes is a community-wide endeavour with the double aim of (i) Understanding volatile cycling at the planetary scale and (ii) Improving global climate models. We present preliminary results from the Trail by Fire expedition that took place between 2015 and 2017. The expedition aimed at providing a snapshot of volatile degassing at the scale of the entire Nazca plate subduction zone by providing remote and direct measurements at nearly twenty degassing volcanoes along the arc. Secondary objectives of the expedition were (i) to acquire $\delta^{13}\text{C}$ measurements in volcanic plumes by Isotope Ratio Infrared Spectroscopy (IRIS), (ii) to acquire simultaneous ground and satellite-based observations and (iii) to perform UAV-based measurements in volcanic plume. An overview of the key findings will be given along with highlights from specific case studies.

Yves Moussallam, Philipson Bani, Aaron Curtis, Talfan Barnie, Manuel Moussallam, Nial Peters, C. Ian Schipper, Alessandro Aiuppa, Gaetano Giudice, Alvaro Amigo, Gabriela Velasquez, Carlos Cardona

Submission 237

Sustaining persistent lava lakes: high-resolution gas measurements at Villarrica volcano, Chile

Persistent lava lakes require a maintained heat supply to sustain a molten state at the Earth's surface. Several mechanisms have been proposed to explain how such heat transfer can operate efficiently. These models assume different magma flow regimes in volcanic conduits and it should, in principle, be possible to differentiate them in terms of gas emissions at the surface. Here we investigate high-frequency SO₂ fluxes, plume composition, thermal emissions and aerial video footage for Villarrica's lava lake in order to interpret the mechanism sustaining its activity. We found that while fluctuations are apparent in all datasets, none shows a stable periodic behaviour. The observations rather suggest a continuous influx of volatiles and magma to the Villarrica lava lake, which points to efficient mixing of ascending volatile-rich and descending degassed magmas within the conduit. We compare our findings to those for other lava lakes where comparable gas emission time-series have been acquired, and suggest that gas flux, magma viscosity and conduit geometry are key parameters that determine flow regime. We consider the broader implications for conduit flow at other volcanoes without lava lakes.

Danielle Moyer, Christine Sealing, Simon Carn, Michael Burton, Loïc Vanderkluysen

Submission 782

Measuring H₂O and CO₂ Emissions in the Mud Volcano region using Open Path FTIR (Yellowstone National Park)

Magma degassing is an important factor in many aspects of monitoring active volcanic zones and mitigating associated hazards. The monitoring of these emissions in concentration, flux, and species ratios is important for detecting signs of unrest as well as understanding the natural cycle and budget of volatile species. However, standard gas measurement methods suffer from either low temporal resolution (e.g., direct sampling of fumaroles) or are limited to measuring a small range of species (e.g., MiniDOAS, MultiGAS). Most remote sensing methods struggle with two key gas emissions that are important to monitoring volcanic activity: carbon dioxide (due to its high atmospheric abundance) and hydrogen sulfide (due to absorption features overlapping with those of water vapor). In order to establish a carbon budget of active gas sources at a volcano with a dynamic hydrothermal system, we carried out a survey of mud pots and fumaroles at Yellowstone National Park using Open-Path Fourier Transform Infrared Spectroscopy, or OP-FTIR, which allows for a temporal resolution as low as one measurement every 10 seconds. We placed an active infrared (IR) source behind the target gas plume and identified gas species from the presence of their absorption feature in measured spectra in the 2.5 to 25 μm range. From these, we derived pathlength concentrations for a wide range of gases, including: water vapor, carbon dioxide, and methane. During our September 2016 campaign in the Mud Volcano thermal area, we measured CO₂ concentrations of 400 ppm in emissions from the Churning Cauldron mud pot, with an H₂O/CO₂ ratio of ~ 8 ; at Sulphur Cauldron, CO₂ concentrations reached 200 ppm above background atmospheric values. We calculated a CO₂ flux of 8.15 T/d and 0.43 T/d, respectively, at these two acid ponds, within range of gas channeling-based estimates from the late 1990s. Previous accumulation chamber studies estimate the CO₂ soil diffuse degassing in the Mud Volcano thermal region at 283.15 T/d, indicating that mud pots are minor contributors of CO₂ emissions in this area, representing $\sim 3\%$ of diffuse emissions. Due to the high acquisition rate and the abundance of water droplets in the plume, spectra were too noisy to reliably detect methane at these locations. Future work will focus on the measurement of trace gases at these same locations by increasing the acquisition time.

Adonara Mucek, Shanaka de Silva, Daniel Miggins, Martin Danišik, Axel Schmitt, Indyo Pratomo

Submission 903

Post-74 ka supereruption magma dynamics at Toba Caldera, Indonesia: Constraints from phase equilibria, $^{40}\text{Ar}/^{39}\text{Ar}$ and (U-Th)/He age determination

The worldwide youngest resurgent caldera, Toba Caldera, Indonesia, entered its current cycle of resurgence after the last caldera eruption 74 ka, producing the Youngest Toba Tuff (YTT). Accompanying the period of resurgence was the uplift and formation of the resurgent dome (Samosir Island) and several lava dome extrusions along ring fractures and faults that cut through the caldera. Previous geochronology for four of these lava dome localities (North Samosir, Tuk Tuk Samosir, North Pardepur, South Pardepur) by combined U-Th-disequilibrium/(U-Th)/He zircon geochronology yielded eruption ages ranging from 69.7 ± 4.5 ka to 56.9 ± 3.9 ka (all errors 2 s.d.), implying resurgent volcanic activity started almost immediately after the climactic eruption and continued for ~ 20 kyrs after. In comparison, $^{40}\text{Ar}/^{39}\text{Ar}$ ages from sanidine and plagioclase feldspar crystals from the same lava domes have returned ages that are contemporaneous with the climactic eruption, between 74.5 ± 6.7 and 73.8 ± 0.9 ka for North Samosir, Tuk Tuk Samosir, and South Pardepur, with only North Pardepur showing a substantially younger $^{40}\text{Ar}/^{39}\text{Ar}$ crystallization age of 57.0 ± 10.2 ka. Matrix glass analyses represented on the quartz-albite-orthoclase (Qz-Ab-Or) ternary plot indicate that the Samosir dome magmas equilibrated over a deeper range of pressures (200-50 MPa) than the YTT (100-50 MPa), while the Pardepur dome magmas record the lowest pressures (50-0.1 MPa). Using Fe-Ti oxide eruption temperatures for these resurgent lava domes between 814 ± 20 and $891 \pm 20^\circ\text{C}$ as calculated from the North and South Pardepur domes and a simple diffusion model, the difference in the (U-Th)/He and $^{40}\text{Ar}/^{39}\text{Ar}$ dating methods can be explained by a difference in closure temperatures between argon and helium. Sanidine and plagioclase feldspar crystals from three lava domes recording the YTT eruption age are interpreted as antecrysts, remaining in the remnant magma system below argon closure temperature (T_c) in sanidine/plagioclase (350°C) and retaining the YTT age, until injection of newer, hotter magma into the system triggered lava eruptions; these are recorded by the (U-Th)/He zircon ages. By contrast, the younger ca 57 ka $^{40}\text{Ar}/^{39}\text{Ar}$ plagioclase age of North Pardepur overlaps with the (U-Th)/He age, implying that plagioclase crystals are either autocrysts formed during the eruption of the North Pardepur dome, or YTT antecrysts that have been reset due to their host magma remaining above argon T_c for >2500 yrs.

Sebastian P. Mueller, Christoph Helo, Franziska Keller, Jacopo Taddeucci, Jonathan Castro

Submission 806

The Atmosphere Strikes Back: Rapid Remelting of Ash by Volcanic Lightning in the Laboratory

Lightning discharge is a common phenomenon associated with volcanic eruption plumes. During the formation of ash plumes, dynamic interaction of ash particles can create electrostatic gradients sufficiently large to cause lightning discharges within the plume or from ground to plume. Given the extreme heat release during the short duration of a discharge, it is likely that the ash particles suspended in a plume are affected by volcanic lightning. Genareau et al. (2015) linked the occurrence of glass spherules and botryoidal aggregates in ash deposits of two explosive eruptions (Eyjafjallajökull, Mt. Redoubt) to rapid melting processes induced by volcanic lightning – in analogy to fulgurite formation.

In order to systematically investigate the potential impact of lightning on air-suspended ash, we have designed an experimental setup, in which an electric arc between two electrodes is generated by a 400 A arc-welding device. Volcanic ash is then blown into the established lightning arc, and a certain proportion of the injected material is rapidly melted due to the high temperatures in and around the plasma channel.

In a reconnaissance study, we have used natural volcanic ash from Sakurajima volcano (Japan) and Chaiten (Chile), as well as homogenized phonolitic glass, to investigate ultra-rapid melting and amalgamation features, and chemical alterations. Spherule and aggregate textures similar to those reported by Genareau et al. (2015) were successfully reproduced during these experiments. Using a 100,000 fps high-speed camera, we further document various processes occurring during the short lightning-ash interaction, including particle melting and rounding, vesiculation and foaming, fragmentation, as well as the particles' thermal evolution.

Genareau K, Wardman JB, Wilson TM, McNutt SR, Izbekov P (2015): Lightning-induced volcanic spherules. *Geology*, doi:10.1130/G36255.1.

Sebastian Mueller, Ulrich Kueppers, Jonathan Ametsbichler, Corrado Cimarelli, Jonathan Merrison, Matthieu Poret, Fabian Wadsworth, Donald Dingwell

Submission 402

Deposition or not? The fate of volcanic ash aggregates

Explosive volcanic eruptions can inject populations of magmatic fragments (on the order of several km³) into Earth's atmosphere. Volcanic ash (< 2 mm) can experience very long atmospheric residence times and commonly achieve global distribution. Numerical modeling of the dispersal of such volcanic ash plumes is a major tool used in routine efforts to mitigate the potential hazards of ash fall for inhabitants, infrastructure and transportation. The accuracy of plume dispersal forecasting has significantly increased, both with respect to temporal resolution and the estimation of ash concentration. Recent tephra dispersal models have been expanded to include descriptions of dynamic ash aggregation processes mostly under wet conditions (i.e. air moisture and water magma content). Although significant progress has been made recently concerning ash aggregation processes, studies of preservation rates of ash aggregates during atmospheric transport are lacking entirely. It follows that current models are forced to regard ash aggregation as irrevocable and therefore likely overestimate aggregation-enhanced sedimentation. First, we have experimentally produced particle aggregates using natural volcanic ash and analogue silicate glass beads. Then, we performed impact tests to study the influence of 1) primary particle size distribution, 2) primary particle surface morphology and 3) particle-particle binder concentration on aggregate impact survival. It returned that aggregate break-up may result from insufficient cementation and/or impact with other particles or aggregates. We also observed experimentally that aggregate stability is enhanced at coarser primary particle sizes (> 50 μm), whereas aggregates composed of finer primary particle sizes (<50 μm) are weaker. Scanning electron microscopy has yielded insights into the mechanisms for the development of strength in aggregates. We offer our analysis of aggregate stability factors to be combined with eruption source parameters for implementation in future tephra dispersal models. As the effective distal ash concentration is a critical parameter for assessing the necessity of immediate first responder actions including air space closure and health protection measures, we anticipate that ash aggregation and disaggregation will greatly benefit the further development of ash dispersal forecasting.

L.J. Patrick Muffler, Andrew T. Calvert, Duane E. Champion, Michael A. Clynne, Drew T. Downs, Robert L. Christiansen

Submission 687

The Cascades volcanic arc between the Lassen Volcanic Center and Mount Shasta, northern California

It has been recognized for at least three decades that the Lassen segment of the Cascades volcanic arc is separated from the segment to the north that includes Mount Shasta by a ~75-km gap that contains very few young volcanic vents. We have carried out coordinated geologic mapping, rock chemistry, $^{40}\text{Ar}/^{39}\text{Ar}$ dating, and paleomagnetic studies (Champion et al., this volume) to elucidate the geologic history of this gap. Our studies confirm that there are no late Quaternary calc-alkaline vents along the axis of the Cascades volcanic arc from Burney Mountain (36 km north of Lassen Peak; Downs et al., this volume) north to nearly Mount Shasta. South of Burney Mountain, the arc is marked by prominent but areally restricted, calc-alkaline, dominantly andesitic edifices of late Pleistocene age that rest on a highly faulted terrain of older (~2.8–1.8 Ma) andesitic rocks. East of these prominent calc-alkaline volcanoes (but west of the Hat Creek fault) are thin, laterally extensive flows of low-potassium olivine tholeiite basalt (LKOT) that range in age from 650 to 24 ka. The LKOTs all flow from south to north, with their termini (occasionally marked by pillow breccias) along the Pit River valley. North of the Pit River, the terrain is dominated by highly weathered, monotonous LKOTs, mostly 1.2–0.8 Ma (but two at 0.3 Ma) that all flow from north to south around ~2.5–2.0 Ma calc-alkaline edifices. The distal termini of these LKOTs are also at the Pit River. The Pit River topographic low is also marked by extensive thick diatomite deposits bracketed by dated LKOTs of 1.8 and 1.0 Ma. The midpoint of the gap has thus been topographically low for at least 1.8 million years.

In detail, the volcanic arc and the gap display significant complexity. Both within and south of the volcanic gap, a few moderate-sized calc-alkaline edifices exist 8–25 km east of the calc-alkaline axis. Also, the youngest volcanism from Burney Mountain south to the Lassen Volcanic Center is expressed by a zone of small-volume, calc-alkaline basalts in a graben just east of the prominent andesitic volcanoes that mark the Cascades axis. Normal faulting probably related to Basin and Range extension has affected volcanic rocks primarily east of the arc axis, with vertical displacements ranging from 33 m on the 24 ka Hat Creek Basalt to ~ 600 m on scarps cutting the early Pleistocene andesitic terrain both north and south of the Pit River.

James Muirhead, Alexa Van Eaton, Nicolas Le Corvec, Giuseppe Re, James White, Michael Ort

Submission 321

The architecture and development of shallow monogenetic feeder systems: perspectives from extinct volcanic fields

The development of networks of shallow intrusions affects the behavior and location of monogenetic eruptions. However, recent examples of monogenetic eruptions are rare, and few have been monitored with the modern techniques (e.g., InSAR, GPS, seismicity) that can ascertain the geometry and interconnectivity of subsurface intrusive feeders. Additionally, physical processes controlling the subsurface geometry of complex feeder systems (e.g., dike-sill-conduit-fissure transitions) are poorly understood. Exposures in extinct fields around the Colorado Plateau provide insights into shallow intrusive processes (<1000 m depth) below monogenetic volcanoes. Here we present field- and satellite-based observations of exposed intrusions in the 7 Ma Hopi Buttes volcanic field (Arizona). Results indicate that many of the eruptions were fed by interconnected dike-sill systems. We suggest that volcanic cone alignment studies are biased to the identification of dike intrusions, and thereby neglect an important contribution of sills to shallow feeder systems. For example, estimates of intruded volumes in fields exhumed in Utah and Arizona show that sills make up 30–90% of the shallow intruded volume within ~1000 m of the paleosurface. These sills likely played a role in modulating eruption styles (e.g., explosive vs effusive) and controlling lateral vent migrations by transporting magma toward or away from eruptive conduits. Field observations, coupled with finite element modeling using COMSOL Multiphysics®, suggest that the mechanical effects of sedimentary layering and stress relaxation during diatreme formation assisted in developing complex intrusive networks that diverted magma laterally. Sill transitions at Hopi Buttes should have produced detectable surface uplifts, and illustrate the importance of geological and numerical modelling studies for informing interpretations of geodetic and seismological data during volcanic unrest.

James Muller, Marc-Antoine Longpré

Submission 723

Tephra dispersal and composition reveal the explosive onset of the CE 1730–1736 Timanfaya eruption, Lanzarote, Canary Islands

Basaltic fissure eruption hazards are chiefly associated with voluminous lava flows and thus are difficult to quantify using the Volcanic Explosivity Index. However, these eruptions can also involve significant explosive activity, with abundant tephra fall deposits. We couple detailed tephrostratigraphy and EPMA and LA-ICP-MS glass geochemistry data from the Timanfaya eruption (Lanzarote, Canary Islands) to better constrain the dynamics of explosive activity at Timanfaya, and the hazards of similar volcanic crises in the future.

Timanfaya was punctuated by 5 main phases of activity [1], each marked by the formation of 1 or more cones along the source fissure. Our field data show that tephra deposition impacted over $\frac{2}{3}$ of the island's surface, sometimes severely and repeatedly. For example, thicknesses of fresh lapilli that overlie a conspicuous orange paleosol commonly exceed 1 m within ~5 km south of the fissure, and tephra sections show multiple beds corresponding to discrete eruption episodes and/or short-lived pulses. Basal-layer isopleth data indicate early eruption column heights in excess of several km. Timanfaya lavas [1] and tephtras sampled at the source vents define a temporal-compositional trend from early basanites to late tholeiites. Marked differences in incompatible trace element enrichment proxies (e.g., Nb/Y 10–100% higher in early vs. late tephtras) and SiO₂ contents are clear despite similar MgO contents in the glasses. We use this to correlate distal tephtras to their respective sources by minimizing the vector distance between vent tephtras and distal samples in Nb/Y–SiO₂ space. Remarkably, most of (~75%) the distal tephtras appear to be derived from the earliest eruptive episodes only. These same tephtras are often coarsest, thickest, and most ubiquitous. Explosive activity thus was confined largely to 1730. However, volumetrically significant lava flows were emplaced throughout the eruption, suggesting that tephtra distribution is not simply a reflection of mass flux. Instead, elevated Nb/Y ratios may be indicative of higher CO₂ contents [2] in the early phase magmas that promoted fragmentation. Our results underscore the potential for explosive episodes during large basaltic fissure eruptions, particularly during onset and early activity, while reaffirming the need for detailed tephrostratigraphy work to customize hazards assessments at individual volcanoes.

[1] Carracedo et al., 1990, *Estudios Geol.*

[2] Sides et al., 2014, *Nat. Geosci.*

Ben Mullet, Paul Segall

Submission 140

Conduit Collapse in Explosive Volcanic Eruptions: A Simple Model to Explain Cessation

Explosive volcanic eruptions can exhibit abrupt changes in physical behavior. In the most extreme cases, high rates of mass discharge are interspaced by dramatic drops in activity and periods of quiescence. Simple models predict exponential decay in overpressure, leading to a gradual tapering of eruptive flux. Abrupt changes in eruptive flux therefore indicate that relief of chamber overpressure cannot be the only control of the evolution of such eruptions. While many physical models focus on steady-state eruptions, the question of what leads to the cessation of an explosive eruption is relatively unexplored. We present a simplified physics-based model of conduit flow during an explosive volcanic eruption that attempts to predict stress-induced conduit collapse linked to co-eruptive pressure loss. The model couples a simple 1-D conduit solution of the continuity and momentum equations with a Mohr-Colomb failure condition for the conduit wall rock. First order models of volatile exsolution and fragmentation are incorporated. Rapid eruptive flux corresponds to a decrease of chamber overpressure and associated drop in conduit pressure, which leads to a critical deviatoric stress condition at the conduit wall. Results indicate that failure is most favorable at the fragmentation depth where stresses change dramatically. Analogous stress distributions have been analyzed for wellbores, where much work has been directed at determining conditions that lead to wellbore failure (e.g. Zoback, 2010) using Mohr-Coulomb failure theory. We extend this framework to cylindrical volcanic conduits, where large deviatoric stresses can develop co-eruptively leading to multiple distinct failure regimes. These failure regimes are categorized and possible implications for conduit flow are discussed, including cessation of eruption. Data from real explosive volcanic systems is analyzed within this framework.

Katherine Mulliken, Cheryl Cameron, Scott Crass, Janet Schaefer, Kristi Wallace

Submission 680

An update on the Alaska Tephra Database

Beginning in 2014, staff at the Alaska Division of Geological & Geophysical Surveys (DGGs) and USGS Alaska Tephra Lab within the Alaska Volcano Observatory (AVO) began developing and populating a component of the Geologic Database of Information on Volcanoes in Alaska (GeoDIVA), called the Alaska Tephra Database. Tephra studies are critical to understanding the eruptive histories of volcanoes and thus are a key component of volcano hazard assessments in Alaska. Currently, the Alaska Tephra Database stores tephra data from more than 600 resources, and includes published data for more than 2,000 tephra samples from Alaska and the Yukon. Information stored in the searchable database includes sample location, location description, sample description, source volcano, named tephra unit, age information, average glass geochemistry, and associated bibliographic references. Challenges during data entry arose from samples having units with complicated nomenclature history, samples considered to be a mix of multiple tephra units, glass geochemistry averages calculated by incorporating data from multiple samples, and units with age discrepancies.

The database contains ~1,300 Alaska tephra samples representing ~175 named tephra units. Named tephra units have varying numbers of individual samples. For example, there are 170 samples from the 1912 Novarupta-Katmai eruption, but many other named tephra units have only one associated sample in the database and hundreds of samples do not have an associated named tephra unit. Thirty-seven of the ~175 named tephra units are from known source volcanoes and eruptions. These 37 tephra units (and their samples) are linked to prehistoric eruptions in the recently expanded eruption database, which includes information for more than 250 prehistoric eruptions from Alaskan volcanoes. Eleven of these 37 tephra units are correlated with caldera-forming eruptions. Lastly, ~800 tephra samples are associated with potential source volcanoes, but not to specific eruption events. The Alaska Tephra Database will continue to be populated as new data becomes available, and we welcome contributions to expand the dataset. Our goal is to make the database the primary repository of Alaska tephra data and an invaluable tool for paleoenvironmental, paleoseismological, and archaeological studies and volcanic eruption history and hazards research in Alaska.

Carolina Munoz-Saez, Michael Manga, Shaul Hurwitz, Maxwell Rudolph, Atsuko Namiki, Seth Saltiel

Submission 1264

What have we learned about geyser dynamics from El Tatio, Chile?

El Tatio, Northern Chile, is the third largest geyser field in the world and the largest in the southern hemisphere. We have been conducting studies in this field since 2012 to better understand the processes controlling geyser eruptions [1,2,3,4]. We have collected measurements at the surface (pressure, temperature, video, microphone, and tilt), and inside geyser conduits (temperature and pressure), collected water samples, and measured physical properties of sinter deposits. We found that high-chloride erupted water originates from a deep geothermal reservoir with a sub-boiling temperature at depth $>260^{\circ}\text{C}$. The reservoir is recharged by non-local meteoric water more than 60 years old. Water ascending from this reservoir boils in the shallow subsurface and steam separates from liquid at $\sim 130^{\circ}\text{C}$. Episodic releases of steam trapped in cavities or shallow reservoirs heat geyser conduits, triggering eruptions. Boiling starts at the top and progresses down as the water column depressurizes. The eruption ends as the conduit is evacuated and cold water begins to recharge it. Irregularities in geyser eruption cycles may reflect complexities in the geometry of the plumbing system. Geysers with longer conduits and shallow reservoirs may have pre-play (minor eruptions) before the main eruptions. Some geysers can be connected to other thermal features by permeable pathways in the subsurface, these geysers are sensitive to pressure variations in the conduits of nearby features. We did not detect variability in eruption cycles in response to changes in temperature, pressure, and solid Earth tides on short time scales (weeks). However, we observed variability in the behavior and location of surface manifestations over time scales of years. Data from El Tatio helps to answer some fundamental questions about geysers dynamics, however questions about the source of the water, geometry of the plumbing system, and natural variability of thermal sources still remain open. These unresolved questions might be addressed by longer and more widespread monitoring.

References

- [1] Namiki et al., 2014, JGR.
- [2] Munoz-Saez et al., 2015, JVGR.
- [3] Munoz-Saez et al., 2015, JGR.
- [4] Munoz-Saez et al., 2016, JVGR.

Arran Murch, James White, Rebecca Carey, Bernd Zimanowski, Ralf Büttner

Submission 594

Generation and deposition of fine ash produced in a deep subaqueous eruption at Havre Volcano

In 2012 Havre volcano produced a rhyolitic eruption at 700-1300 mbsl. This eruption produced a sea surface pumice raft in addition to sea floor effusive and clastic deposits. Post-eruption AUV mapping and ROV observations and sampling make Havre ideal for the study of processes and products of interaction between silicic magma and water. We examine the stratigraphy and particle characteristics of two fine grained proximal clastic units to gain a better understanding of fragmentation, transport and deposition processes.

Subunits 1 (S1) and 2 (S2) are the basal 2 of 4 subunits in the Ash and Lapilli Unit at Havre. S1 and S2 appear texturally related to a giant pumice unit (GP) that they overlie. S1 was deposited over the whole 35 km² study area, draping the caldera, and certainly further beyond. No thickening or fining trends were observed for this subunit. S2 is absent from the north caldera rim however is 1-2 cm thick on the rest of the rim, the subunit thickens to 4-10cm on the caldera floor (~1500 mbsl).

Subunit S1 and S2 have modal grain sizes of 1-2 phi and 5-6 phi, respectively. Grains from both subunits show dominantly blocky and angular morphologies with curvi-planar and stepped fractures common. However, a significant population of grains (5- 20%) have entirely or partially fluidal forms or surfaces. These particles have smooth rounded unbroken surfaces sometimes showing aerodynamic shapes, microtexturally they are glassy with a vesicular core isolated by a dense rim.

Qualitative comparison show distinct microtextures between the GP and grains from S1 and S2.

The distribution of both subunits along with the difference in clast microtextures is not consistent with an origin by abrasion of GP. While the distribution of S1 is consistent with fallout from a plume that must be at least 700 mbsl, the height of the northern caldera wall, that of S2 suggests a source on the southern caldera rim (~900 mbsl) and with deposition down into the caldera (1500 mbsl) occurring from a gravity driven flow limited by local topography.

The fine grain size and dominant clast shapes of S1 and S2 suggest formation during energetic brittle fragmentation. The presence of rhyolite fluidal grains, however, suggests that during eruption magma conditions were locally conducive to fine scale surface tension reshaping of grains; highly unusual for inferred viscosities of rhyolite magma and the highly energetic fragmentation that is suggested by the deposit's fine grain sizes.

Sam Murphy, Dmitri Rouwet, Rob Wright

Submission 941

Color, chemistry and unrest at volcanic crater lakes

The Landsat missions have been taking images of the world's volcanic crater lakes for decades. We delve into this historic archive to quantify the color and temperature of Yugama, Poas and Ruapehu lakes over the last 30 years. The color analysis involved converting from from red-green-blue to hue-saturation-value color space, as the latter more succinctly correlates with the physical properties of the targets. Field measurements of lake chemistry (e.g. pH, Cl, SO₄, Fe) and temperature are available for each lake, as are data on periods of unrest/eruption and precipitation history. We combine this multivariate dataset through machine learning to explore how to differentiate the seasonal from the volcanic, how this might improve our understanding of volcanic processes and in which cases this can help eruption forecasting.

John Murray, Guillermo Caravantes-Gonzales, Hazel Rymer, Glyn Williams-Jones, Fabrizio Ferrucci1

Submission 1013

Recent inflation at Masaya volcano, Nicaragua

A 20 km precise levelling network comprising 81 benchmarks was set up and occupied in 1993, and remeasured in 1994, 2015 and 2017. The method has a vertical height precision of 1.5 mm km⁻¹ on average, and the network covered most of the Masaya caldera, with a reference zero station at the gatehouse of the Masaya National Park, just outside the caldera wall.

Between 2015 and 2017, precise levelling measurements show a pronounced inflation, maximum value +55 mm relative to the gatehouse, centred about 1 km to the west of the 1993-2015 deflation centre. This inflation is almost axisymmetric, with no apparent relation to the shape of the caldera.

Mogi models of calculated vertical displacement resulting from expansion of point sources at different depths were applied to the data. Point source models were used because the relatively small vertical displacements (

The injected volume derived from the best-fit model is just under 1×10^6 m³, which corresponds to a mass of 2.6×10^9 kg. This would correspond to a sphere of 120 m diameter, or an increase in diameter of 2 m for a magma chamber 550 m in diameter. This event is likely to be associated with the appearance of a turbulent lava lake within the summit Santiago crater in December 2016, that has persisted to the present.

This inflation is against the background of long term subsidence of the entire caldera 1993-2015, with greatest subsidence -95 mm near the middle of the western part of the caldera. In the same period there was also a secondary area of subsidence centred on the summit, with a maximum of -77 mm between Santiago and San Fernando craters.

Thomas Murray, Seth Moran, John Ewert

Submission 1287

The Role of US Volcano Observatories in Mitigating the Threats and Risks of Volcanic Unrest and Eruption

The U.S. Geological Survey has the responsibility in the United States to warn and notify the nation of volcanic activity. The USGS undertakes this responsibility through five regional volcano observatories: the Hawaiian Volcano Observatory, Cascades Volcano Observatory, Alaska Volcano Observatory, Yellowstone Volcano Observatory, and California Volcano Observatory. Though all are managed by the USGS Volcano Science Center, considerable responsibility is assigned to each Observatory's Scientist-in-Charge (SIC). In addition to issuing warnings and notifications the SIC is expected to direct activities that communicate volcanic hazards, prepare communities for future eruptions, monitor activity, and undertake research into not only volcanic processes, but into ways to improve eruption response and preparedness. During episodes of unrest, the Observatory provides the best science-based information on the threat posed by a volcano and its current state to local communities and emergency response groups who then take whatever actions they deem necessary to protect the public and mitigate the risk.

Not all of this can be undertaken by an Observatory by itself, nor even with all the resources available to the USGS. The SIC coordinates activities with others to enhance the Observatory's ability to successfully fulfill the goal of reducing risk to the public and economic and social disruption that can be caused by both eruptions or unrest. These activities include being the bridge between the scientific community and the emergency response, which in the case of significant threats will typically be managed under the National Incident Management System. If an Incident Command is established, the SIC may assign one or more technical specialists from the observatory to work with the Incident Command to ensure that information moves quickly between the Incident Command and the Observatory. In parallel, the Observatory coordinates with and solicits information from the greater scientific community, thus ensuring that the Observatory can provide the best scientific guidance to the Incident Command for its operations. The Observatory also plays a critical role when a Joint Information Center (JIC) is established to coordinate the flow of information to the public from various groups involved in the eruption response, ensuring that information coming from the JIC, the Observatory, and the scientific community is consistent and correct.

Euan Mutch, John Maclennan, Marie Edmonds

Submission 250

Timing magma migration through the Icelandic Crust: from the Moho to the surface

The rate of magma transfer throughout the crust, particularly the amount of time it takes for melt to travel from the upper mantle to the surface, is largely unknown. Only one previous study has investigated the timescales of transport of crystals that were in equilibrium with mantle melts [1]. Despite estimating timescales on the order of months to years, the depths from which these crystals were entrained is poorly constrained.

Borgarhraun is an exceptionally well-characterised picrite lava flow in the Theistareykir Volcanic System of Northern Iceland. The crystal-cargo of this lava includes macrocrysts of olivine (Fo₈₆₋₉₀), plagioclase (An₈₄₋₉₀), clinopyroxene and spinel with much rarer wehrlitic nodules. Crystallisation has been estimated to have taken place in deep sub-Moho magma chambers (~24 km). Melt inclusions in primitive olivine macrocrysts (Fo₈₈₋₉₀) are the result of mixing a suite of geochemically distinct mantle melts that were CO₂ undersaturated [2-3]. Zoning in the macrocrysts holds a record of concurrent crystallisation and mixing of these variable mantle melts, as well as ascent through the crust prior to eruption [4]. We have conducted a multi-phase, multi-element approach by applying finite-element diffusion models to wehrlite olivines and plagioclase macrocrysts to constrain the timescales of crystal residence and magma ascent prior to eruption. Model results suggest that at 1250 °C the timescale of final ascent was on the order of 100 days, whilst longer-term plagioclase residence times can exceed 300 years. This analysis shows that magma can ascend from the base of the crust to the surface in under a few months, suggesting picrites such as Borgarhraun are the result of high speed conduits to sub-Moho magma chambers. These rapid ascent timescales have important implications for the physical modelling of primitive magmas as well as for understanding the architecture of magma-plumbing systems in the temporal domain.

References

- [1] Ruprecht, P., & Plank, T. (2013). *Nature*, 500(7460), 68-72.
- [2] Maclennan et al. (2003) *Geochemistry, Geophysics, Geosystems*, 4(11).
- [3] Hauri, E. et al. In AGU Spring Meeting Abstracts (Vol. 1, p. 03).
- [4] Winpenny & Maclennan (2011). *Journal of Petrology*, 52(9), 1791-1812.

Madison Myers, Paul Wallace, Colin Wilson, James Watkins, Yang Liu

Submission 265

Ascent rates of rhyolitic magma in the opening stages of three caldera-forming eruptions

We have investigated the timescales of magma ascent through the initial fall stratigraphy from three rhyolitic supereruptions that show contrasting behavior at eruption onset: (1) 650 km³, 0.77 Ma Bishop Tuff, Long Valley, (2) 530 km³, 25 ka Oruanui eruption, Taupo, and (3) 2,500 km³, 2.1 Ma Huckleberry Ridge Tuff. During ascent, decompression causes volatile exsolution from the host melt into bubbles, leading to H₂O and CO₂ gradients in quartz-hosted reentrants (REs; unsealed inclusions). These gradients are modeled to estimate ascent rates. We present best-fit modeled ascent rates for H₂O and CO₂ profiles for REs in early-erupted products from Bishop (n=10), Oruanui (n=6) and Huckleberry Ridge (n=9). Using a code refined to include an error minimization function, Bishop REs yield ascent rates of 0.7-20 m/s. These values overlap and extend beyond those of the Huckleberry Ridge (0.5-4.7 m/s). Reentrants in Oruanui crystals from the first two eruptive phases (of ten) yield ascent rates of 0.1-0.2 m/s, the slowest measured in this study. Interestingly, these two Oruanui eruption phases are also associated with evidence for eruption initiation and control through rifting. Oruanui ascent rates then increase by an order of magnitude (to 2-5 m/s) into phase three, with a field-verified marked increase in eruption intensity.

In all three eruptions, the interiors of most reentrants appear to have reequilibrated to lower H₂O and CO₂ concentrations when compared to starting melt inclusion values, implying a period of slower ascent prior to the faster, final explosive event. We infer that this slower initial movement reflects movement of magma from storage into a developing conduit system, in which case an assumption of constant decompression conditions from the storage region is not valid. However, there is also an increase in the number of faster ascent rate estimates and deeper starting depths with higher stratigraphic height in all three deposits. We infer that this represents the 'maturing' of the conduit system and the overcoming of any initially sluggish ascent behavior. The ranges presented here agree well with ascent rates that have been estimated using theoretical approximations and numerical modeling for plinian rhyolitic eruptions (0.7-40 m/s)¹. However, these measured rates show that there is valuable information to be gained from placing samples within a field-controlled stratigraphic framework.

1 Rutherford 2008: Rev. Mineral Geochem 69, 241-271.

Naomi Nagata, Keiji Nagatani, Ryosuke Yajima, Tomoyuki Izu, Yasushi Hada, Shigeki Hirose, Noriaki Nakagawa, Toru Shimada

Submission 713

Development of survey technologies for volcanic eruption and lahar, using drone

Lahar occurs frequently where the area volcanic ash deposited during eruption and/or even several years after eruption. It is noted that lahar will effect widespread area which often larger than volcanic ash areas and will cause to terrible damages to the social community around volcanoes. However, it is difficult to get information using for forecasting the lahar occurrences and hazard area because of volcanic activity. In this study, we have developed the new survey technologies that assess the risk for volcanic lahar by observing volcano and those activities from out-side area of regulation region by unmanned devices. This method is likely to be needed for the region where a densely population located nearby active volcanoes such as Japan, Italy and so on.

The new survey technology consists of following steps. First, we collect information about volcanic activities, geographical data and ash fall range. Second, sampling a volcanic ash fall deposited around a volcano and analyzes these features such as grain size, water permeability. Finally, using geographical data and volcanic ash properties, we estimate the damage area in case a lahar occurring. Observation around the volcano during eruption and acquisition of geographical data are carried out using drone that can fly over long distances from outside the entry limits range. Continuous observation of volcanic activity is carried out using an autonomous mobile robot equipped with a high-performance camera. The autonomous mobile robot is transported to the vicinity of the crater by drone. To generate acquisition of terrain data, we use images around the volcano obtained by drone, and create 3D terrain model via some software. Also check the ash fall area based on this information. Volcanic ash is sampled by a full automatic volcanic ash sampling device attaching to the drone. The sampling device is attached to the lower part of the drone. After the drone has moved to the specified sampling point and device reaches the ground then sampling start automatically. Based on the information obtained by the above method, a lahar simulation is carried out and then disaster area is more accurately predicted.

We have carried out many experiments on the development of each technology in active volcanoes in Japan (Asamayama volcano, Unzen-Fugendake volcano, and Sakurajima volcano). In this presentation, we would talk about progress information of this study.

Ailsa Naismith, Matthew Watson, Gustavo Chigna, Helen Thomas, Kerstin Stebel, Robyn Brailey

Submission 18

Using Multiple Datasets to Characterise the Recent Eruptive Activity of Volcán de Fuego, Guatemala

After two decades of quiescence, Volcán de Fuego in Guatemala erupted on 21st May 1999, marking the beginning of a period of activity that continues until the present day. Eruptive behaviour within this period is generally defined by (a) sustained episodes of Strombolian activity, including production of lava flows, fire fountaining and persistent degassing, interspersed with (b) occasional violent paroxysms, consisting of gas- or ash-rich pyroclastic eruptions that generate large eruption columns and pyroclastic flows. Beginning with the eruption of 1999, Fuego has maintained a low level of activity (with the exception of 2006, in which 6 paroxysms occurred). Since 2011, Fuego has become more energetic, producing a greater number of paroxysms each year. Fuego's behaviour during the current eruptive period has frequently caused damage to the people living in the municipalities surrounding the volcano, including provoking the evacuation of 33,000 people after a violent eruption on 13th September 2012.

Eruptive activity at Fuego during 2016 differed noticeably from that of previous years, in both the large number of paroxysmal events observed (16 in total), and in the volcano's distinctive cycle of activity, repeated continuously throughout the year. The cycle began with initial effusive activity, which then increased in energy to mild Strombolian eruptions and fire fountaining, before Fuego eventually produced a violent paroxysm with associated pyroclastic flow(s). Several days of quiescence followed before the cycle resumed.

Here we use information from several sources (including thermal infrared and visual camera images, seismic and webcam data, and archival information) to provide a detailed evaluation of eruptive activity at Volcán de Fuego in 2016, including the intensity and frequency of such activity. We will discuss any observable patterns in activity that this evaluation highlights, and consider possible subsurface processes that could generate the activity observed. Finally, we will discuss what potential this method of research has for long-term monitoring and implementation in disaster risk reduction methods within the municipalities affected by Fuego.

Setsuya Nakada, Ahkmad Zaennudin, Mitsuhiro Yoshimoto, Fukashi Maeno, Yuki Suzuki, Natsumi Hokanishi, Hisashi Sasaki, Masato Iguchi

Submission 163

Growth process of the lava dome/flow complex during 2013--2016 at Sinabung Volcano, Indonesia

The present eruptive activity at Mt. Sinabung which resumed in September 2013, became more active with time. Andesite lava appeared at the summit crater in December 2013, preceded by the summit inflation and elevating seismicity. Since then, the lava effusion has almost continued, being associated with partial collapses of lava, which successively generated pyroclastic density currents (PDCs), and recent cyclic events of vulcanian explosions. The eruptive activity after lava appearance can be divided mainly into three stages, based on the fashion of lava dome/flow growth; that is, (i) lava elongation stage from December of 2013 to the spring of 2014, (ii) lava inflation stage from the spring of 2014 to the summer of 2015, and (iii) vulcanian stage after the summer of 2015. [Lava elongation stage] The lava complex grew first as a lava dome and developed into a lava flow, which extended until the middle of 2014. After repeating partial collapse of lava dome on the steep slope, it flowed rather smoothly, being associated with abundant rock-falls rather than PDC events. When the flow front reached about 3 km from the crater on the gentle slope, the lava flow widened near the front, increasing its thickness (~100 m) without advancing. [Lava inflation stage] Inflation of the whole lava complex began in the middle of 2014 with partial collapses of the both sides and upper-stream. Near the upper portion of the lava complex, new lobes repeatedly appeared and disappeared by collapses on the steep slope before reaching few hundred m. The total volume of this eruption reached about 0.16 km³ (DRE) as of the end of 2015. The discharge rate of lava was largest in the initial stage (>6 m³/s), and it decreased exponentially with time down to ~0.5 m³/s. [Vulcanian stage] Cyclic vulcanian event of a few times/day began after the summer of 2015 when the discharge rate became low (~0.5 m³/s) and, then, was kept unchanged. The composition of the lava became slightly more silicic with time as well as that of the glass chemistry, while the crystallinity slight decreased with time despite of the temporally decreasing discharge rate. It seems that more explosive event in the later stage was led by decreasing permeability in the upper conduit probably owing to shrinkage of the effective conduit diameter.

Mitsuhiro Nakagawa, Akiko Matsumoto, Takeshi Hasegawa, Fukashi Maeno

Submission 578

Diversity and origin of large silicic magma system: Comparative petrological studies of recent caldera-forming eruptions in Japan

It has been widely accepted that large scaled silicic magma eruptions were caused by the mafic injections into the large silicic magma storage system, which was nearly homogeneous. However, we have recognized the possible diversity in the silicic magma from recent large silicic eruptions in Japan, such as 42 ka Shikotsu, 120 ka Kutcharo and 7.3 ka Kikai-Akahoya ones. In these eruptions, voluminous silicic magma erupted with small amount of mafic magma. Thus, it has been concluded that mafic injection occurred before eruption. The silicic magma shows compositional variations, ranging from rhyolite to dacite. In addition, many major and trace elements and isotope ratios exhibit a linear trend in each SiO₂ variation diagram. It should be noted that these linear trends do not continue to the injected mafic magma. Phenocrystic minerals in the silicic magma, such as plagioclase and pyroxenes, show relatively wide variations. In addition, normally and reversely zoned phenocrysts coexist in a single sample. These and linear trends in SiO₂ variation diagrams indicate that the silicic magma is mixing products between two silicic end-member magmas such as rhyolitic and dacitic ones. Considering isotope ratios of the silicic magma, these two end-member magmas were derived from distinct source materials. In addition, these silicic magmas could not be produced by simple differentiation processes from the mafic magmas. Thus, it can be assumed that the silicic magmas could be formed by crustal melting. Although crustal materials are usually heterogeneous, there should exist considerable difference in the region of crustal melting to produce contrasted two silicic end-member magmas. Analysis of compositional zoning profiles of phenocrystic minerals suggests that mixing between silicic magmas had occurred several hundred years before eruption. The mixing could form a zoned, large, silicic magma chamber, in which mafic magma injected just before eruption. On the other hand, eruptions of VEI=5 class, such as AD 1640 Hokkaido-Komagatake and AD 1667 Tarumai ones, also show possible compositional variations of the silicic magma, dacitic one. However, the variations are smaller than those in caldera-forming eruptions. This might correspond to the difference in volume of the region of the crustal melting to form silicic magma.

Masaki Nakahashi, Satoshi Hareyama

Submission 464

Enhancement of volcanic monitoring and observation system of JMA near the crater

Based on the lessons learned from the eruption of Mt. Ontake on 27 September 2014, the Japan Meteorological Agency (JMA) decided to install various instruments near volcanic craters. In general, preceding activities of phreatic eruptions are weak in scale and appear only in the vicinity of the crater. In order to monitor and detect small precursors, JMA decided to install the following instruments near the craters of 48 active volcanoes in Japan: (i) infrared and visible light cameras to monitor thermal activities and change of fumaroles, (ii) broad-band seismometers (CMG-3T, natural period: 120s) and tiltmeters (Denali tiltmeter) to detect low-frequency seismic signals caused by movements of volcanic gas or hydrothermal activities. Since these instruments are installed in high ground around craters, they are often exposed to severe weather conditions such as strong wind and heavy snow. In order to keep stable operations even under severe conditions, JMA has been working on the increase of durability as follows:

- i) adopting wireless system and laying ground loop to make facility structure and apparatus configuration enable to prevent damage due to induced lightning
- ii) enhancing structural strength of cabinet and column against strong wind (60 m/s or more)
- iii) designing power supply to keep instruments operational against the long-time lack of sunlight due to heavy snow that covers solar panels
- iv) controlling instruments remotely by adopting fully IP-based system

With the instruments newly installed near craters, a long-period seismic signal accompanied by a volcanic tremor and slight changes in tiltmeter data was observed around Mt. Ontake on 27 September 2016. Thermal image at the very moment of the eruption of Mt. Aso was also recorded on 8 October 2016. JMA will work on developing techniques for stable operation of these instruments aiming at monitoring and evaluating volcanic activities.

As changes of volcanic gas composition and geomagnetic total intensity were often observed prior to past phreatic eruptions, JMA has installed instruments to observe components of volcanic gas for 4 volcanoes and geomagnetic total intensities for 6 volcanoes (including those under construction) near craters. JMA has been working on developing techniques to use volcanic gas composition data for monitoring volcanic activities as well as to improve in reducing the noise of geomagnetic data, respectively.

Haruhisa Nakamichi, Masato Iguchi, Takeshi Tameguri

Submission 222

Hypocenter distribution of an earthquake swarm associated with rapid magma intrusion into the Sakurajima Volcano on August 2015 using seismic amplitudes

Small to moderate explosive eruptions have frequently occurred at the Showa crater of the Sakurajima Volcano, since 2009. Distinct ground deformation over a half year duration at sites on the flank of the volcano and an increased number of eruptions have been observed in 2010, 2012, and 2015. From the beginning of 2015, distinct ground deformation and eruption activity were observed, and these continued till June 2015, after which, the ground deformation stopped and the number of eruptions suddenly decreased in July 2015. It seemed that the magma supply from a deeper part below the volcano was depleted. However, rapid ground deformation associated with an intense volcano-tectonic (VT) earthquake swarm with one thousand events was observed on August 15, 2015. The pattern of horizontal displacement of GNSS shows an WNW-ESE extension of up to 6 cm on the day, which suggests a rapid opening dike beneath the volcano. Hypocenter locations and their spacio-temporal change can elucidate the evolution process of the intruded dike. However, only a few tens of events were located with arrival times of P and S waves, because their waveforms overlapped each other. Therefore, we applied the amplitudes source location (ASL) method to estimate the hypocenter locations of the VT earthquakes. We estimated site amplitude factors of stations in Sakurajima using regional earthquakes and the coda normalization method. Vertical component velocity seismograms were corrected with the site factors and converted to the RMS amplitude for inputs of the ASL method. A plot of residuals for a hypocenter by the ASL method shows that horizontal locations were well constrained compared to the depths. The epicenters of the earthquakes distribute in and around the dike source, which is estimated by geodetic measurements (Hotta et al., 2016). The epicenters are also located around north-eastern and south-western tips of the dike, partially resembling a “dog-bone” shape. However, the depths of the earthquakes are poorly constrained and widely distribute at -1 to 6 km below sea level. The temporal change of the hypocenter distribution is weakly seen and correlated with the change of rapid ground deformation of tilt and extension meters at two under-ground tunnels. The ground deformation can be divided in to two stages. While the epicenters are concentrated close to the dike source in the first stage, the epicenter distribution spread from the dike source to the north-east and south directions.

Reina Nakaoka, Kazuhiko Kano, Keiko Suzuki-Kamata

Submission 176

Cone-building process in the A.D. 886 eruption on the Niijima Island, Japan

The A.D. 886 rhyolitic eruption on the Niijima Island started with generation of the Habushiura pyroclastic density current (PDC) deposits followed by the growth of the Omine pyroclastic cone and the emplacement of the Mukaiyama lava. Sedimentary structures, emplacement temperatures and ash morphology indicate the Habushiura PDC deposits were generated by shallow marine phreatomagmatic eruptions.

The Habushiura PDC deposits constitute a plateau rising over 100 m above sea level and the Omine pyroclastic cone rises 200 m above the plateau with a basal diameter of 2.7 km, without any indication of significant time break between the plateau and the cone. The summit of the cone is relatively flat, covered with the Mukaiyama lava but at least, five craters occur with a diameter 0.4-0.6 km in the eastern half.

Eruption products of the Omine cone consist of poorly to moderately vesicular blocks and lapilli, blocky-to-platy ash particles, and minor accidental fragments. Juvenile fragments contain elongate vesicles and have a bulk density of 1.6–1.7 g/cm³ in contrast with a smaller bulk density of 0.8–1.3 g/cm³ for the more vesicular juveniles of the Habushiura PDC deposits. These commonly constitute massive, poorly sorted and ash-dominated beds several tens to 120 cm thick with local plastic deformation and disintegration of the beds on the downslope side.

As examined through stepwise thermal demagnetization, the juvenile fragments have a magnetization direction stable and parallel to the direction of the Earth's magnetic field of that time below 350–400°C, suggesting that the juveniles were emplaced below 350–400°C and magnetized while they were cooled to the ambient temperature being accompanied with thermal contraction cracking and disintegration along the cracks.

The Omine pyroclastic cone appear to be composed mainly of PDC deposits and formed by explosive interaction between the hot lava and external water. The Habushiura PDC deposits are also interpreted as the products of explosive interaction between the hot lava and external water but its emplacement temperature is below 300°C as estimated by thermal demagnetization. The emplacement temperature for the Omine PDCs indicates that contribution of external water to the explosive eruptions of the Omine PDCs was smaller than the Habushiura case but the explosive potential was unexpectedly kept at a level to produce PDCs repeatedly. The eruption mechanism of this sort remains as a future research topic.

Shujiro Nakatsuji, Hiroshi Aoyama

Submission 386

An application of the ASL method to seismic activity at Tokachi-dake

Excitations of Low-frequency earthquake (LP events) and continuous tremor at volcano are considered to have close relationships with volcanic fluids such as magma, water, and steam. However, since phase arrivals of these events are usually obscure, it is challenging to determine the hypocenter automatically. To monitor the seismic activity at Tokachi-dake volcano in Hokkaido spatiotemporally, we introduce Amplitude Source Location (ASL) method (Battaglia and Aki, 2003). The ASL method is one of the hypocenter determination techniques that analyzes the amplitude ratio of seismic wave among different stations under the simple assumption on distance attenuation and isotropic radiation of high-frequency seismic signal. Since the ASL method doesn't require precise picking of seismic wave arrivals, it is potentially effective for hypocenter determinations of both LP events and continuous tremor.

For introducing an assumption of isotropic radiation of seismic waves, the ASL method usually treats high-frequency signals over than 5Hz. Since such high-frequency seismic signals are strongly affected by a shallow ground structure, we first estimate site amplification effect at each station at Tokachi-dake by using coda normalization method (e.g., Phillips and Aki, 1986). We used 10 local earthquakes that occurred around Hokkaido in 2013-2016, and estimated site amplification factors at 6 seismic stations. Site amplification factors clearly increase around Taisyo and 62-2 craters, the most active craters at this volcano. As a preliminary analysis, we applied the ASL method to determine the source location of volcanic earthquakes occurred on Oct. 2016, using vertical component data. Here we assumed amplitude decay effects of S-wave caused by geometrical spreading and intrinsic attenuation. The best-fit locations of the analyzed events were distributed beneath the 62-2 crater at the elevation of 1.5km above sea level. This result roughly matches the hypocenter distribution routinely reported by Japan Meteorological Agency. When we changed the number of stations used in the analysis, the estimated source locations are almost stable. This feature indicates that the ASL method is quite effective for estimating source location of volcano-related earthquakes, including small events. We will proceed analysis on LP and tremor events that are excluded from our routine processing, and discuss relation between seismicity and volcanic activity.

Atsuko Namiki, Timothy Willey, Heiko Woith, Eleonora Rivalta, Stefano Parolai, Thomas R. Walter

Submission 392

An elevated volcanic region prevents eruptions but its resonance may trigger an eruption

A complex surface topography leads to stress heterogeneities affecting the orientation of dike propagation. Depending on this stress heterogeneity, the dike propagating tip is expanding or compressing, so that ascending magmas from depth further propagate or accumulate beneath volcanoes, respectively. The mechanisms responsible for arresting and stagnating the buoyant magma to further propagate are not yet well understood, and may be associated to such stress heterogeneities. In specific, arresting and stagnating conditions may be affected by shaking, such as induced from tectonic earthquakes. Large earthquakes have been observed to affect magma transport, sometimes triggering eruptions. However, the 2010 Maule earthquake and the 2011 Tohoku earthquake caused a puzzling subsidence at several volcanic areas (Pritchard et al., 2013; Takada and Fukushima, 2013).

In order to better understand the mechanisms at play during magma ascent beneath the elevated volcanic region and to study the effect of external oscillations, we perform analogue experiments of magma-filled crack propagation inside a mountain-shaped elastic media. We solidify an agar solution in an acrylic box (0.14x0.14 m² in cross-section and < 0.24 m in height) with a triangle roof. By removing the roof, we obtain a mountain-shaped elastic agar with a free surface. We inject a buoyant fluid into the agar mountain in the box from the bottom and shake it by using a shaking table. Our experiments show that, because of the stress deviation inside the agar mountain, the crack tends to propagate laterally, thus preventing a summit eruption. When the fluid contains gas bubbles, the bubbles accumulate at the crack tip and facilitate upward crack propagation so that a summit eruption is enabled. We systematically varied the shaking frequency and found that an external oscillation with a frequency twice the fundamental resonance frequency of the agar mountain can accelerate crack propagation. This could be related to the higher modes modal shape inducing differential deformation at different depth. Therefore, we conjecture that the dynamic, and in particular the direction, of the crack propagation depends on (i) the principal stress pattern, (ii) the density of the fluid, and (iii) the shaking frequency. Our experiments highlight that even a buoyant fluid sometimes descends downward by external oscillations.

Shohei Narita, Makoto Murakami

Submission 159

Ongoing post-eruptive deformation of 2014 phreatic eruption of Ontake volcano, central Japan

L-band InSAR data obtained from ALOS-2 satellite revealed an ongoing post-eruptive deflation of a relatively small area around Jigokudani crater of Ontake volcano, central Japan. The deflation started to manifest just after the 2014 phreatic eruption of the volcano and it still continues. Since no such deformation was seen before the 2014 eruption, we infer that extrusion of hydrothermal fluid from pre-existing reservoir at shallow depth was activated by the eruption. We also infer that hydrothermal fluid had been already accumulated and stored in the reservoir before the eruption. In our study we use InSAR and other geodetic data sets to constrain mechanisms of 2014 eruption and its preparation processes.

The result of InSAR analysis shows that deflation continues with a nearly constant speed during the period between 2014 and 2016. A simple model fitting results using a point source in a half-space elastic medium indicated that the depth of the source is located somewhere between 400-750m beneath the surface and the total amount of volume of the deflation reaches about $7 \times 10^5 \text{m}^3$ as of the end of 2016.

That value is significantly less than that of total water content of emitted plume from the vents between September 2014 to November 2014 (Terada, 2014). This indicates that a large portion of plume emitted from eruptive vents must be originated from not the shallow deflation source but further depth of the volcano.

There is a possibility that the accumulation of hydrothermal fluid in this shallow source was initiated by the 2007 dike intrusion event, which was a major magmatic activity before the 2014 eruption. If this is the case, an increase of GNSS baseline length spanning over the volcano should appear between 2007 and 2014. However, no such increase was observed. This suggests that the accumulation of hydrothermal fluid should have been completed before the 2007 event.

Our InSAR result provides another piece of evidence for the hypothesis that a volcano with high hydrothermal activity can preserve hydrothermal fluid of the order of at least 10^6m^3 at the shallow depth, which may cause a lahar with considerable magnitude in the case that the fluid is released instantaneously, for example, by a sudden collapse of overriding lid triggered by volcanic eruptions or earthquakes.

Lourdes Narváez Medina, Darío Fernando Arcos, Maurizio Battaglia

Submission 67

Twenty years (1990–2010) of geodetic monitoring of Galeras volcano (Colombia) from continuous tilt measurements

Although geodetic monitoring techniques have continually evolved and improved, especially since the introduction of continuous GPS and InSAR, our experience indicates that electronic tiltmeters are very sensitive and can measure changes in ground deformation that would go unobserved by either GPS or InSAR. This characteristic makes tiltmeters very effective in monitoring short term, transient deformation episodes that may be associated with magma intrusions. To support our observation, we present the case study of 20 years of tilt measurements from Galeras (Colombia).

Galeras – an andesitic stratovolcano that is part of the Galeras Volcanic Complex – is one of the most active volcanoes in Colombia. Historic activity is centered on a small-volume cone inside the youngest amphitheater, which breaches the west flank of the volcano. At least 30 confirmed eruption periods have been recorded in the past 480 years, with episodes of unrest ranging from weak fumarolic activity and ash emissions to larger explosive events. The most recent eruption periods, monitored by electronic tiltmeters since 1988, have been characterized by minor explosive eruptions, and the emplacement of three crater domes and small pyroclastic flow deposits. In particular, we focus on three episodes of unrest that occurred in 1991, 2006 and 2008, when the deformation was clearly associated with shallow magma intrusions, and the emplacement and destruction of crater domes. The depth of the intrusions varied from a few hundred meters (August 2005) to two kilometers (January 2009), while the volume change ranged from 10,000 m³ (May-October 2009) to 1,000,000 m³ (January 2009). A comparison with seismic data indicates that the deformation sources were located within the cloud of hypocenters of the volcano-tectonic earthquake events. A lack of a clear correlation between the volume change (and depth) of the sources and the total SO₂ flux could indicate that the unrest at Galeras was related to a larger intrusive event with only a small part of the magma erupted in the form of tephra and lava domes.

Asnawir Nasution, , Y.Yunis, M.Afif, E.Sutaningsih, B.Sulaiman

Submission 301

Recognized Active volcanic and Geothermal Gasses, Case Study of the Anak Ranakah Volcano and the Ulumbu Geothermal Area, West Flores, Indonesia

The Anak-ranakah volcano (2247 m asl.) and the Ulumbu geothermal field (650 m asl.) are located in West-Flores, Eastern part of Indonesia. They are close each other having distance 8 km. After 14,000 years dormancy, the Anak-ranakah erupted and constructed andesitic lava domes in 1987. The released gases (SO₂, HCl) from Anak-ranakah solfatar represent a function of deep magma process, eq. vapour melt separation during coming up generating magma. The existence SO₂ indicates a high temperature magmatic component, rising directly from underlying magma. On the other hand, the Ulumbu's fumaroles have a small amount SO₂, high H₂S and CO₂. The existence H₂S assumed a low temperature gas (400oC) at the deeper level. The H₂, O₂+Ar, CH₄, and NH₃ gases probably indicate a secondary hydrothermal component slowly rising from a two phase, saline brine vapour and covering the magmatic system.

The H₂ to CH₄ and NH₃ shows a decreasing in equilibration for individual species, interpreting slow rate variaties (CH₄ and NH₃) are formed at the depth within the hydrothermal zones. The rapidly rising magmatic component are controlled by the SO₂-H₂S bupper. The H₂S and CH₄ seem to be stable in low temperature rock condition. The acidic condition within the hydrothermal zones of Ulumbu suggests fluid interaction toward surface, where H₂S reacts with rocks. Gas ratio and geothermometry show steam derived from deep sources, having temperature 270oC-280oC. The Ulumbu well (ULB-2), which is a reservoir temperature 230oC, has produced 12-14 MW steam capacity, supplying 4 x 2.5 MW power plants and producing 10 MWe electricity since 2014.

Keywords: Mt. Anak Ranakah solfatar, SO₂ and H₂S, Ulumbu fumarole, Gas Geochemistry, Sub Surface temperature, Geothermal well, power plant.

Christina Neal, Janet Babb, Steven Brantley, James Kauahikaua

Submission 926

Living and working with those at risk: lessons in information coordination from the US Geological Survey's Hawaiian Volcano Observatory

The U.S. Geological Survey's Hawaiian Volcano Observatory (HVO) has a long history of working closely with local authorities and the public to prepare for and respond to volcanic crises and chronic volcanic hazards in Hawai'i. Kīlauea Volcano has been erupting since January of 1983, destroying more than 200 homes and portions of several communities. In 2008, a second vent opened at the Kīlauea summit and it now hosts a 250-m-wide lava lake that attracts large numbers of visitors to Hawai'i Volcanoes National Park. This summit vent is also the main source of significant volcanic air pollution that impacts thousands of people on a daily basis. In 2014 and 2015, Kīlauea's East Rift Zone eruption at Pu'u Ō'ō sent lava flows 20 km downslope to the outskirts of a major community, Pāhoa, resulting in minor infrastructure damage but considerable disruption of thousands of lives, some permanently. Neighboring Mauna Loa Volcano has not erupted since 1984 but for the past ~4 years has seen elevated rates of deformation and seismicity that may portend an eruption in the near future. Tens of thousands of residents and critical infrastructure are potentially at risk of lava inundation during a Mauna Loa eruption.

In addition to its core function of volcano monitoring and hazard assessment in Hawai'i, HVO works in close coordination with Hawai'i County and State Civil Defense agencies, Hawai'i Volcanoes National Park, and other land managers who have ultimate responsibility for public safety. HVO's approach to both crisis response and inter-crisis preparation emphasizes: frequent sharing of scientific monitoring information and updates on the status of the volcanoes; sustained outreach and education through a variety of portals addressing volcano hazards and how individuals and communities can prepare for volcanic eruptions; dissemination of technical products (maps, brochures, fact sheets, web sites) to assist in eruption response, preparedness, and vog impact mitigation; periodic meetings with officials to discuss volcano status, prognosis, and planning. Some efforts are highly collaborative with partners from government and from the community. Each crisis of unrest or eruption provides an opportunity to improve overall coordination and efficacy in mitigating impacts. Strong working relationships among HVO scientists, local officials, and civil protection groups – especially as personnel change and information resources and public expectations evolve – are critical.

David Neave, Olivier Namur, François Holtz

Submission 284

The effect of mantle-derived variability on the mineralogy of primitive basalts: Experimental constraints from Icelandic systems

Subvolcanic magma reservoirs are increasingly recognised as long-lived, geometrically complex and vertically extensive systems. Recognising this complexity is largely due to improvements in analytical techniques and the growth of petrology as a quantitative discipline, and the identification of disequilibrium within isotopically zoned crystals has played a particularly important role in this. Moreover, the crystal stratigraphic approach pioneered by Jon Davidson provides a valuable framework for addressing a range of questions relating to magma assembly. For example, correlations between trace element indicators of mantle-derived enrichment (e.g., Nb/Zr) and the major element content (e.g., Fe, Ca and Na at a given Mg concentration) of Icelandic basalts suggest that crystals may also record mantle-derived variability in their major element contents because, in addition to physical parameters, variability in primary melt Mg, Fe, Ca and Na contents affects mineral-melt equilibria.

In order to isolate the effects of mantle-derived variability from the effects of temperature and pressure, we performed crystallisation experiments on two basaltic compositions from the Reykjanes Peninsula of Iceland. The Háleyjabunga and Stapafell eruptions represent compositional end-members in isotope, trace element and major element spaces: Háleyjabunga is Fe- and Na-poor but Ca-rich, whereas the Stapafell eruption is Fe- and Na-rich but Ca-poor. Experiments were performed in internally heated pressure vessels at temperatures between 1220 °C and 1140 °C, pressures of 1, 3 and 6 kbar and an oxygen fugacity near QFM+1. Although residual liquids largely follow differentiation trends defined by natural Icelandic basalts, there are striking differences in the trajectories of our variably enriched basalts. For example, plagioclase starts to crystallise from depleted melts (Háleyjabunga) at higher temperatures than from enriched melts (Stapafell) (e.g., 1200 °C versus 1160 °C at 3 kbar). Furthermore, high-anorthite plagioclase, which is difficult to model but commonly observed in oceanic basalts, only occurs in low-pressure experiments on depleted compositions; the occurrence of high-anorthite plagioclase in H₂O-poor basalts is a widespread indicator of primary melt heterogeneity. Conversely, by combining information about enrichment from trace elements with plagioclase and clinopyroxene compositions, it is possible to estimate crystallisation conditions for equilibrium crystal assemblages.

Owen Nelson, Tushar Mittal, Brent Delbridge, Noah Randolph-Flagg, Michael Manga

Submission 942

3D flow inside dikes using analog experiments and its control on conduit formation

Dikes are the primary pathways for vertical magma transport. Although significant work has been done developing and testing models of dike propagation involving coupled fracture mechanics and 2D viscous fluid flow (e.g., review by Rivalta et al., 2015), the full 3D flow field inside of a dike has remained largely unexplored (Dahm, 2000). These internal flows affect volatile degassing, dike propagation velocity, solidification, dike geometry, mixing of magmas, and the transport of bubbles and crystals. In this study, we use gelatin as a visco-elastic crustal analog (Di Giuseppe et al., 2009) and oil as a magma analog to image the 3D flow pattern and understand the effects of volatiles, solidification, and flow rate on dike behavior and morphology.

We find changes in the internal 3D flow field that are diagnostic of the processes driving magma ascent in a dike - volatile buoyancy vs source overpressure. Dikes with high volatile content quickly transition to being buoyancy dominated which leads to a relatively narrow dike width and rapid ascent, and distinct laminated morphology. In contrast, magma chamber overpressure produces penny-shaped dikes with rough fracture edges, more complex internal layering, and numerous en-echelon fractures. We argue this difference arises from a competition between crack propagation and flow within the crack and we define characteristic timescales to quantify the two regimes. Once the dike reaches the surface, flow within the dike gets quickly forms a single quasi-cylindrical pathway. This suggests that the transition from dike to conduit can be partially explained by internal flows. We confirm some of these results using semi-analytical solutions for 3D flow in simplified dike geometries. We suggest how to extend these results to outcrops and interpretation of flow textures.

Karoly Nemeth, Jonathan Procter

Submission 707

Pedagogical and indigenous aspects of geoeducation with special reference to the volcanic geoheritage of monogenetic volcanoes

Volcanic geoheritage refers to highly valued volcanic geosites with specific landforms, processes and landscape evolution that influences human societies. Geosites are evaluated by various assessment methods measuring main (scientific, aesthetic, protection) and additional values (function, touristic). While the great diversity of methods applied in evaluating geosites the subjectivity of the measurements and the overrepresentation of geotouristic aspects are common problems. These pitfalls suggest that the geoeducational aspects of some sites may not been looked at in detail or underweighted. In addition, the common geosite evaluation methods are heavily biased toward western cultural values in understanding Earth system and underrepresenting the traditional knowledge of indigenous societies. Volcanoes are common sites where human communities evolved in spite the hazards they pose to the community. To understand and live with volcanoes exploring their geoeducational values to transmit volcanic hazard information to the communities is vital. However, how to do this remains a challenging task especially in those regions where western scientific values meet with traditional knowledge. Small volcanoes (monogenetic) are perfect sites in geoeducational perspective as their size is in human scale and they can demonstrate easily itemized concepts of volcano growth, depositional processes and environmental impacts. The human-scale size and the easy to separate of processes and products concepts provide a good argument to consider Montessori pedagogical methods in geoeducation as it operates an evidence-based start for education leading toward more abstract concepts. Easy itemisation of processes and products associated with small volcanoes fit well with the Montessori Method. In geoeducation designs scaling the information to the public is commonly set to an elementary student level, which is an age group where Montessori Method functions well. In addition indigenous societies are commonly share information by using concrete experiences of sites, materials or items relevant to their everyday life, suggesting a better link to those communities through participatory methods to harvest and utilize such information that can be easily integrated in the Montessori Method. Monogenetic volcanoes where indigenous and western cultures live nearby them can provide perfect test sites to design new ways to communicate volcanic geology, volcanic processes and volcanic hazard.

Jurgen Neuberg, Amy Collinson, Patricia Mothes, Luke Marsden, Dinko Sindija

Submission 1006

Volcano seismicity and tilt in a wide frequency range

Seismic swarms and tilt measurement on active silicic volcanoes have been successfully used to image source processes and assess their eruption potential. Here we show an episode of intriguing eruptive activity on Tungurahua volcano and address the question of shear stress partitioning resulting in both the generation of tilt and low-frequency seismicity in critical phases prior to Vulcanian explosions. Once interpreted together, tilt and seismicity cycles can be explained by an integrated model. On the low-frequency end of the spectrum, a broadband seismometer can be used to measure tilt directly. Once careful data processing has been carried out, a detailed picture of volcanic source processes can be retrieved.

Julia Neukampf, Ben Ellis, Tomas Magna, Olivier Bachmann

Submission 760

Lithium abundance and isotopic variations between phases in a rhyolite (the Mesa Falls Tuff, Yellowstone)

Magmatic differentiation may represent the ultimate mechanism to enrich Li sufficiently to form economically-viable deposits. While demand for Li is increasing, much remains unknown about the behaviour of this volatile element in evolved magmatic systems. To address this, we present the first detailed study of Li concentration and isotopic composition in a rhyolite from Yellowstone (USA). The Yellowstone volcanic field is one of the best-studied areas of rhyolitic volcanism worldwide and provides a natural laboratory to investigate the behaviour of lithium in such differentiated magmas. We focus on one of three Yellowstone caldera-forming eruptions, the Mesa Falls Tuff (MFT), erupted at 1.3 Ma, and completely free of any visible post-eruptive alteration. MFT contains an anhydrous mineral assemblage of sanidine, quartz, plagioclase, clinopyroxene, fayalite, orthopyroxene and the accessory phases Fe-Ti-oxides, zircon and apatite. Individual mineral phases were separated, imaged by SEM, and analysed for (1) major elements concentrations by EMPA and (2) for trace element abundances (including Li) by LA-ICP-MS. Li concentrations of separated minerals were also measured by solution ICP-MS and Li isotopic ratios were determined by solution MC-ICP-MS after purification in cation exchange columns, allowing us to compare trace element abundances with Li concentrations and $\delta^7\text{Li}$ for multiple mineral phases.

Our data indicate a significant variability in Li concentration and $\delta^7\text{Li}$ values between the existing phases. The glass ($\text{SiO}_2=73\text{--}76$ wt.%; $\text{Li}=35.6\text{--}54.8$ ppm) displays the highest lithium concentration and exhibits one of the heaviest $\delta^7\text{Li}$ values ($6.5\pm 0.4\text{‰}$ to $6.9\pm 0.6\text{‰}$) followed by the fayalite (Fa87-88) that incorporated up to 29.7 ppm of lithium ($\delta^7\text{Li}=3.1\pm 0.2\text{‰}$). The $\delta^7\text{Li}$ values of Quartz ($5.7\pm 0.01\text{‰}$ to $7.2\pm 0.2\text{‰}$, $\text{Li}=12.8\text{--}24.5$ ppm) are in the same range as the glass. Early-formed phenocrysts such as the clinopyroxenes (Wo37-42,En15-30,Fs29-45; $\text{Li}=8.9\text{--}12.6$ ppm) and orthopyroxenes (Wo2-4,En22-39,Fs59-75; $\text{Li}=8.0\text{--}10.1$ ppm) show lower Li values and display the lightest $\delta^7\text{Li}$ values ($-0.1\pm 0.2\text{‰}$ to $+1.0\pm 0.2\text{‰}$ and $-2.0\pm 0.4\text{‰}$ to $-2.1\pm 0.3\text{‰}$, respectively). In feldspars, the Li is preferentially incorporated into plagioclase (An18-29,Ab66-73; $\text{Li}=6.1\text{--}28.5$ ppm) over sanidine (Or57-60, Ab38-41; $\text{Li}=2.8\text{--}7.8$ ppm) and shows much less variability in feldspars than other trace elements (e.g. Ba, Sr) that have abundances spanning more than an order of magnitude.

Megan Newcombe, Alexander Lloyd, David Ferguson, Anna Barth, Erik Hauri, Terry Plank

Submission 907

Syneruptive cooling rates and decompression rates of magmas from volcanoes with contrasting eruptive styles

We are constraining the syneruptive P-T-t paths of magmas using a combination of short-timescale cooling and decompression chronometers. Recent work has shown that the thermal histories of crystals in the last few seconds to hours of eruption can be constrained using concentration gradients of MgO inside olivine-hosted melt inclusions (MIs), produced in response to syneruptive cooling and crystallization of olivine on the MI walls [1]. This technique was previously applied to olivine-hosted MIs from pillow rim glasses, a submarine lava flow, and a subaerial hornito eruption. Here, we extend this technique to the study of MIs erupted by arc and ocean island volcanoes, including the subplinian 1974 eruption of Fuego volcano; the 1977 fire-fountain eruption of Seguam volcano; and three eruptions of Kilauea volcano (episode 1 of the 1959 Kilauea Iki fire-fountain eruption, the Keanakākoʻi basal reticulite of the c. 1500 CE vigorous fire-fountain eruption, and the Keanakākoʻi layer 6 deposit of the c. 1650 CE subplinian eruption).

Of the eruptions studied so far, MIs from the 1959 Kilauea Iki fire-fountain eruption record the highest syneruptive cooling rates ($\sim 103\text{--}104$ °C/hr) and the shortest cooling durations ($\sim 100\text{--}102$ s). The largest MIs (radii up to $170\ \mu\text{m}$) from the Kilauea Iki and Seguam fire-fountain eruptions exhibit long plateaus of approximately constant MgO across their centers, suggestive of ascent through the conduit at an approximately constant temperature (or a period of shallow magma stalling) prior to fragmentation. MIs from Fuego record the lowest cooling rates ($\sim 102\text{--}103$ °C/hr) and longest cooling durations ($\sim 102\text{--}103$ s) of the studied eruptions.

The average cooling rates of MIs from the studied eruptions are negatively correlated with magma decompression rates (as determined from volatile gradients in melt embayments [2, 3]). Division of our calculated cooling rates by decompression rates for each eruption allows us to estimate the amount of cooling as a function of magma decompression. Our estimate of ~ 30 °C/kbar for Fuego is consistent with adiabatic ascent of a magma containing $\sim 60\%$ vapor (calculated using the Conflow model of [4]). The high cooling rates inferred for Seguam and Kilauea Iki are consistent with air quenching over ~ 10 s of seconds upon fragmentation and eruption.

[1] Newcombe et al. (2014) *Contrib. Min. Pet.* 168(1); [2] Lloyd et al. (2014) *JVGR* 283;

[3] Ferguson et al. (2016) *Bull. Volc.* 78: 71; [4] Mastin (2002) *G3* 3(7)

Huaiwei Ni

Submission 387

OH diffusion in basaltic and andesitic melts: implication for electrical signature of magma reservoirs

Water dissolved in silicate melts is present in two species, molecular H₂O (neutral) and hydroxyl group OH (charged). Conventional wisdom based on experimental results on felsic melts takes that water diffusion in silicate melts is dominated by molecular H₂O, and that OH is essentially immobile. However, our recent experimental work on water diffusion in basaltic and andesitic melts show that OH diffusivity is smaller than molecular H₂O diffusivity only by less than an order of magnitude. At relatively low water content, it is actually OH that dominates diffusive transport of water. Three major differences between basaltic-andesitic melts and felsic melts may give rise to their different OH mobility. (1) Basaltic and andesitic melts are more depolymerized and less viscous; (2) At the same temperature, pressure and water content, basaltic and andesitic melts contain more OH; (3) A large fraction of OH is bonded with network modifying cations such as Mg and Ca in basaltic-andesitic melts, whereas OH is mostly bonded with network forming cations such as Si and Al in felsic melts. The contribution of OH transport to electrical conductivity of hydrous silicate melts is assessed using the Nernst-Einstein equation. At high water contents (e.g., 4 wt%), the contribution of OH to electrical conductivity even surpasses that of Na. This finding helps to explain the observation from electrical conductivity measurements - water enhances electrical conductivity of basaltic-andesitic melts more effectively than it does for felsic melts. For basaltic-andesitic melts, the effect of water on electrical conductivity is two-fold. (1) The addition of water depresses melt viscosity and facilitates the motion of cations; (2) OH itself serves as an effective charge carrier. Abnormally high electrical conductivity found by magnetotelluric survey may therefore point to active basaltic-andesitic magma reservoirs incorporating significant amount of water.

Cody Nichols, Alison Graettinger

Submission 885

Regional Tectonic Control on the Shape of Maar Craters

This study aims to gain a better understanding of the factors leading to the expressed shape of individual maars in volcanic fields. Maars are volcanic craters formed by the interaction of subsurface magma with the ground water. When the magma makes contact with the water, a phreatomagmatic eruption ensues. Tens to hundreds of these explosions result in the excavation of a volcanic crater ranging in size from a few hundred meters all the way up to six kilometers. The craters produced take on a wide range of shapes including, circular, elliptical, and polyoblate.

The shape of maars varies widely within each volcanic field. Among these maars the existence of one or more axis of elongation is commonplace. Published studies of tephra rings for individual maars suggests the lateral migration of explosion locations during an eruption. In order to determine if the migration of explosion locations and maar crater shape is controlled by regional faults the primary and secondary direction of elongation of maar craters from three different tectonic settings were measured.

Maars for this study were selected based on the criteria that a clear and continuous crater rim be visible by satellite imagery. The Pali Aike volcanic field of Argentina and the Newer Volcanic Province of Australia, San Pablo City volcanic field in the Philippines and Pinacante Mexico, and the Lamongan volcanic field of Indonesia along with the Auckland volcanic field in New Zealand represent intraplate, extensional, and compressional tectonics respectively. The primary angle of elongation was measured by fitting an ellipse within the outline of each maar's crater, such that it occupies the largest possible area without crossing the border. The second direction of elongation is determined similarly, as the longest axis differing by more than 30 degrees from the initial. Using this method, the faults in an area can be compared to the direction of elongation for each maar. While the secondary direction of elongation has not shown any correlation with fault direction, the primary angle is often aligned.

Other studies have investigated maar's geographic location as it relates to regional faulting and found a strong correlation between the occurrence of maars and the presence of fractures in the subsurface. However, this study differs in that it seeks to understand the expression of maars within a field through shape, rather than distribution.

Kuniaki Nishiki, Naomi Nagata, Hiromichi Kanai, Ryuta Furukawa

Submission 157

Estimation methods for the initial population of plinian fall deposits: A case study of the Ta-a and Ta-c2 tephra from Tarumai volcano, southwestern Hokkaido, Japan

Various infrastructure facilities such as power grid transmission network are susceptible to impact of tephra fallout. Therefore, it is important to know where and how much ash falls when a volcano eruption occurs. The simulation code for ash-fall prediction has been developed and used by various research institutions and universities worldwide. On the other hand, it is necessary to input various parameters for the simulation, and the accuracy of the input values also affects the results of the analysis. It is generally difficult to verify those model-dependent input parameters such as volcanic plume height, advection, diffusion, and gravitational fallout process. The parameters such as particle size and density, however, can be verified by the survey and analysis of tephra fall deposits. It is known that the parameters related to the particle size, initial population, for example, affect analytical results of the distribution of thickness (Walker, 1980). However, little is known about its variations.

In this study, we carried out a case study for Tarumai Volcano, Southwest Hokkaido, Japan, to clarify the initial population for tephra of VEI 5 class. The surveyed tephra are "Ta-a" which erupted in 1739 AD, and "Ta-c2" which erupted about 2.5 ka. The geological survey was carried out at several points in the area from the crater to the east of about 300 km, and obtained the bulk density of ejecta, thickness and particle size distribution at each point. Based on these data, in comparison with the estimation techniques by Bonadonna et al. (2005), we proposed a new estimation technique for the initial population by considering the vent distance and the ejecta isopach.

Adriano Nobile, Nicolas d'Oreye, Benoît Smets, Halldor Geirsson, Francois Kervyn de Meerendre

Submission 580

Deep and Shallow Magma Plumbing system interactions at Nyamulagira volcano, Central Africa, revealed by high temporal resolution InSAR time series and GPS

Analyzing ground deformations associated with volcanic eruptions contributes to understand the mechanisms of magma emplacement and characterize the magma plumbing systems.

In regions where in-situ deformation measurements are limited or impossible, because of geographical, economical or political reasons, InSAR may provides crucial information about the surface deformation.

Nyamulagira, an active shield volcano with a central caldera located in the eastern part of the Democratic Republic of Congo along the western branch of the East African Rift System, is characterized by cycle of short-lived flank eruptions (sometimes accompanied with intracrateral activity) every 1-4 yr, and less frequent long-lived eruptions usually emitting larger volumes of lava from eruptive vents most of the time located >8km from the central caldera. The 2011-2012 Nyamulagira eruption, which lasted from November 6 2011 to April 2012, is one of these long-lived events, which are usually also characterized by longer repose time.

SAR images from different satellites (Envisat, COSMO SkyMed, Terrasar-X and Radarsat) allowed measuring pre-, co and post-eruptive ground displacements associated with the eruption. Ground deformation time series obtained with the short revisiting time COSMO SkyMed satellite allowed detecting a very fast (one day) magmatic intrusion below the eastern flank two days prior to the eruption onset. It also allowed the detection of the subsequent intrusion that brought the magma up to the two eruptive vents located 11km ENE from the caldera.

We assessed source parameters and the mechanisms of magma emplacement using analytical models jointly inverting two interferograms in ascending and descending orbits that cover the intrusive period. We tested different type of sources to find the most suitable one for this eruption, given the observed deformation and the volcano-tectonic context. Considering also the few geophysical (seismic and GPS) data available during the eruptive period, our analysis suggest that the eruption is a complex sequence of a deflation of a shallow magma chamber (~3km below the caldera) that fed a sill intrusion toward the ENE direction that twisted into a dyke and brought the magma up to the surface. Furthermore, GPS, InSAR and seismic datasets suggest the presence of a deep magmatic source that possibly fed the shallower magmatic system. This contrasts with classical flank eruptions, which commonly involve the shallow plumbing system only.

Rina Noguchi, Kei Kurita

Submission 281

Geomorphometrical analyses for rootless cones —as natural analogue for dry-wet eruption scaling—

Volcanic pyroclastic cones are one of the most common volcanic morphology in the solar system. They are constructed as a result of deposition of pyroclasts which are ejected from a stable vent. Their smaller and simpler edifices are useful to understand rock fragmentation and transportation mechanism. In planetary science, they are expected to be a key to reveal volcanic activity and internal thermal state when they were formed. Therefore their characterization on remote sensing data is important. Morphometry of pyroclastic cones are influenced by magma properties and eruption environments. Explosions in magmatic eruptions are driven by decompression and expansion of volatiles in ascending magma, then create a conical edifice with slope of the repose angle by ballistic ejection of pyroclasts (scoria cones). In phreatomagmatic eruptions, the vaporization and expansion of external water by magma-water interaction creates significantly explosive phenomena which form cones or rings with narrow angle of slope (maars, tuff cones). The ratio of bottom diameter and crater diameter (hereafter Dcr/Dco) has been used to identify origin of cone features; Dcr/Dco is lower (0.32–0.39) for magmatic scoria cones and is higher (0.49–0.59) for phreatomagmatic tuff rings/cones (Frey and Jarosewich, 1982 and references there in). Nevertheless, phreatomagmatic eruptions contain both of volatile-driven (dry) and external water-driven (wet) explosion mechanisms therefore correlation of cone morphometry and the effect of external water has not been verified.

Rootless cones, which are formed by repeated explosions by lava-water interactions (rootless eruption), have a variety of its geomorphology. Fagents and Thordarson, 2007 showed a variety of styles in rootless eruptions from Surtseyan to Strombolian, and it depends on availability of external water. Since its rock fragmentation simply depends on lava-water interaction, we can verify the correlation of cone morphometry and the effect of external water using rootless cones. In this study we described geomorphometry of rootless cones in Iceland (Noguchi et al., 2016, JVGR) and Kenya using aerial photos. We found rootless cones have very wide range of Dcr/Dco: 0.15–0.88. These wide values should indicate the availability of external water which may reflect in the spatial distribution pattern. We discuss the relevance and present a morphometrical scaling between dry-wet eruptions.

Paraskevi Nomikou, Tim Druitt, Christian Watts, Tamsin Mather, Michele Paulatto, Lara Kalnins, Karim Kelfoun, Dimitris Papanikolaou, Konstantina Bejelou, Danai Lampridou, David Pyle, Steven Carey, Anthony Watts, Benedikt Weiß, Michelle Parks

Submission 316

Post-eruptive flooding of Santorini caldera and implications for tsunami generation

Caldera-forming eruptions of island volcanoes generate tsunamis by the interaction of different eruptive phenomena with the sea. Such tsunamis are a major hazard, but forward models of their impacts are limited by poor understanding of source mechanisms. The 30-80 km³ DRE late Bronze-Age (LBA) eruption of Santorini 3600 years ago was one of the largest of eruptions known worldwide from the past 10,000 years. It evacuated large volumes of magma, causing collapse of the present-day 10 x 7 km sea-flooded caldera. Tsunamis from the eruption are known to have impacted the north coast of Minoan Crete. We present new bathymetric and seismic data for the three breaches connecting the caldera to the open sea. While the two SW breaches are morphologically fresh submarine landslide scars, the 2.0-2.5 km³ NW breach is a 3 km long, 1 km wide, U-shaped submarine channel with a broad arcuate headwall, and is interpreted as having been carved by a combination of regressive landslips and inrushing of seawater into the newly collapsed caldera once the eruption was over. Combining the marine observations with those made onland enables us to reconstruct these events in some detail. Prior to the eruption there existed a lagoonal caldera that had formed 18 ky previously. During the LBA eruption this ancient caldera was cut off from the sea by accumulations of tuff, such that when the caldera re-collapsed it remained dry until the end of the eruption. The sea then broke through the thin barrier of tuffs in the NW corner of the caldera, carving out the NW submarine channel and (from numerical modelling) filling the caldera in less than a couple of days. Caldera collapse associated with the eruption amounted to several hundreds of metres of vertical displacement, and could potentially have generated large tsunamis if it occurred rapidly enough. However, this requires that the caldera was already flooded and connected to the open sea during collapse, which was probably not the case. We conclude that regional-scale tsunamis associated with the LBA eruption were generated by pyroclastic flow inundation, augmented perhaps by mass slumping of rapidly deposited pyroclastic deposits off the seaward slopes of the island volcano. This is consistent with previous tsunami modelling that shows that pyroclastic flows were indeed capable of generating waves of the observed height in northern Crete.

Scott Nooner, William Chadwick, David Caress, Jennifer Paduan, David Clague

Submission 1109

Using high-resolution repeat AUV bathymetry to constrain magma dynamics at Axial Seamount

Axial Seamount is the most active submarine volcano in the NE Pacific, and erupted in 1998, 2011, and 2015. Long-term monitoring at Axial has built a remarkable time-series of bottom pressure observations that have revealed a repeated cycle of inflation and deflation of ± 2 -4 meters that has been used to forecast eruptions with increasing accuracy. The 2015 eruption was the first captured in real time by the OOI Cabled Array and the network of sensors revealed the inner workings of the volcano in unprecedented detail. Nevertheless, we continue to learn more with every eruption and novel techniques are revealing new and surprising phenomena that were previously unknown. An example of this is the use of repeated high-resolution bathymetric mapping using Autonomous Underwater Vehicles (AUVs) to explore whether or not the vertical deformation field extends beyond the summit caldera. The new AUV data are complementary to the pressure measurements in that the AUV surveys are spatially continuous and laterally extensive, whereas the pressure measurements are temporally continuous and have high resolution (1 cm vs. 20 cm), but are spatially limited. AUV repeat bathymetry surveys were carried out in 2014, 2015 and 2016, and are planned for 2017. Comparison of the 2016 data to earlier surveys [Caress et al., 2016] shows some remarkable results including the following: (1) The 2014-2015 comparison (including the large 2015 co-eruption deflation) reveals net subsidence of -1.7 m centered at the caldera center, diminishing away from the center, (2) locally there were abrupt displacements across the caldera faults, and (3) the deformation field at Axial does indeed extend well beyond the caldera. Here we expand on our previous work by using the deformation measured by the AUV repeat bathymetry surveys to model the underlying magma dynamics of Axial Seamount. The best-fitting deflation source for the 2015 eruption agrees with the results from pressure data alone, presented by Nooner and Chadwick [2016] which is best fit by a steeply dipping prolate spheroid centered under the eastern edge of the caldera. We also use the AUV data to calculate the best-fitting post-eruption inflation source and compare to results from the pressure data. Finally we attempt to combine results from the pressure and bathymetry data into a single model.

Diana Núñez, Francisco J Núñez-Cornú, Adán Gómez, Juan Manuel Sandoval, Juan I Pinzón, Elizabeth Trejo-Gómez, Carlos Suárez-Plascencia

Submission 351

Comparison of past and recent seismicity in the Ceboruco Volcano, western Mexico

The Ceboruco volcano is located at the end of the Trans-Mexican Volcanic Belt in Nayarit state. This volcano is the largest (2280 m.a.s.l) of several volcanoes along the Tepic-Zacoalco rift zone and it has a history of effusive-explosive episodes in the recent past with eight eruptions during the last 1000 years, which provides an average of one eruption every 125 years. Since the last eruption occurred in 1870, 147 years ago, the possibility of a new eruption is really high and dangerous due to nearby population centers, important roads and lifelines that traverse the volcano's slopes. This hazards indicates the importance of monitoring the seismicity associated with the Ceboruco volcano whose ongoing activity is evidenced by fumaroles and earthquakes.

The previous seismic studies carried out in this region were registered by just one Lennartz Marslite seismograph featuring a Lennartz Le3D sensor (1 Hz) [Sánchez et al. (2009); Rodríguez Uribe et al. (2013)]. In this study, we compare the seismicity previously obtained with the seismicity obtained by the current semi-permanent network (three Taurus (Nanometrics) and one Q330 Quanterra (Kinematics) digitizers with Lennartz 3Dlite sensors of 1 Hz natural frequency) and one temporary network of 25 Obsidians 4X and 8X (Kinematics). The arrangement of temporary seismic stations covered an area of 16 km x 16 km with one station every 2.5-3 km recording from November 2016 to June 2017.

Francisco J Nuñez-Cornu, Juan I Pinzon-Lopez, Charlotte Rowe

Submission 338

Magma intrusion between Paricutin Volcano and Tancitaro Volcano: Evidence from seismic analysis.

An earthquake swarm occurred on the Michoacan monogenetic volcanic field in Mexico near Paricutin volcano, between May and June 2006. This seismic activity was recorded by a temporary seismic deployment known as the MARS network. We located ~1000 events from this seismic swarm. Previous earthquake swarms in the area were reported in the years 1997, 1999 and 2000. We relocate and analyze the evolution and properties of the 2006 earthquake swarm, employing a waveform cross-correlation-based phase repicking technique. Hypocenters from 911 events were located and divided into eighteen families having a correlation coefficient at or above 0.75. 90% of the earthquakes provide at least sixteen phase picks. We used the single-event location code Hypo71 and the P-wave velocity model used by the Jalisco Seismic and Accelerometer Network to improve hypocenters based on the correlation-adjusted phase arrival times. We relocated 121 earthquakes, which show clearly two clusters, between 9-10 km and 3-4 km depth respectively. The average location error estimates are < 1 km epicentrally, and < 2 km in depth, for the largest event in each cluster. Depths of seismicity migrate upward from 16 to 3.5 km and exhibit a NE-SW trend. The swarm first migrated toward Paricutin Volcano but by mid-June began propagating back toward Tancitaro Volcano. In addition to its persistence, noteworthy aspects of this swarm include a quasi-exponential increase in the rate of activity within the first 15 days; a b-value of 1.47; a jug-shaped hypocenter distribution; a shoaling rate of ~5 km/month within the deeper cluster, and a composite focal mechanism solution indicating largely reverse faulting. These features of the swarm suggest a magmatic source elevating the crustal strain beneath Tancitaro volcano.

Dini Nurfiyani, Anna Foster, Wang Xin, Hendra Gunawan, Dannie Hidayat, Wei Shengji, Benoit Taisne, Caroline Bouvet

Submission 725

Combining petrologic and seismic studies to constrain magma storage conditions beneath Marapi volcano, West Sumatra, Indonesia

At Marapi volcano in West Sumatra, we observed massive basaltic-andesitic pyroclastic flows and (> 30 m) thick phreatic to magmatic deposits on the lower flanks of the volcano. At the summit, we found a large number of fresh-looking volcanic bombs, ranging from 10 cm – 2 m in diameter. These bombs are thought to have been ejected during recent and frequent, small (VEI 1-2) eruptions. Volcano-tectonic earthquakes have been recorded by three short period and seven broadband seismic stations since 2015. Despite a wealth of fresh samples and high-quality seismic data, the processes of magma storage and transport at this volcano are still lacking of study. We focus on reconstructing the plumbing system of the volcano through an interdisciplinary study. A petrologic study of the summit bombs uses pyroxene, plagioclase and glass compositions measured by electron probe microanalyzer (EPMA) to obtain the pre-eruptive crystallinity, pressures and temperatures of magma storage, as well as the volatile contents. Whole rock analyses yield basaltic-andesitic compositions. However, EPMA analyses reveal a significantly more evolved resident magma with a large population of An₄₅₋₅₅ plagioclases hosting rhyodacitic melt inclusions. Some rare plagioclases with An₈₅₋₉₀ were brought by a basaltic magma recharge, while a hybrid population with An₅₅₋₇₅ formed by interaction between the two magmas. Plagioclase-liquid thermometry reveals storage temperatures $\leq 900^{\circ}\text{C}$ assuming 2 wt% H₂O and 200 MPa. We will use pyroxene thermometry and geobarometry to better constrain the temperature and pressure and improve water content estimates from plagioclase compositions. The plumbing system is also being viewed by applying local earthquake tomographic inversion (LOTOS). We ran 9 iterations of velocity modelling and earthquake relocation. The relocated earthquakes are mostly distributed to the west of the volcano, which coincides with the location of the Sumatran fault. The preliminary images obtained from travel-time tomography show an east-west trending area of low velocity, with a particularly low V_p anomaly in the upper 10 km on the western edge of the study region. In order to better image the magma reservoir, we are applying receiver function analysis to the seismic data. Such combined petrologic and geophysical views of the geometry and spatial distribution of magma storage at Marapi will be informative for future periods of unrest and contribute to improve eruption forecasting.

Aprilia Nurmawati, Konstantinos I. Konstantinou

Submission 108

Modeling of volcanic ballistic projectiles during hydrothermal and vulcanian eruptions at Tatun Volcano Group, northern Taiwan

This study investigates the hazard produced by Volcanic Ballistic Projectiles (VBP) at Mt Cising, Tatun Volcano Group, northern Taiwan. VBP is a material with a diameter more than 0.1 m ejected from a vent during an explosive eruption and following nearly parabolic trajectories. Two eruption models are generated: hydrothermal and vulcanian. Hydrothermal explosion model is built based on the parameters known from previous studies which describes the sudden fluid pressure drop to obtain the initial velocity of VBP. These velocities are then used to obtain the ballistic trajectory model for each eruption scenario. The model for a vulcanian eruption considers the energy during rapid decompression when the caprock is blasted. The remaining pressure after fragmentation of caprock is then considered as able to produce energy to eject the caprock. The ballistic equation is used to investigate the distance of VBP which also takes into account the reduced drag zone, wind speed, and VBP diameter of 0.2, 1.0, and 2.0 meters. Hazard maps are generated by mapping the points of impacts according to each scenario. VBP impact on hydrothermal explosions shows that a VBP may reach 576 meters from the fumarole. On the other hand during a vulcanian eruption, the maximum extent of VBPs is 1344 meter with diameter of VBP 2 m. The maps show that the Hsiaoyoukeng Visitor Center and its parking lot are in the hazard zone for all eruption scenarios.

Columbia River versus the Cascade Range volcanic arc—The Columbia River Gorge, Cataclysms, and Cultures

Jim E. O'Connor

Plenary Talk

The Columbia River is one of few world rivers crossing an active volcanic arc. This crossing of paths pits strong fluvial processes of the Columbia River against Cascade Range arc magmatism and related tectonic and geomorphic processes. The east-west trending Columbia River, draining 674,000 km² of western North America, first bisected the north-south trending Cascade Range in the present vicinity of the Columbia River Gorge about 35 million years ago when the Cascadia subduction zone jumped west to its present position and the volcanic arc began building. Early interactions among the river and volcanism are recorded in the paths and character of the far-traveled basalt flows of the Miocene Columbia River Basalt Group. Such volcano-water interactions have continued through the Quaternary, including the ~100 ka river-damming Wind River lava flow, emplacement of ~55 ka Beacon Rock, the remnant of a cinder cone that erupted in the gorge, as well as lahars from Mount Hood and Mount St. Helens. In addition, large landslides have encroached into the valley bottom from the uplifting arc, such as the circa 1450 A.D. Bridge of the Gods landslide. But the Columbia River, powered by the annual snowmelt from half a continent and occasional ice-age megaflooding, persistently incises through these materials, maintaining a near-sea-level path through the arc.

The Columbia River Gorge is the scenic and evolving outcome of these conflicting processes. The resulting dynamic environment hosts rich and diverse ecosystems, including historic runs of millions of anadromous salmon that have supported regional human habitation for more than 10,000 years. Such resources and the natural transportation corridor through the Cascade Range created a nexus of commerce, transportation, and cultural exchange. The first fisheries took advantage of geologic choke points such as Cascade Rapids, a remnant of the Bridge of the Gods landslide dam, and at The Dalles of the Columbia, the historic locus of valley-bottom incision. Now hydroelectric dams take advantage of the constrictions and hydrologic head of these sites, distributing the river's power throughout the west. And interstate road, railroads, and shipping through the gorge connect the interior of the continent with the Pacific coast and beyond. But this infrastructure, modeled after that of other large rivers in quieter geologic settings, is now enjoying a geological reprieve. Ultimately, the river and arc will battle once again.

Sean O'Donnell, Benjamin Andrews, James E Gardner

Submission 352

Effects on air entrainment and lift-off through interaction of two pyroclastic density currents

Most pyroclastic density currents (PDCs) only interact with the ambient air. Yet evidence from some eruptions shows the possibility of interaction between separate PDCs. It has been suggested that the lateral blast of the May 18th, 1980 eruption of Mt. St. Helens eruption actually consisted of two explosions that created two different PDCs. In this scenario, the trailing PDC caught up with the leading current. Evidence from the 1997 eruption of Soufrière Hills shows that multiple PDCs travelled down the same ghaunt with only a few minutes of separation. To gain insight into how PDCs interact with one another, we performed scaled laboratory experiments of dilute, particle-laden, density currents. The scaling of these density currents corresponds with dilute natural PDCs, thus the behavior of the experiments is analogous to that of pyroclastic surges. Heated 20 μ m talc powder was fed from a conveyor belt into an 8.5 \times 6 \times 2.6 meter open-air tank, to create pairs of density currents. Three laser sheets illuminated the density currents in three different planes, video was recorded, and temperature was measured at different heights above the floor and along the runout. We applied a feature-tracking velocimetry program to determine two-dimensional velocity fields within each illuminated plane. Leading currents entered the tank at a constant discharge, where they began to entrain, heat, and expand ambient air before lifting off; lift-off generally occurred at a position 1.5 – 2 meters from the inlet. After a specified pause, an identical trailing current was introduced to follow the same path as the leading current. We repeated this process at different temperatures and pauses between currents. Visual observations show that the trailing current lifted off either at the same position as the leading current or just before it. The temperature data substantiate this observation. The trailing currents with the shortest pauses (five and ten seconds) lifted off sooner than the trailing currents with longer pauses (30 seconds). Once the trailing current began to lift-off, the plume ascended faster than the plume of the leading current in almost all experiments. These results suggest that as the trailing current entrains air heated by the leading current, less entrainment and expansion is required to achieve buoyancy, and thus the current expends less thermal energy heating the surrounding air, allowing it to lift off sooner and rise faster than the leading current and plume.

Daniel O'Hara, Leif Karlstrom, Paul Richardson

Submission 1130

How Does Intrusive Magmatism Influence Landscape Evolution?

Landscape evolution in long-lived volcanic provinces integrates tectonics, erosion, and magmatism. While interactions between tectonics and erosion have long been studied, the influence of magmatism remains relatively unexplored. We focus here on intrusive magmatism. Intrusions emplaced in the shallow crust alter landscape form by constructing surface topography on short timescales that disrupt drainage basin configurations. Rapid uplift can split drainage basins, forming transient, internally-drained regions upstream of the intrusion and cause nearby drainage divides to subsequently migrate toward the basin, like a topographic lens. The amount of this disruption and divide migration is controlled by intrusion size, uplift rate, and initial configuration of the drainage basin upstream of the intrusion. In addition to affecting surface slopes and drainage area, exhuming crystallized intruded bodies may modify landscape erodibility on longer timescales by introducing rock that is harder to erode than surrounding country rock, and alter regional uplift by changing the crustal density structure. These processes induce transient topographic response within the landscape, which may persist for ~1 to 10s of millions of years, depending on erodibility, climate, and tectonic forcing. Time evolution of magmatically-driven uplift might thus be burned into the landscape, so that landscape morphology encodes upper-crustal magmatic flux through time in volcanic settings.

Using a landscape evolution model, we analyze surface response to a distribution of shallow inflating magma bodies. We simulate isolated intrusion form using an elastic model that accounts for the variable influence of gravitational body forces and flexure on uplift shape, and incorporate depth-dependent surface erodibility to model exhumation of intrusions. Global data compiled from laccoliths and InSAR-derived active deformation constrain the distribution of expected intrusion sizes, depths, and local uplift rates. We vary the frequency-magnitude relationship of intrusions as well as their spatial clustering to test sensitivity of land surface evolution to magmatic flux, and determine conditions under which steady state topographic form balances magmatic uplift and surface erosion in the absence of tectonics. This study identifies a new class of long-term landscape forcing mechanisms, and develops a framework for future use in inferring magmatic and erosive processes from topography.

Masatoshi Ohashi, Mie Ichihara, Shiori Takeda, Osamu Kuwano, Atsushi Toramaru

Submission 224

Shape evolution of bubble during solidification -exploring the history of tube pumice-

Tube pumice including elongated bubbles is a common product of explosive silicic eruptions forming calderas. We expect that tube pumice records information about the process leading to a caldera eruption. In order to explore the history of tube pumice, a numerical model is developed. The model is based on the deformation model (Jackson and Tucker, 2003) which predicts the transient shape evolution of an ellipsoidal bubble due to external shear flow and surface tension of the bubble. Adding the effect of exponential viscosity increase, we apply the model to predict deformation of a bubble in solidifying fluid. Processes of forced elongation, shape relaxation, and solidification that are expected for a bubble in tube pumice are simulated.

The behavior of the model depends on two non-dimensional numbers. The first one is the capillary number ($Ca = \frac{R\eta_0 \dot{\epsilon}}{\Gamma}$) which is the ratio between the timescale of shape relaxation due to surface tension and that of shear deformation due to external shear field. R is the bubble radius, η_0 is the viscosity of the liquid surrounding the bubbles, $\dot{\epsilon}$ is the shear rate, and Γ is the surface tension. According to the previous works, the more elongated bubbles are observed with the larger Ca in steady states.

The second non-dimensional number represents the competition between the timescale of solidification and that of shape relaxation. We call this new number the pumice number ($Pu = \frac{R\dot{\eta}_0}{\Gamma}$). $\dot{\eta}_0$ is the rate of viscosity increase of the liquid. A bubble deformed by flow would be relaxed to a sphere if it has enough time in the stress-free condition before solidification of the pumice. Qualitatively, the elongated bubble shape is preserved in the pumice if the pumice number is large.

The results of numerical calculation show that the final bubble shape after solidification is less elongated as Pu increases, even though the shape after forced elongation is better preserved with larger Pu . It is found that the amount of forced elongation mainly depends on the external strain in transient states, and the amount of applied strain decreases as Pu increases.

In conclusion pumice records bubble elongation at the end of the last shear deformation when Pu is large enough. Tube pumice indicates that the last shear deformation has occurred with sufficiently large Ca and sufficiently large strain.

Tsukasa Ohba, Takumi Imura, Yusuke Minami, Keita Ito, Kenta Horikoshi

Submission 367

Interaction between volcanic fluid and magma inferred from altered volcanic ash particles: examples from arc composite cones in Japan

Non-magmatic lithic fragments are abundant in volcanic products of phreatomagmatic, phreatic, hydrothermal, and magmatic-hydrothermal eruptions at arc composite cones. The lithic fragments undergo various degrees of alteration, ranging from very weak hydration to complete silicification. The variety of alteration mineral assemblages implies that the ash was derived from various alteration zones with different physicochemical conditions (temperature, pressure, and fluid chemistry). We have observed non-magmatic volcanic ash, focusing on alteration mineral assemblages of individual ash grains, from some composite cones in the Japan arc: Tokachi, Akita Yakeyama, Kurikoma, Azuma, and Ontake. The observation revealed that advanced argillic alteration (AAA) is the commonest alteration type. Alteration minerals in volcanic ash from Tokachi are silica mineral (cristobalite and quartz), alunite, and kaolin, indicating that they were derived from a shallow part of AAA zone, or alteration temperature is relatively low. Eruptive deposits from Akita Yakeyama, Kurikoma, and Azuma abundantly contain ash grains with the assemblage of quartz + pyrophyllite, indicating a deeper or hotter part of the AAA zone. Volcanic ash of the 2014 Ontake eruption is also abundant in AAA ash particles, accompanying different types of alteration: sericite and potassic alterations. This series of alteration types observed in the volcanic ash from Ontake is correlated with the typical geologic structure of porphyry copper systems which is the interior of the ancient composite cone. Degrees of alteration vary broadly regarding abundances of unaltered/weakly-altered volcanic ash. Some unaltered rock fragments are derived from old lava, whereas others originated from newly intruded magma bodies. At Tokachi and Azuma volcanoes, abundances of unaltered rock fragments increased with stratigraphy. These temporal variations indicate that magmatic contribution to eruptions increased, resulting in the change of eruption type from hydrothermal to magmatic-hydrothermal and phreatomagmatic eruptions.

Masayuki Oishi, Nobuo Geshi, Ryuta Furukawa, Takahiro Yamamoto, Yoshihiro Ishizuka, Teruki Oikawa, Futoshi Nanayama

Submission 468

Distribution patterns of volcanic ash fall deposits from Vulcanian eruptions

This study revealed the distribution, and minimum mass of volcanic ash fall deposits derived from frequent Vulcanian eruptions of the Sakurajima Volcano in southwestern Japan. Surveys were performed every year from 2011 to 2015; however this presentation focuses mainly on the 2014 and 2015 surveys as eruptions were most active. Volcanic ash collectors were set 3-43 km from the crater from which samples were taken in the morning and evening, and after each eruption. Twelve isopleth maps were drawn for each period.

From the data collected, the calculated minimum mass of deposits for each period ranged from a few tens to several tens of thousands of tons. Moreover, during periods without any records of eruptions, continuous emissions of plumes less than 1000 m high occurred. The rate of emission during such periods was estimated to range from several hundreds to several thousands of tons per hour.

Furthermore, we estimated the effect of meteorological conditions on the shapes of isopleths. Firstly, the isopleth becomes narrower as wind speeds increase. Secondly, the difference between wind directions and isopleth axes is larger for smaller mass isopleths. This suggests that, while the shape of a larger mass isopleth is influenced by local wind direction, the shape of a smaller mass isopleth is influenced by complicated wind variations, including wind direction variability from low to high levels. Lastly, the direction of an isopleth axis is influenced the most by wind direction at higher altitudes.

In addition, the isopleth drawn of March 7, 2012, a day subject to wet weather, shows a second maximum deposit by mass, approximately 40 km from the crater. It was expected that the decrease of mass of deposits with distance from the crater would be greater than that during dry conditions. However, the data showing the relationship between mass and distance from the crater does not support this hypothesis.

Avtandil Okrostsvaridze, Nino Popkhadze, Sun-Lin Chung

Submission 1131

Zircons U-Pb dating of Mtkvari canyon volcanic flow (Georgia) and destructive processes of Vardzia cave city hewn into this flow

In the Southern Georgia, along the River Mtkvari canyon outcrops andesitic-dacitic pyroclastic flow. The thickness of the flow varies between 30 - 80 m. The flow represents a lower part of so called Goderdzi subaeral volcanic suite (thickness 600-900 m) [1] and it is outcrops at 35 km, from Nialla valey till the Khertvisi castle [2]. The Goderdzi suite is a part of the Samtskhe-Javakheti volcanic highland (5000 km²; 1500-2500 m a.s.l.), which was formed at Late Cenozoic in the central part of the Lesser Caucasus.

First time, by us, was dating the zircons age by U-Pb method, using LA-ICP-MS equipment of this pyroclastic flow. The samples were taken from three main parts of the flow: in the end of the flow (at 35 km), near the Khertvisi castle (13GEO-04), in the central part of the flow (at 15 km) near the Vardzia cave city (13GEO-05) and at the beginning of the flow (at 2 km) near the Arzameti castle (13GEO-06). The results are as follows: 13GEO-04 = 7.50±0.42 Ma; 13GEO-05 = 7.54±0.21 Ma; 13GEO-06 = 7.52 ± 0.21 Ma; which indicates in very reliable results. Thus, according to this dating, the Mtkvari volcanic flow represents the late Miocene formation.

In the central part of the this volcanic flow, in the 12th century unique cave city of Vardzia was incaved, which with Khertvisi castle, in 1999 is included in the UNESCO World Heritage list. In 1283, after a strong earthquake, the cave complex was severely damaged, but it did not cease its operation. The results of the geological investigation, which was conducted by us, showed, that the Vardzia area has a complex geological structure. It is situated on the eastern slopes of the Erusheti ridge is hewn into the 900 m long tectonic block, which is detached from the main rocks and is gradually subsiding towards the Mtkvari gorge. In addition, the Vardzia block is split into several microblocks by a joint set and thereby its stability lessens. The matter is made worse by the fact that the active deep fault runs along the Vardzia complex in the Mtkvari gorge and presents a potential earthquake source. For this reason, it is clear that the important monument of the World cultural heritage is in danger of natural gradual destruction and earthquake hazards.

References

- [1] Skhirtladze N., 1958. Post-Paleogeneic volcanism of Georgia. Tbilisi, "Metsniereba" 165 p.
- [2] Okrostsvaridze A., Popkhadze N., 2016. Abstr. VI Intern. workshop on collapse calderas. Hokkaido, Japan, p. 42.

Bergrun Oladottir, Evgenia Ilyinskaya, Gudrun Larsen, Magnus Tumi Gudmundsson, Kristin Vogfjord, Emmanuel Pagneux, Bjorn Oddsson, Sara Barsotti

Submission 1193

Catalogue of Icelandic Volcanoes (CIV)

The Catalogue of Icelandic Volcanoes (CIV) is an open-access web resource intended to serve as an official source of information about volcanoes in Iceland for the public and decision makers (<http://icelandicvolcanoes.is>). It contains text and graphic information on all active volcanic systems in Iceland, as well as real-time data from monitoring systems in a format that enables non-specialists to understand the volcanic activity status. The CIV data portal contains scientific data on all eruptions since Eyjafjallajökull 2010 and is an unprecedented endeavour in making volcanological data open and easy to access.

Extensive research has taken place on Icelandic volcanism, and the results reported in numerous scientific papers and other publications. In 2010, the International Civil Aviation Organisation (ICAO) funded a three year project to collate the current state of knowledge and create a comprehensive catalogue readily available to decision makers, stakeholders and the general public. The work on the Catalogue began in 2011, and was then further supported by the Icelandic government and the EU through the FP7 project FUTUREVOLC. CIV also forms a part of an integrated volcanic risk assessment project in Iceland GOSVÁ (commenced in 2012).

The Catalogue is built up of chapters with texts and various mapped information for each of the 32 volcanic systems. The contributions can be classified into three types: 1. Text and other material (including maps and tephra grain size data) on geological aspects and eruption history. This constitutes the bulk of the information presented in the catalogue. 2. Sub-chapters on current alert level and activity status for each volcanic system, updated automatically with information from the IMO monitoring network. 3. Sub-chapters on eruption scenarios, based on the eruption history.

This work is a collaboration of the Icelandic Meteorological Office (IMO), the Institute of Earth Sciences at the University of Iceland, and the Civil Protection Department of the National Commissioner of the Iceland Police, with contributions from a large number of specialists in Iceland and elsewhere.

Bergrun Arna Oladottir, Olgeir Sigmarsson, Gudrun Larsen

Submission 1175

Tephra production and magma plumbing system. The Katla volcanic system, Iceland.

Tephra and lava volume estimates may reveal magma production rate of volcanoes and thereby cast a light on the behavior of the underlying magma plumbing system. Magma chambers, sills and dykes make up the magma plumbing systems that can be of different architecture between volcanoes as well as variable during their lifetime. Tephra studies indicate that the Katla volcano, under the Mýrdalsjökull ice-cap, Iceland, has erupted over 300 times during the last ~8400 years. The activity is characterized by explosive basaltic eruptions and occasional silicic eruptions. Tephra stratigraphy and major element composition has been used to assess the Holocene eruption frequency and compositional variations of the basaltic magma with time suggest evolving magma system configuration at depth, with or without active high-level magma chambers. Over the last 3000 years the tephra composition is interpreted to reflect plumbing system development from an active magma chamber to a non-existing, or inactive, chamber. A large (~18 km³) fissure eruption, the 10th century Eldgjá eruption, took place at the end of an active magma chamber period considerably modifying the plumbing system. Both eruption frequency and tephra production is higher during periods with an active magma chamber and volume estimates reveal up to three times higher tephra production than during the period with no shallow magma chamber. Katla volcano displays a steady-state behavior according to the model of Wadge (1982). Although initially only applied to short time scale (tens of years) in order to infer the architecture of shallow magma plumbing systems, here we apply the same model on much longer time scale (several centuries). This approach gives insight into slower and deeper magma processes operating on longer time scales. Increase in magma production is most likely caused by higher magma flux from a deep-seated reservoir (mantle-crust boundary?) into the shallow magma plumbing system, resulting in erupted magma of less evolved composition (e.g. lower K₂O). The elapsed time for the compositional signature of the deep magma flux to be observed in the volcanic products is controlled by the delay in the shallow plumbing system and thus its configuration.

Cecile Olive-Garcia

Submission 59

The new Chaîne des Puys – Limagne fault résumé: explaining complex geological environments to UNESCO and the international community

Chaîne des Puys – Limagne fault UNESCO World Heritage nomination was first discussed in 2014 to the World Heritage Committee, then in 2016 and will be again in 2018. The proposal was recommended for non-inscription twice by IUCN World Heritage panel reports, but twice upheld as a referral by the World Heritage Committee. The junction of non-inscription and referral twice is unusual for World Heritage, and indicates a difference of opinion between the IUCN and the World Heritage committee. The reason for the support by the committee can be found in the broad support for the nomination from the international scientific community, expressed in letters of support, endorsement and this community's participation and reviews of the nomination material. The lack of support for the project from the IUCN can perhaps be found in the complexity of the nomination's geological environment that goes beyond just a landscape feature and proposed an integrated geological environment of outstanding value (orogenic rift environment). The task for the 2018 submission is to provide, in the most clear and simple way, the environment and the context of the nomination to that the broadest audience of non-specialists can understand it. While this can be done in schematic diagrams and using simple day-to-day phrases, it is still the landscape itself that hold the key to understanding. So the use of the most expressive views, with explanations, which can assist in bring the site's geological significance to the non-specialist and bridge the gap between science and heritage.

Clive Oppenheimer

Submission 1030

Multiproxy evidence for timing and impact of medieval volcanic eruptions

The record of volcanic eruptions in the past is far from complete. Once we lack direct, recorded observations of volcanic events, we rely on evidence provided by the rock record (physical volcanology, tephrochronology), ice core glaciochemistry, paleoclimatic and paleoenvironmental proxies (such as tree rings), and historical sources that may chronicle the indirect consequences of volcanism. Chronology is a critical issue, all the more so when attempts are made to identify the impacts of particular eruptions on the environment, climate and society (i.e., probing causality). I will present several examples of a multidisciplinary approach to identifying volcanic events and their impacts, with a focus on the medieval period.

Julie Oppenheimer, Katharine V. Cashman, Alison Rust, Katherine J. Dobson, Charles Bacon, Amanda Lindoo, Donald B. Dingwell

Submission 1244

A comparison of gas-driven liquid segregation in analogue experiments and andesitic enclave textures

Gas-driven filter pressing is a phenomenon that occurs in crystal-rich magmas: bubble exsolution and growth in a comparatively rigid crystal network drives melt segregation through a pressure gradient. We use analogue experiments to further study the mechanisms by which bubble growth can cause melt segregation, then compare the results to textures in a zoned enclave. In the analogue experiments air was injected into mixtures of syrup and loose beads sandwiched between glass plates. Bubble deformation and coalescence increased significantly when particle fractions increased beyond a critical value. At high particle fractions, bubble growth compacted the particles adjacent to the lobate bubble walls. This caused liquid segregation in patches that disrupt the particle suspension (hereafter “segregation patches”) and into pre-inserted void spaces at the outer edge of experiments (“segregation vesicles”). In prior experiments with fixed particles (e.g. Holtzman et al., 2012), the injected gas propagates by viscous fingering: invasion of the pore-space between immobile particles, generating a finger-like gas front. We compare textures in experiments and in a 58 x 70 x 73 cm³ andesitic enclave from silicic andesite lava flows of Mt. Mazama, Oregon. The enclave has a porous core and a glass-rich rim, and was demonstrated to have undergone gas-driven filter pressing from core to rim (Bacon, 1986). We use 2D (optical microscopy & SEM) and 3D (X-ray tomography) methods to image crystal textures and bubble shapes. The enclave bears signs of both types of gas propagation. Segregation patches bear evidence of an early stage of melt migration in an originally unconsolidated crystal suspension. 3D imaging revealed evidence of fingering in the main crystal network: the porous core has fully connected diktytaxitic voids – angular voids within the crystal networks – which terminate at the core-rim interface in finger-like shapes. Finally, bubbles that interact with microlites in the segregation patches have lobate bubble walls surrounded by compacted microlites, reminiscent of deformed bubbles in experiments. Therefore, melt segregation can occur with both mobile and sealed crystal networks. Gas bubble morphology depends mainly on crystallinity and crystal size; thus viscous fingering may be more common at depth (large crystals) vs. bubble deformation near the surface (microlites). Both processes occur in other crystal-rich magmas and may cause heterogeneity in hand samples.

Clive Oppenheimer

Submission 1029

Dynamics of magmatic degassing observed at lava lakes

Open-path Fourier transform infrared spectroscopy (FTS) is capable of measuring several gaseous molecular species in volcanic plumes. Lava lakes provide a particularly favourable opportunity for FTS when the equipment can be set up on a crater rim with line of sight to the lake. The hot lava surface provides a convenient source of infrared radiation and the typically high plume abundance facilitates measurement of trace species via absorption spectroscopy. Under such circumstances, it is generally possible to measure the two most prevalent volcanic gas species, i.e., water and carbon dioxide, despite their atmospheric background abundances. Two further factors promote the application of the technique for gas geochemical monitoring – the possibility to collect measurements continuously and at high temporal resolution (e.g., every second), and the ability to measure redox sensitive species, notably carbon dioxide, carbon monoxide, sulphur dioxide and carbonyl sulfide. These permit detailed modelling of gas redox equilibria and can reveal remarkable variability, even on short timescales. I will present a number of examples.

Milton Iván Ordóñez Villota, Cristian Mauricio López, Maurizio Battaglia

Submission 70

Ground Deformation at Nevado Del Ruiz (Caldas, Colombia) and its Correlation with the Present Episode of Volcanic Unrest

Nevado del Ruiz is an andesitic–dacitic stratovolcano that is part of the Ruiz–Tolima volcanic massif, a group of five ice-capped volcanoes (Ruiz, Tolima, Santa Isabel, Quindio and Machin). The modern volcano's edifice comprises five lava domes, all within the caldera of an ancestral Ruiz volcano. Historical activity has consisted primarily of explosive eruptions from the central vent, followed by lahars. Ruiz is known for the tragic eruption and lahar of November 13, 1985 that completely destroyed the town of Armero.

Analysis of seismic and deformation data identifies a complex plumbing system within the Tolima-Ruiz massif; magma accumulates in a deeper reservoir midway between Ruiz and Santa Isabel then moves along regional faults towards Ruiz. Magmatic fluids flow from the base of Ruiz into the shallower reservoir beneath the main Arenas crater that is feeding the current episode of unrest.

After 8 years of quiescence, unrest at Ruiz resumed in 2009. The geodetic monitoring system (tiltmeters and permanent GPS sites) recorded aseismic deflation that continued until late 2011, consistent with spreading caused by gravitational collapse of the volcano's edifice.

Seismicity increased significantly in March 2012, together with gas and ash emissions and constant inflation. The volcano erupted in May 29 and June 30, 2012 (VEI = 3). After the eruptions, Ruiz remained in a state of unrest with high seismicity rates, inflation and intermittent emissions of water vapor, SO₂ and ash until August 2015. Deformation stopped in September 2015 and a lava dome was emplaced at the bottom of the main crater. During the last months of 2015, 2016 and first months of 2017, the volcano's unrest was characterized by seismicity (i.e., seismic tremor) with repeated emissions of gas and ash.

Before the explosive eruptions of May/June 2012, deformation was consistent with the migration of small volume of magma to a shallow source located beneath the crater (depth ≈ 2 km and $\Delta V \approx 0.6 \times 10^6$ m³). The inflation observed by GPS after the June 2012 was consistent with a deeper source, located midway between volcano Santa Isabel and Ruiz. Between June 2012 and December 2014 this source ascended from a depth of 17 to 7 km, with a volume change of approximately 1.5×10^6 m³. Interferograms processed by the Jet Propulsion Laboratory confirmed the location, depth and volume change of this deeper source.

Michael H. Ort, Guido Giordano, Elena Zanella, Roberto Isaia, Kayla Iacovino

Submission 684

The Role of Atmospheric Incorporation in Dilute Pyroclastic Density Currents

Pyroclastic currents erupt with a large gas volume fraction and can subsequently incorporate atmospheric gases. In small-volume, short-lived pyroclastic density currents (PDCs), the front is an important part of the total current. This results in significant incorporation of air in the eruption column and some at the front of the current, as shown by low temperatures of emplacement determined from partial thermal demagnetization. Large PDCs may be long lived and contact between the current (behind the head) and the atmosphere is reduced to the side of a collapsing column (if there is one) and the top of the PDC. Large-volume dense PDCs (e.g. Cerro Galan Ignimbrite) show emplacement temperatures above 580 °C. We investigated emplacement temperatures of the 40 ka Campanian Ignimbrite (CI), which erupted from the Campi Flegrei caldera near Naples, Italy. We used partial thermal demagnetization on lithic fragments from 13 CI sites, along several lateral transects from proximal to distal localities (to 75 km from vent), including two sites that required the PDC to flow across ~35 km of open sea (perhaps covered by pumice fall) to reach. The lithic fragments were deposited above 580 °C (magnetite unblocking temperature). Fisher et al. (1993) and later workers showed the CI was emplaced from a density-stratified current with a dilute transport system and a denser depositional system. Some of the PDC overtopped 1600-m-high ridges, with the depositional system re-forming on the far side, but the lower portion of the PDC was blocked and flowed back toward the vent. Modeling suggests dilute PDCs can pass over obstacles up to 1.5X their thickness, implying that the CI PDC was about 1 km thick for much of its emplacement period. Where did the gases come from to inflate this flow? Previous anisotropy of magnetic susceptibility work shows the deposits were emplaced by currents flowing downhill, rather than radially from the vent, and facies variations imply deposition from unsteady currents. However, the deposit is only a few meters thick beyond the first ridgeline of the Apennine Mountains, implying that particle concentration in the ridge-overtopping currents was very low or deposition was brief. We argue that the ~150 km³ CI was emplaced over a short time period (minutes), as longer lived currents need more incorporated air (and cooling) to stay inflated. This requires very high discharge, which may be a requirement to make large dilute PDCs.

Karin Orth, Christopher Phillips, Julie Hollis, Michael Wingate

Submission 1307

The remnant Paleoproterozoic Hart-Carson LIP of north Western Australia

The Carson Volcanics are the only volcanic unit in the Kimberley Basin in northern Western Australia. Together with the Hart Dolerite they comprise the Hart-Carson Large Igneous Province (LIP). New work reveals the age, composition, internal architecture and relationships between some of the intrusive and extrusive portions of the LIP.

U-Pb zircon and baddeleyite dating from differentiated portions of the Hart Dolerite indicate that the LIP is 1797 ± 11 Ma. The remnant LIP covers an area of over 200,000 km². The combined volume of the intrusive and extrusive portions of the Hart-Carson LIP is 300,000 km³, similar to estimates for the volume of the Columbia River Basalts, but significantly less than estimates for the Deccan or Siberian Traps. The extrusive rocks make up 17% of the volume.

The lavas are basalt to basaltic andesite typical of continental tholeiites. In comparison to other LIPs, the Hart-Carson volcanic rocks all have low TiO₂ (all less than 1.7%, but most less than 1.35 wt%). A region-wide dichotomy is evident in the geochemistry. The lower lavas contain less TiO₂ than 1 wt%, whereas the upper lavas have more TiO₂ than 1wt%.

The internal facies architecture of the Carson Volcanics is dominated by extensive pahoehoe lava flows, which are up to 40 m thick in places. Lavas display thick upper crusts, upper ropy surfaces, basal pipe vesicles and internal zonation characteristic of other LIP basalts. Most lavas have polygonal (hackly) jointing common to entablature with only rare examples of well-developed columnar joints. Gentle, open folds are typical across most of the region. So, despite the antiquity of the succession, the lavas create a step-like topography. Intercalated lenses of sedimentary rock are consistent with deposition in a shallow marine to emergent shelf environment over the whole of the Kimberley Basin. Stromalites form in localised pockets at the end of the eruption cycle. Local pillow lava breccia indicate that basalt lava erupted in, or flowed into a subaqueous environment.

Although, eruptive centres have not been located, an interesting signature in the magnetic dataset suggest that sills of Hart Dolerite intruded to high levels in the underlying sandstone, with the potential for volcanism in areas that are now removed by erosion.

Adrien Oth, Julien Barrière, Nicolas Bakundukize, Georges Mavonga, Josue Subira, Niche Mashagiro, Benjamin Kafudu, Silvanos Fiama, Gilles Celli, Jean de Dieu Bigirande, Alain Joseph Ntenge, Laurent Habonimana, Charles Bakundukize, François Kervyn

Submission 310

KivuSNet: A broadband seismic network for the Lake Kivu & Virunga Volcanic Region, Democratic Republic of the Congo

The Kivu Basin is located in the bordering region of the Democratic Republic of Congo and Rwanda, in the Western branch of the East African Rift. Here the active volcanoes Nyamulagira (the most active in Africa) and Nyiragongo (host to the largest persistent lava lake on Earth) threaten the city of Goma and neighbouring agglomerations. For many years already, urbanisation in that region undergoes sustained rapid growth, and Goma counts 1 million inhabitants today. In 1977 and 2002, eruptions of Nyiragongo caused major disasters. Destructive earthquakes can also affect the region, as was the case in 2002 in Kalehe (Mw 6.2) along the western shore of Lake Kivu, or in 2008 in Bukavu (Mw 5.9), south of Lake Kivu. At the same time, until recently modern seismic monitoring infrastructure was lacking in the area, leaving many aspects about the volcanic activity and seismicity up to speculations.

In the framework of several Belgo-Luxembourgish collaborative research projects (the most recent one being RESIST: “Remote Sensing and In Situ Tracking of geohazards”, funded by the Belgian Science Policy and the Luxembourg National Research Fund), we deployed the first dense real-time telemetered broadband seismic network in the region, with the first two stations in 2012 and 2013. It is now a network of 15 stations and still under continuous development. Many KivuSNet stations are co-located with GNSS KivuGNet stations, and three KivuSNet sites are in addition equipped with infrasound arrays.

We present an introduction to the key features of the network and an overview of the first scientific results, including unprecedented insights into tectonic and volcanic seismicity patterns and initial structural investigations (1D velocity model determination). KivuSNet opens a new window for the state of knowledge on the seismic and volcanic activity in this highly-threatened region and represents an indispensable tool for monitoring operations of the Goma Volcano Observatory.

Shizuka Otsuki, Nobuo Geshi, Satoshi Okumura, Michihiko Nakamura, Osamu Sasaki

Submission 1012

Microstructural relaxation of andesitic magma foam

Interfacial tension-driven relaxation is a primary process in the microstructural evolution of bubble-bearing magma. Although several studies have examined the interfacial tension effect for bubble coalescence (e.g., Castro et al., 2012), few have discussed the effect for the microstructure of foamed magma (Otsuki et al., 2015; Kennedy et al., 2016). Otsuki et al. (2015) conducted heating experiments of andesitic pumice cubes and determined that interfacial tension-induced densification (self-contraction) occurred in the sample. In a larger system, multiple-contraction units form melt globs and interglob pores inside the run products. The latter may affect the permeability of magma; thus, the microstructural relaxation process controls outgassing within a shallow volcanic conduit.

To understand the pore microstructure and outgassing evolution of magma, we examined the three-dimensional microstructure and permeability of the heating experiment run products by using andesitic pumice clasts of the Sakurajima 1914 Plinian eruption as starting materials. To investigate the size effect, we prepared two types of starting materials: shaped cubes of 9 mm and non-shaped clasts of 3–6 cm³. The pumices were heated to 1000°C and ≤ 0.1 MPa vapor pressure for up to 32 h in silica glass tubes. The pore microstructure was investigated by using micro X-ray computed tomography, and the permeability of the sample was measured according Takeuchi et al. (2009).

The pumice clast permeability was about 10^{-13} – 10^{-11} m². In the 9 mm cube run products, samples heated ≤ 2 h had a wide range of permeability, at 10^{-16} – 10^{-11} m², whereas those heated 8–32 h had low permeability, at 10^{-16} – 10^{-15} m². In the short run duration of ~ 30 min, the permeable run products exhibited inter-glob pores formed by multiple contractions. However, no outgassing pathway appeared in the impermeable run products of long run at 8–32 h. The interglob pores disappeared likely owing to gravitational deformation and healing of the melt glob boundaries. In larger samples of 3–6 cm³, however, some run products did not become impermeable even in long run durations owing to the maintenance of interglob pores. We consider that the lengths of the interglob pores in the larger samples were longer than those in the 9 mm samples and that the time scale of permeability reduction was longer. We are now investigating the relationship between the length scale of interglob pores and its residence time.

Jacqueline Owen, Thomas Shea, Hugh Tuffen

Submission 931

The role of magma degassing during the explosive subglacial basaltic eruption of Katla (Iceland) in 1918

The ice-covered Katla volcano in southern Iceland is notorious for its powerful subglacial eruptions of basalt. The last major eruption, in 1918, took just two hours to melt though 400 m of overlying ice¹ and triggered a highly destructive >300,000 m³s⁻¹ meltwater flood (jökulhlaup)¹, with airbourne ash deposited over half of Iceland². Why was this eruption so powerful? Was explosivity purely fuelled by magma-meltwater interaction or did magmatic vesiculation also play a role?

To investigate we present detailed textural analysis of pyroclastic material from the 1918 event. Textures in juvenile clasts from jökulhlaup and air-fall tephra deposits were imaged using an electron microprobe in back-scattered electron (BSE) mode at the University of Hawai'i. Thresholded BSE images of thin sections were then input into FOAMS3 and ImageJ to quantify bubble and crystal textures.

Jökulhlaup samples have higher bubble number densities and vesicularities (~300-900 mm⁻² and >60% respectively) than air-fall samples (~2 and

Our results suggest that volatiles played a major role in fueling explosivity, especially for material deposited in the jökulhlaup. This may help to explain why the ice was melted so quickly, and why such a powerful flood developed. Insights into the relative roles of degassing and phreatomagmatic fragmentation during the Katla 1918 eruption could be useful for predicting the eruptive behavior and likely clast type produced during future Katla eruptions, with important implications for jökulhlaup hazards, ash dispersal and the aviation industry.

1. Tómasson H (1996) The jökulhlaup from Katla in 1918, *Ann Glaciol*, 22, 249-254
2. Larsen G (2010) Katla: tephrochronology and eruption history, *Dev Quaternary Sci*, 13: 23-49
3. Shea T et al (2010) Textural studies of vesicles in volcanic rocks: an integrated methodology, *J Volcanol Geotherm Res*, 258, 143-162

Constance Ozimek, Leif Karlstrom

Submission 865

A Thermo-mechanical-chemical magma chamber forward model for the prediction of eruptive cycles and chemical evolution

Magma chambers are a fundamental component of crustal magma transport modulating erupted volumes, compositions, and timing of surface eruptions. However we understand little about how eruption episodicity relates to magma chamber evolution or tectonic setting. The many influences on composition make inference of crustal processes from erupted compositions difficult, but there are patterns of chemical and eruptive evolution in well-characterized systems that suggest something systematic is going on.

In a magma chamber undergoing recharge, evacuation, assimilation and fractional crystallization, recharge often has a predominant affect on melt compositional evolution. In a recharge dominated system, highly compatible elements preferentially partition into the crystal phase and reach steady state before highly incompatible elements, which are concentrated in the melt. We have developed a coupled thermo-mechanical-chemical model in order to characterize melt evolution through cycles of magma chamber filling, rupture, and drainage in a thermally evolving, viscoelastic crust. We consider a sill-like chamber under a free surface subject to influx from a deep source, calculating pressure, temperature, volume, elemental concentration, partitioning between crystals, melt, and bubbles, crustal temperature and rheology through time.

Mechanical regimes of chamber evolution depend on initial chamber volume, injection rates, and crustal properties such as viscosity and diffusivity, which evolve in response to magmatism. Over many rupture cycles the crust tends to evolve from dominantly elastic to dominantly viscous response (see also Karlstrom et al., this meeting). Chambers in the elastic regime tend to be smaller and thus eruption sizes are smaller. As the host rock heats up and crustal viscosity decreases, the time between successive rupture events increases and eventually the chamber is stable to subsequent influx. Chemical composition of the chamber reaches steady state faster in an elastic regime where mass overturns quickly through large recharge and eruption rates. We characterize the dependence of trace element concentrations on mechanical parameters and influx rates, exploring the dependence on chamber depth in an initially normal geotherm, total volatile content, primary and crustal composition. These results should be important for constraining physical controls on eruption episodicity and predictions of instability at magmatic centers.

Germán D. Padilla, Eleazar Padrón, Pedro A. Hernández, Roberto Quevedo, Nemesio M. Pérez, José Barrancos, Gladys V. Melián, María Asensio-Ramos

Submission 1003

Soil ^{222}Rn and CO_2 efflux continuous measurements for the geochemical monitoring of the oceanic active volcano island of Gran Canaria, Canary Islands

Radon (^{222}Rn) and thoron (^{220}Rn) are two radioactive isotopes of radon with a half-life of 3.8 days and 54.4 seconds, respectively. Both isotopes can diffuse easily through the soil and can be detected at very low concentrations, but their migration in large scales, ten to hundreds of meters, is supported by advection (pressure changes) and is related to the existence of a carrier gas source (geothermal fluids or fluids linked to magmatic and metamorphic phenomena), and to the existence of preferential routes for degassing (deep faults). Monitoring of ^{222}Rn and ^{220}Rn in ground and surface waters has become in the last decades an important tool to forecast earthquakes and volcanic eruptions. Gran Canaria is one of the central islands of the Canary Archipelago located off the West African continental margin. The island can be considered volcanically active, as testified by numerous prehistoric basaltic scoria cones, maars, and lava flows with the two younger eruptions dated at ca. 3,000 years B.P. With the aim of improving the volcanic surveillance program of Gran Canaria, an automatic geochemical station was installed at the end of February 2017 for the continuous monitoring of ^{222}Rn , ^{220}Rn , CO_2 and H_2S efflux in the village of Teror, northern part of the island. The instrument is a SARAD RTM2200 equipped with ^{222}Rn , ^{220}Rn , CO_2 and H_2S sensors. Each hour and during 20 minutes the instrument pumps fresh air taken from outside the room to clean the internal volume of a chamber that is completely buried at 1 m depth in the soil and opened on its lower side. The other 40 minutes, the instrument pumps the soil gas continuously in a closed loop from the chamber. The quantification of gas emission is based on observing the increase of their concentration related to the gas volume of the chamber during 40 minutes. In the monitoring period, ^{222}Rn and ^{220}Rn emissions have ranged from 257 and 65 $\text{mBq m}^{-2} \text{ s}^{-1}$ to 569 and 261 $\text{mBq m}^{-2} \text{ s}^{-1}$, respectively, while CO_2 efflux has ranged between 3.8 and 5.7 $\text{g m}^{-2} \text{ d}^{-1}$ and H_2S efflux has remained negligible. The special characteristics of the accumulation chamber (buried at 1 m depth) allow obtaining a very stable CO_2 emission time series, with minimum diurnal and semidiurnal fluctuations. This promising seismo-volcanic monitoring multi-gas technique has provided so far a baseline of gas emission for surveillance purposes of the northern part of Gran Canaria Island in a quiescence period.

Eleazar Padrón, Pedro A. Hernández, Germán D. Padilla, Gladys V. Melián, Nemesio M. Pérez, Carlo Arcilla, Alfredo Mahar Lagmay, Fátima Rodríguez, Mar Alonso, Maria Criselda Baldago, Gerald Quina, Mario A. Aurelio

Submission 834

Monitoring diffuse CO₂ degassing for the volcanic surveillance of Taal volcano, Philippines

Taal Volcano in Southwest Luzon, Philippines, lies between a volcanic arc front facing the subduction zone along the Manila Trench and a volcanic field formed from extension beyond the arc front. Taal Volcano Island is formed by a main tuff cone surrounded by several smaller tuff cones, tuff rings and scoria cones. This island is located in the center of the 30 km wide Taal Caldera, now filled by Taal Lake. To monitor the volcanic activity of Taal volcano is a priority task in the Philippines, because several million people live within a 20-km radius of Taal's caldera rim. Diffuse CO degassing surveys at the surface of the main crater lake of Taal has demonstrated to be sensitive to processes of magmatic intrusion beneath the volcano. Observing changes in the discharge rate of carbon dioxide (CO₂) is an important part of volcanic monitoring programs, because CO₂ is released by progressive depressurization of magma during ascent and reach the surface well before their parental magma. The maximum CO₂ emission rate measured to date occurred two months before the strongest seismic activity recorded during a seismo-volcani unrest period (Arpa et al., 2013, Bull Volcanol 75:747). In January 2016, an automatic geochemical station was installed at the northern portion of the main crater rim to monitor in a continuous mode the diffuse CO₂ degassing and to improve the early warning system at the volcano. The 2016 time series show CO₂ efflux values in the range 20-690 g m⁻² d⁻¹. Although short-temp fluctuations in the diffuse CO₂ emission time series were partially driven by meteorological parameters, the main CO₂ efflux changes were not driven by fluctuations of meteorological variables such as wind speed or barometric pressure and seem clearly to be associated with fluid pressure fluctuations in the volcanic system. Since 14 March, 2017, at 22:00 hours (Philippine time) the station measured a sharp increase of CO₂ emission from ~0.1 up to 1.1 kg m⁻² d⁻¹ in 9 hours. The CO₂ emission survey carried out on 16 March at the surface of Taal crater lake, showed a value of 1,763 t d⁻¹, a value 2.8 times higher than the average value measured in the period 2012-2017. These two geochemical observations might suggest the occurrence of a magmatic intrusion beneath Taal volcano at the middle of March 2017. Other geophysical or geochemical evidences are needed to support this statement.

Engielle Mae Paguican, Matthieu Kervyn

Submission 377

Quantitative analogue modelling of volcano landscape evolution in response to tectonics and erosion

Volcanoes span diverse climate regimes, and underlying tectonics influence their architecture. Tectonically controlled landforms such as volcanoes develop morphologic features that are useful in investigating deformation and landscape evolution. Analogue experiments can help show how edifices are eroded by rainfall and tectonic movement, and the implications for sediment budgets. They are also applicable for understanding the morphological evolution of volcano edifices through time, and the implications for hazard assessment. Identifying morphological features associated with erosion and tectonics is critical for identifying the dominant aggradation and degradation processes.

We present an experimental investigation that links erosion (by rainfall) and deformation (by movement of underlying faults) to the overall evolution and development of volcano edifices. The quantitative evolution of models of four end-member tectonic deformation regimes were analyzed: no tectonics, compression, extension, and strike-slip. We systematically varied the ratio of deformation to rainfall, and used different mixtures of silica sand and flour. Our approach combines these analogue models with photogrammetric 3D topography reconstructions. Digital elevation model differencing and morphometric measurements quantify the changes in size, plan and profile shape of edifices and evolution of morphological features. The series of analogue models link surface erosion and deformation features to tectonic and rainfall rates.

Results indicate that volcano erosional valleys form from surface runoffs that develop into drainage systems. They then widen and deepen into gullies, and as more material is removed from the head scarp, they widen to form amphitheatre-shaped valleys that narrow downstream. Morphological features form continuously, but their lifetime is generally short as erosion and sedimentation processes destroy or bury them. Erosion can mask features of deformed edifices that are prone to flank and summit collapse, thus compromising volcano hazard assessments. In tectonically active volcanoes, however, underlying tectonics control the formation of erosional patterns.

Rebecca Paisley, Kim Berlo, Bassam Ghaleb, Hugh Tuffen

Submission 1048

Isotope and trace element constraints on the role of tuffisite veins as degassing pathways during rhyolitic hybrid activity at Chaitén and Cordón Caulle, Chile

Efficient outgassing of magmatic volatiles is key to diffusing explosive eruptive behaviour. The existence of degassed lavas in the geological record confirms this can occur during rhyolitic eruptions, but degassing mechanisms have remained enigmatic due to the lack of observed activity. Recent eruptions at Chaitén (2008-09) and Cordón Caulle (2011-12) in Chile offer unprecedented opportunities to better constrain how rhyolitic magma degasses. Simultaneous lava effusion and vulcanian explosions were observed; hybrid activity that requires a new paradigm to explain behavioural transitions during high-silicic eruptions. Particle-filled fracture networks (tuffisite veins) have been preserved in aphyric bombs from the hybrid phases of both eruptions. It is proposed that fractures provide transient gas escape pathways, with textures recording multi-stage degassing within the shallow volcanic conduit. The major volatile components of exsolved magmatic vapour (H₂O, CO₂, S, Cl, F) act as ligands or carrier gases for low concentration, volatile trace elements (e.g. Pb, Tl, Cu, Rn, Hg) that are enriched in plumes and fumaroles. Here we use spatial variations of short-lived radioactive nuclides and trace-elements in bombs to constrain gas movement through fracture networks.

In volcanic rocks, ²²⁶Ra-²¹⁰Pb disequilibria have been attributed to the degassing and accumulation of ²²²Rn, the precursor to ²¹⁰Pb. At both volcanoes, the (²¹⁰Pb)/(²²⁶Ra) of most samples are within error of 1 suggesting no continuous, reservoir-scale degassing occurred prior to each eruption. At Cordón Caulle, depletion of ²¹⁰Pb in a tuffisite vein with respect to its host suggests this vein tapped a pocket of isolated magma that had continuously degassed for ²¹⁰Pb suggesting limited or no disequilibrium during syn-eruptive degassing, but Cu enrichment suggests reabsorption of metals did occur. These contrasting findings help constrain the volume of volatile-rich magma that degassed during the vein's short lifetime. Our results suggest gas fluxing can produce different kinds of melt heterogeneity depending on eruption conditions. They further support the model that gas fluxes are concentrated through highly permeable fracture zones that are capable of degassing catchments of deeper, volatile-rich magma.

John Pallister, Paolo Papale, Charles Mandeville, John Eichelberger

Submission 856

Recommendations of the Volcano Observatory Best Practices (VOBP) workshops

Under the aegis of IAVCEI and its commission, the World Organization of Volcano Observatories (WOVO), the Istituto Nazionale di Geofisica e Vulcanologia (INGV), the United States Geological Survey (USGS) and the USGS-USAID Volcano Disaster Assistance Program (VDAP) have convened a series of Volcano Observatory Best Practices (VOBP) workshops. These are the only international meetings specifically designed for leaders of the world's volcano observatories to meet, discuss common issues, and develop best practice recommendations. VOBP1 on Near-term Eruption Forecasting took place in 2011, VOBP2 on Communicating Volcanic Hazards, took place in 2013 and VOBP3 on Long-term Hazard Assessment took place in 2016. VOBP4 on Volcano Observatory Crisis Operations is being planned. A few examples of recommendations (out of many) include: VOBP1 (Short-term Eruption Forecasting) - Eruptions involve complex natural processes that are difficult to forecast with certainty. Consequently, probabilistic forecasts should be used and communicated in appropriate ways along with their inherent uncertainties. VOBP2 (Communication of Volcanic Hazards) - To mitigate risk, observatories and their civil defense partners should communicate directly and regularly. To build a common language and understanding, observatories should engage with stakeholders (from civil authorities to the general public) at all phases of the emergency cycle, including periods of quiescence. In addition, there was a general consensus on the need to clearly identify the separated roles and responsibilities of scientists and decision-makers. VOBP3 (Long-term Hazard Assessment) - Hazard maps are but one component of a portfolio of products, which constitute a complete hazard assessment. A next generation of global databases (e.g., with data on volcanic unrest, eruption precursors and outcomes) is required to inform and validate long-term (and short-term) hazard assessments, and to extend geological data from individual volcanoes. Use of models that embed statistical analysis or simple models that can be used in a statistical way are recommended when conducting long-term hazard assessment. More complex numerical models are recommended to inform understanding of processes, help explore hazardous scenarios, visualize the full range of hazardous phenomena, and inform simpler models. These and other best practice recommendations are summarized in a report compiled by the organizers.

Ayla Pamukcu, Blair Schoene, Chad Deering

Submission 573

Compositional heterogeneity in the Lake City magmatic system (CO, USA) revealed by zircon U-Pb TIMS-TEA

The 23 Ma Lake City caldera and Sunshine Peak Tuff (CO, USA) is an excellent system to explore questions of volcano-pluton connections and magma body heterogeneity. Erupted products of the SPT range from crystal-poor high-silica rhyolite to crystal-rich trachyte, and resurgent porphyritic syenite and quartz monzonite/dacite intrusions are exposed in the center and on the eastern flank of the caldera. Field relations, bulk rock geochemistry, and phenocryst compositions have led to models suggesting: (1) the magmatic system was compositionally variable, and multiple magma batches were involved in the eruption; (2) the rhyolites were derived from a mush (represented by the syenite), and the trachytes are remobilized portions of this cumulate.

We investigate this system further using zircon U-Pb CA-ID-TIMS-TEA to obtain high precision age and trace element information from individual zircon crystals. Zircons are first separated, divided into broad size groupings (large, medium, small), and imaged with CL. Aliquots containing U, Pb and trace elements (TEA) are then separated from individual dissolved and spiked crystals. The U-Pb aliquot is analyzed for an age by TIMS; the TEA aliquot is analyzed for trace element contents by solution ICP-MS.

Zircon ages and trace element contents from all units (except quartz monzonites) overlap, consistent with the hypothesis that the rhyolite was derived from the trachyte (remobilized syenite). Trace element trends (e.g., Hf v. Sm/Yb) are consistent with fractionation and are akin to those seen in other systems that follow the mush model (e.g., Peach Spring Tuff). Yet, these trends are not born out in age-trace element comparisons. Relationships between size and age/composition are also complex – large- and medium-sized grains encompass the range of measured Hf contents, but small grains have neither the most nor the least evolved compositions. CL images reveal dark cores in many the low-Hf crystals; further investigation of these grains and hosted melt inclusion by in situ methods will reveal if these are the source of the low Hf signal and elucidate more about the heterogeneity and evolution of the melt. We interpret the lack of compositional trends with time as reflective of heterogeneity in the state of crystallization and differentiation in different areas of the magmatic system at different points in time; this could be explained by variable temperature conditions in a cooling mush prior to melt extraction and eruption.

Bo Pan, Shanaka de Silva, Jiandong Xu

Submission 218

Magmatic and eruption processes of the Millennium eruption at Changbaishan Tianchi volcano, China/North Korea

Field relations, petrography, bulk and micro-scale chemistry reveal that the most recent history of hazardous Changbaishan Tianchi volcano should be revised with important implications for volcanic hazard in NE Asia. Currently, the two most recent eruptions are identified as a VEI 5 trachytic Baguamiao eruption (BGM) and the much heralded VEI 7, 946 AD “Millennium” eruption (ME) of comendite. However, we find that the former is part of the latter based on the following evidence: (1) trachytic fallout of the BGM lies directly on the comendite tephra of ME without any indication of depositional hiatus; (2) abundant mingled trachyte-comendite pumice in the tephra deposits; (3) similar chemistry of mingled pumice and its components to those in the main BGM and ME products; (4) correlation of bimodal glass shard compositions in the distal ‘B-Tm’ ash from the Japan Sea with comendite and trachyte glass from BGM and ME products. Based on the above evidence, we suggest that the great Millennium eruption of 946 ± 3 AD should be revised to include the BGM trachyte as its final stage.

The deposits attributed to two other trachytic eruptions in 1668 or 1702, and 1903 referred to in historic accounts were also examined. Our field observations, petrography, bulk and micro-scale chemistry combined with previously published Ra/Th ages indicate that all these trachytes are either primary deposits of ME or its reworked deposits. Thus our findings do not support two separate post-ME eruptions and require that volcanic hazard assessment include this new interpretation.

Recent published geochronological data is integrated with our new volcanological framework to inform magma dynamics leading to the ME. The ME comendite, derived from a parental trachyte similar to BGM started accumulating at shallow levels around 12 ka to 8 ka. Around 4 to 1.6 ka the BGM trachyte *sensu strictu* separated from its source and started accumulating and crystallizing beneath the ME comendite. The strong evidence for mixing in the eruption products, suggests that overturn and mixing of this layered comendite-trachyte system occurred during the Millennium eruption ~ 1 ka. The presence of deposits of mixed comendite-trachyte eruptions in the last 100 ky at Changbaishan suggests that these magma dynamics may recur cyclically leading to catastrophic eruption there.

This research was supported by the China National Science Foundation (41302267) and the Special Projects of the Institute of Geology, CEA (IGCEA1505).

Stephen Pansino, Benoit Taisne

Submission 987

Communicating through stress, in the intimacy of a dynamic magmatic system

When dikes propagate near a magma chamber, they can be affected in complex, sometimes counter-intuitive ways. An over- or under-pressurized magma chamber induces a stress field in the surrounding crust, in which the minimum compressive stress is oriented either radially or tangentially to the magma chamber. This controls the orientation, and thus path, of any nearby, propagating dike.

We perform a set of analogue experiments demonstrating some of these interactions. We use gelatin to simulate the earth's crust, since it is an elastic, transparent medium. A balloon is used to create a cavity in the gelatin, which then is pressurized (or depressurized) via hydrostatic forces. The stresses due to this pressure can be visualized using polarized film, allowing us to track how a dike moves through a stress gradient. We produce dikes in different initial orientations (e.g. radial or tangential) to see how they respond to a stress gradient (e.g. growing asymmetrically, bending, or twisting). Preliminary results indicate that over-pressure magma chambers have attractive qualities for dikes, "pulling" them in via different mechanisms, which has partially been shown in previous numerical studies. Under-pressure magma chambers have repelling qualities, preventing dikes from coming too close. This has obvious implications for natural systems, in that dikes are demonstrated to move towards a pressurized systems, which could trigger an eruption, or can be repelled by a deflated system and circumvent the chamber. In the case of an underpressure system, depending on the dike orientation, dikes may prefer to form concentric shells, which in turn could favor growth of the chamber in an onion-like fashion.

Paolo Papale

Submission 1313

Communication of volcanic hazards in urbanized areas, and the roles of scientists and decision makers

The growing complexities of the societies impose that increasing attention is given to the roles and relationships between those who possess and manage scientific knowledge, and those who use that knowledge to make decisions impacting the society. Decision making is a political issue, and as such, it brings elements that depend on the political and cultural set up of the different countries. In most western countries the separation of responsibilities between scientists and decision makers is an accepted principle, but the practices are still far from it. Communications from volcano monitoring centers largely continue to reflect the decades old, pioneering times when volcano scientists were trusted as the sole authority capable of providing direct guidance on societal response to volcanic hazards; one of the most striking evidence is the common definition of current alert level by volcano observatories, that I analyse here, and that result in the assumption of roles and responsibilities that largely exceed those of scientists. Conversely, alert level systems have a meaning and relevance solely in terms of their societal impact, and decisions thereby should be exclusive responsibility of political decision makers. Decision makers should cooperate with experts from many disciplines far beyond volcanology and including social science, engineering, economics, urban planning, risk management, etc., in order to inform their decisions and construct a robust system of progressive actions aimed at minimizing the impact of volcanic unrests and eruptions in urbanized areas, and maximize the resilience of the population and the country.

Lucia Pappalardo, Gianmarco Buono, Paola Petrosino

Submission 1103

X-ray microtomographic investigation to explore trigger mechanisms of plinian eruptions: a Somma-Vesuvius volcano case study.

The knowledge of trigger mechanisms and syn-eruptive dynamic of high-magnitude eruptions is a primary goal in volcanology, due to the influence of these sub-volcanic processes on the behavior of precursory phenomena that are detected by monitoring systems during volcanic crises. In fact a severe difficulty in volcanic forecast is to correlate the evolution of the geochemical and geophysical signals recorded at the surface with the magma transfer at depth and then determine whether the magma would be able to erupt. In the last decades quantitative textural studies on volcanic rocks have proved to be a fundamental approach in exploring the conditions related to magma ascent in volcanic conduit and allowed to improve our ability to interpret volcano-monitoring signals and perform hazard assessments. In more densely populated regions, as the Neapolitan high-risk volcanic area, this information would be essential to avoid a major volcanic disaster. In this case study we have explored the internal microstructure of pyroclasts erupted during the first and most intense plinian eruption of Somma-Vesuvius, by generating high-resolution three-dimensional digital maps via X-ray microtomography. A peculiar aspect of this eruption, that delineates the passage to the explosive character of the volcano as well as the beginning of caldera collapse, is its high intensity that remained stable during all the course of the sustained phase despite the strong magma compositional variation towards mafic composition, thus requiring that additional mechanisms may have acted at sub-volcanic level and magnified the eruption intensity. Our 3D quantitative textural data combined with Sr and Nd isotopic investigations on both separated minerals and matrix-glass, have demonstrated that the transfer of magma towards the surface was accelerated by the occurrence of rapid vesiculation pulses driven by limestone assimilation during magma ascent through the carbonatic bedrock. These findings demonstrate, for the first time on natural volcanic rocks, that limestone assimilation can be a syn-eruptive process, able to trigger further gas release and rapid bubble nucleation in the final stage of magma ascent with deep impact on eruption intensity, thus influencing the hazard of active volcanic systems developed within calcareous substrate, widespread worldwide in several tectonic settings.

Carolyn Parcheta, Aaron Parness, Jeremy Nash, Karl Mitchell

Submission 608

VolcanoBot: Imaging volcanic fissure conduits from the inside out, with implications for lava fountain dynamics.

Volcanic conduits play a fundamental role in shaping the nature of eruptions, thus requiring a more accurate understanding of their geometric constraints to fully understand controls on volcanic activity. Creating and developing VolcanoBot addresses conduit geometry documentation for fissure eruptions by integrating robotics and computer vision with observational field geology and numerical fluid dynamic modeling. Previously, there was no technique to adequately document, quantify, and investigate volcanic fissure conduits (if preserved and exposed) at a centimeter scale. VolcanoBot (a new form of ground-based, subterranean remote sensing) provides centimeter scale resolution of fissures by mapping them in 3D from within the exposed conduits. It is optimally designed for mapping near vertical cracks ($\pm 30^\circ$) by repelling off a tether from a surface base station with minimal risk to the operators. We collected the first-of-its-kind data from a post eruptive fissure conduit at Mauna Ulu, Hawaii over three deployments in 2014-2016. We also created a custom 3D modeling software, called Vmapper, which advances state of the art open source packages by leveraging global optimization algorithms and spatial hashing to speed up the processing pipeline. Our data shows that the fissure conduit has many irregularities throughout the 30 m depth that we mapped, while maintaining a steady width of 30-50 cm. The shape of the irregularities changes with depth, implying that they may be controlled by the underlying stratigraphy. This is further supported by the significant number of piercing points across opposing walls. In order to understand the fluid dynamics of lava fountains erupting through this geometry, first we calculated the speed of sound within vesicular basaltic magma. The speed of sound is ~ 15 m/s for the vesicularity range of 20-80%. The estimated eruption velocities during the Mauna Ulu eruption were 20-30 m/s at 64% vesicularity, implying the lava fountains exceeded their internal speed of sound. This provides a more robust mechanism for fluid basaltic fragmentation as well as a possible explanation for the pulsatory behavior of lava fountains. At the point that a supersonic transition occurs, a shock wave should be produced within the lava fountain, causing a pulse in the lava fountain and potentially providing enough energy and force to fragment the magma. Our ongoing work is focused on this behavior and its influence on vent flaring.

Federica Pardini, Mike Burton, Fabio Arzilli, Giuseppe La spina

Submission 650

SO₂ fluxes from explosive eruptions: a novel numerical approach based on satellite images applied to the Calbuco 2015 eruption.

Quantifying the manner of release of sulphur dioxide (SO₂) from explosive eruptions is of great value for both characterization of volcanic activity and volcanic hazard mitigation. Despite SO₂ is routinely measured from space, difficulties are still present in retrieving injection heights time-series and fluxes at a volcanic vent position. Here we present a new numerical method based on a back-trajectory approach able to fully characterize volcanic SO₂ clouds as seen from space. The numerical tool operates on satellite images of SO₂ clouds through the integration of the HYSPLIT software with custom-designed Python routines which make our procedure completely automated. Injection heights time series and fluxes are computed at high temporal frequency and with low computational cost.

We apply our numerical method to satellite images of SO₂ emitted by the recent Calbuco eruption (Chile, April 2015). Two sub-Plinian events occurred in about 12 hours, a first short event (from 21:00 to 22:30 on the 22nd April) and a second longer one (from 04:00 to 10:00 on the 23rd April). Results show a mean injection height at the vent position of ~15 km for the two pulses, with peaks of 20 km especially for the first event. We infer 0.41 Tg of SO₂ released during the two phases, where 0.19 Tg associated with the first event and 0.22 Tg to the second one. From the retrieved SO₂ budget and injection heights time-series we derived SO₂ fluxes emitted during the two events. Our numerical results show an SO₂ flux with a sharp increase during all the first phase, while a lower average flux smoothly increasing characterizes the second phase.

Finally, we compare our numerical results with sulphur concentrations measured from microprobe analysis of melt inclusions in plagioclase phenocrysts and groundmass glass (residual melt) of tephra samples. Preliminary results show an excess of sulphur gas phase (exsolved from deep unerupted magma) which was already present at shallow depths before the eruption. We hypothesize that the presence of abundant sulphur gas phase at shallow depths could have contributed to generate the overpressure which, eventually, could have triggered the sub-Plinian eruption.

Natalia Pardo, Bernardo Pulgarín, Valentina Betancourt, Federico Lucchi, Llerónimo Valencia

Submission 152

Volcano geological mapping at low-latitudes: successful application of Unconformity-bounded units at the Doña Juana Volcanic Complex, SW-Colombia

We present the Doña Juana Volcanic Complex geological map, stratigraphy, and Ar/Ar-and-C14 geochronology resulting from a pilot-mapping project in Colombia, as a study-case for the application of the geological field techniques currently discussed within the IAVCEI Volcano-Geology Commission. Geomorphology, lithostratigraphy and lithofacies analysis, lithosomes, unconformity-bounded units, and geochronology were successfully integrated. The geological evolution of the DJVC was reconstructed and interpreted in terms of eruption behaviour, stating the basis for realistic, long-term hazard assessment.

The DJVC is a calc-alkaline dacitic composite volcano within the Central Cordillera of Colombia, which started its activity about 1125.4 ± 4.4 ka ago (Ar/Ar age). It comprises four spatially overlapped edifices, and three adventice cones, which unconformably overlay Lower Cretaceous, metasedimentary and volcanic rocks of oceanic affinity. We recognized four major-rank unconformity-bounded units corresponding to five Eruptive Epochs of DJVC. In proximal areas, these unconformities mostly correspond to angular unconformities corresponding to various volcano-tectonic structures and sector collapses affecting the subsequent stages of construction of DJVC. Towards the distal areas, they pass into their correlative disconformities.

In contrast to high-latitude volcanoes, the correlation of the unconformities within the typical Colombian equatorial-climate and socio-political conditions frequently requires a high interpretative component because of the dense vegetation, abrupt topography, and the national armed conflict, which limits access to many sectors of the study area. For instance, this made necessary to introduce some informal geomorphological units to identify volcanic bodies with a clear 3D geometry that are completely inaccessible in the field. In addition, the recognition of well-developed, widespread paleosols and the adoption of the morphostructural relationships of lithologically distinctive terraces at different elevations along the main river valleys were extremely useful for correlation.

The Holocene record has been mostly characterised by the emission of lava-domes, which have collapsed to originate block-and-ash flows, surges, and lahars. The corresponding eruptive products have drained along the present river basins to the NE and SW of the DJVC summit, forming morphological terraces currently populated by nearly 49,000 rural-and-urban inhabitants.

Joali Paredes, Bettina Scheu, Cristian Montanaro, Alejandra Arciniega, Donald B. Dingwell, Diego Perugini

Submission 320

Effects of particles size, componentry and conduit geometry on fragmentation processes.

The grain size distribution (GSD) is an important tool to characterize a volcanic deposit and to link it to eruptive processes. The GSD of a deposit is a complex product of primary processes such as fragmentation of magma to tephra, and secondary processes such as abrasion and comminution within the conduit until the material is expelled to the surface. In particular, the continuous interaction between tephra particles, together with the conduit geometry, play a crucial role in these secondary processes bearing the potential to significantly alter the GSD of the ejected mixture in relation to the GSD derived from primary processes only.

Loose material collected from the Pomici Principale eruption fall deposit (10.3 ka, Campi Flegrei) was used for the experiments. A physical separation allowed for the discrimination of two main groups; 1) pumiceous fraction, and 2) dense fraction. We report the result of particle-size distributions from a series of rapid decompression experiments. The sample material was slowly pressurized to 10MPa using argon gas and then rapidly decompressed. A transparent autoclave and sample holder were used to optimize the visual observation of particle's acceleration, collision and eventual fragmentation.

The study aimed to evaluate the individual influence of three parameters; initial particle size and lithology, together with conduit geometry on size-reducing processes (gas-driven fragmentation, collision, abrasion). To do so, these parameters were altered throughout a range of experiments e.g. 1) particles of 4, 2.8 and 2 mm were prepared in populations with a unique grain size and with two different size fractions (unimodal and bimodal); 2) the ratio pumice/dense fraction in the initial samples were 1:0, 1:1 and 2:1; and 3) two series of experiments were implemented, one maintaining a constant internal diameter along the length of the autoclave, and a second with an inner ring reducing the diameter in one section of the apparatus.

Our first results suggest that 1) an increasing amount of dense clasts in the initial particle mixture produced an increased percentage of fines; 2) a significant amount of very fine material (<63 μ m) is produced independently of the presence of dense clasts, and 3) a reduction on the conduit diameter (analogous to obstacles within the conduit walls) is likely to further reduce the average diameter of individual clasts and increase the generation of very fine material even further.

Martin Parham, Simon Day, Richard Teeuw

Submission 682

To evaluate changes in school children's perceptions of multiple hazards in Dominica, Caribbean: impact of education programs upon hazard awareness before and after local natural disasters

This project aims to assess school students' changing perception of both volcanic and other natural hazards through use of the SurPRISM interviews. We look at spatial differences in perception across four geographically and socially different schools on the island of Dominica in the Caribbean. The SurPRISM interviews are part of a five-year longitudinal study to understand the changing hazard perception of geography students, with non-geography students forming a control group. These interviews will inform a redesign of the hazards' curriculum in schools to improve awareness. This new methodology is adapted from one used in clinical practice to assess patient perceptions of illness and treatment (Büchi and Sensky 1999). This novel measure is essentially non-verbal and uses spatial positions of moveable markers ("object") on a board, relative to a fixed marker that represents the subject ("self"), as a visual metaphor for the importance of the object to the subject. Subjects explain their reasons for placing markers as well as give qualitative socio-economic information about themselves. The SurPRISM data produces statistics on perceptions and qualitative data about each subject.

This presentation focuses on changing perceptions of multiple hazards since 2013. We use the impact of recent disasters (such as Tropical Storm Erica in September 2015) to chart students' changing perceptions. This is combined with an evaluation of how different teaching methods alter perceptions and which methods are the most effective to improve understanding. The results have already prompted an assessment of the wider hazard educational provision. The aim of this is to improve the effectiveness of teaching methods, such as fieldwork, to raise awareness. This longitudinal study, using natural disasters as benchmarks, has allowed us to address the question of how a natural disaster can be used as a reference point to enhance education about less frequent hazards, such as volcanic eruptions.

Büchi, S., & Sensky, T. (1999). PRISM: Pictorial Representation of Illness and Self Measure: a brief nonverbal measure of illness impact and therapeutic aid in psychosomatic medicine. *Psychosomatics*, 40(4), 314-320

Raphael Paris, Martina Ulvrova, Karim Kelfoun, Olivier Roche

Submission 127

The challenge of volcanic tsunami modelling

A volcanic tsunami is defined as a tsunami generated by phenomena occurring at a volcano, such as eruptive processes, rapid ground deformation, flank instability and failure. In the historical record, volcanic tsunamis represent a low-frequency hazard (about 5% of all recorded tsunamis) but the largest events are particularly deadly, four of them being ranked in the twenty deadliest volcanic disasters : Oshima-Oshima 1741, Unzen 1792, Krakatau 1883, and Ritter Island 1888. Volcanic tsunamis caused more than 55000 fatalities during the four last centuries, thus representing the third cause of fatal incidents linked to volcanic eruptions. Source mechanisms of volcanic tsunamis include underwater explosion, pyroclastic flow, lava, and lahar entering the water, slope instabilities, volcanic earthquake, and shock wave due to large explosion, caldera subsidence. Volcanic tsunamis are generally characterised by short-period waves, greater dispersion, and limited far-field effects compared to earthquake-generated tsunamis, but the diversity of source mechanisms imply different types of waves. Diversity of waves in terms of amplitude, period, form, dispersion etc. poses difficulties for integration and harmonisation of sources to be used for numerical models and probabilistic tsunami hazard maps.

Modelling volcanic tsunamis is challenging because the source mechanisms are often complex, thus requiring both the tsunami and volcano expertise. We present a brief review of source mechanisms of volcanic tsunamis, referring to past examples and the physical mechanisms implied. Guidelines for parameterizing the models and the sensitivity to these parameters are provided for different types of source mechanisms, together with results of numerical simulations. The more complex source of volcanic tsunami is pyroclastic flow. Indeed, mechanisms of interaction between pyroclastic flow and water as well as the conditions required to generate a tsunami remain partly elusive because the scientific community lacks observations of this complex phenomenon, and because experimental as well as theoretical studies are rare. A new experimental device is being installed in the laboratoire Magmas & Volcans at Clermont-Ferrand, France. Pyroclastic flows were implied in the generation of disastrous volcanic tsunamis (Santorini, Krakatau). The numerical-experimental combined approach will allow a better understanding of tsunami generation by pyroclastic flows and a reliable hazard evaluation.

Aaron Parness, Aaron Curtis

Submission 1140

Rock and ice climbing robots for volcanology

Conducting the business of volcanology entails prolonged presence on steep terrain. Climbing may provide the most appropriate means of robotic mobility for in situ sampling or sensor deployment in settings like a gas vent on a slope, a fissure, lava tube, or fumarolic ice cave. We review robotic systems capable of interacting with steep volcanic terrain, compare them with small unmanned aircraft capabilities, and present recent progress on a climbing robot with emphasis on its new ice climbing capabilities.

JPL has made consistent progress in mechanical rock climbing over the past decade. Continual improvements in microspine rock gripping technology were applied to evolving robotic platforms including Robosimian, MicroClimber, and LEMUR (Kennedy et al., 2006; Parness et al., 2013). The most recent iteration of LEMUR is regularly tested on lava tube walls and is undergoing integration with a suite of instrumentation to conduct biogeochemical investigations. Ongoing enhancements to the perception systems and onboard software are rapidly elevating its level of autonomy. We expect LEMUR will soon produce useful volcanological results, following in the spiny footsteps of VolcanoBot, another JPL robot which recently mapped an eruptive fissure to 25m (Parcheta et al., 2016).

Recent interest in icy environments in both volcanology and planetary science are driving the development of ice climbing capabilities for LEMUR. We are working on a new gripping / anchoring technology for LEMUR called the ice screw end effector (ISEE). We recently tested an ISEE prototype in the fumarolic ice caves of Mt Erebus. We present further progress on ISEE, including addition of an ice sampling system, and the state of ice climbing capability.

Justin Parra, Olac Fuentes, Vladik Kreinovich, Elizabeth Anthony, Vanessa Espejel-Garcia, Octavio Hinojosa de la Garza

Submission 1245

Eruption Forecasting from Seismic Activity using Neural Networks

Accurate eruption forecasting is one of the most important problems in volcanology. Methods based on analysis of precursors, including gas emissions, ground deformation, and seismic activity have been proposed. With the growing amount of sensor data for volcanic monitoring available in real-time, the automation of this forecasting process has become feasible, at least in principle.

We propose an approach for automated eruption forecasting from seismic activity based on neural networks. We generated a dataset of earthquake locations and magnitudes in the vicinity of 37 of the volcanoes in the Aleutian Arc from 1998 to 2016 by querying the ANSS (Advanced National Seismic System) Composite Catalog. The magnitudes of the earthquakes were binned at certain temporal intervals and crater-centered volumes and used as features for a three-layer neural network, which predicted the probability of an eruption. We evaluated our system using a leave-one-out cross-validation approach, testing the predictions with one volcano at a time, while training the network with data from the remaining 36. Using this approach, we could successfully predict the eruptions of Augustine (2006), Okmok (2008), and Redoubt (2009), while having a very low false positive rate.

Karen Pascal

Submission 115

22 years of volcano-deformation monitoring at Soufrière Hills Volcano, Montserrat

In 1995 Soufrière Hills Volcano (Montserrat, West Indies) erupted for the first time after several centuries of quiescence. Since then, five phases of extrusive activity have occurred, lasting between 3 months and roughly 3.5 years. These phases were interrupted by pauses which mainly lasted between 9 months to approximately 2 years. The eruptive activity is punctuated by episodes of dome building, dome collapse, explosions and associated pyroclastic flows as well as ash plumes and lahars. The eruption has been catastrophic for the economy of the island, causing the permanent evacuation of two-thirds of the island, and the emigration of half of the population. After a major dome collapse in February 2010, the extrusive activity has entered its longest pause to date. However, Soufrière Hills Volcano still shows signs of unrest, as confirmed by the degassing of several hundred tonnes of SO₂ per day, and a slow inflation of ~ 1 cm/yr horizontally. Since the beginning of the eruption, the deformation network has been constantly updated and expanded. Here we present the various methods that have been used until now to monitor the deformation of the Soufrière Hills volcano, and how they have helped to broaden our understanding of its magmatic system. These methods include eg campaign, continuous and 'Spider' GPS stations, EDM (baseline) measurements and borehole strainmeters. We also discuss the challenges of measuring and interpreting the slow deformation observed, and the potential developments which could improve the deformation monitoring of the volcano.

Scott Paterson, Katie Ardill, Vali Memeti

Submission 731

Regional scale magma focusing in the central Sierra Nevada, California: Evolving magma chamber and final intrusive sizes, shapes and volumes in the plutonic plumbing beneath volcanic center.

During the Cretaceous, the Sierra Nevada arc underwent a dramatic magmatic and tectonic flare-up (ca. 130 - 85 Ma) while migrating eastward (~3 mm/yr). During these events, at least one magmatic center formed locally due to inward spatio-temporal focusing at an ~100 km scale in the central Sierra Nevada (CSN) from >105 Ma to 85 Ma. This focusing at deeper, plutonic levels mimics examples established at volcanic levels such as the Aucanquilcha Volcanic Cluster and the San Juan Volcanic field, Colorado.

In the CSN a >105-95 Ma ring of plutons with length/width ratios of 1.5 to 15, areas of 1.5 to 350 km² and estimated volumes of ~3 to 1,700 km³ migrated towards the centrally located, 95-85 Ma, 4/1 ratio, ~1,200 km² area and ca. 11,000 km³ volume Tuolumne Intrusive Complex (TIC). The TIC consists of 3 main phases (Kuna Crest, Half Dome, Cathedral Peak), each of which amalgamated from smaller pulses. Spatio-temporal focusing continued during construction of the TIC with the centers of magmatism moving inwards and northwards: the youngest (84.6 to 86 Ma) center is preserved in the NE corner of the Cathedral Peak phase. Estimated maximum volumes of magma chambers in the older peripheral plutons range from 1 to 1,100 km³ (average = 120 km³). In the TIC at least 7 distinct magma chambers existed ranging in volume from 100 to ~3,000 km³.

Thus, in the CSN, a >20 m.y. inward migrating and focusing plutonic system resulted in an increase of the average volumes of peripheral magma chambers and the average area and volume of final intrusive complexes. Lifespans of TIC magma chambers are estimated to last from a few hundred thousand to >1.5 m.y. Estimates of Cretaceous plutonic/volcanic ratios in the CSN vary from 20 to 30/1. Volumes of volcanic eruptions in continental arcs range from 0.1 km³ to more than 1,000 km³ over average durations of ~50 days. Thus, if even 1/5 of the originally available magma chambers in the CSN erupted, the appropriate plutonic/volcanic ratio would have been produced and the total eruptive volumes would match those in actively focusing volcanic fields of similar dimensions and durations. Super-eruptions could possibly have erupted from the largest magma chambers in the center of the focusing zone.

A potential mechanism to drive focusing is explored by Karlstrom et al. (this meeting). The changing petrology and geochemistry in the CSN magma system is explored by Ardill et al. (this meeting).

Matthew Patrick, Tim Orr, Don Swanson

Submission 929

Is Halema`uma`u's lava lake a window into the deeper magmatic system?

It is commonly written that lava lakes provide a valuable “window” into the deeper magmatic system. In the past decade, research at Erebus and Erta Ale volcanoes has supported this premise by showing that fluctuations in lava lake activity appear to reflect changes in magma supply rate. The ongoing lava lake activity in Halema`uma`u Crater, at the summit of Kilauea Volcano, Hawai`i, presents a unique opportunity to test the window concept in more detail using a combination of long-term visual and camera observations coupled with a robust geophysical monitoring network. We focus on four primary lake processes that have been previously documented, and evaluate the degree to which they reflect shallow or deep phenomena: 1) small explosions, 2) daily to monthly lava level changes, 3) gas pistoning, and 4) lake surface motion variations.

First, small explosive events have occurred in the lake, throwing spatter several hundred meters. Webcam and direct observations have demonstrated that these events are triggered by rockfalls into the lake – essentially a top-down process unrelated to the deep system. Second, daily to monthly lava level changes, of tens of meters, have a strong correlation with ground tilt and GPS, indicating that the lake level is a pressure gauge (piezometer) of the deeper magma reservoir. Third, gas pistoning commonly occurs in the lake, with abrupt lake level changes of up to 20 m. Previous work shows that gas pistoning is driven by shallow gas accumulation near the top of the lake surface, perhaps as a foam, in a shallowly driven process. Fourth, the lava lake surface motion shows two types of behavior: a stable flow that occurs most of the time, and a transient unstable, chaotic surface motion. Multidisciplinary observations (surface motion, lava level, tremor) show that stable lake motion is related to lava upwelling from the feeder conduit, while the unstable motion is related to near-surface spattering fluctuations. Lake surface motion appears to have both deep and shallow controls.

These long-term multidisciplinary observations indicate that lake behavior at Halema`uma`u includes both deeply and shallowly driven processes. The shallow processes demonstrate that the lake is much more than a simple “window” on the deeper system; the lake has its own internal dynamics, superimposed upon the deeply driven processes. We speculate that other lava lakes may also exhibit some combination of shallow and deep processes.

Matthew Patrick, Tim Orr

Submission 930

Long-term operational imaging of eruptive activity at Kilauea Volcano

The two sustained eruptions at Kilauea Volcano present a valuable opportunity for understanding effusive volcanism. These eruptions include a large lava lake in Halema`uma`u Crater at the summit (9 years), as well as pahoehoe lava flows erupted around Pu`u `O`o cone on the East Rift Zone (34 years). Stationary, continuously operating webcam (visual, near infrared and thermal infrared) and time-lapse camera systems have become a vital component of HVO's monitoring network, augmented by aerial and ground-based campaigns using handheld cameras (visual and thermal).

Automated algorithms have been essential for maximizing the operational value of stationary, continuously operating thermal cameras observing the summit lava lake and Pu`u `O`o crater.

Algorithms currently track lake level and the surface velocity field of the lava lake in Halema`uma`u Crater, as well as the abundance of spattering, providing an updated dashboard display of recent activity. Data from these algorithms have helped provide new insights into shallow and deep controls on lava lake behavior. The automated routines also include thermal alarms sent to smartphones, which have been helpful in identifying new activity.

Structure from motion (SfM) techniques have been an integral part of monitoring over the past few years, using both normal photographs and thermal images acquired during helicopter overflights. At Halema`uma`u Crater, SfM has provided a lower cost alternative to LiDAR for mapping and measuring the lava lake and evolving crater geometry. At Pu`u `O`o, we use SfM to map the lava flow margins and make georeferenced thermal maps of the entire pahoehoe flow field, providing quantitative constraints on pahoehoe breakout distribution and subsurface lava tube paths.

Currently we are shifting to higher resolution thermal cameras to provide increased detail and precision, and exploring the use of photogrammetric imaging using stationary thermal cameras. In the future, we anticipate a growing role for unmanned aerial systems as an operational imaging platform on Kilauea. Overall, camera systems at Kilauea have played a vital role in both operational monitoring and hazard assessment, as well as process-oriented research.

Luis Miguel Peci Sanchez, Manuel Berrocoso Dominguez, Alberto Fernandez-Ros, Gonçalo Prates, Amos De Gil, Raul Paez, Belen Rosado Moscoso

Submission 567

VALIDATION OF THE MULTIPARAMETRIC SYSTEM FOR VOLCANIC SURVEILLANCE ON DECEPTION ISLAND (ANTARCTICA): VOLCANIC PROCESS 2012-2017.

Volcanoes are complex systems in which the diverse associated physico-chemical processes present a wide spatial variability. In order to study these processes, it is necessary to deploy monitoring networks. The caldera of Deception volcano is submerged and forms an inner bay named Port Foster. This circumstance adds particular characteristics against the rest of the volcanoes. Its location in Antarctica makes its monitoring a challenge. Based on its specific features we have developed a multi-parametric monitoring system to surveil the following parameters in near-real time: ground deformation with three GPS-GNSS stations in BAE Gabriel de Castilla (BEGC), Fumaroles Bay (FUMA) and Pendulum Cove (PEND); thermal anomalies with a thermistor and thermocouple sensors at different depths to get a vertical profile of Cerro Caliente (CECA) and slope distance between two benchmarks (BEGC-CECA) with electromagnetic distance meter surveying (EDM). Two additional parameters are obtained: instantaneous sea level and temperature measurements of Port Foster with a tide gage station (DECMAR). These records complement the data for volcanic activity surveillance on Deception Island.

All sensors monitored in near-real time have been integrated in a low-cost system based on embedded systems. These systems show great adaptability to different environments because they are based on open, low-cost, low-consumption systems. This system, which collects data from different sensors, connects them, by WiFi links, to a control centre located in the Spanish station where forecasts of short, medium and long term are provided through the analysis of the time series within the context of the island's geodynamic mechanism. This system is a very useful tool, especially to provide the first information at the beginning of the campaign. Thus, this multi-parametric volcano monitoring system can be said to currently allow the assessment of ground deformation and thermometric anomalies observed in near real time (GNSS-GPS, thermometry, EDM).

During the austral winter of 2012 submarine thermometry detected the beginning of an important process of volcanic activity. This process meant continuous geodynamic behaviour of expansion-elevation until January 2015 when the process turned into compression-subsidence behaviour until January 2017. All these changes have been detected and registered and, therefore, validate this multi-parametric system designed for and established on Deception Island.

Gro Pedersen, A. Höskuldsson, T. Askew, T. Thordarson, I. Jónsdóttir, M. Riishuus, B. Óskarsson, E. Magnússon, M. Gudmundsson, F. Sigmundsson, V. Drouin, C. Gallagher, R. Askew, J. Guðnason, W. Moreland, P. Nikkola, H. Reynolds, J. Schmith, S. Dumont

Submission 396

Lava field evolution and emplacement dynamics of the 2014-2015 basaltic fissure eruption at Holuhraun, Iceland

The 6-month long eruption at Holuhraun (Aug. 2014- Feb.2015) was the largest effusive eruption in Iceland in 230 years with an estimated bulk lava volume of ~1.44 km³. The eruption has been divided into three phases based on the evolution of the lava field.

The first phase (~6 weeks) was dominated by open lava channels and the emplacement of four main lava flows (No. 1 to 4). The lava flows were predominantly cooling limited and the longest is lava flow no. 1, which reached the length of 17 km.

Lava emplacement during the second phase (~6 weeks) was influenced by the formation of a 1 km² lava pond about 1 km downstream of the vent. This pond became the main distribution point for the lava transport during phase 2, controlling the emplacement of three new lava flows. Towards the end of phase 2 lava resurfacing became more predominant and lava tubes developed within lava flow no. 1, resulting in formation of inflation plateaus.

In the third and final phase (3 months), transport of lava through tubes dominated the lava transport and inflating plateaus grew in extent in lava flows (no. 1-2), raising the channel surface by 5-15 m above the surrounding lava. These inflation plateaus were the surface manifestation of a growing lava tube system, which formed as lava ponded upstream in the open lava channels. This created sufficient lavastatic pressure in the fluid lava core to lift the roof of the lava channels. More than 19 km² of the lava field was resurfaced during this period, while lava was transported to the distal part of the lava field.

A suite of lava morphologies (shelly pāhoehoe, slabby pāhoehoe, rubbly pāhoehoe, spiny pāhoehoe and 'a'ā) was observed within the first week of the eruption. During phase 1 and 2 'a'ā was the dominant flow morphology in all main lava flows while spiny pāhoehoe was the typifying lava morphology in phase 3. These changes in surface morphology makes the 2014-2015 Holuhraun lava a paired flow field and the development of lava tubes in the existing channels within the 'a'ā flow may explain why paired lava flows often have similar length.

Kevin G. Pedroza-Aldana, Julie Roberge, Teresa Pi-Puig, José A. Andraca-Adame, Nick Varley, Fernanda Flores-Rios

Submission 699

Petrological monitoring during volcanic eruption using X-Ray diffraction to identify the different ash components (glass vs crystals)

Ash emitted during a volcanic eruption consists of two main components: a crystalline phase (including lithics and individual crystals) and an amorphous phase (volcanic glass; VG), whose abundance is associated with a contribution of juvenile material producing the explosive phase emitting the ash (Strombolian eruption). On the other end, low quantities of VG imply an absence of that contribution (Vulcanian eruption). Furthermore, monitoring the presence of crystals and VG in ash during precursor eruptions can allow the prediction of a major event, as was shown at Mount St. Helens. Here, based on previous works, we modified a semi-quantitative method using X-Ray Powder Diffraction (XRPD) to petrologically monitor a volcanic eruption. This is an accessible, low cost, non-destructive technique that gives results (componentry) in a very short amount of time. The methodology involves 3 steps: (1) sample preparation (sieve and gentle crushing), set up of the sample in a back-side sample holder and measurement in step scan mode (0.002° theta) at 40 sec. integration time; (2) calculation of the amount of VG in the ash samples by identifying and quantifying the scattering of both amorphous and crystalline phases in "crystallinity" terms of the material using standards with known amorphous content. This allows the calculation of the constant background intensity, which is subtracted from the total intensity to obtain the relative abundance of VG; and (3) cross-check that the obtained percentages of VG (of known and approximately constant composition) and crystalline phases are correct using a portable X-Ray Fluorescence (FRX) analyzer (also non-destructive). The whole procedure is estimated to take a maximum of 4 to 5 hours per sample. In addition, a complementary step is proposed that aims at a more robust quantitative analysis, but which involves more processing time: the Rietveld method.

This new methodology was successfully applied to ash from the two most active volcanoes in Mexico: Popocatépetl (2011 eruption) in which the presence of VG barely varies although variation in particle sizes is observed; and Colima (July 2015 eruption) whose ash shows a greater amount of VG at the beginning of the explosive phase, with a decrease with time. Further analysis will be done as new samples are obtained, to confirm and strengthen the results.

Justin Peers, Ashleigh Reeves, Chris Gregg, Michael Lindell, Timothy Joyner, David Johnston

Submission 1262

Official stakeholder mental models of effective volcano evacuation at the Long Valley Caldera and Mono-Inyo Craters volcanic system, eastern California, USA

The term mental model (c.f., schema, symbolic interaction) describes how people think about and mentally conceptualize objects, events, and relationships. This includes how they view volcanic unrest, eruptions, and associated hazards; protective actions such as evacuation; and scientific and emergency management agencies. Mental models facilitate people's ability to organize experiences, attach meaning to current events, evaluate consequences of actions and reactions, and consider constraints on performing actions. They also influence people's predictions about future events. Robust to change, mental models are not easily altered; new information is either dismissed or made to fit within previous beliefs. Research suggests that the more discordant new information is with respect to existing beliefs, the more likely the information is to challenge those beliefs, providing opportunities for change. As part of a multi-university NSF Hazards SEES project, we are conducting a mental model study of effective volcano evacuation around Long Valley Caldera (LVC), CA. LVC has been undergoing change and unrest since 1978. At that time a M5.6 earthquake ended 20 years of seismic quiet. Seismicity continued, followed by significant ground deformation and doming of the caldera floor, increased fumarolic activity, and CO₂ degassing which contributed to tree kills and human fatalities. Beginning in 1980, a volcanic crisis arose from the heightened unrest and scientific and social response to it. Tourists avoided the once popular ski town of Mammoth Lakes, property values plummeted, and businesses closed, leaving local residents with lasting impressions—Mammoth Escape Route highway was constructed for evacuation but the name changed to Mammoth Scenic Loop. These and other experiences shaped residents' mental models of volcanoes and evacuation. To identify and understand factors believed to be important in effective volcano evacuations, in summer 2017 we will perform mental model interviews with resident stakeholders representing county, state and federal agencies, and businesses. Individuals will include elected officials, emergency managers, scientists, and other professionals involved with evacuation (traffic engineers, land use planners, police officers, fire fighters, and employees of tourist facilities). The results can ultimately be used to improve the quality of volcano and evacuation information provided to stakeholder groups, including residents and visitors.

Aline Peltier, Jean-Luc Froger, Nicolas Villeneuve, Thibault Catry, Allan Derrien, Sergey Samsonov, Wanpeng Feng, Halldor Geirsson, Nicolas d'Oreye

Submission 189

Using ground, airborne and spaceborne methods to retrieve magma paths at Piton de la Fournaise (La Réunion Island)

Ground deformation monitoring in volcanic areas covers a broad range of techniques, including field (e.g., tiltmeters, extensometers, strainmeters, leveling), airborne (Structure from Motion photogrammetry), and spaceborne (Interferometric Synthetic Aperture Radar: InSAR) observations. The Global Navigation Satellite System (GNSS) is a hybrid method, based both on receivers in the field (ground segment) and on satellite sensors in space (satellite segment). All these techniques are now jointly used on Piton de la Fournaise to better constrain its plumbing system, from shallow reservoirs to the dykes feeding eruptions, and its flank motion. Continuous ground data and air/spaceborne data are complementary to characterize (i) the high-resolution 3D ground deformation distribution in high spatial resolution (air/spaceborne data), and (ii) the dynamics (ground data) associated with eruptive activity. In addition, the structure from Motion photogrammetry technique enables use of historical aerial photography to achieve high-resolution 3-D terrain models on past activity (post 1950), and evidence a temporal evolution in the deformation and volcano magma influx rate. Tracking all these fluxes and the long-lived preferential eastern motion by all these complementary techniques is crucial to mitigate risks associated to eruptions and flank destabilization on this volcano.

Alessandra Pensa, Lucia Capra, Guido Giordano, Sveva Corrado, Claudia Romano

Submission 527

Using charred trees for the determination of block and ash flow and ash cloud temperatures of the 10-11 July 2015 Colima Volcano eruption (Mexico).

The recent 10-11 July 2015 eruption of Colima Volcano, Mexico, involved the collapse of the summit dome that breached to the south generating PDCs along the Montegrando ravine. While the first episode on the 10th consisted of a “cold” block-and-ash flow (BAF) deposits and an associated ash cloud with no burned vegetation, the 11th event consisted of several pulses that overfilled the ravine, and spread up to 10.5km from the vent burning the vegetation. Trees within the valley were completely burned, buried and uprooted by the BAF, while the trees on the valley edges and overbanks were mainly burned and folded by the ash-cloud. Trees burn degree varies visibly from proximal to distal area. The emplacement temperature of the BAF deposit and the associated ash-cloud were reconstructed using different proxies: Thermal Remanent Magnetization (TRM) of lithic clasts and the Charcoal Reflectance (Ro%) analysis and Raman Spectroscopy applied to the charred wood. A total of 32 sites were sampled for the TRM study and 83 charcoaled wood samples were collected for the Ro% and Raman analyses. Primarily results display for the BAF deposit a T from $\approx 350^{\circ}\text{C}$ in to $\approx 250^{\circ}\text{C}$ from proximal to distal areas. Raman and Ro% analyses indicate higher T for the ash cloud varying from $\approx 400^{\circ}\text{C}$ to 300°C from proximal to distal areas. The study of single charred trees along the valley edges display vertical T variations. Samples collected at different heights from the same trunk show that the base was burned (by the contact with the deposit) at lower T with respect to the higher part of the tree that was came in contact with the ash-cloud. We interpret such unexpected reverse thermal zoning as related to the T disequilibrium carried within the flow by the bimodal grain size distribution of block and ash. Ash is expected to quickly loose T respect to block sized clasts, so that within the deposit, charcoal embedded within the ash matrix acquires the ash thermal fingerprints. Thermal re-equilibration inside the deposit takes in fact longer than the thermal acquisition time for charcoal (Caricchi et al., 2004). By contrast the heat wave released to the ash-cloud by the polycomponent BAF quickly equilibrates in that gas-dominated environment to higher T that average the contribution of block-sized clasts. This study represents the first case of simultaneous reconstruction of T variation of BAF deposit and its associated ash-cloud through Ro% and Raman spectroscopy analyses of organic material.

Nemesio Pérez, Susi Pepe, Francesco Montrond, Claudio De Luca, Pietro Tizzani, Luca D'Auria, Samara Dionis, Paulo Fernandes, Sonia V. Silva, Fátima Rodríguez, Marta García-Merino, Rubén García-Hernández, Eurico Montrond, Vera Alfama, Jeremías Cabral, José

Submission 787

Diffuse degassing and deformation monitoring at the oceanic volcanic island of Brava, Cape Verde

Brava (67 km²) is the southwestern most and the smallest inhabited island of the Cape Verde archipelago. This oceanic active volcanic island is located 18 km west of Fogo Island and rises 976 m from the sea level. Volcanic hazard awareness among the Brava population and the authorities is very low because since no historical eruptions are recorded; therefore, its volcano monitoring program is scarce. A collaborative research on diffuse degassing and deformation monitoring at Brava among different Cape Verde and European institutions has been established. With the aim of providing a multidisciplinary volcano monitoring program for Brava, diffuse CO₂ emission surveys have been carried out since 2010; approximately every 2 years. An increase trend of diffuse CO₂ emission rate from 42 to 681 t d⁻¹ at Brava was observed; just one year before the 2014-2015 Fogo eruption and almost three years before the recent seismic-volcanic crisis on August 2016 with more than 1000 seismic events registered by the Cape Verde INMG on August 1st, 2016 (Bruno Faria, personal communication). Due to this seismic-volcanic crisis, a diffuse CO₂ emission survey at Brava was performed from August 2 to 10, 2016, and the estimated degassing rate yield a value about 72 t d⁻¹; typical background values. An additional survey was carried out from October 22 to November 6, 2016, and the estimated diffuse CO₂ emission showed the highest observed value at Brava with a degassing rate about 1.700 t d⁻¹. To understand the origin of the recent seismic-volcanic crisis the analysis of 24 DInSAR images acquired by Sentinel-1 from May 2015 to February 2017 was performed. The time-series, derived through SBAS technique, show a coherent N-S deformation gradient. In particular most of the ground deformation seems to occur between July and November 2016. A preliminary modeling of the ground deformation shows a possible source, located along the SW coast of the island at a depth of about 3.1 km. The volumetric variation of the source is about 700000 m³. These observed changes on diffuse CO₂ emission and deformation are evidences which seem to support the recent volcanic unrest at Brava.

Michael Perfit, Daniel Fornari, Patricia Gregg, Dorsey Wanless, Matthew Smith, W. Ian Ridley

Submission 1268

Diversity of Lavas from the 8° 20'N Seamount Chain: Windows into Small-scale Geochemical Heterogeneity of the Mantle Proximal to the Northern East Pacific Rise

In order to more fully understand oceanic crustal accretion and the sources and melting systematics that occur at mid-ocean ridges (MORs), we undertook a multidisciplinary field program to survey and sample the 8°20'N Seamount Chain which extends ~160 km westward (~3 Ma crust) from the East Pacific Rise (EPR) - Siqueiros transform intersection (RTI). The OASIS cruise (AT37-05) in November 2016 included recovery of 367 lava samples (145 from 17 dredges and 222 from submersible Alvin) from approximately 15 different volcanic edifices. The geophysical (Gregg et al., this conference) and morpho-structural (Fornari et al. this conference) data combined with petrologic and geochemical data provide an opportunity to test hypotheses of off-axis melt generation, distribution and source variation away from the homogenizing effects of melt delivery at the MOR axis. The 8°20'N seamount lavas are predominantly unaltered pillows with lesser amounts (~ 10%) of lobate and sheet flows. Petrographically, the lavas range from being aphyric to olivine and/or plagioclase phyrlic with up to ~ 15% crystals. Small crystal clots of plagioclase plus olivine and/or pyroxene are relatively common. Preliminary correlations between volcanic morphology and petrography suggest low relief, flat-topped cones adjacent to the larger edifices tend to be aphyric, whereas the larger complex volcanic constructs contain more abundant and larger phenocrysts suggesting more complicated magmatic/petrogenetic histories. Remarkably, preliminary glass compositions range from primitive D-MORB with K/Ti (100*K₂O/TiO₂) ratios 9 wt. % to moderately evolved N-MORB (K/Ti 20 to 1.2 wt. %). Several D-MORB are olivine-phyric and chemically similar to picritic basalts previously recovered from the Siqueiros Transform. The E-MORB have a compositional range as great as that documented for seamounts between 5°N and 15° N within 60 km of the EPR axis. In fact, all three MORB types were recovered during one Alvin dive on adjacent volcanic constructs within a few 100 meters of each other. Our initial results attest to significant (and small-scale) chemical heterogeneity of magmas, and potentially their sources, beneath "normal" oceanic lithosphere. On-going geochemical analyses coupled with geophysical results will provide additional constraints on petrogenetic and geodynamic models for the development of this seamount chain.

Michael Perfit

Submission 1286

Geochemical Diversity of Near-ridge Seamount Chains: What they tell us about mantle sources and melting in the off-axis environment

Near-ridge seamount chains offer a unique view into mantle processes because their lavas record greater mantle heterogeneity than that reflected in lavas erupted at associated ridges. Geochemical data from major near-ridge seamount chains like the Lamont Seamounts west of the northern East Pacific Rise $\sim 10^\circ\text{N}$ and the Vance Seamounts west of the southern Juan de Fuca Ridge (JdFR) $\sim 45^\circ\text{N}$ provide clues to how off-axis mantle melting occurs and what mantle components are involved. Lavas from the Lamont and Vance seamount chains as well as smaller discrete seamounts proximal to the JdFR have more diverse major element compositions, and the lavas on average are more primitive (higher MgO) than lavas erupted along adjacent ridge axes. The seamount lavas, particularly near the JdFR, also have more diverse incompatible trace element compositions in comparison to basalts erupted at the adjacent ridge and range from highly depleted D-MORB to slightly enriched E-MORB. Although there is no systematic spatial change in composition in the Lamont Seamounts, lavas from the most distal Vance Seamount have the most enriched signatures and are more depleted approaching the JdFR axis. In contrast, lavas recently recovered from the $8^\circ 20'$ N seamount (west of the EPR) during the 2016 OASIS cruise (see Gregg et al., Fornari et al., and Perfit et al., this conference) are comprised of lavas that range from primitive (high-MgO) D-MORB to extremely enriched E-MORB (K/Ti values up to ~ 50) – in some cases within the same seamount. Surprisingly, the lavas have a compositional range as great as that documented for seamounts between 5°N and 15°N within 60 km of the EPR axis. The $8^\circ 20'$ chain is a nearly continuous feature (~ 160 km long) that parallels the Siqueiros Transform that may have formed over ~ 3 Ma in contrast to the younger more discrete volcanic cones that comprise Lamont and Vance seamounts that align in a mantle reference frame. In both instances geochemical data indicate that mantle sources varied within the chains as well as within individual seamounts and suggest melting-mixing between at least two sources, one similar to or more depleted than DMM and the other an enriched ocean island (OIB-like) source. New geophysical and morphostructural data combined with geochemical data from the $8^\circ 20'$ chain can provide an opportunity to better constrain off-axis melt generation, and source variation away from the homogenizing effects of on- and near-axis magma chambers.

Tom Pering, Andrew McGonigle, Thomas Wilkes

Submission 808

Linking gas flow fluid dynamics with basaltic volcanic eruption style.

Volcanism is driven by the gases dissolved in underground magmas. In the case of basaltic magmas, which have relatively low viscosities, these gas bubbles are free to move through the melt. Following exsolution, spherical bubbles are formed, which can grow and/or coalesce to generate large conduit width bubbles, termed slugs. In the highest gas volume fraction cases, annular flow develops, such that gas flows through a gaseous core in the conduit, surrounded by a magmatic annulus. This results in a variety of surface eruptive styles, ranging from passive degassing, explosions, and fountaining of magma-gas jets from summit craters. To date numerical and laboratory modelling has been applied to characterising the underground fluid dynamics in operation, mostly for slug flow, and to an extent for the other flow regimes. However, there has been little attention devoted towards characterising transitions between these flow regimes, and the associated surface activity types. Furthermore, the developed models have had almost no input from measurements of gas release at the surface. These are two of the most challenging and exciting current frontiers in volcanology.

In this work, we present research on the use of high speed gas imaging techniques, to resolve basaltic degassing processes in far more detail than possible previously. We shall then document the use of such data, to test and refine fluid dynamic models for how subsurface gas flow drives activity at the surface, hence bringing together two sub-branches of volcanology and providing a far richer understanding of how subterranean fluid dynamics drives surface activity. We furthermore report on development of a model describing the points of transitions between these regimes. In particular, our models point towards the degree to which adjacent bubbles are able to coalesce with one another, being the key driver for transitions between these scenarios, and the associated surface activity types.

This study provides an insight into how basaltic degassing styles and gas flow regimes are intrinsically linked, with implications for our capacity to assess transitioning during basaltic activity.

Brian Perttu, Kyle Bradley

Submission 1302

UAV Rapid Field Assessment, Survey, and Data Processing: an geoscience educational study.

In much of the world finding high resolution DEMs for generating topographic maps of recent land change is impossible. Meanwhile, it is important to have updated topographic maps for field sampling, hazard modeling, and disaster preparation. We conducted UAV mapping of sections of the Inyo Craters, Mono County, California, as a proof of concept, generated a topographic map in the same day, and presented these maps to students to use as a base for field measurements, instructing them on in-field DEM generation and map use.

We used a consumer grade DJI Phantom 3 UAV system using a gimbal mounted 12 megapixel camera firing 1 second time lapse mode, georeferenced against onboard GPS. We decided on the mapping area (covering approximately one square kilometer) based on a fast aerial survey before conducting a manually piloted grid survey using approximately 30%-50% overlap between exposures.

This method has implications for improved hazard management during ongoing volcanic activity.

Anna Perttu, Benoit Taisne, Dorianne Tailpied

Submission 985

Regional Infrasound Detection Capability for Southeast Asian Volcanoes

The field of volcanic infrasound has grown since the August 26th, 1883 eruption of Krakatau, the first recorded infrasound event, to the current use of local infrasound integrated into individual volcano monitoring for explosion detection and plume height estimation, and regional use of the International Monitoring System's (IMS) infrasound network for long range monitoring of volcanic activity. This study focuses on a regional scale, using a subset of the IMS network and regional infrasound arrays to monitor for volcanic activity in Southeast Asia. With over 700 active or potentially active volcanoes in the region it is not practical or cost effective to install instruments on all of them, and with a near constant presence of clouds, satellites cannot always be relied on for eruption confirmation. The use of infrasound and remote seismic was essential in constraining the eruption chronology of the Kelud eruption due to the destruction of the majority of the local monitoring network. However, despite this success, there are limitations to the detection capability of volcanic activity through infrasound in the region. For large volcanic eruptions the infrasound spectral characteristics overlap with several other natural phenomenon. The most persistent of these sources is from the interaction between the oceans and the atmosphere, known as the microbarom. Understanding the spatial and temporal distribution of the microbarom will help understand the detection capability of the regional network. In addition to the noise source distribution, this study combines the spatial distribution and eruption probability of the volcanoes in the region to better understand the strengths and weaknesses of the current geometry of station distribution.

Jeremy Pesicek, Sarah Ogburn, J. Jay Wellik

Submission 364

Toward a global assessment of patterns in precursory and eruptive seismicity for improved eruption forecasting

Eruption forecasting at restless volcanoes commonly relies on comparisons between patterns in observed seismicity and historical seismicity at analogous volcanoes worldwide. However, such comparisons are often performed in an ad-hoc fashion and assessments are highly dependent on the knowledge and experience of the group of experts involved. Rapid statistical assessment of eruption likelihood based on analogous worldwide historical seismicity is not currently feasible because the necessary local data for many eruptions does not exist. For the subset of analogous volcanoes where such data are available, we can search for common patterns in seismic progressions in the hope of revealing probable outcomes. For example, we may want to know how often inter-eruptive changes in seismic activity are followed by proportional changes in explosivity at open-system, basaltic volcanoes. Globally representative answers to such forecasting questions cannot easily be obtained from current databases. However we can answer these types of questions using subsets of volcanoes from places like the U.S and Japan, where local monitoring and detailed eruption chronology data are available. In contrast, simpler forecasting questions can be rapidly answered using global data sources. For example, it would be useful to know how often large magnitude earthquakes precede eruptions at volcanoes with long repose times. Using data from the Global Volcanism Program and the International Seismic Centre, we can rapidly obtain useful statistics such as these. Thus, there is currently a tradeoff between the granularity of the forecasting question and the statistical accuracy of the answer. The USGS Volcano Disaster Assistance Program's Eruption Forecasting Information System (EFIS) is an ongoing effort to statistically answer common forecasting questions using global data. In this study, we present some preliminary answers to 1) some simple forecasting questions easily answerable with global data, and 2) more detailed questions with regionally limited answers. Obtaining truly global answers to many important forecasting questions will require additional local monitoring data and detailed chronology data from worldwide observatories.

Nial Peters, Clive Oppenheimer, Paul Brennan

Submission 651

Novel Radar for Monitoring Lava Lake Level

Some lava lakes are remarkably persistent phenomena. But this overall stability can encompass striking variability and complexity such as abrupt or episodic changes in lake level, gas chemistry and flux, seismic tremor and acoustic signals. One of the most basic parameters to describe a lava lake's activity is one of the least straightforward to measure: the level. Optical methods such as photogrammetry and terrestrial laser scanning are typically hampered by the opacity of circulating fumes. The only long term solution in use currently – at Kīlauea volcano – employs a thermal infrared imager. We report here on an alternative approach to operational monitoring of lava lake level using a bespoke radar system. We outline the instrument design and data processing, and summarise the results of initial field campaigns in which the device was deployed in tandem with other instruments for gas and thermal observations at Erebus and Kīlauea volcanoes. We show that the radar altimeter is capable of high-precision, high-temporal resolution and sustained measurements of lava lake level. The essential elements of the instrument are of relatively low cost, and a robust system with modest power requirements could readily be applied to long-term, operational monitoring.

Chiara Maria Petrone, Martin Mangler

Submission 756

The interplinian activity at Popocatépetl volcano (Mexico): months-scale magma mixing events at a steady-state active volcano.

Popocatépetl volcano in Mexico is one of the most active volcanoes on Earth and it also ranks very high in term of threatened population with more than 20 million people living within 70 Km from the crater. It has had at least six major Plinian eruptions in the last 40 ky. These highly explosive events punctuate periods of quiescence and interplinian activity, similar to the current one, with effusive (dome-building and destruction) and Vulcanian eruptions – a pattern shown by many arc volcanoes.

The 23.5 ky BP White Pumice eruption marks a shift from the older Ventorillo edifice to the modern cone of Popocatépetl, which has been characterised at 14 ky BP by the Tutti Frutti Plinian eruption (TFPE), the most powerful (VEI 6) on record at Popocatépetl. A remarkable homogeneity in whole rock compositions for both effusive and explosive activity of the products between 40 and 14 ky suggests that, despite the sector collapse of the older edifice, there are no significant changes in the volcano's plumbing system, pointing to a long-lived and relatively stable plumbing system, but leaving unanswered the question of what processes control the transition in eruptive style.

In this study, we examine the pyroxene crystal cargo populations from both the interplinian activity pre-TFPE and the Tutti Frutti Plinian eruption, in order to assess the role, frequency and timescales of mafic injections into the plumbing system feeding different eruptive styles, and the transition between the interplinian and Plinian phases. Pyroxene core compositions allow to distinguish between an evolved crystal population type (T1A, opx Mg# 65-74, cpx Mg# 72-77) and a mafic one (T2, opx Mg# 81-88, cpx Mg# 85-88) clearly pointing to two separate storage reservoirs. Intermediate hybrid zoned compositional bands (opx Mg# 73-83, cpx Mg# 75-88) along with evolved rims similar to T1A cores, are common in both types suggesting the occurrence of frequent mixing and hybridisation processes of the mafic and evolved melts in a long-lived steady-state plumbing system.

Magma mixing events have been constrained at T of 950-990 °C and 3-6 km depth, and elemental diffusion chronometry (Petrone et al., 2016 Nat Comms) indicates that interplinian phases are characterized by short magma resident time in the order of days to months, similar to the present-day activity. Plinian eruption records longer and more complex history with mafic magma injections preceding the eruption by years to decades.

Michael Petterson, Paul Taylor

Submission 23

Finding a Volcanic Voice in a Multiple Hazard World: Experience from a Pacific Regional Organisation

Marcus Phua, Sean Pyne-O'Donnell, Hamdi Rifai, Rina Zuraida, Satish Singh, Caroline Bouvet de Maisonneuve

Submission 389

Understanding the eruptive history of Sumatran Volcanoes through Tephrostratigraphy

Sumatra is host to at least 30 of ~130 recently/historically active volcanoes across the vast Indonesian archipelago. These volcanoes lie in close proximity to major cities in Indonesia such as Medan (2.5 M inhabitants), but also not too distant from highly populated countries like Singapore (5.6 M). And yet in spite of the inherent risk, the eruptive history of these volcanoes is poorly known, as only a handful have been studied and regularly monitored. To rectify this, we aim to use tephrostratigraphy as a tool to unravel the history and behaviour of past Sumatran eruptions: their frequency, magnitude and spatial footprint. Tephra/cryptotephra sequences preserved in lacustrine, marine and peatland environments are the focal point of the study. A 17.76 m sediment core MD16-3522 was collected from the north-east Indian Ocean (3.522°N; 92.946°E; 4417m) in July 2016 during the MIRAGE I research cruise. Between 0 and 8.29 m below seafloor, the core contains at least two visible centimetre to decimetre-thick tephra layers that are correlated with magnetic susceptibility, positive K, Mn and Zr peaks and negative Cu, Fe and Ti anomalies acquired with a Multi-Sensor Core Logger (MSCL). Positive K and Zr peaks in tandem with negative Fe and Ti anomalies may indicate a silicic origin for the visible tephra layers. In addition, magnetic susceptibility and a^* (a measure of sediment redness) anomalies, along with positive Zr peaks may potentially indicate the presence of up to seven cryptotephra horizons. Ongoing work on this core is focused on: i) identifying tephra/cryptotephra layers in the remainder of the core using the MSCL, ii) elucidating the geochemical fingerprint of the tephra/cryptotephra through glass shard geochemistry and iii) constraining the age of tephra/cryptotephra horizons using ^{14}C dating and $\delta^{18}\text{O}$ chronostratigraphy. Groundwork has been laid for geophysical surveys and coring activities at identified lakes/peatlands in western Sumatra and is expected to proceed in the Spring/Summer of 2017. Although established in many parts of the world, the use of tephra/cryptotephra as a chronological tool has been largely underutilised in Southeast Asia. Establishing the tephrochronological framework throughout Sumatra is expected to yield much improved knowledge of the eruptive history of Sumatran volcanoes and provide the necessary information required for reliable volcanic hazard assessments that are vital to the mitigation of volcanic risks in the region.

David Pieri, Jorge Andres Diaz, Maria Fabrizia Buongiorno

Submission 1241

Advances in the Application of Unmanned Aerial Technologies to In Situ Airborne Observations at Active Volcanoes

Recent and continuing advances in the application of unmanned aerial vehicle (UAV) technology now permit in situ measurements in volcanic plumes and drifting volcanic clouds that were not possible previously. Thus, in situ measurements proximal to active vents, typically in very hazardous airspace, are feasible, although still not without risk. In situ measurements of gas and aerosols in relatively benign distal regions of volcanic plumes, at altitudes of 6000 m and higher will soon become more routine. We report on our long-term (2012-present) program of systematic UAV-based in situ observations of SO₂, CO₂, and H₂S emissions at Volcan Turrialba (Costa Rica), as well as similar recent observations at Kilauea Volcano (Hawaii, USA; 2017), and at several sites in Italy (e.g., La Solfatara, Volcano; 2014-2016). We discuss our strategies for capturing airborne data from near-vent plumes during restless periods and during eruptions, from distal drifting eruption ash/gas clouds, and from diffuse emissions at very low altitudes, utilizing UAVs (e.g., fixed wing, multi-rotor, aerostat), especially as these data become inputs for reverse models of source flux. This work was carried out, in part, at the Jet Propulsion Laboratory of the California Institute of Technology under contract to NASA.

Aaron Pietruszka, Jared Marske, Michael Garcia, Daniel Heaton, J. Michael Rhodes

Submission 568

An Isotopic Perspective into the Magmatic Architecture and Evolution of the Rift Zones of Kīlauea Volcano

We present Pb, Sr, and Nd isotope ratios for Kīlauea's historical rift zone lavas (n=50) to examine the magmatic architecture and evolution of the volcano's East Rift Zone (ERZ) and Southwest Rift Zone (SWRZ). Our results show that Kīlauea's historical eruptive period was preceded by the delivery of a major batch of magma from the summit reservoir to the ERZ. The timing of this intrusion, most likely in the late 17th century, was probably related to the ~300-yr period of explosive eruptions that followed the formation of the modern caldera (Swanson et al., 2012; JVGR). This rift-stored magma was a component in lavas from lower ERZ (LERZ) eruptions in 1790(?), 1840, 1955, and 1960. The only other components in these LERZ lavas are related to summit lavas erupted (1) after the 1924 collapse of Halemaūmaū and (2) during episodes of high fountaining at Kīlauea Iki in 1959. Thus, the intrusion of magma from the summit reservoir into the LERZ is a rare occurrence that is tied to major volcanological events. Intrusions from the summit reservoir in the 1960s likely flushed most older, stored magma from the upper ERZ (UERZ) and middle ERZ (MERZ), leaving large pockets of 1960s-era magma to serve as a dominant component in many subsequent rift lavas. An increase in the duration of pre-eruptive magma storage from the UERZ (~0-7 yr) to the MERZ (~0-19 yr) to the LERZ (up to ~335 yr) is likely controlled by a decrease in the rate of magma supply to the more distal portions of the ERZ. Lavas from several UERZ eruptions in the 1960s and 1970s have a component of mantle-derived magma that bypassed the summit reservoir. There is no evidence for a summit bypass into the MERZ, LERZ, or the volcanically active portion of the SWRZ. These results support a recent model for Kīlauea's plumbing system (Poland et al., 2014; USGS Prof. Pap. 1801): the ERZ is connected to the deeper "South Caldera" magma body and the volcanic SWRZ is connected to the shallower Halemaūmaū magma body.

Camila Pineda, Julia Hammer, Diego Morata

Submission 1270

Storage conditions of Pudahuel rhyolitic ignimbrite in central Chile

Pudahuel ignimbrite is a rhyolitic, crystal poor deposit (~76% SiO₂) associated to the Maipo volcanic complex and located in the Southern Volcanic Zone in the Andes. Its genesis is associated with the formation of the Diamante caldera and it's inferred that ~450 km³ pumice and ash was emplaced during a single massive eruption 113 ka ago determined from U-Pb zircon chronology (Pineda, 2015). The present study aims to understand the genesis of this ignimbrite through characterization of its pre-eruptive magma storage conditions through application of equilibrium thermometry, hygrometry, and laboratory experiments.

Polarizing light microscopy, back-scattered electron imaging, and energy dispersive X-ray spectroscopy applied to a density-separated crystal concentrate suggest that the mineral phases (plagioclase (~1.6%), biotite (0.5%), magnetite (>1%), ilmenite (tr), zircon (tr), monazite (tr), apatite(tr)) are homogeneous and are in chemical equilibrium with rhyolite glass, with the notable exception of highly porous iron sulfide grains (>>1%).

Experiments will be performed at H₂O-vapor saturated conditions in cold-seal pressure vessels on a representative pumice sample. We will boost the likelihood of encountering crystals in the sectioned run products by incorporating additional grains from the concentrate. Experimental run condition selection will be guided by application of the Ghiorso and Evans (2008) Fe-Ti oxide thermometer, as well as through comparison with phase equilibria established for other high-silica rhyolites (e.g., Katmai; Coombs and Gardner, 2001) and crystal-rich dacites. The Waters and Lange (2015) plagioclase-glass hygrometer will be used to extend our findings to H₂O-undersaturated conditions and define an envelope of pressure-temperature-XH₂Ofl conditions producing the glass and feldspar compositions observed in the natural sample.

References

- Coombs M, Gardner J (2001) Shallow-storage conditions for the rhyolite of the 1912 eruption at Novarupta, Alaska. *Geology* 29
- Ghiorso M, Evans B (2008). Thermodynamics of Rhombohedral Oxide Solid Solutions and a Revision of the Fe-Ti Two-oxide Geothermometer and Oxygen-barometer *American Journal of Science* 308
- Pineda C (2015). Geocronología U/Pb en circones de la Ignimbrita Pudahuel. Memoria para optar al título de geóloga, Universidad de Chile
- Waters L, Lange R (2015) An updated calibration of the plagioclase-liquid hygrometer-thermometer applicable to basalts through rhyolites. *American Mineralogist*, Volume 100

Virginie Pinel, Alexandre Carrara, Servando De la Cruz-Reyna

Submission 137

Remote sensing analysis of the 2014-2015 major lava flows at Colima volcano, Mexico, using Sentinel-1 SAR data and Pleiades DEM

Colima volcano (Mexico), one of the most active volcanoes in North America, showed an increase of activity since the end of 2014. This period was notably marked by the July 2015 Pyroclastic Density Currents (PDCs) emission, which is the most intense event since the last Plinian eruption in 1913. Before and during the July 2015 event, four massive lava flows were emplaced on the Western, South Western, Northern and Southern flanks. The present study aims to mapping and characterizing these flow deposits by remote sensing techniques. We used 38 synthetic aperture radar data, acquired between November 2014 and April 2016 by the new European Satellite Sentinel 1-A, and three Digital Elevation Models (DEMs) in order to map and quantify the volume of the lava flows, as well as their surface displacement fields. First, the areas of the deposits are estimated by measuring changes in the surface backscattering properties based on the coherence estimation. Then, DEM difference is used to precisely map the flows and determine their thicknesses and volumes. InSAR time series inversion has been performed to characterize the subsidence rates recorded on the lava flows. Results show that the Western and South Western flows, which were emplaced before the July event, have a total volume $\sim 18.106 \text{ m}^3$, with an average thickness of $\sim 29 \text{ m}$. The Southern lava flow, emplaced just after the PDCs event, presents a volume of $\sim 5.106 \text{ m}^3$, with an average thickness of $\sim 14 \text{ m}$. An average subsidence rate normalized by the lava thickness of $3.7 \text{ mm.yr}^{-1}.\text{m}^{-1}$ could be recorded after August 2015 on the Western and South Western flows caused by lava flows compaction and loading. Time series shows that these deformation rates decreased with time from $5.4 \text{ mm.yr}^{-1}.\text{m}^{-1}$ in August 2015 to $2.6 \text{ mm.yr}^{-1}.\text{m}^{-1}$ in February 2016. The July 2015 major eruptive phase does not seem to significantly affect the mean extrusion rate, which is around $2\text{-}3 \text{ m}^3/\text{s}$. It is concluded that this event has not drastically modified the shallow plumbing system.

Marco Pistolesi, Federico Di Traglia, Mauro Rosi, Costanza Bonadonna

Submission 313

Dynamics of blast eruptions: insights from the deposits of the 13th century AD Breccia di Commenda phreatic explosion (Island of Vulcano, Italy).

Understanding the dynamics and effects of phreatic eruptions is crucial to the hazard assessment of volcanic and geothermal areas. These eruptions may occur associated with magmatic phases or as isolated events, with the most recent examples being those of Te Maari (Togariro, New Zealand) in 2012 and of Ontake volcano (Japan) in 2014. The active caldera in the northern part of the Island of Vulcano (southern Italy) hosts in its center the cone of La Fossa. During its activity, la Fossa experienced various phreatic eruptions (e.g. in 1444 and in 1727 AD), with the most important event which occurred during the 13th century AD (Breccia di Commenda eruption, BdC). We present a detailed study of the BdC eruption through the integration of the stratigraphic characterization with sedimentological data, which allowed for the reconstruction of both eruption timing and eruptive mechanisms. The BdC event occurred in contemporaneous with the eruption of Rocche Rosse (1230±20 AD) from the neighbouring Island of Lipari, 12 km north of la Fossa; white, rhyolitic ash layers are in fact ubiquitously interfingered with the BdC deposits. The study of about 170 tephra logs revealed that the eruption occurred in three main phases. The opening, north-westerly-dispersed fallout (Phase 1) emplaced grey, altered lithic ash bearing accretionary lapilli. The eruption waxed (Phase 2) with several explosions, producing an asymmetric shower of ballistic blocks and the emplacement of narrowly-dispersed, lithic-rich, stratified pyroclastic density current (PDC) deposits, followed by a radially distributed, topographically-controlled, coarse-grained PDC which represent the main body of the breccia deposit. Finally, the eruption waned with the generation of accretionary lapilli-bearing ash fall deposits (Phase 3). Single PDC units range in volume from 2.1×10^4 m³ to 2.7×10^5 m³, with a total dispersal of ~ 4.5 km². Sedimentological analyses revealed that the eruption occurred with little or null involvement of fresh magma and that the breccia deposit was mostly composed by lava fragments. This latter observation suggests that the crater area prior to eruption was almost filled by lavas, which possibly helped in gas pressure build up. Deposit analyses also reveal that currently inhabited areas could be severely damaged by PDC and ballistic fallout activity during similar events, posing a severe threat to people and infrastructures.

Mattia Pistone

Submission 600

Heating or cooling felsic crystal mushes to extract melt? An experimental evaluation of melt extraction efficiency in shallow volcanic systems

The dynamics and kinetics of melt extraction from rheologically stalled, felsic, crystal mushes (> 50 vol.% crystals) are essential to feeding volcanic eruptions. At shallow depths (4-107 years). Whether felsic mushes are mobilised to erupt or the residual melt alone is extracted from the crystalline framework of the mush is primarily a function of the addition of heat and exsolved volatiles forming bubbles into the mush. Two scenarios are considered: 1) gas injection from hot mafic magmas into felsic mushes (heating scenario), and 2) gas exsolution from a crystallising mush (cooling scenario). In the heating scenario, the addition of water from the crystallising mafic magma to the felsic mush can reduce the liquidus temperature of the mush, leading to an increase in melt volume fraction, and lower its bulk viscosity. In the cooling scenario, the buildup and subsequent release of gas pressure can sustain the filter pressing of the residual melt out the crystal framework of the mush. Laboratory-based experiments on water-saturated (4.2 wt.%) dacite crystal mushes, accompanied by high-spatial resolution analytical investigations, were conducted to simulate several aspects of the two scenarios and the processes therein (gas injection versus gas filter pressing). Specifically, high-pressure and -temperature experiments and in-situ real-time synchrotron-based X-ray tomographic microscopy show that gas injection induced by mafic intrusion into an already volatile-saturated felsic system is not able to generate any substantial melt movement/extraction from the mush within the experimental timescale (3 wt.% water, below which fracturing and subsequent gas escape ends gas filter pressing). The experimental observations of the two scenarios shed light on the physical and chemical conditions and timescales of melt extraction from plutonic mushes in the Earth's crust.

Bradley Pitcher

Submission 732

Geochemical Variability and a Statistically Robust Segmentation of the Cascade Arc

The Cascade Arc of western North America exhibits significant along-arc geochemical variability that may result from mantle heterogeneity, regional tectonics and/or geochemical differences in the overlying lithosphere or subducting slab. Schmidt et al. (2008) divided the arc into four geochemically distinct segments, however, the study does not quantify differences between them and is based on a limited dataset (390 samples) which is spatially biased toward only 13 locations. To better characterize the heterogeneity of the entire arc, we compiled >200,000 isotopic, major, and trace element analyses (glass, WR) from over 12,000 samples. However, inherent sampling bias, in which certain regions are more heavily studied than others, skews data towards the compositions of these select localities and inaccurately represents their regions as a whole. To rectify this, we used a weighted bootstrap Monte Carlo approach in which the probability of each analysis being selected was inversely proportional to the number of samples within its 0.25° latitude bin, thus creating a more uniform posterior distribution with which to compare portions of the arc. Multivariate statistical analysis indicates that the four segments proposed by Schmidt et al. (2008) are, in fact, statistically distinct. However, using a modified hierarchical clustering mechanism, we have established a more statistically robust scheme where the arc is objectively divided into five distinct regions which have inter-segment Mahalanobis distances that are 2-12 times greater than in the previous scheme. Segment means of primitive lavas (MgO wt.% >7, Mg#>60) reveal a striking North to South linear trend towards more evolved Sr and Nd isotopic compositions. Trace element ratios of primitive samples demonstrate a greater subduction fluid influence in the southern two segments (higher Ba/Ce) and the involvement of an enriched mantle source in the north (higher Nb/Yb and La/Yb) which may indicate toroidal flow around the northern slab edge. Although Central Oregon volcanoes are often associated with low-K tholeiitic compositions, bootstrapped means for the region indicate a higher contribution from OIB-like magmatic sources (high Dy/Yb, LREE, Nb/Yb, K₂O and low Ba/Yb). By reducing sampling bias and establishing more statistically robust segments, geochemical trends will be used to infer the factors responsible for the along-arc variability of the Cascades.

Adrian Pittari, April Foote, Aliasgar Kapasi, Roger M. Briggs, Keith Miller, Karoly Nemeth

Submission 709

Volcanic history of the Bombay Volcanic Complex, New Zealand: Long-lived, closely-spaced volcanism in a dispersed monogenetic field.

The occurrence of polygenetic volcanic complexes in monogenetic volcanic fields is becoming increasingly recognised. An important question is whether they represent a closely-spaced cluster of vents, or a centrally-fed composite or shield volcano. The 1.59 – 0.51 Ma South Auckland Volcanic Field (SAVF), North Island, New Zealand, comprises at least 82 single, nested or coalesced volcanic complexes of scoria cones, tuff rings, and lava shields or flow fields. Two distinct basaltic compositions are recognised across the field: subalkaline, silica-undersaturated Group A basalts and alkaline, strongly silica-undersaturated Group B basalts.

The Bombay volcanic complex lies above the N-S-trending Drury Fault and comprises a ~3 km-wide, ~140 m-high lava shield with two summit cones that have a published K-Ar age of 0.59 Ma, underlain by an extensive lava field that also hosts five to seven scoria or spatter cones – mostly Group B basalts. The Bombay Quarry, situated 3 km SSW of the summit cones, has exposed a succession through the lower lava field. This study documents the volcanic history of the Bombay Quarry succession observed in drill core and outcrop, and the petrological characteristics. The quarry has two discrete pits representing two palaeotopographic lows that have been infilled with platy to columnar-jointed lavas up to 70 m thick in the southern pit and 40 m thick in the northern pit. Several spatter and scoria cones occur between the lavas, and a narrow feeder dyke connected to a lava flow was observed in the northern pit. Intervals of silt and fine sand, and buried soils, up to 10 m thick, occur between three basalt lavas in the northern pit, representing periods of repose. The basalt succession in the southern pit is overlain by alluvial sand, ~0.7 m-thick, and then by a ~0.5 m-thick distal rhyolitic tephra, with a published age of 1-1.2 Ma. This is then overlain by a 50 m-thick tuff ring succession comprising interbedded fine ash, medium-bedded coarse ash – medium lapilli, and coarse lapilli with blocks and bombs. All lavas and juvenile clasts within the succession are Group B basalts – consistent with the overall composition of the Bombay volcanic complex. The Bombay volcanic complex was active intermittently for at least the second half of the lifetime of the SAVF from the same mantle source region. However, on a local scale the vents were scattered across the complex, and periodically interacted explosively with groundwater.

Marcela Pizarro, Claudia Cannatelli, Diego Morata

Submission 858

CO₂ budget constraints of Lastarria volcano, Central Volcanic Zone, northern Chile

Gas measurements at active volcanoes can provide valuable information about the current status of volcanic systems. Melt inclusions (MIs) provide insights into the pre-eruptive volatile contents in the magma and define the pattern of degassing at depth. Knowledge of non-degassed and degassed volatile contents help to estimate the total gas budget of a volcanic system. Lastarria volcano is located in northern Chile, in the Central Volcanic Zone (CVZ). Lastarria's fumarolic activity is currently the most important source of gases of the CVZ and the volcano exhibits constant deformation. We have used different approaches to assess the amount of CO₂ released by the volcano: (1) we analyzed the gaseous phases by measuring the CO₂ flux using a LICOR-820 infrared gas analyzer and (2) we determined the pre-eruptive CO₂ content in the magma by analyzing the geochemistry of MIs hosted in feldspars and pyroxenes from 7 samples of lava and pyroclastic rocks of different eruptive periods of the volcano. The CO₂ flux was measured along the NW flank of the volcano and results show a range from 0.3 to 2309 g/m²d and a total flux of 65 t/d, in an area of 0.34 km². The petrographic study of MIs in the pyroclastic rocks shows two types of assemblages (MIAs) in the feldspars: MIA1, located in the core of the crystal, contains homogeneous glass associated with a single bubble, and MIA2, located in the rim of the crystal, shows a homogeneous glass with multiple bubbles. Few MIs appear to be slightly recrystallized. Pyroxene-hosted MIs are almost all recrystallized and randomly located in the crystal. At least 2 MIAs have been described in feldspars from the lava samples: MIA1, completely homogenized, and MIA2 composed of homogeneous glass and 1 or more bubbles. In the pyroxenes, we have observed a wide range of MIAs, showing various degrees of recrystallization, from completely homogenized to totally recrystallized. Most of the anomalies of CO₂ flux show a trend of increasing flux towards the NW, where incipient low temperature fumaroles are located. Preliminary observations of MIs show that MIAs hosted in pyroclastic rocks contain a greater amount of bubbles than MIs hosted in the lava, possibly indicating that a greater degree of volatile saturation can be linked with the explosive phase of Lastarria volcano. Future work will involve extensive analytical work on MIs in order to determine the pre-eruptive CO₂ content and link it with current degassing at Lastarria volcano.

Terry Plank, Daniel Rasmussen, Lindsay Buff, Einat Lev, Diana Roman, Erik Hauri, Kirsten Nicolaysen, Pavel Izbekov

Submission 874

THE ROLE OF SLAB DEPTH IN THE MAGMA INPUT TO VOLCANIC ARCS

It remains unclear which subduction parameters control primary melt production beneath volcanic arcs. The volcanoes of the central Alaska-Aleutian arc (Shishaldin to Cleveland volcanoes) offer the opportunity to explore the effect of slab depth on parental magma composition, at nearly constant convergence rate, azimuth and dip. Here, slab depths range from near the global average (~100 km) in the eastern part of the sector (Shishaldin) to near the global minimum (~65 km) in the western part (Cleveland). Using our own melt inclusion data and compiled whole rock compositions, we find systematic variations in magma composition as a function of slab depth. As the depth to the slab decreases, H₂O/K₂O ratios increase by a factor of four (~3 – 12) in the least degassed melt inclusions. At the same time, Si_{5.0} values (the average SiO₂ concentrations of volcanic rocks with 5.0 +/- 0.5 wt% MgO) increase from basaltic (~50 wt%) to basaltic andesite values (55 wt%). Such variations are expected from consideration of slab and mantle wedge thermal structure. The H₂O/K₂O ratio of slab fluids is known to increase, due to the lower solubility of phengite, with decreasing temperature. Slab-top fluid temperatures are estimated to vary from 650-700°C at 65 km depth to 850°C at 90 km depth, consistent with published slab-top geotherms, but only if the coupling point between the slab and mantle is ~ 50 km (much shallower than the 80 km depth typically assumed). The accompanying decrease in Si_{5.0} is consistent with shallower and cooler mantle-melt equilibration temperatures in the thin and cool mantle wedge occurring at shallow depths above the slab (i.e., only 25 km of mantle between the slab at 65 km and the ~40 km thick crust). The volcanoes overlying shallow depths in the slab (Cleveland and Vsevidof) are also generally smaller in volume (by a factor of 5-10) than those overlying greater depths (Shishaldin, Westdahl), and erupt compositions with a higher median SiO₂ content (55-57 vs 51-53 wt%). These observations point to lower melt production and flux into the crust where the depth to the slab is shallow and the resulting slab fluids and thin mantle wedge are cooler. Thus, the parental magma flux feeding the arc is expected to change significantly along strike, and could affect how magma ascends, stalls and erupts as a function of the depth to the subducting slab.

Pavel Plechov, Nikolay Nekrylov, Vesta Davydova

Submission 480

The source of Sulfur for porphyry-type ore deposits

Published $\delta^{34}\text{S}$ data from a large number of porphyry deposits shows magmatic source of Sulphur [Simon, Ripley, 2011]. S/Cu ratio is close to 2:1 molar ratio in most of the quartz-hosted fluid inclusions of different copper deposits (maximum values are 36:1 for vapors and 10:1 for brines) and it is the feature of both vapor and brine inclusions [Seo, Guillong, Heinrich, 2009]. It is explained as the feature of ore-bearing fluid from which chalcopyrite can precipitate. We will show that Cu content in melt as well as content of other ore elements calculated from quartz-hosted brines reflects common rhyolite source. It's used as an argument for negligible influence of Cu re-equilibration on S/Cu ratio in Q-hosted brine inclusions.

On the other hand S/Cu molar ratio in Cu-porphyry ore deposits (and ore-forming fluid) should be much higher than 2:1 due to other sulfide and sulfate minerals precipitates in a porphyry system. Total amount of sulfur fixed only in anhydrite in El Salvador (Chile) ores as an example can rich up to 109 tons while total amount of Cu estimated for this deposit is no more than $1.5 \cdot 10^7$ tons [Gustafson, Hunt, 1975], that corresponds to S:Cu molar ratio more than 130:1. Such amount of sulfur, which is required for copper deposit formation, can't be extracted from the same magma body and it needed to be an additional source of Sulphur-rich fluid.

We will show some evidences of Sulphur-rich fluid in modern island-arc volcanic systems of Bezmyanny and Tolbachik volcanoes (Kamchatka) and track the Sulphur path from magmatic chambers to the surface through melt inclusions, glass composition and surface gas composition measurements. This work is supported by Russian Science Foundation (grant 16-17-10199).

1. Gustafson L.B., Hunt J.P. The porphyry copper deposit at El Salvador, Chile // *Econ. Geol.* 1975. T. 70. № 5. C. 857–912.
2. Seo J.H., Guillong M., Heinrich C.A. The role of sulfur in the formation of magmatic--hydrothermal copper--gold deposits // *Earth Planet. Sci. Lett.* 2009. T. 282. № 1. C. 323–328.
3. Simon A.C., Ripley E.M. The role of magmatic sulfur in the formation of ore deposits // *Rev. Mineral. Geochemistry.* 2011. T. 73. № 1. C. 513–578.

Brent Poe, Antonio Pasculli

Submission 1040

Point defect equilibria in nominally anhydrous minerals: DFT nudged elastic band calculations

Charge and mass transport processes in minerals are governed by point defects. The presence of hydrogen in nominally anhydrous minerals such as olivine can drastically affect the type and concentration of point defects resulting in strong changes in their physical properties. Hydrogen is incorporated into the olivine structure by bonding to oxygen in defect cation vacancy sites. For example, the charge-neutral hydrogarnet defect, in which four protons occupy a vacant tetrahedral Si site, can undergo dissociation into a negatively charged $3\text{H}(\text{Si})$ species, where a free proton is released and occupies a nearby interstitial site. The energetics of this and other important defect equilibria in olivine and in Fe-free end member forsterite can be investigated using first-principles techniques based on Density Functional Theory (DFT). In this study, calculations were executed with packages from the Quantum Espresso (QE) suite implementing the generalised gradient approximation (GGA) for the exchange-correlation energy within the framework of the Projector Augmented-Wave (PAW) method, which is known to show very good agreement with experimentally determined lattice parameters for forsterite and olivine at 0 GPa and their respective PV equations of state up to 40 GPa. We pay particular attention to the total energy differences of stable defect species involved in a variety of H-bearing and H-free defect equilibria in order to estimate their relative abundances at conditions relevant to the lithosphere. We also use the Nudged Elastic Band method in order to map the atomic scale reaction pathways and energetics required for such processes to occur, which allows us to calculate the mobilities of individual defect types and estimate bulk transport properties such as protonic conductivity. Our results help explain the effective changes in elastic and electrical properties of nominally anhydrous minerals as a function of water incorporation.

Margherita Polacci, Fabio Arzilli, Nolwenn Burton, Giuseppe La Spina, Biao Cai, Margaret Hartley, Danilo Di Genova, Nghia Vo, Sara Nonni, Ed Llewellyn, Robert Atwood, Peter Lee, Mike Burton

Submission 291

4D crystallisation in basaltic magmas

We investigated for the first time the 4D (3D plus time) crystallisation kinetics of the most abundant crystalline phases (plagioclase, pyroxene and oxide) in basaltic melts through fast synchrotron X-ray microtomographic imaging of cooling experiments. The experiments were performed at beamline I12 of Diamond Light Source, the UK synchrotron, Harwell. Remelted anhydrous glasses of natural basaltic material from the Etna 2001 eruption, Italy, were prepared at ambient pressure and high temperatures (1400°C) before beamtime in the laboratories of Rome3 University, Italy, in order to obtain water-free glasses. Small cylindrical chips of these glasses (10 to 20 mg) with a diameter of about 3 mm were heated at the beamline up to 1250°C for 1 hour. For these experiments we used the Alice furnace which was commissioned and successfully used up to 1450°C on I12, with controlled cooling at 0.05°C/s to 0.5°C/s. Two types of cooling experiments were performed: single step and cooling rate experiments. For the former experiments, crystallisation was induced by isobarically decreasing temperature from 1250°C to both 1170°C and 1150°C, and then holding at the final temperature for 4 h. For the latter, crystallisation was induced by isobarically decreasing temperature from 1250°C to both 1100°C and 1150°C at a cooling rate of 0.5°C/min and 0.25°C/min, respectively. One crystallisation experiment was also conducted on a natural basaltic sample from Hawaii, where the sample was heated to 680°C, 700°C, 800°C and 900°C, and held at this temperatures for several minutes to 1h. All experiments were conducted in phase-contrast mode with a detector-sample distance of 230 mm, using monochromatic 53 keV light at a temporal resolution of 3 min per scan and a pixel size of 3.2 microns. Processing and quantitative analysis of tomographic data is now in due course using state-of-the art software for 3D and 4D image analysis. Preliminary results on pyroxene crystal growth in single step cooling experiments of Etna 2001 basaltic melts provide values of 2.0×10^{-8} cm³/sec after 90 min and 1.7×10^{-8} cm³/sec after 180 min. These are the first data ever produced on crystallisation of basaltic magma in 4D. Data on crystallisation of basaltic magma are of fundamental importance to improve our understanding of processing affecting magma ascent and eruption dynamics, and therefore extremely valuable to help us improve our capacity of predicting eruptions and mitigating volcanic hazard.

Michael Poland, Aline Peltier, Alessandro Bonforte, Giuseppe Puglisi

Submission 50

A framework for understanding persistent volcanic flank instability based on Kīlauea, Piton de la Fournaise, and Etna

In 1964, James Moore, of the U.S. Geological Survey, suggested that the south flank of Kīlauea may be unstable on the basis of both flank structure and geodetic data collected during eruptive activity. The years since have demonstrated that seaward motion of Kīlauea's south flank occurs via several means, including stable sliding, short accelerations during slow slip events, and by large offsets during strong earthquakes. These insights have been made possible by the advent of high-spatio-temporal-resolution space geodetic techniques, which have also been used to recognize persistent instability at other large basaltic volcanoes, like Piton de la Fournaise (La Réunion) and Etna (Sicily). When viewed through a comparative lens, the manifestations and mechanisms of persistent flank motion are surprisingly different at the three basaltic volcanoes. The rate of flank motion at Kīlauea is several times that of Etna and Piton de la Fournaise and is accommodated on a slip plane several km deeper than is probably present at the other two volcanoes. Gravity also appears to be the dominant driving force at Kīlauea, whereas magmatic activity plays a larger role in flank deformation at Etna and Piton de la Fournaise. Kīlauea and Etna, however, are both characterized by heavily faulted flanks, while Piton de la Fournaise shows little evidence for flank faulting. The spectrum of persistent flank motion at large basaltic edifices may be best understood through a framework defined by magmatic activity (which encompasses both magma supply and edifice size) and the geologic setting of the volcano (especially the characteristics of the subvolcanic basement or intravolcanic weak zones). A volcano's size and magmatic activity will dictate the extent to which gravitational and magmatic forces can drive motion of an unstable flank (and possibly the level of faulting of that flank), while the volcano's geologic setting governs whether or not a plane of weakness exists beneath or within the edifice and can facilitate flank slip. Examining persistent flank instability using this conceptual structure is an alternative to identifying a single volcano as a "type example"—especially since that example is usually Kīlauea, which defines an extreme end of the magmatic activity and geologic setting spectrum.

Michael Poland, Michael Lisowski, Daniel Dzurisin, Rebecca Kramer, Megan McLay, Benjamin Pauk

Submission 51

A volcano geodesy tour of the Cascade arc

It has generally been assumed that Cascade volcanoes show no signs of geodetic change until they are about to erupt, based on the observation that no volcano-wide deformation nor gravity change was measured prior to the May 18, 1980, eruption of Mount St. Helens, Washington. Several decades of geodetic data, however, tell a different story. Of the 13 major volcanic centers in the arc, 5 are or have recently been deforming (Mount Baker, Mount St. Helens, South Sister, Medicine Lake, and Lassen), 5 show no evidence of deformation over the past few decades (Mount Rainier, Mount Hood, Newberry Volcano, Crater Lake, and Mount Shasta), and 3 do not have the ground-based observations needed to assess their deformation state (Glacier Peak, Mount Adams, and Mount Jefferson). In addition, gravity changes have been detected at 2 of the 3 locations where measurements have been repeated (Mount St. Helens and Mount Baker show changes, while South Sister does not). Broad deformation patterns associated with Cascade volcanoes are generally characterized by low displacement rates, in the range of mm to a few cm per year, and are overprinted by much larger tectonic motions of several cm/yr. Continuous GPS provides the best means of tracking the temporal evolution of volcanic deformation in the Cascades and is also critical for characterizing tectonic signals so that they may be isolated from volcanic sources. Better spatial resolution of volcano deformation can be obtained through campaign GPS and InSAR observations, which leverage the accumulation of displacements over time to improve signal to noise. Deformation source mechanisms in the Cascades are diverse and include magma accumulation and withdrawal, post-emplacement cooling of recent volcanic deposits, magmatic-tectonic interactions, and loss of volatiles plus densification of magma. The Cascade Range thus offers an outstanding opportunity for investigating a wide range of volcanic processes. Indeed, there may still be areas of geodetic change that have yet to be discovered, and there is good potential for addressing a number of important questions about how volcanoes work before, during, and after eruptions by continuing geodetic research in the Cascade Arc.

Meagen Pollock, Benjamin Edwards, Chloe Wallace, Alex Hiatt, Sheila Seaman

Submission 1042

Multiple pillow-forming eruptions under changing water/ice conditions revealed in an ancient pillow-dominated tindar in southwest Iceland

Undirhlíðar ridge is a Weischelian-age pillow-dominated tindar on the Reykjanes Peninsula in southwest Iceland. The ~7 km-long ridge includes Undirhlíðar and Vatnsskarð quarries, separated by ~3 km, with ~100 m-high walls that expose longitudinal and across-axis sections of the ridge. We proposed a model for the construction of Undirhlíðar quarry in which an initial effusive phase is followed by an explosive event and a second effusive phase. Based on variations in trace element ratios (LaN/SmN, Zr/Y) and parallel differentiation trends on major element diagrams (FeO*, CaO), the two effusions were fed by magmas from different mantle sources that experienced separate evolutionary histories. Our study, which now includes the ridge and Vatnsskarð quarry, extends the multiple-eruption model to the rest of the ridge, confirms a shift in mantle source between eruptions, and suggests that the eruptive transition is associated with localized drainage events and ridge-wide resetting of lake levels. Emplacement pressures for 35 samples were calculated based on measurements of H₂O (ranging 0.19 - .40 wt.%) in glassy pillow rinds. In basal pillow units, we observe a pattern of decreasing emplacement pressure with increasing elevation that falls along a hydrostatic curve, indicating that the bulk of the ridge was constructed in a static englacial lake. Uppermost pillow units show emplacement pressures that follow a second hydrostatic curve; these are interpreted to represent a second period of volcanic activity in which lake levels had reset. Between the two eruptive periods is a ~20 m transition zone in which pillows were emplaced under lower pressures than those predicted by hydrostatic conditions. These are interpreted to represent fluctuating lake levels and localized drainage events nearing the end of the first eruptive phase. The drainage events may have led to the emplacement of fragmental material that has been observed between pillow units in the quarries. However, Sr-Nd-Pb isotope data also confirm a change in mantle source between eruptions. The lowest stratigraphic units are fed by a different mantle source than rest of the ridge, which shows compositional variability that is consistent with binary mixing of melts from enriched and depleted mantle components previously identified on the Reykjanes Peninsula. The geochemical variations record complex interactions between the magmatic system and ice conditions during pillow-dominated subglacial eruptions.

Nicholas Pollock, Brittany Brand, Olivier Roche, Pete Rowley, Damiano Sarocchi, Roberto Sulpizio

Submission 1081

Using shear-induced, wave-like depositional features to infer flow conditions of pyroclastic density currents at Mount St Helens, Washington, USA

Due to the difficulty of directly measuring physical parameters of pyroclastic density currents during flow and emplacement, we must use features in their deposits to infer flow conditions at the time of deposition. Recent laboratory experiments demonstrate that granular flows can rework substrate material, occasionally producing vortical mixing features reminiscent of shear-induced Kelvin-Helmholtz instabilities in pure Newtonian fluids (e.g. Rowley et al., 2011). Here, we present recently-identified examples of wave-like features in the pyroclastic density current deposits from the May 18, 1980 eruption of Mount St Helens, Washington that closely resemble the shear mixing features produced experimentally. We also present results from new experiments that investigate the conditions that promote the formation and growth of wave-like features along a granular interface for granular flows in frictional regime or with high gas pore pressure. We compare the dimensions of features found in the deposits to those produced experimentally, observing that the wave-like features in both the deposits and experiments are self-similar in form. By extrapolating from the experimental results and shear instability growth theory, we explore flow conditions (e.g. flow velocity, thickness, and particle concentration) for the 1980 Mount St Helens pyroclastic density currents during deposition. This study provides a means of using depositional features to infer flow parameters that are difficult or impossible to constrain in real time. Understanding these parameters is important for accurately modeling pyroclastic density currents and their associated hazards.

Nino Popkhadze, Robert Moritz, Sergo Kekelia

Submission 659

LateCretaceous phreatomagmatic volcanism and distribution of ore deposits in the Bolnisi district:constraints from the Madneuli polymetallic deposit, Lesser Caucasus, Georgia

The Bolnisi mineral district is a rich metallogenic region in the southern part of Georgia, along the border zone with Armenia. The district is part of the Lesser Caucasus, and is located in the north-western part of the Somkheto-Karabakh island arc. Mineralization in the Bolnisi area is associated with a Late Cretaceous volcanic event, and occurs at different stratigraphic levels. The presently producing Madneuli polymetallic deposit, and the Tsitrli Sopeli, Kvemo Bolnisi and David Gareji prospects are hosted by late Turonian to early Santonian rocks. A second group includes the currently producing Sakdrisi deposit, and the Beqtakari, Bnelikhevi, Samgereti, Imedi and Darbazi prospects, which are hosted by the younger Gasandami volcanic and volcano-sedimentary host rocks of Campanian age. Our detailed investigation is based on physical volcanology and facies analyses of the host rocks of the Madneuli deposit and is a new approach to this region. The host rocks of the Madneuli deposit, which belong to the Mashavera suite consist of stratigraphically lower volcano-sedimentary bedded rocks, which are interfingered with rhyodacitic pumiceous pyroclastic flows. Strongly silicified, bedded fine-grained tuff alternate with vesiculated tuff, very thin ash layers, and with accretionary lapilli-bearing tuff, which are interpreted as a product of a phreatomagmatic eruption. The thickness of volcano-sedimentary facies assemblages is about 200m and predominantly occurs in the open pit. It hosts two ore types: a stockwork vein zone in the western and northern parts and a pyrite-telluride-gold corridor in the eastern part of the open pit. The upper volcanic facies units consist of hyaloclastite, which are associated with a submarine dome structure. All this sequences is cross cut by a rhyodacitic extrusion. An ignimbrite pyroclastic flow outcrops in the uppermost part of the open pit. Recent investigations allowed us to recognize a phreatomagmatic breccia in the Madneuli deposit, which might be connecting with a maar-diatreme system in the Madneuli deposit. The volcanic activity producing the dome structure and the rhyodacitic extrusion in the open pit might be connected to a granodiorite to quartz diorite porphyry intrusion, crosscut by drilling at a depth of 800-900 m beneath the Madneuli deposit.

Sam Poppe, Olivier Galland, Nico Bols, Gert Van Gompel, Eoghan Holohan, Matthias Rosenau, Régis Mourgues, Matthieu Kervyn

Submission 179

An unusual patient: 4D X-ray Computed Tomography of analogue magma intrusion experiments

Although geophysical observations provide insight into the interaction of shallow magma intrusion and host rock deformation at active volcanic systems, we remain unable to observe these processes directly. Understanding these subsurface processes in all their dimensions, possibly by combining geophysical observables with analytical and numerical models, is nevertheless critical for ultimately forecasting volcanic eruption. We present a novel analogue modeling set-up for magma intrusion in brittle rock, based on X-ray Computed Tomography (XCT). Firstly, we quantified in detail the mechanical behavior of the often-used, but poorly-understood, brittle rock analogue sand-and-plaster mixed at a range of ratios. Secondly, we show how varying the mechanical strength of this brittle host material results in variations of magma analogue intrusion geometries. Thirdly, through medical wide beam XCT, we collected a series of 3D scan images of each entire experiment over a sequence of time increments. We then use this 4D (3D + time) imagery to study (1) the interaction of intrusion growth with deformation (i.e. fault growth and displacement) in the host and (2) the deformation at the model surface. The major novelty of our approach is that it extends 4D monitoring and quantification of deformation beyond the model surface deformation by enabling a full quantification of the entire intrusion and host rock system through time. In the example experiment series, we found that host rock strength controls intrusion geometry and propagation mode, and we document the development of the intrusion-induced system of faults and fractures in the host. Our modeling set-up envisions the interpretation of intrusion-induced deformation and seismicity, and potential validation of analytical and numerical models used in geodesy of active volcanic systems.

Matthieu Poret, Antonio Costa, Stefano Corradini, Luca Merucci, Daniele Andronico, Gianfranco Vulpiani, Simona Scollo, Antonio Cristaldi

Submission 993

Tephra dispersal and fallout reconstructed integrating field, ground-based Radar and satellite data: Application to the 23 November 2013 Etna paroxysm

On 23 November 2013 Etna erupted producing a volcanic plume, which rose up to ~10 km a.s.l. and dispersed tephra to the NE from the vent over part of Calabria region, in South Italy. Tephra samples were collected at proximal locations (up to 25 km from Etna) and in Calabria (~160 km), but a light shower of fine-grained ash was observed even in Salento (Apulia region, ~400 km of distance). Furthermore, a pilot transmission reported volcanic ash over the Adriatic Sea (~30 km southwards the Albanian coasts) between 10.9 and 11.5 km a.s.l. on 23 November 2013 at 13:50 which corresponds to the volcanic cloud top made of aerosol and gas.

Here we reconstructed the Eruption Source Parameters (ESP) of the paroxysmal episode, such as column height (H), Mass Eruption Rate (MER), Total Erupted Mass (TEM) and Total Grain-Size Distribution (TGSD). The ESP estimation is made using the FALL3D model by integrating data from field, ground-based Radar, and satellite (MSG-SEVIRI). Such integration is essential to cover the full tephra size range (i.e. from cm to μm). Indeed, field samples help to estimate the bulk erupted mass associated to the TGSD coarse fraction, whereas the Radar provides time-series of H, cloud thickness, mass loading, effective radius, concentration, and MER for particle diameters from 20 mm to 25 μm . The eruption phases are described discretizing MER using camera images (visible and thermal) and Radar data. The satellite window (i.e. 20-1 μm) is used to quantify the fine ash fraction (i.e. PM₂₀), track the plume evolution and its mass transported at distal areas. The fine ash fraction of the TGSD is estimated using the ash mass maps retrieved from the satellite-borne multispectral imager SEVIRI in the thermal infrared range, which represents the finer ash part of the cloud. At medial distances (tens of km), the satellite detects only a portion of the volcanic plume (e.g. containing ash), whereas most of particles are ice/water droplets, and at distal locations two bifurcating lobes are present (e.g. ash and aerosol clouds). The simulations are able to reproduce the diluted ash cloud and the thicker ice/water cloud that follow two different trajectories due to wind shear at different heights in the atmosphere. The best-fit results return a maximum column height of ~11.3 km a.s.l., a maximum MER of ~5.6×10⁶ kg/s, a TEM of ~7.7×10⁹ kg, and a PM₂₀ content of ~7.6% with respect to the TEM.

Matthieu Poret, Antonio Costa, Arnau Folch, Alex Marti

Submission 796

Modelling tephra dispersal and ash aggregation: application to the 26 April 1979 eruption of La Soufrière St. Vincent

On 26 April 1979, La Soufrière St. Vincent volcano (West Indies) erupted producing a tephra fallout that blanked the main island and neighbouring island of Bequia, located southwards. Using deposit measurements and available observations reported in Brazier et al. (1982), we reproduce the main features and processes of the eruption and estimate by best-fit the eruption source parameters such as the Mass Eruption Rate (MER), the Total Erupted Mass (TEM), and validate the Total Grain-Size Distribution (TGSD). Tephra transport and deposition is simulated using the 3D time-dependent Eulerian model FALL3D. The TGSD reconstructed by Brazier et al. (1982) showed a bi-modal pattern having a coarse mode around 0.5 mm and a fine mode around 0.06 mm. Because ash aggregation was significant during the eruption, we perform a comparative study by neglecting and accounting for aggregation using three different aggregation models. The models for ash aggregation in the plume assume wet conditions consistently with the eruptive phreatomagmatic features, considering both the effects of air moisture and magmatic water. The sensitivity to the driving meteorological model (WRF-ARW) is also investigated considering model spatial resolutions of 5 and 1 km showing that, for this kind of eruptions, high-resolution meteorology is pivotal. The optimal best-fit results indicate a column height of ~ 13 km above the vent, a MER of $\sim 7 \times 10^6$ kg/s which, for an eruption duration of 370 seconds, gives a TEM of $\sim 2.7 \times 10^9$ kg. The optimal aggregate mean diameter obtained is 1.5Φ with a density of 520 kg/m³ contributing to ~ 28 % of the deposit loading

Alexandros Poulidis, Tetsuya Takemi, Masato Iguchi, Ian Renfrew

Submission 216

Topographic and meteorological controls on the dispersal and deposition of volcanic ash

Volcanic ash is a major atmospheric hazard that, directly or indirectly, affects life, livelihoods, and infrastructure. Accurate prediction of the transport and deposition of volcanic ash is therefore important for hazard management and mitigation. Dispersal of ash is heavily influenced by local and regional wind fields. Mountainous topography affects atmospheric flow, creating a number of complex phenomena (ie. orographic effects), such as flow spitting, gravity waves and downslope winds, known to affect the deposition of volcanic ash.

In the study presented we examined the impact of orographic effects on the transport and deposition of volcanic ash from the Sakurajima volcano in Kyushu, Japan. Sakurajima is one of Japan's most active and closely monitored volcanoes. The frequent activity, surrounding mountainous topography, and large amount of observational data make Sakurajima an ideal natural laboratory for the study of these effects. On 18th August 2013 Sakurajima erupted at 1631 JST with a plume height of 5 km - the highest plume height recorded since 2006. Ash was advected to the W-NW and ashfall was recorded as far as 90 km to the west. This eruption has been studied in depth using a dynamic meteorology-ash-dispersion model (WRF-chem) configured with sufficient resolution to represent local topographically-forced flows. Simulations were also carried out with zero topography to isolate the influence of orographic effects.

We show that orographic effects can act in two ways: strong gravity wave activity close to the volcano act to keep ash afloat, while downslope winds closer to the surface can advect ash downwards and force deposition. Orographic effects are seen to increase both horizontal and vertical diffusion of volcanic ash. Due to its low residence time, heavy ash is seen to be relatively unaffected by orographic effects: in terms of deposition, the most readily affected size ranges for particles were of grain size between $3-5\phi$ (0.125 and 0.03 mm). Resolving orographic effects can lead to uncertainties: the initial plume height can be changed due to gravity wave activity over the volcano, leading to a different simulated plume height, something that could affect similar simulations, especially for eruptions with low plume heights.

John Power, Diana Roman, John Lyons, Matt Haney

Submission 512

Seismic and Infrasonic Observations of Mount Cleveland, Alaska: An Open Vent Volcano in the Central Aleutian Arc – August 2015 to July 2016

Mount Cleveland is a frequently active volcano in the central-Aleutian arc that has had 43 recorded explosions and produced 10 separate small lava domes since December 2011. We operated a six-station broadband seismic network on the volcano between August 2015 and July 2016 that complemented two permanent seismoacoustic stations operated by the Alaska Volcano Observatory (AVO) since 2014. This network captured three explosive eruptions that occurred on April 16, May 6, and May 15, 2016 and swarms of VT earthquakes in August 2015 and April-May 2016. Preliminary analysis suggests that hypocenters of VT earthquakes concentrate beneath the NE flank of the volcano and range in depth between 2 and 10 km below sea level. Calculated duration magnitudes currently range from 0.0 to 1.6. The explosive events have low seismic/acoustic energy ratios and high absolute infrasound pressures suggesting a very shallow source. Ambient noise coda wave interferometry between a pair of stations crossing the NE flank shows a subtle increase in velocity starting in August/September 2015 followed by a decrease in velocity coincident with the explosions in April and May 2016. This seismic network has also allowed us to locate some earthquakes beneath Tana Volcano, which is located roughly 12 km east of Mount Cleveland.

The VT earthquake swarm observed at Cleveland is unique for frequently active volcanoes in the Aleutian arc. Other frequently active volcanoes such as Pavlof and Shishaldin, which have been monitored by permanent seismic networks operated by AVO since 1996 and 1997 respectively, have not hosted VT swarms. This suggests that magma ascent at Cleveland may involve greater stress perturbations and is perhaps more episodic than at other Aleutian arc volcanoes that are often characterized as open vent systems.

Andrew Prata, Helen Dacre, Keith Shine, Emma Irvine

Submission 804

Volcanic ash dosage calculator: A proof-of-concept tool to support aviation stakeholders during ash events

The volcanic ash clouds produced by Icelandic volcano Eyjafjallajökull in April/May 2010 resulted in 'no fly zones' which paralysed European aircraft activity and cost the airline industry an estimated £1.1 billion. In response to the crisis, the Civil Aviation Authority (CAA), in collaboration with Rolls Royce, produced the 'safe-to-fly' chart. As ash concentrations are the primary output of dispersion model forecasts, the chart was designed to illustrate how engine damage progresses as a function of ash concentration. Concentration thresholds were subsequently derived based on previous ash encounters. Research scientists and aircraft manufactures have since recognised the importance of volcanic ash dosages; the accumulated concentration over time. Dosages are an improvement to concentrations as they can be used to identify pernicious situations where ash concentrations are acceptably low but the exposure time is long enough to cause damage to aircraft engines. Here we present a proof-of-concept volcanic ash dosage calculator; an innovative, web-based research tool, developed in close collaboration with operators and regulators, which utilises interactive data visualisation to communicate the uncertainty inherent in dispersion model simulations and subsequent dosage calculations. To calculate dosages, we use NAME (Numerical Atmospheric-dispersion Modelling Environment) to simulate several Icelandic eruption scenarios, which result in tephra dispersal across the North Atlantic, UK and Europe. Ash encounters are simulated based on flight-optimal routes derived from aircraft routing software. Key outputs of the calculator include: the along-flight dosage, exposure time and peak concentration. The design of the tool allows users to explore the key areas of uncertainty in the dosage calculation and to visualise how this changes as the planned flight path is varied. We expect that this research will result in better informed decisions from key stakeholders during volcanic ash events through a deeper understanding of the associated uncertainties in dosage calculations.

Gonçalo Prates, Manuel Berrocoso, Cristina Torrecillas, Alberto Fernández-Ros, Raúl Páez, Amós De Gil, Belén Rosado, Luis Miguel Peci

Submission 475

Deception volcano's 1967-1970 eruption from visible band imagery (Antarctic Peninsula).

Aerial photography and satellite images are widely recognized as a source of data for the production of maps of large areas of extension. The use of appropriate photogrammetric techniques can provide representative volcano-surface maps and through them the quantification of mass movement, extruded material volume and eruption caused destruction. Stereo-photogrammetry is a recognized mapping tool applied for almost one century, where from several overlapping images of the earth surface both 3D models and orthographic mosaics are obtained.

Contrasting with classical stereo-photogrammetry, structure-from-motion and multi-view-stereo is a nearly automated compilation of strategies that involve the identification of features in individual images, the measurement of its coordinates in the camera reference system and the estimation of camera and features positions in a non-scaled arbitrary coordinate system. Only with ground control points or known positions of the camera centers in an appropriate earth reference system the three-dimensional surface reconstruction is obtained based on massive geometric data over a dense point cloud and corresponding surface mesh. The camera positions and surface reconstruction are then required to correct for the radial displacement of each pixel in the images that form the orthographic mosaic. Therefore, the complete imagery processing can be made with manual interaction almost limited to the ground control points' identification. Today's capability to measure volcano surface changes previous to satellite based remote sensing and global navigation satellite systems geodetic measurements are possible by re-analyzing available photogrammetric frames.

Deception volcano high-resolution imagery (frames and satellite images - visible band) where re-analyzed by structure-from-motion and multi-view-stereo photogrammetry and digital image processing to produce orthographic mosaics and digital elevation models that help to re-evaluate Deception's volcanic eruptions from 1967-1970.

Gonçalo Prates, Manuel Berrocoso, Alberto Fernández-Ros, Luis Miguel Peci, Amós De Gil, Belén Rosado, Raúl Páez

Submission 165

Methodological framework for near real-time volcano monitoring developed on Deception volcano (Antarctic Peninsula).

The Global Navigation Satellite Systems consolidation, the global extension and distribution of the International GNSS Service network, the data accessibility via internet, wireless or telemetry, and the receivers high-rate data acquisition, storage capacity and low power consumption, allows the deployment of additional continuously operating stations and periodic campaign observed benchmarks for the assessment of regional scale geodynamics based on ground-displacement. Real-time data access also allows assessing ground-displacements with a slight latency i.e. near real-time.

The development of data processing strategies, supported on precise products, provide the means for millimeter-level positioning and precise ground-displacement velocities to determine regional tectonic models. Anomalies on measured ground-displacements from the regional tectonic model are related to other processes e.g. to an active volcano. The anomalous ground-displacement velocities associated to the volcano dynamics allow to model the acting processes and structures and from them to establish future scenarios. The detail of the volcano dynamics model is proportional to the number and distribution of sites with measured ground-displacement. The proposed networks are constituted by periodically observed benchmarks added to the continuously observed stations. In the assessment of the volcano dynamics we distinguish between non real-time monitoring - simply monitoring - and near real-time monitoring - surveillance. Monitoring provides the time evolution of the volcano dynamics model, while surveillance provides the near real-time status. Promptness negatively affects the data processing solution precision on short data time-intervals. Near real-time measured ground-displacements requires filtering strategies to enhance its precision, benefiting on higher sampling-rates. The Kalman Filter is applied to reduce noise and possible state evolution. On volcanic unrest, forecasting is a priority to mitigate risk. The acceleration of ground-displacements as precursor to seismicity and magma propagation, and a magma propagation model to establish the location of eruption vents and landslides are applied.

In Deception, every austral summer since 2001, in an inhospitable environment and limited outside communications, the development of methods was experienced through the assessment of regional tectonics, volcano dynamics and evolution, and monitoring, surveillance and forecasting capability.

Stephanie Prejean, Jay Wellik, Jeremy Pesicek, Cheryl Cameron, John Ewert, John Lyons, Wendy McCausland, Randall White

Submission 932

Monitored volcanoes with unforecast eruptions: What are we missing?

When adequate monitoring exists, many volcanic eruptions can be successfully forecast, particularly those at long-dormant (closed) magmatic systems. However, many others remain difficult to forecast. Some are not successfully forecast due to inadequate monitoring or prolonged, confusing precursory unrest episodes, but others simply have no detectable precursors or have precursory unrest periods that are too short to provide sufficient warning to nearby populations at risk. In Alaska, most of these troublesome volcanoes are frequently active (open) systems characterized by magmas with $< \sim 57\% \text{ SiO}_2$.

Here, we focus on seismically monitored volcanoes whose eruptions were not forecast due to short or nonexistent precursors and ask what we can learn from these cases to improve monitoring of such volcanoes in the future. We examine global trends in seismic data before these eruptions for missed clues in pre-eruptive seismicity through reanalysis of earthquake catalogs, such as that from the International Seismic Centre, a literature review, and collective VDAP (USGS Volcano Disaster Assistance Program) experience. We highlight several troublesome Alaskan volcanoes monitored by the Alaska Volcano Observatory. Recent eruptions of Pavlof, Veniaminof, Shishaldin, Cleveland, and Okmok volcanoes were not forecast. These are all frequently active volcanoes though their eruption styles and VEIs (1-4) vary. Seismic precursors of the 2008 Okmok eruption progressed too rapidly to issue a forecast. Otherwise initial quantitative searches of seismic data reveal no subtle precursors that were missed. We explore continuous seismic data in more detail, probing for deep long-period earthquakes and other subtle seismicity. Although seismic data are the common denominator among monitored volcanoes, the application of multi-parametric methods including geophysical, geodetic, and geochemical monitoring to problematic volcanic systems may offer the best chance at increasing the forecastability of these systems.

Richard Price, Shane Cronin, Ian Smith, Anke Zernack

Submission 603

Insights into amphibole-fractionation during early subduction-related volcanism of the Taranaki volcanic lineament, North Island, New Zealand.

In a landmark paper published in 2007, Davidson et al. (*Geology* 35, 787-790) used La/Yb and Dy/Yb ratios to identify and differentiate the effects of amphibole fractionation on the evolution of subduction-related magmas. Since amphibole is rare in andesitic volcanic rocks, the amphibole-dominated trends seen in rare earth element (REE) data were considered to reflect “cryptic amphibole fractionation” and amphibole accumulation within the crust or upper mantle. Amphibole was a common liquidus phase in medium- to high-K basalts, basaltic andesites and andesites erupted over the past 0.5 Ma along the Taranaki volcanic lineament in the western North Island of New Zealand. This contrasts with contemporaneous amphibole-free andesitic volcanic products at Ruapehu volcano in the central North Island. The petrological and chemical contrast between the Ruapehu and Taranaki systems provides insights into the controls on amphibole fractionation and their geochemical effects. Here, volcanic clasts were examined from the Maitahi debris avalanche deposit, and record collapsed portions of the Pouakai volcano dated between 0.21-0.24 Ma. This is the older sibling to Taranaki (Egmont) Volcano, which last erupted between AD1800-1820. The Pouakai rocks comprise medium-K, pyroxene-bearing basalts and amphibole-pyroxene basaltic andesites and andesites. Olivine and orthopyroxene are rare. Compared to younger Mt. Taranaki eruptives, the Pouakai volcanic rocks have lower K, P, Ba, Rb, Sr and Zr and higher Sc and V abundances. Ruapehu eruptives of similar age, are relatively enriched in K, P, Ba, Rb, Sr and Zr and depleted in Sc and V. The two suites (Pouakai and Ruapehu) define distinctly different trends on TiO₂, MgO and K₂O versus SiO₂ variation diagrams. Pouakai and other Taranaki volcanic rocks have REE patterns that are distinctly different from those observed in Ruapehu eruptives and the trends are entirely consistent with the Davidson et al. (2007) “cryptic amphibole fractionation” model. Furthermore, textural evidence and geothermobarometry obtained from mineral compositions and assemblages of the Pouakai rocks indicate that a complex magmatic storage and plumbing system had already developed beneath this volcano before 0.24 Ma, extending through the middle to deep crust where magmas evolved by crystal fractionation and were modified by magma mixing.

Sofyan Primulyana

Submission 558

Gas and ash emissions associated with the 2010-present activity of Sinabung Volcano, Indonesia

Sinabung Volcano (Sumatra, Indonesia) awoke from over 1200 years of dormancy with multiple phreatic explosions in 2010. After a few years of quiescence, Sinabung activity resumed in 2013, producing frequent explosions, lava dome extrusion, and pyroclastic flows from dome collapses, becoming one of the world's most active volcanoes and displacing over 20,000 citizens. This study presents a compilation of the geochemical datasets collected by the Indonesian Center for Volcanology and Geological Hazard Mitigation (CVGHM) from 2010 - current (2016), which provides insights into the evolution of the eruption. Based on observations of SO₂ emissions, ash componentry, leachate chemistry, and bulk ash geochemistry, the eruption can be split into five distinct phases.

The initial stage of phreatic summit explosions occurred from August - September 2010, during which, background SO₂ emissions averaged $\sim 550 \pm 180$ t/d.

An eruptive pause (phase two) starting in October 2010 abruptly ended in September 2013 with a resumption of conduit-clearing eruptions.

This third phase (from September – November 2013) had a relatively modest background SO₂ emission rate (avg. $\sim 410 \pm 275$ t/d) and produced ash consisting entirely of accidental ejecta with high S/Cl leachate ratios (up to 30), suggestive of deep-sourced magma and the incorporation of hydrothermal sulfur-bearing phases.

The most intense phase of the eruption (phase four) occurred from December 2013 to February 2014, when juvenile magma first reached the surface. This period included dozens of large eruptions per day, high SO₂ emission rates (average: $1,100 \pm 1,020$ t/d, peak: $\sim 3,800$ t/d), the onset of lava dome extrusion, and a dramatic drop in S/Cl ash leachates to ratios < 5 , all reflecting increased degassing from shallow magma and the clearing out of sulfurous phases from the old hydrothermal system.

From late February 2014 through this time (March 2017), Sinabung settled into a relatively steady state of activity (phase five). Ash emissions now consist of dominantly juvenile material, and background SO₂ emission averaged $\sim 450 \pm 290$ t/d. Starting August 2016, SO₂ emissions started being measured in a continuous manner using a network of permanent scanning DOAS instruments. SO₂ emissions are average $\sim 263 \pm 200$ t/d, with maximum peak $\sim 3,290$ t/d.

Since early 2014, the long-term SO₂ emission rates have been gradually declining, consistent with an apparent decrease in magma supply. Our degassing model suggests that large explosions and pyroclastic flows could continue in the near-term owing to conduit plugging and dome collapses, remaining a major threat until the magma supply rate further decreases and causes complete sealing of the conduit.

Chad Pritchard, Reed Lewis, Paul O'Sullivan

Submission 64

Bubble transport and vapor phase LREE enrichment of mafic enclaves

Bubble segregation is presented as the mode of transport for mafic enclaves comingling in a rhyolite dome located in south-central ID. Porphyritic mafic enclaves of trachybasalt to trachyandesite contain highly altered plagioclase and anorthoclase as well as sanidine and fayalite xenocrysts from the peralkaline rhyolite. Alkali amphiboles surround enclaves and vesicles and are disseminated through the devitrified rhyolite. Vesicles locally contain kaolinite and secondary La-Nd monazite with sparse fluorite. Vapor phase microcrystallization of low-compatible elements from the magmas was found in vesicles of the alkali-rich mafic enclaves. Bubble transport of mafic enclaves is likely the dominant mixing mechanism as many enclaves are encapsulated by large vesicles that typically show signs of bubble deformation, contain increased vesicles toward the top of enclaves, and generally have smaller and rounded enclaves above larger enclaves. Like extrusive mixed magma and commingled outcrops elsewhere, this outcrop is in-line with a normal fault. Comparison to experimental and natural mixed and commingled magmas suggests that mixing was over a short time, and that bubble transport strongly limited mixing and greatly enhanced mafic enclave transport through a higher-viscosity rhyolite.

Matthew Pritchard, Francisco Delgado, Philipp Ruprecht, Paul Lundgren, Kyle Anderson, Luis Lara, Daniel Bertin, Julia Kubanek

Submission 248

Precursors and evolution of the 2011-2012 rhyodacite eruption of Cordón Caulle, southern Chile

The Puyehue-Cordón Caulle (PCC) volcanic complex in the Southern Andean Volcanic Zone of Chile has erupted a large volume of similar composition crystal poor rhyolite/rhyodacite (>2 km³) in a series of three major explosive-extrusive eruptions (1921-22, 1960, 2011-12) in the last 100 years. The most recent is the only highly silicic eruption with detailed geophysical observations before, during and after the eruption. We combine these geophysical data (geodetic and seismic) with petrological studies of the erupted products. These data show several episodes of ground uplift in the years before the eruption, but also a temporal gap between the maximum uplift rate and the time of eruption. The uplift was likely caused by pressurization of the magmatic system between 4-9 km depth, but the cause of pressurization is under investigation. We suggest one possibility is that the deformation is related to magmatic intrusions with a mafic component – we document mafic enclaves in the erupted lavas that are among the most primitive compositions in the history of the PCC volcanic complex. Previous work showed evidence for mafic intrusions only hundreds of years before the 2011 eruption. The 2011 eruption began explosively on 4 June and after two weeks evolved into a hybrid explosive - lava flow effusion whose volume-time evolution we constrain with a series of Digital Elevation Models collected by the TanDEM-X mission. Our independent data confirm the work of Castro et al., (2016) that showed the intrusion of a large volume laccolith or cryptodome during the first 2.5 months of the extrusive phase. InSAR data spanning the first 3 days of the eruption show clear evidence for two distinct sources of deflation 18 km from each other and up to 10 km from the eruptive vent – suggesting hydraulic connectivity of a large magma mush zone. An additional co-eruptive source of deflation is observed during the extrusive phase of the eruption. Pre-eruptive inflation occurred near two of the three co-eruptive sources. We suggest that these pre-eruptive intrusions helped to remobilize either volatiles or melt in the crystal mush underlying PCC, but the proximal trigger of the 2011-2012 eruption is yet unclear. A volcano-tectonic connection is suspected for at least the 1960 eruption of PCC which began 2 days after the Mw 9.5 Valdivia earthquake in southern Chile.

Matthew Pritchard, Steve McNutt, Jo Gottsmann, Mike West, Shan de Silva, Martyn Unsworth, Steve Sparks, Jon Blundy, Scott Henderson, Estela Minaya, Jon Perkins, Noah Finnegan

Submission 451

Integrated geophysical and petrological constraints on crustal melt at the Altiplano-Puna deformation anomaly

The Central Andes is a key global location to study the enigmatic relation between volcanism and plutonism because it was the site of both large ignimbrite-forming eruptions over the last several million years, and currently hosts the world's largest zone of silicic partial melt in the form of the Altiplano-Puna Magma or Mush Body (APMB). The PLUTONS project focused an inter-disciplinary study on two sites of large-scale surface uplift that represent ongoing movement of magmatic fluids in the mid to upper crust. Here we focus on Uturuncu in Bolivia near the center of the APMB that is the site of a 70 km diameter region of ground uplift (maximum rate about 1 cm/yr) surrounded by a ring of subsidence (maximum rate a few mm/yr) with a diameter of 150 km. We use a suite of geological, geochemical, geophysical (seismology, gravity, surface deformation, and electromagnetic methods), petrological, and geomorphological techniques with numerical modeling to infer the subsurface distribution, quantity, and movements of partial melts, as well as the past history of eruptions. We find separate geophysical anomalies in the upper and mid/lower crust (e.g., low seismic velocity, low resistivity, etc.) indicating multiple distinct reservoirs of magma and/or hydrothermal fluids with different physical properties. The characteristics and depths of the geophysical anomalies differ somewhat depending on the technique used – reflecting the different sensitivity of each method to subsurface melt (or fluid) of different compositions, connectivity, and volatile content constrained by petrology, and highlighting the need for integrated, multi-disciplinary studies. Several different models have been proposed as the cause of the unique deformation pattern at Uturuncu, but the PLUTONS observation of no measureable tilt of the shorelines at lakes around Uturuncu leads us to suggest a reversible pattern of ground uplift and subsidence over centuries. Thus the current deformation is likely one of several episodes of uplift that should eventually be followed by subsidence of equal magnitude related to episodic internal reorganization of the APMB connected to a domed bulge-and-column structure beneath Uturuncu.

Line Probst, Luca Caricchi, Martin Gander, Laura Pioli, Enikő Bali, Glen Wallace, Tom Sheldrake

Submission 826

Genetic profiling of crystals from the Bardarbunga-Holuhraun eruption

Zoned crystals in volcanic products record both temporal and spatial variations in the thermodynamic and chemical conditions within magmatic systems. The specific zoning pattern can be used to identify the dominant pre-eruptive processes. However, crystals in volcanic rocks rarely display a unique zoning pattern, but show an internal variability that could be related to major differences in crystallisation histories. Understanding how the pattern of zonation varies within a group of crystals provides an opportunity to investigate the spatial and temporal heterogeneity, or homogeneity, of a magmatic reservoir. A quantitative method has been developed to use cross-correlation of zoning profiles to identify populations of crystals that have a mutual provenance. A stretching factor is calculated to account for potential biases associated with variations in the orientation of crystals and the algorithm is developed to identify discrete stages of growth from a continuous chemical profile. We present the principles of this empirical approach in the context of clinopyroxene phenocrysts from the 2014-15 Bardarbunga-Holuhraun eruption. We show that by identifying different populations of crystals, and linking this to other geochemical datasets we can begin to disentangle the pre-eruptive history of a volcanic eruption.

Jonathan Procter, Georg Zellmer, Grace Marcroft, Takeshi Kuritani, Braden Walsh, Anke Zernack

Submission 875

Magmatic response to volcano collapse; an example from Mt. Taranaki, New Zealand.

Mt. Taranaki exhibits one of the best long-term records of volcanic growth and destruction of any volcano worldwide, making it ideal for understanding the long-term effects of changing lithostatic pressure, or loading and unloading, on the magma chamber and magma supply. The ring-plain around Mt. Taranaki houses volcanoclastic deposits that provide a near continuous record of the evolution of the volcano, yet these records have remained relatively unexploited when investigating the interrelated cyclical phases of volcano collapse and growth, the geochemical evolution of the centre, and the consequent time-varying hazard potential. In this study, we systematically sampled pumice-rich tephra and pumice-rich mass flow deposits that were stratigraphically immediately before and after the $24,801 \pm 268$ years BP Pungarehu Formation debris avalanche ($\sim 7.5 \text{ km}^3$). Crystals (clinopyroxene and plagioclase) were characterised in detail. Mg-Fe zoning across selected pyroxene crystals from samples erupted pre- and post-debris avalanche were found to have completely equilibrated, yet zoning patterns in Al remained intact and showed major differences in their formation. Variations in zoning patterns have enabled the determination of crystal residence times within the magmatic system. It is intended that this technique will be applied across the stratigraphic record, which contains 14 collapse events. This will provide insights into crustal magma transport and residence times, and thereby the propagation of fissures and the buoyancy of the magma pre- and post-collapse, in order to characterise the evolution of the centre and quantify the long-term relationship between magmatic rise and volcano growth and destruction.

Janire Prudencio, Michael Manga

Submission 828

Subsurface structure of Long Valley caldera imaged with seismic scattering and intrinsic attenuation

We model seismic intrinsic and scattering attenuation (Q) in Long Valley caldera, California by analyzing more than 15000 vertical waveforms. Observed energy envelopes are fit to the diffusion model and Q -images are produced using 2D space-weighting functions. We identify high-intrinsic and high-scattering attenuation anomalies in the fluid-rich western and eastern areas of the caldera. Low-intrinsic and low-scattering attenuation anomalies in the center-south of the caldera, one of which corresponds to the location of an earthquake swarm in 2014. From a comparison with other geophysical images (magnetotellurics, seismic tomography) we attribute these anomalies to a hydrothermal system (high attenuation). Average to high attenuation values are also observed at Mammoth Mountain (south-west of the caldera), and may also have a hydrothermal origin. Seismic tomography imaging provides insights into subsurface structures that are complementary to velocity and conductivity images.

Giuseppe Puglisi, Kristín S. Vogfjörð, Sigurður Fjalar Sigurðarson, Danilo Reitano, Philippe Labazuy, Arnaud Lemarchand, Adelina Geyer, Carlos Primo

Submission 1143

Vulkan: the European gateway for EPOS-IP Volcano Observation Thematic Core Services

Due to their highly heterogeneous nature and broad variety of phenomena, active volcanoes are quite different from other geological environments and the relevant data needs to be characterized and organized according to specific approaches and exploiting the experience of a large community. The European volcano observations community, represented by Volcano Observatories (VO) and Volcano Research Institutions (VRI) participating to the European Plate Observing System Implementation Phase (EPOS-IP) project, will implement services to enable open access to data, data products, software and services (DDSS) provided from the community. Technical implementation of these services starts from the Volcano Observations Thematic Core Service (VO-TCS), which will coordinate activities among the contributing VOs and VRIs to ensure their interoperability with the EPOS Integrated Core services (ICS) and will be realized in the first European volcanic portal. The portal currently has the working title “Vulkan” and will be a smart connection between data providers (e.g. ICS) and common users (researchers, students, industry, enthusiasts, etc.). The role of “Vulkan” is to harmonize different kind of data, products and service and create multidisciplinary environment, supporting specifically standards widely used by the community of European researchers. The goal is to implement a service-oriented architecture (SOA) to guarantee interoperability among the different components of the VO-TCS within EPOS-ICS architecture. The presentation will outline the roadmap for the technical implementation of services in the Volcano Observations TCS.

Leo Pure, Dougal Townsend, Graham Leonard, Colin Wilson, Andrew Calvert, John Gamble

Submission 384

Comprehensive mapping and geochronology of glacial and interglacial lava flows at a stratovolcano: a case example from Tongariro volcano, New Zealand

At stratovolcanoes, eruptive stratigraphies provide an essential framework for reconstructing the evolution of magmatic systems and estimating eruption volumes (and rates), both of which have implications for hazard projections. Simple stratigraphic models proposed for many stratovolcanoes assume or imply that volcanism and glaciation are temporally-isolated processes. However, the presence of glacial ice at some stratovolcanoes, notably Ruapehu (New Zealand) and Mt Rainier (United States), has been shown to strongly dictate the distribution of preserved lavas. These findings bring into question the volumes of erupted lava implicated in cone-growth reconstructions at many glaciated stratovolcanoes. We explore synglacial stratovolcano growth models for Tongariro volcano, New Zealand, compared with previous growth interpretations that do not consider volcanism and glaciation as contemporaneous processes. Our observations suggest that previously estimated volumes of erupted (and eroded) lava at Tongariro were overestimated by a factor of at least 2.

Our study synthesises detailed mapping observations and ~100 new lava samples collected from previously unsampled areas (~40% of the edifice) for geochemical and geochronological study. Ten new high-precision (3-8 relative percent at 2σ) $^{40}\text{Ar}/^{39}\text{Ar}$ lava age determinations, in synthesis with 41 previous K/Ar age determinations, demonstrate that lavas were erupted throughout at least three glacial/interglacial cycles, from ~275 ka to present. Non-dated lavas are chronologically ordered and correlated based on field relations and chemical compositions. The ages and locations of preserved lavas suggest that many high-relief landforms at Tongariro were primarily created and maintained by constructive volcanic processes (rather than destructive erosional processes acting on intact cones). During glacial periods, erupted lavas were impounded by ice, which prevented them from entering valleys, resulting in the construction of elevated planèzes of stacked lavas, whereas during interglacial periods, lavas flowed into and along vacant valley floors. We propose that glacially-regulated lava emplacement processes may persist unrecognised at many stratovolcanoes globally, with implications for the volumes of erupted and eroded lava, for reconstructed vent locations and for unravelling the chronology of erupted lavas.

David Pyle

Submission 360

Curating volcanoes: sharing stories to build engagement

'The night before.. earthquakes were felt for miles around', wrote Giovanni Orlandi in a fly-sheet describing the great eruption of Vesuvius in December 1631, when a 'grim cloud.. of immeasurable size' spread across the city of Naples. This report was published within days of the eruption, and placed the news of the event in the context of the stories of the great eruptions of the 'olden days'. The eruption history of Vesuvius is remarkably long and well-known, and continually augmented over the past two thousand years; and that history had not been forgotten when the volcano burst back to life in 1631.

Stories have been used to frame the communication of hazards and risk for as long as stories have been told. But with the passage of time they may be forgotten, particularly at long-dormant or remote volcanoes. Written accounts may nonetheless be preserved in archives and libraries, perhaps far from the country of origin. The acts of uncovering, interpreting and sharing these accounts can be an important element in empowering communities to confront the nature of the hazards posed by volcanoes, and embracing the challenges of dealing with possible future scenarios. This presentation will offer a perspective on the role that re-discovering and sharing accounts of past eruptions can play in the communications of volcano information, building on public engagement activities developed within and along-side the 'Strengthening Resilience in Volcanic Areas (STREVA)' project, and a recent public exhibition.

Zhipeng Qin, Jenny Suckale

Submission 1208

From the lab to the volcano: Using numerical simulations to generalize bi-directional conduit flow from analogue experiments to magmatic systems.

Many volcanoes erupt significantly less magma than they degas, implying that large quantities of magma must descend back into the plumbing system after degassing. The ascent of volatile-rich, buoyant magma and simultaneous descent of dense, degassed magma creates a bi-directional flow field in the conduit. The different regimes of bi-directional flow in narrow pipes have been mapped out through analogue experiments. In this study, we use a virtual laboratory to generalize the behavior observed in the laboratory to volcanic systems.

Laboratory experiments and theoretical analysis have shown that fluids in bi-directional conduit flow develop instabilities along their interfaces. The associated flow fluctuations may be one factor contributing to the episodic nature of eruptive activity in continually active volcanoes. Translating the behavior observed in experiments such as the dominant wavelength of the interface instability to volcanic conduits, however, is not necessarily straightforward. Limitations include the difficulties of achieving steady state in experimental settings, the absence of thermal effects, and the presence of solid crystals that may separate from the magma and alter the flow dynamics in volcanic conduits.

To complement existing laboratory studies, we use a virtual laboratory. Much like an actual experiment, our numerical method accurately captures the coupled motion of multiple fluids and crystals without requiring simplifying assumptions about interaction forces or settling speeds. We combine a topology-preserving advection scheme for tracking the interface between the rising and sinking fluids with a Distributed-Lagrange-Multipliers approach coupled to an Immersed-Boundary method to represent the solid particles. We also consider the role of the thermal convection in varying the viscosity and density of the magma. We have validated our model by reproducing existing laboratory experiments.

Despite their small size, we find that the presence of crystals in the magmatic melt alters the instability observed for two pure fluids. Our simulations show that crystals and thermal effects tend to suppress the interface instability between ascending and descending magma. Crystals, however, introduce new instabilities into the system that result from the fact that crystal speeds depend on the local volume fraction of crystals. We also find that crystals may enhance mixing along the interface, particularly at low viscosity contrasts.

Steven L. Quane, Benjamin J. Andrews

Submission 653

Bread Crusted Bubbles: a View into Conduit Processes

Here, we describe a new type of pyroclast from the ash sized fraction of a distal, unwelded pyroclastic flow deposit from the ~7 Ma Rattlensake Tuff of eastern Oregon. The clasts comprise discreet, fully intact hollow spheroids composed of high silica rhyolite glass. On average, the particles have radii of ~350 microns and wall thicknesses of ~40 microns. Commonly, fins of glass protrude from the spheroid; when multiple fins are present, they meet at an angle of ~120 degrees, resembling the geometry of magmatic foams. Many bubbles exhibit bread crust texture similar to that found on volcanic bombs. On those spheroids, the bread crust texture manifests as a series of cross cutting cracks ranging in number from 50 on each particle. The individual cracks have apertures of ~5 to ~100 microns, and lengths that often exceed 100 microns.

We interpret that formation of these particles is a result of heterogenous fragmentation of a thick walled magmatic foam that liberated individual intact bubbles. Shortly after fragmentation, the outside few microns of the bubble rind cooled resulting in a slightly stiffer rind. As the erupting mixture decompressed, overpressure inside the bubbles increased until it overcame the tensile strength of the outermost rind resulting in brittle deformation (e.g., crack initiation). Ductile flow of the remaining, fully intact, bubble wall thickness accommodated the remaining overpressure in the volumetrically expanding bubble (e.g., crack expansion), resulting in bread crust texture; note that this process ceases immediately if the bubble wall fully ruptures. By tracing individual cracks on SEM images of each spheroid, we quantify the brittle-ductile strain history recorded in the bread crust texture. Results indicate that the surface area and volume of individual spheroids increased up to ~35% and ~50% respectively. Using calculated values for the viscosity of Rattlesnake Tuff ash and assuming pressures of 1-5 MPa required to fracture the rind, we determine model timescales on the order of 10s to 100s of seconds are required to expand the bubbles if the opening of any given crack is accommodated by the entire spheroid and timescales on the order of 100's to 1000's of seconds if the strain is only accommodated by the area of each bread crust crack. Indeed, the exploitation of these uniquely preserved pyroclasts and their textures allows us to quantify conduit dynamics inaccessible through direct observation.

Manuel Queisser

Submission 44

A new portable remote sensor for 2000 m range for airborne and ground-based measurement of CO₂ flux

As emitted excess CO₂ quickly dilutes into the ~400 ppm ambient CO₂ concentration and degassing often occurs diffusively, measuring geological CO₂ fluxes is challenging. Therefore, fluxes are usually derived from grids of in-situ measurements, which are labour intensive measurements.

Other than a safe measurement distance, active remote sensing offers quick, spatially integrated and thus a more thorough measurement of gas fluxes, combined with operation independent of sunlight or clear sky conditions. Due to their weight and size, active remote sensing platforms for CO₂, such as LIDAR, cannot easily be applied in the field or transported overseas. Moreover, their complexity requires a rather lengthy setup procedure and skilled personal.

To meet the need for a rugged, practical CO₂ remote sensing technique to scan volcanic plumes, we have developed the CO₂ LIDAR. It measures 1-D column densities of CO₂ with sufficient sensitivity to reveal the contribution of volcanic excess CO₂.

The CO₂ LIDAR has been undergone a first successful airborne test measuring atmospheric column CO₂ concentrations between the aircraft and the ground. It was further employed on the ground, scanning CO₂ emissions from Bledug Kuwu mud volcano (Central Java) that have been used to derive the CO₂ flux of this mud volcano for the first time.

During the measurement campaign the CO₂ LIDAR demonstrated reliability, portability, quick set-up time (10 to 15 min) and platform independence.

This new technique opens the possibility of rapid, comprehensive surveys of point source, open-vent CO₂ emissions, as well as emissions from more diffuse sources such as lakes and fumarole fields.

Currently, within the proof-of-concept ERC project CarbSens, a further reduction in size, weight and operational complexity is underway with the goal to commercialize the platform. Areas of potential applications include volcano monitoring and bottom-up quantification of CO₂ fluxes.

Xavier Quidelleur, Julia Ricci, Pierre Lahitte, Carlos Pallares

Submission 744

The K-Ar Cassinot-Gillot technique as a tool to reveal evolution of volcanic systems: Example of Basse-Terre Island (Lesser Antilles)

Thorough characterization of magmatic systems evolution through time requires a versatile geochronometer. The K-Ar method has been used for decades and, when applied on separated groundmass with the unspiked Cassinot-Gillot technique, it remains the most suitable dating system for a large variety of Quaternary volcanic rocks. This is especially the case for young arc basic lavas, with high Ca and relatively low K contents, and a low ^{40}Ar radiogenic yield. Accurate ages are obtained when groundmass is analyzed after a very careful mineralogical separation, in order to remove any possible gain of argon (excess ^{40}Ar) from xenocrysts and/or phenocrysts, and any potassium loss due to weathered fraction.

For the first time, we have combined an extended dataset of more than 120 K-Ar ages, with major and trace elements geochemical analyses, in order to better constrain the volcanic history of Basse-Terre Island (Guadeloupe, French West Indies). Located in the north-western branch of the Lesser Antilles inner arc, it is composed of six main volcanic massifs that followed an overall north to south age progression, from 2.79 ± 0.04 Ma to present. Although, the petrological and geochemical characteristics of andesite and basaltic-andesite rocks appear fairly homogeneous through time, our detailed chronology reveals different magmatic processes. Most variations are principally controlled by crystal-melt fractionation and crystal accumulation, but major and trace elements also highlight episodic magmatic recharge. Some geochemical features suggest a continental crust contribution, as well as mantle input of slab-derived fluids. Trace element ratios argue for the presence of at least two different magmatic sources with a bimodal behavior observed throughout the volcanic history of Basse-Terre Island. In addition, together with geomorphological reconstructions, these numerous ages now available have allowed us to quantify construction and erosion rates for volcanic massifs from southern Basse-Terre Island, and to describe in details the evolution of these massifs. Finally, our results show that the comprehensive time control available here is a valuable tool for reconstructing the dynamics and cycling behavior of volcanic systems, and to help forecasting the nature of future activities.

Erika Rader, Jennifer Heldmann, Robert Wysocki

Submission 100

Comparison of natural, experimental, and numerical spatter clasts: Relating morphology to thermal history.

Natural spatter clasts from Craters of the Moon volcanic field (~49 wt.% SiO₂) exhibit a range of morphological traits including clast length, width, vesicularity, and degree of fusion between clasts. Experimental spatter clasts created at the Syracuse Lava Project (~50 wt.% SiO₂) also range in width, vesicularity, and degree of fusion. Thicker clasts in the natural samples correlated positively with greater vesicularity and vesicle size, however, was negatively correlated with degree of fusion between clasts. Experimental clasts were crafted to see which morphological traits are due to higher initial temperatures or slower cooling rates. To form spatter clasts, crushed starting material was added to molten material and manipulated with a metal paddle to lower the temperature and add volatiles. Temperature was measured with a FLIR camera and multiple thermocouples placed between clasts. Numerical models allow experiments to be extended into lunar conditions of lower gravity and reduced heat loss from convection. Initial results indicate that spatter cools more slowly during transport from the vent to the deposit on the moon than it would on Earth suggesting that lunar eruptions would need to have lower initial temperatures to prevent remobilization of clastogenic material. Additionally, material takes longer to cool upon deposition, likely resulting in more highly-fused deposits in lunar spatter cones. Using the numerical model, typical accumulation rates for spatter cones on Earth can be adjusted for lunar deposits, and total eruption times can be estimated from the height of spatter cones in the Marius Hills region of the moon.

Kristen Rahilly, Tobias Fischer, Tehnuka Ilanko, Louis Scuderi, Laura Crossey

Submission 1077

Spatial distribution of diffuse carbon dioxide degassing at Valles caldera, New Mexico with comparison to other geothermal systems.

Analysis of degassing CO₂ has largely centered around active vents. However, diffuse degassing through soils along the flanks of an active volcanic system can contribute a large proportion of total emitted CO₂. Unlike degassing through active vents, diffuse degassing can be highly spatially variable as subsurface structures influence gas flow. Previous researchers have observed a correlation between the extent of hydrothermal soil alteration and the amount of diffuse CO₂ degassing. Previous studies have mapped hydrothermally altered regions at Valles caldera, a 13-mile wide, circular resurgent caldera within north-central New Mexico. Valles is characterized by two different types of hydrothermally altered soils: acid-sulfate soils in the center of the caldera and travertine or sinter deposits along the perimeters. We have begun to identify further areas of hydrothermal alteration using multispectral satellite imagery. Specifically, we have used the reflectance of known hydrothermally altered regions to identify additional hydrothermal alteration. We then use snow index imagery to correlate areas of elevated hydrothermal alteration with areas of enhanced snow removal due to thermal flux over multiple years.

Using areas of hydrothermal alteration mapped with satellite imagery as the basis of site selection, we have established repetitive surveys of diffuse carbon dioxide emissions within Valles caldera using a PP Systems infrared gas analyzer accumulation chamber. We compare the diffuse degassing of Valles caldera with previously established levels of CO₂ degassing at Yellowstone caldera, USA and Campi Fleigrei caldera, Italy. We find that diffuse carbon dioxide degassing can be highly variable within small areas at Valles, from approximately 2,400 gm⁻² d⁻¹ at high flux areas to background levels below 28 gm⁻² d⁻¹. Carbon isotope values measured using the Delta Ray IR Spectrometer show a magmatic signature of gas samples from areas of high concentration diffuse CO₂, with an average value of -5.5‰ (vs. VPDB). By using kriging to establish a semi-variogram map, CO₂ flux measurements acquired at discrete points can be extrapolated to larger areas. The accuracy of these spatial flux maps is highly dependent on fine delineation of high flux regions, while coarser surveys of background flux levels do not affect accuracy.

Frank Ramos, Jacob Buettner, John Wolff, Alicia Lopez

Submission 408

Ra-Ba Partitioning in Young Trachytic Sanidine at Changbaishan Volcano, China: Variable Ages and Partition Coefficients Determined Using Mass Balance, Measured Crystals, and Theoretical Calculations

Radium isotope dating is becoming more popular for constraining the crystallization and residence ages of young crystals in volcanic rocks erupted in the recent past (<8000 years). Plagioclase and potassium feldspar are usually targeted where resulting ages are highly dependent on radium partition coefficients derived from experimental or theoretical methods. It is very difficult to obtain direct empirical measurements for feldspars because the most accurate estimates originate from rare, zero-aged volcanic crystals (free of melt inclusions or other materials that might retain Ra) with minimal or no residence prior to eruption. We determine Ra and Ba partition coefficients and calculate ages for potassium feldspars from extremely young, alkali-rich trachytes where the melt component (represented by crystal-free pumice) is subtracted from the whole rock (melt plus crystals) to obtain average DRa and DBa values of “bulk” feldspar. We also isolate rim and core portions of potassium feldspars to determine crystal ages using theoretically determined DRa derived from measured crystal DCa, DBa, and DSr and compare theoretical values to experimentally determined values. Partition coefficients and ages are variable with empirical results derived from mass balance determinations offering minimum DRa and DBa for all theoretical and experimental determinations for Or42 sanidine (and resulting ages). We review results and uncertainties regarding calculated ages and their implications for crystallization and residence ages of ~Or42 sanidine in Changbaishan trachytes or other young volcanic systems.

Michael Ramsey, Matthew Watson

Submission 1116

A new orbital concept for measuring passive volcanic degassing and small plumes

Changes in volcanic gas and aerosol flux is important to understand the volcanic system and possibly forecast future eruptions. Detecting and quantifying volcanic gas flux has been accomplished using numerous techniques from direct sampling to orbital remote sensing. Remotely-measured data rely on the absorption properties of a gas species in a certain region of the electromagnetic spectrum. The most notable example is SO₂, measured using ground-based Fourier transform infrared spectroscopy (FTIR) and Differential Optical Absorption Spectroscopy (DOAS), for example. These approaches have been quite successful, but are not always practical nor affordable everywhere. Measurements from space or airborne sensors can be limited by the technical specification of the sensors, none of which were designed to detect and measure volcanic degassing and small plumes. The temporal, spatial and spectral resolution of these sensors is simply inadequate. We have proposed an orbital concept designed to measure the global inventory of volcanic degassing on a repeated schedule. The mission concept named ICAPE and the instrument it carries called ITHemis would acquire high-spatial resolution multispectral thermal infrared (TIR) data specifically tuned to detect SO₂, CO₂, H₂O, and solid phase SiO₂ (ash). With a planned a spatial resolution of ~ 30m/pixel and an SO₂ detection threshold better than 2 g/m², the data would allow passive degassing and proximal plumes to be studied globally. If selected and launched, ITHemis will allow us to quantify the mass and energy flux from these plumes and measure the globally-averaged gas, aerosol and mineral abundance injected by them into the lower atmosphere. The data will also provide TIR data continuity between current and future land imaging sensors. Analysis of this potential future dataset has already begun with the development of a ground-based TIR imaging sensor designed to replicate ITHemis. Data were acquired of the Kilauea plume in early 2017 as part of a NASA-sponsored airborne data campaign and will be presented. The ultimate goal of this ongoing effort is to launch the first orbital instrument dedicated to accurately constraining the global flux of SO₂, other climate-relevant gases, and silicate aerosol flux from passive degassing and active systems. The overarching objectives of this system are improved volcanic monitoring, eruption forecasting, and understanding of the linkage between these species to the regional to global climate.

David Ramsey, Lee Siebert

Submission 221

Spatial and Temporal Database Compilation of Holocene Volcanic Vents in the Western Conterminous United States

A spatial and temporal database compilation of all known Holocene volcanic vents in the western conterminous United States has been assembled that records volcanic vent location (latitude/longitude), vent type (cinder cone, dome, fissure vent, etc.), geologic map unit description, rock type, numeric age and reference (if available), geographic feature name, mapping source, and spatial database source (where available). Primary data sources include: USGS geologic maps, USGS Data Series, the Smithsonian Global Volcanism Program (GVP) Holocene Volcanoes of the World database, and published journal articles. Where possible, descriptive data from geologic map databases were assigned to vent points using the spatial join functionality of GIS. Vent locations were repositioned at a map scale of 1:24,000 by using a combination of the following spatial data for guidance: 1:24,000-scale USGS topographic maps, USGS 30-meter DEMs, USGS 10-meter DEMs, commercially-available high-resolution satellite imagery, National Agriculture Imagery Program (NAIP) aerial photography, and 1-meter lidar data collected by the Puget Sound and Oregon Lidar Consortia and the USGS 3DEP (3-Dimensional Elevation Program). A total of 775 volcanic vents have been identified from 46 volcanoes or volcanic fields spanning ten states. These vents are found along the length of the Cascade arc in the Pacific Northwest, widely around the Basin and Range province, and at the southern margin of the Colorado Plateau into New Mexico. The U.S. Geological Survey (USGS) National Volcano Early Warning System (NVEWS) identifies 28 volcanoes and volcanic centers in the western conterminous U.S. that pose moderate, high, or very high threats to surrounding communities based on their recent eruptive histories and their proximity to vulnerable people, property, and infrastructure. This compilation enhances the understanding of volcano hazards that could threaten people and property by providing the context of where Holocene eruptions have occurred and where future eruptions may occur. Future uses of this database may include: spatial comparison with located seismic events, context for generation of numerical hazard models or hazard zonation buffering, and analyses for spatial and temporal trends in regional volcanism and vent expression.

Noah Randolph-Flagg, Stephen Breen, Andres Hernandez, Michael Manga, Steve Self

Submission 869

Erosional columns in the Bishop Tuff as relicts of boiling in a cooling tuff

A few square km of the exposed Bishop Tuff in eastern California, USA, have evenly spaced columns. These columns are more resistant to erosion due to the precipitation of the low-temperature (100-130 °C) zeolite, mordenite, which is not found in the surrounding tuff. We hypothesize that the geometry of the columns is a result of instabilities at liquid-water and steam interface as cold water seeped into the still-cooling Bishop Tuff. We use two methods to quantitatively assess this hypothesis. First, scaling shows, to first order, which hydrodynamic instabilities exist in the system. Second, to account for the effect of multiphase flow, latent heat, and the finite amplitude and temporal evolution of these instabilities we use two-dimensional numerical models of liquid water infiltrating into hot tuff. These tests highlight several features of boiling hydrothermal systems. 1) The geometry of at least some convection appears to be broadly captured by linear stability theory that neglects reactive transport, heterogeneity of the host rock, and the finite-amplitude of instabilities 2) Flow forced by topography for slopes > 10% sets the wavelength of convection requiring that these columns formed somewhere with relatively gentle topography. 3) For permeabilities > 10-13 m² the wavelength of the instability changes through time, slowing infiltration, while for permeabilities < 15 m² cooling is dominated by conduction. The spacing of stability of columns increases with higher vertical permeability and decreases with higher horizontal permeability. Thus, these columns are a rare window into hydrothermal processes that are probably widespread.

Daniel Rasmussen, Terry Plank, Diana Roman, Pavel Izbekov

Submission 1277

MULTIDISCIPLINARY INSIGHT INTO PETROLOGIC INDICATORS OF ERUPTION RUN-UP

Unraveling the sequence and duration of magmatic events preceding volcanic eruption is central to understanding volcanoes and the hazards they pose. Geophysical observations of volcanic unrest give unparalleled insight into stirrings within a magmatic system. However, translation of the signals into magmatic processes is complex, and only a few volcanoes are monitored. Petrology offers powerful tools to study eruption run-up that benefit from direct response to magmatic forcings and applicability to most eruptions. Developing these tools, and tying them to geophysical observations, will help us identify eruption triggers and understand the significance of real-time signals during unrest.

Towards this goal, we investigate eruption run-up at both volcano and global scales. For the former, we study eruptions at Shishaldin, Westdahl, and Cleveland volcanoes in the Aleutians, which span a range in eruptive style, volume, and composition. Mixing timescales are determined by modeling Fe-Mg interdiffusion in olivine. For Shishaldin, the best monitored eruption, mixing timescales show at least two recharge events, which occurred roughly 9 months and 50 days prior to eruption. They were contemporaneous with a swarm of deep long-period earthquakes and a large (M5.2) shallow earthquake, respectively. Preliminary results for diffusion modeling at Westdahl and Cleveland yield similar timescales. To put these findings in a broader context, we compile timescales of eruption precursors identified globally with petrologic, seismic, geodetic, and gas approaches. Mixing timescales for a variety of eruptions are between 101 to 104 days, consistent with our findings in the Aleutians and generally within the range of run-up times defined using other approaches (10-2 to 103 days). In some cases, multiple mixing events are captured petrologically. Notably, most mixing timescales for mafic to intermediate eruptions are less than 1-2 years. For basaltic eruptions, petrologically defined run-up times are generally skewed to longer timescales than those defined seismically. These results point to recharge events that are initially aseismic. In certain cases, changes in seismic shear-wave splitting or velocity have been observed preceding the onset of precursory seismicity, conforming this observation. Such events that apparently “prime the pump” underscore the importance of carrying out forensic petrology and precursory stress field analysis following monitored eruptions.

Barbara Ratschbacher, C. Brenhin Keller, Blair Schoene, Scott Paterson, Lawford Anderson, David Okaya, Keith Putirka, Rachel Lippoldt

Submission 685

Time scales of construction and compositional evolution of a bimodal shallow crustal magma reservoir and implications for differentiation in the upper crust

The construction duration, cooling timescales and extent of in-situ fractionation of magma reservoirs in the shallow crust has important implications for crustal rheology, the plutonic-volcanic connection, and the formation of continental crust. The Jurassic Guadalupe Igneous complex (GIC), a tilted and bimodal (gabbros and granites) complex in the Sierra Nevada arc, California, presents an exceptional opportunity to study the construction timescales of a subvolcanic (~1-10 km) magma reservoir and to test the extent and time scales of in-situ differentiation to form mafic and felsic rocks.

Field and geochemical work in the upper part of the mafic rocks suggest that the gabbros are dominantly cumulates, which have lost interstitial melts feeding high-silica felsic segregations cropping out in their vicinity. These structures were interpreted to represent a microcosm of pluton-scale differentiation processes in which the mafic rocks represent cumulates complementary to felsic rocks. To test this model, we use high-precision U-Pb ID-TIMS zircon geochronology, combined with Ti-in-zircon temperatures and a Bayesian model to estimate zircon saturation time, duration of crystallization and cooling rates in the mafic to felsic lithologies. The results indicate that the entire complex was constructed over 295 ± 6 ka with ages decreasing towards the top of the complex, nominally consistent with a fractional crystallization model.

We use the geochronological results and field relations as constraints to test the longevity of the GIC magma reservoir with a 2D thermal model. After ~200 ka of emplacement, the maximum size of a melt-present chamber is achieved, occupying ~60-70 % of the final size of the intrusive body. The magma body containing > 30 % melt (lower limit of melt extraction) is smaller and its longevity varies between 500 - 200 ka depending on the choice of parental melt composition and the position in the complex.

We use stable isotopes to further test the fractionation model. New zircon oxygen data increase from sub-mantle values of ~ 4-4.5 ‰ in the lower and upper mafic rocks to mantle-like values in the felsic segregations and uppermost mafic cumulates and values of ~ 6.5 ‰ in the felsic rocks at the top of the GIC. These values demonstrate that the entire felsic part of the GIC could not have formed from fractionation of gabbro cumulates at the emplacement level alone, and that the system was at least partially open to an external oxygen reservoir.

Pamela Rattigan, David Brown

Submission 503

The stratigraphy and emplacement of lava-like and welded ignimbrites on the southern flank of Las Cañadas Caldera, Tenerife, Canary Islands: implications for volcanic hazards in the Canary Islands

Lava-like ignimbrites are the highest-grade deposits of pyroclastic density currents (PDCs), and represent the products of extremely hazardous volcanic eruptions. Similarities between lava-like ignimbrites and lavas (e.g. flow banding and columnar jointing) have resulted in misinterpretation of deposits historically, which poses a threat at active/dormant volcanoes, potentially leading to underestimations of the hazards of future volcanic activity.

The extra-caldera deposits of the southern flank of the Las Cañadas Caldera, Tenerife, belong to the Uncanca Formation, the oldest of the Las Canadas Upper Group (Martí et al, 1994). They extend for ~16 km, and form prominent rusty orange, terraced mountains in the landscape. There is very limited understanding and documentation of these units, which are briefly and loosely referred to in the literature as “lavas” (Ridley, 1969) and later as “welded fall deposits” (Soriano et al, 2002; 2006). However, the units are only partly described with limited evidence of the suggested emplacement model.

A reassessment of the stratigraphy, structure and emplacement of the extra-caldera deposits is presented. We interpret them as lava-like ignimbrites, exhibiting a range of welding and rheomorphic textures. A series of thick, stacked, predominantly lava-like tuffs have been identified, and these are punctuated by lenses of stratified, pumice-rich tuffs, lapilli tuffs and breccias with various degrees of welding. These deposits record four distinct eruption phases, the complex stratigraphy of which can be attributed to the landscape modifying and topography controlled (valley-filling) nature of the PDCs.

These deposits represent a significant period of eruptive history on Tenerife currently absent from the stratigraphy of the island and their interpretation as lava-like ignimbrites is crucial to understanding the potential hazards posed by active volcanism on the island, and in the wider Canary Islands.

Martí, J. et al, 1994. *Geol Mag*, 131, 715-727

Ridley, W, I., 1969. *Contr. Min. and Petrol*, 26, 124-160

Soriano, C. et al, 2002. *GSA Bull*, 114, 883-166.

Soriano, C. et al, 2006. *Bull Volc*, 69, 217-231

Mark Reagan, Heather Handley, Ralf Gertisser, Michael Turner, Kim Berlo, Katie Preece

Submission 655

U-series evidence for ongoing skarnification beneath Merapi Volcano, Indonesia

Lavas erupted from Merapi Volcano in recent decades have several noteworthy features including abundant xenoliths composed largely of calc-silicate minerals. Another noteworthy feature of the Merapi lavas is the magnitude of the excesses of ^{226}Ra over ^{230}Th [$(^{226}\text{Ra}/^{230}\text{Th}) = 2.8\text{-}3.7$; Gauthier and Condomines, 1999, EPSL; Condomines et al., 2005, EPSL; Handley et al., submitted, GCA], which are unusual for lavas as differentiated and incompatible trace element enriched as these. We collected compositionally zoned calc-silicate xenoliths from the 2010 eruption to test the hypothesis that the ^{226}Ra excesses result from ongoing skarnification of limestone blocks within the magma and magma chamber wall-rocks beneath Merapi. One xenolith was sliced into zones based on mineral abundances, characterized compositionally, then analyzed for ^{232}Th , ^{238}U , ^{234}U , ^{230}Th , ^{226}Ra , and ^{210}Pb . The zones include from inside-out: (A) a wollastonite-rich core, (B) a clinopyroxene-rich zone, (C) a fine-grained gray rind, and (D) adjacent lava. Compared with zone D, zone C has similar levels of disequilibrium between the U-series nuclides, but lower concentrations of U and Th by about 25% suggesting that it represents aphyric lava that quenched against the limestone when it was assimilated. Zone A has a significantly higher ($^{230}\text{Th}/^{232}\text{Th}$), ~40% lower U concentration, a small excess of ^{230}Th over ^{238}U , $(^{226}\text{Ra}/^{230}\text{Th}) \approx 0.14$, and a small but measurable excess of ^{210}Pb over ^{226}Ra . Zone B has intermediate compositional values. Our data support the concept that the skarnification of crustal limestones contributed to the ^{226}Ra excesses in Merapi lavas, and that the process is occurring in real time. The data also illustrate that CO_2 is being released consistently into the magma by crustal interaction, and may be a factor in generating explosive eruptions, consistent with earlier findings [e.g. Chadwick et al., 2007, J. Pet.; Deegan et al., 2010, J. Pet.; Troll et al., 2013, JVGR].

Vincent Realmuto, Florian Schwandner, Tamar Elias, Keith Horton, Steven Businger, Lacey Holland

Submission 660

The HypsIRI Preparatory Airborne Science Campaign to Kilauea Volcano: Combining Multi-Sensor Remote Sensing with In-Situ Sampling and Dispersion Modeling to Study Sulfur Dioxide Emissions

The return of eruptive activity to the summit of Kilauea Volcano in 2008 has increased summit emissions of sulfur dioxide (SO₂) gas dramatically, leading to adverse impacts on human health, agriculture, and the natural and built environment in communities downwind of the volcano. The principal threat to air quality and respiratory health is the noxious and acidic suspension of SO₂ and fine-scale (PM_{2.5}) sulfate (SO₄) aerosols known as vog. To help the public minimize their exposure to vog, the Vog Measurement and Prediction Project (VMAP) at the University of Hawaii-Manoa, forecasts SO₂ and SO₄ concentrations for the state of Hawaii. The VMAP forecasts are initialized with rates of SO₂ emission from the source vents as measured by the USGS Hawaiian Volcano Observatory.

NASA's planned HypsIRI satellite mission will provide at least two TIR (day + night) observations at the equator every five days, and at least one VSWIR + TIR observation every 19 days, at a spatial resolution of 60 m. To promote the development, refinement, and validation of procedures to utilize the data anticipated from HypsIRI, the recent HypsIRI Preparatory Airborne Science Campaign to Hawaii (17 January – 3 March 2017) collected AVIRIS and MASTER data over Kilauea Volcano. We use MASTER TIR data to map the initial concentrations of SO₂ at the summit of Kilauea and near-field dispersion of the gas plumes downwind of the summit. To evaluate the impact of our SO₂ concentration maps on the forecasting skill of the VMAP vog model, we initialize the vog model with the SO₂ maps and compare the resulting forecasts to those obtained with the conventional line-source initialization. We use AVIRIS VSWIR data to map changes in the mass concentration and physical properties of the aerosols based on changes in the aerosol optical depth (AOD) of the plumes. Our TIR and VSWIR data products provide better constraints on the rates at which SO₂ converts to SO₄ and map spatial variability in the conversion rate. We validate our data products with ground-based measurements of SO₂ concentration and AOD, and retrievals derived from contemporaneous satellite data. This analysis of data from multiple TIR sensors was enabled by the Plume Tracker toolkit.

Portions of this research were conducted at the Jet Propulsion Laboratory, California Institute of Technology, under contract to NASA. U.S. Government sponsorship acknowledged.

Kevin Reath, Matthew Pritchard, Alison Alcott, Samantha Moruzzi, Dave Pieri, Justin Linick

Submission 676

The ASTER Volcanic Thermal Anomaly Database

Since its launch in 1999, the high spatial resolution of the 90m/pixel thermal infrared (TIR) sensor of the Advanced Spaceborne Thermal Emission and Reflectance Radiometer (ASTER) instrument has recorded low levels of volcanic thermal output that occur during the precursory period of eruption at many volcanoes (e.g. Kliuchevskoi, Sabancaya, Chikurachki). ASTER's TIR high temporal resolution counterparts, the Moderate Resolution Imaging Spectroradiometer (MODIS) and the Advanced Very High Resolution Radiometer (AVHRR) sensors are currently incorporated into monitoring systems such as MODVOLC and V-ADAPT that collect and archive thermal data. Whereas these archives have proven to be a valuable resource for identifying and interpreting volcanic activity occurring during the eruptive cycle, they lack the spatial resolution often needed to detect precursory activity. The ASTER Volcano Archive (AVA) at JPL collects and archives ASTER data acquired over volcanoes and automatically produces volcanic ash, surface alteration, and thermal anomaly data products. Currently, the automatically generated AVA thermal anomaly data product is not optimized to detect lower thermal output anomalies, such as those sometimes produced before eruptions. However, the Cornell ASTER Volcanic Thermal Anomaly Database (AVTAD) can detect and archive subtle thermal anomalies due to the unique way in which these data are collected. A manual search is performed for every ASTER nighttime scene acquired over Holocene volcanoes as identified by the Smithsonian Global Volcanism Program (GVP). AVTAD is currently limited to Latin America with the intention to expand to a global scale.

JPL and Cornell research groups are currently combining AVTAD and AVA capabilities to demonstrate where precursory thermal anomalies are detectable by ASTER as well as limitations of these data. Additionally, AVTAD data will assist in differentiating non-eruptive thermal anomalies and thermal unrest leading to an eruption, as well as quantifying the pre-eruptive time span of unrest on a regional, system-by-system, or volcano-by-volcano basis. The eventual goal is to create an automated system that will capitalize on the AVA archive for retrospective studies of past eruptions, as well as for predictions of future ones. This work was carried out at Cornell University and the Jet Propulsion Laboratory of the California Institute of Technology under contract with the NASA Earth Surface and Interior Focus Area.

Ashleigh Reeves, Christopher Gregg, Michael Lindell, Timothy Joyner, Carla Prater

Submission 891

Assessing stakeholder perceptions and warning confidence at Kīlauea and Mauna Loa volcanoes, Hawai`i

The purpose of this study is to examine resident perceptions among social stakeholder groups and warning confidence on Kīlauea and Mauna Loa volcanoes, Hawai`i. The stakeholder groups include federal, state, and local agencies, and media, in addition to the survey respondents and their relatives, co-workers and friends. Stakeholders were evaluated on traits of knowledge of the hazard, trustworthiness, and protection responsibility. This study explores the correlation between demographical characteristics, hazard zone, community bondedness, and past experience with a lava flow crisis at Kīlauea and elevated alert level at Mauna Loa with stakeholder perceptions and warning confidence. Community bondedness relates to people's social connectedness through membership in community organizations and the influence of trust between community members and organizational institutions. Trust has been shown to be an important factor influencing people's understanding of hazards, perceptions of risk, effective risk communication, and attitudes toward risk management. Demographic characteristics of residents located on Kīlauea's East Rift Zone (ERZ) differ from residents' location on Mauna Loa's Southwest Rift Zone (SWRZ) in regard to race and ethnicity, income, and level of education achieved. In addition to differences in demographic variables, Kīlauea and Mauna Loa also differ in eruption history. The 1983-present eruption of Kīlauea's ERZ has produced a series of lava flow crises, the latest occurring in 2014 and 2015 when lava from a new vent crept northeast towards developed areas in the lower Puna District. In contrast, the last eruption and crisis on nearby Mauna Loa occurred in 1984 and the last eruption and crisis from its Southwest Rift Zone SWRZ was in 1950. Lava flows on the SWRZ typically move much faster than on Kīlauea due to steep topography and high discharge rates, decreasing the time available to respond. Consequently, a crisis on Mauna Loa's SWRZ would likely be much different than the recent crisis on Kīlauea. Results of this study will help to better understand how residents' perceptions of stakeholders influences their confidence in hazard warnings.

Mary Reid, Fidel Costa

Submission 1167

Insights Into Intracontinental Basaltic Magma Sources, Transport, and Storage

Robust constraints on transport rates and storage areas of basaltic magmas are critical to establishing the extent to which they faithfully record mantle source heterogeneity or a host of intracrustal processes. We explored the chemical zoning within populations of olivine phenocrysts from three basalts from the Pleistocene-age Hasan Monogenetic Cluster of Central Anatolia that may reflect different conditions of melt generation and storage. All the chosen basalts are particularly mafic. Melting may have occurred as mantle upwelled to near-Moho depths in an extensional environment. A quartz-normative basalt equilibrated just below the crust-mantle boundary (~38 km depth) and yielded the simplest olivine zoning profiles. Olivine cores ($Fo_{89.4\pm 0.3}$) are normally zoned towards 75, mostly in 30-50 micrometers thick rims. Olivine Ca and Fo correlate negatively and quasi-linearly, consistent with a lack of co-crystallizing augite. Modeling of Mg-Fe and Ca diffusion gives 5–11 versus 37–88 days, respectively, but due to the effects of growth the actual times are likely to be shorter. The absence of multiple olivine populations or reverse Fo zoning suggests that these crystals probably reflect magma transport towards the surface (at >0.1 m/s), with limited intracrustal storage. An equally magnesian, but alkaline, basalt (4 wt.% normative Ne) was derived from a parental melt that equilibrated with the mantle at ~50 km depth and contains clots of augite. Olivines have Mg-rich cores ($Fo_{89.6\pm 0.6}$) and are normally zoned, but inflections in zoning profiles define 40–50 micrometer near-rim zones that complicate determination of diffusion timescales. Judging by Ca–Fo covariations, these zones correspond to the onset of augite co-crystallization, possibly reflecting slower magma ascent at depth. The third basalt, selected because of evidence for deep-seated augite crystallization, also equilibrated with the mantle at ~50 km depth but has olivine with variable core compositions (Fo_{82} to Fo_{87}) and, in all but the most magnesian grain, near-rim plateaus or compositional reversals. These variations are consistent with magma recharge and mixing. Differences between the three sets of olivine records may reflect eruption of the first basalt within an active, fault system-controlled volcanic field, versus eruptions of the latter two basalts on the flanks of medium to large Miocene- to Pliocene-aged stratovolcanoes at the periphery of the volcanic field.

Kerry Reid, Hazel Rymer, Stephen Blake, Glyn Williams-Jones, John Murray

Submission 866

A detailed anatomy of the current degassing cycle at Masaya volcano, Nicaragua.

Masaya volcano, located in Nicaragua, has been relentlessly degassing for ~150 years exhibiting prolonged episodes of passive degassing with periods of intense gas emission “crises”. Over these elevated episodes sulfur dioxide (SO₂) emissions can be as high as 1800 metric t/d, predisposing local residents to chronic ailments, crop failures and the contamination of water sources downwind from the crater. SO₂ measurements have been performed since the 1970’s (Stoiber et al., 1986), with a valuable temporal record for Masaya from the mid 1990’s (e.g. Martin et al., 2010; Nadeau and Williams-Jones, 2009). The current degassing cycle started in 1996.

The average SO₂ flux since 1996 has been 1000 t/d, accounting for ~1–3% of global volcanic SO₂ emissions (Hilton et al., 2002). This study continues to monitor SO₂ emission rates using a mini-UV spectrometer (FLYSPEC). Results demonstrate that relative to the previous 20 year SO₂ flux average the volcano is in a period of reduced degassing, with emission rates for 2015 (58.23 t/d), 2016 (136.11 t/d) and 2017 (217 t/d) significantly lower. However, it is important to note that emissions are steadily increasing, showing potential for emissions to reach an elevated state.

In addition, downwind concentrations have been recorded for communities to establish exposure levels through the use of diffusion tubes. Interestingly, diffusion tube data reveals exposure levels dropping over the 2015-2017 period even though emission rates appear to be intensifying. In 2015, 2016 and 2017, the average downwind concentrations were 737 µg m⁻³, 281 µg m⁻³ and 114 µg m⁻³, respectively. It should be noted that downwind concentrations, as far as 35 km, still continue to exceed the maximum annual SO₂ ambient air quality guidelines of 20 µg m⁻³ (The Air Quality Regulations England, 2000, DEFRA), leaving communities at risk of long-term health implications and environmental degradation.

Hilton et al., 2002, RMG, 47 (1), 319-370.

Martin et al., 2010, JGR, 115 (B9), 215.

Nadeau et al., 2009, BV, 71 (4), 389-400.

Stoiber et al., 1986, JGR, 91(B12), 12215-31.

Shannon Rentz, Gary Michelfelder, Emily Salings, Max Hoffman

Submission 1251

Incremental development of the magma reservoir beneath the Mogollon Datil Volcanic Field, New Mexico: Insights from U-Pb geochronology and trace element geochemistry of zircon

Caldera systems are capable of outputting voluminous quantities of volcanoclastic material with wide ranging negative environmental impacts. Determining the behaviors of previously erupted systems may help inform predictive models used to evaluate hazards and assess risks for analogous currently active volcanic systems. The Mogollon-Datil volcanic field (MDVF) is a 40-20 Ma cluster of caldera activity in southern New Mexico tied to the subduction, and possible delamination, of oceanic lithosphere beneath the North American continental plate. A regional ignimbrite flare up from 36-24 Ma produced at least 28 caldera-forming eruptions. The calc-alkaline magmatism of three calderas in this field (the Mogollon, Bursum, and Gila Cliff Dwellings) produced several voluminous and regionally dispersed ash flow tuffs. Magmatic zircon sampled from these tuffs can record timescales of magmatic accumulation via U-Pb isotopic zonation. This study focuses on analysis of zircon crystals and the utilization of U-Pb isotope ratios as geochronometers for magmatic activity in the MDVF. We present new U-Pb geochronology results obtained via Sensitive High Resolution Ion Microprobe-Reverse Geometry (SHRIMP-RG) analysis of magmatic zircon from five MDVF ignimbrites. We compare previous geochronology results obtained via $^{40}\text{Ar}/^{39}\text{Ar}$ in sanidine to new $^{206}\text{Pb}/^{238}\text{U}$ age dates (1σ error), Pb isotopic ratios, and trace element compositions in the zircon samples.

Javier Reyes, Luis E. Lara, Diego Morata

Submission 1195

Contrasting patterns of magmatic ascent and storage for shield and rejuvenated intraplate volcanism in Juan Fernández Ridge (Nazca plate), SE Pacific

Robinson Crusoe Island is the most outstanding remnant of a compound volcanic structure in the Juan Fernández Ridge, a ~750km-long aseismic ridge located on the Nazca plate in the SE Pacific. Two different volcanic sequences represent both the shield and the rejuvenated stages, the latter emplaced after 3 My of volcanic quiescence and erosion. We here present first order geochemical features for these units and through geothermobarometry and textural analysis we unravel their contrasting ascent and storage history.

The shield stage (~3.70–4.10 Ma, $40\text{Ar}/39\text{Ar}$ in groundmass) is represented by a ~900 m thick sequence of basalt and picrite lava flows forming subsets according their chemistry and mineralogy: 'differentiated', 'near-primitive' and 'olivine-rich' lavas. Pressure estimates for in-equilibrium assemblages are $40\text{Ar}/39\text{Ar}$ in groundmass) with two compositional flavors: the primitive 'high-Mg' group that crystallized clinopyroxene at pressures

We propose the existence of shallow magmatic reservoirs in the shield stage, where the ascending magmas would have been stored and differentiated. On the other hand, rejuvenated magmas experimented rapid ascent with polybaric crystallization and sometimes short-time storage in low-volume reservoirs. Flexural response could control the ascent and storage patterns at the seamount/island scale and hence the resulting eruptive style and volcanic assemblage.

This research was supported by Fondecyt 1110966, Fondecyt 1141303 (both granted to L. E. Lara) and FONDAP-15090013 projects

Dominique Richard, Kai-Uwe Hess, Fabian Wadsworth, Benoît Cordonnier, Joan Marti, Donald Dingwell

Submission 458

A pyroclastic deposit with unusual devitrification features within the Guajara Formation along the Las Cañadas caldera, Tenerife, Canary Islands.

The phonolitic glassy base of a sequence of pyroclastic deposits from the top of the Guajara Formation along the Las Cañadas caldera, Tenerife, in the Canary Islands, exhibits unusual textures that sparked our interest. The ca. 3m-thick volcanic deposit consists of obsidian intermingled with an undefined green phase, and dispersed pumice lapilli and lithic blocks. The base of the deposit is mostly obsidian and the proportion of the green phase increases upward. Calorimetry on the obsidian reveals a low glass transition temperature of ca. 650°C, and higher cooling rates at the base (10-3 K s⁻¹) than in the middle of the deposit (10-6 K s⁻¹). Interestingly, optical microscopy reveals that the green phase is composed of welded and devitrified ash, which suggests this deposit could be a pyroclastic density current. In addition, fragments of the green phase detached brittly and moved from their original position within the deposit as the groundmass was still viscous during emplacement. This study hopefully brings us closer to unravelling the secrets of glassy and devitrified pyroclastic deposits.

Jacob Richardson, James Wilson, Charles Connor, Aurelie Germa, Christopher Perry, Koji Kiyosugi

Submission 1052

Volcanic Event Age Model: Consolidating multiple date models to estimate recurrence rate

Much of volcanology involves reconstruction of the timing, magnitude, and types of eruptions using the incomplete geologic record. We present a new method that utilizes diverse datatypes, including stratigraphy, radiometric age determinations, and the paleomagnetic record, to improve estimates of the timing of eruptions and the uncertainty in eruption timing. The pay-off is clarification of how well recurrence rates of volcanism are known, with implications for interpretation of the geologic record, probabilistic hazard assessments, and improved resolution of volcano stratigraphy.

An algorithm, the Volcanic Event Age Model (VEAM), has been designed that can use many different age-dating techniques and exploits modeled age uncertainty. This algorithm takes an assembled volcanic database that includes 1) identified volcanic events, 2) modeled ages with uncertainty, 3) mapped stratigraphic relationships, and 4) paleomagnetic data. VEAM then estimates the age of each volcanic event many times as a Monte Carlo, governed by the rules that each event is dated based on model age probability density functions and that superposition is never violated. The resulting product is several thousand sets of potential ages for the entire volcanic terrain of interest. These sets are then used to model recurrence rate and, if volume estimates are given for each event, a volume flux.

The VEAM algorithm has been tested on multiple volcanic fields. These include Abu Monogenetic Volcanic Field (SW Japan) using K-Ar dates; Caribou Volcanic Field, California (USA), using K-Ar and $^{40}\text{Ar}/^{39}\text{Ar}$ dates; and Arsia Mons Caldera Volcanic Field, on Mars, using crater retention age-dating. These examples show the flexibility of VEAM and its ability to model timing and uncertainty in the eruption record recurrence rate over time.

Nicole Richter, Jacqueline T. Salzer, Elske de Zeeuw-van Dalfsen, Daniele Perissin, Mehdi Nikkhoo, Thomas R. Walter

Submission 1024

Morphology, dynamics and evolution of a nested volcanic crater system: insights from integrated ground- and spaceborne techniques at Láscar Volcano, Chile

We study the current physical state, the morphology and dynamic behavior, as well as the evolution of the nested summit craters of Láscar Volcano, Chile, one of the most active volcanoes of the continental margin of the Central Volcanic Zone in the Chilean Andes. The volcano's eastern edifice hosts three nested summit craters, the westernmost of which (crater A) is actively degassing and lava dome eruptions have occurred from there in recent decades. A new mechanism to explain the nested crater formation at Láscar Volcano has been proposed recently and suggests that the central crater (crater B) might be a parasitic crater that has formed as a consequence of eruptive activity at crater A. The authors have based their theory on terrestrial laser scanner (TLS) data and analogue modelling (de Zeeuw-van Dalfsen et al., 2017).

We here present the near-3D surface deformation field, i.e. the integrated near-horizontal and near-vertical velocities, for two distinct time periods (between June 2012 and July 2014 and between January 2015 and January 2017) within Láscar's nested summit craters. Our results are derived from high-resolution TerraSAR-X SpotLight interferometry in combination with precise topographic data from joint Pléiades and TLS data. We detect two separate regions of local subsidence occurring within the volcano's summit craters, and an inward slumping of both the central and easternmost craters (i.e. crater B and crater C). We consider these movements to be related to the general geomorphologic setting and structural architecture of the nested summit craters. While the vertical component of our deformation data essentially supports the theory of a parasitic central crater, the horizontal velocities give room for extended interpretation and discussion.

We show the potential and value of combined high-resolution satellite radar and topographic data to (a) quantify small scale and slow surface deformation processes related to morphological changes and (b) complete results obtained from mapping morphological and structural features and analogue modelling. Our results also have implications for the dynamics of nested summit craters elsewhere in the world.

Jenny Riker, Katharine Cashman

Submission 1055

Interpreting crystal size distributions in complex magmatic systems: a case for compositional CSDs

Crystal size distributions (CSDs) are widely employed in studies of volcanic samples to decipher the nature and timescales of eruptive processes. In simple magmatic systems, continuous crystal nucleation and growth yields log linear size distributions that can be quantitatively linked to kinetic parameters such as crystallisation rate or residence time. Most magmatic systems are not simple, however, and the form of CSDs in natural volcanic rocks – commonly curved or kinked – bears this out. Rather, many volcanic rocks are a product of complex crustal magmatic storage regions in which rims grow on antecrystic cores and distributed crystal cargo is reassembled shortly before eruption. Antecrysts frequently display evolved rims that reflect growth from the transporting melt; these rims are compositionally similar to – and likely synchronous with – the accompanying groundmass population. These observations raise questions about the validity of an approach that assumes a unimodal distribution of crystal sizes subject to constant kinetic conditions.

Experiments simulating crystal growth present one means of untangling the complexities of CSD analysis. A large cache of experimental data are now available to describe crystal growth under controlled conditions (both decompression and cooling) for a range of magmatic compositions. Here we use examples from crystallization experiments and natural samples to illustrate the effects of rim growth on CSD form and interpretation. We show how the conventional approach to fitting curved CSDs – with two or more linear segments – results in erroneous interpretations of the kinetics of both early and late-stage crystallisation events. A CSD fit to larger crystal sizes lumps antecrystic cores with later rims, and so does not record a single crystallisation episode; similarly, the magnitude of late-stage crystallisation is underestimated when the rims of antecrysts are excluded from analysis of contemporaneous groundmass. These assumptions can introduce substantial errors into calculations of residence times and decompression or cooling rates. Finally, we show how compositional CSDs can be constructed for minerals such as plagioclase using simple BSE images or more sophisticated element maps, enabling the devolution of kinetic information for discrete crystal populations. Our aim is to encourage more critical, and ultimately more instructive, use of crystal size data to inform interpretations of eruption dynamics.

Eleanora Rivalta, Marco Neri, Francesco Maccaferri, Valerio Acocella, Rosolino Cirrincione

Submission 1308

Crustal magma pathways for Etnean and Hyblean volcanism curved by deepening of Malta Escarpment

A fraction of the volcanic activity on Earth occurs intraplate, challenging our models of melting and magma transfer to the Earth's surface. A prominent example is Mt. Etna in Italy, offset from the proposed asthenospheric tear below the Malta Escarpment. Likewise, the Hyblean volcanism to the south and the overall northward migration of the eastern Sicilian volcanism are still unexplained. Here we backtrack the Sicilian volcanism along simulated magma pathways, accounting for regional tectonic stresses and crustal decompression due to the deepening of the Malta Escarpment. Our models demonstrate that both the Hyblean and Etnean volcanism may have been sourced through inclined pathways from a melt pooling region below the Malta Escarpment and that the migration of volcanism within the Hyblean and Etnean phases may stem from the crustal stress history of Eastern Sicily. Accounting for crustal stresses may elucidate intraplate volcanism and its wandering.

Steven Rizo, Aurelie Germa, Sylvain Charbonnier, Charles Connor

Submission 466

How to improve volume calculation of lava flows to enhance eruption rate estimates and hazard assessment

Accurate volume calculation of lava flows is necessary to constrain their emplacement dynamics and better estimate eruption rates of volcanic events. The most accurate volume calculations are made where the topography before (i.e., basal surface) and after emplacement (i.e., flow surface) is known. When basal and flow surface are not available, volumes are calculated based on planimetric calculations or using interpolated basal surfaces. Planimetric volume calculations are performed by multiplying a uniform flow thickness by the area of the flow. Interpolation of the basal surface is performed using the elevation of the topography within a given distance from the edge of the flow. Basal surfaces are generally obtained with an inverse distance weighted interpolation, and/or by first and second order global polynomial interpolations. Lava flow units of varying composition from the Lassen volcanic field are used to evaluate the accuracy of these methods. Basaltic lava flows have volumes ranging from 0.016 to 0.086 km³. Volumes of basaltic andesites range from 0.0008 to 0.82 km³. Andesitic flows have volumes between 0.1 and 3.9km³. An example using a dacitic lava flow gives a volume of 0.38 km³ when the basal surface is modeled with inverse distance weighting interpolation, and a volume of 0.45km³ when the second-order global polynomial interpolation is used. The wide range of estimated volumes results from over-simplifying the basal surface morphology. A proposed method to verify the accuracy of the basal surface is to use historical case studies that have topography data available from before and after lava flow emplacement (such as the 2014-2015 eruption of Fogo in Cape Verde); model a basal surface using the post-eruption DEM; then compare the modeled and true basal surfaces. Correlations between flow thickness, surface topography and the basal surface of historical case studies will be used to derive a new model to determine the basal surface for flows where this data is missing, and better calculate lava flow volumes. These improved volumes will be crucial to refine models of volcanic processes to fit more realistic data.

Julie Roberge, Alison Rust, Kathy Cashman

Submission 1223

Popocatepetl's shades of grey: a detailed petrology study of ashes from 2008 to 2015

Popocatepetl volcano, Mexico, is renowned for its frequent vulcanian (dome rupture) and occasional strombolian eruptions. A few weeks after a 7.4 earthquake in March 2012, strombolian activity at Popocatepetl sharply increased. Looking at a collection of ashes from January 2008 to March 2015 (previous to, and after the earthquake), the first thing one notices is the wide variety of colors, which range from white to black. These variations in color can be attributed to variations in the componentry, chemistry and/or texture of the clast, which in turn can be related to different volcanic/magmatic processes. We characterized these ash samples both texturally and compositionally, to better constrain magma ascent dynamics and identify pulses of new magma. Grain size and componentry analysis shows that the ash mineralogy does not change through time. What changes are the proportions and the size of the different mineral types. For example, olivine is present in all ash samples, although sometimes it is so small that it is hard to identify. Furthermore, it has always been thought that the "white" ashes form from high concentrations of plagioclase combined with an absence of mafic (dark colored) minerals. Here we show that the pale ashes actually have the same componentry as the darker ashes (same amount of mafic minerals) but that all the minerals are coated in a white glass. High resolution image analysis confirms the consistency in mineral phases through time and shows that variations in their proportion correlate with particle size. We also establish that the presence vs absence of microlites and vesicles directly correlates with the color of the glass. White glass has no microlites, shows textures that suggest reduced viscosity (long, fine elongate shards) and slightly deformed vesicles (oval, squared), whereas black glasses tend to be less vesicular with variable microlite contents. Finally, the chemical composition of the glass (dacite to rhyolite) varies with time but the range of variations is the same within individual samples.

These findings are of great significance for monitoring the volcano. For example, during times of high explosivity at the volcano, the olivine content in the ash is used as an indicator of juvenile magma, and when no olivine is found in the ash, it is thought that no new magma is coming to the surface. Through this work it is now clear that white glass rather than olivine is the indicator of new magma at Popocatepetl's volcano.

Genevieve Robert, Madeline Bruno, Olin Carty, Rebecca Smith, Paige Guevarra, Alan Whittington

Submission 883

The viscosity of low-SiO₂ mixed Na-K aluminosilicate melts, with and without fluorine

While fluorine has a lower abundance than H₂O and CO₂ in most magmatic and volcanic systems, F is as effective as water at reducing the viscosity of silica-rich melts. Previous studies have also shown that, just like water, the effect of F in reducing melt viscosity is strongest in the most highly polymerized melts. It is known from Raman spectroscopy that Na-K mixing along the 75 mol% and 83 mol% SiO₂ joins of the NaAlSiO₄-KAlSiO₄-SiO₂ system lead to the formation of subnetworks. From NMR studies, it is also known that non-bridging oxygen sites exist in metaluminous and peraluminous glasses, their proportion being a function of Al:Si ratio and cation charge. In order to determine how the effect of fluorine varies as a function of Na:K ratio and Al:Si ratio, we measured the viscosity of F-bearing melts of varying Na:K ratio along the jadeite-leucite (Jd-Lct) and nepheline-kalsilite (Ne-Kls) joins of the NaAlSiO₄-KAlSiO₄-SiO₂ system.

In F-free melts, the K-end-member has the highest viscosity and T₁₂ (temperature of the 10¹² Pas isokom), and the mixed-alkali effect results in a viscosity minimum at intermediate compositions. This is in agreement with trends previously observed in the 75 mol% and 83 mol% SiO₂ joins for the same system. For the Na- end-members, the lowest Al:Si ratio melts have the highest viscosity, while available literature data and extrapolation of trends from our measurements suggest there is little difference in viscosity between the K- end-members, at least at temperatures near the glass transition. With increasing Al:Si ratio, more order is required to satisfy the aluminum avoidance principle, but the importance of ordering seems to affect the viscosity of Na-rich and K-rich melts differently.

Fluorine reduces the viscosity of all of the melts we studied, and its effect appears to be approximately independent of Na:K ratio, at least across the Jd-Lct join. Whether this holds true in Ne-Kls melts is less clear. For melts with intermediate Na:K ratios, the magnitude of viscosity reduction seems to be independent of Al:Si ratio in both series. Adding ~8 mol% F to melts with Na/(Na+K) ratio of 0.5 results in a T₁₂ reduction of 186°C relative to F-free melts. The implications of our results thus far are that the complexation of fluorine in peraluminous or metaluminous mixed Na-K aluminosilicate melts does not depend strongly on Al:Si ratio, but may be somewhat dependent on Na:K ratio, at least for the Ne-Kls join.

Gioachino Roberti, Benjamin van Wyk de Vries, Brent Ward, Pierre Friele, John J. Clague, Luigi Perotti, Marco Giardino

Submission 101

From ice melting to multi-phase debris avalanche: the 2010 Mount Meager volcano collapse

Recent climate change has reduced glacier ice cover in high mountains around the world. In combination with the thaw of alpine permafrost, glacier retreat has driven marginally stable slopes to failure. In the case of young volcanic massifs, the poor rock conditions have exacerbated these processes and led to very large landslides. Water from melting snow and ice fills fractures and pores elevating pore water pressures and bringing slopes to the threshold of collapse. The water within the failed rocks can then transform an initial rockslide into a multi-phase, long-runout debris avalanche. In August 2010, Mount Meager, an ice-clad, Plio-Pleistocene volcano in British Columbia, Canada, was the site of one of the largest landslides in Canadian history. Aerial photographs spanning the period 1948-2006 allowed us to document glacier retreat and progressive deformation of the volcanic flank. As Capricorn Glacier, which is located at the foot of the steep south side of Mount Meager, retreated, tension cracks opened across the slope, the toe bulged and precursory smaller landslides occurred. The slope that failed catastrophically in 2010 comprised, from top to bottom, an intrusive rhyodacite plug, block and ash layers, volcanic breccia, and quartz diorite basement. The lower part of the slope was saturated with water, which increased pore water pressures in the breccia and fractured and hydrothermally altered basement rocks, causing those materials to mobilize. Shortly afterwards, several large failures, controlled by lithology and faults, propagated up the slope to the secondary peak of Mount Meager, involving the whole volcanic sequence. The sliding rock masses fractured and spread as water escaped at the front and surface, forming an advance water-rich flow phase. The remaining water-poor mass continued to slide into the valley bottom. The water-rich phase reached higher velocities and superelevated as it ran down the valley of Capricorn Creek, leaving only scattered deposits. The slower water-poor phase did not superelevate and left a continuous hummocky deposit with brittle and ductile structures along Meager Creek and Lillooet River valleys. Future glacier retreat will further debutress the Mount Meager massif and add water to already weakened rocks, leading to other large multi-phase landslides. The high mobility and long runout of these landslides must be taken into account when assessing hazards and risk in downstream communities.

Deborah Robertson, Erouscilla Joseph, Nicolas Fournier

Submission 455

From above or below? What triggered the 2016 Boiling Lake instabilities in Dominica?

The Boiling Lake is a renowned volcano-hydrothermal feature located in an area next to the Valley of Desolation in southern Dominica. The Lake experiences sporadic interruptions in hydrothermal activity, seven (7) instances have been documented since 1876. One of the more recent changes in lake activity was recorded between December 2004 and April 2005. During that time the Lake stopped boiling, repeatedly emptied and refilled, before returning to its long term stable conditions. It was suggested that the instability was as a result of extensional strain induced by an earthquake and its main aftershock that occurred around the same period. In November 2016 the Boiling Lake experienced its eighth sporadic episode, however this one was notably preceded by a landslide on the edge of the lake. So the question is asked: What triggered this latest episode? Is it an indicator of static and/or dynamic changes occurring beneath the Lake or was the emptying triggered by the landslide?

The authors present findings regarding regional activity occurring before and during this episode and compare it with observations from previous episodes.

Philippe Robidoux, Maria Luce Frezzotti, Erik H. Hauri, Alessandro Aiuppa

Submission 814

Shrinkage bubbles: the C-O-H-S magmatic fluid system

New analytical results of the composition of shrinkage bubbles from melt olivine-hosted (forsterite [Fo] <80) glass inclusions advance a novel petrogenesis model on San Cristóbal volcano, Nicaragua. The components found inside the shrinkage bubbles (vapor, liquid, minerals) may represent the relics of early Carbon-Oxygen-Hydrogen-Sulfur (C-O-H-S) fluids exsolved from a magma-hydrothermal system inside the inclusion. To verify this hypothesis, firstly high precision Raman spectroscopy ($\pm 1 \mu\text{m}$) revealed gaseous carbon dioxide ($0.17\text{--}0.31 \text{ g/cm}^3$, number of samples $n = 31$) coexisting with liquid water (7/31) at ambient temperature inside the shrinkage bubble of naturally quenched inclusions. Secondly, the Raman spectra were used to identify mineral phases formed along the bubble/glass rim and those were confirmed by electron retro-diffusion/energy dispersive spectroscopy. The presence of liquid water is revealed with a novel Raman spectrum's subtraction method that isolate the $3460 \pm 60 \text{ cm}^{-1}$ isosbestic liquid water peak. According to major oxides/volatiles contents from inclusions holding a shrinkage bubble (electronic microprobe, nanoscale secondary ion mass spectrometry), liquid water migrates inside the bubbles (0.9–7.0 bubble Vol. %), but those are small contents (only 0.3 wt %) in comparison to the inclusion itself (< 3.3 wt %). Water still represents a principal agent for chemical reactions with other dissolved ionic species (SO_4^{2-} , CO_3^{2-} , Cl^- , etc.) and major elements from the glass inclusion (Mg, Fe, Cu, Si, Al, Na, K, etc.). Such chemical processes occur following pre-eruptive to post-eruptive inclusion cooling with volatile diffusion (1200 down to 250 °C), bubbles nucleation, expansion (1009–1141 °C) and contraction (<530 °C). To conclude, the mineral Fe-Mg-Cu-rich paragenetic sequence found inside the (vapor) shrinkage bubble corresponds to different cooling stages: (A) high-T copper-iron sulfide precipitation (500–700 °C), (B) low-T hydrothermal conditions (<350 °C, magnesite deposition from CO_2 vapor) and finally (C) ambient-low °T mineral precipitation (<150 °C; carbonates, sulfates, liquid water, etc.). Consequently, the C-O-H-S mixture of a shrinkage bubble can represent an ideal closed magmatic-hydrothermal system preserved inside glass inclusions after exsolution of magmatic fluids during cooling.

Joel Robinson, Drew Downs

Submission 643

Integrating Technology and Geologic Mapping

The oldest preserved geologic map is an Egyptian map prepared in 1150 BCE for a Rameses IV quarrying expedition that shows topographic features, location of building stone, and gold deposits. Whereas tools and methods have changed since then, the overall goal remains to create maps showing the locations of landforms and the boundaries (and often orientations) of rocks or geologic strata. Traditionally, the tools of a geologic mapper consisted of a compass, rock hammer, hand lens, notebook, pens and pencils, and a depiction of the Earth's surface, either as topographic maps and/or aerial photos. Whereas these tools are still an integral part of a geologist's toolkit, new tools have been added. Geologists now also use spatial databases or Geographic Information Systems (GIS), laptop computers, mobile devices, GPS units, satellite imagery, and high-resolution topographic models. However, increasing the number of tools does not necessarily correlate with better geologic maps. It is important to consider the most effective way of integrating all these tools and the information gleaned from them into a coherent picture that allows a map to be created and assembled efficiently.

In 2014, the USGS began the process of creating a geologic map of the northernmost ~3,500 square kilometers of Harrat Rahat volcanic field, Saudi Arabia. A GIS database was built to support the project's 11 geologists and to facilitate the use of map information in the field, office, and laboratory. The database organized satellite imagery and high-resolution topographic information, field notes about geologic field relationships, and samples collected for petrographic, geochronologic, geochemical, and paleomagnetic analyses. The GIS needed to move seamlessly between the office and field, so the abilities to display spatial data and location information on a mobile device, directly edit database tables using a standard input format, and easily transfer data between mobile devices and master GIS were deemed essential. The database facilitated data sharing among geologists, spatial awareness of sampling distribution, centralized storage of field data, and organized field observations. This resulted in efficient use of time and resources, facilitated the planning of future field work, and organized priorities for laboratory experiments. Ultimately, the data organization helped geologists turn field observations into geologic map information that will provide a framework for hazard assessments.

Alan Robock, Joanna Slawinska

Submission 919

Volcanic Eruptions as the Cause of the Little Ice Age

Both external forcing (solar radiation, volcanic eruptions) and internal fluctuations have been proposed to explain such multi-centennial perturbations as the Little Ice Age. Confidence in these hypotheses is limited due to the limited number of proxies, as well as only one observed realization of the Last Millennium. Here, we evaluate different hypotheses on the origin of Little Ice Age-like anomalies, focusing in particular on the long-term response of North Atlantic and Arctic climate perturbations to solar and volcanic perturbations. For that, we analyze the Last Millennium Ensemble of climate model simulations carried out with the Community Earth System Model (CESM) at the National Center for Atmospheric Research, supplemented by a range of sensitivity tests performed by us using CESM, focusing in particular on the sensitivity to initial conditions and the strength of solar and volcanic forcing. By comparing the climate response to various combinations of external perturbations, we demonstrate nonlinear interactions that are necessary to explain trends observed in the fully coupled system and discuss physical mechanisms through which these external forcings can trigger multidecadal modes of the Atlantic Multidecadal Oscillation and subsequently lead to a Little-Ice-Age-like regime. For that, we capture and compare patterns of the coupled atmosphere-sea-ice-ocean response as revealed through a range of data analysis techniques. We show that the large 1257 Samalas, 1452 Kuwae, and 1600 Huaynaputina volcanic eruptions were the main causes of the multi-centennial glaciation associated with the Little Ice Age.

Olivier Roche, Siet van den Wildenberg, Renaud Delannay, Anne Mangeney, Alexandre Valance

Submission 194

Basal forces in volcanic granular mass flows – experimental insights

Basal forces are fundamental in controlling the emplacement and the runout distance of volcanic granular mass flows, such as debris avalanches and coarse-grained pyroclastic flows, whose energy dissipation is controlled essentially by particle-particle and particle-substrate interactions. We address the role of basal forces through a series of analogue experiments on granular flows. The device consists of a reservoir connected to an inclined channel and from which particles are released to generate a granular flow. The particles of the flow are collected at the outlet of the channel in a box placed on a weight scale in order to measure the mass flux of the granular flow, which is typically of 1 to 5 kg/s. The flow thickness at the entrance of the channel is controlled by the aperture of the reservoir gate and it is typically of 0.5 to 2 cm. The channel is 1.5 m-long, 0.3 m-wide, and has a smooth base. The particles are glass beads of size 1.5 mm. A plate inserted in the base of the channel is connected to a 3-component sensor that can measure the basal normal (N) as well as the shear longitudinal (S) and transverse components of the particles weight, and an effective friction angle equal to $\text{atan}(S/N)$ can be determined. The forces transmitted by the granular flow to the plate are recorded at a frequency of 3 kHz, with a detection limit of 0.01 N. We report results of experiments at slope angles varying from 13 to 84 degrees. Our first observation is that at low angles (< 20 degrees) the flows are in steady state (constant velocity) but at higher inclinations the flows are accelerating and their velocity at the plate-sensor increases with the channel slope angle. Measurements show that both the normal and longitudinal force components decrease with the slope angle because the flows thin while accelerating downstream. Investigation of the effective friction angle suggest that there may be three regimes: (i) for small slope angles (<20 degrees) the effective friction angle is equal to the slope angle, (ii) for intermediate slope angles (20-50 degrees) the effective friction angle reaches a plateau of 21-22 degrees, (iii) for high slope angles (50-84 degrees) the effective friction angle decreases to 18 degrees.

Olivier Roche, David Buesch, Greg Valentine

Submission 191

The significance of substrate-derived blocks in ignimbrites for parent flow emplacement mechanisms – Example of the Peach Spring Tuff, western USA, and experimental constraints

Field examples show many ignimbrites contain blocks of decimeter to meter size that were captured from the substrate by the parent pyroclastic density currents. Such blocks are likely to provide fundamental insights into the physics of emplacement of the flows. We have investigated the Peach Spring Tuff, formed by the ~18.8 Ma Silver Creek caldera eruption, that has a dense-rock-equivalent volume of ~1300 km³. We report the presence of substrate-derived blocks of size up to ~70-90 cm at reconstructed distances from the source of ~30-150 km west and east of the caldera. Most blocks were picked up by currents on alluvial fans having natural granular substrates. Detailed field mapping reveals transport distances of tens to a several hundreds of meters. Simple analysis shows that the blocks could not be entrained by a dilute turbulent current. Therefore we performed analogue laboratory experiments to study the entrainment mechanisms of substrate particles by dense gas-particle flows. A volume of fine particles (80 microns) with high pore gas pressure was released to generate flows over a granular substrate of coarse particles (1600 microns). Many substrate particles were dragged temporarily at the flow base before ascending into the matrix of fines. These particles were entrained downstream by the gas-particle flows and eventually settled and froze at the base of the aggrading deposits. A key observation was that uplift of particles of given size and density (i.e. weight) occurred at a well-defined critical flow velocity, which we characterized by an empirical relationship. Assuming that the parent flows of the Peach Spring Tuff had a base consisting of a dense gas-particle mixture (overridden by a turbulent ash cloud) we then used our empirical law to infer flow velocities according to the characteristics of the largest blocks observed in the field. We found velocities of ~5-20 m/s, which, taking into account runout distances of ~170 km from caldera, corresponded to minimum flow durations of 2.5-10 hours. These durations and the total volume erupted indicate volume discharge rates of ~10⁷-10⁸ m³/s DRE, in agreement with other caldera-forming eruptions of similar magnitude (e.g. Tambora, 75 ka). The method we present is applicable to other ignimbrites to infer the physics of emplacement and the velocities of the pyroclastic flows as well as the discharge rates of large-volume eruptions.

Mel Rodgers, Patrick J. Smith, Tamsin A. Mather, David M. Pyle

Submission 948

The July 2008 Vulcanian Explosion of Soufrière Hills Volcano, Montserrat: Using seismicity to investigate pre-eruption processes during quiescent-explosive transitions.

Volcanoes often transition between quiescent, effusive, and explosive behaviour during dome-forming eruptions. At Soufrière Hills Volcano (SHV), Montserrat, repeated transitions have occurred with most large explosions occurring during phases of dome growth, or as major dome collapse events. However, the July 2008 Vulcanian explosion occurred at the end of a quiescent phase (Pause 3) and marked the onset of an extrusion phase (Phase 4). This was one of the largest explosions by volume and the largest to occur outside a period of lava extrusion. In this study we analysed the seismicity of the precursory seismic swarm (one of the most intense seismic swarms ever recorded at SHV) to investigate the subsurface processes that resulted in this eruption. We used spectral and multiplet analysis techniques to relate monitoring observations (seismic, SO₂, visual) to subsurface interpretations. In addition we developed machine-learning multi-station waveform classifier to allow systematic re-classification of waveforms. We propose that an initial VT swarm was triggered by ascent of decoupled gas ahead of rising magma. A subsequent LF swarm shows a coincident decrease in spectral content that we interpret as magma ascent through the upper conduit system. An ash-venting event on 27 July may have triggered rapid microlite growth. After peak event rate we observe an increase in the spectral content of the LF swarm, concurrent with a decrease in event rates. This could be interpreted as pressurization of the magmatic system over the final 24hrs, due to inhibited magmatic outgassing. This study demonstrates the use of spectral and multiplet analysis to connect observed seismicity to processes occurring in the volcanic subsurface. Our waveform classification method allows systematic and efficient classification of waveforms and can be used in volcano monitoring and research.

Angelica Rodriguez, Rachel Teasdale

Submission 147

Monitoring hydrothermal water temperature and composition at the Lassen Volcanic Center, Southern Cascades

The Lassen Volcanic Center (LVC) is located at the southern end of the Cascades Volcanic Arc in Northern California. Volcanism associated with the construction of the LVC began approximately 600 ka (Clynne and Muffler, 2010). The original LVC edifice has been altered glacially as well as hydrothermally to form the largest hydrothermal field in the Cascades range. Hydrothermal features include hot springs, fumaroles, mud pots, and boiling pools. This work reports on continuous water temperature measurements within the hydrothermal system of the LVC based on the idea that as magmatic activity changes, the temperature of the hydrothermal systems will also vary. Two sites have been targeted at the LVC, Sulphur Works (SW), and Boiling Springs Lake (BSL) to monitor water temperature and composition. Methods for measuring water temperatures of fumaroles were developed using a CR800 Campbell Scientific data logger and a flexible hermetic sealed PFA RTD sensor probe, which were installed at BSL and SW (Mendes et al., 2008). Water temperature measurements are recorded at half hour intervals and downloaded every 2 months. Water temperature measured at SW correlates with diurnal variations. However water at BSL does not change with diurnal variation. Baseline winter water temperature for SW is approximately 90°C. Water composition at SW from 2008 to 2017 includes, pH of 2.11-2.17. Isotope values of $\delta^{18}\text{O}/^{16}\text{O}$ is -4.29‰ and δD -62.4‰ in the dry season (fall) but are $\delta^{18}\text{O}/^{16}\text{O}$ is -0.29‰ and δD -11.2‰ in the wet season (spring; Mendes et al., 2008). These data indicate meteoric water is an important component for the SW hydrothermal system, and as also indicated by water temperature data, spring run-off overprints hydrothermal fluid temperature and water composition. Ongoing work includes collecting water temperature and composition data at SW and BSL to characterize trends from pre-drought years (2008-2012), through drought years (2012- winter 2016) and a more recent high precipitation and snow pack year (winter - spring 2017).

Lizzette Rodriguez

Submission 688

Preliminary results of grain size and component analysis of pyroclastic deposits from events at Fuego and Santiaguito volcanoes, Guatemala, during the period 2010-2016

Fuego and Santiaguito volcanoes are two of the most active and explosive volcanoes in Guatemala and are the target of this study. Deposits from different events in the period 2010-2016 were studied using grain size and component analysis. This period is considered a period of heightened explosive activity, compared to the last decades. The deposits are from pyroclastic falls, flows and surges. The samples were collected by volcanologists and observers from the Fuego and Santiaguito volcano observatories, from different locations around each volcano. These analyses give us information about the eruptive events and we can compare the deposits produced by different processes. Grain size analysis between -5 phi and 4 phi was conducted on ~5 samples from Santiaguito (from falls and flows in 2010-16) and ~12 samples from Fuego (from falls, flows, and surges in 2012-16). The samples from Fuego showed bimodal and left-skewed grain size distributions. The samples from Santiaguito showed left-skewed grain size distributions, even though one of the samples was from a pyroclastic flow deposit (from the explosive dome collapse of May 9, 2014). Preliminary analysis shows that for the Fuego samples there was a highest abundance of juveniles, followed by crystals, with very few lithic grains identified. The results were very consistent throughout the different events and with time. For Santiaguito there was generally a higher abundance of crystals, followed by juveniles. Density analysis indicated that the densities of Fuego's juvenile and lithic grains were 1.3 and 2.9 g/cm³, respectively. In the case of Santiaguito, the density of the vesicular grains was 2.4 g/cm³. The results of the grain size distribution parameters (median diameter and standard deviation) did not fall into the fields expected for characteristic deposits from previous work (e.g., Walker, 1983). The sorting, however, was very consistent with the process producing the deposits, except for that of the pyroclastic flow deposit from Santiaguito, which was well sorted.

Fátima Rodríguez, Gladys V. Melián, Egbert Jolie, Anna Jentsch, Andrew Rae, Agnes Mazot, Mark Harvey, Eleazar Padrón, Pedro A. Hernández

Submission 1007

Surface geochemical mapping for geothermal exploration research at the Taupo Volcanic Zone, New Zealand

New Zealand is well known for its utilization of high-temperature geothermal fields for geothermal power generation. Almost all of these geothermal fields are located within the Taupo Volcanic Zone (TVZ). However, there are still undeveloped medium- to high-enthalpy geothermal fields in this region. One of these examples is the Reporoa geothermal system, an elongated basin located to the south of Waiotapu, the largest geothermal field in TVZ. The Reporoa system is characterized by several geothermal surface manifestations, with Opaheke hot springs as the largest geothermal area. In other areas of the Reporoa basin further warm springs, pools, and seeps into drains and surface alteration has been observed. It has been discussed for a long time about the possible geo-hydrological link between Reporoa and Waiotapu geothermal system, or if Reporoa represent an individual geothermal system.

During February 2016 a surface geochemical survey was undertaken in a ~ 10 km² area inside the Northern part of the Reporoa system. Carbon dioxide efflux measurements were performed using the accumulation chamber method. Furthermore, an extended soil gas survey was performed by taking soil gas samples and performing chemical analyses (e.g., He, Ar, Ne, H₂, N₂, O₂, CH₄) as well as carbon isotopic analysis of the soil CO₂ ($\delta^{13}\text{C-CO}_2$). Additionally, ²²²Rn (Radon) and ²²⁰Rn (Thoron) activity concentration measurements in soil gas have been performed by alpha spectroscopy. The main goal of the study was to achieve a comprehensive understanding of the diffuse degassing processes and their relation to potential fluid pathways along permeable fault zones that could indicate a possible geo-hydrological link between Waiotapu and Reporoa. According to carbon isotopic analysis, the Opaheke hot springs show a clear volcanic-hydrothermal origin. Moreover, there are other, so far unknown areas showing signals of heavy carbon isotopes being indicative of a volcanic-hydrothermal source. Some of the analysed soil gases show a spatial trend that could confirm a hydraulic link between Waiotapu and Reporoa. Further data analyses and the correlation with other information (e.g., geophysics) will help to discriminate if those signals are indicative of a deep or shallow linkage.

Sara Rodríguez-Molina, María Charco, Ana M. Negredo, Pablo J. González, Mike Poland, David A. Schmidt

Submission 1104

Coupling the effects of conduit magma flow into a viscoelastic chamber to model volcano surface deformation: An application to Three Sisters volcano, Oregon, USA

The Three Sisters volcanic region Oregon (USA) is one of the most active volcanic areas in the Cascade Range and is densely populated with eruptive vents. An extensive area just west of South Sister volcano has been actively uplifting since about 1998. InSAR data from 1992 through 2010 shows an uplift rate in the area of 3-4 cm/yr from 1998 to 2003. After the summer of 2003 the deformation rate decreased considerably -a change that is also supported by leveling and campaign/continuous GPS data. Here, we analyze the temporal behavior of the displacement field using a new analytical model that describes the process of injecting magma into a reservoir surrounded by a viscoelastic shell. Our dynamic model is based on Hagen-Poiseuille flow through a vertical conduit that leads to an increase in pressure within a spherical reservoir and time-dependent surface deformation. We present an inversion methodology using the combination of a genetic algorithm (GA) inversion program and a dynamic model to determine the characteristic parameters of the volcanic deformation. The strategy is to provide a time series of the change in source volume using the parameter estimation technique outlined by González et al. (2013). The observed surface uplift is compared to predictions from the dynamic model to constrain model parameters, namely characteristic Poiseuille and Maxwell time scales, inlet and outlet injection pressure, and source and shell geometries. The modeling approach used here could be used to develop a strategy for including time-series deformation data in the interpretation of volcanic unrest.

Luis Angel Rodriguez-Sedano, Damiano Sarocchi, Lorenzo Borselli, Oscar Augusto Segura-Cisneros, Gamaliel Moreno-Chavez

Submission 1189

Volcano-sedimentary survey of pyroclastic deposits by means of unmanned aerial vehicles.

Unmanned Aerial Vehicles (UAV) have been effectively utilized in many fields of science. Decreased cost, augmented payloads, and availability of smaller cameras with better resolution, have contributed to its widespread usage in many fields of geology.

Although in volcanology drones have been used since the 1980s, their application was limited to video collection and safely documenting eruptive processes from proximal distances. In recent years, the use of drones for quantitative data collection has increased. UAVs are employed for photogrammetric purposes, multi-spectral and thermal image acquisition, infrasound collection, and direct gas sampling of the volcano plume and inaccessible fumaroles areas. The application of drones in volcanology is rapidly spreading and diversifying.

This work presents a new way to carry out quantitative volcano-sedimentary study of pyroclastic deposits by UAV. We use a mod. DJI 900 hexacopter vehicle, (7 kg payload), equipped with two cameras of different resolution and focal length. The measuring method uses two parallel lasers emitted from the UAV to the outcrop wall. Gimbal stabilizers for lasers and camera permit accurate and calibrated image acquisition suitable for analysis. The videos obtained by a GoPro Hero 4 camera, with a wide field rectified lens, are used for the 3D model reconstruction of the outcrop and for photogrammetric purposes. A Sony hdx455/B camera is used for high resolution imaging in order to obtain the best resolution for optical granulometric analysis. Finally, the images are analyzed using image analysis software designed in our labs.

The preliminary results obtained are promising and comparable with results obtained by other texture analysis methods. The resolution we obtain permits the measurement of particles on the order of 1 mm in size, but this limit can be improved to hundreds of microns. This method, developed for volcano-sedimentology purposes, can also be useful in other sedimentary research as well as structural geology and geotechnical applications.

Evelyn Roeloffs, Joshua P. Jones

Submission 1138

The March 30, 2014 Mw4.8 earthquake near Norris Geyser Basin, Yellowstone National Park: Co- and post-seismic deformation from Plate Boundary Observatory borehole strainmeters

On March 30, 2014, a Mw4.8 earthquake at 7.6 km depth near Norris Geyser Basin in Yellowstone National Park (USA) produced coseismic strain offsets at two Plate Boundary Observatory borehole strainmeters (BSMs): B950 and B206, 6 km south and 15 km southeast of the epicenter, respectively. B950 also recorded at least several days of post-seismic strain. Before this earthquake, the largest at Yellowstone in over 30 years, seismic activity in Yellowstone had begun to increase in September, 2013, and the surface uplift rate of GPS station NRWY near Norris had increased to a peak rate of 15 cm/year in late November, 2013. Seismicity intensified within 10 km of Norris in early February, 2014. Several days after the earthquake on March 30, 2014, vertical movement at NRWY reversed to subsidence, suggesting that a locus of pressurization near Norris Geyser Basin was relieved by the Mw4.8 earthquake rupture. Similar "fault-valve" behavior has been attributed to the largest earthquakes in swarms at Long Valley caldera, California, an interpretation supported by the initiation of strain-rate transients following those events. We examine the Yellowstone BSM data for analogous signals following the March 30, 2014 Mw4.8 earthquake, which had an 87% double-couple moment tensor combining strike slip and normal faulting. Coseismic strains at B950 and B206 agree well with those calculated from the double-couple portion of the moment tensor, except that the coseismic offset in engineering shear strain at B950 (1.1 ± 0.1 microstrain) is about five times larger than calculated. B950 also recorded continued increasing engineering shear strain, totaling approximately 0.2 microstrain, in the five days following the Mw4.8 event, a time period when uplift at NRWY continued and seismicity at Norris propagated to shallower depths. The coseismic engineering shear strain offset at B950 can be accounted for by adding a tensile fault adjacent to the double-couple shear fault: the post-seismic strain is then consistent with continued growth of this tensile fault for about five days. Longer-term post-earthquake strain-rate changes at B950 are difficult to distinguish from seasonal variations, like those subsequently recorded between April and mid-May of 2015 and 2016. The strain record from B950 is consistent with the Mw4.8 earthquake rupture breaching an impermeable zone and facilitating the pressure release inferred from GPS-documented subsidence.

Ben Rogers, Håvard S. Bertelsen, Olivier Galland

Submission 489

Magma intrusion in viscoelastic media: a laboratory model of coeval brittle and ductile deformation

The Earth's crust and upper mantle are zones of strong textural, compositional and structural heterogeneity. Host rocks intruded by magma should therefore be considered as complex materials that exhibit contrasting rheological behaviour in different settings. The mode and form of magma intrusion is largely controlled by this rheological complexity. End member elastic conditions are understood to produce blade-like dikes through tensile hydrofracturing whereas visco-plastic conditions are suggested to produce rounded plutons through diapirism. While dikes have been studied at length due to their prevalence in volcanic systems and diapiric plutons are often considered when studying magma intrusion at depth, the form of magma bodies intruding into intermediate viscoelastic hosts is poorly constrained.

Here we present a laboratory model of magma intrusion into a visco-elasto-plastic host that aims to bridge this gap in magma intrusion theory. Our model consists of a two dimensional Hele-Shaw cell in which oil and water (magma analogues) are injected into Laponite, a colloidal suspension of synthetic smectite clay which forms a viscoelastic and photoelastic a gel (a crustal analogue). The experiments are imaged using a polariscope which highlights the local stress-strain patterns as first order birefringence. Digital image correlation is then applied to quantify the stress-strain relationships in the host and map the distribution of deformation accommodating magma emplacement. The intrusions formed broad, lobe-like Rayleigh-Taylor fingers and narrow, magma-filled fractures in viscous and elastic host materials respectively, while more complex intrusion geometries were formed in intermediate visco-elasto-plastic host conditions.

This method allows for the observation of intrusion morphology in association with carefully controlled host rheology. Furthermore, the experiments imply that intrusions that appear to propagate through dominantly viscous processes can in fact exhibit elastic stress patterns and fracturing. Therefore, these experiments provide valuable insight into the complex mechanics of magma intrusion in viscoelastic settings.

Kurt Roggensack, Gordon Moore

Submission 1166

New and Improved H₂O-CO₂ Solubility Models: Comparing Basalt and Basaltic Andesite Solubility Relationships

Volatiles greatly influence physical properties of magmas (density, viscosity), phase equilibria and crystallization processes, and also the style and force of eruptions. While melt inclusions have provided a window into the subsurface conditions of pre-eruptive magmas, ultimately the interpretation of melt inclusion data relies on volatile solubility relationships. We've conducted fluid-saturated (H₂O-CO₂) experiments to determine the solubility in two mafic magma compositions commonly found in convergent margin settings. The results of the experiments on basalt and basaltic andesite are useful for interpreting olivine-hosted melt inclusions (MIs) and place important constraints on arc volcanism. While many experimental studies have investigated H₂O and CO₂ solubility in basalts, the slightly more evolved basaltic andesite has received less attention. Further, recent studies have shown that considerable CO₂ is often present in MI vapor bubbles indicating a need to explore CO₂ solubility at greater crustal depth. We present the results of new volatile-saturated, mixed-fluid (H₂O-CO₂) experiments using a piston-cylinder, AuPd capsules and operating at pressures from 300 to 600 MPa. Post-run the experimental capsules were punctured under vacuum and capsule fluids were condensed and separated and measured by manometry. Glasses were analyzed by FTIR to determine dissolved H₂O and CO₂. New results for basalt are in general agreement with published experiments at low pressures, but at higher pressures the solubility of CO₂ exceeds the levels predicted by current solubility models. The new experiments also show that the solubility of CO₂ in basaltic andesite is roughly 25% lower than basalt at 400 MPa.

Aleksei Rogozin

Submission 595

Giant Pliocene-Pleistocene explosive eruptions within the Karymshinsky-Zhirovsky area (South Kamchatka): episodicity and stages of volcanism

Kamchatka volcanic arc hosts numerous calderas. Middle-Pleistocene-Holocene calderas are well expressed in topography whereas the older ones can be identified only with the help of detailed field mapping of related deposits. In South Kamchatka volcanic rocks of acidic composition are widely developed, mainly tuffs and ignimbrites which were formed during large-scale explosive eruptions, which sources have not yet been established or are problematic.

In recent years, the study of sections of volcanic deposits and Ar-Ar dating of the region's rocks was carried out, as a result of which the Karymshina super-caldera, the largest caldera on the peninsula, was first documented [Leonov, Rogozin, 2007]. In the plane it has an oval shape (25x15 km). The volume of igneous products amounted to ~ 825 km³. The age of the caldera is 1.78 Ma.

Later studies have allowed to separate volcanogenic strata of the area into three units of welded tuffs erupted in three pulses between 4.01 and 1.39 Ma [Leonov, Rogozin, 2009; Bindeman et al., 2010]. Further mapping allowed more detailed mapping of the deposits of each unit. The most ancient stage of acidic volcanism (4.01-3.7 Ma) in the area is represented by dacite, rhyolite and rhyodacite lavas, tuffs, tuff breccias and ignimbrites. The rocks are distinguished by the bimodal distribution of the composition: andesidicite-dacite (62.3 – 65.1 wt.% SiO₂) and rhyodacites (69.4 – 72.6 wt.% SiO₂). The ignimbrites belonging to this stage are mapped in 35 km to SE from the edge of the caldera in the sides of river basins of Fal'shivaya River and Zhirovaya River. The age of ignimbrites of this stage is 4.01 Ma [Leonov et al., 2013]. Another outburst of acidic volcanism is associated with the formation of the Karymshina caldera. Ignimbrites and crystalloclastic tuffs filling the caldera have Eopleistocene age (1.78-1.39 Ma). Their composition varies from andesites to rhyolites (60.3 - 74.5 wt.% SiO₂). The area of their distribution is confined to the upper reaches of the Karymchina, Karymshina, Bannaya and Levaya Bystraya rivers. Their minimum thickness, uncovered in the left side of the Karymshina river, is more than 1000 m. During fieldwork in 2012-2016 a vast field of ignimbrites, traces of a large pyroclastic flow. The maximum thickness of the flow exceeds 500 m. Ignimbrites were found at a distance up to 35-40 km to the west from the edge of the caldera.

The study was supported by the Russian Science Foundation (project 16-17-10035).

Diana Roman

Submission 879

Automated detection and characterization of harmonic tremor at Popocatepetl Volcano, Mexico

Seismic harmonic tremor has long been associated with volcanic unrest. Most notably, it has functioned as an important short-term precursor to some major volcanic eruptions. However, major eruptions have also occurred without any apparent precursory harmonic tremor, and at other volcanoes, harmonic tremor appears to occur as a background or syneruptive (as opposed to precursory) process. It is unclear why only particular phases of eruption at particular volcanoes exhibit harmonic tremor – whether it is an artifact of differing detection protocols or a reflection of underlying physical processes. Thus, a systematic tool for assessing harmonic tremor would be useful for understanding the relationship of harmonic tremor relationship to eruptive activity and its value as an eruption precursor. Because harmonic tremor shares structural characteristics with speech and music, digital signal processing techniques developed to analyze these signals can be adapted to detect and analyze harmonic tremor. I developed a novel algorithm for detection of harmonic tremor by combining pitch-detection techniques with an assessment of the power of all hypothetical overtones to automatically identify occurrences of harmonic tremor and characterize their frequency content. The algorithm is then applied to continuous seismic data from Popocatepetl Volcano, Mexico, during a six-month period of heightened eruptive activity from December 2014-May 2015. During this period, major explosions (in terms of largest seismic energy release) occurred on December 23 and 25, January 6, February 25, April 3, 4, 18, and 18, and May 25 and 29. The algorithm detected a total of 1586 minutes of strong harmonic tremor during this six-month period. The majority of the harmonic tremor (1542 minutes) occurred during the five months with major explosions, with only 44 minutes of tremor detected in the relatively volcanically quiet month of January. Thus, harmonic tremor is generally correlated with periods of heightened eruptive activity. However, comparison of the timing of individual harmonic tremor episodes with individual explosions indicates a complex temporal relationship between harmonic tremor and volcanic activity. The results from Popocatepetl demonstrates the algorithm's ability to accurately detect and characterize harmonic tremor in near-real time while highlighting the need for additional work to understand the causes and implications of harmonic tremor at restless volcanoes.

Erika Ronchin, Steffi Burchardt, Tobias Mattsson, Christoph Hieronymus

Submission 418

Modeling of magma emplacement processes during laccolith growth

Understanding the processes that occur in active magma reservoirs is fundamental in estimating volcanic hazards. Unfortunately, active magma reservoirs are not accessible. Therefore, our understanding of what happens in active reservoirs before an eruption is limited to indirect information, mainly provided by geophysical and geodetic monitoring methods (e.g., seismic tomography, earthquake types and distributions, GPS, InSAR). However, the interpretation of geodetic and geophysical surface signals in terms of subsurface processes is not straightforward and the models that should provide this link may ignore or underestimate some key processes within the reservoir.

More direct observation of the processes occurring inside the magma reservoirs is provided by relict exposed reservoirs. The solidified intrusions contain evidence of the physical processes during magma emplacement. Here we target the emplacement of laccoliths, mushroom-shaped magma reservoirs that form when viscous magma intrudes and updomes the overlying rocks. New field evidence of subsolidus deformation of magma during laccolith emplacement (see Burchardt et al. and Mattsson et al., this conference) indicates that magma inflow and crystallization, laccolith growth, and host-rock deformation dynamically interact.

We address this interplay through Finite Element Method models built in Comsol Multiphysics with shapes and dimensions taken from natural benchmark examples. We model magma flow patterns in space and (relative) time and implement the physical properties of the magma from experimental and empirical relationships. We simulate dynamic magma behavior in a magmatic system in which the expansion of the reservoir is coupled with the accommodation of the deforming host rock. Preliminary results highlight the importance of magma viscosity in driving magma ascent and flow dynamics, as well as the influence of the solid fraction on the effective viscosity and flow patterns.

Tyrone Rooney

Submission 833

Flood Basalts and Pulsed Magmatism in East Africa

Cenozoic magmatism in East Africa results from the interplay between lithospheric extension and material upwelling from the African large low-velocity shear velocity province (LLSVP). The modern focusing of East African magmatism into oceanic spreading centers and continental rifts highlights the modern control of lithospheric thinning in magma generation processes, however the widespread, and volumetrically significant flood basalt events of the Eocene to Early Miocene suggest a significant role for material upwelling from the African LLSVP. The slow relative motion of the African plate during the Cenozoic has resulted in significant spatial overlap in lavas derived from different magmatic events. This complexity is being resolved with enhanced geochronological precision and a focus on the geochemical characteristics of the volcanic products. It is now apparent that there are three distinct pulses of basaltic volcanism, followed by either by bimodal lavas or silicic volcanic products during this period: (A) Eocene Initial Phase from 45-34 Ma. This is a period of dominantly basaltic volcanism focused in Southern Ethiopia and Northern Kenya (Turkana). (B) Oligocene Traps phase from ~33.9-27 Ma. This period coincides with a significant increase in the aerial extent of volcanism with broadly age equivalent 1 to 2 km thick sequences of dominantly basalt centered on the NW Ethiopian Plateau and Yemen, but also Turkana. (C) Early Miocene resurgence phase from ~26.9-22 Ma. This resurgence in basaltic volcanism that is seen throughout the region at ca. 24-23 Ma, but is less volumetrically significant than the prior two basaltic pulses. With our developing understanding of the persistence of LLSVP anomalies within the mantle, I propose that the three basaltic pulses are ostensibly manifestations of the same plume-lithosphere interaction, requiring revision to the duration, magmatic extent, and magma volume of the African-Arabian Large Igneous Province.

Christophe Komorowski

Submission 516

Three-Dimensional structure of the La Soufrière de Guadeloupe shallow hydrothermal system from muon tomography, gravity and electrical resistivity data

The La Soufrière de Guadeloupe volcano comprises a strongly developed and prolonged hydrothermal system related to the intense precipitation regime averaging 7 m/y and to sustained degassing and periodic magmatic eruptions in the last 10 000 years. This hydrothermal system is the source of several hazards including laterally directed explosions due to over-pressurisation, sulfur and halogen-rich degassing, mudflows and partial edifice collapse of the lava dome. A three-dimensional density model of the dome including the shallow part of the hydrothermal system was obtained from the joint inversion of gravity data and outgoing muon flux data from 3 muon telescopes measuring simultaneously in different points around the dome. The linear, smoothness-constrained, least-squares inversion we perform compensates for the influence of the acquisition geometry in the model regularization matrix. The resulting density model shows several low and high density anomalies. In the surface, they correlate to regions of highly altered and non-altered rock, respectively. Subsurface low density anomalies in the southern part of the summit and flanks correspond to the presently most active part of the hydrothermal system characterized by high-flux fumarolic degassing and the presence of hot, acid fluids. We compare and jointly interpret the density model with a three-dimensional electrical conductivity model obtained from the inversion of electrical resistivity tomography data, geochemical, and geological data. Our density model constitutes the basis for the development of a three-dimensional monitoring strategy of active hydrothermal systems using simultaneous muon telescopes measurements combined with other geophysical observables.

William I Rose, Erika Vye

Submission 161

Keweenaw Geoheritage: How to develop a Global Geopark in the US?

Earth science education in US schools is minimal; yet through prioritizing Earth science literacy heightened awareness of cultural linkages to the Earth can be achieved. Grassroots commitment to a geopark designation therefore requires a comprehensive public education and outreach strategy. With a strong geoheritage, low population and two national parks, the Keweenaw and Isle Royale offer advantages for education and outreach over other sites. We concentrated on communicating simple messages with the public through many geopark partners over the past four years, such as schools, businesses, politicians. We present our message (paragraph below) through presentations, field trips, geoconservation efforts, outdoor and indoor exhibits, educational books, films and more.

Just over 1 billion years ago a huge "hot spot" moved vast amounts of material upward under what is now the Lake Superior Basin bounded by the Keweenaw and Isle Royale. This profound event split Earth's largest continent and created extraordinary ponded flood basalts that filled a rift extending thousands of miles and was marked by millenia long magma oceans. Rifting and heat led to a massive hydrothermal system that produced Earth's only known major native copper. The rift event was disturbed and ended by continental collisions. Volcanism changed to redbed rift-filling and massive thrust faulting that moved the lavas and hydrothermal zones upward within the crust by miles. Much later, continental glaciers stripped away miles of rock layers and exposed the unique native copper along the Midcontinent Rift basin. The glacier then retreated to the north as humans migrated to America from Asia. People found the projecting copper right away and started the "American bronze age" 9000 years ago. Earth's largest freshwater lake (Superior) stabilized within the rift basin. Copper riches led to large scale industrial development and immigration which helped the young country to grow and develop industry. During the mining industry, geology - then a young science - was focused on the Keweenaw region. This resulted in global discoveries in mineralogy, geochemistry, structural and mining geology.

Geological interpretation of treasure from the deep earth adds understanding, appreciation and value to existing tourism programs. Keweenaw and Isle Royale geosites, geostories, and the abundant human overprint offer a compelling story that enhances existing parks' infrastructure through the lens of geotourism.

William I Rose

Submission 1266

Keweenaw Geoheritage: How to develop a Global Geopark in the US?

Earth science education in US schools is minimal; yet through prioritizing Earth science literacy a heightened awareness of cultural linkages to the Earth can be achieved. Grassroots commitment to a geopark designation therefore requires a comprehensive public education and outreach strategy. With a strong geoheritage, low population and two national parks, the Keweenaw and Isle Royale offer advantages for education and outreach over other sites. We have concentrated on communicating simple messages with the public through a multitude of geopark partners over the past four years, such as schools, businesses, politicians. We present this message through presentations, field trips, geoconservation efforts, outdoor and indoor exhibits, educational books and films and more.

Just over 1 billion years ago a huge "hot spot" moved vast amounts of material upward under what is now the Lake Superior Basin bounded by the Keweenaw and Isle Royale. This profound event split Earth's largest continent and created extraordinary ponded flood basalts that filled a rift extending thousands of miles and was marked by millenia long magma oceans. Rifting and heat led to a massive hydrothermal system that produced Earth's only known major native copper. The rift event was disturbed and ended by continental collisions. Volcanism changed to redbed rift-filling and massive thrust faulting that moved the lavas and hydrothermal zones upward within the crust by miles. Much later, continental glaciers stripped away miles of rock layers and exposed the unique native copper along the Midcontinent Rift basin. The glacier then retreated to the north as humans migrated to America from Asia. People found the projecting copper right away and started the "American bronze age" 9000 years ago. Earth's largest freshwater lake (Superior) stabilized within the rift basin. Copper riches led to large scale industrial development and immigration which helped the young country to grow and develop industry. During the mining industry, geology - then a young science - was focused on the unique Keweenaw region. This resulted in global discoveries in mineralogy, geochemistry, structural and mining geology.

Geological interpretation of treasure from the deep earth adds understanding, appreciation and value to existing tourism programs. Keweenaw & Isle Royale geosites, geostories, & the abundant human overprint offer a compelling story that enhances existing parks' infrastructure through the lens of geotourism.

Pierre-Simon Ross, Patrick Hayman, Gerardo Carrasco Núñez

Submission 96

Felsic diatremes, a volcanological overview

Felsic maar-diatreme volcanoes have been largely ignored by volcanologists, but commonly host major ore deposits, most commonly epithermal Au-Ag. Meanwhile, economic geologists have been studying mineralized felsic diatremes for decades. Using what we believe to be the five best described felsic diatremes based on publically available information (Cerro de Pasco in Peru, Kelian in Indonesia, Montana Tunnels in the USA, Mt. Rawdon in Australia, and Wau in Papua New Guinea), and new data on Mt. Rawdon, we present an overview of their characteristics and emplacement processes. The ejecta ring portion of the volcano is also briefly discussed, based on Wau and on two rhyolitic Mexican tuff rings, Hoya de Estrada and Tepexitl, to build a complete overview of felsic maar-diatremes volcanoes. We then compare these volcanoes to their ultramafic to mafic counterparts, as well as to lava domes and to small calderas. We conclude that felsic maar-diatremes are probably formed by dome-like eruptions (with limited eruptive rates, and mostly poorly vesicular magma), but strongly modified by phreatomagmatism.

Holly Rotman, Tehnuka Ilanko, Clive Oppenheimer, Philip Kyle

Submission 863

Seismic and gas geochemical observations during an episode of increased explosive activity at Erebus volcano, Antarctica

Erebus volcano is renowned for its persistent lava lake and intra- to inter-annual episodes of heightened Strombolian activity. Explosions occur at the lava lake itself (large gas bubble ruptures) and from adjacent vents within the summit crater. Explosions are detected throughout the year from seismic observations. The reasons for the variability in frequency and size of explosive events remain unclear.

Here we examine the first ~9 months of an episode of increased explosive activity from June 2013 to April 2014, using a combination of seismic observations and gas composition data obtained by open-path FTIR spectroscopy. The number of explosions sourced at the lava lake increased gradually from 0-1 explosions/day in mid-June 2013 to 2-3 explosions/day by mid-October 2013. Between late December 2013 and early April 2014, there were on average 2-4 lava lake explosions per day (with a maximum of 16 on January 14). This ~3 month interval of increased activity was also characterized by 'ash venting' or jetting events from vents around the lava lake. After a period of inactivity, one of these, informally called the "Active vent", was the site of around 50 explosions between January 8 and March 13, 2014. The duration of these events was up to 30 s, considerably longer than the near-instantaneous lava lake explosions.

In December 2013, around 20 bubble bursts in the lake were captured by FTIR spectroscopic observations. These events varied from meter- to decameter-sized bubbles. The larger bubbles ejected much of the lava from the lake as meter-sized bombs. The gas composition of the larger bubbles is relatively rich in carbon dioxide, one of seven molecular species quantified in the volcanic emissions. Contemporaneous seismic records enable quantification of the nature and size of the bubble burst events. This permits a detailed investigation of the variation of gas composition with gas volume for each event. Our current results suggest that although the CO₂/HCl ratio appears invariant with gas volume, the SO₂/CO₂ and CO₂/H₂O ratios increase with gas volume size.

Stefanie Rott, Bettina Scheu, Klaus Mayer, Tim I. Yilmaz, H. Albert Gilg, Erouscilla P. Joseph, Cristian Montanaro, Donald B. Dingwell

Submission 852

Phreatic activity, hydrothermal alteration and related hazards at Boiling Lake and the Valley of Desolation, Dominica

The Boiling Lake (BL) and the Valley of Desolation (VoD) are areas of high hydrothermal activity and very popular tourist attractions at Dominica, where several small phreatic eruption have been reported, as for instance in 1997. During two field campaigns we mapped the hydrothermal activity as well as its surficial phenomena, further we investigated alteration processes and their effects on outgassing and the propensity for phreatic eruptions in both areas. Petrophysical properties (density, permeability, strength) of clay-rich unconsolidated samples were obtained in situ by field-based characterization. These unconsolidated samples, together with consolidated rocks have been collected and further investigated in the laboratory in order to characterize a range of rocks affected by supergene and hydrothermal alteration. The degree of alteration was quantified based on the geochemical composition (XRF, XRD), which correlated well with the degradation of rock mechanical properties. Our results show that alteration leads to an increasing abundance of clay minerals and a decrease in both strength and permeability of the rocks. For VoD we found that in the immediate vicinity of outgassing acid-sulphate fluids, advanced argillic alteration yields mineral zoning further influenced by the presence of groundwater. The water-saturated basal zone is dominated by kaolinite whereas alunite formation is favored at and above the groundwater table where atmospheric oxidation of H_2S to H_2SO_4 occurs. This alteration type may in turn inhibit outgassing at the surface, increasing the potential for pressurization in the subsurface and thus the propensity of phreatic eruptions. The alteration observed at BL is very similar to VoD, however here we also evaluate lake drainage and landslides can act as trigger for phreatic eruptions. Rapid decompression experiments in the laboratory, together with ballistic trajectory calculations allow us to constrain the conditions prior to the recent small-scale phreatic event in the Valley of Desolation in 1997 and evaluate the hazard potential for both areas. Furthermore our results contribute to a better understanding of the hazard potential of hydrothermally active areas in general.

Michael Rowe, Yuli Heled, Isabelle Chambefort, Colin Wilson

Submission 1293

Vapour phase alteration and cooling of compound ignimbrite sheets: the silica story

Many large ignimbrite sheets that are welded show vapour-phase alteration in addition to the initial crystallisation of the formerly glassy matrix. We present new data on silica polymorphs created by alteration processes during cooling and emplacement of compound ignimbrites. Prior investigations into the cooling history of thick, high-T ignimbrite sheets indicated that there was a change in silica polymorphs and associated groundmass textures. Silica polymorph distribution through the ignimbrite was consistent with cooling profiles from numerical modelling. Here, we utilise X-ray diffraction and SEM imaging to examine changes in groundmass texture and mineralogy through selected sections in two compound ignimbrites: the Bishop Tuff (USA) and Whakamaru Ignimbrite (New Zealand). Two transects through the Bishop Tuff exposed in Owens Gorge, linked to previously documented stratigraphic packages and welding zones, provide a basis for comparison to the Whakamaru Ignimbrite at the Maraetai Dam section on the Waikato River. Calculated using a newly developed software routine, samples from both localities generally contain only 10-30% amorphous material, consistent with the welded nature of the samples. Interestingly, silica polymorphs indicate a mineralogical change from cristobalite to tridymite at, and just above, the contact between the flow sheets for two of the three sections investigated. In contrast, for the Bishop section containing a fall deposit intercalation, no tridymite is observed. A density profile through the Whakamaru section shows no significant variation in the presence of tridymite. In contrast, for the Bishop section, there is a significant change in density at the contact between ignimbrite packages. The systematic stratigraphic location of the tridymite at the contact of flow units suggests that the presence of tridymite is not related to cooling rate. In the case of the Whakamaru ignimbrite, the presence of tridymite also corresponds to a distinctive horizontal fracture pattern. We propose that groundmass tridymite is related to localised vapour phase alteration and that the upper flow material served as a “cap” for vapour accumulation, resulting in tridymite crystallization only where the two ignimbrite sheets are in direct contact. The correlation of compound ignimbrite structures and silica polymorphs may prove a valuable exploration tool for understanding potential fluid flow along ignimbrite structures in geothermal systems.

Colin Rowell, Steven McNutt, David Fee, Mark Jellinek

Submission 705

Ground-coupled airwave based site-assessment for detection of volcanic explosions at regional seismic stations in Alaska

Ground-coupled airwaves (GCA) occur where an atmospherically propagating pressure wave impinges on the ground surface to induce seismic shaking. For volcano monitoring networks, GCA signals serve to fill a data gap in cases where acoustic sensors are sparse or inactive, and provide confirmation of surface eruptive activity associated with seismic signals. The explosive phase of the 2009 eruption of Redoubt Volcano, Alaska, produced 19 explosions that were recorded at local and regional seismic and acoustic sensors. Spectral analysis and band-pass filtering of seismic data reveals GCA signals at regional distances of up to 245 km previously undetected in raw waveforms. These airwaves are generally only recorded at stations northeast of the source, consistent with ducting of sound by seasonal tropospheric or stratospheric winds. Coherency of signals between seismic stations is poor, and GCA signal amplitudes do not always scale with pressure sensor amplitudes. In line with similar studies [e.g. Fee et al., 2016; De Angelis et al., 2012], GCA signal detection and characteristics are governed as much by atmospheric conditions and efficiency of acoustic-to-seismic coupling as by initial source conditions or distance.

Following our initial observations at Redoubt, we perform an expanded analysis on eruption signals and ground-coupled airwaves from select volcanoes in Alaska and the Aleutian Islands over the past 10 years. Our analysis consists of three components: (1) Ray trace modelling provides a first order prediction for which stations will receive signals based on seasonal wind and temperature profiles. Coupling efficiency can then be estimated as a function of incidence angle and site substrate [e.g. Garces and McNutt, 2000, Appendix C]. (2) We detect GCA's via acoustic propagation velocities and envelope cross-correlation, and where sensor density allows, f-k beamforming. (3) GCA signals are analyzed using Principle Component Analysis (PCA) to isolate signal contributions, which are compared against model predictions and spatio-temporal detection patterns from steps (1) and (2) to assess the relative importance of source conditions, propagation effects, and coupling. Successful predictions provide a framework for which sensors in the regional network can be used to detect and analyze ground-coupled airwave signals from these volcanoes.

Scott Rowland, Andrew Harris, Nicolas Villeneuve, Thorvaldur Thordarson

Submission 963

THERE IS ALWAYS SOMETHING TO LEARN FROM THOSE INTERESTING BUT PUZZLING LAVA-FLOW OUTCROPS THAT EVERYBODY COMES ACROSS EVERY NOW AND THEN

Over the past 40 years our knowledge of lava flows has improved markedly. We understand how they cool, how tubes, channels, and various surfaces develop, and how these can be interpreted with respect to emplacement conditions. We can even write computer models that replicate known flows. What's a field volcanologist to do? The answer is obvious, of course: keep going into the field and recording your observations. Turn your notes, photographs, and interpretations into a published manuscript, and don't fear that it doesn't contain a quantitative model. But be sure to check the older (likely non-digital) literature first! Many of those old-timers (e.g., H. Stearns, R. Nichols, etc.) were excellent observers and published about almost everything they observed. What we ask you not to do, however, is give the object of your study a new lava-type name – one practice we feel the old-timers were a little too eager to do. Every volcanologist has come across lava-flow features that s/he isn't familiar with and which may defy explanation, at least initially. Such features likely hold information about a (perhaps infrequent) process, and guaranteed someday you'll have to try and explain them during a field trip. We offer a few examples that we don't fully understand: Accretionary lava balls occur on some 'a'ā flows and supposedly develop as surface rubble coats itself with fluid core lava, yet they occur on flows in which the core almost certainly was not sufficiently fluid to form a coating. Jagged fins of lava in the middle of 'a'ā flows (described by R. Nichols and K. Krauskopf) form partly by spreading of the flow core after it has been emplaced, but they stick up above the clinker surface and show grooves that were produced by vertical motion – what causes them to rise? Bulges on some pāhoehoe flows suggest that the flow direction alternated between left and right – do they hold information about crustal growth rates?

Scott Rowland, John Sinton

Submission 1218

KA'ĀPAHU, A THICK BENMOREITE FLOW SEQUENCE ON EAST MOLOKA'I VOLCANO, HAWAI'I

Ka'āpahu (the truncation) is a steep ridge on the south slope of East Moloka'i volcano consisting of 5-6 3-4 m-thick mugearite lava flows overlain by 3-4 10-20 m-thick benmoreite lava flows. They appear to have all erupted from approximately the same vent location during late post-shield activity of the volcano. We present data on the benmoreite, the longest flow of which extends 2000 m down a 14° slope. It has 58 wt. % SiO₂, is non-vesicular, and contains numerous plagioclase phenocrysts, plus olivine, magnetite, brown amphibole (locally altered to an anhydrous assemblage) and clinopyroxene. Ka'āpahu is obvious because it stands higher than the rest of the shield surface nearby and because ~1.3 million years of sub-tropical weathering have altered the benmoreite to distinctive shades of light and dark grey. Unfortunately, this same weathering has also degraded flow margins, contacts, and internal flow structures, making mapping difficult both in the field and with imagery. Original flow widths are unknown but were likely 250-350 m at most. The current area of benmoreite is ~0.3 km² and its volume is ~0.004 km³. Using the formula of G. Hulme (1974), yield strengths for 10 and 20 m-thick flows with a density of 1600 kg m⁻³ on a 14° slope are 35,000 and 70,000 N m⁻², respectively. The benmoreite flows show a progression from longest to shortest with relative age, giving the along-flow topographic profile a stepped shape. This temporal shortening of the flows was likely due to a combination of decreasing eruption rate and increasing yield strength and viscosity.

Ken Rubin, Robert Embley, David Clague, William Chadwick

Submission 1265

Eruption styles at 1.2 km deep West Mata Submarine Volcano summit revealed by video observations and deposit mapping

West Mata Seamount is an active submarine volcano between the NE Lau Basin and the Tofua Arc, between Fiji and Samoa in the SW Pacific (Resing et al., *Nat. Geosci.*, 2011, doi:10.1038/ngeo1275; Clague et al., 2011; doi:10.1029/2011GC003791). It has erupted from its 1200 m deep summit and from deeper flank vents over the past decade (Embley et al., *G-cubed*, 2014, doi: 10.1002/2014GC005387). In 2009, we made direct observations of its eruptions with a remotely operated vehicle (ROV), including the first observations of active deep sea lava flows and the first historical observation of boninite magma being erupted on Earth. In this video-intensive presentation, we document and discuss the range of explosive and effusive eruptive conditions that were observed, the deposit types they produced, and relations to the different volcanic vent structures that were active during our observations. High crystallinity (40-50%) lava was documented erupting effusively and explosively in a range of styles, producing lava flow, sand, and tephra/scoria deposits. Observed eruptive styles varied widely, particularly with respect to conditions, extent, and locus of fragmentation, which all varied in space and time during our 4 days of observations in 2009. Four distinct fragmentation mechanisms operated: (1) gas-driven, (2) by external water in the conduit, (3) post vent mechanical eject breakup and (4) quench granulation occurring above or on the sea bed. Our group revisited the volcano with an ROV in 2012, finding major changes at the summit (pit crater formation, mass wasting, and cessation or hiatus in active volcanism). Collectively, observations made during the 2009 and 2012 surveys, plus deposit mapping and lava dating, allow us to reconstruct variations in eruption conditions and styles before, during, and after the period of direct observations, revealing apparent waxing and waning of eruption intensity and its effect on the distributions of eruption products.

Julian Rüdiger, J. Maarten de Moor, Lukas Hoffmann, Nicole Bobrowski, Alexandra Gutmann, Marcello Liotta, Marco Liuzzo, Jorge Andres Diaz, Alfred Alan, Ernesto Corrales, Fiona D'Arcy, John Stix, Thorsten Hoffmann

Submission 888

Comprehensive application of Unmanned Aerial Vehicles (UAV) for volcanic gas emission studies

Volcanoes are a substantial source for several atmospheric trace gases including sulfur and halogen containing species, as well as CO₂. Monitoring the composition and flux of these gases is an important part of volcano monitoring. Besides remote sensing methods (e.g. UV-spectroscopy), plume gas compositions are often obtained in-situ, exposing scientists to hazardous conditions or making measurements during periods of high activity impossible. The rapid development and widespread availability of unmanned aerial vehicles (UAVs) in recent years has made its applications in volcanic environments easily feasible and represents a useful tool for personnel risk avoidance.

Herein, we demonstrate the deployment of multirotor UAVs (quadro- and octocopters) with custom-made lightweight payloads for the compositional analysis and flux estimation of volcanic plumes. Field applications were performed at Stromboli Volcano (Italy), Turrialba Volcano (Costa Rica) and Masaya Volcano (Nicaragua). Multiple in-situ gas measuring systems, based on electrochemical and optical detection principles, were used for the determination of CO₂, SO₂ and H₂S and compared with established methods. Besides the mixing ratios of these gases, temperature, pressure, relative humidity and GPS position were recorded. All parameters were both stored onboard the UAV and transmitted by telemetry. For total SO₂ flux estimations a small differential optical absorption spectroscopy (DOAS) system measured SO₂ column amounts on transversal flights below the plume, showing the potential to replace manned or car-based operations.

The UAV system also enables the investigation of gaseous halogen species (e.g. HCl, HBr, BrO(H), Br₂, Cl₂, and BrCl) and their compositional variation in the plume with distance from the source (plume aging in air), which requires airborne sampling. To shed light on the halogen speciation in the aging plume, a gas diffusion denuder-sampling unit (including a SO₂ sensor) was mounted on the UAV, allowing the determination of halogen species in the lower ppb range at various distances (up to 2.5 km) to the active volcanic vent. Our data collected at three volcanoes during heightened activity show that UAV-based campaign gas measurements are a valuable contribution to volcano monitoring and provide unique insights into volcanic degassing processes.

Max Rudolph, Rob Sohn

Submission 1147

A model for internal oscillations in geysers, with application to Old Faithful (Yellowstone, USA)

We present a mechanical model for internal oscillations in geysers with “bubble trap” configurations, where ascending gas or vapor becomes trapped beneath the roof of a cavity that is laterally offset from the eruption conduit. Such a configuration has been inferred for many geysers worldwide, including Old Faithful Geyser of Yellowstone National Park, on the basis of in-situ video observations and geophysical measurements. We consider two cases, one in which the trapped gas behaves as an isothermal ideal gas, and one where it is treated as isenthalpic steam. In both cases the system behaves as a damped, harmonic oscillator with a resonant frequency that is sensitive to the conduit geometries and fluid volumes. We use the model to predict internal oscillation frequencies for Old Faithful geyser, in Yellowstone, USA, using conduit geometry constraints from the literature, and find that the frequencies predicted by the model are consistent with observations (~ 1 Hz). We show that systematic frequency increases during the recharge cycle, when the fluid volume of the system is increasing due to recharge, are consistent with either a decrease in the amount (both volume and mass) of trapped gas or vapor, a decrease in the eruption conduit cross-sectional area, or a combination of both.

Elise Rumpf, Einat Lev

Submission 30

Experimental Investigation of the Influence of Small-Scale Topography on Lava Flow Advance

A quantitative understanding of lava flow emplacement is integral to the safety of communities and infrastructure surrounding active volcanoes and for the interpretation of planetary and historical emplacement conditions. The influence of small-scale topography is not currently accounted for in flow prediction models despite evidence that topographic features on the order of flow thickness will affect flow dynamics. To quantify this influence, we completed three sets of experiments that investigated the effects of pre-existing small-scale topography (on the order of flow height or less) on lava flow emplacement dynamics. To represent the complicated rheology of natural lava, we used three materials: corn syrup, polyethylene glycol (PEG), and molten basalt. Syrup and PEG experiments were completed at the Fluid Mechanics Laboratory at Columbia University. Both materials were extruded onto a sloped plane covered in a series of beds of four varying grain sizes. Basalt experiments were completed at the Syracuse University Lava Project facility. Basalt was heated to >1200 degrees Celsius and poured onto a series of sloping beds of six different grain sizes.

For all three materials, flow advance rates were affected by substrate roughness. Flow front advance rates decreased with increasing bed grain size, with decreases equivalent to up to an order of magnitude increase in effective viscosity. The difference in flow front advance rate decreased with time after experiment initialization. The decrease in velocity is due to mechanical and thermal influences of the substrate. A rough substrate disrupts smooth fluid emplacement, promoting downward movement of material into void spaces between substrate grains and lateral movement of material through the development of breakouts. These effects decrease the volume of material moving directly downslope. Additionally, the increased surface area of a rough substrate will increase initial rates of heat conduction from the base of the lava flow, lowering internal flow temperatures, thereby increasing flow viscosity. These effects diminish with time after flow initialization as a basal boundary layer develops. We recommend that a roughness factor is included in future lava flow emplacement models to increase prediction accuracy. In addition, the topographic roughness of regions prone to lava flows should be characterized ahead of flow emplacement using techniques such as photogrammetry and LIDAR.

Philipp Ruprecht, Heather Winslow, Matthew Pritchard, Daniel Basualto, Francisco Garcia

Submission 716

Recharge of silicic magmatic systems - Mafic magmas driving the 2011 Puyehue-Cordón Caulle eruption?

Over the last 69 kyr Volcán Puyehue-Cordón Caulle (PCC) in the Southern Volcanic Zone of the Chilean Andes erupted basalt (~50 wt% SiO₂ and >8 wt% MgO) to rhyodacite (~70 wt% SiO₂ and ~3 wt% K₂O; Singer et al. 2008) with episodes that were dominated by more mafic magmas as well as others by silicic eruption products. In recent history the volcano has increasingly erupted silicic magmas suggesting that any mafic input is cryptic and hybridized at depth below the shallow silicic storage region.

The recent activity culminated in three explosive-effusive crystal-poor rhyodacite eruptions (1921-22, 1960, 2011). Among these, the 2011 eruption was extensively monitored geodetically and seismically prior, during, and after the eruption. This provides a unique opportunity to address magma mass transfer through the crust associated with the 2011 eruption and the potential role for deeper, mafic magmas to replenish the silicic system and trigger the eruption. However, previous petrologic studies of the 2011 eruption have reported a very limited involvement of mafic magma, found in the form of xenocrystic calcic plagioclase and mafic minerals. As a result, triggering of this eruption has been enigmatic especially in light of the 1960 eruption that serves as the best example for a megathrust-earthquake triggered eruption (as it was 2 days after the Mw 9.5 Valdivia earthquake).

We present new petrologic results from the 2011 eruption that highlights the presence of mafic magmas in the form of mafic enclaves as part of the mostly rhyodacite magma. Such mafic recharge magmas may solve how this eruption was triggered. These mafic enclaves are rare but ubiquitous within the 2011 lavas and compositionally fall near the most mafic-end member (~50 wt% SiO₂; ~8 wt% MgO) defined through PCCs eruptive history suggesting that deeper primitive magmas directly feed the silicic system. Generally, whole rock geochemistry shows that these enclaves have not fractionated significant amounts of plagioclase given the lack of a Eu anomaly. However, in a few examples plagioclase accumulation indicated by small positive Eu anomalies suggests a remobilized mush origin for some of these mafic magmas. Further study of the mineral chemistry will constrain the P-T conditions of the primitive recharge magmas and will provide new petrologic constraints for the interpretation of pre-, syn-, and post-eruptive monitoring signals.

Philipp Ruprecht, Einat Lev, Alexander S. Lloyd

Submission 724

A tale of two flows -- A field study at Quizapu Volcano, Chile

Quizapu volcano, in the Chilean Southern Volcanic Zone, erupted effusively in 1846-47 and explosively in 1932. This sequence of events formed a terrain comprised of large andesitic to dacitic lava flows covered by a layer of pumice. This unique environment provides volcanologists studying lava flows with an opportunity to test field methods and assumptions that are often difficult to assess in the rugged conditions of expansive silicic flows. In 2016 a bi-national team of students and researchers from Chile and the US explored the Quizapu area, focusing on two major flow lobes from the 1846-47 eruption. Despite originating from the same eruption, and traversing similar topography, the lobes exhibit different large-scale morphology. The southern flow lobe (SF) has a uniform, smooth, almost straight geometry (earning it the nickname "the highway"), while the northern flow lobe (NF) has undulating boundaries and irregular width and thickness.

The team collected an extensive set of 68 samples (29 NF, 39 SF), spanning areas from to 4.6 to 7.9 km (NF) and 2.5 to 7.6 km (SF) from the vent. Sampling covered both the main channels and the levees, in a systematic grid pattern. Samples were analyzed for 3D structure, crystallinity, and vesicularity using X-ray microtomography, and for major and trace element composition using XRF. UAV-based aerial photographs collected during sampling were used to construct digital elevation models.

Our results reveal that SF has a remarkably uniform chemical composition and shows little variation in microstructure. NF, on the other hand, shows gradients in vesicularity, decreasing from 21% to 3% down flow, in addition to changes in composition. SiO₂ content decreases from ~63.5 to 62 wt%, accompanied by along-flow trends in MnO, MgO, and CaO. The two flows have distinct chemical composition, with an average of 63 wt% SiO₂ content for NF compared with 68 wt% for SF. The overall compositional diversity of this eruption has been studied previously to constrain sub-volcanic magma mixing processes.

Our findings provide an example for the extent of chemical and morphological variability in both individual flow lobes and between multiple flows from a single eruption. This insight should guide sampling efforts in the future for single- and multi-flow effusive eruptions, and inform the assessment of previous studies based on extensive or limited sampling. Furthermore, the results provide new constraints for models of along-flow lava evolution.

Alison Rust, Katharine Cashman

Submission 79

Spatial variations in ash properties – controls from petrology to sedimentation

Real-time tracking and predictive modelling of volcanic ash dispersion and deposition relies on simple assumptions of ash properties. We collate data from tephra deposits that record changes in ash properties with distance, particularly distal and ultra-distal deposits that provide information on far-travelled ash. Not only does ash grain size vary substantially with distance, but also the components, composition, shapes, and densities of particles.

The bulk compositions of erupted magmas vary, as do their crystal and bubble contents. The ash derived from fragmentation of the magma can thus have components that are glassy or crystalline, and dense or vesicular. The size, shape and abundance of crystals and bubbles in turn depend on the storage and decompression history of the magma. Where the fragmenting magma is very low-crystallinity (near-liquidus temperature and often H₂O-poor), the glassy ash has the same composition as the bulk magma except for volatile species. However, if magma crystallizes as it ascends, the residual melt evolves in composition; consequently the chemistry of glassy ash particles is typically different from the bulk chemistry of the parent magma, and due to variations in the proportion of crystals sedimented, the composition of tephra varies with distance from source. Importantly, the glass component of intermediate-composition eruptions is generally more evolved than the bulk magma. Magmas with ~63 wt% SiO₂ are susceptible to ascent-driven crystallization, generating a broad range of glass chemistries despite a uniform magma composition.

Very fine ash from eruptions of intermediate to silicic composition is therefore likely to be rhyolitic regardless of the parent magma composition. This is a consequence of both the prevalence of rhyolite glass and early deposition of crystals, which form relatively dense, compact particles. Consequently ash shape and bubble content are important determinants for long-range transport. Data from distal and ultra-distal ash particles suggest that far-travelled ash is variably vesicular and often highly anisotropic in shape (e.g. platy). Furthermore, a substantial proportion of the mass of far-travelled ash can reside in particles too large to be detectable by most optical particle counters or passive remote sensing techniques.

Regis Rutarindwa, Elaine Spiller, Marcus Bursik, Andrea Bevilacqua

Submission 911

A probabilistic hazard mapping tool for the Long Valley volcanic region (CA, USA)

Probabilistic hazard maps are used to graphically represent forecasts of potentially hazardous volcanic processes associated with an eruption. The construction of a probabilistic hazard map requires the characterization of all possible scenarios (aleatoric variability) that might lead to an event of interest. These scenarios then must be “fed in” to a physical model of the geophysical process which are typically computationally expensive to exercise.

We present a hazard-mapping tool for the Long Valley region of California. This tool utilizes statistical surrogates of the physical model (in this demonstration, TITAN2D simulations of pyroclastic density currents) to perform rapid hazard assessment. It effectively replaces simulations that take $O(\text{min})$ - $O(\text{hours})$ with function evaluation which take a fraction of a second to exercise. This speed up enables tremendous flexibility in scenario modeling as we can quickly construct and compare probabilistic hazard maps under a variety of scenario models. Furthermore, we can quickly update a probabilistic hazard map as new data or emergent situations arise.

Amy Ryan, Elizabeth Friedlander, Kelly Russell, Michael Heap, Lori Kennedy

Submission 523

Hot pressing of gouge during the 2004-2008 eruption of Mount St. Helens

We present results from a study designed to constrain the timescales, conditions and mechanisms for densification of volcanic gouge at Mount St. Helens (MSH) during the 2004-2008 eruption. During that time MSH produced 7 lava spines that were each mantled by gouge, a fine crystal-rich rock powder containing little to no glass, created by fracturing and cataclasis at the conduit-wall rock interface. The gouge carapaces are texturally diverse: at spine 4 the gouge transitions from unconsolidated to indurated material, then cohesive cataclasite; at spine 7 there is a sharp contact between indurated gouge and dense ultracataclasite. The juxtaposition of these rocks suggests that the unconsolidated gouge is densified and lithified during ascent to the surface. At present the conditions, timescales and mechanisms for densification of these glass-poor materials are unknown. We use observational data (mass flux and extrusion rates, eruption duration) to reconstruct the pre-2004 magma column and to model the ascent of the magma that fed each spine. The modeled residence time for spine 7 is > 100 days longer than for spine 4, and we attribute the formation of the ultracataclasite to the extra time the gouge remained at high temperature (T) in the conduit. We hypothesize that solid-state sintering, a process whereby crystalline particles are fused together as a result of atomic diffusion (i.e., the same process responsible for the production of ceramics by hot (isostatic) pressing), drives densification during ascent. To test this idea we have conducted high-T uniaxial deformation experiments using MSH gouge as the starting material. The experiments test the feasibility of experimentally densifying gouge by hot pressing, and constrain the effects of T, axial differential stress (σ) and experiment time (t) on densification efficiency, rates and mechanisms. Our experimental conditions include $T \leq 900^\circ\text{C}$ (melting), $\sigma \leq 25$ MPa, and $t \leq 90$ hours. The physical properties of the experimental products will be compared to those of natural densified gouge, tying the results from the laboratory to the natural system. Initial results show an increase in sample shortening (axial strain (ϵ)) and shortening rate between experiments completed at 650 and 850°C (for the same t). This change in ϵ -t curves with increasing T suggests there is a second densification process, aside from mechanical compaction, at elevated T. We propose that this process is solid-state sintering.

Juliet Ryan-Davis, Judy Fierstein

Submission 531

Evidence for mafic magma injection associated with the high-silica rhyolite, postglacial plinian eruption at the Laguna del Maule volcanic field, Chile

Analyses of a suite of basaltic to andesitic comagmatic ejecta (bulk SiO₂ ~53–62 wt%) from the dominantly high-silica crystal poor rhyolite ignimbrite and airfall tephra of the rhyolite of Laguna del Maule (rdm, bulk SiO₂ ~76–77 wt. %) indicate mingling of two to three distinct melts just prior to eruption. Evidence for mingling is recognizable in hand samples and electron microprobe analyses of hornblende and olivine phenocrysts.

Laguna del Maule volcanic field is a long-lived Andean rear-arc system with a notably high number of postglacial silicic eruptions. Postglacial rdm primary deposits, exposed radially around Laguna del Maule, contain several types of denser cauliflower-shaped clasts. Clasts consist of olivine basalts, olivine + hornblende basaltic andesites, and hornblende andesites; all include plagioclase ±clinopyroxene ±minor phases. The ejected clasts, once considered accessory lithics but here recognized as comagmatic liquids, are volumetrically minor but are conspicuous throughout the otherwise wholly rhyolitic eruption—estimated to be ~20 km³ of pyroclastic material.

A narrow range of rhyolite composition and inclusion textures indicate that basaltic and andesitic liquids coexisted with rhyolitic melt but did not mix effectively. Rhyolite pumice clasts include chilled mafic enclaves with olivine that is chemically identical to the olivine found in basalt and basaltic andesite clasts. The rhyolite also uncommonly includes streaks of the third pumiceous, buff-colored hornblende andesite. Olivines (Fo_{78.5-80}) are virtually unzoned, and embayments and melt inclusions suggest undercooled crystallization. Hornblendes in basaltic andesite clasts are rounded, occasionally have reaction rims, and overlap in composition with those in the andesite, as well as with rare hornblende in the rhyolite.

Basalt textures provide evidence that the basalt was liquid when it came in contact with the lower temperature rhyolite. Rhyolite pumice adhering to the outermost crenulate surfaces of the basaltic clasts fills the outermost crenulations and vesicles, where there are thin (<1 mm) quenched basaltic margins. Vesicles in the cores of basaltic clasts are typically rounder and larger than sheared, finer, and fewer vesicles toward their outer margins. These textures indicate mingling of coexisting liquids that came into contact just prior to eruption, either as eruption-triggering replenishment(s) or as additional melts drawn into the conduit during ascent.

Hazel Rymer, Glyn Williams-Jones, John Murray, Pierre Delmelle, Kerry Reid, Guillermo Caravantes-Gonzalez

Submission 841

Precursors to the current activity at Masaya volcano, Nicaragua

Activity at Masaya volcano has been confined within the Santiago pit crater since 1772. Adjacent craters hosted earlier lava lakes and overflowed to produce extensive lava flows. The presently active crater complex is located within a large elongated caldera which is associated with 6-7 ka basaltic Plinian eruptions. In February 1994, there was an elongate 12 metre glowing open vent in the bottom of the Santiago pit crater, with strombolian activity. Between 1995 and 2015, apart from a few small isolated vent-clearing explosions, activity was restricted to passive degassing and magma was not visible. In December 2015, a lava lake became visible and it rose until April 2016, since when it has remained at about the same level. The lava surface, visible inside a vent about 50 metres wide, is in a constant state of rapid turbulent motion with continuous bursting of gas bubbles and ejection of spatter against the vent walls.

Over the period 1993 to the present, we have monitored ground deformation, microgravity, gas flux and sulphur deposition. We have found that against a context of overall long-term (1993-2015) deflation, there has been recent local inflation consistent with magma intrusion. The gas flux and gravity data show cyclic behaviour with an approximately 10-year period. After almost 10 years of gravity decrease with associated SO₂ flux increase (1993-2000), a period of relative stability was observed until 2010. Following this, a steady increase in gravity at points close to the summit craters as well as consistent increases in SO₂ flux has proceeded until the present time. Furthermore, a proxy for the environmental impact of this persistent activity can be gained from S deposition downwind of the craters and we have detected this as far away as the coastline.

This paper integrates the various geophysical data sets to provide evidence for internal magmatic processes and environmental impact which are much longer lived than the activity visible at the surface.

Ugan Saing

Submission 610

The first permanent Multi-GAS stations in Indonesia: monitoring hydrothermal gas emissions from Timbang and Sileri craters (Dieng Volcanic Complex, Central Java), May 2013 – March 2017

Dieng Volcanic Complex (DVC) is located in Dieng Plateau in Central Java, Indonesia. In this volcanic complex, there are more than 20 small Pleistocene to Holocene age volcanic craters and cones that cover an area of more than 6×14 km. The Dieng region of central Java is densely populated and is an important region for agriculture and tourism. Timbang and Sileri craters have been two of the most active craters in the last 10 years. Timbang crater is located in the western part of the DVC and Sileri is in the eastern part. The primary hazard from Timbang crater is the periodic expulsion of dense, ground-hugging gas clouds with lethal concentrations of CO₂. These gas clouds can travel >1 km downhill across major roads and cultivated agricultural land. Sileri crater features a ~50°C bubbling lake (pH ~6) that last had a phreatic explosion in September 2009. In order to supplement existing monitoring techniques (seismic, temperature, and pH of the crater lake, periodic discrete gas measurements), a joint CVGHM-USGS team installed two permanent, fully autonomous, telemetered Multi-GAS (Multiple Gas Analyzer System) stations at the rim of Timbang and Sileri craters in May 2013. Timbang station is equipped with a CO₂ gas sensor with a range of 0-30%, which draws sample gases out of the crater by a 60 meter-long tube. Sileri station samples plume gases and is equipped with CO₂ (0-5000 ppm), SO₂ (0-50 ppm), and H₂S (0-50 ppm) sensors, plus meteorological sensors (wind speed & direction, ambient temperature, pressure, relative humidity). Data have been collected continuously since May 2013 from Timbang crater. In spring 2013, Timbang crater experienced unrest and from the end of May 2013 to the end of July 2013 the concentrations of CO₂ emitted from Timbang vent often exceeded 30% (sensor saturated). From July 2013 to July 2014, the average CO₂ concentrations decreased gradually to 0.1-0.3% (ambient CO₂ value in the crater) and activity has remained low. The Sileri Multi-GAS has experienced intermittent power and telemetry problems, resulting in data gaps from 20 February 2015 to 27 July 2016. Activity, however, has been low and gas concentrations from the lake have been stable. Measured CO₂ is typically 390-500 ppmv and H₂S values up to ~7 ppmv have been recorded. SO₂ has not been detected. The gas data from Timbang and Sileri craters have shown us that both craters are in a quiescent condition at this time.

Genji Saito, Isoji Miyagi, Yoshihisa Kawanabe

Submission 93

Depth of the magma chamber of the Kikai-Akahoya caldera-forming eruption of Satsuma-Iojima volcano, Japan, based on petrological observation and melt-inclusion analysis.

Depth of a magma chamber is important information for understanding the eruption mechanism. Petrological observation of pyroclastic rocks and chemical analyses of melt inclusions were carried out in order to investigate depth of the magma chamber of Kikai-Akahoya caldera-forming eruption (7.3 ka, VEI=7) of Satsuma-Iojima volcano, Japan. Samples were collected from two pyroclastic units formed by the eruption; Koya-Funakura air-fall pumice deposit (KFA; 2-3m thick) and nonwelded Takeshima pyroclastic flow deposit (TPF; ~30m thick; Ono et al., 1982). XRF analyses indicate the pumices in the KFA have rhyolite composition (SiO₂=71-72 wt.%). The TPF also consists of similar rhyolite pumices and vitric ash, however the upper unit of the TPF contain andesite scoria (SiO₂=58-61 wt.%). Two-pyroxene thermometry applied to the pyroxene-pairs in the pumices and the scoria indicate magma temperature of 940-1009°C for the rhyolite and 1048°C for the andesite. Major elements, S and Cl contents of the melt inclusions (MIs) in plagioclases and pyroxenes in the pumices and the scoria were measured by EPMA, and H₂O and CO₂ by SIMS. Major element composition of MIs in the pumices and the scoria is similar to that of groundmass of them, respectively, indicating the melt entrapment just before the eruption. Rhyolite MIs in the KFA and TPF have volatile contents of 2.4-6.0 wt.% H₂O, 0.007-0.061 wt.% CO₂, 0.003-0.029 wt.% S and 0.073-0.171 wt.% Cl. The large variation in H₂O and CO₂ contents is not related to the major element contents. Comparison of the H₂O and CO₂ contents of the MIs with the solubility of H₂O and CO₂ in a rhyolite melt suggests that the variation could be caused by addition of CO₂-rich gas to the gas-saturated rhyolite magma at the pressure of 100-280 MPa. Dacite MIs in the andesite scoria in the TPF have 2.2-4.8 wt.% H₂O, 0.014-0.058 wt.% CO₂, 0.023-0.119 wt.% S and 0.070-0.118 wt.% Cl. The variation in H₂O and CO₂ contents of the dacite MIs could be caused by degassing of andesite magma with pressure decrease from 180 to 80 MPa. Our results suggest that the magma chamber was located at the depth of 4-11 km (assuming the density of crust of 2500 kg/m³) and CO₂-rich gas and andesite magma injected to the gas-saturated rhyolite magma in the chamber just before the caldera-forming eruption.

Flavia Maria Salani, Silvina Eugenia Luro

Submission 693

Stratigraphy and Geochemistry of Cerro Escorioso Volcanic Field, Miocene, Patagonia, Argentina.

The Cerro Escorioso Volcanic Field (CEVF) forms the basaltic magmatism, which covers an extension of 140 km² and developed in the extraandean Patagonia of Argentina, southwestern part of the Somún Curá Plateau. This sequence corresponds to the postume stage of the Neogene extensional volcanism in the area. Lavas outpoured over volcanic Mesozoic units as Triassic Garamilla Formation and Jurassic Lonco Trapial Group, Cenozoic volcanics of Sarmiento Group and Miocene acidic lavas of Pire Mahuida Volcanic Complex. Analytical determinations (K-Ar 17 ± 1 Ma and 14.3 ± 0.6 Ma) pointed to a Miocene age.

This basaltic field is the product of small centers, which correspond to very eroded or dismantled scoria cones, sometimes buried by lava flows, which make it difficult to study. However, seven vents have been identified, of which two have a good degree of preservation: the Cerro Escorioso and Cerro Negro (42° 14' 24.31" S; 68° 48' 41.96" W). The former stands out from the rest of the cones and it is one that gives the name of the field. Cerro Escorioso is the largest scoria cone, 34.5 m height, 764.5 m in diameter, with 13,10° slopes and show a well exposed sequence of decimeters to 1 m thick levels composed by lapilli and bombs accumulation. The levels exhibit a moderate to dense welding, and could originate clastogenic lavas. The effusive facies associated with the eruption centers are lava flows that extended far away from the vents.

The volcano stratigraphic study allowed distinguishing three types of basalts that correspond to three identifiable lithochemical units. At the base of the sequence, basaltic flows with olivine and clinopyroxene microphenocrysts, a groundmass composed by olivine, clinopyroxene and nepheline occur. These flows are followed by basaltic lavas with orthopyroxene nodules (with clinopyroxene and olivine coronae), showing intergranular groundmass composed by clinopyroxene, olivine and plagioclase. Finally, the basaltic lava flows at the top of the sequence are characterized by a mineral assemblage mainly constituted of orthopyroxene crystals with clinopyroxene rims, plagioclase, opaque minerals and glass, defining intergranular and intersertal textures. The stratigraphic position of each basaltic type matches from base to top with subsaturated basalts, saturated alkaline basalts and subalkaline lavas. These contrasting petrographic and chemical features suggest different sources and/or complex processes involved in the magmatic evolution.

Hillarie J. Sales, Martin J. Streck, William C. McIntosh

Submission 959

Spectacular co-eruption of crystal-poor rhyolite and Fe-rich andesite and its implication for mafic underpinnings to voluminous A-type rhyolites: The Wildcat Creek Tuff, eastern Oregon

The Wildcat Creek Tuff is a thin (≤ 5 m), rhyolitic to andesitic ash-flow tuff with a minimal extent of 1500 km² in Malheur county, eastern Oregon. The previously undated tuff yielded a single crystal (anorthoclase) ⁴⁰Ar/³⁹Ar date of 15.49 ± 0.02 Ma and thus is closely related to mafic and silicic volcanism of the Columbia River Province. The tuff texturally stands out by its high proportion of co-mingled mafic inclusions appearing as dark, scoriaceous, and phenocryst-poor components, and their proportion dictate bulk tuff compositions ranging from rhyolite (74 wt% SiO₂) to andesite (59 wt% SiO₂). Glass analyses confirm the rhyolite end member at 74-75 wt% SiO₂ and two more mafic members, one at 59-60 wt% and the other at 56-57 wt% SiO₂. Rare plagioclase and even rarer pyroxene phenocrysts with compositions clustering at An₆₀₋₇₄ and An₃₅₋₄₅, and Mg# of ~ 72 and ~ 60 , respectively, similarly suggest two andesitic magmas. The 60% SiO₂ member is the dominant andesitic component and has distinctly lower TiO₂ and CaO, slightly lower FeO*, but comparable Al₂O₃, MgO, and alkalis than the basaltic andesite. Compositional bimodality between rhyolite and andesite is indicated by the observed gap of ~ 14 wt% SiO₂ based on glass analyses.

Other ash-flow tuffs from eastern Oregon (Rattlesnake, Dinner Creek, Devine Canyon, and others) also erupted crystal-poor dacitic to basaltic-andesitic cognate components, but the high proportion in the Wildcat Creek Tuff seems unrivaled. The co-eruption of andesitic magmas with rhyolite implies that all magmas were tapped from a common reservoir. The proportion of intermediate magmas increased during the eruption(s) up to the point where nearly all deposited tuff material consisted of andesite. This is consistent with progressively deeper magma withdrawal, in turn implying that andesitic magmas resided below the rhyolites as discrete magma batch.

Wildcat Creek Tuff data argue against the interpretation that intermediate components of rhyolitic tuffs are sampling remelted crystal mush after extraction of rhyolites, and that rhyolites evolved from these by fractionation dominated processes. To the contrary, small negative Eu anomalies, normal Ba and Sr concentrations, and nearly aphyric nature are consistent with a large contribution of mixing between Wildcat Creek Tuff rhyolites and regional mid Miocene, Fe-rich, and crystal-poor basaltic andesite magmas that occur ubiquitously as lava flows.

Emily Salings, Gary Michelfelder, Shannon Rentz

Submission 1121

The Bloodgood Canyon Tuff, Mogollon-Datil Volcanic Field, New Mexico: Relic of Thermal Destabilization in a Crystal Mush

The Mogollon-Datil volcanic field (MDVF), located in southern New Mexico, is the remnant of extreme and punctuated volcanism over ~12 m.y. of activity. The Bursum caldera is the youngest of three nested calderas in the Mogollon Mountains in the western MDVF. Here we present data from a high-silica, large volume ignimbrite sheet associated with the Bursum caldera, the Bloodgood Canyon Tuff (BCT; 28.0 Ma; >1300 km³). Extensive mapping and regional studies by previous workers have provided a limited whole rock geochemical dataset and descriptions of the unit, but a detailed study had not been conducted. We present new whole-rock major- and trace-element analyses, Sr, Nd, and Pb isotope ratios, mineral chemistry, and petrographic textures to suggest an evolution model for the BCT. We suggest a model of assimilation and fractional crystallization of a dacite composition magma followed by the remobilization of a crystal mush by the upwelling of mafic magma at the peak of ignimbrite flare-up in southern New Mexico. Sanidine phenocrysts in the BCT record three crystallization periods through trace element concentrations and crystal size distributions. Thermal disequilibrium induced by an intrusion of high-temperature mafic magma initiated the eruption of the BCT, and remobilization of this mush mixed with rhyolitic composition magma lenses within the mush that interacted locally with the amphibolitic-composition crust. Further destabilization of the magma chamber initiated a trapdoor style collapse of the Bursum caldera and erupted most of the remaining eruptible magma.

Vincent Salters, Justin Mandeville, Peter Larson, Thomas Sisson, Michael Clynne

Submission 318

What do the magmas of Indian Heaven and Mounts St. Helens, Cascades Arc, have in common?

Recent geophysical studies of the subsurface of the Cascade Range near Mount St. Helens (MSH) have indicated the possibility of a zone with distributed melt in the lower crust east of MSH directly below the Indian Heaven (IH) volcanic field (Kiser et al. 2016). This is in addition to upper crustal magma pathways directly beneath MSH. Furthermore, the seismic contrast between crust and mantle directly beneath MSH is small. This lack of seismic contrast is interpreted as the presence of serpentinized (cold) mantle lithosphere, which would be a potential barrier for magma transport and further argue for eastward origin of MSH magmas which would then be below the IH volcanic field and indicate co-location of IH and MSH magmas (Hansen et al. 2016).

We present new trace element and high precision isotope data on MSH and the Quaternary IH to its east. We restricted our MSH analyses to rocks from the Castle Creek period (2200-1700 BP) as those encompass the entire range of magma compositions of the volcano. IH volcanism is diffuse with mostly basaltic and basaltic andesite lavas. Trace element compositions of all IH lavas show typical arc-like signatures with depletions in Nb, Ta, and Ti and enrichments in Sr (to 1200 ppm) and Ba (to 600 ppm) and U. IH lavas are LREE and incompatible element enriched, similar to MSH lavas. Few IH basalts have Sr, Ba and LREE enrichments that exceed the enrichments of the MSH lavas, but the trace element patterns of the two volcanic fields are very similar.

MSH and IH overlap in radiogenic isotopic (Sr, Nd, Pb and Hf) composition and are distinct from nearby Cascades magmas. For both MSH and IH the correlation between Nd and Hf-isotopic composition is poor while $^{176}\text{Hf}/^{177}\text{Hf}$ and $^{206}\text{Pb}/^{204}\text{Pb}$ are well correlated, overlap, and are distinct from nearby Mt. Adams. Preliminary

$\delta^{18}\text{O}$ data for IH olivines range from 5.0-5.7‰, which are lower than MSH lavas, which range down to 5.7‰. The trace element and radiogenic isotopes indicate that some of the IH and MSH magmas can have similar mafic parents, but that the more evolved magmas at MSH have a significant crustal influence.

References:

- Hansen, S. M., et al (2016). Nature Comm. DOI: 10.1038/ncomms13242
Kiser, E., et al (2016). Geology 44(6): 411-414.

Rebecca O. Salvage, Javier F. Pacheco

Submission 153

Seismicity associated with the ongoing (2014 to present) eruption of Volcan Turrialba, Costa Rica

After almost 150 years of quiescence, Volcan Turrialba (Costa Rica) showed signs of increased seismicity and degassing in 1996, culminating in a number of phreatic explosions in 2010. A more energetic phase of this eruption began in October 2014, which has resulted in the closing of the international airport near San Jose (SJO), approximately 50 km south-west of the volcano, on a number of occasions due to the presence of ash. The ongoing eruptive activity from Volcan Turrialba is dangerous to the population, industry and agriculture, particularly due to the emission of ash and fluctuations in gases and seismicity.

The characterisation of seismicity in volcanic settings is important for understanding the evolving magmatic system at depth, and can aid in forecasting attempts for different volcanic scenarios. Consequently, an automated detection and classification system of seismic events based on a Hidden Markov Model (HMM) is currently being implemented for events at Volcan Turrialba. The HMM is trained to detect different seismic events from the continuous seismic record and classify them according to their spectral and waveform characteristics. The training database contains over 2200 pre-categorised seismic events to which the incoming seismic data is compared. The automatic classification of events is a necessary first step for further analysis of the seismicity generated at Volcan Turrialba.

Some low frequency seismic events detected with the HMM at Volcan Turrialba show remarkable similarity to one another. The number of families of similar events varies each day: on some days there are a number of families; on others there are no similar events at all. These identified families are located at shallow depths beneath the active crater, suggestive of movement of fluid towards the surface. On some occasions, these similar seismic events have progressed into "drumbeats"; the systematic repetition of very similar events. The most recent drumbeat signal occurred on 27 January 2017, lasted less than 3 hours in duration and contained hundreds of events. Approximately 8 hours later, a small eruption with an ash plume of less than 200m above the crater occurred. Although drumbeats have often been thought of as a precursor to eruptions, most eruptions at Volcan Turrialba occur without their presence. We present a detailed insight into the seismicity at Volcan Turrialba and its connection with the current eruptive phase of this volcanic complex.

Sergey Samoylenko, Natalia Gorbach

Submission 431

Shallow magma chamber beneath Young Shiveluch volcano (Kamchatka): preliminary results of physical modeling

Young Shiveluch is the most productive andesitic volcano of Kamchatka with magma discharge rates of ca. 36 Mt/year, an order of magnitude higher than typical island arc volcanoes [1]. Characteristic feature of this volcano is small compositional variability of erupted magmas. About 60% of the Holocene tephra (42 of 60 major tephra units) are represented by amphibole-bearing andesites with silica content of 60-62 wt. % [2]. Recently erupted magmas (1964-2016) have similar composition [3]. These observations suggest that the Young Shiveluch magma plumbing system may be in a stationary or at least in quasi-steady state during the last ca. 10 ka and consists of a shallow magma chamber fed by more primitive magmas from depth.

Based on the available extensive tephrostratigraphical and volcanological background [2] and known petrological and geochemical data [e.g., 3,4,5] we attempted to estimate the volume and shape of the shallow Shiveluch magmatic chamber. We used orthogonal ellipsoidal coordinate system, which allowed us to estimate both the eccentricity and the volume of the chamber without adding unknown parameter of the feeding conduit radius. Our results suggest that the shallow magma chamber of Young Shiveluch volcano may have a shape of a flatten sphere with dimensions of 1400 x 3000 m and volume of ca. 8-12 km³. The chamber is located at the depth of ~ 5 km judging from petrological data. These results provide basis for further analysis of the Shiveluch volcano plumbing system and comparison with geophysical data.

This work was supported by the Russian Foundation for Basic Research (grant # 15-05-06640)

Referenses:

- [1] Melekestsev, I. V., 1991. Active volcanoes of Kamchatka. 1, 84-92.;
- [2] Ponomareva, V.V. et al., 2007. AGU Geophysical Monograph, 172, 263-282.;
- [3] Gorbach et al., 2016. Volcanol Seismol, 10 (6), 360-381;
- [4] Humphreys M. et al., 2006. Journal of Petrology. 47 (12), 2303-2334;
- [5] Ponomareva, V.V. et al., 2015. International Journal of Earth Sciences, 104, 1459–1482.

Richard Sanderson, Robin Matoza, David Fee, Matt Haney, John Lyons

Submission 733

Remote explosive volcanic eruption detection, location, and characterization using the EarthScope Transportable Array in Alaska.

The ongoing deployment of the EarthScope Transportable Array (TA) in Alaska affords an unprecedented opportunity to study explosive volcanic eruptions using a dense regional seismo-acoustic network. Active volcanism in the Aleutian Arc poses a risk to both regional and international aircraft. Infrasound monitoring has demonstrated utility for the detection of remote explosive volcanism, but previous studies have utilized relatively sparse networks of infrasound stations in comparison to the TA in Alaska. We are developing capabilities for the detection, location, and characterization of remote explosive volcanic eruptions in the seismic, infrasonic, and ground-coupled airwave regimes. Data used incorporate both that from the TA and additional regional networks such as those of the Alaska Volcano Observatory (AVO) and Alaska Earthquake Center (AEC). Here we implement a Reverse Time Migration (RTM) technique to locate explosive eruptions in Alaska, with a focus on the recent explosive activity at locally-unmonitored Bogoslof volcano (active since mid-December 2016). Numerous large eruptive events from Bogoslof provide a unique calibration dataset allowing experimentation and optimization of different RTM strategies. Tuning the RTM algorithm is key to its success, but many challenges exist such as varying signal durations and amplitudes, as well as the typical source-station distributions and most volcanic eruptions occurring outside the network. Our methods cater to both event detection using real-time data as well as scanning of data archives for detecting and discriminating volcanic and non-volcanic events. The TA's rich records of infrasound from volcanic eruptions allow comparison with plume heights derived from other instruments and may help constrain models on eruptive processes and improve future forecasts of ash dispersal.

Laura Sandri, Karen Strehlow, Jo Gottsmann, Alison Rust, Geoff Kilgour, Roberto Tonini

Submission 1072

On the occurrence of phreatic eruptions at Ruapehu: statistics and probabilistic hazard forecast for ballistics

Although phreatic eruptions pose a serious threat to people in crater proximity (as it has been recently demonstrated at Ontake and Etna volcanoes), they are often underestimated and have been comparatively understudied. The detailed eruption catalogue for Ruapehu Volcano in New Zealand provides an exceptional opportunity to study the statistics of the occurrence of phreatic explosions at a crater lake volcano.

In this view, we first performed a statistical analysis on this database, which suggests that phreatic events at Ruapehu tend to cluster in time. We argue that this may be linked to an increase in the heat flow during periods of a more shallow-seated magma column. According to Ruapehu's eruption catalogue, the average monthly probability for a phreatic explosion to occur is about 10%. However, the frequency of phreatic explosions is significantly higher than the background level in the years preceding magmatic eruptions.

Secondly, we combined the output of 60,000 clast-ejection simulations with a Bayesian event tree tool (PyBetVH), in order to perform a probabilistic assessment of the hazard due to ballistic ejecta in the summit area of Ruapehu, which is frequently visited by hikers and skiers. The resulting hazard assessment shows that the probability for the summit to be affected by a ballistic impact density potentially lethal to people within the next month is up to 6%. The hazard is especially high on the northern lakeshore, where the only mountain refuge is located.

We believe that our results contribute to quantify the local hazard due to ballistics, as well as to increase the general perception of hazards due to steam-driven explosions.

Kyohei Sano, Eiichi Sato, Keiji Wada

Submission 712

Oxidation state and outgassing process of obsidian lava inferred from microRaman spectroscopy

Silicic volcanism ranges from explosive to effusive. Understanding what controls in such activity is an important issue to explain the explosive-effusive transition. The recent observation on Cordón Caulle (Chile, 2011–12) revealed the explosive-effusive hybrid activity (Schipper et al., 2013) and the oxidation state in volcanic products have attracted attention to reveal the effusive-explosive transition during magma ascent, especially on viscous magma eruptions (e.g. Castro et al., 2014). The Laser Raman spectroscopy is expected to give information about micro-scale oxidation state based on the specification of oxide microlite and glass amorphous structure in volcanic rocks.

We can observe the red-colored oxidized obsidian mingled with black-colored obsidian at the Akaishiyama obsidian lava on Shirataki, northern Hokkaido, Japan. The mingled texture shows various contrasts and distributions on the hand specimen, and we can consider that such a various oxidation texture reflect the different mechanisms of outgassing process during the eruption. In this study, we used the microRaman spectroscopy to characterize the oxidation state in the obsidian, using a JASCO NRS-7100 Laser Raman Spectrometer with 514 nm excitation at Kobe University Research Facility Center for Science and Technology, Japan. We obtained the 2 types of Raman spectra of oxide microlites in red and black obsidians, respectively. Compared with referential spectra, we identified captured spectrum as magnetite and hematite. Based on the analytical results of microRaman Spectrometer and distribution pattern of oxidation texture, we reveal the formation process of heterogeneous oxidation textures during the eruption.

Cristian Santacoloma, Rosa Alpala, Oscar Cadena

Submission 801

FRACTAL DIMENSION CORRELATION (D2) AND GENERAL HURST EXPONENT (H) CALCULATIONS APPLIED TO NEVADO DEL HUILA VOLCANO SEISMIC ACTIVITY DURING 2007 – 2010.

Nevado del Huila volcano experienced an important increase in its activity between 2007 and 2010, exhibiting several stages in its behavior that led to two phreatic eruptions and a dome extrusion. Seismic activity displayed temporal variations in fractal dimension correlation. In several cases a decrease in fractal dimension correlation before main activity peaks was observed. This was related to a grouping behavior of the seismic activity to form clusters, which were linked to a dominant process within the volcanic system that is traceable. In all cases an important decrease in this coefficient after eruptions was obtained. This period of time was also characterized by changes in the Hurst exponent, which had a strong tendency in the eruptive process to be of statistical noise. This is because the system was dominated by processes like magma bodies ascending to the surface affecting the clustering of earthquakes and the degassing of the volcanic structure.

Fractal dimension; Hurst Exponent; Clustering

Damiano Sarocchi, Gamaliel Moreno-Chavez, Lorenzo Borselli, Luis Angel Rodriguez-Sedano, Brittany Brand, Nicholas Pollock, Roberto Sulpizio, Trevor Hawkins, Patrick Zrelak

Submission 971

Quantitative texture analysis through remote imaging and automated image analysis: A case study from Mount St Helens, WA (USA).

Quantitative texture analysis (QTA) is crucial instrument for the modern study of pyroclastic deposits. Using remote imaging and image analysis coupled with stereology, permit this analysis of granulometric texture in a complete, fast, automatic and accurate way. The method provides critical information regarding the fragmentation efficiency of an eruption, segregation and bulking processes, flow dynamics during transport, as well as flow directions and deposition mechanisms.

During last decades we developed a series of hardware and software tools dedicated to QTA, which provides optical granulometry data, morphological clast descriptors, and clast fabric information. The analyses are based on scaled images acquired remotely (by drones or telephotography) processed in order to extract the maximum information. The images, properly segmented, are analyzed with image analysis programs developed in our labs. Diverse texture parameters, including optical granulometry, clast morphology and grain shape fabric, are calculated. In all cases, the output information consists in localized data or thematic profiles and maps. All the developed software are freely available.

We will present an overview of our methods, and show preliminary analysis of the textural data collected during five campaigns at Mt St Helens where we applied QTA to study 40 m thick exposures through debris avalanche and pyroclastic flow deposits from the 18 May 1980 eruption of Mount St Helens (WA). Textural data obtained are used as complement to classic volcano-sedimentology information and, together, allows an integral study of each depositional unit. Such analyses show vertical and longitudinal variation along any of the depositional units and can be useful to decipher the complex depositional scenario. Fluctuation in texture parameters and changes in fabric indicators, suggest the mixing of different pyroclastic density currents, forced to diverge or merge due to the presence of debris avalanche hummocks along their paths.

May Sas, Noriyuki Kawasaki, Phil Shane, Naoya Sakamoto, Hisayoshi Yurimoto, Georg Zellmer

Submission 81

Developing high resolution analysis of $^{87}\text{Sr}/^{86}\text{Sr}$ in plagioclase using SIMS, and application to deposits from Okataina volcano, New Zealand

Plagioclase is an abundant igneous mineral that crystallizes over a large range of pressures and temperatures, is sensitive to fluctuations in intensive conditions, and records compositional variations during growth. Thus, it may be used to determine pre-eruptive conditions of magmas. Coupling elemental and textural zoning with isotopic compositions of plagioclase helps determine the degree of crustal contamination, identify the occurrence of magmatic recharge events, and ultimately decipher the processes that lead to eruption. Increasing the resolution at which isotopic compositions can be determined therefore improves our understanding of rates of magmatic change.

Current techniques utilized to determine Sr isotopic compositions in plagioclase include thermal ionization mass spectrometry (TIMS) and laser ablation multi-collector inductively-coupled plasma mass spectrometry (LA-MC-ICPMS). The precision of TIMS is unparalleled by other currently available techniques, but sample preparation, which includes microdrilling and chemical separation, is time consuming. While LA-MC-ICPMS allows for in-situ analysis of plagioclase, the diameter of ablation spots (commonly 100 μm) limits the size of crystal domains that can be analysed. Furthermore, major issues for all techniques include diffusion and averaging of Sr isotopes across the analysed region. To investigate the potential for improved resolution of isotope zoning, $^{87}\text{Sr}/^{86}\text{Sr}$ ratios were measured in plagioclase using a CAMECA IMS 1280-HR multi-collector secondary ion mass spectrometer (MC-SIMS) at Hokkaido University. Run conditions include $\sim 10\mu\text{m}$ in diameter $^{16}\text{O}^-$ primary ion beam (6 nA, 23 keV), mass resolving power ($M/\Delta M$) of 7,000, and 400 s total count time per spot. ^{85}Rb and $^{40}\text{Ca}_2$ were measured in order to determine contribution of interferences of ^{87}Rb and Ca dimers to $^{86}\text{Sr}^+$ and $^{87}\text{Sr}^+$. Anorthite from Miyakejima volcano, Japan, with homogeneous $^{87}\text{Sr}/^{86}\text{Sr}$ was used as a standard with average external precision of ± 0.0005 (2σ). Crystals from 3 rhyolite Okataina volcano deposits were examined, Kaharoa (0.7 ka), Rotoma (9.5 ka) and Rotoiti (45 ka). Generally, isotopic ratios decrease from core to rim in Kaharoa crystals, show slight variability in Rotoma plagioclase, and have variable trends in Rotoiti crystals. Future work includes improving analytical precision, locating additional natural plagioclase to use as standards (homogeneous $^{87}\text{Sr}/^{86}\text{Sr}$ and An70-30), and analysing compositionally variable crystals.

Yoichi Sasai, Makoto Uyeshima, Jacques Zlotnicki

Submission 112

Magnetic variations associated with the tilt-step events during the 2000 eruption of Miyake-jima volcano revisited

A new caldera was formed at the summit during the 2000 eruption of Miyake-jima Volcano, central Japan. It began with the collapse on the top and was finally built up until the August 18 largest eruption. During the caldera formation, the ground deformation called the tilt-step occurred once or twice a day. The velocity wave form of the tilt-step was the seismic VLP event with 50 seconds duration. Although the amplitude of VLP event was different one by one, its duration was always constant. Associated with the tilt-step events, the geomagnetic and electric field variations were observed. The magnetic change was an abrupt step-like one similar to the tilt-step itself, while the SP variation had a single wave form with 100 seconds duration. Two different models were proposed for the generating mechanism of the tilt-step, i.e. Kumagai model (Kumagai et al., 2001: a cylindrical piston entering into the magma reservoir) and Kikuchi model (Kikuchi et al., 2001: underground explosion of a vapor reservoir injecting fluids into the surrounding rocks). The total intensity changes were explained as due to the piezomagnetic effect accompanying the Mogi model. Forced injection of fluids produced the SP variation owing to the electrokinetic effect (Sasai et al., 2002; Zlotnicki et al., 2003). However, a new study on the cause of SP variation was presented by Kuwano et al. (2015), in which the fluid flow was induced within the poroelastic medium by the strain field of the tilt-step source. They employed the Kumagai model, which was approximated by a vertical tensile crack. Recently, we obtained the 3-component magnetometer data at two sites on the NE and SE slope of the volcano. Based on new magnetic data as well as a different idea on the tilt-step proposed by Kuwano et al., we reexamined our previous model for the magnetic variations. We found that the Mogi model cannot explain the observed D component variations, which were opposite in sign between the two sites. The 3-component magnetic data contain apparent changes due to the rotation of the sensor in the geomagnetic main field, which are of the same order of magnitude as the piezomagnetic changes. A vertical tensile fault is preferable as the source because the sensor rotation effect can explain the opposite sign of the D component.

Hisashi Sasaki, Shino Naruke, Tatsuro Chiba, Hiroyuki Yamada

Submission 636

Investigation and analysis of damage caused by lapilli fall during the eruption of Aso Volcano, Japan on October 8, 2016

We investigated and analyzed the characteristics of damage caused by lapilli fall during the eruption of Aso Volcano on October 8, 2016 in Japan. Lapilli fall arrived at a remote residential area more than 4 km away from the Nakadake crater of the Aso volcano, and damaged buildings and agriculture facilities. A windowpane and a screen door of the National Aso Youth Friendship Center (approximately 4.5 km northeast of the Nakadake crater) were damaged by lapilli of approximately 3 cm in diameter. According to the relative position of a hole on the screen door and collision trace of the windowpane, lapilli came flying from the north side. This direction of projection does not align with the direction of the Nakadake crater. It is suggested that this stone did not fly in direct ballistic trajectory from the Nakadake crater. The lapilli fall created a large number of holes on a polycarbonate board installed at the roofed passage connecting buildings of the National Aso Youth Friendship Center. Many holes were formed because the polycarbonate board was deteriorated by ultraviolet rays. Damage to more than 1000 solar panels was also confirmed in an area approximately 6.5 km northeast of the Nakadake crater. Furthermore, in the neighboring areas, holes were found in the vinyl film of a plastic greenhouse. It is important to investigate the relationships between the collision energy of lapilli fall and strength of glass and polycarbonate boards.

Hisashi Sasaki, Shino Naruke, Suguru Fujita, Ichiro Nagashima

Submission 1039

Techniques for probabilistic estimation of damage to buildings by ballistic projectiles

In Japan, damage to buildings by natural disasters is classified under complete destruction, large-scale partial destruction, and partial destruction. Authorized standards of building damage have been established for earthquakes, floods, and tornadoes, but there is no such standard for volcanoes. Some residential areas in Japan exist in the vicinity of volcanic craters. As such, buildings are more likely to be damaged when such volcanoes erupt. However, most studies on ballistic projectiles have not been conducted considering buildings in residential areas close to craters. In this study, we attempted to perform probabilistic evaluation of building damage caused by ballistic projectiles from phreatic eruption. Estimates of eruption probability, crater formation probability, distribution probability, and damage probability are necessary for the probabilistic evaluation. Therefore, eruption probability was estimated using Brownian passage time and Poisson distribution from a past eruption record. Crater formation probability was estimated using kernel density based on a past eruption position. The distribution probability of cinder was estimated on the basis of past eruptions for which the spatial distribution of ballistic projectiles have been researched well. Damage probability was evaluated for every wooden construction, steel-frame construction, and reinforced concrete construction using laboratory data on collisions from previous studies. Wooden and steel-frame constructions were found to be most vulnerable to penetration by cinder. In reinforced concrete construction, cracks, scabbing, and penetration of concrete boards occur. Damage to reinforced concrete constructions vary depending on the size and collision speed of ballistic projectiles. For a probabilistic evaluation of building damage by ballistic projectiles, we multiplied these probabilities, and illustrate the analysis results on maps using GIS.

Shin Sato, Masao Ban, Yuki Nishi, Teruki Oikawa, Seiko Yamasaki

Submission 158

Temporal change of magma plumbing system in flourish time of Zao volcano, NE Japan

The Zao volcano is one of representative stratovolcano in NE Japan, having about 1 m.y. eruption history. The activity is divided into six stages. The eruption rate reached maximum in stage three. We investigated this stage products to reveal the magma feeding system of the maximum eruption rate.

The products are divided into lower, middle, and upper units. These are mainly composed of piles of lava flows. Rocks of these three units are quartz bearing two pyroxene andesite, two pyroxene andesite, and two pyroxene basaltic andesite, respectively. All rocks belong to medium-K calc-alkaline series and have disequilibrium features showing magma mixing. The whole rock compositions of lower and middle units show linear trends in silica variation diagrams. In some diagrams, the trends of these units are different. These trends converge at silica-richer part, but diverge in silica-poorer part. The compositions of the upper unit plot on silica poorer extension of the middle unit trend. These data suggest new mafic magma started to ascent in the period of the middle unit. Phenocrystic compositions show different features among units. Histograms of Mg#s of opx and cpx cores show the unimodal distribution in lower and upper units, but the peak compositions are higher in upper (Mg# of opx, cpx = 70~74, 70~72) than in lower (Mg# of opx, cpx = 62~63, 67~68). In the middle unit, both peaks coexist. In terms of plagioclase, An-poorer and richer ones coexist in all rocks. An-contents of the richer ones are always around An90. Whereas, peak compositions of the poorer ones are An55 in the lower unit and An72 in the upper unit. Both peaks coexist in the middle unit.

Judging from the compositions, An-poorer plagioclases and all pyroxenes derived from felsic end-member magma and An-rich plagioclase was from mafic end-ember magma. Pyroxene thermometer calculations applied on Mg-lower and higher pyroxene pairs gave ca. 960 and 1030 degrees C. These data indicate new higher temperature felsic end-member was formed in the period of the middle unit. Repeated infusions of the new mafic magma converted the lower temperature felsic end-member of the lower unit to higher temperature one. In the period of the middle unit, both of lower and higher felsic magmas were involved in the mixing, afterwards the former was no longer active. Such transition of the plumbing system would reflect higher rate of the infusion of the mafic magma.

Eiichi Sato, Keiichi Fukui, Toshiki Shimbori, Kensuke Ishii, Tetsuo Tokumoto, Masayuki Maki, Masato Iguchi

Submission 225

Fine structure of volcanic ash plume observed by advanced weather radars

It is expected that polarimetric weather radars can obtain information about GSD (Grain Size Distribution) or PSD (Particle Size Distribution) inside volcanic ash plume. Generally, polarimetric radars transmit horizontal and vertical radio waves at the same time, and receive the backscattered waves, thus, we can get the ratio and the correlation coefficient of two components. We think these parameters are important for Quantitative Ash Estimation (QAE). On the other hand, fast-scan radars can get a 3D image of a volcanic ash plume in a moment. We believe that data obtained by fast-scan radars can contribute to clarification of volcanic ash plume dynamics.

Meteorological Research Institute (MRI) installed an X-band multi-parameter (polarimetric) radar (MRI-XMP) and a Ku-band fast-scan radar (MRI-Ku) near Sakurajima volcano, located in the southern part of Kyushu, and started observation from March, 2016. On April 29th, 2016, we successfully captured a volcanic eruption by MRI-XMP and MRI-Ku simultaneously. The maximum value of the correlation coefficient (ρ_{hv}/CC) which was observed by MRI-XMP is higher than 0.95, which is higher value than we thought. On the other hand, MRI-Ku captured vortices inside volcanic ash plume.

In this presentation, we will show the fine structure of the volcanic ash plume observed by these radars.

Acknowledgement

This work is supported by Integrated Program for Next Generation Volcano Research and Human Resource Development.

Keiko Sato, Yoshinori Takebe, Seiko Yamasaki, Hidenori Kumagai, Naoyoshi Iwata, Masao Ban

Submission 624

The noble gas isotope anomaly in the newest-stage products of Zao volcano, NE Japan

Noble gases have unique characteristics that they are rarely combined with other chemicals as their very stable nature. Because its main reservoir is atmosphere, their isotopic composition is well defined and believed to be uniform all over the world, i.e. insensitive to geological disturbance. Whereas, the chemical composition of igneous rock, magmatic processes, and eruptive condition affect to the noble gas composition. Hence, the noble gas isotopic ratios and abundances are powerful tool to study the magmatic and volcanic processes of eruption products.

The Zao volcano, one of the representative stratovolcanoes in NE Japan and has been active since ca. 1 Ma. The newest stage started at about 35 ka and dominated by pyroclastic rocks. These are divided into the Kumanodake pyroclastic rocks, the Komakusadaira pyroclastic rocks, the Kattadake pyroclastic rocks, the Umanose agglutinate, and the Goshikidake pyroclastic rocks. Their chemical composition ranges from basaltic andesite to andesite, belonging to medium-K, calc-alkaline series.

We have performed the K-Ar dating on these pyroclastic rocks and obtained 57-30 ka, 13 ka, and 5 ka ages for the Komakusadaira, the Kattadake pyroclastic rocks, and the Umanose agglutinate, respectively. Samples from the Komakusadaira and the Goshikidake pyroclastic rocks (bubbled and less-bubbled samples for Ar, Kr, Xe isotopes) and the neighboring hot spring waters (for He isotopes) were analyzed by standard noble gas analysis method using GVI-5400He in JAMSTEC. We also analyzed international age standard of Sori93B, Bern4B, HD-B1 and two domestic standards (YZ-1, ca. 227 ka, e.g. Takaoka, 1989; MZ-94, ca. 326 ka, Iwata et al., 2009) from Zao volcano. The He isotope ratio was calibrated by the Kaminoyama hot spring gas collected in 1983 (e.g. Hanyu and Kaneoka, 1987).

Kr and Xe isotope ratios of all samples are similar to the atmospheric ratio regardless of their much concentrated abundance, i.e. 10-100 times higher than the atmospheric value. The YZ and MZ94 show similar Ar feature in spite of the heavier noble gas concentration. The bubbled samples show higher initial $^{38}\text{Ar}/^{36}\text{Ar}$ ratios than those of less-bubbled samples. Preliminary result of He isotopic ratio of the water samples suggests some contributions of mantle component. We discuss the contributions of deep magma and the process which can explain the high Kr and Xe concentrations, and excess Ar.

Eiichi Sato, Kyohei Sano, Masami Izuho, Andrei V. Grebennikov, Keiji Wada

Submission 718

Internal structure and magma ascent process of obsidian lavas in the south of Kamchatka Peninsula, Russia

In the south of Kamchatka Peninsula (53.04N, 157.78E), obsidian lavas are exposed from north-northeast to south-southwest direction over 400 m. The cross-section of the obsidian lavas is divided into upper and lower parts. Each part is about 15 m thick. The internal structure of the upper part is divided into two parts. The surface part is composed of rhyolite lava (A) and the interior part comprises alternating pumiceous (C) and three massive obsidian layers (B, D, and E). On the other hand, the internal structure of the lower part consists of alternating pumiceous and obsidian layers. The obsidian layers are classified into at least three layers.

Typical structure of obsidian lava is thought to consist of an outer obsidian region and an interior rhyolite region (Cas and Wright, 1987; Stevenson et al., 1994; Sano et al., 2015; Wada and Sano, 2015). In general, the rhyolite has perlitic cracks in the glass and contains some amounts of crystalline materials, namely, spherulite and lithophysae, whereas the obsidian contains none of such features and materials. In the study area, however, the internal structure of the obsidian lavas is complex and different from the typical structure.

The obsidian rock samples were collected from the three massive obsidian layers (B, D, and E) in the upper part and from one obsidian layer (F) in the lower part. We estimated glass compositions and water contents of the four obsidian samples (B, D, E, and F). The glass compositions of B, D, and E are divided into three regions according to FeO contents and that of F shows the intermediate compositions between D and E. Water contents in the four obsidian samples are following; 0.52-0.54 [wt.%] in E, 0.33-0.37 [wt.%] in F, 0.04-0.18 [wt.%] in B, and 0.04-0.10 [wt.%] in D. The four obsidian samples are different in the glass compositions and water contents. Therefore, the obsidian lava in this region may be formed by ascent of heterogeneous magma in the conduit with the different chemical compositions and water contents.

Kate Saunders, Ester Jolis, Duncan Muir, Valentin Troll, Frances Deegan, David Hilton, Chris Harris

Submission 315

Petrogenesis of Sumatran Andesite volcanoes

Arc volcanism in Sumatra is characterised by a chain of dominantly andesite volcanoes that run the length of the island. Recent explosive eruptions at Sinabung, northern Sumatra have demonstrated the potential hazard that andesite volcanoes pose to local and regional communities, but only limited geochemical data if any exist for many of these volcanoes.

The genesis of andesites is a contentious topic with the debate surrounding whether melts are contaminated within the mantle or the overriding crust. Here we report major, minor and trace element, Sr-Nd-Pb-O-He isotopes of whole rock and mineral separates of 14 volcanoes along the Sumatra arc segment (from north to south Sinabung, Sibayak, Toba, Bual Buali, Sorik Marapi, Marapi, Talang, Kerici, Berang, Kaba, Dempo, Sekincau, Ratai and Rajabasa) to provide insights into andesite magma genesis and to better understand magmatic processes in the region.

Erupted lavas are generally porphyritic with plagioclase and pyroxene crystals as the dominant phases. Differences in degree of differentiation can be observed at each volcanic centre. Combined with the crystal rich nature of the majority of the samples, this observation indicates that fractional crystallisation was an important processes in the genesis of these andesites.

Little along arc bulk rock geochemical variation is observed. However, whole rock and mineral specific geochemistry reveals two groups of andesites: 1) a central and southern grouping and 2) a northern volcano group that commences north of Bual Buali. Andesites in the central and southern Sumatra region show dominantly mantle-like geochemical signatures. In contrast, those in the northern group show dominantly crustal geochemical signatures indicating that additional crustal processes are relevant in the genesis of andesites in northern Sumatra.

Theresa Sawi, Michael Manga

Submission 552

Revisiting Earthquake-Triggered Volcanic Eruptions

Analyses of global volcanic and seismic records since 1500AD have shown that explosive eruptions (VEI2 or larger) are preceded within days by nearby major earthquakes (M8 or larger) about four times more often than expected due to coincidence, suggesting that earthquakes can trigger eruptions (e.g., Linde and Sacks, 1998; Manga and Brodsky, 2006). We expand the definition of a triggered eruption to include the possibility of M6 or greater earthquakes within five days and 800 km of a VEI 2 or greater eruption. Removing pre-1964 records, we find ~50 volcanoes that at some point experienced a potentially triggered eruption and define these volcanoes as “sensitive volcanoes”. Within this group of sensitive volcanoes, normalized distributions of volcano-centric factors such as tectonic setting, dominant rock type, and type of volcano are practically indistinguishable from those of “insensitive volcanoes” (ones that have never had a triggered eruption). These distributions are almost indistinguishable from those of sensitive volcanoes in which the time of eruption has been randomized. The only notable difference between sensitive volcanoes and insensitive volcanoes is a shorter time interval between all explosive eruptions for sensitive volcanoes, indicating that sensitive volcanoes erupt more frequently. The potentially triggered eruptions do not show a magnitude-distance relationship expected from seismically triggered events, and eruptions are no more likely to happen in the days after than the days before the earthquake. These same analyses performed on the population of sensitive volcanoes using the original parameters (M8 or larger earthquake) but a longer span of time (post-1500AD) result in similar outcomes as with the extended parameters described above. The most statistically robust indication of triggered volcanism is a significantly higher number of explosive eruptions in the 1000 days following major earthquakes than in the 1000 days preceding them, a trend that only gets stronger as the data becomes more recent, and a finding that is consistent with results obtained from previous studies. We conclude that short-term seismically triggered eruptions occur less frequently than previously inferred.

Michael Sawlan

Submission 1238

Discrimination of magmatic and alteration signatures in Columbia River flood basalts provides new insights into their chemostratigraphy and petrogenesis

Accurate characterization of the original magmatic compositions of flood basalts is fundamental to interpretations of magma genesis, stratigraphy, and correlation across the extensive igneous provinces they form. Critical evaluation of the geochemistry of the Sentinel Bluffs Member (SB) of the Grande Ronde Basalt (GRB), Columbia River Basalt Group (CRBG), demonstrates that a mass-analysis methodology, similar to that routinely used in studies of weathering and soil formation, enables the identification of subtle and previously unrecognized low-temperature alteration, and thus the determination of primary magmatic geochemical compositions in rocks modified by secondary processes. This methodology, here termed "mass analysis", employs concentrations and ratios of immobile elements to show that alteration has resulted in the loss of rock mass due to mineral dissolution in anoxic groundwater. The methodology enables determination of the amount of mass change, quantitative correction of immobile-element abundances, determination of the composition of material transported from altered lava and, hence, calculation of the magmatic major-element composition of altered lava. Immobile-element abundances corrected for mass loss indicate that SB lavas have a high degree of homogeneity, which permits the identification and regional correlation of individual flows and flow packages. The methodology developed with SB lavas is applicable to other lavas of the CRBG and most likely to other volcanic provinces in which lavas have undergone long-term interaction with groundwater.

Mass-balance models, using magmatic SB compositions and accounting for stratigraphic constraints, indicate that $\leq 10\%$ Cpx+Pl fractionation played a dominant role in generating the chemical variations within compositionally distinct batches of SB magma. The SB chemical trends within magma batches are similar to those resulting from more extensive Cpx+Pl fractionation in fractional crystallization experiments on tholeiitic basalt at 0.7 GPa (Villiger et al., 2007, *J. Pet.*). This fractionation of SB magmas undoubtedly represents the last phase in a long differentiation history of these evolved (mg# 42-38) magmas. Chemical trends similar to those of SB lavas are observed in other GRB members, suggesting that that Cpx+Pl fractionation at lower crustal pressures is a process common to magmas of the CRBG.

Jennifer Saxby, Katharine Cashman, Alison Rust, Frances Beckett

Submission 317

From needles to plates: extreme volcanic ash shape and implications for ash dispersion modelling

The transport of particles in a volcanic ash cloud depends on meteorological variables and the physical properties of the particles. Particle shape affects fall velocity and therefore residence time in the atmosphere, which in turn determines atmospheric ash loading. This study investigates the relationship between particle shape and settling velocity where shape significantly deviates from the spherical standard used in most volcanic ash dispersion models.

Sedimentation schemes in dispersion models that do not approximate ash as spherical generally adjust drag coefficients based on a single shape factor, most commonly sphericity, the ratio of particle surface area to that of an equivalent-volume sphere. However, due to difficulties in characterising fine volcanic particles in three dimensions, a 2D measure is often used as a substitute. To evaluate published drag coefficients and shape factors, we have measured the fall velocity of idealised particle shapes over a Reynolds number (Re) range realistic for fine distal volcanic ash. The results highlight the accuracy of the Ganser (1993) sedimentation scheme compared to alternatives, and illustrate the sensitivity of the scheme to the accuracy of particle shape descriptors. Importantly, using a 2D shape parameter increases the mean error on terminal velocity from 19.2% to 32.9%, comparable to the mean error expected from modelling particles as equivalent-volume spheres.

As a case study, we have performed a detailed morphological analysis of 838 ash grains from three distinctive and widespread silicic tephra layers from Katla volcano in Iceland, known as the 'needle layers' for their abundant elongated grains. These ash particles have an average sphericity of 0.2 – 0.6, far lower than the range typically assumed for volcanic ash. Parameterising this shape in the atmospheric dispersion model NAME using the Ganser (1993) sedimentation scheme for non-spherical particles causes model particles to travel up to twice the maximum distance predicted using the spherical default scheme (White, 1974). This suggests a significantly greater maximum travel distance for extremely non-spherical ash particles. One consequence is that the default particle size distribution used operationally in NAME may need to be extended where shape is extreme, as larger particles will travel far enough to be important for long-range distal ash forecasting.

Micah Angeli Sayco, Maurizio Battaglia, Alain Bernard, Ma. Antonia Bornas, Edgardo Villacorte, Renato Solidum

Submission 715

Insights on Recent Ground Deformation of Taal Volcano based on continuous GPS Measurements

Six Global Positioning System stations around the active Taal Volcano caldera complex on Volcano Island (Philippines) detected an uplift event between December 2014 and May 2015. The greatest deformation was measured south of Main Crater Lake (MCL). The event preceded swarms of volcano-tectonic earthquakes (VTs) beneath Volcano Island. Along with seismicity, flux rates of CO₂ dissolved in the waters of MCL rose gradually, reaching saturation point by March 2015. Taal Lake's water level similarly increased. According to GPS observation data, Taal Volcano has slowly deflated since June 2015. Likewise, seismicity and water levels decreased to baseline levels by October 2015. Volcano deformation during this period of unrest is most consistent with pressurization of Taal Volcano's hydrothermal system rather than direct magma processes, in agreement with seismicity and gas monitoring. We modeled the continuous GPS deformation velocities to estimate the location, depth and volume change of the deformation source before and after the episode of unrest. We inverted the deformation velocities using an analytical model that assumes an elastic, homogeneous and isotropic crust.

Piergiorgio Scarlato, Elisabetta Del Bello, Laura Spina, Damien Gaudin, Jacopo Taddeucci, Tullio Ricci

Submission 1014

Exploring the variability of Strombolian explosions at Batu Tara volcano (Indonesia) using infrasound and high speed imagery

A field experiment was held in Batu Tara Volcano (Indonesia) in September 2014 aimed at studying its Strombolian eruptions dynamics. Using a combination of thermal images, acquired at 50-200 fps with an infrared (FLIR) camera deployed in direct view of the active vent, and synchronized acoustic signals acquired at 10 kHz with two broadband microphones (freq. range of kHz to 0.1 Hz), we analysed a sequence of explosive events recorded in a time interval of 28 hours. Thermal images characterization was performed by integrating the amplitude of the thermal images in a box above the vent, and then correcting for the background, obtaining a thermal amplitude signal variation over time. From this, 146 peak events were discriminated by using a trigger algorithm based on a percentile threshold of 20. Thermally characterised events show a broad unimodal distribution in terms of event duration, and a bimodal distribution of amplitudes. According to the different eruptive conditions, each explosion can be characterized by a single peak or by a sequence of pulses. The explosions were also discriminated according to their infrasonic features. Different families of waveforms were retrieved based on a cross correlation method. Some explosions are characterized by a first, high amplitude transient, with a first positive peak pressure followed by rapid dampening, typical of a Strombolian eruption, while others are characterized by an emergent signal. Such two distinct waveforms types are sometimes overlapping reflecting the variations in 1) the timing and ejection of large spatters and bombs, ii) the presence of secondary pulses, and also iii) the amount of ash involved. The different evolutions suggest that there are at least two repeatable explosion dynamics occurring in the conduit, with comparable gas overpressure, source depth and amount of gas involved.

Lauren Schaefer, Ben Kennedy, Marlene Villeneuve, Stefan Cook, Harry Keys, Graham Leonard, Art Jolly

Submission 609

Geotechnical characterization and numerical modeling of crater rim stability at Mt. Ruapehu, New Zealand

Lahars are among the deadliest of volcanic phenomena, having killed 40,000 people worldwide since the late 1700's. The active Mt. Ruapehu volcano in New Zealand hosts a 106 m³ lake in the summit crater, making it prone to lahar hazards due to the volume of water stored behind a narrow outlet dam. In 1953 and 2007, portions of the crater lake outlet dams failed and partially drained the lake to form lahars. To understand the hazard of future dam-break lahars, in which partial or complete collapse of the crater lake outlet dam occurs, it is necessary to understand the geotechnical characteristics of the material currently composing the outlet dam. This includes characterizing prehistoric lavas and breccias and historic tephra, and evaluating the response of these materials to different loading conditions. For this study, materials comprising the outlet dam were sampled and analyzed using rock and soil physical and mechanical laboratory tests to determine porosity, permeability, strength, and stiffness. The challenge of characterizing the strength of a brecciated and poorly lithified deposit, considered to be the weakest material at the outlet dam, is discussed. These geomechanical characteristics were used to model the stability of the outlet dam under different instability triggers such as lake level change and seismic loading using limit equilibrium and finite element modeling. Response signals from local and regional earthquake events sourced from nearby stations were used in a Newmark stability analysis to determine critical slip surfaces and displacements for different sized input events. A sensitivity analysis of the material properties was also conducted to analyze the effects of hydrothermal alteration and weakening of the material over time. Our modeling indicates that major volcano-tectonic earthquakes could result in failure of the outlet dam, leading to drainage that could lower the crater lake up to 4 m. We plan to expand this work to the whole lake-filled crater to determine the boundaries for size and triggering of failure beyond the outlet area. Engineering-focused studies such as these can reveal the influential variables in volcanic stability, the forces required for volcanic material to fail, and the size and direction of possible mass flows.

Janet Schaefer, Katherine Mulliken, Cheryl Cameron, Kristi Wallace

Submission 677

Digitizing Alaska's ashfall record: a tephra geospatial database

Tephra studies are vital in understanding the frequency and magnitude of volcanic eruptions and are a key component of volcano-hazard assessments and a multitude of interdisciplinary studies that rely on tephra deposits as time-stratigraphic markers. Information on tephra deposits in Alaska is distributed amongst hundreds of publications that span numerous research disciplines. In order to streamline tephra occurrence data, these disparate publications have been compiled into one comprehensive geospatial dataset within the Alaska Tephra Database module of the Alaska Volcano Observatory's (AVO) Geologic Database of Information on Volcanoes in Alaska (GeoDIVA).

We have digitized tephra deposit geospatial information for more than 120 published resources, including peer-reviewed articles, reports, and theses/dissertations, which includes ~40 eruptions from ~20 volcanoes in Alaska. Fields in the geodatabase include source volcano, eruption identification number (allowing these data to be linked to existing tables in the GeoDIVA eruption database), deposit name, deposit age, deposit thickness, isopach and isomass contours, bibliographic reference, and a description of what was digitized (bibliographic reference figure number, figure scale, figure caption). Once complete, we intend to distribute this data through a web-based interactive map interface, freely available to the public.

Jenny Schauroth, Fabian Ben Wadsworth, Bettina Scheu, Jeremie Vasseur, Katherine J Dobson, Donald Bruce Dingwell, Yan Lavallee

Submission 906

Sealing off outgassing pathways: Fracture healing timescales resolved by sintering obsidian under surface tension

Highly silicic volcanoes can undergo rapid switches between explosive and effusive eruption styles. Fractures in magma are believed to act as the primary pathways through which volatiles outgas during eruptions. The opening or sealing of these fractures may contribute to changes in eruptive style. Tuffisites and tuffisitic breccias, ubiquitous in obsidian, are likely to represent the preserved record of these outgassing channels and are filled with a pack of variably deformed clasts and sintered ash. The timescales of tuffisite sealing determine the efficacy and duration of local outgassing events, and are dependent on the physics of sintering and welding of the fracture fill.

Here we use a combination of experimental techniques to estimate fracture healing timescales. We performed isothermal sintering experiments of obsidian clasts and ash using optical dilatometry in a regime where surface tension dominates over buoyancy forces. We used crushed obsidian from Hrafninnuhryggur (Krafla, Iceland) packed into free-standing cylinders with a known initial inter-particle porosity. We then tracked the continuous evolution of the sample volume during sintering and closure of the pore network. We finally used X-ray computed tomography with sub-micron spatial resolution to assess the porosity at various sintering stages. The final porosities experimentally obtained are compared to natural fracture healing textures from Hrafninnuhryggur.

During sintering, the powder cylinders densify due to porosity loss until volume equilibrium beyond which no further porosity loss was observed. At this point (i.e., a critical percolation threshold porosity) the pore network transitioned from a connected pore network to isolated bubbles suspended in the samples. Upon further temperature increase these isolated bubbles started to expand in volume. The percolation threshold porosity represents the critical transition to a non-outgassing system and we therefore parameterize the temperature-dependent timescale required to reach this point. We propose that the tuffisite sintering timescales explored here are relevant to the outgassing timescales at obsidian forming volcanoes.

Stephen P. Scheidt, Jacob E. Bleacher, Christopher W. Hamilton, Patrick L. Whelley, William B. Garry, Joana Voigt, Sarah Sutton

Submission 924

Anatomy of streamlined volcanic islands using multi-view stereophotogrammetry, Kilauea volcano, Hawaii

Flows of either lava or water have been inferred on the surface of Mars based on the occurrence of sinuous and anabranching channels as well as the occurrence of streamlined islands. Streamlined islands identified in planetary image data typically have teardrop shapes in planview. Examples have been identified in many locations associated with the Tharsis Volcanic and Elysium Volcanic Provinces. Streamlined islands are frequently interpreted as the products of erosion by the overland flows of water due to its low viscosity and erosion potential. However, some long basaltic lava flows on Mars could suggest high rates of effusion and/or low viscosity of the lava, which could produce similar streamlined landforms due to interactions with high-standing topographic obstacles such as tumuli, knolls, or impact craters.

We conducted fieldwork in Hawaii on the December 1974 lava flow to produce digital terrain models (0.5–10 cm/pixel) of five volcanic streamlined islands (ranging from 5–50 m in length) using multi-view stereophotogrammetry from ground-based and aerial photography. We present in detail the shape, texture and facies associated with five streamlined islands and use these terrestrial analogs to help establish a baseline for testing hypotheses of fluvial versus volcanic origin of similar landforms on Mars.

Based on our observations of constructional features in terrestrial lava flows, it is clear that the presence of streamlined islands alone are not indicative of erosion, and additional geomorphic evidence must support that interpretation. For example, the presence of fluvial bedforms, depositional bars, and/or cut bank erosion would support a fluvial interpretation, where lobate flow margins, platy surfaces, and lava high stands (i.e., "bathtub rings") would indicate volcanic processes. Subsequent aeolian or fluvial activity can easily modify or entirely obscure these geomorphic details; therefore, it is critical to conduct the "outcrop" scale analyses enabled in high-resolution data.

With high-resolution datasets such as Mars Reconnaissance Orbiter CTX (6 m/pixel) and HiRISE (0.3 m/pixel), it is possible to observe supporting geomorphic indicators (e.g., shape and texture) to correctly distinguish between hydrodynamically streamlined islands formed by water erosion and teardrop-shaped constructional features formed by the emplacement of lava around high-standing obstacles.

Bettina Scheu, Cristian Montanaro, Donald B. Dingwell

Submission 851

Phreatic & hydrothermal eruptions: Insights into energy budget and eruption dynamics based on field and laboratory studies.

Phreatic and hydrothermal eruptions are amongst the most common and most diverse eruption types on earth. Heating and/or decompression leads groundwater or hydrothermal fluids to rapidly flash to steam triggering these types of eruptions. Their diversity and complexity arises from the variety of (1) rock types and host rocks that can be involved, (2) ways to seal possible degassing pathways, (3) alteration type and degree of rocks involved, and finally (4) P-T-t conditions possible. In addition phreatic and hydrothermal eruptions are very difficult to predict in terms of timing and magnitude bearing important consequences, especially in densely populated regions or popular hiking / recreation destinations. Despite of their hazard potential, phreatic and hydrothermal eruptions have been understudied in volcanology compared to their magmatic counterparts. Recent violent eruptions as for instance the 2012 Upper TeMaari eruption (NZ) and especially the 2014 Ontake eruption (Japan) spotlighted this eruption type and triggered various studies, combining for instance field and experimental approaches.

Here we present conclusions from several case-studies, representing weak to violent eruption behavior. Further we give insights into the effect of host rock lithology and alteration on the eruption likelihood and dynamics. Field studies revealed insights into the eruption dynamics, for instance based on detailed mapping of the deposits and or the ballistic strew field of a hydrothermal eruption. The main lithology types identified for an eruption were characterized for their petrophysical properties and degree of alteration. Then these lithology types were used for rapid decompression experiments mimicking hydrothermal explosions under realistic P-T conditions (from 110 °C & 0.3 MPa up to 400°C & 25 MPa). Experimental studies of this kind facilitate better constraints on the eruption dynamics as for instance the ejection of ballistics or amount of ash produced and their associated hazard. Furthermore they shed light on the energy conversion and partitioning during hydrothermal explosions. Such field and experimental studies provide an important step towards a realistic estimation of hazards posed by phreatic and hydrothermal eruption.

C Ian Schipper, Jonathan M Castro, Ben Kennedy, Jack Whattam, Hugh Tuffen

Submission 937

Multiple obsidians, multiple fates: Textural variability in co-erupted effusive and explosive products at Cordón Caulle (2011-12, Chile)

Eruption styles and the processes that drive them are often described in binary terms, such as: explosive versus effusive or closed-system versus open-system. Recent observations of complex eruptions and modern tools for scrutinizing eruptive products are now demonstrating that the lines between endmember processes are fuzzy. The 2011-12 eruption of Cordón Caulle volcano (Chile) provided an exceptional example of hybrid explosive-effusive eruption dynamics, and the opportunity to study a representative suite of the resulting products. We present a textural (by μ -CT) and volatile (H₂O and Cl by FTIR and EPMA) content analysis of ballistic bombs and lava that were co-erupted, and investigate the dynamic and heterogeneous processes of conduit flow and degassing that led to the production of each. Bomb textures cover the complete spectrum of vesicularity: from dense obsidians through to pumice, although whole bombs made up of these endmembers are rare. Most common are composite bombs, comprising different proportions of rewelded ash, pumice, and obsidian, that ultimately foamed and breadcrusted en masse as singular heterogeneous entities during eruption. We discuss a common origin for both dense and foamed composite bombs, formed by in-conduit fragmentation and annealing of variably degassed melt domains in the portions of the conduit that fed explosive blasts. Conversely, textural evidence for in-conduit brecciation is more nuanced in the lava, suggesting that it formed from a more continuous melt body, with the caveat that evidence for brecciation and annealing was overprinted during flow emplacement. For the flow to have been emplaced simultaneously with the bombs implies dramatic and traceable variability in flow dynamics and melt coherency across a relatively small conduit cross-section. We highlight the vast variability in flow conditions that can exist within a single conduit, the perils in equating closed-system degassing with explosivity, and the importance of accounting for multi-parameter heterogeneity in explaining complex hybrid silicic eruptions.

W. Kirk Schleichfarth, Mary Reid, Michael Cosca

Submission 1300

The Central Anatolia Volcanic Province: Spatio-temporal constraints on an evolving tectonic and magmatic province

The time progression of volcanism in the Central Anatolian Volcanic Province provides essential constraints on the timing of transtensional basin development, propagation of fault activity, changes in deformation style in the region, and the migration of mantle melting. Previous work identified several volcanic lineaments and recognized the distribution of volcanic centers along regional transtensional fault zones. However, poor constraints on the inception and duration of volcanism throughout the province have inhibited detailed tectono-magmatic models. Strategically-selected samples from the Central Anatolia Fault Zone yield >20 new $^{40}\text{Ar}/^{39}\text{Ar}$ ages that help constrain the inception of volcanism at several individual centers and for the entire province. Coupling these new ages with a comprehensive compilation of published radiometric ages enables us to formulate a tectono-magmatic model. We find that all of the volcanic centers of Central Anatolia occur in lineaments that are associated with either the Tuz Golu Fault Zone or the Central Anatolia Fault Zone and the basins they developed. Three distinct time-progressive lineaments are observed, each migrating from the north and northeast towards the south and southwest: (1) Tuz Golu Basin volcanic centers migrated from Kekikalesi (predecessor to Hasandag) at ~ 8.3 Ma towards the southwest through Pliocene time, synchronous with migration of deformation in the basin; (2) The Derinkuyu Basin volcanic centers initiated in the north near the source of the Cappadocian ignimbrites at ~ 10.5 Ma and migrated south across the basin and along the Golludag Fault through early Pliocene time, synchronous with the proposed timing of basin development and fault activity; (3) The inception of Sultansazligi (Erciyes) Basin volcanism along the Central Anatolia Fault Zone began at Tekgozkopru at ~ 10.4 Ma and migrated along the western margin of the basin towards the SSW through early Pliocene time during a major shift in the kinematics of this fault zone. The apparent time progression of volcanic activity in Central Anatolia suggests that volcanic activity and crustal deformation are intimately linked in Central Anatolia. We suggest that removal and steepening of the complex and torn African slab towards the SSW led to asthenospheric upwelling, mantle melting, and corresponding migration of volcanism.

Tyler Schlieder, Kari Cooper, Richard Bradshaw, Adam Kent, Christian Huber

Submission 729

Quantifying thermal history for the 1980-86 and 2004-05 eruptions of Mount St. Helens, USA

The processes involved in the formation and storage of magma within upper crustal reservoirs is of fundamental importance to volcanology, and yet the physical and thermal conditions governing magma storage and remobilization remain poorly understood. We report new ^{238}U - ^{230}Th - ^{226}Ra disequilibria data and trace-element diffusion timescales from the Mount St. Helens (MSH) 1980 cryptodome and 2004-5 dacite domes. These timescales are interpreted in light of previously collected U-series isotopic data to quantify pre-eruptive thermal conditions of magma storage (i.e., thermal history) within the MSH magma reservoir.

U-Th-Ra data imply significant compositional and age diversity within the crystal cargo sampled during both the 1980-86 and 2004-5 eruptive episodes, with isotopically distinct crystal populations sampled by lavas erupted less than one month apart. Crystal heterogeneity is further supported by elevated plagioclase ($^{230}\text{Th}/^{232}\text{Th}$) relative to the host glass within one sample which can only be explained by a significant foreign (i.e., antecrystic or xenocrystic) plagioclase component. Preservation of ^{230}Th - ^{226}Ra disequilibria in all measured MSH samples, excluding one 2004-5 dome, is consistent with some portion of plagioclase crystallization occurring less than 10 ka. However, low plagioclase ($^{230}\text{Th}/^{232}\text{Th}$) for all 2004-5 eruptive products require a component of old plagioclase greater than 10 kyr old. Conservative estimates for the proportion of the old component entrained in 2004-5 dacites range from 25-40%. U-series analysis of 1980 cryptodome dacite is in progress.

Preliminary Sr-in-plagioclase diffusion timescales indicate MSH 2004-5 magmas spent 750°C prior to eruption (Bradshaw pers. comm.). When compared to a minimum crystal residence time of 10 kyr for the old plagioclase component, these data suggest MSH crystals involved in the 2004-5 eruptive phase have spent 50% (crystals) that experience rapid “defrosting” and accumulation of mobile magma shortly prior to eruption.

Advancing volcano seismology with large-N seismic arrays

Brandon Schmandt

Plenary Talk

Seismology provides key insights into the occurrence of rapid localized deformation and the large scale physical structure of magmatic systems. Observational strategies in volcano seismology are subject to tradeoffs between a small number of very high-quality long-term installations and a much larger number of lower-quality shorter-term installations. The former deployment strategy (small-N, long-term) has been dominant, which is pragmatic given the need to monitor the evolution of hazardous magmatic systems on time scales of years to decades. However, there may be increasingly important roles for the latter strategy (large-N, short-term) as volcano seismology aspires to reach higher levels of resolution and test hypotheses that have been raised with small network observations but are difficult or impossible to test without a change in observational scale. In volcanic settings without existing seismic arrays, it may also be advantageous to use short-term high-density arrays to optimally design or evaluate the need for long-term observatories. In the presentation, these perspectives on volcano seismology will be motivated by results from a 2-week deployment of ~900 cable-free geophones within ~12 km of Mount St. Helens in 2014. The large-N pilot experiment had the advantages of being embedded within a sparser long-term seismic observatory run by the USGS Cascades Volcano Observatory and the Pacific Northwest Seismic Network, and augmented by temporary passive and active source seismic arrays from the multi-institution iMUSH project funded by NSF GeoPRISMS. Capabilities of the dense geophone array for investigations of volcanic-tectonic and long period seismicity and structural imaging will be presented and used to identify potential strategies for future experiments. Strengths of the large-N geophone array include discrimination of surface and subsurface sources of long-period signals, evaluation of the relative contributions of source and path effects, and identification of low signal-to-noise reflected arrivals from controlled source explosions.

Mariek Schmidt, Alicia Thomas, Lucy Thompson, Ralf Gellert

Submission 504

Diverse igneous protolith contributions to sediments in Gale Crater: Implications for a variably metasomatised Mars mantle

Igneous float rocks and least altered sedimentary bedrock examined in Gale Crater by the Mars Science Laboratory (MSL) rover Curiosity provide insight to the petrogenesis of the crystalline basement. The MSL Alpha Particle X-ray Spectrometer (APXS) determines concentrations of an element suite that includes minor (K, P, Ti) and trace elements (Cr, Ni) of varying compatibility in basaltic melts, allowing petrologic modelling of igneous histories and character of the mantle source.

Igneous floats examined by the APXS include: 1) Jake M class (n=13) phonotephritic to trachyandesitic blocks and cobbles that likely derive from conglomeratic bedrock and are rich in Na and Al (up to 16.9% Al₂O₃) and low in Ni and Cr; 2) a basaltic, fine-grained cobble called Nova that is enriched in P₂O₅ (3.2 wt%); and 3) Pogy, a basaltic cobble with low K₂O and super-chondritic CaO/Al₂O₃, linking it to the SNC meteorites. Least altered basaltic sedimentary bedrock includes: 1) Bathurst Inlet class (n=13) comprising dark-toned potassic siltstone sandstone, to matrix-supported conglomerate of the Bradbury Group with enrichments in Zn and Ni (up to 4681 and 516 ppm, respectively) thought to reflect enrichment in the sediment source; and 2) Ronan class (n=19) comprising least altered, basaltic sandstone of the Stimson Formation with compositions similar to local soils, but more variable and ranging to lower K₂O and higher Ni. The CheMin X-Ray Diffractometer has identified mineral assemblages in the least altered sediments dominated by igneous minerals and an amorphous component.

The SNC-like composition of Pogy rock is consistent with ~5% partial melting of normal Mars mantle. Elevated K and compatible metals (Ni and Cr) observed in least altered basaltic sediments (Bathurst and Ronan classes) cannot be attributed to partial melting of typical Mars mantle. Instead, the character of the Gale mantle is likely alkali and Ni-enriched by an oxidizing metasomatic event. Both alkali contents and oxidation state are variable in the Mars interior.

The Jake M class and Nova demonstrate that Mars generates diverse evolved alkaline magmas. Variable alkali contents over a limited range in SiO₂ among Jake M rocks (4.1-7.1 wt% Na₂O, 0.7-6.0 K₂O/TiO₂, and 49-53 wt% SiO₂) are probably not a result of fractional crystallization of a single parental magma. More likely, Jake M rocks and Nova are a product of fractional crystallization of a range of parental magmas with variable alkali and P.

Anja Schmidt, Michael Mills, Steven Ghan, Jonathan Gregory, Richard Allan, Timothy Andrews, Andrew Conley, Piers Forster, Andrew Gettelman, Susan Solomon, Brian Toon

Submission 341

Current and near-future volcanic forcing of global climate change

To quantify the impacts of man-made climate change and the effectiveness of mitigation strategies it is essential to accurately attribute changes of surface temperature over recent and future decades not only to anthropogenic, but also to natural climate forcing agents such as volcanic eruptions. Here we use a volcanic sulfur dioxide emission inventory in a comprehensive aerosol-climate model to derive an improved time series of global-mean volcanic forcing since 1990. Our model simulations suggest that the widely used relation between volcanic forcing and volcanic stratospheric aerosol optical depth (SAOD) overestimates the forcing from 1991 Mt.-Pinatubo-magnitude eruptions by ~30% when aerosol-cloud interactions are considered. We calculate a time-mean global-mean volcanic forcing of -0.10 W m^{-2} during 2005-2015 relative to the 1999-2002 time-mean, attributed to a high frequency of small-to-moderate magnitude eruptions after 2005. An overestimate in near-term warming projections is identified when assuming volcanically quiescent conditions, which are statistically rarer than periods of frequent small-to-moderate magnitude eruptions. We will discuss how the climate modelling community could make near-term climate projections more consistent with the frequent occurrence of small-to-moderate magnitude eruptions and the expected low occurrence probability of large-magnitude eruptions such as 1991 Mt. Pinatubo.

Tobias Schmiedel, Olivier Galland, Christoph Breitzkreuz

Submission 471

The control of host rock strength on sill and laccolith emplacement: insights from quantitative laboratory models

Igneous intrusions in sedimentary basins exhibit a great diversity of shapes from thin sheets (e.g. sills, cone sheets), to massive intrusions (e.g. laccoliths, plugs). Presently, two distinct types of mechanical models exist to address the general mechanisms of magma emplacement in the brittle crust. On one hand, models for sheet intrusions consider “relatively low” (often neglected) viscosity magma into elastic rock. On the other hand, models for massive intrusions consider very viscous magma intruding into a weak plastic host rock. However, natural rocks are complex elasto-plastic materials, and field observations and seismic data evidence that both elastic and plastic deformation commonly accommodate the emplacement of magma. Therefore, none of the established models of magma emplacement has the capability to simulate the diversity of intrusion shapes.

In this study, we present new results of quantitative laboratory models of magma emplacement in the brittle crust. Our experimental series uses dry Coulomb granular materials of variable cohesion (= shear strength) as model host rock and molten vegetable oil, which solidifies after the end of the experiments, as model magma. In the models, a horizontal flexible net positioned right above the injection inlet represents a weak layer, along which the oil initially intrudes. We investigated the effects on magma emplacement through a series of experiments, in which we systematically varied: (1) the cohesion of the host, (2) the injection depth, and (3) the flow rate. We show that when the host rock is strong (high cohesion) and/or the overburden thick, the resulting intrusions are thin, flat-lying saucer-shaped sills, and their emplacement is dominantly accommodated by elastic bending of the host. Conversely, when the host rock is weak (low cohesion) and/or the overburden thin, the resulting intrusions are massive laccolithic plugs and their emplacement is dominantly accommodated by shear failure of the host. Our experiments also suggest that the emplacement of cone sheets is controlled by a combination of elastic/shear failure deformation mechanisms. Our experiments are the first that spontaneously simulate diverse, geological relevant intrusion shapes. Thus, we infer that accounting for the complex elasto-plastic behavior of the host rock is essential for unraveling the complex dynamics of magma emplacement in the Earth’s brittle crust.

Hans-Ulrich Schmincke, Mari Sumita, Deniz Cukur

Submission 887

A large-volume explosive basaltic eruption: The 80 ka Incekaya system in eastern Turkey

Subaerial and lacustrine deposits of the 80 ka Incekaya eruption within and outside huge Lake Van (eastern Turkey) represent one of the largest explosive basaltic eruptions known. Progression of onshore scoria cones along a 5 km fissure ended at the fault-bound lake shore with a >400m high hyaloclastite edifice (Incekaya Volcano) made up of lower crudely banked altered (unit A) capped by ca. 30 m bedded hyaloclastites (B). The lithostratigraphy of a 2 m onshore hyaloclastite section (VTTS) 13 km east of Incekaya is correlated in detail to a ca. 2 m bedded hyaloclastite unit drilled at intralake Site 2 (ICDP) 27 km N of Incekaya both thought to correlate to Incekaya unit B. The drilled hyaloclastite unit represents the most widespread seismic reflector (X) (>1,100 km², minimum volume ~1.5 km³) in Lake Van (>2 km³ tephra together with onshore sections). Seismic evidence for at least one 300 m intralake (hyaloclastite ?) cone plus a major seismically chaotic unit, on average 50 m thick and traceable seismically for a minimum of 250 km², immediately beneath reflector X, are interpreted as hyaloclastite mass flow deposits probably fed from the intralake continuation of the fissure. The total volume of hyaloclastites including (a) Incekaya cone, (b) the bedded intralake and onshore deposits, (c) the subaqueous cone(s) and (d) widespread intralake mass flow deposits is estimated as roughly 20 km³ (5 km³ magma). Interaction of voluminous and rapid magma supply and water >>300 m below present lake level above a rapidly propagating ca. 15-20 km long fissure were the dominating factors.

Olivine and plagioclase microphenocrysts, many skeletal, (203). Dominant S/SW wind directions are inferred from areal distribution of tephra layers but umbrella cloud dispersal is also suggested. Wet conditions are reflected in abundant accretionary lapilli. Absence of background carbonate varves within the 2 m drilled bedded hyaloclastite deposit indicate a short pulsating highly energetic eruption. Instantaneous deposition of a >2 m hyaloclastite blanket in the now densely populated coastal areas of western Lake Van would represent a significant hazard and risk and may have also been a major boundary in the regional and intralake biosphere evolution at 80 ka.

David Schneider, Michael Pavolonis, Alexa Van Eaton, Kristi Wallace

Submission 909

Characteristics of volcanic clouds from a water-rich eruptive process: Satellite observations of the 2016-2017 eruption of Bogoslof volcano, Alaska

Explosive eruptions that incorporate large amounts of water from oceanic, lacustrine or glacial sources produce volcanic clouds with distinctive characteristics that affect their properties in satellite images, fallout and dispersion, and generation of lightning. Bogoslof volcano in the Central Aleutian Islands began erupting in mid-December 2016. The vent(s) for most of the explosive events has been in the shallow ocean and/or a crater lake, resulting in entrainment of large amounts of water into the subsequent volcanic clouds. Through mid-March 2017 there have been 37 explosive events. Two-thirds of the events produced volcanic clouds that were visible in meteorological satellite data. The remaining events either produced clouds that were too small to be detected or were obscured by meteorological clouds. Volcanic cloud altitude varied from 5 to 11 km above sea level, and disrupted some air traffic, primarily to the city of Unalaska, about 100 km east of Bogoslof. As is typical for volcanic clouds from water-rich eruptions, the thermal-IR brightness temperature difference technique was poorly suited for discriminating volcanic ash. This is likely due to ice formation on ash particles, changing the spectral properties of the cloud. Two explosive events that showed no ash signature in satellite data produced ash fall that could be collected (the others dispersed over the ocean and remote islands), supporting the hypothesis that satellite-based discrimination of volcanic ash was masked by ice formation. Although both of these ash-fall events occurred during eruption sequences that likely transitioned from a submerged vent to a subaerial event (as interpreted from infrasound, seismic, and high spatial-resolution satellite data), neither cloud had a multispectral volcanic ash signal. The volcanic clouds were manually identified during eruption response primarily by their sudden onset, growth, temperature (i.e. height), and location over the volcano. Fourteen of the events were detected by the automated NOAA VOLCAT cloud-growth algorithm that identifies anomalous growth rate indicative of energetic explosive eruptions. Twenty-one of the explosive events were accompanied by volcanogenic lightning, further suggesting the presence of ice/hail in the eruption column. Scavenging of fine-grained volcanic ash due to ice formation complicated ash fall and dispersion modeling, as AVO's operational model is not designed for submarine vents or significant ice formation.

Dayana Andrea Schonwalder Angel, Fidel Costa Rodriguez, Rusell Blong

Submission 950

The atmospheric SO₂ budget emitted by the 'Tibito Tephra' eruption (middle 17th Century). Long Island volcano, Papua New Guinea

The Tibito Tephra eruption is considered to be one of the sixth largest eruptions of the last few hundred years. The most recent (unpublished) date of this VEI 6 eruption places it in the range 1640-1660 A.D. The deposits of this basaltic-andesitic (55.4 wt.% SiO₂) eruption covered an area of at least 85000 km² with a total tephra fall volume of at least 11 km³ [1]. Given the size of the eruption, and its mafic composition a significant amount of SO₂ could have been released to the atmosphere, in which case it should be recognizable in the ice cores records of Greenland and the Antarctic. We did a petrological study of the proximal eruption products focused on the determination of the S concentration of the interstitial glass and glass inclusions trapped in plagioclase and clinopyroxene phenocrysts. We found that the mean concentrations of interstitial glass is 0.041 wt% S (Std dev. 0.02) and the mean concentration in the glass inclusions in minerals is 0.068 wt% S (Std dev. 0.04). Mass balance calculation using the erupted volume and the difference between S concentration in the glass inclusions and the residual glass allowed us to identify that the Tibito Tephra eruption released to the atmosphere a minimum mass of S of 4.75×10^9 Kg. At present, we are unable to reconcile the known 'size' of this eruption and the newly determined S mass with any substantial S peaks in the Greenland and Antarctic ice core records.

[1]. Blong, R.J., *The Time of Darkness. Local legends and volcanic reality in Papua New Guinea*. 1982, Canberra: Australian National University Press.

Kevin Schrecengost, Kari Cooper, Philipp Ruprecht, Adam J.R. Kent, Christian Huber

Submission 1199

Storage and Rejuvenation of Large Homogenous Dacitic Eruptions: a case study from the 1846/47 and 1932 Eruptions of Volcán Quizapu, Chile

The thermal conditions of magma storage and remobilization are poorly understood; yet, they control the rheology and, therefore, affect eruption and mixing dynamics. Recent studies of smaller andesite-dacitic systems (eruptive products 3) suggest that magmas are stored at cool, near-solidus temperatures for long periods of time within a rheologically locked crystal mush prior to remobilization and eruption. Volcanic systems that produce large eruptive volumes may have magma storage volumes that are either maintained at higher temperature prior to eruption or have much higher thermal fluxes prior to eruption.

Volcán Quizapu, Chile is a basaltic andesite-dacite stratovolcano that has produced two of the largest historic eruptions in South America (1846-47, 1932; 4-5 km³ each). These eruptive products have been modeled as extracted interstitial liquids from a long-lasting homogenous andesitic mush at elevated temperatures and maintained by periodic recharge. Zircon U-Th crystal ages, Ti-in-zircon thermometry, and trace element compositions from 1846-47 and 1932 dacite provide additional constraints on the pre-eruptive thermal conditions and contrast with crystallization histories from Mt. St. Helens and Lassen Volcanic Center, which record more prolonged, heterogeneous crystallization histories and variable trace-element compositions that are inconsistent with crystallization within their host magma. Integrating zircon ages with plagioclase ²³⁰Th-²²⁶Ra ages show that zircon from both eruptions, while generally young (zero age to 26 ka; N = 29), significantly predate bulk plagioclase Ra-Th residence ages of 1-6 ka. Five zircons produce older ages (>125 ka). Zircon crystallization temperatures average 764°C (727-829°C), cooler than previously determined storage and eruption temperatures based on major phases. Dacitic plagioclase, predominantly An₃₀₋₄₀, require exceedingly wet conditions (≥7 wt% H₂O) to stabilize at such low temperatures, which are incompatible with water concentrations determined from amphibole (~4 wt% H₂O). If zircon crystallization is representative of long-term storage conditions, the eruptive products must have been reheated by ~40-230°C prior to remobilization and eruption, as required by Fe-Ti oxide thermometry. These observations suggest that major and trace phase crystal records are both spatially and temporally decoupled within the reservoir providing insight to the chemical, thermal, and physical architecture of the reservoir.

Hans F. Schwaiger, Kristi L. Wallace

Submission 1123

Forecasting resuspension of volcanic ash from the 1912 Novarupta eruption

The 1912 eruption of Novarupta-Katmai was the world's most voluminous eruption since the 1815 eruption of Tombora. Much of the proximal deposit remains un-vegetated and provides a source region for tephra to be resuspended in times of high winds and dry conditions, as is often the case in the autumn months. The Alaska Volcano Observatory (AVO) has logged a few dozen of these events since 2003, a few of which have produced ash clouds observed in satellite imagery extending a few hundred km downwind at altitudes of several km above sea level. There is growing concern for the potential hazards that these resuspension events can pose to both regional air traffic and air quality on Kodiak Island. To forecast these events, we have modified the USGS ash dispersion model, Ash3d, to include resuspension of ash deposits based on boundary layer meteorological conditions. For each of the few dozen events over the past 14 years, we have used the Weather Research and Forecasting (WRF) model to calculate meteorological conditions on a high-resolution grid (6 km regionally, 2 km over the deposit). Using the WRF output with the Ash3d forecast model, together with satellite retrievals of ash cloud load and height, we constrain the parameters of the resuspension source term. For a few of the recent events, we can verify the model using air quality measurements (PM10) from instruments we deployed on Kodiak Island. To bring this model into AVO operations, we use the high-resolution (5.9 km, hourly) North American Mesoscale (NAM) model from NCEP for the Alaska region to provide daily Ash3d forecasts of ash resuspension. The NAM meteorological model is evaluated for conditions favorable for resuspension (friction velocity > 0.75 m/s, precipitation rate

Florian M. Schwandner, Michael R Gunson, Charles E Podolske, Simon A Carn, Annmarie Eldering, Thomas Krings, David S Schimel, Hai M Nguyen, David Crisp, Christopher W O'Dell, Gregory B Osterman, Laura T Iraci, James R Podolske, Kristal R. Verhulst

Submission 119

Space-Borne Detection of Volcanic Carbon Dioxide

Remote sensing may help in the unambiguous identification of earliest signals heralding volcanic unrest: precursors that reflect deviation of magmatic systems from metastable background activity. Ascent and emplacement of new basaltic magma at depth may precede eruptions by weeks to months and transient localized carbon dioxide (CO₂) emissions have been observed weeks to months ahead of magmatic surface activity. Detecting such CO₂ precursors by continuous ground-based monitoring operations is unfortunately not a widely implemented method yet, save a handful of volcanoes. Detecting CO₂ emissions from space offers obvious advantages – however it is technologically challenging, not the least due to the increasing atmospheric burden of CO₂, against which a surface emission signal is hard to discern.

Singular continuous point source plumes from volcanoes and other point sources like power plants, turbulently mix into their proximal background fields. In contrast, plumes of aggregate point sources such as cities, and transportation or fossil fuel distribution networks, mix into each other and may therefore result in broader and more persistent excess signals of total column averaged CO₂ (XCO₂).

NASA's first satellite dedicated to atmospheric CO₂ observation, the Orbiting Carbon Observatory-2 (OCO-2), launched in July 2014 and now leads the afternoon constellation of satellites (A-Train). While continuously collecting measurements in eight footprints across a narrow (2-sensitive TIR imaging data (ASTER). This approach offers a path toward automating plume detections with subsequent matching and mining of OCO-2 data. We found several distinct singular source CO₂ signals. For aggregate point sources, we investigated whether OCO-2's multi-sounding swath observing geometry can reveal intra-urban spatial emission structures in the observed variability of XCO₂ data. OCO-2 data demonstrate that we can detect localized excess XCO₂ signals of 2 to 6 ppm against suburban and rural backgrounds.

Darin Schwartz, Dorsey Wanless, Adam Soule, Meghan Jones, Daniel Fornari

Submission 1237

Petrogenesis of Interisland Seamounts in the Galápagos Archipelago

The Galápagos Archipelago is an intraplate volcanic chain that consists of nine major islands on top a broad volcanic platform, which rises 3000 m from the abyssal plain to depths Alucia (8/2015) mapped and sampled seamounts in previously unexplored areas of the shallow volcanic platform. Seamounts that were sampled are from the central platform, between the islands of Santiago and Santa Cruz (N=11); the western platform, south of Fernandina Island (N=4); and the southern platform, west of Floreana Island (N=7). We analyzed major and trace element concentrations by XRF and solution ICP-MS on 105 basalts collected from 22 seamounts to determine if lavas from each region are related to a single magmatic episode. Homogeneity of trace element ratios at each seamount indicates that nearly all are formed from monogenetic basaltic eruptions (e.g., RSD of [La/Sm]_N at 19 seamounts N= 0.74-1.55 in Santiago, 1.4-4.9 in Floreana and 1.6-2.2 in Fernandina). Thus, we suggest that lava fields associated with the seamounts in the different areas are constructed over multiple monogenetic events. Seamounts from each geographic region have chemical characteristics that suggest linkages to the larger plumbing system of nearby islands. For example, extreme variability in [La/Ba]_N of seamounts in the Floreana region (0.50-2.4) is a characteristic unique to lavas erupted on that island. The compositional variability within and between groups of seamounts on the platform provides insight into the complex magmatic systems from which they are sourced.

Brad Scott

Submission 1204

Creating volcano activity catalogues from historic records; A case study from Ruapehu and Te Maari volcanoes, Tongariro National Park, New Zealand

The desire to better understand the hazards and risk to infrastructure and visitors to Tongariro National Park has resulted in several risk assessments. To make these as robust as possible the catalogues of eruptive activity also needed to be revised. This presentation brings to you a case study of the methodologies and results from revising the historic eruption catalogues for Ruapehu and Te Maari volcanoes in New Zealand. The new catalogues document over 700 days of eruptive activity whereas pre-existing catalogues only documented 60-100 days. Several previously unrecorded eruptions are now documented and we are more able to classify the styles and magnitude of eruptive activity and volcanic unrest; better relating them to impacts and risk. Risk assessments and calculations are now more robust. The problem of relating historic catalogues and geological records remains.

The delineation of volcanic hazards and the calculation of risk created by those hazards has become an important and powerful tool in the volcanology tool box. Detailed geological studies are improving our knowledge of eruptions preserved in the geological record, however the details of the historic activity are not always treated in the same detail. This is partially a consequence of these studies been conducted by other science sectors and the difficulty in accessing written and oral records. Eruptive activity catalogues if they exist are usually focussed on the stronger or more damaging phases of an eruptive episode, rarely do they record or use data about the lesser pulses of activity that accumulate to produce the phases and episodes.

Robust risk assessments require good input data sets as well as methodologies. The advent of digital data capture, of newspapers, government records, institutional annual reports and more general organisational records has created a new source of accessible and reliable data. Careful analysis of these records allows the creation of data sets about historic eruptive activity to a level of detail not previously possible. These data can be used to infill existing catalogues with data about smaller pulses of activity, capturing activity and sometimes anecdotal data on impacts.

Paul Segall, Sigrún Hreinsdóttir

Submission 86

Pressurization and Stressing of Magma Chambers with Viscoelastic Aureoles: Application to Grímsvötn volcano, Iceland

Elevated temperature surrounding long-lived magma chambers should lead to viscoelastic behavior of the surrounding crust, influencing surface deformation and conditions for eruption onset. We employ an analytical solution for a spherical magma chamber surrounded by a Maxwell viscoelastic shell in an elastic half-space, following a sudden decrease in chamber pressure from an explosive eruption. Mass flux into the chamber is proportional to the pressure difference between a deep reservoir and the chamber. In the no-recharge limit the system exhibits either post-eruptive deflation or, for sufficiently incompressible magmas, partial re-inflation. More generally, whether initial post-eruptive response is deflation/inflation depends on melt compressibility, and the ratio of Maxwell to elastic-refilling time. Short relaxation times delay recovery of chamber pressure to pre-eruptive values. In some cases, the pressure recovers before co-eruptive deflation measured at earth's surface.

Following eruption, radial stress in the shell decays monotonically, however hoop stresses, which are initially compressive, go through a local (relative tension) maximum. The magma pressure in excess of the dike normal compression at the chamber wall can recover to pre-eruptive values well before the chamber pressure or erupted mass recovers. This suggests that dikes could nucleate at the chamber margin well before enough pressure has recovered to drive them far from the chamber. For some parameters, co-eruptive deflation has not fully recovered when the overpressure is everywhere restored to pre-eruptive values, a condition assumed to be sufficient for eruption.

We apply the model to Grímsvötn volcano, Iceland, which erupted explosively in 2004 and 2011. Horizontal GPS data from a station 6 km SE of the vent are corrected for tectonic strain, and rotated into radial/tangential coordinates. The time series is truncated at the start of the 2014 Bárðarbunga intrusion. The data exhibit rapid re-inflation following eruptions, with time scales of ~ 1 month, followed by quasi-linear inflation. We conduct Markov Chain Monte Carlo estimation of model parameters, assuming a random walk covariance, consistent with the tangential displacements. Results indicate viscosity in excess of 10^{16} Pa-s, and require a relatively incompressible magma. The latter contrasts with inferences made during the 2011 eruption, and may indicate substantial degassing during, or shortly after, the eruption.

Kaori Seki, Takeshi Ohba, Shinnosuke Aoyama, Yuichiro Ueno, Hirochika Sumino, Wataru Kanda, Muga Yaguchi, Toshiya Tanbo

Submission 240

The isotopic values and chemical compositions from the the hydrothermal system beneath the Jigokudani Valley, Tateyama Volcano, Japan

Tateyama Volcano has an active solfatara field called Jigokudani Valley (JV). The JV was formed by repeated phreatic eruptions about 40,000 years ago. These situations are suggestive of the presence of a well-developed hydrothermal system beneath the JV because phreatic eruptions mostly occur within the hydrothermal system. The recent state of the hydrothermal system in the JV was clarified by the resistivity structure and the geochemical analyses of hot-spring waters (Seki et al., 2016), but comprehensive studies on volcanic gases have not been conducted for a long time. Therefore, it is necessary to examine the geochemistry of volcanic gases for a better understanding of the whole magma-hydrothermal system in addition to the hot-spring water analysis. Fumarolic gases and hot-spring waters in the JV were sampled at 7 sites and 12 sites in 2016, respectively. The measured fumarolic temperatures showed from 91.6 to 113.6 °C, most of which are higher than the boiling point of water in this area. We measured the anion concentrations and isotopic ratios ($\delta^{18}\text{O}_{\text{water}}$, $\delta\text{D}_{\text{water}}$, $\delta^{34}\text{S}_{\text{sulfate}}$, and $\delta^{33}\text{S}_{\text{sulfate}}$) of hot spring water, and the chemical compositions and isotopic ratios ($\delta^{18}\text{O}$, δD , $3\text{He}/4\text{He}$, $\delta^{34}\text{S}$, and $\delta^{33}\text{S}$) of volcanic gases. We found that the fumarolic gases containing HCl were discharged in the highly active geothermal area of the JV, where the compositions of the hot-spring waters showed high Cl^- concentration (~20,000 ppm). The fumarolic gases showing high $\text{H}_2\text{S}/\text{SO}_2$ ratios were sampled in the areas where the hot-spring waters were mainly composed of SO_4^{2-} containing almost no Cl^- and $\delta^{34}\text{S}$ showed low values. This indicates that SO_4^{2-} is derived from the oxidation of H_2S . $3\text{He}/4\text{He}$ ratios of the fumarolic gases were from 6.8 to 7.7 RA, which suggests that He is derived from the volcanic gas of magmatic origin. Comparison of the results of the geochemical analysis with the resistivity structure (Seki et al., 2016) indicates that all hot springs of the JV are formed within the depth of 500 m. Some of hot spring waters showed large time variations in $\text{Cl}^-/\text{SO}_4^{2-}$ concentration ratios. We inferred that these changes occurred by decrease of Cl^- concentration caused by the change in the temperature condition of the hydrothermal system. We will update the model of hydrothermal system beneath the JV in consideration of results of volcanic gas analyses and such time variations of hot spring waters.

Daisuke Sekine, Takeshi Hasegawa

Submission 1274

Eruption history and magma processes of pyroclastic deposits around Kamafusayama, southern Fukushima, Japan

Rhyolitic to dacitic Shirakawa pyroclastic flow deposits (SPfd) from early Pleistocene caldera volcanoes (1.51~0.92Ma) are widely distributed in the south part of northeast Japan arc. On the other hand, andesitic to basaltic Nasu stratovolcanic group (NSG) was formed and is still active since 0.54 Ma in this area. The Kamafusayama pyroclastic deposit (KfPD) has intermediate characteristics with respect to: 1) eruption age (0.59~0.41Ma), 2) distribution and 3) compositions (dacite to andesite) compared to the SPFD and NSG. Although clarifying the eruption history and magma processes of KfPD is essential for understanding the volcanism and magmatism in this area, detailed stratigraphy and the source area have not been clearly revealed. Therefore, we did a geological and petrological study to reveal the stratigraphy and magmatic process.

KfPD consist of alternative units of pyroclastic flow and fall deposit, which can be divided into two stages separated by a paleosol layer (Eruption Stage1 and 2, composed of 7 and 13 units, respectively). A debris avalanche deposit (KfDAD) was found at the top of Eruption Stage1.

Juvenile materials of KfPD consist of white pumice, gray pumice, scoria and banded pumice or scoria. Phenocryst minerals include Pl, Opx, Cpx, Opq, \pm Qtz. Major elemental chemistry of whole rock samples show andesitic to dacitic compositions ($\text{SiO}_2 = 57.4\sim 65.7$ wt%). On a plot of SiO_2 vs. K_2O , each eruptive stage forms a slightly distinct, subparallel linear trend that cross the boundary of Medium-K and Low-K. The existence of banded pumice, along with the linear trends of the eruptive stages on chemical variation diagrams, suggest that magma mixing was a common process in each stage of KfPD. The most mafic sample of KfPD has similar petrological features to eruptive products of Kashiasahidake volcano (the oldest volcano in NSG). Estimated composition of the silicic end-member with mixing lines of KfPD overlaps with the compositional field of the Ashino pyroclastic flow (one of the members of SPFD) on Harker diagrams. It can be considered that KfPD magmas were products from the mixing of those of Ashino pyroclastic flow and Kashiasahidake Volcano.

Stephen Self, Anne Jay, Loïc Vanderkluyzen

Submission 544

Physical characteristics of Deccan basalt lavas in the Central Western Ghats, India

A fairly robust, geochemically based, stratigraphy has been developed for lavas of the central parts of the Western Ghats, which provides some of the best exposures of the Deccan Basalt/Volcanic Group. This chemo–stratigraphy, which has been established for ~ 30 years, breaks the lava sequence into three sub-groups, from oldest to youngest, Kalsubai, Lonavala, and Wai. Each sub-group has been further divided into formations (fm), again based mainly upon geochemical criteria. We have logged, sampled, and provided geochemical recognition of representative sequences from each formation in order to study the physical characteristics of the lava flows constituting the formations. Various other workers have also examined parts of the same, but geographically, lava sequences. All formations examined so far are dominated by pahoehoe (phh) lavas, except for aa flows recognized in the Thakurvadi Fm (mid-Kalsubai Sub-group) NE of our main study region, and occasionally reported elsewhere. There is a spectrum of phh types, with end-members being small, non-inflated lobes in the decimeter to meter size-range up to inflated sheet lobes several km in length and up to 70 m thick. Rubbly phh flow-lobes are rare. The various fms are dominated by these phh types: the three lower formations of the Kalsubai Sub-Group show mainly small-phh flows but with some sheet lobes; Thakurvadi has small to moderate-size phh lobes arranged in thick packages (possibly eruptive units); the upper Kalsubai formations is sheet-lobe dominated in the study area. The lower Lonavala Sub-group formation (Khandala) is also composed of sheet-lobes but the upper one (Bushe) has both small phh and sheet-lobe facies, with the former being more common. The three large-volume fms of the Wai Sub-group are mainly composed of sheet-lobes. Limitations on interpretation such as lateral variability within an eruptive package are imposed by a general inability to correlate individual eruptive packages within a formation between adjacent locations (several to 10s of km apart). Also, with only a limited appreciation of source areas for the various formations, it is difficult to say if there are proximal or distal characteristics for the lava sequences, if such differences exist.

Sally Sennert, Erik Klemetti, Deanne Bird

Submission 426

Role of Social Media and Networking in Volcanic Crises and Communication

The growth of social media as a primary, and often preferred, news source has led to the rapid dissemination of information about volcanic eruptions and potential volcanic crises. This information comes from a variety of sources: news organisations, emergency management agencies, individuals (both public and official), and volcano monitoring observatories. Once posted, this information is easily shared, increasing its reach to a population much broader than more traditional forms of media, such as radio, television, and newspapers. The popularity of social media as a vehicle for dissemination of eruption information presents benefits as well as challenges, therefore it is important for organizations to develop and state their plans for social-media use. For instance volcano observatories might use official social media channels to distribute activity statements and forecasts, in addition to sharing images and data. We explore two examples of projects that collect/disseminate information regarding volcanic crises and eruptive activity via social media sources: the Smithsonian Institution/U.S. Geological Survey Weekly Volcanic Activity Report and the 'Eruptions' blog. Based on these experiences, recommendations are made to volcanic observatories in how to better use social media as a communication tool. These recommendations include: using social media as a two-way dialogue to communicate and receive information directly from the public and other sources; stating that the social media account is from an official source; and posting types of information that users want to see, such as images, videos, and figures.

Gilles Seropian, John Stix

Submission 1160

Monitoring and forecasting fault development at actively forming calderas: an experimental study

Caldera collapse events can be sudden and violent in the case of large explosive volcanic eruptions or incremental in the case of long-lived eruptions. Faults nucleating during collapse are associated with seismic hazards, but also potential economic resources. Yet the timing, location, and evolution of newly formed faults are poorly constrained. We conducted a series of sandbox experiments using a series of piezoelectric sensors to monitor stress perturbations during caldera collapse. We found excellent spatial and temporal correlations among (a) fault nucleation, inferred from the stress sensor data, (b) the appearance of faults on the surface, and (c) final fault structure, obtained via cross-sections. We estimated fault propagation rates for early inner faults, which scale with the evacuation rates. We applied our experimental results to seismic data from natural caldera-forming episodes in order to estimate rates of fault propagation for these systems. Our experiments are consistent with en masse caldera collapse events, such as at Katmai in 1912 and Pinatubo in 1991.

Winchelle Ian Sevilla, Christian Joseph Clarito, April Angelique Dominguiano, Allan Loza, Paolo Reniva, Juan Cordon, Lawrence Aaron Banes, Ricardo Seda

Submission 764

Imaging the seismic velocity structure under Taal Volcano, Philippines

Taal Volcano, one of the most active of the Philippines' 24 active volcanoes, is located inside a large fresh-water lake set within a 30 × 25 kilometer-wide caldera. This volcanic complex is part of the Macolod Corridor, a 40–km wide zone of active Quaternary volcanism and extensional faulting that crosses southwestern Luzon island in a N-S and NE-SW directions. To the west is the eastward dipping Manila trench with Wadati–Benioff zone dipping almost vertical down to ~250 km in the vicinity of the study area. This slab does not underlie the volcanic fields of the corridor including Taal Volcano, hence some studies attributed the source of volcanisms to rifting rather than the subduction process. However, isotope geochemistry studies on volcanic eruptive products indicate that the mantle wedge below the volcanoes are contaminated by slab–derived melts or slab–derived fluids or both. We conducted P-wave tomography study to image the subsurface velocity structure under Taal Volcano. Our aim is to map the magma source and storage region using travel time picks from the local seismic networks. Imaging the subsurface can provide critical constraints on the current status of the magma reservoir that can aid in evaluating the eruption potential of Taal Volcano.

Sarah Shallcross, Graham Mann, Anja Schmidt, Ryan Neely, Sandip Dhomse, Jim Haywood, Andrew Jones

Submission 519

The role of ash in the dispersion of the 1991 Mount Pinatubo plume: An observational and model intercomparison study.

Explosive volcanic eruptions are capable of injecting huge quantities of sulphur dioxide (SO₂) and ash into the atmosphere, which cause significant enhancement to the stratospheric aerosol layer and have complex effects on Earth's climate. Sulphuric acid aerosols, converted from emitted SO₂, and ash both act to reduce solar radiation reaching the Earth's surface through increased scattering, thus having a cooling effect. The magnitude of this cooling is dependent on the particle size distribution of the volcanically-enhanced stratospheric aerosol layer. Volcanic ash particles have restricted residence time in the atmosphere due to their larger sizes, hence the general belief that they have a negligible climatic effect.

Balloon-borne and aircraft measurements, following the 1991 Mount Pinatubo eruption, indicate that fine ash particles (diameters of 2.5-10 µm) can stay in the atmosphere for several months after eruptions. Ash particles have also been found in modelling studies to have a local, short-lived climate impact. This impact differs for eruptions at differing latitudes, but appears to affect the volcanic cloud itself and, therefore, its dispersion.

The UK Met Office United Kingdom Climate and Aerosol Model (UM-UKCA) is a composition climate model with coupled sulphuric chemistry and aerosol microphysics. Studies such as Dhomse et al. (2014) show good qualitative agreement with satellite data on the progression of the 1991 Mount Pinatubo aerosol plume to the Northern hemisphere. However, as is common with most other interactive aerosol models, Southern hemisphere transport is less well simulated compared to observations of SAGE II satellite Aerosol Optical Depth (AOD).

This study aims to investigate the role of fine ash in affecting the global dispersion of the 1991 Mount Pinatubo plume. This involves introducing a source of ultra-fine ash into UM-UKCA and comparing simulations with and without ash-sulphuric interactions against ground-based lidar observations from near-tropical, mid and high latitude locations through the post-1991 period.

Hannah Shamloo, Christy Till

Submission 1089

Petrologic Insights into the Timing and Triggering Mechanism of the Lava Creek Tuff Supereruption, Yellowstone Caldera, WY, USA

The Yellowstone caldera is infamous for its most recent supereruption ~630,000 years ago, which deposited >1000 km³ of rhyolite ash across the contiguous US known as the Lava Creek Tuff (LCT), however, little petrologic work has been done on the LCT. The aim of this study is to use LCT fallout ash to investigate the magmatic events that lead to eruption and over what timescale these events took place. The LCT fallout ash contains zoned sanidine and quartz phenocrysts with minor plagioclase and clinopyroxene and oxides along with lithic fragments and glass shards. Scanning electron microscope cathodoluminescent imaging of sanidine reveals three distinct populations; Pop. 1 has single thick (~200-600 μm) bright outermost rims and dark interiors; Pop.2 shows a more diverse zoning pattern with multiple bright and dark zones and thinner (~50-200 μm) outermost rims; Pop.3 are unzoned and nearly homogenous. Electron microprobe major element and NanoSIMS trace element analyses and feldspar-liquid thermometry performed on Pop. 1 and 2 sanidine (Or48-55) reveal hotter (~25°C) and Ba and Sr-rich, chemically less-evolved, outermost crystal rims relative to the crystal interiors suggesting the LCT experienced at least one rejuvenation event shortly before its eruption. Rhyolite-MELTS phase-equilibria modeling best agrees with the mineral compositions for a bulk water content of ~1 wt.% H₂O and a storage pressure of 3 kbar. NanoSIMS analyses reveal core-rim Ba and Sr concentration profiles of similar widths that require a formation mechanism dominated by crystal growth rather than diffusion, similar to that observed by Till et al. (2015) in Yellowstone post-caldera lavas. The slowest experimentally-derived sanidine growth rates (10-10 cm/s: Swanson et al., 1989) suggest conservative estimates of a few years to a couple of decades to grow the 50-600 μm Pop 1 and 2 sanidine rims after the rejuvenation and/or remelting of feldspar and mafic phases that chemically-altered the melt composition. Thus it seems likely that a reheating event contributed to the LCT's eruption in the years leading to the eruption.

Phil Shane, Victoria Smith, Sonja Storm, Axel Schmitt

Submission 102

Long-lived crystal mushes, short-lived eruptible magmas, and various crystal records: Okataina rhyolite volcano

Rhyolite magma systems are commonly thought to reside as a 'crystal mush' prior to eruption. However, the longevity of such systems and the transition to eruptible magma are poorly constrained and estimates vary greatly. This partly reflects differing growth and elemental diffusion rates, and closure temperatures for various minerals. At Okataina volcano, U-Th disequilibrium dating of zircon demonstrate crystallization over the last 300 ka. Age-depth profiling of individual crystals reveal prolonged growth (100 ka) that is commonly punctuated by hiatuses of up to 40 ka. The crystals have been periodically liberated from sub-solidus conditions or resorbed by thermal events. Overall, zircon temporal-compositional patterns became more diverse following the last caldera-forming event (~45 ka), reflecting the development of isolated melt bodies following emptying of the magma reservoir. During intra-caldera activity over the last 22 ka, some zircon growth was relatively continuous and there is a lack of signals associated with intervening eruptions. This reflects long periods of warm crystal mush buffered from change during eruption disturbances. A similar conclusion is reached from amphibole. The mostly non-zoned crystals record a range of temperatures (~700-900C) in all eruptions indicating the mush zone has a long-lived thermal gradient regardless of eruption tempo. Significant crystal transport and mixing must occur during eruption. Plagioclase growth is more responsive to rapid changes in melt composition, temperature and water content, but is difficult to directly date. Following the 45 ka caldera event, erupted plagioclase record frequent resorption and regrowth events associated magma recharge. A change to cooler, higher-SiO₂ magmas occurred in the last 25 ka. Erupted plagioclase record simpler histories comprising resorbed cores and rims formed during fractional crystallization. The overall pattern is consistent with redevelopment of an upper crustal magma reservoir. The concepts of long-term warm storage versus rapid remobilization from cold storage is strongly influenced by the intrinsic properties of the minerals being investigated. Neither rapidly nor slowly diffusing minerals provide the complete picture of timescales. The competing concepts of magma storage has implications for hazard assessment.

Thomas Shea

Submission 269

Probing olivine for chemical zoning and timescales: insights from crystallization experiments in natural basalt

Olivine is the go-to phase for a cornucopia of studies aiming to extract P-T-t information from the products of volcanic eruptions. Even though olivine has been the petrologist's drosophilia [1] for phase equilibria, crystallization and diffusion studies for decades, our understanding of its morphological and chemical development during crystal growth and diffusive re-equilibration has changed significantly in the last few years. It is now thought that olivine phenocrysts often start their magmatic journey as rapidly grown skeletal frameworks that then mature into faceted, polyhedral crystals with time. Such rapid, non-concentric growth changes the way in which we interpret zoning patterns in the major, minor and trace elements in olivine, and directly affects petrological applications that are based on element partitioning and diffusion.

To investigate how chemical zoning is acquired and modified during olivine growth, series of 1-atm crystallization experiments were performed using a natural Kilauea basalt (MgO=11.5 wt.%) as starting material. Charges seeded with loose olivine were heated to slightly above (1290°C) or below (1277°C) the liquidus for 24h, then cooled to final temperatures 1240-1270°C (undercoolings $\Delta T \approx 10-40^\circ\text{C}$) and left at these conditions for up to 4 days. Two types of crystals were obtained: crystals that nucleated and grew during/after the cooling step, and crystals that had residual cores from initial olivine seeds in addition to newly grown rims. The first type were used to examine the composition of olivine under rapid growth conditions, while the seeded crystals were used to characterize the diffusion behavior of Fe-Mg, Ni, Ca, and Cr. The important questions addressed by this study are: (1) Can olivine phenocrysts resembling natural crystals grow in a few hours? (2) Are the degrees of undercooling required to cause rapid, skeletal growth and the P-enrichment patterns observed in many natural crystals unrealistically high? (3) Does rapid olivine growth induce changes in element partitioning relative to slow, near-equilibrium growth? (4) Does rapid growth result in changes in rates of cation diffusion? (Cheat sheet: Yes, No, Yes, Probably). Solving these questions is critical in order to validate the use of olivine as a faithful time, pressure, and temperature capsule for volcanologists.

[1] Chakraborty (2008) Diffusion in solid silicates: A tool to track timescales of processes comes of age. *Annu Rev Earth Planet Sci* 36:153-190

Tom Sheldrake, Luca Caricchi

Submission 817

Tectonic and thermal controls on the magnitude and rate of eruptive activity at convergent margins

We present an analysis of eruptive activity in 15 volcanic arcs (total arc length analysed of 15,000 km) and explore how the architecture of subduction zones influences the magnitude of volcanic eruptions (M) and volumetric eruption rate (VER). To explore the role of the tectonic variables we complement the statistical analysis with thermal modelling of magma transfer through the crust. The results of the thermal modelling indicate that increases in crustal magma fluxes lead to an increase in both M and VER, which results in a systematic relationship between the two volcanic parameters. However, when the thermal model accounts for heat loss from the magmatic system, for constant magma flux the VER can decrease in time and the maximum value of M be limited. This is especially the case for reservoirs that are thermally inefficient, for example, where the diameter of the magmatic system and/or the inter-eruptive timescale is large. This competing behaviour between enthalpy accumulation associated with magma flux, and heat loss from the reservoir, is observed in the distribution of volcanic parameters and associated tectonic variables. In tectonic settings where the parallel component of subduction is low, enthalpy accumulation appears dominant over heat loss. Consequently, both volcanic parameters increase with crustal fluxes, which we interpret to be related to the rate of normal subduction and age of the subducting slab. However, where the parallel component of subduction is high, the role of crustal fluxes is muddied due to the poor thermal efficiency of magmatic systems in these tectonic settings. The influence of inter-eruptive timescale is observed in regions where magma fluxes are low but crustal thickness is large, in which the value of M is high but VER low. The combined analysis of tectonic parameters and basic thermal modelling allows us to unravel the fundamental relationships between the architecture of convergent margins and the characteristic rate and size of volcanic eruptions.

David Sherrod

Submission 695

Diamond Craters, Oregon: the transition of a Holocene subaerial dry eruption to phreatomagmatic

Basaltic phreatomagmatic eruptions commonly dry out as eruption proceeds. Causative factors include an exhausted supply of saturated shallow sediment, reduced aquifer supply or permeability, or shielding of the eruptive conduit by the heated aureole developed around the fissure. Conversely, an eruption may become phreatomagmatic when a fissure propagates into a water-laden environment, such as lake or ocean. But how might the change to phreatomagmatism occur if the geographic extent remains unchanged?

Diamond Craters lava field of southeastern Oregon, age about 7,500 cal BP, made the change after first producing 1.45 km³ of pāhoehoe lava. The stress field apparently changed suitably during the eruption that magma could migrate along a regionally prominent structural grain, injecting the lava field to create elongate endogenous antiforms (domes) 2-3 km in length on a WNW-ESE trend. Structural relief is as great as 120 m and injected volume, about 0.6 km³. Shallow magma injection, near or just below the sediment-lava field contact, is indicated by abruptly steepened ropy pāhoehoe surfaces along the dome margins. Crestal grabens crown some antiforms, whereas others are slivered by numerous gaping cracks. All the antiforms are dotted by collapse craters. Two craters, east and west Twin Craters, held their own small lava ponds.

In this setting the eruption became phreatomagmatic, blasting out unconsolidated sediment, bedrock blocks as large as 3 m, and juvenile basaltic ash (0.14 km³ tephra total, about half as juvenile magmatic component). The resulting deposit, as thick as 20 m near the central vent, thins abruptly toward the edge of the lava field 4-5 km away. The sequence of structural events, progressing back, is demonstrated by tephra burying the flat-floored collapse craters (tops of small lava ponds) that themselves are set in the tilted flanks of the young lava antiforms. Post-tephra eruptions were sparse, extruding scattered pāhoehoe pads whose volume is less than 1 percent of the total erupted volume.

Why the change? I propose sudden (hours to days) addition of water by a mechanism seen in 2010 in southeastern Oregon, when an unusually wet spring season filled an otherwise arid basin dammed by the lava. The drain in 2010 was an open crack in pre-Diamond Craters lava that was accepting water at rates in excess of 1,100 liters per minute, with nowhere to go but beneath the young lava, into the underlying shallow floodplain deposits of the Blitzen River.

Taketo Shimano, Masato Iguchi, Setsuya Nakada, Yuki Suzuki, Fukashi Maeno, Mitsuhiro Yoshimoto, Akhmad Zaennudin, Natsumi Hokanishi

Submission 75

Detection of transition in eruption style by spectrophotometric colorimetry of time-series ash samples during long-lasting eruptions

For forecasting and understanding the sequence of volcanic eruption, it is mentioned important more often than before to know eruptive materials continuously as well as geophysical data. Eruptions produce various types of materials of different grain size, shape, crystallinity, vesicularity, and chemical composition, probably reflecting eruption styles or processes at depths. Especially, long-lasting eruptions such as those at Stromboli and Sakurajima usually emit ash particles with different ratio of particles systematically reflecting changes in styles. But so far, the description of these materials has been a hard work to derive simple and immediate data continuously and sustainably to interpret, for instance, magma condition during the eruption. Here we used spectrophotometer to describe the color of ash samples in CIE L*a*b* system easily and sustainably for long term monitoring. We collected these data at several active volcanoes in Japan and Indonesia to derive a universal database.

The bulk ash samples have wide variations in color even among samples within a week, but the values, in terms of time-series data, change systematically with changes in dominant eruption style and also with some geophysical data. Microscopic investigation of ash particles indicates that the color change is due to changes in relative amount of vesicular, glassy, crystalline, and accidental particles. The colors also change with grain size even in one sample. Thus we also analyzed color by classifying into some size fractions and found that the finer the ash the brighter and more vivid the color.

Quantitative description of color enables also comparison among volcanoes. The database shows that similar major variation trends exist with positive correlation among L, a*, and b*. For example, long lasting activity with frequent explosions leads to L* (brightness) increase as a result of crystallization of microlites. Increase of black dense blocky particles by vulcanian explosions lowers these values whereas increase of glassy brown vesicular particles by strombolian eruptions raises the values. Vent enlargement results in higher b* value due to accidental particles. Thus, the database of the ashfall color would be useful for immediate assessment to monitor eruption styles.*

Hironao Shinjoe, Yuji Orihashi, Tomoaki Sumii

Submission 956

Boron and other trace element constraints on the slab-derived component of high-Mg andesite; implications for short-lived forearc magmatism in Miocene SW Japan

In Middle Miocene Southwest Japan arc, intensive magmatism occurred in the region closer to the Nankai trench than Quaternary volcanic front. Distribution of the igneous rocks of the magmatism is up to 800 km along arc, 150 km across arc directions, respectively. The Setouchi Volcanic Rocks (SVR) are one of the member of this forearc magmatism, and the existence of high-Mg andesite which can coexist in equilibrium with the mantle peridotite has been drawing attention.

We present a dataset of boron and other trace element contents for basalts and high-Mg andesites (HMA) obtained from the SVR. Most of elements were analyzed on XRF and ICPMS. Boron contents were determined by prompt gamma-ray analysis, and arsenic and antimony contents by epithermal neutron activation analysis using the research reactor JRR-3 of JAEA. In the previous geochemical studies on HMA and basalt, contribution of subducting sediment, particularly partial melt of terrigenous sediments to the magma source was discussed mainly based on their Sr, Nd, Pb isotopic compositions.

Analyzed samples show a large negative Nb and Ta anomalies, and enrichment of LILE and Pb, which are features of typical island arc volcanic rocks. Boron contents of basalts and HMA are highly variable (7 – 71 ppm). Trace element compositions of altered oceanic crust-derived fluid, sediment-derived fluid, and sediment melt are modeled, and resultant fluid mobile/immobile element ratios (e.g., B/Nb, Ba/Nb, Pb/Nb, and K/Nb) are used to examine slab-derived component to mantle source. Most of element ratios are explained by

Origin of the Miocene forearc magmatism in SW Japan arc is usually ascribed to the subduction of young hence hot Shikoku Basin of the Philippine Sea plate, because it was almost coeval with the initiation of the subduction of Shikoku Basin of the Philippine Sea plate, immediately after the opening of the Japan Sea and clockwise rotation of Southwest Japan. Tectonic implication of the slab melting is discussed along with review of recent radiometric dating results of Setouchi volcanic rocks.

Kei Shirai, Hiroaki Shiraishi, Satoshi Tanaka, Hideki Murakami, Jun Oikawa, Yoshiaki Ishihara, Masahiko Hayakawa, Takahide Mizuno, Ken Goto, Masanobu Ozaki, Kazuhiko Yamada, Ryuhei Yamada

Submission 105

Development of penetrator probe for volcano monitoring deployed from unmanned aerial vehicle

Currently the conditions to deploy an urgent monitoring system for volcano signal right after the onset of eruption are limited. The constraint is of concern for human safety in approaching to the volcanic activity, more likely as closest as possible. Our goal is to develop supplemental method that will allow to monitor volcano activities considering both volcanic surveillance and safety concerns capable to be deployed from an unmanned aerial vehicle (UAV).

To achieve this goal, we are developing a penetrator probe for monitoring the volcanic activity. The probe is designed to remotely operate for prolonged period of time (more than 3 months) in remote, acquiring data after penetrating into the ground dropped from fixed-wing UAV in a free-fall manner. Collected data as well as parameters for pre-processing of raw data and statics summaries will be sent and received as telemetry and command through the commercial Iridium satellite network system. Our prototype probe, with

We have tested components for this volcanic monitoring system onboard the penetrator probe will withstand the impact shock (speed to ground: 90 m/sec) through actual drop experiments of the probe at altitude up to 400 meters in the field using the UAV. We expect to complete this development and deploy this penetrator probe to Suwanose-jima Volcano, Ryukyu Islands (Japan) in mid/late-2017.

Stefania Sicola, Danilo Di Genova, Claudia Romano, Alessandro Vona, Sara Fanara, Kai-Uwe Hess, Donald B. Dingwell, Patrizia Landi

Submission 1053

Raman spectra of hydrous volcanic glasses: effects of chemical composition on water content estimation

Water is the most abundant volatile dissolved in silicate melts and strongly affects melt structure and properties, magma transport and eruptive style. Raman spectroscopy can give insight into the silicate structure, and water content of silicate melts. This technique presents several advantages such as: 1) high-spatial resolution; 2) non-destructive character; 3) minor sample preparation 4) detection of crystal phases; and 5) possibility of in-situ investigations at high temperature and pressure.

Several approaches to estimate the water content of silicate glasses (mostly iron-free) and melt inclusions have been presented based on internal and/or external calibration. Here, we discuss these different approaches using a wide range of chemical composition of glasses. We used 24 natural samples from basaltic to rhyolitic in composition and water content up to 4.5 wt% . By using two different Raman spectrometers we also explore potential instrumental effects in the quantification of water content and discuss the correct choice of the analytical procedure for spectra analyses. The proposed model takes into account chemical composition of the glasses, as well as variation in iron content and oxidation state. The presence of iron oxides at the nanoscale is also taken into account in the proposed model in order to make it suitable for natural systems.

Claus Siebe, Sergio Salinas, Lilia Arana-Salinas, José Luis Macías, James Gardner, Rosanna Bonasia

Submission 38

Popocatepetl's White Pumice Plinian eruption (~27,800 cal BP) and associated debris avalanche: Implications for hazard evaluations

Popocatepetl's White Pumice (WP) is one of the most voluminous Plinian fallouts produced in Mexico during the Late Pleistocene-Holocene. Its eruption ~23,500 14C y BP (27,800 cal BP) was triggered by the catastrophic failure of the SW flank of the volcano. The resulting debris avalanche reached 72 km from the cone with an apparent coefficient of friction (L/H) of 0.06. The deposit covers an area of ~1200 km² and has a volume of 10.4 km³. This gigantic landslide, characterized by exceptionally large hummocks (>400 m) provoked the sudden decompression of the hydrothermal and magmatic systems, which produced an initial lateral blast followed by the rise of a Plinian column that reached an altitude of ~33 km. The isopach map allows the recognition of a dispersal axis pointing toward the south, where an area of ~2490 km² was covered by >10 cm of pumice and ash. The total volume of the pumice fallout is estimated at ~1.9 km³ DRE. Pumice clasts are dacitic (62-66 wt.% SiO₂, anhydrous basis), highly vesicular (55-88 vol.%) and display a seriate texture with phenocrysts of plag + hbl + cpx + opx.

As the eruption progressed, discharge rates became intermittent and the height of the column fluctuated and finally collapsed, generating pumice-and-ash flows that were emplaced around the volcano. This short but intense activity was followed during subsequent years by rain-induced lahars that reached great distances. At the same time, more degassed andesitic-dacitic (61-65 wt.% SiO₂) magma was erupted effusively (4.4 km³, DRE) in the new horseshoe-shaped ~5 km-wide crater from which the Tochmilco lava flow descended toward the SSE, where it inundated an area of ~68 km² and reached ~22 km. Since then, multiple eruptions have reconstructed the summit cone, almost obliterating the horseshoe-shaped crater.

During the course of this catastrophic eruption (VEI=5) a total volume of ~6.3 km³ (DRE) of juvenile magma (pumice and lava) was emitted and an additional ~10 km³ of pre-existing rocks (debris avalanche) mobilized. It surpasses in magnitude most other known Plinian eruptions from Popocatepetl and can be envisaged as an example for a worst-case scenario for hazard evaluations. It dramatically changed the morphology of the volcano and had profound effects beyond its vicinity on the rivers draining the surrounding plains as well as on the lacustrine basin to the NE. A repeat of such an eruption in this densely populated region would cause a calamity of unprecedented dimensions.

Lee Siebert, James W. Vallance

Submission 249

LARGE-VOLUME EDIFICE FAILURES IN THE CASCADE RANGE OF SOUTHERN BRITISH COLUMBIA TO NORTHERN CALIFORNIA

The common global phenomenon of large-scale volcanic edifice failure with resulting catastrophic debris avalanches and debris flows is also prominent in the Cascade Range from southern British Columbia to northern California. Four dozen Quaternary collapse events in excess of 0.01 km³ have been recorded, with nearly two-thirds of these larger than 0.1 km³. Collapse deposits exceeding a cubic kilometer have taken place at volcanoes in Washington, Oregon, and California, with the Pleistocene collapse of Mount Shasta attaining a volume of ~45 km³ deposited over an area of 675 km². The vast majority of documented collapses occurred during the Holocene, in part reflecting potential burial of Pleistocene deposits. Seven events occurred in historical time; with the exception of the 1980 Mount St. Helens collapse, all were relatively small flank collapses (0.01-0.1 km³) at Mount Meager in southern British Columbia (most recently in 2010) and Mounts Baker and Rainier in Washington. Preliminary data suggest an average Holocene recurrence interval in the Cascade Range of about 250 years for ≥ 0.01 km³ collapse events and about 450 years for events ≥ 0.1 km³. Edifice failures in the Cascade Range most commonly involve collapse of the upper edifice and central conduit areas of steep-sided, glacier-clad stratovolcanoes, but they also include smaller-volume flank collapses and failures at a low-angle shield volcano, lava domes, as well as multiple large-scale collapses of Crater Lake caldera walls leaving deposits clearly identifiable in lake bathymetry. A half dozen or more Holocene events have occurred at Mounts Meager, Baker, and Rainier. Cascade Range volcanoes do not show a preferred failure direction as observed in some other volcanic arc settings. Failure style includes water-poor debris avalanches such as at Mount St. Helens in 1980 and Chaos Crags at the Lassen volcanic center about 300 years ago, but is dominated in the Cascade Range by wetter debris avalanches that transformed directly to lahars. Both syn-eruptive and non-eruptive collapse events have occurred. Long-runout debris avalanches and lahars from edifice collapses in mountainous terrain commonly form barriers at tributary drainages creating ephemeral lakes. Subsequent lake-breakout lahars are common at Cascade Range volcanoes, reflecting a significant secondary impact of edifice-collapse events.

Daniel Sierra, Francisco Vásquez, Marco Almeida, Daniel Andrade, Patricia Mothes

Submission 669

Characterization of lahar deposits corresponding to Cotopaxi Volcano's historical eruptions along the eastern drainage (Ecuador)

Cotopaxi is an active stratovolcano, located 60 km SE of Quito, capital of Ecuador. Due to the presence of a voluminous ice-cap and the volcano's closeness to several populated centers it's considered one of the most dangerous in the country. During historical times, Cotopaxi has presented at least 5 main eruptive cycles triggering major lahars descending through its three principal drainages: Pita (North), Cutuchi (South) and Tambo-Tamboya (East).

Northern and southern lahar deposits have captured the attention of researchers who have exhaustively studied them through decades. Despite the fact that eastern lahars could cause affectation on many human settlements, such as Puerto Napo, their deposits have not been properly described. Since this area was poorly inhabited in the past centuries, only few written reports can be found showing that the 1744, 1768 and 1877 eruptions affected it.

Once formed, those lahars crossed the eastern cordillera through narrow canyons where deposition is scarce. Finally, they spread out more than 100km downstream, upon the Amazon lowlands. As a consequence of this long transport, these lahars present a very different behavior and properties of those of the northern and southern zones.

Two different deposits were identified at the eastern lowlands; the younger one seems to correspond to the 1877 eruption, meanwhile the older one might correspond to one of the 18th Century events. Our team collected samples in the deposits of the proximal and distal zones. Then, chemical, granulometric and componentry analyses were performed. The analyses allowed us to characterize the deposit and gave us in a better understanding of flow, and its erosional patterns, particularly since clasts of Cordilleran metamorphic basement rocks are amply represented.

In addition, our fieldwork lead us to delimitate the inundation areas and estimate a deposit's volume. By stablishing a comparison between our results and those for the northern and southern area we expected to acquire a better knowledge of the eastern lahar's dynamics and the possible consequences of the occurrence of similar events on the future.

Olgeir Sigmarsson, Gaelle Mollex

Submission 981

Short magma mixing timescales before and during the Eyjafjallajökull 2010 eruption

How fast mafic and silicic magmas are mixed together and homogenized at depth is not well understood. The summit eruption of Eyjafjallajökull volcano, Iceland, 14 April to 23 May 2010 was preceded by approximately 300 days of excess volatile accumulation in a basalt beneath a silicic magma as inferred from ^{210}Po - ^{210}Pb disequilibria. A seismic swarm spring and summer 2009 corresponds in time with the initial volatile release at depth and formation of the mafic intrusion that stalled beneath the silicic magma body. The intrusion of evolved basalt, with an excess vapor phase, into a residual alkaline rhyolite coincides with a single larger earthquake at approximately 6 km depth the night before the summit eruption and after three weeks of relatively primitive alkali basalt ($\text{MgO} \sim 8\%$) flank eruption. The flank basalt brought up olivine, which melt inclusions and compositional zonation suggest basalt magma mixing on a timescale of a month. The explosive eruption on 14 April from the summit crater produced tephra with three glass compositions, namely the residual 1823 alkali rhyolite, relatively evolved and vesicular basalt together with variably mingled benmoreite glass. These three glass types were only erupted over the first three days during the initial explosive phase. The magma discharge rate decreased over the next two weeks, and its compositional range retracted over the first week from 50-71 to 57-60 % SiO_2 but only from 348-787 to 442-742 ppm for the slow-diffusing Zr. Deep seismicity started late 3 May, resulting in increased eruption plume height and the emission of tephra, early 5 May, with increased glass compositional variations (SiO_2 : 58-67%). That tephra contains olivine with primitive core (Fo80) and presenting Fe-Mg zonation down to Fo50 at the crystal rim. Both the olivine zonation and a Hopper-structure olivine reacting to hypersthene suggest a transfer time of approximately one day between the mafic recharge into the evolved magma and eruption. The glass compositional range decreased during the following days but increased again, a day after a mafic magma recharge as inferred from renewed deep seismicity (SiO_2 : 58-68%). These variability fluctuations of glass composition continued until the end of the eruption and were present in tephra that erupted a day after a deep seismic crisis. Taken together, after the initial phase when the magma system was being remobilized the glass mixing timescale was approximately a week.

Freysteinn Sigmundsson, Vincent Drouin, Michelle Brandsdottir, Stéphanie Dumont, Siqi Li, Andrew Hooper, Benedikt G. Ofeigsson, Sigrun Hreinsdottir, Halldor Geirsson, Pall Einarsson, Magnus Tumi Gudmundsson, Kristin Jonsdottir, Kristin Vogfjord, Saemundur

Submission 1176

Magma domain models of Icelandic volcanoes: Reconciling volcano geodesy with multidisciplinary constraints

We reevaluate how extensive volcano geodesy results at Icelandic volcanoes can be better reconciled with results from other disciplines, including geology and volcano history, seismicity, petrology and geochemistry, geothermal activity, borehole observations and drilling, gravity and electrical imaging of volcano interiors. The combined data is interpreted in terms of magma domain models, which we consider to represent the crustal volume hosting magma at a shallow level. It may be of variable size and shape, containing variable amounts of magma, melts and crystals and comprising magma bodies with variable connectivity. The largest signals due to magma transfer observed are within the Bardarbunga volcanic system during 2014-2015, where results from geodesy, seismicity, petrology and geochemistry fit an integrated model. About 2 km³ of basaltic magma drained from beneath the Bardarbunga caldera, at an inferred depth of about 10 km, during coupled caldera collapse of 65 meters, lateral dyking, and the largest effusive lava eruption in Iceland since 1784. However, the most extensive dataset in Iceland in terms of multiple constraints on magma plumbing is at Krafla volcano where all of the aforementioned constraints can be applied, including direct constraints from drilling into rhyolitic magma at 2.1 km depth. At Krafla caldera we interpret the data in terms of at least two magma bodies at shallow depth: (i) a basaltic magma body with a pressure center near the center of the Krafla caldera in the 3-5 km depth range, contributing to S-wave shadows and influencing seismic propagation, as well as being responsible for an inflation/deflation pattern during the 1975-1984 Krafla rifting episode, and (ii) a shallower body of rhyolitic magma with an upper surface at 2.1 km underlying the main geothermal area within the Krafla caldera. This rhyolitic body was inactive during 1975-1984, but also contributes to S-wave shadows. It has been drilled close to or into multiple times and is responsible for superheated steams near the bottom of several geothermal wells. During the rifting episode the shallow basaltic magma body received continuous inflow from a deeper magma body. Continuing work aims at resolving the magma bodies better, including further interpretation of electrical imaging considering the relative influence of alteration minerals compared to that of basaltic and rhyolitic magmas on the electrical signal, constrained by laboratory measurements.

Edwin Simbaña, Francisco Vásquez, Anais Vásquez, Ernesto Meza, Daniel Andrade

Submission 539

Evidences of the destruction of pre-Hispanic populations by lahars from Cayambe volcano (Ecuador) and implications for future eruptive periods

Since approx. 800 A.D. until Inca invasion in 1500, the Caranqui culture occupied the region where nowadays the city of Cayambe (Ecuador) is located. Their settlements expanded uphill along the western flanks of the Cayambe volcano, following the Blanco River, where agricultural land is most productive. Cayambe volcano, with several eruptions over the last 4000 years, must have posed many challenges to pre-Hispanic populations inhabiting this zone. The Blanco River is one of the main drainage systems of the volcano and, in case of an eruption, it is very plausible to assume that lahars flowed down the river and gravely affected nearby settlements.

The aim of this study was to prove this hypothesis by inspecting “La Remonta” area, which is located over the right margin of the Blanco River and which is currently being rapidly urbanized by the growing city of Cayambe. During fieldwork various lithic fragments made in obsidian and andesite (e.g. arrowheads, scrapers, splinters and millstones) and ceramics (pottery) were found within a lahar deposit. Most of the collected fragments are not indicative of a specific culture. Nevertheless, the absence of decorations, their smooth and simple surface, their thick walls (9-20mm) and carbon particles found within them suggest that they were of domestic use and that the population they were used by lived off of agriculture, hunting and aquaculture.

Some ceramic fragments with red paint and slip, and the specific shape of other elements are similar to one type of vessel that belongs to the first phase of the Caranqui culture (800-1250 A.D.). This finding allows determining a relative age of this destructive event, which could be most likely linked to the strong volcanic eruption of the Cayambe in 880 A.D.

In depth investigations of this archeological site, which would serve to retrace the exact location and extent of this Caranqui settlement, are currently impeded by rapidly growing agricultural lands and urban zones. Nonetheless, the findings of this study are very valuable to the community since they embody the hazard that could await settlements downstream of the Blanco River – taking into account that the Cayambe volcano has shown unrest since mid-June, 2016.

Jack Simmons, Ray Cas, Tim Druitt, Rebecca Carey

Submission 227

Precursors to explosive volcanic eruptions at Santorini caldera, Greece: perspectives from the geological record

Identifying the signals and predicting the eruptive behaviours that precede climactic explosive eruptions are essential for modern appraisals of volcanic hazard and risk. These signals, or precursor events, can be studied with a range of ground-based monitoring equipment (e.g., seismometers, GPS, COSPEC) and remotely with satellites (e.g., InSAR geodetic monitoring). Although these techniques are useful for studying the precursors to modern volcanic eruptions, only a narrow range of volcanic activity has been recorded since the inception of this technology. Pre-historic and early historic records, in the form of volcanic deposits, detail a more complete range of volcanic activity, including the precursors to major explosive eruptions. Deposits of the three largest rhyodacitic explosive eruptions at Santorini, in particular, record a combination of both simple and complex precursory phenomena. So-called simple precursor deposits, at the base of the 172 ka Lower Pumice 2 and 3.6 ka Minoan eruption sequences, record discreet, short-lived, low intensity explosive events that occur hours to days before the main climactic event. These precursor eruptions produced localised pyroclastic surges and/or small volcanic plumes (<10 km high) that deposited thin beds of rhyodacitic pumice and ash (up to tens of centimetres thick) at proximal locations to the vent. In contrast, the precursor deposits of the 184 ka Lower Pumice 1 plinian eruption are significantly thicker (tens of centimetres to several metres), more variable in composition (precursor pumice - dacitic and moderately crystal-rich vs. plinian pumice - rhyodacitic and crystal-poor), lithologically complex, widely dispersed and incipiently bioturbated. These deposit characteristics reflect pauses in eruptive activity and rapid transitions in eruption style (from magmatic to phreatomagmatic, and including pyroclastic fall, flow and surge events) in the months to years preceding the main explosive event, while small-scale faults, which terminate at the top of the complex precursor sequence, record a period of heightened seismicity. Research on precursor deposits and their association with the climactic eruption phase is still in its infancy and poorly understood. Further research is thus needed to identify typical volcanic precursors for a single volcanic centre and for eruptions of a specific magnitude.

Isla Catherine Simmons, Melissa Anne Pfeffer, Eliza Shona Calder, Bo Galle, Santiago Arellano, Diego Coppola, Sara Barsotti

Submission 21

Extended SO₂ outgassing from the 2014-2015 Holuhraun lava field, Iceland

The 2014-2015 Holuhraun eruption was the largest fissure eruption in Iceland in the last 200 years. This flood basalt eruption produced ~1.6 km³ of lava, forming a lava field covering an area of ~84 km². Over the six-month course of the eruption ~12 Mt of SO₂ were released from the eruption vents as well as from the cooling lava field. This presentation will discuss the SO₂ emitted by the Holuhraun lava field, providing the first study of the extent and relative importance of the outgassing of a lava field after emplacement.

Scanning differential optical absorption spectroscopy (DOAS) instruments were installed at the eruption site to monitor the flux of SO₂, and data were analysed to estimate the SO₂ emissions from the lava field. It was found that the SO₂ flux from the lava field decreased during the final month of the eruption, from 7 kg/s in January to 4 kg/s in February. The lava field then continued to release SO₂ at a flux of 2 kg/s for at least four months after the end of the eruption. While the lava field was not a significant contributor to the total SO₂ emissions released during the eruption, it was still an important polluter and caused high concentrations of SO₂ at ground level in Iceland both during the eruption and after lava effusion ceased. The results of this work will be discussed in the context of gas hazards caused by lava flows and the mechanisms of gas release from a lava flow post-deposition.

Kenneth WW Sims

Submission 521

The “zero-age sample”: Using lava lake samples from Mt Erebus, Antarctica and Nyiragongo, DR Congo to determine the time scales of magmatic processes in alkaline volcanic systems.

Knowledge of the timescales of shallow magmatic processes coupled with constraints on magmatic cyclicity is critical for producing better models for eruption forecasting. Measurements of U- and Th- decay series isotopes provide a unique perspective on the time scales of magmatic processes including the rates of solid mantle upwelling, magma differentiation, and magma degassing. However, because some of these nuclides have very short half-lives (as short as 138 days), modeling these processes requires that we know explicitly the eruption age of the sample (i.e. when the sample solidified) and that it is young relative to the half-life of the shortest lived daughter nuclide being measured.

Because lava lake samples can be collected molten, or as just solidified overflow and/or bombs, they provide a rare opportunity to use U-series measurements to understand the timescales of magmatic processes. Here we present ^{238}U – ^{234}U – ^{230}Th – ^{226}Ra – ^{210}Pb – ^{210}Po and ^{232}Th – ^{228}Th – ^{228}Ra and ^{235}U – ^{231}Pa – ^{227}Ac coupled with Sr, Nd, Hf and Pb long-lived radiogenic isotopes and major- and trace-element chemistries for lava lake samples collected from Mt Erebus, Antarctica and Nyiragongo, DR Congo. These measurements have enabled us to determine magma residence times and crystallization rates as well as the timescales of magma recharge and magmatic degassing. These zero age samples are also providing us with a necessary baseline for using U-series measurements for dating older lavas, which is essential for determining the timescales of magmatic cycles.

Christine Simurda, Michael Ramsey, Stephen Scheidt, David Crown

Submission 967

Surface Roughness and Block Size Distribution on Silicic Lava Flows

The property of thermal inertia (TI) represents the resistance of a material to natural changes in temperature over the diurnal cycle. It can be used to estimate surface properties such as particle size, moisture content, and cementation. TI is calculated directly from the thermal conductivity, thermal capacity, and density of the material. Because these variables cannot be measured using remote sensing data, apparent thermal inertia (ATI) is commonly utilized as an approximation of TI. However, the detection of coarse particles may be obscured by fines, so it is critical to improve the identification of the particle size distribution and whether a region on the ground is dominated by mantling or checkboard mixing of larger blocks plus fines in low-lying regions. Also, shadowing created by large block sizes will lower the visible albedo and daytime temperature, which combine to artificially raise ATI values. Thus, understanding the block size distribution within each pixel using thermal inertia and high spatial resolution visible data will improve our understanding of flow emplacement for older and active flows and domes. Our study area focused on the rhyolite flows in the Mono Domes system (California). The North Coulee flow is covered in areas with thick tephra deposits from younger eruptions and the surface size distribution ranges from ashy to blocky. To accurately assess the subpixel distribution of blocks, multispectral data from orbital sensors with spatial resolutions ranging from 1.85 to 90 m/pixel were analyzed, along with samples, GPS, and photogrammetry data acquired during mapping. Subpixel distributions and shadowing were evaluated and quantified for the surface of the dome to determine the accuracy at each spatial resolution and compare to the ATI data to evaluate the relationship between block size, shadowing and temperature. Analysis of samples and field observations confirmed the composition and grain size concentrations. Ultimately, this method constrained the relationship between thermal inertia and block size, demonstrating that even publically available lower spatial resolution data can be used to accurately interpret the thermophysical and surface properties of silicic lava flows. This method can be used to understand surface changes with time during future active flow emplacement as well as being applicable to lava flow regions on other planets such as Mars.

Graeme Alexander William Sinclair, Jennie Gilbert, Nigel Clark

Submission 654

Topography and Topologies of Policy Mobility in Volcanic Risk Reduction

An estimated 800 million people worldwide are exposed to disaster risk from volcanic activity. Elected governments are generally responsible for reducing such volcanic risk within their territories through the development and implementation of public policy (Smith and Petley, 2009).

Volcanic risk reduction (VRR) policy varies between jurisdictions, dependent on a variety of volcanic and socioeconomic factors (Wilkinson, 2013). The pursuit of 'best practice' VRR remains a long-term goal of volcanology and global disaster risk reduction (UNISDR, 2015). The international mobilisation of policy, expertise and resources has shaped VRR to date, with some approaches proving more successful and influential than others (Macias and Aguirre, 2006). Such international exchanges will very likely continue to influence VRR.

This study seeks understanding of the movement of policy and knowledge in VRR through the introduction of policy mobility studies. This field examines the processes that accompany policies and knowledge around the globe in order to determine "how, why, where and with what effects policies are mobilised, circulated, learned, reformed and reassembled" (McCann and Ward, 2012). The mobilities field aims to understand how certain approaches come to be identified as 'best practices' at an international level and their impact in new jurisdictions.

Policy mobility investigations typically 'follow' case studies chronologically, constructing narratives from archival research, interviews and observations to document and map the events, agents and networks that shape policies and their movement and reception (Peck and Theodore, 2012). We present a depiction of the global policy field of VRR (Hannigan, 2012); a dynamic collective of separate-but-interrelated networks of knowledge and policy exchange that have shaped diverse policy approaches to volcanic risk to date and their potential to create new topologies, i.e. whereby geographically disparate volcanoes may be 'brought together' (subverting topography, the existing geo-spatial distribution of volcanic risk) in order to exchange lessons on coping with specific, shared risks.

Brad Singer, H  l  ne Le M  vel, Joseph M. Licciardi Licciardi, Loreto C  rdova, Basil Tikoff, Nicolas Garibaldi, Angela K. Diefenbach, Nathan L. Andersen

Submission 538

Integrating geomorphology, geochronology, and numerical modeling of 60 meter surface inflation to reveal Holocene growth of the silicic magma reservoir beneath Laguna del Maule, Chile

The Laguna del Maule (LdM) Volcanic Field comprises an unusually large concentration of silicic eruptions surrounding a 23x17 km lake basin atop the southern Andes. Since 2007 the crust has been inflating at >20 cm/y. Geology, petrology, and geophysics suggest that the silicic vents have tapped an extensive, but ephemeral, layer of rhyolitic melt that began to form atop a mush zone by ~20 ka, with a renewed phase of rhyolite eruptions concentrated around the southern flank of the basin since 14.5 ka. The Espejos coul  e, $^{40}\text{Ar}/^{39}\text{Ar}$ -dated at 19.0 ± 0.7 ka, dammed the northern outlet of LdM and raised its level ~200 m to form a prominent basin-wide shoreline. Subsidiary shorelines lower than the highstand are poorly preserved. ^{36}Cl measurements of wave-cut Pleistocene rhyodacite and andesite, where multiple shoreline horizons occur between 2376 and 2386 masl, yield ages of 9.4 ± 0.2 , 8.8 ± 0.3 , 7.5 ± 0.2 , 6.6 ± 0.3 , and 4.2 ± 0.1 ka. We infer that the lake level dropped at 9.4 ka, and that the younger dates reflect variable surface erosion, or lower shorelines, following the initial drop in lake level. This interpretation is bolstered by a ^{36}Cl age of 8.4 ± 0.6 ka and $^{40}\text{Ar}/^{39}\text{Ar}$ age of 5.6 ± 1.1 ka from lavas that erupted onto the highstand shoreline.

GPS positions of 64 sites on the highstand surface were measured with cm-scale vertical precision (rapid-static mode). These data are augmented by a photogrammetrically-generated 1 m resolution DEM. The geodesy reveals a 62 m elevation difference between the SE and NW highstand shoreline surface. The elevation gradient and spatial distribution are consistent with an inflating magma source located SE of the lake, but may include minor displacement on faults. To investigate the origin of the deformed shoreline, we use analytical and numerical models of repeated magma injections into a long-lived reservoir and calculate the resulting surface displacement over 9.4 ka. Assuming the vertical displacement reflects intrusions of magma corresponding to episodes of non-eruptive inflation, similar to unrest of the past decade, we can quantify the total volume of magma feeding the system during the Holocene. Modeling the geomorphic signal offers a rare opportunity to provide the ratio of intrusion to eruption in a silicic system by comparing simulated magma recharge volumes to measured volumes of erupted rhyolite. Moreover, the growth rate of the reservoir can be estimated over a time period well beyond the brief historical record of unrest.

Emma Singh, Tetsuya Okada, Christina Magill

Submission 385

Exposure of roads to volcanic ash from a future eruption from Mount Fuji, Japan: Implications for evacuation.

Volcanic eruptions can produce a variety of hazards, impact areas far from source, and have the potential to persist over weeks or months. Hazards such as lava flows, lahars, pyroclastic density currents and tephra falls can occur simultaneously or consecutively, and can cause damage and disruption to society and built environments. Volcanic ash in particular can be heavy, highly abrasive, corrosive and conductive and can spread far and wide. Only millimetres are needed to disrupt essential services and critical infrastructure, such as electricity, water supply, waste systems, communications and transportation. These lifelines are essential for maintaining modern society's socioeconomic activities and, importantly for the interests of this study, controlling emergency response and assisting post-event recovery.

To better prepare for future hazard events, potential impacts on critical infrastructure need to be included in scenario development and vulnerability assessment. There is a need to understand the behaviour and interconnectedness of critical infrastructures and to identify populations and services that rely on their operation. Therefore, critical infrastructure vulnerability needs to be considered alongside social dimensions that take into account the ability of populations to adapt or cope with infrastructure disruption.

Using both ashfall dispersal modelling and graph theory techniques we demonstrate the impact that ash induced road closures might have on emergency response during, and recovery following, a future volcanic eruption at Mount Fuji, Japan. In particular these techniques will be used to assess the impacts of ashfall on the evacuation plans for Yamanashi Prefecture with regards to a future 1707 Hiei type eruption at Mount Fuji. These techniques may be applied to various hazard scenarios and may inform disaster mitigation programs, emergency response and community recovery.

Lloyd Singura, Tsukasa Ohba

Submission 768

Quaternary explosive eruptions of Rabaul and its tephra evolution and distribution in the New Ireland Basin-Petrological assessments of sedimented and recent tephra deposits

To evaluate preserved Quaternary Rabaul tephra in this region, we conducted fieldwork at two localities. These included 1) Rasirik (a distal site >65 kilometres NNE of Rabaul on west coast Namatanai-New Ireland Province), an uplifted tephra in marine turbidites southwest of New Ireland Basin, 2) Rabaul caldera flank (proximal sites to source at Kokopo beach, the Blue Lagun tunnel ignimbrite along the Kokopo-Rabaul road) and at the base of Tavurvur cone. Tephra grains were correlated to previous seafloor tephra cored northwest of the New Ireland basin (>100 kilometres from Rabaul). Sedimented-to-recently deposited tephra were acquired in the form of volcanic sand/air-fall ash, pumice, and few volcanic rocks which were brought to Akita University's analytical laboratory for geochemical analysis. The ash was sieved using 500-63 micron sieves. Microscopic observations of sieved grains reveal common rock forming minerals of pyroxene, olivine, hornblende and magnetite as accessory with minor felsic volcanic glass shards typical of Rabaul's basaltic-basaltic andesite to high silica dacitic and rhyolitic lavas. The exposures of Rabaul like lavas in these proximal and distal tephra shards deduce catastrophic volcanic eruptions relative to caldera forming events that disseminate tephra far into the New Ireland Basin. This is valuable to document the tephra provenance, evolution and distribution for the region which is significant to evaluating future air-fall tephra and related volcanic disasters in Papua New Guinea. Completion of geochemical analysis and dating of the samples will make considerable contributions to the study of the Rabaul caldera forming events and add to the reconstruction of the tephra stratigraphy of the Rabaul-New Ireland settings.

Tom Sisson, John Power, Matt Haney

Submission 920

The deep-crustal roots of arc stratovolcanoes illuminated by long-period seismicity caused by degassing and fluid-enhanced wallrock embrittlement

Proximity of deep long-period (DLP) seismicity to volcanoes [1-4], spectral similarities to events attributed to fluid motion, and temporal associations with some eruptions prompt the interpretation that DLPs indicate magmas newly arrived into the mid and lower crust. However, DLPs are commonly offset from directly beneath their respective volcanoes and may result from gradually exsolved magmatic volatiles +/- residual liquids that elevate pore pressures and embrittle otherwise ductile rocks and largely solidified magmas. Considered in composite, >2000 mid-crustal to upper-mantle DLP events from the Alaska-Aleutian arc cluster beneath the respective volcanoes at 15-30 km depths but are less common directly beneath the volcanoes at greater depths. DLP events become abundant at radial distances of 4-10 km at depths >20 km. This distribution suggests a seismogenic region surrounding or offset from the lower crustal axis of the arc magmatic systems.

An origin of DLPs by degassing of newly arrived magma is not supported because CO₂ concentrations are low, and H₂O's high solubility at deep crustal pressures delays degassing until advanced solidification, which is slow due to high ambient temperatures in the deep crust. Isotherms propagate with the square root of time around the mid- to deep-crustal portions of magmatic systems, so over the 1-5×10⁵ yr durations of convergent-margin volcanoes, temperatures are appreciably elevated only at distances <10 km. The deep magmatic systems are encased in relatively thin thermal sheaths, outside of which temperatures drop sharply to near ambient and rock strengths increase accordingly. Collectively, these observations support a scenario wherein magmas that intrude and crystallize in the roots of arc volcanic systems gradually exsolve vapor, some of which percolates out into wallrocks. Beyond some critical isotherm, rock strength increases sufficiently for fluid-enhanced brittle failure of otherwise ductile materials when stressed by nearby magma replenishments and ordinary tectonic forces. Exsolved fluids and residual melts create and transit these fractures, generating DLP signals. If true, the spatial distribution of DLPs indicates that the hot, active roots of arc stratovolcanoes are typically narrow (≤5 km) and are sheathed by a cooler region (≤10 km) laced by veins and, possibly, aplite/pegmatite dikes.

1. Pitt et al. 2002 *Seis Res Lett*; 2. Power et al. 2004 *JVGR*; 3. Aso & Tsai 2014 *JGR*; 4. Nichols et al. 2011 *JVGR*

Ian Skilling, David McGarvie

Submission 1018

Jokulhlaup Deposition on Actively Inflating Subaerial Basaltic Lava Flows: A New Model for the Sida Formation, SE Iceland

The Plio-Pleistocene Sida Formation occurs in the same region of south-eastern Iceland as the large volume Laki 1783-84 and Eldgja 934 basaltic lava eruptions, and broadly comprises up to nine stacked groups that consist of a basal glacial diamicton, overlain by basaltic lavas up to 20m thick and capped by up to 150m thickness of vitriclastic sediments (hyaloclastites). The upper surfaces of the Sida lavas locally display distinctive fluidal and dike-like apophyses to several metres in length into the overlying hyaloclastite, where they are associated with peperite domains. The formation has been interpreted as having been emplaced either in a dominantly submarine setting (Bergh and Sigvaldason, 1991) or a dominantly subglacial one (Smellie, 2008; Banik et al., 2014). Following recent work, we have re-interpreted the Sida Formation as comprising large-volume subaerial lava flows emplaced into active river channels and dry interfluves on glacial outwash plains (sandur), with glacial advances between the eruptive episodes. The active lavas were "drowned" by large volumes of rapidly emplaced subaerial sediment (hyaloclastite) from water floods across the outwash plains. The source of the water is most likely sub-ice (jokulhlaup), but could also be from an ice-margin or rift lake. The vent area(s) for the Sida Formation are not exposed, but we argue that it was erupted from a fissure or fissures in the region of the Laki fissure, with part of the fissure under water (probably ice-confined) and part of it subaerial. The hyaloclastite was generated by explosive eruptions in an area of dammed water in the subaqueous section and the lavas from the subaerial part. We suggest that the apophyses from the upper surfaces of the lavas develop when inflation of the lavas gives rise to intrusion into the overlying sediment, the nature of which will depend on sediment thickness, density, rheology, hydrology etc. Such ice-margin glaciovolcanic sequences may be characteristic of "deglaciation-triggering" in this part of Iceland, but occur in any areas on Earth and Mars where there is a coincidence of large volume active basaltic lava flows adjacent to ice-caps. Similar inflation-driven intrusions may also occur in other settings associated with "catastrophic" sedimentation, such as alluvial or submarine fans.

Jakub Sliwinski, Olivier Bachmann, Marcel Guillong, Matthew Zimmerer, Peter Lipman

Submission 772

Geochemical and geochronological comparison of cogenetic crystal-rich dacites and crystal-poor rhyolites in the Southern Rocky Mountain Volcanic Field, CO

The Tertiary Southern Rocky Mountain Volcanic Field in Colorado, USA, is well known for its magmatic productivity, manifested as a diversity of erupted and intruded igneous rocks. These include some of the largest silicic eruptions in the geological record in two flavors: monotonous intermediates (e.g. Fish Canyon Tuff; 5,000 km³ crystal-rich dacite) and zoned ignimbrites (e.g. Carpenter Ridge Tuff; 1,000 km³ crystal-poor rhyolite/crystal-rich dacite). Zoned ignimbrites, despite their heterogeneity in eruptive products, are hypothesized to derive from the same magma reservoir, due to their coincident spatial distribution, complementary geochemistry and near-simultaneous eruption (rhyolites nearly always precede dacites). If rhyolites are indeed the extracted residual melts from dacitic mushes, then a first-order hypothesis would suggest that mineral crystallization should be roughly contemporaneous. Here, we examine zircon U-Pb ages and geochemistry by laser ablation inductively-coupled-plasma mass spectrometry from co-erupted dacites and rhyolites of four units in Colorado: the zoned Rat Creek, Carpenter Ridge, Bonanza and Nelson Mountain Tuffs. Results suggest that while ages and geochemistry of zircon populations are overlapping in the dacitic and rhyolitic members of the Carpenter Ridge and Bonanza Tuffs, the Rat Creek and Nelson Mountain Tuffs show more complex characteristics, necessitating further consideration of issues such as inheritance and the timing of zircon crystallization relative to melt-solid segregation. In particular, some zircons from the rhyolitic Rat Creek and Nelson Mountain Tuffs record much lower Hf and Yb/Dy and higher Ti (i.e., higher temperature) than any of the dacitic units and display little to no Eu anomaly, indicating crystallization from a less evolved melt than the rhyolite they sit in.

Lara Smale, Christopher Kilburn, Stephen Edwards

Submission 477

A Crustal Damage Model for Coupling the Magmatic and Hydrothermal System and the Control on Ground Movements at Campi Flegrei Caldera, Italy

We propose a new model to interpret ground deformation at Campi Flegrei in terms of interaction between its magmatic and hydrothermal systems. The caldera is one of the highest risk volcanoes in the world with a population of 360 000. Since 1950 it has been in a state of unrest similar to behaviour in the 100 years before the last eruption at Monte Nuovo in 1538. There is thus an elevated concern for renewed magma transport to shallow levels.

To assess eruption potential, it is essential to differentiate deformation due to magma intrusion from that caused by a disturbance of the hydrothermal system. A critical step in defining future scenarios of unrest is establishing a robust model of mass-energy transfer between the magmatic and hydrothermal systems. Between 1950-1984, three short-term rapid uplifts (c.1 m yr⁻¹) elevated the centre of the caldera by c.4 m. After uplift in 1982-1984, long-term subsidence from 1985-2005 lowered the ground by c.0.6 m. This deformation has virtually been recovered by slow uplift since 2005. Previous models of the hydrothermal system focus on the post-1982 sequence and primarily attribute uplifts to pressurisation of the hydrothermal system owing to a transfer of deep magmatic fluids. A key assumption is that the subsidence was caused by an outflow of fluids from the hydrothermal system and represented a return to equilibrium conditions.

We suggest that the hydrothermal system was disturbed in 1982-1984 when a magma intrusion fractured a low-permeability horizon below the hydrothermal system and allowed the influx of fluids from an underlying supercritical reservoir. Once intrusion and fracturing ended, self-sealing processes reduced permeability and mass-energy transfer rates returned to background values. Subsidence occurred between 1985-2000 because elevated pressure in the hydrothermal system allowed decompression from fluid outflow to dominate pressurisation by fluid influx. The current uplift is attributed to a continued adjustment of the system to the initial disturbance. Contrary to conventional studies, our model suggests the system was disturbed from equilibrium from 1984-2005 and that uplift since 2005 represents a return to conditions prevailing in 1982-1984. Unless Campi Flegrei is disturbed by a new shallow intrusion, we expect the current uplift rate will either decay to a static equilibrium or, through a repeated sealing-rupture mechanism, continue its post-1984 behaviour in a new regime of slow ground oscillation.

Jean-François Smekens, Mathieu Gouhier

Submission 645

Investigating Degassing Processes with a Ground-based Hyperspectral TIR Imager: A Case Study at Stromboli Volcano

Thermal infrared (TIR) imaging is a common tool for the monitoring of volcanic activity. Broadband cameras with increasing sampling frequency give great insight into the physical processes taking place during effusive and explosive event, while Fourier transform infrared (FTIR) methods provide high resolution spectral information used to assess the composition of volcanic gases but are often limited to a single point of interest. Multispectral imagers, equipped with bandpass filters, have been used to quantify both ash and sulfur dioxide (SO₂) emissions by volcanoes from the ground. Continuing developments in detector technology have given rise to a new class of hyperspectral imagers combining both approaches. In this work we present the results of our observations of volcanic activity at Stromboli volcano with a ground-based imager, the Telops Hyper-Cam LW. The instrument features a cooled mercury-cadmium-telluride (MCT) detector (320×256 pixels) and uses a FTIR method to produce data cubes with a user-selectable spectral resolution of up to 0.25 cm⁻¹ over the spectral range 875-1315 cm⁻¹ (7.7-11.8 μm). Using datasets collected from two different vantage points, and reflecting a series of atmospheric conditions, we investigate the effects of those parameters on the efficacy of simple Brightness Temperature Difference (BTD) indicators, often used to identify potential pixels of interest in large volumes of data produced by multispectral instruments. Our results show that quickly changing conditions at the vent – including but not limited to the presence of summit fog – render the establishment of meaningful thresholds for BTD indicators practically impossible. As a result, we have developed an innovative technique based on curve-fitting and principle component analysis (PCA) to quickly extract spectral information from high-resolution datasets and implement fast and reliable identification of sulfur dioxide. We also explore ways to use this spectral information to improve detection and quantification methods in the TIR - specifically with multispectral imagers - and move toward semi-autonomous algorithms for continuous monitoring.

Benoît Smets, Nicolas d'Oreye, Matthieu Kervyn, François Kervyn

Submission 27

The Nyiragongo lava lake (D.R. Congo): current state of knowledge and perspectives

Nyiragongo volcano, in North Kivu, Democratic Republic of Congo, is among the most active volcanoes in Africa and on Earth. Since the first European observations in the late 19th Century, its eruptive activity mostly concentrated into its main crater, with the presence of a persistent lava lake from at least 1928 to 1977 and since 2002. The size, shape and elevation of this lava lake have evolved through time, modifying the topography of the main crater. In January 1977 and 2002, the uppermost magmatic system of Nyiragongo, including the lava lake, was drained during flank eruptions. Like any other persistent lava lake system, the Nyiragongo lava lake is a unique opportunity to directly monitor the dynamics of the upper magmatic system of the volcano. Monitoring the Nyiragongo lava lake also offers a chance to detect any change in the magmatic activity that could lead to a hazardous flank eruption. In this presentation, we focus on the dynamics of the Nyiragongo lava lake level and its relationship with the volcanic plumbing system, by describing the historical and most recent lava lake activity, and presenting new quantitative observations using close-range photogrammetry, a Stereographic Time-Lapse Camera (STLC) system and high-resolution satellite SAR and InSAR remote sensing. Results highlight that, contrary to some interpretations in the literature, the lava lake drainages appear to be the consequence and not the cause of the 1977 and 2002 flank eruptions. Two types of short-term lava lake level variations are observed. The first one corresponds to cyclic metre-scale variations attributed to gas piston activity. First STLC records in September 2011 show hour-scale gas piston cycles reaching up to 3.8 m, which are interpreted to be related to gas accumulation and release in the lava lake itself. The second type of variations corresponds to sporadic decametre-scale level rises or falls, which are related to major pressure changes in the upper magmatic system and may be responsible for topographic changes or ground deformation in the main crater. Finally, preliminary results of a large scientific expedition focused on the study of the Nyiragongo lava lake, which is planned in June 2017, will be presented, in order to highlight the perspective of new multidisciplinary studies on this remote persistent lava lake.

Victoria Smith, Madeleine Humphreys, Michael Stock, Roberto Isaia, Takehiko Suzuki, Danielle McLean, Paul Albert

Submission 641

An apatite for tephrochronology

Evaluation of the tempo, magnitude and ash dispersal during explosive eruptions relies on building robust event stratigraphies by correlating proximal and distal tephra sequences. In the distal environment, the physical characteristics of these sequences are not distinctive enough to allow for robust correlations. Since the 1980s, major element glass chemistry has been employed to make correlations allowing distal and proximal records to be integrated. However, some volcanic centres produce eruption deposits with similar major element glass chemistries over thousands of years and thus it is difficult to correlate distal occurrences to their proximal equivalents. This has been largely circumvented by acquiring trace element compositions of the glass shards but sometimes the problem of not having a unique glass chemical fingerprint still exists. Some crystal phases (e.g., Fe-Ti oxides and biotite) are useful for correlating tephra deposits when the glass compositions are similar, or if the glasses are too microlite-rich or altered, but are not always present. Apatite is a common accessory phase in evolved eruption deposits. It can incorporate both volatiles and trace elements (e.g., rare earth elements) into its crystal structure, and has been shown to be useful in correlating K-bentonites of altered, Ordovician tephra deposits in North America (e.g., Sell et al., 2015). However, there are no detailed studies to show whether apatite compositions can be used to distinguish successive eruption deposits from the same volcano. We have extracted apatite microphenocrysts from eruption sequences comprising multiple eruption events (including large caldera-forming and smaller explosive events) from various volcanoes around the world and analysed the major, volatile and trace element compositions to determine which elements are the most reliable for correlating the eruption deposits. We will present data from these eruptions and discuss the other information that can be gleaned from these apatite compositions.

References:

Sell et al. (2015). Geological Society of America Bulletin.
<http://doi.org/10.1130/B31194.1>

Gregory Smith, Rebecca Williams, Peter Rowley, Daniel Parsons

Submission 816

Pyroclastic Density Currents: The Influence of Variable Fluidisation

Pyroclastic Density Currents (PDCs) are hot, density driven mixtures of gas and volcanic particles formed during explosive volcanic eruptions. They are capable of depositing large ignimbrite sheets, which can exhibit a variety of sedimentary structures.

Due to their inherent nature, the direct observation of the deposition of ignimbrites by PDCs is incredibly challenging, and our knowledge of the internal processes of PDCs comes largely from physical and numerical modelling. PDCs are known to have high gas pore pressures due to various possible mechanisms of fluidisation, and this is thought to explain their greater than expected runout distances.

This series of experiments further examines the effect of fluidisation on analogue currents. Previous work has shown how sustained, fluidised currents not only aggrade deposits thicker than the current itself but have much longer runout distances than non-fluidised currents. Here, we use a novel flume apparatus that not only allows the simulation of high pore pressures by fluidising the current through a basal gas flux, but which can provide different fluxes to three different divisions of the flume channel. This allows the modelling of different degrees of fluidisation within the same current, which is significant as PDCs are intrinsically heterogeneous in time and space.

The results of these variable fluidisation experiments will be discussed, and a sensitivity analysis of how parameters including slope angle and current volume as well as fluidisation states affect the current dynamics will be presented. This work will inform future experiments in the same flume, examining the effects of complex topography and variable grain size on bedform formation.

Cassandra Smith, Stephen McNutt, Sonja Behnke, Alexa Van Eaton, Ronald Thomas, Harald Edens

Submission 495

Volcanic lightning as an indicator of ash parameters: A case study of Sakurajima Volcano, Japan, May-June 2015

Volcanic lightning is an emerging field of study for monitoring explosive, ash-producing eruptions. Volcanic ash is hazardous to aviation as well as local communities. Using volcanic lightning to monitor ongoing ash emissions, however, requires a better understanding of how volcanic lightning develops, and whether or not lightning can be used as an indicator for specific ash characteristics.

Volcanic lightning is common at Sakurajima Volcano, Japan. During the summer of 2015 we deployed a 9 station Lightning Mapping Array (LMA), developed by New Mexico Institute of Mining and Technology, within 20 km of Sakurajima Volcano to detect the very high-frequency electromagnetic radiation generated by volcanic lightning. Of the eruptions analyzed so far the two main types of electrical signals recorded were near vent-lightning and continuous radio frequencies (CRF).

In addition to the LMA data we collected samples of actively falling ash during a ten-day observation period from May 29th-June 7th 2015. Eruptive events were also recorded on a Trillium broadband three-component seismometer. Ash samples were characterized in terms of componentry, plagioclase microlite number density, laser diffraction particle size analysis, and particle morphology using a PharmaVision 830. The ash parameters were compared with maximum vertical seismic amplitudes and the electrical discharge statistics of the respective explosive events. We have begun to determine the relationships that exist between quantifiable ash characteristics and volcanic electrification, especially the occurrence of CRF.

We have found that CRF occurred during events where ash samples were composed of greater than 60% glass with less than 10% lithics. CRF was also present during eruptions whose samples have high mean roundness but maintain a distribution tail of acicular grains. Finally, CRF occurred in more explosive events as defined by higher seismic amplitudes ($>7\mu\text{m}$). We infer from these relationships that CRF is generated in highly explosive events by a combination of initial and secondary fragmentation of the ash as it is generated and travels up the conduit.

Richard Smith

Submission 1186

Developing a mechanism for successful, multiagency, volcano science advice and research coordination: facilitation across the boundaries of disaster risk research, policy, and practice in New Zealand

Volcanic crises create myriad challenges for the volcanology community. There are very high demands for information and advice from the public and emergency management officials, typically in an environment of significant ambiguity and uncertainty. Professional and institutional tensions can arise during eruptions or unrest from the competing demands of 24/7 hazard monitoring functions, provision of science advice in a politically charged environment, and capturing the 'once-in-a-career' research opportunity.

The role of the volcano scientist (and associated hazard monitoring capabilities) in technical risk assessments to inform official decision making is reasonably well defined, and tried and tested in many recent volcanic crises. However, servicing critical science and risk communication needs and fulfilling the high value research opportunities associated with the event make resourcing potentially problematic, especially for long-lived events. In many instances it will require capacity and capability from individuals and institutions outside the science agency with the formal 'crisis response' mandate (such as a geological survey). Such "scaling-up" requirements on the volcanology community dictate the need for strong relationships of trust among science institutions (and between peers) well before any coordinated response is called upon.

International good practice in disaster risk management identifies the importance of authoritative, well communicated science advice that is well integrated with the emergency response. Past experience also shows the strategic and operational benefits derived from well-coordinated, pre-planned science investigations of the event that contribute not just to advances in knowledge, but to inform future planning and improvements in disaster risk reduction and to underpin risk transfer approaches.

To achieve these outcomes, a national New Zealand Volcanic Science Advisory Panel (NZVSAP) has been established that encompasses all available expertise in volcanic processes and impacts in New Zealand. The main benefits of the NZVSAP are to pool the breadth and depth of national volcanic science expertise from relevant science agencies, and to integrate research and monitoring capabilities such that the provision of science advice and research activities in response to a volcanic crisis is high quality, co-ordinated, well-communicated and sustainable.

Ian E M Smith

Submission 111

The Geochemical Behaviour of small scale basaltic systems: the example of intraplate monogenetic systems.

Fields of basaltic volcanoes express the activity of small-scale mantle-sourced magmatic systems. These systems have their origin in the upper mantle in both plate boundary and intraplate tectonic settings. A key feature of such systems is that the volumes of magma involved are extremely small and so their ascent through the crust must therefore be rapid enough to overcome the consequences of cooling and solidification. A feature of small-scale basaltic systems is that individual volcanoes represent the eruption of discrete batches of magma which, although characteristic of the field of which they are a part, individually show distinct chemical compositions indicating that subtly different processes were involved in their genesis. It is significant that the compositions of the monogenetic volcanoes of these systems carry the chemical signature of processes that operate at or near their upper mantle sources. The Auckland Volcanic field is an example of a small-scale magmatic system in an intraplate tectonic environment in which erupted rocks show the signature of deep seated processes. Three processes are recognised: progressive partial melting of a heterogeneous asthenospheric source, near-source fractionation of high pressure crystalline phases and sequential monogenetic eruptions separated by a clear time interval. In other monogenetic volcanic fields mixing of chemically discrete magma batches has also been observed. The importance of these small-scale monogenetic volcanic systems is that their compositions provide an insight into how the mantle behaves. One variable is the degree of partial melting of the source – of the order of 3-7%. A second variable is the pressure (depth) range within which melt extraction occurs. A third parameter is the modal nature of the source – whether simple lherzolitic mantle or a more complicated mixture of lherzolite together with an eclogitic component. An important consideration is the process by which an aliquot of mantle undergoes melting on this small scale. Generally, adiabatic melting associated with mantle convection is appropriate at least for intraplate systems such as the Auckland Volcanic Field. However, individual volcanoes in a monogenetic field are unlikely to represent individual melting events. Rather, the source of individual magma batches is probably a crystal-liquid mush from which compositionally discrete melts are extracted at intervals which are determined by external tectonic events.

Diane Smith, William Leeman

Submission 200

Basaltic lavas of Mount St. Helens: evidence for diverse mantle sources and mixing with evolved magmas at shallow depth

Activity at Mount St. Helens (MSH) began ca. 300 ka and continued intermittently to the present (Mullineaux and Crandell, 1981, USGS Prof. Paper 1250; Clynne et al., 2008, USGS Prof. Paper 1750). MSH eruptive products are dominated by dacitic compositions, with subordinate andesite and basalt. Although mafic magmas are thought to play a significant role at MSH, actual effusion of basaltic lavas was restricted to the relatively brief Castle Creek eruptive episode (ca. 2200-1900 yrs B.P.) and from separate vents located within a few kilometers of each other. These lavas define two distinct compositional groups: low-K tholeiitic basalt [LKT], and high-K intraplate basalt [IPB]. Primitive lavas in each group (MgO contents up to ~7.5 wt %) have ~0.5 wt % K₂O [LKT] and ~1.5 wt % K₂O [IPB, some of which are ne-normative]. With decreasing MgO, both groups form continuous and curvilinear trends that converge toward the composition of MSH andesites (~1 wt % K₂O and 5 wt % MgO). Similar arrays observed in variation diagrams for nominally incompatible elements are attributed to magma mixing processes. New SEM/EMP studies document that olivine analyses restricted to phenocryst cores span large compositional ranges (up to 23 mole % Fo, with an average of 13 mole %) in individual samples. The occurrence of olivines with core compositions more Fo-rich than predicted from bulk-rock Mg# suggests that MSH basalts are derived from even more primitive liquids, similar to LKT and IPB basalts from the Indian Heaven lava field located ~40 km southeast from MSH. Olivine phenocrysts with core compositions of Fo₆₀₋₇₂ exhibit embayed textures and/or overgrowth rims of orthopyroxene with Mg#s ~65-70. These observations confirm that olivine populations comprise mixtures of crystals from different magmas that subsequently reacted to partially re-equilibrate with more evolved magmas in the shallow conduit system. Despite the close proximity of vents for MSH basaltic lavas, we see no evidence of mingling or mixing between LKT and IPB basalt types, which erupted within a short time interval (< 300 years), and conclude that they ascended vertically from different magma source regions along narrowly separated conduit systems. These magmas are inferred to have originated from depths as great as 60-70 km. Geophysical and petrologic studies are consistent with intermittent presence of mid-to-lower crustal magma reservoirs that impede ascent of mantle-derived mafic magmas.

Katharine Solada, Shanaka de Silva, Adonara Mucek, Indyo Pratomo, Jade Bowers, Rendi Jamil, Sinung Baskoro

Submission 683

Rates of resurgent uplift of Samosir Island in Toba Caldera, Indonesia constrained by lake sediment chronology

Large silicic calderas like Yellowstone, U.S.A., or Campi Flegrei, Italy, undergo resurgence after their catastrophic caldera forming eruptions. One of the youngest of these is Toba Caldera in Sumatra, Indonesia, erupting ~74 ka to produce the Youngest Toba Tuff (YTT) and its associated caldera (Chesner and Rose, 1991, *Bulletin Volcanology*, 53, 343-356). Post-caldera resurgence has resulted in the uplifted dome, Samosir Island, now elevated 700 m above lake level at its eastern margin. The upper surface of Samosir is covered with up to 100 m of lake sediment that preserves a rich post-eruption history. To constrain this history of uplift at Samosir Island, sediment from sections covering the entire island were collected; 27 of these have been dated using ¹⁴C dating. Lake sediment collected at the boundary of the Youngest Toba Tuff and the lake sediment is dated at ~38.7 ka, indicating that sediment accumulation is recorded at least since that time. Older sediment ages have not been obtained, but stratigraphic correlation suggests older sediment in other locations. Paleomagnetic correlation is being conducted to assess the sediment history older than 38.7 ka. Focusing on the uppermost sedimentary layers that yielded coherent ¹⁴C ages, six ¹⁴C ages from these layers provide the youngest possible ages, revealing an increasing age progression from the west at 953 m at 15.1 ka to the top of the fault 1700 m at 33.7 ka. This suggests differential uplift of Samosir progressed from east to west, consistent with the westward tilt of the island. Uplift rates were calculated assuming that the age reflects the most recent submergence of Samosir. Since lake level has remained constant post the YTT eruption, an uplift rate can be calculated by elevation above the lake/age (de Silva et al., 2015, *Frontiers in Earth Science*, 3, 6-15). These data reveal 1) locally rates vary from 0.22 cm/yr to as high as 18.7 cm/yr; and 2) sectorially distinct uplift histories. Maximum cumulative uplift occurred along the Samosir fault zone and uplift rates here decrease with age from ~5 cm/yr at 33 ka to ¹⁴C ages in combination with paleomagnetic analysis will provide further insight into the age-elevation history of Samosir.

Arianna Soldati, Alan Whittington, Lucia Gurioli, Andrew Harris, Maeva Rhéty, Nicolas Villeneuve

Submission 251

Does lava remember its own thermal history? A new experimental approach to investigate subliquidus rheology applied to the December 2010 eruption of Piton de La Fournaise (La Réunion)

The classical experimental protocol for investigating the subliquidus rheology of lava entails reaching and maintaining superliquidus temperatures first, in order to eliminate crystal nuclei. The target temperature is then approached from above, with homogeneous crystallization occurring along the liquid line of descent. However, in nature lava rarely experiences superliquidus conditions. Crystal nuclei (and often phenocrysts) are typically present, and can act as nucleation sites for microlites. We therefore developed a new experimental protocol in which the target temperature is approached from below, avoiding complete remelting and thus obtaining data directly relevant to field observations. We compared textures and crystal fractions obtained with the two protocols, and concluded that they are equivalent. This new experimental approach has the key advantages of being simpler and, critically, expanding the range of compositions that can be investigated at subliquidus temperatures, since it does not require heating through the critical reduction zone (~1450-1550 °C). We used the new protocol to measure the subliquidus rheology of recent lava flows from Piton de La Fournaise (December 2010 eruption). During the eruption four separate flows were emplaced. All flows were fed by the same fissure over about 15 hours, but then flowed in slightly different directions. This provided us with a unique chance to address the long-standing question of how pre-existing topography controls lava flow system structure. The critical parameter is not the absolute slope value, but rather the slope variation, so that a transition from a steep to a shallow slope results in braided flow, while a transition from a shallow to a steep slope leads to a single channel flow. We were able to assess the rheological evolution of the studied flows through a combination of topographic effect quantification and novel laboratory viscosity measurements. The findings of this study allow us to interpret and explain the observed flow structure, and advance our ability to mitigate hazards associated with future flows.

Ingo Sonder, Andrew G. Harp, Alison H. Graettinger, Gregory A. Valentine, Pranabendu Moitra, Ralf Büttner, Bernd Zimanowski

Submission 1156

Explosive Magma-Water Interaction Experiments: Premix Conditions on Decimeter Scale

The explosive interaction of magma and external water drives volcanic eruptions in a variety of settings such as maar-diatreme volcanoes, eruptions comparable in size to the 2010 Eyjafjallajökull eruption, or possibly large scale phreatoplinian systems. Explosive magma-water interaction is driven by rapid heat transfer ($\sim 10^6$ K/s) which causes brittle failure of magma close to the magma-water interface. The magmas' brittle failure is a central component of this violent heat transfer mechanism, since it acts at high speeds as massive feedback loop by exponentially increasing the magma-water interfacial area. Previous experiments revealed those fundamental steps in this process, which is termed "Molten Fuel Coolant Interaction". They also reveal the great difficulties for the analysis in the context of real world volcanic settings: Water needs to be pre-mixed with the magma body as a liquid prior to the explosion start; timing was shown to play a major role. The length scale of brittle reaction for each water domain is not well understood. The size limitations of closed room laboratory experiments impose a maximum experiment size of about 15 cm for the magma, and several cm for the mixed-in liquid water. Such limitations make it hard to derive robust scale independent quantities such as the often discussed magma to water mass ratio.

Here we present first experimental results of a setup that was built as a logical next step to address above limitations. Experiments are based on a ~ 60 kg, 25–30 L magma body, which is held in a container and made of re-molten volcanic rock. Our first results consist of a correlation of ejected magma size and speed with the available water, the mixing speed, and the timing relative to the explosions' trigger.

Jean Soubestre, Nikolai Shapiro, Léonard Seydoux, Julien de Rosny, Dimitry Droznin, Svetlana Droznina, Sergey Senyukov, Evgeny Gordeev

Submission 1069

Detecting seismo-volcanic signals and classifying volcanic tremor sources at the Klyuchevskoy volcanic group (Kamchatka) from the seismic network covariance matrix analysis

Seismic signals associated with volcanic unrest are generated by different physical processes such as vibrations due to explosions, stresses induced by ascending magma and released in form of volcano-tectonic (VT) earthquakes, and longer-period seismicity in form of long-period (LP) earthquakes or tremors induced by fluid movement within the volcano plumbing or hydrothermal systems. The main goal of the present work is to develop a seismic network-based method for the detection of those seismo-volcanic signals, and the automatic classification of sources of volcanic tremor which constitutes one of the most important attribute of volcanic unrest.

The method is applied on four and a half years of seismic data continuously recorded by the permanent monitoring network composed of 19 stations operated in the vicinity of the Klyuchevskoy volcanic group (KVG) in Kamchatka, Russia. The KVG is composed of 13 stratovolcanoes located in an approximately 70 km diameter zone, with three of them (Klyuchevskoy, Bezymianny and Tolbachik) being very active during last decades. In addition, two other active volcanoes, Shiveluch and Kizimen, are respectively located north and south of KVG.

The method is based on the analysis of eigenvalues and eigenvectors of the array covariance matrix. As a first step, following Seydoux et al. (2016), the width of the array covariance matrix eigenvalues distribution is used to detect the most coherent signals of the recorded wavefield corresponding to prominent sources. Volcanic sources such as explosion, VT and LP earthquakes, and tremors are efficiently detected, together with other types of seismic sources from oceanic and tectonic origins. As a second step, the array covariance matrix's first eigenvector computed every day is analyzed, making the assumption that it represents the principal component of the daily seismic wavefield and, for days with tremor activity, characterizes the dominant tremor sources. Those first eigenvectors can therefore be used as network-based fingerprints of tremor sources. A clustering process is developed to analyze this collection of first eigenvectors, using correlation coefficient as a measure of their similarity. This automatic procedure identifies seven clusters associated with different periods of tremor of four volcanoes, some of them not being detected by the previous analysis based on eigenvalues. The developed method does not require a priori knowledge, and is fully automatic and adaptive.

Adam Soule, Dana Yoerger, Meghan Jones, Rebecca Carey, Mark Kurz, Dorsey Wanless

Submission 1154

Autonomous Underwater Vehicles in Submarine Volcanic Studies

Autonomous underwater vehicle technology has advanced rapidly over the last decade and now is routinely deployed in the study of submarine volcanic systems. High resolution acoustic mapping of the seafloor, geophysical measurements, water column properties, and visual imagery can — in some cases — all be collected contemporaneously during autonomous surveys. This presentation will provide an overview of the key enabling technologies employed by AUVs that allow positioning and situational awareness during missions and discuss the details three studies in unique submarine environments that have used AUVs to aid submarine volcanic studies. First, I will describe surveys conducted at Havre Volcano in the Kermadec Arc using the US National Deep Submergence Facility AUV Sentry. A 1-m resolution bathymetric map of the ~6 km wide calder and rim was constructed from 11 Sentry deployments in 2015. Combined with earlier ship-based bathymetric mapping, these data allowed the volume of material erupted in the 2012 to be evaluated. In addition, seafloor magnetization data collected by AUV helped to define the subsurface structure of the Havre caldera. Next, I will describe surveys of the shallow submarine Galápagos volcanic platform using a REMUS 600 AUV operated by the WHOI Oceanographic Systems Laboratory used to construct sub-meter resolution bathymetric and sidescan sonar backscatter maps of seamounts around the Galápagos Islands in 2015. These data, combined with seafloor observations, are used to resolve volcanic and sedimentary features that reflect the interaction of sea-level change with volcanic construction and subsidence. Lastly, I will describe a study using the AUV Sentry to map portions of the axial valley of the Mid-Atlantic Ridge in 2016 that illuminate the variations in volcanism and tectonism as a function of magma supply rate to the ridge. These three studies, which include a mid-ocean ridge at ~4000m depth, a submarine arc volcano at ~2000m depth, and an ocean island platform at ~500m depth, each present a unique set of challenges and opportunities that autonomous platforms are well-suited to address. Lastly, I will provide an overview of the coming advances in AUV technology (e.g., increased endurance, enhanced onboard processing power, co-robotics, and autonomous sampling mechanisms) that are likely to influence our use of AUVs in future submarine volcanic studies.

Delphine Roselyne Nathalie Sourisseau, José Luis MACIAS, Denis R. AVELLAN, Juan Pablo BERNAL URUCHURTU, Giovanni SOSA CEBALLOS

Submission 1257

Stratigraphy of the post-caldera explosive volcanism of the La Primavera Caldera, Jalisco Mexico

The La Primavera caldera is a rhyolitic complex located at the intersection between the Sierra Madre Occidental (SMO) and the Trans-Mexican-Volcanic-Belt (TMVB). La Primavera caldera was formed 95 ky ago with the eruption that produced the Tala Tuff (Mahood, 1980; 1981). The depression formed during the eruption formed a lake that recorded fluvio-lacustrine sedimentation and post-caldera pyroclastic and effusive activity. Although post-caldera stratigraphy was partly studied by Walker et al. (1991) and Mahood (1980; 1981) several gaps of information still need to be solved regarding the sources, distribution, and correlation of explosive pyroclastic activity. With this purpose in mind, we carried out detailed fieldwork with the description of stratigraphic columns, granulometry, componentry, and chemistry of juvenile particles. This correlation was assisted by $^{258}\text{U}/\text{Th}$ dating in zircons.

The Tala Tuff and the Giant Pumice bed (emplaced during the lake sedimentation) were used as marker horizons to correlate deposits. At least five plinian to subplinian subaereal deposits were found on top of the GPb. These deposits were dated between 78 and 57 ky with isochrone and model ages calculated in zircons. These fallouts are separated by paleosols or volcanoclastic deposits (lahar or fluvatile). Field evidence, chemical analyses of pumice and lava domes indicate that the possible sources of these eruptions are the domes of San Miguel (92.0-60.5 ky; Mahood and Drake, 1982), and Las Planillas (61.3-60.5 ky; Mahood and Drake, 1982), although, further studies are being conducted.

Thin sections and componentry analysis showed aphyric pumices and pumices with up to 10% of crystals. Pumice deposits dated between 70 and 60 ka have 2-10 % of crystal that consists of microphenocrysts ($\leq 250\mu\text{m}$) of quartz \geq sanidine \gg clinopyroxene-amphibole $>$ fayalite $>$ Fe-Ti oxides with biotite. All samples are peralkaline rhyolites (72.5-74.7 wt.% SiO_2 ; and 3.95-4.8 wt.% K_2O).

Viviane Souty, Sylvie Vergnolle, Christelle Zielinski, Philipson Bani, Alexis Le Pichon, Michel Lardy, Philippe Millier, Pascal Herry, Sylvain Todman

Submission 97

Insights on eruptive patterns at open-vent volcanoes from simultaneous infrasonic, thermal and seismic records at Yasur volcano (Vanuatu)

Strombolian activity at open-vent volcanoes is often characterized by series of explosions due to gas slugs which rise the conduit and then burst at the surface of the magma. The strength and the number of explosions can vary significantly with time. These fluctuations can help us to better understand the processes occurring at shallow depths. These processes involve both gas flow and variable fraction of ejecta. This complexity is better studied by combining several geophysical techniques.

The relatively simple access to Yasur volcano (Vanuatu) and its large number of strong explosions (a few per minutes) make of this volcano an ideal candidate for continuous records. Infrasonic, seismic and thermal measurements were simultaneously performed for a few weeks in June 2009 and again in Sept-Nov 2016. Infrasonic records can be used to estimate gas volumes (10^2 - 10^4 m³), while thermal measurements are indicative of the ejecta volume. The delay between the arrival times can be used to estimate the gas velocity and the depth of the top of the magma column. The acoustic-seismic ratio of energy and their delay can also provide information about the variation of the depth of the explosions. The activity in June 2009 was relatively quiet and steady. The infrasonic, seismic and thermal powers per explosion did not show any obvious correlation (acoustic: 104-107W; seismic: 104-107W; thermal: 102-104W). The top of the magma column is very shallow (108W. Significant variations in the strength and in the number of explosions during this period also exist (from alert level 2 to level 3). The differences observed during a quiet and a vigorous activity will be discussed in detail.

Stephen Sparks, Jonathan Rougier, Katharine Cashman, Natalia Delinge, Sarah Brown

Submission 185

Analysis of LaMEVE database for large magnitude explosive eruptions: implications for under-recording and magnitude-frequency relationship.

The database on Large Magnitude Explosive Eruptions (LaMEVE) provides a resource to understand biases in the geological and historical records of volcanism (under-recording), and to estimate global and regional return magnitude-frequency relationships. We use a non-parametric statistical analysis to assess the global recording rate for large (M4+) explosive eruptions. This approach imposes minimal structure on the shape of the recording rate through time. Recording rates have declined rapidly: prior to the year 1600 AD they are 6.5 (corrected for under-recording) suggests that the magnitude-frequency relationship departs from the power law derived from lower magnitude eruptions such that frequency drops farther below the extrapolation of the power law as magnitude increases, with an asymptotic limit at about $M = 9.3$. Reasons for this change could include variations in the likelihood of forming large magma chambers in different geodynamic settings.

Zack Spica, Mathieu Perton, Denis Legrand

Submission 259

Architecture of the Colima volcano magmatic plumbing system

Although extensively studied, the internal structure and deep magmatic system of the Colima volcano remain unknown. Our research gives new clues to understand how and where magmas are produced and stored at depth. Using ambient seismic noise, we jointly invert for Rayleigh and Love wave dispersion curves for both phase and group velocity, which is applied for the first time in a volcanic environment. We invert for both the shear wave velocity and radial anisotropy. The 3D high resolution shear wave velocity model shows a deep, large and well-delineated elliptic-shape magmatic reservoir below the Colima volcano complex at a depth of about 15 km. On the other hand, the radial anisotropy model shows a significant negative feature (i.e., $V_{SV} > V_{SH}$) revealed from ≥ 35 km depth until the top of the magma reservoir at about 12 km depth. The latter suggests the presence of numerous vertical fractures where fluids, rooting from a well-known mantle window, can easily migrate upward and then accumulate in the magma reservoir. Furthermore, the convergence of both a low velocity zone and a negative anisotropy suggests that the magma is mainly stored in conduits or inter-fingered dykes as opposed to horizontally stratified magma reservoir.

Ales Spicak, Jiri Vanek

Submission 1001

Magma migration beneath submarine volcanic arcs revealed by earthquake swarm analysis

This contribution reveals rate of magma migration beneath submarine volcanic arcs. Migration of magma in the Earth's crust beneath submarine volcanic domains belongs to processes that are difficult to observe and quantify. Extent and rate of magma migration have been determined only rarely, by interpreting the earthquake occurrence beneath sites monitored by dense local networks of seismic stations. Here we show that magma unrest can be followed beneath remote submarine volcanic domains also by an analysis of teleseismically recorded earthquake swarms. Swarms have been frequently observed beneath submarine volcanic arcs above subducting slabs at two areas of our interest: in the Andaman Sea region and in southern Ryukyu. Seismicity of both areas is covered by global catalogs of hypocenter parameters: the EHB catalog 1960 – 2008 and the new catalog of the International Seismological Center 2009 – 2013. In addition, southern Ryukyu is covered by the catalog of the Japan Meteorological Agency 1967 - 2014. The swarms recorded by these agencies consist of several tens to more than a hundred events in the body-wave magnitude range from the lower threshold value of about 4.0 to 5.7 and the depth range between several km to 50 km. Positions of earthquake swarm epicenters typically correlates with seamounts and seamount ranges. The swarms develop in a non-random manner: epicenters of swarm earthquakes migrate laterally at a rate of several kilometers per hour. The rate of lateral migration of swarm earthquakes can be determined by means of simple time-distance plots. The rate corresponds e.g. to the rate of migration of earthquake occurrence before the well-known eruption of the Icelandic Bardarbunga volcano in 2014 monitored by a dense network of local stations. The repeated occurrence of relatively strong, teleseismically recorded earthquake swarms probably reflects fluid and/or magma ascent through the plumbing system of the submarine volcanic arcs, points to brittle character of the lithospheric wedge at respective depths and favors the studied areas – the Andaman Sea region and the southern Ryukyu area – to be potential sites of submarine volcanic activity. Last but not least, the study documents high accuracy of hypocenter parameters published by data centers such as ISC and JMA, and the usefulness of the EHB relocation procedure.

*Volkhard Spiess, Lena Steinmann, Marco Sacchi, Giuseppe De Natale, -
MagellanPlus Workshop participants*

Submission 1157

Understanding the dynamics of an active caldera at the land-sea interface: Strategies for an amphibious IODP/ICDP drilling initiative at the Campi Flegrei caldera

Caldera-forming explosive eruptions are among the most catastrophic natural events to affect the Earth's surface. Hence, associated hazards and risks are important to assess and predict. It had been recommended to target calderas with IODP drilling; therefore a MagellanPlus Workshop was held in Naples (Italy; Feb 2017) to discuss a community-based strategy for drilling an active caldera at the land-sea interface or in a marine setting.

During the workshop, it was agreed that the Campi Flegrei caldera (CFc), featuring processes such as (1) recent unrest, (2) post-caldera eruptions (last eruption in 1538 AD), (3) long-term caldera resurgence, (4) hydrothermal activity, as well as (5) prehistoric large-scale ignimbritic eruptions, represents a globally unique key site to study the dynamics of an active caldera. The partially submerged CFc, result of two large-scale eruptions, the Campanian Ignimbrite (CI; 39 ka) and the Neapolitan Yellow Tuff (NYT; 15 ka), represents an extremely active volcanic area with recent intense uplift episodes. Its shoreline location and the unknown role of large volumes of water in the subsurface make the volcanic system particularly unpredictable.

While ICDP drilling (Campi Flegrei Deep Drilling; CFDDP) is ongoing, an amphibious approach, comprising marine IODP drilling, opens the opportunity to utilize a 3D seismic data set to target particular elements of the hydrothermal and magmatic system as well as land-sea gradients. In detail, the influence of internal (i.e. hydrothermalism, magmatism) as well as external (i.e. tectonism, sea-level variations) forcings on unrest and eruptions shall be examined to reveal the eruption potential and assess volcanic hazards. Furthermore, the marine drilling will provide a complete stratigraphic record of the largely unknown CFc eruption history and elucidate the climatic and environmental impact of large ignimbritic eruptions and the subsequent recovery of life. Using multichannel reflection seismic data from the marine caldera portion, isolated borehole observations can then be spatially extended, thereby providing novel insights on the caldera architecture and potential magma/fluid pathways. Furthermore, new technologies for deep borehole and seafloor monitoring shall be integrated into the existing observation network. Ultimately, in-situ borehole observations are urgently needed to verify analogue and numerical caldera models for reliable risk assessment.

Laura Spina, Daniele Morgavi, Antonio Costa, Bettina Scheu, Donald Dingwell, Diego Perugini

Submission 737

Degassing in Stratified Magmas: Experimental Investigation on the Effects of Physical Properties and Decompression Rate

Volcanic conduit systems are often characterized by the coexistence of magmas with different rheological properties, either evolved at different stages or resulting from cooling and degassing-driven crystallization of the uppermost section of the magma column. This is quite common during lava dome eruptions. Different stratified rheological heterogeneities result in various mixing/mingling fingerprints on the textural features of the ejecta, and likely influence eruptive behaviours (e.g. Lautze and Houghton, 2005). In order to investigate the effects of such magma rheological contrasts, we performed a set of laboratory experiments to explore the role of physical properties and decompression rate on different stratified analogue magmatic systems. We used silicone oil with viscosities of 10 and 1000 Pa s mixed with glass beads as a proxy for crystals. Samples were mounted in a transparent autoclave, having the lower viscosity at the bottom and the higher on the top. Next the samples were fully saturated with argon gas at 10 MPa and finally decompressed. The degassing behaviour of the analogue systems during decompression was monitored through high speed cameras as well as pressure sensors located at the top and bottom of the autoclave. We performed three sets of experiments 1) by varying the decompression rate (either ca. 10⁻² or 10³ MPa/s) to confine the effect of different ascent history; 2) by varying the amount of analogue spherical crystals (0, 10, 30, 70 vol%) added to the 1000 Pa s silicone oil basis to investigate the role of crystal fraction; 3) by differentiating the volume ratio between the two analogue magmas, with the aim of isolating the effect of heterogeneities thickness.

Results enabled us to quantify the strong dependence of degassing style -in terms of expansive response of the two analogue magmas, ascent speed and time-scales of outgassing- on decompression rate and solid loading. For the same experimental conditions, the time-scale of outgassing changes of up to two orders of magnitude with decompression rate. Similarly, solid loading is able to modulate both the ascent speed during initial expansion phase and the time-scale of outgassing.

Courtney Sprain, Paul Renne, Isabel Fendley, Loyc Vanderkluyzen, Kanchan Pande, Steve Self, Mark Richards

Submission 1275

Timing, Tempo, and Transitions in the Deccan Volcanic Sequence

Within the basalt sequence of the Deccan Traps of India, major transitions have been documented in lava flow morphology, basalt composition, and feeder dike orientation, indicating rapid and extensive reorganizations of the magmatic system. The timing of these transitions, however, remains to be thoroughly investigated. High-precision $^{40}\text{Ar}/^{39}\text{Ar}$ geochronology is increasingly revealing the tempo of Deccan volcanism in the Western Ghats (WG), where the most complete record of this massive lava extrusion event is preserved. This study aims at determining the timing of these transitions, and that of the time-stratigraphic horizon corresponding to the Cretaceous-Paleogene boundary (KPB) within the eruptive sequence. An additional (and challenging) goal is to develop an accurate record of province-wide magma volume extrusion history. Results thus far reveal a quasi-continuous record of volcanism in the WG from about 66.4 to at least 65.5 Ma, with no hiatuses longer than ~ 50 ka. As a consequence, the persistent concept of three discrete pulses of eruptions in the WG is erroneous and should be abandoned. Available data place the KPB time horizon (66.04 ± 0.04 Ma) within or near the Lonavala subgroup in the WG, wherein a fundamental change in magma chemistry and eruptive tempo characterize the transition to eruptions of the most voluminous, widespread and compositionally monotonous tholeiite lavas of the Wai Subgroup. This transition likely represents a state shift in the magma plumbing system, mantle melting processes and magma interaction with the crust. Coincidence with the KPB suggests a causal relationship between the state shift and the Chicxulub impact, which is unambiguously synchronous with the KPB, possibly a result of seismically induced permeability increase and volatile exsolution. New data are presented which further clarify the tempo of WG volcanism, delineate more precisely the timing of the state shift relative to the KPB, and begin to clarify the extent to which the chemical stratigraphy defined in the WG can be extended to distal regions of the Deccan province.

Patricia Sruoga, Manuela Elissondo, Mario Rosas, Judy Fierstein, Bradley Singer, Nathan Andersen

Submission 1062

CERRO BARRANCAS, LAGUNA DEL MAULE VOLCANIC FIELD, CHILE: eruptive stratigraphy and hazard assessment

The postglacial record of the Laguna del Maule Volcanic Field (LMVF) (36° 10'S, 70° 30' W) includes rhyolite and rhyodacite lava flows, domes, tephra falls and pyroclastic flows related to 16 multi-vent eruptive centers. Ongoing uplift of >20 cm/year since 2007 near the youngest of those centers makes unraveling its recent eruptive history imperative in a hazard assessment. The Barrancas center in the southeastern part of LMVF has been an especially productive and long-lived vent complex. Much of its ~6 km³ postglacial eruptive volume is preserved in the headwaters of Río Barrancas, Argentina. Detailed mapping, combined with petrographic, grain-size, textural and geochemical analyses and new Ar/Ar dating reveal a complex eruptive stratigraphy. An early episode of multi-stage dome building has been dated between ~14.5 ka and ~11.4 ka. A series of dome collapses in quick succession produced block-and-ash flows that traveled up to 13 km from source, filled the upper Barrancas valley with deposits ~60 m thick and created the plateau called Pampa del Rayo. Effects of hydrothermal alteration and associated mineralization are seen in both the dome and the blocks included in the block-and-ash deposits suggesting that the late hydrothermal system may have triggered the explosive event. A younger, partly overlapping volcanic sequence includes 9 obsidian flows, 2 of which have been dated at 5.6 ka and 1.85 ka, and a thick package of tephra falls and intercalated pyroclastic flows related to the activity of at least 3 pumice cones. Tentatively, two nearby monogenetic mafic cones may be related to the Barrancas system. Future studies will undoubtedly improve our understanding of this volcano which—if it were to erupt again—could have widespread effects in Chile and Argentina, particularly in southern Mendoza and northern Neuquen provinces. Due to the remote location of Cerro Barrancas, hazard assessment is focused on tephra fall and pyroclastic flow distal impact. Particularly, Laguna Fea and Laguna Negra, which have been dammed by the block-and-ash deposits, are highlighted as a major threat in case of renewed volcanic activity or by catastrophic failure of the pyroclastic dam.

Amanda Stadermann, Christopher Hamilton, Catherine Neish

Submission 1122

Mapping Lunar Impact Melt Around Giordano Bruno Crater

Impact melt is a fundamental part of the impact cratering process. Impact cratering causes melting of the target material over a wide range of temperatures, including superheated liquids. For this reason (and others), impact melt flows are fundamentally different than lava flows, which typically erupt near the liquidus. In some circumstances, impact melts exhibit unusual fluid flow behaviors and morphologies that are distinct from traditional lava flows. On the Moon, impact melts are relatively well preserved because they are only altered by further impacts into the target. There are no hydrologic or atmospheric processes to disturb or alter the impact melt-bearing rocks. In this study, we seek to constrain volume, viscosity, and relative emplacement time of impact melt.

We achieve these goals by geologically mapping the young lunar crater Giordano Bruno, focusing on its interior and exterior impact melt. We categorize the melt into different facies (or morphologic flow types), such as channels, veneers, and ponds. In the interior of Giordano Bruno, ponding is extensive, but there are also veneers and channels on crater walls. Exterior to the rim of Giordano Bruno, we also observe veneers, ponds, and channels, with the addition lobate flows. We use several different data sets to aid in our investigation of the Giordano Bruno impact melts, including data from the Lunar Reconnaissance Orbiter (LRO) Narrow Angle Camera (NAC) and Wide Angle Camera (WAC) to map out facies changes. To supplement this data, we use SELenological and ENgineering Explorer "KAGUYA" (SELENE) mosaics to infill gaps in coverage of high resolution data sets. Topographic maps created from LROC WAC and NAC, LRO Lunar Orbiter Laser Altimeter, and KAGUYA Terrain Camera data aid in our understanding of how the facies change with slope. Lastly, we use LRO Mini-RF S-Band circular polarization ratio data to constrain the locations and physical properties of the impact melt. Through this work, we characterize impact melt distributions and facies types to learn about its emplacement mechanisms and related impact cratering processes. Specifically, we determine if changes in facies are related to changes in viscosity as the impact melt cools in the near-vacuum environment of the Moon.

D. Sarah Stamps, Elifuraha Saria, J. Robert Jones, Kang-Hyeun Ji, Mike Daniels, Dave Mencin, Daud Ntambila

Submission 1049

Potential volcanic deformation signals at Ol Doinyo Lengai in 2017: detection and response

Monitoring of volcanoes and data collection in real-time has increased over the past decade as the transmission and cyberinfrastructure capabilities continue to improve. In June 2016 we initiated the first phase of Tanzania's first volcano observatory at the active Ol Doinyo Lengai volcano (TZVOLCANO), which includes 5 continuous and telemetered GNSS/GPS sensors of which 2 produce real-time PPP-AR position solutions. We developed a simple program to use EarthCube's Cloud HOSted Real-time Data Services for the geosciences (CHORDS, NSF ICER #1639750) for visualization and easy access to the data (tzvolcano.CHORDSrt.com). On January 17, 2017 we observed the first of a series of potential volcanic signals at Ol Doinyo Lengai through the time-series generated in near real time. In response, we rapidly deployed a field team to assess the stability of our GNSS/GPS stations and determined that our positioning sensors were functioning properly in January 2017. Further, local team members of the Engaresero village reported (1) low magnitude seismicity, (2) changes in crater geometry, and (3) increased ash emissions after the initial January 2017 signals were observed via CHORDS. We report about these events, our subsequent actions, and the implications for volcanic hazards assessment in Tanzania.

Alexander Steele, Christopher Kilburn, Agust Gudmundsson

Submission 508

Unrest and Eruption at Large Calderas: Campi Flegrei, Southern Italy

We present numerical simulations to investigate critical amounts of uplift before eruptions at large calderas. These have been applied to the Campi Flegrei caldera in southern Italy, because it is currently in unrest and poses an increased threat from eruption to its population of 360,000 people. The last eruption in 1538 occurred after 100 years of caldera-wide uplift, which raised Pozzuoli, a town at the centre of the caldera, by 17 m. Ground uplift recommenced in the 1950s, since when Pozzuoli has been raised by almost 4 m. A crucial goal for emergency management is to determine whether 17 m of uplift at Pozzuoli must again be reached before an eruption can occur.

Uplift and volcano-tectonic seismicity since 1950 are consistent with the repeated intrusion of magma about 3 km beneath Pozzuoli and an accumulation of stress in the overlying crust. A laterally-extended geometry is the preferred shape for the intrusion, either as a single sill that is being episodically replenished or as a succession of independent sills. Our first simulations have explored the stress fields and surface displacements generated by a single sill at 3 km depth. They were constrained by physical conditions appropriate for Campi Flegrei: sill radii of 3 km or less; maximum overpressures of 20 MPa; and a maximum of 10 MPa for the tensile strength of the crust. Simulations were run for both a homogeneous and layered elastic-brittle crust. Following the approach by Pollard and Johnson, layers were permitted to slip with frictional resistance modelled as the equivalent of stiffnesses from 0.1 to 10 MPa per m.

The results show that a homogeneous crust in tension will fail between a sill's margin and the surface at a maximum uplift of 8 m. They also show that layered crusts can accommodate larger amounts of uplift before bulk failure, the amount increasing with a greater number of layers and a smaller frictional resistance. However, all the layered crusts failed only after uplifts significantly greater than 17 m. Additional factors must therefore operate to favour an eruption after an uplift of 17 m. These include the interaction of a sill with caldera ring faults, or the development of the shallow magmatic system as a collection of sills, rather than a single intrusion.

Andri Stefánsson, David R. Hilton, Árný E. Sveinbjörnsdóttir, Peter Torssander, Jan Heinemeier, Jaime D. Barnes, Shuhei Ono, Sæmundur A. Halldórsson, Jens Fiebig

Submission 628

SOURCES AND REACTIONS OF VOLATILES IN ICELANDIC THERMAL FLUID

Thermal fluids in Iceland range in temperature from 440°C and are dominated by water (>97 mol%) with chloride concentration from 20,000 ppm. The isotope systematics of the fluids reveal many important features of the source(s) and transport of volatiles from the mantle beneath Iceland and through the crust to surface. Studies spanning over four decades have shown a large range of values for δD (-131 to +3.3‰), tritium (-0.4 to +13.8 TU) and $\delta^{18}O$ (-20.8 to +2.3‰) for H₂O, $^3He/^4He$ (+3.1 to +30.4 RA), $\delta^{11}B$ (-6.7 to +25.0‰), $\delta^{13}C(CO_2)$ (-27.4 to +4.6‰), $^{14}C(CO_2)$ (+0.6 to +118 pMC), $\delta^{13}C(CH_4)$ (-52.3 to -17.8‰), $\delta^{15}N$ (-10.5 to +3.0‰), $\delta^{34}S(H_2S)$ (-10.9 to +3.4‰), $\delta^{34}S(SO_4)$ (-2.0 to +21.2‰) and $\delta^{37}Cl$ (-1.0 to +2.1‰) in both liquid and vapor phases. Based on this isotopic and chemical dataset, it can be concluded that the thermal fluids originates from meteoric and/or seawater. For other volatiles, degassing of mantle-derived melts contribute to He, CO₂ and possibly also to Cl in the fluids whereas water-rock interaction also contributes to CO₂ and is the major source of H₂S, SO₄, Cl and B in the fluids. Air-water interaction mainly controls N₂, Ar and Ne concentrations. The large range of many non-reactive volatile isotope ratios, such as $\delta^{37}Cl$ and $^3He/^4He$, are considered to indicate heterogeneity of the mantle and derived melts beneath Iceland. In contrast, the large range of many reactive isotope elements, such as CO₂ and H₂S, are heavily affected by processes occurring within the geothermal systems, including fluid-rock interaction, depressurization boiling, and isotopic fractionation between secondary minerals and the aqueous and vapor species. Variations due to these geothermal processes may exceed any differences observed among various sources highlighting the importance and effects of chemical reactions on the isotope systematics of reactive elements.

Ashley Steiner, John Wolff

Submission 703

The chemical composition of pumice vs. whole-rock ignimbrite samples: does it matter? A detailed portable XRF study of the Bandelier Tuff.

Volcanologists and petrologists who study the geochemistry of ignimbrites have been aware of potential problems arising from analyzing whole rocks at least since Walker (1972) showed that ashy tuff matrices are typically enriched in crystals compared to suspended pumice clasts. Lithic fragments in ignimbrites also contribute to divergence of bulk and magmatic compositions. For non-welded ignimbrites, the problem is usually avoided by sampling pumice (assumed to represent magma) and ignoring the matrix. This is more difficult for welded ignimbrites, necessitating careful removal of fiamme from the welded matrix. For very densely welded, rheomorphic and lava-like ignimbrites in which original matrix and larger pyroclasts cannot be distinguished, the problem is intractable. Despite long awareness of this issue, there have been few systematic attempts to assess the actual results of analyzing matrix, pumice-matrix mixtures and whole-rock samples from ignimbrites. Here, we report major, minor and trace element concentrations analyzed with a portable X-Ray fluorescence spectrometer (Steiner et al., 2017) for more than 1,600 non-welded matrix and 2,600 pumice samples collected from the 1.60 Ma high-silica rhyolite Otowi Member of the Bandelier Tuff, Valles caldera, New Mexico, USA. The phenocryst assemblage is sanidine + quartz + Fe-clinopyroxene + titanomagnetite ± fayalite ± allanite ± chevkinite ± zircon ± britholite ± apatite. Lithic fragments are dominated by andesite. The Otowi Member has a strongly differentiated, near-haplogranite composition; consequently, the general effect of contributions from excess crystals and micro-lithics in the matrix is to increase concentrations of compatible elements and hence render bulk compositions less evolved than the true magmatic composition. In addition, we find selective enrichment in trace elements which partition very strongly into accessory mineral phases (e.g. Zr in zircon, REE in allanite and chevkinite). Concentrations of Ti, Fe, Ca, P, Sr, Ba, Zr and Ce in the ignimbrite matrix are variably (up to 15-fold in the case of Sr) and non-systematically enriched compared to those in pumice. Strongly incompatible elements (e.g. Y, Nb, Th) are least affected, and provide the most robust measure of magmatic evolution obtainable from ignimbrite whole-rock data.

References: GPL Walker (1972) *Cont Min Pet* 36, 135-146; AE Steiner, RM Conrey, JA Wolff (2017) *Chem Geol* 453, 35–54.

Lena Steinmann, Volkhard Spiess, Marco Sacchi

Submission 1125

Stratigraphy, architecture and volcanic evolution of an amphibious caldera – Insights from a 3D high-resolution multichannel seismic survey at the Campi Flegrei caldera

The partly submerged Campi Flegrei caldera (CFc) represents one of the world's maximum volcanic risk areas due to its history of large-scale explosive eruptions, its ongoing episodes of unrest, and its high population density with ~2.5 million people living in close vicinity. Despite ample research, the mechanisms for unrest (hydrothermal vs. magmatic) as well as the volcanic evolution and overall caldera architecture remain controversial, with three prevailing hypotheses describing the CFc as either (1) a nested-caldera complex formed by the Campanian Ignimbrite (CI) and the Neapolitan Yellow Tuff (NYT) eruptions at 39 and 15 ka, respectively, (2) a single caldera formed by the NYT eruption, or (3) no caldera at all. On our poster, we present a 3D grid of high-resolution multichannel seismic data (line spacing 75-100 m) from the marine caldera portion, providing novel information on its shallow (<250 mbsf) subsurface. Volcanic deposits and edifices were seismically distinguished from sedimentary successions and the regional stratigraphy could be refined and extended back to the CI eruption.

In detail, the seismic data revealed the existence of a nested-caldera complex formed by the CI and NYT eruptions with a resurgent dome and associated apical normal faults in its centre. The clearly imaged inner caldera fault was initially activated during the CI collapse and later reactivated during the NYT collapse with different amounts of subsidence. The NYT eruption was associated with subsidence in the range of ~75 m in the marine portion. The NYT caldera is filled with on average 61 m reworked sediment deposited between 15 and 8.6 ka. Furthermore, we found that the inner caldera fault has acted as a pathway for the post-collapse ascent of gases/fluids possibly originating from a deeper (~2 km) hydrothermal system. This implies that structural features such as faults may have an immediate effect on the degassing of the hydrothermal system, which in return may have direct implications for the interpretation of unrest. The occurrence of shallow gas/fluid-rich patches south of the inner caldera fault suggests the existence of a deeper (>250 m) fracture zone likely related to an outer caldera fault formed during the CI collapse.

With respect to the evaluation of volcanic hazards, the identified major caldera faults could potentially facilitate the ascent of magma, thereby representing potential future eruption sites, and should thus be considered in forecasting models.

Pete Stelling, Lisa Shevenell, Nick Hinz, Mark Coolbaugh

Submission 904

Volcanic characteristics and surface features as indicators of geothermal potential on active subduction zone volcanoes

A database of key geologic factors expected to be indicative of productive geothermal systems in a global training set has been developed. This database includes all 74 subduction zone volcanic centers world-wide with current or proven power production capability. The focus of the work was to evaluate volcanic centers individually and as a group in these arcs by correlating various geologic characteristics with known potential to host electricity grade geothermal systems at the volcanic centers. Importantly, this data set only contains data from subduction zone volcanoes and contains no negative cases, limiting the populations of any statistical groups. Regardless, this is the most robust geothermal benchmark training set for magmatic-heated geothermal systems to date that has been made public. The work reported here is part of a larger project to establish favorability rankings for geothermal sites based on play fairway analysis of development risk. This paper describes volcano characteristics, compositions and eruption ages and trends along with surface manifestation observations and temperatures as they relate to known power producing systems. Our findings show a strong correlation between the presence and size of active flank fumarole areas and installed power production. Additionally, the majority of volcanic characteristics, including long-held anecdotal correlations related to magmatic composition or size, have limited to no correlation with power production potential. Notable exceptions are correlations between greater power yield from geothermal systems associated with older (Pleistocene) caldera systems than systems hosted by Holocene calderas or non-caldera volcanic centers. Power-hosting volcanic centers that have erupted within the last 160 years supply 50% of the global installed geothermal power in subduction zones, and nearly all of these systems are generally mafic (basaltic or andesitic) in average composition. Volcanic centers erupting between 160 and 900 years ago are dominated by felsic volcanic systems, and provide 47% of the global power from volcanic arcs. Only 3% of geothermal power produced in subduction zones are hosted by volcanic center erupting more than 900 years ago. We anticipate that these results may be able to help guide future geothermal exploration efforts.

Mark Stelten, Kari Cooper

Submission 667

Petrologic evidence for the current state of Yellowstone's magmatic system

The Yellowstone Plateau Volcanic Field in northwestern Wyoming is one of the world's largest, active silicic volcanic centers, and has produced three caldera forming eruptions in the past 2.1 Myr. Following the most recent caldera collapse at ca. 631 ka, which produced the Lava Creek Tuff, Yellowstone's magmatic system has been characterized by a series of dominantly effusive events, the most recent of which produced the Central Plateau Member rhyolites from ca. 170 to 70 ka. Recent work has focused on quantifying the age, trace-element, and isotopic composition of zircons, glass, and major phases from the Central Plateau Member rhyolites. These studies have led to competing models for rhyolite generation at Yellowstone, which range from partial melting of previously erupted Yellowstone rhyolites to extraction of melt from a long-lived, crystal-rich reservoir. Despite these recent advances, several fundamental questions regarding the nature of the magmatic system at Yellowstone Plateau remain to be addressed. Such questions include, (1) what is the physical state of the present day magmatic system, and is the system waning, suggesting smaller and/or fewer future eruptions, and (2) what might be precursory signals for future eruptions. To address these questions and better constrain the T-t-x evolution of the magmatic system in the recent past, we examine temporal trends in several crystal-based thermometers and in the trace-element composition of zircons, glasses, and major phases hosted in rhyolites from the Central Plateau Member eruptive episode. We compare these data to recent melting/crystallization experiments performed on Yellowstone rhyolites, and to recent gravity, seismic tomography, and strain-field studies at Yellowstone that identify a low V_p and low-density body beneath Yellowstone caldera. Through integration of these various techniques we present a model for the current state of Yellowstone's magmatic system, and hypothesize about the future eruptive potential of Yellowstone caldera.

Kirsten Stephens, Susanna Ebmeier, Nicola Young, Christelle Wauthier, Juliet Biggs

Submission 652

Uncovering the mysteries behind lava lake deformation source mechanisms: a case study of the ephemeral lava lake at Masaya volcano, Nicaragua

Masaya volcano exhibits persistent degassing, an ephemeral lava lake, and explosive eruptions with little to no magma erupted. Here, we present a case study examining three different periods of lava lake activity at Masaya volcano using high temporal and spatial resolution Synthetic Aperture Radar (SAR) data (ALOS-1 2007-2010; COSMO-SkyMed 2012; CSK, ALOS-2, RSAT2, Sentinel-1 2015-present). COSMO-SkyMed (CSK) data spanned a period of explosive eruption (30 April – 17 May 2012), during which there was no lava lake present in the Santiago crater pit. Our results showed line-of-sight (LOS) uplift within 2 km of the summit prior to the explosive period, reaching peak uplift ~27 days before the onset of explosive activity, followed by subsidence of ~5 mm leading up to the onset. The closeness of the deformation to the summit suggests that it was due to shallow conduit processes, and that the pre-eruptive deformation sequence was potentially caused by the flow of magma through a constriction within the shallow conduit system. Finite element modeling of the InSAR results suggests a pressurized conduit 450 m below the surface vent (radius 160 m and length 700 m), surrounded by a halo of brecciated material. In contrast, the earliest InSAR study using ALOS-1 data suggested ~2 cm/yr subsidence in the southern sector of the inferred large ring fault during a period of lava lake activity and phreatomagmatic eruptions (2007-2010). More recent observations (CSK, ALOS-2, RADARSAT-2, Sentinel-1) have shown LOS uplift patterns during the first ~9 months of the lava lake reappearance at the Santiago crater pit (December 2015). This suggests that this deformation may be due to a pressurized source that is linked to the lava lake present at the surface.

Carol Stewart, Natalia Deligne, Thomas Wilson, Alistair Davies, Priyan Perera, Rob Buxton, Emily Grace

Submission 459

Investigating volcanic eruption impacts on water infrastructure using a scenario approach: damage to networks, outage maps and potential public health consequences

Critical infrastructure systems provide essential services to modern societies. Water supply and wastewater networks (known as water infrastructure) are critically important for firefighting, public health and sanitation, habitability, the provision of health care services, and business continuity. We use a new multi-hazard scenario of a small basaltic eruption in the Auckland Volcanic Field, New Zealand, to explore consequences for the water infrastructure of Auckland; Auckland is New Zealand's largest city with a third of the national population. In partnership with water utility managers, we developed 'Level of Service (LoS)' metrics for the water infrastructure networks. These metrics range from full service to no service. We used a series of network status maps to summarise impacts of the hypothetical eruption sequence on the networks' physical assets. The maps also account for evacuation zone considerations and the cascading impacts of concurrent power outages. For example, not all pumping stations have backup power generation; evacuation cordons may prevent utility personnel from manually starting generators. We then created a series of regional maps showing the LoS for water supply and wastewater over the course of the eruption and recovery period. For water supply, despite relatively localised damage to the network, service interruptions could last over a year over the entire city, well beyond the end of the month-long eruption. Auckland's wastewater network is severely affected by this scenario given the eruption location, with the city's wastewater treatment plant lying within the zone of heavy damage to complete destruction. Its estimated repair time is 2-3 years. During this time, there could be extended duration discharges of untreated and partially treated sewage to the city's waterways, necessitating public health measures such as imposing bans on recreational contact and food gathering in receiving waters. A concerted and sustained environmental and public health response would be necessary to manage the substantial risks to public health. Our findings highlight the complexity and challenges of managing water infrastructure during and after a volcanic eruption.

John Stix

Submission 164

Understanding unrest at ramp-down and ramp-up volcanoes

Ramp-down volcanoes re-activate, erupt, and then quiet down quickly, commonly in the space of a year or less. Some examples include Pinatubo 1991, Chaiten 2008-2009, and Merapi 2010. Repose intervals are commonly long, while the eruptions are sudden and highly explosive. Timescales of precursory activity appear to be on the order of several months. Post-paroxysmal activity may continue for several years, but the main activity ceases rapidly, sometimes on the order of days. The magmatic plumbing network generally comprises a well-established magma reservoir or reservoirs, and the magmas are commonly highly mobile owing to their elevated temperatures, high volatile contents, and crystal-poor nature.

By contrast, ramp-up volcanoes re-activate slowly initially and then gain in intensity, commonly on yearly to decadal scales. Examples include Soufrière Hills (1995 to today) and Turrialba (mid-1990's to today). Their behaviour is characterized by significant geophysical unrest and gas release but small eruptions. During the early stages of re-activation, it is commonly difficult to decide whether the system is being driven magmatically, or whether some lesser process is at work, such as structural re-organization of the plumbing system, hydrothermal activity, etc. In the final stages, it is likewise difficult to determine when activity ends. Magmatic systems appear to comprise a poorly-defined plexus of connected and unconnected pathways, while the magmas are sluggish owing to their crystal-rich and gas-poor character.

We might consider ramp-down volcanoes as "active systems" and ramp-up volcanoes as "stagnant systems", although this may be misleading. For both types, the role of deeper magma inputs appears to be important in driving activity, but in some instances the evidence for such inputs is either cryptic or not clearly present. Likewise, tectonic influences also appear to play a significant role in many instances, channeling magma and triggering eruptions. For both volcano types, forecasting their behaviour can be extremely difficult, with many surprises for scientists. For ramp-down volcanoes, the short precursory window is highly problematic. For ramp-up volcanoes, early recognition of a re-activating magmatic system is challenging.

Michael Stock, Madeleine Humphreys, Victoria Smith, Roberto Isaia, Richard Brooker, David Pyle

Submission 395

Tracking pre-eruptive volatile behaviour at Campi Flegrei, Italy, through integrated analysis of apatite and glass

Volatile elements play an important role in controlling physical and chemical processes within magmatic systems in the build-up to volcanic eruptions. However, determining volatile behaviour in sub-volcanic systems remains challenging using established petrologic techniques (e.g. melt inclusions), particularly during the final stages of magma storage and onset of ascent. Igneous apatite crystals incorporate all major magmatic volatile species (i.e. H₂O, CO₂, SO₂, F, Cl) into their crystal structure and may preserve important information about the behaviour of these elements during magmatic evolution. However, the complexity of the apatite-melt volatile relationship has previously inhibited application of apatite as a magmatic volatile 'probe'. In this study, we compare natural apatite analyses with new thermodynamic models that predict the evolution crystal compositions during different fractional crystallisation scenarios. This allows us to decipher to the record of magmatic volatile evolution preserved by apatite. Through integrating 'textural-constrained' apatite and glass analyses (i.e. inclusions and matrix phases), we are able to create a spatially- and temporally-resolved picture of pre-eruptive fluid systematics, which we use to gain new insights into pre-eruptive processes in the Campi Flegrei system, Italy.

We find that clinopyroxene- and biotite-hosted apatite inclusions from Campi Flegrei ubiquitously preserve trends consistent with persistent volatile-undersaturated crystallisation until late in magmatic evolution. In contrast, apatite microphenocrysts show considerably more compositional diversity, which is interpreted to record volatile-undersaturated crystallisation; H₂O-saturation within a deep magmatic storage region shortly before eruption; and cooling or degassing during ascent. The same general trends are preserved by apatite crystals from different explosive eruptions of Campi Flegrei in the past 15 kyr, regardless of the eruption date, magnitude or composition. Clinopyroxene-hosted melt inclusions consistently have low H₂O concentrations and have re-equilibrated on ascent, during short-term magma storage at 1-3 km, similar to the depth of sill emplacement during recent seismic crises at Campi Flegrei. Matrix glasses have almost entirely degassed. This study demonstrates the potential utility of combined apatite and glass analysis for constraining the behaviour of volatile species in sub-volcanic systems during magmatic evolution.

Wendy Stovall, Elizabeth Westby

Submission 805

Keeping It Real with @USGSVolcanoes

An estimated 2.5 billion people worldwide participate in online social networks. Users stay in touch with friends, seek out entertainment, share opinions and stay up-to-date with news and current events relevant to their lives. The majority of adults (upwards of 85% by some estimates) expect organizations to have a social media presence that offers timely and interesting content.

The USGS Volcano Hazards Program operates social media accounts on both Facebook and Twitter. We post and share images, videos, volcanic activity notifications, scientific research, and Observatory events. The accounts have become our de facto news channel, providing users with access to factual, interesting (share-worthy), and time-critical information, and rumor control. When deviations from normal or background levels of monitoring data are detected, we aim to get ahead of the conventional news cycle by posting internally-vetted findings. Such timely outreach has caused our posts to ‘trend’ (i.e., be highlighted by the platform as a topic of immediate interest), and therefore reach more people.

When scientific organizations operate social media accounts, there is an implied expectation for trustworthy, reliable, and compelling information. The primary tenets of the USGS Volcanoes social media plan are to 1) post near real-time volcano activity notifications, 2) convey volcano hazards information, 3) make volcano science more accessible, and 4) maintain a two-way dialogue with account followers. Success is measured quantitatively via numbers of reactions, shares, and followers, combined with the qualitative content of comments. The most effective posts include videos or graphics depicting changes in volcanic behavior.

Daily presentation of timely volcano science to our USGS Volcanoes social media accounts supports public trust in the USGS as the authoritative voice in the U.S. regarding volcanic activity. This both lays the groundwork for effective communication during future volcanic crises and results in greater numbers of people informed about volcanic phenomena.

Martin Streck, William Mcintosh, Mark Ferns

Submission 17

Columbia River Rhyolites: age-distribution patterns and their implications for arrival, location, and dispersion of flood basalt magmas in the crust

The long-held view of Columbia River province magmatism was that flood basalts are not associated with abundant contemporaneous rhyolites and the first rhyolites of note were those at the McDermitt volcanic field, SE Oregon from where the Snake River Plain (SRP) rhyolite progression started. This has changed and it is now clear that basaltic lavas of the Columbia River Basalt Group (CRBG) are associated with rhyolites erupting over a wide area. We focused on unknown or little studied rhyolite occurrences in eastern Oregon and our new data complement recent studies along the Oregon, Idaho and Nevada state borders. Along this southern periphery, $^{40}\text{Ar}/^{39}\text{Ar}$ geochronology revealed voluminous rhyolite activity started at ~ 16.5 Ma and lasted until ~ 15 Ma. Our currently oldest rhyolite $^{40}\text{Ar}/^{39}\text{Ar}$ ages of 16.53 ± 0.14 , 16.69 ± 0.01 , and 17.00 ± 0.12 were obtained on the northernmost rhyolites from the greater Dooley Mountain area, near Baker City, NE Oregon. Furthermore, rhyolite activity was most extensive and voluminous from 16.3 to 15.5 Ma and waned thereafter, eventually leading to the two age-progressive rhyolite trends of the SRP, Idaho and the High Lava Plains, Oregon.

Our and literature data suggest following rhyolite age-distribution patterns that in turn have implications for arrival, location, and dispersion of flood basalt magmas in the crust. Earliest rhyolites (≥ 16.4 Ma) appear in the south and north of the province with an apparent initial gap in between. This is consistent with the arrival of the earliest CRBG magmas of the Steens Basalt in the south and Imnaha Basalt in the north. Most voluminous and widespread rhyolite volcanism around 16 Ma clearly coincides with the most voluminous CRBG unit, the Grande Ronde Basalt (GRB). Although main GRB activity from the Chief Joseph dike swarm seems to have ceased by ~ 15.9 Ma, enough GRB magmas may have stalled in the crust to support rhyolite centers from 15.9 to 15 Ma. Samples of such late and evolved GRB magmas erupted along with rhyolite in co-mingled eruptions as preserved in the youngest unit of the Dinner Creek Tuff and the Wildcat Creek Tuff but also locally in purely mafic eruptions.

The existence of crustal CRBG reservoirs beneath rhyolites seems inevitable particularly for GRB magmas that then travelled in dikes northward to their main eruption sites. These age-distributions patterns also question the significance of the apparent time-progressive CRBG volcanism.

Karen Strehlow, Joachim Gottsmann, Alison Rust

Submission 1064

Hydrological responses to volcanic strain and the arising capabilities for volcano monitoring

Many volcanic processes are associated with crustal deformation. Because of their poroelastic nature, aquifers in volcanic regions respond to the applied strain with changes in pore pressure and groundwater flow patterns. These variations are mirrored in well water levels, which can therefore provide important constraints on the subsurface processes causing the deformation.

We developed numerical models that simulate crustal deformation due to different volcanic strain sources and the dynamic poroelastic aquifer response with finite element analysis. The models are applied to two case studies. The first investigates possible deformation sources for strain-induced well level changes by up to 10 m preceding the 2000 eruption of Usu volcano (Japan). We propose that these were induced by the pressurization of both the magma chamber at 4 km depth and a large, shallow hydrothermal system.

The second case study simulates water level changes in the Belham valley on Montserrat over the course of two years (2004-2006). In this case, the aquifer responds to both gradual and rapid transient strain sources associated with the eruption of Soufrière Hills volcano (Montserrat). Repeated lahar sedimentation in the valley leads to a steadily increasing sediment load and thereby rising aquifer pressures. The wholesale dome collapse in May 2006 on the other hand induced significant dilatational strain and thereby a short-term water level drop.

The presented models are a significantly improved tool for the interpretation of well level signals in volcanic areas that can provide valuable constraints for volcanic strain sources and thereby complement other monitoring systems.

Erik Sturkell, Halldór Ólafsson, Eysteinn Tryggvason, Halldór Geirsson, Ásta Rut Hjartardóttir, Páll Einarsson, Freysteinn Sigmundsson, Talfan Barnie

Submission 481

Fifty years of tilt measurements in Iceland: Lessons learned

Half a century of tilt measurements in Iceland has provided numerous important results. The tilt program began 1966 with six optical leveling lines 2-10 km long. In total, 41 lines and 29 circular stations have been installed. Trials with mobile water tube tiltmeters were performed, but optical measurements (dry-tilt) were found to obtain the same accuracy and were easier to make. At Krafla, Askja, and Hekla volcanoes, tilt measurements have been successfully interpreted in terms of key parameters of the underlying magmatic systems, including location, depth, and volume change of pressure sources interpreted as magma reservoirs. The longer leveling lines display subsidence along the central axis of the rift zones in Iceland. The uncertainty in tilt at optical leveling stations depends on the distance between its end points. In a ring setup the lower limit is 3 μrad , and for lines it is 2 μrad . A stationary liquid tiltmeter was set up in the Krafla power station at the start of the 1975-1984 Krafla rifting episode to enable continuous monitoring of tilt, which is not possible with dry-tilt measurements. It is located about 2 km horizontally from the center of a shallow magma chamber, inferred from regional tilt measurements to be at 2.5 km depth. At this distance the surface tilt signal is strongest, and the tiltmeter data together with seismic observations proved invaluable to follow magma flow in and out of the reservoir. Currently, a single electronic tiltmeter is in continuous operation at Grímsvötn volcano, which was used together with GPS observations to constrain a deflating pressure source during the 2011 eruption, interpreted as a magma chamber. Continuous tiltmeters (water-tube and electronic tilt) tend to lack the long-term stability of the dry-tilt measurements. Leveling is labor intensive and many of the tilt stations in Iceland are not currently in use except a handful of stations that have proven sensitive and with long time series. Today only two lines and one circle station are measured annually. About ten circular stations are measured every several years, and some lines e.g. Surtsey and Thingvellir are measured every 10 – 15 years. The continued use of leveling lines lies in the fact they give independent results from space-geodetic observations, and it is known which stations are useful. Both the tilt stations and long leveling lines, which have proven to be sensitive, are a thus good complement to today's wide array of techniques.

Carlos Suarez-Plascencia, Francisco-Javier Nuñez-Cornu, Digna Ahtziri Carrillo Gonzalez, Bianca Valeria Sarez-Gonzalez

Submission 555

THE ERUPTIVE PROCESS 2015-2017 DEL VOLCÁN COLIMA, MEXICO AND UPDATING THE MAP OF RISK.

The Colima volcano, located in western Mexico (19 30.696N, 103 37.026W), showed a notable increase in activity since June 2015, which was characterized by the formation of a new dome, the emission of voluminous lava flows, explosive episodes with duration of at least 8 weeks that destroyed the dome and generated pyroclastic flows, ballistic fall and ash. The geochemical analysis shows a 2% increase in SiO₂ content in ashes emitted in June 2005 with respect to the events of 2015 and 2017.

The pyroclastic activity of 2015 was the most important since January 20, 1913. On July 10, two flows were formed by collapse of the lava front, channeled through the Monte Grande and San Antonio gullies, reaching a distance of 11 km, devastating part of the forest and killing some cows, the January 2017 flows were channeled through the La Arena ravine, where they flowed for 4.5 km without causing any damage. The eruptive columns in this period reached up to 4000 m above the crater level, causing ash to fall to NE, W, SW and SE, affecting nearby towns such as Ciudad Guzman, Zapotiltic, Huescalapa, Colima and small towns.

In the last ten years, the piedmont of the volcano and the Nevado de Colima, present an important change of land use, with the substitution of traditional sugar cane, corn and coniferous forests for avocado and berries, which cover Gradually the slopes located from 700 to 3000 masl, these activities have required the hiring of a large number of agricultural workers, in addition to the construction of balers and the expansion of the highway Guadalajara-Manzanillo, in order to give output to these products To the international market.

The explosive evolution, accompanied by an increase in pyroclastic activity, the constant fall of ash and the development of socio-economic activities, motivate the updating of the risk map of the Colima volcano, elaborated in the 2000, using information technologies Geographic, that will allow to determine the vulnerability and the current hazard, the iteration of both elements allow us to quantify the levels of volcanic risk. The results obtained will directly impact the Operation Plan of the Colima volcano applied by the Jalisco State Civil Protection, which aims to reduce the impact of an explosion type January 1913 (VEI 4) of the volcano.

Jenny Suckale, Tobias Keller

Submission 1136

Huffing and puffing: Modeling the physics of passive degassing, puffing, and Strombolian eruptions in basaltic volcanoes

Basaltic volcanism is driven primarily by the exsolution and buoyant ascent of gas. Observations from basaltic volcanoes like Stromboli identify three different regimes of degassing: passive degassing from a distributed area, puffing from active conduits, and Strombolian eruptions. Here we study how the coupled interactions between crystals, bubbles and magmatic melt in the upper portion of the Strombolian plumbing system lead to three different degassing regimes of increasing intensity. While we focus on Stromboli as an example, we argue that our insights could generalize to other volcanic systems characterized by low-viscosity melts.

Degassing and crystallization from dehydration during ascent govern the properties of the magmatic mush in the upper plumbing system at Stromboli. To characterize the three-phase interactions between crystals, bubbles and melt in the uppermost 1000 m, we link a 1D steady state model of dehydration and crystallization to a 2D dynamic model of flow through a deforming volcanic mush. Our setup implies that the deeper magma processing system provides a steady flux of well-mixed magma with approximately constant temperature, water content, and crystallinity into this shallow part of the plumbing system.

Our model exhibits three dynamic regimes, which we propose are representative of the three commonly observed degassing regimes at Stromboli. In the first regime, indicative of passive degassing, gas percolation is continuous and pervasive. It does not cause movement of magma or buildup of overpressure. Since gas percolation is the primary means of heat transport through the mush, it tends to localize in hot pathways of high gas flux and mobile magma. In the second regime, decompaction waves form in the hot flow zones created by passive degassing. Decompaction waves manifest themselves on the surface as small gas pulses emerging from active vents in short succession much like the puffing observed at Stromboli. If the mush residing in the upper conduit is crystalline enough to form a load-bearing matrix over tens and hundreds of meters, overpressure buildup during gas ascent may be significant. In addition, edifice-scale stresses impart tensile shear stresses on the mush. These conditions define the third behavioral regime, which is characterized by the onset of tensile fracture ahead of large gas pulses. Propagation through fracturing leads to rapid ascent speeds and magma entrainment, reminiscent of Strombolian eruptions.

Masafumi Sudo, Manfred Strecker, Andrea Friese, Kai Hahne, Simon Riedl, Tito Lopeyok, Geoffrey Mibei

Submission 1096

Temporal change in geochemistry of volcanic rocks along the volcano-tectonic axis of the northern Kenya Rift: Insights from the Ar/Ar geochronology and whole-rock chemistry at Paka

Six Quaternary volcanic centers located in the northern Kenya rift, mainly erupted basalts and trachytes and form the trachytic shield volcanoes. Paka, one of those volcanic centers, was investigated by systematic $^{40}\text{Ar}/^{39}\text{Ar}$ dating of 32 latest fresh volcanic rocks mostly from lava flows, and was found that the eruptive activities range continuously from 0.58 Ma to 0.012 Ma. Three relatively pronounced eruptive periods were found as around 0.4 Ma, 0.15 Ma and younger than 0.05 Ma by the relative frequency of eruption events. The division of whole Paka eruptive events to three episodes as 0.6-0.35 Ma (I), 0.35-0.1 Ma (II) and 0.1-0 Ma (III) based on those pronounced periods shows that the spatial change of eruptive vents gradually converge to NNE-SSW direction, which is similar to that of the Kenya Rift.

The volcanic activity of Paka started at 0.58 Ma by the eruption of the nepheline-normative basalt (Lower Basalt), meanwhile hypersthene-normative basalts, widely distributed around Paka, erupted together with nepheline-normative basalts only in the period from 0.3 to 0.1 Ma during the continuous trachytic eruptions lasted since 0.43 Ma to 0.01 Ma. Dunkley et al. (1993), however, previously deduced that Paka sits on and is also overlain by the hypersthene-normative basaltic lava flows, in which the latter (Young Basalt) distributes among volcanic centers of Paka, Silali and Korosi.

Nevertheless, this newly found eruptive order could more easily be explained by a simple model with the single hot mantle-diapir uprised beneath Paka. The diapir separates firstly smaller amounts of nepheline-normative basaltic magmas under higher pressures, then more voluminous hypersthene-normative basaltic magmas at shallower depth and by the higher degree of melting. Furthermore, Nb/Zr ratios in all the rocks gradually decrease along the above three episodes, reflecting the possible repeating segregation of basaltic magmas by fractional melting from the single mantle-diapir and their subsequent differentiation to trachytes, because the partitioning coefficients of Zr against mantle minerals are slightly higher than those of Nb. Although the flood basalts and trachytic shield volcanoes in the northern Kenya Rift are often considered separately, our results imply that those magmas could be derived from a single magma plumbing system or volcano in some cases.

Reference: Dunkley et al. (1993): International Series, Research Report SC/93/1, 185pp, British Geological Survey

Roberto Sulpizio, Damiano Sarocchi, Luis Angel Rodriguez-Sedano, Brittany Brand, Nicholas Pollock, Gerardo Campos

Submission 827

On the entrapment mechanisms of volcanic granular flows from laboratory experiments and comparison with natural exposures

Most of our current knowledge on hazardous volcanic granular-type mass flows stems from interpreting resulting deposits because direct observations are largely limited. Current sediment transport and deposition models (underlying these interpretations) are still in their infancies and are also largely debated. This is because of the complex and hitherto poorly understood physics of granular matter. Here we present laboratory experiments on poly-disperse granular flows of volcanic material designed to bridge this gap. The experimental results highlight some important characteristics of internal organization and general kinematics of granular flows that can be extended to the generality of poly-dispersed, flowing granular matter. In particular, we find that decelerating volcanic granular flows can entrap loose material from the base due to high shear stress exerted from the flow base. The difference in velocity between the moving flow and the loose material at its base imparts rotation, which results in formation of vortexes similar to Kelvin-Helmholtz instabilities in fluids. The shear induced laboratory structures were compared with natural exposures of concentrated pyroclastic density currents of May 18, 1980 eruption of Mount St. Helens. The comparison and the data collected in the laboratory allowed the formulation of a shear-dependent model of entrapment for decelerating volcanic granular flows. These results may have impact on many field of research in Earth science, physics, engineering and industry.

Roberto Sulpizio

Submission 665

On the use of field data for defining eruptive scenarios and drawing of hazard maps

Geological data are essential in the description of the volcanic history, in the comprehension of volcanic evolution, in the geological interpretation of the phases of construction and erosion on volcanic edifices and of volcanic unrest. Volcanology has made great advances in the last three decades, becoming a modern interdisciplinary science for quantifying volcanic processes, their associated hazards and impacts on society and the environment.

The geology of volcanic areas represents the unavoidable baseline for all the studies dealing with volcanic activity, because the geological record witnesses to the reality, and provides the measure against which the applicability of observations from other sources (e.g. numerical simulations) must be ultimately assessed.

What are geological data collectable on volcanoes? The stratigraphy of a volcano, the description of lithofacies association and architecture, the morphology of volcanic landscapes, the geological mapping of volcanic deposits, the volcano-tectonics interactions. All these data are essential for defining eruptive scenarios and drawing of hazard maps, which are the basic tools in volcanic hazard mitigation. This presentation will review the use of geological data for understanding volcanic processes and behaviour, and their use for hazard mitigation purposes.

Mari Sumita, Hans-Ulrich Schmincke

Submission 884

600 000 years of continuous eruptive record of Nemrut and Süphan volcanoes, eastern Anatolia: onshore and offshore tephrochronology of Lake Van area (Paleovan ICDP Drilling project)

Chronological, chemical, mineralogical, volcanological and sedimentological data obtained on ca. 250 of a total of ca. 450-500 tephra layers from Site 2 of the ICDP Paleovan project are compared with similar data from the ca. 570 ka onshore record of Nemrut Volcano adjacent to, and underlying, Lake Van.

Nemrut explosive activity extends from ca. 570 ka to historic onshore and from ca. 580 ka to Holocene in the core. Most tephra layers are slightly peralkaline trachytes, larger volumes of rhyolitic tephra having been erupted at intervals of 30-40 ka. Fallout deposits dominate while larger rhyolite eruptions are generally associated with ignimbrites onshore, thick massive tephra deposits drilled being interpreted as syn-ignimbrite turbidites. Stages of caldera collapse were associated with large-volume rhyolitic eruptions. Most larger eruptions are compositionally zoned from evolved to more mafic, magma mingling being ubiquitous.

Eruptive rates at Nemrut volcano increased in time. Tephra from adjacent subalkalic Süphan volcano dominate the felsic tephra in the core prior to about 200 ka. Nemrut volcanic explosive activity was roughly periodic while that of Süphan was episodic with external forcing (seismic, hydroclastic) having been characteristic forcing mechanisms. Dominantly high-Al basaltic tephra in the lower ca. 100 m of the core are of subaqueous origin and may represent parent magma to the subalkalic Süphan system.

We estimate about 30 % of the cored tephra layers to be reworked. Wind-transported tephra, most common and associated with dry climate intervals, contain many xenocrysts and other nonvolcanic particles. Thick fallout deposits of fine-grained basal tephra and rounded pumice at the top are pumice raft deposits reflecting prolonged abrasion in pumice rafts. Poorly sorted reworked tephra deposits with abundant organic debris and gypsum crystals are interpreted as recording extended periods of low lake levels and correlate with seismically defined low lake level periods. Such intervals may be used as independent criteria for recording significant lake level changes.

The precise stratigraphic and temporal correlation of the upper cores from sites 1 and 2, as well as with the onshore tephra record as based on fallout tephra defined by chemical composition and highly concordant $^{40}\text{Ar}/^{39}\text{Ar}$ ages. There is a tentative correlation of higher eruption frequency with warm climate periods.

Ikuro Sumita, Nao Yasuda, Moe Mizuno, Heiko Woith, Eleonora Rivalta

Submission 156

Experiments on shaking-induced fluidization in a liquid-immersed granular medium : implications for triggering eruptions

Earthquakes may liquefy crystal-bearing magma as well as mud to trigger eruption. However the shaking conditions needed for such phenomena to occur are still poorly known. Here we conduct laboratory experiments in which a liquid-immersed granular medium is shaken sinusoidally and also using earthquake waveforms. Here we use a layered granular medium such that the upper layer consists of fine-grained glass beads forming a permeable barrier. The shaking condition is characterized by a dimensionless acceleration $\Gamma = a / (\Delta \rho g / \rho)$ and frequency (f). (i) Vertical shaking [1, 2]: We find that there is a critical Γ_c for liquefaction and subsequent Rayleigh-Taylor (R-T) instability to occur. Experiments conducted at $f = 10 - 5000$ Hz indicate that Γ_c is minimum at 100 Hz. At high f , liquefaction is suppressed because of smaller shaking energy. At low f it is suppressed because the period of shaking is longer than d/V_s (d : particle size, V_s : Stokes' velocity). This indicates that not only acceleration but also the velocity is important for liquefaction. Experiments conducted using a more viscous liquid indicate that although the growth of the instability is slower, Γ_c is reduced and the frequency band for liquefaction to occur is broadened. We interpret this result as a consequence of viscous lubrication and a smaller V_s . Experiments with a thicker upper layer reduces the growth rate of the instability. (ii) Horizontal shaking : We find that R-T instability, similar to those observed in (i) occurs at 10 Hz. However at 1 Hz, sloshing occurs because it is close to the resonant frequency of the container used [3]. As a result, initially graded layers are flipped over and an inverse grading forms. At 1-10 Hz we find a coexistence of R-T instability and sloshing. Since 1-10 Hz correspond to the seismic band, we conducted experiments using waveforms of earthquakes with different characteristic f . We confirmed that R-T instability occurs only when the high f component is present. We also measured the sound and pore water pressure in the granular medium. At 10 Hz and $\Gamma > 1$, we detected sound and negative pore water pressure, suggesting particle collision and dilatancy. Application to magma and mud suggests that under specific shaking conditions, vesiculation by decompression may occur.

[1] Yasuda & Sumita, 2014, PEPS, 1:13, [2] Ibid., 2016, PRE, 93, 022901, [3] Namiki et al., 2016, JVGR, 320, 156, [4] youtube : geodynlab.

Ivan Suñe Puchol, Gerardo de Jesus Aguirre Diaz, Pablo Davila Harris, Dario Pedrazzi, Eduardo Gutierrez, Walter Hernandez, Daniel Miggins, Antonio Costa

Submission 1221

THE VOLUMINOUS 1.5 Ma OLOCUILTA IGNIMBRITE: A PRE-COLAPSE FISSURE SUPERERUPTION OF ILOPANGO CALDERA, EL SALVADOR

The Olocuilta Ignimbrite dated at ~ 1.53 Ma (U-Pb zircon age), is the first of several large eruptions of the long-lived Ilopango caldera, an active volcano along the Central America Volcanic Arc, in El Salvador. It is rhyolitic in composition, pink-red, partly to densely welded, and composed mostly of pumice clasts, lithics and ash matrix, with quartz and plagioclase phenocrysts. Preliminary estimates for the eruption volume of the Olocuilta Ignimbrite suggest that it is larger than 100 km³ of Dense Rock Equivalent (DRE). This number depends on the volume of the co-ignimbritic ash dispersed in the far-field. This widespread pyroclastic deposit extends for more than 1000 km² within the central part of El Salvador. It forms an extensive plateau at the southern flank of the Ilopango caldera, with preserved thicknesses of more than 100 meters measured along the canyons of the main N-S rivers. The upper part of the ignimbrite outflow sheet (8 to 10 m) is strongly welded, presenting classic eutaxitic textures and columnar jointing. Geologic and stratigraphic features of Olocuilta Ignimbrite indicate a strong tectonic control on and a fissure origin of the eruption. Evidences includes: 1) the absence of initial plinian deposits, which is a characteristic of several fissure ignimbrites in Mexico (Aguirre-Díaz and Labarthe-Hernández, *Geology* 2003), that have been interpreted as eruptions triggered by regional faults; 2) lack of co-ignimbritic lithic lag breccias around the Ilopango caldera, which suggests a strong extensional field and that there was not a caldera collapse associated to this eruption, 3) this ignimbrite is not observed in the inner walls of the current caldera, and 4) the San Vicente fault as possible feeder for Olocuilta ignimbrite, which is a major fault of the El Salvador Fault System, with right strike-slip faults linked with the transtensional tectonics crossing the country from W to E. An example of this relationship between the volcanism of the Ilopango caldera and the regional tectonics, is the last eruption occurred in 1879, when a dacitic dome was extruded in the middle of Ilopango Lake, just after a series of earthquakes caused by the San Vicente fault (Golombek and Carr, 1978). This study was financed by CONACYT-CB grant 240447 and logistically supported by MARN-El Salvador.

Young Sunwoo, Doyoon Kim, Yoo Jung Kim, Jae Eun Park, Hyerim Park

Submission 1247

3-Dimensional Chemical Transport Model Application for Risk Assessment of Potential Volcanic Disaster around Korean Peninsula

Many volcanos are located within 1,500 km of Korea which implies that a potential disaster is always possible. Several eruption precursors were observed rather recently at Mt. Baekdu, which has sparked intensive research on volcanic disasters in Korea.

For assessment of potential volcanic hazard in Korea, we developed classification method of volcanic eruption Worst-case scenarios using the HYSPLIT-4 regarding air quality impact. And we conducted 3-dimensional chemistry transport modeling for selected eruption scenarios

The Community Multi-scale Air Quality (CMAQ) modeling system was employed for 3-dimensional chemical transport modeling. We estimates volcanic ash emission using ERUPT-3 modeling results, and SO₂ emission was estimated by using VSI (Volcanic Sulfur Index). Emissions of other gases calculated by mole fractions of volatiles from arc volcanoes(Fischer 2008). For adjustments of volcanic plume shape in CMAQ, we calculated vertical mass fractions using conventional 'umbrella shape' suggested by Stuefer et. al (2013).

Sarah S. Sutton, Christopher W. Hamilton, Jacob E. Bleacher, David A. Williams

Submission 461

Channelized Flows East of Olympus Mons, Mars

The flexural moat around Olympus Mons is infilled with Late Amazonian-age lava flows, and contains a diversity of channelized flows, low shields, vents, and fissures. We examine two channel systems east of Olympus Mons, which source from separate fissures. Located 50 km apart, the channels, as well as their related fissures, display contrasting morphologies.

Both channel systems extend NNW for 10s to 100s of km. They are situated in a relatively smooth region with a $<1^\circ$ downward slope, inclined towards the base of the Olympus Mons scarp. This area, between the older Olympus Mons aureole deposits and the basal scarp, is on the northern portion of a regional drainage divide. The northern channel system (17.5° N, 233.0° E) displays volcanic features such as leveed channels with rough inner margins. The southern system (17.3° N, 235.0° E) displays fluvial characteristics such as streamlined islands, cutbank erosion, and a scoured channel bed. The fissures associated with each channel system are also distinct. The fissure associated with the northern channel system is linear, and parallels other fissures in the region, which are oriented radially to Olympus Mons. The southern system is associated with a fissure system that consists of branching, arcuate segments. Relationships between the fissures and channels are also considered, both as potential source regions and as crosscutting features.

We use regional topographic data from the Mars Orbiter Laser Altimeter, as well as Mars Reconnaissance Orbiter Context Camera (CTX) and High Resolution Imaging Science Experiment (HiRISE) images and stereo-derived digital terrain models (DTMs) to map geologic units and facies. The geologic map describes the Olympus Mons edifice and aureole units, Late Amazonian plains lavas, and the Ulysses Fossae unit. The facies map includes fissures, vents, channels, craters, and low shields. We use high-resolution DTMs to constrain models of lava and aqueous flow emplacement in this region in order to determine the nature of the fluid(s) involved in the formation of each system.

The distinct channel morphologies are minimally modified or overprinted by other processes, making this site ideal to study some of the youngest surface expressions of magmatic and subsurface aqueous activity on Mars. We examine the superposition of features to understand the relative timing of volcanic and aqueous events in the context of the volcano-tectonic evolution of the Tharsis region and its hydrology.

Takehiko Suzuki, Masanori Murata

Submission 978

Tephrochronological study of the long-term explosive eruption history in the Northeast Japan Arc

Eruptions rated at a VEI of 6–8 strongly influence human activity via huge pyroclastic flows and widely distributed fall-out tephtras. To evaluate their impacts, ages, repose periods, distributions and sequences of tephtras are crucial. However, even though both major and minor tephtras have been prominently deposited in proximal areas, their stratigraphy is sometimes incomplete due to several reasons. Large-volume tephtras tend to be distributed broadly. Therefore, the correlation of distal fall-out tephtras with proximal ignimbrites is effective to complete the eruptive sequence. Moreover, the identification of distal tephtras contributes to the determination of not only a reliable erupted volume but also the precise age because it can be crosschecked by integrated time-scales based on many methods.

To establish the eruption history in the Northeast Japan Arc, a typical island arc originated by subduction, we had revised Quaternary tephrochronology. Here, we focus on two million years sequence of large-volume tephtras (VEI=7), together with showing long-term changes in eruption rate and repose periods of huge eruptions. Quaternary volcanoes in the area are grouped into eight volcanic regions (VRs), and some of them are characterized by both calderas and strato-volcano formations since Late Miocene. During the period from 2.0 Ma to 0.7 Ma, three VRs had provided at least seven large-volume tephtras (VEI: 7) by caldera-forming eruptions. In ascending order, they are two tephtras from the Sengan geothermal VR (Tmg-R4 tephtra: 2.0 Ma, Kd44-Naka: 1.968–1.781Ma) (Suzuki & Nakayama, 2007), four from the Aizu VR (Sr-Kmd: 1.542–1.504 Ma, Sr-Aki-Kd18: 1.522–1.460 Ma, Sr-Asn-Kd8: 1.219 Ma, Sr-Kc-U8: 0.922–0.910 Ma) and one from the Towada-Hakkoda VR (Hkd-Ku: 0.76 Ma) (Suzuki et al., 2005). All of them are composed of distal fall-out tephtras and proximal ignimbrite. We re-examined their ages considering the stratigraphic positions of the distal tephtras identified in the Kanto region where biostratigraphic and magneto-stratigraphic frameworks are available. Considering these data and smaller ignimbrites (VEI: 6), it is concluded that at least three of eight VRs have a specific period characterized by repeated caldera-forming eruptions (VEI: 7), lasting for 0.1 to 0.6 myr. After 0.7 Ma, occurrences of caldera-forming eruptions have been limited in Towada-Hakkoda and Kurikoma-Onikobe VRs where eruptions of VEI=6 associated with smaller ignimbrites had repeatedly occurred.

Yujiro Suzuki, Masato Iguchi

Submission 56

Determination of the mass eruption rate for the 2014 Mount Kelud eruption using three-dimensional numerical simulations of volcanic plumes

The 13 February 2014 eruptions of Mount Kelud, Indonesia, had a mass eruption rate of $\sim 10^7$ kg s⁻¹ at the vent. In such an intensity of eruption, the eruption column generally rises almost vertically and the umbrella cloud can be controlled by both the gravity current of umbrella cloud and advection due to atmospheric wind. Because of these multiple predominant factors, the eruptions with a moderate intensity cannot be reproduced by the previous simple models (e.g., Woods, 1988). Therefore, we present three-dimensional (3D) numerical simulations of the development of a volcanic eruption column and umbrella cloud formed during the 2014 Kelud eruption, and determine the eruption conditions through comparisons between the simulation results and the observed data.

The 3D numerical simulations were designed to reproduce the injection of a mixture of pyroclasts and volcanic gas from a circular vent located at 1500 m asl. We used a combination of a pseudo-gas model for fluid motion and a Lagrangian model for particle motion. We carried out eight simulations of eruption plumes with variable mass eruption rate (MER), which ranges 5×10^5 to 1×10^8 kg s⁻¹. The other parameters were kept fixed in all of the simulations.

The model used in this study quantitatively reproduces the observed data and, in particular, the plume height and the horizontal expansion level and rate of the umbrella cloud. The simulation results suggest that on the basis of the plume height and structures and the horizontal expansion level of the umbrella cloud the mass eruption rate (MER) for the 2014 Kelud eruptions was 3×10^7 to 4×10^7 kg s⁻¹. On the basis of the horizontal expansion rate of the umbrella cloud, on the other hand, the estimated MER was 1×10^8 kg s⁻¹. The difference between these two estimates implies the strong diffusion in the umbrella cloud or the efficient entrainment of ambient air by eruption column.

Yuki Suzuki

Submission 283

Magma plumbing system of Fuji volcano inferred from product of latest summit eruption (Yufune-2 scoria)

The Fuji volcano has been dormant since 1707. Therefore, petrological studies of past ejecta are important. At an outcrop locating 10 km from the summit, I have divided the Yufune-2 scoria deposit (2.2 ka) into 5 units (a-e). The scoria size increases toward unit-b, but decreases in the upper units. Bulk composition of scoria (ca. 51 wt.% SiO₂) does not change with eruptive unit. I have analyzed thin sections of 4-6 scoriae for each unit. Except xenoliths of basaltic lava (Suzuki and Fujii, 2010 JVGR), scoriae seem almost homogeneous. Phenocrysts of olivine and plagioclase (less than 2mm) are euhedral and lack in reaction rims. Compositional distribution of phenocryst cores are distinctive in each unit. All scoriae of unit-b and c are dominated by low-Fo (85) and high-Fo (>76), although some scoriae show wide Fo extending to 73. In unit-a scoriae and rest of unit-d scoriae, cores of phenocrysts show wide range (Fo73-80, An65-92). The degree of compositional variety is due to two types of phenocrysts. High Fo (>76) and low Fo (85) is homogeneous and is characterized by small crystal size (less than 500 μ m). Low An plagioclase (85) region that closely resembles the high An type in size. Scoriae having only high Fo and high An types (e.g. unit-d) have lower amount of phenocrysts (3 vol.%) than scoriae having only low Fo and low An types (19 vol.%). These lines of evidence indicate that 1) magmas with different degree of crystallization, but with the same bulk composition, were present, and 2) the two endmembers were erupted independently or mixed; mixed magma in unit-a, followed by the high-crystallinity magma in the climax (unit-b and unit-c), ended with less-crystallized magma accompanied by mixed magma. The high crystallinity magma was derived from the less crystallized magma. The identification of the parts that crystallized when crystallinity of magma was low is possible only for plagioclase, because of much more sluggish diffusion of CaAl-NaSi in plagioclase in comparison with Mg-Fe in olivine. More examination of diffusion profiles is necessary in order to constrain the timescale of storage of the high-crystallinity magma, and to constrain the timescale from final mixing to eruption.

Elliot Swallow, Colin Wilson, Madison Myers, Paul Wallace, Katie Collins, Euan Smith

Submission 449

The onset of caldera-collapse in a supereruption captured in glass and mineral chemistries

Stratigraphically constrained geochemical analyses spanning the transition between initial fall activity and the onset of widespread ignimbrite deposition in caldera-forming silicic eruptions shed light on the parental magma system. Early deposits of some eruptions show that their initiation and magmatic systems can be complex^{1,2}, but how do such complex systems escalate into caldera-collapse? The 2.08 Ma, ~2,500 km³ Huckleberry Ridge Tuff (HRT) consists of widespread initial fall deposits^{3,4} followed by three ignimbrite members³: A, B and C3. Myers et al.² demonstrated the episodic and multi-vent initiation of the HRT in the initial fall deposits, with sequential tapping of three discrete melt bodies, the last of which became dominant within the later fall deposits. We use matrix glass and mineral chemistry to focus on the subsequent transition from the fall deposit into widespread ignimbrite (member A) deposition. Trace element analyses of glass shards in basal ignimbrite A reveals clustering of compositions and signifies a continuation of, and escalation in, the tapping of multiple melt domains from four during the fall deposit to nine in the basal ignimbrite. These earliest flows tapped a range of melts, from highly evolved (as in the fall deposits) to hotter, less evolved material not seen in the fall deposits. Variations are greatest in Ba (10-900 ppm), Sr/Rb ratios (0.005-0.09) and degrees of LREE depletion. However there is an absence of geographical variation, with proximal and distal locations both north and south of the subsequent caldera exhibiting similar ranges of glass composition from inferred penecontemporaneous flow deposition. These observations indicate that a complex magmatic system (comprising multiple melt/magma domains) was not just limited to the earliest tapped materials. Pairing of melt and mineral chemistries shows two compositionally distinct upper-crustal lineages within the broader magmatic system. Widespread ignimbrite deposition, inferred to reflect caldera-collapse, occurred after ~50km³ magma had been discharged. Although external tectonic controls were important as an eruption trigger², subsequent depressurisation of the system through magma withdrawal led to caldera-collapse, opening of multiple vents and tapping of numerous discrete melt-dominant bodies.

¹Pistolesi et al. (2016): *Geology* 44, 487; ²Myers et al. (2016): *EPSL* 451, 285;

³Christiansen (2001): USGS Prof Pap 729-G; ⁴Izett & Wilcox (1982), USGS Map I-1325.

Donald Swanson, Matt Patrick, Tim Orr

Submission 206

Slowly pulsing magma supply inferred from changes in level of the lava lake in Overlook crater, Kīlauea

The persistence and accessibility of the lava lake in Overlook crater provide an opportunity to track changes in lake level and relate them to other monitored parameters at Kīlauea. It is well documented that lake level falls and rises during summit-wide deflation-inflation (DI) events. The amplitudes of such level changes are typically 20–30 m, and the durations 2–4 days. In addition, gas-piston activity causes changes of a few meters in lake level with typical durations of tens of minutes to hours.

Largely obscured by these shallow-seated, relatively rapid changes in lake level is a long-term pattern that can be seen when monthly averages of lake level are examined. Since near-daily laser rangefinder measurements to the lake surface were started in July 2013, we recognize at least seven periods lasting several months when average lake level rose and then fell a few meters. Such a pattern correlates with monthly-averaged vertical motion measured at 5 GPS stations around Kīlauea summit. The stations move upward when lake level rises or uplift rate increases, and they subside or slow their uplift when the level drops.

The monthly-averaged lake level also correlates with the mass of juvenile ejecta collected in 10 buckets on the caldera floor above the lake. Not surprisingly, more ejecta mass accumulates when lake level is high and less when it is low. Thus the variation of tephra accumulation with time can be used as a proxy for lake level before laser rangefinder measurements became routine. Using this proxy, we recognize 4–6 cycles between late 2008 and 2013.

The simplest explanation for the dozen or so cycles in lake level and tephra accumulation is a slowly pulsing supply rate of magma entering the summit magma reservoir complex. The entire summit GPS network responds similarly during the cycles (with one exception), so it is unlikely that magma is simply being transferred from one part of the reservoir complex to another. Most likely, the pulsing magma supply is reflecting a deeper process or processes, which could range from fluctuating rates of melting in the mantle to complexities along the 80–100-km-long transport path between the mantle and the shallow reservoir system. Pulsing magma supply over several-month periods has not been recognized previously at Kīlauea. We suspect that magma supply may be changing on all time scales, even at times when there is no obvious surge as in 2003–2007.

Kristin Sweeney, Jon Major

Submission 214

Quantifying the role of initial conditions in drainage network configuration, Mount St. Helens, WA

The 1980 eruption of Mount St. Helens (MSH) buried the North Fork Toutle River (NFTR) valley in up to 150 m of deposits from a debris avalanche, pyroclastic flows, and lahars. This exceptional fill largely erased the headwater drainage network. More than thirty-five years after the eruption, sediment yield from the NFTR remains elevated over background levels, and erosion is a major factor influencing the trajectory of ecological recovery. Channel processes dominate sediment transport in the NFTR. Thus, the configuration of the post-eruption drainage network controls the spatial distribution of erosion (and by extension ecological activity). Determining the factors controlling drainage network topology is central to predicting the continuing geomorphic and ecological response to the eruption. Past analysis of aerial photographs shows wide variability in mechanisms of channel initiation in the NFTR. Fill-and-spill of closed depressions occurs in the hummocky debris avalanche and headward incision and subsequent avulsion dominate the planar Pumice Plain. We hypothesize that these early patterns are driven by differences in surface roughness, erodibility, and topographic confinement among the 1980 deposits. However, it is unclear whether this spatial heterogeneity persists or is overprinted by (a) autogenic processes such as drainage area competition between neighboring channels, or (b) large-magnitude flows that are relatively insensitive to local topographic roughness. To test the importance of initial conditions in the early stages of drainage network formation (1980 – 86) and examine the persistence of initial patterns in the modern network, we generated a series of six digital surface models (DSMs) using vertical aerial photos and Structure-from-Motion photogrammetry software. We extracted the channel network from these DSMs and from 2009 lidar, and compared channel formation and evolution among areas of distinct initial surface roughness and topographic confinement. Our preliminary results confirm that channel initiation processes correlate well with initial surface roughness and erodibility. Geometry of the current network, however, is best explained by the influence of large flows (post-1980 lahars and floods) and 1982 – 1985 pumping of nearby Spirit Lake; excess shear stress enabled rapid vertical incision, which subsequently fostered lateral erosion in the main channel but reduced overall topologic rates of change.

Matthew Sweeney, Greg Valentine

Submission 131

Impact zone dynamics of polydisperse multiphase jets and their implications for the initial conditions of pyroclastic density currents and their subsequent deposits

The fluid dynamics at the zone where a collapsing eruption column impacts the ground dictate the initial conditions for pyroclastic density currents as they move across the landscape and form deposits. However, our understanding of this impact zone is limited due to the inability to directly observe and measure it in nature. As a collapsing multiphase jet (gas + particles) approaches the ground, particles decelerate via drag with the carrier gas. The particles' inertia works against these drag interactions, resulting in a competition between these two forces, which is described by an impact Stokes number. The impact Stokes number determines how easily particles of a given size or density class make the transition from an axial to radial flow at the impact zone. Our multifield numerical modeling of impinging jets shows that particle behavior is sensitive to whether a jet is monodisperse or polydisperse. For instance, a particle with $d=0.01$ m, which is relatively poorly coupled to the gas phase in a monodisperse mixture, becomes better coupled when in the presence of particles with $d=0.0001$ m due to particle-particle drag. However, there is a limit to this phenomenon. In situations where particles are sufficiently poorly coupled that they are not as affected by the interphase particle-particle drag of the smaller particles, they can pack at the impact site. This increase in particle volume fraction means a decrease in gas volume fraction, which can result in a sort of expulsion of gas downstream of the impact zone. If fine particles are present, they can be expelled with the gas, resulting in a dilute density current preceding the main flow. Furthermore, we quantify the length scales at which particles decelerate as they approach the ground, which is highly sensitive to the mixture sound speed. In cases where the collapsing jet is supersonic, a standing shock develops at the impact zone, which results in a much smaller length scale and thus a greater impact Stokes number. This work suggests that modeling done with a single particle size can be misleading when taken in the context of volcanic flows with a range of particle sizes and densities. In addition, volume fraction dependent compressibility effects must also be considered when analyzing deposits.

Dawn Sweeney Ruth, Fidel Costa

Submission 952

Unraveling processes and time scales recorded by multiply zoned plagioclase crystals

Many basaltic andesite open vent volcanoes (e.g. Mayon, Stromboli, Etna) erupt plagioclase rich lavas. Their phenocrysts show very similar textures and compositions, including multiple dissolution zones riddled with glass and mineral inclusion that are associated with high Ca/Na zones. The recurrent high Ca/Na excursions and dissolution zones in single crystals are a record of the pre-eruptive processes occurring at these volcanoes, either repetitive magma intrusions between eruptions, or/and convection in the reservoir/conduit that allows for the permanent degassing. Here we have started a detailed textural and compositional analysis of this type plagioclase found in lavas from Mayon volcano to gain insight into the processes and time scales they record.

Lavas from the 2000 eruption contain plagioclase phenocrysts with An zones alternating between An₈₀₋₉₀ and ~An₆₀. The rimward edges of zones show sharp boundaries where An-rich regions drop suddenly to An-poor regions. An content in diffuse boundaries gently increase from An-poor to An-rich. Electron microprobe and LA-ICPMS analyses of Sr, Mg, and Ti show that these trace elements change accordingly with the An. However, most An correlates negatively with Mg content and show mirror images in profile traverses, indicating that Mg has probably fully re-equilibrated by diffusion. The relationships between An and Fe and Ti, respectively, are more complex with observed positive and negative correlations. In some crystals, Ti transition zones in profile traverses are sharp with widths of < 5 μm . Other crystals, however, do not have distinct zones with respect to Ti content.

Sr content also changes with An. Calculated liquids in equilibrium with high An cores are higher than those in equilibrium with the rims, and thus they have not been reequilibrated by diffusion. The width of the transition zones of Sr concentrations are generally < 5 micrometers, which, if taken as indication as the diffusion length scale, suggests times between the An changes and eruption less than 6 months. Such time scales are comparable to those we have obtained from modelling of Fe-Mg zoning in orthopyroxene, and suggest multiple intrusions and volatile pressure variations are the main processes recorded by the plagioclase crystals. The pyroxene and plagioclase datasets combined, indicate that multiple intrusions occur below Mayon volcano prior to eruption, in accord with some indication that not every unrest episode leads to eruption.

Devy Kamil Syahbana, Martanto Martanto, Novia Abdul-Manaf, Heruningtyas Desi Purnamasari, Annisa Prastanti, Nia Haerani, Iing Kusnadi, Ferry Rusmawan, Aditya Sebastian Andreas, Oktory Prambada, Ugan Boyson Saing, Yudhi Wahyudi, Syarif Abdul-Manaf, David A

Submission 824

Eruption precursors: A case study from volcanoes in eastern region of Indonesia

The main goal of volcano monitoring is to mitigate disaster risk caused by volcanic eruptions. Studying the precursory signatures of volcanic eruptions is one of the most important steps carried out by volcanologists to achieve the goal. A multidisciplinary volcano monitoring method has been applied at volcanoes to detect changes in the geophysical, geochemical, and geodetic behavior preceding, during, and following the eruptions. A long-term volcano monitoring data help volcanologists to define some common signatures of volcanic activities which may culminate in an eruption.

Here we present results of our study aiming at understanding volcanic eruption precursors from several unrests in eastern Indonesia volcanoes. We use seismic data from our monitoring network in Indonesia as the basis of this study, while other data obtained from other methods are also complementary used. We make comparison of monitoring data from an individual volcano between different unrests. We also compare monitoring data between different volcanoes during their unrests. We find similar eruption precursors of an individual volcano, which is consistent with their eruption style. However, we suggest that common eruption precursors implied from studies of an individual volcano may not be generalized to infer the global volcanic eruption precursors. Even at the same volcano, our experience from one unrest could not directly be applied to another situation. The results of our study may contribute to the effort in the prediction of the behavior of future eruptions, and to volcanic hazards assessment, and therefore to volcanic disaster risk mitigation.

Dawid Szymanowski, Jörn-Frederik Wotzlaw, Ben S. Ellis, Olivier Bachmann, Marcel Guillong, Albrecht von Quadt

Submission 98

Zircon–titanite constraints on pre-eruptive storage conditions in large magma reservoirs

Building supereruptive magma reservoirs in the cold, upper parts of the Earth's crust requires a significant flux of magma into the magmatic system extended for a period sufficiently long for its accumulation, differentiation and periodic eruption. Some models favour magma storage in a 'cold' non-eruptible state, requiring extensive reactivation of the reservoirs before eruption, while others suggest storage at higher temperature and lower crystallinity, implying that magma in such reservoirs is readily eruptible. Consequently, constraining hazards related to large volcanic eruptions requires observations directly linking magma residence timescales to the thermal state and crystallinity during storage. We present a method for simultaneously determining crystallisation temperatures and ages of co-genetic magmatic crystals of zircon and titanite, allowing us to place tight constraints on the long-term thermal evolution of magma reservoirs. High-precision ID–TIMS U–Pb dates of zircon and titanite in the > 900 km³ Kneeling Nun Tuff (New Mexico, USA) independently record > 600,000 years of magma assembly while their trace element contents allow us to constrain the dominant storage conditions to low temperatures between the solidus (680–700 °C) and the temperature of the onset of titanite crystallisation (726 ± 22 °C). Similar zircon–titanite systematics including the lack of near-solidus titanite in a suite of supereruptions suggest that protracted low-temperature 'mushy' storage culminating in late-stage reheating is a widespread feature of large crystal-rich eruptions.

Jacopo Taddeucci, Miguel Angel Alatorre Ibarquengoitia, Omar Vázquez, Elisabetta Del Bello, Piergiorgio Scarlato, Tullio Ricci

Submission 1032

The in-flight dynamics of Volcanic Ballistic Projectiles: An high-speed imaging perspective.

Centimeter to meter-sized volcanic ballistic projectiles from explosive eruptions jeopardize people and properties at kilometers from the volcano, but they also witness past eruptions. Traditionally, projectile trajectory is modeled using simplified ballistic theory, accounting for gravity and drag forces only and assuming simply-shaped projectiles free-moving through air. Recently, collisions between projectiles and interactions with plumes are starting to be considered. Beside theory, experimental studies and field mapping have so far dominated volcanic projectile research, with only limited observations.

The introduction of high-speed, high-definition imaging has opened a new spatial and temporal scale of observation, illuminating in-flight processes not considered before. We can now document and parameterize a variety of in-flight dynamics that control the trajectory of volcanic projectiles from different eruptions. In-flight collisions are promoted by the occurrence of multiple, syn-eruptive ejection pulses, new pulses ejecting faster projectiles amongst previously ejected, already decelerating ones. Collision outcome depend on projectile mechanical properties, bouncing and breaking dominating brittle blocks, stretching, merging and deforming dominating ductile bombs. Blocks and bombs often deform and fragment both on landing and in flight, due to air drag and fast spinning. Projectile spinning and deformation result in variable settling velocity, shifting the 'terminal fall velocity' paradigm. Combining the trajectory of selected projectiles, the first field-derived parameterization of drag deceleration is offered, including revised drag coefficient analysis.

The diffuse fragmentation of bomb-sized pyroclasts both in-flight and on landing implies, for instance, that the grain size distribution of proximal tephra deposits of mafic composition may significantly differ from that originated at the vent. Finally, we offer a new parameterization of processes that include drag deceleration, projectile rotation and spinning, and in-flight collisions. These new perspectives shed light on projectile fallout hazard mapping and forecasting and on the interpretation of projectile deposits from past eruptions, both on Earth and on other planets.

Kimiko Taguchi, Hiroyuki Kumagai, Yuta Maeda, Roberto Torres

Submission 41

Resonator size and fluid properties of long-period events inferred from an analytical formula for crack resonance frequencies

The geometry and fluid acoustic properties of the resonator at the source of the long-period (LP) event have been estimated by the comparison of observed frequencies with resonance frequencies of the crack model (Chouet, JGR, 1986). Recently an analytical formula for the crack resonance frequencies was proposed by Maeda and Kumagai (GRL, 2013; GJI, 2017), which enables the comparison in a simple and systematic way. Taguchi et al. (AGU meeting, 2016) showed that all the crack model parameters, which explained several peak frequencies of LP events at Kusatsu-Shirane and Galeras volcanoes, were estimated by using this formula. In this study we analyzed further events that occurred from August 1992 to January 1993 at Kusatsu-Shirane and from 6 to 10 January 1993 at Galeras. Assuming misty and dusty gases at Kusatsu-Shirane and Galeras, respectively, our analysis results indicated that the crack volume increased as increasing gas weight fraction of the fluid in the crack at both volcanoes. At Kusatsu-Shirane, the crack volume increased from 10^{-1} m³ to 103 m³ and gas weight fraction also increased from 10^{-2} to about 1 between August and November 1992. Then both the crack volume and gas weight fraction decreased to about 10^{-1} m³ and to 10^{-2} , respectively, in January 1993. An increase in gas weight fraction at Kusatsu-Shirane was indicated by Kumagai et al. (JGR, 2002), but our study showed that the remarkable increase in the crack volume also occurred in this period. At Galeras volcano, the crack volume decreased from 103 m³ to 10^{-1} m³ and gas weight fraction decreased from 10^{-1} to 10^{-3} between 7 and 10 January 1993. This tendency was not shown by previous studies. Since a magma eruption was observed at Galeras after a few days from the latest event analyzed in this study, the temporal variation of the crack volume and gas weight fraction may be caused by precursor processes of the magma eruption. In this study we demonstrated that our method using the analytical formula of the crack resonance frequencies contributes to constrain the source processes of LP events and to monitor the state of fluids under volcanoes.

Dorianne Tailpied, Benoit Taisne, Anna Perttu

Submission 986

Listening for volcanoes in SE ASIA: regional detection capability for infrasound using realistic atmospheric specifications

Southeast Asia is home to over 700 active or potentially active volcanoes. Eruptive plumes from these volcanoes can have an adverse impact on regional air traffic. Satellite based remote sensing of these volcanoes is complicated by tropical weather and year round near constant partial cloud cover of the region. In a five year study of cloud cover for Sumatra, the clearest day had 40% cloud cover. Infrasound offers a cloud cover independent additional tool to monitor for eruptions of these volcanoes. The February 2014 eruption of Kelud Volcano in Indonesia, produced a major stratospheric ash injection. Remote seismic and infrasound detections of this event were critical for identifying the eruption chronology due to the destruction of the majority of the local instruments. This project uses realistic atmospheric conditions along the infrasound propagation path, source frequency and noise levels at the station. Case studies like Kelud are used as a verification tool in order to better define the regional detection capability in terms of VEI from given regions. They are also used as benchmarks to find optimal locations for additional regional infrasound arrays to increase detection capability of smaller VEI events which have the potential to impact regional airports, causing disruption to the aviation sector.

Taka'aki Taira, Adrian Borsa, Florent Brenguier, John Vidale

Submission 847

Ambient-noise time-lapse monitoring of seismic velocity at Newberry Volcano, Oregon

In combination with surface geodetic measurement, the time-lapse monitoring of seismic velocity can provide unique insights into the time-dependent deformation field and its relationship to the dynamics of volcanic system. Seismic interferometry has become one of the most powerful seismological tools for time-lapse monitoring of seismic velocity [Haney et al., 2015, Encyclopedia of Earthquake Engineering]. We investigate the temporal evolution of seismic velocity at Newberry Volcano by using seismic interferometry with ambient noise. Although the seismic activity at Newberry Volcano has been low in the last decades, this volcano is a “very high threat volcano” [Ewert et al., 2006, U.S. Geological Survey Fact Sheet]. We apply a single-station cross-correlation method [Hobiger et al., 2014, Geophys. J. Int.] in which velocity changes are determined by cross-correlating different sensor components (e.g., vertical-north component). At the Newberry volcanic area, over 10 seismic stations are maintained by University of Washington and Cascadia Volcano Observatory (CVO). In particular, six CVO broadband stations are collocated with GPS sites, which allows us to directly compare geodetic and seismic observations at each site for understanding time-dependent crustal deformation. We analyzed continuous waveform collected from 2012 through 2016 to obtain temporal evolution of velocity changes at frequencies from 0.1 to 8.0 Hz. We find seasonal variations in seismic velocity from all six CVO broadband sites. Station ASBU (located at Astronaut Butte, ~15 km northwest from the Newberry caldera) exhibits the most marked seasonal velocity variation ($\pm 0.4\%$ in the frequency band of 1-4 Hz) in which the seismic velocity is consistently increased during September-October. The collocated GPS site also displays a season vertical deformation (upward deformation in September-October). There is variability in the amplitude and phase of the seasonal cycles among those 6 stations. Thermoelastic stress change and hydrological loading (including snow and lake reservoir loadings) are the most likely drivers of the seasonal velocity changes. We investigate the effect of hydrological loading by calculating the time-varying load strain at Newberry Volcano from GPS estimates of regional terrestrial water storage [Borsa et al., 2014, Science], modeling the predicted effect on seismic velocities, and cross-correlating modeled and observed velocity changes.

Benoit Taisne, Anna Perttu, Patrick Whelley, Wei Ming Chong

Submission 769

Ash in the air! From morphological study to weather variability, which region is the most likely to impact your next trip?

Containing just shy of a thousand of volcanoes, South East Asia is one of the most volcanically active regions on Earth. Combining this with a boom in local and international air-traffic, makes it a prime location to study hazards linked to volcanic ash in the atmosphere. In order to estimate the hazard in a large region, one needs to update the list of known volcanoes, as well as their potential to erupt, and then needs to estimate where the injected ash is going to be transported. While resolving these questions, 26 new volcanoes were identified and classified according to their morphological characteristics. An assumption is made that volcanoes with similar morphologies have had similar eruption histories, and well-studied volcanoes within each morphologic classification are used as a proxy for the understudied or unknown volcanoes within the group. We then group volcanoes into a set of geographic zones that have an apparent eruption probability derived from the volcanoes within each zone. For each zone, 8 eruptive scenarios are run every day for 6 years using historical reanalyzed winds. With approximately 150 TB of data, the long term and long range probability is estimated. But which zone is contributing the most? Which season is the most favorable to fly across South China Sea? This study aims to understand not only the decadal probability of volcanic ash in the atmosphere that can affect aviation, but also to identify which zones contribute the most ash and as well as the potential effect of seasonal weather on a given region of interest.

Yasuhisa Tajima, Toshiaki Hasenaka, Masayuki Torii

Submission 77

Effects of 2016 Kumamoto earthquakes on the Aso volcanic edifice

Large earthquakes occurred in the central part of Kumamoto prefecture on April 14–16, 2016, causing strong disaster along the northern segment of Hinagu faults and the eastern segment of Futagawa faults. The major earthquakes analyzed the Mj 7.3 occurring along the eastern segment of the Futagawa faults on April 16 at 1:25 JST (Headquarters for Earthquake Research Promotion, 2016). The Futagawa fault and related faults (Watanabe et al., 1979) included in the Futagawa segment, which are oriented NE–SW on the western flank of Aso caldera, affected central cones of Aso volcano.

Earthquake surface ruptures appeared on the Aso volcanic edifice, which in turn generated landslides. We conducted landform change analysis of the central cones of Aso volcano using aerial photographs published on April 16 by Google Earth (Google Earth ©2016 ZENRIN 2016) together with photographs obtained on May 30 and 31 by the Geospatial Information Authority of Japan (2016). First, we categorized the topographical change as scarps, arc-shaped cracks, and linear cracks. Field survey indicated the causes of scarps, arc-shaped cracks to be landslides, and linear cracks to be faulting, respectively. We discovered a surface ruptures concentration zone (RCZ) in which concentrations of many earthquake surface ruptures and landslides propagating from the west foot to the center of the Aso volcanic edifice. The geomorphological variations caused by the Kumamoto earthquakes created a RCZ with a core composed of Aso-N, Aso-C, and Aso-S rupture bands (C-RCZ) and north and south margin of RCZ (NM-RCZ, SM-RVZ).

In particular, very strong agreement was indicated between recent magmatic vent distribution and NM-RCZ distribution. Additionally, the Nakadake crater correlates with the C-RCZ. Aso-N·C rupture bands suddenly become obscure in the east Kusasenrigahama region. We assumed the Aso-N·C rupture bands turned into shallow depth at the east side of Kusasenrigahama. And we consider this rupture band shallowing process across the magma storage region was important for causing the magma to pass eastward, exiting at the Nakadake crater. These results indicate a strong correlation between the major faulting and volcanic activity in central cones of Aso volcano. The parallel lines of rupture bands as fault structures that are created by terminal extension faulting of the Futagawa faults.

Akimichi Takagi, Nagaoka Yutaka, Keiichi Fukui, Shinobu Ando, Kazuhiro Kimura, Hiroaki Tsuchiyama

Submission 226

Monitoring of the 2013–2015 Nishinoshima Eruption, Japan

The island of Nishinoshima, located ~940 km south of Tokyo, belongs to the volcanic front of the Izu-Bonin arc-trench system. The 2013–15 Nishinoshima eruptive episode began in November 2013 when a new island was created just south of the main island. The new island continued to spew large amounts of lava. After one month, lavas from the new island got to the main island. Later, lavas had merged with and covered much of the main island.

Since Nishinoshima Island is uninhabited, this eruption caused no damage. However, this eruptive episode is volcanologically interesting because it is the first reported eruption to maintain an effusion rate of 105 m³/d for around two years. Monitoring of the eruptive activity at Nishinoshima included observations from a research vessel and analyses of various remote-sensing datasets from multiple satellites.

We summarize observations and analytical results in six chapters of this presentation: (1) visual observations of eruptive activity, (2) plume activity recorded by optical-sensor satellites, (3) thermal activity recorded by geostationary meteorological satellites, (4) lava effusion and ground deformation recorded by the advanced land observing satellite (ALOS-2), (5) SO₂ emissions in volcanic plumes, and (6) seismicity recorded by ocean bottom seismometers. Temporal variations of these datasets have been synchronized. All observed activity decreased gradually from June to July 2015.

Results in this work indicate that a multidisciplinary approach facilitates eruption monitoring, even in the case of isolated volcanic islands such as Nishinoshima. Remote sensing observations and analyses proved to be especially effective.

Shinji Takarada, Hideo Hoshizumi

Submission 232

Depositional features and emplacement mechanism of pyroclastic density currents at Unzen, Hokkaido Komagatake and Aso volcanoes, Japan

Pyroclastic density currents (PDCs) cause devastations in and around areas near volcanoes. The emplacement mechanisms of PDCs have been debated in the last few decades. The PDC emplacement mechanisms in this study are discussed based on field data of small-scale 1991-95 Unzen block-and-ash flow deposit (single flow volume; 104-106m³), middle-scale 1929 Hokkaido Komagatake pumice flow deposit (106-107m³) and large-scale 90ka Aso-4 ignimbrite (108-109m³) in Japan. Many 30cm to 1m thick flow units are observed in the Unzen PDC deposits. Large lithics (5-20cm in diameter) in the flow units sometimes show horizontal alignments at 10-30cm intervals. Many 30cm to 5m thick flow units with pumice-concentration zone at the top are observed in the Hokkaido Komagatake PDC deposits. Pumices (5-15cm) in the flow units sometimes show horizontal alignments at 10-50cm intervals. The orientations of elongated pumices are parallel to the flow direction from the bottom to the higher levels of the flow unit. Lobes and levees are observed on the surface. Several 1 to 20m thick flow units are observed in the Aso-4 PDC deposits. Large pumices (20-85cm) in the flow units sometimes show horizontal alignments at 30cm to 2m intervals.

The horizontal alignments of large lithics or pumices in the flow units of these PDC deposits suggest that PDCs were not formed in mass freezing, but formed incrementally at 10cm–2m thick intervals from the bottom (depositional subunits; DSU). The alignments of large lithics or pumices at the upper part of DSUs suggest (1) lithics or pumices were concentrated at the bottom of the turbulent PDC boundary layer, (2) increased interactions between the lithics or pumices, and (3) the formation of concentration zone at the top of the DSUs. The elongated pumices parallel to the flow direction in almost all levels of Komagatake PDC also suggest that the pumices were aligned due to shear stress within the turbulent PDC boundary layer.

The accumulation rate per m² at the bottom of these PDCs were determined based on estimated volume and arrival time. The accumulation rates are 10⁻³-10⁻² m/s, 10⁻²-10⁻¹ m/s, and 10⁻¹-100 m/s in Unzen, Komagatake and Aso PDCs, respectively, indicating large turbulence differences. Therefore, the major differences of depositional features (e.g. thickness of DSUs) among these PDCs were caused by the large differences of turbulence and accumulation rates at the bottom of the PDCs due to large differences of volumes and eruption rates.

Shinji Takarada, Joel Bandibas, G-EVER Promotion Team

Submission 223

Asia-Pacific region earthquake and volcanic hazards mapping project and G-EVER volcanic hazard assessment support system

The Asia-Pacific region earthquake and volcanic hazards mapping project aims to develop an advanced online hazard information system (<http://ccop-geoinfo.org/G-EVER>) that provides past and recent earthquake and volcanic hazards information online. The information system shows distribution of calderas, tephra falls, tsunami inundation areas, active faults and fatalities in an interactive and user-friendly interface. Links to major volcanic eruptions databases, such as Smithsonian, VOGRIPA, ASTER satellite images, Volcanoes of Japan and WOVodat are available on each volcano in the system. This project is implemented with the cooperation of major research institutes and organizations in the Asia-Pacific region.

The Eastern Asia Earthquake and Volcanic Hazards Information Map, published in 2016, is a collaborative product of the G-EVER Promotion Team in the Geological Survey of Japan, AIST and several geological institutes in Southeast Asia. The Map contains information about geohazards in the area as well as its geology and tectonics: the distribution of Holocene volcanoes, calderas, large-scale ignimbrites, ash falls, active faults, earthquake hypocenters and source areas; and the fatalities in major volcanic events, in major earthquakes and in tsunami hazards. The fatalities in volcanic eruptions and earthquakes are classified by the main cause of the death and graphically illustrated to facilitate visual understanding of the magnitude of the damage from these disasters. The GIS contents of the map can be downloaded on the Asia-Pacific Region Earthquake and Volcanic Hazard Information System.

The G-EVER volcanic hazard assessment support system (<http://volcano.g-ever1.org/>) is developed based on eruption history, volcanic eruption database and numerical simulations. The volcano hazard assessment support system using Energy Cone, Titan2D and Tephra2 simulations can predict the area that would be affected by volcanic eruptions, such as pyroclastic flow, debris avalanche and tephra falls. The system can assess any Quaternary volcano in the world (>3,000) using ASTER Global DEM. Using the volcano hazard assessment system, the area that would be affected by volcanic eruptions at any locations near the volcano can be evaluated. The system could estimate volcanic hazard risks by overlaying the distributions of volcanic deposits on major roads, houses and evacuation areas using WebGIS.

Minoru Takeo, Takao Ohminato, Mie Ichihara, Masanao Shinohara, Kiyoshi Baba, Atsushi Watanabe, Hiroko Sugioka, Yozo Hamano

Submission 397

Geophysical observations at a new volcanic island Nishinoshima, Ogasawara, Japan

In November 2013, an island-forming eruption started near Nishinoshima island, Ogasawara, Japan. By the end of the eruption in late 2015, the island area and the erupted volume reached 2.7 km² and 1.6 ×10⁸ m³, respectively. During the eruption, scientific observations of the island were limited to using remote methods due to the restricted area of 1.5 km from the active vent set by Japan Meteorological Agency. Several types of remote geophysical observations were conducted by various universities and institutions during the period when the restricted area of 1.5 km was set. For example, ocean bottom seismometers (OBSs) and ocean bottom electro magnetometers (OBEMs) were deployed outside of the restricted area. Infrasound sensors were deployed at Chichijima island 130 km to the east of Nishinoshima. Visual observations were also conducted by unmanned small helicopter operated from a ship outside the restricted area.

In August 2016, responding to a decline in volcanic activity, the restricted area was reduced from 1.5 km to 0.5 km so that observations in the vicinity of the island including landing were possible. We carried out geophysical observations using a research vessel Shinseimaru in October 2016. In the observations, we landed on the island and installed a solar powered observation system composed of a broadband seismometer, an infrasound sensor, and a satellite telemetry device. We also conducted a visual and infrasound observation using a small vessel named Wave Glider, an observation system that travels on the sea-surface autonomously exploiting the sea wave energy. Observations using OBSs and OBEMs were continued at closer distances to the island.

The observations initiated during the Shinseimaru cruise will offer new insights on volcanic processes at Nishinoshima. For example, the newly installed seismic and infrasound station in the island would contribute to monitoring the volcanic activity more clearly and promptly than the remote observations. The configuration of the OBEMs was designed so as to be sensitive to a shallow magma chamber beneath the island. Together with the geochemical information from the rock samples collected during the landing survey, the electric conductivity structure would contribute to restricting the depth range at which the island-forming magma was stored beneath the island.

Shingo Takeuchi, Kiyoshi Toshida, Daisuke Miura, Shimpei Uesawa, Hisatoshi Ito

Submission 381

The association of eruption magnitude with magmatic properties: Evidence from Magma database of volcanic eruptions in Japan during the last one hundred thousand years

Several global databases of eruption properties have been developed in recent years including Volcanoes of the World (Global Volcanism Program, 2013), Large Magnitude Explosive Volcanic Eruptions (LaMEVE; Croweller et al., 2012), Collapse Caldera Database (Geyer and Marti, 2008) and DomeHaz (Ogburn et al., 2015). These databases contain various eruption properties; eruption age, eruption magnitude, eruption style and volcanic explosivity index. However, magmatic properties inferred from petrological analysis have not been treated quantitatively. In order to explore association between magmatic and eruption properties, this study constructed a new database of magmatic properties and combined it with existing eruption databases of volcanic eruptions in Japan during the last one hundred thousand years (Hayakawa, 1995-, Kudo and Hoshizumi, 2006-, Yamamoto, 2015). We sampled and analyzed the erupted products of about one hundred eruptions to construct the database. The erupted magmas were characterized by preeruptive melt SiO₂ (groundmass SiO₂) and phenocryst contents, for there is ineligible discrepancy between bulk and melt SiO₂ contents for phenocryst rich magmas. Eruption magnitude, M , are used as the most representative eruption property. In the database, large eruptions of $M \geq 6$ were exhaustively analyzed as possible. In contrast, small eruptions of $M < 2$ content, phenocryst content and eruption magnitude. Although there is a large scatter, the association shows that eruption magnitude tends to increase one order of magnitude with increasing melt SiO₂ content by 10 wt% or decreasing phenocryst content by 30 vol%. Caldera-forming eruptions of phenocryst-poor magma with rhyolitic melt have the maximum magnitude with $M > 7$ in this database. In order to examine the universality of the plane-like pattern, we compared the result for Japanese volcanoes with that for global volcanoes. The melt SiO₂ and phenocryst content data for global eruptions in Takeuchi (2011) were combined with the eruption magnitude data from the LaMEVE. Despite different tectonic settings, the association for the global eruptions shows similar pattern to that for the Japanese eruptions. Notable outliers are super-eruptions ($M > 7$) of rhyolitic melt with abundant phenocryst occurring more than a million years ago, called monotonous intermediate.

Giancarlo Tamburello, Séverine Moune, Patrick Allard, Swetha Venugopal, Vincent Robert, Marina Rosas-Carbajal, Thierry Kitou, Francois Beauducel, Jean-Christophe Komorowski

Submission 566

Spatio-temporal relationships between fumarolic degassing, hydrothermal fluid circulation and lava dome deformation at La Soufrière volcano, Guadeloupe (Lesser Antilles)

Surveying fumarolic gas emissions on dormant volcanoes in hydrothermal stage is important to decipher the evolution of magma-derived volatile supply and its interactions with the hydrothermal system. Here we report on improved measurements of fumarolic gas compositions and gas fluxes at La Soufrière volcano (Guadeloupe) in 2016, during an ongoing period of degassing unrest initiated in 1992. We operated simultaneously three portable MultiGAS sensing devices in the field to determine the chemical proportions and the mass flux of the main volatile species (H₂O, CO₂, H₂S, SO₂, H₂) emitted from the different vents currently active on top of La Soufrière lava dome. Our results reveal compositional differences among the fumarolic vents that depend on both their respective location with respect to the 3D-distribution of fluids of the hydrothermal system, as imaged from detailed electrical resistivity tomography, as well as secondary processes (S-scrubbing and precipitation, steam condensation) affecting the uprising gas mixtures. Our data set demonstrates the persistency of an increased bulk gas emission rate from the volcano over the past ten years, but with a marked spatial shift of the fumarolic activity from the centre of the lava dome towards the east (SE, NE, N) and along the NW-SE trending fault-controlled Breislack fracture, characterized by the reactivation of former fumaroles or/and the opening of new pressurized fumaroles as well as the northward progression of a thermal anomaly front through the substratum. These observations fit well with both seismic and extensometric evidence of increased opening of fractures cutting the eastern part of La Soufrière lava dome. Our study thus reveals a close spatio-temporal relationship between fumarolic degassing, ground deformation, seismic activity and the hydrothermal system on an active volcano in a stage of moderate yet persistent and evolving unrest.

Giancarlo Tamburello, Vincent Robert, Jean-Christophe Komorowski, Thierry Kitou, Patrick Allard, Arnaud Lemarchand, Celine Dessert, Anne Le Friant

Submission 569

Real-time gas monitoring of a fumarolic field: application at La Soufrière of Guadeloupe (Lesser Antilles)

Fumarolic fields of closed-conduit volcanoes are often characterized by heterogeneous chemical compositions in response to varying hydrothermal/magmatic inputs. Monitoring in real-time how this contribution varies spatially and temporally may contribute to evaluate improve the understanding and assessment of future volcanic unrest. Here we report on the first deployment of a MultiGAS network for measuring the H₂O-CO₂-H₂S-SO₂ gas molar fractions in the major fumaroles of the La Soufrière volcano of Guadeloupe island (Lesser Antilles) which is characterized by the intensification of decadal fumarolic emissions after the 1976-1977 non-magmatic eruptive crisis. Data from this continuous telemetered MultiGAS network will be complementary to in-situ fumarole gas sampling performed by the OVSG since 1979 and to periodic MultiGAS surveys through the gas plume. High-frequency gas surveys at La Soufrière will provide key insights into pre- and syn-eruptive volcanic processes, will help refine/implement models of the dynamics of the magmatic/hydrothermal system, as well as provide better constraints on the source mechanisms controlling degassing, thermal and seismic energy release in the context of moderate yet persistent and evolving unrest since 1992.

Chiou Ting Tan, Benoit Taisne, Jurgen Neuberg

Submission 472

Magma On The Move! Monitoring Magma Migration Using Synthetic Seismic Amplitude Ratio Analysis

Volcanic eruptions are often heralded by magma movement, thus it is important for observatories to detect such motion, and as early as possible. Tracking the magma per se is challenging, but a good proxy for it is to track the seismicity that is reflecting the stress perturbations induced by the migrating magma. This can be done using Seismic Amplitude Ratio Analysis (SARA), a simple method which tracks the time evolution of the ratios of seismic amplitudes recorded at different seismic stations in a network in real time. Changes in amplitude ratios signify changes in location of the seismic activity, implying magma movement. We improve upon the SARA method by adding steps to 1) quantitatively determine whether amplitude ratios are changing, 2) trigger an alert system automatically when seismic migration is detected, and 3) make the method more robust for application across most volcanic systems and seismic networks with different migration time scales. To develop and test our improved method, we applied it to synthetic seismograms simulating seismic migration. Using synthetics not only provides a controlled environment for us to observe how changes in different parameters affect the amplitude ratios, but also the means to examine a variety of scenarios, including migration in different directions, and migration amidst various degrees and spread of background events. Our results show that we are able to clearly pick up the start and end of a migration episode, as well as distinguish between the magma gushing out at the surface and the magmatic injection stalling at depth in a failed attempt to reach the surface. We also used real seismic data which has known magma migration to validate our methodology. An application of our improved SARA method was done on recent seismic data from Gede volcano, a volcano in western Java. Seismic swarms periodically happen at Gede volcano, which neither culminate in eruptions nor detectable inflation. Preliminary results suggest that the driving forces behind these swarms do not involve magma migration, but more techniques need to be tested to completely rule out the involvement of magma.

Akiko Tanaka, Paul Lundgren

Submission 474

Source model for Kuchinoerabujima volcano, Japan, constrained by interferometric synthetic aperture radar observations

Kuchinoerabujima is an active volcanic island located on the volcanic front of the Ryukyu island arc. After 34 years of dormancy, the volcano erupted on 3 August 2014 and on 29 May 2015. Japan Meteorological Agency reported that an explosive and phreatomagmatic eruption generated an ash plume reaching 9-km high above Shindake Crater's rim, and pyroclastic flows descended the southwest flank and reached the coast on the northwest flank. Ground displacements near the summit area of Shindake were detected by InSAR analysis using the ALOS-2/PALSAR-2 data [e.g., http://www.eorc.jaxa.jp/ALOS-2/en/img_up/dis_pal2_kuchinoerabu_20140821.htm].

Before these eruptions, seismic swarms were accompanied by a radial outward pattern from the summit crater repeated almost every two years since 1999 [Iguchi, 2007] and eruptive activities of Kuchinoerabujima volcano occurred at two active craters of Shindake and Furudake. InSAR analysis using the ALOS/PALSAR data [e.g., Yamamoto, 2009; Tanaka and Lundgren, 2013] also detected ground displacements near the summit area of Shindake.

We applied the InSAR time-series analysis using the software package StaMPS/MTI [Hooper, 2010] to the ALOS/PALSAR data acquired on both ascending and descending orbits from May 2006 to March 2011. The line-of-sight (LOS) displacements show a rather complicated pattern compared with previous results obtained using GPS measurements and InSAR analysis. The mean velocity maps show two focused areas of LOS shortening located beneath Shindake and Furudake at a rate of 20 mm/year, confirming the inflation trend. The observed deformation near the summit area of Shindake was consistent with previous results. Also, it suggests another deformation source beneath Furudake, which was not clearly accounted for previously. We model the Kuchinoerabujima volcano sources that produced clear and distinct fringe patterns with rectangular dislocations and compound dislocation models [Nikkhoo et al., 2017].

Ryo Tanaka, Takeshi Hashimoto, Nobuo Matsushima, Tsuneo Ishido

Submission 376

Numerical investigation of temporal changes in magnetic total field and ground deformation associated with volcanic hydrothermal systems

Localized temporal changes in the magnetic field and coincident ground deformation are often observed at volcanoes. This study focuses on two mechanisms that may bring about some changes in hydrothermal system during inter-eruptive stages: (1) permeability reduction at a shallow part of the conduit, and (2) fluctuation of hydrothermal fluid flux from a deeper part. We classify the pattern of temperature and pore pressure changes that are associated with the conduit constriction and/or fluctuating flux of hydrothermal fluid by means of hydrothermal numerical simulation.

We used the hydrothermal numerical simulator that enabled us to calculate the heat and mass flow rate of H₂O and air. The calculation region was set as axisymmetric 2D to represent a simplified conical edifice with a uniform porosity and permeability. Meteoric recharge was injected at the land surface at a constant rate and a constant heat flow was supplied at the base of the model. The high-permeability conduit was introduced at the axis of symmetry. Hydrothermal fluid is injected at the bottom of the conduit. After reaching a quasi-steady condition, an abrupt reduction of permeability at a particular depth (PCB) in the conduit and/or an increase in flux of hydrothermal fluid were imposed, and the system response was observed.

Conduit obstruction caused reduction in temperature and pore pressure above PCB, as well as heating and pressurization below it. In contrast, increase in the fluid supply from the bottom resulted in heat accumulation and pore pressure increase throughout the conduit. When the two mechanisms were introduced at the same time, patterns of temperature and pore pressure changes were found to be controlled by the degree of permeability reduction and by the amplitude of stepwise increase in the fluid flux. When the permeability at PCB decrease to the smaller level than that of host rock, significant cooling and depressurization were seen above PCB regardless of the amount of fluid flux elevation.

These classifications provide useful clues for understanding the mechanisms of total magnetic field accompanied with ground deformation during inter-eruptive stages. The hydrothermal system may experience some change in state prior to eruptions. However, changes in the hydrothermal system do not always lead to explosive surface manifestations. Improved understanding of such changes contributes to the assessment of whether an eruption is likely or not.

Kenichiro Tani, Osamu Ishizuka, Iona McIntosh, Alexander Nichols, Yuka Masaki, Fumihiko Ikegami, Hirochika Sumino, Takashi Toyofuku

Submission 564

Oomurodashi Volcano, northern Izu-Bonin Arc: Long term edifice growth under shallow sea environment and its potential hazards

Oomurodashi is a bathymetric high located at the northern end of the Izu-Bonin Arc. Using the 200 m bathymetric contour to define its summit dimensions, the diameter of Oomurodashi is ~20 km, making it one of the largest edifices among the Izu-Bonin Arc volcanoes. Oomurodashi has been regarded as inactive, largely because it has a vast flat-topped summit at ~100 meters below sea level (mbsl).

During a research cruise in 2007, we conducted a dive survey in a small crater, Oomuro Hole, located in the center of the flat-topped summit, using a remotely-operated vehicle (ROV). The heat flow measurement conducted on the floor of Oomuro Hole during this dive recorded an anomalously high value of 4,200 mW/m². Furthermore, ROV observations revealed that the southwestern wall of Oomuro Hole consists of fresh rhyolitic lavas.

These findings suggest that Oomurodashi is an active silicic submarine volcano. To confirm this hypothesis, we conducted detailed ROV and geophysical surveys of Oomurodashi in 2012 and 2016. The ROV surveys revealed numerous active hydrothermal vents on the floor of Oomuro Hole, at ~200 mbsl; the maximum water temperature recorded at the hydrothermal vents was 202°C. ROV observations revealed that the area surrounding Oomuro Hole on the flat-topped summit of Oomurodashi is covered by extensive fresh rhyolitic lava and pumice clasts, suggesting recent explosive eruption(s) from the Hole.

These findings strongly indicate that Oomurodashi is an active silicic submarine volcano. Since the summit of Oomurodashi is in shallow water, it is possible that eruption columns can breach the sea surface and generate subaerial plumes. A ~10 ka pumiceous tephra layer with identical geochemical characteristics to the rhyolites recovered during the dives has been discovered in the subaerial outcrops of the neighboring islands of Izu-Oshima and Toshima, strongly suggesting that these tephra deposits originated from Oomuro Hole.

The deeper slopes of Oomurodashi are composed of effusive and intrusive rocks that are bimodal in composition, with basaltic dikes and lavas on the northern flank and dacite volcanoclastics on the eastern flank. This suggests that Oomurodashi is a complex of smaller edifices of various magma types.

We will provide a geological overview of Oomurodashi Volcano and edifice growth history based on the ROV observations, and discuss its potential hazards on the basis of shallow submarine silicic eruptions.

Sarah Tapscott, Þorvaldur Þórðarson

Submission 877

Clast density comparison between the rooted cone tephra and the Grámelur rootless cone tephra of the Nesjahraun lava flow, Þingvellir, SW Iceland

Comparison between the tephra that form rootless cones versus the associated primary rooted cones is required to identify the physical properties that allow for robust distinction between these geometrically similar volcanic formations. Such identification will assist in developing a straightforward classification of rootless cone tephra in comparison to rooted or primary tephra. This contribution focusses on the comparison of clast densities of the primary versus rootless cone tephra from the Holocene Nesjahraun fissure eruption and its potential for underpinning identification and classification scheme for rootless cone deposits.

The Nesjahraun lava flow, located on the southern shore of Þingvallavatn, SW Iceland, is a basaltic lava flow that erupted 1880 ± 65 before present from a 5-km-long vent system trending 030° and is made up of a row of spatter and scoria cones. The lava flow extends approximately 1.5km into Þingvallavatn and lava-water interactions on the shoreline initiated explosive water to lava interactions, generating the rootless cones Grámelur and Eldborg.

Samples, with focus on the northern, onshore portion of the eruption, were taken from a spatter cone vent and the rootless cone Grámelur. Clast densities were obtained using the water immersion method.

The results show that vent tephra is typified by low clast densities, where the average density for the samples are $280 \pm 69 \text{ kg/m}^3$ (1-sigma standard deviation) and $500 \pm 103 \text{ kg/m}^3$, reflecting high (80-90%) vesicularity and thus efficient magma degassing during venting of the magma.

In contrast, the Grámelur rootless tephra are typified by normal distributions and significantly higher average densities of $1660 \pm 150 \text{ kg/m}^3$, $1700 \pm 200 \text{ kg/m}^3$ and $1860 \pm 190 \text{ kg/m}^3$. These results signify lower clast vesicularity for the rootless tephra in the range 30-40%. This result is not unexpected as the lava involved in the rootless eruptions is largely degassed at the time of the explosive lava to water interactions, but also provides a platform for distinguishing between primary versus rootless tephra.

Additional results will be presented following a comparative vesicle size distribution analysis. Preliminary investigation shows that the vent tephra features evenly distributed spherical vesicles resting in a microlite-rich glassy matrix. In comparison, the Grámelur rootless tephra clasts are characterized by jagged, irregular shape, unevenly distributed vesicles sitting in a holocrystalline matrix of microlites.

Inga Tarasenko, Pierre Delmelle, Charles Biolders, Alicia Guevara

Submission 922

Crusting of volcanic tephra deposits: an experimental study

Surface crusting of fresh tephra deposits is a common phenomenon occurring after a rain event. Tephra crusting may lead to a decrease in soil water infiltration and an increase in runoff and erosion. It also may hamper seed germination and depress plant growth, thereby posing problems to farmers. Although tephra crusting has long been observed, its formation mechanism and the controlling factors have not been investigated.

We present the results of a study in which tephra crusting was studied experimentally. Tephra samples from three eruptions, i.e. Eyjafjallajökull 2010 (EYJA), Mt. Merapi 2010 (MER) and San Cristobal 2000 (SC) were tested. The particle size distribution of these tephra samples differ: MER contains the largest contents of silt- and clay-sized particles, whereas EYJA is the coarsest sample. SC has lower amounts of silt-sized and clay-sized particles than MER. Besides, this sample also contains significant amounts of soluble sulphate and halide salts. A rainfall simulator was used to apply 5, 10, 15 and 20 mm of rain to reconstructed tephra deposits. All treatments were performed in triplicates. Polished sections of the treated samples were examined using optical and electron microscopy. Crust thickness and porosity were estimated using an image analysis software.

Exposure of MER and SC tephra to 5, 10, 15 and 20 mm of rain always led to surface crust formation. However, crusting of EYJA tephra was erratic. Crust thickness ranges from 0.05 to 0.99 mm and from 0.09 to 0.68 mm in MER and SC tephra, respectively, and correlates positively with the amount of rain applied. Porosity of the surface crust is typically lower (by a factor of up to 2.6) than that measured deeper in the tephra deposit. The crust that formed on top of MER tephra deposit showed a “washed out” and a “washed in” layer. These features are interpreted as the result of particle sorting. In contrast, crusting of SC tephra may be the consequence of compaction due to interaction of raindrops with the deposit surface. There is no evidence of chemically cemented particles in the SC tephra deposit. We suggest that the particle size distribution of a tephra deposit plays a key role in crust formation.

Franco Tassi, Mariano Agosto, Clara Lamberti, Alberto Caselli, Giovannella Pecoraino, Chiara Caponi, Juliana Szentiványi, Stefania Venturi, Jimena Presa

Submission 239

The 2012-2016 eruptive cycle at Copahue volcano (Argentina): hints from the temporal evolution of the chemical and isotopic features of hydrothermal-type gas discharges

This study presents the chemical and isotopic compositions of hydrothermal gases collected from fumaroles located in the surroundings of Copahue volcano (Argentina). In this volcano, a new eruptive cycle, characterized by occasional phreatic and phreatomagmatic eruptions, started on July 19, 2012 and it is still ongoing. Gas samples, including those from two fumaroles from the summit of the active crater, were collected during surveys carried out by different researcher teams from 1976 to February 2016. The time-series of H₂, CO and light hydrocarbons showed episodic increases in correspondence of the main eruptive events, likely caused by enhanced inputs of hot magmatic fluids affecting the hydrothermal reservoir. In 2012-2014, these evidences were apparently in contrast with the temporal variations of the R_c/R_a and δ¹³C-CO₂ values, which indicated increasing inputs from a crustal fluid source. In 2015-2016, the isotopic parameters showed opposite trends, consistent with the gas chemistry, since they were approaching the compositional features of the two summit fumaroles, which were possibly corresponding to those of the deep magmatic-related end-member. The delayed and smoothed compositional changes of the peripheral hydrothermal fluid discharges in response to the 2012-2016 eruptive events suggest that geochemical surveys of these emissions can unlikely provide premonitory signals of volcanic unrest if the volcanic activity will keep centered in the main crater. At Copahue volcano, seismic activity and ground deformation seem to represent the most reliable approaches for monitoring purposes. However, the relative compositional stability of the hydrothermal reservoir is a great advantage in terms of geothermal resource exploitation, encouraging new investments in the Copahue geothermal project abandoned in the 1990's.

Isabelle A Taylor, James Preston, Elisa Carboni, Tamsin A Mather, Roy G Grainger, Nicolas Theys, Silvana Hidalgo, Brendan McCormick Kilbride

Submission 394

Using the Infrared Atmospheric Sounding Interferometer to detect volcanic emissions of sulphur dioxide

Monitoring volcanic emissions of sulphur dioxide (SO₂) offers insight into processes taking place beneath volcanoes. It is also important for assessing the hazard presented by these gases, and any accompanying ash, to local communities and the aviation industry, and for understanding the impact on the environment and climate. Satellite instruments have been widely used for this purpose but monitoring of emissions into the troposphere, such as those from smaller explosive eruptions and non-eruptive volcanic activity, has been most commonly measured with ultraviolet instruments. Two retrievals developed at the University of Oxford for the Infrared Atmospheric Sounding Interferometer (IASI) show some promise at detecting and retrieving the properties of both lower altitude plumes and SO₂ clouds of lower concentration. Here, a 'fast' linear retrieval was applied globally to detect sources of SO₂. The results were dominated by emissions from large scale eruptions but elevated signals can also be identified from smaller eruptions, strong non-eruptive volcanic sources, and industrial centres suggesting the technique has promise for detecting lower altitude emissions and smaller SO₂ mass loadings. The speed of this technique facilitates its use for near real time monitoring and for identifying interesting signals for further study with the full iterative retrieval which can quantify the amount of gas released. SO₂ emissions were persistently detected at volcanoes in Ecuador and Kamchatka and so these were selected for further study with the iterative retrieval. Across both regions, SO₂ emissions identified with IASI corresponded well with reports of volcanic activity from other sources. At Tungurahua, it was possible to compare the IASI observations against those from the ultraviolet Ozone Monitoring Instrument and ground based SO₂ flux measurements. The results were promising with each dataset showing similar trends. This demonstrates that the IASI retrievals can detect and quantify tropospheric SO₂ emissions, including those from non-eruptive volcanic activity, which if used alongside other datasets could be a valuable contribution to volcanic monitoring.

Paul Taylor

Submission 53

The 1946 Eruption of Niuafou'ou Island, Kingdom of Tonga: Was an Evacuation Really Warranted?

Niuafou'ou is Tonga's remotest island, located 450 km north of Tongatapu at latitude 15.60oS, longitude 175.63oW and is home to about 800 Niuafou'ouans who live in 8 villages. Niuafou'ou is the most active volcano in the Kingdom and its history has been dominated by periods of both lava-producing (effusive) and ash-producing (explosive) activity. Although the majority of the 10 reported eruptions have only resulted in damage to dwellings and crops, during the 1853 event at least 25 Niuafou'ouans may have perished. Since the most recent eruption in September 1946, the volcano has remained dormant, except for a seismic swarm on 21-22 March 1985. A volcanic hazard assessment completed in the mid-1990s suggested that Niuafou'ou must still be considered a dangerous volcanic system.

The 1946 eruption occurred during the period 09-18 September producing a small lava field that covered 0.3km² of land along the north coast. A series of four en-echelon fissures opened propagating in an eastward direction with the eastern-most fissure opening directly under Angaha village. There were no known fatalities that were directly attributed to eruption. Other than the partial destruction of structures in Angaha there was no effect on the other villages or farmlands in other parts in the island. However, as a result of the eruption the Government directed that a complete evacuation be undertaken at the best possible time. The evacuation was completed by December 1946. Following the evacuation although several small groups of copra cutters were permitted on the island during the intervening period, resettlement was only permitted in 1958 but it was on the condition that residents returned without Government support. Since the evacuation the inhabitants have endured a considerable degree of cultural and economic hardship and even today still harbor considerable resentment toward the Government.

Was this evacuation really warranted? In volcanological terms the eruption was a minor event, however, it did result in the destruction of the main Government village of Angaha, on the north coast. There are no known records that a volcanic hazard assessment of any kind was conducted following the eruption and whilst a recent assessment conducted by the author indicated that Niuafou'ou should be considered a dangerous volcano, the evacuation was not necessary. Although a plebiscite (referendum) was conducted, the final decision to evacuate was made purely for political reasons.

Paul Taylor

Submission 52

The 1943 Eruption of Niuafu'ou: An Eruption Chronology and the Effects of Volcanic Pollution as Provided by Local Informants

Subaerial back-arc volcanoes are rare; however, the island volcano of Niuafu'ou, the northern-most outlier of the Tongan Group, is one such example which has allowed the nature of volcanic processes of this unique volcanic environment to be studied.

Niuafu'ou lies some 650 kms north of Tongatapu, mid-way between Fiji and the Samoan Islands, and is the most isolated island of the Tongan Group. Since the early 1800's at least ten volcanic eruptions on the island of Niuafu'ou have resulted in the destruction of property and, in some cases, loss of life has also occurred. The activity that has occurred during historic times has been predominantly effusive events, e.g. 1853, 1867, 1912, 1929, 1935-36, 1943 and 1946, which have covered large areas of the lower flanks of the island with lava fields. As well as lava flows other associated phenomena that have also occurred during periods of activity has included tephra fall, pyroclastic surges, volcanic earthquakes, ground fracturing, subsidence and the effects of volcanic gases.

The eruption that commenced on 26 September 1943, although in volcanological terms a relatively minor event, it is clear from the few accounts that are available it had a devastating effect on the island and its population. Lava flows have flowed downslope from the vents, commonly entering the sea at numerous locations where they have created extensive columns of steam, ash and gas. Whilst the activity was located in an uninhabited area, it resulted in most of the island's vegetation, including the majority of the food crops, being destroyed. During the weeks/months that followed, the population experienced a period of severe famine.

When eruptions are not witnessed by scientists it is sometimes difficult to assess the extent and effects of the eruption and therefore it is important to draw information from all available sources. Due to the paucity of information, descriptions provided by local informants, some witnessing the eruption, remain the only source of information.

This paper will draw on the few available descriptions of the activity to develop a chronology of the 1943 eruption, provide detail of the character and extent of the activity, and then will assess the impact of the associated hazards that occurred, particularly volcanic pollution (laze and vog), and its effect on both the landscape and the local population.

Rachel Teasdale, Kaatje van der Hoeven Kraft, Michael Poland

Submission 142

Use of real data in the classroom: Monitoring Mount St. Helens 2004 dome growth

Authentic datasets are an increasingly common tool available for teaching students and the public about Earth processes, particularly in the field of geohazards. Creating teachable content from these vast data sets is a time-consuming prospect, but data are available in several formats online, including collections hosted by National Association of Geoscience Teaching (NAGT). We recently developed a classroom activity exploring the 2004 dome growth at Mount St. Helens (MSH) and tested undergraduate student learning at multiple institution types and university grade levels. In the activity, students first work in small groups to learn and interpret one of three data types that were used by USGS scientists (earthquake epicenters, RSAM, or GPS data) from September through November 2004. Later, students reorganize into mixed expertise groups to teach one another about the characteristics of the data they just learned and assess the emerging magmatic activity as an interdisciplinary team. Ultimately, student teams determine the appropriate USGS Volcano Alert Level as of November 2004. As in our similar activity in which students examine the Pu'u Ō'ō June 2007 "Father's Day" event (Episode 56; <http://serc.carleton.edu/48383>), the MSH lesson puts students in the role of USGS scientists. Pre- and post-activity student survey data for the MSH activity indicates that a majority of students learned about new techniques affiliated with volcanic monitoring and effectively taught new information to their peers. Increased student knowledge also includes an improved sophistication of language in descriptions of their interpretation of data. The greatest increase in student confidence occurred for their use of multiple data types when assessing volcanic activity (average increase of 2 points on a 5 point Likert scale). Results indicate the strength of developing classroom lessons that incorporate real-world data and put students in the role of professional geologists at the time of emerging volcanic crises. Use of real monitoring data is not only useful and effective as a teaching tool, the authentic data highlight state-of-the-art technology, demonstrate the dynamic nature of volcanoes, the importance of multiple types of monitoring, and promotes excitement about the process of scientific discovery through hands-on learning.

Maria Luisa Tejada, Sandra Catane, Catherine Lit, Allan Mandanas, Hannah Mirabueno, Renato Solidum, Maria Carmencita Arpa, Alyssa Peleo-Alampay, Allan Fernando

Submission 323

Tracing large volcanic eruptions from marine tephra layers in Philippine marginal basins

Majority of the Philippines' most active volcanoes are located along the eastern and central part of Luzon, most notably the Bicol arc where Mayon volcano is the best known among them. Communities near the volcanic edifices in Bicol region, are in constant threat to volcanic hazards. The reconstruction of the eruptive history of these volcanoes in the last one million years is important, not only for hazards assessment but also for understanding the magmatic evolution of the Philippine arc. Although there had been several studies in the past describing and characterizing the volcanic products of volcanoes in this region, there had been no detailed reconstruction of volcanic eruptions with time, in terms of the volume and size, extent of volcanic deposits, and impact on marine environment. Piston coring in the Sibuyan and Bohol seas in the Philippines recovered several marine tephra layers that may provide an archive of explosive eruptions and magmatic activities from the nearby Bicol volcanic arc. The glass fragments in these ash deposits exhibit bubble-wall-type morphology typical of co-ignimbrite ash deposits, suggesting that they are primary distal deposits of explosive eruptions on land. In-situ geochemical microanalyses of the glass fragments reveal that they have compositions that form tight clusters in major element data plots, supporting their primary depositional origin. The ash layers appear to have a bimodal distribution in terms of major element geochemistry: one group having andesitic to dacitic composition (55-64 SiO₂ wt%) and the other one having rhyolitic composition (69-78 SiO₂ wt%). This bimodal grouping in terms of major elements is also supported by distinct trace element compositions of the glass fragments in representative ash layers, which can be traced back to possible sources on land that display similar geochemical attributes, such as Mayon and Irosin volcanoes. The persistence of rhyolitic ash layers in the cores suggests that they could be correlatable to the newly identified widespread tephra marker in the Bicol arc (Mirabueno et al., *Quat. Intl.* 2011). However, more detailed and extensive tephrochronological work is needed to establish the chronology and frequency of explosive eruption events from these volcanoes to assist volcanic hazards evaluation and disaster prevention planning from explosive volcanic eruptions in the future.

Virginia Tenorio, Wendy McCausland, Randall White

Submission 855

Seismic precursors to the 2015-2016 eruption of Momotombo volcano, Nicaragua

Momotombo volcano began erupting on 1 December 2015, following more than 110 years of repose. A process-based model of pre-eruptive seismic patterns was used by the Instituto Nicaragüense de Estudios Territoriales (INETER) to forecast the eruption onset, subsequent explosions, and lava flow, and to issue warnings to the Nicaraguan Civil Protection Agency. The first significant seismic swarm at Momotombo since regional seismic monitoring began occurred in September 1975 with > 250 distal volcano tectonic (VT) earthquakes with magnitudes between M1.3 and M3. Distal VT swarms increased significantly again between 1997 and 2013, with swarms of magnitudes M3 distal VTs occurring including an M4.7 on November 24. When on 1 December the first significant tremor was recorded, INETER forecast an eruption could occur in hours to days. Seismicity was then dominated by tremor and preceded strombolian explosions and the eruption of lava at the summit. Coincident with the onset of the eruption was a dramatic increase in well-pressure over a couple of days. By January and February 2016, the explosions were vulcanian and produced pyroclastic flows to the north and northwest that reached up to 2.2 km.

Frank Tepley

Submission 876

The development of isotopic microsampling at the Los Angeles Volcano Observatory (LAVO)

The use of isotopic analysis to trace magmatic sources and processes is a common analytical technique. At the Los Angeles Volcano Observatory (LAVO), Dr. Jon Davidson and his students helped develop and refine a new technique that allowed for isotopic fingerprinting of magmatic components at the crystal and sub-crystal scale. These microsampling techniques were developed to extract isotopic and geochemical compositions that whole-rock and whole-crystal analyses could not obtain thus allowing researchers to more thoroughly constrain the petrogenetic histories of volcanic and plutonic systems. The new technique involved micromilling growth zones of crystals in situ and low-blank chemical processing. Isotopic microsampling, when used in concert with Nomarski Interferometry (NDIC) to enhance compositionally dependent textural features of crystals, and electron microprobe analyses to determine compositional variations in target crystals, provided a combined textural, chemical and isotopic relationship that was used to diagnose open system processes such as magma mixing, contamination and recharge. With the development of isotopic microsampling, Davidson-led research delved into geological problems answerable only through the use of these techniques. From these studies, it became clear that mineral phases are not always in isotopic equilibrium with other co-existing phases and/or their host groundmass. Additionally, it was found that intracrystalline isotopic heterogeneity is common reflecting crystal growth in a progressively changing magmatic system. I review several of the studies originating in the LAVO under Davidson's tutelage illustrating the impact that isotopic microsampling has had on our understanding of magmatic evolutionary processes.

Gabrielle Tepp, Matthew Haney, John Lyons, William Chadwick, Susan Merle, Robert Dziak, Delwayne Bohnenstiehl

Submission 549

Hydroacoustic and Seismic Observations of the 2014 Submarine Eruption at Ahyi Seamount, Mariana Arc

When signs of an eruption in the Northern Mariana Islands (NMI) were first recognized in April 2014, hydroacoustic signals detected by the International Monitoring System (IMS) Wake Island hydrophones were key to pinpointing the source as Ahyi Seamount, located ~2250 km from the IMS arrays. Several thousand underwater explosions occurred throughout a 2-week period beginning on April 23 with sporadic activity observed until May 17. Hydroacoustic signals from these explosions were also detected by the land-based NMI seismic network and regional seismometers, with some signals even reaching as far as 12,000 km distant at the IMS Juan Fernandez Islands hydrophone arrays. During the first few days of the eruption, a NOAA coral reef monitoring expedition in the region reported seeing orange-yellow mats on the sea surface and hearing explosions while scuba diving at nearby Farallón de Pájaros island. Confirmation that the activity was centered at Ahyi Seamount was provided by post-eruption repeat bathymetric mapping, which identified a new crater at the volcano summit and large landslide chute on the south flank.

We aim to better describe the 2014 Ahyi eruptive episode through analysis of hydroacoustic and seismic observations. We consider event rates, waveform similarity, and amplitudes among other characteristics. While most of the detected events were explosions, possible signals relating to the large landslide or other activity may be identified. The rate of events detected by both seismic and hydroacoustic networks is similar though the character of the signals recorded on each differs. Furthermore, a comparison of hydroacoustic and seismic recordings of the same events provides information about wave conversion and detection that may have implications for future monitoring efforts of submarine volcanoes.

Brian Terbush

Submission 1083

Successes, challenges, and strategies for effective communication with emergency managers

The Washington State Emergency Management Division (WA EMD) serves as a coordinator and facilitator between the scientific community, the emergency management community, and the public, specifically regarding the state's natural hazards, including five active volcanoes. This work involves ensuring that state residents and visitors, as well as local, county, and Tribal governments, all directly benefit from the most relevant risk information. In Washington, EMD uses research from contracted and partner scientific organizations directly for public outreach, to develop and revise comprehensive emergency coordination plans, conduct accurate and effective training and exercises, and to recommend policy changes within the state at a legislative level. Due to this function, WA EMD has a history of experience serving as a communication interface of geologic hazard information between the scientific community and the public. While the majority of experiences are successful, the process of receiving the necessary information does not always go smoothly.

Members of the emergency management community rely on the expertise provided by scientific researchers, but it is essential that this information be communicated effectively to a wider audience. There are several communication best practices that would help improve this exchange of information. A few of them include: summarized clear and concise talking points communicating the new information in lay language, illustrative graphical representations which can be used to present the information to many different audiences, and ways that this new information could be applied. To illustrate these concepts in practice, we present several examples of success stories, as well as some of the challenges WA EMD has experienced in communication with the scientific community, and how communications could have been improved to better meet the needs of stakeholders.

Weston Thelen, Seth Moran, David Shelly

Submission 440

The Cascade Volcanoes Are Alive With The Sound of Earthquakes

Volcanoes in the Cascade Range of the United States exhibit significant variability in their background seismicity rates in part due to differences in seismic detection thresholds, but much of it is real and likely reflects differences in conditions in the underlying magmatic-hydrothermal systems at each volcano and the local tectonic stresses. Here we consider the seismicity around each of the ten Very High Threat Cascade volcanoes, as defined by the National Volcanic Early Warning System (NVEWS) threat assessment, in order to determine what critical factors or processes may be affecting the observed seismic behavior. Of these ten, four volcanoes are consistently seismogenic when considering earthquakes within 10 km of the volcanic center or caldera edge (Mount Rainier, Mount St. Helens, Mount Hood, Lassen Volcanic Center (LVC)). Other Very High Threat volcanoes (South Sister, Mount Baker, Glacier Peak, Crater Lake, Newberry Caldera and Mount Shasta) have comparatively low rates of seismicity and/or not enough recorded earthquakes to provide meaningful catalog statistics.

Among the four volcanic centers that are consistently seismogenic, we find that interevent times are similar at Mount Rainier, Mount Hood and LVC; in contrast, interevent times at Mount St. Helens during non-eruptive periods appear to have a different probability density distribution at shorter interevent times. Though not a unique explanation, the difference may be explained as the signature of magmatic recharge, which is present at Mount St. Helens during periods of repose. We examine swarms of earthquakes (defined as three or more located earthquakes per day above the maximum magnitude of completeness for all catalogs) and find that earthquakes within a swarm account for about 60% of seismicity at Mount St. Helens, Mount Hood and the LVC, but only 16% of the earthquakes at Mount Rainier. We also find that seismicity within the upper 2-3 km tends to be more constant in rate whereas deeper earthquakes tend to be “swarmier.” Such behavior could reflect different rheologic properties in the crust (e.g., higher strain rates are required at greater depths) or different processes occurring in the shallower (primarily hydrothermal) vs deeper (primarily magmatic) parts of the magmatic systems.

Sam Thiele, Alexander Cruden, Steven Micklethwaite, Jozua van Otterloo

Submission 28

House of Cards: The role of load-bearing dyke networks in volcanic edifice instabilities

The island of La Palma (Spain) is well known for large collapse events, the most recent of which removed a significant portion of the Cumbre Nueva edifice at ca. 550 ka. Erosion of this collapse scar has formed extensive cliffs within Caldera de Taburiente, exposing thousands of dykes in an approximately radial swarm. The role of these dykes in the edifice instability and eventual failure remains largely unexplored.

We present UAV-based 3D modelling, mapping and field observations of the dykes in Caldera de Taburiente, where near-continuous exposure provides an ideal field locality to investigate the distribution of dykes within volcanic edifices and their potential effect on edifice mechanics. Our results highlight the large number of dykes involved, illustrate their relationships to the collapse geometry and provide quantification of key geotechnical parameters (e.g., fracture intensity and dyke spacing). Furthermore, observations of internal dyke-parallel joint sets and multiple-dykes in weak host rocks with internal glassy chill margins provide structural evidence for local stress concentration within solidified dykes, and hence a broader contribution to edifice mechanics and deformation than has previously been recognised.

We suggest that solidified dykes with different mechanical properties to their hosts have the potential to significantly affect volcanic edifice strength, and hence stability. If dykes behave in a more rigid fashion than their surroundings, they will act to support the edifice weight, “channelling” and locally concentrating gravitational stresses. This effect can improve edifice strength, allowing steeper slopes. Conversely, it could also provide a potentially catastrophic weakening mechanism because progressive hydrothermal alteration or strain softening (due to fracturing or eventual dyke truncation) reduces the ability of dykes to support a load. Interactions between dykes and edifice hydrogeology are also likely to have significant implications for instability formation and development.

Jennifer Thines, Ingrid Ukstins Peate, David Peate

Submission 456

Using mineral chemistry from Afro-Arabian flood volcanics to quantify formation mechanisms of large volume silicic pyroclastic eruptions

Flood volcanic provinces represent some of the largest volumetric accumulations of magmatism on the planet following mid-ocean ridges (Coffin and Eldholm, 1992). The Oligocene Afro-Arabian bimodal flood volcanic province is located in Yemen and Ethiopia. In recent years, several studies including $^{40}\text{Ar}/^{39}\text{Ar}$ geochronology of Ethiopian tephras (Rooney et al., 2012), major and trace geochemistry of Ethiopian Oligocene volcanic strata (Rooney et al., 2013), and analyses of atmospheric CO_2 in relation to Oligocene Afro-Arabian volcanism have been conducted (Prave et al., 2016). However, research into the Yemen conjugate rifted margin remains sparse. Previous work has established the presence of at least 8 major silicic eruptive units (ca. 1,500 to 3,000 km^3 dense rock equivalent) and four minor successions ranging in age from 30.2 to 27.7 Ma in Northern Yemen (Ukstins Peate, 2003; Baker et al., 1996; Ukstins et al., 2002; Riisager et al., 2005). Locally, silicic units represent up to 50% of the volcanic stratigraphy and have been divided into three groups based on whole rock geochemistry and detailed field observations: Main Basalts (31 to 29.7 Ma), Main Silicics (29.7 to 27.7 Ma), and Upper Bimodal (29.5 to 27.7 Ma) (Ukstins Peate, 2003). The Yemen section is unique in that correlated oceanic tephras indicate extreme geochemical heterogeneity in individual eruption events which can span from 43 to 75 wt% SiO_2 (Ukstins Peate et al., 2008). The main silicic units have yielded dense rock equivalent estimates of $\sim 3,100 \text{ km}^3$ for a single eruption with ash fall-out over areas $> 1 \times 10^7 \text{ km}^2$ (Ukstins Peate, 2003). Whole rock geochemistry from Inductively Coupled Mass Spectrometry (ICP-MS) shows vertical and lateral compositional heterogeneity within individual units as well as between units. Preliminary analyses of feldspar and clinopyroxene with the Electron Probe Microanalyzer (EPMA) also show vertical compositional heterogeneity. Detailed mineral chemistry will continue to be performed on pyroxene and feldspar in conjunction with ilmenite-magnetite thermometry in order to assess the crystallization temperatures and fine-scale chemical variations within the 12 units from 8 sample localities in Northern Yemen. The geochemical heterogeneity preserved in these deposits provides important insight into the formation mechanisms for large-volume silicic magmas in continental rifting environments.

Simon Thivet, Lucia Gurioli, Andrea Di Muro, Guillaume Boudoire, Andrew Harris

Submission 335

Eruption of a stratified basaltic sill: insights from the June 2014 and July 2015 eruptions of Piton de La Fournaise

Small-volume proximal eruptions are common at Piton de la Fournaise (La Reunion Island, France). However, the mechanisms driving such basaltic eruptions are still not completely understood. To gain insight, we focused on a well-constrained multidisciplinary dataset for the two short-lived (~2 day-long) eruptions of June 2014 (0.4 million m³) and July 2015 (2 million m³), which occurred near the SE rim, and on the NE flank, of the central cone, respectively. These two events were part of a new eruptive cycle that began in June 2014 following 3.5 years of quiescence. The approach involves integration of physical measurements (e.g., time-averaged discharge rate, TADR), physical and textural analyses of pyroclasts and lava, and chemical analyses. Based on this approach four main groups of pyroclasts were identified in both eruptions: "golden pumice", "fluidal scoria", "spiny-glassy scoria" and "spiny-opaque scoria". The first two groups are predominant at the beginning of each eruption, during Hawaiian phases characterized by highest TADR (30 m³.s⁻¹ for July 2015). These products are highly vesicular (700 kg.m⁻³), with isolated vesicles (up to 38 % vol.) and very low crystal contents. Their abundance decreases with time in favor of "spiny" products during the course of each eruption. These spiny scoria are thus more abundant towards the end of an eruption, coinciding with decreasing TADR (1-5 m³.s⁻¹), and are (i) denser (1300 kg.m⁻³) than the golden pumice and fluidal products, (ii) have larger, more connected vesicles and (iii) have higher crystal contents (up to 50% vol., corrected for vesicularity). The higher crystallinity is both in terms of microcrysts and mesocrysts. However, bulk composition remains homogeneous, with only some minor glass chemistry variations reflecting different degrees of late-stage crystallization. We thus suggest that these short-lived eruptions involve single batches of magma. Progressive textural variations are due to magma extraction from a horizontally stratified sill. A gas-rich foam layer, formed at the top of the sill, first feeds an initial phase of annular flow at a high ascent rates during dyke propagation. This drives the opening phase of Hawaiian-style activity. The sill is progressively emptied to tap more degassed magma, with lower ascent rates leading to bubble coalescence and microcrystallization characteristic of a less intense Strombolian-style, or purely effusive activity, towards the end of the eruption.

Helen Thomas, Ailsa Naismith, Robyn Brailey, Gustavo Chigna, Kerstin Stebel, Fred Prata, Matt Watson

Submission 403

Multi-spectral infrared cameras for long-term observations of degassing and volcanic activity: a case-study from Volcán de Fuego, Guatemala

Volcán de Fuego, Guatemala, situated 45km WSW of Guatemala City, typically exhibits high levels of activity with regular Vulcanian and Strombolian eruptive phases. In 2015, the volcano began to demonstrate a new eruptive pattern with ongoing and regular Vulcanian eruptions, interspersed with paroxysmal phases approximately every three weeks (15 in 2015 and 16 in 2016). As a result of the enhanced activity, national and international flights have been significantly disrupted and the La Aurora international airport has been forced to close on a number of occasions. Measurements of emissions from Fuego to better characterise its ongoing behaviour have been so far limited, with ground-based remote sensing measurements typically restricted to individual field campaigns. Due to the high density of volcanoes in the region, satellite sensors often struggle to differentiate between them and emissions are attributed to a number of potential sources.

Since February 2016, a multi-spectral, infrared (IR) imaging camera has been semi-permanently positioned 7 km south-east of the Fuego summit. The imaging camera, with band pass filters with central wavelengths at 8.6, 10.0 and 11 μm has the ability to retrieve quantitative estimates of SO₂ emission rates and plume ash content, as well as information available from standard IR cameras (such as temperature and plume altitude). Here we use this unprecedented time-series of data, along with additional data-sets from field campaigns in January 2016 and February/March 2017 to investigate the relationships between SO₂ emission rates, eruptive energy, repose intervals and ash emissions within the paroxysmal cycles. We will also discuss the potential future application of IR imaging cameras for long-term measurement campaigns and hazard mitigation.

Nicole Thomas, Tobias Fischer, Adrian Brearley

Submission 1254

Magma Injection Triggers Earthquake Swarm and Eruption: Mineralogical Indications of Magma Mixing, 2007-8 Eruption at Oldoinyo Lengai, Tanzania, Africa.

The world's only active natrocarbonatite volcano, Oldoinyo Lengai, in Tanzania, Africa had its most explosive eruption on Sept 24, 2007, with a sub-plinian plume rising ~12km high (VAAC,2008). The assumed anhydrous nature of the primary nephelinite magma at Lengai, does not explain this highly explosive behavior. InSAR elastic modeling (Baer et al, 2008) demonstrates magma chamber pressurization and increased inflation after the peak seismic event (5.9 Mag on July 17, 2007), followed by dyke propagation, with subsequent eruption deflation. Injection of magma from a source as deep as 15km is inferred from the Geophysical InSAR elastic model. Here we present geochemical evidence in support of a deeper magma source behind this highly pyroclastic eruption at Lengai.

In this geochemical study of the eruptive ash products, electron microprobe (EMPA at University of New Mexico) and mass spectrometry (LA- ICP-MS at University of Columbia Lamont-Doherty Earth Observatory) analyses confirm the presence of more than one nephelinite magma in the 2007-8 eruption. Two distinct nephelinite magma assemblages were identified in this mineralogical analyses of the ash erupta: a highly evolved nephelinite, with less than 3% glass from the primary nephelinite magma chamber, as indicated by the highly peralkalinitic feldspathoid: combeite ($\text{Na}_2\text{Ca}_2\text{Si}_3\text{O}_9$), commonly found in Lengai eruptive products (Dawson 1966, 1998), and a less evolved nephelinite magma, with up to 18% glass that did not contain combeite, with significantly higher Si, Al, Mg and Mn content.

Magma mixing of the two nephelinites is evidenced in sudden changes in the melt chemistry in both ash sample sets. This can be seen in resorption rims, disequilibrium textures, stepwise zoning, mineral instability in addition to REE and trace element distribution. Phase abundances, mineral formulas and endmember components for both assemblages represent varying cooling histories, chemical contributions and phase distributions. Melt compositions from the glass analyses of the two assemblages demonstrate the presence of two distinct melt compositions, both peralkalinitic nephelinites one Al enriched and one Ca enriched.

Helen Thomas, Matthew Watson, Rory Clarkson, Helen Dacre, Colin Hord

Submission 499

Volcanic Ash and Aviation: Knowledge Exchange for Improved Hazard Mitigation

Volcanic ash in the atmosphere poses a threat to both commercial and military aviation operations. Since the eruption of Eyjafjallajökull in 2010, the enhanced research effort and level of interest in the issues surrounding volcanic ash for the aviation community have led to some major changes in policy and practice, particularly within Europe. Of these, the shift from total avoidance to permitting flight under certain ash concentrations is one of the most significant. However, it is apparent that some of the more recent developments in research science, including the application of probabilistic dispersion modelling and forecasting and research investigating a dose-based approach to volcanic ash avoidance are not yet integrated into operational policy. Both could have significant implications for flight planning, improving safety and minimising the economic impact of ash in the atmosphere.

Ensuring that policy and practice within the aviation industry is underpinned by the most relevant, up to date and sound science requires close collaboration and strong relationships between the stakeholders involved. Not only are there areas where science can be applied more effectively to policy, but improving scientists' understanding of how operational decisions are made is key for directing research. This project aims to address some of the current disparity between the various stakeholders using effective knowledge exchange. In this context, we will discuss recent progress of the project, including impact already achieved as well as highlighting some of the hurdles associated with stakeholder engagement and changing industrial perceptions of academia. Through this work, we aim to strengthen existing relationships between industrial, governmental and academic stakeholders as well as foster new connections to improve the application of scientific research in practice.

Ellen Thomas, Paula Tartell, Hilary Brumberg, Robert Reynolds, Gregory Mulder, Johan Varekamp

Submission 1259

The twin crater lakes of Newberry Volcano, OR: analogs of ancient environments?

Newberry Volcano (OR) has twin crater lakes, separated by a 6000 year old, narrow volcanic ridge. East Lake is a terminal lake with a volcanic gas input of CO₂, H₂S, and Hg, a pH 6.5-7 and ~ 135 ppm HCO₃⁻. Paulina Lake has an outlet (Paulina Creek), and subaqueous hot fluid inputs. It has a pH ~ 8, 400 ppm HCO₃⁻ and 15 ppb As. The lakes have active ecosystems, with diatoms abundant among primary producers. Most material input in the ecosystem is provided by the volcano: CO₂, P, Si, and trace elements, but nitrogen is locally fixed by cyanobacteria (*Nostoc*), and energy provided by sunlight. These "geophytic" lakes receive toxic volcanic inputs: arsenic in Paulina Lake, mercury in East Lake, the latter accumulating in the sediment at a rate of ~5 kg/yr. We used a small subaqueous ROVER (ongoing work) to locate hot springs on the Paulina Lake bottom, the source of Si, ferrous Fe, Mn, P and As. The ferrous iron is oxidized in the lake waters, leading to precipitation of hydrous Fe-oxides, which scavenge dissolved P and As, which are jointly deposited in the sediment. Sedimentary organic matter reduces these oxides, releasing the elements into the pore waters and leading to precipitation of vivianite (Fe₃(PO₄)₂·8H₂O). Part of the P in the vivianite may be replaced by As. Dried sediment has an intense blue-green color from the abundant vivianite crystals. The Paulina Lake sediment contains up to 60% SiO₂ (diatom frustules, hydrothermal silica) and up to 14% Fe₂O₃. This Fe-Si combination resembles that of Precambrian Banded Iron Formation, and the common cyanobacterial colonies enhance the similarity to 'ancient environments'. East Lake sediment consists of diatomaceous silica and volcanic ash, with up to 12% organic matter, and only 1-2 % Fe₂O₃. This lake releases 40-50 Mg CO₂/day through diffusive degassing. The volcanic Hg(o) is oxidized to Hg²⁺ and H₂S is oxidized to SO₄⁼, the latter in concentrations of ~ 65 ppm. Sulfate-reducing bacteria methylate the Hg²⁺; the methyl-Hg is taken up by diatoms and biomagnified at higher levels in the ecosystem. The largest predators, Kokanee salmon, thus have Hg concentrations of 3-4 ppm. We used meteorological and O-H stable isotope data to create lake water budgets, and found that in summer the small water sheds inside the crater deliver almost no water, while a substantial hydrothermal fluid input is needed to provide mass balance for Paulina Lake and its outflow creek.

James Thompson, Michael Ramsey

Submission 671

Identifying silicic lava surface textures and flow relationships using multispectral thermal infrared data

Multispectral thermal infrared (TIR) remote sensing data is used to detect and map distinct surface textures on silicic lava flow surfaces at Medicine Lake Volcano, CA. The results allow emplacement processes to be inferred and the potential for explosive volcanic activity at future eruptions to be better understood. The identification of the type and distribution of vesicular surface textures and their variability with successive lava flows is relevant to calculate possible changes in the active flow's thermo-rheology and volatile content. Vesicularity produces variability in TIR emissivity spectra that can be identified and quantified using spectral modeling approaches such as linear deconvolution. This model assumes that emissivity spectra are a linear mixture of spectral end-members based on their areal percentage in a given pixel in the data. The basis of this assumption relies on the dominance of surface scattering in the TIR, meaning that spectral components sum linearly due to the single photon and grain interaction. Therefore, the mixed spectrum from each pixel can be linearly unmixed using a library of those end-members. To determine the distribution of vesicularity, two spectral end-members were used, a non-vesicular obsidian glass and a blackbody that has a constant emissivity of 1.0 at all wavelengths. Multispectral TIR data acquired using the MODIS/ASTER Airborne Simulator (MASTER) instrument were analyzed, from Medicine Lake Volcano. Distinct regions of interest (ROI) were defined in the MASTER data and the spectra from those as well as laboratory hyperspectral data were analyzed, to determine more subtle lava compositional variations. The model results demonstrate that surface vesicularity increased with lava silica content and proximity to vents, which is consistent with previous geological mapping and the analysis of collected rock samples. The same techniques can also be applied to more recent silicic lava flows such as the 2008-2009 rhyolitic eruption of Chaitén Volcano (Chile). Orbital TIR data acquired during the eruption is being evaluated to map the surface textural distribution throughout the flow emplacement period. The ability to ultimately constrain surface textural and compositional distributions on silicic lava flows and domes using multispectral TIR data will improve our understanding during emplacement and of potential hazards.

Ren Thompson, Kenzie Turner, Michael Cosca, Ben Drenth, Leah Morgan, V.J.S. Grauch

Submission 535

Eruptive history of the Taos Plateau volcanic field and links to extensional tectonism of the northern Rio Grande rift, USA

The Pliocene Taos Plateau Volcanic Field (TPVF) is the largest volcanic field of the Rio Grande rift. Deposits of the TPVF are distributed across ~4500 km² in the southern part of the ~12,000 km² San Luis Valley in southern Colorado and northern New Mexico constituting a major component of the structural San Luis Basin (SLB) fill. Exposed deposit thicknesses range from a few meters near the distal termini of basaltic lava flows to ~170 m in the Rio Grande gorge near Taos, NM. New geologic mapping in combination with ~150 high-resolution ⁴⁰Ar/³⁹Ar age determinations reveals a complex distribution of >60 exposed eruptive centers ranging in composition from basalt to rhyolite. Total eruptive volume, estimated from geologic map relations, geophysical modeling of basin geometry and subsurface distribution of basaltic deposits, are approximately 300 km³ and consists of 66% Servilleta Basalt (tholeiite), 3% mildly alkaline trachybasalt and trachyandesite, 12% olivine andesite, 17% dacite, and 3 erupted volume typical) monogenetic andesitic shield volcanoes (~5-4.4 Ma); which are north-south aligned and distributed along the central axis of the SLB, parallel to major intrabasin faults. Large (up to 21 km³ erupted volume) zoned dacitic lava dome complexes (~5 Ma Guadalupe Mountain/Cerro Negro, ~3.9 Ma Ute Mountain, and ~3 Ma San Antonio Mountain) reach elevations of 3300 m, ~770 m above the valley floor and each is spatially and temporally associated with fault-bounded sub-basins superposed on the broader structural SLB. Locally, coeval Pliocene fault-slip rates are ~2.5 times the long-term rates determined for the SLB confirming the temporal association of local intrabasin extensional faulting and eruptive centers.

Thor Thordarson, Ármann Höskuldsson, Ingibjörg Jónsdóttir and the FES and IES Volacno and Hazard Group

Submission 776

The magma discharge and the volume of lava erupted during the 2014-15 eruption on Dyngjusandur, North Iceland as determined by geometric measurements

The August 31st 2014 to February 27th 2015 lava-producing eruption on Dyngjusandur produced a lava flow-field with an area of 84 km² and a bulk volume of 1.45±0.04 km³ as determined from post eruption approximately 0.5-m-resolution digital elevation model (DEM). This volume is equivalent to 1.2±0.1 km³ when calculated as dense rock. This volume makes the eruption at Dyngjusandur the largest eruption in Iceland since the Laki flood lava eruption in 1783-4 (volume, 15 km³; area, 600 km²). As such, this event provided the volcanological community with an excellent opportunity to observe and study the formation of moderate-size basaltic lava flow-field that was emplaced on effectively flat ground (3/s) and a near halt of activity on day 15, when discharge dropped to 30 m³/s. Activity picked up over the next 5 days with TADR reaching a second peak of 440 m³/s on day 20. From then on the TADR dropped steadily, in roughly exponential fashion, until the end of the eruption. The relationship between TADR and lava advance will be explored in relation to potential hazards posed by basaltic lava flows.

Clifford Thurber, Crystal Wespestad, Carlos Cardona, Bethany Vanderhoof, Ninfa Bennington, Xiangfang Zeng, Federica Lanza, Katie Keranen

Submission 1084

Seismic investigation of the rhyolitic magma system beneath the Laguna del Maule volcanic field, Chile

The Laguna del Maule volcanic field, straddling the Chile-Argentina border at 36° S, is currently the subject of a multi-disciplinary collaborative investigation supported primarily by the U.S. National Science Foundation Integrated Earth Systems program and the Observatorio Volcanológico de Los Andes del Sur (OVDAS) of SERNAGEOMIN. At least 50 post-glacial (younger than 20 ka) eruptions from more than two dozen vents encircling the 25x17 km lake basin have produced rhyodacitic-rhyolitic lava flows and ash deposits totaling >30 km³, suggesting that a large, active, silicic magma reservoir fuels this system. Since 2007, GPS and INSAR geodesy reveals that Laguna del Maule has been experiencing rapid uplift at 20 to 25 cm/year centered within the ring of silicic vents. Moreover, a deformed paleoshoreline that has been ³⁶Cl-dated implies magma-driven surface uplift of >60 m and that growth of this large shallow reservoir has occurred over at least the past 9,400 years. The University of Wisconsin-Madison, Cornell University, and OVDAS have deployed a seismic array covering 450 km² that surrounds the lake basin. The array consisted of 18 broadband stations in 2015, and was enlarged to 47 stations in 2016 (37 broadband, 10 short-period). The full array will remain in place until early 2018.

A variety of seismic studies are planned for the seismic array data, including body-wave tomography, surface-wave tomography (from ambient noise), attenuation tomography, teleseismic tomography, receiver function analysis, seismic interferometry, and focal mechanism and moment tensor determination. The main goals are to detect the magma chamber underlying Laguna del Maule and characterize its dimensions and properties.

We report on preliminary results from body-wave and ambient noise tomography, and compare the results to those from other geophysical techniques. Both the preliminary body-wave (V_p and V_s) and ambient noise (V_s) images show evidence of upper crustal low velocity anomalies. One such anomaly is present in both models along the southwest side of the lake, close to the estimated source area for the uplift measured by InSAR and GPS. A Bouguer gravity low, interpreted to reflect a crystal-rich magma reservoir, occupies the same area. In contrast, magnetotelluric results image the largest low-resistivity zone near the north side of the lake. We will present refined tomographic models, including preliminary results from a joint body wave-surface wave inversion.

Christy Till

Submission 1229

An Integrated Approach for Identifying the P-T-X-t Histories and Eruption Triggers for Silicic Magmas; An Example Examining the Scaup Lake Rhyolite, Yellowstone Caldera, WY

The crystal cargoes from past eruptions provide petrologic records of the pressure, temperature and composition of a magma body preceding eruption. Recent advances in diffusion chronometry also now enable us to reconstruct the timing of magmatic events shortly before eruption. Here these techniques are combined to unlock detailed P-T-X-t histories of silicic magma bodies leading to eruption, using the ca. 260 ka Scaup Lake rhyolite lava (SCL) from Yellowstone caldera as an example. The SCL contains ~30% phenocrysts of reversely zoned quartz, clinopyroxene, orthopyroxene, plagioclase and sanidine. SCL sanidine and plagioclase reveal ubiquitous bright rims that are enriched in Ba, Sr, Ca and in some cases Mg and Ti relative to the grain interior. Major element transects across the full width of the sanidine rims reveal two pronounced changes in composition that can be equated to heating events (older +10-30°C, younger +40-100°C) using sanidine-liquid thermometry and compositional relationships predicted by Rhyolite-MELTS. Renewed precipitation of sanidine at higher temperatures could reflect magma ascent and concomitant exsolution of dissolved H₂O, the addition of CO₂ by new magma, and/or the addition of K-Na-enriched melt derived from melting sanidine-rich cumulates. The increase in magmaphile elements associated with the 10-30°C heating event indicate this episode of feldspar growth resulted from the injection of a hotter, less evolved magma ~10-40 yrs prior to eruption based on diffusion chronometry (Till et al., *Geology*, 2015). The younger, heating event of ≤100°C is recorded in the outermost 50-75 microns of the crystal rim and associated with a variety of trace element behavior (e.g., wt.% Ba constant, increases or decreases) in different crystals. Conservative estimates using natural and experimental crystal growth rates suggest this second heating event occurred within 1.5-2 yrs of eruption, consistent with a subset of the diffusion chronometry results that indicate rejuvenation-eruption timescales of <10 mo.s. Thermodynamic calculations suggest depressurization of 200-300 MPa could produce ≤25-30°C of heating, requiring additional processes to explain the late stage heating event. Thus the feldspar record suggests a widespread rejuvenation event that unlocked a significant portion of the crystal mush several decades before eruption, followed by a second more localized rejuvenation event in the year or two before eruption.

Christy Till, Adam Kent, Geoffrey Abers

Submission 1226

An interdisciplinary synthesis of mantle conditions, crustal storage and seismic velocities in the Southern-Central Cascades Arc

One of the most fundamental unanswered questions in subduction system science is the cause of the observed diversity in volcanic arc style at an arc-segment to whole-arc scale. Specifically, we have yet to distinguish the predominant mantle and crustal processes responsible for the diversity of arc volcanic phenomenon, including the presence of central volcanoes vs. dispersed volcanism; observed episodicity in volcanic fluxes in time and space; variations in magma chemistry; and differences in the extent of magmatic focusing. We focus on the Southern-Central Cascades arc, a well-studied and “hot” end-member in active subduction systems, using an interdisciplinary approach that combines mantle and crust thermobarometry of arc magmas with the V_s velocity structures from ambient noise tomography for the crust and upper mantle. A suite of primitive basalt thermobarometry from between 40-47°N latitude suggests variations in mantle wedge temperature of ~200-250°C at depths of last mantle equilibration between ~30-60 km. Melt inclusion saturation pressures, mineral barometry, and experimental constraints published to date suggest a range of crustal storage depths with considerable shallow magma residence at <~10 km. The primitive arc magmas temperatures of last equilibration vary up to ~100°C at similar depths beneath individual arc volcanoes (e.g., beneath Newberry volcano in Central Oregon) and maximum crustal storage depths vary up to 20 km as recorded by a given barometric method (e.g., melt inclusion saturation vs. experimental constraints). In addition, there appears to be a broad correlation between low velocity regions and the location primitive melt Re: Revised Abstract equilibration in the mantle along strike. However, differences in the location of low velocity regions along the Cascade arc-axis between different surface wave-based V_s models necessitate revisiting these inversions before comparing them with petrologic calculations of temperature, pressure, and melt extent. Overall preliminary evidence suggests three variables play important roles in producing volcanic arc diversity: the prevalence of primitive arc magmas at a given arc segment, their pressure and temperature of mantle equilibration, and magmatic focusing in the upper crust.

Andrea Todde, Rafeollo Cioni, Karoly Nemeth, Marco Pistolesi, Nobuo Geshi, Costanza Bonadonna, Sébastien Biass

Submission 923

Understanding complex evolution of intermediate to silicic linear-source Plinian eruptions: Sakurajima volcano (Japan) and Tarawera Volcanic Complex (New Zealand) as case studies

Plinian eruptions are commonly fed by intermediate to silicic magmas and originate both from single central vent and from km-long eruptive fissures defined by alignments of several vents. In the latter case, multiple vents can be active at the same time or sequentially, producing a complex stratigraphy of proximal deposits in which relations between the vent(s) source and tephra beds in medial area are difficult to establish. In addition, changes in the eruptive style may occur, overlapping or following the main sustained Plinian phase, making the reconstruction of eruptions behavior over time hard to constrain. Detailed field studies of tephra deposits, together with sedimentological and textural characterization of the erupted materials can provide wide datasets to understand complex eruptive sequences often associated with linear-source Plinian eruptions. In this context we investigate the stratigraphy of the AD 1914 Taisho eruption, the most recent Plinian eruptive episode of Sakurajima Volcano (Japan). The reconstruction of the Taisho eruption, based on the chronicles and the re-interpretation of the tephra deposits, depicts an eruptive scenario in which the eruption began with a Plinian explosive phase characterized by the rise of two convective columns simultaneously from two parallel, newly-opened, fissures located on two opposite sides of the volcano. After 36-48 hours, the eruption evolved toward an effusive activity with the outpouring of andesitic lava flows for several months, accompanied by ash emissions and minor discrete Vulcanian explosions. This field-based methodology can be extended to more silicic and larger volume eruptions, as for example the ~ AD 1315 Kaharoa eruption, the youngest rhyolitic Plinian eruption of the Tarawera Volcanic Complex (New Zealand). The eruption developed from multiple vents along an 8 km linear zone and exhibited a complex succession of different eruptive styles, intensities, and dynamics over an estimated ~ 5-year period of time, including initial phreatomagmatic and Plinian explosions with associated pyroclastic density currents, extrusions of lava domes and block and ash flows. The field-based approach is an essential and rapid tool to understand the complex evolution of volcanic eruptions in various time-scales, to establish eruptive scenarios and to define potential volcanic risk associated to the large spectrum of eruptive styles presented by these eruptions.

Filip Tomek, Jiří Žák, Martin Svojtka, Friedrich Finger, Michael Waitzinger, Vladislav Rappich

Submission 139

Emplacement dynamics of syn-collapse ring dikes: an example from the Altenberg-Teplice caldera, Bohemian Massif

The late Carboniferous Altenberg–Teplice volcanic complex (Bohemian Massif, Czech Republic and Germany) is a ~NNW–SSE-elongated, eastward dipping trap-door collapse caldera (~18 × 35 km) exposing (1) a pre-caldera monzogranite pluton, (2) a ~700 m thick sequence of pre-caldera dacite and rhyolite tuffs, ignimbrites and lavas, (3) an up to 1.5 km thick sequence of caldera rhyolite ignimbrites and lavas, (4) a porphyritic microgranite caldera ring dikes, and (5) a late subvolcanic Li-mica granite pluton. We focus on the emplacement mechanisms of caldera ring dikes using integrated structural and textural analysis, anisotropy of magnetic susceptibility (AMS), geochemistry and U–Pb zircon geochronology. The porphyritic microgranite is characterized by rapidly quenched fine- to coarse-grained quartz-feldspar microgranitic to granophyric texture with K-feldspar, oligoclase to andesine and resorbed quartz phenocrysts and glomerocrysts. Weak feldspar foliation and lineation measured are mostly parallel to the AMS fabrics. The AMS signal is dominated by multi-domain titanomagnetite and maghemite microphenocrysts dispersed in the matrix or embedded in feldspar and biotite grains. Three ring dike segments delineate the subsided portion of the caldera from the W, NW and E, whereas its southern portion is covered by younger sediments. The western segment is dominated by oblate AMS ellipsoids, eastern by prolate ellipsoids, and both ellipsoid shapes alternate in the NW. In addition, four domains with vertical lineations were identified and the fabric intensity is stronger in the center and in thinner parts of the dikes. We interpret this complex fabric pattern as reflecting simultaneous magma ascent within the ring dike, with eastward trapdoor collapse triggered by magma chamber withdrawal during/after the last ignimbrite eruptions. The vertical lineation domains represent ascent paths from which the magma was distributed laterally to the other parts of the ring dike. Magma stretching (prolate fabric) which corresponds to longer magma ascent paths along the eastern segment switch to magma flattening (oblate fabric) along the western segment caused by compression from the hinged caldera floor. Moreover, this hypothesis is supported by a close geochemical signature of the youngest ignimbrites and lavas with ring dikes, and also corroborated by the newly obtained U-Pb zircon ages indicating magma crystallization at ~312 Ma to produce coeval pyroclastic and dike rocks.

Akihiko Tomiya, Yoshihiko Goto, Tohru Danhara, Shanaka de Silva

Submission 122

Magmatic conditions and preeruptive magma processes of the catastrophic eruption of high-silica rhyolite from Toya caldera, Japan

Toya caldera, Japan, erupted a large amount of high-silica rhyolite (Toya ignimbrite; VEI 7; SiO₂=77-78 wt.%) at 112-115 ka (e.g., Machida and Arai, 2003). To investigate the production and eruption processes of the high-silica rhyolite, we analyzed Toya ignimbrite, using XRF and ICP-MS for bulk rock compositions and electron microprobe and LA-ICP-MS for compositions and textures of the minerals.

Most of pumice in Toya ignimbrite is well-vesiculated homogeneous white pumice, whose crystal content is only 3-4 vol.%. White pumice typically contains low-An plagioclase (pl) (An₁₀₋₁₃), low-Mg opx (Mg# 25-28), quartz (qz), and low-Mg magnetite (mt) (Mg/Mn=0.23-0.26). We call this association type-A phenocrysts, which is in equilibrium with the high-silica rhyolite. In the later stage of the eruption, heterogeneous pumice and less-vesiculated mafic pumice also appear. Mafic pumice contains high-An pl (An_{>76}), high-Mg opx (Mg#>60 and MnO<1wt%), cpx, and high-Mg mt (Mg/Mn>5.5), which we call type-B phenocrysts. Heterogeneous pumice contains both type-A and type-B phenocrysts, and also contains other type of phenocrysts (type-C), namely mid-An pl, mid-Mg opx, amphibole (amp), mid-Mg mt, and ilmenite (ilm). The coexistence of three types of phenocrysts is evidence that magmas with type-B and type-C phenocrysts mixed into the rhyolite.

The temperatures of type-A, B, and C associations are <810°C, ca. 880°C, and ca. 810-860°C, respectively, according to the Fe-Ti oxide and two-pyroxene geothermometry. We estimated the temperature and pressure of the high-silica rhyolite to be 790-810°C and 100-150 MPa, respectively, where type-A phenocrysts were in equilibrium with the melt under water-saturated condition, using Rhyolite-MELTS (Gualda et al., 2012).

The magma mixing occurred just prior to the eruption because there is virtually no reverse zoning in type-A phenocrysts. Type-A magnetite has a zoning profile within only ca.10 microns from the rim, corresponding only a few days from mixing to eruption if it is a diffusion profile. Therefore, the Toya ignimbrite eruption started abruptly.

There was a long time, however, between the injection of the mafic magma into the magma reservoir and the eruption because type-B pl has a mantle with a hundred microns in width, indicating a time for crystal growth. According to diffusion analysis for Mg in plagioclase, the time from the injection to the eruption was hundreds of years.

Roberto Torres, Diego Gomez

Submission 775

Characterization of volcanic activity at Galeras Volcano, Colombia

Galeras Volcano, composed mostly of andesite, is 4500 years old and is considered the most active volcano in Colombia due to frequent eruptions. Most of these eruptions are categorized as Vulcanian-type with small erupting columns (≤ 12 km high), producing mainly pyroclastic fall deposits. A typical feature is the extrusion of lava domes and their emplacement at the bottom of the crater. Lava cooling and solidification contributes to sealing vents and conduits to inhibit gas escape, with the consequential generation of overpressure triggering an eruption. A multiparameter data set including measurements of seismic data, deformation, SO₂ flux emission, and thermal imagery has been used to characterize diverse volcanic activity at Galeras since 1989. Four stages of activity have been identified. The first is the “quiet or resting stage”. It is characterized by low levels of earthquake occurrence with low seismic energy, low amount of gas emissions and no deformation in the volcano edifice. The second stage is the “clean-up and conduit opening stage,” where an increase in the diversity of volcano-seismic signals and the amount of released energy occurs. In this stage, gas emissions, ash and explosive eruptions of non-juvenile magma occur, where the hydrothermal system plays a fundamental role. The third stage is the “magma intrusion and/or dome construction stage”, this is characterized by deformation of the volcanic edifice accompanied with the increase of LP event occurrence and SO₂ emissions. In this stage, the hydrothermal system has dried out and there are minor eruptions, predominantly of ash. It generally ends with the emplacement of a lava dome at the surface. The fourth stage is the “dome destruction stage” which begins with a decrease in volcano-seismic signals. There are no manifestations of progressive volcanic deformations (except during major eruptions, where a fast deformation occurs), and there is a low emission of gases preceding explosive eruptions with a predominant magma component. Prior of most of these eruptions, a special type of LP events are recorded called “Tornillos”. A typical feature of these events is observed in the temporal evolution of the dominant frequencies which decrease while the signals increase their durations.

Manuela Tost, Shane Cronin, Marco Brenna, Ian Smith, Simon Barker, Mathieu Colombier, Brendan Hall

Submission 670

The formation of the youngest volcanic cone in the world: Hunga Tonga-Hunga Ha'apai

Surtseyan volcanic deposits have been identified in all parts of the world, but observations of their formation linked with field studies are rare. Between December 2014 and January 2015, volcanic activity was observed between the two volcanic islands Hunga Tonga and Hunga Ha'apai, Kingdom of Tonga. The eruption started as a shallow submarine event (th of January 2015, magma-water interaction gradually decreased and the eruptions produced massive, poorly sorted and fine to coarse-grained deposits, which become gradually coarser towards the top. The eruptions were accompanied by up to 10 km high black ash plumes. The subaerial cone units comprise subrounded juvenile lapilli and up to 30 cm-sized bombs with finely vesicular exterior rims and large hollow cores, which were ejected up to 400 m above the sea surface. These deposits make up most of the subaerial lapilli-tuff cone, suggesting early-on shielding of the melt from the surrounding sea water. The later stage of the eruption was characterized by energetic, fine-grained, and planar to cross-bedded pyroclastic surge deposits, indicating a further phase of dominantly phreatomagmatic activity. This sudden shift in eruptive style might be related to a failure of the southern cone flank prior to the 19th of January 2015, which created an amphitheatre-type structure open towards the sea. Just before the 28th of January 2015, activity ceased and eruptions became smaller, with tephra and surge deposits limited to the inner crater wall.

Conner Toth, Mikkel Louis, Wendy Bohrson, Sylvana Bendaña, Nicole Moore, Anita Grunder

Submission 576

Open-System Origin of Giant Plagioclase in the Steens Basalt, SE Oregon, USA: Assimilation of Plagioclase Mush or Entrainment of Plagioclase Antecrysts?

Exceptionally large (>2 cm) and abundant (up to 40 modal %) plagioclase crystals in the Steens Basalt, the oldest and most mafic major unit of the Columbia River Basalt Province, provide strong evidence for incorporation of plagioclase-rich material into basaltic melt. Hypotheses for the nature of this material include entrainment of antecrysts or assimilation of plagioclase-rich mush (crystals+melt) or cumulate. Major and trace elements of ~100 plagioclase that represent its range of textures, sizes, and compositions from 16 samples of 2 stratigraphic traverses at Steens Mtn. record core-rim chemical changes and allow these hypotheses to be explored.

Steens basalts have whole-rock MgO of 3.5-12 wt.%, and phyrlic samples are dominated by plagioclase and olivine, plus clinopyroxene in the more evolved samples. Plagioclase modes range from ~6 wt.%. Sparsely phyrlic samples contain occasional crystals no larger than 1 cm.

Average plagioclase anorthite (An) content is 64, with 72% of analyses between An60 and An70. Zoning is typically modest, with 84% of core-rim differences less than 10 An. Zoning among trace elements (e.g., Ba, La, Pb, Sr) is also modest. Oscillatory zoning is ubiquitous, and where compositional zoning exists, both normal and reverse zoning are present. Distinct resorption boundaries (sieved zones and crystallized melt inclusions) are uncommon.

Phase equilibria modeling using MELTS (see Louis et al., this meeting) indicates plagioclase crystallization begins at ~7 wt.% MgO. However, samples with more MgO also contain large plagioclase, suggesting an antecryst entrainment origin for plagioclase in the most mafic samples. In magmas where plagioclase is stable, entrained crystals may have experienced textural maturation as plagioclase-rich mush is assimilated. Heterogeneous LA-ICP-MS plagioclase $^{87}\text{Sr}/^{86}\text{Sr}$ in Steens Basalt samples (Ramos et al. 2013) suggest that open-system processes (i.e. recharge, assimilation) are important. In-situ core vs. rim $^{87}\text{Sr}/^{86}\text{Sr}$ analyses (by microdrilling and TIMS) permit investigation of $^{87}\text{Sr}/^{86}\text{Sr}$ variations as a function of whole-rock composition and plagioclase texture, composition, and size, allowing us to further elucidate the origin and growth history of giant plagioclase.

Pierre-Yves Tournigand, Jacopo Taddeucci, Damien Gaudin, Juan José Peña Fernández, Diego Perugini, Elisabetta Del Bello, Piergiorgio Scarlato, Joern Sesterhenn

Submission 789

Initial transient ash plume dynamics: new insights from combined high-speed imagery, computer vision techniques and fractal analysis.

Transient volcanic plumes, typically generated by Strombolian and Vulcanian eruptions, are time-dependent features characterized by rise and development time scales similar to the eruption duration. Their dynamical properties are thus strongly related to the source conditions and evolution over time. In this study, the initial dynamics of transient volcanic plumes and their relation with discharge history have been investigated using high-speed and high-resolution visible and thermal videos from eruptions of Stromboli (Italy), Fuego (Guatemala) and Sakurajima (Japan) volcanoes.

Physical parametrization of the plumes has been performed by defining their front velocity, volume and apparent surface temperature. Optical flow computer vision tool and shape analysis were applied in order to extract plume velocity field and shape complexity evolution over time. Shape complexity was assessed using two different methods. The first one estimates the ratio between perimeters of the plume boundary and the smallest box able to contain the plume. The second one determines the Hausdorff fractal dimension based on the box-counting procedure. The ejection of the gas-pyroclasts mixture at the erupting vents has been also characterized, both qualitatively, in terms of number, location, duration, and frequency of individual ejection pulses, and quantitatively, in terms of time-resolved mass eruption rate.

Front velocity displays twofold trends resulting from the initial gas-thrust and later buoyant phases. Plume volume over time follows a power law trend, common to all volcanoes, with coefficients varying with vent discharge history. The velocity field of the plumes highlights different features, including initial jets, ring vortex formation and air entrainment. Shape complexity increase and discontinuities over time reveal the formation of vortexes at different scales and the impact of secondary ejection phases, respectively. Time-resolved mass eruption rates may vary up to two orders of magnitude within a few seconds from the onset of the eruption.

New imaging tools and image processing techniques development allow higher time and space resolution observation of volcanic eruptive events, such as transient plumes. This enables more detailed dynamical characterization and shed light on 1) the crucial impact of discharge history upon the initial and, possibly, later evolution of transient plumes, and 2) source condition information held by their shape evolution.

Meredith Townsend, David Pollard

Submission 819

Re-examining the “level of neutral buoyancy” and its role in dike stability

The “level of neutral buoyancy” (LNB) is thought to govern the depth of magma storage in the crust as well as the geometry, depth, and dynamics of lateral dike injection from shallow reservoirs. The standard conception of the LNB is a horizon at which the large-scale, in-situ density of magma and host rock is equal (Ryan, 1987). For dikes, we can understand vertical stability and the role of neutral buoyancy by applying principles of fracture mechanics. Dikes will vertically arrest when the stress intensity at the upper and lower tips is between zero and the host-rock fracture toughness ($0 < K_{Ic} < 100 \text{ MPa}\sqrt{\text{m}}$). If the magma density is greater than the host-rock density near the top of a dike, but less than the host-rock density near the bottom, vertical gradients in pressure will act to trap the dike even if the host rock is very weak ($K_{Ic} = 0$). However, the level at which dikes become trapped by this mechanism is extremely sensitive to the density structure of the host rock. Models for crustal density as determined by seismic surveys typically are expressed as discrete layers representing lithologic and/or rheologic boundaries (e.g. Zucca et al., 1982); in other models, density is a continuous function of depth, perhaps resulting from compaction of pore space with increasing pressure (e.g. Head and Wilson, 1992). The depths and geometries of stable dike configurations are dramatically different for these two models. In addition, the vertical stability of dikes is very sensitive to dike height, magma overpressure, and host-rock strength. Here we review how the LNB has been employed in various models for dikes, and we use a new analytical model to explore how this level compares with the depths at which dikes are predicted to be stable when taking into account the effects of dike height and the density structure of the host rock. This analysis has implications for the depths at which magma is stored, and the lateral propagation pathways of dikes, which in turn affects the architecture and evolution of shallow magmatic plumbing systems.

Samantha Tramontano, Marc-Antoine Longpré, Eveling Espinoza, Armando Saballos

Submission 946

The timing and longevity of a mafic magma recharge event prior to the 2015-2016 eruption at Momotombo volcano, Nicaragua

Understanding the nature and timescales of triggering mechanisms of volcanic eruptions, particularly for systems that reactivate after a long period of quiescence, is paramount for improved hazard assessment. Post hoc petrologic reconstructions of eruption products allow for backtracking of the temporal evolution of magma bodies leading up to eruption. These reconstructions may be compared to monitoring data to better link magmatic processes (occurring at depth) to geophysical and geochemical signals observed at the surface. Here, we focus on the most recent eruption of Momotombo volcano, Nicaragua, which began on December 1, 2015, after a repose period of 110 years and lasted four months, with the aim of constraining pre-eruptive magmatic processes, their timescales, and potential relationships with detected pre-eruptive seismicity [1]. To develop our petrologic reconstruction, we collect major and trace element abundances in core-to-rim traverses in mineral grains using an electron microprobe. Olivine crystals from the primary trachy-basaltic ash falls (with assemblage plagioclase-olivine-orthopyroxene-clinopyroxene) display polyhedral to skeletal morphologies and are predominantly reversely zoned (87% of analyzed olivines), averaging Fo80.9 in the cores to Fo82.4+ in the rims. Normally zoned crystals, averaging Fo81.5 in the cores and Fo80.6 in the rims, are also occasionally observed (13% of analyzed olivines). In detail, reversely zoned rims (20–100 μm wide), with or without plateau, are complex, and there is typically a change to normal zoning at the outermost 10–40 μm of the rims. In addition, zoning in Fe-Mg is accompanied by variations in Ni, Ca, and P at different length scales. The observed textures and chemically zoned rims imply rapid olivine crystallization from a more primitive (or more oxidized) melt at a late-stage prior to eruption, which we tentatively attribute to a mafic magma recharge event triggering the eruption. Seismic data are consistent with the reactivation of Momotombo on timescales of weeks to years in the lead-up to the December 2015 eruption [1]. By modeling the diffusion of elements across the reversely zoned boundaries within olivines, we estimate the timing and longevity of the postulated mafic recharge event prior to the 2015 Momotombo eruption, potentially allowing for a link between seismic precursors and eruption triggers.

[1] La Femina et al. (2016), AGU Abstract.

Elizabeth Trejo-Gomez, Francisco Javier Nuñez-Cornu, CARLOS SUAREZ-PLASCENCIA, DIANA NUÑEZ, JUANA MARTINEZ-ALVAREZ, JUAN MANUEL SANDOVAL-HERNANDEZ, ADAN GOMEZ-HERNANDEZ

Submission 422

Vulnerability estimation at Ceboruco Volcano, Nayarit, Mexico.

The Ceboruco Volcano is located in Nayarit State, Mexico, at 21.125° N and 104.508° W, has been characterized in the past by episodes of effusive-explosive eruptions. The most recent eruption of the Ceboruco Volcano was in 1870, and current activity is evidenced by seismicity and various fumaroles. Nelson (1986) identifies eight eruptions in the last 1000 years which correspond to one eruption on average every 125 years, and suggests that new eruptions are very likely.

Ceboruco eruptions presents different phases as strombolian and plinian. The composition of lava shows different rocks types: dacite, ryodacite, andesite and basalt. The most important eruptions of Ceboruco occurred between years AD 990-1020, and other sites with evidence of activity prior to these eruptions (Gardner JE, Tait S., 2000).

We estimate vulnerability at the Ceboruco Volcano region, for hazards such as ash fall, flows (lava and pyroclastic), based on the study of Suárez-Plascencia (1998). The hypothesis of this work is that the volcano continues active implying potential hazards to related to adjacent communities, the economic activities developed on its slopes, the roads and vital lines communications.

The vulnerability in the affected area due to these has been estimated using the criteria of CENAPRED (2011) and CEPAL (2003), with available information and generated by INEGI (Census, 2010) and the Directorio Estadístico Nacional de Unidades Económicas (DENUE, 2016). We calculated a projection of population growth, population density, economically active population for year 2015, type of dwelling and the economic activity sites for 2016. Finally, all these vulnerability data were integrated into GIS for maps.

Marine Tridon

Submission 743

Inversion of Coeval Shear and Normal Stress of Piton de la Fournaise Flank Displacement

The April 2007 eruption of Piton de la Fournaise was the biggest volcano eruptive crisis of the 20th and 21st centuries. InSAR captured a large (1.4 m) co-eruptive seaward slip of the volcano's eastern flank, which continued for more than a year at a decreasing rate after the end of the eruption. Co-eruptive uplift and post-eruptive subsidence were also observed. While it is generally agreed that volcano flank displacement might be induced by fault slip, we investigate whether this flank displacement might have been induced by a sheared sill, as suggested by observations of sheared sills at Piton des Neiges. To test this hypothesis, we develop a new method to invert a quadrangular curved source submitted to co-eruptive pressure and shear stress changes. This method, based on boundary elements, is applied to co-eruptive and post-eruptive InSAR data. Post-eruptive displacement is well explained by slip and closure of a large fracture subparallel to the topography (5 km by 8 km), and probably coincident with a lithological discontinuity. The amount of closure is too large and the closure time too short to be explained by a thermally compacting sill, allowing to rule out the sill hypothesis. Co-eruptive displacement can be explained by a smaller (2 km by 2 km) fracture at the same location, submitted to a zero overpressure and a 3 MPa shear stress drop, which confirms that the determined structure is not a sill. We conclude that the fracture is a detachment fold, shallow enough to induce the observed co-eruptive uplift. This finding confirms a previous determination obtained using a decision tree based on ratios of maximum displacements. The determined shear stress change of 3 MPa is consistent with the eastern flank loaded by previously intruded rift dikes.

Barbara Tripoli, Benoit Cordonnier, Daniele Giordano, Peter Ulmer

Submission 586

Hidden magma reservoirs under active volcanoes

Seismic tomography performed under active volcanoes usually reveals low velocity zones interpreted as magma chambers feeding volcanic eruptions. However, some volcanoes, such as Teide in Tenerife, Canary Islands, lack evidences of a large magmatic reservoir. Measurements of seismic velocities at high pressure and high temperature performed on hydrous silicate melts are of critical importance to the interpretation of seismic tomography images. In order to better constrain the geometrical features of the Teide volcanic system, new laboratory measurements of seismic velocities of natural hydrous phonolite have been performed at pressure from 150 to 300 MPa and temperature from 100 to 550°C. The experimental data recorded in the region characterized by liquid-like behavior have been extrapolated to magmatic temperatures (up to 1100°C) and upscaled to natural frequency (10 Hz). We then combined these data to calculated seismic properties of prominent phenocrysts in two possible compositions of magma chamber under Teide: phonolite and phonotephrite. Our calculations confirm the hypothesis that the magma chamber producing phonolitic liquid may not be visible on seismic tomography depending on mineral assemblage, temperature, crystal content and water concentration dissolved in the melt. Indeed, the seismic velocities of a cold, aphyric or partially crystallized, magma chamber, are indistinguishable from the seismic velocities of a hot magma chamber with a phonotephritic composition that contains a crystal fraction in excess of 0.45.

Juliana Troch, Ben Ellis, Chris Harris, Peter Ulmer, Olivier Bachmann, Anne-Sophie Bouvier, Lukas Baumgartner

Submission 790

The role of melting during the generation of low- $\delta^{18}\text{O}$ rhyolites in the Yellowstone province

In the Yellowstone volcanic field, low- $\delta^{18}\text{O}$ rhyolite lavas (+0.1 to +5.8‰) are interpreted to be the consequence of bulk melting of previously deposited and hydrothermally altered volcanics in the down-dropping roof following caldera collapse. In the absence of compositional and experimental data, the “self-cannibalisation bulk melting”-theory relies on the assumption that hydrothermally altered materials are near-cotectic and hydrous (>3 wt% H₂O) and will therefore rapidly melt at temperatures

We examined hydrothermally altered rhyolite from three USGS drillcores from Yellowstone as well as hydrothermally altered granitoid and rhyolite from the Idaho batholith and Challis volcanic field, in order to characterise possible hydrothermally altered source materials in terms of mineralogy, major and trace elements, oxygen isotopes and water contents. Additionally, we performed melting experiments at conditions of 850-1000°C and 1 kbar in externally heated HCM cold-seal vessels on two of these altered, low- $\delta^{18}\text{O}$ rhyolitic and granitoid starting materials.

Our results indicate that bulk $\delta^{18}\text{O}$ values of surface samples do not necessarily represent the variation in altered rhyolite at depth, which can vary from “normal” (+5.8 to 6.1‰) to as low as -5‰ at depths of 100 to 160 m. Alteration is independent of bulk composition and water content. With >75% of the altered samples having 2O, water is the main limiting factor during remelting and assimilation of these materials.

Modelled melting curves via rhyolite-MELTS suggest that at 850°C, an average of 35% melt could be created and that bulk melting would require temperatures >1100°C. These findings are consistent with the observed melt fractions from the experiments. Preliminary $\delta^{18}\text{O}$ values from experimental glasses suggests that they mostly inherit the bulk oxygen isotope composition from the starting material, even when individual mineral phases show stark isotopic contrast (e.g. quartz at +7.6‰ and k-feldspar at -7.1‰ on mineral separates).

Our findings indicate that bulk melting without an external water source would require unrealistically high temperatures and that low- $\delta^{18}\text{O}$ rhyolite lavas are more likely the result of mixing between a low- $\delta^{18}\text{O}$ crustal partial melt and a normal- $\delta^{18}\text{O}$ fractionation-derived melt component from the main reservoir, as supported by isotopic mass-balance models and thermal and volumetric constraints.

Matteo Trolese, Matteo Cerminara, Tomaso Esposti Ongaro, Guido Giordano

Submission 235

Controls of column collapse regime on initial temperature of pyroclastic density currents

According to emplacement temperatures of ignimbrites reported in literature, pyroclastic density currents (PDCs) may travel for several tens of kilometers far from the vent without significant heat loss of the pyroclasts, even more where they are topographically controlled. At the same time, there are several cases where the temperature of PDCs deposits even in proximal regions is significantly lower than the eruptive magmatic temperature, whereas other deposits are extensively welded and maintain very high temperature even in distal localities. This brings up questions about the controlling factors that may affect the thermal state of PDCs at their formation – i.e. if and how different eruption styles may affect the initial temperature of PDCs. To address this question, here we simulated variable collapse regimes of volcanic columns using a compressible three-dimensional multiphase equilibrium-Eulerian model. For our parametric study, we considered three constant mass discharge rates at source corresponding to typical estimates for sub-plinian (107 kg/s), plinian (108 kg/s) and ultra-plinian (1.5×10^9 kg/s) eruptions, adopting equal amount of particles of two different sizes (i.e. 1.5 and 50 μm). We then varied a set of independent mixture variables at the conduit exit, such as gas pressure and total water content, and computed analytically the flow conditions after decompression above the vent by assuming an adiabatic and nearly isothermal transformation of a choked-flow. Our results show that the initial temperature of PDCs is strongly correlated with the amount of mass involved into the collapse. This is due to the effect of air entrainment eroding thermally the jet phase, inducing up to 40% of temperature decrease respect to initial magmatic temperature. Smaller erosions are associated with larger proportion of collapse, whereas lower values are not observed, suggesting that larger thermal erosions result in buoyant columns.

Jen Truby, Ed Llewellyn, Jacopo Taddeucci, Mike Dungan

Submission 631

Mobilizing a magma mush through bubble growth – rheological triggering of the largest eruptions

Magma crystallizes as it cools and degasses. Once its crystal content exceeds a critical value, the crystals jam against one another, forming an immobile magma mush. Counterintuitively, many of the largest explosive volcanic eruptions involve magma that has a crystal content above the critical jamming value. How is such a mush mobilized? We propose that the pervasive formation and growth of bubbles of magmatic gas pushes the crystals apart, unjamming the mush. We test our model using analogue suspensions, and demonstrate that the growth of bubbles alone is sufficient to mobilize an initially jammed particle suspension. Processes that have previously been proposed for mush mobilization include underplating by a recharge magma, decompression related to tectonic stresses, and seismic shaking, all of which may trigger bubble nucleation; consequently, our model provides a fundamental mechanism that reconciles previous models. Our model also allows us to identify conditions under which mobilization by bubble growth does not occur, in which case pluton formation will be favoured over eruption.

Kaori Tsukamoto, Koki Aizawa, Wataru Kanda, Makoto Uyeshima, Kaori Seki, Takahiro Kishita, Mitsuru Utsugi, Takao Koyama

Submission 758

Shallow resistivity structure and its relation to hypocenters and deformation sources: Iwo-yama Volcano, Kirishima Volcanic Complex, Japan

Phreatic eruptions are thought to occur when groundwater is heated and boiled by a heat source; however, recent studies of resistivity structure suggest that explosive phreatic eruptions also occur under other conditions. Previous magnetotelluric surveys have detected a shallow electrically conductive layer beneath volcanoes, interpreted as a hydrothermally altered clay cap layer (e.g., Nurhasan et al., 2006; Aizawa et al., 2008, 2009; Kanda et al., 2008; Yamaya et al., 2013). It has been proposed that phreatic eruptions occur when the accumulated pressure beneath this clay cap layer is relieved by some form of trigger. Therefore, imaging the shape, size, and location of the clay cap layer may be the key to assessing the potential for a phreatic eruption to occur.

Iwo-yama is an active volcano in the Kirishima Volcanic Complex, located on Southern Kyushu Island, Japan. Around Iwo-yama, shallow (<2 km) tectonic earthquakes have increased since December 2013, and volcanic tremors have occasionally occurred since July 2015 (Japan Meteorological Agency, 2015). Furthermore, fumarolic gases were detected in December 2015 for the first time in 12 years. A leveling survey detected ground uplift during June to December 2015, and the pressure source was estimated to be at a depth of 700 m, 150 m east of the crater (Matsushima et al., 2015). This evidence indicates the increasing likelihood of a phreatic eruption.

To investigate the underlying mechanism of these volcanic activities and the potential for future eruptions, we acquired broadband (0.005–3000 s) magnetotelluric (MT) measurements around Iwo-yama in April 2016. We recorded two components of the electric field at 20 observation sites, and five components of the electric and magnetic fields at 7 observation sites. Inversion of the MT data revealed that the shallow earthquakes occur beneath an electrically conductive layer, interpreted as a hydrothermally altered clay-dominated unit. The pressure source identified by the leveling survey corresponds to the base of this electrically conductive layer. This spatial relationship suggests that the supply of high-temperature fluids has increased beneath Iwo-yama, causing an increase in pore pressure beneath the clay layer, and resulting in an increase in tectonic activity and ground inflation. In this presentation, we will further examine the precise locations of these earthquakes and investigate the relationship of such events to the shallow conductive layer.

Kae Tsunematsu, Rebecca Fitzgerald, Ben Kennedy, Christopher Gomez, Jean-Luc Falcone, Bastien Chopard

Submission 29

Open Source 3D Multiparticle Ballistic Simulator "Ballista"

Ballistic projectiles are emitted from the vent of the volcano when an explosive eruption occurs. Their sizes range from a few centimeters to several meters, and the landing velocity of these pyroclasts can exceed 100 km/h. Therefore, for hazards and disaster risk management, it is essential to estimate the affected area of ballistic projectiles. To reach this goal the ballistic trajectory simulator "Ballista" was developed. This model can calculate the trajectory and deposition condition of multiple ballistic particles in three dimensions using a momentum equation including air friction and an equation to simulate the particle transport. The momentum equation which is a second-order differential equation is solved with the Runge-Kutta method, and particle transport is simulated using the Lagrangian method. It was programmed using Java to increase portability and to easily include topographic effect.

In this presentation, we show how the estimation of ejection conditions varies when we include the topography at the Tongariro Upper TeMaari crater, the Ontake Jigokudani crater, and the Auckland Volcanic Field. When the crater is inside a valley for example the Ontake Jigokudani crater, the natural wall prevents particles from exiting the valley. On the other hand, if particles are ejected from the crater on the slope of the mountain, for example the Upper TeMaari crater, the travel distance of particles become greater and the block landing area become larger. In cases of flat topography, for example the Auckland Volcanic Field, simulated distances do not significantly vary. Therefore, it is essential to include the topography when the crater is located in a valley or on the slope of an interfluvium. The ejection angle is also a very important factor constraining which areas ballistic particles are deposited in.

We demonstrate how to run the model using the graphical user interface (GUI), present how to plot the distribution of simulated particles in GIS, and how to draw the trajectories using Matlab. The source code and a distribution version of this software "Ballista" are planned to be available online soon.

Tomoki Tsutsui, Masato Iguchi, Takeshi Tameguri, Haruhisa Nakamichi

Submission 209

Evolving seismic reflectors and magma supply system in Sakurajima Volcano and Aira Caldera, Japan

Evolving seismic reflectors beneath Sakurajima Volcano and Aira Caldera from 2008 through 2016 will be presented, which are detected through seismic experiments, and magma supply system of Sakurajima Volcano will be discussed.

Sakurajima Volcano is one of the most active volcanoes in Japan. Sakurajima stands in the southern margin of Aira Caldera in south Kyushu (Aramaki, 1984). A flank crater, Showa Crater, resumed in June 2006 after decreasing Vulcanian activity at the summit crater of Minamidake. After then, four major intrusion events, Events 2009 (from 2009 through 2010), 2011 (from 2011 through 2012), 2015A (early 2015), and 2015B (15 August 2015), were observed. Vulcanian activity at Showa Crater has decreased down after the latest event, 2015B, to the present.

Two series of controlled source seismic experiments have been carried out since 2008 for probing Sakurajima Volcano and Aira Caldera.

The first seismic series across Aira caldera was carried out for investigating caldera structure in 2008 and 2013. Two significant later arrivals are observed for the shot point in northwest of Aira Caldera as followings;

- 1) a clear PP reflection in 6.3 to 7.2 seconds after the shot time appears in southern Sakurajima through Osumi Peninsular,
- 2) another clear PS converted reflection in 7.9 to 8.8 seconds after the shot time appears in northern shore of Sakurajima.

Both the reflections originate in coincident location and were explained with an interface at 11 km depth in the center of Aira Caldera where pressure source region by Mogi (1958) locates.

The second seismic series was carried out since 2009 for investigating structural evolution beneath the volcano. The seismic rounds until 2014 revealed an evolving reflector Alpha in the depth of 5.8 km below sea level (Tsutsui et al., 2016). The reflectivity variation at Alpha can be explained by change in magma property at the depth during the series (Tsutsui et al., 2016).

Following three clear later arrivals are found in cross-line shooting seismograms;

- 3) a PS converted reflection from 5.8 km below sea level,
- 4) a PP reflection from 4.7 km below sea level,
- 5) another PP reflection from 2.4 km below sea level.

All of their origin are modeled at 2 km south of reflector Alpha, and locate in known pressure source beneath northeast flank of Sakurajima Volcano (Iguchi et al. 2013). It should be noted that three later arrivals show temporal changes in its intensity. The seismic experiments reveals magma movement successfully.

Hugh Tuffen, Ellen McGowan, Mike James

Submission 958

Rhyolitic dyke evolution from pyroclastic pathways to dense magmatic plugs

Rhyolitic dykes deliver magma towards the surface in some of the largest volcanic eruptions on Earth, yet surprisingly little is known about their formation and evolution prior to and during magma transport. Dissected Icelandic central volcanoes provide a rich source of information on the architecture of magmatic plumbing systems, and we use detailed characterisation of Tertiary and Quaternary dykes at Husafell and Torfajökull to reconstruct their evolution.

At a depth of hundreds of metres at Husafell, propagating dykes initially advanced via the intrusive injection of vanguard pyroclastic material into fracture networks within damaged country rock. The local mechanical properties of the country rock strongly influenced this phase. Coalescence of fractures and erosion of country rock then created broader pathways for magmatic ascent, which were later narrowed and smoothed by progressive aggregation of welded pyroclasts onto dyke walls. Incorporation of lithics into this aggregating material preserved permeability in otherwise densely compacting, melt-rich magma. Dyke centres were finally filled by late-stage magma that failed to fragment and became the locus of crystallisation and magmatic fluid circulation.

By contrast, at shallower depths of only tens of metres at Torfajökull, late-stage magmatic processes involved transient fracturing and brecciation events in welding and compacting foams, which decoupled gas from magma and potentially fed hybrid explosive-effusive activity. Low dissolved water concentrations indicate efficient gas removal to sub-lithostatic pressure. The striking parallels between processes recorded in Torfajökull dykes and those occurring in recent Chilean eruptions allow bridging of the gap between surface observations and the subsurface geological record.

Evidence from such fossil systems includes structure and texture over a broad range of spatial scales, together with petrology and geochemistry. It provides key perspective on the magma movement that can only currently be tracked from the surface, insights into the origin of geophysical signals such as microseismicity, and parameter constraints for improved models of silicic magma ascent within dykes.

Andrew Tupper

Submission 972

Getting real – making the International Airways Volcano Watch work for everybody

The International Airways Volcano Watch (IAVW), administered by the International Civil Aviation Organisation (ICAO) on behalf of all signatories to the Chicago Convention, requires countries with active volcanoes to monitor them for aviation purposes, and defines an international system of advice, warnings, and response from officials and airlines. Procedures around the warning system have been greatly strengthened since the 2010 Eyjafjallajökull and 2011 Cordon Caulle eruptions respectively affected the Northern and Southern Hemispheres. International and national volcanic ash exercises have significantly improved procedures and understandings, including in Europe and Southeast Asia. Rapidly evolving communication technologies, including internet messaging platforms, have been used in innovative ways to overtake more ‘traditional’ operational communication and to provide solutions appropriate to operational conditions, in some cases racing ahead of ICT policy processes and demonstrating the difficulty of converging on any one global communication solution.

Despite this, the consistency of IAVW coverage remains starkly uneven, with large deficiencies in basic volcanic monitoring and the functionality of communications and warning mechanisms. If anything, local capability gaps between neighbours may be increasing, potentially confounding aviation industry expectations of globally improving service, and the potential to link the IAVW strongly to local warning arrangements for non-aviation services. Much of the world remains in non-compliance of ICAO requirements, with some areas of particular concern, and despite the potential for cost-recovery from the aviation industry to assist in improving the situation. The challenge, therefore, is to learn from recent improvements and apply new best practice processes universally, including for civil defence, to raise the overall level of preparedness for volcanic crisis. The discussion will show examples from Indonesia and Papua New Guinea.

Nicolas Turner, Bruce Houghton, Ryan Perroy, Jacopo Taddeucci, Marina Bisson

Submission 711

Volcanic hazard monitoring with a small unmanned aerial system: structure-from-motion based studies of lava flows and explosive volcanism

Rapid advances in low-cost robotics and powerful computer vision based techniques are greatly improving our ability to monitor and assess volcanic hazards during ongoing eruptions. Two recent case studies are presented, the 2014-2015 Pāhoā lava flow crisis on Kīlauea, Hawai'i and a 2016 mapping campaign at Stromboli, Italy. Stromboli and Kīlauea are the most continuously active volcanoes on earth and provide two important end-member datasets for Hawaiian/effusive and Strombolian eruptions. During the Pāhoā crisis an active pāhoehoe lava flow was repeatedly mapped with a small unmanned aerial system (sUAS) to produce a time-series of high spatial resolution (6 cm) orthomosaics and associated digital point clouds using structure-from-motion (SfM) software. Survey-grade positional control was provided by ground control points with differential GPS. The forest environment surrounding the flow proved challenging to completely filter of vegetation. However, a series of lidar processing algorithms from LAStools were used on the dense point cloud data and a 1 m bare-earth digital elevation model (DEM) was extracted that better reflected microtopography. The resulting DEMs show an increased number of detected 'paths of steepest descent' over a conventional 10 m DEM. The sUAS-derived DEM also captured dynamic changes caused by the inflated pāhoehoe flow, which will significantly redirect the paths of future flows in the Pāhoā area. SfM-based measurements of an active pāhoehoe flow enhances both short-term and long-term hazard assessments.

At Stromboli volcano sUAS were used to map the crater terrace and provide detailed measurements of vent geometry and depth, which are otherwise difficult to constrain due to emission of gas and large ejecta creating a hazardous environment to human life. The survey required multiple repeat flights with the sUAS to acquire enough imagery to construct a high resolution 10 cm DEM of the active NE and SW craters using SfM. The 2016 SfM-based DEM was then compared to 2012 and 2005 lidar surveys of the crater terrace. Utilizing both SfM and lidar datasets has allowed us to measure the evolution of vent location and crater morphology over a decade, a period which included two paroxysms that significantly altered the morphology of the crater terrace. SfM techniques and low-cost sUAS technology are effective in filling critical gaps in real-time monitoring and greatly improve our ability to assess volcanic hazards during ongoing eruptions.

Victoria Tweedie, John Stix

Submission 434

Calibration of non-radiometric FLIR Vue Pro thermal camera for use on a UAV

UAVs provide exciting opportunities to collect high-resolution thermal data to monitor volcanic activities, such as dome growth and collapse, which are hazardous or otherwise inaccessible. The FLIR Vue Pro camera is a lightweight (113.4g) thermal infrared camera suitable for use on drones. The camera measures the emission of long wave infrared radiation (LWIR) of objects. Using Automatic Gain Control (AGC) the camera displays thermal information in shades of grey. The FLIR Vue Pro is a non-radiometric thermal camera and is not intended to measure exact temperature measurements. However, we attempted to calibrate the camera in the lab and field. Laboratory-controlled experiments were conducted to establish the relationship between actual and FLIR-measured temperatures of a blackbody at two different distances of 26 cm and 153 cm. Temperatures were measured approximately every 5 degrees Celsius from 0 to 150 degrees Celsius. Actual temperature measurements were made using a temperature monitor connected to the blackbody, whereas FLIR-temperature measurements were collected as JPG images saved to a micro-SD card using a Bluetooth tablet. Collected images were loaded into FLIR Tools+. Measurements were made on each image at approximately 3 cm from all four corners. Corner measurements were averaged to determine a FLIR-measured temperature for each image. FLIR-measured temperatures were compared to actual temperatures to establish a predictive relationship. No significant difference was observed between measurements at different distances. The relationship between actual temperature and FLIR-temperature measurements is best fit by a second order polynomial. Further temperature experiments will be conducted outside at different elevations by securing the FLIR Vue Pro to the body of a Turbo Ace Matrix-i UAV with adhesive tape and zip ties. These results provide promise that the FLIR Vue Pro camera can be used onboard a UAV for temperature monitoring and mapping purposes.

Teresa Ubide, Balz S. Kamber

Submission 616

Clinopyroxene trace element zoning records eruption triggers at Mount Etna, Sicily

Mt. Etna is one of the most active volcanoes on Earth and has experienced enhanced eruptive activity since the 1970s. This has been attributed to the arrival of a primitive, volatile-rich, more alkaline magma in its feeding system^{1,2}. The volcano typically produces porphyritic basalts with varying fractions of mm-sized plagioclase, olivine and clinopyroxene crystals all showing growth zoning in response to polybaric crystallisation of hydrous magma^{3,4,5}. Clinopyroxene is studied here to explore its potential to record magma history as it crystallises from deep (>27 km) to shallow depths⁵, and because chemical diffusion is relatively slow⁶, potentially preserving protracted processes. We apply high-resolution laser ablation ICP-MS mapping⁷ to clinopyroxene crystals from lavas spanning 40 years of eruptive activity (1974-2014). Compositional zoning reflects pronounced, punctuated episodes of invasion of primitive magma into resident crystal-melt mushes, recorded as zones enriched in chromium and other transition metals. Statistical analysis of the zoning in 287 crystals shows that magma was not effectively stirred. Instead, fresh injections appear to have triggered mobilisation and volcanic eruption very rapidly. Considering clinopyroxene growth rates⁵, the time elapsed between recharge and eruption may be as short as ca. 2 weeks, in agreement with previous minimum estimates from diffusion chronometry in olivine⁴. We observe an increase in the occurrence of chromium-rich crystal zones with time as magma invasion migrated from the eccentric, deep-dyke-fed plumbing system into the main central conduits. This supports the theory that Mt. Etna is more likely to remain highly active rather than reverting to its previous relative quiescence. We propose that detailed analysis of clinopyroxene zoning provides new insights into deep, complex magma histories and may constitute a novel tool to estimate eruption-triggering mechanisms in basaltic to intermediate volcanic systems.

1. Condomines et al. (1995), *Earth Planet Sci Lett*. 2. Corsaro et al. (2009), *JGR: Solid Earth*. 3. Giacomoni et al. (2014), *Earth Sci Rev*. 4. Kahl et al. (2015), *J Petrol*. 5. Armienti et al. (2013), *J Petrol*. 6. Costa & Morgan (2011), *Timescales of Magmatic Processes: From Core to Atmosphere*. 7. Ubide et al. (2015), *Chem Geol*.

Hideki Ueda, Masashi Nagai, Toshikazu Tanada

Submission 270

Research for eruption forecast of volcanic eruption in Iwojima volcano, Japan

Iwojima Island is an active caldera volcano located about 1,200 km to the south of Tokyo, Japan. We are monitoring by seismometers and GPS to develop a technique to forecast eruption in the island. Phreatic eruptions sometimes occur in the vicinity of the coast such as 2001 and 2012, and very small eruptions frequently occur at geothermal areas. This technique will contribute to securing the safety of residents.

About 50 years of observation by NIED shows that volcanic activity of Iwojima can be classified into three phases. In phase 1, subsidence and contraction at the central part of the caldera dominate, and activities of earthquakes and phreatic eruption are weak. In phase 2, a large uplift of the island dominates. Earthquake occurrence rate increases in proportion to the uplift rate. Very small phreatic eruptions are also seen in this phase. In Phase 3, small phreatic eruption takes place after a rapid uplift and severe earthquake activity, and a subsidence is observed after the phreatic eruption. In the end of April 2012, we observed 10 cm uplift and more than 400 earthquakes in one day. The rapid uplift and subsidence during phase 3 can be explained by inflation and deflation of a shallow sill-like source about 1 km beneath the center of the caldera. The results of the geological survey show that the central part of the caldera is mostly filled with alternating layers of lava flow and tuff (Nagai and Kobayashi, 2015), suggesting that the hot water in the tuff sandwiched between the lava flows suddenly expands causing the phreatic eruption. These results show that continuous monitoring of seismic activity and crustal deformation is effective for forecasting phreatic eruption in Iwojima.

The existence of the tuff and the lava flow in Iwojima shows that a devastating magmatic eruption has occurred. The geological survey shows that a massive eruption occurred in the caldera about 2700 years ago and then magma eruptions occurred at the southwest of the island several times afterwards. However, magmatic eruptions have not been observed since people started living. To make this prediction, other caldera volcano activities will be helpful. International data sharing efforts such as the WOVOdat database should contribute. In Japan, we are also developing a data sharing system in Japan through the project from 2016. We would like to develop a comprehensive forecasting technology including magmatic eruption of Iwojima through international data sharing.

Shimpei Uesawa, Mitsuhiro Nakagawa, Akane Umetsu

Submission 215

Eruptive history, structure and magmatic change at Yotei Volcano, southwest Hokkaido, Japan

It is difficult to perform geochronological study especially on a young cone shape stratovolcano such as Yotei Volcano. To understand whole eruptive history, structure and magmatic evolution of Yotei Volcano, we carried out chronological study of the volcano with correlation between tephra units distributed in its base and the volcanic edifice using petrological characteristics. Based on the stratigraphic relations and petrological characteristics, Yotei volcanic edifice can be distinguished into three groups: Yotei volcanic edifice I to III in ascending order (YE-I- to III). Whole-rock compositions show progressively higher in incompatible elements (Na_2O , P_2O_5 , Zr and Y) from YE-I to YE-III. Based on the characteristics of whole-rock compositions, these three groups are correlated to Yotei tephra group I, Yotei tephra group II-2, and Yotei tephra group II-3 in ascending order, respectively. However, Yotei tephra group II-1 is not correlated to any volcanic edifice group because the volcanic edifice, which could be correlated to tephra group II-1, might be totally buried by subsequent ejecta. As a result, Yotei volcano can be divided into two stages: Stage I Stage II separated by long dormancy (~8,000). Moreover, Stage II Yotei Volcano consists of three stages separated by dormancy (for 2,000–5000 years) namely II-1, 2 and 3. Based on the chronology and calculation of eruptive products volumes, it is revealed that eruption rates of Stage I (lasted from ca.50 to ca. 46 cal. ka BP), Stage II-1 and 2 (lasted from ca. 37.9 to ca. 21.2 cal. ka BP) were high (1.9–3.6 km^3/ky DRE and 0.3–1 km^3/ky DRE), whereas that of Stage II-3 (lasted from ca. 16.6 to ca. 2–3 cal. ka BP) was low (0.04 km^3/ky DRE). Thus, changes in eruption rate of the volcano have occurred associated with changes in magma types. These relationships imply that magmas beneath the volcano controls the growth process of the stratovolcano.

Ingrid Ukstins, Shangguan Shimai, Wei Tian

Submission 601

Volcanic stratigraphy and near-vent deposits of the Tarim flood basalts, NW China.

The early Permian Tarim flood volcanics (NW China) are composed of a bimodal suite of effusive and explosive mafic and silicic eruptive units, plus associated dikes, sills and intrusions of ultramafic to granitic composition, ranging in age from ~358 to 205 Ma. While the bulk of the province (>99 %) underlies the Takelamakan Desert, the main outcrop in Keping exposes ~100 km of laterally continuous mafic lavas and volcanoclastic deposits, with intercalated silicic pyroclastic units. The lower Kupukuziman Fm (KP) is composed of 2 basalts, mafic volcanoclastic deposits, silicic airfall tuffs and ignimbrite. The upper Kaipazileike Fm (KZ) is laterally variable, with up to 12 mafic lavas separated by 15-30 m thick qtz- and fsp-rich sandstones. Major and trace element data show a range of compositions from 41.6 to 49.4 wt % SiO₂. KP basalts are distinguished from KZ by their higher Nb/Zr and Th/La ratios. Six distinct groups can be recognized and traced laterally, two in KP and four in KZ. Two KP lava groups have different TiO₂ (~3.2% vs. ~3.9%) and incompatible elements (e.g. Nb: 25 ppm vs. 30 ppm, Ta: 1.5 ppm vs. 1.8 ppm). KZ lavas can be divided into four groups based on Mg# (~30 to ~43), Lu/Hf ratio (0.079 to 0.086), and incompatible elements (e.g. Zr: ~450 to ~250 ppm, Nb: ~42 to ~25 ppm, Sm/Yb: ~2.8 to ~2.3). A megacrystic plagioclase lava in the KZ section has been used as a correlation marker, but compositional data suggests it may not be the same lava. Between the KP and KZ Fms is an 800 m thick sequence of siltstone and sandstone informally referred to as the FP Fm. Depositional textures and localized coal beds suggest sediments are deltaic to fluvial. Lavas are ropy to rubbly inflated pahoehoe flows (3 to 70 m), forming localized intense peperite deposits along basal layers emplaced onto sand. Mafic volcanoclastic deposits are abundant in the KP. They consist of bedded, sorted fine-grained ash in the east, transition to massive, fine-grained, and bomb-bearing (bombs 5-15 cm), and massive accretionary lapilli bearing tuffs with bombs (bombs 20-40 cm) intercalated with thin and fine-grained, finely laminated tephra in the west. Deposit morphology and variability suggest concentrated and dilute pyroclastic density currents and ballistic fallout originated from vent sites near the western-most Tarim outcrops; we postulate this was a vent area for the lower KP Fm. Upper KZ lavas appear to originate distally.

Carl Ulberg, Kenneth Creager, Seth Bachmann, Geoffrey Abers, Kayla Crosbie, Robert Crosson, Roger Denlinger, Weston Thelen, Steven Hansen, Brandon Schmandt, Eric Kiser, Alan Levander, Olivier Bachmann

Submission 1127

Local Earthquake Tomography at Mount St. Helens with the iMUSH Broadband Array

We deployed 70 broadband seismometers in the summer of 2014 to image the seismic velocity structure beneath Mount St. Helens (MSH), Washington, as part of the collaborative imaging Magma Under St. Helens (iMUSH) project. The broadband array had a ~100 km diameter centered on MSH with an average station spacing of 10 km, and was active for 2 years through summer 2016, augmented by dozens of permanent stations in the area. We determine P-wave and S-wave arrival times recorded on the broadband array and also incorporate picks from the permanent network. More than 300 local events $>M0.5$ occurred during the deployment, providing over 11,000 P-wave and 4500 S-wave arrival times to date. In addition, we incorporate 23 active shots in 2014 that were part of the active-source component of iMUSH. These were recorded with good signal-to-noise ratios across the entire array. We use the program struct3DP to invert travel times to obtain a 3-D seismic velocity model and relocate hypocenters, with travel times computed using a 3-D eikonal-equation solver. The preliminary 3-D model shows low P- and S-wave velocities along the St. Helens seismic Zone (SHZ), striking NNW-SSE of MSH from near the surface to where we lose resolution at 15–20 km depth. The SHZ coincides with a sharp boundary in Moho reflectivity that has been interpreted as the eastern boundary of a serpentinized mantle wedge (Hansen et al, 2016). We speculate that the SHZ and low wave speeds are related to fluids rising from the eastern boundary of the wedge. Other features in the model include a low-velocity region beneath MSH at depths of 10–20 km, possibly indicating a magma storage zone and another low-velocity region 20 km NE of MSH at depths of 10–20 km. We also find a general trend at mid-crustal depths of high velocities to the west and low velocities to the east consistent with the presence of cold, accreted mafic Siletz terrane to the west and higher temperatures to the east.

Masashi Ushioda, Isoji Miyagi, Toshihiro Suzuki, Eiichi Takahashi

Submission 1298

Pre-eruptive P-T conditions and H₂O concentration of Aso-4 silicic magma based on high pressure experiments

Aso-4 is the largest and recent caldera forming eruption (>600km³) in the Aso volcano, Japan. Determining the physical and chemical conditions (P, T, XH₂O, fO₂) in the magma chamber enables us to constrain trends of crystal differentiation and compare the data with geophysical observations. Kaneko et al.(2007) carried out petrological analyses for Aso-4 products systematically and discussed the conditions of magma chamber. However, pressure of the pre-eruptive conditions, which is an important parameter for the comparison to various observations, for Aso-4 products was not determined by petrological study. In this study, the purpose was determination of pre-eruptive conditions (P, T, XH₂O, fO₂) of Aso-4 silicic magma chamber. Reproduction of phenocryst assemblage and compositions of Aso-4A pumice (KJ5665: Hoshizumi, personal communication), which had the most silicic composition and was considered as the felsic end member, was carried out using high-P and high-T experiments.

KJ5665 pumice had plagioclase, orthopyroxene, magnetite, and ilmenite and trace of hornblende phenocrysts. All frequent distributions of core compositions for these phenocrysts were unimodal. Core compositions of plagioclase and orthopyroxene ranged from An₃₀ and Mg₇₂ to An₅₀ and Mg₇₅, respectively. Temperature and fO₂ were 870~880°C and FMQ+2, respectively, estimated by thermometer and oxygen barometer using equilibrium between magnetite and ilmenite (Lepage 2003; Andersen and Lindsley 1985). Three hydrous glasses (2, 3.5, and 6 wt.% H₂O) were synthesized using the powder of KJ5665 for starting materials. Melting experiments were performed in temperatures between 810 and 930 °C at 200, 400, and 700MPa under NNO-buffered condition using IHPVs (SMC8600 and HARM200 installed at Tokyo Tech and GSJ, AIST, respectively). Plagioclase, orthopyroxene and/or K-feldspar crystallized with small amount of Fe-Ti oxides in the lower H₂O content of run products, while orthopyroxene did not crystallize and biotite crystallized in the higher H₂O content of run products. At 200 MPa and 900 °C and under low H₂O content (~2wt.%) of run products, plagioclase and orthopyroxene which compositions fell within the range of that of phenocrysts crystallized. In the experiments, hornblende which existed rarely as phenocrysts in the KJ5665 pumice did not crystallize. Origin of hornblende phenocrysts need to be carefully considered using various petrological features.

Sri Budhi Utami, Fidel Costa, Christina Widiwijayanti, Hanik Humaida

Submission 765

Petrologic data and timescales of magmatic processes leading up to the 1990 Kelud eruptions and its relation to volcanic unrest

Explosive eruptions at Kelud volcano in Indonesia escalate rapidly, as exemplified in the 1990 and 2014 events where major unrest only occurred hours to days before eruption. This is very different from other volcanoes from subduction zones that produce similar magmas (e.g. Merapi), and thus the plumbing system and processes that lead to eruption are probably different. Here we report the results of a combined petrologic and volcanic unrest study of the 1990 eruption. Pumice from the main Plinian phase of the eruption is porphyritic basaltic andesite, with glomerocrysts and phenocrysts (33 vol.%) set in a glassy, vesicular groundmass (67 vol. %). Phenocryst are plagioclase (Plag) + orthopyroxene (Opx) + clinopyroxene (Cpx) + Fe-Ti oxides (magnetite \pm spinel \pm \ddot{u} lvospinel), with rare apatite. Plag (An₃₉₋₉₁) show concentric oscillatory zoning with up to three distinct inner zones hosting melt inclusions, yet all have normal rim zones; in some crystals inner zones are also irregular and partially resorbed. Calculated magma water contents and temperatures range from 2.5-8.0 wt.% and 950-960°C based on plagioclase-melt hygrometry and geothermometry, respectively. Opx-Cpx geothermobarometry show they crystallized at 930-950°C and 5 - 9 kbars, corresponding to 21-36 km depths below surface. Some Opx (Mg# 52-60) crystals display high Mg/Fe bands close to their outer rims. Modeling the transition zone between high and low Mg/Fe bands using diffusion laws gives a range of timescales between 2-10 days for most of the crystals, with one example of about 30 days. Seismic unrest records leading up to the 1990 eruption shows two distinct seismic swarms occurring 3 months and one month before eruption. The latter could perhaps be recorded in one of our crystals and could reflect magma intrusion into a shallow reservoir. However, as most of the times recorded by the high Mg/Fe bands are only up to 10 days, they likely correspond to magma movement between reservoirs or towards the surface. In this scenario, the high Mg/Fe bands result from oxidation of the system (and preferential uptake of Mg from Fe³⁺ by Opx) due to volatile degassing and magma movement, rather than magma intrusion as is typically proposed in many other studies.

Ivan Utkin

Submission 238

Exploring the features of meshless methods in application to lava flow modeling

To assess the hazards associated with the propagation of lava flows during volcanic eruptions, it is necessary to develop models which allow correct prediction of lava flow path and depth. Mathematical modeling based on CFD becomes more and more popular as computing power increases.

It is known that parameters of the flow are significantly influenced by the presence of the solid crust, which is formed due to the heat exchange of the lava surface with the atmosphere. In traditional mesh-based methods temperature and stress boundary conditions must be specified on an unknown free surface of the flow. In recent years, mesh-free numerical methods, which make it possible to overcome the drawbacks of traditional approaches, are actively developed.

One of the most popular and established meshless methods is SPH (Smoothed Particle Hydrodynamics) was originally developed for astrophysical applications. Since then it has been modified and successfully applied to a wide range of problems. For a lava flow, important factors influencing the choice of numerical methods are high viscosity, low speed of propagation and large characteristic times of order of days to weeks. Therefore, to use SPH it might be necessary to modify existing methods, and develop new techniques allowing accurate reproduction all physical processes of interest.

The aim of this study is to test the capabilities of SPH in application to of lava flows in the presence of a temperature dependent viscosity, to determine the problems the method, possible ways of solution, and a further direction of research. For this purpose, a software was developed that implements several different formulations of the SPH method, and several numerical experiments were performed with values of parameters typical for lava flows. It was shown that the results are in a good agreement with known analytical solutions, and the ability of the method to reproduce the effects observed on real lava flows, for example, breaking the crust when a low-viscosity lava is injected into a region filled with high-viscosity lava.

Sebastien Valade, Maurizio Ripepe, Dario Tedesco, Giovanni Giuffrida, Francesco Pandolfo, Gabriele Erba, Celestin Kasereka Mahinda, Katcho Karume

Submission 1185

Mount Nyiragongo lava lake dynamics inferred from geophysical observations

Nyiragongo volcano (Democratic Republic of the Congo) hosts the largest lava lake on Earth. In late February 2016, a new eruptive vent opened near the active lava lake, marking the onset of an unusual phase of activity. A field campaign was organized in April 2016, during which we deployed an infrasonic array and an infrared thermal camera. The volcanic activity was characterized by two distinct features: (i) the lava lake, confined within a pit crater on the lowest crater terrace, and (ii) the newly created spatter cone, where cyclic Strombolian activity fed a lava flow which cascaded in the lava lake. Insights into the lake dynamics was provided by the analysis of the surface crust motion using optical flow algorithms. The results reveal a complex interplay between regions of upwelling (where the arrival of magma from depth is accommodated by radial spreading of the crust), and regions of downwelling (where persistent bubble bursting creates a depression towards which the surrounding crust is dragged into). Despite the complexity of the system, where multiple convective cells coexist, we show that upwelling is on average positioned in the lake center, and downwelling along the lake margins. Moreover, we observe short timescale fluctuations of both the surface velocities and the lake level, which likely reflect characteristic flow properties. Our observations complement those reported on a number of other lava lakes, and allow us to refine existing conceptual models of active lava lakes.

Gueugneau Valentin, Kelfoun Karim, Druitt Tim

Submission 334

Numerical modelling of the surge-derived pyroclastic flow of 25 June 1997 at Soufriere Hills Volcano, Montserrat.

Deposits from ash-cloud surges associated with dome-collapse block-and-ash flows can, under some conditions, be immediately remobilized to form dense, surge-derived pyroclastic flows (SDPF). SDPFs, such as that generated on 25 June 1997 at Soufrière Hills, Montserrat, are hazardous because they can follow drainages different from those exploited by the block-and-ash flows.

We investigate by numerical modelling the conditions that favor the generation of SDPFs during dome-collapse events. We developed a new version of the numerical model VolcFlow that simulates both components of a block-and-ash flow: the basal avalanche and the overriding ash-cloud surge. In the model, mass transfer into the ash cloud is caused by particle entrainment from the basal avalanche, while particle sedimentation from the ash cloud transfers mass in the opposite sense. The dense pyroclastic flows (block-and-ash flows and SDPFs) are assumed to have a plastic rheology, as suggested by earlier modelling work. If the deposit from the ash-cloud surge is thick enough to exceed the plastic limit, then the ash will remobilize and amalgamate to form a SDPF.

The parameter governing entrainment from the block-and-ash flow to the overriding ash cloud is poorly constrained, and is being measured using laboratory experiments. We generate a dilute mixture of air and particles (analogous to the surge) by passage of air through an agitated bed of hot volcanic particles (analogous to the block and ash flow), and use the system to quantify the mass exchange parameters.

Application of the model to the 25 June 1997 dome collapse at Soufrière Hills successfully reproduces the extent and thickness of deposits formed by the block-and-ash flow, the ash-cloud surge, and the SDPF. The formation of the SDPF is, however, highly dependent on topography. The modelled ash-cloud surge detaches from the block-and-ash flow at a bend in Mosquito Ghaut (a river valley). This allows the surge to sediment over a large area with steep slopes, and the deposit is locally thick enough to remobilize and amalgamate to form the observed 3 km long SDPF in the Dyer's River Valley. The detachment of the ash-cloud surge from the block-and-ash flow, combined with the sedimentation on steep slopes, is the most likely mechanism that led to the formation of a SDPF. Our work aims to generate physically robust models that can be used for hazard forecasting of surge-derived pyroclastic flows.

Gueugneau Valentin, Kelfoun Karim, Roche Olivier, Chupin Laurent

Submission 229

Effects of pore pressure in pyroclastic flows: numerical simulation and experimental validation

Pyroclastic flows are mixtures of volcanic gases and particles that can be very hazardous owing to their fluid-like behavior. One possible mechanism to explain this behavior is the reduction of particles friction due to the internal gas pore pressure.

We present a new version of the numerical model VolcFlow, which was modified to take into account gas pressure advection, gas pressure diffusion, and the effect of gas on the basal and the internal friction angles. Before testing our hypothesis by confronting field data to a numerical model on real topography, we should ensure that the model is able to reproduce the emplacement of laboratory granular flows with interstitial gas pore pressure. We carried out experiments on dam-break gas-particle flows in a horizontal flume. A granular media with an high initial pore pressure was released suddenly, which generated a gas-particle flow that lose pore pressure progressively through pressure diffusion. Flow properties was recorded (such as the velocity, runout, and surface profile variation with time). We show that our new numerical model reproduces accurately the temporal variation of the flow front velocity and of the surface flow profile as well as the final shape of deposit.

Then, the numerical code is applied to pyroclastic flows of Lascar volcano (1993 eruption, Chile). Our model reproduces the runout and the morphological features of the deposits, with lateral levées, a central channel and a lobate front, better than previous rheologies (dry Coulomb and plastic behavior). Our results support the hypothesis of the role of gas pore pressure in pyroclastic flows and explain both the fluid-like behavior of the flows and the formation of lateral levees.

Greg Valentine, Alison Graettinger, James White, Pierre-Simon Ross

Submission 88

Updates to concepts on phreatomagmatic maar-diatremes and their pyroclastic deposits

A grand challenge in volcanology is the need to advance our understanding of the mechanisms and effects of the interaction of magma with externally derived water. Maar-diatremes provide key natural experiments on these problems, as they are the type example of volcanoes that are dominated by explosive phreatomagmatic activity. Recent field research, experiments, and modeling have provided important new insights into the dynamics of maar-diatreme eruptions. These have implications for field observations and significantly modify inferences that have been prevalent in the maar-diatreme literature. In previous models, explosions were often inferred to take place at the base of a diatreme (root zone), with progressive downward growth due to a cone of depression in the host aquifer. However, it is likely that diatremes themselves contain much water that is heterogeneously distributed, and field evidence supports the existence of explosion sites at many vertical and lateral locations (intradiatreme fragmentation zones). Conceptual models have sometimes assumed that diatremes hosted by “soft substrate” (e.g., unconsolidated sediments) would have shallower walls than those hosted by competent rock, but this now appears only to apply to the subaerial crater, not the subsurface structure. Crater sizes have been used to estimate explosion energies, but this can only work for single-explosion craters where the depth of explosion is known. Compounding this is the multi-explosion nature of maar-diatremes. Deep-seated lithic clasts in tephra ring beds have been taken to indicate the depth of the explosion that produced that bed, but modeling and experiments show that only relatively shallow explosions actually vent to the surface. Deep-seated lithics are gradually brought to shallow depths through step-wise mixing of multiple subsurface explosions. Tephra ring deposits are often inferred to be indicators of fragmentation, with finer-grained deposit representing more efficient fragmentation during the explosion that emplaced it. However, there are other factors that strongly influence deposit grain size, including the depth of an explosion with respect to its energy, the interaction of an erupting jet with topography around a vent (e.g., crater), and the fact that much of what is ejected might have been recycled in the vent/diatreme such that grain size partly reflects the cumulative effects of multiple explosions.

Brennan van Alderwerelt

Submission 910

Diverse minor volcanism across the central Andean arc

Fault-controlled monogenetic lavas across the Central Andes at ~23°S illuminate the magmatic diversity of the arc, evidenced by whole-rock, melt inclusion, and mineral compositions. The Altiplano-Puna region is dominated by bimodal, felsic-intermediate volcanism and mafic lavas are notoriously rare as they are impeded by thickened crust (55–65 km) and > 500,000 km³ of mid-crustal magma. As a result, the nature of parental magmas has been poorly constrained. However, small volumes of less-evolved lava have been erupted along zones of crustal weakness and faulting, representing compositions commonly obscured due to crustal assimilation and/or extended storage in sub-volcanic magma chambers. These minor lavas display geochemical evidence for arc magmas generated by decompression and fore-arc subduction erosion and provide important constraints on parental compositions. These minor lavas approximate different end-member compositions from which the range of intermediate main arc volcanism in the Altiplano-Puna is ultimately derived. The location of these geochemically diverse minor eruptions are correlated with intersecting orogen-parallel thrust faults and orogen-oblique transverse lineaments which accommodate regional crustal shortening. Olivine-rich basaltic andesite (54 wt% SiO₂, 7.4 wt% MgO; 87Sr/86Sr = 0.7061) near the arc axis at Cerro Overo maar is a regional mafic end-member and approximates the composition of arc magmas in the partially-molten lower crust (MASH zones). Olivine-hosted melt inclusions from Cerro Overo suggest mobilization of MASH magma by injection(s) of basaltic melt. In the Cordon de Puntas Negras at the eastern margin of the arc, olivine-cpx basaltic andesite (53 wt% SiO₂, 6.7 wt% MgO; 87Sr/86Sr = 0.7059) is another regional endmember, transitional between fluid flux and intraplate magmatism. The Tilocalar Group at the western margin of the arc are aphyric, intermediate (59–63 wt% SiO₂, 2.4–3.6 wt% MgO) lavas with Adakite-like signatures (e.g. high Sr/Y and Sm/Yb) and originate from small melt fractions of metabasaltic material at high P. Evolved isotopic compositions (87Sr/86Sr = 0.7065 – 0.7070) support generation by melting of metabasaltic lower crust, potentially related to forearc subduction erosion or foundering of the lithospheric root, and not by direct melting of the subducted slab. The nature and origin of magmas generated in the central Andes is clearly more complex than large-volume ignimbrites and stratovolcanoes has revealed thus far.

Alexa Van Eaton, David Schneider, Peter Cervelli, Robert Holzworth, John Lyons, Matthew Haney, Kristi Wallace, David Fee, Larry Mastin

Submission 935

Volcanic lightning during the shallow submarine eruption of Bogoslof volcano, Alaska

Lightning in volcanic plumes provides a promising way to monitor ash-producing eruptions and investigate their dynamics. Among the many methods of lightning detection are global networks of electromagnetic sensors, which use radio waves in the very low frequency band. These signals propagate thousands of kilometers at the speed of light, providing an opportunity for rapid detection of explosive volcanism anywhere in the world. Lightning is particularly valuable as a near real-time indicator of ash-rich plumes that are hazardous to aviation. But under what conditions does electrical activity in volcanic plumes become powerful, detectable lightning? And inversely, can we use lightning to illuminate key eruption processes and hazards?

Bogoslof is a shallow submarine volcano ~50 km northwest of the Aleutian Arc front in Alaska. Since December 2016, it has produced >36 explosive events with plume heights from a few km to 11 km above sea level. The eruption has resulted in lightning-rich (~60% of events) and lightning-poor events, providing a superb example to investigate the conditions favorable for lightning generation. For instance, two of the most energetic and well-recorded events on Jan 31st and March 8th 2017 produced abundant lightning—hundreds of strokes detected by the World Wide Lightning Location Network (WWLLN). Both examples show evidence for a general drying out of the vent(s) through time, as inferred from satellite observations and seismoacoustic signals. In this study, we compare the evolution of the volcanic lightning (stroke rates, locations, and energies) with satellite, seismic, infrasound, and volcanic ash observations to explore relationships between eruption behavior and electrical activity. Our overall aim is to advance a conceptual model for how lightning evolves and responds to physical processes during shallow submarine volcanism.

Jozua van Otterloo, Alexander R. Cruden

Submission 219

Magma pathways in interconnected multi-dyke and sill systems

Magma transport networks comprise multiple pathways of interconnected intrusive sheets of dykes and sills. Although it is important for volcanic systems and intrusion-hosted economic deposits, it is not well understood how magma flow in such networks is affected by multiple intrusion events whilst the network has not been sealed yet, or by continued intrusion in a complex multi-dyke and sill network. At many volcanic centres, multiple magma batches use the same dyke-vent system to erupt; at some of these, multiple magma batches erupt from the same system simultaneously.

Here we present the results of laboratory experiments simulating multiple interconnected sheet-like intrusions using water (the magma analogue) into solid gelatine (the elastic host-rock analogue) to show how sheet-like magma pathways might develop in upper crustal transport networks. The experiments find that only a narrow connection is sufficient to channel magma from one intrusive sheet into another and that this opening length is only ~10% of the maximum intrusion width. When an intrusive sheet ruptures the free surface its length is ~20% of the maximum intrusion width. Once a surface rupture is formed, magma migration in multi-pulse intrusive systems transitions from sheet-like to channelized pathways. These experiments, however, do not consider the effects of cooling-induced crystallization and solidification or any related changes in viscosity. Nonetheless, these experiments provide new insight in the first-order dynamics of fluid flow in a network of multiple dykes and sills.

Jozua van Otterloo, Alexander R. Cruden

Submission 220

Unique intra-vent folded dyke and peperite: new mechanism for magma-water mixing

Efficient mixing of magma and water is required for explosive molten fuel-coolant interaction and resulting phreatomagmatic explosions. Water needs to be trapped by the magma whilst simultaneously retaining a steam film that insulates the magma and prevents flash heating of the water. Steam film collapse and flash heating can only result in phreatomagmatic explosions if the water is trapped by the magma. However, to mix these immiscible fluids in such a way is difficult. Impure coolants or slurries (mixtures of water and sediment) increase the miscibility, and therefore the efficiency, which provide a useful explanation for the onset of phreatomagmatic eruptions, but not necessarily the occurrence of a final phreatomagmatic explosion after a predominantly magmatic eruption.

A new mechanism for magma-water mixing is found at a folded dyke in one bud of French Butte, Hopi Buttes Volcanic Field, Arizona. Four buds exist along an 800-m dyke system. Each of these buds are marked by extensive peperite formed by quench fragmentation and mixing with surrounding fine sand and silt deposits from a playa-lake environment. At one bud the interior is filled by a vertically folded dyke with peperite margins thus trapping the peperite in the folds. Analogue experiments with sand-coated silicon gum show that this folded section is the result of a collapsed intrusive sheet. This collapse is the result of gravitational pull after the magmatic pressure dropped and dyke could not sustain itself anymore; this is typical when eruptive activity ceases. Efficient magma-water mixing and phreatomagmatic activity at the close of an otherwise magmatic eruption can be explained by gravitational collapse of the intrusive trapping water-hosting sediment and peperite.

Benjamin van Wyk de Vries

Submission 60

Monogenetic volcanism and geoheritage: the case for a broad recognition at World Heritage

Monogenetic volcanoes and volcanic fields are widespread and found in all geological environments from the sea floor, through arcs, rifts and transform faults to uplifted plateau and continental interiors. They reflect each and every tectonic environment through their landforms and by their distribution within the fields where they are grouped. Monogenetic fields meld into landscapes that have evolved over many millions of years, and record the changes related to the geological processes in this evolution, thus even highly eroded fields (like the Bohemian Paradise volcanoes) tell an important story. Monogenetic volcanoes are thus an essential geological feature, that should be represented at all levels of geoheritage, including, and especially World Heritage. We look at the world-wide spread of monogenetic volcanism and we compare and contrast fields for their diversity, complexity, and their tectonic, geological and landscape environment. Several fields stand out as the most diverse, and these also cover the main tectonic environments. These fields are characterised by a close spacing of volcanoes, diverse landforms and compositions. They are not isolated features, and their geoheritage value is often inseparable from their associated geological environment. We describe just a few of the most diverse continental examples: the Chaîne des Puys (orogen-related rift margin), Saudi Arabian volcanoes (post ocean-opening continental plateau), San Francisco (delamination related continental plateau) and Meidob (continental hot spot), to illustrate the diversity. Basaltic fields, while compositionally restricted, are no less important in illustrating the interaction with monogenetic volcanism and landscape, and some like Diamond craters (Oregon), or The Moroccan central Atlas volcanoes, provide exceptional landscapes for basaltic monogenetic volcanism. Basaltic volcanoes like Auckland or the Xitle, Mexico are important for their interaction with the urban environment. In the final count, monogenetic volcanoes and volcanic fields are an indispensable element to be included in geoheritage sites representing the major tectonic environments, and deserve a specific inclusion at World Heritage in their own right.

Benjamin van Wyk de Vries

Submission 58

Geological Environments and the place of volcanoes in global geoheritage

Any geological site needs to be seen in the context of the global geological system if its relevance is to be fully appreciated. This is as true for research as for geoheritage and the educational and touristic relevance. A global geological framework can provide the necessary context, and in this presentation I review those frameworks that exist and propose one that could be adopted as a standard to be used internationally for geosciences and geoscience outreach. The value of the framework is that it allows to place a site clearly and simply in its setting, and can be used to compare and contrast sites. It also provide a quick and easy appreciation of the broader Earth system. We provide three types of representation that can be used together. The first is a table, which holds all geological environments and processes in a generalised way. The second is a schematic cut through the Earth showing the different geological spheres and their interactions. The third is a system diagram that diagrammatically depicts the links and evolution of the system in question. To illustrate the use and demonstrate the methodology we provide examples for UNESCO World Heritage sites where such a framework is indispensable for comparing sites. We use Grand Canyon, The Chaîne des Puys - Limagne fault nomination, Iceland World Heritage, and Kamchatka as examples to show how the framework can be used to discriminate between sites and to represent their value for geoheritage.

Benjamin van Wyk de Vries, Catherine Lit

Submission 379

Eruption dynamics and landform development – an 8,000 year old record of landscape reaction to a trachytic monogenetic eruption

The Puy Chopine volcano erupted about 8,000 years ago in the Chaîne des Puys, Auvergne, France. The volcano has fascinated geologists since the 18th Century, due to its distinctive shape, with a steep spine of trachyte in a horse shoe-shaped scar. A small-steep sided breccia ring occupies the north-east side of the scar, and constrains the spine. Additional small craters and depressions occur to the south and north of the main one. The area for about 3 km to the north and north-east is covered by surge and dense pyroclastic flows, and a probable small debris avalanche. Recent Lidar coverage by the city of Clermont-Ferrand (CRAIG open data) has brought to light fingered flow fronts 1.5 km east of the volcano. These form a lobe that passed between the Chaumont Scoria cone and a small granite hill. The lobe is cut by a broad, steep-sided, flat bottomed gully that merges up stream into a network of rills extending from the pumice plain immediately at the base of the breccia ring. Below the flow fingers, the gully broadens and lead to a drainage that descends to a Neolithic site (Mozac) where an abandoned camp was covered by laharic material from the eruption. The discovery of the fingers, and gully, as well as detailed mapping of the breccia cone allows the eruptive and post eruptive sequence to be described. The subtle eruptive features have survived the highly erosive context after the eruption and have been protected by several thousand years of pastoralism to provide an exceptional record of a monogenetic cryptodome intrusion, flank collapse, explosive eruption and subsequent environmental impact. This provides a possible scenario for a future eruption in the area.

Marit van Zalinge, Steve Sparks, Darren Mark, Frances Cooper

Submission 476

Petrogenesis and temporal evolution of the 21.9 Ma large-volume Cardones ignimbrite, Central Andes; implications for a complex magma-mush system

The Cardones ignimbrite is part of the early Miocene Oxaya Formation located on the western Central Andean slope in northernmost Chile. The Cardones ignimbrite is a crystal-rich (ca. 40 vol%) rhyolite with an extra-caldera volume of >1260 km³ and a maximum thickness of 1000 m. Cores from multiple drill holes through the ignimbrite allowed us to sample pumice from the full stratigraphy. Modal analyses in combination with EPMA show that the pumice can be related to two distinct magma types: 1) Sanidine-poor magma that is amphibole-bearing, has a Ba-rich melt phase (400-1000 ppm) and temperatures between 850-750°C; and 2) sanidine-rich magma that has a Ba-poor melt phase (40Ar/39Ar geochronology on 42 individual sanidine crystals from a single pumice clast give a weighted mean eruption age of ca. 21.931 Ma (n23). However, 19 sanidine crystals give ages that are older than the eruption age, ranging between 22 and 28 Ma. We interpret these older sanidine crystals as antecrysts that represent the incubation time for the formation of a large silicic reservoir (Annen et al., 2015) that coincided with a significant increase in convergence rate between the Nazca and South American Plates (Somoza, 1998). We suggest that the abundant antecrystic sanidine crystals and the absence of a systematic relationship between pumice composition and ignimbrite stratigraphy indicate that major destabilization of the magmatic system resulted in the amalgamation and mixing of different magma layers and surrounding crystal-mush to form a large heterogeneous eruptible magma body.

References: Annen, et al., 2015, *Lithos*; Somoza, 1998, *Journal of South American Earth Sciences*

Loïc Vanderkluysen, Erika Rader, Hetu Sheth, Stephen Self, Amanda Clarke, Danielle Moyer

Submission 204

Variability of lava flow morphologies in the Deccan Traps large igneous province (India)

In continental flood basalt provinces (CFBs), lava flow morphologies have traditionally been classified into two distinct types recognizable in the field: (a) “compound” lava flows dominated by meter to decimeter-sized pāhoehoe toes and lobes, and (b) “simple” flows, dominated by inflated sheet lobes tens to >100 m in thickness, and tens of meters to kilometers in lateral extent. Temporal (i.e., stratigraphic) transitions between these two types of flows have been recognized in many CFBs worldwide and seem to be a fundamental feature. However, lateral and temporal variations in these morphologies remain poorly studied and understood. Two principal hypotheses have been proposed to account for possible lateral variations in lava flow facies in CFBs: smaller toes and lobes occur in distal regions of flow fields, representing breakouts at the edges of sheet lobe-dominated flow fields; or, alternatively, smaller toes and lobes represent proximal facies. We conducted a field study focusing on two Deccan formations, the Khandala and the Poladpur, located in the middle and upper sections of the province’s defined chemostratigraphy. We studied nine sections along a ~600 km long E-W transect, with the easternmost sections representing the most distal outcrops, ≥ 500 km away from inferred vent areas in the western Deccan. The Khandala Formation is traditionally described as a sequence of 3-4 inflated sheet lobes in well-exposed medial sections ~300 km from their inferred source. However, in proximal sections, we find the Khandala to be much thicker overall, with half of its thickness dominated by small, meter-sized toes and lobes. Inflated sheet lobes of the Khandala are thinner on average in the proximal sections than in more distal ones. In the Poladpur, the average thickness of inflated sheet lobes is greater in distal outcrops in the eastern Deccan relative to those closer to inferred vents. We interpret these results as an indication that smaller, meter-sized toes and lobes are indicative of proximal facies, whereas parts of flow fields dominated by thicker (> 10 m) inflated sheet lobes are much more likely to have reached the far edges of the province. We also carried out wax analogue experiments to shed some light on the eruption conditions necessary for the development of these morphologies. The experiments reveal that pulsatory effusion rates are required for inflation, with implications for the eruptive tempo during the emplacement of CFB provinces.

Tiziana Vanorio

Submission 162

Cementing Roman Concrete to a Caldera: A Physicochemical Process Impacting Rock Strength and Fracture Toughness

Ancient concrete would seem to have little to do with volcano geology. In this presentation, I will show similarities between the caprock of the Campi Flegrei caldera (Italy), the lid of this hydrothermal system, and the Roman-era concrete for which the region was known. Both materials require a similar set of chemical reactions to give it the high durability and strength caused by microstructures of intertwining fibrous minerals. The presence of this natural, fibrous rock is utterly fascinating because it highlights the existence of physicochemical processes that help explain the dynamics and the geophysical observations in this caldera.

On the one hand, the presence of this concrete-like rock helps explain the ability of the caldera to withstand periods of delayed seismic response despite the high-rate uplift (~2 m in two years), which always posed an interesting rock physics question of how certain rocks are capable of accommodating such deformation without immediately releasing the stored energy through rock fracturing or cracking. From a mechanical perspective, the formation of fibrous minerals by intertwining filaments confers strength to the caprock of this hydrothermal system, contributing to its ductility and increased resistance to fracture. On the other hand, this fibrous rock testifies the presence of a natural process reflecting that characterizing the cementitious pastes in modern and Roman concrete (i.e., the “cement” making stage). This stage, however, can be undermined by an overabundance of CO₂, which leads to carbonation and cracking of the cementitious binder – a process which has long been recognized to cause chemomechanical changes affecting the integrity of cement pastes. This finding opens new perspectives for understanding the role of chemical processes in caldera systems, which may take place in addition to changes in mechanical stress exerted by pore pressure buildup.

Johan Varekamp, Hilary Brumberg, Lena Capece, Paula Tartell

Submission 1073

Carbon dioxide emissions from East Lake, Newberry Volcano, Oregon

East Lake, one of the twin crater lakes at Newberry Volcano, OR, has a volcanic CO₂ input at its ~ 50 m deep bottom. This terminal lake has a pH of 6.5-7 and 135 ppm HCO₃. A gas-accumulation float chamber, connected to a LICOR CO₂ analyzer was used for CO₂ flux measurements, and the chamber contents were sampled for C isotope analyses. The CO₂ fluxes are obtained from the rate of CO₂ build-up in the chamber, which then contains a mixture of ambient and lake CO₂. We developed an alternative, the draw-down method, where we inserted a CO₂ trap after the LICOR, and pumped the chamber down to a CO₂ steady state concentration. From the pump rate and the chamber steady state CO₂ concentration, the CO₂ flux is constrained, and the gas inside the chamber is then almost pure lake CO₂. We simulated both methods with known CO₂ inputs and the float chamber in a kiddie pool, and we constructed a degassing cell to simulate CO₂ fluxes and isotope fractionation under controlled conditions (LABLAKE experiment). The field CO₂ fluxes from East Lake were measured in summer 2015 and 2016 at 100 locations spread over the lake. The mean flux value was ~0.2 mole CO₂ / m²day (range 0.1-0.9), and the East Lake flux for the two years was 40-50 Mg CO₂ per day. Sequential Gaussian Simulations created a flux map for the lake, with high values near hot springs caused by discrete CO₂ bubble escape. We also calculated CO₂ fluxes from gas evasion equations using calculated deltaPCO₂ values. All field, theory, and lab methods yielded similar results. We obtained a five year record of d¹³C(DIC) in lake water profiles and analyzed d¹³C (CO₂-gas) in lake gas, ambient air, and LABLAKE headspace samples. The mean lake CO₂ had -10.5 ‰ VPDB, whereas calculated d¹³C(CO₂-aq) is -1 to -3 ‰, suggesting a degassing fractionation of ~ 9 ‰. The d¹³C(DIC) profiles show a strong depth gradient from +5 ‰ at the surface to +1 ‰ at depth. A two box degassing model was constructed, based on C mass balance (volcanic CO₂ input = photosynthetic C removal + CO₂ degassing) to simulate the d¹³C(DIC) gradients. During the winter the lake is frozen over, volcanic CO₂ builds up (no degassing or photosynthesis), and during the summer the lake degasses, creating together with biological productivity the d¹³C(DIC) gradient in the water column. The steepest gradients were measured in the late fall, which are then reset to zero during lake turnover and freezing in the winter, to start building up again in the spring upon thawing.

Dulce Vargas-Bracamontes, Mauricio Mora, Alejandro Nava, Gabriel Reyes-Dávila, Raúl Arámbula, Carlos Navarro, Alejandro Martínez, Miguel González

Submission 571

Detection of significant changes in the 2015-2017 seismicity of Volcán de Colima, Mexico

Volcán de Colima is an andesitic stratovolcano located in western Mexico. It is considered the most active volcano in Mexico, with activity characterized mainly by intermittent effusive and explosive episodes. On July 10th-11th 2015, Volcán de Colima underwent its most intense eruptive phase since its Subplinian-Plinian eruption in 1913. A partial collapse of the dome and of the crater's wall generated several pyroclastic density currents (PDCs), the largest of which reached 10.3 km to the south of the volcano. Lava flows along with incandescent rockfalls descended through various flanks of the volcanic edifice, and the ashfall affected people up to 40 km from the volcano's summit. Inhabitants from the small villages closest to the volcano were evacuated and authorities sealed off a 12 km area. In the following months, an explosive stage of vulcanian eruptions was predominant along with the presence of a small dome which appeared in February 2016. Then, a new phase of effusive activity began by the end of September 2016 after the rapid emplacement of a lava dome which overspilled the southern rim and fed a lava flow. Intermittent explosions destroyed most of this recently emplaced dome until early November 2016 when another pulse of magma resumed the formation of a new dome which was subsequently destroyed by frequent vulcanian explosions. An increase in the intensity of the explosions began on the 7th of January 2017, some of them considered as moderate to large, produced shock waves that were reported in the city of Colima and PDCs by column collapse that reached up to 4.5 km from the crater.

We present an analysis of the precursory, eruptive and post-eruptive seismicity related to this near constant activity of Volcán de Colima. In particular, we focus on the search of temporal information within the spectral content of volcanic signals, employing common time-frequency representations such as Fourier and wavelet transforms, but also more recent techniques proposed for the analysis of non-stationary signals, such as the synchrosqueezed transform and Yule-Walker autoregressive method. Then, we applied Akaike information criterion for the detection of changes in the time series. We present results of their performances and discuss the potential use of each technique to characterize and quantify spectral changes which could be used to forecast future eruptive events and to evaluate the course of volcanic processes during ongoing eruptions.

Nick Varley, Sam Thiele

Submission 171

Gentle dome growth to catastrophic collapse: variations in effusive activity at Volcán de Colima

The eruptive intensity at Volcán de Colima, Mexico has increased in recent years with frequent transitions between different styles. The current episode commenced in Jan. 2013 and since we have witnessed at least 8 distinct phases of effusion with large variations in the intensity of explosive activity. This period included two critical periods with evacuations: in July 2015 as a result of an enigmatic eruption, resulting in an extraordinary large pyroclastic density current (PDC); and in Sept. 2016 with the rapid emplacement of a gas-rich magma batch.

2013 – 2015 included some remarkable variations in the summit morphology, highlighted using photogrammetry using both aerial photos and thermal images. The latter allows improved imaging during conditions when either gas emission or clouds reduces the visibility for photos. Activity included a rapidly extending lava flow, with a 2nd pulse creating a composite flow; subsidence, with a considerable volume reduction before a new lobe was emplaced; simultaneous subsidence and growth of different parts of the dome.

The July 2015 eruption was preceded by dome growth supplied from two vents. This resulted in 2 lava flows to the N and S, which had contrasting appearances, suggesting different rheologies and sources. A large magma pulse with minimal precursory activity produced the largest volume PDC in >100 years. It flowed for 10.7 km, so remarkably mobile. Although increased gas-contents of the magma batch increased mobility, the development of an eruption column was suppressed with efficient fragmentation maintaining a higher density with material rapidly collapsing to form the relatively large volume PDC, with two phases in two days. The volume of the flow was increased due to the contribution of the collapse of a part of the crater rim. This was followed by a passively emplaced lava flow.

Large volumes of SO₂ accompanied the Sept. 2016 dome emplacement, but notoriously there was no explosion. The crater was quickly filled to the point where the magma could again overflow. No collapse occurred.

These events require some new scenarios to be established for risk evaluation at Volcán de Colima. The eruption mechanism needs defining with rapidly changing magma properties again pointing to presence of multiple reservoirs. Petrological results will help to establish variations in magma properties, which have manifested themselves as the wide variation in dome emplacement styles, as well as explosion characteristics.

Matthew Varnam, Mike Burton, Giuseppe Salerno

Submission 1063

Continuous volcanic monitoring using the SO₂ camera

Volcanic activity is driven through the exsolution, expansion and release of gas from ascending magma, and measuring gas fluxes from volcanoes is key in understanding the dynamics of such systems. A powerful technique for observing SO₂ is through UV imaging. SO₂ is an ideal target gas due to its strong UV absorption, high volcanic gas concentration, and crucially, unlike like the most abundant constituents of volcanic gas (CO₂ and H₂O), it has a low background atmospheric concentration. The development of the SO₂ camera is creating significant improvements in the temporal resolution of SO₂ flux measurement, allowing the changes in volcanic plume SO₂ to be observed during short-lived explosive events.

Higher temporal resolution opens the possibility of improved integration with geophysical monitoring techniques, such as seismic and deformation, which further enhances our ability to forecast and track eruptions. Previous studies using the SO₂ camera have mostly been limited to several short-term deployments, for example at Stromboli or Sakurajima, but provided significant insights into individual explosive events. Mt. Etna, in Sicily, is one of the first volcanoes to be routinely observed by the SO₂ camera, so presents a wealth of data for further understanding volcanic gas processes, alongside an opportunity to develop SO₂ camera.

Bhuvan Varugu, Falk Amelung

Submission 1107

InSAR revealed deformation at Mauna Loa and inflation-earthquake interaction

Since the last quarter of 2013, Mauna Loa has started to show signs of significant inflation which is continuing at a steady rate. This sudden activity after a long gap is alarming as it is also accompanied with increased shallow seismicity in the south west rift zone, close to the caldera, where significant magma activity is perceived. To evaluate these, we used InSAR observations from COSMO SkyMED during 2013 - 2017 and inverted them using analytical models for magma sources. Our analysis suggests a close relation between the inflation and increased no. of earthquakes. In this study, we explain how inflating magma has triggered earthquakes (M 4.0 in September 2016 & other M>3.0 earthquakes) and in turn how these earthquakes are altering the magma sources. We further revisit the Amelung et al. 2007 source models to see the impact of earthquakes on the magma sources. For a better understanding of the magma chamber and characterization of stresses, we intend to develop a Finite Element model incorporating the effect of Mauna Loa's huge topography.

Francisco Vásquez, Daniel Sierra, Daniel Andrade, Emilia Saltos, Patricio Ramón, Patricia Mothes

Submission 532

Morphology of Cotopaxi volcano's crater (Ecuador) before and after the 1877 major eruption and its potential influence in future eruptive scenarios

Major volcanic eruptions usually cause significant changes in the morphology of volcanic craters. Explosive eruptions can easily erode crater walls, while ballistic blocks, proximal tephra fallout and other pyroclastic materials could partially or totally fill it. Effusive eruptions, either by lava-dome or -flow emplacement, can as well produce new morphologies in stratovolcano craters. Cotopaxi is an active stratovolcano located 60 km south-east of Quito, capital of Ecuador. It has presented at least 5 major eruptive cycles during historical times (1532-present). Some of those eruptions could have drastically changed the morphology of the crater.

Some written reports and historical photography provide evidence about the past morphology of the Cotopaxi. That information was used to rebuild the crater morphology before the major eruption of June 26th, 1877. This event generated several primary lahars, which descended through nearly all the principal drainages of Cotopaxi, due to the partial melting of the glacier cap by boiling over pyroclastic flows.

The behavior of moving pyroclastic flows is highly influenced by the topography. A Digital Terrain Model (DTM) representing the current topography of Cotopaxi has been used to rebuild the approximate pre-1877 crater morphology from which the 1877 boiling over eruption scenario has been numerically modeled. The VolcFlow code was used to reproduce the pyroclastic flows derived from the reconstructed crater.

Pyroclastic flows trigger primary lahar formation in glacier-clad volcanoes and Cotopaxi is characterized by a large massive ice cap of 14 km² which offers plenty input of water. In this particular case the Cotopaxi's lahars magnitude (i.e. peak discharge) can be considered as a proxy of the pyroclastic flow magnitude. Thus, the distribution of pyroclastic flows obtained by the simulations were compared with estimations of lahar peak discharges of the 1877 eruption performed around the cone, in the proximal zones, to corroborate the accurateness of our crater reconstruction.

Once calibrated parameters were obtained for modelization, new simulations were performed using the current crater morphology in order to simulate a future 1877 eruption type. The results of such simulations suggest that the current crater shape favors flows descending towards the eastern and western flanks of Cotopaxi and consequently major probabilities of primary lahars affecting certain drainages more than others.

Jeremie Vasseur, Fabian Wadsworth, Michael Heap, Ian Main, Yan Lavallée, Donald Dingwell

Submission 785

Forecasting the brittle failure of heterogeneous magma

Heterogeneity develops in magmas during ascent and is dominated by the development of bubble populations or pore-network clusters which grow, interact, localize, coalesce, outgas and resorb. As a first step, we numerically construct 3D volumes that are populated by randomly generated heterogeneous and polydisperse spheres that are permitted to overlap. These systems are designed to represent the random growth and interaction of bubbles in a liquid volume. We use these simulated geometries to show that statistical predications of the inter-bubble lengthscales and evolving bubble surface area or cluster densities can be made based on fundamental theory. As a second step, we take a range of well constrained random heterogeneous volcanic rock samples including andesites, synthetic partially sintered glass bead samples, and intact glass samples and subject them to a variety of stress loading conditions at a range of temperatures until failure. We record in real time the evolution of the number of acoustic events that precede failure and show that in all scenarios, the acoustic event rate accelerates toward failure, consistent with previous findings. Applying tools designed to forecast the failure time based on these precursory signals, we constrain the absolute error on the forecast time. We find that for all sample types, the error associated with an accurate forecast of failure scales non-linearly with our metric: the lengthscale between the pore clusters in the material. Moreover, using a simple micromechanical model for the deformation of porous elastic bodies, we show that the ratio between the equilibrium sub-critical crack length emanating from the pore clusters relative to the inter-pore lengthscale, provides a scaling for the error on forecast accuracy. We propose that low-frequency, long period volcanic earthquakes – that are thought to originate in magma rupture events – could elucidate the characteristic inter-flaw lengthscales for case-study volcanic conduit scenarios, and effectively scale our findings to natural cases.

R. Greg Vaughan, Laszlo Keszthelyi, Ashley Davies

Submission 849

A calibrated, high-speed, multispectral VNIR camera for remotely retrieving lava eruption temperature at Kilauea

The surface of molten lava can cool very quickly when it is first exposed - hundreds of degrees per second. Hence, remotely measuring the eruption temperature is an attempt to record something that is visible for only a fraction of a second, and typically present in just a fraction of a pixel. Previous observations and models have demonstrated that remotely determining peak lava temperatures can have hundreds of degrees of uncertainty. The ultimate goal of this NASA-funded research is to design an instrument capable of reliably measuring the temperature of active lava on Jupiter's moon, Io. The results of this work will also establish the validity of measurement and data processing methods that could be applied to satellite, airborne, and ground-based remote sensing data sets for terrestrial volcano monitoring. In December, 2016, we conducted our 3rd field imaging experiment on Kilauea Volcano, HI, with a calibrated, high-speed, visible - near infrared camera to test techniques for accurately retrieving lava eruption temperatures. Essentially an optical imaging pyrometer, the camera acquires simultaneous image data in 3 channels (GRN, RED, and NIR) at 50 frames per second. The camera was calibrated by making a series of measurements, at 50 °C intervals, of a high-temperature blackbody source that ranges in temperature from 600-1500 °C, while systematically varying the gain, F-stop, frame rate, and exposure time settings. From the calibration data, we developed a series of equations to (1) convert DN values measured by the camera to brightness temperature for each channel, assuming unity emissivity; and (2) relate DN ratios (e.g., NIR/RED) to a color temperature, which is the temperature of a blackbody emitting the same brightness ratio at two wavelengths. Applying the data processing to the calibration images, for temperatures ranging from 900-1250 °C, the retrieved NIR and RED brightness temperatures were within 25 °C of the actual temperature. The accuracy of the retrieved GRN brightness temperatures were within 10 °C of the actual temperature, but only at the highest temperatures (1100-1250 °C). The retrieved NIR/RED color temperatures were within 85 °C of the actual temperature. In the field, we collected unsaturated image data of active breakouts from the 61g lava flow, and retrieved brightness temperatures within 25°C, and color temperatures within 70 °C, of the thermocouple-measured lava temperature of 1136 °C.

Swetha Venugopal, Séverine Moune, Glyn Williams-Jones, Alexander Wilson, Kelly Russell

Submission 244

Gas emissions and magma source of the Mount Meager Volcanic Complex, Garibaldi Volcanic Belt, BC

The Garibaldi Volcanic Belt (GVB), located in western Canada, is a Quaternary-aged glaciovolcanic belt created by the subduction of the young (3 of rhyodacite magma was extruded during this singular Holocene eruption, including a 9-km long valley filling pyroclastic and lava flow assemblage.

Although Mount Meager is considered dormant, starting in February 2016 reports were made of gas emanating from pockets of hot ground as well as the appearance of several new summit fumaroles. Due to the low level of volcanic activity and limited access, there have been no comprehensive degassing surveys in the GVB. As such, this study aims to address this knowledge gap by combining direct sampling of the Mount Meager summit fumaroles with melt inclusion analyses in order to characterize the magmatic system beneath the MMVC.

Gas surveys of the summit fumaroles were performed with a portable Multi-GAS instrument and showed predominantly H₂O, CO₂ and H₂S (CO₂/H₂S 4-5.97 and H₂O/H₂S 4.3-50). Olivine-hosted melt inclusions were sampled from the most recent eruption and analyzed for major, trace and volatile elements using Electron Microprobe, LA-ICP-MS and SIMS. These primitive inclusions (0.50-0.95 K₂O wt%) are uniquely alkalic, which is consistent with previous whole rock studies depicting a transition from calc-alkaline magma in the southern segment to alkaline beneath the northern segment of the arc, namely Salal Creek and Bridge River. This transition is attributed to the younger age of the downgoing slab in the north as well as asthenospheric upwelling due to slab rollback.

The main implications of this study are the estimation of the MMVC volatile budget through the combination of melt inclusions and gas surveys as well as the characterization of the magma source. This work also provides valuable baseline data in the event of any future unrest within the GVB.

Edward Venzke, Benjamin Andrews

Submission 1145

Expanded content and availability of the Volcanoes of the World database

The Volcanoes of the World (VOTW) database, maintained by the Smithsonian's Global Volcanism Program (GVP), has provided the most comprehensive catalog available of Holocene volcanoes and their eruptions for more than 45 years. Recent work has focused on expanding the types of data available, reviewing the Holocene or Pleistocene classifications, and improving data access methods. Information for updates comes from a variety of sources, including published research, the Smithsonian/USGS Weekly Volcanic Activity Report, and reports in the Bulletin of the Global Volcanism Network, which are compiled using multiple sources (e.g. observatories, satellites, aviation notices) by GVP staff to provide a narrative of recent activity.

Schema and administrative changes during a database conversion project completed in 2013 were done with future flexibility and collaboration as a major consideration. The revised volcano numbering system enables linking VOTW to other databases and websites that have used the volcano number as a key in their own databases and website code. During 2017, the long-term goal of allowing automated data updates from the VOTW and downloads in various formats was accomplished with a GeoServer webservices portal.

Building on the schema flexibility, significant projects were completed in the past year that enable emissions and deformation specialists to provide data for import into the VOTW. The first datasets have been made available alongside the existing eruptions data, both through volcano profile pages and the search/download features on the GVP website (118 volcanoes with emissions data, 199 with deformation). In addition, the "Eruptions, Earthquakes, & Emissions" web application was launched in 2016. This time-lapse map or globe-based animation of volcanic eruptions and earthquakes since 1960 also shows volcanic sulfur dioxide emissions since 1978, the first year satellites were available to provide global monitoring of SO₂.

In addition, smaller projects were completed in the past two years, including connecting Smithsonian physical samples to their source volcanoes and making geolocated volcanic subfeatures available in Google Earth placemarks. A preliminary list of Pleistocene volcanoes and profile pages, originally published in the 2010 Volcanoes of the World book, was put on the website in 2016; work to identify, validate, and describe those volcanoes (currently over 1,150) is ongoing.

Camila Vera, Angelo Castruccio, Yarko Niño, Aldo Tamburrino, Olivier Roche

Submission 1205

Analogue modeling of cooling viscous lava flows: using a new thermo-rheological material.

Previous studies of lava flow dynamics, rheological analysis and morphological features of lava flows have shown that lava behaves as a non-Newtonian fluid with a strain-rate dependent on viscosity. Analogue experiments on lava flows use simple materials, mostly Newtonian fluids with a solidification temperature and crust formation of the flow. Another approach is the use of Bingham isothermal models in order to study the effects of a yield strength. Most of these experiments have been used to either model low viscosity lavas such as Hawaiian basalts or lava domes with high viscosities, leaving a range of lava compositions out of the analysis.

In this study we introduce a temperature dependent material characterized with a Herschel Bulkley constitutive law to model a range of viscous lava flow compositions. A specific type of commercial sweet condensed milk caramel was tested and used for this study. We obtained the rheology of the material with a rotational rheometer at different temperatures. The consistency, yield strength and flow index evolve continuously as temperature drops while the flow is in contact with air at ambient temperature. We carried out experiments in order to model simple lava flows in an unconfined, inclined surface, with constant flow rates. These experiments were recorded with regular and thermal cameras to study the emplacement dynamics of the flow and surface temperature variation as motion ceased. Resulting flows showed good symmetry and oval shape. Scaling and dimensionless analysis is consistent with known values for natural lavas, ensuring laminar behavior and Bingham number close to 1. Structure from motion technique was used to develop DEM models of the final flow morphology, showing features also seen in real lava flows: lateral levee formation and a channeled flow with ridges and larger thicknesses of the flow at the front. Final geometry of the flows show important variation of maximum width and basal area related to different flow rates.

This study brings a new inexpensive and easy to handle material for modeling viscous lava flows in the laboratory, including a complex rheology with a non-Newtonian behavior that varies with time and temperature, unifying relevant characteristics of natural lava flows in a single model.

Sylvie Vergnolle, Christelle Zielinski, Viviane Souty, Philipson Bani, Alexis Le Pichon, Michel Lardy, Philippe Millier, Pascal Herry, Sylvain Todman

Submission 393

Insights into eruptive dynamics at open-vents volcanoes from quasi-continuous infrasonic records (2003-2014) at Yasur (Vanuatu)

Open-vents volcanoes, often presenting series of Strombolian explosions of various intensity, are responding, although with a delay, to any changes in the degassing pattern within a shallow magma reservoir. Hence, they are providing a quasi-direct route to phenomena occurring at depth, where eruptions are initiated. Open-vents volcanoes display a persistent volcanic activity, although of variable intensity. Their phases of enhanced activity could therefore be interpreted as analogous to eruptive phases of a volcano alternating between eruptions and quiescence periods. Long-times series at open-vents volcanoes could therefore be key measurements to unravel physical processes at the origin of eruptions and be crucial for monitoring.

Continuous infrasonic records can be used to estimate the gas volume expelled at the vent, both during explosions and between explosions. Long-time series of quasi-continuous infrasonic measurements, performed at one open-vent volcano, Yasur (Vanuatu), between 2003 and 2014, are analysed. The first observation is that the active gas volume, due to explosions (overpressurised gas), only represents a few percents of the total gas volume emitted between explosions, due to their short duration (1s). The second observation is that various types of enhanced activity exist at Yasur, explaining the difficulty in monitoring. The periods of enhanced activity, marked by a large number of explosions and/or large infrasonic pressures, are sometimes long (a few weeks) and start by a gradual build-up or very short and associated with a fast rising time. The transitions between low and vigorous activity, when sharp, are characteristic of an instability, which is triggered by a gas flux exceeding a critical value, equal to $1900 \text{ m}^3/\text{s}$ at atmospheric pressure. Furthermore the observation that the critical gas flux is equal to the mean gas flux, could explain why the activity is persistent at Yasur. We also discuss the use of these observations for monitoring and the potential physical mechanisms based on the analysis of several of these enhanced phases.

Andrea Verolino, James White, Bernd Zimanowski

Submission 357

EXPERIMENTAL SUBAQUEOUS SURTSEYAN ERUPTIONS

Shallow subaqueous volcanic eruptions are natural events that typically include a variety of explosive interactions between magma and surface water. These eruptions have been widely described where the eruption breaches the surface (e.g. Surtsey, Capelinhos), which may be hours or weeks after eruption initiation depending on water depth and eruption rate. Little is known, however, about the fully subaqueous onset of these eruptions. Geoscientists attempt to understand dynamics of these initial phases by studying the primary deposits formed from them. An alternative is to tackle the problem through modelling or experimental work. Here, we present results from bench-scale underwater experiments aimed at understanding the dynamics of the subaqueous part of a Surtseyan eruption with, for the first time, a focus on the behaviour of particles (volcanic and non-). For these experiments, argon is the expanding gas, and forces a population of particles, under known driving pressures, into a container filled with water (32x32x32 cm). Each run was recorded at 1 Mpx/frame and 1000 fps. Two types of run were done: 1) initially dry particles driven into water (analogous to particles formed in a subaqueous explosion), and 2) particles initially in water forced into a water-filled container (analogous to particles propelled away from an explosion in or beneath them). Across the range of particles used, and for both types of runs, we observed a consistent sequence of events: a) initial doming; b) a main decompressing gas expansion, and; c) a phase of “necking”, when a forced plume separated from the initial driving jet. Both the jet and the forced plume comprise clouds of bubbles and particles, rather than a simple bubble/cavity, and ascend at rates much greater than if buoyancy driven. Manual and automatic tracking highlight the different behaviours of the particles in every individual stage, both for wet and dry particles, and for different materials. An important observation is that during necking, many particles are ‘stranded’ in the water column to later settle or descend in gravity currents. Some particles are in contrast re-entrained into the forced plume.

Marco Viccaro, Marisa Giuffrida, Luisa Ottolini

Submission 810

Ultra-fast sin-eruptive degassing and ascent of Etna magmas from Li gradients in plagioclase

The investigation of lithium in plagioclase is becoming an important tool to track and quantify the temporal development of degassing processes of magmas ascending toward surface. We present SIMS data of Li in plagioclase crystals from products of Mount Etna (Italy) in an attempt to investigate the late-stage ascent and degassing processes leading to or accompanying the most energetic, paroxysmal eruptions occurred at the volcano in the period 2011-2013. The investigated plagioclase crystals have shown trends of decreasing lithium concentrations from the crystal interior toward the edge, with localized changes to higher Li contents. The general rim-ward decline of Li in plagioclase implies significant diffusive disequilibrium during the final stage of crystal growth, which reflects in turn Li loss from the melt through sin-eruptive degassing driven by decompression. In contrast, the occurrence of localized lithium spikes/enrichments along the plagioclase rims may be evidence of transient, dynamic processes associated with gas exsolution from deep portions of the volcano plumbing system and consequent flushing at shallow depths. Modeling the Li diffusion between plagioclase and its hosting melt allows determination of the timescales of decompression-driven magma degassing just before and during the eruption culminating with the paroxysmal phenomenology. Diffusion calculations yield timescales on the order of minutes or less. Our improved knowledge on depths of storage levels beneath the volcano, based on seismic signals, has led us to quantify extremely fast final magma ascent rates for these paroxysmal eruptions at Etna. Importance of our results consists in the application of methods, recently used exclusively for closed-system volcanoes producing violent eruptions, also to open-conduit systems that have generally quiet eruptive periods of activity sometimes interrupted by sudden re-awakening and production of anomalous energetic eruptions.

Celine Vidal, Yves Moussallam, Clive Oppenheimer, Gezahegn Yirgu, Asfawossen Asrat, Karen Fontijn, Frances Williams, Paul Mohr

Submission 484

Timing and characteristics of Middle Pleistocene caldera-forming eruptions in the Ethiopian Rift

Homo sapiens first evolved circa 200,000 years ago (i.e. during the Middle Pleistocene) in the East African Rift, where the dynamic landscapes and ecosystems provided an important evolutionary stimulus for our species. While numerous hypotheses have been proposed to link characteristics of the Rift environment and climatic change to hominin distribution, speciation, and extinction, little attention has been paid to the role that volcanism would have played in shaping the Rift habitability. The Ethiopian Rift hosts a dozen of quaternary caldera volcanic complexes, at least five of which are suspected to have formed 300,000-200,000 years ago during a major pulse of explosive activity. These eruptions produced widespread tephra fallout deposits and filled the Rift valley with ignimbrite, which drastically remodelled the landscapes and disrupted ecosystems and hydrological systems, and potentially isolated hominin populations in regions of the Rift. Timing and erupted volumes of most of these colossal eruptions are very poorly constrained, with hitherto unexplored feedbacks. We are integrating stratigraphy and geochemical analysis of whole-rocks and glasses of erupted products with new Ar-Ar dating to quantify the size and age of the caldera forming eruptions of Fentale, Kone, Gedemsa and Shala volcanoes. Reconstructing the tephra dispersal of these eruptions relies on chronologic and geochemical correlations of proximal deposits with distal tephra horizons identified at key paleoarchaeological sites in the Ethiopian Rift and beyond. The outcome of these reconstructions will constitute a robust database for modelling of ecosystem impacts of these eruptions, and the implications for contemporary human populations.

Olga K. Vilmundardóttir, Friðþór S. Sigurmundsson, Gro B.M. Pedersen, Fadi Kizel, Nicola Falco, Joaquín M.C. Belart, Guðrún Gísladóttir, Jón A. Benediktsson

Submission 231

Examining primary succession for the past 850 yrs on the lava-chronosequence of Hekla volcano in south Iceland

Mt. Hekla is among Iceland's most active volcanoes, erupting at least 23 times since the island was settled in c.871 AD. It is located on the highland margin bordering the Southern lowlands, the largest and most productive farmlands in Iceland. Hekla is a ridge shaped stratovolcano, producing both tephra and lava during eruptions. Due to the mountain's proximity to inhabited lands, its historical eruptions have been contemporarily documented. Tephra deposited during eruptions is often preserved in soils. Tephrochronologists have accurately dated the lava fields of Hekla by linking together the historical descriptions of Hekla eruptions and tephra layers found in soil profiles. The objective of this study was to study primary vegetation succession spanning over 800 yrs by the means of Hekla's lava-chronosequence. Field data was collected in summer 2015-2016, within lava fields formed in 1158, 1206, 1300, 1389-90, 1554, 1693, 1725, 1766-68, 1845, 1878, 1913, 1947, 1970, 1980-81, 1991 and 2000. Vegetation and soil parameters were measured around the mountain with elevation range 100-800 m a.s.l. DCA ordination was applied to investigate primary succession stages. Regression models were used to analyze the relation between lava age and vegetation and soil parameters.

Preliminary results show three succession stages: Stage 1(a) is the initial succession found on lavas *Racomitrium* moss mat with dwarf shrubs. This stage was found on lavas 300-700 yrs of age. Stage 3 represents the most developed vegetation where birch shrubland is forming. This stage was only found on the oldest lavas >600 yrs. An additional stage was identified, Stage 1(b) representing areas heavily affected by tephra deposition where succession is reset and tephra now favors establishment of vascular plants. The Hekla lavas are mostly covered by the moss *Racomitrium lanuginosum*. Regression analysis shows that *Raco.lanu.* cover does not significantly change with lava age, yet its thickness seemingly reaches maximum in lavas between 400-600 yrs of age, coinciding with the intermediate 2nd succession stage. This supports the inhibition model, where the thick moss mat prohibits the establishment of vascular plants in the lavas. The development of birch woodland, the climax ecosystem of Iceland, takes several centuries under the conditions southwest of Hekla.

Marija Voloschina, Gert Lube, Jonathan Procter, Anja Moebis

Submission 961

Developing a multi-hazard eruptive record for Mt. Ruapehu, New Zealand

To forecast the impacts of volcanic hazards, individual hazard processes are traditionally studied in isolation. This approach proved successful to better understand underlying physical processes. However, recent eruptive events showed that uncertainties and spatio-temporal dependencies strongly affect predictive models. This is due to the wide possible range of eruption scales and styles over the time span of a multi-stage multi-hazard eruption. This complexity often leads to severe underestimation of hazard intensities and time-scales, and, because of unexpected changes in hazard dynamics, may result in a high degree of unpreparedness. Sudden changes in eruptive behaviour are particularly notorious at long-lived and frequently active andesitic composite cones, such as Mt. Ruapehu in New Zealand.

This research aims at developing a high-resolution multi-hazard record of Ruapehu's eruption history for the past few thousand years. This encapsulates two broad research questions: Is Ruapehu dominated by single-staged or multi-staged eruption episodes; and which processes from magma generation to eruption are responsible for switches in eruption behaviour? To achieve this we have started to create a framework of proximal-medial tephra sequences and to relate them to other deposits of concurrent and successive effusive and explosive events. Our preliminary results for the past 2,000 years show that the eruptive history is more complex than previously assumed. Nineteen earlier defined tephra fall members represent multi-staged eruption episodes events rather than assumed single-stage eruptions. We also identified at least ten additional multi-stage eruption episodes. These observations increase the existing eruption frequency by almost an order of magnitude. Importantly, tephra units show a broad range of dry magmatic to phreatomagmatic eruption styles. They also include dome-forming events and PDCs, previously thought to be absent or extremely rare in this 2,000 years eruption record.

We will show how our dataset can be used to define sequence, number, style and magnitude of eruptions in an episode. We will give examples on how patterns within an eruption sequence (including sudden changes in behaviour) can be identified and discuss our approaches to relate these patterns to physico-chemical processes of the volcanic system.

Felix von Aulock, Yan Lavallée, Silvio De Angelis, Jackie Kendrick, Anthony Lamur, Andreas Rietbrock, Oliver Lamb, Adrian Hornby

Submission 1078

Recording syn-eruptive morphological changes of Santiaguito volcano (Guatemala) with an unmanned aerial vehicle (UAV)

Santiaguito volcano in Guatemala has been continuously active for almost 100 years, producing several domes and frequent explosions. This explosive activity has recently undergone a transition from minor degassing events to major vent clearing explosions and back. Combining observations of eruption rates of magma at different stages of dome growth with classification of concurrent explosive behaviour of the volcano will help us understand continuous effusive eruptions that are accompanied by explosive events.

We captured videos and still images of the active dome of Caliente across three campaigns from 2015 to early 2017. We compared both the visual appearance of the dome surface before, during and after explosions from an unmanned aerial vehicle (UAV; DJI Phantom 2 and Mavic Pro) and from the summit of nearby Santa Maria volcano. Three-dimensional reconstructions of the topography through Structure-from-motion algorithms let us estimate morphological changes of the dome surface over a range of timescales.

Comparison of 3D point clouds show gas-and-ash eruption through complex fractures, explosion pits forming during minor degassing explosions on the timescale of ~1 h, fault formation and extrusion on the dome surface during timescales up to a week and significant changes to the volcanic edifice over the course of 1 year, during which larger vent clearing eruptions took place.

UAVs are becoming an important tool for volcano monitoring and data collection. Using these tools to observe, illustrate and measure morphological changes at active volcanoes can help us estimate eruption rates, locate degassing pathways, analyse structural changes and understand eruption mechanisms.

Matthew R Von Lintig, Jeffrey Bruce Johnson, Alex J C Miller

Submission 678

Quiescence at Sakurajima quantified through infrasound detection: the relationship between sealed vents and explosions

Volcanic infrasound arrays are used to detect infrasound and determine the direction of incident acoustic waves. Coherent infrasound energy originating from a volcano vent is typically an indicator of explosive or degassing activity. Infrasound array data thus permit quantification of when a vent may be openly degassing and help to identify 'open' and 'closed' periods and their relationship to volcanic explosions. Precise determination of periods when a vent is sealed, or not radiating infrasound, permits improved identification of quiescent 'repose' periods, allowing quantitative statistical analysis. For instance, at Sakurajima Volcano (Japan) observations suggest that Vulcanian explosions are preceded by time periods when the vent is sealed.

We identify open-vent periods at Sakurajima Volcano using infrasound recorded on two small arrays located 3.5 and 3.8 km from the active Showa Crater during the week of July 18-25, 2013. The array at 3.5 km (KUR) consisted of 6 microphones with a small (25 m) aperture and situated with line-of-sight to the active crater rim. The array (HAR) at 3.8 km consisted of three elements located in the lee of substantial topography and detections there are less comprehensive. We have tested array processing techniques including cross correlation, beamforming, filtering, and delay-and-sum stacking to maximize the identification of open-vent activity and minimize false detections due to (wind) noise or other non-crater-sourced infrasound, such as echoes and microbaroms. Preliminary observations of infrasound detections show that pre-explosion repose intervals average about five hours and can surpass ten hours. This contrasts with mean quiescent intervals of eight minutes, which typically terminate in periods of non-explosive, open-vent degassing. We construct a regression tree to identify event characteristics that precede explosive eruptions. Explosion likelihood is described by the proportion of pre-explosion quiescent intervals that 'survive' as a function of increasing time. Preliminary results show that probabilistic forecasting derived from the quantification of vent activity can be used to anticipate episodic eruptions at Sakurajima.

Alessandro Vona, Andrea Di Piazza, Eugenio Nicotra, Claudia Romano, Marco Viccaro, Guido Giordano

Submission 1060

The complex rheology of megacryst-rich magmas

Multiphase magma rheological properties play a fundamental role on lava flow transport, emplacement and morphology. We present here a series of high-temperature experiments designed to investigate the multiphase (melt + crystals + bubbles) rheology of a mugearitic megacryst-bearing lava from Mt. Etna. A peculiar textural feature of this magma is the abundance of cm-size plagioclase crystals (megacrysts) together with smaller size crystals (phenocrysts and microlites), yielding a very wide crystal size distribution. Different experimental techniques (rotational and compressional rheometry) were combined to investigate the rheology of this natural lava under different degrees of partial melting at subliquidus conditions. Results indicate that natural megacryst-bearing mugearite magmas from Mt. Etna display a wide range of behaviors as a function of temperature ($T = 1000 - 1200$ °C) and crystal content ($\phi_x = 0.2 - 0.7$). In the investigated T range, the deformation mechanism of these magmas varies from mainly brittle ($T < 1085$ °C). At $T = 1075$ °C, both ductile and brittle behaviors have been observed. In the ductile regime, these magmas behave as non-Newtonian fluids (at least up to $T = 1100$ °C) showing marked apparent shear thinning behavior. The observed rheological behavior is due to a complex response related to a non-homogenous deformation of the natural sample (e.g. viscous and/or brittle shear localization), favored by the presence of bubbles. Consequently, the obtained flow parameters can be considered as representative of the bulk rheology of natural magmas, commonly characterized by similar non-homogeneous deformation styles. Rheological modeling indicates that at eruptive temperatures, the presence of a pre-eruptive crystal cargo and bubbles facilitates the achievement of critical crystal content during flow and cooling ultimately controlling lava transport and emplacement. Flow conditions can be maintained in the presence of an efficient insulation and, importantly, of deformable vesicles promoting and enhancing shear localization.

Charlotte Vye-Brown, Sue Loughlin, Julia Crummy, Murray Lark, Richard Brown, Sam Engwell, Katie Preece, Jenni Barclay, Kay Smith

Submission 998

Development of a volcanic hazard assessment methodology for Ascension Island, South Atlantic

Ascension Island is the northernmost volcanic island of the British Overseas Territory in the South Atlantic, situated ~1300 km northwest of St Helena, ~90 km west of the Mid Atlantic Ridge, ~1600 km from Africa and ~2250 km from South America. Recent volcanological, geochemical and petrological research on the subaerial volcanic deposits on Ascension has revealed new insights into the volcanic stratigraphy, and styles and timing of past volcanism. The research was designed to fill some knowledge gaps and enable a volcanic hazard assessment of the island. There are nevertheless considerable uncertainties typical of small island settings for example, the limited preservation of pyroclastic deposits, limited exposure of the stratigraphy and limited extents of all onshore deposits. Calculation of frequency-magnitude relationships is therefore a particular challenge in such settings. We present the development of a methodology to deliver a volcanic hazard assessment that is cognisant of these limitations. The method includes an expert elicitation using the SHELF method to elicit probability density functions for the numbers of events and the frequency of events of different magnitude. These are used in modelling of selected volcanic hazards (dispersion of ash and inundation by lava flows) that pose the highest possible impact on lives, livelihoods and well-being on the island and to populate an event tree showing the likelihoods of different eruption outcomes. This new information will be used for long-term planning and preparation by the Ascension Island Government.

Keiji Wada, Kyohei Sano

Submission 960

Emplacement mechanism of obsidian-rhyolite magma: observation of whole internal section of the Shirataki obsidian lava, northern Hokkaido, Japan

Formation process of obsidian and rhyolite during emplacement of silicic magmas was studied through the observation of internal structure of obsidian-rhyolite lava from Shirataki, northern Hokkaido, Japan. In the Shirataki monogenetic volcano field (2.2 Ma) there are many outcrops of densely compact obsidian zones ($\text{SiO}_2=76.7-77.4$ wt.%) (Wada and Sano, 2015; Sano et al., 2015). Among them, whole internal section of Akaishiyama lava from the top to the bottom can be seen along the valley continuously.

The Akaishiyama obsidian-rhyolite lava shows good exposures of internal sections with thickness of about 190 meters, showing the symmetrical structure comprising an upper clastic zone (UCZ; 5m thick), an upper dense obsidian zone (UDO; 15m), an upper banded obsidian zone (UBO; 70-80m), a central rhyolite zone (CR; 65m), a lower banded obsidian zone (LBO; 15m), a lower dense obsidian zone (LDO; 20m), and a lower clastic zone (LCZ; 3m). The dense obsidian is composed of >98 % glass containing a small amount of H_2O (<0.1wt.%) with magnetite microlites. Obsidian and rhyolite have similar bulk-rock compositions and number density of microlites, although the rhyolite contains glass with perlitic cracks and a large amount of crystalline material (spherulites and lithophysae).

The UBO zone is characterized by spherulite concentration layers with tuffisite veins and rhyolite enclaves. Spherulites (<12cm in diameter) are clustered in the dense obsidian. The variety of spherulite morphology is probably due to difference in the number density and the connectivity of vesicles, and subsequent outgassing. Tuffisite veins show brecciated obsidians in tuffaceous matrix, showing an outgassing path during the emplacement of obsidian-rhyolite lava. Perpendicular dip of spherulite concentration layers with parallel lines indicates the UBO zone itself was probably the domain of vent area. From the observation of these occurrences in the internal section and rock texture, we show the qualitative formation model of Shirataki obsidian-rhyolite lava.

Fabian Wadsworth, Jeremie Vasseur, Ed Llewellyn, Jim Gardner, Danilo Di Genova, Felix von Aulock, Kai-Uwe Hess, Donald Dingwell

Submission 1075

Water disequilibrium during welding of rhyolitic volcanic ash

Silicic magma fractures to produce efficient outgassing networks in shallow conduits. Volcanic ash transported through such fractures can clog them by sticking to the fracture walls and to each other, leading to a time-dependent sealing of the outgassing network. While this is happening, the volcanic ash is subject to mass transfer of volatiles that leads to a competition between diffusive processes and sintering or sticking processes. We examine this system both theoretically and experimentally by producing hydrous silicate glass particles and allowing them to sinter together. We use a 1D solution to Fick's diffusion equation – extended for polydisperse arrays of particles – to predict how quickly bulk water could move into or out of our particle populations. We then compare this with the capillary time that is characteristic of the sintering process. This permits us to explore regimes of behaviour where, (1) the diffusive equilibration of water is fast compared with sintering, or (2) sintering is fast compared with diffusion. For both end-member scenarios, we show that the fully welded system will be relatively homogeneous in water distribution. However, while in (1) the system will be in water equilibrium at that pressure and temperature, in (2) the system will remain in disequilibrium and could vesiculate after welding. Transitional behaviour is characterized by a locally heterogeneous water distribution in the welded particle pack at the completion of sintering. These complexities are captured by a spatially averaged Capillary-Peclet number, which determines the relative dominance of either diffusion or sintering. This work implicates the particle size as a primary control in determining whether fragmented ash can equilibrate before welding a fracture network closed or not. We propose that where water disequilibrium can be preserved in welded systems, subsequent vesiculation and bubble growth can lead to fragmentation and explosive activity, whereas efficient degassing and outgassing before the completion of sintering may result in less explosive potential.

Gregory Waite, Kyle Brill, Monica Castro-Escobar

Submission 1231

The persistent eruptive activity at Fuego volcano, Guatemala: a multi-instrumental evaluation of processes with timescales from seconds to months

Magmatic processes produce a rich variety of deformation signals, ranging over orders of magnitude in frequency. We report on interpretations of several field deployments that included tiltmeter, broadband seismic, infrasound, and time-lapse recordings of Fuego volcano between 2008 and 2016. A 3800 m basaltic to basaltic andesite stratovolcano in the western Guatemala, Fuego is an excellent laboratory for study of broadband deformation due to its persistent unrest. The open-vent activity since 1999 is characterized by continuous background degassing from the summit crater, frequent explosions (0.5-5 per hour) of varying style, and intermittent lava effusion. The Instituto Nacional de Sismología, Vulcanología, Meteorología e Hidrología maintains a permanent three component seismometer and two web cams. We augmented the INSIVUMEH observatories with repeated short-term (weeks to months) deployments to refine ideas about the eruption process.

LP events with similar, short duration waveforms are seen in data years apart. They are much more frequent than explosive eruptions and are located high in the conduit, though they are not associated with eruptions. LPs are dominated by a Rayleigh wave arrival preceded by a weak P wave. VLP events and much longer period tilt, accompany explosive eruptions and gas puffing. Full waveform source inversions suggest a crack-like mechanism for data in the 30-10 s period band, but inclusion of much longer period, tilt-affected waveforms indicates a pipe-like feature. At some stations, particle motions change from dominantly radial to tangential with increasing period. This is confirmed by tilt data from a station located on the ridge north of the summit. The dominant tilt direction is nearly tangential. Tilt often begins 30 minutes prior to an explosive eruption and continues at a constant rate until a few minutes prior to an eruption. The rate of tilt decreases or even reverses in the minutes prior to an explosion, then rapidly drops immediately after. Observations of pre-explosion tilt highlight a quasi cyclic nature of Fuego activity. Days to weeks of less frequent explosions build to periods of more frequent, more explosive eruptions with short-lived lava flows approximately monthly. We propose models for processes over the range of timescales of repeating events.

Richard B. Waitt, Richard P. Hoblitt

Submission 363

The 18 May 1980 Pyroclastic Surge at Mount St. Helens as Two Separate Events

In 1980 and for years later the forest-felling pyroclastic surge from Mount St. Helens on 18 May 1980 was thought a single event. But there came enough photographs and satellite records of the plume, sedimentologic and stratigraphic data, and eyewitness accounts to suggest two surges, each initiated during a series of large explosions—two such series spaced more than a minute apart. Hoblitt (2000, *Phil. R. Soc. London A* 358) explored these lines of evidence.

More recent stratigraphic data reinforce this view. The coarse lower part of the surge deposit in proximal areas commonly comprises two graded beds, the upper one thicker. And several eyewitness accounts now finely detailed in Waitt (2015, *In the Path of Destruction*, Wash. St. U. Press) require a second large surge. Two accounts in the northwest (McNerney and Smart; Scymancky) could not play out as they did across many minutes unless the surges were two and separated in time. The first surge originated during the first and second gigantic landslides. The second surge began more than a minute after the first, unleashed during the start of the third of the three great landslides. This second surge was the larger, more energetic, and faster—the one that flattened most of the forest and ran out to the limits of surge. Though explosions initiated both surges, eyewitness photographs suggest they flowed off the volcano and far beyond driven partly, perhaps mostly, by gravity. Numerical and other theoretical models of the Mount St. Helens surge, to be entirely valid, should incorporate the idea of two distinct surges separated in time.

Joseph Walder

Submission 133

Energetics of Surtseyan eruptions: insights from the fluid dynamics and phenomenology of underwater chemical explosions

Perhaps the most distinctive feature of Surtseyan eruptions is the “tephra jet”. The subaerial eruptive column comprises an aggregate of such jets, commonly with a volcanic bomb at the tip moving on a ballistic trajectory. Yet “tephra jet” seems an odd name for a phenomenon that was first described as follows in relation to the 1952 Myojinsho eruption:

The sea surface...suddenly domed up nearly to 20 m in height...A number of blocks followed by dark water tails, mixtures of water and rock fragments, broke through the crest of the dome like plumes. These numerous plumes of dark mixture of water and rocks were ejected to the heights of 400 m or more....(Morimoto & Oosaka, 1955, Bull. Earthq. Res. Inst. Tokyo Univ., vol. 33, pp. 221–250).

It is implausible that trails of water tens to hundreds of m long can be dragged in the wake of a volcanic bomb as it passes through the water surface. Moreover, it is easy to show that an individual volcanic bomb ejected from an underwater vent cannot pass through water and continue on a subaerial ballistic trajectory unless hydrodynamic drag is radically reduced from normal by presence of a continuous vapor film. Yet such a film tends to be unstable and collapse. Nor is a tephra jet likely to arise from a submarine vapor/pyroclast jet except for very shallow eruptive vents, as the vapor will condense. As an alternate explanation, I propose that Surtseyan eruption phenomena be interpreted by analogy with observations of the effects of detonating an underwater explosive (UNDEX). In this context, watery tephra jets are understood as hydrodynamic phenomena associated with discrete phreatomagmatic explosions, and UNDEX physics and phenomenology are used to make inferences about the energetics of Surtseyan explosions. Data for tephra-jet characteristics from subaqueous basaltic eruptions can be brought into agreement with UNDEX data only if the enthalpy release during the volcanic explosions is at most a few percent of the available enthalpy of the erupted magma. Comparable “inefficiency” has been found in a range of experiments on molten fuel/coolant interactions. UNDEX studies also provide a framework for understanding some perplexing sedimentological aspects of explosive subaqueous eruptions, such as the presence of clasts that seem to have been deposited subaqueously in a dry state.

Brett Walker, Michael Garcia, Tim Orr

Submission 944

PETROLOGIC INSIGHTS INTO RIFT-ZONE MAGMATIC INTERACTIONS UNDER KILAUEA'S NAPAU CRATER (1963-2011)

The high frequency of historical eruptions at Kilauea volcano presents an exceptional opportunity to address fundamental questions related to the transport, storage, and interaction of magmas within rift zones. The Napau Crater area on Kilauea's East Rift Zone (ERZ) has experienced frequent historical fissure eruptions (eight within 50 years). Repeated intrusion and eruption into this region suggest that the Napau Crater area serves as a magma mixing 'depot' within the ERZ. Lava from historical Napau eruptions was interpreted to represent mixing between rift-zone stored magmas and new, summit-derived magma (Thornber et al. 2015; Orr et al. 2015). Whole-rock, glass, and mineral compositions were determined for a newly collected suite of samples from the 1963, 1965, 1968, 1983, 1997, and 2011 eruptions to better understand potential mixing processes within the ERZ. These data are used to elucidate the pre-eruptive history and temporal evolution of lavas from Napau Crater's most recent episode, the March 2011 Kamoamoia eruption. Whole-rock XRF data reveal two geochemically distinct magma batches for the 2011 eruption: a first more evolved (6.5-6.6 wt. % MgO), and a second less evolved (6.1-6.3 wt. % MgO) end-member. Incompatible element ratio plots (e.g. Nb/Y vs. K/Y, Nb/Y vs. Ba/Y) also indicate two magma batches present in Kamoamoia lavas. Olivine crystals from both batches show normal and reversed zoning indicating mixing and short-term storage prior to the March 2011 eruption. Least-squares regression calculations were made to evaluate whether residual magmas from the 1963-1997 Napau eruptions and Pu'u 'O'o lavas were mixing components for the 2011 eruption. These results confirm the possibility of mixing between summit-derived magma and residual magma from the January 1997 Napau eruption. The composition of summit-derived magma was inferred from compositions of Pu'u 'O'o lava that erupted within six months prior to the Kamoamoia eruption. Insights from these fissure outbreaks are important for understanding if and how magmas from different periods interact within rift zones at basaltic volcanoes.

Laura Walkup, Kari Prassack, William Hart, Elmira Wan

Submission 369

Geochemistry and tephrostratigraphy of Pliocene tephra in Hagerman Fossil Beds National Monument, Idaho, USA

Hagerman Fossil Beds National Monument contains diverse, internationally significant Pliocene faunal and floral assemblages. Within the monument and surrounding areas, the Glens Ferry Formation preserves lacustrine and fluvial deposits interbedded with tephra and lava flows. This study focuses on the geochemistry of the tephra, as well as their use in establishing spatial and geochronologic context for fossil sites within the Glens Ferry Formation in the national monument. Over 150 animal and plant fossils, including many type specimens, have been discovered in the Hagerman Fossil Beds. The ages of type specimens are especially important because they represent the first, and sometimes only, known occurrence of a species in the fossil record. New tephra identifications and geochemical correlations provide a refined temporal framework for several sites containing fossils of particular taxonomic and paleoenvironmental interest.

Previous studies were focused in two small areas (Fossil Gulch and Peters Gulch) within the national monument and identified four silicic tephra (informally named the lower lapilli, peters gulch ash, fossil gulch ash, and horse quarry ash by previous workers) and five basaltic tephra (informally named beds F, G, H, I, and J) at these localities. Using single-shard electron microprobe (EMP) and inductively coupled plasma – mass spectrometry (ICP–MS) techniques, new major, minor, and trace elemental analytical data were obtained, which permitted extension of the mapped areal distribution and correlation of tephra layers and associated fossil sites across eight kilometers. These new data also provide hitherto unknown information about the spectrum of chemical variability within these tephra. Furthermore, the geochemical signatures of the silicic tephra allowed determination of proximal and distal eruptive source areas for these tephra – respectively, in the Yellowstone hotspot/Snake River Plain region, and the Cascade Range.

Kellie Wall, Anita Grunder

Submission 1128

New age and compositional constraints on the evolution of Goat Rocks Volcano, WA

This work investigates the location, longevity, and cyclicity of volcanic activity at the deeply eroded Pliocene-Pleistocene Goat Rocks Volcano in the southern Washington Cascades. Goat Rocks Volcano lies ~35 km north of Mount Adams and is the northernmost major edifice on the linear arc axis extending through Mount Adams to Mount Mazama. Activity precedes and overlaps with that of neighboring Mount Adams, St. Helens, and Rainier (Hildreth, 2007). This composite volcano was built on the margin of a 3.2-Ma rhyolite caldera. Erosional unconformities separate five eruptive stages of andesitic to rhyodacitic lavas and tephras (Clayton, 1983; Swanson, 1996 and unpub.). From oldest to youngest, these stages are Tieton Peak, Qgr1, Qgr2, Qgr3, and Qgr4. Previous work constrains the eruptive timeline of Goat Rocks and peripheral vents to between 3.2 Ma and ~0.25 Ma, using field relations, magnetic polarity, a few radiometric ages, and compositional data (Clayton, 1983; Swanson, 1996, unpub.; Pringle, 2008; Hammond, 2013; Gusey et al., 2016; Yntema et al., 2016; Ayers et al., 2016; Wall et al., 2016).

We present an updated record of the evolution of Goat Rocks Volcano with new age and compositional data including zircon U-Pb ages and trace element compositions, $^{40}\text{Ar}/^{39}\text{Ar}$ ages, and XRF and ICP-MS bulk compositions. Textures, compositions, and U-Pb ages of zircons from two samples reveal complexity in crystallization and magma storage preceding eruption. Ten spots on 9 zircons from sample GR16-30 (basal Qgr2) include a dominant population of relatively uniform texture and trace element composition, with mean age and combined 1σ standard deviation of 0.97 ± 0.16 Ma, plus two zircons with distinctive texture and/or composition and slightly older ages. Eight zircons from sample GR16-38 (Qgr4) record two populations with differing texture/morphology, separate differentiation trends in U-Hf space, and different mean ages 0.55 ± 0.04 Ma and 0.43 ± 0.02 Ma (combined 1σ standard deviation). We add to the eruptive timeline with eight $^{40}\text{Ar}/^{39}\text{Ar}$ ages of plagioclase and groundmass separates from a basalt near Bear Creek Mountain and andesite-dacite lava flows erupted from central Goat Rocks and Old Snowy Mountain. In addition, we present bulk compositions of 24 samples from the Goat Lake and Old Snowy Mountain areas, building a detailed record of changing magmatic conditions and processes during the multi-stage life of this volcano.

Paul Wallace, Kristina Walowski, Ellen Aster

Submission 1191

Determining H₂O and CO₂ contents of basaltic arc magmas using melt inclusions: Diffusive H loss, shrinkage bubble formation, and the CO₂ contents of primary melts

The volatiles H₂O and CO₂ play a major role in arc magmatism, and tracking their return flux from the subducted slab to the Earth's surface is important for understanding global geochemical cycles. Melt inclusions (MIs) are a commonly used tool for measuring the concentrations of volatiles in magmas. However, recent studies have shown that MIs are imperfect storage containers that can lose H by diffusion through the mineral host and CO₂ due to formation of a vapor bubble in the inclusion. Here, we use data for MIs from primitive basaltic magmas in the Lassen region of the Cascade arc [1] to show how post-entrapment processes can be distinguished from magmatic variability. Using the highest measured H₂O from MIs at each volcanic center, we use correlations of volatile and trace element ratios (H₂O/Ce, Cl/Nb, Sr/Nd) to demonstrate that primary geochemical variability results from variable addition of a hydrous subduction component to the mantle wedge. However, volcanic centers in the Lassen region and at nearby Mt. Shasta with the highest Sr/Nd, and therefore largest amount of a subduction component, have low H₂O/Ce, suggesting that MIs in the most H₂O-rich magmas were affected by diffusive H loss after trapping. Extrapolation of the correlation between H₂O, Cl and trace elements predicts 8-10 wt% H₂O in Mt. Shasta high-Mg andesite magma, in agreement with phase equilibria and amphibole compositions [2]. For CO₂ in MIs, we correct for the loss of CO₂ to a vapor bubble formed by post-entrapment crystallization and thermal contraction [3]. The results suggest minimum magmatic values of 1500-4500 ppm CO₂, but these likely reflect the depths of stalling and crystallization in the crust rather than primary magma values. Our data indicate minimum CO₂/Nb values for Cascade magma source regions that are similar (~500) to 3x higher (~1500) than for depleted MORB mantle. Our CO₂ results are similar to estimates for other arc volcanoes that range up to 4000 ppm CO₂ (Fuego [4]), 3800 ppm (Klyuchevskoy [5]) and 7000 ppm (Jorullo [3]). The highest of these values overlap with the estimate of 0.6 – 1.3 wt% CO₂ in primary arc magmas inferred from arc volcano CO₂ emissions [5].

[1] Walowski et al. 2016, EPSL; [2] Krawczynski et al. 2012, CMP; [3] Aster et al. 2016, JVGR; [4] Moore et al. 2015, Am. Min.; [5] Mironov et al. 2015, EPSL; [5] Wallace 2005, JVGR.

Kristi Wallace, Leslie Hayden, Janet Schaefer, Katherine Mulliken, Cheryl Cameron, Christina Neal

Submission 541

Tephra marker horizons of the Aleutian Arc – A tephrochronology of largest eruptions in Alaska.

Deposition of volcanic ash onto a landscape is essentially instantaneous in geologic time. If the ages of volcanic-ash layers are known or if the ashes can be correlated to deposits of known age, they are excellent time-stratigraphic markers used in volcanology, archaeology, and paleoclimate research. Volcanic-ash deposits from large tephra-producing eruptions (e.g. caldera-forming eruptions) are most likely to be widely-distributed and therefore more often encountered in field studies. Compilation of physical and chemical characteristics, geospatial distribution, and age of these deposits can support research in many disciplines across large regions and even across continents.

As part of a larger effort to construct a comprehensive database of Alaska tephtras, this work is intended to highlight Holocene-age tephra deposits of the largest eruptions from Alaska volcanoes. We have constructed a thorough list of the largest Holocene-age tephra-producing eruptions from approximately 26 source volcanoes, digitized geospatial data on tephra distributions, collected new glass geochemistry for approximately 13 deposits, and are evaluating existing age information to provide improved age estimates. Many of these deposits do not yet have glass geochemistry, which is needed to conclusively correlate deposits. Therefore, we are working to obtain samples from both proximal and distal locations for each deposit and geochemically analyze these samples to aid in improving correlation potential with other unidentified deposits.

We envision that researchers will be able to query our database online using text or spatial searches and quickly download and visualize these data from large eruptions that may have impacted their area of study. This product will aid those working on tephra-related stratigraphic issues in Alaska to enable rapid and confident determinations of which tephra deposits are relevant to a given study area and what geochronologic constraints are currently possible. Information from the database will be useful for assessing tephra-fall hazards associated with these large and important eruptions.

Paul A. Wallace, Jackie E. Kendrick, Sarah H. De Angelis, James D. Ashworth, Rebecca Coats, Takahiro Miwa, Elisabetta Mariani, Yan Lavallée

Submission 1016

Late-stage magmatic heating and deformation during the 1994 spine extrusion at Unzen volcano, Japan

Lava dome eruptions are commonly accompanied by the extrusion of a spine, a typical manifestation of increasing viscosity inhibiting magma flow commonly marking the cessation of a prolonged eruptive episode. Protraction of a spine during the closing stages of the 1991-95 dome eruption at Unzen volcano (Japan) has provided the unique opportunity to explore the role of late-stage magmatic heating and deformation on magma ascent. We focus on a 6 m wide shear zone consisting of four structurally discrete units including gouge, a highly sheared zone grading to a moderately sheared zone and a relatively undeformed core. We present the first systematic study of the microstructures, mineralogy, crystal stability, crystal size distribution and magnetic properties across this shear zone. The data is complimented by high-temperature high-velocity rotary shear experiments to simulate the deformation evolution during shear. The dacitic, crystal-rich (>70 vol.%) spine preserves an abundant record of both brittle and ductile deformation. A decrease in crystal size with increasing shear indicates brittle processes dominate adjacent to the spine margins. The porous network varies significantly, with pore size decreasing with increasing shear, a result of shear-enhanced compaction, a process recreated experimentally during shearing. The interaction of crystals further facilitates stress localisation and strain partitioning along the conduit margin, leading to crystal-plastic deformation. Electron backscatter diffraction (EBSD) reveals significant strain localisation in the gouge and high shear zones, with most strain being accommodated in the weak phenocryst phases (i.e. biotite) and groundmass plagioclase microlites. Mineral destabilisation is evident across the entire shear zone, with groundmass amphibole displaying breakdown rims suggesting late-stage disequilibrium conditions, with granular rims only present in the gouge and symplectic rims in the sheared and undeformed magma. A gradual increase in rim thickness towards the gouge, magnetic susceptibility measurements as well as an increase in microlite crystallisation and glass devitrification towards the spine margins suggest the likely effect of thermal input due to strain localisation may be the contributing factor. The evidence presented implies a late-stage magmatic heating event as a consequence of frictional and shear processes in the shallow conduit.

Braden Walsh, Arthur Jolly, Jonathan Procter

Submission 378

Geophysical analysis of the 27 April 2016 Whakaari/White Island, New Zealand eruption: Insights into eruption dynamics and vent characteristics.

Using a combination of multiple geophysical techniques, we set out to determine the eruption characteristics of the phreatic eruption that occurred on Whakaari Island, New Zealand on April 27 2016. The eruption occurred at ~9:30 UTC with a very-long period earthquake precursor before the most energetic portion of the eruption at ~9:53 UTC. Through the use of both acoustic and seismic data multiple eruptive pulses were determined to have occurred over a 30 min time period with tremor lasting ~2 hours after the pulsing sequence. The pulses had separation intervals of ~7 min. To estimate locations for the eruptive vents, coherence methods (i.e. back projection and semblance) were used with infrasound data along with an amplitude source location (ASL) method for determining locations with seismic data. Through the use of these techniques, multiple excitation locations on or near the active crater were discovered during the eruptive pulse sequence. Furthermore, location results for the late tremor generally located at a singular point. The locations of the eruptive pulse sequence originated at depths between ~0-200 m, with the late tremor excitations locating at a constant depth of ~100 m. We show here that combining data sources and using multiple geophysical techniques, the characteristics and locations of volcanic eruptions can be better understood when using a joint investigation with several data sources.

Ting Wang, Jiancang Zhuang, Koji Kiyosugi

Submission 279

Replenishing eruption records for robust hazard estimation

Records of geophysical events such as earthquakes and volcanic eruptions, which are usually modeled as point processes, often have missing data that result in underestimate of corresponding hazard. We present a fast approach for replenishing missing data in the record of volcanic eruptions with time-independent marks (magnitudes). This method carries out a bi-scale empirical transformation of the event times and marks and then reconstructs the record of volcanic eruptions using simulation. After testing this method on a synthetic data set, we analysed the eruption record of Hakone Volcano with minimum magnitude 4. Hakone is an active volcano located at the northern boundary zone of the Izu-Mariana volcanic arc in central Japan. We did a sensitivity test by carrying out 100 simulations and then estimating the hazard rate after each simulation. The results show that about 54% (95% CI: 40%-68%) of data are missing in the original record. The estimated cumulative number of events for the reconstructed dataset shows a remarkable jump around 180 ka. This increased proportion of replenished events is caused by the presence of a cluster of large (magnitude 6) events in the record at 178 ka, 181 ka, 185 ka and 190 ka, which boosted the number of smaller magnitude events around that time period. The ages of events at Hakone Volcano are still under discussion, and hence the replenished data around 180 ka may be an overestimate. This result is based on the assumption that eruptions with a magnitude of 5.7 or above are complete in the record, and that the record is complete since 105ka. This algorithm also provides a useful way to adjust the underestimation of future hazard.

Maren Wanke, Ozge Karakas, Olivier Bachmann

Submission 469

The magmatic plumbing system beneath Mount St. Helens

The eruptive products of Mount St. Helens (MSH) volcano range from basalt to rhyodacite, but dacite is the most abundant rock type. The dacites are most frequently interpreted as a result of melting metabasaltic lower crust by injection of mafic magmas from the mantle. Here we present new thermal and petrologic constraints that suggest limited (<15-20 %) contributions from melting such metabasaltic lower crust. Simple fractional crystallization models can reproduce both major and trace element patterns of dacites after ~55-60 % crystallization of a basaltic andesite parent (one of the three main types of mafic magma erupted at MSH), while thermal models highlight the challenge of melting and assimilating large amounts of mafic subsolidus lithologies in the lower crust, even during injection of hot mantle-derived material. Mineral thermobarometry (particularly using amphiboles), along with recent geophysical imaging of the whole crust in the MSH region, confirms polybaric storage, with a lower crustal mafic mush zone, and subvolcanic storage of dominantly dacitic magmas. We suggest that MSH dacites are generated by: (1) mantle-derived arc magma evolving by AFC to intermediate compositions in a lower crustal magma reservoir and (2) ascent of these intermediate magmas, along an inclined path, to an upper crustal reservoir, where they reach high crystallinity without significant crystal-melt separation (negligible amounts of rhyodacite/rhyolite, in contrast to neighbouring volcanoes such as Mt. Baker and Mt. Mazama). The subvolcanic magma reservoir was (and will likely continue to be) frequently recharged by different magma types, leading to the complex mineral assemblages and mingling/mixing textures that are observed in most of the intermediate magmas of MSH.

V. Dorsey Wanless, Mark Behn

Submission 646

Geochemical and thermal constraints on magma storage and crystallization along the global mid-ocean ridge system

Geophysical observations and numerical models indicate that mid-ocean ridges with variable magma supplies have dramatically different crustal architectures, which should have a profound influence on the depths of magma storage and crystallization. Here we use two global datasets (basalts and melt inclusions) and three different approaches (vapor-saturation pressures, major element geobarometers, and fractional crystallization models) to constrain pressures of crystallization along the global mid-ocean ridge system. We compare these results to thermal models and geophysical observations to create a comprehensive model for crystallization at mid-ocean ridges with variable magma flux.

We present volatile (CO₂, H₂O, F, S, Cl), major, and trace element data from >450 naturally glassy, olivine-hosted, melt inclusions erupted on five mid-ocean ridges that span the range of spreading rates. We use equilibrium CO₂-H₂O concentrations to determine vapor-saturation pressures for each melt inclusion, which are converted to depths of crystallization. These are combined with crystallization pressures calculated using MELTS thermodynamic models and major element geobarometers on >9,500 MORB glasses from 195 mid-ocean ridge segments to produce a global model for melt storage, crystallization and accretion. Comparing these results to thermal models and geophysical observations we find that crystallization occurs from the mantle to the seafloor at all ridges, but is enhanced at major thermal/rheological boundaries. We observe pronounced peaks in distributions of crystallization that correlate with magma chamber depths (when present) and the base of the lithosphere at all ridges. Furthermore, the distributions of crystallization deepen with decreasing magma supply, consistent with thicker lithosphere and cooler thermal regimes at slower spreading ridges. These results indicate that storage and crystallization is strongly influenced by the thermal and crustal structure at all spreading rates.

Leighton M. Watson, Eric M. Dunham, Jeffrey B. Johnson, Hugo David Ortiz Erazo, Alex J. C. Miller, Mario Ruiz

Submission 706

Infrasonic Resonance of Volcanic Craters

Harmonic infrasound signals, with a pronounced fundamental tone, have been observed at a number of open-vent volcanic systems including Cotopaxi, Erebus, Villarrica, Telica, Masaya, and Kilauea, where outgassing or explosive bubble bursts excite acoustic waves and resonant modes of a crater. Infrasound records contain information about the properties of the volcano, such as the geometry of the crater, spectral content of the acoustic source, and volumetric flux of fluid ejected at the bottom of the crater.

We develop a model of the acoustic waves inside the volcanic crater in order to extract information about crater geometry and crater floor gas flux. Our model links the volumetric flux from the base of the crater to the excess pressure at the vent and at typical recording sites situated kilometers from the crater. We consider axisymmetric craters that are deep and narrow, where the radius is less than the wavelengths of interest.

We calculate crater transfer functions, which include resonant modes and quality factors, which are related to damping of the resonant tones. Inside the crater, we solve the quasi one-dimensional linear acoustics equations in the frequency domain to determine the transfer function that maps the volumetric flux at the base of the crater to that at the outlet. Outside the crater, we treat the acoustic source as a circular piston embedded in an infinite baffle and calculate the transfer function that relates volumetric flux at the outlet to the excess pressure at specified distance in an assumed homogenous atmosphere. The two transfer functions are combined linearly to relate the volumetric source flux to the excess pressure at distance.

Previous work has used analytical solutions for the resonant frequencies of horns, originally developed for the study of musical instruments, to investigate harmonic infrasound observations (e.g., Richardson et al., 2014). Our numerical model generalizes this approach in two ways. Firstly, our model can handle arbitrary axisymmetric crater profiles. Secondly, we compute the transfer function between inlet volumetric flux and excess pressure as a function of frequency.

This model can be used to invert for the crater geometry by making assumptions about the nature of the acoustic source. Alternatively, infrasound observations can be inverted to determine the acoustic source if the crater geometry is known.

Kathryn Watts, David John, Joseph Colgan, Christopher Henry

Submission 570

Probing the volcanic-plutonic connection in the deeply dissected Caetano caldera in the Nevada Great Basin, U.S.A.: Source of the late Eocene Caetano Tuff

Silicic calderas are an extreme manifestation of crustal magmatism. They are important research targets for understanding volcanic hazards, and in some cases, the formation of economically valuable mineral and geothermal resources. However, our understanding of the magmatic plumbing systems that give rise to them, specifically how silicic plutons may connect to caldera-forming eruptions at the surface, is limited by coarse geophysical techniques in modern calderas and incomplete records in the geologic past. The exceptionally well-preserved 34 Ma Caetano caldera in north-central Nevada has been tectonically exposed by basin-and-range extension to a paleodepth of ~5 km. The caldera floor, thick (~3-4 km) intracaldera Caetano Tuff, a tuff dike, two generations of resurgent plutons, ring-fracture intrusions, pre- and post-caldera lavas, and extracaldera dikes and domes associated with large Carlin-type gold deposits comprise the caldera stratigraphy. Integrating geologic mapping with geochronological, petrological, geochemical and isotopic studies of whole rocks and minerals, we define the evolution of the magmatic system that sourced the >1,100 km³ Caetano Tuff. Our data point to: (1) shallow (<15 km) anatexis of isotopically diverse metasedimentary basement crust, (2) protracted assembly, homogenization, and distillation of rhyolite to form a ~5-9 km thick, crystal-rich (~30-45 vol. %), chemically zoned (~71-77 wt% SiO₂) magma chamber, (3) multiple episodes of magma recharge, (4) rapid eruption of the Caetano Tuff and emplacement of plutons and small intrusions (within a span of <100 ka based on ⁴⁰Ar/³⁹Ar ages). All lines of evidence indicate that the voluminous plutonic caldera rocks are genetically equivalent to the least evolved part of the intracaldera Caetano Tuff and represent residual cumulate-rich "mush" that remained in the chamber after caldera collapse. Resurgent plutons intruded into caldera fill to depths <1 km locally. Insights from this extraordinarily exposed caldera system may be important for evaluating and revising existing paradigms of silicic magma generation in the upper crust.

Christelle Wauthier, Benoît Smets, Andy Hooper, François Kervyn, Nicolas d'Oreye

Submission 1099

Steady-rate and long-term ground deformation associated with dry gas vents in the Lake Kivu area

Dry gas vents correspond to an increasing lethal hazard to the local population in the Goma region in the Lake Kivu area (Democratic Republic of Congo). We processed a time series (« StaMPS » [Hooper, 2008]) of an ENVISAT ASAR dataset comprising 47 SAR scenes spanning 16 January 2003 to 25 March 2010, acquired along descending orbits. We identified new deforming areas on the northern shore of Lake Kivu, characterized by line of sight steady ground subsidence of ~ 15 mm/year. Two distinct areas can be identified : one centered on the Rumoka volcanic cone which was built during the 1912 eruption at Nyamulagira volcano, and another one, broader spatially and centered in the Bulengo area. Both areas include dry gas vents that are topographic depressions which release substantive amount of gases (mainly CO₂ and CH₄). The inversion of the StaMPS geodetic dataset led us to infer the presence of at least two deflating hydrothermal reservoirs accounting for the observed deformation. These findings provide crucial information about the deformation behavior and patterns associated with hazardous gas emanations areas in the populated Lake Kivu area and thus bear important implications for natural hazard assessment.

Christopher Waythomas, David Schneider, Kim Van Eaton, William Burton, Cheryl Cameron, Peter Cervelli, Michelle Coombs, Pavel Izbekov, Jessica Larsen, Larry Mastin, Robert McGimsey, Janet Schaefer, Alexa Van Eaton, Kristi Wallace, Rick Wessels

Submission 546

2016-17 Shallow Submarine Eruption of Bogoslof Volcano, Alaska—Preliminary Observations and Eruptive Products at a Back-Arc Volcano in the Southern Bering Sea

Bogoslof volcano is a 75 km³ submarine volcano in the southern Bering Sea near Dutch Harbor, Alaska that began erupting in mid-December, 2016, 24 years after its last eruption in 1992. By mid-March, 2017, the volcano has produced at least 37 explosive events. Analysis of satellite images since mid-December, 2016, show changes in the configuration of Bogoslof Island resulting from proximal deposition of pyroclastic material and wave erosion of the coastline. Eye-witness and satellite observations of volcanic clouds indicate that they typically appear dark at the base, due to ash content, but the upper, higher parts of the cloud are almost always white and ice rich. So far, volcanic clouds have reached altitudes of 6–11 km above sea level, and many plumes have produced abundant lightning (>200 strokes).

Bogoslof Island is the top of a submarine edifice and consists of lava domes and pyroclastic deposits from prior historical eruptions. The pre-eruption area of the island was about 0.3 km². Explosive events have occurred from two or more submerged (2. The eruptive deposits appear fine grained; though full characterization must wait until we visit the island.

Eruptive events on January 30–31 and March 7–8 lasted 1–2.5 hrs. and were among the longest, most energetic events thus far. The January 30–31 event produced a trace amount of crystal-rich ash fall on Unalaska Island 60–100 km east of the volcano and about 0.18 km² of blocky ejecta (up to 2 m diameter) on Bogoslof Island. The March 7–8 event also produced ash fall on Unalaska Island and deposited blocky fallout on Bogoslof Island. It is possible that these longer, more energetic events may have had a greater juvenile magmatic component and produced enough new material to temporarily build a drier vent. Most of the eruptive activity has involved magma-water interactions, though the role of water in individual events may have varied. It is also possible that the events on January 30–31 and March 7–8 could have been the result of shallow Vulcanian explosions.

Cameron Webb, Hugh Tuffen, Jacqueline Owen, Jonathan Castro, Kim Berlo, C. Ian Schipper, Katia Wehbe

Submission 925

Mid-loaf crisis: internal breadcrust surfaces in rhyolitic bombs from Chaitén

Breadcrust bombs ejected in Vulcanian explosions provide useful insights into the state of partially degassed magma within silicic conduits^{1,2}. Dense bomb margins are conventionally thought to reflect rapid thermal quenching of air-cooled magma, with slower cooling of expanded interiors permitting significant post-fragmentation vesiculation in volatile-rich bombs^{1,2}. However, pumiceous rhyolitic bombs emitted in the hybrid phase of the 2008-09 Chaitén eruption exhibit a striking, interconnected network of both external and internal breadcrusted surfaces, which cannot reflect thermal effects alone.

Internal breadcrusted surfaces comprise intersecting curvilinear veins of fine-grained tuffitic material μm - mm in thickness, flanked by dense obsidian selvages that are thickest (to $>500 \mu\text{m}$) where veins intersect. Dense obsidian selvages display strong diffusive H_2O depletion to 0.2-0.3 wt % from a far-field 0.7 wt % in neighbouring expanded domains. Experimental vesiculation at 825 °C and 1Atm confirms suppression of vesiculation beneath a threshold of 0.6 wt % H_2O , and best model fits to measured H_2O diffusion profiles indicate degassing over ~ 4 hours, consistent with plausible bomb cooling timescales. Internal breadcrusting therefore reflects a degassing quench triggered by post-fragmentation gas loss into fracture networks within ejected bombs.

We present a model in which a fragmentation event damaged a shallow magmatic plug, creating a network of fractures that defined bombs but failed to cause complete disaggregation. The fractures created highly localised permeable pathways within initially-dense, low-permeability magma³. This facilitated open-system degassing to near-atmospheric pressure less than a millimetre from parcels of inflating magma undergoing predominantly closed-system degassing. The correlation between thickest dense selvages and the greatest density of intersecting fractures suggests that small-scale spatial variations in permeability within fracture networks, which reflect fracture apertures and connectedness, strongly influence the local efficiency of degassing⁴.

Bomb textures and chemistry provide an illuminating snapshot of transient fracture-mediated degassing, and demonstrate that breadcrust textures may be generated by chemical as well as thermal quenching.

[1] Wright et al 2007 Bull Volc 69, 281-300.

[2] Giachetti et al 2010 JVGR 193, 215-231.

[3] Castro et al 2012 EPSL 333–334, 63–69.

[4] Heap & Kennedy 2016 EPSL 447, 139–150.

Brian Webb, Martin Streck, Mark Ferns, William McIntosh

Submission 1187

Flow units of the Littlefield Rhyolite, eastern Oregon, constraining age and storage sites of Grande Ronde Basalt magmas

The Littlefield Rhyolite consists of widespread, high-temperature, hotspot-related rhyolitic lavas that erupted in eastern Oregon contemporaneous to late-stage Grande Ronde Basalt lavas. The estimated total volume of erupted rhyolites is $\sim 100 \text{ km}^3$ covering $\sim 850 \text{ km}^2$.

This study investigated the stratigraphy and petrology of the Littlefield Rhyolite and whether field and geochemical relationships exist to help constrain the timing and storage sites of Grande Ronde magmas. Although indistinguishable in the field, our data reveal that the Littlefield Rhyolite consists of two geochemically distinct rhyolite flow packages that are designated here as lower and upper Littlefield Rhyolite, according to stratigraphic relationships in the Malheur Gorge. Rarely viewed in sequence, these rhyolites are distinguished by Zr, Ba, Nb, TiO_2 and FeO contents and $^{40}\text{Ar}/^{39}\text{Ar}$ ages (16.12 ± 0.04 vs 16.05 ± 0.04).

Rhyolites known either as 'rhyolite of Cottonwood Mountain' or 'rhyolite of Bully Creek Canyon', and which are exposed around Cottonwood Mountain, NW of Vale, have identical compositions to samples of lower Littlefield Rhyolite. Additionally, single crystal $^{40}\text{Ar}/^{39}\text{Ar}$ ages of two samples (16.12 ± 0.07 , 16.20 ± 0.08) are statistically indistinguishable. Together, this provides unequivocal evidence that lower Littlefield Rhyolite erupted over a minimal distance of 40 km from vents observed within the Malheur River Gorge in the south, to Cottonwood Mountain in the north.

Among units sandwiched between the lower and upper Littlefield Rhyolite are several lava flows and a one-meter thick agglutinated spatter deposit of local Grande Ronde Basalt. The spatter deposit thickens to 10s of meters over a distance of 800 m where the deposit is strongly welded. We now recognize this as a venting site of Grande Ronde Basalt. Ages of Littlefield Rhyolite flow units constrain eruption of local Grande Ronde Basalt to an age span of $\sim 100\text{k}$ years, between 16.05 – 16.12 Ma.

One local variant of late-stage Grande Ronde Basalt is icelanditic ($\sim 61 \text{ wt. } \% \text{ SiO}_2$) and is found at a number of places including a location near the southern extent of the upper Littlefield Rhyolite. Geochemical modeling strongly suggests that icelandite lavas resulted from mixing of Grande Ronde and upper Littlefield Rhyolite magmas, thereby tying a Grande Ronde magma storage site to within the greater Malheur River Gorge area, and indicating contemporaneity of rhyolitic and Grande Ronde magma reservoirs.

Gregor Weber, Luca Caricchi, José Luis Arce

Submission 656

Temporal evolution and pre-eruptive processes at Nevado de Toluca volcano, Mexico

Linking pre-eruptive processes to the frequency at which eruptions of different magnitudes occur is essential to understand the underlying factors controlling the behaviour of volcanoes. To attempt to establish this link it is necessary to study in detail the long-term evolution of magmatic systems.

For this study we sampled the entire ~ 1.5 Ma spanning eruptive history of Nevado de Toluca in Mexico, a subduction-related volcano with well documented effusive and explosive eruptions. We use a combination of whole rock and mineral chemistry, as well as cross-correlation of crystal zoning profiles and high precision U-Th zircon geochronology to compare eruptions of different magnitude, size and style. The first results show that Nevado de Toluca is characterized by a remarkably homogeneous dacitic major element composition, even for contrasting eruptive styles, throughout its eruptive history. This indicates that similar processes in favour of production and extrusion of this magma type must operate on long timescales beneath the volcano. Trace element patterns are also rather restricted in variability for eruptions of different style through time and show enrichment of LREE over HREE. Larger variability is observed for monogenetic cones in the vicinity of the volcano. Interestingly, Nevado de Toluca is characterized by high Sr/Y of up to 90 showing an adakite-like signature. Further work will provide quantitative insights on petrogenetic processes and on the frequency at which intensive parameters changed within the magma reservoir before the eruptions. Our results will be integrated in a global database including other volcanic systems and literature data in an attempt to identify similarities and differences between magmatic reservoirs feeding volcanic eruptions of different magnitudes. The final target of this project is to constrain the physical factors controlling the recurrence rate of volcanic eruptions at regional and global scale.

Gregor Weber, Luca Caricchi, Thomas Sheldrake

Submission 658

The variability of magma compositions sampled by volcanoes: Linking statistical geochemistry and thermal modelling

The chemical diversity observed in genetically related rock suites at individual volcanoes often reflects differentiation processes. However, while some system erupt magmas covering a wide spectrum of geochemical compositions, other volcanoes produce magmas with rather monotonous chemistry. Such different behavior must reflect different processes or maturation stages. While the bulk of compositions erupted can be used to classify particular volcanoes (e.g. andesitic or dacitic volcanoes) and therefore roughly approximate potential eruptive behavior, the underlying reasons why single volcanoes preferentially sample certain ranges of the magmatic spectrum remains enigmatic. We address this problem by taking advantage of the large number of published whole rock analyses for volcanic products from the GEOROC database. We quantify the compositional variability for a large number of volcanoes (n=248) for which abundant high quality major element data is available by calculating a set of statistical parameters that can be used to characterize the chemical diversity of each particular eruptive center. In order to identify differences and similarities between compositionally diverse volcanoes we link these statistical data to a number of system specific variables. First, we evaluate the role of regional scale tectonic and crustal parameter that could potentially influence the chemical diversity of volcanoes. As the compositional variability within individual volcanic regions and at neighboring volcanoes can be comprehensive, local factors at the scale of individual volcanoes need to be considered. We use thermal modelling coupled with published experimental phase equilibria to explore how magma fluxes could be linked to magma diversity at individual eruptive centers. Our study is an attempt to link the chemistry of erupted magmas to specific tectonic parameters, plumbing system architecture and thermal evolution of magma reservoirs.

Peter Webley, Catherine Cahill, Marty Rogers, Michael Hatfield

Submission 543

**Alaska Center for Unmanned Aircraft Systems Integration (ACUASI):
Operational Support and Geoscience Research**

Unmanned Aircraft Systems (UAS) have enormous potential for use in geoscience research and supporting operational needs from natural hazard assessment to the mitigation of critical infrastructure failure. They provide a new tool for universities, local, state, federal, and military organizations to collect new measurements not readily available from other sensors. We will present on the UAS capabilities and research of the Alaska Center for Unmanned Aircraft Systems Integration (ACUASI, <http://acuasi.alaska.edu/>). Our UAS range from the Responder with its dual visible/infrared payload that can provide simultaneous data to our new SeaHunter UAS with 90 lb. payload and multiple hour flight time. ACUASI, as a designated US Federal Aviation Administration (FAA) test center, works closely with the FAA on integrating UAS into the national airspace. ACUASI covers all aspects of working with UAS from pilot training, airspace navigation, flight operations, and remote sensing analysis to payload design and integration engineers and policy experts. In addition to using built in payloads on our UAS, we have developed our small UAS Ptarmigan to include a small FLIR and high precision dual frequency GPS that can provide decimeter precision mosaiced maps and develop digital surface models of the volcanic landscape. Also, we have been working on including optical particle counters and mini-gas sensors to measure ash particle size fraction and gas content respectively, as well as infrared thermal cameras with neutral density and narrow band filters to record temperatures higher than the current limits of small infrared cameras and measure the brightness temperatures at different wavelengths to develop multispectral maps of the surface. We will demonstrate how UAS can be integrated in operational support systems and at the same time be used in geoscience research projects to provide high precision, accurate, and reliable observations.

Aaron Wech, Matt Haney

Submission 1148

Probing Bogoslof volcano eruption dynamics using a catalog of repeating earthquakes

Bogoslof volcano, a submarine backarc stratovolcano in the Bering Sea, began erupting in December 2016 after 25 years of inactivity. The eruption sequence has so far consisted of >37 significant explosions recorded by seismic and infrasound sensors on the nearby islands 50-100 km away. Explosive episodes have varied in duration and seismic amplitude, and observable seismicity has been characterized by a combination of discrete earthquakes and continuous tremor. Several explosions have been preceded by sequences of repeating earthquakes from 10s of minutes to hours before the eruption, enabling short-term eruption forecasting. The repeating earthquakes often show linearly decreasing inter-event times and inverse moment rates as the events merge into a continuous tremor signal with distinct spectral properties compared to co-eruptive tremor. Some explosions have coincided with earthquakes occurring during phases of co-eruptive tremor, and occasionally post-eruption. Many of these earthquakes have been located by AVO analysts with magnitudes of $ML \sim 1-1.5$. Here we present the results of a match-filter analysis using templates derived from phase-weighted stacks of known event clusters in the AVO earthquake catalog. We apply this method to a single station ~ 73 km from Bogoslof between September 1 and March 15 to detect thousands of earthquakes ranging from $ML \sim 0.3-1.8$. Location uncertainties suffer from poor network coverage owing to distal stations to the south, and no stations north, of Bogoslof. However, the magnitude variability and temporal resolution of the match-filter catalog offers a detailed investigation of pre-, co- and post-eruption dynamics for dozens of distinct explosions and is a valuable tool for understanding the overall evolution of the system throughout its months-long eruption sequence.

Anne Weit, Olivier Roche, Thierry Dubois, Michael Manga

Submission 180

Experimental study of the solid phase concentration in volcanic turbulent gas-particle mixtures

Volcanic gas-particle mixtures such as plumes and pyroclastic density currents may have a wide range of particle concentrations. This work addresses the dynamics of dilute mixtures in which the particles are carried by the turbulent gas. Though previous studies suggest that such mixtures have particle concentrations of the order of one volume percent the dependence of the solid concentration with the Reynolds number is unclear. We addressed this issue through laboratory experiments performed in a vertical tube where gas-particle mixtures were created by injecting a turbulent air flow. Monodisperse mixtures of glass beads of different grain sizes (77 μm , 206 μm , 307 μm , 467 μm , 705 μm , 1.5 mm) were used with varying mean concentrations from 0.025 to 8 vol. %. The particles were injected stepwise between runs. To create a stable homogenous mixture, the mean air velocity was set to match the terminal particle settling velocity for the different grain sizes. Thus air velocities of 0.5-9.6 m/s and corresponding Reynolds numbers of ~ 3000 -60000 were used. Pressure values at the base of the tube nearly matched the weight of the particles divided by the cross sectional area of the tube. This suggests that the weight of the particles was transmitted through the gas phase even for very dilute mixtures down to 0.025 vol.%. Above a critical particle concentration, at which all the particles were carried by the turbulent flow, subsequent injected particles were not maintained in the mixture and instead settled to the base of the tube to form a dense fluidized bed. This critical concentration was found by two different methods: (1) using a ball with a slightly lower density than that of a dense bed, which was placed at the base of the tube before the air flowed, and (2) with an additional pressure sensor placed above the top of the dense bed. For the first method the ball rose once the dense bed formed when the turbulent mixture above it reached the critical particle concentration. For the second method the pressure values were similar to those at the base until the critical concentration of the mixture above the sensor was reached and then the pressure was constant. Both methods yielded similar critical concentrations of 1.7 ± 0.2 vol.% independent of the Reynolds number. This result gives insights into the maximum particle concentrations of volcanic dilute gas-particle mixtures.

Jay Wellik, Sarah Ogburn, Jeremy Pesicek, Stephanie Prejean, Weston Thelen

Submission 547

Analyzing the temporal relationship between changes in seismic rate, seismic energy release, and eruptive behavior at U.S. volcanoes

The United States Geological Survey Volcano Disaster Assistance Program (USGS-VDAP) uses multi-disciplinary conceptual models in order to interpret and synthesize geologic and monitoring data for the purpose of generating probabilistic eruption forecasts. In the conceptual progression of seismic activity preceding eruptions, distal volcano tectonic swarms are usually the first detected signs of unrest, followed by proximal volcano tectonic swarms, then followed by low frequency and hybrid events below the summit. This model has been developed primarily to explain seismicity preceding the first vent opening eruption after a significant repose, but here we test its utility to explain major changes in intra-eruptive behavior as well. Specifically, we seek to determine whether seismic rate changes or cumulative seismic moment changes reliably precede changes in eruptive behavior during intra-eruptive time periods. We use eruption chronologies from all monitored eruptions in the U.S., which includes eruptions at stratovolcanoes, shield volcanoes, and caldera systems. We search for similarities and differences between pre-eruptive and syn-eruptive seismic patterns as well as overall similarities and differences in behavior between volcanoes with long-repose periods (i.e., “closed system” volcanoes) and volcanoes with frequent or prolonged eruptions (“open system” volcanoes). We present a simple methodology that uses eruption chronologies and earthquake catalogs in hopes that our test can be replicated in other regions where data are sufficient. This work is part of the Eruption Forecasting Information System (EFIS) project – an ongoing initiative by VDAP to quantitatively test the success rate of the conceptual models employed for eruption forecasting through the use of databases, monitoring data, and statistical analysis.

Cenozoic tectonic evolution of the Cascadia convergent margin, western North America

Ray E. Wells

Plenary Talk

The Cascadia convergent margin consists of a young Juan de Fuca plate subducting northeast at about 40 mm/yr beneath western North America to produce the Cascade volcanic arc, extending more than 1000 km from British Columbia to N. California. The arc is built across the suture between Paleogene oceanic tholeiite of the Siletz terrane in the forearc and older Mesozoic rocks of the continent. The history of this margin highlights a basic question: is magmatism mainly a response to plate motions – mantle flow driven by subduction, slab rollback, and passive spreading, or is it driven in part by a deep-seated, long lived Yellowstone Hotspot (YHS)? I use geologic mapping, geochronology, paleomagnetism, geodetic (GPS) data, and a modern plate motion model to construct a 4-part history that examines possible roles of mantle flow and a long-lived YHS: 1) Origin and accretion of Siletzia – U-Pb and $^{40}\text{Ar}/^{39}\text{Ar}$ ages, global coccolith zones, and paleomagnetism show that the basalts were erupted offshore 56–49 Ma, and accretion was completed between 51 and 49 Ma in Oregon. Siletzia's composition, 17-30 km crustal thickness, rapid eruption, location, and timing of accretion are consistent with formation as an oceanic plateau at the location of a fixed YHS. 2) Post accretion forearc rifting and magmatism – 8 m.y. after accretion, margin-parallel extension of the forearc and regional dike swarms fed voluminous tholeiitic to alkalic basalts of the Tillamook magmatic episode (41.6 Ma), which interfinger with coal bearing strata and arc-derived tuffs. 3) The Cascade arc – initiated at about 40 Ma. Paleogene arc rocks of the Western Cascades are buried to the east by younger volcanics of the modern arc. The southern arc is dominantly extensional, with numerous basaltic vents; the northern arc is built on uplifted pre-Tertiary basement. Plutons of the Miocene arc axis are offset clockwise from the present arc, indicating 4) Clockwise rotation and dextral shear of Cascadia, as documented by paleomagnetism, GPS velocities, and seismicity. Block rotation and slab rollback driven by toroidal and return mantle flow contribute to arc migration outboard of an expanding Basin and Range province. Siletzia's 56 Ma origin and the 42 Ma Tillamook episode on the leading edge of N. America both coincide with the location of a fixed YHS in a plate motion model that includes PNW rotation. Later arc migration and Newberry trend magmatism are consistent with plate-driven mantle flow.

Cynthia Werner, Christoph Kern, Diego Coppola, Daniel Rasmussen, Peter Kelly, John Lyons, Kristi Wallace, David Schneider, Rick Wessels

Submission 453

Linking gas emissions, lava extrusion, and melt S contents for a better understanding of shallow magmatic processes at Mount Cleveland volcano, Alaska

Mount Cleveland (1730 m) is one of the most active volcanoes in the Aleutian arc and has erupted at least 21 times in the last century. Open-vent activity at the volcano in recent years has been characterized by elevated temperatures in the summit area as observed in satellite data, nearly continuous degassing, intermittent minor explosions, and periodic dome growth. To better understand the shallow magmatic system, we combine measurements of volcanic gas compositions and emission rates from August 2015 and July 2016, lava extrusion rates calculated from thermal output in satellite data (2011 to 2015), and the first estimates of primary S contents from olivine-hosted melt inclusions. SO₂ emission rates measured with helicopter-borne DOAS were 600 ± 39 t/d in 2015, and 324 ± 55 t/d in 2016. CO₂/SO₂ ratios measured with an airborne Multi-GAS system were 2S was not detected, consistent with degassing from shallow magma. Higher emissions in 2015 are consistent with the extrusion of a dome in the weeks preceding the degassing measurements, as opposed to the 2016 measurement period when no dome growth occurred in months preceding the measurements. Thermal anomalies derived from MODIS data from 2011 to 2015 had an average repose time of only four days, pointing to continual shallow magmatic activity. Rapid increases in the thermal output were often coincident with visual observations of dome growth in satellite images. The average rate of lava extrusion calculated for nine such periods between 2011 and 2015 was $0.28 \text{ m}^3 \text{ s}^{-1}$, and the total volume extruded was between 1.9 and 5.8 million m³. The thermal output from these observed events of lava extrusion, however, only accounts for roughly half of the cumulative thermal budget, suggesting an additional low-level heat source that is most likely shallow magma. Assuming that 600 t/d of SO₂ was released from the lava supplying the July 2015 lava extrusion event (0.16 – 0.48 million m³), we calculate a primary S content of 0.3 - 1 wt. %. This estimate is greater than the highest S content (0.15 wt. %) measured in olivine-hosted melt inclusions from recently erupted tephra. Thus, we suggest that convection of magma to the upper conduit can account for both the excess degassing and heat loss at Mount Cleveland.

Elizabeth Westby

Submission 435

“Reality” social media engages viewers and builds a following: USGS Volcanoes Mount St. Helens eruption anniversary series delivers an insider’s perspective on the events surrounding May 18, 1980.

For the 35th anniversary of the May 18, 1980 eruption of Mount St. Helens, USGS Volcanoes Facebook took followers behind the scenes to experience what it was like to be a scientist as events unfolded. Daily posts included details about changes in volcanic activity, how scientists responded, and the challenges faced in communicating eruption uncertainties with the media and the public. The 96-post series gave a significant boost to the newly-established USGS Volcanoes Facebook page, nearly doubling the total page Likes in two months. Telling the eruption’s backstory elevated the page as an authoritative source of information, established rapport with a multi-generational audience, and firmly rooted USGS Volcanoes in the social media community.

The posts began on March 19 and continued for 74 days—the duration of the run-up to the eruption and two weeks of aftermath. The posts extracted chronologies and descriptions of events from the book by USGS scientist Richard Waitt “In the Path of Destruction, Eyewitness Chronicles of Mount St. Helens”. These were combined with USGS images, graphics, b-roll video of scientists’ recollections and scanned newspaper articles. In total, 119 photos, 34 newspaper scans, 19 videos, and 16 graphics were shared with viewers. On May 18, 21 posts were scheduled throughout the day to coincide with the timing of key events, from an early morning radio check with David Johnston at Coldwater II, to the landslide, lateral blast, accounts of eruption survivors, and the final realization that Coldwater II was gone. The posts concluded May 31 with a final emphasis on lessons learned.

USGS Volcanoes responded to comments throughout, correcting misperceptions and supplementing historical accounts with current information on volcanic hazards and monitoring. Written comments also provided insight into how the posts were received, with viewers expressing appreciation for the re-telling of an enthralling story. Many shared where they were on May 18 or how Mount St. Helens has affected their lives and families.

Our experience shows that consecutive multi-media posts are an effective social media content strategy. During the series, page Likes grew from 8,600 to over 15,700. The daily total Reach ranged from 5,400 to 575,000. A video post of the eruption column on May 18 had a Reach of 253,000, was viewed 81,000 times and shared nearly 1,800 times. Since then, page Likes continue to steadily increase, now at 46,000.

Patrick Whalen, Frank Ettensohn

Submission 1222

THE OLIGOCENE WEST ELK BRECCIA: EVIDENCE FOR MASSIVE VOLCANIC DEBRIS AVALANCHES IN THE EASTERN GUNNISON RIVER VALLEY, WEST-CENTRAL COLORADO, U.S.A.

The West Elk Breccia has been known and studied since the late 1800's and many interpretations have been suggested. Inasmuch as the unit represents several types of volcanoclastic sedimentation, several interpretations may be warranted for various parts of the unit. However, one type of sedimentation that has not been broached is the possibility of debris-avalanche deposits, and close examination of the West Elk deposits in this study has recognized evidence for debris-avalanche deposits at three different scales: volcano scale, outcrop scale, and intra-outcrop scale. At the volcano scale, a preserved scarp in basal parts of the old volcano reveals underlying Mesozoic bedrock, suggesting the likelihood of mass movement as debris avalanches. At the outcrop scale, a series of mega-blocks, some as large as hundreds of meters in maximum length, retain bedding formed proximally, have atypical orientations, and are surrounded by a tuffaceous conglomeratic material that served as a matrix during movement. Contacts between mega-blocks and matrix occur at irregular, commonly high angles. At the intra-outcrop scale, matrix is "injected" into fractures at all scales, resulting in jigsaw-fit fracturing, an indication of non-turbulent flow that allowed the flows to rip up and preserve clasts of soft shale seen in the distalmost matrix deposits. From medial-to-distal matrix deposits, volcanoclast content decreases by 23%; Paleozoic and Mesozoic clasts increase by 5%; and the overall size of mega-blocks decreases. The geochemical and petrographic signatures of this very heterogeneous formation reveal a pyroxene-andesite composition for the breccia with a more silicic matrix facies, along with accompanying andesitic to dacitic tuffs in the east Elk Creek Tuff, all of which corroborate previous work on this northern extension of the San Juan volcanic field. The study area includes about 100 km², and measured sections allow for an estimation of total breccia volume at about 8.5 km³.

Patrick Whelley, Stephen P. Scheidt, W. Brent Garry, Jacob Richardson, Christopher W. Hamilton, Jacob Bleacher

Submission 497

Comparison and fusion of ultra-high-resolution topographic data at Kīlauea volcano, Hawaii

We acquired ultra-high-resolution (~10 cm/pixel) digital elevation models (DEMs) of the December 1974 lava flow on Kīlauea Volcano using Terrestrial Laser Scanning (TLS) and kite-based systems. Each data set covers ~1 km² and helps to understand the emplacement and modification of this deposit. However, the topographic measurements were acquired using vastly different technologies and perspectives (TLS from the surface and kite-based imaging from the sky). We seek to quantify the similarities and differences of the resulting products, including the quality of the data acquired by each method individually, and the gains made by fusing both products.

TLS is an active remote sensor, using a near infrared laser that enables line-of-sight observations even within regions that lack illumination, which are undetectable to passive camera systems. TLS provides point clouds with observations on vertical faces and inside caves, but horizontal resolution drastically decreases with distance from the scanner due to occultation of the laser by high-standing topography. Kite-based (or another airborne platform) photography is downward viewing, overcoming the data-gap limitation of TLS, but lacking observations where surfaces are occulted from a near-nadir view (i.e., beneath overhanging ledges). Kite images are used to generate DTMs through Multi-View Stereo-Photogrammetry (MVSP). Both TLS and MVSP products use Differential GPS for accurate georeferencing; therefore, these data can be combined.

We assessed DEM reliability by quantifying uncertainty in the model's source point cloud. Point density is a proxy for uncertainty: fewer observed points correspond to greater uncertainty at the location of interest. Uncertainty is calibrated using Monte Carlo Resampling in high point density areas. Known DGPS tie point locations are used to co-locate DEMs, which are then merged by averaging elevation values, weighted by their modeled uncertainties.

Each method has advantages and disadvantages and the best system to choose depends on the application, and resources. A DEM made using both has fewer occultation holes than TLS alone and includes more vertical faces, shadowed regions, and cave interiors than MVSP alone. By quantifying uncertainty in individual DEMs and in a fused DEM we can evaluate past data collection efforts and better allocate resources for future field campaigns to study volcano morphology with ultra-high-resolution topography.

Patrick Whelley, W. Brent Garry, Christopher W. Hamilton, Jacob Richardson, Jacob Bleacher

Submission 492

Using roughness patterns to study volcanic deposit textures in remotely sensed topographic data

For the experienced field geologist, volcanic deposit morphology provides a rapid and reliable basis for identifying the nature and geologic histories of these materials. Planar sheet-like pyroclastic deposits are smooth at the meter to decameter scales and are indicative of high-velocity flows of small particles (mostly ash-sized). Lobate pyroclastic deposits bound by levees are rough at the meter scale and are indicative of comparatively lower flow velocities and higher concentrations of larger pumices. In contrast, *aa* lava deposits commonly contain levees and clinkers, are rough at the millimeter to decameter scales, and are indicative of high flow velocities or higher viscosity. Pāhoehoe deposits are lobate and smooth at the decameter scale and are indicative of low flow velocity or lower viscosity. These simple relationships are useful in the field, but are insufficient when using remote-sensing data alone to assess deposit morphology. A reliable tool for quantitatively identifying and differentiating volcanic deposits would improve volcanic mapping efforts in remote regions on Earth and would produce a significant advancement in planetary volcanology.

Surface roughness patterns provide a quantitative method for evaluating volcanic deposits by using co-occurrence statistics to measure entropy (ENT) and homogeneity (HOM) in deposit topography. At the meter scale, lobate pyroclastic deposits from the Mount St. Helens (MSH) 1980 eruption have low ENT and high HOM. *aa* lava from the Muliwai a Pele lava channel, Mauna Ulu, Hawai'i, has high ENT and low HOM while pāhoehoe lava adjacent to the channel has lower ENT and higher HOM and is less rough than the MSH pyroclastics. Using these sites as analogs for planetary examples and newly available meter scale topography from the High Resolution Imaging Science Experiment we evaluate volcanic deposits on Mars. Roughness patterns surrounding a lava channel near the Tartarus Colles in Elysium Planitia (171.25° E, 24.85°N) Mars are consistent with pāhoehoe lava suggesting low emplacement velocities or viscosities. A lava flow within an impact crater in another region of Elysium Planitia (159.77° E, 01.04° S) contains both patches of high ENT with low HOM and low ENT with high HOM suggesting a complex emplacement history with episodes of both slow and fast moving lava.

We use these statistical measures to evaluate emplacement and degradation histories of volcanic deposits across a variety of volcanoes.

Robert White, Marie Edmonds, John MacLennan, Jennifer Jenkins

Submission 36

Deep Crustal Magma Plumbing in Iceland from seismicity, geochemistry and petrology

We have mapped magma transport paths from the deep (20 km) to the shallow (6 km) crust and in two cases to eventual surface eruption under several Icelandic rift volcanoes (Askja, Bardarbunga, Eyjafjallajökull, Upptyppingar). We use microearthquakes caused by brittle fracture to map magma on the move and tomographic seismic studies of velocity perturbations beneath volcanoes to map the magma storage regions. High-frequency brittle failure earthquakes with magnitudes of typically 0-2 occur where melt is forcing its way through the country rock, or where previously frozen melt is repeatedly re-broken in conduits and dykes. The Icelandic crust on the rift zones where these earthquakes occur is normally ductile at depths greater than 8 km beneath the surface, so the occurrence of brittle failure seismicity at depths as great as 20 km is indicative of high strain rates, for which magma movement is the most likely explanation. We suggest that fractionation of magma and consequent high vapour pressures caused by the exsolution of carbon dioxide-rich fluids in the deep crust is driving magma movement through cracks and dykes connecting deep crustal sills. Moment tensor solutions of the seismic events show they are often caused by opening cracks. We compare the depths of deep crustal sills mapped using microseismicity with petrological barometers of storage depths determined from the solidified products of Icelandic eruptions and find that both measures consistently show that melt resides at many different depths in the crust. Seismic velocity constraints from seismic refraction, tomography and receiver function studies can also be reproduced by modelling fractionation histories of primitive melts injected into the Icelandic crust.

We thank members of the Cambridge Volcano Seismology Group for incalculable assistance in both fieldwork in Iceland and in processing the recorded seismic data over the last decade.

Alan Whittington, Arianna Soldati, Jordon Beem, Tim Robertson, Francisco Gomez

Submission 257

Reconstructing a Monogenetic Eruption: Rheology and Morphology of a ~7ka Flow from the Cima Volcanic Field (CA)

We present a rheological and morphological study of a Holocene lava flow emitted by a monogenetic cinder cone in the Cima Volcanic Field, eastern California. Our field observations focused on surface morphology, which transitions from smooth pahoehoe ropes near the vent to jagged blocks over the majority of the flow, and on channel and levée dimensions. We collected airborne photogrammetry data and used it to generate a digital elevation model. From this, the total flow volume was estimated and surface roughness was quantified in terms of standard deviation of the real surface (5cm resolution) from the software-generated 1m-average plane. Sample textural analyses revealed that the near-vent portion of the flow is significantly more crystalline ($f_{xtal}=0.95\pm 0.04$) than the main flow body ($f_{xtal}=0.66\pm 0.11$). The rheology of Cima lavas was determined experimentally by concentric cylinder viscometry between 1550 °C and 1160 °C, including the first subliquidus rheology measurements for a continental intraplate trachybasaltic lava. The experimentally determined effective viscosity increases from 54 Pa·s to 1,361 Pa·s during cooling from the liquidus (~1230 °C) to 1160 °C, where crystal fraction is 0.11. Flow curves fitted to measurements at different strain rates indicate a Herschel-Bulkley rheological behavior, combining shear-thinning with a yield strength negligible at the higher measured temperatures but increasing up to 357 ± 41 Pa at 1160 °C. The lava viscosity over this range is still lower than most basaltic melts, due to the high alkali content of Cima lavas (~6 wt% Na₂O+K₂O). By combining field observations and experimental results, we reconstructed the emplacement history of the Cima flow. We determined that the morphological pahoehoe to blocks transition of this trachybasalt occurs at a temperature of 1160 ± 10 °C, similar to that observed for Hawaiian tholeiitic lavas, but at higher apparent viscosity values. Monogenetic volcanism in the Western United States is typically characterized by low effusion rates and eruption on sub-horizontal desert plains. Under these low strain-rate conditions, the pahoehoe to blocks transition is likely to occur abruptly upon minimal cooling, i.e. very close to the vent, but lava tubes may transport fluid lava to flow fronts rapidly, allowing breakouts to extend the flow length, as we infer happened for the Cima flow.

Christina Widiwijayanti, Fidel Costa, Nang Thin Zar Win, Erickson Fajiculay, Christopher G. Newhall, Antonius Ratdomopurbo, WOVO Observatories

Submission 969

WOVOdat As A Localhost Solution For Archiving, Retrieving, And Visualizing Volcano Monitoring Data

Most volcanic eruptions are preceded and accompanied by a period of unrest. But volcanoes behave differently, not all give sign of unrest, and not all signs are necessarily followed by an eruption. During periods of volcanic unrest, volcanologists need to interpret monitoring data to be able to forecast whether an eruption is likely to occur, to better anticipate the eruption outcome, and implement timely mitigation measures. The advances in monitoring techniques now allow collecting large amounts of multi-parameter data and information in a short time, which generates an increasing volume of data to archive and process. Therefore, an efficient and robust system of managing, archiving, and processing large volume of data is crucial to achieve good quality surveillance and successful crisis response. WOVOdat (www.wovodat.org) has developed a stand-alone monitoring database system at volcano observatory level for: (1) Efficient and systematic data archiving system, (2) interactive retrieval and display of historical and current data, including synchronized time plots of changes in various parameters, (3) Comparisons of unrest within or between analogous volcanoes.

A standalone package, an open source system, is freely available for observatories that wish to adopt WOVOdat and develop their own database for managing volcano monitoring data. We provide a ready installable MySQL database template as well as interactive tools for user to submit, query, and visualize data. Users may consult and download documentation (user manual, SQL schema, XML format, table formats). The WOVOdat standalone version is operational and being used in PHIVOLCS (Philippines), CVGHM (Indonesia), RVO (Papua New Guinea), and NIED (Japan). We welcome collaboration with other - observatories.

Thomas Wilkes, Tom Pering, Andrew McGonigle, Jon Willmott

Submission 797

The application of low-cost imaging sensors to the remote sensing of volcanogenic sulphur dioxide

The quantification of volcanic SO₂ flux plays a key role in the monitoring and research efforts at active volcanoes. In particular, ultraviolet (UV) remote sensing techniques are applied, such as the spectroscopic differential absorption spectroscopy (DOAS) and UV imaging (e.g., the SO₂ camera). DOAS retrievals, using UV spectrometers, can provide accurate SO₂ column densities, where the high spectral resolution facilitates the correction of certain radiative transfer effects. More recently, the advent of SO₂ cameras has provided much higher spatial and temporal resolutions, enabling integration with other geophysical datasets, allowing detailed investigation of eruption dynamics and subsurface processes. Although nominally cheap (\$1,000-10,000s), the cost inhibits the widespread proliferation of these instruments to aid with volcanic hazard assessment, particularly given that a large proportion of active volcanoes are located in developing countries, where funds are limited.

Here, we detail the modification of a low-cost camera sensor, primarily designed for the smartphone market, to increase its sensitivity to UV radiation. We have designed optical systems around the Raspberry Pi-based sensor, to manufacture both low-cost UV cameras (for use as an SO₂ camera) and spectrometers (for DOAS retrievals). In both instances, optical housings were 3D printed using a publicly available selective laser sintering service. A side-by-side comparison of our SO₂ camera with a JAI system which is routinely deployed for volcanic SO₂ measurements indicates that our system performs remarkably well, with flux measurements on Mount Etna, Italy, showing a strong linear relationship between the two units ($r^2=0.92$). Preliminary tests of the spectrometer show that it has sufficient signal and spectral resolution to perform DOAS retrievals, and deployment at Drax Power Station, UK, corroborates this. With costs for each instrument approximately an order of magnitude, or more, cheaper than their commercial counterpart, the good performance of these low-cost alternatives highlights that they could greatly benefit the volcano research and monitoring community. Ongoing development of a user-friendly, open-source, Python code to accompany the systems, which aids in data acquisition and analysis, will allow non-specialist personnel to operate the instruments with relative ease.

George Williams, Colin Frewan, Sterling Morgan, Ben Kennedy, Thomas Wilson, Allan Scott, Alex Watson

Submission 916

Ballistic cannon experiments quantify the vulnerability of buildings impacted in a multi-hazard ballistic and ash fall context

Recent volcanic eruptions with little useful warning have created a ballistic hazard leading to a number of casualties and building damage. This has heightened the need for effective assessment and management of volcanic ballistic risk. Attempts to produce quantitative ballistic risk assessments which can adequately predict likely impacts have been limited by 1) insufficient building vulnerability data and 2) an overly simplistic approach of assessing the damage caused by ballistic impacts in isolation, without consideration of the potential for multiple volcanic hazards to either exacerbate or reduce total damage. An improved, quantitative understanding of how different building types perform under ballistic impacts in conjunction with other volcanic hazards such as tephra fall is vital for informing risk models and appropriate life safety actions.

To address this lack of quantitative vulnerability data we conducted a series of experiments using a pneumatic cannon to simulate ballistic impacts to tephra covered, reinforced concrete and sheet metal roofs. We found that tephra deposits over 100 mm thick were able to increase a structure's resistance to ballistic damage by increasing the relative thickness of material being impacted and by providing a compactable energy absorption barrier. Tephra deposits of various thicknesses, compositions and grain size distributions were used to assess the energy absorption capacities of deposits likely to accumulate on roofs by a range of ballistic producing eruption styles.

Our experiments show that as the thickness of a tephra deposit on top of a roof increases, the risk of roof perforation by ballistics is reduced. However, increasing tephra thicknesses on roofs also brings increased risk of roof collapse due to overloading. In cases where ballistics perforate tephra covered roofing materials, large amounts of tephra surrounding the perforation are able to enter the building causing further damage to the building interior. These experiments provide evidence of how buildings might perform differently when they are impacted by multiple, compounding and interacting volcanic hazards compared to impacts from individual hazards. The ability tephra deposits have to increase a building's impact resistance to ballistics could be utilised as a means of reducing the risk of death by ballistics during eruptions but further investigation into appropriate mitigation measures is required.

Rebecca Williams, Michael Branney, Tiffany Barry, Michael Norry

Submission 905

Mapping the interaction of a pyroclastic density current with irregular topography: the chemically-zoned, low aspect-ratio Green Tuff ignimbrite, Pantelleria, Italy

Near circular ignimbrites are emplaced by particularly hazardous, radial, high-velocity pyroclastic density currents from large-scale eruptions. Their circular distribution has been inferred to record simultaneous flow in all directions from source, overtopping hills rather than passively flowing down valleys. We used detailed chemical mapping to show how the response of an individual pyroclastic current to topographic barriers changed with time – the current first flowing around hills, and later (during peak flow) overtopping them. The pristine, welded Green Tuff ignimbrite (aspect ratio ~1:3125) was deposited over irregular topography during the most recent (c. 46 ka) large explosive eruption on Pantelleria, Italy. The main (low aspect-ratio) ignimbrite flow-unit is gradationally zoned, systematically from pantellerite (base) to trachyte (top), and indicates that the composition of the pyroclastic density current gradually changed with time. Different geographic distributions of the individual compositional zones within the ignimbrite have enabled us to reconstruct a succession of snapshots of the current's evolution. The geographic 'footprint' of the current changed with time as the current gradually waxed and later waned (Williams et al. 2014). When the current initially encountered a hill or barrier, it was not able to overtop the hill. First it was blocked, reflected, or deflected around the lower flanks of barriers, including conical hills and transverse ridges. But as the current waxed, it progressively inundated, and then overtopped hills, during peak flow conditions. Later, as the current waned, it gradually retreated from summits, and once again became blocked or reflected by the hills. Such incrementally shifting responses of a pyroclastic density current to topography is consistent with shifting depositional patterns recorded in ignimbrites elsewhere (e.g. Poris ignimbrite, Tenerife; Brown and Branney 2013). Such behaviour would probably be easily overlooked in ignimbrites that do not show compositional zoning, but is to be expected wherever density currents are sustained, and should probably be considered when assessing hazards at explosive volcanoes.

Brown RJ, Branney MJ 2013. doi 10.1007/s00445-013-0727-0

Williams R, Branney MJ, Barry TL 2014. doi 10.1130/G34830.1

Marie-Claude Williamson, Gordon N. Oakey

Submission 702

Comparative geochemical and geophysical studies of volcanic rocks from the High Arctic Large Igneous Province (HALIP) and the Alpha Ridge, Arctic Ocean

The Canadian portion of the High Arctic Large Igneous Province (HALIP), exposed on Axel Heiberg Island and northern Ellesmere Island, consists of continental flood basalts, sills and dykes (~125-90 Ma); ferrobasaltic lava flows and associated intrusions (~92 Ma); and bimodal alkaline igneous rocks (~88-80 Ma). The HALIP magmatic event was triggered by tectonic rejuvenation of the Sverdrup Basin and the opening of the Arctic Ocean in the Early Cretaceous. Offshore, the Alpha-Mendeleev Ridge Complex (AMRC) is a first-order physiographic and geological feature of the Amerasia Basin that is characterized by high amplitude “chaotic” magnetic anomalies associated with large-scale regional magmatism. The approximate areal extent of the AMRC is $\sim 1.3 \times 10^6$ km², suggesting a total volume of igneous rocks of $\sim 20 \times 10^6$ km³. The only dated volcanic rock sample recovered from the Alpha Ridge is ~ 89 Ma.

The Hansen Point Rift Volcanics (HPRV) consist of bimodal alkaline igneous rocks that were emplaced during the waning stages of the HALIP event. Previous studies have shown that lava flows consist of picritic basalt, alkali basalt, trachyandesite, trachyte and peralkaline rhyolite erupted from central vents. Whole rock geochemical analyses acquired for this study suggest that high-MgO lava flows (8.5-13.3 wt.%) have FeO* values of 8.9-10.7 wt.%; TiO₂ values of 1.2-2.4 wt.%; are LREE-enriched (LaN/SmN: 3-5); and have low contents of HREE (e.g. Lu: 0.26-0.37). The most magnesian lava flow analysed so far is a ferropicrite with olivine (Fo₈₄₋₈₇) and Ti-rich diopside phenocrysts set in a glassy matrix. This result is of interest to us because ferropicrites of Phanerozoic age occur as low volume lava flows or thin dykes associated with continental flood basalt provinces. They typically show high values of MgO, FeO*, Ni and Cr; moderate values of SiO₂, and low values of Al₂O₃ and HREE, and are interpreted as Fe-rich melts generated from a mantle plume.

In August 2016, approximately 100 kg of volcanic rocks were successfully dredged from the Alpha Ridge during a collaborative Canada-Sweden Polar Expedition under Canada’s UNCLOS (United Nations Convention on Law of the Sea) Program. We present new mineralogical, geochemical and magnetic susceptibility data for the onshore HPRV and volcanic rocks dredged from the Alpha Ridge. The results highlight the petrological significance of ferropicrites with implications for the magmatic evolution of the onshore HALIP and offshore AMRC.

Colin Wilson, Elliot Swallow, Bruce Charlier, John Gamble

Submission 230

Diverse and contrasting mafic influences on the magmatic systems of the 2.08 Ma Huckleberry Ridge eruption, Yellowstone

The Yellowstone Plateau volcanic field (YPVF) is the currently active focus of the Yellowstone-Snake River Plain (YSRP) volcanic province. The YSRP is a quintessential example of bimodal volcanism¹, with mantle-derived olivine tholeiites providing the thermal and volatile fluxes to generate the voluminous rhyolitic volcanism [2]. However there are also scattered lavas of contrasting compositions, dominantly trachybasalts and trachyandesites but ranging continuously up to high-Ba rhyolite, which collectively define a Craters of the Moon (COM) trend. The COM eruptives are often found at the edges of the YSRP and are interpreted to represent small-volume magma batches derived by extreme mid-crustal fractionation of a tholeiitic parent [1,3-4].

The ~2,500 km³ Huckleberry Ridge Tuff (HRT), the first of three caldera-forming eruptions in the YPVF, consists of initial fall deposits, followed by three ignimbrite members (A, B and C) and with further fall deposits between ignimbrites B and C₂. The HRT was preceded and followed by the eruption of YSRP olivine tholeiites from an area spanning the inferred caldera². Previously identified² aphyric scoria in ignimbrite B, and a newly identified juvenile mafic component in ignimbrite A are compositionally similar to each other, with Ba to 3500 ppm, Zr to 1850 ppm and P₂O₅ to 1.8 wt%. These mafic compositions define a 'HRT-COM' trend, parallel to but offset to higher Ba from that defined by younger surficial COM lava flows west of the HRT caldera.

We here summarise major, trace and isotopic data from these three mafic suites, which temporally bracket the HRT eruption. We compare them with other data from the COM suite and evaluate interpretations for their genesis, which range from extreme fractional crystallisation to melts from metasomatised mantle. We propose that the most likely source for the 'HRT-COM' magmas, in close spatial proximity to olivine tholeiites, is heterogeneously enriched portions of the sub-continental lithospheric mantle. These portions were enriched by solute-rich fluids/partial melts derived from the underlying subducted Farallon slab in a high temperature and high pressure regime. Our data highlight the complexity of mafic root zones underlying the supereruption-scale HRT rhyolitic bodies during the initiation of the YPVF.

1 Christiansen & McCurry (2009): Bull Volc 70, 251

2 Christiansen (2001): USGS Prof Paper 729-G

3 Whitaker et al. (2008): Bull Volc 70, 417

4 Putirka et al. (2009): J Petrol 50, 1639

Thomas Wilson, Carol Stewart, Natalia Deligne, Graham Leonard, Susanna Jenkins, Joshua Hayes, Daniel Blake, Alec Wild

Submission 1291

Assessing Volcanic Impacts to Society

Volcanic eruptions can cause a range of societal impacts from local to global scales. The severity of impact is typically a function of the hazard intensity (e.g. ashfall load), what societal elements are exposed (e.g. people, buildings, crops, etc.), and the vulnerability of those elements.

Assessing volcanic impacts and how to reduce their effects forms a cornerstone of volcanic disaster risk reduction. However, a) the broad range of potential volcanic hazards, hazard intensities, durations, and the complex interaction between these hazards, b) the vast array of societal elements exposed to volcanic hazards and their vulnerability or resilience, and c) the broad range of possible pre-, syn-, or post-event mitigation actions all creates considerable challenges for robust assessment of likely impacts/risks and identifying potentially credible and useful mitigation measures.

This presentation will explore efforts to develop quantitative risk models which integrate hazard, exposure and vulnerability. It will focus on the development and application of fragility and vulnerability models derived from the rich catalogue of (mostly qualitative) field based observations, and the more recent drive towards empirical (mostly quantitative) investigations of volcanic impacts in controlled laboratory settings. The presentation will also explore the benefits and challenges of co-creating risk assessments with stakeholders which are focused on what affected communities may experience, such as duration of evacuation and loss of infrastructure services, as well as direct damage to the built environment. Finally, it will explore future challenges in this field and some of the exciting initiatives which will hopefully help address them.

Amelia Winner, Ken Ferrier, Josef Dufek, William Guinn

Submission 901

Experimental and Numerical Determination of Bed Force Distributions in Concentrated Pyroclastic Density Currents

Pyroclastic density currents (PDCs) are highly energetic gravity currents composed of hot gas, juvenile eruptive material, and lithics eroded from the bed and vent. Erosion and entrainment of bed material into the current can greatly impact flow dynamics, mobility, and thus hazards associated with PDCs. While PDCs are recognized as some of the most dangerous geological flows, the mechanisms of erosion and material entrainment remain poorly constrained. Proposed mechanisms include increased bed stresses due to force chain formation, discrete particle impacts, pore pressure evolution, and frictional interactions between particles. Instrumentation and measurement of real-time PDCs is nearly impossible due to their infrequent occurrence and hostile characteristics, as flows are capable of reaching temperatures of $> 800^{\circ}\text{C}$ and velocities of up to 200 m/s. This study employs a combination of laboratory experiments and numerical simulations to quantify the forces imposed on the bed by PDCs. Our experimental apparatus consists of a rotating cylindrical flume, capable of generating linear velocities of up to 10 m/s. With this experimental setup, we are able to simulate long-duration flows and observe impact forces at the bed over timescales comparable to the flow duration of natural PDCs. By applying particle imaging velocimetry to flows of 5 mm spherical glass beads, we are able to measure velocity gradients as high as 48 s^{-1} within the flow. To measure the distribution of bed-normal forces imparted by the flow on the bed, we embedded force sensor arrays on the bed that are capable of measuring stresses up to 350 kPa. The distribution of forces imparted on the bed by the flow will be explored over a parameter space described by naturally occurring PDCs. These experiments will be used to validate a numerical discrete element model, which we will use in future work to model the bed forces produced by a wide range of granular flows. These models will allow us to better constrain the supply of bed material entrained by overlying density currents and feedbacks between bed entrainment and flow dynamics. The combination of these laboratory and numerical experiments will provide a means for exploring the sensitivity of basal forces to macroscopic flow properties such as grain size, particle concentration, and shear rate.

Heather Winslow, Philipp Ruprecht

Submission 704

Petrochemical constraints for primitive magmas in the Southern Andean Volcanic Zone from Volcán Manantial Pelado's eruptive history

Volcán Manantial Pelado (35.5 °S; 70.8 °W) lies within the transitional zone of the Southern Andean Volcanic Zone as one of the more mafic centers in this part of the Andes. It stands in contrast to the otherwise regional voluminous silicic magmatism that is expressed most recently in the 1846-47 and 1932 Quizapu eruptions, but also extends into the Pleistocene at the Calabozos Caldera and the Volcán Descabezado Grande-Cerro Azul (DG-CA) Volcanic Cluster. The diversity of parent magmas feeding these silicic systems has yet to be fully constrained through space and time. Manantial Pelado (~15 km NW of Volcán Quizapu) is a great study site to explore the diversity within parental magmas. Its strongly dissected nature allows access to a long history of mafic magmatism. Samples were collected from glacially-carved valleys throughout the volcano's stratigraphy focusing on the effusive history.

Manantial Pelado is made up of mostly porphyritic, holocrystalline basaltic andesite to andesite with large mafic phenocrysts of pyroxene (2-4 mm) and olivine (1-3 mm) occurring in variable proportions. Plagioclase (1-2 mm) is the most abundant phenocrystic phase. Hydrous phases are absent suggesting overall dry and/or shallow conditions. Microlites are dominantly plagioclase and Ca-rich pyroxenes. Preliminary results show that olivines are homogenous with narrow, weak normal zoning near the rim (Fo ~80-70) and frequent pyroxene overgrowth. Within the uniform cores (Fo ~80) Cr-spinel inclusions are common with Cr# ranging from 0.3 to 0.7 suggesting that spinels retain some primitive parentage, while olivines (and spinels) are affected by Fe-Mg equilibration during magma evolution. Clinopyroxene is abundant with Mg# of 75, while orthopyroxene is much less frequent and typically resorbed. Plagioclase textures vary with some crystals having anorthitic cores of An85. Rims are more sodic (An55) and similar to groundmass plagioclase microlites.

These samples provide new constraints on the regional primitive magmas feeding the DG-CA Volcanic Cluster. While they clearly show some fractionation and hybridization, they still contain some primitive mineral signatures that allow us to characterize the diversity of parental magmas. Information from whole rock geochemistry and additional mineral-scale data will further constrain how Manantial Pelado's primitive history connects to the silicic magmatism in this region.

Claire Witham, Sara Barsotti, Stephanie Dumont

Submission 193

“Katla Erupts”: A transboundary exercise conducted by FUTUREVOLC

One of the challenges in responding to large eruptions is the international nature of their impacts and the requirement for coordinated response. Adequately representing these crises in an exercise requires complex and long-lasting scenarios and the involvement of institutions from many countries. In January 2016 the EU FP7 FUTUREVOLC project conducted a three day exercise in which 26 European project partners, together with additional Stakeholders, were involved in responding to an evolving eruption scenario at Katla volcano. Katla was chosen as it is one of Iceland’s most active volcanoes and poses a multi-hazard threat due to its location under the Mýrdalsjökull ice-cap in South Iceland. In this area the population (locals and tourists) exposed to possible volcanic hazards varies strongly with the season, from several hundred on a standard day in January up to thousands in August. Experts from outside of the project were engaged in planning a realistic scenario, which evolved from a small glacial flood on day 1, to an explosive eruption on day 2 and dome growth leading to a rock-fall on day 3.

The detailed scenario enabled all participants to practice and test their response procedures. In Iceland, a Scientific Advisory Board was formed, procedures were practiced for sending monitoring teams into the field and the set-up of new equipment was tested. International partners were able to practice real time interpretation of monitoring data from a wide range of equipment and sources. To evaluate cross-border dissemination of information, the exercise included the London VAAC and representatives from international media and civil protection. The international make-up of these stakeholder organisations means that good communications will be vital in any eruption and the exercise tested new ways of sharing and discussing data.

This is the first exercise of this magnitude and scope for an eruption in Iceland and was a successful test of the response to such an eruption. Following the exercise 90% of partners said they felt better prepared for the next eruption. As with any exercise, it also identified areas where further development is required and improvements can be made to procedures. This presentation will highlight how the exercise scenario was developed and run, and discuss the key lessons learned.

Kendall Wnuk, Christelle Wauthier

Submission 642

Temporal evolution of magma sources and surface deformation at Pacaya Volcano, Guatemala revealed by InSAR

Pacaya Volcano, Guatemala is a continuously active, basaltic volcano whose western flank is unstable. Despite continuous activity since 1961, a lack of high temporal resolution geodetic surveying has prevented detailed modeling of Pacaya's underlying magmatic plumbing system. A new, temporally dense dataset of Interferometric Synthetic Aperture Radar (InSAR) RADARSAT-2 images, spanning December 2012 to March 2014, shows magmatic deformation before and during major eruptions in January and March 2014. Inversion of InSAR surface displacements using simple analytical forward models suggest that three magma bodies are responsible for the observed deformation: (1) a ~4 km deep spherical reservoir located northwest of the summit, (2) a ~0.4 km deep spherical source located directly west of the summit, and (3) a shallow dike below the summit. Periods of heightened volcanic activity are instigated by magma pulses at depth, resulting in rapid inflation of the edifice. We observe an intrusion cycle at Pacaya that consists of deflation of one or both magma reservoirs followed by dike intrusion. Intrusion volumes are proportional to reservoir volume loss and do not always result in an eruption. Periods of increased activity culminate with larger dike-fed eruptions. Large eruptions are followed by inter-eruptive periods marked by a decrease in crater explosions and a lack of detected deformation. Co-eruptive flank motion appears to have initiated a new stage of volcanic rifting at Pacaya defined by repeated NW-SE oriented dike intrusions. This creates a positive feedback relationship whereby magmatic forcing from eruptive dike intrusions induce flank motion.

Julia Woitischek, Marie Edmonds, Andrew W Woods, Clive Oppenheimer

Submission 337

Experimental insights into degassing of open-vent basaltic volcanoes

Open vent basaltic volcanism is characterised by the continuous release of gas, which may manifest itself through the intermittent release of gas slugs or more quiescent high frequency degassing of small bubbles. Prior efforts to understand the controls on the phenomena have focussed on two-phase (liquid-gas) flows, in which the stability of a foam in a magma chamber has a key role on the form of gas venting at the surface. However, it has become clear that in many cases the magma may be highly crystalline, leading to important differences in the rheology of the melt-crystal mixture, and in turn this may also influence the style of degassing.

Here we report a series of novel three-phase (liquid-solid-gas) analogue experiments aimed at probing how the dynamics of gas flow through a particle suspension varies with the particle load as an analogue for the effect of different crystal content on open vent degassing. The small-scale experimental setup consists of a long vertical Perspex tube filled with mixtures of glycerol and water of varying viscosity together with cellulose acetate particles to represent crystals. Gas is introduced via a pump at the base of the cylinder and the nature of the flow has been investigated for various gas flow rates, particle loading and liquid viscosity.

Measurements of the volume, rise speed, and number density of bubbles, show systematic trends in the frequency and size of the bubbles as the particle loading is increased. For the same gas flux and liquid viscosity with the high frequency release of small bubbles being reminiscent of quiescent degassing at Halema'ūma'u (Kilauea, Hawaii) while the lower frequency release of large gas bubbles may represent episodic bursting of gas bubbles as seen in Strombolian style systems.

Using scaling arguments, we compare our findings with observations of open vent degassing from a series of natural systems.

John A. Wolff, Frank C. Ramos, Corey Dimond

Submission 437

Melt inclusion and single crystal isotopic record of a large rhyolitic magma system between two super-eruptions

Jon Davidson was a leader in the application of isotope ratio micro-analysis to problems of igneous petrogenesis. Much of his early work in this field focused on rhyolitic systems. Here, we apply single-crystal and melt inclusion analysis to high-silica rhyolites erupted from the Valles caldera, New Mexico. The Valle Toledo Member of the Cerro Toledo Formation, Jemez Mountains volcanic field, consists of a series of rhyolite domes, pumice fallout and pyroclastic flow deposits emplaced between the major caldera-forming, compositionally zoned eruptions of the Otowi Member (1.60 Ma, 380 ± 170 km³) and Tshirege Member (1.24 Ma, ~ 400 km³) of the Bandelier Tuff. Valle Toledo units represent much smaller volumes of magma (order 1 – 10 km³) that provide, in some measure, a record of the state of the evolving system between the two major eruptions. Whole-rock data present an uncomplicated picture; increasing incompatible element concentrations and decreasing ¹⁴³Nd/¹⁴⁴Nd with time are consistent with a straightforward assimilation-fractional crystallization process in rhyolite magma. However variations of trace elements, ⁸⁷Sr/⁸⁶Sr and Pb isotopes in feldspars and melt inclusions do not support this simple hypothesis. Although ⁸⁷Sr/⁸⁶Sr in feldspar shows an overall upward increase, several units exhibit internal variations, and melt inclusions in quartz are both quite different and more variable than feldspars. For example, Pb isotope ratios of individual melt inclusion-bearing quartz crystals from the basal unit, erupted immediately after the Otowi Member, show extreme variations that encompass almost the entire range of values found for the Jemez Mountains volcanic field. Although whole-rock trace element abundances in the basal unit are restricted and similar to the last-erupted Otowi compositions, melt inclusions have a range similar to that of the entire Otowi whole-rock suite, suggesting thorough stirring of the system during Otowi eruption and caldera collapse. These relations are interpreted in terms of spatially decoupled assimilation, fractionation, recharge and cumulate melting during the 360,000 years between the two major compositionally zoned caldera-forming eruptions.

Ying-Qi Wong

Submission 169

Constraining the magmatic system at Mount St. Helens (2004-2008) using Bayesian inversion with physics-based models including gas escape and crystallization

Physics-based models of volcanic eruptions allow us to integrate diverse volcanological datasets to constrain important parameters of magmatic systems and to track their evolution during eruptions. We have extended the 1D cylindrical conduit model of Anderson and Segall [2011] to include equilibrium crystallization, as well as vertical and lateral degassing. Excess pressure in the magma chamber drives Newtonian flow until the viscous resistance to flow exceeds the rate-dependent frictional strength on the conduit wall, at which point viscous flow naturally transitions to plug flow. We investigate steady-state solutions to the governing equations, and compare with the quasi-steady dome growth phase of Mount St. Helens between March and December 2005. Magma chamber pressure, initial water content, conduit radius, wall friction coefficient, magma permeability and percolation threshold, which is the minimum porosity required for degassing, are treated as unknown model parameters. We specify the wall rock permeability using Manning and Ingebritsen [1999]. Crystallization and gas loss produce complex behavior particularly in the shallow conduit, with degassing acting as a strong control on mass flux. We use this physics-based model in a Bayesian inversion to link data including dome rock porosity estimated from hand samples, extrusion rate from photogrammetry, plug depth from the maximum depth of drumbeat earthquakes, and crystallization pressure from petrologic data to determine probability density functions of the model parameters and their correlations. Magma permeability is well constrained to maintain the balance between chamber water content and observed dome rock porosity at the surface. Low frictional resistance is required to allow extrusion at the observed rate while maintaining reasonable magma chamber pressures. This could arise from low coefficient of friction (<0.3) or effective normal stress.

Preliminary work on transient conduit behavior shows that as chamber overpressure declines during eruption, the solidus and magma percolation threshold deepen since these properties are primarily influenced by conduit pressure. Crystallization and gas loss increase density and viscosity, likely contributing to the end of an eruption. This time-dependent physics-based model will allow us to incorporate time-evolving geodetic and extrusion flux data into future Bayesian inversion.

Daniel Woodell, Martin Schöpfer, Bernhard Grasemann

Submission 807

Distinct Element Method (DEM) numerical models of restless calderas

Large caldera collapses with cataclysmic eruptions of over 1000 km³ of magma ('super-volcanoes') constitute a major hazard to humanity, and still-active calderas often lie adjacent to or under large population centers. After collapse, volcanoes often undergo uplift ('resurgence') due to recharge of the magma reservoir. This re-supply of magma at depth causes uplift of the subsided part of the caldera and leads to faulting and new eruptions at the surface. Over several years to 100's of years these post-collapse deformation cycles can manifest as numerous 'unrest episodes' of meter-scale uplift and subsidence that are punctuated by faulting and eruption.

An acute problem for accurate assessment of hazard potential is the persistent uncertainty and debate about how caldera collapse is triggered, how it evolves, and how it is structurally accommodated. Researchers have consequently turned to physical and numerical models of caldera collapse to gain further insights into the initiation, development, and final geometry of caldera structures. New numerical modeling techniques such as the Distinct Element Method (DEM), are currently providing increased insight into these critical questions.

The principle advantage of using the DEM over more commonly used continuum models (e.g. Finite Elements) to model large strain volcanic deformation is that it can not only precisely calculate displacements, stresses, and strains based on realistic rock properties, but it can also directly and accurately model the initiation, growth, rupture, and reactivation of complex discontinuities like faults, key to assessing eruption and hazard potential.

We generate realistic models of restless calderas, including pre-collapse inflation (tumescence), followed by collapse and later by resurgence (characteristic for restless calderas), and analyze the model results. We investigate if faults formed during previous stages of the evolution of a restless caldera are reactivated during a subsequent stage, as well as the development of structures during different stages of caldera unrest and what effect various pre-stage structures and magma reservoir geometries may have. Our models help shed light on the mechanics at work underneath active calderas and improve volcanic hazard assessment.

Taylor Woods, Kimberly Genareau, Shelby Cloer

Submission 255

Effects of Grain Size and Shape on Volcanic Ash Electrical Conductivity

The exact mechanisms of electric charge generation and transmission in explosive eruption columns and plumes are poorly understood. Ash is a probable charge carrier, and thus, the physical properties of ash may factor into charge generation and transmission. Specifically, the shape and size of ash grains may be contributing factors. To examine the relationship between volcanic ash electrical conductivity and grain size/shape, this research compares conductivity measurements to grain size distribution and shape parameters from several volcanic centers: Five minimally processed ash samples collected from explosive eruptions in Alaska, U.S.A. (Katmai, 1912; Crater Peak, 1992; Augustine, 2006; Okmok, 2008; Redoubt, 2009), and a set of homogenized (with respect to grain size and shape) ash samples from Lathrop Wells (Nevada, U.S.A.), Taupo (New Zealand), and the Valles Caldera (New Mexico, U.S.A.). Grain size distribution was measured using a Malvern 3000 laser diffractometer particle size analyzer (LDPSA) and grain shapes (aspect ratios, concavity indices) were characterized using backscattered electron images that were processed with ImageJ freeware. Bulk composition of all samples was determined using X-ray fluorescence (XRF). The volume resistivity of minimally compressed samples was measured at controlled temperature (25-30 °C) and relative humidity (25 %) using a current amplifier and converted to conductivity. A general effective media (GEM) equation was then applied to account for variations in grain packing, grain shape, and sample porosity. Preliminary analyses suggest that particle size distribution controls ash conductivity, as samples with higher proportions of fine particles (greater surface area, smaller mean volume) have higher conductivity values. Although all ash samples are electrically insulating, homogenized samples provide maximum conductivity measurements that range over roughly five orders of magnitude (10^{-7} - 10^{-12} ($\Omega \cdot \text{cm}$)⁻¹) and non-homogenized Alaskan samples range over roughly seven orders of magnitude (10^{-7} - 10^{-14} ($\Omega \cdot \text{cm}$)⁻¹). There was no observed relationship between bulk ash composition and conductivity, suggesting that magma chemistry does not play a role. Instead, the efficiency of magma fragmentation during explosive eruptions, and the resulting proportion of fine ash particles generated, controls the bulk electrical conductivity of volcanic ash.

Gerhard Wörner, Magdalena Blum-Oeste, John Hora, Axel K Schmitt, Wencke Wegner

Submission 462

Changing regimes in central Andean magma systems

Magma composition, eruption rate and lifetime (Ma - ka) are variable in magma systems feeding stratovolcanoes in the central Andes. P-T-t data constrain the evolution of two strongly contrasting magmatic regimes at Taapaca and Parinacota volcanoes in northern Chile. Taapaca is a long-lived (1.5 Ma) intermittently active dacite dome cluster. P-T conditions of crystallisation, enclave and amphibole compositions indicate mixing of resident rhyodacite magma (750-840°C) and hotter mafic magmas (900-1050°C) at 6 to 15 km. Uniform dacite compositions indicate constant end-member proportions for 1.5 Ma.

Parinacota “Old Cone” erupted a range of compositions from basalt to rhyolite over 50 ka. Most lavas have two distinct amphibole populations and their depth and temperature of crystallisation completely overlap with those at Taapaca. Sector collapse at 8 ka was followed by increased eruption rates and re-building of a “Young Cone” by uniform mafic, amphibole-free cpx-opx andesites that crystallized between 6 and 30 km from deeper reservoirs after the collapse. Late fissure eruptions at the base of the volcano produced two distinct mafic andesites that correspond closely to end-member compositions of mafic enclaves at Taapaca volcano.

Ba-in sanidine diffusion modelling, zircon U-series-dating and (published) bulk rock U-series data demonstrate residence times up to hundreds of ka at shallow pressures for the rhyodacite end-member. By contrast, U-series disequilibrium in Young Cone lavas (published data) suggest magma transfer from deep sources in less than a few ka.

These distinct magmatic regimes are controlled by variable recharge rates of mafic magma into the rhyodacite reservoir. Low recharge rates keep the crustal reservoir “alive”, without eruption (“resident regime”). Increased recharge to a critical value occurs at irregular intervals to overcome the activation threshold of the viscous rhyodacite resulting in dacites with uniform mixing proportions (“critical activation regime”). Variably higher recharge rates produce (Old Cone) compositions from dacites to amphibole andesites and more mafic cpx-opx andesites (“mobilization regime”). After eruption rates increased dramatically (Young Cone) mafic recharge from greater depths essentially flushed the shallow magma reservoir (“break-through regime”). Finally, fissure eruptions at the base of Parinacota erupted the two distinct mafic recharge magmas without interaction with the shallow reservoir (“single batch regime”).

Robert Wright, Estelle Bonny

Submission 1271

An assessment of three satellite-based methods to retrieve lava discharge rate

One of the most important parameters required to study active lava flows is the lava discharge rate. Satellite remote sensing data arguably allow for higher temporal resolution (and logistically easier) sampling of discharge rates than do in-situ measurements. Three methods have been defined in the literature to retrieve time-averaged discharge rate (TADR) using thermal infrared satellite data: i) the Harris et al. (1997) method using 11 micron radiance and heat flux balance, ii) Wright et al. (2001) method that simplify the previous technique to a simple linear relationship between active lava area and TADR, and iii) Coppola et al. (2012) method using measurements of 4 micron radiance. These different methods have been used interchangeably and are generally assumed to give similar results. We used NASA's MODerate Resolution Imaging Spectroradiometer (MODIS) thermal data to estimate TADRs from all lava-flow forming eruptions around the world from 2000 to 2015 to determine the relative performance of each approach. To be able to see which method yields results that are closest to field measurements ("ground-truth"), we extracted the total volume of lava produced by each of the 105 eruptions from 34 volcanoes that composed our database by integrating the TADR over time. We compared the volumes from Harris et al. (1997) and Coppola et al. (2012) methods to those found in the literature (estimated with different techniques ranging from InSAR to field measurements). The method of Wright et al. 2001 is a simplification of the method from Harris et al., 1997 and we found that the results follow the same trend as the latter with a small offset; we therefore concentrated only on the first and last methods. We noted an interesting feature, mostly at Nyamuragira volcano, where the TADR time series shows a turnaround towards the end of the eruption with the first method becoming higher than the third, which might arise from the better sensibility of the 11 micron radiance to colder lava temperatures. We found that generally the method from Harris et al. (1997) yields results that are closer to the volumes found in the literature than Coppola et al. (2012) are, although the latter is more often encompassing the ground-truth value due to its larger uncertainty.

Heather Wright, Marco Rivera, Jessica Vela, Chris Harpel

Submission 1144

Explosive eruptive history of Ubinas volcano, Peru, over the past 14 ka

Ubinas volcano, a stratovolcano located ~65km east of Arequipa, Peru, is the most historically active volcano in the country. Its current eruptive period (since 2006) has consisted of a series of Vulcanian and phreatomagmatic explosive eruptions ($VEI \leq 2$) producing ashfall and ejecting ballistic bombs. Here we explore the prehistoric eruptive record from Ubinas and document at least 12 subPlinian to Plinian tephra-fall deposits. These units vary non-monotonically in bulk composition from high-K calc-alkaline andesite to rhyolite. The largest and oldest Plinian eruption (~14 ka) was rhyolitic in composition.

Whole rock, glass, and Fe-Ti oxide compositions plus petrographic and sedimentologic characteristics are used to fingerprint individual units, aiding in correlation between tephra deposits dispersed across the landscape. Bulk compositions of Ubinas tephra units are geochemically distinct from neighboring volcanoes' eruptive products, where trace element concentrations in Ubinas rocks are comparatively enriched. For example, a distinct white, lithic-poor, fine-lapilli tephra-fall deposit blankets the entire area around Ubinas, but it is geochemically distinct from Ubinas tephra. This marker unit was erupted between 7 ka and 1 ka from a volcano south of Ubinas.

Groundmass glass compositions of all explosive units from Ubinas are rhyolitic, due to microlite crystallization that has driven up the SiO₂ content of residual melt in intermediate composition magmas. Melt inclusions are dacitic to rhyolitic in composition. The least evolved inclusions (~69 wt% SiO₂) contain up to 0.19 wt% SO₃. Pre-eruptive temperatures, based on compositions of touching oxide pairs in intermediate composition tephra units, range from 800 to 900°C (except two high temperature outliers; using the Andersen and Lindsley geothermometer). Oxide pairs further indicate oxygen fugacities of $\log fO_2 = NNO + 3$.

Jiandong Xu, Hongmei Yu

Submission 391

Probabilistic Assessment of Tephra Fallout Hazard for the Nuclear Power Plants (NPPS) of China – A Case of Taishan NPP

Starting from the 1980's of last century, China has launched the national plan of constructing nuclear power plants along the coastline region in east China. Currently, for some of these candidate sites, nuclear facilities have been installed and in operation, but for some others nuclear power plants are still under construction or in site evaluation. To meet the safety standards for volcanic hazard, we follow the IAEA SSG-21 guidelines, and develop a simple and practical diffusion program in order to evaluate the potential volcanic hazard caused by tephra fallout from the explosive eruptions which are within the distance of several hundreds kilometers away from the candidate site.

Taishan Nuclear Power Plant (TNPP), Guandong Province, China, is geographically located at Yaogu village of Chixi town at Taishan city, Guandong Province, China. The designed capacity of the TNPP is six Areva's 1,750 megawatt (MW) European Pressurized Reactor (EPR) units. In geology, the TNPP site is located in the continental margin of South China. To the south is the South China Sea, which consists of the oceanic basin, two rifted margins, one transform margin and one subduction zone. In about 350 km SW to the TNPP, the Quaternary volcanism in north Hainan Island is characterized by multi periodic activity, in which the most recent eruption is dated in about 4,000a B.P. According to IAEA SSG-21, a capable volcano is one for which both (i) a future eruption or related volcanic event is credible; and (ii) such an event has the potential to produce phenomena that may affect a site. Therefore, the Hainan volcano field is capable of producing hazardous phenomena that may reach the TNPP.

The input parameters for the simulation of tephra fallout from the future eruption of Hainan volcano, such as the size, density and shape of the tephra, the bulk volume and column height, the diffusion parameter $P(z)$, wind direction and intensity, were obtained by field investigation and laboratory analysis. We carried out more than 10,000 tephra fallout simulations using a statistical dataset of wind profiles which are obtained from China Meteorological Data Sharing Service System (CMDSSS). Tephra fallout hazard probability maps were constructed for two tephra thickness thresholds of 10cm and 1 cm. Our results show that the tephra produced by the future large-scale explosive eruption from Hainan volcanoes can only affect the area in a range about 250 km away from the eruption center.

Xueming Xue, Jeffrey Freymueller

Submission 65

An unscented Kalman filter combining GPS and InSAR for time-dependent modeling of volcanic deformation

The Kalman filter is an effective tool for time-dependent inversion of geodetic data. Based on a Mogi point source model, an unscented Kalman filter (UKF) was developed for volcanic source modeling using GPS observations. The UKF allows retrieval of the time-dependent history of both source strength and source location. We have expanded the UKF to be able to integrate Interferometric Synthetic Aperture Radar (InSAR) observations. Before applying the UKF, it is necessary to estimate the uncertainty of the InSAR data and find appropriate relative weights between GPS and InSAR observations. We remove a time-independent Mogi source and phase ramp from every InSAR image and use the residual to obtain its variance-covariance information. If there are GPS observations at the same time, we then determine the optimal weight to the corresponding InSAR image using Variance Component Estimation. The GPS and InSAR time series can then be combined using the UKF. We apply this approach to the post-eruptive inflation of Okmok volcano, Alaska. We use GPS data from 4 continuous sites and 11 campaign sites and InSAR data from 4 different acquisition tracks of TerraSAR-X and Envisat satellites throughout the 2008-2014 time period. Continuous GPS data indicates that Okmok started inflating soon after the 2008 eruption. The inflation then slowed down, but suddenly sped up again in the middle of 2013.

Taishi Yamada, Hiroshi Aoyama

Submission 373

A numerical study on the onset of explosion earthquakes

Vulcanian eruption is characterized by sudden ejection of volcanic fragments, excitation of shock wave and explosion earthquake. A volume change source or a vertical single force are major candidates of source mechanism that explains observed waveforms of explosion earthquakes. Since the mechanism obtained from inverse analysis only represents macroscopic force system at the source region, it is still challenging to infer the dynamics in the volcanic conduit directly.

Magma fragmentation and ejection accompanying Vulcanian eruption are often modeled by the shock tube theory. To obtain fundamental characteristics of explosion earthquakes, we examine displacement field induced by the shock tube problem of ideal gas in an elastic pipe adopting OpenFOAM. Computational region is a fan-shaped column of 4 km length, consisting of a vertical fluid pipe with the radius of 20 m and surrounding elastic media with the radius of 4 km. As the initial condition, a diaphragm dividing different pressure regions in the pipe is assumed at the focal depth of explosion earthquakes at some volcanoes. We set the pressure difference at the diaphragm referring estimated overpressure of Vulcanian eruptions.

Our numerical simulation shows that the elastic wave propagates from fluid-solid boundary at the depth of the diaphragm. The polarity of the elastic wave has a nodal plane about 30° upward from the horizontal plane. Since the compressional polarity is seen above the nodal plane, surface displacement waveforms at the vicinity of the pipe have the compressional onset. Contrary, displacement waveforms at the far side from the pipe have the dilatational onset because the nodal plane crosses the surface. The pressure change in the pipe below the diaphragm (decreasing) is almost twice of that above the diaphragm (increasing). Therefore, the angle of the nodal plane may reflect the amplitude ratio of transient pressure change in the pipe.

Yamada et al. (2016) reported that the focal depth of explosion earthquakes at Lokon-Empung volcano in Indonesia is about 1 km beneath the active vent. The polarity of the onset is compressional at all stations ranging 1.7-6.9 km from the active vent. Our simulation shows that the compressional onset is seen only at up to 1.5 km from the pipe assuming the diaphragm at the depth of 1 km. Therefore, it is suggested that additional source process has to be considered to reproduce the initial compressional wave at all stations.

Kazuya Yamakawa, Mie Ichihara

Submission 181

Characterization and modeling of sound generated by a bubble vibrating on liquid surface

Bubble sounds are measured with active degassing at volcanoes. It has been used to estimate the gas flux considering a specific mechanism of sound generation: Bouche et al. (2010) assumed bubble sound due to vibration on the surface of magma (we call it as Vergniolle bubble sound referring to Vergniolle and Brandeis, 1996), while Johnson et al. (2008) assumed bubble bursting. However it is challenging to specify the mechanism of acoustic signals observed at volcanoes where we cannot always look into the source. In laboratory experiments, we have found that Vergniolle bubble sound had identifiable features that include frequency gliding upward and spindle-shaped envelopes. We examine the mechanism of Vergniolle bubble sound in detail by a model calculation and summarize notable characteristics to distinguish it from other mechanisms in acoustic data.

We follow the experiments by Lyons et al. (2013) which used a viscoelastic transparent gel solution. Bubbles rise in the fluid with coalescence and oscillation, and finally escape from the surface. The sequences are recorded by microphones and a high speed camera. We find two main processes generating sound: (1) bubble detaching from a nozzle and (2) rising bubble above the fluid surface. In this experiments, no acoustic signal is detected with bubble bursting. The signal of (2) is Vergniolle bubble sound and we focus such signals.

We develop a model referring to Vergniolle and Brandeis (1996). We call the part of a bubble above the fluid surface as the 'head', and the part below the surface as the 'tail'. As the bubble rises on the surface, the head grows while the tail shrinks. The tail-to-head volume transfer is incorporated in the model. It enables the oscillation to start and grow without an external excitation and explains a half of the frequency gliding. The remaining frequency increase is expected to be due to thinning of the bubble film by gravitational flow. The model also suggests that in order to generate a sufficiently large acoustic signal as observed in the experiment a bubble needs additional excitation before it starts appearing on the surface.

Both amplitude and frequency of Vergniolle bubble sound increase due to the tail-to-head volume transfer. After the tail disappears, the amplitude decays while the frequency keeps growing due to thinning of the bubble film. Thus, it is important to observe evolution of the amplitude and the frequency in order to identify Vergniolle bubble sound.

Seiko Yamasaki, Hideo Hoshizumi, Daniel P. Miggins, Anthony A.P. Koppers, Shanaka de Silva, Akikazu Matsumoto

Submission 720

Reconstruction of the Growth History of Kuju Volcanic Complex, Southwest Japan: Estimation of Magma Discharge Rates by Unspiked K-Ar and $^{40}\text{Ar}/^{39}\text{Ar}$ Dating

Kuju volcanic complex is located on the junction of the volcanic front on the Ryukyu Arc and the Beppu-Shimabara Graben on Kyushu Island, southwest Japan. This volcanic complex comprises small stratovolcanoes and lava domes that are surrounded by gentle slopes composed of pyroclastic flow, debris avalanche and debris flow deposits. The onset of the Kuju volcanism was ca. 200 ka, and the last phreatic eruption occurred in 1995-96 after at least 333 years of dormancy. Constructing the growth history and magma discharge rates of this active volcano is important for understanding the spatial/temporal change of magma plumbing system of the arc volcanic system, assessing the possible eruptive pattern and forecasting of the eruptive activity in the future.

We reconstructed the growth history from western to central portions of Kuju volcanic complex based on the unspiked K-Ar and $^{40}\text{Ar}/^{39}\text{Ar}$ dating. The unspiked K-Ar dating procedure enables the correction for the mass fractionated initial $^{40}\text{Ar}/^{36}\text{Ar}$ ratios. This technique has been successfully applied to young volcanic samples, especially younger than 0.5 Ma. The resulting ages are consistent with stratigraphic relationships, as well as concordant with reported conventional K-Ar, Thermo Luminescence, Fission Track and ^{14}C ages.

The unspiked K-Ar ages for the small andesitic-dacitic volcanoes of Stage I yielded with two age groups ca. 160-150 and ca. 90-80 ka. During Stage III after the largest eruption associated with the Handa Pyroclastic Flow Deposit (Stage II), some lava domes and smaller stratovolcanoes in the central part were built up from 54 to 34 ka. A project is underway to apply incremental heating $^{40}\text{Ar}/^{39}\text{Ar}$ dating at Oregon State University using multicollector ARGUS-VI mass spectrometry, for comparison with the unspiked K-Ar ages and for improving the precision in eruption ages.

Based on the ages and estimated volume for each volcanic unit, we calculated magma discharge rates during each volcanic stage and for all stages of the growth history. The geographical feature of the exposed product and the thickness information from the boring cores were used for the estimation of the volume for each unit. The calculated magma discharge rates for Stage I, III and IV are 0.09, 0.12 and 0.18 km^3/ky , respectively, indicating that the activity has increased slightly. All stages together yield a discharge rate of 0.12 km^3/ky which is similar to Aso and Unzen volcanoes located west of this complex.

Yasuhiro Yanagida, Michihiko Nakamura, Atsushi YASUDA, Takeyoshi YOSHIDA

Submission 559

Melt inclusions in amphibole-bearing gabbroic xenoliths from the Ichinomegata maar, NE Japan: Snapshot of hydrous arc magma differentiation in the deep crust

We report chemical compositions of melt inclusions hosted in amphibole-bearing gabbroic xenoliths from the Ichinomegata maar located on the back-arc side of northeast Japan. Andesitic magma erupted 0.06–0.08 Ma, with abundant deep-crustal and mantle xenoliths. We selected eight amphibole gabbroic xenoliths composed of medium-grained amphibole (tschermakite) and plagioclase (An_{80–93}) with minor amounts of apatite and magnetite. Little- and non-crystallized glasses were preserved as inclusions <50–200 μm in diameter in plagioclase, magnetite, and apatite. Amphibole geobarometry yielded 4–6 kbar, corresponding to 15–24 km depth, which is consistent with the seismologically estimated petrologic structure beneath the Ichinomegata maar (Nishimoto et al., 2008). The calculated temperature range (880–980°C) is slightly higher than the dehydration melting solidus and is consistent with the presence of melt inclusions in the gabbro. The melt inclusions calculated as anhydrous show dacitic to rhyolitic compositions with 63.9–72.9 wt% SiO₂ in plagioclase, 64.8–73.0 in apatite, and 69.0–74.0 in magnetite. The SiO₂ content of coexisting liquid is estimated to be 63.8 to 69.1 wt% on the basis of a chemometric method using amphibole chemistry (Ridolfi and Renzulli, 2012). This result is consistent with the melt-inclusion data. The distribution coefficients of Fe-Mg between amphibole and melt inclusions satisfy the equilibrium test of Putirka (2016), except for some inclusions in apatite and magnetite. Analyzed melt-inclusion compositions match very well with melt compositions in crystallization experiments of hydrous arc basalt at 0.7 GPa (Nandedkar et al., 2014). The melt inclusions in anorthite-rich plagioclase (An_{81–90}) have low CaO/NaO weight ratios (0.6–1.9) and very high $KD = (Ca/Na)_{plg}/(Ca/Na)_{liq}$, as found in differentiation experiments with hydrous melt (8–15 wt% H₂O). These features indicate that the silicic melt was formed in equilibrium with the amphibole gabbro in middle to lower crust beneath the Ichinomegata maar, in the presence of extremely hydrous melt (~10 wt% H₂O) during late-stage differentiation of hydrous arc magmas in the deep crust. The water contents of melt inclusions were measured with FT-IR micro-reflectance spectroscopy to be up to 7.4 wt%; this supports the hydrous nature of the silicic melt, given that the melt inclusions include bubbles.

Keywords: xenolith; amphibole gabbro; plagioclase; melt inclusion; silicic melt

Jiaming Yang, Maxwell Rudolph, Leif Karlstrom

Submission 1168

Melting in the Mantle Wedge: Quantifying the effects of crustal thickening and viscous decoupling on melt production with application to the Cascadia subduction zone

Arc magmatism is sustained by the complex interactions between the subducting slab, the overriding plate, and the mantle wedge. Partial melting of mantle peridotite is achieved by fluid-induced flux melting and decompression melting due to upward flow. The distribution of melting is sensitive to temperature, the pattern of flow, and the pressure in the mantle wedge. The arc front is the surface manifestation of partial melting in the mantle wedge and is characterized by a narrow chain of active volcanoes that migrate in time. The conventional interpretation is that changes in slab dip angle lead to changes in the arc front position relative to the trench. We explore an alternative hypothesis: evolution of the overlying plate, specifically thickening of the arc root, causes arc front migration. We investigate the effects of crustal thickening and viscous decoupling of the shallow slab-mantle interface on melt production using 2D numerical models involving a stationary overriding plate, a subducting plate with prescribed motion, and a dynamic mantle wedge. Melt production is quantified using a hydrous melting parameterization. We conclude that crustal thickening beneath the arc front decreases the rate of melt production and induces a separation in forearc and back-arc mantle melt generation; and viscous decoupling limits the trenchward extent of melt production.

Qingyuan Yang, Marcus Bursik, Bruce Pitman

Submission 374

A new method to estimate the dispersal axis and vent location of tephra fall deposits

The thickness distribution of tephra fall deposits can be described with a semi-empirical model as a cone that is stretched and rotated along the dispersal axis. Such models can effectively estimate the total eruption volume given their straightforward mathematic expression. To extend the application of such models, we examine if they can be used to infer the source vent location of tephra fall deposits with thickness and maximum clast size measurements. The model is realized and tested by combining a first-order gradient descent method with two published semi-empirical implementations separately. Our method is applied to Beds 1, 2, and 3 of the North Mono eruption for evaluation. Given sufficient data (>70 sample sites), the estimated vent locations from a semi-empirical model with a power-law decay agree well with the hand-drawn isopach maps, while the estimated vent location for Bed 1 is beyond the extent of the bed when the exponential model is used. This can be explained by a sudden change in decay rate for the deposit, and insufficient sample sites in the upwind area. However, it is worth noting that the known source vent lies on the dispersal axis estimated with the exponential model.

After using the entire dataset, we take subsets of data for further testing. When the input observations are fewer and farther from the vent (with 30-40 observations), both of the semi-empirical models fail to make a correct prediction of vent location, but most of the estimated dispersal axes are consistent with hand-drawn maps, and cut through the respective source vents. This can be partly explained by the complex decay rate of tephra thickness and maximum clast size. Ideal performance in predicting the dispersal axis can be explained by the presence of strong wind, which makes the uncertainty from other factors negligible. Applying the method to clusters of observations (sample sites close to each other; 10-15 observations) reveals slight and gradual changes in the dispersal axis as the input sample sites get farther away from the vent, which perhaps is due to variability of atmospheric conditions during the eruption. Our work provides an objective method (with scripts written in R) that is proven to be effective in identifying the dispersal axis of fall deposits, and that often provides excellent estimates of vent location. Our tests do imply that semi-empirical models need to be used with caution given limited observations.

Ya-Min Yang, Sheng-Rong Song, Kenneth Rubin

Submission 273

U–Th–Ra Isotope Dating to Constrain the Youngest Eruption of Tatun Volcanic Group

Seismological studies revealed a magma reservoir beneath the Taipei metropolis last year, in which the Tatun Volcanic Group (TVG) in Taiwan lies, creating a large concern to if and when the volcanoes will erupt again. Recent U–Th–Ra isotope analyses conducted on morphologically young lava dome of TVG present crystallization ages as young as 1,370 years or less; this is a relatively young age compared to previous dating done on TVG, which suggested ages from tens of thousands to hundreds of thousands of years. The young age is much more plausible, as the terrain of the volcanoes have not been heavily eroded despite abundant rainfall, but also defines the TVG as active. The discordance in age can be explained by admixing of xenocrysts from older rocks into new lava, meaning the rocks will appear older in the results most previous dating methods yield. With a combination of ^{238}U – ^{230}Th and ^{226}Ra – ^{230}Th dating on plagioclase, pyroxene, amphibole, magnetite mineral separates, and whole rock, previous studies were able to constrain the crystallization ages of two samples. Therefore, we will be conducting U–Th–Ra isotope analyses on various lava flow samples in the area in hopes of obtaining the age of the youngest eruption and the connection between crystallization and eruption ages of the volcanoes of TVG. Meanwhile, fission track analyses and Ar–Ar dating will be done alongside for comparison.

Yuki Yasuda

Submission 380

Collapse mechanism of small calderas: a case study of the Ohachidaira caldera, Hokkaido, Japan

In order to elucidate the formation mechanism of small calderas, we have investigated the 30 ka Sounkyo eruption (VEI 5) during which the Ohachidaira caldera (2 km in diameter) formed. At distal sites, the Sounkyo eruption products comprise a pumice-fall deposit and the overlying Sounkyo ignimbrite. The proximal products which crop out around the caldera consist of five units, from base to top: pumice and scoria-fall deposit (SK-A), climactic ignimbrite (SK-B), lithic breccia (SK-C), scoria-fall deposit (SK-D), and ignimbrite (SK-E). A thin fine-ash layer caps SK-C lithic breccia and is overlain by SK-D, indicating a short hiatus after ejection of the lithic breccia. The distal pumice-fall deposit and the Sounkyo ignimbrite correlate with the proximal fall unit SK-A and ignimbrite units SK-B and -E, respectively, on the basis of their lithological and petrological characteristics and paleomagnetic directions. The total lithic volume ejected during the eruption is comparable to the present caldera volume, suggesting that the Ohachidaira caldera formed mainly by explosive reaming rather than caldera collapse. This casts doubt on the common interpretation that lithic breccias associated with caldera-forming eruptions represent the marker of caldera collapse. The diversity of lithic component of the lithic breccias ejected in large caldera-forming eruptions, such as at Crater Lake, Santorini, and Phlegraean Fields, may record the opening of multiple vents. Moreover, the significant volume of the deep-origin lithics as well as the shallow-origin ones in the lithic breccias suggests conduit erosion over a wide depth range, which is consistent with the interpretation of the lithic breccias. In the case of small caldera-forming eruptions, such as at Ceboruco and Ohachidaira, however, the deep-origin lithic content in the lithic breccias decreases, compared to the preceding deposits of the same eruption, at the expense of the shallow-origin lithics, indicating that the lithic breccias reflect a change of the shallow part of the conduit system. Considering that SK-C lithic breccia was followed by the eruptive hiatus, we hypothesize that SK-C lithic breccia marks a collapse or widening of the shallow part of the conduit and vent that (1) produced abundant lithics, (2) choked the conduit, and (3) stopped the eruption. We conclude that the presence of lithic breccias at small caldera-forming eruptions does not necessarily reflect the presence of caldera collapse.

Akihiko Yokoo, Kyoka Ishii, Takahiro Ohkura, Takahito Kazama

Submission 1301

Monotonic infrasound waves at the 2014–2015 eruption of Aso Volcano, Japan

At Aso volcano in Japan, 160-days long magmatic eruption occurred in 2014–2015 after a 20-years dormancy. This eruption was the first event that we could monitor by our infrasound network deployed around the crater. During a whole period of this eruption, in both cases when ash venting and Strombolian explosions occurred, monotonic infrasound waves were observed almost everyday. Estimated source location of the signals by considering topographic effect and atmospheric condition were highly stable at the active vent. Peak frequency of the signals 0.4–0.7 Hz varied with time, however, had no good correlation with difference of eruption style. We speculate that these signals were related to resonant frequencies of a void in the conduit, uppermost part inside the vent. For simplicity, we assumed that shape of the void was a open-ends conical pipe. At the end of April, length of the pipe determined from analysis of ballistic trajectories was 200-250 m. This indicates that sound speed in the pipe occupying by volcanic gases was 400-500 m/s, which suggests temperature of the gases was 450-550 K. These results corresponds results of independent seismo-acoustic analysis and were considered as reasonable. Because we successfully measured time evolution of size of the eruptive vent, radius of the exit, we could also estimate both length and base radius of the tube. We thus constrained sound velocity inside the vent as 300-400 m/s for the first one-month of the 2014–2015 eruption when continuous ash emissions were observed. This value can be accounted for by significant gas mass fraction of the ash plume, a few tens wt.%. Since ash plume do not have a chance to increase the gas mass fraction before it reaches to the atmosphere from its original value as the gas content in the magma, contribution of additional gases from excess degassing in magma supply system of the volcano was inferred. We also estimated volume of the pipe at the end of the eruption when crater bottom was collapsed on 3 May 2015, as $2\text{--}4 \times 10^5 \text{ m}^3$. This volume is the same order of, - however, is insufficient relative to -, total subsidence measured from photo-based digital elevation models. This discrepancy indicates that the collapse might be triggered by drain-back of magma with a volume of $1\text{--}3 \times 10^5 \text{ m}^3$. Then, collapsed materials filled the space of the vent including the space where escaping magma had filled, which resulted in perfect cease the magmatic eruption activity.

Nicola Young, Joachim Gottsmann

Submission 479

Inversion of Bouguer data at Campi Flegrei: Imaging the Hydrothermal Plume

We present the results of a high spatial density gravity survey of Solfatara tuff cone and the surrounding area within Campi Flegrei, Italy. Campi Flegrei experienced deformation on the order of meters in the 1970's and 80's and numerous mini-uplift events on the order of centimetres have occurred since. This deformation has been attributed to magmatic intrusions, perturbations to the hydrothermal system and a combination of both instigators. Hydrothermal fluids and gases are released most vigorously at Solfatara and at Pisciarelli nearby. Thermo-hydro-mechanical models explaining the measured fumarole emissions and mini-uplift events require a plume of ascending hot H₂O vapour and CO₂ from depth. Geophysical techniques such as electromagnetism, electrical resistivity, and active seismic imaging have resolved the subsurface architecture to depths between a few hundred meters to 3 km depth at Solfatara, but no gravity survey has been carried out since 1968. We used a Scintrex CG5 gravimeter and simultaneous benchmark localisation using a GNSS system to create a dense survey grid of 51 stations within Solfatara crater, and a reduced coverage network of 36 further stations outside the crater to 4 km distance. Results show an overall broad negative local Bouguer anomaly ~5 km in width with an amplitude of ~10 mGal centered approximately 1 km NW of Solfatara. Localised short wavelength (100 m) negative Bouguer anomalies within the Solfatara crater reach ~1 mGal in amplitude. We perform a 3D inversion of the local Bouguer anomaly to image the spatial density distribution. We interpret a low density body imaged to around 250 m depth beneath Pisciarelli as the current center of the Solfatara hydrothermal plume.

Elham Yousefzadeh, Adrian Pittari, David J. Lowe, Beth R.S. Fox

Submission 698

Physical characteristics of the matrix of the 1.2 Ma Ongatiti Ignimbrite: implications for fine-scale eruption and emplacement processes in voluminous pyroclastic flows

The widespread rhyodacitic to rhyolitic Ongatiti Ignimbrite was emplaced during a supereruption 1.2 Ma ago in the central North Island (New Zealand). The Mangakino Caldera, the oldest volcanic centre in the Taupo Volcanic Zone (TVZ), is recognized as the main source of the Ongatiti Ignimbrite. The Oparau Tephra and (informal) unit K12 of the Kauroa Ash sequence have been recognised as the distal equivalents of the Ongatiti Ignimbrite. This study focuses on the textural characteristics and components of the ignimbrite matrix to better understand the magma fragmentation process, to assess the transportational and depositional dynamics of the gas-ash fluid, and also to assess the post-emplacement process. The microtextures of ignimbrite matrix samples were described and quantified using optical petrography, scanning electron microscopy (SEM), back-scattered electron imaging (BSEI), and elemental analyses (EDS). The matrix is poorly sorted and is characterised by variations in the size and texture of pumice fragments, glass shards, crystals and lithic clasts. Glass shards range in shape between dominantly platy, Y-shaped, and complex shapes and in size from a few microns to about 900 microns. Due to the degree of devitrification and chemical alteration, shards range in colour from colourless to dark brown. Glass shards transition into complex pumice clasts at larger sizes. The main pumice textures are fibrous, dense, spherical and elongate vesicular and mixed textures. The matrix is crystal-rich and comprises primary volcanic crystals that are mostly subhedral to anhedral in shape. These crystals range between 100 microns to a few 1000 microns in size and comprise plagioclase, quartz, pyroxene, hornblende, and Ti-Fe oxides. The eutaxitic texture and degree of welding in the matrix are defined by crystal-crystal contacts and deformation of glass shards around particles, and the highest degree of welding is shown by moderately deformed shards. In addition, the ignimbrite matrix shows devitrification and vapour phase alteration at some sites. The range of juvenile particle size and morphology indicate that the microstructure of the erupting magma foam was heterogeneous. This variable aggregate of particles also shows the complexity of particle size and shape in the pyroclastic flow ash-gas fluid.

Sung-Hyo Yun, Cheol-Woo Chang

Submission 445

Pyroclastic Density Current Simulation using TITAN2D for Jeju Volcanic Island, Korea

In order to determine the runout range of pyroclastic density currents on Jeju volcanic island, column collapse on Dodubong, Suwolbong, Songaksan, and Ilchulbong monogenetic volcanoes and lava dome collapse on 8 locations of outer rim of summit baekrokdam crater were simulated by TITAN2D numerical simulation program. We set the internal friction angle of the pyroclastic density currents as 35° and bed friction angle as 15° for column collapse, internal friction angle as 30° and bed friction angle as 20° for lava dome collapse. Then we set the eruption column height, vent radius, height and radius of lava dome, initial speed of collapse and simulation times. And we carried out numerical simulations for a total of 288 scenarios. The result shows that the maximum runout range was 6.2 km in case of column collapse with VEI 3, and 13.4 km in case of lava dome collapse. This study can be used database for manufacturing of hazard map to minimize damages caused by pyroclastic density currents occurred on Jeju island. This research was supported by a grant [MPSS-NH-2015-81] through the Disaster and Safety Management Institute funded by Ministry of Public Safety and Security of Korean government.

David Zakharov, Ilya Bindeman

Submission 349

Triple oxygen systematics of hydrothermally altered rocks: A new tool in studying water-rock interaction

Intrusion of magma into subsurface layers of crust induces hydrothermal systems that are charged with groundwater, meteoric water or oceanic water. Traditionally, $\delta^{18}\text{O}$ and $\delta^2\text{H}$ in hydrothermally altered rocks are used to derive the isotopic composition of hydrothermal fluids and to trace the source of the fluids. However, rocks that experienced post-depositional alteration through secondary hydration, formation of clays or metamorphism represent a challenge for traditional stable isotope approaches. To tackle this challenge we explore a novel approach that is based on triple oxygen isotope systematics in hydrothermally altered rocks. In our laboratory we use high-precision mass spectrometry and newly developed effective gas purification technique to detect variations in the relationship between $\delta^{17}\text{O}$ and $\delta^{18}\text{O}$. Simultaneous measurements of triple oxygen isotopes in terrestrial materials show that the mass-dependent fractionation leads to slight but systematic variations in relationship between $^{17}\text{O}/^{16}\text{O}$ and $^{18}\text{O}/^{16}\text{O}$. Hydrothermal alteration in shallow hydrothermal systems represents mixing between silicates and meteoric or oceanic water. Simultaneous measurements of $\delta^{17}\text{O}$ and $\delta^{18}\text{O}$ allows to derive isotopic composition of original water involved in hydrothermal alteration. Original isotopic equilibrium between hydrothermal minerals does not need to be preserved in order to estimate $\delta^{18}\text{O}$ of original hydrothermal fluid. Triple oxygen isotope systematics constrains the water-to-rock ratios at which hydrothermally altered rocks were formed. To test the usefulness of the triple oxygen isotope approach we analyze hydrothermally altered rocks Iceland, Crater Lake in Oregon and Precambrian rocks, including some of the lowest terrestrial $\delta^{18}\text{O}$ rocks (-27‰ VSMOW) from subglacial Paleoproterozoic hydrothermal systems. We discover the involvement of meteoric water with $\delta^{18}\text{O}$ of -40‰ (essentially glacial melt waters) during an episode of snowball Earth in amphibolite-facies rocks from the Baltic Shield using triple oxygen isotopes. We analyzed remarkably well-preserved Paleoproterozoic submarine basalts for conventional $\delta^{18}\text{O}$ and $\delta^2\text{H}$ as well as triple oxygen isotopes to derive $\delta^{18}\text{O}$ of the 2.4 Ga ocean. The results of conventional analyzes and triple oxygen isotope analysis compare well. Triple oxygen isotopic approach in hydrothermally altered rocks is a new tool that can be used in the study of rock-water interaction in fossil hydrothermal systems and ore deposits.

Brian Zambri, Alan Robock, Anja Schmidt, Michael Mills

Submission 862

Modeling Climate Impacts of the 1783-1784 Laki Eruption in Iceland

The Laki eruption in Iceland, which began in June 1783, was followed by many of the typical climate responses to volcanic eruptions: suppressed precipitation and droughts, crop failure, and surface cooling lasting two to three years. In contrast to the observed cooling in 1784-1786, the summer of 1783 was anomalously warm in western Europe, with July temperatures reaching more than 3°C above the mean in some areas. While climate models can generally reproduce the surface cooling and decreased rainfall associated with volcanic eruptions, model studies have failed to reproduce the extreme warming in western Europe that followed the Laki eruption. As a result of the inability to reproduce the anomalous warming, the question remains as to whether this phenomenon was a response to the eruption, or merely an example of internal climate variability. Using the Community Earth System Model from the National Center for Atmospheric Research, we investigate the role of the aerosol indirect effect of the “Laki haze,” and the effect of the eruption on Europe’s climate. Results indicate that the extreme summer temperatures may be attributed to natural variability. On the other hand, the unusually cold winter in Europe appears to have been due to the eruption, which forced a negative phase of the North Atlantic Oscillation in conjunction with a positive phase of the El Niño Southern Oscillation. Understanding the cause of this anomaly is important not only for historical purposes, but also for understanding and predicting possible climate responses to future high-latitude volcanic eruptions.

John Zayac, Marc-Antoine Longpré, Eveling Espinoza, Armando Saballos

Submission 1164

Eruptive History and Mafic-to-Silicic Magma Interactions at Monte Galán and Momotombo Volcanoes, Nicaragua

Momotombo volcano, one of Nicaragua's most iconic volcanic landmarks, erupted in 2015–2016 after 110 years of quiescence. In this work, we use field and geochemical data to reconstruct the volcanic history and magmatic system evolution of Momotombo and neighboring Monte Galán caldera. Monte Galán is a relatively unstudied collapse structure, 4.5 km in diameter, that intersects the northwest flanks of Momotombo, whose recent lavas in turn overlap the caldera walls, indicating that the two centers have intertwined eruptive histories. We recently discovered a thus far undocumented outcrop — located in a quarry 2.5 km west of the caldera rim, near Loma La Chistata — that provides clear exposure of several tephra falls interbedded with pyroclastic flow deposits. The two thickest plinian pumice fall units (6 m and 3 m thick) are preliminarily interpreted to record rhyodacitic, caldera-forming eruption(s) at Monte Galán. In the stratigraphic sequence leading up to the first major plinian pumice fall deposit, we observe interbedded basaltic ash and more silicic pumice that lack mingling textures but also appear to have been deposited continuously, indicating close temporal and spatial eruption of varying magma types. The region surrounding the caldera is blanketed with thick dacitic to rhyolitic tephra falls and ignimbrite deposits. Early work on these deposit suggested that they originated from a series of volcanic centers located in the La Paz Centro and Puerto Momotombo area [1]. Recent work has suggested that they actually originate largely from the concealed Malpaisillo caldera structure to the north [2]. Highway construction to the southwest of the caldera has uncovered new road cuts with excellent exposures of the structural and temporal relationships between these units, including spectacular unconformities marked by paleosols, indicating protracted felsic volcanism in the region. Our work expands upon both of these studies to identify the deposits of Monte Galán in these outcrops and discuss the impact of the caldera forming eruption in the evolution of the region. We also geochemically investigate the possible interactions between the magmatic system(s) feeding Momotombo and Monte Galán.

[1] Hradecky et al. (2001), CGU/INETER report.

[2] Stoppa (2015), M.Sc. Thesis, University of Fribourg.

Georg Zellmer, Jun-Ichi Kimura, Qing Chang, Gregory Shellnutt, May Sas, Phil Shane

Submission 73

Sr and Pb isotopic compositions of variably altered feldspars in the 1.14 Ga Great Abitibi Dyke: implications for isotopic studies and dating of giant radiating dyke swarms and ancient plutonic rocks

Radioisotope analysis and geochronology of plutonic rocks is an important method for deriving the provenance and age of ancient magmatic episodes, and the petrogenetic processes operating during emplacement of giant radiating mafic dyke swarms and associated deposits. Sr isotopic compositions of unaltered and variably altered feldspar from the 1.14 Ga gabbroic Great Abitibi Dyke (GAD), Ontario, Canada, obtained via laser ablation inductively-coupled plasma mass spectrometry (LA-ICPMS), allow us to distinguish the effects of progressive alteration on feldspar isotopic compositions. The data display an alteration trend between fresh, low-Rb plagioclase with $^{87}\text{Sr}/^{86}\text{Sr}$ ratios of circa 0.70445 and high-Rb alkali feldspar with $^{87}\text{Sr}/^{86}\text{Sr}$ ratios of 0.7059. This alteration trend is incompatible with simple mixing between low- and high-Rb domains, and instead has an age significance. Feldspar Rb-Sr ages range from concordant with the baddeleyite U-Pb emplacement age of the dyke to a few hundred million years post-emplacement. Pb isotopic compositions of fresh GAD plagioclase were also obtained, producing a growth curve that yields an age of circa 1 Ga, approximately consistent with the emplacement age, and a μ value of 8.3. Average initial $^{87}\text{Sr}/^{86}\text{Sr}$ of fresh GAD plagioclase ($t \sim 1$ Ga) of 0.70445 is almost that of the chondritic uniform reservoir (CHUR) of the present day (0.70452). Using a single stage evolution model, the Rb/Sr ratio of the GAD source would thus need to be circa 1.27 times higher than that of CHUR to accomplish the observed radiogenic Sr at circa 1 Ga. This study highlights the need for microanalysis to differentiate between alteration and magmatic processes when doing Sr isotope work, and shows the potential of this technique for rapid age estimation of plutonic rocks as well as for constraining mantle compositional variations through space and time.

Ling Zeng, Lili Cheng, Jason Herrin, Fidel Costa

Submission 618

CE 1.0: A MATLAB-based software for computational phenocryst extraction and statistical petrology

It is nowadays possible to collect large-area backscattered electron images of entire standard thin sections in a matter of a few hours. These greyscale images can be calibrated for the compositions some minerals (e.g. plagioclase) with a small number of electron microprobe analysis, and thus provide a wealth of quantitative data for hundreds of crystals. However, to effectively make use of the textures and compositions of large numbers of crystals to understand magmatic processes we need to be able to automatically outline and segregate the crystals of interest from the rest of the sample. Here, we present CE 1.0, a set of MATLAB routines using dilation methods to outline plagioclase crystals in grayscale images of volcanic rocks. Users are able to outline crystals by setting several parameters such as number of voids, grayscale threshold values, and the number of crystals of interest. The crystals extracted from the image could then be saved either as individual images or collectively in one image that could be used for crystal size and zoning studies. By calibrating image grayscales to plagioclase compositions, users can acquire composition distribution maps useful for statistical analysis. An example of this methodology is provided for electron images of a sample from the 1947 eruption of the Mayon volcano, Philippines to demonstrate use of CE 1.0 to outline plagioclase crystals from this basaltic andesite sample, and then to obtain the compositional distributions. These data can then be used in combination with statistical analysis (Cheng et al., 2017) to unravel crystal populations.

Cheng, L., Costa, F., Carniel, R. (2017) Unraveling the presence of multiple plagioclase populations and identification of representative two dimensional sections using a statistical and numerical approach. *American Mineralogist*, doi: 10.2138/am-2017-5929CCBYNCND

Anke Verena Zernack, Jonathan Procter, Shane Cronin, Emma Singh

Submission 934

A complex interplay of sediment erosion and deposition during the 18 March 2007 crater-lake breakout lahar at Mt. Ruapehu, New Zealand

The long-anticipated 2007 Ruapehu Crater Lake breakout lahar provided a unique opportunity to capture a complete dataset of a single mass-flow event. On 18 March 2017, the tephra dam that had been blocking the lake outlet collapsed, releasing 1.3 million m³ of water into the Whangaehu River channel. The generated flow reached its maximum sediment-carrying capacity at 22 km from source and continued to travel as fully-bulked lahar for at least another 40 km along the Whangaehu River. We focus on medial reaches, following attainment of the highest sediment concentrations (25-40 km) to evaluate sedimentary processes during the lahar passage by combining the depositional record with high-precision, pre- and post-event LiDAR topographic data and detailed observations of flow height, velocity and seismic energy.

LiDAR data reveal a broad alternating pattern of erosion and deposition along this sinuous river stretch with net-erosion dominating in straight sections and deposition mainly occurring on outer channel bends. The deposits comprise several discrete units that differ in grainsize, texture, thickness and distribution depending on local channel conditions and time-variant flow rheology. The dynamic flow data show a rapidly rising watery bow-wave ahead of the lahar, which emplaced bedded, moderately-sorted medium sands on middle- to high-level banks. High flow velocity and turbulence promoted erosion in near-channel sites. Overlying massive, reversely graded, very poorly-sorted sandy gravels were deposited by the highly sediment-charged main lahar body. Decrease in stage height and retreat of the concentrated flow back into the channel ceased deposition on the upper banks and initiated near-channel accumulation of thick, normally graded gravelly units at channel bends and a thin coarse sandy layer along straight sections. The final depositional stage was marked by bedded, moderately- to poorly-sorted sandy deposits in near-channel sites and initially on middle slopes, with pulses in the waning flow producing alternating layers of coarse and medium sands. The step-wise drop in flow stage resulted in simultaneous erosion of the previously deposited sediments and successive cutting of terraces.

The 2007 lahar event has provided more specific constraints on erosion and deposition rates and processes in relation to tempo-spatial flow variations and local river channel morphology that could help mitigate future risks to communities and infrastructure from such events.

Yan Zhan, Patricia M. Gregg, Estelle Chaussard, Yosuke Aoki

Submission 346

Investigation of volcanic unrest in Indonesia using statistical data assimilation with a two-source magma chamber model

A critical goal in the field of volcanology is to identify the precursory information that provides the best indication of eruption likelihood. In this study, a 3D, statistical data assimilation framework is used to combine InSAR deformation data with magma chamber models to investigate six restless volcanoes in the west Sunda Arc of Indonesia. Of the six inflating volcanoes, three had eruptions following inflation and three did not. The Ensemble Kalman Filter (EnKF) method is used to combine InSAR observations of surface deformation with geodynamic models to search for precursory signals that may provide an indication of eruption potential. To represent the multi-component deformation observations, a two-source analytical model is established that simulates both the surface uplift by an inflating shallow magma chamber and the subsidence resulting from the deflation of a deeper source. The models are updated by assimilating InSAR line of sight (LOS) data collected from the ALOS-1 satellite between 2007-2011. By conducting a two-step EnKF analysis, model parameters are estimated throughout the time span of the InSAR coverage providing updates to the model trajectory as new data becomes available. The depth of the shallow sources for the six volcanoes is predicted to vary from 500 m to 3000 m below sea level and generally, models for the three erupting volcanoes (Sinabung, Kerinci, and Slamet) predict shallower sources than at the three volcanoes that inflated but did not erupt (Lawu, Lamongan, and Agung). Furthermore, all six volcanoes exhibit continuous volume inflation, except for Kerinci, which stagnates after its eruption in 2009, indicating a possible stability of the magma storage system. From the first application of EnKF with real InSAR data, we find that the EnKF performs well to track the shallower chamber. However, the EnKF has difficulty determining the parameters of the deeper sources to explain subsidence around the edifices of Kerinci, Lamongan, Lawu, and Sinabung. The InSAR data was corrected for topography-related atmospheric errors that could affect the inflation signal within the edifice, but the subsidence signal observed outside of the volcanic edifices with inconsistent temporal patterns might be affected by atmospheric contamination. Therefore, further work is necessary to better constrain InSAR data error so that the EnKF can distinguish volcanic subsidence from interference associated with atmospheric phase delays.

Li Zhang, Huaiwei Ni

Submission 786

A general model of water diffusivity in calc-alkaline silicate melts and glasses

Water diffusivity governs the transport of water in silicate melts throughout the process of magma differentiation, all the way to the rate of bubble growth during volcanic eruption and hydration of volcanic glass on Earth's surface. Igneous rocks along the calc-alkaline series (basalt, andesite, dacite, and rhyolite) are commonly found in volcanic arcs at water-rich subduction zones. In the past several decades, continuous efforts have been devoted to collect experimental data of water diffusivity in calc-alkaline silicate melts and glasses and to understand the underlying physical mechanism. Significant progresses in this field now make it possible to develop a unified, mechanistic and quantitative model of water diffusion and diffusivity in calc-alkaline silicate melts and glasses. After compiling a significant amount of literature data, we develop a general water diffusivity model that accounts for the combined influence of temperature, pressure and melt composition on water diffusivity. This model considers the contribution of both molecular H₂O (H₂O_m) and hydroxyl (OH) to water diffusion. Mole fraction of Si among all cations is found to be a good index of melt composition. This general water diffusivity model, which can reproduce nearly all experimental data within a factor of 2.5, is recommended for use in future applications.

Yunjun Zhang, Falk Amelung, Yosuke Aoki

Submission 160

Diverse volcanic deformation in Kyushu, SW Japan from a decade of L-Band InSAR time series analysis

With advance in spaceborne geodetic technique, such as time series InSAR, now we can dive into decades of satellite data archive and see ground displacement changing through time. This approach provides us a relative comprehensive (high-resolution in 3D space and relative continuous low-resolution in time) way to examine temporal evolution of ground behavior on the surface. Here we show our time series InSAR results exploited from a decade of L-band SAR observation using ALOS and ALOS-2 on Kyushu, southwest Japan. Widespread volcanic deformations are found during both eruptive cycle and inter-eruptive period, summarized into following three types.

1) Volcanic inflation and deflation due to magmatic activity on Kirishima and Sakurajima volcanoes. (a) Both pre- and co-eruptive deformation due to its VEI=2 eruption in 2011 January 26 are captured by ALOS, as shown in Fig. 1. Two sources are identified: a shallow source at mean sea level beneath the summit, which corresponds to the 2008-2010 phreatic events; and a deep magmatic chamber at ~10 km depth ~5 km away to the west of Shinmoe-dake, corresponding to the 2011 eruptive event, it started inflating ~1 year before the eruption with a linear velocity of ~4 cm/yr in LOS (Line-of-Sight) direction. The volume change associated to the pre-eruptive deformation is close in amplitude to the volume change related to the co-eruptive deformation. It means that the amount of new magma that enters into the magma chamber was transferred to the surface to feed the eruption, indicating that the shallow reservoir is not a large magma storage zone but acts more as a transfer zone between deep source and surface.

(b) Sakurajima shows very complex deformation patterns (Fig. 2). Three individual dike intrusion events are identified in 2010, 2011 and 2015 using ALOS and ALOS-2 data, as shown in Fig. 2(b-d); sudden inflation on the north flank starting at the beginning of 2011; and the long term inflation around the Aira caldera ring.

2) Subsidence due to cooling magma bodies, lava flow or hydrothermal activities are found in Kuju, Unzen, Aso, Kirishima and Sakurajima volcanoes (Fig. 1-3).

3) Subsidence due to geothermal activities: Hatchobaru geothermal power plant near Kuju volcano (Fig. 3b), Yamagawa geothermal power plant near Ata caldera (Fig. 3e) and Yunotani Nagano hot spring, or onsen, near Aso caldera (Fig. 3d).

All InSAR time series product are available through our web viewer (<http://insarmaps.miami.edu>).

Brian Zimmer, Piotr Arlukowicz, Grant Montieth, Lauren Richardson

Submission 63

High-Precision Photogrammetry for Change Detection in Non-Georeferenced Data Sets

Structure from Motion (SfM) uses photogrammetry and computer software to construct 3-dimensional models from a series of 2-dimensional digital photos. This technique can be easily applied to georeferenced data sets to detect changes in landscape morphology over time for large scale (>1m³) areas and if permanent control points can be established, such as rebar spikes, change detection is possible on smaller scale (3) areas. However, it becomes significantly more complicated to quantifiably detect change when permanent control points are either missing or not possible. This paper describes a method to determine the resolution of change-detection software when no reference frame data is available. The technique uses Agisoft Photoscan Pro, Cloud Compare, and Blender animation software to identify and quantify mm-scale erosional changes in decimeter-scale features. Using this technique we are able to identify both where erosion is occurring as well as the rate of change. The method can also be applied to larger structures, such as volcanoes, as an inexpensive method of monitoring for ground deformation or dome growth even in the absence of precise GPS data.

Matthew Zimmerer, Matthew Heizler, William McIntosh

Submission 1220

An age-based assessment of volcanic hazards within the Rio Grande Rift and along the Jemez Lineament, New Mexico, U.S.A.

Nearly 200 new Ar/Ar ages of late Quaternary (i.e., < 500 ka) eruptive centers in New Mexico provide important information about eruption frequency and vent migration patterns that are vital for hazard assessment. Ages were determined using the ARGUS VI high-sensitivity multi-collector mass spectrometer, which yields more than an order of magnitude increase in precision compared to the older generation mass spectrometers that determined many of the previous age constraints for the region. Late Quaternary volcanism in the Rio Grande Rift and along the Jemez Lineament is distributed into approximately 12 major volcanic fields and is predominantly mafic in composition with the exception of silicic eruptions at the Valles caldera. The average eruption frequency for individual fields during the late Quaternary ranges from as rapid as one eruption per 10 ka to as little as one per 45 ka. All fields show significant pulses in activity where the ages of individual eruptions cannot be distinguished at current levels of precision. Calculating a statewide eruption frequency during the last 500 ka is challenging because of the incomplete nature of the volcanic record. However, the youngest vents in the region are well identified and an accurate recurrence rate can be calculated for just the last 100 ka, which indicates a frequency of 1 eruption per 3.7 ka. This eruption frequency suggests that the current eruptive hiatus (3.9 ± 1.2 ka defined by the youngest eruption in NM) is not necessarily indicative of waning activity, but is instead a characteristic tempo of activity in the region. New ages, together with published ages, have also identified a previously unrecognized temporal-spatial pattern of volcanism. Most fields display a west-to-east migration in volcanism at rates that could be explained by the motion of the North American plate over a relative fixed source. This newly discovered migration pattern only pertains to vents that erupted in the last 1-3 Ma; older vents do not appear to display the same migration in volcanism. Time-space patterns suggest that the most likely location for future eruptive activity is near or east of the youngest vents within each of the late Quaternary monogenetic basaltic volcanic fields. This research showcases why similar studies should be expanded to other late Quaternary centers in the southwestern United States to better characterize the volcanic hazards throughout the region.

Jacques Zlotnicki, Yoichi Sasai, Malcolm Johnston, George Vargemezis, PHIVOLCS EM (E. Villacorte, P. Reniva, P. Alanis, Juan M. Gordon Jr) Team

Submission 123

Taal volcano in Philippines: What is the future?

The last three eruptions of Taal volcano in the Philippines occurred in 1911 (VEI=3), 1965 (VEI=4), and 1977. In 1911, deposits devastated the Island and the western part of the prehistorical caldera in which the Island is lying. Ash fell on Manila city located 60 km away from the volcano. The 1965 eruption opened a new crater in the southwestern part of Island. Violent base surges happened. Ash columns reached 20 km in altitude and spread ash up to 80 km to the west. About 90 Mm³ of ejecta were expelled. The activity continued episodically until October 1977. Almost 40 years have passed, and the period without an eruption is one of the longest in historical time.

However, Taal regularly suffers large seismic crises. The most important crises occurred between Feb. 14 and 28, 1992 and between March 11 and May 31, 1994. More than 2500 and 1550 earthquakes were recorded in a day in 1992 and 1994, respectively. Up to 400 m long fissures opened near the northern crater rim. Uplift of the northern part of the volcano was estimated to be 20 cm and 15 cm in 1992 and 1994, respectively. Between 2000 and 2004, cyclic inflation and deflation processes of some month's duration were identified and the source of deformation was estimated to be at about 5 km depth. The volcano entered into a new phase of seismic activity after April 19, 2010.

Since 2005, EMSEV (<http://www.emsev-iugg.org/emsev/>) and PHIVOLCS (<http://www.phivolcs.dost.gov.ph/>) make efforts to understand the geological setting and the plumbing system, as well as to continuously monitor the activity with electromagnetic and others geophysical methods. A huge hydrothermal system (HS) lies at about 2.5 km depth below this Island. This HS relays and possibly buffers upwelling magmatic fluids and thermal transfers, and induced ground deformation by pore pressure changes. Several studies of the location of the deformation source(s) feeding the HS and responsible for the primary indicate that the average depth could be between 4 and 6 km, with a location that seems to fluctuate with time.

Two key issues arise that will be discussed during the session. First, do we observe changes in the activity during the past 12 years of joint EMSEV-PHIVOLCS cooperation? Second, are we able to identify where further activity will take place and why? To approach these difficult questions, we will discuss the latest results obtained with EM and temperatures surveys.

Jeffrey Zurek, Glyn Williams-Jones, Isabelle Lépine

Submission 662

Geologically-constrained geophysical inversions of the Renard kimberlite pipes, northern Québec, Canada

Located in northern Québec, Canada, the Renard Diamond Mine consists of a cluster of nine diamondiferous kimberlite bodies emplaced (~640 Ma) into Archean migmatite, gneiss and granite of the southeastern Superior Province. Exploration and delineation of the Renard 2 pipe by Stornoway Diamond Corporation involved extensive drilling (~44,000 m) as well as airborne, ground and borehole geophysics (e.g., electromagnetic, total magnetic field, magnetic susceptibility). A comprehensive 3D geological model of the Renard 2 pipe was developed to guide mine development, and can be leveraged for a retrospective study focused on geologically-constrained geophysical models.

Using the GOCAD Mining Suite, in conjunction with VPmg geophysical code, 3D modeling of the magnetic data showed that current geological constraints for the Renard 2 and 3 pipes can effectively reproduce the geophysical signal, after accounting for remanent magnetization. Using only the geophysical datasets, the misfit on inversions suggest that the data is best fit by a cylinder (rather than the typical tapering kimberlite pipe shape), and that this shape continues to the bottom of the inversion model at a depth of 500 m. This is significantly more information than was available in the original exploration model, which saw maximum drill depths of ~100 m and ~250 m in the first and second campaigns, respectively. As such, this novel cost effective methodology can optimize the interpretation of near surface geophysical data to enhance effective target determination and assessment. Modelling also identified a currently unexplained near vertical linear feature which intersects Renard 2 and is not constrained by the drilling.

Furthermore, this study has enabled the development and testing of a methodology that utilizes the geophysical data, with only limited a priori geological constraints, to resolve exploration challenges elsewhere within the Renard kimberlite cluster. Iterative inversion models have been used to investigate depth and geometry for a range of different geophysical anomalies that are in various stages of development and exploration. Current inversion models for the anomaly associated with the Renard 1 kimberlite also suggest a body that continues beyond 500 m depth with a shape that does not taper significantly. Renard 1 is not currently in the mine plan and has seen only about 2,500 m of drilling.